64TH INTERNATIONAL CONFERENCE FOR STUDENTS OF PHYSICS AND NATURAL SCIENCES

OPEN READINGS 2021

MARCH 16-19 VILNIUS LITHUANIA

ABSTRACT BOOK

VILNIUS UNIVERSITY PRESS

Editors
Šarūnas Mickus
Rasa Platakytė
Simona Pūkienė

Cover and Interior design
Rasa Platakytė

Vilnius University Press
9 Saulėtekio Av., Building III, LT-10222 Vilnius
info@leidykla.vu.lt, www.leidykla.vu.lt

Bibliographic data of the book is provided in
Martynas Mažvydas National Library
of Lithuania's National Bibliography Data Bank (NBDB).

ISBN 978-609-07-0590-2 (PDF)

© Vilnius University, 2021

Dear participants,

Last year, as we were writing the opening word for “Open Readings 2020”, we still had hopes to see you all in Vilnius. That hope remains for next year, and for now we are still happy to meet you all virtually. It’s incredibly exciting to see that so many young scientists are eager to participate and share their work and passion with others.

We hope that you will enjoy this online conference experiment. The oral and poster sessions, the invited speakers’ lectures, the social events all remain. As long as you treat yourself to a cup of coffee during the breaks, hopefully it will feel just as any other “Open Readings” conference before this. And just like science experiments, we hope it will be about adjusting and adapting, and never giving up. We aim to help you find inspiration in the talks by world-class scientists and joy in exchanging ideas with your peers.

Yours sincerely,

“Open Readings” organizing team

Conference Chair:

Rasa Platakytė, *Faculty of Physics, Vilnius University, OSA and SPIE Chapters of Vilnius University*

Organizing Committee:

Simona Pūkienė, *Center for Physical Sciences and Technology, OSA and SPIE Chapters of Vilnius University*

Dovilė Lengvinaitė, *Faculty of Physics, Vilnius University, and OSA Chapter of Vilnius University*

Martynas Velička, *Faculty of Physics, Vilnius University*

Bernadeta Balčiukynaitė, *Faculty of Physics, Vilnius University, and SPIE Chapter of Vilnius University*

Gabrielė Kareivaitė, *Faculty of Physics, Vilnius University*

Kornelijus Pūkas, *Faculty of Physics, Vilnius University*

Laura Tauraitė, *Faculty of Physics, Vilnius University, OSA and SPIE Chapters of Vilnius University*

Lukas Naimovičius, *Faculty of Physics, Vilnius University*

Rimantė Bandzevičiūtė, *Faculty of Physics, Vilnius University, OSA and SPIE Chapters of Vilnius University*

Šarūnas Mickus, *Faculty of Physics, Vilnius University*

Vaida Marčiulionytė, *Faculty of Physics, Vilnius University, and SPIE Chapter of Vilnius University*

Živilė Čerškutė, *Faculty of Physics, Vilnius University, OSA and SPIE Chapters of Vilnius University*

Programme Committee:

dr. Kastytis Zubovas, *Fundamental Research Department, Center for Physical Sciences and Technology*

dr. Aurimas Vyšniauskas, *Department of Molecular Compound Physics, Center for Physical Sciences and Technology*

dr. Danielis Rutkauskas, *Department of Molecular Compound Physics, Center for Physical Sciences and Technology*

dr. Algirdas Mikalkėnas, *Institute of Biosciences, Life Sciences Center*

dr. Ramūnas Aleksiejūnas, *Institute of Photonics and Nanotechnology, Faculty of Physics, Vilnius University*

Enrika Celitan, *Institute of Biosciences, Life Sciences Center*

dr. Julius Vengelis, *Laser Research Center, Faculty of Physics, Vilnius University*

dr. Jonas Berzinš, *Light Conversion*

dr. Rasa Pauliukaitė, *Department of Nanoengineering, Center for Physical Sciences and Technology*

dr. Justina Gaidukevič, *Institute of Chemistry, Faculty of Chemistry and Geosciences, Vilnius University*

dr. Andrius Gelžinis, *Institute of Chemical Physics, Faculty of Physics, Vilnius University*

dr. Jurga Juodkazytė, *Department of Chemical Engineering and Technology, Center for Physical Sciences and Technology*

dr. Linas Vilčiauskas, *Department of Chemical Engineering and Technology, Center for Physical Sciences and Technology*

dr. Jurga Būdienė, *Department of Organic chemistry, Center for Physical Sciences and Technology*

dr. Aldona Balčiūnaitė, *Department of Catalysis, Center for Physical Sciences and Technology*

dr. Rasa Garjonytė, *Department of Organic chemistry, Center for Physical Sciences and Technology*

dr. Ilja Ignatjev, *Department of Organic chemistry, Center for Physical Sciences and Technology*

dr. Justinas Čeponkus, *Institute of Chemical Physics, Faculty of Physics, Vilnius University*

dr. Vytautas Jakštas, *Department of Physical Technologies, Center for Physical Sciences and Technology*

dr. Tomas Šalkus, *Institute of Applied Electrodynamics and Telecommunications, Faculty of Physics, Vilnius University*

dr. Vilma Kavaliukė, *Institute of Applied Electrodynamics and Telecommunications, Faculty of Physics, Vilnius University*

dr. Paulius Baronas, *Institute of Photonics and Nanotechnology, Faculty of Physics, Vilnius University*

dr. Rūta Kananavičiūtė, *Institute of Biosciences, Life Sciences Center*

dr. Marius Treideris, *Department of Physical Technologies, Center for Physical Sciences and Technology*

dr. Martynas Velička, *Institute of Chemical Physics, Faculty of Physics, Vilnius University*

dr. Virginijus Bukauskas, *Department of Physical Technologies, Center for Physical Sciences and Technology*

Ernesta Bužavaitė – Vertelienė, *Department of Laser Technologies, Center for Physical Sciences and Technology*

Chairmen:

dr. Linas Vilčiauskas, *Department of Chemical Engineering and Technology, Center for Physical Sciences and Technology*

dr. Linas Minkevičius, *Department of Optoelectronics, Center for Physical Sciences and Technology*

dr. Aidas Matijošius, *Laser Research Center, Faculty of Physics, Vilnius University*

dr. Aurimas Vyšniauskas, *Faculty of Chemistry and Geosciences, Vilnius University*

prof. Gintaras Valušis, *Department of Optoelectronics, Center for Physical Sciences and Technology*

dr. Mažena Mackoit-Sinkevičienė, *Department of Optoelectronics, Center for Physical Sciences and Technology*

res. prof. Aurelijus Rinkevičius, *Experimental nuclear and particle physics center, Faculty of Physics, Vilnius University*

Mihir Pendharkar

Stanford University,

USA

TOPOLOGICAL QUANTUM COMPUTING: A MATERIALS PERSPECTIVE

A quantum computer is theorized to aid in simulating nature quantum mechanically and various approaches to building a quantum computer are actively being pursued. Common to all approaches is the requirement for building a fault tolerance from errors due to external environmental perturbations (noise). Inherent fault tolerance is only native to one approach – topological quantum computation. This approach is based upon Majorana Zero Modes which are quasi-particles with no measurable charge or mass, that are bound to zero-energy. Quantum information is said to be stored non-locally in interactions of MZMs. These MZMs have been predicted to arise at the ends of 1D chain of electrons with strong spin-orbit coupling, when such a chain is transparently coupled to an s-wave superconductor and an external magnetic field is applied along the length of the chain. Signatures of MZMs were first reported in 2012 [1].

This talk will focus on the materials aspects of the challenge of topological quantum computing focusing primarily on exploring new superconductors and semiconductors for use in super-semi hybrid systems. Semiconductors like InAs and InSb when coupled to a superconductor like aluminum (Al), have been claimed to show zero energy end modes reminiscent of MZMs, though further proof is necessary. Increasing spin-orbit interaction in the host semiconductor is one proposed way of increasing topological protection from the environment [2]. InAsSb is one such compound semiconductor and this talk will discuss the growth of 1D nanowires and 2D quantum wells in this material system. On the same lines, increasing the superconducting energy gap is another parallel pathway to increasing topological protection. This talk will discuss the observation of two electron charging in superconducting tin, the first such reported observation after aluminum [3]. As tin offers a larger superconducting gap and higher in-plane critical field than aluminum, it is presented as a robust alternative for next generation super-semi devices. While confirming the observation of MZMs remains an outstanding challenge, exploration of novel superconductor-semiconductor combinations may help find the elusive Majoranas.

[1] V. Mourik, et al., *Science* **336** (6084), pp. 1003-1007 (2012)
[2] J.D. Sau, et al., *Phys. Rev. B* **85**, 064512 (2012)
[3] M. Pendharkar, B. Zhang, H. Wu, A. Zarassi, P. Zhang, et al., arXiv:1912.06071 (2019)

Chennupati Jagadish

Research School of Physics, Australian National University

Australia

SEMICONDUCTOR NANOSTRUCTURES FOR OPTOELECTRONICS APPLICATIONS

Semiconductors have played an important role in the development of information and communications technology, solar cells, solid state lighting. Nanowires are considered as building blocks for the next generation electronics and optoelectronics. In this talk, I will introduce the importance of nanowires and their potential applications and discuss about how these nanowires can be synthesized and how the shape, size and composition of the nanowires influence their structural and optical properties. I will present results on axial and radial heterostructures and how one can engineer the optical properties to obtain high performance lasers, THz detectors, solar cells and to engineer neuronal networks. Future prospects of the semiconductor nanowires will be discussed.

Klaus-Dieter Kreuer

Physical Chemistry of Solids, Max Planck Institute for Solid State Research

Germany

ENABLING HYDROGEN AS FUTURE ENERGY CARRIER: FROM THE LITHUANIA CRADLE TO WHERE WE ARE TODAY

The expected end of the “oil age” (for environmental reasons) will lead to increasing focus and reliance on alternative energy conversion devices and ways for storing energy. Future scenarios may comprise “hydrogen” as an energy carrier with high energy density and potentially high conversion efficiency into electric energy and vice versa [1]. A lot will depend on further progress in PEM (polymer electrolyte membrane) electrolyzer and fuel cell technology with many fundamental and engineering problems waiting to be solved.

The first who actually proposed a theory on the decomposition of water into hydrogen and oxygen by means of “électricité galvanique” [2] was the Lithuanian Freiherr Christian Johann Dietrich Theodor von Grotthuß. He introduced a concept of ionic conductivity which already captured in a qualitative way what 100 years later was described by the Nernst-Einstein relationship.In my presentation, I will tell the story starting from von Grotthuß all the way to state of the art research in an anecdotic way. I will touch upon i) the long standing issue of understanding proton conduction phenomena as an example of a process which, by no means, is unidirectional in nature, ii) the complex issue of developing materials with high performance, longevity and environmental benignity meeting critical cost targets and iii) exciting recent findings (fresh out of the lab) narrowing the gap between our visions and facts proven by good scientific practice.

[1] K. D. Kreuer ed.: Fuel Cells, Springer 2013, ISBN 978-1-4614-5785-5

[2] C. J. T. de Grotthuss: Mémoire sur la décomposition de l’eau et des corps qu’elle tient en dissolution à l’acide de l’électricité galvanique, Annales Chim. (Paris) vol. 58, 1806, 54 - 74

Tomas Tamulevičius

Institute of Materials Science, Kaunas University of Technology

Lithuania

SELF – ASSEMBLED NANOPHOTONICS

Noble metal-related resonant optical effects were puzzling humankind for centuries. In the modern era, plasmonics and related nanotechnologies gain even more attention. The peculiarities of localized surface plasmon resonances (LSPR) observed in nanostructures of silver, gold, copper, aluminum, and several more materials are well documented these days. However, the breakthrough necessary for bringing LSPR based consumer products is still on the way. The necessary precision and repeatability of manufacturing are the main technological bottlenecks impeding the scaling up. Bottom-up nanomaterial synthesis methods were always up-and-coming because of the resulting qualities and yields, but they were rarely capable of providing positional control, repeatability. A templated deposition is bridging the advantages of the two worlds, the high monodisperse and superb optical quality wet synthesized nanostructures are following deposition sites with the clean-room lithography-defined positional accuracies. Such artificially manmade two-dimensional materials or metasurfaces become functioning nano-optics devices. On-demand light absorption and scattering properties open new pathways for novel emerging applications in energy harvesting, light-filtering, nanolasing, sensing, and many others.

Urtė Neniškytė

Department of Neurobiology and Biophysics, Life Sciences Center

Lithuania

GARDENING THE BRAIN: INTERDISCIPLINARY APPROACH TO INVESTIGATE SYNAPTIC PRUNING IN DEVELOPING BRAIN

The mature brain connectome emerges through synaptic pruning of superfluous connections in developing brain. Microglia have central role in this process: they refine neuronal circuitry by phagocytosis and trogocytosis of synaptic structures. While a range of microglial receptors and soluble proteins have been identified to mediate synaptic pruning, up until now there has been limited data on neuronal „eat-me“ molecules that would label unnecessary synapses for microglial elimination. Since exposed phosphatidylserine is a well-established „eat-me“ signal for phagocytosis, we investigated the role of phosphatidylserine scrambling in synaptic pruning. We found that phosphatidylserine was preferentially exposed on synaptic structures and promoted microglia-synapse interaction. Phosphatidylserine exposure was developmentally upregulated and required the activity of Xkr8 – a major phospholipid scramblase, which was expressed throughout the brain and was developmentally upregulated after birth.

Conditional Xkr8 knock-out in excitatory neurons diminished axonal bouton trogocytosis and caused insufficient elimination of excitatory synapses. Furthermore, Xkr8 cKO brains had significantly higher axonal density in corticospinal tracts of pyramidal neurons, indicating reduced elimination of the whole axons. These morphological aberrations were followed by abnormal electrophysiological profiles of Xkr8-deficient neurons that exhibited increased spontaneous activity and the failure of functional synaptic maturation. Finally, Xkr8 deficiency led to increased global connectivity of the brain that was maintained into adulthood, as measured by functional MRI. This is the first evidence that mammalian synaptic pruning requires developmental phosphatidylserine exposure via scramblase activity, identifying the first „eat-me“ signal that is exposed on unnecessary synapses for their developmental removal.

Eglė Čekanavičiūtė

Space Biosciences Research Branch, NASA Ames

USA

NEUROIMMUNE RESPONSES TO SPACE RADIATION

The main health risks of human deep space exploration involve the damage to the central nervous system (CNS) and the immune system caused by exposure to ionizing radiation beyond the protective magnetic field of the Earth. The extent of CNS damage is partially mediated by the blood-brain barrier, which regulates interactions between CNS and the rest of the body. However, studies on blood-brain barrier in regulating CNS responses to ionizing radiation have been limited, especially in human tissue/organ analogs. Therefore, we developed a high-throughput 3D organ-on-a-chip system to study human blood-brain barrier impairments caused by deep space radiation, and here will present our first results using this system. Furthermore, in our lab we have been exploring the individual variability, genomic associations and secreted biomarkers of immune responses to space radiation, all of which might be used to address personalized health risks for astronauts. Ultimately, we aim to expand upon these results to uncover novel cellular and mechanistic targets for countermeasure development to reduce human CNS and immune damage in deep space exploration.

Daniele Faccio

School of Physics and Astronomy, University of Glasgow

United Kingdom

IMAGING WITH TIME: FROM MULTIPATH IMAGING TO HEALTHCARE APPLICATIONS

I will review some of our work in the area of computational imaging based on, or inspired by quantum technologies for light detection. The key aspect we have been investigating is the role of temporal (time-of-flight) information that can be recorded using single photon counting (and other) techniques. This temporal information allows a range of applications such as non-line-of-sight imaging or tracking, which I will briefly overview as in introduction to more general "multi-path" imaging, i.e. use of return echoes from a scene that have bounced multiple times between objects before being detected. Temporal information alone of multipath echoes can be sufficient to reconstruct a full 3D image of the scene and can be equally applied to light, radar and acoustic sensing. An extreme example of multipath information is diffuse imaging, i.e. imaging through highly scattering media with potential applications for through-body imaging (e.g. imaging inside the brain) and remote heart activity monitoring.

16 March, TUESDAY

09:00	Mihir Pendharkar TOPOLOGICAL QUANTUM COMPUTING: A MATERIALS PERSPECTIVE		
10:00	BREAK		
	ORAL SESSION O1		p.
10:15	Algita Stankevičiūtė, Łukasz Wyrzykowski EXPLORING BLACK HOLES WITH MICADO - THE FIRST LIGHT IMAGER OF E-ELT	O1-1	33
10:30	Matas Tartėnas, Kastytis Zubovas IMPROVING BLACK HOLE ACCRETION TREATMENT IN NUMERICAL SIMULATIONS	O1-2	34
10:45	Kasparas Karlauskas, Vidas Dobrovolskas, Arūnas Kučinskas EUROPIUM ABUNDANCE IN THE RED-GIANT BRANCH STARS OF GALACTIC GLOBULAR CLUSTER 47 TUCANAE	O1-3	35
11:00	Marcos Muñiz Cueli, Laura Bonavera, Joaquín González-Nuevo González, Andrea Lapi A DIRECT AND ROBUST METHOD TO OBSERVATIONALLY CONSTRAIN THE HALO MASS FUNCTION	O1-4	36
11:15	Martynas Laužikas, Kastytis Zubovas EVOLUTION OF TWO-PHASE GAS SYSTEM: IMPACT OF AGN-DRIVEN OUTFLOWS ON FRAGMENTATION OF TURBULENT MOLECULAR CLOUDS	O1-5	37
	ORAL SESSION O2		
10:15	Egle Ezerskyte, Arturas Katelnikovas SYNTHESIS AND OPTICAL PROPERTIES INVESTIGATION OF MULTI-COLOUR EMITTING $GDPO_4:CE^{3+}/TB^{3+},EU^{3+}$ NANOPARTICLES	O2-1	38
10:30	Did not participate	O2-2	39
10:45	Paulius Gaigalas, Vaclovas Klimas, Arūnas Jagminas IMPACT OF L-CYSTEINE ON THE COMPOSITION AND ELECTROCATALYTIC PROPERTIES OF MoS_2 FILMS	O2-3	40
11:00	Kernius Vilkevičius, Evaldas Stankevičius FEMTOSECOND LASER GENERATION OF MICROBUMPS ON GOLD THIN FILMS	O2-4	41
11:15	Lukas Naimovičius, Edvinas Radiunas, Barbara Chatinovska, Augustina Jozeliūnaitė, Edvinas Orentas, Karolis Kazlauskas DYKETOPYRROLOPYRROLE EMITTERS FOR NIR-TO-VISIBLE PHOTON UPCONVERSION	O2-5	42
11:30	BREAK		
	ORAL SESSION O3		
11:45	Did not participate	O3-1	43
12:00	Mantas Vaičiulis, Kazimieras Nomeika, Ramūnas Aleksiejūnas CARRIER LOCALIZATION IN InGaN STRUCTURES INVESTIGATED BY LIGHT-INDUCED TRANSIENT GRATING TECHNIQUE	O3-2	44
12:15	Daniil Pashnev, Tommi Kaplas, Vadym Korotyeyev, Vytautas Janonis, Andrzej Urbanowicz, Justinas Jorudas and Irmantas Kašalynas TEMPERATURE DEPENDENT ELECTRON EFFECTIVE MASS IN AlGaN/GaN HETEROSTRUCTURES MEASURED VIA THz SPECTROSCOPY OF 2D PLASMONS	O3-3	45
12:30	Justinas Jorudas, Artūr Šimukovič, Irmantas Kašalynas ELECTRICAL CHARACTERISTICS OF „BUFFER-FREE“ AlGaN/GaN HETEROSTRUCTURES	O3-4	46
12:45	Ričardas Norkus, Jan Devenson, Remigijus Juškėnas, Arūnas Krotkus TERAHERTZ EMISSION FROM ULTRATHIN BISMUTH LAYERS	O3-5	47
13:00	Evelina Dudutienė, Dominykas Sanda, Algirdas Jasinskas, Joshya Shyamala Rajagopal, Hélène Carrere, Bronislovas Čechavičius, Renata Butkutė PHOTOLUMINESCENCE STUDY OF GaAsBi/GaAs QUANTUM WELLS	O3-6	48
	ORAL SESSION O4		
11:45	Maciej Nowagiel, Mateusz J. Samsel, Tomasz K. Pietrzak IMPROVING SODIUM BATTERIES CATHODES: THERMAL NANOCRYSTALLIZATION OF GLASSY ALLUAUDITES	O4-1	49
12:00	Maryna Dryhailo, Yuliia Taranets RESEARCH OF IMPACT OF PRESENCE OF VITAMINS B2, B3, AND C ON CALCIUM OXALATE MONOHYDRATE CRYSTALLIZATION PROCESSES IN SIMULATED BODY FLUID	O4-2	50
12:15	Ondrej Friedrich, Jan Valtera FREQUENCY CONTROLLED AC ELECTROSPINNING FOR ENHANCED NANOFIBER PRODUCTION	O4-3	51
12:30	Magdalena Bartolewska, Matej Buzgo, Aiva Simaite BLEND ELECTROSPINNING OF CONTROLLED-RELEASE DRUG DELIVERY SYSTEMS WITH MMP INHIBITORS	O4-4	52
12:45	Renata Butrimienė, Vesta Skrodenytė-Arbačiauskienė, Danguolė Montvydienė, Živilė Jurgelėnė, Dalius Butkauskas, Nijolė Kazlauskienė EFFECTS OF Cd BASED, Cd FREE QUANTUM DOTS AND Cd^{2+} ON ISOLATED GUT MICROBIOTA OF *Salmo trutta* FRY	O4-5	53
13:00	Mona Fadel, M.P. Fernandez-Garcia, Pedro Gorria, Jesus A. Blanco, David Martinez-Blanco, Fabian Suarez-Garcia, Julian Martin-Jimeno, and Alaa Adawy CHARACTERIZATION OF CARBONACEOUS MATERIALS WITH CONTROLLED POROSITY AND MORPHOLOGY	O4-6	54

13:15	**TIME FOR INDUSTRY**
15:00	BREAK
15:15-16:00	**POSTER SESSION P1**
16:00	BREAK
16:15-17:00	**POSTER SESSION P2**
17:00	**Social event: "ITER – Future energy"**

17 March, WEDNESDAY

09:00	Chennupati Jagadish SEMICONDUCTOR NANOSTRUCTURES FOR OPTOELECTRONICS APPLICATIONS		
10:00	BREAK		
	ORAL SESSION O5		p.
10:15	Justina Jaseliūnaitė INTERFERENCE OF ANTIPHASE-SYNCHRONIZED VORTEX SHEDDING IN FLOW PAST AN INLINE MICRO-CYLINDER ARRAY	O5-1	55
10:30	Marijus Ambrozas, Andrius Juodagalvis IMPROVED FAKE LEPTON BACKGROUND ESTIMATION FOR THE DRELL-YAN DIFFERENTIAL CROSS SECTION MEASUREMENT USING 2016 CERN CMS DATA	O5-2	56
10:45	Anton Kunčinas, Per Osland, Margarida Nesbitt Rebelo MULTI-HIGGS DOUBLET MODELS AND GROUP THEORY	O5-3	57
11:00	Giedrius Žlabys, Chu-hui Fan, Egidijus Anisimovas, Krzysztof Sacha ENGINEERING TIME-SPACE CRYSTALLINE STRUCTURES	O5-4	58
11:15	Kazimieras Tamoliūnas, Jevgenij Chmeliov, Andrius Gelžinis MODELLING OF INTERACTION BETWEEN PHOTOSYNTHETIC PIGMENTS USING QUANTUM CHEMISTRY METHODS	O5-5	59
	ORAL SESSION O6		
10:15	Deimante Vaitukaityte, Cristina Momblona, Kasparas Rakstys, Albertus Adrian Sutanto, Bin Ding, Vygintas Jankauskas, Alytis Gruodis, Tadas Malinauskas, Abdullah M. Asiri, Paul J. Dyson, Vytautas Getautis, Mohammad Khaja Nazeeruddin ENAMINE-DERIVED SPIROBIFLUORENES AS HOLE TRANSPORTING MATERIALS FOR PEROVSKITE SOLAR CELLS	O6-1	60
10:30	Jakub Wręczycki, Grzegorz Mlostoń, Katarzyna Urbaniak, Dariusz M. Bieliński THE FLUORIDE ANION CATALYZED SULFURIZATION OF THIOKETONES WITH ELEMENTAL SULFUR LEADING TO SULFUR-RICH HETEROCYCLES	O6-2	61
10:45	Mantas Marcinskas, Tadas Malinauskas SYNTHESIS AND INVESTIGATION OF ORGANOMETALLIC PRECURSORS FOR CONVENIENT COPPER (I) THIOCYANATE LAYER DEPOSITION	O6-3	62
11:00	Ieva Agne Cechanaviciute, Wolfgang Schuhmann HIGH ENTROPY ALLOYS AS CATALYSTS FOR SELECTIVE GLYCEROL OXIDATION	O6-4	63
11:15	Augustina Jozeliunaite, Edvinas Orentas AN EFFICIANT HETEROGENOUS CARBON-BASED PHOTOCATALYST FOR SELECTIVE SULFIDE OXIDATION TO SULFOXIDES	O6-5	64
11:30	BREAK		
	ORAL SESSION O7		
11:45	Mantas Drazdys, Darija Astrauskytė, Ramutis Drazdys INVESTIGATION OF INITIAL GROWTH RATE OF DIELECTRICAL THIN FILMS DEPOSITED BY ATOMIC LAYER DEPOSITION	O7-1	65
12:00	Did not participate	O7-2	66
12:15	Kamilė Bareikaitė, Rokas Skaisgiris, Jelena Dodonova, Sigitas Tumkevičius, Saulius Juršėnas PHOTOPHYSICAL PROPERTIES OF PYRIMIDINE-BASED TADF EMITTERS	O7-3	67
12:30	Rusnė Ivaškevičiūtė-Povilauskienė, Dalius Seliuta, Alesia Paddubskaya, Domas Jokubauskis, Linas Minkevičius, Andrzej Urbanowicz, Ieva Matulaitienė, Lina Mikoliūnaitė, Gintaras Valušis OPTICAL MODULATION OF MONO AND BI-LAYER GRAPHENE	O7-4	68
12:45	Rokas Jasiūnas, Vidmantas Jašinskas, Huotian Zhang, Feng Gao, Vidmantas Gulbinas CHARGE CARRIER TRANSPORT IN CLOSE TO REAL WORKING CONDITIONS OF ORGANIC SOLAR CELLS	O7-5	69
13:00	Nerijus Jurkūnas, Algirdas Jasinskas, Simona Pūkienė, Andrius Bičiūnas, Bronislovas Čechavičius, Virginijus Bukauskas and Renata Butkutė GROWTH AND INVESTIGATION OF Bi-CONTAINING COMPOUND *PIN* STRUCTURES	O7-6	70

	ORAL SESSION O8		
11:45	Austėja Mikalčiūtė, Andrius Gelžinis, Jevgenij Chmeliov CRYSTALLOGRAPHY-BASED MODELLING OF THE INTER-PIGMENT INTERACTION IN THE FUCOXANTHIN–CHLOROPHYLL PROTEIN COMPLEX	O8-1	71
12:00	Daria Pashneva, Julija Pauraite, Agnė Minderytė, Vadimas Dudoitis, Kristina Plauškaitė, Inga Garbarienė, Lina Davulienė, Steigvilė Byčenkienė OUTDOOR AND INDOOR LEVELS OF BLACK CARBON IN AN URBAN ENVIRONMENT	O8-2	72
12:15	Monika Baublytė, Edita Garškaitė, Denis Sokol, Ramūnas Skaudžius IN SITU $GdPO_4$:Eu HYDROTHERMAL SYNTHESIS IN WOODS MATRIX	O8-3	73
12:30	Jan Albert Zienkiewicz, Dorota Kowalska, Katarzyna Fedoruk, Mariusz Stefański, Adam Pikul, Maciej Ptak NOVEL HYBRID ORGANIC-INORGANIC PEROVSKITE WITH PROTONATED UNSYMMETRICAL DIMETHYLHYDRAZINE – SYNTHESIS AND PHYSICOCHEMICAL CHARACTERIZATION	O8-4	74
12:45	Joanna Stocka, Rasa Platakytė, Justinas Čeponkus, Valdas Šablinskas, Gamil A. Guirgis, Paweł Rodziewicz COMPUTATIONAL AND EXPERIMENTAL VIBRATIONAL STUDY OF 1-CHLOROMETHYL-1-FLUOROSILACYCLOHEXANE CONFORMATIONS AND ITS REARRANGEMENTS	O8-5	75
13:00	Sridhar Hariharaputran, Arul Murugan Natarajan, Zilvinas Rinkevicius, Patrick Norman MODELING OF STRUCTURAL AND PHOTOPHYSICAL PROPERTIES OF AN OPTICAL PROBE IN AQUEOUS AND MEMBRANE ENVIRONMENTS	O8-6	76
13:15	BREAK		
14:00	Klaus-Dieter Kreuer ENABLING HYDROGEN AS FUTURE ENERGY CARRIER: FROM THE LITHUANIA CRADLE TO WHERE WE ARE TODAY		
15:00	BREAK		
15:15-16:00	**POSTER SESSION P3**		
16:00	BREAK		
16:15-17:00	**POSTER SESSION P4**		
17:00	**Social event - discussion: "Life after Science"** Simona Liukaitytė, Renata Butkutė, Paulius Saudargas (Goda Raibytė)		

18 March, THURSDAY

09:00	Tomas Tamulevičius SELF-ASSEMBLED NANOPHOTONICS		
10:00	BREAK		
	ORAL SESSION O9		p.
10:15	Vytautas Paura, Virginijus Marcinkevičius HYPERSPECTRAL UNMIXING: ALGORITHMS REVIEW AND BENCHMARKING	O9-1	77
10:30	Rugilė Lukaševičiūtė, Lena Golubewa, Renata Karpicz CHARACTERIZATION OF BORON NITRIDE QUANTUM DOTS SYNTHESIZED BY A SINGLE STEP HYDROTHERMAL METHOD	O9-2	78
10:45	Cristina Mendez-Lopez, Luis J. Fernandez-Menendez, Cristina Gonzalez-Gago, Jorge Pisonero, Nerea Bordel EFFECTS OF NEBULIZED CALCIUM NITRITE CONCENTRATION ON A LASER-INDUCED PLASMA EMISSION AND PARAMETERS	O9-3	79
11:00	Reinis Lazda, Laima Bušaite, Florians Gahbauers, Andris Bērziņš, Mārcis Auziņš MEASURING THE VECTOR OF A MAGNETIC FIELD USING A DIAMOND CRYSTAL.	O9-4	80
	ORAL SESSION O10		
10:15	Inga Songailiene, Jonas Juozapaitis , Giedre Tamulaitiene, Audrone Ruksenaite, Sigitas Sulcius, Giedrius Sasnauskas, Ceslovas Venclovas , Virginijus Siksnys HEPN-MNT TOXIN-ANTITOXIN SYSTEM AS A PROPOSED BACTERIAL ATP SENSOR	O10-1	81
10:30	Justina Kavaliauskaitė, Auksė Kazlauskaitė, Juozas Lazutka, Arūnas Stirkė ACTIVATION OF NUCLEAR FACTOR NF-κB RECOGNITION PROMOTER-CONTROLLED REPORTER GENE TRANSCRIPTION BY PULSED ELECTRIC FIELD TREATMENT IN VIABLE HEP-2C AND CHO-K1 CELLS	O10-2	82
10:45	Ewa Borowska, Mateusz Abram, Joanna Kargul NOVEL APPROACH ON APPLICATION OF AN EXTREMOPHILIC RED ALGA CYANIDIOSCHYZON MEROLAE IN PHYTOREMEDIATION	O10-3	83
11:00	Greta Gančytė, Povilas Šimonis, Arūnas Stirkė INVESTIGATION OF OSMOTIC SHOCK EFFECTS ON YEAST CELL RESPONSES TO PULSED ELECTRIC FIELD TREATMENT	O10-4	84
11:15	Agne Rimkute, Dovile Stravinskiene, Gintautas Zvirblis BIOSYNTHESIS OF RECOMBINANT ALLERGENS USING MAMMALIAN CELLS EXPRESSION SYSTEM	O10-5	85

11:30 BREAK

ORAL SESSION O11

11:45	Karolina Maleckaitė, Jelena Dodonova, Stepas Toliautas, Rugilė Žilėnaitė, Džiugas Jurgutis, Vitalijus Karabanovas, Sigitas Tumkevičius, Aurimas Vyšniauskas DESIGNING A VISCOSITY-SENSITIVE BODIPY FLUOROPHORE FOR A LIVE CELL IMAGING	O11-1	86
12:00	Julija Grigorjevaite, Arturas Katelnikovas OPTICAL PROPERTIES INVESTIGATION OF BLUE-EXCITABLE RED-EMITTING $K_2Bi(PO_4)(MoO_4):PR^{3+}$ POWDERS	O11-2	87
12:15	Agata Jarocka, Paweł Dębowski, Tomasz K. Pietrzak, Marek Wasiucionek INFLUENCE ANALYSIS OF SELECTED FACTORS ON THE EUROPIUM IONS REDUCTION IN THE GLASSY MATRIX	O11-3	88
12:30	Katarzyna Polak, Andrzej Sitkiewicz, Arkadiusz Leniart, Paweł Majewski THERMAL ANNEALING OF PS-B-PMMA DIBLOCK COPOLYMER THIN FILMS	O11-4	89
12:45	Eimantas Duda, David Hall, Sergey Bagnich, Cameron Carpenter-Warren, Rishabh Saxena, Michael Y. Wong, David B. Cordes, Alexandra M. Z. Slawin, David Beljonne, Yoann Olivier, Eli Zysman-Colman, and Anna Koehler DOES EXTENDING THE DONOR GROUP ENHANCE THERMALLY ACTIVATED DELAYED FLUORESCENCE PROPERTIES?	O11-5	90
13:00	Agnieszka Anna Wiciak, Wolfgang M. Klesse, Davide Spirito OPTIMIZATION OF FABRICATION OF THz GERMANIUM MICROANTENNAS	O11-6	91

ORAL SESSION O12

11:45	Vytautas Rudokas, Gintautas Žvirblis, Aurelija Žvirblienė DEVELOPMENT OF MONOCLONAL ANTIBODIES AGAINST HOUSE DUST MITE ALLERGEN DER P 21 FOR THE QUANTIFICATION OF ALLERGEN COMPONENT IN ALLERGEN EXTRACTS	O12-1	92
12:00	Džiugas Jurgutis, Greta Jarockytė, Aurimas Vyšniauskas, Vitalijus Karabanovas, Ričardas Rotomskis. DETERMINING THE PROPERTIES OF VISCOSITY-SENSITIVE MOLECULAR ROTOR IN HUMAN MESENCHYMAL STEM CELLS AND THEIR DIFFERENTIATED COUNTERPARTS	O12-2	93
12:15	Sergio Sanjurjo Montero, Irene Corral Lorences, Luis Javier Secades López-Cancio A FLEXIBLE MATHEMATICAL SYSTEM TO MODEL EPIDEMICS AND SOME PREDICTIONS FOR ITALIAN COVID-19 PANDEMIC	O12-3	94
12:30	Carl A. Fogarty, Elisa Fadda THE OLIGOMANNOSE N-GLYCANS 3D ARCHITECTURE AND ITS RESPONSE TO THE FCΓRIIIA STRUCTURAL LANDSCAPE.	O12-4	95
12:45	Mykolas Mačiulis, Viktoras Mažeika, Martynas Riauka, Lukas Kontenis, Danutė Bulotienė, Vitalijus Karabanovas, Edvardas Žurauskas, Virginijus Barzda THIRD–HARMONIC GENERATION MICROSCOPY OF COLLAGEN IN BIOLOGICAL TISSUES STAINED WITH HEMATOXYLIN AND EOSIN	O12-5	96
13:00	Did not participate	O12-6	97

13:15 BREAK

14:00 Urtė Neniškytė
GARDENING THE BRAIN: INTERDISCIPLINARY APPROACH TO INVESTIGATE SYNAPTIC PRUNING IN DEVELOPING BRAIN

15:00 BREAK

15:15-16:00 **POSTER SESSION P5**

16:00 BREAK

16:15-17:00 **POSTER SESSION P6**

19 March, FRIDAY

09:00 Eglė Čechanavičiūtė
NEUROIMMUNE RESPONSES TO SPACE RADIATION

10:00 BREAK

ORAL SESSION O13

			p.
10:15	Evaldas Kažukauskas, Simas Butkus, Piotr Tokarski, Vytautas Jukna, Carlos Vytautas Diamond Manikas, Martynas Barkauskas, Valdas Sirutkaitis. MICROMACHINING OF TRANSPARENT BIOCOMPATIBLE POLYMERS APPLIED IN MEDICINE USING BURSTS OF FEMTOSECOND LASER PULSES	O13-1	98

10:30	Vytenis Girdauskas, Paulius Mackonis, Augustinas Petrulėnas, Aleksėj Rodin TOWARDS 50 FS SWIR PULSES BY TRANSIENT STIMULATED RAMAN CHIRPED-PULSE AMPLIFICATION WITH SPECTRUM SYNTHESIS	O13-2	99
10:45	Andrea Zelioli, Algirdas Jasinskas, Ada Gajauskaitė, Simona Pūkienė, Lukas Jočionis, Evelina Dudutienė, Bronislovas Čechavičius and Renata Butkutė OPTIMIZATION OF GaInAs/GaAs QUANTUM WELL TECHNOLOGY FOR APPLICATIONS IN NEAR INFRARED VERTICAL-EXTERNAL-CAVITY SURFACE-EMITTING LASERS	O13-3	100
11:00	Did not participate	O13-4	101
11:15	Diana Gonzalez-Hernandez, Simonas Varapnickas, Mangirdas Malinauskas FABRICATION OF THREE-DIMENSIONAL MICROELEMENTS BY TWO-PHOTON LITHOGRAPHY FOR REFRACTIVE INDEX MEASUREMENTS	O13-5	102
	ORAL SESSION O14		
10:15	Kristina Mašalaitė, Asta Lučiūnaitė, Indrė Dalgėdienė, Aurelija Žvirblienė NLRP3 INFLAMMASOME ACTIVATION BY VIRAL-LIKE PARTICLES IN MACROPHAGES	O14-1	103
10:30	Mantas Adomaitis, Grita Skujienė IVESTIGATION OF A NEW ORGANIC CONTROL MEASURE AGAINST INVASIVE SLUGS	O14-2	104
10:45	Karolina Zilionyte, Ugne Bagdzeviciute, Elena Urbstaite, Agata Mlynska, Emilija Paberale, Neringa Dobrovolskiene, Vita Pasukoniene MOLECULAR BIOMAKERS OF MOUSE TUMOR IMMUNOGENICITY AND PREDICTION OF RESPONSE TO DENDRITIC CELL VACCINES AND ANTI-PD-1 TREATMENT	O14-3	105
11:00	Aistė Zentelytė, Elizabet Beržanskytė, Giedrė Valiulienė, Rūta Navakauskienė NEUROGENIC DIFFERENTIATION OF HUMAN AMNIOTIC FLUID STEM CELLS FROM HEALTHY AND FETUS AFFECTED PREGNANCIES	O14-4	106
11:15	Radvilė Markevičiūtė SPECIES OF THE GENUS ANTOCHA OSTEN SACKEN 1860 (DIPTERA: LIMONIIDAE) IN SICHUAN (CHINA)	O14-5	107
11:30	BREAK		
	ORAL SESSION O15		
11:45	Robertas Grigutis, Vytautas Jukna, Marius Navickas, Gintaras Tamošauskas, Kęstutis Staliūnas, Audrius Dubietis CONICAL THIRD HARMONIC GENERATION FROM FEMTOSECOND LASER INDUCED NANOGRATING IN TRANSPARENT MATERIALS DURING FILAMENTATION AT HIGH REPETITION RATES	O15-1	108
12:00	Indre Meskelaite, Darius Gailevicius, Martynas Peckus, Lina Grineviciute, Ruslan A. Lymarenko, Victor B. Taranenko, Kestutis Staliunas AXISYMMETRIC DIFFRACTIVE REFLECTOR FOR BEAM SUPER-COLLIMATION	O15-2	109
12:15	Sara Piotrowska, Mateusz Król, Katarzyna Rechcińska, Rafał Mirek, Rafał Mazur, Przemysław Morawiak, Przemysław Kula, Wiktor Piecek, Barbara Piętka, Jacek Szczytko HYBRID LIQUID CRYSTAL MICROCAVITY AS A PHOTONIC DEVICE TO CONTROL SYNTHETIC OPTICAL SPIN-ORBIT INTERACTIONS	O15-3	110
12:30	Kristians Draguns, Inga Brice, Toms Salgals, Janis Alnis DISPERSION ENGINEERING OF WHISPERING GALLERY MODE RESONATORS FOR FREQUENCY COMB GENERATION AND TELECOMMUNICATION APPLICATIONS	O15-4	111
12:45	Diana Klezovich COMPARATIVE NONLINEAR DYNAMICS OF HIGH-POWER FEMTOSECOND LASER PULSES IN KERR MEDIA DEPENDING ON THEIR TOPOLOGICAL CHARGE	O15-5	112
13:00	Danas Buožius, Giedrius Balčas, Viktorija Tamulienė TERAHERTZ WAVE GENERATION IN AIR PLASMA OPTIMISATION USING BICHROMATIC FEMTOSECOND LASER PULSES	O15-6	113
	ORAL SESSION O16		
11:45	Magdalena Łabowska, Izabela Michalak, Jerzy Detyna INFLUENCE OF pH ON SWELLING PROPERTIES OF ALGINATE HYDROGEL AS A POTENTIAL MATERIAL FOR DRUG DELIVERY SYSTEM	O16-1	114
12:00	Justyna Rewak-Soroczynska, Paulina Sobierajska, Rafal J. Wiglusz ANTIFUNGAL ACTIVITY OF FLUCONAZOLE INCORPORATED INTO HYDROGELS MODIFIED WITH NANOHYDROXYAPATITE	O16-2	115
12:15	Vasyl Velykyi, Maria Stupchuk, Tatyana Voznesenskaya MODULATION SIRT-1 ACTIVITY IN IMMUNE CELLS UNDER OXIDATIVE STRESS: CELL DEATH AND SURVIVAL	O16-3	116
12:30	Vėjūnė Pukenytė, Raimondas Šiukšta, Tatjana Čėsnienė EVALUATION OF POLLUTED SOIL-INDUCED OXIDATIVE STRESS USING VICIA FABA CHLOROPHYLL MORPHOSES AS A MODEL SYSTEM	O16-4	117
12:45	Vidmante Fuchs, Michael Kutza, Sven Wischnewski, Nikolaus Deigendesch, Luc Lutz, Laila Kulsvehagen, Gerda Ricken, Ludwig Kappos, Alexandar Tzankov, Simon Hametner, Stephan Frank, Lucas Schirmer, Anne-Katrin Pröbstel PRESENCE OF SARS-COV-2 TRANSCRIPTS IN THE CHOROID PLEXUS OF MS AND NON-MS PATIENTS WITH COVID-19	O16-5	118
13:00	Anastasiya Kanunnikova, Artem Goliusov, Arina Mamatova, Yuliya Prosmytskaya, Daniil Lappo, Yury Linnik	O16-6	119

	THE COMPARISON OF DIFFERENT MODELS FOR INDUCING EXPERIMENTAL PERITONEAL ADHESIONS IN RATS
13:15	BREAK
14:00	Daniele Faccio IMAGING WITH TIME: FROM MULTIPATH IMAGING TO HEALTHCARE APPLICATIONS
15:00	BREAK
15:15-16:00	**POSTER SESSION P5**
16:00	BREAK
16:15-17:00	**POSTER SESSION P6**
17:00	Closing remarks

List of poster presentations

16 March, TUESDAY

15:15-16:00 POSTER SESSION P1

		p.
Gerda Klimaitė, Domantas Peckus, Tomas Tamulevicius, Jaunius Mykolaitis, Mindaugas Juodėnas, Asta Tamulevičienė, Algirdas Lazauskas, Sigitas Tamulevičius ULTRAFAST LOCALIZED SURFACE PLASMON RELAXATION DYNAMICS OF PLASMONIC METAL NANOPARTICLES BY MEANS OF TRANSIENT ABSORPTION SPECTROSCOPY	P1-1	120
Ieva Stašaitytė, Andrius Vitkauskas, Agnė Šulčiūtė, Simas Račkauskas ZnO TETRAPODS MORPHOLOGY AND STRUCTURE INFLUENCE ON ELECTROCHEMICAL PROPERTIES	P1-2	121
Ema Baliūnaitė, Almira Ramanavičienė APPLICATION OF MAGNETIC GOLD-COATED NANOPARTICLES FOR THE DETERMINATION OF HUMAN GROWTH HORMONE	P1-3	122
Julianija Nikitina, Tomas Tolenis, Darius Gailevičius, Kęstutis Staliūnas, Lina Grinevičiūtė DEPOSITION OF THIN FILMS ON STRUCTURED SURFACES	P1-4	123
Benediktas Brasiunas, Anton Popov, Almira Ramanaviciene THE EVALUATION OF KINETIC OPTICAL REDUCING SUGAR SENSOR BASED ON GOLD NANOPARTICLE FORMATION	P1-5	124
Anatoly Pushkarev LEAD HALIDE PEROVSKITE NANO- AND MICROLASERS FOR GAS SENSING APPLICATIONS	P1-6	125
Justina Gaidukevič, Rasa Pauliukaitė N-DOPED REDUCED GRAPHENE OXIDE AS ELECTRODE MATERIAL FOR HYDROGEN PEROXIDE ELECTROCHEMICAL SENSOR	P1-7	126
Paulius Dolmantas, Aušrinė Jurkevičiūtė, Asta Tamulevičienė, Andrius Vasiliauskas, Šarūnas Meškinis, Tomas Tamulevičius AMORPHOUS DIAMOND-LIKE CARBON AS A MATRIX FOR NANOCOMPOSITE PLASMONIC LIGHT ABSORBING ANTI-REFLECTIVE COATINGS	P1-8	127
Eimantas Bucmys, Viktorija Lisyte, Anton Popov EVALUATION OF ANTIBODIES IMMOBILIZATION ON GOLD-COATED MAGNETIC NANOPARTICLES.	P1-9	128
Laurynas Tumėnas, Skirmantas Norkus, Brigita Abakevičienė THE TEMPERATURE INFLUENCE ON ULTRA-HIGH MOLECULAR WEIGHT POLYETHYLENE STRUCTURAL PROPERTIES	P1-10	129
Juzef Kucinski, Mindaugas Gicevicius, Lina Mikoliunaite DEVELOPMENT OF ELASTIC PEDOT:PSS-BASED ELECTROCHROMIC COMPOSITES FOR STRETCHABLE ELECTRONICS APPLICATIONS	P1-11	130
Paulina Andriunaite, Vesta Navikaite-Snipaitiene, Ramune Rutkaite ADSORPTION OF DICLOFENAC FROM AQUEOUS MEDIUM ON CHEMICALLY MODIFIED STARCH	P1-12	131
Kristina Bunevičienė, Meda Pašvenskaitė GRANULATION OF INDUSTRIAL WASTE AND ANALYSIS OF THE OBTAINED GRANULES	P1-13	132
Md. Reazuddin Repon, Daiva Mikučionienė HEATING BEHAVIOUR INVESTIGATION OF AG/PA BASED KNITTED FABRICS	P1-14	133
Karolina Almonaityte, Joana Bendoraitiene, Greta Cizauskaite, Diana Masiulionyte, Dovile Liudvinaviciute, Ramune Rutkaite PECULIARITIES OF POTATO, CORN AND WHEAT STARCHES CROSS-LINKING	P1-15	134
Rugilė Žilėnaitė, Karolina Maleckaitė, Jelena Dodonova, Sigitas Tumkevičius, Aurimas Vyšniauskas SPECTROSCOPIC CHARACTERISATION OF BODIPY-BASED NEW FLUORESCENT VISCOSITY SENSORS	P1-16	135
Zygimantas Augys, Vesta Navikaite-Snipaitiene ENCAPSULATION OF ANTHOCYANINS AND CINNAMALDEHYDE IN STARCH OCTENYLSUCCINATE	P1-17	136
Maliha Parvin, Milda Petrulevičienė, Irena Savickaja, Benjaminas Šebeka, Arnas Naujokaitis, Vidas Pakštas, Renata Karpicz, Jurga Juodkazytė INVESTIGATION OF PHOTOANODIC PROCESSES ON WO_3 ELECTRODE IN DIFFERENT ELECTROLYTES	P1-18	137
Lukas Bardėnas, Rokas Skaisgiris, Dace Cirule, Maris Turks, Saulius Juršėnas METAL IONS SENSING FOR BIOLOGICAL APPLICATIONS BASED ON ORGANIC SEMICONDUCTORS	P1-19	138
Dovile Liudvinaviciute, Karolina Almonaityte, Joana Bendoraitiene, Ramunė Rutkaite COMPLEX FORMATION BETWEEN ANTHOCYANINS AND SODIUM ALGINATES USING ADSORPTION PROCESS AND INVESTIGATION OF PROPERTIES OF FORMED COMPLEXES	P1-20	139
Vilius Samuolis, Vytautas Getautis, Artiom Magomedov ORGANIC DYES WITH FUNCTIONAL AMMONIUM GROUPS FOR THE 2D PEROVSKITES	P1-21	140
Andrius Kamarauskas, Gediminas Šlekas, Dalius Seliuta, Žilvinas Kancleris MULTIPLE FANO RESONANCES IN A MIRRORED ARRAY OF SPLIT-RING RESONATORS	P1-22	141
Jorūnas Dobilas, Voitech Stankevic CONSTRUCTION OF A PULSED MAGNET FOR CLOSED CYCLE HELIUM GAS CRYOCOOLER	P1-23	142
Mindaugas Janušauskas, Povilas Adomėnas, Ona Adomėnienė, Regimantas Komskis, Saulius Juršėnas TUNING THE EMISSION IN CARBAZOLE - BIPYRIDINE MOLECULAR SYSTEMS FOR TADF APPLICATIONS	P1-24	143
Milita Užgirytė, Povilas Adomėnas, Ona Adomėnienė, Regimantas Komskis, Saulius Juršėnas HIGHLY EFFICIENT EMISSION OF CHARGE TRANSFER STATES IN CARBAZOLE - PYRIDINE MOLECULAR SYSTEMS FOR TADF APPLICATIONS	P1-25	144
Samanta Lipkevičiūtė, Džiugas Litvinas, Regimantas Komskis, Saulius Juršėnas STIMULATED GREEN EMISSION IN LEAD BROMIDE PEROVSKITES	P1-26	145
Dovydas Banevičius, Gediminas Kreiza, Domantas Berenis, Tomas Javorskis, Edvinas Orentas, Saulius Antanas Juršėnas, Karolis Kazlauskas SUBSTANTIAL TADF OLED PERFORMANCE IMPROVEMENT BY SIMPLE EMITTER STRUCTURE MODIFICATION	P1-27	146
Modestas Čeikauskas, Voitech Stankevič TESTING OF CMR-B-SCALAR SENSORS USING MICROSECONDS DURATION HIGH PULSED MAGNETIC FIELDS	P1-28	147

Agata Jarocka, Dominika Wąs, Jakub Płachta, Tomasz K. Pietrzak INVESTIGATION OF OPTICAL PROPERTIES OF $CaAlBO_3F_2$ GLASSY MATRIX DOPED WITH EUROPIUM AND SAMARIUM IONS	P1-29	148
Did not participate	P1-30	149
Justina Savickytė, Povilas Adomėnas, Ona Adomėnienė, Regimantas Komskis, Saulius Juršėnas CARBAZOLE - PYRIMIDINE MOLECULAR SYSTEMS FOR TADF APPLICATIONS	P1-31	150
Nerijus Karlonas COMPARISON OF SOLID-PHASE EXTRACTION SORBENTS FOR THE DETERMINATION OF SEDATIVE-HYPNOTICS DRUGS IN BIOLOGICAL SPECIMENS	P1-32	151
Kristaps Saršūns, Aleksejs Karziņins, Kaspars Leduskrasts, Agris Bērziņš, Toms Rēķis FORMATION OF SOLID SOLUTION IN XANTHONE DERIVATIVE SYSTEMS EXHIBITING LUMINESCENCE PROPERTIES	P1-33	152
Lukas Dvylys, Rasa Keruckiene, Juozas Vidas Grazulevicius NAPHTHYRIDINE AND CARBAZOLE DERIVATIVES AS ELECTROACTIVE MATERIALS	P1-34	153
Sonata Pleskytė, Ieva Uogintė INVESTIGATION OF MICROPLASTIC CONTAMINATION IN WASTEWATER SAMPLES	P1-35	154
Zane Čerpakovska, Kristaps Saršūns, Agris Bērziņš INVESTIGATION OF POSSIBILITIES TO CONTROL THE POLYMORPH OBTAINED IN CRYSTALLIZATION OF 3-HYDROXYBENZOIC ACID	P1-36	155
Huda Alghamdi, Anna M. Hogan, Jeremy D. Glennon. PREPARATION OF A NOVEL STATIONARY PHASE FOR ION EXCHANGE SEPARATION IN LIQUID CHROMATOGRAPHY	P1-37	156
Touqeer Gill, Julija Pauraitė, Steigvilė Byčenkienė and Kristina Plauškaitė LONG TERM SUBMICRON AEROSOL CHEMICAL CHARACTERIZATION IN RŪGŠTELIŠKIS (LITHUANIA) RURAL ENVIRONMENT	P1-38	157
Lena Marciniak, Justyna Anna Adamczyk, Adam Marek Pieczonka, Michał Rachwalski SYNTHESIS OF HYDRAZIDE HYDRAZONES WITH LUMINESCENT PROPERTIES	P1-39	158
Dušica Jovanović, Tamara Ivetić, Nina Finčur THE EFFICIENCY OF ZnO NANOPOWDERS MODIFIED BY GRINGING AND DOPING WITH Mg(II) IONS IN THE PHOTOCATALYTIC DEGRADATION OF CIPROFLOXACIN	P1-40	159
Laura Sakalauskiene, Anton Popov, Asta Kausaite-Minkstimiene, Almira Ramanaviciene DEVELOPMENT OF GLUCOSE BIOSENSOR: IMMOBILIZATION OF GLUCOSE OXIDASE ON DENDRITIC GOLD NANOSTRUCTURES	P1-41	160
Veronika S. Karpushenkova, Hanna M. Maltanava ELECTROCHEMICAL SYNTHESIS OF TiO_2 PEO-COATINGS ON THE ALUMINUM SURFACE	P1-42	161
Did not participate	P1-43	162
Benas Balandis, Vaida Paketurytė, Tomas Šinkūnas, Daumantas Matulis, Asta Zubrienė, Vytautas Mickevičius SYNTHESIS OF BENZENESULFONAMIDE-BEARING B,Г-AMINO ACID DERIVATIVES AS HUMAN CARBONIC ANHYDRASE INHIBITORS	P1-44	163
Daria Łuczak, Adam Marek Pieczonka GREEN APPROACH IN THE SYNTHESIS OF N-ACYLPYRAZOLES	P1-45	164
Karolina Koselak, Stanisław Porwański, Anna Zawisza SUGAR ORGANOCATALYSTS WITH UREA FRAGMENT	P1-46	165
Žyginta Einorytė, Kęstutis Aidas MODELLING ^{17}O NMR SPECTRA OF TAUTOMERIC FORMS OF CITRININ	P1-47	166
Martyna Malinowska, Anna Zawisza, Stanisław Leśniak ASYMMETRIC BETTI REACTION - SEARCHING FOR NEW LIGANDS	P1-48	167
Aldona Balčiūnaitė, Dovydas Vdovinskis, Loreta Tamašauskaitė-Tamašiūnaitė, Eugenijus Norkus HYDROGEN PRODUCTION FROM WATER SPLITTING USING PEROVSKITE NANOPARTICLES	P1-49	168
Oleksandr Navozenko, Valeriy Yashchuk, Mykhaylo Losytskyy, Yuriy Slominskii, Dalius Gudeika THE SPECTRAL PROPERTIES OF BORON-CONTAINING DYES AT LOW TEMPERATURES	P1-50	169

Robert Poenaru, Apolodor Aristotel Raduta SINGLE-PARTICLE MOTION IN A WOBBLING NUCLEUS - A CASE-STUDY FOR ODD-MASS ISOTOPES	P2-1	
Izolda Marcinonienė EXTREMELY HEAVY RAIN AND VERY STRONG SQUALLS OVER LITHUANIA IN 1961-2020 PERIOD: ANALYSIS AND CLIMATOLOGY	P2-2	171
Darya Kisuryna, Ulyana Hatkevich, Danyil Voloshchuk, Zlata Lepenkova, George Pitsevich, Valdas Sablinskas THEORETICAL ANALYSIS OF THE CONFORMATIONS AND IR SPECTRA OF THE HYDROGEN TRIOXIDE (HOOOH) DIMERS	P2-3	172
Anton Serko, Pavel Peretruhin, Alex Malevich, George Pitsevich, Dmitry Shender, Darya Kisuryna, Vitas Balevicius THE TRANSITION FROM NON EQUIDISTANT TO EQUIDISTANT GRID FOR THE TORSION COORDINATE OF THE CH_3 GROUP WHEN CALCULATING MULTIDIMENSIONAL POTENTIAL ENERGY SURFACES	P2-4	173
Uladzimir Lazicki, Egor Molokanov, Alex Malevich, George Pitsevich, Olga Soroka, Aleksandr Shastin, Darya Kisuryna, Vitas Balevicius HYDROXYL AND METHYL GROUPS TUNNELING PROBABILITY IN THE HOOCH3 MOLECULE CALCULATED AT MP2/CC-PVQZ LEVEL OF THEORY TAKING INTO ACCOUNT ZPVE	P2-5	174
Tomas Klinavičius, Mindaugas Juodėnas, Andrius Žutautas, Tomas Tamulevičius REFRACTIVE INDEX SENSOR FOR LIQUIDS BASED ON DIFFRACTION EFFICIENCY MEASUREMENT	P2-6	175
Zoya Tsoy, Artūras Jukna IDENTIFICATION OF NUMBER, FREQUENCY, AND POWER OF SOURCES OF ELECTROMAGNETIC RADIATION IN THE HUMAN LIVING AREA	P2-7	176
Anastasija Supranovič, Akvilė Zabiliūtė-Karaliūnė, Artūras Katelnikovas, Pranciškus Vitta CHARACTERIZATION AND SPECTRAL PROPERTIES OF THERMOGRAPHIC PHOSPHORS FOR OPTICAL THERMOMETRY APPLICATIONS	P2-8	177
Domantas Dunajevas, Agnė Zdaniauskienė, Martynas Talaikis, Rita Sadzevičienė, Gediminas Niaura STUDY OF SAM WITH IMIDAZOLE FUNCTIONAL GROUP BY SURFACE AND SHELL-ISOLATED NANOPARTICLE ENHANCED RAMAN SPECTROSCOPY	P2-9	178
Gerda Mickūnaitė, Aida Kamarauskienė, Justinas Čeponkus, Eglė Lastauskienė, Rimantė Bandzevičiūtė STUDY OF PATHOGENIC BACTERIA AND FUNGI BY MEANS OF FTIR ATR SPECTROSCOPY	P2-10	179

Aušrinė Jurkevičiūtė, Paulius Dolmantas, Tomas Tamulevičius, Juris Prikulis SPECTROSCOPIC ELLIPSOMETRY INVESTIGATION OF UNIFORMITY OF DIAMOND-LIKE CARBON AND SILVER NANOCOMPOSITE THIN FILM	P2-11	180
Rimantė Bandzevičiūtė, Gediminas Platkevičius, Justinas Čeponkus, Gerda Mickūnaitė, Albertas Čekauskas, Arūnas Želvys, Valdas Šablinskas DETECTION OF MALIGNANT HUMAN BLADDER TISSUE BY MEANS OF FIBER BASED ATR IR SPECTROSCOPY	P2-12	181
Did not participate	P2-13	182
Morta Stadulytė, Rasa Platakytė, Justinas Čeponkus, Vaidas Pudžaitis LIBRARY OF RED PIGMENT RAMAN SPECTRA AND PIGMENT IDENTIFICATION IN PAINTED WORKS OF ART	P2-14	183
Živilė Čerškutė, Žydrūnas Podlipskas, Gintautas Tamulaitis RELATIONSHIP OF SPATIAL AND KINETIC CATHODOLUMINESCENCE PROPERTIES IN NONPOLAR InGaN QUANTUM WELLS	P2-15	184
Kasparas Dryžas, Laura Tauraitė, Antanas Urbas, Sergejus Orlovas RAMAN SPECTROSCOPY ANALYSIS OF FS LASER INDUCED STRUCTURAL DAMAGE ON SODA LIME AND ALUMINOSILICATE GLASSES.	P2-16	185
Vitaliy Romanenko, Galina Lujanienė, Sergej Šemčuk, Mažeika Jonas, Elena Ezhova, Galina Garnaga-Budrė DISTRIBUTION OF 241AM ACTIVITY CONCENTRATIONS IN THE BALTIC SEA SEDIMENTS	P2-17	186
Roberts Berkis, Janis Alnis , Kristians Draguns, Aigars Atvars , Inga Brice , Pauls Kristaps Reinis. PMMA WGM MICRO RESONATOR MODE FAMILY ANALYSIS USING SPOT INTENSITY CHANGES FROM IMAGE PROCESSING.	P2-18	187
Mateusz J. Samsel, Tomasz K. Pietrzak, Maciej Nowagiel HOLDER FOR IMPEDANCE SPECTROSCOPY MEASUREMENTS OF MIXED CONDUCTORS IN INERT GAS ATMOSPHERE	P2-19	188
Mohammad Nour ALSAMSAM, Kazimieras Nomeika, Žydrūnas Podlipskas, Jonas Jurkevičius, Ramūnas Aleksiejūnas ENHANCED DETECTION OF UV-INDUCED FREE-CARRIERS BY MULTIPLE PROBE BEAM PASSES INSIDE A CO-DOPED GAGG CRYSTAL	P2-20	189
Dominykas Dumbrė, Vytautas Jakštas, Vladislovas Čižas, Mindaugas Karaliūnas METAL GRATING DEPOSITION, CHARACTERIZATION AND IMPACT ON OPTICAL RESPONSE OF GaAs/AlGaAs NANOSTRUCTURES	P2-21	190
Sundar Arumugam Krishnan Nagarajan, Shalini Murugesan OBSTRUCTIVE SLEEP APNEA PREVENTING AND TREATING BED	P2-22	191
Daina Afanovaitė, Martynas Velička ANALYSIS OF INKS AND WRITTEN TEXTS USING SURFACE ENHANCED RAMAN SPECTROSCOPY	P2-23	192
Erika Putincevaitė, Natalija German THE CHOOSE OF OPTIMAL CONDITIONS FOR THE DEVELOPMENT OF GLUCOSE BIOLOGICAL SENSOR BASED ON INSOLUBLE ELECTRON TRANSFER MEDIATOR	P2-24	193
Rugile Chmieliauskaite, Natalija German THE ENZYME-ASSISTED SYNTHESIS OF POLYMERIC NANOCOMPOSITES AND THEIR INVESTIGATIONS	P2-25	194
Aliaksandra Radchanka, Varvara Hrybouskaya, Tatiana Terpinskaya EFFECT OF BETULINIC ACID IN THE POLYMERIC SHELL OF ENCAPSULATED QUANTUM DOTS ON THEIR INTERACTION WITH CELLS	P2-26	195
Urtė Ciganė, Arvydas Palevičius RESEARCH AND DEVELOPMENT OF INNOVATIVE FUNCTIONAL NANOMEMBRANES IN BIOENGINEERING	P2-27	196
Vincentas Maciulis, Silvija Juciute, Uldis Malinovskis, Donats Erts, Arunas Ramanavicius, Almira Ramanaviciene, Saulius Balevicius, Ieva Plikusiene TOWARDS SPECTROSCOPIC ELLIPSOMETRY BASED BIOSENSOR: EVALUATION OF HUMAN SERUM ALBUMIN ADSORPTION TO POROUS ALUMINIUM OXIDE	P2-28	197
Paulius Laurikėnas, Mindaugas Ilickas, Tomas Tamulevičius, Simas Račkauskas ZnO NANOPARTICLES FOR ANTI-REFLECTIVE APPLICATIONS	P2-29	198
Mantas Mikalkevičius, Mindaugas Juodėnas, Tomas Tamulevičius, Asta Tamulevičienė CONTROL OF THE STAINLESS STEEL WETTABILITY VIA VARYING FEMTOSECOND LASER PARAMETERS USED FOR IMPOSING LASER-INDUCED PERIODIC SURFACE STRUCTURES	P2-30	199
Katsiaryna Charniakova, Arunas Jagminas, Igor Vrublevsky EFFECT OF SUBSTRATE NATURE ON CELL MORPHOLOGY OF THIN ANODIC ALUMINA FILMS FORMED IN THE SULFURIC ACID SOLUTION	P2-31	200
Vita Petrikaitė, Evaldas Stankevičius SYNTHESIS OF GOLD–SILVER NANOPARTICLES USING NANOSECOND LASER AND THIN METALLIC FILMS	P2-32	201
Raman Novikau, Galina Lujanienė, Vidas Pakštas, Martynas Talaikis, Audrius Drabavičius, Arnas Naujokaitis DEVELOPMENT OF NANOCOMPOSITES BASED ON CLAY, GRAPHENE OXIDE AND MAGNETITE/MAGHEMITE	P2-33	202
Did not participate	P2-34	203
Ernesta Lubinaite, Benediktas Brasiunas, Anton Popov, Asta Kausaite-Minkstimiene, Jonas Labutis, Almira Ramanaviciene THE IMPACT OF GOLD NANOPARTICLE SIZE ON SPECTROPHOTOMETRIC DETECTION OF HEPARIN	P2-35	204
Aleksandra Wosztyl, Krzysztof Fronc, Bożena Sikora, Tomasz Wojciechowski, Roman Minikayev, Wojciech Paszkowicz, Kamil Sobczak, Przemysław Kowalik, Katarzyna Łysiak, Danek Elbaum, Jacek Szczytko, Izabela Kamińska UPCONVERTING NANOPARTICLES - SYNTHESIS AND CHARACTERIZATION	P2-36	205
Gytis Babaitis, Darius Dobrovolskas INVESTIGATION OF InGaN/GaN QUANTUM WELLS PHOTOLUMINESCENCE AND SURFACE TOPOGRAPHY	P2-37	206
Did not participate	P2-38	207
Nadzeya Khinevich, Juodenas Mindaugas, Tomas Tamulevicius, Sigitas Tamulevicius DEVELOPMENT OF A POROUS SILICON BASED GUIDE MODE RESONATOR AS A TEMPLATE FOR SERS-APPLICATION	P2-39	208
Mindaugas Kazlauskas, Danguolė Montvydienė, Živilė Jurgelėnė, Sergej Šemčuk, Kęstutis Jokšas, Nijolė Kazlauskienė EFFECTS OF GRAPHENE OXIDE NANOSTRUCTURES AND METAL MIXTURES ON LEPIDIUM SATIVUM	P2-40	209
Edith Flora Joel, Galina Lujaniene, Sandra Stanionytė, Loreta Levinskaitė GRAPHENE OXIDE / CHITOSAN / COPPER NANOCOMPOSITES FOR ANTIBACTERIAL STUDIES	P2-41	210
Did not participate	P2-42	211
Monika Puzerytė, Aušra Simanaitienė, Nerita Žmuidzinavičienė, Simona Ostachavičiūtė, Dovilė Sinkevičiūtė, Agnė Šulčiūtė SPINEL TYPE $ZnCO_2O_4$ COATINGS FORMATION AND ELECTROCHEMICAL PERFORMANCE	P2-43	212
Jovita Grigonytė, Simona Ostachavičiūtė, Dovilė Sinkevičiūtė, Nerita Žmuidzinavičienė, Algirdas Šulčius, Agnė Šulčiūtė DEPOSITION METHOD INFLUENCE ON MORPHOLOGY AND PHOTOELECTROCHEMICAL PROPERTIES OF ZnO FILMS	P2-44	213

Eimantas Kriščiūnas, Vladas Vansevičius STAR CLUSTERS IN THE ANDROMEDA GALAXY	P2-45	214
Karlis Pukitis, Miroslaw Schmidt, Ryszard Szczerba, Jinhua He MODELLING CIRCUMSTELLAR MOLECULAR LINE VARIABILITY IN IRC +10216	P2-46	215
Edgaras Kolomiecas, Vidas Dobrovolskas, Arūnas Kučinskas ABUNDANCE OF ZIRCONIUM IN THE ATMOSPHERES OF RED GIANTS IN GALACTIC GLOBULAR CLUSTER 47 TUC	P2-47	216
Jorge Perez Gonzalez, Enrique Diez Alonso, Faustino Garcia CHARACTERIZATION OF THE VARIABLE STAR EPIC 246257206 DISCOVERED WITH OBSERVATIONS OF THE K2-C12-FOV TAKEN BY THE KEPLER SPACE TELESCOPE.	P2-48	217
Edvinas Navakauskas and Simona Strazdaitė COMPARISON OF DIFFERENT DEUTERATED DIPALMITOYL PHOSPHATIDYLCHOLINE MONOLAYERS USING SUM-FREQUENCY GENERATION SPECTROSCOPY	P2-49	218
Aliaksandr Miadzvetski, Valery Plakhodzka, Anastasiya Shcherbovich, Natalie Savastenko PLASMA-INDUCED MODIFICATION OF ZnO-BASED CATALYSTS DOPED WITH Ag PLASMON NANOPARTICLES FOR PHOTODEGRADATION OF PHARMACOLOGICAL WASTE	P2-50	219

17 March, WEDNESDAY

15:15-16:00 **POSTER SESSION P3**

		p.
Daniele Costa da Silva Alves, Luiz Antônio de Almeida Pinto, Tito Roberto Sant'Anna Cadaval Junior, Carmel Bernadette Breslin DEVELOPMENT OF CHITOSAN SPONGE MODIFIED WITH CARBON NANOTUBES FOR PHENOL ADSORPTION	P3-1	220
Mohamed Abdelkader THE USE OF MACHINE LEARNING IN ORTHOTROPIC MATERIALS CLASSIFICATION VIA MODAL ANALYSIS	P3-2	221
Mindaugas Ilickas, Simas Račkauskas, Brigita Abakevičienė SYNTHESIS AND INVESTIGATION OF FUNCTIONAL PROPERTIES OF ZINC OXIDE NANOPOWDERS	P3-3	222
Avtushko Kirill Valentinovich, Sadov Vasily Sergeevich STEGANOGRAPHIC INTEGRATION OF COMMUNICATION SCHEMES IN MAPS	P3-4	223
Justas Ciganas, Giedrius Janušas INNOVATIVE TECHNOLOGIES FOR THE FORMATION OF MICROSTRUCTURES IN FUNCTIONAL MATERIALS	P3-5	224
Mohaiminul Quayum, Md. Reazuddin Repon IMPROVEMENT OF FLAME RETARDANCY AND EVALUATION OF PHYSICAL PROPERTIES OF JUTE FABRIC USING COMBINED CHEMICAL	P3-6	225
Gintarė Plečkaitytė, Jurgis Pilipavičius, Jurga Juodkazytė, Linas Vilčiauskas INVESTIGATION OF $Na_4Fe_3(PO_4)_2(P_2O_7)$ AS CATHODE FOR AQUEOUS NA-ION BATTERIES	P3-7	226
Eduardas Pečiulis, Jūratė Simokaitienė, Juozas Vidas Gražulevičius SYNTHESYS AND PROPERTIES OF METHOXYPHENYL OR METHYLTHIOPHENYL SUBSTITUTED CARBAZOLE DERIVATIVES AS HOLE-TRANSPORTING MATERIALS	P3-8	227
Karolis Leitonas, Dmytro Volyniuk, Viktorija Andruleviciene, Pavel Arsenyan, Brigita Vigante, Juozas Vidas Grazulevicius TADF BEHAVIOUR OF CARBAZOLE AND PHENOTHIAZINE SUBSTITUTED PYRIDINES TOWARDS OLED APLICATIONS	P3-9	228
Greta Motiekaityte, Aukse Navaruckiene, Jolita Ostrauskaite REAL-TIME PHOTORHEOMETRY STUDY OF DUAL PHOTOCURING KINETICS OF BIO-BASED MONOMERS	P3-10	229
Sandesh Mysore Sathyaraj, Harsha Dyanesh , Veeraraghavan Rajagopalan THE CONTROL OF THERMAL BEHAVIOR COIR MIXED GLASS FIBER SPUR GEAR DURING MESHING PROCESS (HAND-LAYUP METHOD)	P3-11	230
Dominik Suwala, Grzegorz Wryk, Aleksandra Szymanska, Krzysztof Domanski, Alicja Kalucka, Ola Bednarczyk, Dana BinczukWojciech Mech, Adam Wincukiewicz, Maciej Krajewski, Joanna Sitnicka, Krzysztof P. Korona, Maria Kaminska PRODUCTION OF VARIOUS SIZE ORGANIC PHOTOVOLTAIC CELLS WITH P3HT:PC61BM AS AN ACTIVE LAYER	P3-12	231
Aukse Navaruckiene, Danguole Bridziuviene, Vita Raudoniene, Jolita Ostrauskaite VANILLIN ACRYLATE-BASED POLYMERS: INFLUENCE OF RESIN COMPOSITION TO PHOTOCURING KINETICS AND PROPERTIES OF THE RESULTING POLYMERS	P3-13	232
Justinas Jaras, Aukse Navaruckiene, Jolita Ostrauskaite SYNTHESIS AND INVESTIGATION OF TRIDECYL METHACRYLATE-BASED PHOTOCROSS-LINKED POLYMERS	P3-14	233
Eglė Tankelevičiūtė, Paulius Baronas, Regimantas Komskis, Povilas Adomėnas, Ona Adomėnienė, and Saulius Juršėnas HELICITY INDUCED SPIN-ORBIT COUPLING FOR ULTRAFAST ISC IN ALKYNE BRIDGED BIFLUORENES	P3-15	234
Mykyta Kovalenko, Daniela Senkevič, Karolina Lapkauskaitė,Andrius Dzedzickis, Vytautas Bučinskas DEVELOPMENT OF MEDICAL PLANT DRYING METHOD BASED ON THE CONTROL OF RELATIVE HUMIDITY	P3-16	235
Ada Steponavičiūtė, Karolis Stravinskas, Aušra Selskienė, Genrik Mordas PROCESS PARAMETER INFLUENCE ON SURFACE ROUGHNESS OF ADDITIVELY MANUFACTURED STAINLESS STEEL PARTS	P3-17	236
Nikita Edgar Sitiajev, Vaiva Trečiokaitė, Ernestas Šutinys EXPERIMENTAL RESEARCH OF FORCE/PRESSURE SENSOR STATIC AND DYNAMIC ACCURACY AND REPEATABILITY	P3-18	237
Jurga Jeršovaitė, Edvinas Skliutas, Giedrė Grigalevičiūtė, Daiva Baltriukienė, Mangirdas Malinauskas OPTICALLY 3D PRINTED SCAFFOLDS BIOCOMPATIBILITY EVALUATION AND IMPROVEMENT	P3-19	238
Norina Asfand, Virginija Daukantienė INFLUENCE OF FIBER CONTENT ON THE BENDING STIFFNESS OF FUNCTIONAL TEXTILES	P3-20	239
Did not participate	P3-21	240
Skirmantas Norkus, Osvaldas Grubys, Simona Raugalaite, Brigita Abakeviciene, Ramunas Valiokas 3D PRINTED HYDROXYAPATITE – PROPERTIES AND APPLICATIONS AS SCAFFOLD MATERIAL FOR BONE REGENERATION	P3-22	241
Romualdas Jonas Čepas, Lukas Kukulas, Gytis Juška, Kristijonas Genevičius RECOMBINATION OF CHARGE CARRIERS IN BULK HETEROJUNCTION SOLAR CELLS	P3-23	242
Algirdas Petronis, Tomas Januškevičius, Kęstutis Dumbrava, Karolina Lapkauskaitė, Andrius Dzedzickis, Vytautas Bučinskas IMPROVING DISPLACEMENT ESTIMATION BY MEMS ACCELEROMETER USING DEEP Q-LEARNING ALGORITHM	P3-24	243
Egidijus Kamarauskas, Romualdas Jonas Čepas, Kristijonas Genevičius CELIV TECHNIQUE FOR INVESTIGATION OF PHOTO-GENERATED CHARGE CARRIERS MOBILITY IN THIN FILMS	P3-25	244
Dominykas Augulis, Kazimieras Badokas, Arūnas Kadys, Simonas Strumskis, Ilja Ignatjev, Giedrius Juška, Jūras Mickevičius and Tadas Malinauskas THE INFLUENCE OF GRAPHENE SURFACE TREATMENT ON REMOTE EPITAXY OF GALLIUM NITRIDE	P3-26	245
Julija Jokšaitė, Andrius Vasiliauskas, Aušrinė Jurkevičiūtė, Asta Tamulevičienė INVESTIGATION OF THE STRUCTURE AND OPTICAL PROPERTIES OF DIAMOND LIKE CARBON THIN FILMS	P3-27	246
Kristina Radinović, Jadranka Milikić, Aldona Balčiūnaitė, Zita Sukackienė, Loreta Tamašauskaitė-Tamašiūnaitė and Biljana Šljukić ARSENIC DETECTION BY GOLD COBALT ELECTRODE IN AQUEOUS MEDIA	P3-28	247
Greta Merkininkaitė, Edvinas Aleksandravičius, Mangirdas Malinauskas, Darius Gailevičius, Simas Šakirzanovas LASER ADDITIVE MANUFACTURING OF CRYSTALLINE 3D NANOSTRUCTURES	P3-29	248
Nadežda Traškina, Jurgis Pilipavičius, Milda Petrulevičienė, Jurga Juodkazytė, Linas Vilčiauskas OPTIMIZATION OF ANODE PREPARATION PROCESS FOR AQUEOUS NA-ION BATTERIES	P3-30	249
Karolis Stravinskas, Genrik Mordas, Alireza Shahidi, Romuald Petkevič SELECTIVE LASER – MATERIAL POWDER MELTING	P3-31	250
Agata Jarocka, Przemysław P. Michalski, Jacek Ryl, Tomasz K. Pietrzak, Marek Wasiucionek XPS STUDIES OF VANADIUM-DOPED LITHIUM-MANGANESE-BORATE GLASSES AND NANOCOMPOSITES	P3-32	251
Sikander Abbas Basra, Zeeshan Azam, Norina Asfand CHARACTERIZATION OF TENSILE PROPERTIES OF KNITTED UNI-DIRECTIONAL THERMOPLASTIC PREPREG COMPOSITES	P3-33	252

Kristine Kalnica-Dorosenko, Aiga Svede VISUAL ACUITY EXAMINATION AT HOME DURING COVID-19	P3-34	253
Did not participate	P3-35	254
Anna Marini, Bianca Bottino GADOLINIUM LOADED ORGANIC DETECTOR FOR THE DARKSIDE EXPERIMENT	P3-36	255
Romuald Petkevič, Sergejus Borodinas, Genrik Mordas CENTERED METAL POWDER FLOW FOR PRECISION LASER METAL POWDER DEPOSITION	P3-37	256
Did not participate	P3-38	257
Natalija Tetervenoka, Kaspars Traskovskis, Aivars Vembris OPTICAL AND ELECTROLUMINESCENCE PROPERTIES OF SOLUTION PROCESSIBLE IR(PPY)3 DERIVATIVES WITH ADDED TRIPHENYLMETHANE GROUPS	P3-39	258
Vitalij Fiodorov, Karolis Ratautas, Zenius Mockus LASER-ASSISTED SELECTIVE FABRICATION OF COPPER TRACES ON POLYMERS BY ELECTROPLATING	P3-40	259
Arsenii Kovalenko WIRELESS COMMUNICATION IN THE INTERNET OF THINGS	P3-41	260
Linda Krauze, Vita Konosonoka, Kristiana Zizlane, Tatjana Pladere, Gunta Krumina GAZE PARAMETERS WHEN VIEWING IMAGES ON THE MULTI-PLANE VOLUMETRIC DISPLAY	P3-42	261
Shalini Murugesan, Sundar Arumugam Krishnan Nagarajan, Virginija Gylienė, Valdas Eidukynas, Giedrius Gylys IMPROVEMENT OF HEARING PROTHESES AND AIDS BY USING CAD/CAE TECHNIQUES	P3-43	262
Aida Drevilkauskaitė, Amran Al-Ashouri, Steve Albrecht, Vytautas Getautis, Artiom Magomedov CARBAZOLE-BASED MONOLAYERS FOR PEROVSKITE SOLAR CELLS	P3-44	263
Kazimieras Baltrusaitis, Anna Sytchkova, Remigijus Juškėnas, Vitalija Jasulaitienė, Rimantas Simniškis, Viktoras Vaičikauskas, Alexandr Belosludtsev INVESTIGATION OF CHROMIUM THIN FILMS FOR OPTICAL APPLICATIONS	P3-45	264
Vaiva Soriūtė, Patrik Ščajev CARRIER TRANSPORT PROCESSES IN MIXED CATION LEAD HALIDE PEROVSKITE MATERIALS	P3-46	265
Miglė Stančiauskaitė, Tomas Murauskas, Valentina Plaušinaitienė, Virgaudas Kubilius THIN PEROVSKITE La:$BaSnO_3$ FILMS - TOWARDS NOVEL OPTOELECTRONIC MATERIALS	P3-47	266
Did not participate	P3-48	267
Did not participate	P3-49	268
Eugene V. Petrenko, Lyudmila V. Omelchenko, Andrei L. Solovjov FLUCTUATION CONDUCTIVITY IN $YBa_2Cu_3O_{7-\delta}$ SINGLE CRYSTALS UNDER ELECTRON IRRADIATION	P3-50	269

16:15-17:00 **POSTER SESSION P4**

Sandesh Mysore Sathyaraj, Veeraraghavan Rajagopalan, Harsha Dyanesh FABRICATION OF COMPOSITE HELMET USING BANANA FIBER AND FLY ASH	P4-1	270
Robert Poenaru DESCRIBING THE WOBBLING MOTION IN ^{163}LU THROUGH A SEMI-CLASSICAL APPROACH	P4-2	271
Simonas Draukšas, Thomas Gajdosik RENORMALIZING THE NEUTRINO MIXING MATRIX IN THE GRIMUS-NEUFELD MODEL	P4-3	272
Simas Jankauskas, Ugnė Šilingaitė, Simonas Draukšas HEAVY GAUGE BOSON W' SEARCH IN MUON CHANNEL USING "MADMINER" PACKAGE	P4-4	273
Domantas Čiapas, Aurelijus Rinkevičius. ANALYSIS OF Z BOSON DECAY TO NEUTRINOS USING LHC	P4-5	274
Ignas Kazakevičius, Vygintas Gontis APPROXIMATION OF BURST DURATION'S PDFS OF BIRTH-DEATH PROCESSES	P4-6	275
Valery Kapshai, Anton Talkachov, Anton Shamyna ANALYSIS OF THE TOTAL RADIATION POWER OF THE SECOND–HARMONIC GENERATION FROM A LINEAR STRUCTURE OF LONG CYLINDRICAL DIELECTRIC PARTICLES	P4-7	276
Mario Graml , Dominik Kreil , Helga M. Böhm NONLINEAR RESPONSE THEORY IN ULTRA-THIN ELECTRON LAYERS	P4-8	277
Dominykas Orlovas, Aurelijus Rinkevičius Z BOSON DECAY CLASSIFICATION USING ARTIFICIAL INTELLIGENCE WITH LHC	P4-9	278
Simona Breidokaite, Gediminas Stankunas COMPARISON OF NEUTRON FLUX IN EU DEMO DIVERTOR PLASMA-FACING COMPONENTS USING WCLL AND HCPB BREEDING BLANKET MODELS	P4-10	279
José Carlos Lozano OVERESTIMATION OF SPAIN'S SUMMER TEMPERATURES DUE TO REGIONAL CLIMATE MODELS NON-STATIONARY BIASES.	P4-11	280
Laimonas Deveikis, Tomas Čeponis, Eugenijus Gaubas STUDY OF ELECTRICAL CHARACTERISTICS OF SiGe AND CdZnTe MATERIALS APPLICABLE TO RADIATION DETECTION	P4-12	281
Rokas Kondrotas, Arūnas Krotkus, Saulius Tumėnas, Bronislovas Cechavicius, Maarja Grossberg, Marit Kauk-Kuusik, Xiaofeng Li CHALCOGENIDE-PEROVSKITES FOR MULTIJUNCTION SOLAR CELL APPLICATION	P4-13	282
Elena Valkiūnaitė, Jūras Mickevičius INVESTIGATION OF TWO LUMINESCENCE BANDS IN NONPOLAR InGaN/GaN MULTIPLE QUANTUM WELLS SPECTRA	P4-14	283
Mariamija Nikitina MICROSCOPIC LUMINESCENCE PROPERTIES OF VARIOUS POLARITY InGaN QUANTUM STRUCTURES	P4-15	284
Monika Jokubauskaitė, Evelina Dudutienė, Ramūnas Nedzinskas, Liuwen Chang, Mitch Chou TEMPERATURE-DEPENDENT PHOTOLUMINESCENCE OF ROCKSALT $Zn_{1-x}Mg_xO$ EPILAYERS	P4-16	285
Kornelijus Pūkas, Tomas Čeponis, Eugenijus Gaubas TCAD SIMULATIONS OF P-TYPE Si AND $Si_{1-x}Ge_x$ LOW GAIN AVALANCHE DETECTOR CHARACTERISTICS	P4-17	286

Aleksandra Širvinskytė, Jūras Mickevičius PHOTOLUMINESCENCE STUDIES OF GaN EPITAXIAL LAYERS	P4-18	287
Tomas Grinys, Kristupas Razas MODELING OF P-N JUNCTION OF III GROUP NITRIDE BY FINITE DIFFERENCE METHOD	P4-19	288
Jonas Gradauskas, Steponas Ašmontas, Algirdas Sužiedėlis, Aldis Šilėnas, Aurimas Čerškus, Ovidijus Žalys, Oleksandr Masalskyi HOT CARRIER EVIDENCE IN A SOLAR CELL	P4-20	289
Manvydas Dapkevičius, Edvinas Radiunas, Saulius Juršėnas, Steponas Raišys, Karolis Kazlauskas TRIPLET EXCITON DIFFUSION IN PHOTON UPCONVERTING RUBRENE FILMS	P4-21	290
Lukas Matulis and Pranciškus Vitta HYPERSPECTRAL IMAGING TECHNOLOGY WITH A SMARTPHONE AND MULTICOLOUR FLASH	P4-22	291
Did not participate	P4-23	292
Vaiva Soriūtė, Patrik Ščajev, Pavels Onufrijevs, Arturs Medvids, Hung-Hsiang Cheng OPTOELECTRONIC PROPERTIES OF GERMANIUM-TIN LAYER	P4-24	293
Gustas Liaugminas, Julijanas Želudevičius, Kęstutis Regelskis OPTICAL FREQUENCY CONVERSION TO VISIBLE AND NEAR-IR RANGES USING PHOTONIC CRYSTAL FIBERS	P4-25	294
Did not participate	P4-26	295
Marius Navickas, Robertas Grigutis, Gintaras Tamošauskas, Vytautas Jukna, Audrius Dubietis HIGH REPETITION RATE LASER-INDUCED PERIODIC STRUCTURES IN TRANSPARENT DIELECTRIC MATERIALS	P4-27	296
Ernestas Nacius, Benas Stanionis, Pavel Gotovski, Orestas Ulčinas,Sergej Orlov, Vytautas Jukna LASER MICRO-MACHINING OF TRANSPARENT MATERIAL WITH BESSEL BEAMS GENERATED BY SPATIALLY DISPLACED AXICONS	P4-28	297
Rycard Lebed, Aleksej M. Rodin Nd:YVO_4 AMPLIFIERS SEEDED WITH Nd:YAP AND Nd:YVO_4 LASER PULSES AT 1.34 μm FOR NON-INVASIVE BLOOD DIAGNOSTICS	P4-29	298
Miglė Kuliešaitė, Jokūbas Pimpė, Vygandas Jarutis, Julius Vengelis UV-VISIBLE LIGHT GENERATION IN PHOTONIC CRYSTAL FIBER PUMPED BY IR 110 FS PUMP PULSES	P4-30	299
Did not participate	P4-31	300
Mantas Drazdys, Darija Astrauskytė, Vitalija Jasulaitienė, Ramutis Drazdys ATOMIC LAYER DEPOSITION OF SiO_2 USING OXYGEN PLASMA AND OZONE	P4-32	301
Justas Kudirka, Erminas Kozlovskis, Antanas Urbas COMPARISON OF FIRST-ORDER SELECTIVE DIFFRACTION EFFICIENCIES OF VOLUME BRAGG GRATINGS IN THREE DIFFERENT TYPES OF GLASS	P4-33	302
Vaida Marčiulionytė, Vytautas Jukna, Gintaras Tamošauskas, Audrius Dubietis SUPERCONTINUUM GENERATION IN CaF_2 CRYSTAL PUMPED BY HIGH REPETITION RATE GREEN FEMTOSECOND LASER PULSES	P4-34	303
Ramūnas Logminas, Arūnas Varanavičius MULTI-PLATE CONTINUUM GENERATORS FOR FEW CYCLE PULSE FORMATION	P4-35	304
Akvilė Bunkevičiūtė, Balys Momgaudis, Mikas Vengris INVESTIGATION OF IMPURITIES IN LASER MEDIA: CATHODOLUMINESCENCE AND FILAMENT INDUCEDLUMINESCENCE COMPARISON	P4-36	305
Jonas Banys, Julius Vengelis CONSTRUCTION AND INVESTIGATION OF ROD-TYPE FIBER AMPLIFIER SYSTEM FOR FEMTOSECOND YB:KGW OSCILLATOR	P4-37	306
Aivaras Pečiulis, Mikas Vengris INVESTIGATION OF THE DYNAMICS OF OPTICAL DAMAGE USING PUMP-PROBE SPECTROSCOPY	P4-38	307
Gaudenis Jansonas, Rimantas Budriūnas, Arūnas Varanavičius NUMERICALLY PROCESSED INTERFEROMETRIC NONLINEAR REFRACTIVE INDEX MEASUREMENTS AT 3240nm	P4-39	308
Danielius Samsonas, Lukas Kontenis, Mikas Vengris LABEL-FREE IMAGING OF BIOLOGICAL TISSUE USING WIDEFIELD SECOND-HARMONIC GENERATION MICROSCOPY	P4-40	309
Emanuelis Lazauskas, Lina Grinevičiūtė, Gabija Petrauskaitė, Lukas Ramalis and Tomas Tolenis INVESTIGATION OF OPTIMIZATION AND MANUFACTURE POTENTIAL FOR SCULPTURED THIN FILM BASED ACHROMATIC WAVEPLATES	P4-41	310
Ugnė Norkutė, Lukas Ramalis, Rytis Buzelis, Tomas Tolenis INVESTIGATION OF RELATION BETWEEN OPTICAL RESISTIVITY AND STORING CONDITIONS OF POROUS SILICA BASED MULTILAYER COATINGS	P4-42	311
Darija Astrauskytė, Mantas Drazdys, Ramutis Drazdys CRYSTALLIZATION BEHAVIOR OF TITANIUM OXIDE THIN FILMS DEPOSITED BY PLASMA ENHANCED AND OZONE-BASED ATOMIC LAYER DEPOSITION	P4-43	312
Simonas Driukas, Gabrielė Kavaliauskaitė, Raminta Skačkauskaitė, Kasparas Rakštys, Marius Franckevičius, Vidmantas Gulbinas PASSIVATION OF $FA_{0.95}Cs_{0.05}PbI_3$ PEROVSKITE WITH (PHENYLENE)DI(ETHYLAMMONIUM) ORTO-, META-, PARA- CATIONS IMPROVES CHARGE CARRIER EXTRACTION	P4-44	313
Gabriele Stanionyte, Julius Vengelis CONSTRUCTION AND INVESTIGATION OF SUBNANOSECOND OPG/OPA	P4-45	314
Simas Melnikas, Lukas Ramalis, Simonas Kičas, Tomas Tolenis, INCLUSION OF SCULPTURED TOP LAYER IN CHIRPED MIRROR DESIGN FOR REDUCED GROUP DELAY DISPERSION OSCILLATIONS	P4-46	315
Pauls Kristaps Reinis, Lase Milgrave, Kristians Draguns, Inga Brice, Janis Alnis, Aigars Atvars LISSAJOUS FIGURES AS DATA PROCESSING METHOD FOR OPTICAL WAVELENGTH SHIFT BASED SENSORS	P4-47	316
Karolis Adomavičius, Ieva Žičkienė, Egidijus Auksorius, Dawid Borycki, SlawomirTomczewski, Maciej Wojtkowski ULTRAFAST VOLUMETRIC (3D) HUMAN RETINA IMAGING WITH FOURIER-DOMAIN FULL-FIELD OPTICAL COHERENCE TOMOGRAPHY	P4-48	317
Vytautas Gradauskas, Justina Anulytė, Ernesta Bužavaitė-Vertelienė, Ieva Plikusienė, Zigmas Balevičius; (IN-SITU) STUDY OF IMMOBILIZED RECEPTOR BINDING KINETICS BY USING PLANAR PHOTONIC-PLASMONIC NANOSTRUCTURES FOR BIOSENSING	P4-49	318

18 March, THURSDAY

15:15-16:00 POSTER SESSION P5

		p.
Did not participate	P5-1	319
Gelminė Vansevičiūtė, Milda Stankevičiūtė THE GENOTOXIC IMPACT TO PERIPHERAL BLOOD CELLS OF PERCA FLUVIATILIS INDUCED BY MULTIPLE STRESSORS. COMET ASSAY AND NUCLEAR ABNORMALITIES ANALYSIS	P5-2	320
Evelina Griniuk, Irena Savickaja, Arnas Naujokaitis, Jurga Juodkazytė, Milda Petrulevičienė OPTIMIZATION OF SOL-GEL SYNTHESIS PROCEDURE OF TUNGSTEN (VI) OXIDE COATINGS FOR EFFICIENT PHOTOELECTROCHEMICAL PRODUCTION OF HYPOCHLORITE	P5-3	321
Vitalijus Stirkė, Linas Balčiauskas, Laima Balčiauskienė, Raminta Skipitytė, Andrius Garbaras TROPHIC ECOLOGY OF SMALL MAMMALS IN COMMERCIAL ORCHARDS: INSIGHTS FROM STABLE ISOTOPE STUDIES	P5-4	322
Ieva Vaicekauskaitė, Diana Žilovič, Rūta Čiurlienė, Rasa Sabaliauskaitė, Sonata Jarmalaitė *ARID1A* MUTATIONS IN UTERINE LAVAGE FLUID INDICATES EARLY ENDOMETRIAL AND OVARIAN CANCERS	P5-5	323
M. Gedgaudas, A. Mickevičiūtė, A. Brukštus, D. Matulis, E. Kazlauskas HIGH AFFINITY BINDING INHIBITORS OF PROTOZOAN PARASITE HSP90	P5-6	324
Veronika Malyško, Vitalij Novickij, Auksė Zinkevičienė, Jurij Novickij, Julita Kulbacka, Nina Rembialkowska, Irutė Girkontaitė PREDICTION OF CANCER CELL VIABILITY AND COMPROMISED MEMBRANE INTEGRITY AFTER PULSED ELECTRIC FIELD TREATMENT USING LUMINESCENCE	P5-7	325
Nataliya Kozak, Lubov Atramentova REPRODUCTIVE CHARACTERISTICS AND SELECTION INDEXES OF CRIMEAN TATAR WOMEN ACCORDING TO THEIR SUB-ETHNIC GROUPS	P5-8	326
Gabija Žalpytė THE EFFECT OF NAPHTHYLACETIC ACID ON CREEPING GLOXINIA	P5-9	327
Tomas Makaras and Milda Stankevičiūtė ACCLIMATION EFFECT ON SALMONIDS (ONCORHYNCHUS MYKISS AND SALMO SALAR) SWIMMING BEHAVIOUR: DETERMINATION OF APPROPRIATE ACCLIMATION PERIOD	P5-10	328
Eivina Radzevičiūtė, Austėja Balevičiūtė, Augustinas Želvys, Vitalij Novickij, Karolina Žilionytė, Irutė Girkontaitė THE INFLUENCE OF NANOSECOND ELECTROPORATION ON THE DEVELOPMENT OF ANTIBODIES AGAINST TUMOR CELLS	P5-11	329
Eglė Žalytė, Veronika Dedonytė, Benediktas Kurlinkus, Audrius Šileikis, Peter Schemmer, Mindaugas Valius ESTABLISHMENT AND CHARACTERIZATION OF A NEW PANCREATIC DUCTAL ADENOCARCINOMA CELL LINE CAPAN-26	P5-12	330
Agnė Bučaitė, Milda Stankevičiūtė, Janina Pažusienė GENOTOXIC AND CYTOTOXIC EFFECTS OF MICROPLASTICS ON ONCORHYNCHUS MYKISS: EXPLORATORY DATA ANALYSIS USING MACHINE LEARNING	P5-13	331
Gerda Skinderytė, Saulius Serva, Aleksandras Konovalovas DEVELOPMENT OF FLUORESCENCE-BASED TRANSPOSITION ASSAY FOR SACCHAROMYCES CEREVISIAE	P5-14	332
Yuliia Khmelnytska, Olena Perepelytsina, Mykhailo Sydorenko INVESTIGATION OF ANTICANCER DRUGS INFLUENCE ON BREAST CANCER CELL MODELS	P5-15	333
Justina Gaizevska, Ausra Stumbryte-Kaminskiene, Rasa Sabaliauskaite, Sonata Jarmalaite INSIGHT INTO THE HETEROGENEITY OF BREAST CANCER THROUGH NEXT GENERATION SEQUENCING	P5-16	334
Edgaras Tamelis, Lauryna Ragauskaitė, Dalia Gelvonauskienė, Danas Baniulis REDOX ENZYMES INVOLVED IN ARABIDOPSIS THALIANA (L.) HEYNH. SEEDLING RESPONSE TO COLD PLASMA TREATMENT OF SEEDS	P5-17	335
Augustas Morkvėnas, Živilė Jurgelėnė, Sergej Šemčiuk, Nijolė Kazlauskienė, Vitalijus Karabanovas BIOACCUMULATION OF GRAPHENE OXIDE NANOSTRUCTURES IN SALMO TRUTTA AT EARLY DEVELOPMENT STAGES	P5-18	336
Reda Nalivaikienė, Virginija Kalcienė, Aleksandras Rybakovas, Žilvinas Pūtys, Giedrė Višinskienė, Laura Butrimavičienė GENO- AND CYTOTOXIC RESPONSES IN FLOUNDER (PLATICHTHYS FLESUS) FROM THE LITHUANIAN COASTAL ZONE (BALTIC SEA)	P5-19	337
Eglė Žymantaitė, Jan Aleksander Kraśko, Agata Mlynska, Emilija Paberalė DENDRITIC CELL VACCINE MODULATION IN VITRO WITH CHARACTERISED EPITHELIAL OVARIAN CANCER CELL LINE LYSATE	P5-20	338
Joelis Verdingas, Asta Stapulionytė EVALUATION OF PH INFLUENCE ON ONION ROOT GROWTH AND GENOTOXICITY INDICES BY ALLIUM CEPA ASSAYS	P5-21	339
Mariia Naumova, Lilia Savinska INFLUENCE OF THE ISOFORM P85 S6K1 ON THE ACTIVITY OF OTHER ISOFORMS IN CELLS WITH CRISPR-EDITED EXPRESSION OF S6K1.	P5-22	340
Benita Buragaite-Staponkiene, Kristina Snipaitiene, Adomas Rovas, Ruta Matuleviciute, Egle Punceviciene, Irena Butrimiene, Alina Puriene, Sonata Jarmalaite CIRCULATING MIRNAS AS DIAGNOSTIC BIOMARKERS FOR PERIODONTITIS	P5-23	341
Andrius Burdulis, Danguolė Žiogienė, Alma Gedvilaitė CONSTRUCTION OF SACCHAROMYCES CEREVISIAE DOLICHOL KINASE MUTANTS USING CRISPR-CAS9 SYSTEM AND INVESTIGATION OF THEIR GLYCOSYLATION PROPERTIES	P5-24	342
Vilius Mensonas, Raimondas Šiukšta, Violeta Kleizaitė INVESTIGATION OF ALUMINUM TOXICITY RESPONSE OF NEWLY CREATED LITHUANIAN BARLEY CULTIVARS	P5-25	343
Indrė Juodviršytė, Justina Kaziūnienė, Audrius Gegeckas ISOLATION AND CHARACTERIZATION OF CELLULASE PRODUCING MICROORGANISMS FROM BIOGAS DIGESTATE	P5-26	344
Lina Anulevičiūtė, Gintarė Sauliutė, Arvydas Markuckas, Živilė Jurgelėnė, Milda Stankevičiūtė TOXICOLOGICAL EFFECTS OF TIRE FIRE EFFLUENTS: CATALASE AND METALLOTHIONEIN INDUCTION IN RAINBOW TROUT (ONCORHYNCHUS MYKISS) LARVAE	P5-27	345
Augustė Vipartaitė, Kristina Žukauskaitė, Rasa Sabaliauskaitė, Sonata Jarmalaitė IDENTIFICATION OF CRITICAL GENETIC EVENT OF CLEAR CELL RENAL CELL CARCINOMA BASED ON PLASMA MRNA LEVELS	P5-28	346
Dominyka Breimelytė, Asta Stapulionytė EVALUATION OF CYTOTOXICITY AND GENOTOXICITY OF ZINC OXIDE NANOPARTICLES BY ALLIUM CEPA TEST	P5-29	347
Raminta Saulėnaitė, Jolanta Patamsytė GENETIC DIVERSITY ANALYSIS OF HERACLEUM SOSNOWSKYI IN VILNIUS CITY AND SURROUDINGS USING ISSR MOLECULAR MARKERS	P5-30	348
Justinas Baleišis, Romualdas Rudys. PHOTOMECHANICAL EFFECT INDUCED ON INDRADERMAL TATTOO PIGMENTS WITH PICOSECOND ND:YAG LASER	P5-31	349

Donata Stancelytė, Irena Nedveckytė ALLELOPATHIC ACTIVITY OF INVASIVE PLANT CANADIAN GOLDENROD (SOLIDAGO CANADENSIS L.)	P5-32	350
Gabrielė Dzimitravičiūtė, Kristina Daniūnaitė ANALYSIS OF CIRCULATING MIRNA LEVELS IN BLOOD OF WOMEN DIAGNOSED WITH GESTATIONAL DIABETES	P5-33	351
Svetlana OhiienkoRoman TrokhymchukYuliia IlchenkoNadiia Zolotarova EVALUATING OF TWO ELISA ASSAYS IN KHARKIV OBLAST	P5-34	352
Gabrielė Bumbulytė, Vincas Būda NATURAL REPELLENTS FOR MEALWORM (TENEBRIO MOLITOR L.) LARVAE	P5-35	353
Greta Meidutė, Rūta Maleckaitė, Kristina Daniūnaitė GENE EXPRESSION ANALYSIS OF HISTONE METHYLATION ASSOCIATED GENES IN PROSTATE TUMORS	P5-36	354
Paulina Šlimaitė, Elias Maccioni, Vilma Petrikaitė EVALUATION OF ANTICANCER ACTIVITY OF KINASE INHIBITORS IN MDA-MB-231 BREAST CANCER CELL LINE	P5-37	355
Liucija Kamaitytė-Bukelskienė, Jurgita Butkuvienė, Donatas Naugžemys IMPACT OF WATER TRANSPORT ON WATER COURSES WITH RANUNCULION VEGETATION – HABITAT TYPE OF EUROPEAN IMPORTANCE 3260	P5-38	356
Ieva Calkaite, Algimanta Kundrotaite, Karolina Barcauskaite DETERMINATION OF BIOLOGICALLY ACTIVE COMPOUNDS AND ITS RADICAL SCAVENGING ACTIVITY IN CANNABIS SATIVA L. MORPHOLOGICAL PARTS	P5-39	357
Indre Zakiene, Gintare Ziukaite, Juozas Grigas, Arnoldas Pautienius, Judita Zymantiene POST-EXTRACTION SITE WOUND HEALING USING PLATELET-RICH-FIBRIN IN DOGS	P5-40	358
Laura Jurkaitytė, Ieva Dumšytė, Alisa Gricajeva, Lukas Stasiulionis, Lilija Kalėdienė INFLUENCE OF ANTIMICROBIAL PHOTOINACTIVATION ON MONOCULTURAL BACTERIAL BIOFILMS	P5-41	359
Girstautė Dabkevičiūtė, Elias Maccioni, Vilma Petrikaitė ANTICANCER ACTIVITY OF SUNITINIB ANALOGUES IN BRAIN CANCER MODELS	P5-42	360
Did not participate	P5-43	361
Did not participate	P5-44	362
Kristina Khudaleeva, Nikolay Abolmasov APPLICATION OF A MULTIFUNCTIONAL LASER DIAGNOSTIC COMPLEX "LAKK-M"IN DENTISTRY	P5-45	363
Anastasia Derevtsova, Svetlana Derevtsova PHYSICS IN MEDICINE: DISORDERS OF MICROCIRCULATORY PROCESSES IN THE MUSCLE AND THEIR DIAGNOSIS IN DISEASES OF THE NERVOUS SYSTEM	P5-46	364
Did not participate	P5-47	365
Ugne Imbrasaite, Bronius Buckus THE ROLE OF LAPAROSCOPY IN THE MANAGEMENT OF ABDOMINAL TRAUMA	P5-48	366
Did not participate	P5-49	367
Pranas Grigaitis, Ibrahim El-Semman, Angelica Rodrigues Prado, Manuel Garcia Albornoz, Victoria Harman, Stephen Holman, Johan van Heerden, Simon Hubbard, Rob Beynon, Frank J. Bruggeman, Pascale Daran-Lapujade, Nikolaus Sonnenschein, Jens Nielsen, Bas Teus COMPARTMENT-SPECIFIC PROTEOME CONSTRAINTS DRIVE CHANGES IN YEAST METABOLISM	P5-50	368

16:15-17:00 POSTER SESSION P6

Sandra Barysaitė, Andrius Gelzinis, Jevgenij Chmeliov, Leonas Valkunas MODELING OF CONCENTRATION QUENCHING IN TWO-DIMENSIONAL SYSTEMS	P6-1	369
Elžbieta Počobut, Tadas Malinauskas SYNTHESIS AND IVESTIGATION OF NEW ORGANIC SEMICONDUCTORS WITH AMIDE AND REACTIVE FUNCTIONAL GROUPS	P6-2	370
Lauryna Monika Svirskaitė, Tadas Malinauskas SYNTHESIS AND INVESTIGATION OF N-TYPE ORGANIC SEMICONDUCTORS CONTAINING ANCHORING GROUPS	P6-3	371
Birutė Bugelytė, Ingrida Jurkutė, Vida Vičkačkaitė DEEP EUTECTIC SOLVENTS FOR HEADSPACE GAS CHROMATOGRAPHIC DETERMINATION OF HEXANAL	P6-4	372
Aleksandra Buchcic, Anna Zawisza, Stanisław Leśniak, Michał Rachwalski ASYMMETRIC FRIEDEL-CRAFTS ALKYLATION OF INDOLES CATALYZED BY CHIRAL PHOSPHINE-AZIRIDINES	P6-5	373
Rūta Aukštakojytė, Justina Gaidukevič, Jurgis Barkauskas THE THERMAL DECOMPOSITION OF GRAPHENE OXIDE IN THE PRESENCE OF CARBON SUBOXIDE	P6-6	374
Gabriele Rankelyte, Jevgenij Chmeliov MODELING OF SINGLET-SINGLET ANNIHILATION IN ONE-DIMENSIONAL MOLECULAR LATTICE	P6-7	375
Silvija Juciute, Ieva Plikusiene, Vincentas Maciulis, Almira Ramanaviciene, Zigmas Balevicius, Ernesta Buzavaite-Verteliene, Evaldas Ciplys, Rimantas Slibinskas, Martynas Simanavicius, Aurelija Zvirbliene, Arunas Ramanavicius TOTAL INTERNAL REFLECTION ELLIPSOMETRY FOR THE INVESTIGATION OF SARS-COV-2 NUCLEOCAPSID PROTEIN AND SPECIFIC ANTIBODY BINDING KINETICS	P6-8	376
Audrius Sadaunykas, Audrius Zolumskis, Evaldas Naujalis DEVELOPMENT OF ADD-ON PROTOTYPE FOR GC OVEN COOLING	P6-9	377
Ugnė Rimkaitė, Ieva Karpavičienė, Edvinas Orentas SYNTHESIS OF ASYMMETRIC NAPHTHALENE DIIMIDE AS A MODEL PHOTOCATALYST FOR MULTICOMPONENT PHOTOREDOX REACTIONS	P6-10	378
Agnė Zdaniauskienė, Tatjana Charkova, Rita Sadzevičienė, Gediminas Niaura IN-SITU SHINERS ANALYSIS OF IMIDAZOLE RING TERMINATED MONOLAYER AT ELECTROCHEMICAL INTERFACE	P6-11	379
Justyna Anna Adamczyk, Lena Marciniak, Adam Marek Pieczonka, Michał Rachwalski NONSYMMETRICAL AZINES WITH AGGREGATION INDUCED EMISSION ENHANCEMENT	P6-12	380
Agne Kizalaite, Aleksej Zarkov HYDROTHERMAL SYNTHESIS OF ZINC WHITLOCKITE	P6-13	381

Greta Inkrataitė, Ramūnas Skaudžius SYNTHESIS AND INVESTIGATION OF LuAG:Pr,B COATINGS ON QUARTZ SUBSTRATE OBTAINED BY SOL-GEL SPIN COATING TECHNIQUE	P6-14	382
Povilas Luizys, Maryte Daskeviciene, Kasparas Rakstys, Vygintas Jankauskas, Egidijus Kamarauskas SYNTHESIS AND CHARACTERISTICS OF ORGANIC SEMICONDUCTORS WITH N-CARBAZOLYL-BASED CHROMOPHORES	P6-15	383
Dovydas Karoblis, Aleksej Zarkov, Kestutis Mazeika, Dalis Baltrunas, Gediminas Niaura, Aldona Beganskiene, Aivaras Kareiva STRUCTURAL AND MAGNETIC STUDY OF $YFeO_3$-$GdFeO_3$ SOLID SOLUTIONS	P6-16	384
Žyginta Einorytė, Greta Majauskaitė, Kęstutis Aidas MODELLING BINARY SYSTEMS OF ACETIC ACID AND DIMETHYL SULFOXIDE: STRUCTURAL ANALYSIS AND ^{1}H NMR SPECTRA	P6-17	385
Milica Ilić, Ivana Kuzminac, Marija Sakač COMPARATIVE STUDY OF IN SILLICO TOOLS TO PREDICT THE ADME PROFILING FOR SELECTED 5,6-OXYGENATED D-HOMO STEROIDS	P6-18	386
Gabija Kavaliauskaitė, Povilas Virbickas, Aušra Valiūnienė, Urtė Samukaitė - Bubnienė YEAST CELL MODIFICATION WITH PRUSSIAN BLUE	P6-19	387
Ljubica Brenjo, Srđan Bjedov SYNTHESIS OF BILE ACID PRECURSOR FOR NEW GLUCOCORTICOID DERIVATIVES	P6-20	388
Edita Daublytė, Agnė Zdaniauskienė, Tatjana Charkova MICROWAVE-ASSISTED SYNTHESIS OF SILVER NANOPARTICLES WITH POLYOLS	P6-21	389
Karolina Karalevičiūtė , Galina Lujanienė , Raman Novikau , Vidas Pakštas , Audrius Drabavičius , Arnas Naujokaitis SYNTHESIS, CHARACTERIZATION AND APPLICATION OF CHITOSAN-CLAY-BASED NANOCOMPOSITES FOR SORPTION OF METALS/RADIONUCLIDES	P6-22	390
Ella Duvanova Ella, Serhii Radio, Georgiy Rozantsev INTERACTION OF COPPER(II) WITH ACIDIFIED SODIUM ORTOTUNGSTATE AQUEOUS SOLUTIONS	P6-23	391
Ruta Juodvalkyte, Monika Skruodiene, Ramunas Skaudzius SYNTHESIS AND ANALYSIS OF YTTRIUM ALUMINIUM GARNET DOPED WITH TANTALUM, CALCIUM AND EUROPIUM OR CERIUM	P6-24	392
Lukas Neverdauskas, Paulina Kaziukonytė, Algirdas Brukštus SYNTHESIS OF BENZIMIDAZOLE DERIVATIVES AS POTENTIAL INHIBITORS FOR HSP90	P6-25	393
Martyna Malinowska, Anna Zawisza, Stanisław Leśniak AZIRIDIN-2-YL METHANOLS AS CHIRAL SOLVATING AGENTS FOR CARBOXYLIC ACIDS	P6-26	394
Irina Fiodorova, Tomas Serevičius, Rokas Skaisgiris, Gediminas Kreiza, Dovydas Banevičius, Karolis Kazlauskas, Saulius Juršėnas, Sigitas Tumkevičius STRUCTURE OPTIMIZATION AND TADF PROPERTIES OF NOVEL ACRIDINE-PYRIMIDINE DERIVATIVES	P6-27	395
Raimonda Boguzaite, Vilma Ratautaite, Ernestas Brazys, Arunas Ramanavicius THE PPY LAYER THICKNESS CONTROL FOR THE DEVELOPMENT OF THE SENSOR	P6-28	396
Kamilė Tulaitė, Justina Jovaišaitė, Jelena Tamulienė, Jonas Šarlauskas, Narimantas Čėnas and Saulius Juršėnas. PHOTOPHYSICAL STUDY OF TIRAPAZAMINE BASED COMPOUNDS	P6-29	397
Migle Lebedevaite, Jolita Ostrauskaite INVESTIGATION OF PHOTOCROSS-LINKING KINETICS OF ACRYLATED SOYBEAN OIL WITH DIFFERENT PHOTOINITIATORS AND PROPERTIES OF THE RESULTING POLYMERS	P6-30	398
Kristina Tot, Anita Lazić, Tatjana Đaković Sekulić EXAMINATION OF NEW SPIROHYDANTOINS AND THEIR MOLECULAR DESCRIPTORS RELATED TO THEIR BIOACTIVITY AND TOXICITY	P6-31	399
Paulina Nemaniutė, Dalia Bražinskienė, Svajus Asadauskas INDUCTION OF VISCOSITY INCREASE DURING POLYGLYCOL ADDITION TO ISOCYANATES	P6-32	400
Yuliia Oleksii, Serhii Radio, Eugeni Get'man ISOMORPHOUS SUBSTITUTION AND STABILITY OF SOLID SOLUTIONS IN THE $La_{1-X}Ln_XF_3$, LN = CE – HO SYSTEMS	P6-33	401
Karolina Aleknaite, Laura Peciulyte, Deimante Rosliuk, Ramune Rutkaite APPLICATION OF STARCH ACETATE FOR REMOVAL OF ALKYL PARABENS FROM AQUEOUS MEDIUM	P6-34	402
Audrė Kalinauskaitė, Marijus Jurkūnas, Svajus Asadauskas MEASUREMENT OF STORAGE MODULUS IN UNCURED ELASTOMERS USING PLATE-PLATE AND MOVING DIE TECHNIQUES	P6-35	403
Loreta Tamašauskaitė-Tamašiūnaitė, Eivilė Budrytė, Aldona Balčiūnaitė, Jūratė Vaičiūnienė, Eugenijus Norkus SYNTHESIS, CHARACTERISATION AND INVESTIGATION OF NITROGEN-DOPED CARBON SUPPORTED MANGANESE-COBALT NANOPARTICLES	P6-36	404
Aldona Balčiūnaitė, Titas Stanevičius, Loreta Tamašauskaitė-Tamašiūnaitė, Eugenijus Norkus INVESTIGATION OF HYDROGEN PEROXIDE REDUCTION ON COPPER-NICKEL FOAMS	P6-37	405
Daina Upskuvienė, Jūratė Vaičiūnienė, Ivar Kruusenberg, Katlin Kaare, Aleksandrs Volperts, Galina Dobele, Aivars Zurins, Loreta Tamašauskaitė-Tamašiūnaitė, Eugenijus Norkus NITROGEN-DOPED CARBON SUPPORTED WITH GOLD NANOPARTICLES AS AN EFFICIENT CATALYST FOR GLUCOSE ELECTRO-OXIDATION	P6-38	406
Laurynas Butkus, Rūta Barisevičiūtė, Justina Šapolaitė, Žilvinas Ežerinskis, Evaldas Maceika, Algirdas Pabedinskas, Andrius Garbaras, Vidmantas Remeikis ASSESSMENT OF THE IGNALINA NUCLEAR POWER PLANT INFLUENCE ON RADIOCARBON CONCENTRATION IN LAKE DRUKSIAI	P6-39	407
Goda Gudinskaitė, Danguolė Jakimavičiūtė, Rasa Šlinkšienė INFLUENCE OF PEAT EXTRACT ON THE PROPERTIES OF LIQUID FERTILIZERS	P6-40	408
Hanna Maltanava, Nikita Belko, Michael Samtsov, Sergey Poznyak OPTICAL AND REDOX PROPERTIES OF POLYMETHINE DYES	P6-41	409
Did not participate	P6-42	410
Mantas Norkus, Gediminas Niaura, Ramūnas Skaudžius FABRICATION OF PHOSPHOR IN GLASS MATRIX MATERIALS UTILIZING NOVEL LOW MELTING TEMPERATURE PHOSPHATE GLASSES	P6-43	411
Gytaute Sirgedaite, Lina Mikoliunaite A MICROWAVE-FACILITATED SYNTHESIS OF MAGNETIC FE_3O_4 NANOPARTICLES	P6-44	412
Did not participate	P6-45	413
Sarune Daskeviciute, Cristina Momblona, Kasparas Rakstys, Albertus Adrian Sutanto, Maryte Daskeviciene, Vygintas Jankauskas, Alytis Gruoodis, Giedre Bubniene, Vytautas Getautis, Mohammad Khaja Nazeeruddin FLUORENE-BASED ENAMINES AS LOW-COST AND DOPANT-FREE HOLE TRANSPORTING MATERIALS FOR HIGH PERFORMANCE AND STABLE PEROVSKITE SOLAR CELLS	P6-46	414

Did not participate	P6-47	415
Maryia Drobysh, Viktorija Liustrovaite, Alma Rucinskiene, Martynas Simanavicius, Aurelija Zvirbliene, Rimantas Slibinskas, Ieva Plikusiene, Evaldas Ciplys, Arunas Ramanavicius MODELING OF ELECTROCHEMICAL-BASED IMMUNOSENSORS FOR THE DETECTION OF SPECIFIC ANTIBODIES	P6-48	416
Donatas Pleškys, Irena Savickaja, Vidas Pakštas, Arnas Naujokaitis, Jurga Juodkazytė, Milda Petrulevičienė THE EFFECT OF STABILIZING AGENTS IN SOL-GEL SYNTHESIS OF $BiVO_4$ COATINGS	P6-49	417
Laura Michailova, Irena Savickaja, Gintarė Plečkaitytė, Arnas Naujokaitis, Vidas Pakštas, Milda Petrulevičienė, Jurga Juodkazytė, Rimantas Ramanauskas MODIFICATION OF $BiVO_4$ AND INVESTIGATION OF PHOTOELECTROCHEMICAL ACTIVITY	P6-50	418

19 March, FRIDAY

15:15-16:00 POSTER SESSION P7

		p.
Simas Macionis, Dalius Gudeika, Dmytro Volyniuk, Oleksandr Bezvikonnyi, Jiun Haw Lee, Pei-Hsi Lee, Chia-Hsun Chen, Tien-Lung Chiu, Juozas V. Grazulevicius NEW BIPOLAR HOSTS FOR HIGH EFFICIENCY OLEDs	P7-1	419
Povilas Virbickas, Aušra Valiūnienė, Gabija Kavaliauskaitė, Gerda Žižiūnaitė THE APPLICATIONS OF PRUSSIAN BLUE IN PH SENSING	P7-2	420
Viktorija Liustrovaite, Ausra Valiuniene, Gintaras Valincius, Arunas Ramanavicius CHLOROPHYLL a IMMOBILIZATION INTO TETHERED BILAYER LIPID MEMBRANE	P7-3	421
Joana Sinkevičiūtė, Remigijus Ivanauskas, Ingrida Ancutienė, Algimantas Ivanauskas STUDY OF FORMATION OF TIN SULFIDE LAYERS ON POLYAMIDE SHEET	P7-4	422
Megija Neimane, Vitālijs Lazarenko, Māris Bērtiņš, Arturs Vīksna, Dagnija Lazdiņa, Kristaps Makovskis, Ilze Kārkliņa, Andis Lazdiņš VARIATIONS OF RARE EARTH ELEMENTS IN THE BOTTOM AND FLY WOOD ASH	P7-5	423
Nojus Radzevičius, Linas Vilčiauskas AB INITIO CALCULATIONS OF $Na_{1+2X}Mn_XTi_{2-X}(PO_4)_3$ (x = 0.0; 1.0) RAMAN SPECTRA	P7-6	424
Tomas Janeliunas, Malek Mahmoudi, Melika Ghasemi, Dalius Gudeika, Dmytro Volyniuk, Juozas V. Grazulevicius SYNTHESIS AND CHARACTERIZATION OF DIBENZOTHIOPHENE DERIVATIVES AS THERMALLY ACTIVATED DELAYED FLUORESCENCE EMITTERS	P7-7	425
Naveen Masimukku, Dalius Gudeika, Oleksandr Bezvikonnyi, Dmytro Volyniuk, Juozas Vidas Grazulevicius 1,8-NAPHTHALIMIDE DERIVATIVES EXHIBITING THERMALLY ACTIVATED DELAYED FLUORESCENCE	P7-8	426
Liucija Urbelytė, Birutė Grybaitė, Vytautas Mickevičius SYNTHESIS OF NOVEL 2-[(2,6-DICHLORO-4-SULFAMOYLPHENYL)AMINO]ACETIC ACID DERIVATIVES	P7-9	427
Andrius Pakalniškis, Ramūnas Skaudžius, Tomas Murauskas, Siarhei I. Latushka, Denis Alikin, Algirdas Selskis, Dmitry Karpinsky, Aivaras Kareiva INSPECTION OF THE MORPHOTROPIC PHASE BOURANDY IN SAMARIUM SUBSTITUTED $BiFeO_3$	P7-10	428
Birutė Serapinienė, Jurga Juodkazytė, Laima Gudavičiūtė, Algirdas Selskis, Rimantas Ramanauskas ELECTROCHEMICALLY ACTIVE SURFACE AREA MEASUREMENT OF HONEYCOMB-LIKE COPPER FOAM ELECTRODE	P7-11	429
Barbara Chatinovska, Augustina Jozeliūnaitė, Edvinas Radiunas, Lukas Naimovičius, Karolis Kazlauskas, Edvinas Orentas MACROMOLECULAR DIKETOPYRROLOPYRROLE AS THE ANNIHILATOR IN UPCONVERTING ORGANIC FILMS	P7-12	430
Adrian Vicent-Claramunt, Evaldas Naujalis CORRELATION BETWEEN PYRIDINE AND FURFURYL ALCOHOL INGESTION AND THEIR PRESENCE IN BREATH	P7-13	431
Davit Tediashvili, Linas Vilčiauskas A RRDE STUDY OF MN-BASED CATHODE MATERIAL DEGRADATION IN AQUEOUS NA -ION BATTERIES	P7-14	432
Diana Griesiute, Agne Kizalaite, Hanna Klipan, Aleksej Zarkov SYNTHESIS OF Cu CONTAINING CALCIUM PHOSPHATE WITH WHITLOCKITE STRUCTURE THROUGH THE LOW-TEMPERATURE DISSOLUTION-PRECIPITATION PROCESS	P7-15	433
Oleksandra Mariichak, Georgii Rozantsev, Serhii Radio SYNTHESIS AND CRYSTAL STRUCTURES OF SAMARIUM(III)–CONTAINING HETEROPOLY SALTS WITH PEACOCK–WEAKLEY TYPE ANION $Na_{9-x}H_x[Sm(W_5O_{18})_2]\cdot nH_2O$	P7-16	434
Indrė Misiūnaitė, Karolis Žigas, Ieva Karpavičienė DETERMINATION OF COMPOUNDS STRUCTURES FORMED DURING ELECTROPHILIC CYCLIZATION REACTIONS OF BENZIMIDAZOL-2-YL ALKYNES USING NMR	P7-17	435
Sabina Pavliukovič, Povilas Šimonis, Rasa Garjonytė, Arūnas Stirkė INVESTIGATION OF ELECTROPORATION EFFECTS BY MEDIATED AMPEROMETRY AT YEAST MODIFIED ELECTRODES	P7-18	436
Miglė Bartkutė, Audrius Sadaunykas, Evaldas Naujalis HPLC METHOD DEVELOPMENT AND VALIDATION FOR MAIN CANNABINOIDS DETERMINATION IN HEMP BIOMASS AND OIL	P7-19	437
Aistė Jegorovė, Marytė Daškevičienė, Vytautas Jankauskas, Egidijus Kamarauskas, Vytautas Getautis NEW FLUORENE CLASS SEMICONDUCTORS AS HOLE TRANSPORTING MATERIALS FOR PEROVSKITE SOLAR CELLS	P7-20	438
Yasmina Halabi , Chaimae Nasri, Hicham Harhar, Abdelkebir Bellaouchou, Mohamed Tabyaoui DATE SEED: A GREAT SOURCE OF BIOACTIVE COMPOUNDS WITH ANTIOXIDANT POTENTIAL	P7-21	439
Yuliya Prosmytskaya, Anastasiya Kanunnikova EVALUATION OF THE POLYMER FILMS DEGRADATION IN VITRO	P7-22	440
Artem Bezfamilnyi, Stela Georgieva, Anton. Georgiev DEVELOPMENT OF A VOLTAMMETRIC METHOD FOR THE DETERMINATION OF CU (II) IONS IN AQUEOUS SAMPLES USING NOVEL AZO-AZOMETHINE COMPOUNDS AS COMPLEXING AGENTS	P7-23	441
Žana Činčienė, Aldona Balčiūnaitė, Loreta Tamašauskaitė-Tamašiūnaitė, Eugenijus Norkus 3D METALLIC COPPER-NICKELFOAMS AS CATALYSTS FOR THE ELECTROOXIDATION OF SODIUM BOROHYDRIDE	P7-24	442
Eglė Šidlauskaitė, Andrius Merkys METHODS FOR THE DETERMINATION OF COVALENT BONDS IN SMALL MOLECULE CRYSTALS	P7-25	443
Giedrė Karzaitė, Mahboubeh Eskandari, Tautgirdas Ruzgas CHARACTERISATION OF LOW MOLECULAR WEIGHT BIOMARKERS OF INFLAMMATION AND CANCER	P7-26	444
Edita Kodytė, Rūta Gruškienė, Jolanta Sereikaitė THE EFFECT OF STORAGE TIME ON THE LOADING EFFICIENCY OF NISIN-LOADED ULVAN PARTICLES	P7-27	445
Mantas Žiaunys, Andrius Sakalauskas, Vytautas Smirnovas IDENTIFYING INSULIN FIBRIL CONFORMATIONAL DIFFERENCES BY THIOFLAVIN-T BINDING CHARACTERISTICS	P7-28	446
Aida Šermukšnytė, Ingrida Tumosienė, Kristina Kantminienė. *S*-SUBSTITUTED 5-(2-((4-ETHOXYPHENYL)AMINO)ETHYL)-4-PHENYL-2,4-DIHYDRO-3*H*-1,2,4-TRIAZOLE-3-THIONE DERIVATIVES AS POTENTIAL ANTIOXIDANT AGENTS	P7-29	447
Raimonda Mažylytė, Justina Kaziūnienė, Eglė Lastauskienė, Audrius Gegeckas ISOLATION OF PHOSPHATE SOLUBILIZING MICROORGANISM AND INDUSTRIAL FERMENTATION PROCESS OPTIMIZATION	P7-30	448

Jurga Andrėja Kazlauskaitė, Jurga Bernatonienė ANTIOXIDANT ACTIVITY IN *TRIFOLIUM PRATENSE* L. BLOSSOMS USING DIFFERENT EXTRACTION METHODS	P7-31	449
Inga Matulytė, Akvilė Mataraitė, Jurga Bernatonienė ANTIOXIDANT ACTIVITY OF NUTMEG ESSENTIAL OIL (PURE, WITH MAGNESIUM ALUMINOMETASILICATE AS EXCIPIENT AND THEIR MIXTURE IN A RATIO OF 1:1)	P7-32	450
Aistė Kairytė, Inga Matijošytė, Arnoldas Kaunietis DEVELOPMENT OF CONTROLLED GENE EXPRESSION SYSTEM FOR (PARA)GEOBACILLUS SPP. BACTERIA	P7-33	451
Akvilė Vilpišauskaitė, Saulė Ulinauskaitė, Algirdas Kaupinis, Mindaugas Valius, Arnoldas Kaunietis HETEROLOGOUS EXPRESSION OF NOVEL BACTERIOCIN FROM THERMOPHILIC BACTERIA	P7-34	452
Ernesta Augustinienė, Naglis Malys IDENTIFICATION AND CHARACTERIZATION OF L- AND D-LACTIC ACID-INDUCIBLE SYSTEMS FOR TRANSCRIPTION FACTOR-BASED BIOSENSOR DEVELOPMENT	P7-35	453
Milda Bulotaitė, Vilma Kaškonienė, Rūta Mickienė, Audrius Maruška CHANGES IN THE TOTAL MICROBIAL COUNT AND ANTIBACTERIAL ACTIVITY OF KOMBUCHA PREPARED WITH HERBAL TEAS	P7-36	454
Kamilė Šimelytė, Augustė Rastenienė, Jolanta Sereikaitė, Ramunė Stanevičienė, Elena Servienė. SCREENING OF PURIFICATION METHODS FOR ANTIMICROBIAL PEPTIDE FROM PEDIOCOCCUS ACIDILACTICI JEM-1	P7-37	455
Justina Kaziūnienė, Raimonda Mažylytė, Audrius Gegeckas ISOLATION AND SCREENING OF DIAZOTROPHIC MICROORGANISMS WHICH ARE SIGNIFICANT FOR SUSTAINABLE AGRICULTURE	P7-38	456
Tautvydas Kojis, Aurelija Mickevičiūtė, Lina Baranauskienė PRODUCTION OF RECOMBINANT MOUSE CARBONIC ANHYDRASE XIV PROTEIN	P7-39	457
Mantė Rakauskaitė, Arnoldas Kaunietis, Marija Jankunec ANTIMICROBIAL EFFECT OF GEOBACILLIN 26 BY ATOMIC FORCE MICROSCOPY	P7-40	458
Agnė Savickaitė, Renata Gudiukaitė *IN SILICO* ANALYSIS OF CUTINASE FROM *STREPTOMYCES SCABIEI* 87.22	P7-41	459
Jolita Pachaleva, Ruta Gruskiene, Alma Bockuviene, Jolanta Sereikaite. THE ANTIOXIDANT ACTIVITY OF NISIN-LOADED PECTIN-CHITOOLIGOSACCHARIDES PARTICLES	P7-42	460
Elvyra Gumbinaitė, Povilas Šimonis, Aušra Linkevičiūtė, Arūnas Stirkė ELECTROPORATION ASSISTED IMPROVEMENT OF FREEZING TOLERANCE IN YEAST CELLS	P7-43	461
Martynas Raila, Eivydas Andriukonis, Arūnas Ramanavičius SLA 3D PRINTING APPLICATION FOR FAST ELECTROCHEMICAL DEVICE PROTOTYPING	P7-44	462
Delianas Palinauskas, Gintautas Bagdžiūnas ELECTROCHEMICAL INVESTIGATION OF ADSORBED CYCLODEXTRINS ON ITO ELECTRODE FOR POTENTIAL HYSTAMINE SENSING	P7-45	463
Evelina Jankaitytė, Zigmantas Toleikis, Vytautas Smirnovas, Gintaras Valinčius, Rima Budvytytė STUDY OF THE INTERACTION OF MISFOLDED PROTEINS WITH MEMBRANE MODEL SYSTEMS	P7-46	464
Tomas Urbaitis, Giedrius Gasiūnas, Joshua K. Young, Monika Jasnauskaitė, Mantvyda Grušytė, Sushmitha Paulraj, Jennifer L. Curcuru, Megumu Mabuchi, Ryan T. Fuchs, Ezra Schildkraut, G. Brett Robb and Virginijus Šikšnys HARNESSING THE DIVERSITY OF CAS9 ORTHOLOGS FOR GENOME EDITING	P7-47	465
Justinas Babinskas, Jerica Sabotič, Inga Matijošytė SYNTHESIS AND INVESTIGATION OF OLIGOMERIZED AROMATIC AMINE FOR LACCASE ACTIVITY ASSAY	P7-48	466
Eivydas Andriukonis, Marius Butkevičius HYDROGEL BASED MICRO AG/AGCL REFERENCE ELECTRODES. QUICK PROTOTYPING OF REFERENCE ELECTRODES	P7-49	467

16:15-17:00 POSTER SESSION P8

Egle Plukaite, Vilmantas Pupkis, Indre Lapeikaite, Vilma Kisnieriene ACTION POTENTIAL PROPAGATION VELOCITY IN *NITELLOPSIS OBTUSA*	P8-1	468
Margarita Poderyte, Ausra Valiuniene, Inga Gabriunaite APPLICATION OF SCANNING ELECTROCHEMICAL IMPEDANCE MICROSCOPE FOR INVESTIGATION OF ELECTROPORATION PROCESS	P8-2	469
Algimantas Kaminskas, Asta Kausaite-Minkstimiene TOWARD TO AN ENZYMATIC BIOFUEL CELL POWERED BY GLUCOSE	P8-3	470
Benas Kužmarskis, Vilmantas Pupkis, Vilma Kisnierienė, Indrė Lapeikaitė ACTION POTENTIALS OF PLANTS: EFFECTS OF CHLORIDE CHANNELS' INHIBITION	P8-4	471
Akvilė Milašiutė, Rima Budvytytė, Gintaras Valinčius STUDY OF THE INTERACTION OF HSP70 WITH UNILAMELLAR VESICLES	P8-5	472
Arūnas Stirkė, Raimonda Celiesiūtė-Germanienė, Aurelijus Zimkus, Nerija Žurauskienė, Povilas Šimonis, Aldas Dervinis, Arūnas Ramanavičius, Saulius Balevičius, Klaudija Mačiūtė, Justina Kriovaitė INVESTIGATION OF YEAST CELL WALL BARRIER FUNCTIONS AFTER PEF TREATMENT	P8-6	473
Ona Bartininkaitė, Aleksandras Konovalovas, Justas Lazutka, Elena Servienė, Saulius Serva CHARACTERIZATION OF VIRUS-LIKE PARTICLES OF *TORULASPORA DELBRUECKII* VIRUS TDV-1 PRODUCED IN *SACCHAROMYCES CEREVISIAE*	P8-7	474
Jolita Jagelaviciute, Dalia Cizeikiene ANTIOXIDANT ACTIVITY AND RESISTANCE TO LOW PH OF STRAINS BELONGING TO LACTOBACILLUS AND BIFIDOBACTERIUM GENERA	P8-8	475
Katazyna Blazevic, Juste Rozene, Vakare Guoba Sataite, Inga Morkvenaite-Vilkonciene BAKER'S YEAST-BASED QUINONES-MEDIATED MICROBIAL FUEL CELL	P8-9	476
Kristupas Paulius, Aleksandras Konovalovas, Saulius Serva SACCHAROMYCETALES AND THEIR ALLIES IN BIOLOGICAL VERSATILITY	P8-10	477
Katarzyna Dziergowska, Izabela Michalak METAL-OXIDE NANOPARTICLES SYNTHESIS FROM MACROALGAL EXTRACTS	P8-11	478
Rimgailė Tamulytė, Evelina Jankaitytė, Zigmantas Toleikis, Marija Jankunec STUDY OF THE INTERACTION OF S100A9 PROTEIN WITH LIPID MEMBRANES	P8-12	479

Aušrinė Venckaitytė, Vilma Kaškonienė, Rūta Mickienė, Audrius Maruška APPLICATION OF ENZYMATIC AND BACTERIAL HYDROLYSIS FOR INCREASE OF THE BIOLOGICAL ACTIVITY OF RAW PLANT MATERIAL	P8-13	480
Emilija Januškaitė, Osvaldas Vilutis, Agnė Kalnaitytė THE PHOTOSTABILITY OF CdSe/ZnS-COOH QUANTUM DOTS IN AQUEOUS AND BIOLOGICAL MEDIA	P8-14	481
Danas Klimavičius, Dalia Smalakyte, Abhishek Pateria, Matthias Bochtler, Gintautas Tamulaitis CONSTRUCTION OF TYPE III-A CRISPR-CAS EFFECTOR COMPLEX FOR TRANSPORTATION INTO THE ZEBRAFISH NUCLEUS	P8-15	482
Marius Butkevičius, Audrius Laurynėnas APPLICATION OF MARCUS THEORY TO ANALYSIS OF GLUCOSE OXIDASE CATALYZED REDUCTION REACTION	P8-16	483
Gintarė Povilaitytė, Lilija Kalėdienė, Alisa Gricajeva PREPARATION OF IMMOBILIZED MICROBIAL LIPOLYTIC ENZYMES APPLICABLE FOR THE SYNTHESIS OF FLAVOR ESTERS	P8-17	484
Tomas Mockaitis, Vida Mildažienė, Rasa Žūkienė EFFECTS OF COLD PLASMA ON THE AMOUNT OF STEVIOL GLYCOSIDES IN STEVIA REBAUDIANA BERTONI LEAVES	P8-18	485
Viktoras Mažeika, Mykolas Mačiulis, Martynas Riauka, Lukas Kontenis, Edvardas Žurauskas, Virginijus Barzda POLARIMETRIC NONLINEAR MICROSCOPY WITH TEXTURE ANALYSIS FOR COLON CANCER DIAGNOSTICS	P8-19	486
Vilmantas Pedišius, Audrius Maruška, Irena Vaškevičienė PHYTOCHEMICAL ANALYSIS OF *ARTEMISIA DUBIA* WALL. SECONDARY METABOLITES AND ITS SOLID PELLET CALORIFIC VALUE	P8-20	487
Martynas Riauka, Viktoras Mazeika, Mykolas Maciulis, Edvardas Zurauskas, Lukas Kontenis, Virginijus Barzda COLLAGEN ULTRASTRUCTURE CHANGES IN LENTIGINOUS MELANOMA CHARACTERIZED BY SECOND-HARMONIC GENERATION MICROSCOPY	P8-21	488
Gytis Martusevičius, Gintarė Sauliutė, Janina Pažusienė, Živilė Jurgelėnė, Sergej Šemčuk, Milda Stankevičiūtė INVESTIGATIONS OF BIOLOGICAL EFFECTS OF GRAPHENE OXIDE NANOSTRUCTURES ON BROWN TROUT (*SALMO TRUTTA*)	P8-22	489
Anatolii Ivankov, Rasa Žukienė, Zita Naučienė, Laima Degutyte-Fomins, Irina Filatova, Veronika Lyushkevich, Vida Mildažienė IMPACT OF RED CLOVER SEED COLOR ON GERMINATION, MORPHOMETRY, AND ROOT NODULATION AFTER SEED TREATMENT WITH COLD PLASMA AND ELECTROMAGNETIC FIELD	P8-23	490
Karolina Lankaitė, Rūta Mickienė, Vilma Kaškonienė, Audrius Sigitas Maruška ANALYSIS OF SECONDARY METABOLITES OF MEDICAL PLANTS *Levandula* L. AND *Helichrysum* L.	P8-24	491
Laurynas Vaškevičius, Vilius Malūnavičius, Marija Jankunec, Renata Gudiukaitė ANALYSIS OF THE BIOCONSOLIDATION POTENTIAL OF *STAPHYLOCOCCUS* SP. H6	P8-25	492
Did not participate	P8-26	493
Justė Tamošiūnaitė, Simona Streckaitė CONCENTRATION QUENCHING OF ZINC-PHTHALOCYANINE IN SOLUTIONS	P8-27	494
Did not participate	P8-28	495
Augusta Jankutė, Simona Guobužaitė, Ronaldas Jakubovskis, Viktor Gribniak, Jaunius Urbonavičius. THE POTENTIAL OF *BACILLUS PSEUDOFIRMUS* AS HEALING AGENT OF BIOLOGICAL SELF-HEALING CONCRETE IN NORTH EUROPE REGION	P8-29	496
Anastasiia Tsymbaliuk, Viktoriia Stetska, Taisa Dovbynchuk, Oleksandr Gorbach, Ganna Tolstanova, Alexander Zholos THE ROLE OF TRPV4 CATION CHANNELS IN SMOOTH MUSCLE CONTRACTILE ACTIVITY IN RATS WITH PARKINSON`S DISEASE	P8-30	497
Konstanty Keda, Giedre Tamulaitiene, Irmantas Mogila, Virginijus Siksnys, Gintautas Tamulaitis CRYSTALISATION OF CRISPR-CAS RELATED TOXIN	P8-31	498
Raminta Reškevičiūtė, Indrė Dalgėdienė, Aurelija Žirblienė, Milda Plečkaitytė INVESTIGATION OF *GARDNERELLA SPP*. CNA PROTEIN USING IMMUNOLOGICAL METHODS	P8-32	499
Kornelija Buivydaitė, Marijus Plečkaitis, Ričardas Rotomskis PH DEPENDENT SELF-ASSEMBLING OF H_2TPPS_4 IN AQUEOUS SOLUTIONS	P8-33	500
Eglė Vitkūnaitė, Lina Baranauskienė INTRINSIC THERMODYNAMIC PARAMETERS OF HUMAN CARBONIC ANHYDRASE II AND ACETAZOLAMIDE INTERACTION	P8-34	501
Denis Baronas, Auksė Kazlauskaitė, Paulius Sasnauskas, Povilas Šėporaitis, Kamilė Vainiūtė ONFLOW: A SOFTWARE TOOL THAT PREDICTS LATERAL FLOW ASSAY PARAMETERS	P8-35	502
Edvardas Timoščenka, Aurelija Mickevičiūtė, Lina Baranauskienė PRODUCTION OF RECOMBINANT MOUSE CARBONIC ANHYDRASES CAR I, CAR II, CAR III, CAR VII AND CAR XIII	P8-36	503
Andrius Sakalauskas, Vytautas Smirnovas FLAVONE OXIDATION DERIVATIVES ACT AS INHIBITORS OF AMYLOID-BETA AGGREGATION	P8-37	504
Kamile Mikalauskaite, Mantas Ziaunys, Tomas Sneideris, Vytautas Smirnovas EFFECT OF IONIC STRENGTH ON THIOFLAVIN-T AFFINITY TO AMYLOID FIBRILS AND ITS FLUORESCENCE INTENSITY	P8-38	505
Laura Kiaušaitė, Laurynas Alijošius, Eugenijus Šimoliūnas, Aurelija Zajančkauskaitė, Martynas Skapas, Lidija Truncaitė SELF-ASSEMBLED NANOSTRUCTURES FORMED BY RECOMBINANT PROTEINS OF BACTERIOPHAGE VIRIONS	P8-39	506
Mehdi Alizadeh, Fayez Habach, Margarete K. Akens, Agne Kalnaityte, Saulius Bagdonas, Virginijus Barzda POLARIMETRIC SECOND HARMONIC GENERATION RESPONSE OF COMPLEX BIOLOGICAL STRUCTURES IN THE FOCAL VOLUME OF THE MICROSCOPE	P8-40	507
Did not participate	P8-41	508
Rugilė Bareikaitė, Deimantė Purytė, Irina Buchovec OPTICAL STUDY OF PHOTOACTIVE ANTIBACTERIAL AGENTS: RIBOFLAVIN AND CHLOROPHYLLIN.	P8-42	509
Timas Merkelis, Kasparas Kizys, Antanas Zinovicius, Juste Rozene, Inga Morkvenaite-Vilkonciene, Arunas Ramanavicius MICROBIAL BIOFUEL CELL BASED ON BAKER'S YEAST TREATED BY 9, 10-PHENANTHRENEQUINONE	P8-43	510
Patricija Izabelė Kaulakytė, Lilija Kalėdienė, Alisa Gricajeva IDENTIFICATION OF A NOVEL FAMILY OF BACTERIAL LIPOLYTIC ENZYMES	P8-44	511
Aleksandrs Petjukevics, Natalja Skute RAMAN LIGHT SCATTERING FROM THE LEAVES PLATES OF AQUATIC MACROPHYTE ELODEA CANADENSIS (MICHX. 1803) UNDER THE INFLUENCE OF MULTILEVEL SALINITY IN VIVO.	P8-45	512
Radvilas Bendorys, Bernadeta Masiulionytė, Beatričė Milda Balaišytė,Stasė Gasiulė, Vaidotas Stankevičius OPTIMIZATION OF GENOME PRIME EDITING IN MURINE EMBRYONIC CELLS	P8-46	513
Ilya Navitski, Nadezda Amaegberi, Galina Semenkova, Oleg Shadyro PALMITOXYACETONE, A PRODUCT OF FREE RADICAL LYSOPHOSPHOLIPIDS DESTRUCTION, REGULATES H_2O_2 PRODUCTION BY NEUTROPHILS	P8-47	514

Valeriya Klopava, Jan Panada, Tatsiana Kulahava, Nina Frolova, Yaroslav Faletrov, Vladimir Shkumatov THE EFFECT OF INDOLE-CONTAINING STEROIDS ON THE MITOCHONDRIAL MEMBRANE POTENTIAL OF C6 GLIOMA CELLS	P8-48	515
Justas Martūnas, Alisa Gricajeva, Arnoldas Kaunietis NEW LINEAR AZOL(IN)E CONTAINING ANTIMICROBIAL PEPTIDE IDENTIFICATION IN THERMOPHILIC BACTERIUM	P8-49	516
Julija Jurevičiūtė, Martynas Malikėnas NEW ADOMET ANALOGUES WITH FLUORESCENT MOIETIES. RESEARCH ON SYNTHESIS OF FLUORESCEINCARBOXY MOIETY POSSESSING ALKYNE AND PREPARATION OF 6-AZIDOHEX-2-YN-1-YL NOSYLATE	P8-50	517

EXPLORING BLACK HOLES WITH MICADO - THE FIRST LIGHT IMAGER OF E-ELT

Algita Stankevičiūtė[1], Łukasz Wyrzykowski[1]

[1]Astronomical Observatory of the University of Warsaw, Poland
algita@astrouw.edu.pl, atigla@gmail.com

Intermediate Mass Black Holes (IMBHs) are hypothetical missing building blocks of larger black holes, Super-Massive Black Holes (SMBH), which are found in the centres of galaxies [1,2]. The left-over population of IMBHs should be discoverable in the present Universe, however, current attempts resulted only in weak candidates [3].

Firstly, we have to rely on the unique and up-to-date methods that can find, explore and quantify the traces of IMBHs. Among the most persuasive techniques, the Gravitational Microlensing phenomenon [4] becomes a very powerful probing technique which can be used to study the structure of the Milky Way no matter how faint objects are [5]. This method is based on Einstein's general relativity theory which means that incoming light wavefront can bend around massive object (e.g., black hole) as a consequence of its gravity when so called "lensing star" is passing by [6].

However, missing piece of information in microlensing is the separation between the lensed images, as they are of order of milliarcseconds. First high resolution imaging of microlensed images was obtained with ESO's (European Southern Observatory) VLTI (Very Large Telescope Interferometer) instrument GRAVITY [7]. Nevertheless, to get more information and details of our desired astronomical object, we must have telescope with bigger diameter in order to reach to more common but weaker sources. The bigger the telescope, the higher angular resolution that we can get. ESO's E-ELT (Europe's Extremely Large Telescope) will be the biggest "eye" on Earth in 2025 with 39.3 m diameter primary segmented mirror [8].

In this research, we are presenting the capabilities of detecting IMBHs with E-ELT first light imager MICADO (Multi-Adaptive Optics Imaging Camera for Deep Observations) (the set-up is showed in Fig. 1). By applying, multi-adaptive optics systems, we can be able to resolve images without a huge impact coming from atmosphere but the we must to get a proper calibration of the instrument. This work will present the factors that determine the difficulties faced by the calibration.

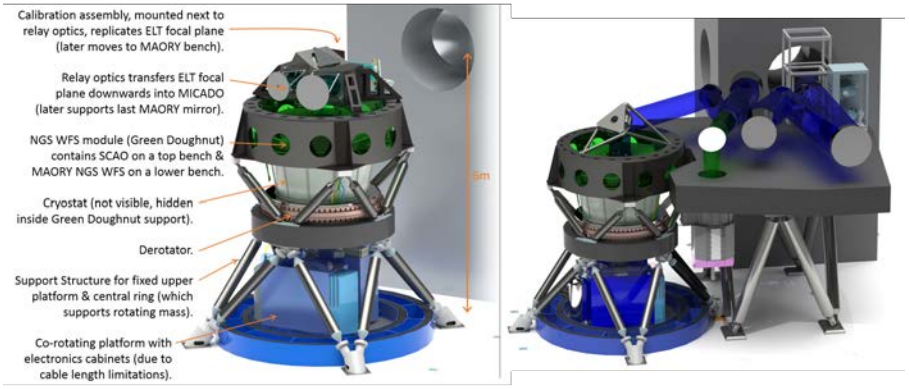

Fig. 1. The overview of MICADO instrument.

In summary, MICADO will be able to perform high resolution (5 - 12 milliarcsec) near infrared observations and it is very promising future instrument to detect microlensed candidates of IMBHs. In the future, we are hoping to simulate the probability of IMBHs candidates with milliarcsec resolution of MICADO and get required spectroscopic information from the research that we presented.

We would like to acknowledge dr. Gabriele Rodeghiero (INAF OAS Bologna, Italy), dr. Robert J. Harris and dr. Jörg-Uwe (Max Planck Institute for Astronomy, Heidelberg, Germany) for contribution in working with MICADO calibration assembly.

[1] D. Batcheldor, A. Robinson, D. J. Axon, E. S. Perlman and D. Merritt, A DISPLACED SUPERMASSIVE BLACK HOLE IN M87, The Astrophysical Journal Letters **717**, L6–L10 (2010).
[2] M. Mezcua, Observational evidence for intermediate-mass black holes, International Journal of Modern Physics D **26**, 1730021-1-51 (2017)
[3] J. E. Greene, J. Strader and L. C. Ho, Intermediate-Mass Black Holes, Annual Review of Astronomy and Astrophysics **58**, 257-312 (2020)
[4] B. Paczynski, Gravitational Microlensing: Black Holes, Planets; OGLE, VLTI, HST and Space Probes, **arXiv:astro-ph/0306564 [astro-ph.SR]** (2003)
[5] Ł. Wyrzykowski, et al., OGLE-III Microlensing Events and the Structure of the Galactic Bulge, The Astrophysical Journal Supplement Series **216:12**, 17pp (2016)
[6] Ł. Wyrzykowski, Z. Kostrzewa-Rutkowska, K. Rybicki, Microlensing by single black-holes in the Galaxy, **arXiv:1601.02830 [astro-ph.SR]** (2016)
[7] S. Dong, et al., First Resolution of Microlensed Images, The Astrophysics Journal **871:70**, 11pp (2019)
[8] R. Gilmozzi and J. Spyromilio, The European extremely large telescope (E-ELT), The Messenger **127:11**, 3pp (2007)

IMPROVING BLACK HOLE ACCRETION TREATMENT IN NUMERICAL SIMULATIONS

Matas Tartėnas[1], Kastytis Zubovas[1,2]

[1]Department of Fundamental Research, Center for Physical Sciences and Technology, Lithuania
[2]Astronomical Observatory, Vilnius University, Lithuania
matas.tartenas@gmail.com

Gas accretion on to a supermassive black hole (SMBH) is the engine supporting active galactic nuclei (AGN). Most of the luminosity is generated by a sub-parsec scale accretion disc which forms if a significant amount of gas comes close to the SMBH, but to fully understand how activity is initiated and supported over a longer period of time, we have to study gas dynamics on various galactic spatial scales. Gas from kiloparsec scales is observed to migrate toward the centre and is seen to be accumulated in $\sim 10-100$ pc circumnuclear rings [1], which, as seen in recent ALMA local AGN observations, may become the reservoirs of gas feeding the SMBH [2].

One of the most important tools in studying gas dynamics are 3D hydrodynamical models. But current models have trouble accurately simulating phenomena that occur on vastly different spatial scales, e.g. ranging from the circumnuclear gas reservoir at $\sim$10 pc from the SMBH to the accretion disc at $<$0.01 pc. Our aim is to improve simulations of the vicinity of AGN by adding a more detailed model of accretion. We do this by implementing a sub-grid accretion disc coupled to the black hole particle. We use a standard thin α-prescription [3] that consists of a number of concentric rings and is dynamically evolved with a separate time criterion than the hydrodynamic simulation as a whole.

We test our approach by simulating a several-parsec-wide region with conditions similar to those at the centre of our Galaxy using 3D hydrodynamical code Gadget-3. The model consists of three main components: the central SMBH ($M_{\rm bh} = 4\times10^6\,{\rm M}_\odot$), the Circumnuclear Ring-like toroidal gas ring ($M_{\rm r} = 10^5\,{\rm M}_\odot$, $R_{\rm in} = 1.5\,{\rm pc}$, $R_{\rm out} = 4\,{\rm pc}$) and an infalling molecular cloud ($M_{\rm mc} = 10^5\,{\rm M}_\odot$, $R_{\rm mc} = 3\,{\rm pc}$). A retrograde collision between the molecular cloud and the gas ring results in significant accretion, where the accretion disc is fed by the gas that crosses a sink boundary ($r_{\rm sink} = 0.01\,{\rm pc}$) in the hydrodynamical model.

Initial results show promise. The more detailed accretion prescription does not significantly increase the computational cost. Accretion occurs more smoothly over a longer period of time as the gas moves through the viscous disc (Fig. 1, left). Various parameters of the accretion disc can be followed over time (e.g. the surface density in Fig. 1, right), which allows us to add a more precise prescription for feedback and mass loss due to luminosity exceeding the Eddington rate, which we plan to do in the future.

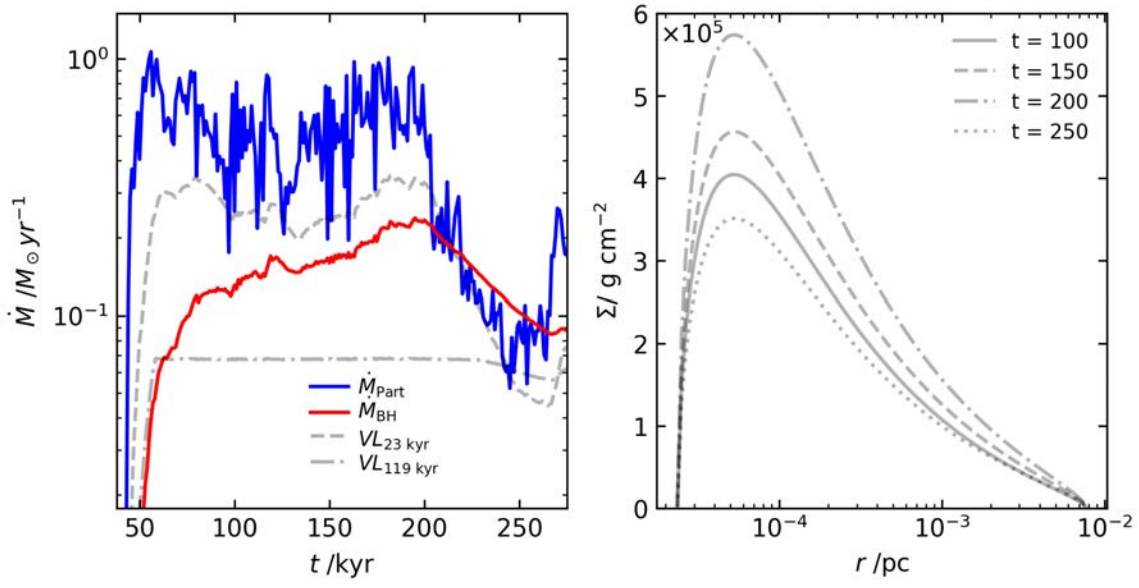

Fig. 1. Left: mass accretion rate on to the disc particle (blue) and SMBH mediated by the accretion disc (red). Grey lines show results from a simple two-state accretion model limited by the constant accretion disc viscosity timescale. Right: surface density of the accretion disc at various times during the simulation run.

[1] N. Butterfield, A. Barnes et al, Investigating the gas in the Galactic Bar: the missing link between the Galactic Disc and the Central Molecular Zone, Bulletin of the American Astronomical Society 51, 3, 460 (2019)
[2] A. Audibert and F. Combes, ALMA captures feeding and feedback from the active galactic nucleus in NGC 613, Astronomy & Astrophysics 632, A33 (2019).
[3] J. E. Pringle, Accretion discs in astrophysics, Annual Review of Astronomy and Astrophysics 19, 137-162 (1981).

EUROPIUM ABUNDANCE IN THE RED-GIANT BRANCH STARS OF GALACTIC GLOBULAR CLUSTER 47 TUCANAE

Kasparas Karlauskas[1], Vidas Dobrovolskas[2], Arūnas Kučinskas[2]

[1]Faculty of Physics, Vilnius University, Saulėtekio al. 9, LT-10222, Lithuania
[2]Institute of Theoretical Physics and Astronomy, Vilnius University, Saulėtekio al. 3, LT-10257, Lithuania
kasparas.karlauskas@ff.stud.vu.lt

Galactic globular clusters (GGCs) were long thought to be simple stellar populations – stellar populations that have the same age and initial chemical composition. This view has changed with the discovery of multiple populations (MP) in the GGCs: *first population* (1P) with the chemical composition of Galactic field stars, and *second population* (2P) with anomalous chemical composition (enhanced He, N, Na and depleted O, C) [1]. It is therefore thought that the chemical composition of 2P stars has been modified during the cluster evolution. However, it is unclear how this could have happened because none of the mechanisms proposed so far is capable of explaining all observable properties of MPs in the GGCs [2].

Further and more stringent constraints on the possible evolutionary scenarios of the GCCs could be obtained by investigating abundance patterns of chemical elements that were produced by various processes of stellar nucleosynthesis, including those synthesised by neutron capture reactions. In this context, correlations between the elemental abundances may hint at their common origin and may help to identify the most likely evolutionary scenarios of the GGCs.

In this study we used `ATLAS9` 1D stellar atmosphere models and spectrum synthesis package `SYNTHE` [3] to determine europium abundance in the atmospheres of 93 red-giant branch (RGB) stars in Galactic globular cluster 47 Tucanae. Our results suggest the existence of weak but statistically significant [Eu/Fe]–[Na/Fe] correlation (Fig. 1). This is the first observational evidence that the 2P stars in the GGCs could have been enriched with the r-process elements. These r-process elements should have been synthesised by the same polluters that enriched the 2P stars with the light chemical elements. Because europium is produced only during explosive nucleosynthesis events (e.g. in Type II supernovae), this sets a new constraint on the candidate evolutionary scenarios of the GGCs, i.e. they should be capable of explaining the enrichment of 2P stars in *both* the light and r-process elements simultaneously.

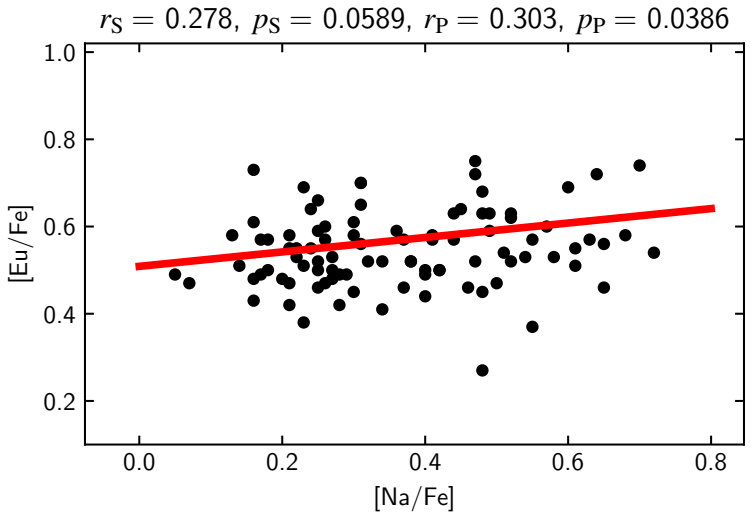

Fig. 1. Abundance of europium determined in the sample of 93 RGB stars in Galactic globular cluster 47 Tuc, plotted in the [Eu/Fe]–[Na/Fe] plane (full circles). Red solid line is linear best fit to the data. Pearson's and Spearman's correlation coefficients, as well as the corresponding p-values, are indicated at the top of the figure.

[1] R. Gratton, A. Bragaglia, E. Carretta, C.'D'Orazi, S. Lucatello, A. Sollima, What is a globular cluster? An observational perspective, Astronomy and Astrophysics Review, **27**, 8 (2019)
[2] N. Bastian, & C. Lardo, Multiple Stellar Populations in Globular Clusters, Annual Review of Astronomy and Astrophysics **56**, 83-136 (2018).
[3] L. Sbordone, Kurucz's codes under GNU-Linux, Memorie della Societa Astronomica Italiana Supplementi, **8**, 61-63 (2005).

A DIRECT AND ROBUST METHOD TO OBSERVATIONALLY CONSTRAIN THE HALO MASS FUNCTION

Marcos Muñiz Cueli[1], Laura Bonavera[1], Joaquín González-Nuevo González[1], Andrea Lapi[2]

[1]Departamento de Física, Universidad de Oviedo, C. Federico García Lorca 18, Oviedo, Spain
[2]International School for Advances Studies (SISSA), Via Bonomea 265, Trieste, Italy
mcueli@uniovi.es

Within the standard paradigm of cosmology, the hierarchical growth of dark matter perturbations is an essential assumption to explain galaxy formation. As a consequence, the relevance of dark matter halos for probing large-scale structure has motivated the search for a quantitative understanding of their mass distribution. Although computational cosmology has so far been the main arena for determining the number density of halos, numerical simulations are subject to systematic differences regarding, for instance, the modeling of baryon physics. The present proof of concept thus pursues the objective of determining the halo mass function (HMF) through the observation of the (weak lensing) magnification bias effect on high-redshift submillimeter galaxies, given the suitability of these sources for a study of this kind.

In essence, in this work [1] we have measured the angular cross-correlation function between a foreground sample of GAMA galaxies $(0.2 < z < 0.8)$ and a background sample of H-ATLAS submillimeter galaxies $(1.2 < z < 4.0)$ via a modified version of the Landy & Szalay estimator. This measurement is then checked against the theoretical prediction within the halo model picture, which yields

$$w(\theta) = 2(\beta - 1) \int_0^\infty \frac{dz}{\chi^2(z)} n_f(z) W^{lens}(z) \int_0^\infty \frac{dl}{2\pi} l P_{g-dm}\left(\frac{l}{\chi(z)}, z\right) J_0(l\theta), \tag{1}$$

where β is the logarithmic slope of the background source number counts, $\chi(z)$ is the comoving distance up to redshift z, $n_f(z)$ is the unit-normalized foreground redshift distribution, $W^{lens}(z)$ is the so-called lensing kernel, J_0 is the zeroth-order Bessel function and P_{g-dm} is the galaxy-dark matter cross-power spectrum.

Within the halo model formalism, the cross-power spectrum contains information about the number density of dark matter halos (via the HMF and the parameters characterizing it) and about the mean number of galaxies which populate these halos (via the so-called halo occupation distribution (HOD) parameters). By means of a Markov chain Monte Carlo algorithm, we have derived posterior probability distributions for the HMF and HOD parameters (both jointly and fixing the latter to common literature values) following two well-known HMF models, namely the Sheth and Tormen (ST) [2] and Tinker [3] templates. For the former model, we have also relaxed the usual assumptions about normalization and allowed negative values for one of its parameters (what we call the "free" ST fit). Sampling these distributions, we have obtained Bayesian credible intervals for the $z = 0$ HMF at different halo masses, as shown in Fig 1.

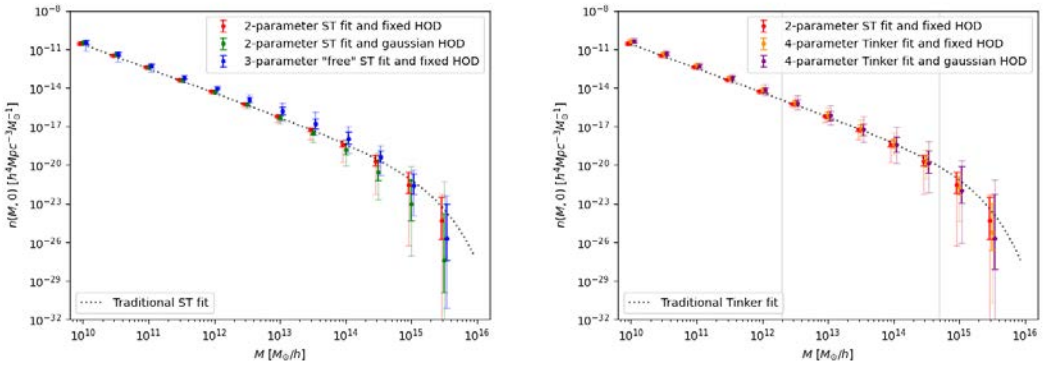

Fig. 1. Credible intervals (68% in bold and 95% in faint colors) for the $z = 0$ HMF at different mass values. For each mass, the results from the three different cases shown in each legend are displaced horizontally and in order.

Under the assumption that all HMF parameters are positive, the ST fit only seems to fully explain the data by forcing the mean number of satellite galaxies in a halo (captured by one HOD parameter) to increase substantially from its prior mean value. The Tinker fit, on the other hand, provides a robust description of the data without relevant changes in the HOD parameters, but with some dependence on the prior range of two of its parameters. While all cases are in agreement with numerical simulations, the involved parameters are, however, better determined by considering the "free" ST model.

[1] M. M. Cueli, L. Bonavera, J. González-Nuevo and A. Lapi, A direct and robust method to observationally constrain the halo mass function via the submillimeter magnification bias: Proof of concept, A&A **645**, A126,(2021).
[2] R. K. Sheth and G. Tormen, Large scale bias and the peak background split, MNRAS **308**, 119-126 (1999).
[3] J. Tinker, A. V. Kravstov, A. Klypin et al., Toward a Halo Mass Function for Precision Cosmology: The Limits of Universality, The Astrophysical Journal **688**, 2, 709-728 (2008).

EVOLUTION OF TWO-PHASE GAS SYSTEM: IMPACT OF AGN-DRIVEN OUTFLOWS ON FRAGMENTATION OF TURBULENT MOLECULAR CLOUDS

Martynas Laužikas[1], Kastytis Zubovas[1,2]

[1]Astronomical Observatory, Vilnius University, Saulėtekio al. 3, Vilnius LT-10257, Lithuania
[2]Center for Physical Sciences and Technology, Saulėtekio al. 3, Vilnius LT-10257, Lithuania
martynas.lauzikas@ftmc.lt

It is well established, that nearly every galaxy had multiple episodes of activity during its evolution. During this period matter is accreted by the central super massive black hole (SMBH) and an associated increase in brightness is observed. During such events outflows of hot matter, powered by accretion, sweep through the inner parts of the galaxy interacting with gas and dust on its way. Outflows cool, condense and lose momentum as they reach the outer regions. During this process interactions with denser molecular clouds (MC) take place. Molecular clouds are usually in delicate equilibrium with the surrounding medium and evolve relatively slowly but interactions with outflows change this equilibrium. These clouds are cradles for stars, responsible for the chemical evolution of the galaxy as a whole. Young massive stars evolve rapidly, dispersing newly created elements into the surrounding medium. It is typically assumed that AGN-driven outflows tend to be destructive and inhibit star formation. However, the result of the interaction can be very different depending on the properties of the outflow, such as gas temperature and momentum. Therefore, it is of particular interest to explore interaction of MCs with outflows of low momentum.

The analysis of such interaction is not new. While there are numerous models, a common approach is to reduce number of unknowns in the system. Such simplifications are useful as they help isolate certain evolutionary effects. But to make models more realistic, as much physical processes as possible must be included. It is very tempting to build a method that is suitable for a wide variety of systems and account for as many as physical processes as possible.

We use Arepo [1], a modern hydrodynamical code, which utilises a moving mesh to discretize the flow of matter. The code flexibility, combined with numerical accuracy and availability of different modules makes this tool a good candidate for this task. A model can be described as a virtual wind tunnel - an elongated volume with periodic boundary conditions on the sides and special boundaries at the ends. On the central axis, a turbulent molecular cloud of uniform density is placed with no initial velocity. The rest of the volume is filled with interstellar medium (ISM). We tested a range of ISM and cloud parameters: ISM temperatures $10^4 - 10^7$ K and velocities 10 - 100 km s^{-1}; cloud masses $10^3 - 10^5$ M$_\odot$. Figure 1 illustrates one of the modelled systems. There is a tendency for faster flows to destroy clouds, while hotter flows compress them. The effect of cloud mass (coupled with density and radius) is to be determined.

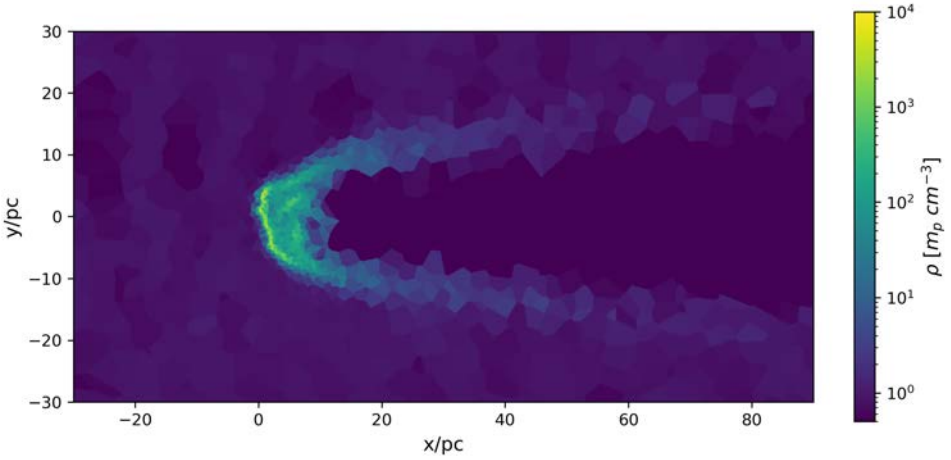

Fig. 1. Density slice of evolved system. MC is ablated by hot wind, and dense compressed threads of material are visible. They will become birthplace of stars.

Modeled processes include gravity, cooling and heating, ionisation reactions, turbulence and, soon, star formation. The final goal is to map a parameter space where a boundary could be drawn separating destructive and nondestructive flows. A side product of simulations with the thermo-chemistry package is a possibility to trace chemical elements and ionisation states, which enables a more direct connection with observations.

[1] V. Springel, *E pur si muove:* Galilean-invariant cosmological hydrodynamical simulations on a moving mesh, MNRAS **000**, 000-000 (2009).

SYNTHESIS AND OPTICAL PROPERTIES INVESTIGATION OF MULTI-COLOUR EMITTING $GdPO_4:Ce^{3+}/Tb^{3+},Eu^{3+}$ NANOPARTICLES

Egle Ezerskyte, Arturas Katelnikovas

Institute of Chemistry, Faculty of Chemistry and Geosciences, Vilnius University, Lithuania
egle.ezerskyte@chgf.stud.vu.lt

Hydrothermal reaction synthesis method was chosen to produce undoped $GdPO_4$ samples in order to determine optimal synthesis conditions (Gd:P molar ratio and pH value of the reaction mixture) seeking to obtain nano-scale particles. As depicted in Fig. 1, $GdPO_4$ nanorods (approx. 80 nm in length and 20 nm in width) are produced if the Gd:P molar ratio is equal to 1:10 and the pH value of the reaction mixture is equal to 10.

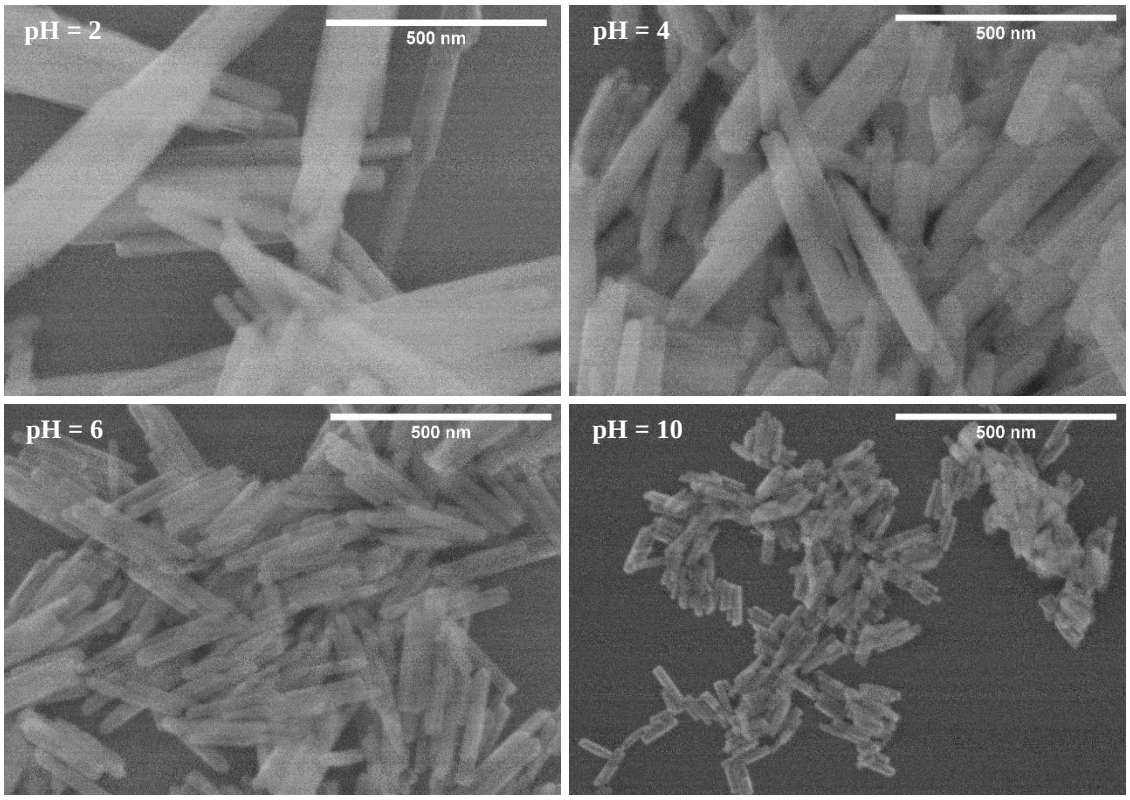

Fig. 1. SEM images of $GdPO_4$ particles synthesized at a constant Gd:P molar ratio (1:10) but under different pH values of the reaction mixture.

Further on our research focused on producing $GdPO_4$ nanorods doped with Ce^{3+}, Tb^{3+} and Eu^{3+} ions individually and in different two-ion combinations under fixed synthesis conditions (Gd:P = 1:10, pH = 10) following by the characterization of structural and optical properties of the obtained compounds.

Thus, detailed analysis and obtained results of XRD patterns, SEM images, reflection, excitation and emission spectra of $GdPO_4:Ce^{3+},Tb^{3+},Eu^{3+}$ and $GdPO_4:Ce^{3+}/Tb^{3+},Eu^{3+}$ phosphors will be presented.

Acknowledgements: This project has received funding from European Social Fund (project No. 09.3.3-LMT-K-712-22-0271) under grant agreement with the Research Council of Lithuania (LMTLT).

O2-2

DID NOT PARTICIPATE

IMPACT OF L-CYSTEINE ON THE COMPOSITION AND ELECTROCATALYTIC PROPERTIES OF MoS_2 FILMS

Paulius Gaigalas[1], Vaclovas Klimas[1], ArÎnas Jagminas[1]

[1] State Research Institute Center for Physical Sciences and Technology, Saulãtekio ave. 3, LT-10257, Vilnius, Lithuania

paulius.gaigalas@ftmc.lt

Clean and renewable energy sources currently are of great interest for many researchers, due to the ever-growing demand of energy and current reliance on fossil fuel consumption. Hydrogen gas (H_2) is considered one of the cleanest energy sources available, which can be obtained by using noble metal electrocatalysts for water splitting. However, the scarcity and cost of noble metals is a hindrance to successful application of water splitting for hydrogen generation on an industrial scale [1]. Therefore, alternative electrocatalysts are thoroughly investigated, with molybdenum disulfide (MoS_2) being recognized as a promising replacement for noble metal electrocatalysts [2].

In this study, nanoplatelet-shaped hybrid MoS_2 films were fabricated onto anodized Ti substrates *via* hydrothermal synthesis from a solution consisting of thiourea, ammonium heptamolybdate and L-cysteine. Hydrothermal synthesis was carried out at 220 Ñ2 °C for 5 to 10 h using a Teflon-lined steel autoclave.

SEM images of fabricated MoS_2 nanostructures (Fig. 1a.) reveal that molybdenum disulfide films, synthesized both with and without L-cysteine possess a nanoplatelet morphology deposited onto the surface of titanium nanotubes (Fig 1a. Inset) formed by Ti anodizing, which is consistent with our previous findings. Electrocatalytic properties of hybrid MoS_2 films were assessed by linear sweep voltammetry measurements in 0.5 mol/L H_2SO_4 using a three-electrode setup. From these cyclic voltammograms (Fig. 1b.), it can be seen that addition of L-cysteine to the synthesis solution leads to an increase of current density, reaching approximately 65 mA/cm^2 at -0.35 V. Furthermore, hybrid MoS_2 electrocatalysts synthesized with L-cysteine display much better electrocatalytic stability with the current density decreasing by ~8% after 2000 cycles, whereas samples without L-cysteine exhibit a decrease of about 70% of initial current density after just 250 cycles.

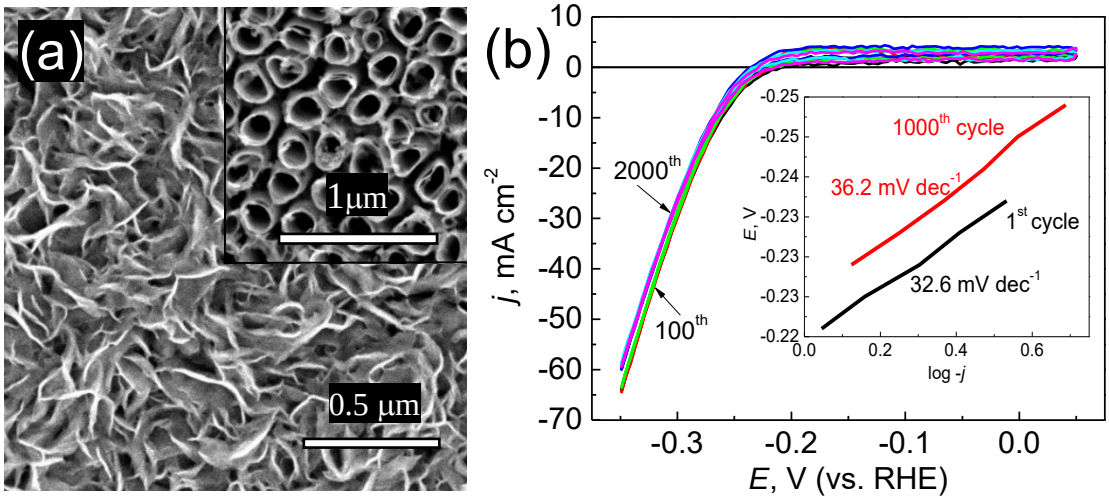

Fig. 1 Top-side SEM view (a) and cyclic voltammograms (b) of MoS_2 film fabricated onto the anodized Ti substrate *via* hydrothermal synthesis in the solution: 5 ammonium heptamolybdate, 90 thiourea and 3 mmol L^{-1} of L-cysteine at 220 ÁC for 5 h.

The Tafel slopes (Fig. 1b. Inset) of samples with L-cysteine were found to be close to that of Pt/C, which is considered an ideal HER electrocatalyst. XPS analysis suggests that HER stabilty and activity of MoS_2/L-cysteine electrocatalysts increase are related to the formation of a 2D composite composed of a dominating metallic and highly active 1T-MoS_2 and MoO_2 phases interfaced with the semiconducting 2H-MoS_2 and MoO_3 phases. Additional research is to be undertaken in order to gain further insight on the influence of amino acids on the formation mechanism of hybrid MoS_2 films.

[1] M.G. Walter, E.L. Warren, J.R. McKone, S.W. Boettcher, Q. Mi, E.A. Santori, N.S. Lewis, Solar water splitting cells, Chem. Rev. 110, 6446ï 6473 (2010)

[2] W. Sheng *et al.*, Correlating hydrogen oxidation and evolution activity on platinum at different pH with measured hydrogen binding energy, Nat. Commun., 6, 5848 (2015)

FEMTOSECOND LASER GENERATION OF MICROBUMPS ON GOLD THIN FILMS

Kernius Vilkevičius, Evaldas Stankevičius

Department of Laser Technologies, Center for Physical Sciences and Technology, Lithuania
kernius.vilkevicius@ftmc.lt

The processing of material with ultrashort laser pulses induces the formation of wavelength-size microstructures. Due to the high elasticity of gold, using single pulses of femtosecond laser complex structures on a metal surface can be generated. With relatively small energies, just above film modification energy, microscopic protrusions called microbumps can be produced. These hollow structures are formed due to the melting and solidification processes of the irradiated gold layer [1].

Arrayed microstructures of noble metals like gold and silver exhibit unique optical properties one of which is surface plasmon resonance phenomena [2]. When irradiated, in the periodic gold microstructures surface plasmons are excited and the resonant wavelength is absorbed.

Usually, such microstructures are fabricated using lithography methods which are a fast and efficient way to produce small periodic arrays [3]. However, the diameter of the beam limits the area of the array and microstructures are not identical due to the energy distribution profile of the beam. Thus, another direct laser writing method is used for the formation of similar and high reproducibility microbumps in a periodic array. The produced grating and several microbumps are represented by a scanning electron microscope (SEM) in Fig. 1.

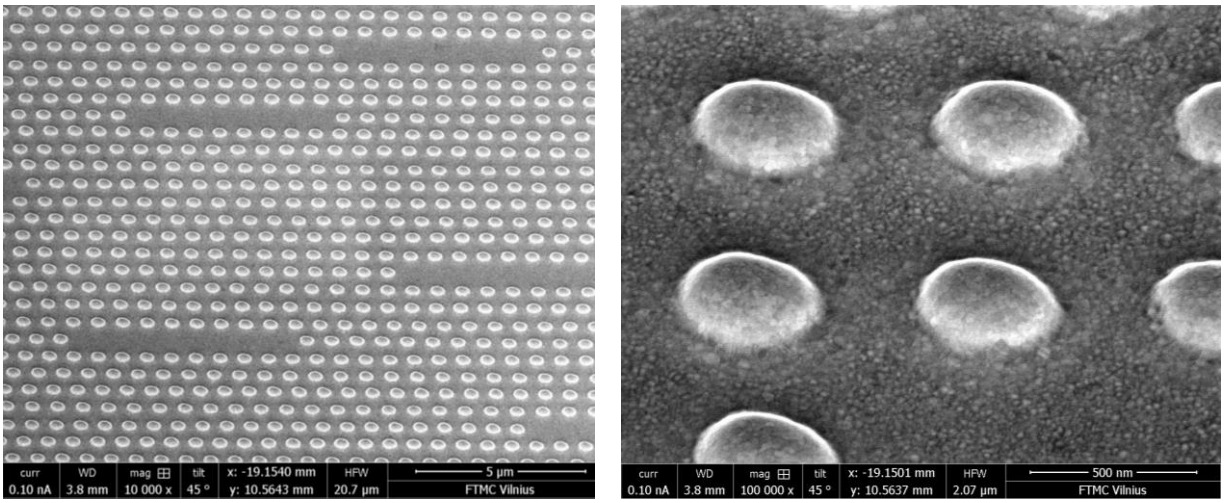

Fig. 1. SEM micrograph of microbump array tilted by 45° (left) and a zoomed view of several microbumps tilted by 45° (right).

The periodic arrays of microbumps were investigated using spectrophotometer and measuring excited plasmon resonances. The gratings demonstrated the hybrid lattice plasmon polaritons in the visible/near-infrared (VIS/NIR) range. There was investigated resonant wavelength dependence on the period of the array, polarization of incident light, and angle of incidence. It was found out that depending on the polarization of incident light different diffractive resonance modes were excited – one resonance strongly dependent on the angle of the incidence and another almost fixed resonance. Also, the grating period influence was observed – with higher period plasmon resonance shifts to higher wavelengths.

To compare practical values and determine the nature of excited plasmons, the theoretical model was used for calculating the resonant wavelength of the diffraction grating. The measured values were in good agreement with the theoretical estimation.

[1] Y.P. Meshcheryakov, N.M. Bulgakova. Thermoelastic modeling of microbump and nanojet formation on nanosize gold films under femtosecond laser irradiation, Applied Physics A **82(2)**, 363–368 (2006).

[2] V.G. Kravets, et al. Plasmonic Surface Lattice Resonances: A Review of Properties and Applications. Chemical Reviews **118(12)**, 5912–5951 (2018).

[3] B. Voisiat, et al. Flexible Microstructuring of Thin Films Using Multi-beam Interference Ablation with Ultrashort Lasers. Journal of Laser Micro/Nanoengineering **6(3)**, 185–190 (2011).

DYKETOPYRROLOPYRROLE EMITTERS FOR NIR-TO-VISIBLE PHOTON UPCONVERSION

Lukas Naimovi̧ius[1], Edvinas Radiunas[1], Barbara Chatinovska[2], Augustina Jozeli Î naitā[2], Edvinas Orentas[2], Karolis Kazlauskas[1]

[1]Institute of Photonics and Nanotechnology, Faculty of Physics, Vilnius University, Lithuania
[2]Department of Organic Chemistry, Faculty of Chemistry and Geosciences, Vilnius University, Lithuania
lukas.naimovicius@ff.vu.lt

Triplet-triplet annihilation (TTA) mediated NIR-to-visible photon upconversion (UC) is a rapidly advancing field of photonics with numerous potential applications. [1] The most promising TTA-UC applications include photovoltaics, photocatalysis, night vision, targeted drug delivery and bio-imaging. [1-3] UC systems are typically composed of a sensitizer and an emitter. The sensitizer is responsible for absorption of low energy photons and triplet generation via intersystem crossing, whereas the emitter - for accumulation of triplets and TTA, which is followed by emission of higher energy photons. However, several challenges related to a lack of TTA emitters in NIR range, their tendency to aggregate and low UC quantum yield are yet to be overcome. From this point of view, diketopyrrolopyrrole (DPP) emitters seem to be an attractive alternative to a widely used rubrene [1] or perylene diimide [3].

The work is focused on revealing the impact of different side-moieties of DPP compounds on the aggregation-caused emission quenching, and subsequently, UC performance. To this end, photophysical properties of ethylhexyl-substituted compound (DPPeh) as well as of alkyl chain strapped compound (DPPc) were thoroughly assessed. Essentially, the DPP derivatives expressed high FL quantum yield (91%) in the isolated form and demonstrated the feasibility for TTA in a solution. UC measurements of DPP solutions admixed with phthalocyanine (PdPc) sensitizer in oxygen-free atmosphere revealed NIR-to-vis upconversion with UC quantum yield of 2.9% (Fig. 1). Although the introduction of different side-moieties into DPP did not alter its aggregation noticeably (Fig. 2), the obtained efficient UC confirmed the potential of these derivatives for TTA-UC application.

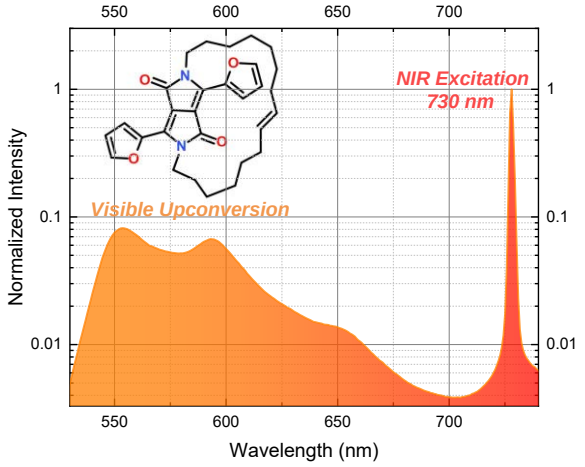

Fig. 1 UC spectra of DPPc/PdPc (8 mM/15ε M) in toluene.

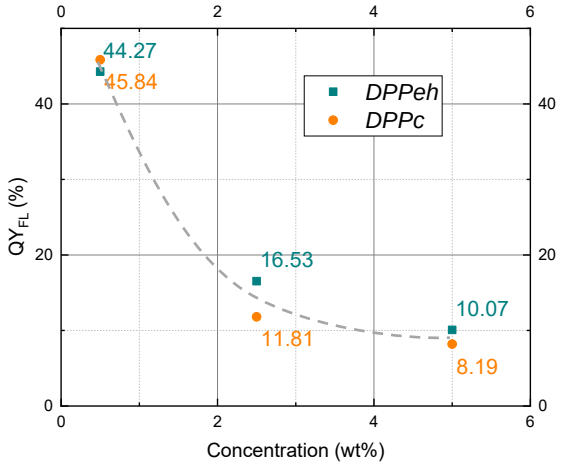

Fig. 2 FL quantum yield of DPPc and DPPeh as a function of their concentration in polystyrene.

[1] M. Wu et al., ñSolid-state infrared-to-visible upconversion sensitized by colloidal nanocrystals,ò Nat. Photonics, vol. 10, no. 1, pp. 31ï 34, (2016)
[2] Radiunas, E. et al., Impact of: T-butyl substitution in a rubrene emitter for solid state NIR-to-visible photon upconversion. Phys. Chem. Chem. Phys. 22, 7392ï 7403 (2020).
[3] Bharmoria, P. et al., Triplet-triplet annihilation based near infrared to visible molecular photon upconversion. Chem. Soc. Rev. 49, 6529ï 6554 (2020).

O3-1

DID NOT PARTICIPATE

CARRIER LOCALIZATION IN InGaN STRUCTURES INVESTIGATED BY LIGHT-INDUCED TRANSIENT GRATING TECHNIQUE

Mantas Vaiļiulis, Kazimieras Nomeika, RamÎnas AleksiejÎnas

[1] Institute of Photonics and Nanotechnology, Faculty of Physics, Vilnius University, Saulãtekis Av. 3, LT-10257 Vilnius, Lithuania
mantas.vaiciulis@ff.stud.vu.lt

Localization of charge carriers in shallow potential minima just below the band edges is typical for materials and structures with some level of disorder. This process is well known in III-nitrides alloys where it is believed to be the main reason for high internal quantum efficiency, despite high defect density [1]. The exact effect of carrier localization to carrier transport and recombination is difficult to analyze. Quantum wells of ternary nitride alloys is a very complex structure; thus, investigation of carrier localization demands a computational-heavy modelling [2] and sophisticated experimental methods [3].

One way to experimentally study the carrier localization is by observing the properties of carrier diffusion. In this presentation, we report the results obtained by Light-Induced Transient Grating (LITG) technique in InGaN/GaN/sapphire structures grown by MOCVD technique along the polar (*c*) crystallographic directions. We carry out LITG experiments to measure the ambipolar diffusion coefficient (*D*) of photoexcited carriers in quantum wells and thick layers. From the dependencies of *D* on carrier density and photoexcitation wavelength, we analyze the impact of carrier localization on their transport and recombination pathways.

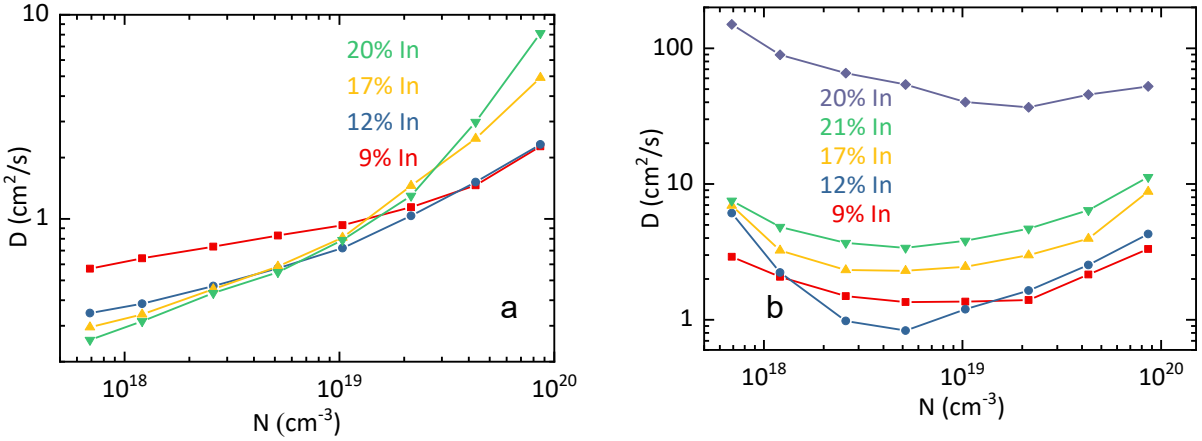

Fig. 1: Diffusion dependence in QWs (a) and layers (b) with different In content on carrier density. QW samples consist of ten 3 nm thick quantum wells, while layer samples are single 50 nm thick layer, except for 21% In sample, which is only 25 nm thick.

In QWs *D*(N) dependence can be divided into two regions of carrier densities. The first region can be described by simplified Einstein relation, valid for nondegenerate semiconductor at equilibrium condition. The increase of *D* with carrier density in the second region can be attributed to carrier degeneracy, when quasi-Fermi level approaches the bands [4], however, it has been shown recently that degeneracy alone is not enough to account for the *D*(*N*) dependence in InGaN. Carrier localization to local potential minima formed by random alloy fluctuations [5] as well as carrier delocalization [6] are also contributing factors in explaining *D*(N).

In layers high diffusion coefficient at low carrier densities could be explained by percolation theory and the decrease of diffusion with the increase of carrier density could be explained by Coulomb blocking in the percolative paths. As the carrier density in these percolative paths increases, so does the Coulomb interaction between the charge carriers which hinders their movement [7]. The center region of slow diffusion coefficient change can be described by Einstein relation. The increase of diffusion coefficient at high carrier densities can be attributed to hole diffusion in a degenerate semiconductor with disorder [5].

[1] S. Chichibu et al., Spatially resolved cathodoluminescence spectra of InGaN quantum wells, Appl. Phys. Lett. **71**, 2346ï 2348 (1997).
[2] C.-K Li et al., Localization landscape theory of disorder in semiconductors. III. Application to carrier transport and recombination in light emitting diodes, Phys. Rev. B **95**, 144206 (2017).
[3] W. Hahn et al., Evidence of nanoscale Anderson localization induced by intrinsic compositional disorder in InGaN/GaN quantum wells by scanning tunneling luminescence spectroscopy. Phys. Rev. B **98**, 045305 (2018).
[4] T. Malinauskas et al., Diffusion and recombination of degenerate carrier plasma in GaN, Physica Status Solidi (C) Current Topics in Solid State Physics, **6**(SUPPL. 2), 743ï 746 (2009).
[5] R. AleksiejÎnas et al., Impact of Alloy-Disorder-Induced Localization on Hole Diffusion in Highly Excited c -Plane and m -Plane (In,Ga)N Quantum Wells, Physical Review Applied, **14**(5), 1ï 11 (2020)
[6] K. Nomeika et al., Impact of carrier localization and diffusion on photoluminescence in highly excited cyan and green InGaN LED structures, Journal of Luminescence, **188**, 301ï 306 (2017).
[7] H. E. Romero et al., Coulomb Blockade and Hopping Conduction in PbSe Quantum Dots, Phys. Rev. Lett. **95**, 156801 (2005).

TEMPERATURE DEPENDENT ELECTRON EFFECTIVE MASS IN AlGaN/GAN HETEROSTRUCTURES MEASURED VIA THz SPECTROSCOPY OF 2D PLASMONS

Daniil Pashnev, Tommi Kaplas, Vadym Korotyeyev, Vytautas Janonis, Andrzej Urbanowicz, Justinas Jorudas and Irmantas Kaġalynas

THz photonics laboratory, Department of Optoelectronics, Center for Physical Sciences and Technology, Vilnius, Lithuania
daniil.pashnev@ftmc.lt

The AlGaN/GaN heterostructures are widely used as main elements of many optoelectronic devices, including detectors [1] and modulators [2] of THz radiation. The high electron mobility transistor (HEMT) structures based on AlGaN/GaN with a two-dimensional electron gas (2DEG) possessing mobility of 19 000 (for 77 K) and 2200 cm^2/Vs (for 300 K) [3, 4] are promising for the development of resonant THz detectors and emitters based on the plasma waves phenomena [5, 6]. Despite the considerable interest, the electron effective mass contains significant uncertainties in these heterostructures with value increase from 0.19-0.25 m_e (m_e free electron mass) at cryogenic temperatures up to 0.33-0.36 m_e at room temperature [7].

Grating-coupled AlGaN/GaN HEMT structures exhibit resonant behaviour due to a 2D plasmons excitation in the THz range [3,8]. The position of the resonances depends on the electron concentration, effective mass, and the wave vector in the lattice in accordance to analytical models [8ï 9], while the full width at half maximum of the resonance peak can be related to the electron scattering time. The resonant 2D plasmon features can be observed in both amplitude and phase spectra measured by the THz time-domain spectroscopy (TDS) system [3]. Thus, THz TDS allows direct investigation of the electron effective mass dependence on carrier density or temperature in plasmonic structures [8, 10].

The AlGaN/GaN heterostructures were grown on a 500 ε m thick semi-insulating SiC substrate. Periodical metal gratings for excitation of 2D plasmons were fabricated on the heterostructure surface in an area of 2x2 mm^2. Four samples with grating parameters of the width/period of 350/600 440/800, 530/1030, and 830/1000 in nanometers were investigated in transmission geometry using a commercial spectrometer T-SPEC 800 (TeraVil) in the frequency range 0.1-4 THz at various temperatures provided by a liquid nitrogen cryostat.

Plasmons were excited in all samples in the frequency range 1-3 THz. The resonant features of 2D plasmons under the grating were found as a pronounced minimum and an inflection point in the power and phase spectra, respectively. The position of the resonance redshifted with an increase of grating period in an agreement with theory [4, 8, 10], for example, the plasmons were excited at 2.2 and 1.4 THz in the samples with grating periods of 600 and 1000 nm, respectively. Resonance features remain visible in both power and phase spectra up to 220 K and 300 K for samples with the same grating period of 1000 nm but different filing factor 50% and 80%, respectively. Moreover, with the temperature increase, 2D plasmon resonances experienced the red-shift in the transmission spectra of all samples. For a case of 80% filling factor, the position changed was largest from 1.38 THz at 80 K to 1.13 THz at 300 K. It was noticed that the concentration of electrons at room temperature increased up to 10% of the low-temperature value which in turn should blue shift the resonance position. Thus, the phenomenon was attributed to the renormalization of electron effective mass, which deviation starts at 134K and at 295K increased up to 55% of its nominal value, following the phenomenological dependence of $m^*(T) = m_e [1+ 0.01(T/134)^5]$.

Acknowledgement: This work was supported by the Research Council of Lithuania (Lietuvos mokslo taryba) under the ñTERAGANWIREò Project (Grant No. S-LL-19-1).

[1] W. Knap, V. Kachorovskii, Y. Deng, S. Rumyantsev, J. Q. Lu, R. Gaska, M.S. Shur, G. Simin, X. Hu, M. A. Khan, C.A. Saylor, L.C.Brunel, òNonresonant detection of terahertz radiation in field-effect transistorsò Journal of Applied Physics 91(11), 9346 (2002). DOI:10.1063/1.1468257

[2] X. Zhang, Y. Xing, Q. Zhang, Y. Gu, Y. Su, Ch. Ma ñHigh speed terahertz modulator based on the single channel AlGaN/GaN high electron mobility transistorò Solid-State Electronics146, 9-12 (2018). DOI: 10.1016/j.sse.2018.04.011

[3] D. Pashnev, T. Kaplas, V. Korotyeyev, V. Janonis, A. Urbanowicz, J. Jorudas, and I. Kaġalynas, ñTerahertz time-domain spectroscopy of two-dimensional plasmons in AlGaN/GaN heterostructures,ò Appl. Phys. Lett. 117, 051105 (2020).

[4] J.-T. Chen, J. Bergsten, J. Lu, E. Janz®n, M. Thorsell, L. Hultman, N. Rorsman, and O. Kordina, ñA GaN-SiC hybrid material for high-frequency and power electronics,ò Appl. Phys. Lett. 113, 041605 (2018).

[5] N. Dyakonova, P. Faltermeier, D. B. But, D. Coquillat, S. D. Ganichev, W. Knap, K. Szkudlarek, and G. Cywinski, ñSaturation of photoresponse to intense THz radiation in AlGaN/GaN HEMT detector,ò J. Appl. Phys. 120, 164507(2016).

[6] V. A. Shalygin, M. D. Moldavskaya, M. Y. Vinnichenko, K. V. Maremyanin, A. A. Artemyev, V. Y. Panevin, L. E. Vorobjev, D. A. Firsov, V. V. Korotyeyev, A. V. Sakharov, E. E. Zavarin, D. S. Arteev, W. V. Lundin, A. F. Tsatsulnikov, S. Suihkonen, and C. Kauppinen, ñSelective terahertz emission due to electrically excited 2D plasmons in AlGaN/GaN heterostructure,ò J. Appl. Phys. 126, 183104 (2019).

[7] T. Hofmann, P. K¿hne, S. Sch che, J.-T. Chen, U. Forsberg, E. Janz®n, N. Ben Sedrine, C. M. Herzinger, J. A. Woollam, M. Schubert, and V. Darakchieva, ñTemperature dependent effective mass in AlGaN/GaN high electron mobility transistor structuresò, Appl. Phys. Lett.,101,192102 (2012). DOI:10.1063/1.4765351

[8] D. Tsui, S. Allen, R. Logan, A. Kamgar, and S. Coppersmith, ñHigh frequency conductivity in silicon inversion layers: Drude relaxation, 2D plasmons and minigaps in a surface superlattice,ò Surf. Sci. 73, 419ï 433 (1978).

[9] A. V. Chaplik, ñAbsorption and emission of electromagnetic waves by two dimensional plasmons,ò Surf. Sci. Rep. 5, 289ï 335 (1985).

[10] D. Pashnev, V. V. Korotyeyev, J. Jorudas, T. Kaplas, V. Janonis, A. Urbanowicz, and I. Kaġalynas, ñExperimental evidence of temperature dependent effective mass in AlGaN/GaN heterostructures observed via THz spectroscopy of 2D plasmons,ò Appl. Phys. Lett.,117, 162101(2020). DOI:10.1063/5.0022600R

ELECTRICAL CHARACTERISTICS OF ĂBUFFER-FREEñ AlGaN/GaN HETEROSTRUCTURES

Justinas Jorudas[1*], ArtÎr Ġimukoviļ[2], Irmantas Kaġalynas[1]

[1] Terahertz photonics laboratory, Center for Physical Sciences and Technology (FTMC), Lithuania
[2] Fluctuation research laboratory, Center for Physical Sciences and Technology (FTMC), Lithuania
justinas.joruas@ftmc.lt

The AlGaN/GaN high electron mobility transistors (HEMTs) used in high power and high frequency applications usually are grown on silicon carbide (SiC) substrate. The common approach to compensate for the lattice mismatch and to reduce the dislocation density in these structures is to grow thick GaN buffer doped with deep acceptors such as Fe or C which compensate residual doping of an *n*-type GaN on top of the AlN nucleation layer (NL). However, this approach reduces the advantage of SiC high thermal conductivity. Also, the acceptor-type impurities in a thick GaN buffer introduce the deep charge trapping centers resulting in the increase of low-frequency noise [1]. To solve this, a new heteroepitaxy approach has been developed recently, which is based on the hot-wall metalorganic vapor deposition (MOCVD) and allows to grow high structural quality AlGaN/GaN HEMT structures without thick GaN buffer [2]. It could be expected that this technology will reduce effects of traps from GaN:C buffer, but thick acceptor doped GaN buffer is important for reduction of threading dislocations density.

In this work, the ñbuffer-freeò AlGaN/GaN heterostructure was used to develop Schottky barrier diodes (SBDs) and HEMTs studying the performance of realistic devices under high DC voltages and in radio frequency (RF) regimes. The voltage-current, the noise, and the gain characteristics demonstrated the improved thermal stability of ñbuffer-freeò AlGaN/GaN heterostructure in comparison to a standard AlGaN/GaN heterostructures but with thick GaN buffer [1,3]. The SBDs demonstrated the breakdown fields up to 0.8 MV/cm. Hall measurements revealed thermally stable two-dimensional electron gas (2DEG) density $N_{2DEG} = 10^{13}$ cm^{-2} in the range from room temperature (300 K) down to liquid nitrogen (77 K) with the respective mobility values of ε = 1.7Ã10^3 cm^2/VÃs and ε = 1.0Ã10^4 cm^2/VÃs. Meanwhile the HEMTs demonstrated a maximum drain current and the transconductance values to be as high as 0.5 A/mm and 150 mS/mm, respectively for the transistors with the gate length L_G = 5 εm. Low-frequency noise characterization of HEMTs revealed the effective trap density values to be below 10^{19} cm^{-3}eV^{-1}. The analysis of transistors RF characteristics revealed f_T and f_{max} values to be up to 1.3 GHz and 6.7 GHz, respectively, demonstrating the figure of merit FOM=f_TÏ L_G to be up to 6.7 GHzÃm.

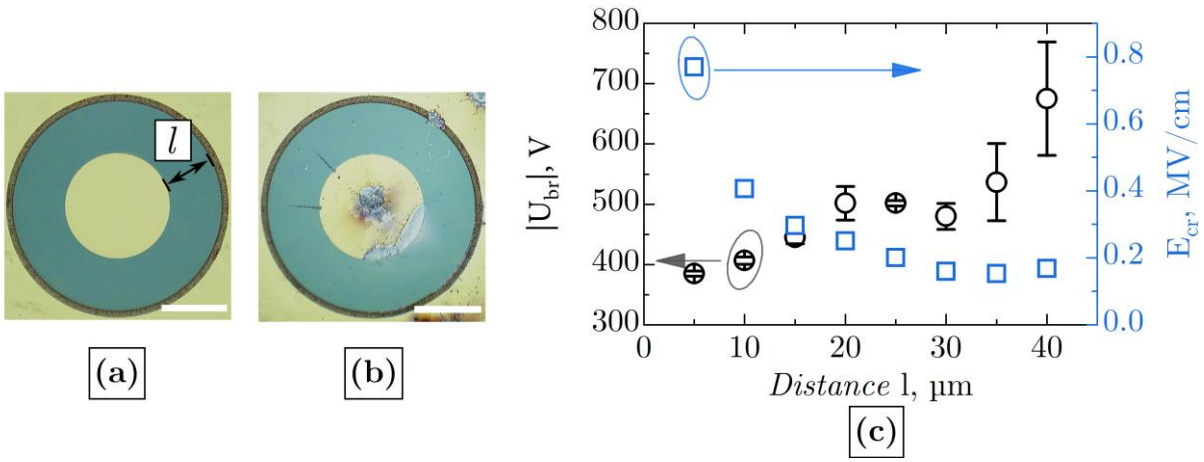

Fig. 1. Schottky barrier diodes (SBDs) fabricated from ñbuffer-freeò AlGaN HEMT. Optical microscope images of l=40 εm contact separation SBDs before (a) and after (b) breakdown. (c) Breakdown voltage U_{br} and critical field E_{cr} dependence on contact separation distance l of SBDs

Acknowledgement The work was supported by the Research Council of Lithuania (Lietuvos mokslo taryba) under the ñTERAGANWIREò project (grant No. S-LL-19-1).

[1] P. Sai *et al.*, ñLow frequency noise and trap density in GaN/AlGaN field effect transistors,ò *Appl. Phys. Lett.*, vol. 115, no. 18, p. 183501, Oct. 2019.
[2] J.-T. Chen *et al.*, ñA GaNï SiC hybrid material for high-frequency and power electronics,ò *Appl. Phys. Lett.*, vol. 113, no. 4, p. 041605, Jul. 2018.
[3] J. Jorudas *et al.*, ñAlGaN/GaN on SiC Devices without a GaN Buffer Layer: Electrical and Noise Characteristics,ò *Micromachines*, vol. 11, no. 12, p. 1131, Dec. 2020.

TERAHERTZ EMISSION FROM ULTRATHIN BISMUTH LAYERS

Ričardas Norkus, Jan Devenson, Remigijus Juškėnas, Arūnas Krotkus

Center for Physical Sciences and Technology, Saulėtekio av. 3, LT-10257, Vilnius, Lithuania
ricardas.norkus@ftmc.lt

Terahertz (THz) frequency range measurement techniques have greatly improved over the last decades and are applied in many different application areas such as sensing, spectroscopy, imaging, and material characterization. THz emission spectroscopy (TES) is becoming popular technique for material characterization. THz pulses are generated on the material surface when it is photoexcited by femtosecond laser pulses. Laser pulses are inducing ultrafast changing photocurrents, which cause electrical dipoles radiating in the THz frequency range. THz pulse emission induced by femtosecond optical pulses has been observed in different semiconductors, gases and liquids. TES can be used to determine some parameters of the semiconductor band structure. These include direct band gap [1], subsidiary valley position [2] and conduction band offset position of heterojunctions [3].

In this work, we describe the effect of femtosecond optical pulse induced THz emission from thin bismuth layers. Thin bismuth (Bi) films are an interesting research object because of their rich variety of physical properties. Previously THz pulses were used for investigating bismuth only in two contributions [4,5]. In both works much thicker Bi samples were used.

Several Bi samples were grown on (111) oriented Si substrates using Molecular beam epitaxy system (MBE). The main difference in technological conditions between investigate samples was different substrate temperatures. It was equal to 100 °C for the layer VS001 and 20 °C for VS002.

The structure of the layers was studied by In-plane X-Ray diffraction (XRD) and their thickness by X-ray reflectivity (XRR). thickness of the both Bi films was approximately the same: 7.7 ± 0.5 and 8.8 ± 0.5 nm for VS001 and VS002 respectively. Measurements also showed that VS001 sample resembles polycrystalline film, while VS002 epitaxial layer is monocrystalline, with the hexagonal plane coinciding with sample's surface.

THz pulse emission from the Bi layers was investigated using femtosecond optical pulses from OPA Orpheus (Light Conversion). THZ emission spectra (fig 1 a) shows It can be seen that THz emission sets-on when the photon energy becomes larger than ~0.45 eV, which suggests that the energy band gap of these layers, and monotonously increases at higher photon energies. THz emission could be explained by photoexcited lateral currents in hexagonal crystals, such currents can be excited by optical beams polarized perpendicular to the main c axis. Both samples has an azimuthal angle dependence (fig 1 b), which is more pronounced in vs002 sample. This could be explained by shift current.

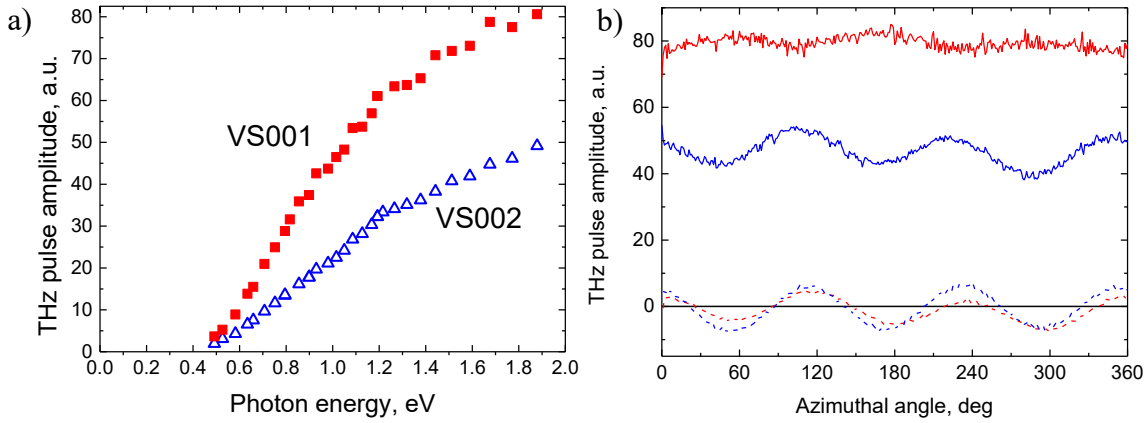

Fig. 1. a) THz emission spectra of thin Bi layers, b) Azimuthal angle dependence of those layers, while the incidence angle is 30 degrees (full line) and 0 degrees (dotted line)

[1] I.Nevinskas, R.Norkus, A.Geižutis, L.Kulyuk, A.Miku, K.Sushkevich and A Krotkus, „Terahertz pulse emission from photoexcited bulk crystals of transition metal dichalcogenides“ J. Phys. D: Appl. Phys. 54 115105 (2020)

[2] A. Arlauskas and A. Krotkus, "THz excitation spectra of AIIIBV semiconductors", Semicond. Sci. Technol., 27, 115015 (2012).

[3] V. Karpus, R. Norkus, R. Butkutė, S. Stanionytė, B. Čechavičius, and A. Krotkus, "THz-excitation spectroscopy technique for band-offset determination", Optics Express, 26, 33807 (2018).

[4] I. E. Ilyakov, B. V. Shishkin, D. A. Fadeev, I. V. Oladyshkin, V. V. Chernov, A. I. Okhapkin, P. A. Yunin, V. A. Mironov, and R. A.Akhmedzhanov, "Terahertz radiation from bismuth surface induced by femtosecond laser pulses", Opt. Lett., 41, 4289 (2016).

[5] Y. Hirai, N. Yoshikawa, H. Hirose, M. Kawaguchi, M. Hayashi, and R. Shimano, "Terahertz Emission from Bismuth Thin Films Induced by Excitation with Circularly Polarized Light", Phys. Rev. Appl., 14, 064015 (2020).

PHOTOLUMINESCENCE STUDY OF GaAsBi/GaAs QUANTUM WELLS

Evelina Dudutienė[1], Dominykas Sanda[1], Algirdas Jasinskas[1], Joshya Shyamala Rajagopal[2], Hélène Carrere[2], Bronislovas Čechavičius[1], Renata Butkutė[1]

[1] Department of Optoelectronics, State research institute Center for Physical Sciences and Technology, Lithuania
[2] LPCNO, Institut National Des Sciences Appliquées, Toulouse, France
evelina.dudutiene@ftmc.lt

GaAsBi heterostructures are an attractive candidate to develop GaAs-based applications for long wavelength optoelectronics, such as infrared lasers, photodetectors, solar cells, terahertz devices [1], etc. This is mainly due to the large band gap reduction possible with incorporation of small amounts of Bi, relatively temperature insensitive band gap, high electron mobility, and large spin–orbit splitting. However, the exploitation of those GaAsBi heterostructures has been hampered by the practical difficulties of growing GaAsBi quantum wells with high emission at room temperature.

This work presents temperature- and excitation-dependent photoluminescence (PL) study of three GaAsBi/GaAs multi-quantum wells (MQW) structures grown by molecular beam epitaxy. All three MQW structures exhibits exceptionally high room temperature emission. Temperature-dependent PL measurements were used to explore optical interband transitions at temperature from 3 K to 300 K (see Fig. 1 a-c). PL peak position versus temperature (Fig. 1 d) were analysed using Varshni equation [2] or combined Varshni–Eliseev equations [3]. A broad PL emission band at room temperature together with S-shape character of PL peak position variation with temperature indicated effect of carrier localisation. As further matter, activation energies derived from PL measurements provided in-sight into thermal quenching processes of luminescence. Moreover, room temperature time-resolved photoluminescence spectroscopy (TRPL) was applied for study of carrier recombination in GaAsBi MQWs.

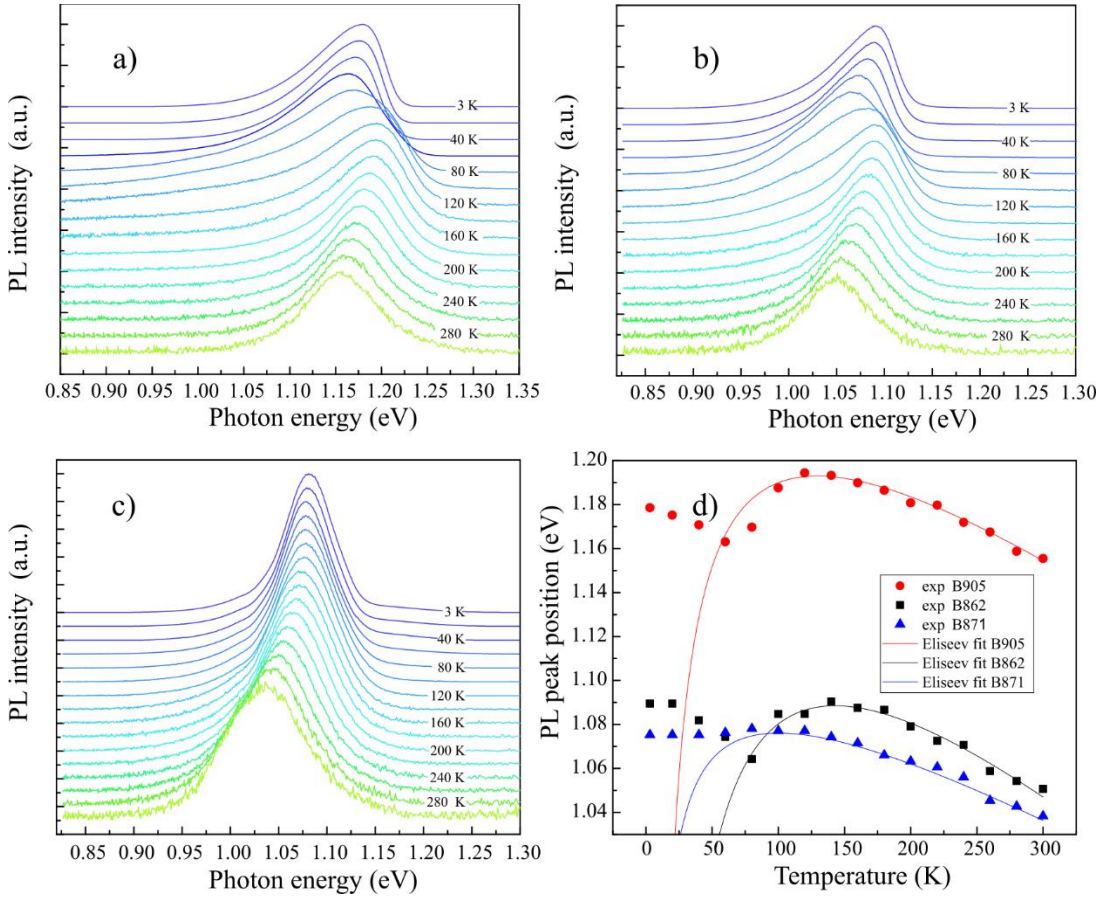

Fig. 1. Temperature – dependent PL spectra of GaAsBi/GaAs MQW PL measured for sample B905 with 3.9 % of Bi (a), sample B862 with 4.5% of Bi (b) and sample B871 with 4.6% of Bi (c). GaAsBi/GaAs MQW structures PL peak position at maximum intensity dependences on temperature (d).

[1] S. Wang, L. Pengfei, eds. *Bismuth-Containing Alloys and Nanostructures* (Springer, Singapore, 2019).
[2] Y. P. Varshni, Temperature dependence of the energy gap in semiconductors. Physica **34**(1), 149-154 (1967).
[3] P. G. Eliseev, et al., 'Blue' temperature-induced shift and band-tail emission in InGaN based light sources. Applied Physics Letters **71**, 569–71(1997)

IMPROVING SODIUM BATTERIES CATHODES: THERMAL NANOCRYSTALLIZATION OF GLASSY ALLUAUDITES

Maciej Nowagiel, Mateusz J. Samsel, Tomasz K. Pietrzak

Faculty of Physics, Warsaw University of Technology, Poland
maciej.nowagiel.stud@pw.edu.pl

Application of renewable power sources carries new challenges concerning energy storage. Wind and solar plants are susceptible to atmospheric conditions. For example – wind farms produce energy only when sufficiently strong wind blows. One of the remedies to stabilize their output is utilization of battery storage stations. In this field, sodium-ion batteries are expected to be sustainable and cheap alternative to lithium ones [1].

Alluaudites, which structure was first described by Fisher in 1955 [2], are among potential cathode materials. $Na_xMnFe_2(PO_4)_3$ attracted much interest of Trad and co-workers, since its theoretical gravimetric capacity could be close to 170 mAh/g if reversibly cycled between x = 0 and 3 [3]. Poor electrical conductivity ($\sigma(275°C) = 9.7 \cdot 10^{-7}$ S/cm [4]) is one of the main obstacles to their implementation.

Alluaudite structure can be adopted by various compounds. In our research, we were studying materials with nominal composition of $Na_2Fe_3(PO_4)_3$, $Na_2Fe_2V(PO_4)_3$ and $Na_2FeMnV(PO_4)_3$. Some of these compositions have been synthesized for the first time, as no such reports in the literature have been found. Thermal treatment of glassy samples led to nanocrystallization of alluaudite phase [5]. Previous studies on amorphous analogs of cathode materials for Li-ion batteries show significant increase of electrical conductivity as a result of their thermal nanocrystallization, due to occuring of preferable conditions for polaron hopping mechanism of conduction [6]. We have shown that similar procedure can be successfully applied to sodium compounds as well. In preliminary measurements, we observed a significant (5 orders of magnitude) and irreversible increase of conductivity, which resulted in receiving nanomaterial with $\sigma(25°C) \approx 10^{-3}$ S/cm (Fig. 1).

We observed some impurity phases in the samples, though. Therefore, in this work, we strived to elaborate optimal syntheses conditions to obtain alluaudite-like nanomaterials with maximum possible phase purity. The following parameters were taken into account: reagents used, presynthesis of the reagents, cooling rate, role of reducing atmosphere.

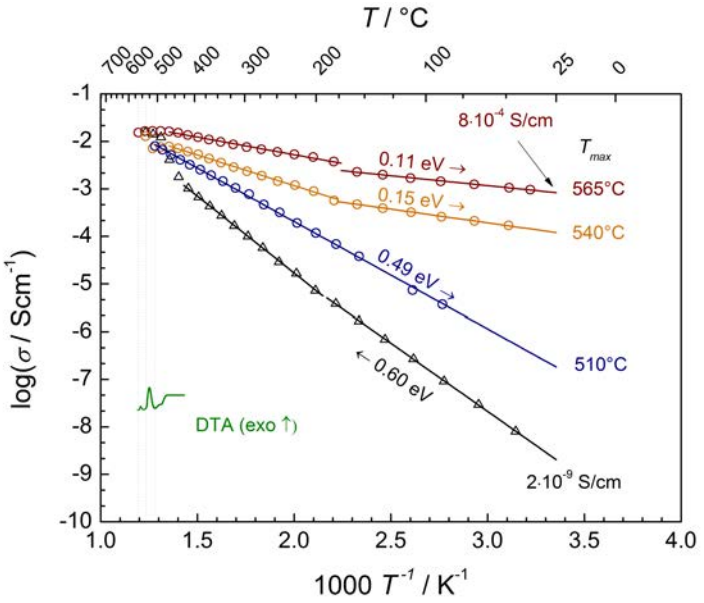

Fig. 1. Arrhenius plot for an as-prepared glassy $Na_2Fe_2V(PO_4)_3$ sample (triangles) and heated to different maximum temperatures (circles) within 510–565°C range. DTA curve is given for comparison.

[1] V. Palomares et al., Energy & Environmental Science **5** (2012), 5884–5901.
[2] D.J. Fisher, American Mineralogist **40** (1955), 1100–1109.
[3] K. Trad et al., Chemistry of Materials **22** (2010), 5554–5562.
[4] A. Daidouh et al., Solid State Sciences **4** (2002), 541–548.
[5] A.E. Chamryga et al., Journal of Non-Crystalline Solids **526** (2019), 119721.
[6] T.K. Pietrzak et al., Materials Science and Engineering **B 213** (2016), 140–147.

RESEARCH OF IMPACT OF PRESENCE OF VITAMINS B2, B3, AND C ON CALCIUM OXALATE MOHOHYDRATE CRYSTALLIZATION PROCESSES IN SIMULATED BODY FLUID

Maryna Dryhailo[1], Yuliia Taranets[2]

[1] Faculty of Physics, V. N. Karazin Kharkiv National University, Ukraine
[2] Department of non-linear crystals, Institute for Single Crystals of the National Academy of Sciences of Ukraine, Ukraine
mkdryhailo25@gmail.com

Urolithiasis is one of the most common diseases of human urinal tract. Crystals of mineral origin have the propensities for renal calculi, or kidney stones formation. The reviewed example of these crystals is calcium oxalate monohydrate CaC2O4IH2O (COM) [1]. Nowadays the crystallization of COM under influence of various compounds that come to human organism with food is not fully studied and analyzed. Scientists are interested in impact on crystallization COM of amino acids, food supplements, and especially vitamins [2].

The main purpose of this work is modelling COM crystallization processes in simulated body fluid with presence of water-soluble vitamins B2, B3, and C and examining their influence on the nucleation processes, morphology, and size of COM crystals. The temperature during the experiments was 37ÁC, pH = 5.8, and I = 0.15 (NaCl).

The structure and the phase composition of the synthesized calcium oxalate precipitates were determined using the methods of X-ray phase analysis and IR spectroscopy. The morphology of the crystals was examined applying scanning electron microscopy. The crystallization kinetics for the model COM solutions was studied by measuring the solution turbidity.

[1] Rez. P., What does the crystallography of stones tell us about their formation?, Urolithiasis **45(1)**, 11-18 (2017).
[2] Taranets Y. V. et al., Effect of amino acids and B-group vitamins on nucleation of calcium oxalate monohydrate crystals, Journal of Crystal Growth **531**, 125368 (2020).

FREQUENCY CONTROLLED AC ELECTROSPINNING FOR ENHANCED NANOFIBER PRODUCTION

Ondrej Friedrich[1], Jan Valtera [1]

[1] Department of Textile Machine Design, Technical University of Liberec, Czech Republic
ondrej.friedrich@tul.cz

Nanofiber materials are characterized by high specific surfaces, advantageous for applications in the field of filtration, tissue engineering, etc. There are several methods of preparing polymeric nanofibers out of which electrospinning is the most used one. In this technology, fibres are formed due to electric forces created by means of electric potential difference between an electrode and a collector. Till now, two types of electrospinning have been developed: spinning in the constant electrical field "DC electrospinning" and spinning in the alternating electrical field "AC electrospinning" [1]. Unlike the first one, the AC electrospinning does not require any physical collector and the plume of nanofibers can be collected by various means, e.g. non-conductive rotating core yarn [2]. Ions emitted from the spinneret form a so-called ñvirtual collectorò in its vicinity that works as a highly efficient collector for oppositely charged ions emitted in the next period [3]. Velocity of fibers drawn by electric field falls suddenly after reaching the area of the virtual collector. Even though some studies have been carried out [4], the behaviour of the virtual collector under different input signal conditions and its influence on fibres productivity has not yet been fully investigated.

This work focuses on analysis of fibre velocity in between the electrode and the virtual collector under various signal conditions. Furthermore, the aim is to design a new electrode capable of flat nanofibrous material production with appropriate signal parameters applied in order to improve the efficiency and homogeneity. For this purpose the laboratory AC electrospinning device was built. It comprises one or several thin rotary discs as a spinning electrode, see Fig 1. The device enables the setting of input electrical signals (waveform, amplitude, frequency and offset), while recording the fibres movement by high-speed camera. The effect of various signal parameters upon the collector distance R, fibres production and morphology was measured and analysed.

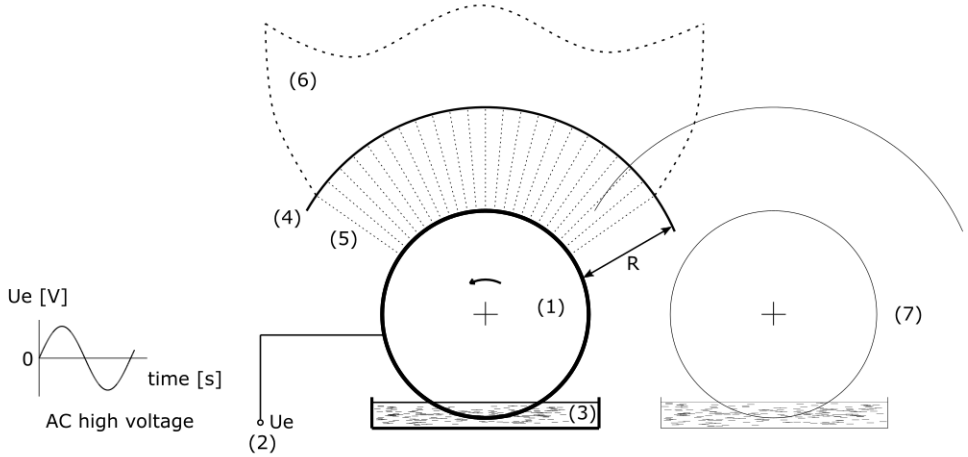

Fig. 1. Schematic of the process of forming nanofibrous material: electrode (thin rotary disc) (1), high AC voltage source (2), polymeric solution (3), virtual collector (4), area of fast moving fibres (5), area of slowly rising nanofibrous material (6), illustration of multi-disc configuration (7)

Results of carried out tests proved considerable effect of frequency, amplitude and waveform (*sine* vs *square*) on the distance R. In a multi-disc configuration, it was observed that spinning under lower frequencies improves the interconnection of nanofibers from individual discs and enables production of a single flat nanofibrous structure. Acquired results from single/multi-disc AC electrodes will be further used for improvement of homogeneity that is required for medical, hygiene or filtration application.

This publication was written at the Technical University of Liberec as part of the project with the support of the Specific University Research Grant 2021-5029, as provided by the Ministry of Education, Youth and Sports of the Czech Republic in the year 2021.

[1] Balogh, Attila, Farkas, Bal ázs, Verreck, Geert, Mensch, J ürgen, Borb ás, Enik ő, Nagy, Brigitta, Marosi, Gy örgy, Nagy, Zsombor Krist óf, AC and DC electrospinning of hydroxypropylmethylcellulose with polyethyleneoxides as secondary polymer for improved drug dissolution. International Journal of Pharmaceutics http://dx.doi.org/10.1016/j.ijpharm.2016.03.024

[2] J. Valtera, T. Kalous, P. Pokorny, O. Batka, M. Bilek, J. Chvojka, P. Mikes, E.K. Kostakova, P. Zabka, J. Ornstova, J. Beran, A. Stanishevsky, D. Lukas, Fabrication of dual-functional composite yarns with a nanofibrous envelope using high throughput AC needleless and collectorless electrospinning, Sci. Rep. 9 (2019). doi:10.1038/s41598-019-38557-z.

[3] P. Pokorny, E. Kostakova, F. Sanetrnik, P. Mikes, J. Chvojka, T. Kalous, M. Bilek, K. Pejchar, J. Valtera, D. Lukas, Effective AC needleless and collectorless electrospinning for yarn production, 2014. doi:10.1039/c4cp04346d.

[4] Maheshwari, Siddharth. (2009). Assembly of Multi-Stranded Nanofiber Threads through AC Electrospinning. Advanced Materials - ADVAN MATER. 21. 349-354. doi.org/10.1002/adma.200800722.

BLEND ELECTROSPINNING OF CONTROLLED-RELEASE DRUG DELIVERY SYSTEMS WITH MMP INHIBITORS

Magdalena Bartolewska[1,2], Matej Buzgo[2], Aiva Simaite[2]

[1] Faculty of Physics, University of Warsaw, Pasteura 5, 02-093 Warsaw, Poland
[2] InoCure s.r.o., R&D lab, Prumyslov§ 1960, 250 88 Cel§kovice, Czech Republic
bartolewskamagdalena@gmail.com

Bone fractures associated with osteoporosis are a serious worldwide problem, especially among the elderly. Despite significant advances in the treatment of osteoporosis over the past few decades, osteoporotic fractures remain a major clinical challenge in the elderly population due to impaired healing. Matrix metalloproteinases (MMPs) are a family of host-derived proteolytic enzymes that play a key role in tissue-destroying inflammatory diseases and has also shown to play role in osteoporosis. Chlorhexidine (CHX) is a compound capable of inhibiting MMP by binding calcium and zinc ions necessary for proteolytic activity. To allow the tissue to heal efficiently in patients with reduced regenerative capacity, the active molecules, such as cyclohexidine, can be encapsulated in the fibers and implanted in the affected site.

The electrospinning technique has been widely recognized as an effective and convenient method of producing functional biomaterials from nanofibers. Electro-spun polymer-ceramic composites have gained interest as scaffolding in bone engineering applications. Electro-spun fibers have many advantages when it comes to their use as drug delivery systems (DDS), such as biocompatibility. Tunable biodegradability, drug release rate.

The research aimed to create fibrous scaffolds made of polyethylene oxide (PEO) and polycaprolactone (PCL) of different proportions with the encapsulation of chlorhexidine as MMP modulators. The timed release of active molecules can lead to faster and more complete healing. To control the release rate of the MMP modulatore, the amount of PEO in PCL-PEO fibers can varied. In this work, we investigated the influence of the PCL:PEO ration on the release rate of the small molecules from electrospun nanofibers.

EFFECTS OF Cd BASED, Cd FREE QUANTUM DOTS AND Cd^{2+} ON ISOLATED GUT MICROBIOTA OF *Salmo trutta* FRY

Renata Butrimienė[1], Vesta Skrodenytė-Arbačiauskienė[1], Danguolė Montvydienė[1], Živilė Jurgelėnė[1], Dalius Butkauskas[1], Nijolė Kazlauskienė[1]

[1] Nature Research Centre, Vilnius, Lithuania
renata.butrimiene@gamtc.lt

The most prevalent commercial nanomaterial products are widely released into the environment. Some nanomaterials are toxic to various aquatic organisms, but their influence on the aquatic organismŏs gut microbiota remains unknown [1]. One of the nanomaterials which effects on organisms and environment are quantum dots (QDs). Concentration of QDs in the compounds of aquatic environment is still unknown [2]. The ecotoxicological impact of QDs on aquatic organisms is an emerging problem, especially due to their nano-specific properties, physico-chemical transformation in the environment and release of toxic metals, such as Cd, from QDs structure [2]. Studies have shown that metals exposure alters the composition and metabolic profile of the gut microbiota at the functional level, and in turn, the gut microbiota alters the uptake and metabolism of metals and could cause the dysbiosis [3, 4].

The aim of the study was to examine the effects of commercially available semiconductors Cd based QDs (CdSe/ZnS-COOH. 4 nM), Cd free QDs (CuInS/ZnS-COOH, 4 nM) and Cd^{2+} (50 and 80 mg/L) on isolated gut bacteria of S*almo trutta* fry depending on temperature and to evaluate the changes of microbiota.

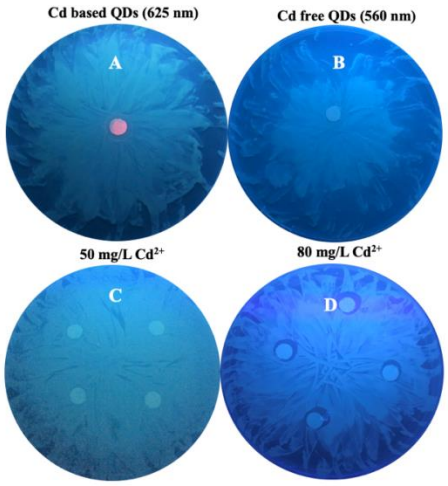

Fig. 1. Effects of 4 nM concentrations of Cd based (A) and Cd free (B) QDs and 50 (C) and 80 mg/L (D) concentrations of Cd^{2+} on gut bacteria of S*almo trutta* fry.

Isolates were identified by polymerase chain reaction and sequencing of 16S rRNA 1500 nt. Sequences of isolates AL13 and AL20 closely related to *Aeromonas salmonicida* subsp. *salmonicida* (similarity 99%), AL8 ï to *Aeromonas* sp. (similarity 100%), AL2 ï to *Aeromonas popoffii* (similarity 99%) and AL18 ï to *Shewanella putrefaciens* (similarity 99%). Minimum inhibitory concentrations of Cd^{2+} against isolated *Salmo trutta* fry gut bacteria were determined by agar disc dilution method. Different concentrations were prepared and dispensed at 10 Õl in each disc (6 mm diameter) of the bacterium-seeded tryptone soya agar plate and were incubated at 15ÜC and 25ÜC for 48 h aerobically.

The data obtained showed that the concentrations of tested QDs and 50 mg/L Cd^{2+} did not cause statistically significant inhibitory effect on isolated gut bacteria of *Salmo trutta* fry and this effect did not depend on temperature [Fig. 1 A; B; C]. Minimum inhibitory concentrations (MIC) value of Cd^{2+} was assessed by determining the lowest concentration of metal ion that caused growth inhibition of bacteria. The MIC value for isolated *Aeromonas* sp. (AL8), *Aeromonas salmonicida* subsp. *salmonicida* (AL13, AL20), *Aeromonas popoffii* (AL2) and *Shewanella putrefaciens* (AL18) was 80 mg/L Cd^{2+} concentration [Fig. 1 D].

This study of isolated gut microbiota of *Salmo trutta* fry after Cd-based and Cd-free QDs exposure in the future will allow predicting the potential health risk to aquatic organisms.

This work was funded by the Research Council of Lithuania, Project No. S-MIP-20-22.

[1] Y. Ma et al., Sex dependent effects of silver nanoparticles on the zebrafish gut microbiota, Environmental Science: Nano, **5,** 740-751 (2018).
[2] T. L. Rocha et al., Environmental behaviour and ecotoxicity of quantum dots at various trophic levels: A review, Environment International, **98**, 1-17 (2017).
[3] H. Duan et al., Gut microbiota: A target for heavy metal toxicity and a probiotic protective strategy, Science of The Total Environment, **742**(10), 140429 (2020).
[4] O. Adamovsky et al., The Gut Microbiome and Aquatic Toxicology: An Emerging Concept for Environmental Health, Environmental Toxicology and Chemistry, **37**(11), 2758-2775 (2018).

CHARACTERIZATION OF CARBONACEOUS MATERIALS WITH CONTROLLED POROSITY AND MORPHOLOGY

Mona Fadel[1], M.P. Fernandez-Garcia[1], Pedro Gorria[1], Jesus A. Blanco[1], David Martinez-Blanco[2], Fabian Suarez-Garcia[3], Julian Martin-Jimeno[3], and Alaa Adawy[2]

[1] Department of Physics, University of Oviedo, 33007, Oviedo, Spain
[2] Scientific-Technical Services, University of Oviedo, 33006 Oviedo, Spain
[3] National Institute of carbon CSIC, 33080, Oviedo, spain
uo273017@uniovi.es

Carbonaceous materials that include metallic nanoparticles (NPs) have attracted extensive interest during the last decades, especially those of metals like Ni and NiO in core/ shell morphologies. However, in order to improve NiO properties for those applications, a correlated analysis of its microstructure and magnetic properties, should be done.

In particular, Nickel oxide is widely studied due to its importance in technological applications (i.e., catalysis, batteries, ceramics, etc). To achieve this purpose, we have prepared five samples of 2-methylimidazole Nickel (NIOF) nanoparticles with carbonization temperatures between 400ºC and 600ºC; characterized their crystal structure and microstructure by X-Ray diffraction (XRD) and high resolution transmission electron microscopy (HRTEM). Additionaly, their magnetic properties were studied by SQUID magnetometer through ZFC-FC and M(H) curves.

The samples exhibit two crystallographic phases of Ni: face centered cubic-FCC and hexagonal compact phase-HCP. Additionally, at the lowest carbonization temperature Ni_3C was also detected. XRD peaks become narrower and symmetrical as the carbonization temperature raises, suggesting that the Ni-NPs mean diameter increases. Inter planar distances were measured by analysing into detail HRTEM images. These studies corroborate XRD results and the existence of Ni_3C phase on samples synthesized at the lowest carbonization temperature.

The analysis of M(H) curves recorded at room temperature, reveal that the saturation magnetization is low on samples that contain antiferromagnetic Ni_3C or NiO phases. Besides, the saturation magnetization values (Ms) and mean blocking temperature values (TB) increases as the carbonization temperature rises because larger NPs are synthesized in those conditions.

From the magnetic analysis, we suggest that each NPs can be described as consisting of a metallic Ni core, surrounded by very thin shell of NiO.

INTERFERENCE OF ANTIPHASE-SYNCHRONIZED VORTEX SHEDDING IN FLOW PAST AN INLINE MICRO-CYLINDER ARRAY

Justina JaseliÎ naitä

Laboratory of Nuclear Installation Safety, Lithuanian Energy Institute, Lithuania
Justina.Jaseliunaite@lei.lt

Unsteady and turbulent flow around an array of cylinders is encountered in many engineering applications, e. g., fuel and control rods in nuclear reactors, oil and gas pipelines, high-rise buildings, heat exchangers etc. Flow over two circular cylinders in a tandem, staggered, side-by-side arrangements is well investigated [1]. Nevertheless, as the number of obstacles increases, flow becomes progressively more complex. Existing research is limited to investigation of wake of the cylinder array but does not analyse the gap flow between the cylinders [2]. The coupling effect between cylinders induce wake interference, vortex synchronization, boundary layer/shear layer/wake/cylinder/vortex/gap flow interactions [3], which give rise to flow-induced vibration phenomenon causing severe challenges to the design and exploitation as a result of occurrence of loads and large amplitudes.

In this work computational fluid dynamics simulation of the flow in micro-channel is reported. Numerical 2D simulation was performed using OpenFOAM software. Validation was performed according to Renfer experiment [4], the coincidence of modelling and experimental data on average exceeds 90 %. The flow structure is dependent on gap-spacing ratio $P_{L/T}/D$, where P is the cylinder centre-to-centre spacing ratio, L and T are longitudinal and transverse separation, respectively, D is the diameter of a cylinder, in this case - $P_L/D = 2$, $P_T/D = 3$.

Investigated configuration at certain Reynolds numbers Re_d experience interference of antiphase-synchronized pattern of gap flow, which is shown in Fig. 1., here $Re_d = u_m D/\nu$, where u_m is the mean velocity of fluid between the cylinders and is ν the kinematic viscosity of fluid. Due to low P_L/D ratio and higher P_T/D ratio, recirculation zones lose their strength and shed alternating von Karman vortices. As the phase difference between each gap flow is ´, it results in anti-phase synchronized vortex shedding, where wake zones interact with each other constructively (see Fig. 1 b)). This phenomenon leads to decreased pressure and higher kinetic energy and vorticity zones, which have abrupt gradients. Maximum speed in these zones is 40 % higher than the maximum speed at the end of channel, where the in-phase vortex-shedding is observed (see Fig. 1 c)). The interference gives rise to coupled vortices and instabilities in the gap flow and wakes, which can lead to a strong increase or decrease of drag and lift forces and Strouhal number of the obstacles. In all cases vortex shedding leads to more or less fluctuating forces on the cylinders and can cause structural vibrations, resonance, acoustic noise, which can provoke failure of structure.

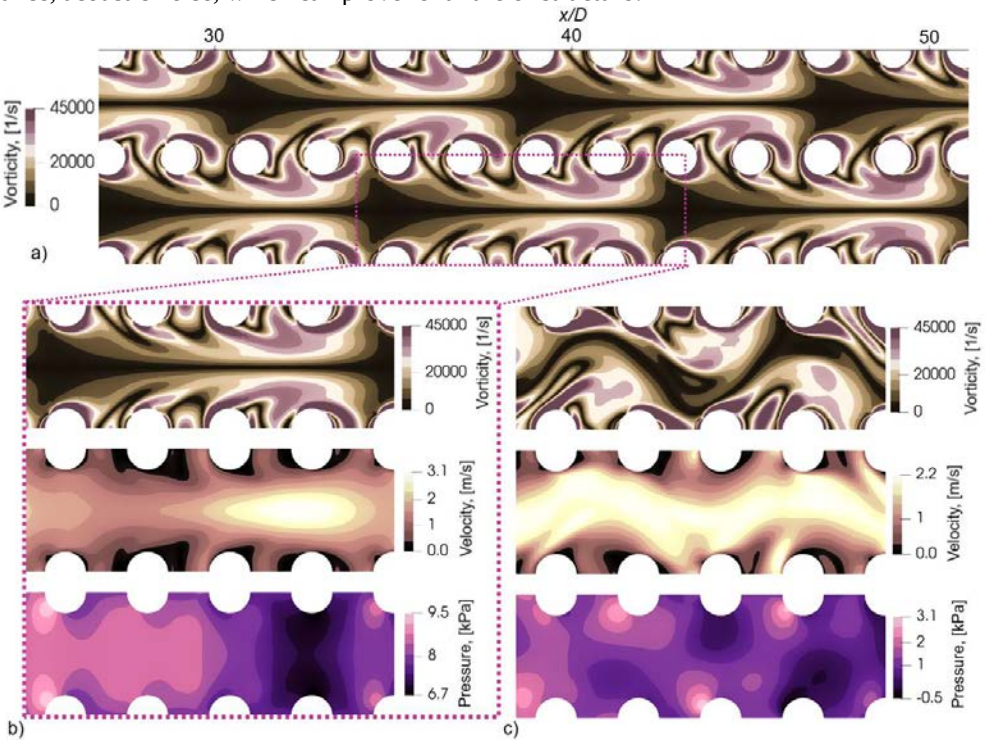

Fig 1. $Re_d = 180$, $t = 0.1$ s, a) vorticity contours, b) and c) vorticity, velocity, pressure fields starting from $x/D = 34$ and 94, respectively

[1] Y. Zhou & Md. M. Alam, Wake of two interacting circular cylinders: A review, International Journal of Heat and Fluid Flow **62**, 510-537 (2016).
[2] T. Tang, P. Yu, X. Shan et al., On the transition behavior of laminar flow through and a multi-cylinder array, Physics of Fluids **32**, 013601 (2020).
[3] Md. M. Alam & J. P. Meyer, Two interacting cylinders in cross flow, Physical Review **84**, 056304 (2011).
[4] A. Renfer, M. K. Tiwari, T. Brunschwiler et al. Experimental investigation into vortex structure and pressure drop across microcavities in 3D integrated electronics, Experiments in Fluids **51**, 731-741 (2011).

IMPROVED FAKE LEPTON BACKGROUND ESTIMATION FOR THE DRELL-YAN DIFFERENTIAL CROSS SECTION MEASUREMENT USING 2016 CERN CMS DATA

Marijus Ambrozas, Andrius Juodagalvis

Institute of Theoretical Physics and Astronomy, Faculty of Physics, Vilnius University, Lithuania
marijus.ambrozas@gmail.com

The Large Hadron Collider (LHC) at CERN accelerates protons to almost the speed of light and collides them together with 13 TeV collision energy. Short-lived heavy particles may be produced during such collisions, and investigation of these events allows physicists to further push the frontier of our understanding about the Universe. Colliding protons can be described as two opposite flows of quarks and gluons, according to the parton model. Any two (or more) partons may interact during the collision, producing new particles. There are different probabilities of different outcomes, which initially depend on the parton distribution functions (PDFs). PDFs describe probabilities of existence and energy fraction of specific partons inside a proton. PDFs must be measured with high precision in order to make correct predictions about proton interactions.

The Drell-Yan process takes place during a proton-proton collision, when a quark and an antiquark annihilate to create a *Z* boson or a virtual photon which nearly instantly decays into a charged lepton-antilepton pair (dilepton for short) [1]. Dilepton center-of-mass properties depend directly on four-momenta of the annihilating quarks. Therefore, precise measurements of Drell-Yan process differential cross sections are used to constrain the PDFs [2]. These measurements are also useful for testing the validity of higher-order corrections of the standard model as well as for a number of other experimental measurements where the Drell-Yan process is considered a background [3-5].

Charged leptons created during the Drell-Yan process usually have a high momentum and leave tracks that are well separated from tracks of other particles. This type of leptons is usually called ñprompt.ò There also are other processes that may produce prompt lepton pairs just like the Drell-Yan process. We refer to these processes as prompt lepton backgrounds. There is also a possibility that a poorly isolated lepton emerging from a hadronic jet or even the jet itself will be misreconstructed as a prompt lepton. This type of leptons is called ñfake.ò Typical fake lepton backgrounds are the *W*+Jets (one lepton is prompt and one is fake) and the *QCD* multijet (both leptons are fake) processes.

Fake lepton events have very large cross sections and very low probabilities to be selected as Drell-Yan event candidates. Therefore, the simulated fake lepton background predictions are usually inaccurate. Data-driven techniques are exploited to estimate such background yields. The ñfake rateò method relies on measuring the fake lepton selection efficiency. The measured efficiency is applied on events containing fake leptons that have failed the selection to estimate the number of events that have passed it. In theory, a more sophisticated method is the ñmatrix method,ò which additionally measures the prompt lepton selection efficiency. Both methods will be presented and compared in the context of the Drell-Yan differential cross section measurement using 2016 CERN CMS data recorded at $\sqrt{s}$ = 13 TeV.

Collaboration with CERN CMS experiment is supported by the Lithuanian Academy of Sciences. This work was also partially supported by a scholarship from Vilnius University Experimental Nuclear and Particle Physics Center and done in collaboration with scientists from Universit® libre de Bruxelles, Yonsei University, and the University of Nebraska in Lincoln.

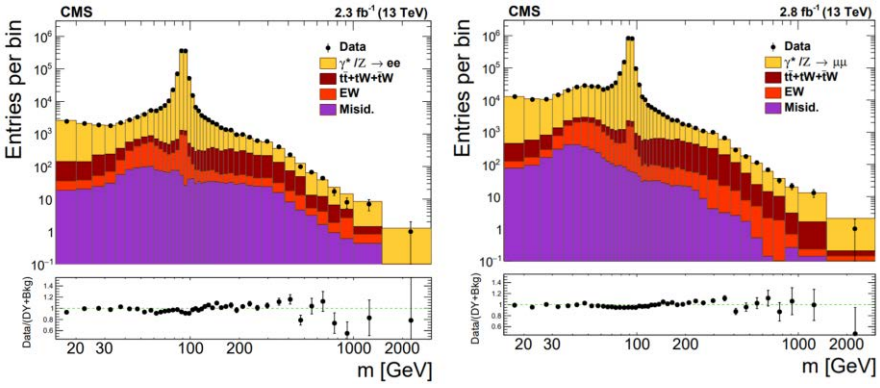

Fig. 1. Dielectron (left) and dimuon (right) invariant mass distributions measured using 2015 CERN CMS data [2]. Black dots denote event yields measured with the CMS detector. Yellow bars mark simulated Drell-Yan process ñEWò marks prompt lepton backgrounds. ñMisid.ò denotes fake lepton backgrounds, estimated using the ñfake rateò method.

[1] S. D. Drell, T. M. Yan, Massive Lepton Pair Production in Hadron-Hadron Collisions at High-Energies, Phys. Rev. Lett. **25**, 316 (1970).

[2] CMS Collaboration, Measurement of the differential Drell-Yan cross section in proton-proton collisions at $\sqrt{s}$ = 13 TeV, JHEP **12** 059 (2019).

[3] ATLAS Collaboration. A search for the dimuon decay of the Standard Model Higgs boson with the ATLAS detector. Phys. Lett. B **812**, 135980 (2021).

[4] CMS Collaboration. Search for high-mass resonances in dilepton final states in proton-proton collisions at $\sqrt{s}$ = 13 TeV. JHEP **06** 120 (2018).

[5] CMS Collaboration. Search for top squark pair production using dilepton final states in pp collision data collected at $\sqrt{s}$ = 13 TeV. Eur. Phys. J. C **81** 3 (2021).

MULTI-HIGGS DOUBLET MODELS AND GROUP THEORY

Anton Kunčinas[1], Per Osland[2], Margarida Nesbitt Rebelo[1]

[1]Centro de Física Teórica de Partículas – CFTP and Dept de Física Instituto Superior Técnico – IST, Universidade de Lisboa, Av. Rovisco Pais, P-1049-001 Lisboa, Portugal
[2]Department of Physics and Technology, University of Bergen, Postboks 7803, N-5020 Bergen, Norway
Anton.Kuncinas@protonmail.com

The Standard Model (SM) of particle physics has been extensively tested for a few decades and is the most successful description of Nature. Nearly all theoretical SM predictions have been experimentally verified and the last missing piece, the Higgs boson, was discovered in 2012 [1, 2]. This is undoubtedly a fascinating discovery in the field of particle physics and might be the final missing piece. Nevertheless, there is no experimental verification that it is the only Higgs boson, and it will be tested at the LHC and future colliders. It is widely accepted that the SM is an effective low-energy theory, which is capable of explaining physics at low energies, $\mathcal{O}(100)$ GeV, but fails at high energies. While the SM of particle physics keeps on triumphing, there is a vast amount of both theoretical and experimental phenomena that cannot be resolved within the SM framework, some of which are: neutrino oscillations, asymmetry of matter-antimatter, the strong CP problem, *etc*. From the cosmological point of view the overall SM situation is daunting as it fails to describe not only gravity and dark energy, but also nearly 85% of the matter in the Universe, which is constituted by Dark Matter (DM). The multi-Higgs models could resolve some of the issues and are commonly invoked when models beyond the SM are constructed. Thus, we propose and are motivated that such extension could potentially solve several problems.

The SM uses the minimal Brout-Englert-Higgs mechanism [3, 4, 5], where a single complex SU(2) doublet is considered. The simplest extension of the SM electroweak sector is the Two-Higgs-Doublet Model (2HDM) [6, 7]. In the 2HDM a second SU(2) doublet is added to the SM-like doublet. Such extension predicts a rich scalar spectrum: two additional neutral states $h_{(1,2)}$, and a charged state $h^{\pm}$. The second SU(2) doublet can be further on constrained to result in a viable DM candidate [8]. There are many possibilities to extended the scalar sector by not only the SU(2) doublet but a general n-tuplet, each with its own advantages. A non-minimal scalar sector is well motivated in both Supersymmetry and Grand Unified Theories, where extension of the scalar sector is inevitable.

With limitless possibilities to extend the scalar sector it is crucial not to oversaturate a model with an endless list of free parameters. Let us consider the most general NHDM model. The number of free real parameters is given by $N_{\text{tot}} = N^2\left(N^2+3\right)/2$ [9]. With the number of additional SU(2) doublets, the total amount of free parameters grows rapidly, and a specific model loses predictiveness. Symmetries play an important role in controlling the number of free parameters, therefore increasing the predictability of such extensions. For example, the most general 3HDM scalar potential results in 54 free real parameters. However, if we impose a discrete S_3 symmetry [10, 11, 12, 13] *ad hoc*, the number of free parameters decreases to up to ten. In the multi-Higgs extensions some of the problems of the SM, such as the need for new sources of CP violation, which are required to account for the observed baryon asymmetry, can be addressed. An important feature of multi-Higgs extensions of the SM is the possibility of having spontaneous CP violation. Imposing additional symmetries may eliminate the possibility of having spontaneous CP violation.

During the talk we shall cover the 2HDM and the 3HDM models. In particular, we shall present results of Ref. [14], where implications of a mass degeneracy among scalar states and possible symmetries of the 2HDM scalar potential were presented. Moreover, we shall discuss what happens to CP violation in the scalar sector when symmetries are imposed. Also, we introduce a basic principle of how to construct an S_3-symmetric 3HDM and how symmetries can lead to massless states [15, 16].

[1] G. Aad *et al.* [ATLAS], "Observation of a new particle in the search for the Standard Model Higgs boson with the ATLAS detector at the LHC," Phys. Lett. B **716** (2012), 1-29 doi:10.1016/j.physletb.2012.08.020 [arXiv:1207.7214 [hep-ex]].
[2] S. Chatrchyan *et al.* [CMS], "Observation of a New Boson at a Mass of 125 GeV with the CMS Experiment at the LHC," Phys. Lett. B **716** (2012), 30-61 doi:10.1016/j.physletb.2012.08.021 [arXiv:1207.7235 [hep-ex]].
[3] F. Englert and R. Brout, Phys. Rev. Lett. **13** (1964), 321-323 doi:10.1103/PhysRevLett.13.321
[4] P. W. Higgs, Phys. Lett. **12** (1964), 132-133 doi:10.1016/0031-9163(64)91136-9
[5] G. S. Guralnik, C. R. Hagen and T. W. B. Kibble, Phys. Rev. Lett. **13** (1964), 585-587 doi:10.1103/PhysRevLett.13.585
[6] T. D. Lee, Phys. Rev. D **8** (1973), 1226-1239 doi:10.1103/PhysRevD.8.1226
[7] G. C. Branco, P. M. Ferreira, L. Lavoura, M. N. Rebelo, M. Sher and J. P. Silva, Phys. Rept. **516** (2012), 1-102 doi:10.1016/j.physrep.2012.02.002 [arXiv:1106.0034 [hep-ph]].
[8] N. G. Deshpande and E. Ma, Phys. Rev. D **18** (1978), 2574 doi:10.1103/PhysRevD.18.2574
[9] K. Olaussen, P. Osland and M. A. Solberg, JHEP **07** (2011), 020 doi:10.1007/JHEP07(2011)020 [arXiv:1007.1424 [hep-ph]].
[10] S. Pakvasa and H. Sugawara, Phys. Lett. B **73** (1978), 61-64 doi:10.1016/0370-2693(78)90172-7
[11] E. Derman, Phys. Rev. D **19** (1979), 317-329 doi:10.1103/PhysRevD.19.317
[12] E. Derman and H. S. Tsao, Phys. Rev. D **20** (1979), 1207 doi:10.1103/PhysRevD.20.1207
[13] J. Kubo, H. Okada and F. Sakamaki, Phys. Rev. D **70** (2004), 036007 doi:10.1103/PhysRevD.70.036007 [arXiv:hep-ph/0402089 [hep-ph]].
[14] H. E. Haber, O. M. Ogreid, P. Osland and M. N. Rebelo, JHEP **01** (2019), 042 doi:10.1007/JHEP01(2019)042 [arXiv:1808.08629 [hep-ph]].
[15] D. Emmanuel-Costa, O. M. Ogreid, P. Osland and M. N. Rebelo, JHEP **02** (2016), 154 [erratum: JHEP **08** (2016), 169] doi:10.1007/JHEP08(2016)169 [arXiv:1601.04654 [hep-ph]].
[16] A. Kunčinas, O. M. Ogreid, P. Osland and M. N. Rebelo, Phys. Rev. D **101** (2020) no.7, 075052 doi:10.1103/PhysRevD.101.075052 [arXiv:2001.01994 [hep-ph]].

ENGINEERING TIME-SPACE CRYSTALLINE STRUCTURES

Giedrius Žlabys[1], Chu-hui Fan[2], Egidijus Anisimovas[1], Krzysztof Sacha[2]

[1]Institute of Theoretical Physics and Astronomy, Vilnius University, Saulėtekio 3, LT-10257 Vilnius, Lithuania
[2]Instytut Fizyki Teoretycznej, Uniwersytet Jagielloński, ulica Profesora Stanisława Łojasiewicza 11, PL-30-348 Kraków, Poland
giedrius.zlabys@tfai.vu.lt

Regular space crystals are described by a spatially periodic distribution of particles observed at a fixed moment of time. To form time crystals [1, 2], the roles between time and space are interchanged. In this case the periodicity is observed in time by fixing a position in space and measuring the periodic detection of particles during the experimental time frame. Time crystal behavior can emerge spontaneously in many-body systems and can also be engineered by suitable external time-periodic driving. This allows to realize a variety of condensed-matter phenomena in the time domain [3, 4].

In this presentation, we demonstrate the notion of time-space crystalline structures (TSCS) which merge the ideas of time and space crystals to form systems that are both temporally and spatially periodic [5]. Starting with a particle in a one-dimensional periodic potential, an external periodic and resonant driving can be used to engineer a crystalline time structure at each potential well of the spatial lattice thus effectively forming a two-dimensional TSCS. This allows us to construct a system where each spatially orthogonal one-dimensional periodic potential comes equipped with a periodic structure in time. For a three-dimensional lattice with a proper choice of driving this leads to a six-dimensional TSCS. Realization of a six-dimensional crystalline structure paves the way towards investigation of higher-dimensional condensed-matter phases.

[1] A. Shapere, F. Wilczek, Classical Time Crystals, Phys. Rev. Lett. **109**, 160402 (2012)
[2] F. Wilczek, Quantum Time Crystals, Phys. Rev. Lett. **109**, 160401 (2012).
[3] K. Sacha, J. Zakrzewski, Time crystals: a review, Rep. Prog. Phys. **81**, 016401 (2017)
[4] L. Guo, P. Liang, Condensed matter physics in time crystals , New J. Phys. **22**, 075003 (2020)
[5] G. Žlabys, C.-h. Fan, E. Anisimovas, K. Sacha, Six-dimensional time-space crystals, arXiv:2012.02783 (2020)

MODELLING OF INTERACTION BETWEEN PHOTOSYNTHETIC PIGMENTS USING QUANTUM CHEMISTRY METHODS

Kazimieras TamoliÎnas[1], Jevgenij Chmeliov[1, 2], Andrius Gelģinis[1, 2]

[1]Institute of Chemical Physics, Faculty of Physics, Vilnius University, Lithuania
[2]Department of Molecular Compound Physics, Center for Physical Sciences and Technology, Lithuania
kazimieras.tamoliunas@ff.stud.vu.lt

Photosystem (PSII), one of many pigment-protein supercomplexes located inside the thylakoid membrane of the plantôs organelle chloroplast, takes an important part in the photosynthetic reactions. PSII participates in the light harvesting as well as the charge transfer processes while also contributing to the plantôs defensive mechanisms [1]. It was recognised that the LHCII protein complex, which comprises the PSII protein, is highly involved in the process of nonphotochemical quenching (NPQ) ï one of the main plantôs defensive resources. In cases when the rate of photon absorption exceeds the transfer rate towards the reaction centre, certain quenching sites appear within the LHCII complex, allowing it to dissipate the excess excitation energy as heat [2].

In search for the description of the NPQ process, a study suggested that the close-lying chlorophyll (Chl) molecules can form the charge transfer (CT) states, which are able to act as the excitation energy quenchers [3]. Meanwhile, others argued that the CT states are related to the red-shifted state (700-720 nm) with respect to the main state (680 nm) of the LHCII complex [4]. Even though the mechanism and precise location of the NPQ was not clarified, the studies imply the possibility that the CT states might contribute to the process. The close-lying Chla610, Chla611 and Chla612 structures inside the LHCII complex excel in the lowest excited-state energies as well as the highest interaction energies, which are the inherent characteristics of the CT states [5]. On this basis, the triplet was central to the present investigation.

High resolution LHCII protein structure [6] and plenty of experimental data [3, 4] allowed to search for the CT states using quantum chemistry computational methods. The density functional theory (DFT) was applied to probe the ground-state properties while the time-dependent DFT (TDDFT) formalism was used to investigate the properties of the excited-states. Coulomb attenuating hybrid exchange-correlation functional (CAM-B3LYP) was selected with cc-pVDZ basis set. The structures were picked out of the LHCII structure and optimised at the DFT/CAM-B3LYP level of theory. The optimised monomers were then assembled into dimers with respect to their original locations and a number of excited states (8 for monomer and 16 for dimer structures) were calculated at the TDDFT/CAM-B3LYP level of theory.

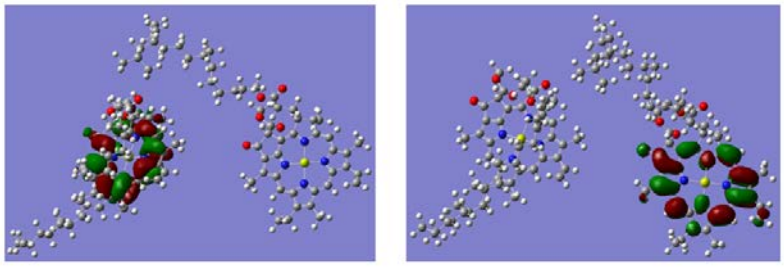

Fig. 1. The contribution of the molecular orbital transition to the seventh excited state of the Chla610ï Chla611 dimer.

The excited-state properties were presented using the molecular orbital contributions to the different excited states, transition energies and dipole moments. The candidate CT states for all the dimer structures were found to lie among the higher order excited states. They were recognised as either non-local transitions or transitions with some proportion of excitonic coupling. Transition dipole moments further validated the existence of CT states showing characteristic zero (Fig. 1) or nearly vanishing transition dipole moment.

In conclusion, the computational study at the (TD)DFT/CAM-B3LYP level of theory is able to reproduce the experimental results. This implies that further models can be tested to verify that the existence of the CT states is a real physical phenomenon, invariant of chosen methodology. Furthermore, the environmental effects, which are thought to possess a huge effect on the NPQ mechanism can be incorporated to varying degree in order to achieve a more realistic picture.

[1] J. M. Berg, J. L. Tymoczko, L. Stryer, Biochemistry, 5th edition, W. H. Freeman and Company, 2002.
[2] A. V. Ruban, Nonphotochemical Chlorophyll Fluorescence Quenching: Mechanism and Effectiveness in Protecting Plants from Photodamage. PP, 170(4), (2016), 1903ï 1916.
[3] Y. Miloslavina, A. Wehner, P.H. Lambrev, E. Wientjes, M. Reus, G. Garab, R. Croce, A.R. Holzwarth, Far-red fluorescence: a direct spectroscopic marker for LHCII oligomer formation in non-photochemical quenching, FEBS Lett. 582(25-26) (2008), 3625ï 3631.
[4] J. Chmeliov, A. Gelzinis, E. Songaila, R. Augulis, C. D. P. Duffy, A. V. Ruban, & L. Valkunas, The nature of self-regulation in photosynthetic light-harvesting antenna. Nature Plants, 2(5), (2016), 16045.
[5] J. Chmeliov, (2015), Excitation evolution and self-regulation ability of photosynthetic light-harvesting systems, doctoral dissertation, Vilnius University.
[6] Y. Umena, K. Kawakami, J.-R. Shen, & N. Kamiya, Crystal structure of oxygen-evolving photosystem II at a resolution of 1.9 A. Nature, 473(7345), (2011), 55ï 60.

ENAMINE-DERIVED SPIROBIFLUORENES AS HOLE TRANSPORTING MATERIALS FOR PEROVSKITE SOLAR CELLS

Deimante Vaitukaityte[1], Cristina Momblona[2], Kasparas Rakstys[1], Albertus Adrian Sutanto[2], Bin Ding[2], Vygintas Jankauskas[3], Alytis Gruodis[3], Tadas Malinauskas[1], Abdullah M. Asiri[4], Paul J. Dyson[2], Vytautas Getautis[1], Mohammad Khaja Nazeeruddin[2]

[1] Department of Organic Chemistry, Kaunas University of Technology, Lithuania
[2] Institute of Chemical Sciences and Engineering, £cole Polytechnique F®d®rale de Lausanne, Switzerland
[3] Institute of Chemical Physics, Vilnius University, Lithuania
[4] Center of Excellence for Advanced Materials Research, King Abdulaziz University, Saudi Arabia
deimante.vaitukaityte@ktu.lt

Perovskite solar cells (PSCs) require high efficiency and good long-term stability that must come at low costs to achieve the commercial viability. Counting more than 20 years, spiro-OMeTAD now dominates the field of PSCs and is the hole-transporting material (HTM) routinely employed as highly efficient reference material for the research interests despite its high price (~250 $/g) [1]. Although PSCs have recently achieved certified power conversion efficiency (PCE) exceeding 25%, one major bottleneck of stabilizing the performance is the lack of stable HTMs, which extract positive charges from the active perovskite light absorber and transmit them to the electrode [2].

In this work, four HTMs containing well-established spirobifluorene core with introduced enamine arms were synthesized by simple and straightforward condensation reaction that in contrary to spiro-OMeTAD does not require expensive palladium catalysts and water is the only by-product. In addition, simple product workup and purification may result in significantly reduced synthesis costs.

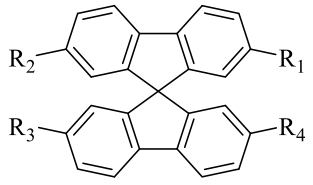

V1305: R_1 = BDDE, $R_2 = R_3 = R_4$ = H
V1306: $R_1 = R_3$ = BDDE, $R_2 = R_4$ = H
V1307: $R_1 = R_2 = R_3 = R_4$ = BDDE
V1308: $R_1 = R_2$ = BDDE, $R_3 = R_4$ = H

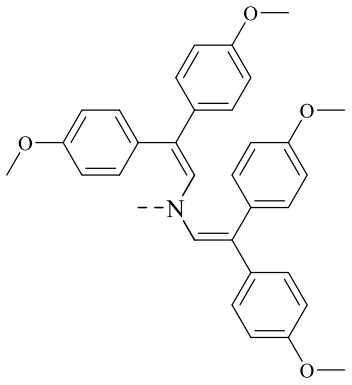

bisdimethoxydiphenylenamine (BDDE)

Fig. 1. Structures of enamine-based hole transporting materials **V1305**, **V1306**, **V1307** and **V1308**.

To investigate photoelectrical properties of synthesized HTMs hole drift mobility ($\tilde{O}$) and ionization potential (I_P) were measured. Solid-state I_P was measured using the electron photoemission in the air (PESA) to study the HOMO energy level of spiro-enamine HTMs. Ionization potential values of **V1305**, **V1306** that have one and two enamine arms, respectively, tetra-substituted **V1307** and trans-configurated **V1308** were found to be 5.33, 5.37, 5.46, and 5.46 eV, respectively, which is significantly stabilized comparing to that of spiro-OMeTAD (5.00 eV). Based on the solid-state optical gap and I_P values electron affinities were calculated to be 2.43, 2.53, 2.63, and 2.68 eV for **V1305**, **V1306**, **V1307** and **V1308**, respectively. It is important that the electron affinities are smaller comparing with the conduction band (CB) energy of the perovskite (-4.10 eV), therefore effective electron blocking from the perovskite to the electrode should be ensured. Xerographic time of flight (XTOF) technique was used to determine the charge mobility of investigated HTMs layers. **V1308** and **V1307** exhibited the highest zero-field $\tilde{O}_0$ among the series having the values of 9.4 Ǐ 10^{-4} and 6.4 Ǐ 10^{-4} cm^2/Vs, respectively, both outperforming that of spiro-OMeTAD ($\tilde{O}_0$ = 1.3Ǐ 10^{-4} cm^2/Vs).

n-i-p solar cells were fabricated with the device layout FTO/c-TiO_2/m-TiO_2/SnO_2/perovskite/HTM/Au to test novel materials as HTMs. The most efficient devices containing **V1305**, **V1307** and **V1308** presented similar power conversion efficiency values of 19.0, 19.2 and 19.1%, respectively. Data analysis confirms the correlation between hole drift mobility and device performance, being most efficient the devices containing the HTM with higher hole mobility values following the order: **V1306**’ **V1305**’ **V1308**’ **=V1307**. This work shows that simple enamine condensation protocol could be used as universal approach achieving HTMs for highly efficient and stable PSCs.

[1] K. Jiang, F. Wu, G. Zhang et al., Efficient Perovskite Solar Cells Based on Dopant Free Spiro OMeTAD Processed With Halogen Free Green Solvent, Solar RRL **3**, 1900061 (2019).
[2] K. Rakstys, M. Saliba, P. Gao et al., Highly Efficient Perovskite Solar Cells Employing an Easily Attainable Bifluorenylidene Based Hole Transporting Material, Angewandte Chemie International Edition **55**, 7464-7468 (2016).

THE FLUORIDE ANION CATALYZED SULFURIZATION OF THIOKETONES WITH ELEMENTAL SULFUR LEADING TO SULFUR-RICH HETEROCYCLES

Jakub Wrńczycki[1], Grzegorz MlostoŒ[2], Katarzyna Urbaniak[2], Dariusz M. BieliŒski[1]

[1] Institute of Polymer and Dye Technology, Faculty of Chemistry, Lodz University of Technology, 12/16 Stefanowskiego Street, 90-924, Lodz, Poland
[2] Department of Organic and Applied Chemistry, Faculty of Chemistry, University of Lodz, 12 Tamka Street, 91-403, Lodz, Poland
jakub.wreczycki@dokt.p.lodz.pl

The elemental sulfur (S_8) based organic synthesis constitutes an interesting and practically relevant topic in the current organic chemistry [1]. Utilization of sulfur excess, mainly manufactured as a side product of the petroleum industry processes, for the production of useful organic or polymeric materials is of primary interest to sustain the proper cycle of sulfur conversion [2]. In our continuous studies on nucleophilic carbenes (NHCs) reactions with elemental sulfur are aimed at the synthesis of practically useful, on-enolizable imidazole-2-thiones [3].

It is well established that sulfurization reactions of thioketones such as aryl, hetaryl or cycloaliphatic thioketones ($R_2C=S$) with the use of S_8 attracts attention of researchers since sulfur-rich heterocycles are of interest for medicinal chemistry, in fragrances, agrochemical production, etc. [4,5]. In the past, various nucleophilic species have been applied for the S_8 activation. However, one of the unorthodox approach, presented in our work, is the usage of easily accessible fluoride anion F^- as a potent activator of elemental sulfur [6]. Tentatively, we propose that the reactive sulfurizing reagents formed thereby are in situ generated, nucleophilic fluoropolysulfide anions $FS_{(8-x)}^-$.

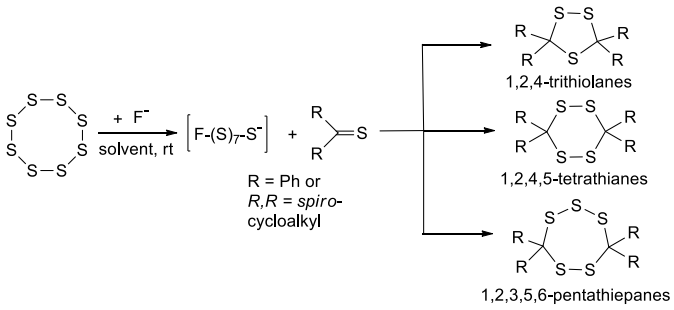

Fig. 1. Ring cleavage of the S_8 crown in the presence of fluoride anion and further pathway reactions of the generated fluoropolysulfide anions with thioketones leading to sulfur-rich heterocycles.

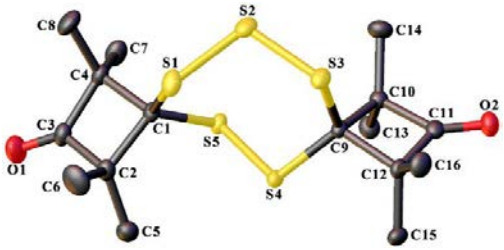

Fig. 2. X-Ray structure of an 1,2,3-5,6-pentathiepane (R,R = *spiro*-2,2,4,4-tetramethylcyclobutanone)

In our ongoing research, we found that the in situ-generated fluoropolysulfide anions act as powerful sulfurizing reagents of cycloaliphatic and selected aromatic thioketones leading to diverse sulfur-rich heterocycles (Fig. 1.) Moreover, depending on the molar ratio of the starting materials (i.e. thioketone/[S]), formation of sulfur-rich heterocycles with variable ring size was observed. A novel, unique and efficient method for the *S*-transfer to the C=S bond *via* activation of S_8 with fluoride anion as well as mechanisms of the formation of sulfur rich-heterocycles, including dithiiranes existing in an equilibrium with the ring-opened isomeric species (diradicals/zwitterions) as a key intermediates, will be discussed.

Acknowledgement: Authors acknowledge financial support by the National Centre for Research and Development (Warsaw, Poland) within the grant InterChemMed (WND-POWR.03.02.00-00-I029/16-01). GM and KU acknowledge partial support by the National Science Center (Cracow) within the Grant Beethoven-2 (#2016/23/G/ST5/04115/l).

[1] T. B. Nguyen, Recent advances in organic reactions involving elemental sulfur, Advanced Synthesis & Catalysis **359**, 1066ï 1130 (2017).
[2] W. J. Chung, J.J. Griebel, E. T. Kim et al. The use of elemental sulfur as an alternative feedstock for polymeric materials, Nature Chemistry **5**, 518ï 524 (2013).
[3] G. MlostoŒ, M. Celeda, W. Poper, M. Kowalczyk, K. Gach-Janczak, A. Janecka, M. JasiŒski, Synthesis, selected transformations, and biological activity of alkoxy analogues of lepidilines A and C. Materials **13,** e4190**,** (2020).
[4] R. Huisgen, J. Rapp, The conversion of thioketones to 1,2,4,5-tetrathianes and its mechanism, Heterocycles **45**, 507-525 (1997)
[5] R. Huisgen, J. Rapp, J, H. Huber, Sulfurization of thiones: 2,2,4,4-tetramethyl-3-thioxocyclobutanone, Liebigs Annalen/Recueil **7**, 1517ï 1523 (1997).
[6] V. A. Petrov, W. Marshall, Remarkable effect of metal fluoride catalyst on reaction of hexafluoropropene, sulfur and vinyl ethers. Convenient synthesis of 2,2-bis(trifluoromethyl)-4-R-thietanes, 3,3-bis(trifluoromethyl)-5-R-1,2-dithiolanes and 2,2-bis(trifluoromethyl)-4-R-1,3-dithiolanes. Journal of Fluorine Chemistry **131**, 1144ï 1155 (2010).

SYNTHESIS AND IVESTIGATION OF ORGANOMETALLIC PRECURSORS FOR CONVENIENT COPPER (I) THIOCYANATE LAYER DEPOSITION

Mantas Marį inskas, Tadas Malinauskas

Faculty of Chemical Technology, Kaunas University of Technology, Lithuania
mantas.marcinskas@ktu.edu

Over the last decade perovskite solar cells (PSCs) received large amount of attention from scientists and the efficiency of these devices was increased up to 25.5 % [1]. Consequently, PSC became one of the most promising future photovoltaic technologies. At this moment, large effort is being made towards commercialization, by improving the long-term stability and finding the balance between the device performance and overall manufacturing costs. Large part of cost-effectiveness in PSC relies on the charge transporting materials, therefore, many researchers have focused their attention on development of optimal hole transporting materials (HTMs).

Inorganic semiconductors, such as transition metal oxides, copper or nickel derivatives offer beneficial physical and chemical properties. Among them, copper (I) thiocyanate (CuSCN) can be highlighted as one of the most promising HTMs, because of its low-cost, large bandgap (>3.5eV), optical transparency and relatively high hole mobility (up to 0.1 $cm^2V^{-1}s^{-1}$). Furthermore, CuSCN is solution processable and its layer can be deposited even at low temperatures. These benefits make CuSCN perspective semiconductor for application not only for PSCs, but also in other optoelectronics, e.g. organic light-emitting diodes or CdTe solar cells. However, CuSCN is insoluble in most of widely used solvents, therefore current CuSCN solution processing technologies are limited to only a few solvents, such as ammonia solution or diethyl sulfide (DES). Both of them can damage perovskite layer, additionally DES has strong emetic effect, so its elimination would be advantageous, especially in larger scale application [2-4].

In this research, a series of different organometallic complexes were synthesized as CuSCN precursors to improve its deposition procedure. All synthesized compounds were obtained in one-step synthesis, purified by quick and inexpensive methods and most of them are characterized by relatively low thermal decomposition temperatures. These precursors thermally decompose to form CuSCN and volatile organic byproducts which evaporate during the layer formation step, as shown in Scheme 1.

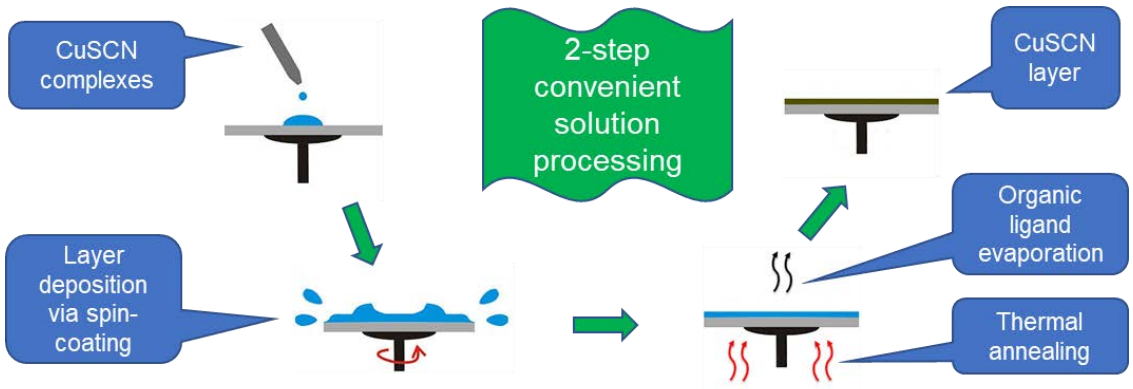

Scheme 1. The formation of CuSCN layer by spin-coating and heating

Large part of synthesized CuSCN complexes, investigated in this work, are soluble in dimethyl sulfoxide, which is considered as a green solvent and can be used as a replacement for DES. Moreover, several precursors have demonstrated solubility in other organic solvents such as chloroform and tetrahydrofuran, hence their usability can be expanded to various PSCs architectures, as well as other optoelectronics.

[1] NREL solar cells efficiency chart: https://www.nrel.gov/pv/assets/pdfs/best-research-cell-efficiencies.20200104.pdf
[2] N. R. Paudel, Y. Yan. Application of copper thiocyanate for high open circuit voltages of CdTe solar cells. Progress in Photovoltaics **24** (1), 94-101.
[3] N. Wijeyasinghe, T. Anthopoulos. Copper(I) thiocyanate (CuSCN) as a hole-transport material for large-area opto/electronics. Semicond. Sci. Technol. **30**, 104002.
[4] N. Wijeyasinghe, A. Regoutz et. al. Copper(I) Thiocyanate (CuSCN) Hole-Transport Layers Processed from Aqueous Precursor Solutions and Their Application in Thin-Film Transistors and Highly Efficient Organic and Organometal Halide Perovskite Solar Cells. Adv. Funct. Mater. **2017**, 1701818.

HIGH-ENTROPY ALLOYS AS CATALYSTS FOR SELECTIVE GLYCEROL OXIDATION

Ieva Agne Cechanaviciute[1], Wolfgang Schuhmann[2]

[1] Faculty of Chemistry and Geosciences, Vilnius University, Naugarduko str. 24, Vilnius, Lithuania
[2] Analytical Chemistryð Center for Electrochemical Sciences (CES), Faculty of Chemistry and Biochemistry, Ruhr University Bochum, Universit[a] tsstrasse 150, 44780 Bochum, Germany
ievaagne@gmail.com

Hydrogen synthesis through water electrolysis is strongly limited by the high overpotentials associated with the anodic oxygen evolution reaction (OER). One of the alternatives could be replacing oxygen evolution with the oxidation of a more readily oxidized species like alcohols [1]. Through recent years increased production of biodiesel of which glycerol is the main byproduct (10 wt%) increased glycerolôs availability and made it a perfect candidate for the alternative anode reactions to value-added products [2].

High-entropy alloys (HEAs) are alloys that are formed by mixing comparatively large or even equal proportions of usually five elements. Due to the multiatomic composition a unique alloy structure, with various active binding sites and improved catalytical properties can be achieved [3]. For this research HEAs were obtained using aerosol-based spraying synthesis route and limited to a maximum of two noble metals in the structure. To find the best HEA for glycerol oxidation both elemental composition and elemental ratio in the alloy were varied consistently.

HEA suitability for glycerol electrooxidation was firstly investigated by evaluating its catalytical activity. It was done by performing potential cycling between 0 and 0.7 V, 10 mV/s, for 3 cycles in 1 M KOH and 0.1 M glycerol solution in 1 M KOH. For electrochemical measurements, a three-electrode system where the working electrode was modified with catalyst suspension was used. In pure electrolyte solution, oxygen evolution reaction was monitored and later compared to the alcohol oxidation reaction occurring in the glycerol solution by comparing the current density and overpotential values (Fig. 1). This way over 40 catalysts were scanned and their catalytical activity assessed.

Catalysts that demonstrated sufficiently high current densities and suitable overpotential values were further used to investigate their selectivity for glycerol oxidation. This was done using a closed system flow-through cell where glycerol and 1 M KOH solutions were used for the circulation in modified with catalyst working electrode and counter electrode compartments simultaneously. Compartments were separated using ion-exchange membrane. Samples of oxidized glycerol solution were taken at fixed time intervals through the time span of 48 h and analyzed using high performance liquid chromatography (HPLC).

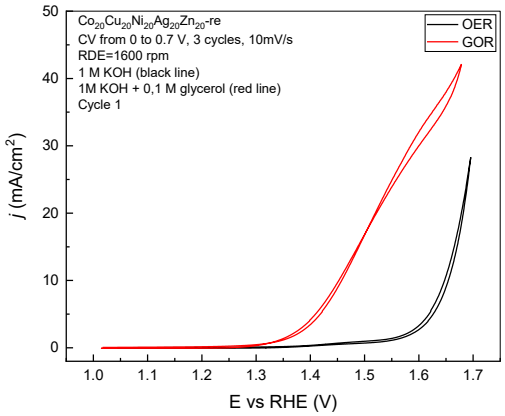

Fig. 1. Electrochemical measurements using $Co_{20}Cu_{20}Ni_{20}Ag_{20}Zn_{20}$ catalyst

Multiple selectivity measurements revealed that the main products of glycerol oxidation were lactic, oxalic, tartronic, formic, acetic, glycolic and glyceric acids. The influence of different elements and their ratio to the selectivity were also evaluated. It was noted that varying the composition of HEAs may lead to a higher selectivity towards particular product formation. This leads a promising way for future research where conversion of certain molecules can be easily shifted towards a desirable direction by ease manipulation of HEAs.

[1] M. A. Lijie Du, Y. Sun, B. You, Hybrid water electrolysis: Replacing oxygen evolution reaction for energy-efficient hydrogen production and beyond, Materials Reports: Energy, 100004 (2020).
[2] M. R. Monteiro, C. L. Kugelmeier, R. S. Pinheiro, et al. Glycerol from biodiesel production: Technological paths for sustainability, Renewable and Sustainable Energy Reviews, 88, 109-122 (2018).
[3] Diao, H., Santodonato, L.J., Tang, Z. et al. Local Structures of High-Entropy Alloys (HEAs) on Atomic Scales: An Overview, 67, 2321ï 2325 (2015)

AN EFFICIANT HETEROGENOUS CARBON-BASED PHOTOCATALYST FOR SELECTIVE SULFIDE OXIDATION TO SULFOXIDES

Augustina JozeliÎnaitā[1], Edvinas Orentas[1]

[1] Department of Organic Chemistry, Vilnius University, Lithuania
augustina.jozeliunaite@chgf.vu.lt

Oxidation of sulfides plays a significant role in numerous fields such as wastewater treatment, chemical warfare agent disposal, fossil fuels desulfurization and preparation of various pharmaceuticals. Therefore, the tremendous effort has been made to develop chemoselective transformation of sulfides to sulfoxides. Most common synthetic approaches rely either on hazardous oxidizing agents like peroxides and hypervalent iodine reagents, require expensive and toxic transition metals as catalysts or photosensitizers such as Rose Bengal, Eosin Y, Bodipy, etc. Nevertheless, poor chemoselectivity and low catalytic activity still limit their prospective application [1].

Visible-light mediated metal-free heterogenous catalysts have been extensively pursued in hopes of enabling more efficient and environmentally sustainable chemical transformations. Hence, we propose unmodified fullerene soot and fullerene C_{60} nanodispersion as a low-cost heterogenous photocatalysts for chemoselective sulfides oxidation to sulfoxides in ethanol without further overoxidation to sulfones. Since C_{60} is well-known good electron acceptor and is easily excited by blue light, the photooxidation can take place by two different mechanisms: either by excited C_{60} state generating singlet oxygen or by an electron-transfer mechanism employing triplet oxygen.

The fullerene soot possesses the huge advantage amongst other reusable catalyst because it can be easily recovered by simple filtration and reused many times without losing its intrinsic properties. Additionally, it does not require any modification or catalyst immobilization onto heterogenous supports such as resins or insoluble polymers, it is available from multiple suppliers and is very cheap. In addition, larger scale reactions were carried out in excellent yields using a flow reactor with a non-immobilized heterogenous fullerene soot.

The wider applicability of fullerene nanodispersion as a heterogenous photocatalyst was successfully demonstrated in radical cyclization, boronic acid oxidation and imine formation reactions [2].

[1] D.-Y. Zheng, E.-X. Chen, C.-R. Ye, X.-C. Huang, High-efficiency photo-oxidation of thioethers over C60@PCN-222 under air, J. Mater. Chem. A, **7**, 22084-22091 (2019).

[2] A.Jozeliunaite, D. Valceckas, E. Orentas, Fullerene soot and a fullerene nanodispersion as recyclable heterogeneous off-the-shelf photocatalysts, RSC Adv, **11**, 4104-4111 (2021).

INVESTIGATION OF INITIAL GROWTH RATE OF DIELECTRICAL THIN FILMS DEPOSITED BY ATOMIC LAYER DEPOTION

Mantas Drazdys[1], Darija Astrauskytã[1], Ramutis Drazdys[1]

[1]Microoptical components laboratory, Center for Physical Sciences and Technology, Lithuania
mantas.drazdys@ftmc.lt

Continuous development of lasers and laser technologies create higher requirements for optical components and thin film coatings. Thin films can be deposited by using variety of methods including physical vapour deposition (PVD), sol-gel techniques, sputtering and chemical vapour deposition. However, with the decreasing size of optics and increasing demand for complex 3D shape optical substrates atomic layer deposition (ALD) became one of the promising technologies that could be used for manufacturing of optical coatings.

ALD is based on the principle of self-limiting sequential chemical reactions between gas-phase precursors and a surface. The self-limiting growth mechanism allows accurate thin film thickness control even on more complex 3D substrates. As ALD is a chemical deposition method, the quality and properties of resulting films are dictated by the precursor and surface reactions [1].

The initial growth rate of layer is a key factor in manufacturing precise ultrathin films whose accuracy define the characteristics of optical coatings. It has been shown that depending on the surface species, on which film is being deposited, the initial growth rate might vary. This variation can be observed during the first 10 to 30 cycles [2]. These variations of growth rate do not have a significant impact on average thickness precision of thicker films. However, while deposition ultrathin films, the variation of initial growth rate can result in apparent discrepancy of final thickness precision.

In this work we investigated the initial growth of HfO_2, TiO_2, Ta_2O_5 and Al_2O_3 thin films on various surface species by using ALD thermal process and in-situ quartz crystal microbalance (QCM) monitoring. Each ALD cycle consisted of four steps which were as follows: metalorganic precursor pulse, purge, water pulse, purge (Fig. 1). For this investigation we used metalorganic precursors and deionized water to deposit films at 120 and 150 .

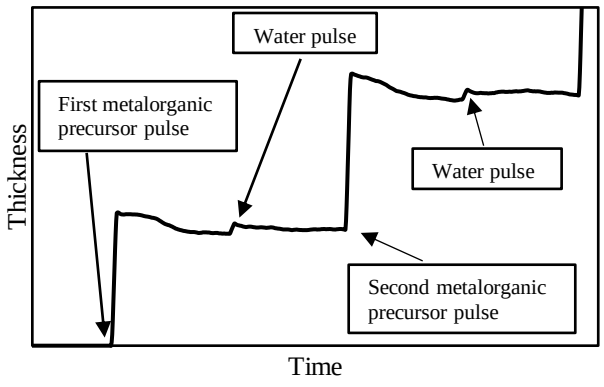

Fig. 1. QCM measurements of two ALD cycles.

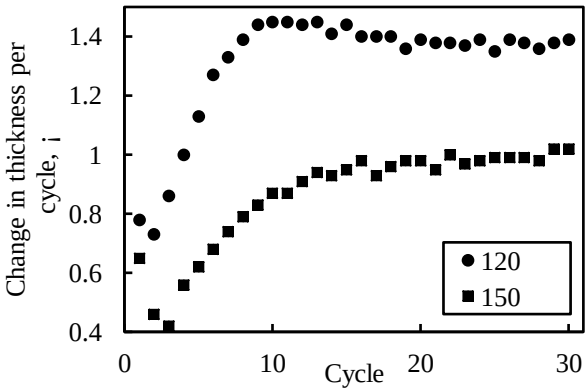

Fig. 2. HfO_2 growth on SiO_2.

Experimental investigation led to conclusions, that in some cases the initial growth rate can be more than twice lower compared to the stable growth rate (Fig. 2). On the contrary, when deposition Ta_2O_5, Al_2O_3 sublayer barely influences the initial growth rate. We found that in most cases linear growth of thin films begins after 10 ï 15 cycles.

[1] H. Tiznado et al., TiO_2 and Al_2O_3 ultra-thin nanolaminates growth by ALD; instrument automation and films characterization, Rev. Mex. Fis. **58**, 459-465 (2012).
[2] C. W. Wiegand et al., Understanding the growth mechanisms of multi-layered systems in atomic layer deposition process, Chem. Mater. **30**, 1971-1979 (2018).

O7-2

DID NOT PARTICIPATE

PHOTOPHYSICAL PROPERTIES OF PYRIMIDINE-BASED TADF EMITTERS

Kamilã Bareikaitã[1], Rokas Skaisgiris[1], Jelena Dodonova[2], Sigitas Tumkeviļius[2], Saulius Jurģãnas[1]

[1] Institute of Photonics and Nanotechnology, Faculty of Physics, Vilnius University, Lithuania
[2] Institute of Chemistry, Faculty of Chemistry and Geosciences, Vilnius University, Lithuania
kamile.bareikaite@ff.stud.vu.lt

Organic light emitting diodes (OLEDs) are devices of great potential and interest. However, 75% of electrically injected charge in the OLED ends up in non-emissive triplet states. Triplets can be harvested through the mechanism of thermally activated delayed fluorescence (TADF), where thermal energy is exploited to upconvert triplets to emissive singlet state. As a result, it is possible to achieve up to 100% internal efficiency, without the use of any heavy metals as it is usual in efficient phosphorescent devices [1]. To achieve efficient TADF, the energy gap between the lowest singlet and triplet states (ΔE_{ST}) should be minimized, this is usually reached by spatially separating the HOMO and LUMO states in charge transfer compounds, composed of electron donor and acceptor [2].

In this work, photophysical properties of new pyrimidine-based emitters were investigated - a pyrimidine acceptor with a tert-butyl carbazole donor attached to it at different places (fig. 1). Standard photophysical properties analysis was conducted - absorption, emission, time-resolved fluorescence experiments - in air or vacuum and in room temperature as well as 50K. The obtained data revealed that attaching donor at different positions leads to emission wavelength shift from 483 nm in compound CP2 to 437 nm in compound CP6. Moreover, the molecule with donors at the *ortho* and *meta* positions (CP2) shows the smallest ΔE_{ST} gap (135meV) while for the other compounds it was above 250meV. This may be the result of sterically crowding of donor units leading to larger twist angles and in turn larger separation of HOMO ï LUMO orbitals [3]. The reduced ΔE_{ST} led to CP2 having the largest amount of delayed emission ï 68% compared to 58% and 20% for compounds CP4 and CP6, respectively. The origin of delayed fluorescence was attributed to TADF emission due to being quenched in low temperature of 50 K (fig 1. decay kinetic).

In conclusion, carefully selecting the point of attachments for donor units can lead to superior TADF emission properties.

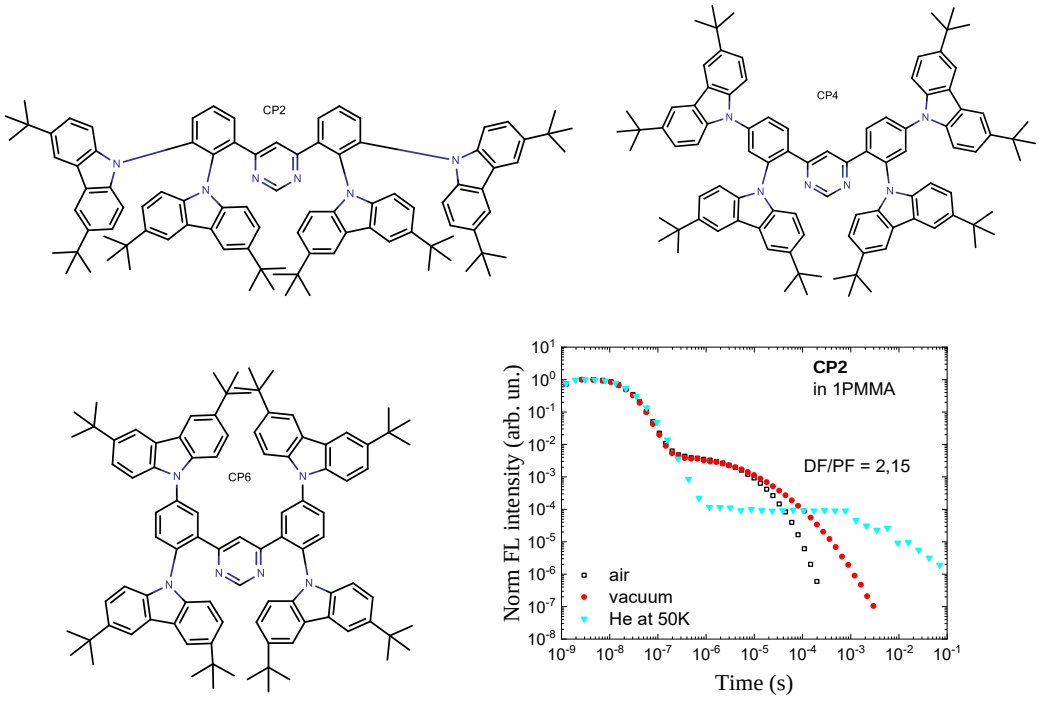

Fig. 1 Pyrimidine ï carbazole TADF compounds analyzed in this work and the decay kinetics of compound CP2 in 1 wt% PMMA films at room temperature in air and vacuum ambient and at 50 K temperature.

[1] K. Goushi, K. Yoshida, K. Sato, C. Adachi, Organic light-emitting diodes employing efficient reverse intersystem crossing for triplet-to-singlet state conversion, Nature Photonics **6**, 253ï 258 (2012).
[2] F. B. Dias et al., Photophysics of thermally activated delayed fluorescence molecules, Methods and Applications in Fluorescence **5**, 012001 (2017).
[3] T. Sereviļius, R. Skaisgiris, J. Dodonova, L. Jagintaviļius, J. Buceviļius, K. Kazlauskas, S. Jurģãnas, S. Tumkeviļius, Emission wavelength dependence on the rISC rate in TADF compounds with large conformational disorder, Chemical Communications **55**, 1975-1978 (2019).

OPTICAL MODULATION OF MONO AND BI-LAYER GRAPHENE

Rusnė Ivaškevičiūtė-Povilauskienė[1], Dalius Seliuta[1], Alesia Paddubskaya[2], Domas Jokubauskis[1], Linas Minkevičius[1], Andrzej Urbanowicz[1], Ieva Matulaitienė[3], Lina Mikolišiūnaitė[3], Gintaras Valušis[1]

[1] Department of Optoelectronics, Center for Physical Sciences and Technology, Lithuania
[2] Institute for Nuclear Problems, Belarusian State University, Belarus
[3]Department of Organic Chemistry, Center for Physical Sciences and Technology, Lithuania
rusne.ivaskeviciute@ftmc.lt

Terahertz (THz) imaging systems are currently one of the most attractive topics in optoelectronics. As all systems active elements are getting smaller, passive optical components as well required to be more compact. In this case optical properties and compactness of graphene makes it suitable for this application. To make a functional diffractive element, graphene requires to absorb THz radiation. Since it is almost completely transparent in this frequency range, grapheneõs transmittance can be controlled by using chemical, electrical or optical doping [1].

In this work optical modulation is chosen as contactless method.

Three types of samples were fabricated in order to investigate optical modulation of mono and bi-layer graphene. As graphene is not a free-standing material, it was transferred on silicon (Si) substrate, which is transparent in THz range. Therefore, the first sample is a single graphene layer on Si. The second sample is two graphene layers on Si which were transferred one by one. The third sample is pure Si wafer which served as a reference to the first two samples.

Optical modulation was achieved by using pumping laser to generate free carriers in Si substrate. Carriers are transferred to graphene layer and due to its higher carrier mobility, grapheneõs transmittance of THz radiation is reduced [2].

In order to evaluate modulation depth of all three samples, transmittance spectra were measured using THz frequency-domain spectrometer. Spectra are depicted in Fig. 1. Results showed that due to photoexcitation, the modulation depth of bi-layer graphene goes up to 42%.

Photo-modulation features of graphene-on-silicon prepared using different technological approaches will be discussed in details.

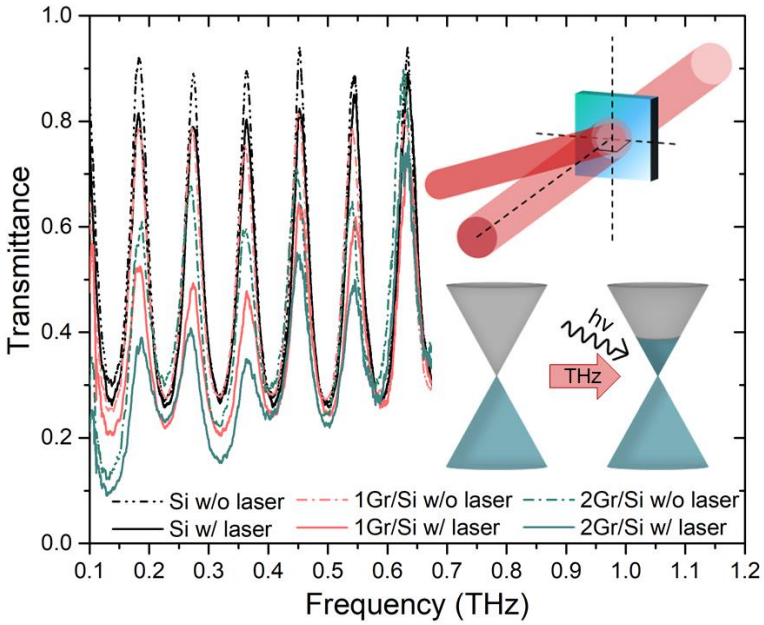

Fig. 1. Transmittance spectrum of Si and different graphene layers. Inset depicts optical modulation scheme and grapheneõs Dirac cones before and after photoexcitation.

[1] R. Binder, *Optical Properties of Graphene* (University of Arizona, USA, 2016).
[2] M. Fu, X. Wang, S. Wang, Z. Xie, S. Feng, W. Sun, J. Ye, P. Han, Y. Zhang, Efficient terahertz modulator based on photoexcited graphene, Opt. Mater. **66**, 381-385 (2017).

CHARGE CARRIER TRANSPORT IN CLOSE TO REAL WORKING CONDITIONS OF ORGANIC SOLAR CELLS

Rokas JasiÎnas[1], Vidmantas Jaġinskas[1], Huotian Zhang[2], Feng Gao[2], Vidmantas Gulbinas[1]

[1]Department of Molecular Compound Physics, Center for Physical Sciences and Technology, Saulãtekio av. 3, LT-10257 Vilnius, Lithuania

[2]Department of Physics Chemistry and Biology (IFM), Linköping University, Linköping SE-58183, Sweden

rokas.jasiunas@ftmc.lt

Ever since organic photovoltaic devices have been introduced to scientific community decades ago, debates about underlaying physics of charge transport ignited and continue to flourish to this day. Charge carrier mobility is one of the main parameters determining carrier extraction and recombination. Thus, not surprising that complex and still poorly understood it becomes the center of debates.

It has been demonstrated in several publications that charge carrier mobility in an active layer of the organic solar cell decreases with time after photogeneration by several orders of magnitude [1-5]. On the other hand, there are also works showing that steady-state mobility analysis can be successfully applied to organic photovoltaic devices[6-9]. Recently, it was argued that carrier mobility in operating solar cells is indeed constant and that transient methods showing time-dependent carrier mobility, such as transient photocurrent, where the sample is excited by a short laser pulse, are inadequate because carrier traps remain almost empty [10]. While under constant Solar illumination carrier traps become populated, therefore mobility does not decrease while the carrier is drifting.

In this work, we have experimentally investigated carrier extraction dynamics in TQ1:$PC_{71}BM$, one of a standard model of polymer-fullerene solar cells, and highly effective non-fullerene acceptor based PBDB-T:Y1 organic photovoltaic devices. We employed several transient methods, covering the wide temporal window from ps to Õs, and numerical modelling to address carrier transport in close to real working conditions of a solar cell. To evaluate the role of trapped carriers, we compared carrier extraction dynamics under excitation of samples by weak laser pulses when trap states were nonpopulated and with additional 1 Sun illumination populating the trap states.

We showed that mobility decay during initial carrier drift is the same when carriers are either continuously generated by steady-state illumination or by a short laser pulse. Nevertheless, steady-state illumination alters carrier transport in Õs timescale differently, depending on active layer materials. For fullerene-based device, continuous illumination repeals mobility decay present in case of periodic excitation; however, in highly effective non-fullerene devices due to extremely low trap population mobility decay in Õs timescale is marginal in both cases.

[1] Deviġis, A.; Serbenta, A.; Meerholz, K.; Hertel, D.; Gulbinas, V. Ultrafast Dynamics of Carrier Mobility in a Conjugated Polymer Probed at Molecular and Microscopic Length Scales. *Phys. Rev. Lett.* **2009**, *103* (2), 027404.

[2] Jasiunas, R.; Zhang, H.; Yuan, J.; Zhou, X.; Qian, D.; Zou, Y.; Deviġis, A.; Sulskus, J.; Gao, F.; Gulbinas, V. From Generation to Extraction: A Time-Resolved Investigation of Photophysical Processes in Non-Fullerene Organic Solar Cells. *J. Phys. Chem. C* **2020**,

[3] Melianas, A.; Pranculis, V.; Deviġis, A.; Gulbinas, V.; Inganª s, O.; Kemerink, M. Dispersion Dominated Photocurrent in Polymer:Fullerene Solar Cells. *Adv. Funct. Mater.* **2014**, *24* (28), 4507ï 4514.

[4] Abramaviļius, V.; Amarasinghe Vithanage, D.; Deviġis, A.; Infahsaeng, Y.; Bruno, A.; Foster, S.; Keivanidis, P. E.; Abramaviļius, D.; Nelson, J.; Yartsev, A.; Sundstrº m, V.; Gulbinas, V. Carrier Motion in As-Spun and Annealed P3HT:PCBM Blends Revealed by Ultrafast Optical Electric Field Probing and Monte Carlo Simulations. *Phys. Chem. Chem. Phys.* **2014**, *16* (6), 2686.

[5] Augulis, R.; Deviġis, A.; Peckus, D.; Gulbinas, V.; Hertel, D.; Meerholz, K. High Electron Mobility and Its Role in Charge Carrier Generation in Merocyanine/Fullerene Blends. *J. Phys. Chem. C* **2015**, *119* (11), 5761ï 5770.

[6] Mihailetchi, V. D.; Xie, H. X.; de Boer, B.; Koster, L. J. A.; Blom, P. W. M. Charge Transport and Photocurrent Generation in Poly(3-Hexylthiophene): Methanofullerene Bulk-Heterojunction Solar Cells. Adv. Funct. Mater. **2006**, 16 (5), 699ï 708.

[7] Bartelt, J. A.; Lam, D.; Burke, T. M.; Sweetnam, S. M.; McGehee, M. D. Charge-Carrier Mobility Requirements for Bulk Heterojunction Solar Cells with High Fill Factor and External Quantum Efficiency >90%. Adv. Energy Mater**. 2015**, 5 (15), 1500577.

[8] Bartesaghi, D.; Pérez, I. del C.; Kniepert, J.; Roland, S.; Turbiez, M.; Neher, D.; Koster, L. J. A. Competition between Recombination and Extraction of Free Charges Determines the Fill Factor of Organic Solar Cells. Nat. Commun. **2015**, 6 (1), 7083.

[9] Proctor, C. M.; Love, J. A.; Nguyen, T.-Q. Mobility Guidelines for High Fill Factor Solution-Processed Small Molecule Solar Cells. Adv. Mater. **2014**, 26 (34), 5957ï 5961.

[10] Le Corre, V. M.; Chatri, A. R.; Doumon, N. Y.; Koster, L. J. A. Charge Carrier Extraction in Organic Solar Cells Governed by Steady-State Mobilities. Adv. Energy Mater. **2017**, 7 (22), 1701138.

GROWTH AND INVESTIGATION OF Bi-CONTAINING COMPOUND *PIN* STRUCTURES

Nerijus JurkÎnas[*1, 2], Algirdas Jasinskas[1], Simona PÎkienã[1], Arnas Pukinskas[1, 2], Andrius Biļiînas[1], Bronislovas Ļechaviļius[1], Virginijus Bukauskas[1] and Renata Butkutã[1, 2]

[1]Optoelectronics Dept., Center for Physical Sciences and Technology, Saulãtekio av. 3, LT-10257 Vilnius, Lithuania
[2]Faculty of Physics, Vilnius University, Saulãtekio av. 9, III building, LT-10222 Vilnius, Lithuania
nerijus.jurkunas@ff.stud.vu.lt

The last decade huge interest in devices, operating in telecommunication wavelengths window (from 1 εm to 1.5 εm) was observed. Traditionally the active area of such components is fabricated using heterostructures of A3-B5 semiconductor compounds, such as InGaAsP or InGaAlAs. These devises are sensitive to temperature, and stabilization of parameters require external coolers [1]. To obviate disadvantages and fulfill the main requirements for semiconductors technologies - high efficiency and low costs, the performances of components must be improved. This could be achieved replacing usual heterostructures by new more attractive material.

GaAsBi, namely bismide alloy, exhibit unique physical properties, including a large energy bowing effect, less temperature sensitive bandgap, large SO split energy and negligible influence on electron and hole mobility. The partial substitution of As by larger Bi atoms into the lattice of GaAs allows to reduce the band gap from 60 meV to 88 meV for Bi% [2, 3]. Theoretic outlook of bismide compounds attracts attention of scientists working in both material engineering as well research and commercial device application directions. Several attempts to fabricate bismide-based near infrared (NIR) sources, light emitting diodes (LEDs) and laser diodes (LDs), were demonstrated in Ref. [4-6].

This study aims to growth technology and complex investigation of multiple quantum well (MQW) structures for LEDs exhibiting luminescent properties in spectral range from 1 εm to 1.5 εm. A new concept of LED design was proofed. Combining two earlier demonstrated by our group ideas [7, 8], *pin* structures with insulating layer cotaining Bi quantum dots in the wells sandwiched by parabolic quantum barriers were fabricated. The optimization of MQWs was performed by MBE, varying Bi content, QW and barrier thickness, *in-situ* annealing temperature and time. Photoluminescence and voltage-current measurements of MQW structures and LEDs have been carried out to evaluate the optical and electrical properties and served as a feed-back for epitaxy optimum conditions mapping. The complex characterization of samples (see Fig. 1) permitted to reveal the dominating recombination mechanisms in bismides MQWs, and define key parameters influencing to LEDs performances.

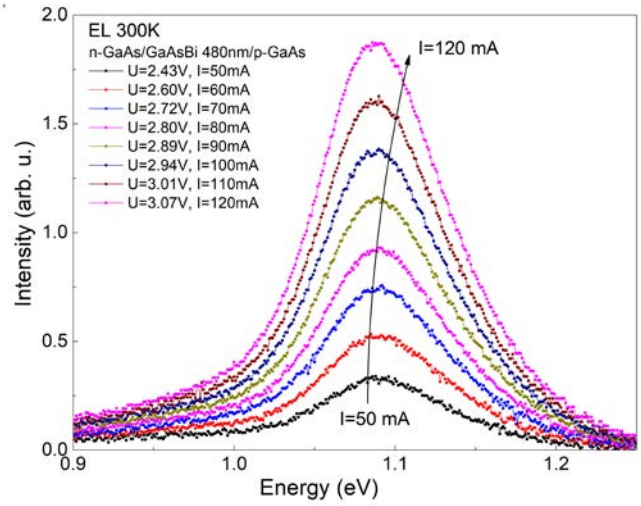

Fig. 1. Room temperature electroluminescence spectra measured for GaAsBi based pin structure using different injection currents.

[1] Hiroyuki Ichikawa, et al., Analysis of GaInAsP Laser Diodes Degraded by Light Absorption at an Active Layer of the Facet Electronics and Communications in Japan, 93, No. 2, p.32 (2010).
[2] Kunishige Oe, et al., New Semiconductor Alloy $GaAs_{1-x}Bi_x$ Grown by Metal Organic Vapor Phase Epitaxy, Jpn. J. Appl. Phys., **37**, L1283 (1998).
[3] K. Bertulis, et al., GaBiAs: A material for optoelectronic terahertz devices, Appl. Phys. Lett. **88**, p. 201112 (2006).
[4] Robert Douglas Richards, et al., Telecommunication wavelength GaAsBi light emitting diodes, IET Optoelectron., **10**, Iss. 2, p. 34 (2016).
[5] Ludewig, P., et al., Electrical injection Ga(AsBi)/(AlGa) as single quantum well laser, Appl. Phys. Lett., **102**, (24), p. 242115 (2013).
[6] R. Butkutã et al., Multi quantum well Ga(AsBi)/GaAs laser diodes with more than 6% of bismuth, ELECTRONICS LETTERS, **50**, No. 16 p. 1155ï 1157 (2014).
[7] R. Butkutã et al., AlAs as a Bi blocking barrier in GaAsBi multi-quantum wells: structural analysis, Lithuanian Journal of Physics **57** (1), 2 (2017); R. Butkutã et al., Bismuth quantum dots in annealed GaAsBi/AlAs quantum wells, Nanoscale research letters, **12**, 436, 3 (2017).
[8] S PÎkienã et al., Enhancement of photoluminescence of GaAsBi quantum wells by parabolic design of AlGaAs barriers, Nanotechnology, Vol. 30, p. 455001 (2019).

CRYSTALLOGRAPHY-BASED MODELLING OF THE INTER-PIGMENT INTERACTION IN THE FUCOXANTHIN–CHLOROPHYLL PROTEIN COMPLEX

Austėja Mikalčiūtė[1], Andrius Gelžinis[1,2], Jevgenij Chmeliov[1,2]

[1]Institute of Chemical Physics, Faculty of Physics, Vilnius University, Lithuania
[2]Department of Molecular Compound Physics, Centre for Physical Sciences and Technology, Lithuania
austeja.mikalciute@ff.stud.vu.lt

Photosynthesis is undoubtedly one of the most important biochemical interactions in nature, which allows for the coexistence of countless life forms. Organisms, which carry out photosynthesis, have adapted to live in various ecological niches throughout the millions of years of evolution, which has resulted in roughly the same amount of net primary production executed on land and in water. Diatoms are a wide-spread species of algae, that performs approximately 20% of photosynthesis on Earth. Diatoms have a unique light-harvesting complex – fucoxanthin-chlorophyll protein (FCP), which has such chromophores as chlorophyll (Chl) *c* or fucoxanthin, that are not present in light-harvesting complexes in higher plants. These exceptional chromophores enable diatoms to survive in water, where penetrated light is mostly in the blue-green visible region. FCP complexes are not only responsible for light harvesting, but their chromophores also participate in the quenching of the photosystem in order to minimize the damage done by intensive light and therefore serves as an interesting research material due to systematic differences in their mechanisms from light harvesting complexes of higher plants.

Only in 2019 two crystallographic structures of FCP were determined from *Phaeodactylum triconutum* [1] and *Chaetoceros gracilis* [2]. In this work interaction energy by point dipole approximation was calculated for various Chl *a* and *c* pairs in FCP monomers and FCP-A tetramer from the determined crystallographic structures. Transition dipole moment was formed in the direction from N_B to N_D atom (representing direction of the Chl Q_y transition) and the center of the dipole was chosen the Mg atom in the center of porphyrin ring of chlorophylls. Results of the study indicate that for chromophore pairs present in all monomers interaction energy is really similar (Fig. 1), however, differences occur, when additional pigments are present in some of the monomers. These additional pigments interact strongly with some chlorophylls in the system. Strong interactions between chlorophyll *c* and chlorophyll *a* align well with the results from spectroscopic data [3]: there is a fast energy transfer channel (50 fs) from Chl *c* to Chl *a*. Notwithstanding, that does not have an impact on Q_y peak position in absorption spectra and differences in absorption strength can be explained by the amount of pigments present in the monomer. Currently the chromophores of FCP are being modelled using Density Functional Theory and it is hoped that these calculations will provide some new insights about the system in the near future.

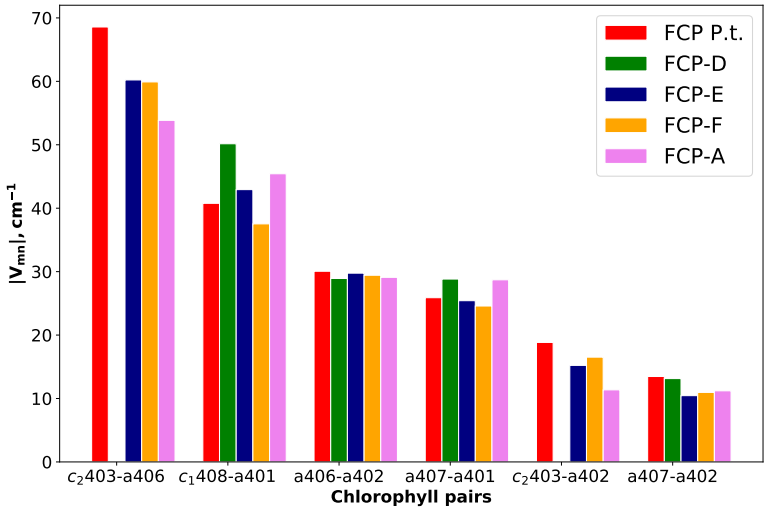

Fig. 1. Interaction energies comparison of some chlorophyll pairs in different FCP monomers

[1] W. Wang et al., Structural basis for blue-green light harvesting and energy dissipation in diatoms, Science, **363**, 1–8 (2019).
[2] X. Pi et al., The pigment-protein network of a diatom photosystem II–light-harvesting antenna supercomplex, Science, **365**, 1–10 (2019).
[3] A. Gelžinis et al., Confronting FCP structure with ultrafast spectroscopy data: Evidence for structural variations, Physical Chemistry Chemical Physics, **23**, 806-821, 2021.

OUTDOOR AND INDOOR LEVELS OF BLACK CARBON IN AN URBAN ENVIRONMENT

Daria Pashneva, Julija Pauraite, Agnã Minderytã, Vadimas Dudoitis,
Kristina Plaugkaitã, Inga Garbarienã, Lina Davulienã, Steigvilã Byl enkienã

Department of Environmental Research, Center for Physical Sciences and Technology, Vilnius, Lithuania
daria.pashneva@ftmc.lt

Black carbon (BC) is the most strongly light absorbing component of particulate matter (PM) with short atmospheric lifetime (on the order of a few days to weeks) and thus BC not only has impacts on climate change but also has the potential to affect human health. The main sources of BC in urban environments come from incomplete combustion of fossil fuels and biomass burning. Due to its small size (less than 2.5 ε m), BC can be inhaled deep into the lungs reaching alveoli and penetrate bloodstream causing cardiovascular, respiratory and other diseases [1, 2]. In the modern world, people spend 90% of their time indoors (home, offices etc.) where energy-efficient buildings can create risks for indoor air quality and health [3]. This study aims to investigate influence of outdoor-to-indoor exchange to indoor levels of BC. Continuous real-time measurements of optical absorption by aerosol particles were investigated in the urban region of Vilnius during the cold period (from October to December 2020). Equivalent black carbon (eBC) mass concentration was measured by an Aethalometer (Magee Scientific, model AE-31). The optical transmission of carbonaceous aerosol particles was measured sequentially at 7 wavelengths (ə= 370, 470, 520, 590, 660, 880 and 950 nm), where the eBC mass concentration was derived from the light absorption coefficient ($ů_{ab}$) at a 880 nm wavelength.

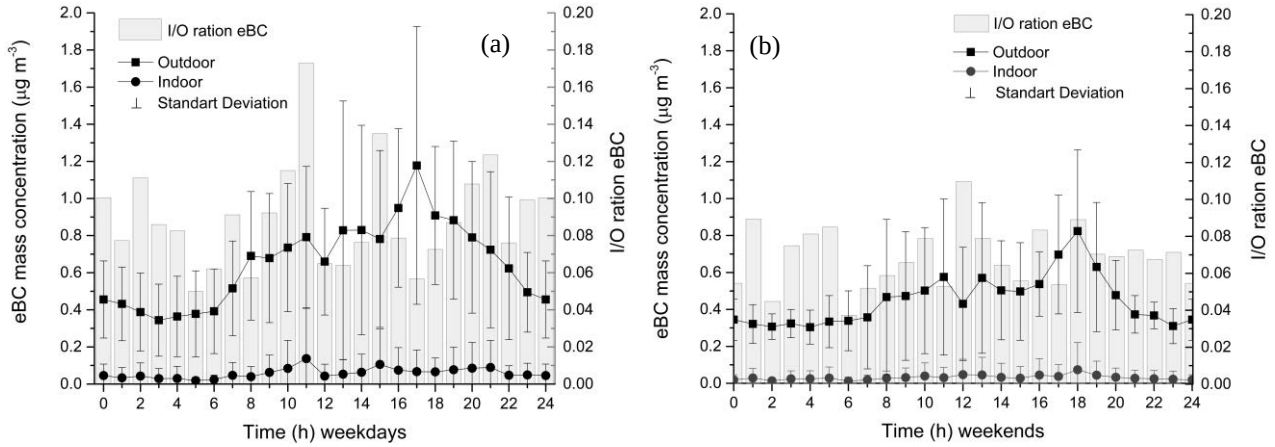

Fig. 1. Daily cycle of outdoor and indoor eBC mass concentration for (a) weekdays and (b) weekend.

The results (figure 1 (a, b)) show a moderate influence of outdoor eBC emissions on the indoor eBC level. The weekend levels of eBC mass concentration were lower than in weekdays. Hourly mean mass concentrations of eBC for weekdays and weekends shows daily cycles, this can be explained by periodicity of traffic intensity and heating activities. The highest outdoor eBC mass concentrations (1.2 μg m^{-3}) were observed between 16:00 and 18:00. Mean indoor/outdoor (I/O) ratios of the eBC mass concentration for the entire measurement period (calculated on a sample-by-sample basis) were found to be 0.12 (standard deviation - 0.26).

[1] U.S. EPA, ñReport to Congress on Black Carbon,ò Dep. Inter. Environ. Relat. Agencies Appropriations Act, 2010, no. March, p. 388, 2012, [Online]. Available: https://www3.epa.gov/airquality/blackcarbon/2012report/fullreport.pdf.

[2] S. K. Pani, S. H. Wang, N. H. Lin, S. Chantara, C. Te Lee, and D. Thepnuan, ñBlack carbon over an urban atmosphere in northern peninsular Southeast Asia: Characteristics, source apportionment, and associated health risks,ò Environ. Pollut., vol. 259, Apr. 2020, doi: 10.1016/j.envpol.2019.113871.

[3] E. Cheek, V. Guercio, C. Shrubsole, and S. Dimitroulopoulou, ñPortable air purification: review of impacts on indoor air quality and health,ò Sci. T 2020

IN SITU $GdPO_4$:Eu HYDROTHERMAL SYNTHESIS IN WOODS MATRIX

Monika Baublytė[1], Ramūnas Skaudžius[1], Edita Gargaitė[2]

[1]Department of Inorganic Chemistry, Faculty of Chemistry, Vilnius University, Naugarduko st. 24, LT- 03225 Vilnius
[2]Wood Science and Engineering, Luleå University of Technology, Forskargatan 1, 931 87 Skellefteå, Sweden
monika.baublyte@mb.vu.lt

Wood is one of the most abundant building materials used in residential and non-residential buildings, furniture constructions, and decoration. Due to high sustainability, thermal and electrical insulating properties and aesthetics, wood demand is increasing every year [1].

Nevertheless, the wood used in listed industries, require high resistance to mechanical and chemical damage. One of the main challenges is resistance to fire - retardancy. At highly elevated temperatures wood burns producing flammable volatiles which are followed by ignition and flame spread across the surface increasing the rate of heat transfer to deeper layers of wood. Scientists are creating materials to encounter minor issue – usually organic compounds (phosphorus-based, phosphorus-nitrogen, phosphorus-halogen compounds) are used to impregnate the wood, though, it can produce toxic volatile compounds during pyrolysis. Growing awareness of the toxicity of such compounds leads to further investigation of new materials, systems and methods which could improve wood retardancy. This work proposes an inorganic $GdPO_4$ compound produced by in situ hydrothermal synthesis in woods matrix as a new alternative and innovative method to increase retardancy [2-4].

Samples of soft wood were prepared by in situ hydrothermal synthesis at 110ºC initially retaining wood in a vacuum and later introduced to precursor solutions of $GdNO_3·6H_2O$/$EuNO_3·6H_2O$ (VNP) and $NH_3H_2PO_4$ (VPN). Characteristics of samples after synthesis were observed by scanning electron microscopy (SEM), optical properties (Fig. 1) were used to determine if wood surface contains the desired ceramics, thermogravimetric (TG) analysis was performed to inspect $GdPO_4$ impact on woods retardancy.

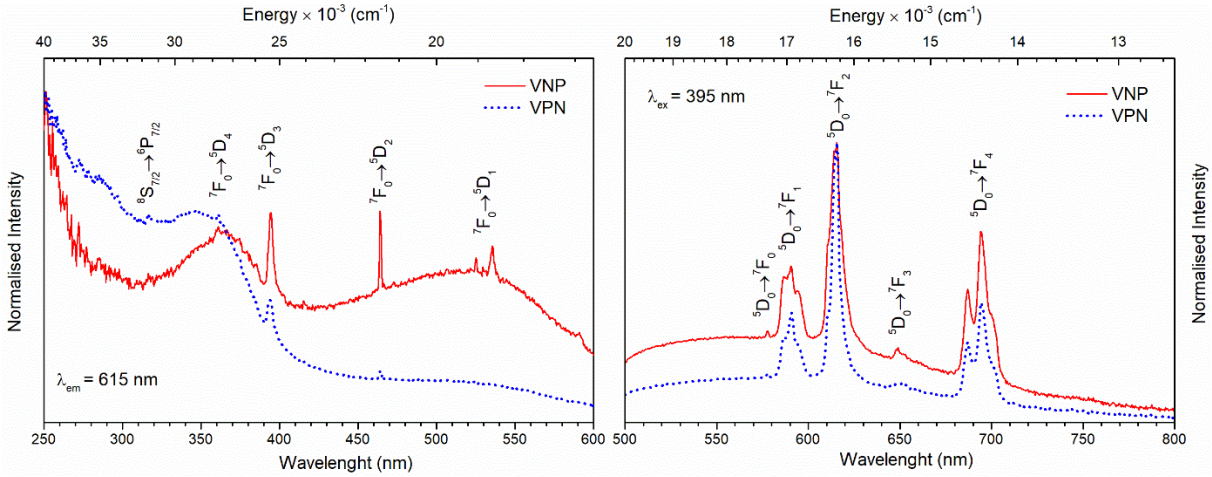

Fig. 1. Excitation and emission spectra of woods matrix after in situ $GdPO_4$:Eu hydrothermal synthesis.

[1] R. C. Pettersen, The Chemical Composition of Wood, The Chemistry of Solid Wood **207**, 57–126 (1984).
[2] M. Nikolaeva and T. Kärki, A Review of Fire Retardant Processes and Chemistry, with Discussion of the Case of Wood-plastic Composites, Balt. For. **17** 13 (2011).
[3] F. Lionetto, R. Del Sole, D. Cannoletta, G. Vasapollo, and A. Maffezzoli, Monitoring Wood Degradation during Weathering by Cellulose Crystallinity, Materials **5**, 10 1910–1922 (2012).
[4] L. A. Lowden, T. R. Hull. Flammability Behaviour of Wood and a Review of the Methods for its Reduction, Lowden and Hull Fire Science Reviews **2** (2013).

NOVEL HYBRID ORGANIC-INORGANIC PEROVSKITE WITH PROTONATED UNSYMMETRICAL DIMETHYLHYDRAZINE ï SYNTHESIS AND PHYSICOCHEMICAL CHARACTERIZATION

Jan Albert Zienkiewicz[1], Dorota Kowalska[1], Katarzyna Fedoruk[2], Mariusz StefaCski[1], Adam Pikul[1], Maciej Ptak[1]

[1] Institute of Low Temperature and Structure Research, Polish Academy of Sciences, Ok· lna 2 str., 50-422 Wroclaw, Poland

[2] Institute of Physics, Wrocğaw University of Technology, WybrzeÕe WyspiaCskiego 27, 50-370 Wrocğaw, Poland

j.zienkiewicz@intibs.pl

One of the subclasses of metal-organic frameworks (MOFs) with very interesting physicochemical properties are metal-formates templated by ammonium ions. They are classified as hybrid organic-inorganic perovskites (HOIPs), because most of them adopt perovskite-like architecture, described by general formula $AB(HCOO)_3$, where sites A and B and are occupied by an ammonium ion and metal ion (i.e. Mn^{2+}, Co^{2+}, Ni^{2+} or Zn^{2+}), respectively [1].

Depending on their structure and crystal symmetry, there are known examples of formate HOIPs that exhibit luminescent, ferroelastic, ferroelectric, dielectric, magnetic or multiferroic properties. Our particular attention was caught by amines with varying number of methyl groups.

An increasing number of methyl groups affects the steric hindrance, order of hydrogen bonds and thus crystal structure and physicochemical parameters, such as phase transitions (PTs) temperatures or ferroic ordering. For example, manganese(II) hydrazinium formate, **[Hy]Mn(HCOO)$_3$**, is a multiferroic material, which crystallizes in the orthorhombic *Pna*2$_1$ space group. At 355 K, it undergoes PT to the *Pnma* centrosymmetric phase [2]. The methylhydrazinium analogue, **[MHy]Mn(HCOO)$_3$**, experiences two PTs upon cooling, i.e., at 310 K from dynamically disordered high-temperature (HT) $R\bar{3}c$ phase to the partially ordered room-temperature (RT) ferroelectric *R*3*c* phase and at 224 K to the *P*1 phase. The ferroelectric nature of the RT phase was confirmed by pyroelectric measurements [3]. It is worth emphasizing that the methylhydrazinium cation was recently shown to be an interesting agent that can be used as a templated cation or spacer in design of novel non-centrosymmetric 3D or 2D lead halide perovskites [4,5].

In view of the above, the 1,1-dimethylhydrazinium cation caught our huge attention. In presented work, synthesis and physicochemical properties of 1,1-dimethylhydrazinium analogue, **[DMHy]Mn(HCOO)$_3$** (Fig. 1.), are described and compared to results obtained for hydrazinium and methylhydrazinium analogues. The title compound has been investigated using methods of differential scanning calorimetry (DSC), Raman, infrared (IR) and UV-VIS spectroscopy, powder and single-crystal X-Ray diffraction (XRD), magnetic measurements and broadband dielectric spectroscopy (BDS).

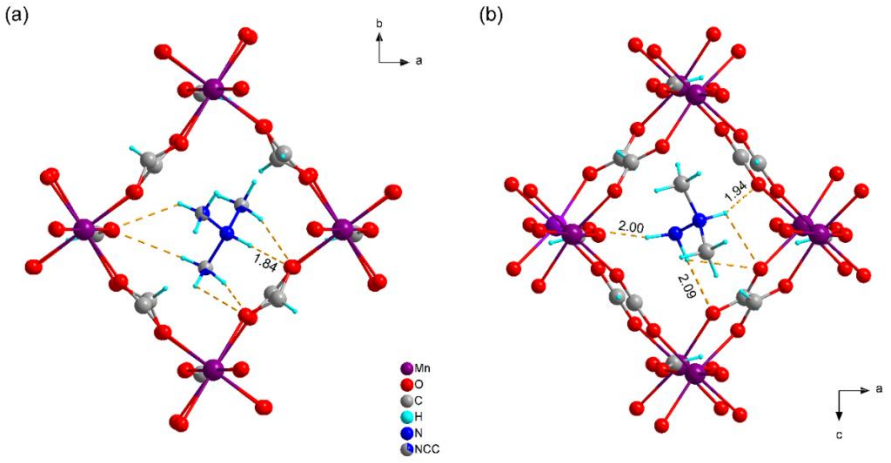

Fig. 1. The details of the crystal structure of room temperature (a) and low temperature (b) phase. The dashed lines designate Nï HïO hydrogen bonds (lengths given in ¡)

[1] G.P. Nagabhushana, R. Shivaramaiah, A. Navrotsky, Thermochemistry of multiferroic organic-inorganic hybrid perovskites $[(CH_3)_2NH_2][M(HCOO)_3]$ (M = Mn, Co, Ni, and Zn), J. Am. Chem. Soc. **137**, 10351ï 10356 (2015).

[2] S. Chen, R. Shang, K.L. Hu et al., $[NH_2NH_3][M(HCOO)_3]$ (M = Mn^{2+}, Zn^{2+}, Co^{2+} and Mg^{2+}): structural phase transitions, prominent dielectric anomalies and negative thermal expansion, and magnetic ordering, Inorg. Chem. Front. **1**, 83ï 98 (2014)

[3] M. MĹczka, A. GĹgor, M. Ptak, et al., A. Phase Transitions and Coexistence of Magnetic and Electric Orders in the Methylhydrazinium Metal Formate Frameworks, Chem. Mater. **29**, 2264ï 2275 (2017)

[4] M. MĹczka, M. Ptak, A. GĹgor, et al., A. Methylhydrazinium Lead Bromide: Noncentrosymmetric Three-Dimensional Perovskite with Exceptionally Large Framework Distortion and Green Photoluminescence, Chem. Mater. **32**, 1667ï 1673 (2020)

[5] M. MĹczka, A. GĹgor, J.K. Zarľba, et al., A. Three-Dimensional Perovskite Methylhydrazinium Lead Chloride with Two Polar Phases and Unusual Second-Harmonic Generation Bistability above Room Temperature, Chem. Mater. **32**, 4072ï 4082 (2020)

COMPUTATIONAL AND EXPERIMENTAL VIBRATIONAL STUDY OF 1-CHLOROMETHYL-1-FLUOROSILACYCLOHEXANE CONFORMATIONS AND ITS REARRANGEMENTS

Joanna Stocka[1], Rasa Platakytė[1], Justinas Ceponkus[1], Valdas Sablinskas[1], Gamil A. Guirgis[2], Paweł Rodziewicz[3]

[1] Chemical Physics Institute, Vilnius University, Saulėtekio al. 3, 10257 Vilnius, Lithuania
[2] Department of Chemistry and Biochemistry, College of Charleston, Charleston, SC 29424, USA
[3] Institute of Chemistry, Jan Kochanowski University, 15G świętokrzyska St., 25-406, Kielce, Poland
joana.stocka@gmail.com

Organosilicon compounds are rather attractive in the field of surface science. Cyclic hydrocarbon films have good surface adhesion properties which are mostly related to a ´ electron orbital[1]. Substituting one carbon atom in the ring with a silicon atom enhances adhesion since it acts as hydrolytically sensitive center that can react with inorganic substrates such as glass to form stable covalent bonds[2]. 1-chloromethyl-1-fluorosilacyclohexane is a newly synthesized cyclic organic compound with unknown structural parameters and conformational diversity.

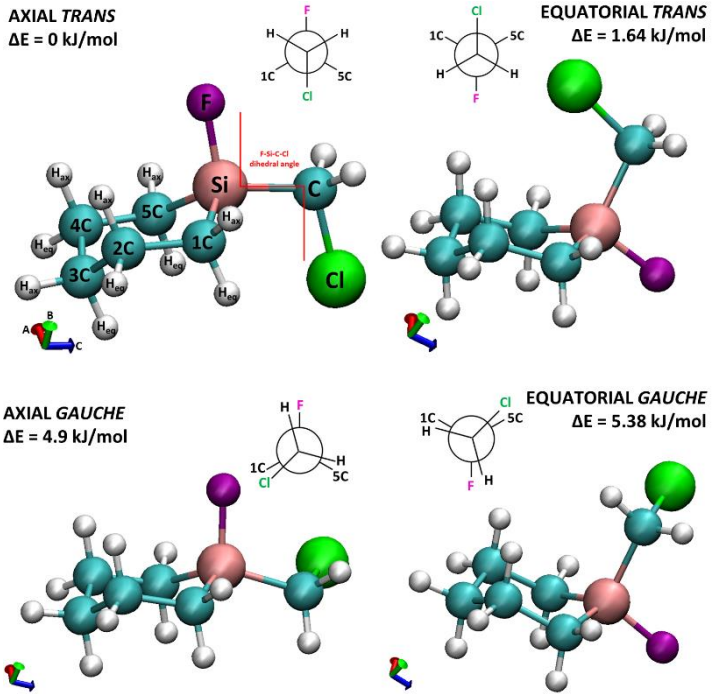

Fig. 1. Structures of four lowest energy conformers of 1-chloromethyl-1-fluorosilacyclohexane and the respective DFT/B3LYP relative energies. The F-Si-C-Cl dihedral angle change is shown as Newman projection. Internal axes are marked as: A (red), B (green), C (blue).

Several different vibrational spectroscopy methods were employed to analyze the properties of this molecule. Infrared and Raman spectra were recorded for the sample in liquid phase. Additionally, IR absorption spectra were registered in gaseous phase and as low temperature solid with the molecules isolated in argon and nitrogen matrices. In order to control thermodynamic equilibrium between the conformers hot nozzle technique was used during the deposition of the gaseous matrix mixture.. DFT calculations were performed utilizing B3LYP functional and augmented Dunning correlation-consistent valence double zeta basis set. The 1-fluoro-1-chlormethyl-silacyclohexane molecule can reveal twelve conformations out of which the chair-axial-trans one has the lowest energy. However, there are also three two more chair type conformers that are stable enough to possibly be observed in experimental spectra.

[1] H. Butt, K Graf, M. Kappl, Physics and Chemistry of Interfaces, Wiley, 2003
[2] J. Ceponkus, V. Sablinskas, V.Aleksa, M.Pucetaite, R.Platakyte, C.W.Reed, C.Cotter, G.Guirgis, Vibrational Spectroscopy, 81, 136-143, 2015

MODELING OF STRUCTURAL AND PHOTOPHYSICAL PROPERTIES OF AN OPTICAL PROBE IN AQUEOUS AND MEMBRANE ENVIRONMENTS

Sridhar Hariharaputran, Arul Murugan Natarajan, Zilvinas Rinkevicius, Patrick Norman

Faculty of Mathematics and Natural Sciences, Department of Physics, Kaunas University of Technology, StudentÔ str. 50, LT-51368 Kaunas, Lithuania,
Division of Theoretical Chemistry and Biology, KTH Royal Institute of Technology, Stockholm, Sweden
sryjyo@gmail.com

Motivation: Gram-negative bacteria causing chronic and biofilm associated infections have become resistant to multiple drugs and is a concern across the globe. It is of paramount importance to develop diagnostic agents and curative molecules for combating such bacterial infections. **Problem:** To develop such molecules suitable for diagnosis and therapy, bacterial membrane /envelope serves as a suitable target and it is important to understand the interactions of bacterial envelopes to small molecules to design drugs and to develop microbial coatings. Theoretical and experimental studies in the past decades have discovered and analysed the structure of gram-negative bacteria. Results from these studies lead to the understanding that the shape and structure of the outer membrane has a significant role in drug design that can penetrate the impermeable membrane.[1] Another key topic of relevance is to design molecules suitable for bacterial imaging. Many molecular probes have been developed and optical probes are one of the diagnostic agents and in this imaging is done by fluorescent tracers that target or illuminate bacteria. **Our approach:** involves building membrane models to analyse small organic molecules interaction with Gram-negative bacterial cell membranes. The basic membrane complex models are built using CHARMM-GUI web-based platforms. Based on the previous research works on gram-negative bacteria we developed membrane systems using heterogeneous lipid combinations consisting of POPE (phosphatidylethanolamine) and POPG (phosphatidylglycerol) lipids following the steps in the platform. Further molecular dynamics simulations were performed. The trajectories from the production run were used for further analysis. Next is to study the structure of vancomycin and fluorescein tagged vancomycin within membrane and to study the photophysics of vancomycin and fluorescein tagged vancomycin when they are bound to membrane compared to in aqueous environment. Further aim is to study conformational dynamics and optical properties of fluorescein tagged vancomycin in water and in the membrane environment. **Results:** During the simulation of 100 ns time scale, the fluorescein tagged vancomycin able to bind to the membrane and get inserted suggesting that the studied vancomycin tagged fluorescein can become a potential molecular probe for membrane imaging. Further, structural properties of the systems such as area per lipid, volume, density, electron density and other properties were analysed. We also aim to carry out QM/MM calculations as implemented in Veloxchem[2] for the probe in the water and membrane environment to study its optical properties.

Lipid type	System	Upper Leaflet	Lower Leaflet	Total number of Lipids
POPE:POPG	1:1	21:21	21:21	42:42
POPE:POPG	3:1	33:11	33:11	44:44
POPE:POPG	5:1	40:08	40:08	48:48
POPE:POPG		41:123	41:123	164:164

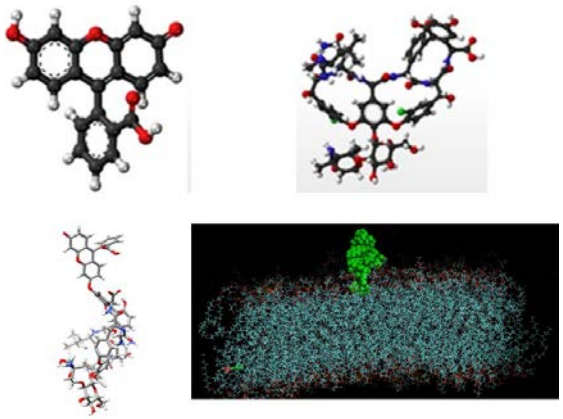

Figure. 1 (**A**). Summary of different membrane systems using heterogeneous lipids (**B**). Top - Fluorescein, Vancomycin, Bottom: Fluorescein tagged vancomycin, Probe binding to the membrane.

Conclusions: Through understanding the photophysical (absorption, fluorescence) properties of optical probes in a membrane-like environment, we can optimize them in a way that they can be used to probe membrane structure.

Acknowledgements: The work has been partly performed under the Project HPC-EUROPA3 (INFRAIA-2016-1-730897), with the support of the EC Research Innovation Action under the H2020 Programme; the first author gratefully acknowledges the support of KTH Royal Institute of Technology, Department of Theoretical Chemistry and Biology S-106 91 Stockholm, Sweden and for the computer resources and technical support provided by PDC centre for High Performance Computing at KTH, Sweden, Kaunas University of Technology. The Swedish National Infrastructure for Computing (SNIC), Sweden, National Supercomputer Centre (NSC) at Link° ping University, Sweden, Funding agencies ï Research Council of Lithuania (LMT), European Structural Funds, Government of the Republic of Lithuania.

Correspondence address: murugan@theochem.kth.se , zilvinas.rinkevicius@ktu.lt, panor@kth.se

[1] Hariharaputran S et al., *In:* Medical Physics in the Baltic States / [ed] Adliene, D, KTU Press, 2019, p. 102-104
[2] Rinkevicius Z et al., WIREs Computational Molecular Science, 10:e:1457, 2020

HYPERSPECTRAL UNMIXING: ALGORITHMS REVIEW AND BENCHMARKING

Vytautas Paura[1], Virginijus Marcinkevičius[1]

[1]Institute of Data Science and Digital Technologies, Vilnius University, Lithuania
vytautas.paura@mif.stud.vu.lt

Hyperpsectral imaging is an emerging technology used in remote sensing for acquiring images on hundreds of spectral bands at the same time. Often hyperspectral cameras have a small spatial resolution compared to RGB cameras, which often creates mixed pixels. Hyperpsectral unmixing algorithms aim to estimate the pure spectral pixels and their abundances in hyperspectral imagery. Developed unmixing algorithms are used to solve three main steps of the spectral unmixing problem: 1) accurately estimating the possible endmembers in a hyperspectral image or dataset; 2) finding the spectral signatures in the extracted endmembers; 3) calculating the abundances of each endmember in all of the pixels of a hyperspectral image.

Many of the available spectral unmixing algorithms are not capable of performing all of the main unmixing steps or struggle to do so resulting in an inadequate unmixing accuracy. While using an algorithms capable of completing all three steps with high enough accuracy greatly reduces errors between steps, integration and development times. Many of the available algorithms fall into three main categories:

- Sparse regression models. E. g.: CLSUnSAL [1] an upgraded algorithm based on *alternating direction method of multipliers* that achieved a signal reconstruction error (SRE) score on synthetic data of 21.47 dB and 8.79 dB for 2 and 6 endmembers respectively (with signal-to-noise ration (SNR) of 40 dB).
- Non-negative matrix factorization. E. g.: TV-RSNMF [2] a blind hyperspectral unmixing algorithm implemented with sparse and total variation regularizers. On synthetic dataset algorithm got spectral angle distance (SAD) of 0.0452 (SNR 10 dB) and 0.0060 (SNR 40 dB).
- Autoencoder networks. E. g.: DeepGUn [3] a network made from generative adversarial network and variational autoencoders to use spatial and spectral information of a hyperspectral cube. Reconstruction root mean squared error (RMSE) metric was used to test the performance of this algorithm and a value of 0.0448 was achieved on a synthetic dataset.

Many of these algorithms not only use different base methods to solve the unmixing problem but also these authors create different methodologies and datasets (e.g. synthetic data created from USGS spectral library [5]) to test their methods against each other, because a standardised experiments and universal datasets are not available. This creates a problem when trying to compare the algorithms against each other and trying select the best quality algorithms for any of the three steps. In turn selecting and improving the best available unmixing algorithm is difficult.

In this paper we review the most popular and newest hyperspectral unmixing algorithms, and create a standardised algorithm testing methodology to benchmark hyperpsctral unmixing algorithms. To accurately compare them, the algorithms are tested using three different metrics and five different datasets to more accurately asses the performance of solving any of the three unmixing problems. Used datasets: 1) an artificially created dataset in a laboratory [4]; 2) synthetic dataset create from USGS spectral library [5]; 3) IEEE GRSS 2018 data fusion contest hyperspectral dataset; 4) USGS created Cuprite dataset; 5) USGS created Urban dataset. The metric that are used: RMSE; SAD; SRE. In this paper an experiment using this methodology is conducted to test the algorithm robustness to a change in a number of endmembers and the results of this experiment will be presented.

[1] M. Iordache, J. M. Bioucas-Dias, and A. Plaza, "Collaborative sparse regression for hyperspectral unmixing," IEEE Transactions on Geoscience and Remote Sensing, vol. 52, no. 1, pp. 341–354, 2014.

[2] W. He, H. Zhang, and L. Zhang, "Total variation regularized reweighted sparse nonnegative matrix factorization for hyperspectral unmixing," IEEE Transactions on Geoscience and Remote Sensing, vol. 55, no. 7, pp. 3909–3921, 2017.

[3] R. A. Borsoi, T. Imbiriba, and J. C. M. Bermudez, "Deep generative endmember modeling: An application to unsupervised spectral unmixing," IEEE Transactions on Computational Imaging, vol. 6, pp. 374–384, 2020.

[4] M. Zhao, J. Chen, and Z. He, "A laboratory-created dataset with ground-truth for hyperspectral unmixing evaluation, "CoRR, vol. abs/1902.08347, 2019. [Online]. Available: http://arxiv.org/abs/1902.08347

[5] R. F. Kokaly, R. N. Clark, G. A. Swayze, K. E. Livo, T. M. Hoefen,N. C. Pearson, R. A. Wise, W. M. Benzel, H. A. Lowers, R. L. Driscoll, and A. J. Klein, *Usgs spectral library version 7* Reston, VA, Tech.Rep., 2017, report. [Online]. Available: https://doi.org/10.3133/ds1035

CHARACTERIZATION OF BORON NITRIDE QUANTUM DOTS SYNTHESIZED BY A SINGLE STEP HYDROTHERMAL METHOD

Rugilė Lukaševičiūtė[1,2], Lena Golubewa[2,3], Renata Karpicz[2]

[1] Department of Physics, Vilnius University, Lithuania
[2] Department of Molecular Compounds Physics, Center for Physical Sciences and Technology, Lithuania
[3] Department of Nanoelectromagnetics, Institute for Nuclear Physics of BSU, Belarus
rugile.lukaseviciute@gmail.com

Quantum dots (QDs) exhibit extraordinary optical and physical properties, and, thus, have proven themselves in various fields of research including bio-imaging, biological labeling, drug delivery, photocatalyst, electrical devices and sensors [1].

One of the most promising types of QDs are boron nitride quantum dots (BNQDs), as they exhibit the unique physical and chemical properties [2], including excellent mechanical strength, high thermal stability, luminescent properties, large surface area, superb oxidation resistance, which provide extremely high drug-loading capacity, making them good candidates for various bio-medical applications. Therefore, significant attention has been paid recently towards the synthesis and fabrication of stable non-toxic BNQDs with controllable and scalable properties.

In this work BNQDs were synthesized via hydrothermal treatment of the mixture of boric acid and ammonia solution at 200ÁC for 12 h. Two-step purification was performed: (i) the large tracts were removed via filtration through 0,22 Õm microporous membrane, (ii) solvent replacement for water was provided via evaporation at RT. The final solution was a stable transparent suspension without visible agglomerates. The spectroscopic properties of synthesized BNQDs solution were investigated by using steady-state and Raman spectroscopy. From UV-vis spectrum, the maximum absorption wavelength of BNQDs was found to be 265 nm as shown in Fig. 1. The wide emission peak is located at 430 nm under 375-nm excitation. Fluorescence quantum yield of BNQDs was calculated using Stilbene 420 as a reference and is about 6%.

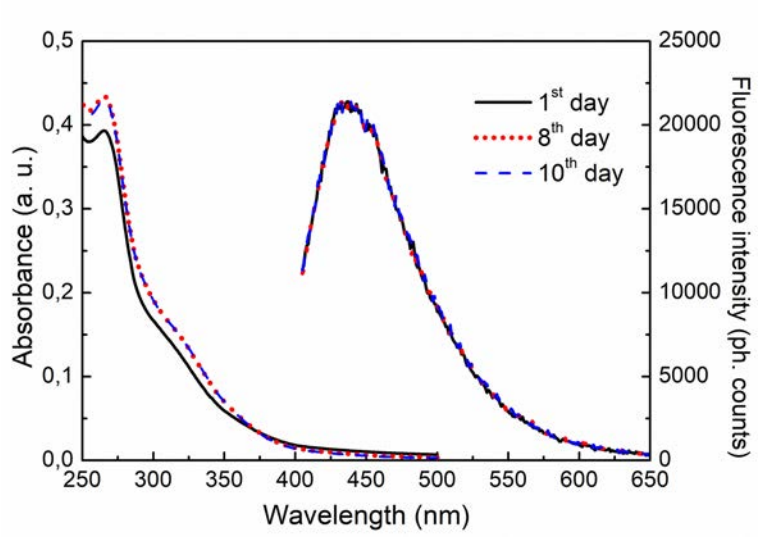

Fig. 1. Absorption and fluorescence spectra of the BNQDs water solutions. Excitation wavelength λ_{ex} = 375 nm, emission range λ_{em} = 390-650 nm.

Due to specific hexagonal BN atomic structure, anticancer drugs of the quinone-like structure are among the most suitable therapeutic agents that could be effectively delivered inside the cancer cell with BNQD „shuttle“. Thus, synthesized BNQDs will be used further for optically guided delivery of quinone drugs and their subsequent controllable release inside the cancer cells.

[1] R. Jerome, Ashok K. Sundramoorthy, Hydrothermal Synthesis of Boron Nitride Quantum Dots/Poly(Luminol) Nanocomposite for Selective Detection of Ascorbic Acid, J. Electrochem. Soc. **166**, B3017 (2019).
[2] C.R. Dean, A.F. Young, I. Meric, C. Lee et al., Boron nitride substrates for high-quality graphene electronics, Nat. Nanotechnol. **5**, 722-726 (2010).

EFFECTS OF NEBULIZED CALCIUM NITRITE CONCENTRATION ON A LASER-INDUCED PLASMA EMISSION AND PARAMETERS

Cristina M®ndez-L· pez[1], Luis Javier Fern§ndez-Men®ndez[1], Cristina Gonz§lez-Gago[1], Jorge Pisonero[1], Nerea Bordel[1]

[1] Department of Physics, University of Oviedo, Spain
mendezcristina@uniovi.es

The determination of halogens is a challenging task in Laser-Induced Breakdown Spectroscopy because these species have low excitation efficiencies, with their most intense emission lines being in vacuum-UV. Different strategies have been developed to increase sensitivity of detection, either involving the use of a noble gas atmosphere or the detection of molecular emission from species that recombine in the plasma (i.e. halogen and an alkaline earth metal). A particular case would be the detection of fluorine via emission of CaF [1]. However, this requires the sample to contain the alkaline earth metal; in order to surpass this circumstance, a nebulization method was developed. This method introduces calcium on a F-containing sample by directing a Ca-containing solution aerosol towards the laserôs incidence spot. [2].

The physical effects of the nebulization components (i.e. Ar carrier, ultrapure water matrix, Ca nitrite solution) were later studied in a sequential manner on a F-free model sample (Cu), observing a strong alteration of the plasma plume shape and emission when the aqueous Ca-solution was introduced [3]. These studies were done with spatio-temporal resolution along the vertical axis of the plasma.

In the present work, with the purpose of further characterize the effects on the plasma, a double-detection experimental set-up was implemented. This way, a high-resolution spectrometer with both diffraction gratings and a mirror is used for precise spatio-temporal measurements while the overall emission (spatial and temporally integrated) is collected via optical fiber into a broad-range (200-600 nm) non-gated spectrometer. This double system can be used to monitor overall changes on the plasma while a specific parameter is studied. A schematized view of the complete experimental set-up is shown in Figure 1.

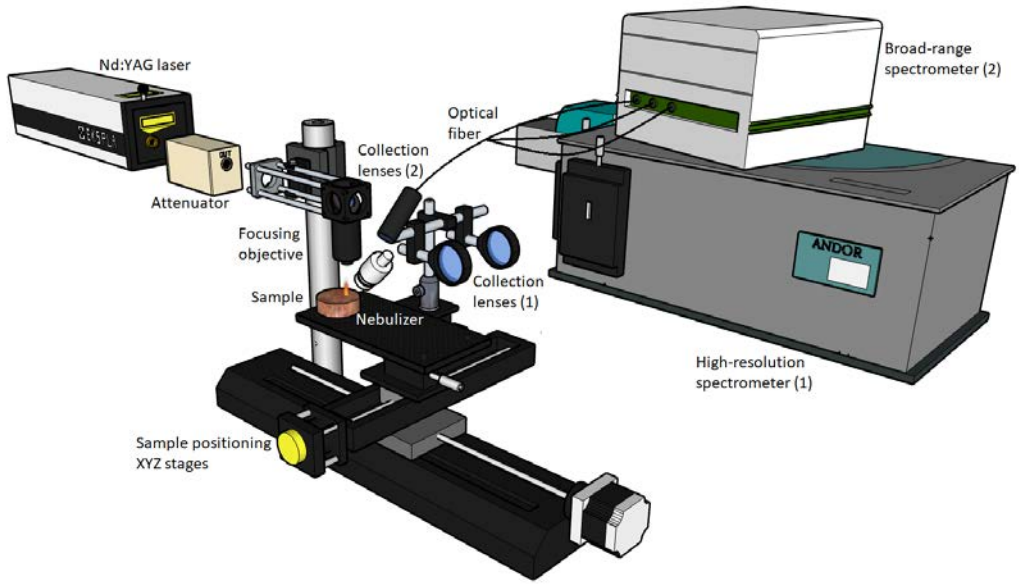

Fig. 1. Main elements of the experimental set-up

The studies carried out to characterize the nebulization effect on the plasma were performed for different Ca-solution concentrations (ranging from 0% to 15%) as well as without nebulization, as reference. As a first step, the double system was used to obtain excitation temperatures from both detection systems. One of them requires multiple spectra to cover all the wavelength exposures necessary to collect all emission lines, while the other allows for a full spectrum at each shot. Afterwards, electronic densities were obtained via Stark-widening of H-alpha emission line while monitoring the full emission. The results show a decrease on excitation temperatures that is dependent on the increasing amount of Ca and an alteration of the electronic density in the plasma, regarding both spatial distribution and numerical values.

[1] C. Ćlvarez-Llamas, J. Pisonero and N. Bordel. Quantification of fluorine traces in solid samples using CaF molecular emission bands in atmospheric air laser-induced breakdown spectroscopy. Spectrochim. Acta ï Part B: At. Spectrosc., **123** (2016) 157-162.
[2] C. Ćlvarez-Llamas, J. Pisonero and N. Bordel. A novel approach for quantitative LIBS fluorine analysis using CaF emission in calcium-free samples. J. Anal. At. Spectrom. **32.1** (2017) 162-166
[3] C. M®ndez-L· pez, R. Ćlvarez-Garc²a, C. Ćlvarez-Llamas, et al. Laser Induced plasmas at different nebulization conditions: spatio-temporal distribution of emission signals and excitation temperatures. Spectrochim. Acta ï Part B: At. Spectrosc., **170** (2020) 105906

MEASURING THE VECTOR OF A MAGNETIC FIELD USING A DIAMOND CRYSTAL.

Reinis Lazda[1], Laima Bušaite[1], Florians Gahbauers[1], Andris Bērziņš[1], Mārcis Auziņš[1]

[1]Laser Centre, University of Latvia
reinis.lazda@lu.lv

In this work we are using nitrogen–vacancy (NV) centers (Fig. 1 Left) in diamond to measure the vector [1] (magnitude and direction) of a magnetic field.

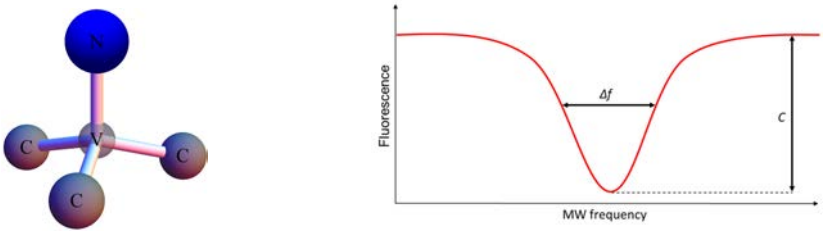

Fig. 1. Left: NV center, a C_{3v} symmetric structure in a diamond crystal carbon lattice consisting of a carbon atom substituting nitrogen atom and a lattice vacancy adjacent to it. Right: Continuous wave ODMR magnetic field measurement sensitivity.

The sensitivity of a magnetic field measurement [2] can be estimated by the following relation:

$$\eta_{sensitivity} \approx \frac{\Delta f}{C\sqrt{N_P}}. \tag{1}$$

The main parameters are Δf - the full width at half maximum (FWHM), C - the optically detected magnetic resonance (ODMR) contrast, N_P - the number of received photons per second (see Fig. 1 Right).

This work is focused on creating a compact magnetometer prototype device (with a magnetic field sensitivity on the order of 100 pT/Hz$^{1/2}$) as a part of a feasibility study project with the European Space Agency (see Fig. 2).

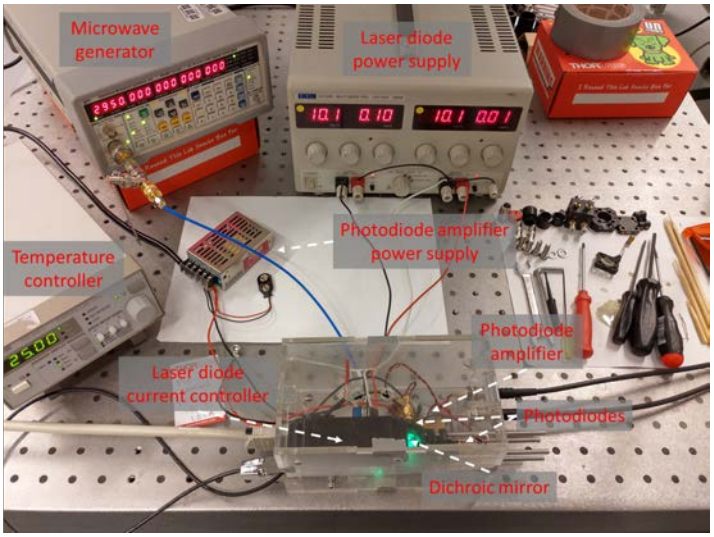

Fig. 2. Experimental setup showing a compact optical system design (laser excitation, fluorescence collection and microwave delivery) encased in a small volume.

Acknowledgements

We acknowledge the financial support from the Base/Performance Funding Project Nr. ZD2010/AZ27, AAP2015/B013 of the University of Latvia. This activity is carried out under a programme of, and funded by, the European Space Agency, ESA Contract No. 4000129670/20/NL/SC, "Feasibility study of spacecraft magnetometers based on nitrogen-vacancy centres in diamond". The view expressed in this publications can in no way be taken to reflect the official opinion of the European Space Agency.

[1] Jennifer M. Schloss, John F. Barry, Matthew J. Turner, and Ronald L. Walsworth, Phys. Rev. Applied **10**, 034044 (2018).
[2] John F. Barry, Jennifer M. Schloss, Erik Bauch, Matthew J. Turner, Connor A. Hart, Linh M. Pham, and Ronald L. Walsworth, Rev. Mod. Phys. **92**, 015004 (2020).

HEPN-MNT TOXIN-ANTITOXIN SYSTEM AS A PROPOSED BACTERIAL ATP SENSOR

Songailiene Inga[1], Juozapaitis Jonas[1], Tamulaitiene Giedre[1], Ruksenaite Audrone[1], Ġulį ius Sigitas[2], Sasnauskas Giedrius[1], Venclovas Į eslovas[1], Ġikėnys Virginijus[1]

[1] Institute of Biotechnology, Life Sciences Center, Vilnius University, Lithuania
[2] Laboratory of Algology and Microbial Ecology, Nature Research Centre, Vilnius, Lithuania
inga.songailiene@bti.vu.lt

Prokaryotic toxin-antitoxin systems (TA) are composed of a toxin, capable of interfering with key cellular processes, and its neutralizing antidote, the antitoxin.

Here, we focus on the HEPN-MNT TA system encoded in the vicinity of a I-D CRISPR-Cas system in cyanobacterium *Aphanizomenon flos-aquae*. MNT stands for minimal nucleotidyltransferase, while HEPN represents a group of higher eukaryotes and prokaryotes binding domain-proteins, mostly known as active RNases [1],[2]. We showed that HEPN toxin acts as an RNase with an unusual target specificity and cleaves off 4 nt from the 3Ń end in a subset of tRNAs, thereby interfering with translation [3].

Moreover, we found that the MNT antitoxin inhibits HEPN RNase through enzymatic reaction. MNT performs covalent di-AMPylation (diadenylation) of a conserved tyrosine Y109 residue in the active site loop of HEPN toxin. Furthermore, we present crystallographic snapshots of the di-AMPylation reaction at different stages that explain the mechanism of HEPN RNase inactivation. Finally, we propose that HEPN-MNT system functions as a primitive cellular ATP sensor which monitors ATP homeostasis and at low ATP levels releases active HEPN toxin [3].

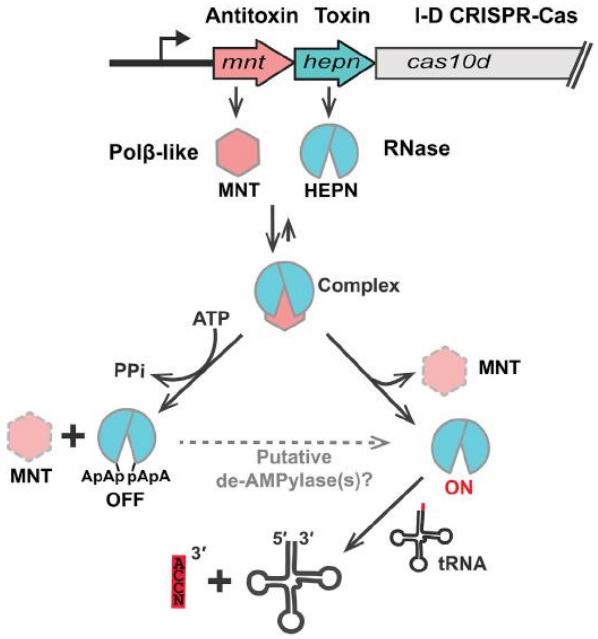

Fig 1. Proposed mechanism of action of *A. flos-aquae* HEPN-MNT toxin-antitoxin system. After translation HEPN and MNT form a toxin-antitoxin (TA) complex. Under normal cellular ATP concentrations, MNT antitoxin di-AMPylates HEPN in the complex resulting in RNase inactivation and TA complex dissociation; released relatively unstable MNT is likely degraded. At low ATP levels caused by phage infection or other stress conditions that change ATP homeostasis, active HEPN RNase remains unmodified and may escape from the complex. Resultant cleavage of 4 nt from the tRNA 3Ń end abolishes aminoacylation and disrupts translation. Alternatively, di-AMPylated HEPN RNase may be reactivated by as yet unknown cellular de-AMPylase(s).

[1] V. Anantharaman, KS. Makarova, AM. Burroughs, EV. Koonin, L. Aravind, *Comprehensive analysis of the HEPN superfamily: identification of novel roles in intra-genomic conflicts, defense, pathogenesis and RNA processing.* Biol Direct. 2013 Jun 15;8:15.doi: 10.1186/1745-6150-8-15.

[2] L. Aravind, EV. Koonin, *DNA polymerase beta-like nucleotidyltransferase superfamily identification of three new families, classification and evolutionary history.* Nucleic Acids Res. 1999 Apr 1;27(7):1609-18. doi: 10.1093/nar/27.7.1609.

[3] I. Songailiene, J. Juozapaitis, G.Tamulaitiene, A.Ruksenaite,1 S. Sulcius, G. Sasnauskas, Į. Venclovas and V. Siksnys, *HEPN-MNT Toxin-Antitoxin System: The HEPN Ribonuclease Is Neutralized by OligoAMPylation*. Mol Cell. 2020 Dec 17;80(6):955-970.e7. doi: 10.1016/j.molcel.2020.11.034.

ACTIVATION OF NUCLEAR FACTOR NF-κB RECOGNITION PROMOTER-CONTROLLED REPORTER GENE TRANSCRIPTION BY PULSED ELECTRIC FIELD TREATMENT IN VIABLE HEP-2C AND CHO-K1 CELLS

Justina Kavaliauskaitė[1], Auksė Kazlauskaitė[1,2], Juozas Lazutka[2], Arūnas Stirkė[1]

[1] Laboratory of Bioelectrics, State Research Institute Center for Physical Sciences and Technology, Lithuania
[2] Bioscience Institute, Life Sciences Center, Vilnius University, Lithuania.
justina.kavaliauskaite@ftmc.lt

A significant number of human disease phenotypes are linked to mutations in over 4000 genes (as per OMIM Gene Map Statistics, 2020). This has created a base for therapeutic strategies that can modify nucleic acids within disease-affected cells, eg., gene therapy, and many genes have been investigated as potential candidates for such strategies. However, effects of transgene medicinal agents depend on the dosage, therefore, both for laboratory and therapeutic applications, a regulated gene expression is a potential requirement. In this context, pulsed electric field technology could be a candidate for non-invasive, biophysical activator of the induction of gene expression.

The aim of this study is to examine the use of microsecond pulsed electric field (μsPEF) stimulation as a proof-of-concept for potential non-ligand physically triggered inducer of gene expression in viable mammalian cells. We report here the response and activation of heterologous transcription system, which consists of NF-κB controlled synthetic promoter and a reporter gene (pNF-κB-SEAP) in viable human cervix carcinoma cells (Hep-2c) and Cricetulus griseus ovarian tissue (CHO-K1) cells. The conditions for treatment were selected based on published data [1, 2]. The rectangular electric pulses with different amplitude, fixed pulse frequency (1 Hz) and pulse duration (100 μs) was used. Results are reported in relative expression of SEAP in folds 24- and 48-hours post-pulsation. The cellular metabolic activity was assessed 24- and 48-hours post-pulsation and was expressed as a percentage relative to the untreated control cells.

pNF-κB-SEAP transfected Hep-2c cell line exposure to μsPEF of 0.25, 0.3 and 0.4 kV/cm resulted in increased levels of relative expression of SEAP (approximately 1.7-fold compared to the control) 24 hours post pulsation. However, μsPEF of 0.165 kV/cm showed the highest peak of relative expression of SEAP in Hep-2c cell line 24 hours post-pulsation – 2-fold in comparison to control. No gene expression activation was detected in Hep-2c cell line 48 hours post-pulsation. Conversely, no activation of gene expression was detected in all experimental setup in CHO-K1 cell line 24 hours post-pulsation, but μsPEF of 0.3 kV/cm resulted in increased levels of relative expression of SEAP (approximately 1.2-fold compared to the control) 48 hours post-pulsation. All experimental setup resulted in high viability of both cell lines.

We conclude the activation of NF-κB in Hep-2c cells is achieved by μsPEF treatment of cell suspension reaching the peak at 0.165 kV/cm 24 hours post-pulsation. The activation of CHO-K1 is achieved at lower levels at 0.3 kV/cm with a time delay and is detected 48 hours post-pulsation. Experimental setup of PEF application does not have a significant impact on viability of treated cells. To our knowledge, this is the first experimental study that demonstrates μsPEF can act as the inducer of target promoter.

[1] Pavlin, M.; Kandušer, M., New Insights into the Mechanisms of Gene Electrotransfer – Experimental and Theoretical Analysis. Sci. Rep. **5**, 9132 (2015).
[2] Šatkauskas, S., André, F., Bureau, M. F., Scherman, D., Miklavčič, D., Mir, L. M., Electrophoretic Component of Electric Pulses Determines the Efficacy of In Vivo DNA Electrotransfer. Hum. Gene Ther., **16 (10)**, 1194-1201 (2005).

NOVEL APPROACH ON APPLICATION OF AN EXTREMOPHILIC RED ALGA *CYANIDIOSCHYZON MEROLAE* IN PHYTOREMEDIATION

Ewa Borowska[1], Mateusz Abram[2], Joanna Kargul[2]

[1] The College of Inter-Faculty Individual Studies in Mathematics and Natural Sciences (MISMaP), University of Warsaw, Poland
[2] Solar Fuels Laboratory, Centre of New Technologies, University of Warsaw, Poland
e.borowska@biol.uw.edu.pl, ewa.borowska86@gmail.com

In our present world, water pollution and bioremediation are among the most important issues facing our society and our planet. Scientists are endeavoring to discover novel methods for removing pollutants from water or clean sludges for safely reusing contaminated waters. Most of these environmental hazards are created in the human sphere, such as acid and metalliferous drainage, which also contain heavy metals. Acidic and eutrophic waters can determine further dangerous conditions for biodiversity as an increase of either biogenic elements or the acidity of ground and sea waters. Organisms, especially those that can thrive in naturally polluted habitats, give us a great possibility to use their features for understanding, cleaning, transforming, and removing toxic processes [1].

One of the possibilities for reducing toxicity of waste is to apply microorganisms in bioremediation. Thus, the best opportunity is to use relevant organisms with a wide spectrum of activity and adaptation to harmful conditions, such as with extremophiles.

Cyanidioschyzon merolae is a red microalgae, one of the most primitive algae in fact, which naturally exist in sulphate-rich hot springs habitat (pH 1.5, at 45 ï 56 ÁC) associated with high heavy metal concentrations [2, 3]. In this research, we present the first steps to assess the bioremediation potential of *C. merolae*. We measured cell survivability in the presence of selected high salt concentrations at two growth temperatures (42 ÁC and 25 ÁC). It is worth mentioning that this research introduces a new cell strain of *Cyanidioschyzon merolae* based on the NIES-1332 strain (Microbial Culture Collection from the National Institute for Environmental Studies (Tsukuba, Japan)), which is adapted to various pH and capable of being an effective growth under pH conditions in the range of 2.5 to 6.7. Likewise, it can be cultivated in temperature ranges of 25 ï 65 ÁC, although the optimal range is 40 ï 42 ÁC.

Our research implies a new facet to cope with such peculiar pollution with a different pH range. This research is based on Patent notification by Polish Patent Office: No. P.432684.

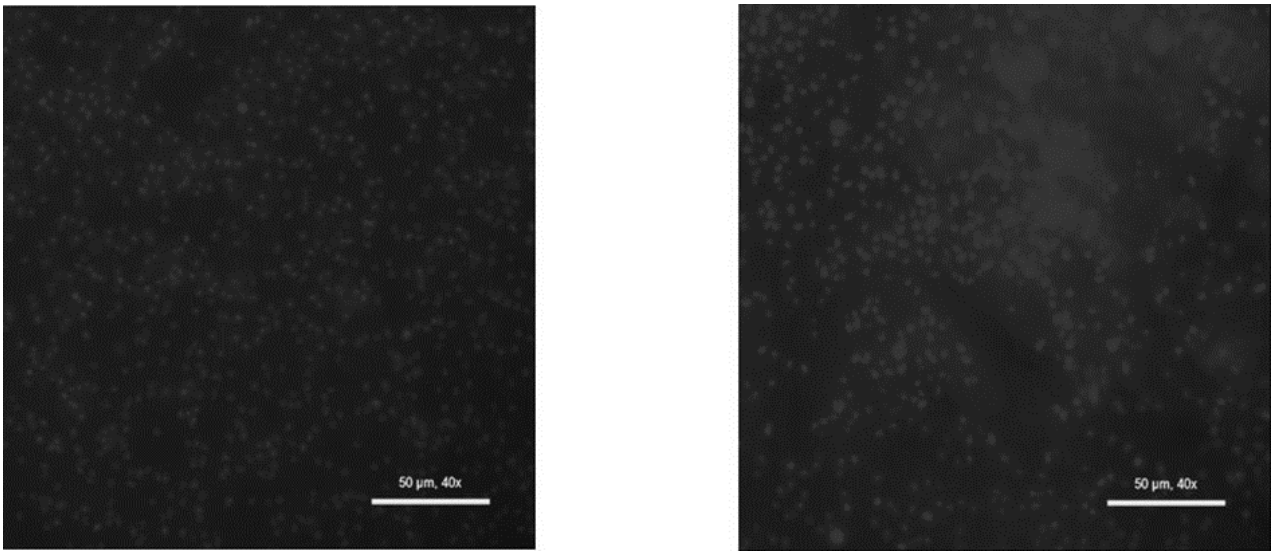

Fig. 1. Fluorescence microscopy images of chlorophyll emissions from *C. merolae* cells cultured at different pH: (a) 2.5 (b) >6.

We discovered important differences between cells in varying pH conditions such as their size and shape shown in Fig. 1. Microscopic analysis was performed via LS720 fluorescence microscope (Etaluma) at 40x magnification and chlorophyll excitation at 580 ï 598 nm. 50 ÕM scale. Both micrographs show the fluorescence of individual chloroplasts in *C. merolae* cells. This shows the cell viability in both cultures.

In summation, this preliminary data and new cell strain open further possibilities of investigation for the bioremediation potential of *C. merolae*.

[1] S. K. Gupta. *Application of Microalgae in Wastewater Treatment* (Springer, Switzerland, 2019).
[2] T. Kuroiwa, et al. *Cyanidioschyzon merolae. A New Model Eukaryote for Cell and Organelle Biology* (Springer, Singapore, 2017).
[3] P. De Luca, et al. *Cyanidioschyzon merolae* a new alga of thermal acidic environments. Journal of Plant Taxonomy and Geography **31** (1978).

INVESTIGATION OF OSMOTIC SHOCK EFFECTS ON YEAST CELL RESPONSES TO PULSED ELECTRIC FIELD TREATMENT

Greta Ganį ytą̄[1], Povilas Ġimonis[1], ArÎ nas Stirką̄[1]

[1] Laboratory of Bioelectrics,
Center for Physical Sciences and Technology,
Saulą̄tekio al. 3, Vilnius, Lithuania
greta.gancyte@gmail.com

Saccharomyces cerevisiae yeasts are single-celled eucaryotic fungus microorganisms. Since ancient times they have been used in baking, winemaking and brewing. They also have been widely used as a model organisms for a number of reasons including similar internal cell and gene structure to higher eukaryotes, fast doubling time and low maintenance requirements [1]. During the course of evolution yeast adapted to employ the HOG pathway to recover after dangerous cell shape modifications and intracellular water disbalance caused by environmental osmotic pressure changes [2]. Pulsed electric field (PEF) treatment is known to cause plasma membrane permeabilization, an effect known as electroporation, yet at the moment there is no information on whether biochemical pathways responsible for intracellular osmotic balance have a role in yeast response to PEF treatment [3].

In this study we investigated if osmotic pressure change has any effect on cell viability and whether HOG pathway plays a role in recovery after PEF treatment. Experiments were performed with wild type Y00000 yeast and a mutant strain derived from WT, Y02724, with no active *HOG1* gene. Yeast from respective strains will be referred as WT and HOG. Cells were grown until 1 OD, transferred to electroporation buffer (20 mM TRIS, 1 M sorbitol, pH = 7.4), yeast suspension was exposed to single electric field pulse with duration of 150 Õs and field strength of up to 10 kV/cm. Electroporation buffer was used as a reference point to represent isoosmotic conditions. After PEF treatment cells were immediately transferred to hyperosmotic (1.5 M sorbitol), isoosmotic or hypoosmotic (0.5 M sorbitol) solution, incubated for 5 minutes and plated on agaric YPD media. Swift osmotic pressure change will be defined as osmotic shock. After two days of incubation in 30 ºC colonies were counted.

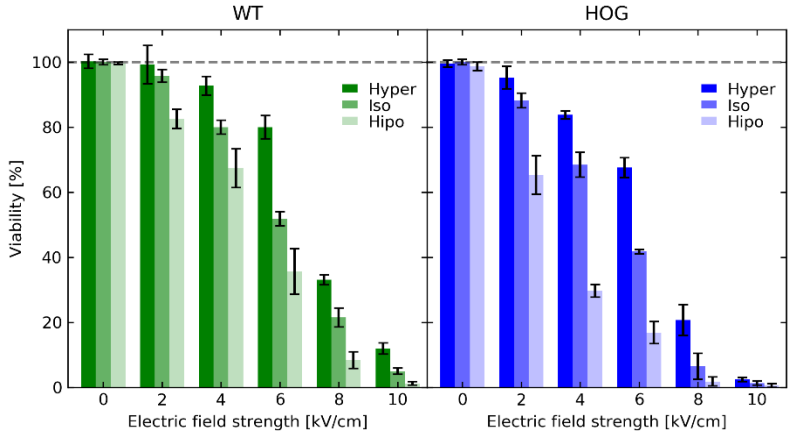

Fig. 1. Yeast viability dependence on osmotic shock treatment after PEF. WT viability is depicted on the left side in green colour, HOG viability is depicted on the right side in blue colour. Opacity of the respective colour represents osmotic shock applied: darkest for hyperosmotic, lightest for hipoosmotic.

It was shown that cellsô viability decreases with the increase of elecric field strength. Transfer of PEF treated cells to solutions with different osmotic composition significantly influenced yeast cell viability (Fig. 1.). Most notable viability changes were spotted after 4 and 6 kV/cm. After 4 kV/cm hyperosmotic shock increased WT and HOG viability by 13% and 15%, hypoosmotic ï decreased by 12% and 39% respectively. After 6 kV/cm hyperosmotic shock increased WT and HOG cell viability by 28% and 26%, hypoosmotic ï decreased by 16% and 25% respectively, relative to no (isoosmotic) shock treatment. To further investigate the influence of osmotic shock treatment leakage of intracellular compounds was evaluated. Absorbtion at wawelengths of 260 nm and 280 nm revealed that the amount of intracellular components in the media decreased after hiperosmotic shock and increased after hipoosmotic shock, supporting the hypothesis that mechanical cell shape alteration influences cellsô reaction to PEF. Furthermore, statistical analysis confirmed that HOG strain was more sensitive to beforementioned treatments suggesting that HOG pathway is of relevance to recovery after electroporation.

To summarise, yeast cell viability after exposure to PEF can be altered by subsequent change in osmolarity of media. HOG pathway involvement was linked to recovery after electroporation.

[1] M. Parapouli, A. Vasileiadis, A.-S. Afendra, and E. Hatziloukas, ñSaccharomyces cerevisiae and its industrial applicationsò, AIMS Microbiol. 6(1): 1ï 31 (2020)
[2] S. Hohmann, ñControl of high osmolarity signalling in the yeast Saccharomyces cerevisiaeò, FEBS Lett. 17;583(24):4025-9, (2009)
[3 A. Stirke, R. Celiesiute-Germaniene, A. Zimkus, N. Zurauskiene, P. Simonis, A. Dervinis, A. Ramanavicius, and S. Balevicius, ñThe link between yeast cell wall porosity and plasma membrane permeability after PEF treatment.ò Scientific reports vol. 9,1 14731, (2019)

BIOSYNTHESIS OF RECOMBINANT ALLERGENS USING MAMMALIAN CELLS EXPRESSION SYSTEM

Agne Rimkute[1], Dovile Stravinskiene[1], Gintautas Zvirblis[2]

[1]Department of Immunology and Cell Biology, Life Sciences Center, Vilnius University, Vilnius, Lithuania
[2]Department of Eukaryote Gene Engineering, Life Sciences Center, Vilnius University, Vilnius, Lithuania
agne.rimkute@gmc.vu.lt

IgE-mediated allergic reactions are the most common hypersensitivity disorders affecting up to 30% of the population worldwide and still rising. Due to the high prevalence of these diseases, accurate diagnosis is critical to ensure the most effective treatment. Immunological test systems for allergy diagnostics currently mostly involve allergen extracts, which are a heterogeneous mixture of various allergic and non-allergic components. Levels of the main allergen and the additional substances could vary among different batches of the product. In contrast, recombinant allergens can be produced as defined molecules with known immunologic and biological features [1]. The usage of purified recombinant allergens instead of allergen extracts could increase the accuracy of allergic reaction detection, as well as reduce cross-reactions. Recombinant proteins could be produced using various expression systems, including mammalian cells. The ability to perform post-translational modifications that are not present in proteins produced in prokaryotes makes mammalian cells expression system an advantageous production platform [2].

This study aimed to produce recombinant secreted maltose-binding protein (MBP) fused wasp‘s allergen Ves v 2 (rVes v 2-MBP) and cow‘s milk allergen Bos d 4 (rBos d 4-MBP) in mammalian cells. Synthetic DNA fragments coding these allergens were cloned to mammalian expression vector and transiently transfected into Chinese hamster ovary (CHO) cells. Secreted rBos d 4-MBP was purified using MBP affinity tag and confirmed using immunoblotting and indirect enzyme-linked immunosorbent assay using monoclonal antibodies against MBP. However, recombinant Ves v 2 allergen was not secreted into cells growth media but was detected in intracellular compartment of the cell. To determine if synthesized recombinant protein antigenicity is similar to natural allergen, blood serum samples from patients allergic to cow‘s milk were tested with rBos d 4-MBP. Also, blood serum samples were tested using the same recombinant allergen produced in *E. coli*.

Results show that serum samples with allergen-specific IgE recognizes rBos d 4-MBP antigen produced in CHO cells, suggesting that recombinant protein contains IgE-binding epitopes. Nevertheless, rBos d 4-MBP protein produced in *E. coli* was not recognized by specific IgE.

In conclusion, recombinant Bos d 4 fused with MBP expressed in mammalian cells is most likely to be similar to native protein as compared to the same recombinant allergen produced in *E. coli*. These results indicate that mammalian cells expression system is suitable for eukaryotic protein production and synthesized recombinant proteins could be used for improving molecular allergology tests *in vitro*.

[1] R. Valenta, A. Karaulov, V. Niederberger, Y. Zhernov, O. Elisyutina, R. Campana, M. Focke-Tejkl, M. Curin, L. Namazova-Baranova, J. Y. Wang, R. Pawankar, M. Khaitov, Allergen Extracts for In Vivo Diagnosis and Treatment of Allergy: Is There a Future? J Allergy Clin Immunol Pract, 1845–1855 (2018).
[2] M. Curin, V. Garib, R. Valenta, Single recombinant and purified major allergens and peptides How they are made and how they change allergy diagnosis and treatment, Ann Allergy Asthma Immunol, 119(3): 201–209 (2017).

DESIGNING A VISCOSITY-SENSITIVE BODIPY FLUOROPHORE FOR A LIVE CELL IMAGING

Karolina Maleckaitė[1], Jelena Dodonova[2], Stepas Toliautas[3], Rugilė Gylėnaitė[1,2], Dėiugas Jurgutis[4], Vitalijus Karabanovas[4,5], Sigitas Tumkevičius[2], Aurimas Vyšniauskas[1]

[1] Center of Physical Sciences and Technology, Saulėtekio av. 3, Vilnius, LT-10257, Lithuania.
[2] Institute of Chemistry, Faculty of Chemistry and Geosciences, Vilnius University, Naugarduko str. 24, Vilnius, LT-03225, Lithuania
[3] Institute of Chemical Physics, Faculty of Physics, Vilnius University, Saulėtekio av. 9-III, 10222 Vilnius, Lithuania
[4] Biomedical Physics Laboratory, National Cancer Institute, P. Baublio str. 3b, LT-08406 Vilnius, Lithuania
[5] Department of Chemistry and Bioengineering, Vilnius Gediminas Technical University, Sauletekio av. 11, LT-10223, Vilnius, Lithuania
karolina.maleckaite@ftmc.lt

Viscosity imaging at a microscopic scale can reveal information about the diffusion-controlled processes in biosystems. Determining a microviscosity change can indicate the development of atherosclerosis, diabetes, and Alzheimerôs disease.[1] ôMolecular rotorsôare viscosity-sensitive fluorophores that provide one of the easiest methods to image microviscosity. These fluorophores have been employed for imaging microviscosity in polymers, living cells and lipid bilayers.[1] The concept of molecular rotors mechanism is based on a changing fluorescence signal, which emerges from the competition between intramolecular rotation and emitted photons. The nature of the electronically excited state is changed by the rotation causing a faster non-radiative relaxation. Therefore, a longer fluorescence lifetime of the molecule is observed in a high viscosity environment.[2]

One of the most widely-used molecular rotors is BODIPY-C_{10} (Fig. 1A). This standout molecule displays the monoexponential fluorescence decay, which simplifies the data analysis. Unfortunately, the green absorbance and fluorescence wavelengths are the greatest drawbacks of the BODIPY-C_{10}. It is well known, that the longer wavelengths are desired for viscosity imaging of the biological sample. It is possible to achieve longer wavelengths by introducing conjugated substituents and extending the conjugation length within the fluorophore.[3] However, we have to ensure that the new red-emitting BODIPY molecule remains viscosity-sensitive.

To avoid a time-consuming synthesis of a large number of fluorophores with various modifications, we show how density functional theory (DFT) calculations can help to determine viscosity-sensitive properties of the molecule before its synthesis. In this work, we investigate four phenyl-substituted BODIPY molecular rotors (Fig. 1A): without any additional moieties on *b*-phenyls (BP-PH), with two methyl (BP-PH-2M) or isopropyl (BP-PH-ISO) groups on each *b*-phenyl ring, and methyl-substituted *b*-phenyls with a nitro-substituted *meso*-phenyl (BP-PH-2M-NO_2). In this case, adding *b*-phenyls increases moleculeôs conjugation and red-shifts fluorescence spectra to biologically-friendly wavelengths.

The research consists of quantum chemical calculations, absorption and fluorescence spectra measurements, fluorescence lifetime evaluation, and live cells imaging using lipid vesicles. Dependencies regarding the molecular structure, activation energy barrier, increasing solvent viscosity, polarity, and temperature were investigated. Quantum chemical calculations showed that an increase in an activation energy barrier (Fig. 1B) results in red-shifted fluorescence spectra. Moreover, DFT-based calculations allowed us to create a red-emitting probe by introducing a nitro group, which reduces the barrier and increases viscosity-sensitivity of the molecule (Fig. 1C).[4]

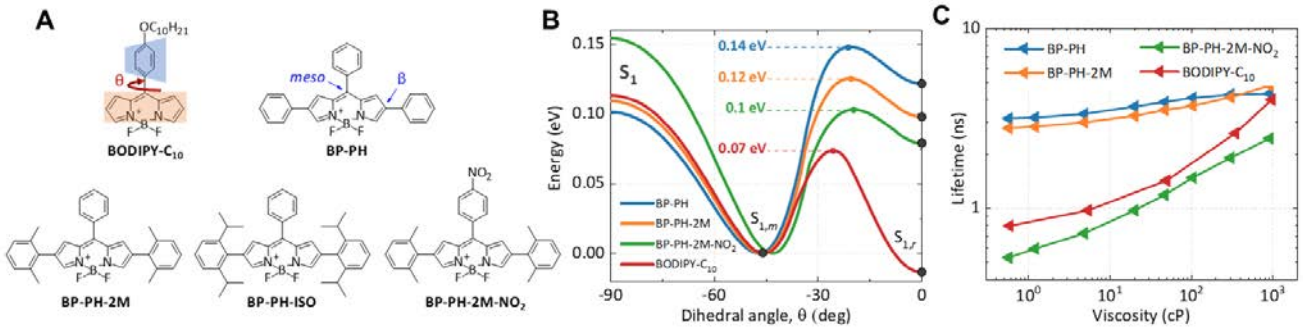

Fig. 1. (A) The structures of the molecular rotors used in this work, and the rotor mechanism showed on BODIPY-C_{10}. TD-DFT calculated potential energy surface curves (B) and viscosity-dependent fluorescence lifetimes (C) of BP-PH (blue), BP-PH-2M (yellow), BP-PH-2M-NO_2 (green), and BODIPY-C_{10} (red).

[1] M. K. Kuimova, Physical Chemistry Chemical Physics, 2012, 14, 12671ï 12686.
[2] M. A. Haidekker and E. A. Theodorakis, Organic and Biomolecular Chemistry, 2007, 5, 1669ï 1678.
[3] D. Zhang et al., Physical Chemistry Chemical Physics, 2011, 13, 13026ï 13033.
[4] S. Toliautas et al., Chemistry ï A European Journal, 2019, 25, 10342ï 10349.

OPTICAL PROPERTIES INVESTIGATION OF BLUE-EXCITABLE RED-EMITTING $K_2Bi(PO_4)(MoO_4):Pr^{3+}$ POWDERS

Julija Grigorjevaite[1], Arturas Katelnikovas[1]

[1] Institute of Chemistry, Department of Chemistry and Geosciences, Vilnius University, Lithuania
julija.grigorjevaite@chf.vu.lt

The direct transitions from ^3P_J (J = 0, 1, 2) or $^1D_2$ excited levels to the ground states (^3H_J) results in sharp lines in the Pr^{3+} emission spectra. Besides, in some host matrices, the energy migration from ^3P_J to $^1D_2$ levels can be observed yielding exclusively red emission [1]. In our studied host matrix, namely, $K_2Bi(PO_4)(MoO_4)$, only intraconfigurational (4f Ÿ 4f) transitions were observed. Also, cross-relaxation processes are very common in inorganic materials doped with trivalent praseodymium ions and this process is responsible for the emission quenching, especially as a function of dopant concentration. The cross-relaxation process can be directly measured by examining the fluorescence intensity decay after the pulsed excitation.

For the aforementioned reasons, Pr^{3+} doped $K_2Bi(PO_4)(MoO_4)$ synthesis and optical measurements were performed. Moreover, the luminescence properties of rare-earth ions are determined by their environment in the host lattice. In most cases, molybdate based compounds are used as luminescent ion hosts in order to obtain well-defined emission properties [2].

In this research, the $K_2Bi(PO_4)(MoO_4):Pr^{3+}$ phosphors were prepared by a solid state reaction method at relatively low temperature (873.15 K). The optical properties of synthesized samples were consistently studied as a function of Pr^{3+} concentration and temperature. The given presentation will include XRD and SEM measurements, reflection, excitation, emission spectra, PL decay curves, luminous efficacies at room temperature; and emission spectra, PL decay curves, as well as CIE 1931 color coordinates in 77 ï 500 K temperature interval.

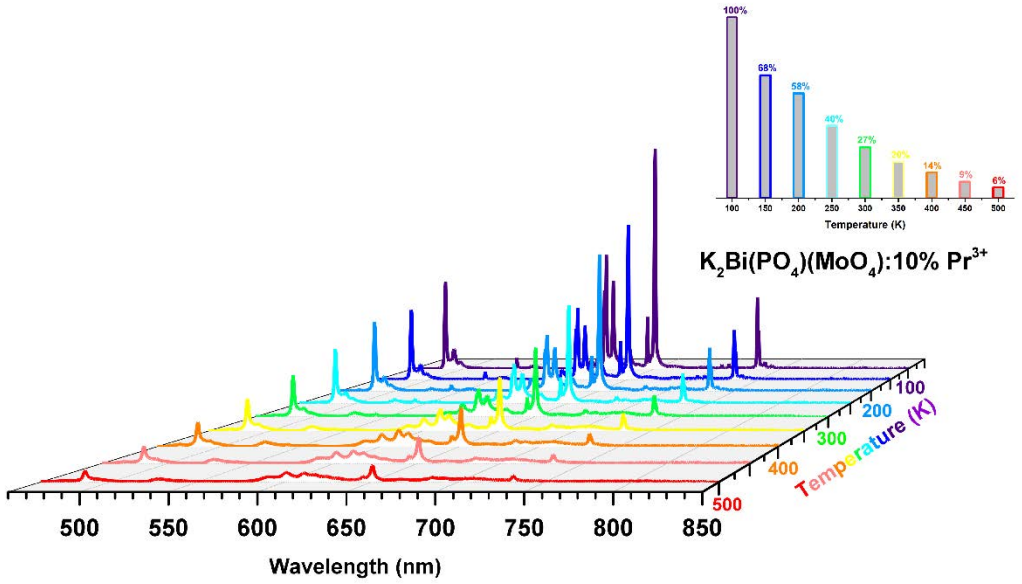

Fig. 1. Temperature dependent emission (λ_{ex} = 448 nm) spectra of $K_2Bi(PO_4)(MoO_4)$ doped with 10% Pr^{3+} ranging from 100 K to 500 K with inset of the integrated emission intensity at different temperatures.

The thermal quenching behavior for the sample doped with 10% Pr^{3+} ions is shown in Fig. 1. The inset of this figure represents the integrated emission intensity at different temperatures which obviously decreases when the temperature increases. It was observed that PL intensity decreases exponentially with increasing temperature. Low (100 K) temperature emission spectra are dominated by $^3P_0$ Ÿ $^3H_4$, $^1D_2$ Ÿ $^3H_4$, $^3P_0$ Ÿ $^3H_6$ and $^3P_0$ Ÿ $^3F_4$ transitions. However, when temperature was increased to 500 K all transitions from $^3P_0$ and $^1D_2$ almost disappeared. This feature is expected, because of cross-relaxation and $^1D_2$ level is absolutely vanished in non-radiative pathway, and only emission from $^3P_0$ Ÿ $^3H_4$, $^3H_6$, and $^3F_4$ transitions at 590 nm, 601 nm and 740 nm are seen in the spectra at 500 K temperature.

Finally, our determined optical features show possibility to use synthesized materials in display and security pigments industry.

[1] P. Boutinaud, E. Pinel, M. Oubaha, R. Mahiou, E. Cavalli, M. Bettinelli, Making red emitting phosphors with Pr^{3+}, Opt Mater, 2006;28:9-13.
[2] J. Grigorjevaite, A. Katelnikovas, Synthesis and Optical Properties Investigation of Blue-Excitable Red-Emitting $K_2Bi(PO_4)(MoO_4):Pr^{3+}$ Powders, Journal of Materials Research and Technology, 2020, 9, 6, 15779-15787 (doi: 10.1016/j.jmrt.2020.11.054).

INFLUENCE ANALYSIS OF SELECTED FACTORS ON THE EUROPIUM IONS REDUCTION IN THE GLASSY MATRIX

Agata Jarocka[1], PaweğDñbowski[1], Tomasz K. Pietrzak[1], Marek Wasiucionek[1]

[1] Faculty of Physics, Warsaw University of Technology, Koszykowa 75, 00-662 Warsaw, Poland
agata.jarocka.dokt@pw.edu.pl

Over the past years, our group has been working on amorphous and nanocrystallised materials towards finding possible new cathode materials for Li-ion and Na-ion batteries [1], syntheses of glasses and their thermal nanocrystallisation, as well as methods to avoid oxidation of transition metals involved. Based on that experience, it was proposed to produce transparent glassy matrices doped with rare earth elements (REE), such as e.g. Eu, Pr. We studied the effects of the synthesesô conditions on REE ions reduction and adopted these correlations to control photoluminescence properties of samples.

Our recent work [2] proved that it is possible to synthesize REE-doped glassy materials whose photoluminescence spectrum can be tuned depending on synthesis conditions by using melt-quenching process. During that work we found out that one can control the relative Eu^{3+}/Eu^{2+} ions concentrations. As both Eu^{3+}/Eu^{2+} are photoluminescent in different parts of the visible range, the possibility of controlling their relative concentrations means that it is possible to "tuneò photoluminescence spectrum of the material. Furthermore, emission can be ñlikenò to the natural light and strong UV/blue component which is present in spectra of many of todayôs white LEDs can be suppressed. This would make white LEDs more comfortable and healthier for the eyes than they are today [3]. It is also possible to adjust phosphors to other needed colors.

In this research, a glassy matrices based on borate and phosphate glasses were successfully synthesized by a melt-quenching process, using a double crucible method [4]. Samples obtained at different synthesis conditions were carefully investigated using X-ray diffractometry (XRD),), photoluminescence spectroscopy (PL), photoluminescence excitation (PLE) and absorption spectroscopy.

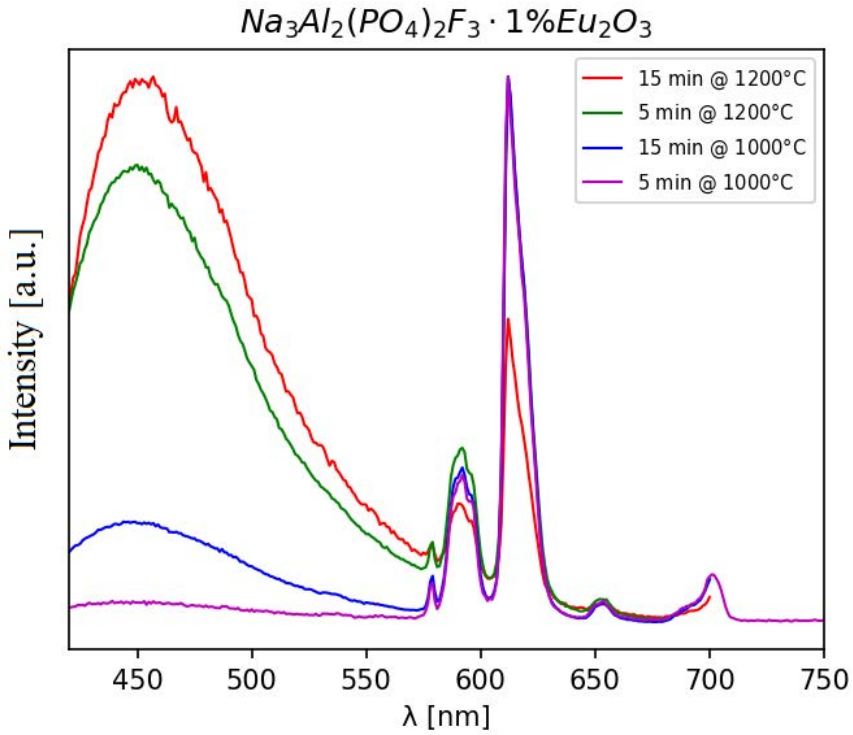

Fig. 1. PL studies of 4 glassy samples $Na_3Al_2(PO_4)_2F_3$ doped with Eu_2O_3 excited with 396 nm. Different synthesis parameters (time and temperature) are given in the plots.

[1] T.K. Pietrzak *et al*., Materials Science and Engineering B 213 (2016) 140-147.
[2] T.K. Pietrzak, A. Goğbiewska *et al*., Journal of Luminescence 208 (2019) 322ï 326.
[3] E. Chamorro *et al*., Photochemistry and Photobiology, 89 (2013) 468ï 473.
[4] K. Hirose *et al*., Solid State Ionics, 178 (2007) 801ï 807.

THERMAL ANNEALING OF PS-B-PMMA DIBLOCK COPOLYMER THIN FILMS

Katarzyna Polak[1], Andrzej Sitkiewicz[1], Arkadiusz Leniart[1], Paweł Majewski[1]

[1] Section of Theoretical Chemistry and Crystallography, Faculty of Chemistry, University of Warsaw, Pasteura 1, 02-093 Warsaw, Poland
ka.polak2@student.uw.edu.pl

Block copolymers (BCPs) are self-assembling materials able to form diverse morphologies (like lamellae, cylinders, spheres etc.) depending on the relative volume fraction of the two blocks. Thermal annealing is one of the methods used to enhance kinetics of self-assembling BCP. The orientation of the phase in thin films can be influenced by many factors e.g. substrate surface energy or film thickness.

We examine the effect of vacuum oven annealing on two lamellae-forming polystyrene-block-poly(methyl methacrylate) (PS-b-PMMA) diblock copolymer with molecular mass 74 kg/mol (L74) and 104 kg/mol (L104). To prepare the surface Si wafer was activated with oxygen plasma. Then to orient BCP phase vertically film of rand-PS-b-PMMA solution was spin coated and baked in 220oC for 5 minutes and the rest was rinsed with toluene. Films were prepared via flow coating onto the surface. Thermal annealing of the sample was performed by baking the wafer in 200oC for 16 hours.

Visualization with atomic force microscopy AFM was used to characterize a morphology of BCP. To generate film that can be imaged with AFM the PMMA phase in diblock copolymer was removed with exposure to UV light for 5 minutes and immersing in glacial acetic acid for another 5 minutes. Right now we are working on a relationship between the thickness of PS-b-PMMA film and the periodicity in obtained morphology.

DOES EXTENDING THE DONOR GROUP ENHANCE THERMALLY ACTIVATED DELAYED FLUORESCENCE PROPERTIES?

Eimantas Duda[1], David Hall[2,3], Sergey Bagnich[1], Cameron Carpenter-Warren[2], Rishabh Saxena[1], Michael Y. Wong[2], David B. Cordes[2], Alexandra M. Z. Slawin[2], David Beljonne[3], Yoann Olivier[4], Eli Zysman-Colman[2*], and Anna K° hler[1*]

[1]Soft Matter Optoelectronics, BIMF & BPI, University of Bayreuth, Germany
[2]Organic Semiconductor Centre, EaStCHEM School of Chemistry, University of St Andrews, UK
[3]Laboratory for Chemistry of Novel Materials, University of Mons, Belgium
[4]Unit®de Chimie Physique Th®orique et Structurale & Laboratoire de Physique du Solide, Namur Institute of Structured Matter, Universit®de Namur, Belgium
eimantas.duda@uni-bayreuth.de

In order to better understand how the photophysical properties change with the extension of the donor group, we selected a well-known thermally activated delayed fluorescence (TADF) emitter **2CzPN** [1-3] as a reference and synthesized a series of molecules with extended donor groups that include carbazole (Cz), diphenylamine (*t*BuDPA) and phenoxazine-based (PXZ) units. **2CzPN** itself consists of an electron-withdrawing phthalonitrile core with two carbazole donor moieties attached. The additional donor units can be substituted comparatively easily at the 3,6-positions of carbazole, allowing for the conjugated ´-system to extend. **2CzPN** is thus ideally suited to study the impact of hole wavefunction delocalization on the singlet-triplet gap and TADF performance. By systematic investigation of photophysics in toluene solution and mCP film complemented with density functional theory (DFT) calculations, we demonstrate that extending the donor group essentially decreases the singlet-triplet gap at the cost of decreased PLQY or TADF property. In the case of **Cz-2CzPN** and ***t*BuDPA-2CzPN**, the singlet-triplet gap is successfully reduced yet stronger non-radiative losses are present compared to **2CzPN**. In the case of **PXZ-2CzPN**, the oscillator strength becomes negligible indicating a too high HOMO LUMO decoupling. Here we not only report positive effects behind the extension of the donor group but also perform a comprehensive study to understand the energy loss channels in extended **2CzPN** systems.

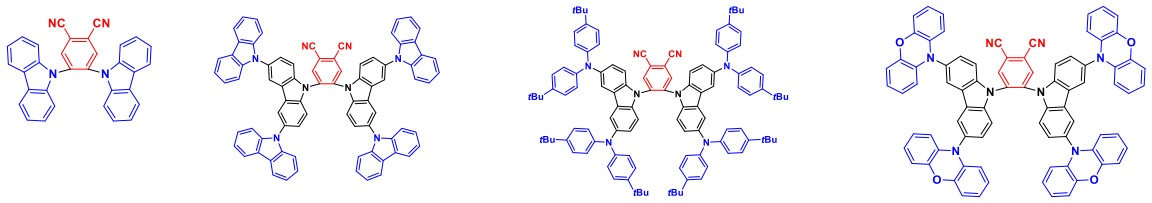

2CzPN **Cz-2CzPN** ***t*BuDPA-2CzPN** **PXZ-2CzPN**

Fig. 1. Chemical structures of the compounds investigated.

[1] Uoyama, H.; Goushi, K.; Shizu, K.; Nomura, H.; Adachi, C., Highly efficient organic light-emitting diodes from delayed fluorescence. Nature, 492 (7428), 234-238 (2012).
[2] Kim, G. H.; Lampande, R.; Im, J. B.; Lee, J. M.; Lee, J. Y.; Kwon, J. H., Controlling the exciton lifetime of blue thermally activated delayed fluorescence emitters using a heteroatom-containing pyridoindole donor moiety. Materials Horizons, 4 (4), 619-624 (2017).
[3] Wong, M. Y.; Krotkus, S.; Copley, G.; Li, W.; Murawski, C.; Hall, D.; Hedley, G. J.; Jaricot, M.; Cordes, D. B.; Slawin, A. M. Z.; Olivier, Y.; Beljonne, D.; Muccioli, L.; Moral, M.; Sancho-Garcia, J.-C.; Gather, M. C.; Samuel, I. D. W.; Zysman-Colman, E., Deep-Blue Oxadiazole-Containing Thermally Activated Delayed Fluorescence Emitters for Organic Light-Emitting Diodes. ACS Applied Materials & Interfaces, 10 (39), 33360-33372 (2018).

OPTIMIZATION OF FABRICATION OF THZ ï GERMANIUM MICROANTENNAS

Agnieszka Anna Wiciak[1], Wolfgang M. Klesse[1], Davide Spirito[1]

[1] IHPï Leibniz-Institut f¿r innovative Mikroelektronik, Im Technologiepark 25, 15236 Frankfurt (Oder) (Germany)
wiciak@ihp-microelectronics.com

Terahertz (THz) spectroscopy is an effective method for the detection of organic and biochemical molecules. Nonetheless, in the current state, the use of THz spectroscopy in biochemical applications is limited to high concentrations of substances because of low sensitivity. Using plasmonic resonators (antennas) gives the opportunity to increase the sensitivity and allows to measure dilute substances.

Typical and well-known materials for plasmonics biosensors are noble metals, however they unsuitable for use in CMOS foundries. Highly doped semiconductors are promising in this wavelength range, as they show plasmonic behavior with limited losses. Here, we chose n-doped germanium as basis material for fabrication of microantennas and slots, whose resonance can yield the desired field enhancement at THz frequencies. Furthermore, germanium has the relevant advantage that it can be readily integrated in semiconductor foundry processes and thus offers potential for mass production, provided an optimization of the antenna response.

We have studied the material and fabrication parameters, as well as the antenna design, to target specific resonance frequency in the range 0.1-10 THz with the optimal quality factor. These features can be tuned by changing the size and geometry of the antenna. In order to choose the optimal Ge doping, the absorption of the material in the THz and IR range has been examined.^We employ maskless photolithography for fabrication, which enables flexibility in pattering of different resonator geometries. The microstructures are subsequently defined via reactive ion etching or wet etching. Optimization of these processes is assessed with Scanning Electron Microscopy (SEM) and Atomic Force Microscopy (AFM). Finally, the performance of the antennas is studied by THz-time domain spectroscopy (TDS).

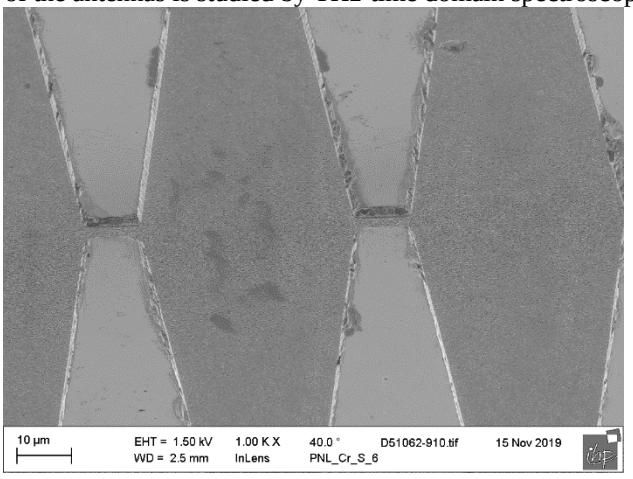

Fig. 1. SEM image of bow-tie THz-microantennas.

We will show these results for microantennas and slot antennas in two types of shape: (1) a dipole design with two rectangular arms and (2) bow-tie design with trapezoid arms. Moreover we studied the influence of the shape and distribution of resonator arrays on the antenna performance.

The THz-TDS data demonstrates that the shape of plasmonic antennas has an important impact on their optical properties. At least two resonant modes can be distinguished by observation in reflectance or transmittance geometry with an electric field polarization oriented along the short axis (high-frequency resonance) or the long axis (low-frequency resonance) of the resonators. In arrays, higher-order, coupled and collective resonances can be observed by increasing the number of resonators and manipulating their particular geometry.

THz-TDS measurements reveal that both the maximum absorption and the resonance of our slot antennas are sensitive to the mass concentration of Ŭ-lactose solutions in a range below 1 g/ml. This provides a proof-of-principle that this type of antenna is suitable for quantitative detection of biomolecules.

DEVELOPMENT OF MONOCLONAL ANTIBODIES AGAINST HOUSE DUST MITE ALLERGEN DER P 21 FOR THE QUANTIFICATION OF ALLERGEN COMPONENT IN ALLERGEN EXTRACTS

Vytautas Rudokas, Gintautas Ţvirblis, Aurelija Ţvirblienė

Institute of Biotechnology, Life Sciences Center, Vilnius University, Lithuania
vytautas.rudokas@gmc.vu.lt

Allergy is a type I hypersensitivity reaction to the environmental antigens that usually cause little or no problem to most people. The house dust mite (HDM) is one of the most important and widely spread allergen sources causing allergy and its related complications, such as bronchial asthma. Recombinant allergens are being used in molecular allergy diagnostics systems and can also be employed in the development of monoclonal antibodies (MAbs). Since the allergen extracts from different manufacturers lack proper standardization regarding to its composition [1], MAbs against specific allergen components can be used for the quantification of allergen components in allergen extracts.

This study aimed to purify recombinant HDM allergens and then develop, characterize and apply MAbs against one of the purified allergens. Here, we studied 9 allergens from HDM *Dermatophagoides pteronyssinus* and *Dermatophagoides farinae*, which were previously fused with maltose binding protein (MBP), expressed in *E. coli* and were purified using affinity liquid chromatography of MBP-passenger proteins. The allergens were Der f 1, Der f 2, Der p 10, Der p 21, Der p 23, Der p 24, Der p 26, Der p 30 and Der p 36. A TEV protease hydrolysis sequence was inserted in between each allergen and its MBP sequence. MBP and TEV also had 6 histidine sequence inserted. Hydrolysis reaction was optimized to detach MBP from purified allergens and one selected allergen ï rDer p 21 was purified using second step affinity liquid Ni-NTA chromatography. Blood serum from HDM allergic patients was analyzed and complex formation, between rDer p 21 and IgE (antibodies against native allergens), was observed. These results led to the development of MAbs against purified rDer p 21. Five hybridoma cell lines producing high affinity MAbs of IgG isotype were generated using hybridoma technology [2]. The MAbs were grouped into two categories according to their recognized epitopes and a sandwich enzyme-linked immunosorbent assay (Fig. 1) system for the quantification of Der p 21 was developed and optimized.

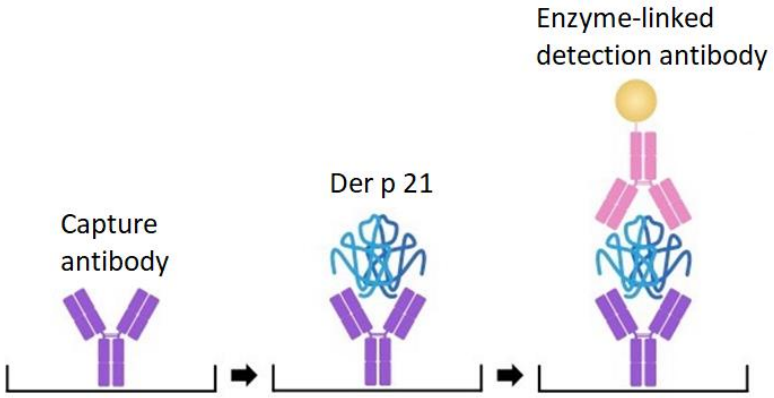

Fig. 1. Scheme of sandwich enzyme-linked immunosorbent assay.

[1] A. Casset, A. Mari, A. Purohit et al., Varying allergen composition and content affects the in vivo allergenic activity of commercial Dermatophagoides pteronyssinus extracts, International Archives of Allergy and Immunology **159**, 253-262 (2012).
[2] G. Kº hler, C. Milstein, Continuous cultures of fused cells secreting antibody of predefined specificity, Nature **256**, 495-497 (1975).

DETERMINING THE PROPERTIES OF VISCOSITY-SENSITIVE MOLECULAR ROTOR IN HUMAN MESENCHYMAL STEM CELLS AND THEIR DIFFERENTIATED COUNTERPARTS

Dģiugas Jurgutis[1, 2], Greta Jarockytā[1, 2], Aurimas Vyģniauskas[3],
Vitalijus Karabanovas[1, 4], Riļardas Rotomskis[1, 5]

[1] Biomedical Physics Laboratory of National Cancer Institute, Baublio 3B, Vilnius, Lithuania;
[2] Life Sciences Center, Vilnius University, Saulātekio av. 7, Vilnius, Lithuania;
[3] Center for Physical Sciences and Technology, Saulātekio av. 3, Vilnius, Lithuania;
[4] Department of Chemistry and Bioengineering, Vilnius Gediminas Technical University, Vilnius, Lithuania;
[5] Biophotonics group of Laser Research Centre, Vilnius University, Vilnius, Lithuania
dziugas.jurgutis@nvi.lt

Differentiation of cells completely alters their morphological and biochemical profiles. While the aforementioned profiles have been sufficiently characterised, the biomechanical remodelling, such as the change of viscosity within cell structure and organelles, remains unmonitored. Determining viscosity during and after differentiation may provide deeper insight into the vital process, especially for stem cells, e.g. mesenchymal stem cells (MSC) that are capable of differentiating into fat, bone, cartilage or other connective tissue. Therefore, a state-of-the-art method is essential for a spatial resolved quantitative intracellular viscosity ómappingô in MSC and their differentiated counterparts.

Molecular rotors are viscosity-sensitive fluorophores that may be utilized in monitoring intracellular viscosity. One of such molecules - BODIPY-h (BDP-h) is based on BODIPY (*4,4-difluoro-4-bora-3a,4a-diaza-s-indacene)* fluorescent dye. The molecule was tested in methanol-glycerol and toluene-castor oil mixtures and its sensitivity to viscosity was confirmed [1]. BDP-h phenyl ringôs rotation depends on the viscosity of the surrounding micro-environment (Fig. 1): more viscous medium inhibits intramolecular rotation, which leads to slower deactivation from the fluorescent state via non-radiative energy transition, thus resulting in a longer fluorescence (FL) lifetime and vice versa [2].

The aim of our study was to determine the photophysical properties of BDP-h in aqueous media, such as phosphate-buffered saline (PBS) or cell growth medium - Dulbecco's Modified Eagle Medium (DMEM) with or without fetal bovine serum (FBS), together with the uptake of the molecular rotor in human skin MSC and their differentiated counterparts: adipocytes, osteocytes and chondrocytes.

Absorption, fluorescence spectra and fluorescence lifetimes of BDP-h were measured in distilled water, PBS and DMEM with or without FBS. For the uptake evaluation, StemPro differentiation kits (Gibco, US), were applied for specific differentiation of MSC. Cells were stained with 9 ε M BODIPY-h solution diluted with DMEM (1:1000) (Gibco, US) and incubated for 120 min. The accumulation of dye was observed using Nikon Eclipse Te2000-S confocal microscope (Nikon, Japan).

Our findings indicate that molecular rotor BDP-h interacts with serum proteins, which results in a slight red shift of both BDP-h absorption and fluorescence spectra by 6 nm and 4 nm, respectively. Inclusion of protein molecules also results in longer fluorescence lifetimes, which increases from 0.22 ns to 4.7 ns. BDP-h uptake evaluation revealed that dye accumulates both in fixed and live MSC. The molecular rotor diffuses through the membrane and stains membrane-bound organelles without passing the nuclear membrane. In differentiated MSC the intracellular distribution is different: in adipocytes BDP-h accumulates in lipid droplets, while in chondrocytes and osteocytes the dye exhibits cytosolic staining.

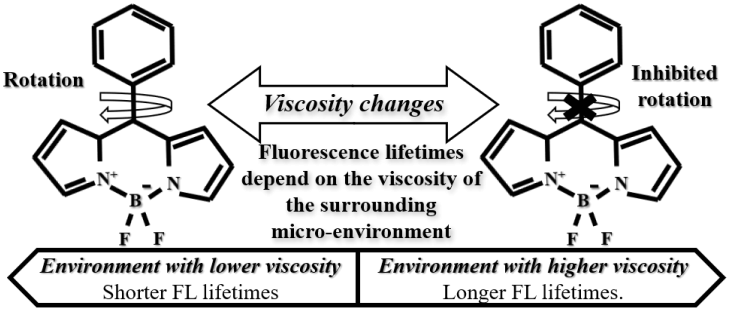

Fig. 1. The mechanism of molecular rotors demonstrated with BDP-h.

[1] Toliautas, S. et al. Enhancing the Viscosity-Sensitive Range of a BODIPY Molecular Rotor by Two Orders of Magnitude. Chemistry ï A European Journal 25, 10342ï 10349 (2019).
[2] Kuimova, M. K. Mapping viscosity in cells using molecular rotors. Phys. Chem. Chem. Phys. 14, 12671ï 12686 (2012).

A FLEXIBLE MATHEMATICAL SYSTEM TO MODEL EPIDEMICS AND SOME PREDICTIONS FOR ITALIAN COVID-19 PANDEMIC

Sergio Sanjurjo Montero, Irene Corral Lorences, Luis Javier Secades López-Cancio

Science Faculty, University of Oviedo, Spain
uo276361@uniovi.es

Our study consists of a theoretical model that allows predictions of epidemic evolution. It has high flexibility to adapt to a wide range of circumstances via a calibration process made with real data. In this paper, we study the Italian COVID-19 pandemic. Employing data from the first half of 2020, we got a forecast for the second half of that year.

The model presented consists of a mix of established and acknowledged epidemic evolution modelling, of which [1] is a clear and engaging introduction, and our personal view of the subject. We have opted for a complex model with a fair amount of rates to enhance flexibility at the cost of simplicity.

Every person of the whole population gets classified into one of four types: susceptible (S), infected (I), recovered (R) and asymptomatic (A). S can contract the illness by getting in contact with I or A, turning himself I or R depending on his resistance to the disease. I can recover entirely becoming R, or overcome the disease while still spreading it, becoming A in this case. R can lose immunity going back to I. A can lose the capacity to transmit the illness, finally achieving R. Every one of these transitions is controlled by an evolution rate, which needs calibration with real data.

To calibrate these rates, we have used real data from the first wave of Italian COVID-19 pandemic. From there, we have used numerical integration of the differential equations model to predict the impact of easing containment measures, ultimately leading to the second wave, as seen in Fig. 1.

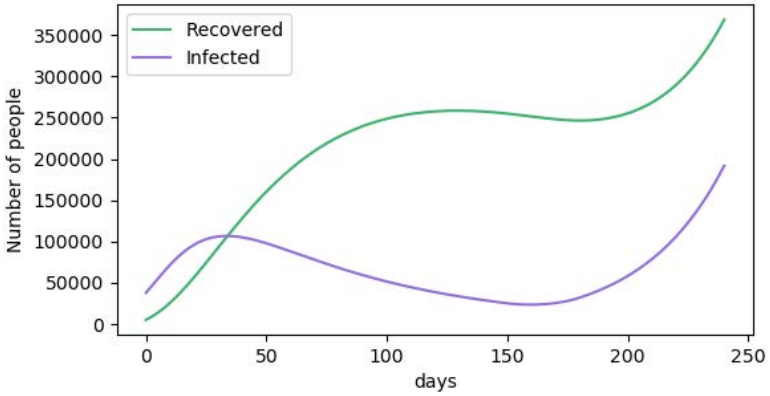

Fig. 1. Temporal evolution of the number of recovered and infected people.

The most concerning issue when mathematically modelling an epidemic is its periodic behaviour (the so-called waves). We have considered a manual tweak of the rates to solve this problem, taking into account government decisions and population reaction to them.

However, this need for a precise selection of the parameters can be a double-edged sword. In our case, it was simple to choose rates that would fit reality because we knew the results beforehand, though it could get tricky to select adequate parameters to achieve real predictions of the future of an epidemic.

Nowadays, with the new possibilities granted by technology, we have reached a clear conclusion. The complex epidemiological models are the best way to transform existing data into predictions of the future. Its only disadvantage is the accuracy required in its parameters.

Nevertheless, neural networks with deep learning methods could accomplish this fine-tuning by intense training of this artificial intelligence. Now, with the COVID-19 pandemic at its peak, we are collecting a large amount of useful data every day. It is mandatory to take this opportunity to create a strong understanding of the evolution of epidemics, as well as a capacity to predict and contain them.

[1] E. C. Pliego, A. Fraguela, *Modelos Epidemiológicos de Enfermedades Virales Infecciosas* (Epidemiological Models of Infectious Viral Diseases), Meritorious Autonomous University of Puebla. Undergraduate thesis, 2017.

THE OLIGOMANOSE N-GLYCANS 3D ARCHITECTURE AND ITS RESPONSE TO THE FCγRIIIA STRUCTURAL LANDSCAPE.

Carl Aaron Fogarty[1], Elisa Fadda[1]

[1]Department of Chemistry, Maynooth University, Ireland.
carl.fogarty.2016@mumail.ie

Oligomannoses are evolutionarily the oldest class of N-glycans, where the arms of the common pentasaccharide unit, i.e. Manα(1-6)-[Manα(1-3)]-Manβ(1-4)-GlcNAcβ(1-4)-GlcNAcβ1-Asn, are functionalized exclusively with branched arrangements of mannose (Man) monosaccharide units. In mammalian species oligomannose N-glycans can have up to 9 Man, meanwhile structures can grow to over 200 units in yeast mannan. The highly dynamic nature, branching complexity and 3D structure of oligomannoses have been recently highlighted for their roles in immune escape and infectivity of enveloped viruses, such as SARS-CoV2 and HIV-1. The architectural features that allow these N-glycans to perform their functions is yet unclear, due to their intrinsically disordered nature that hinders their structural characterization. In this work we will discuss the results of over 54 μs of cumulative sampling by molecular dynamics (MD) simulations of differently processed, unlinked oligomannose N-glycans common in vertebrates. We then discuss the effects of a complex protein surface on their structural equilibria based on over 4 μs cumulative MD sampling of the fully glycosylated CD16a Fc gamma receptor (FcγRIIIa), where the type of glycosylation is known to modulate its binding affinity for IgG1s, regulating the antibody-dependent cellular cytotoxicity (ADCC). Our results show that the protein's structural constraints shift the oligomannoses conformational ensemble to promote conformers that satisfy the steric requirements and hydrogen bonding networks demanded by the protein's surface landscape. More importantly, we find that the protein does not actively distort the N-glycans into structures not populated in the unlinked forms in solution. Ultimately, the highly populated conformations of the Man5 linked glycans support experimental evidence of high levels of hybrid complex forms at N45 and show a specific presentation of the arms at N162, which may be involved in mediating binding affinity to the IgG1 Fc.

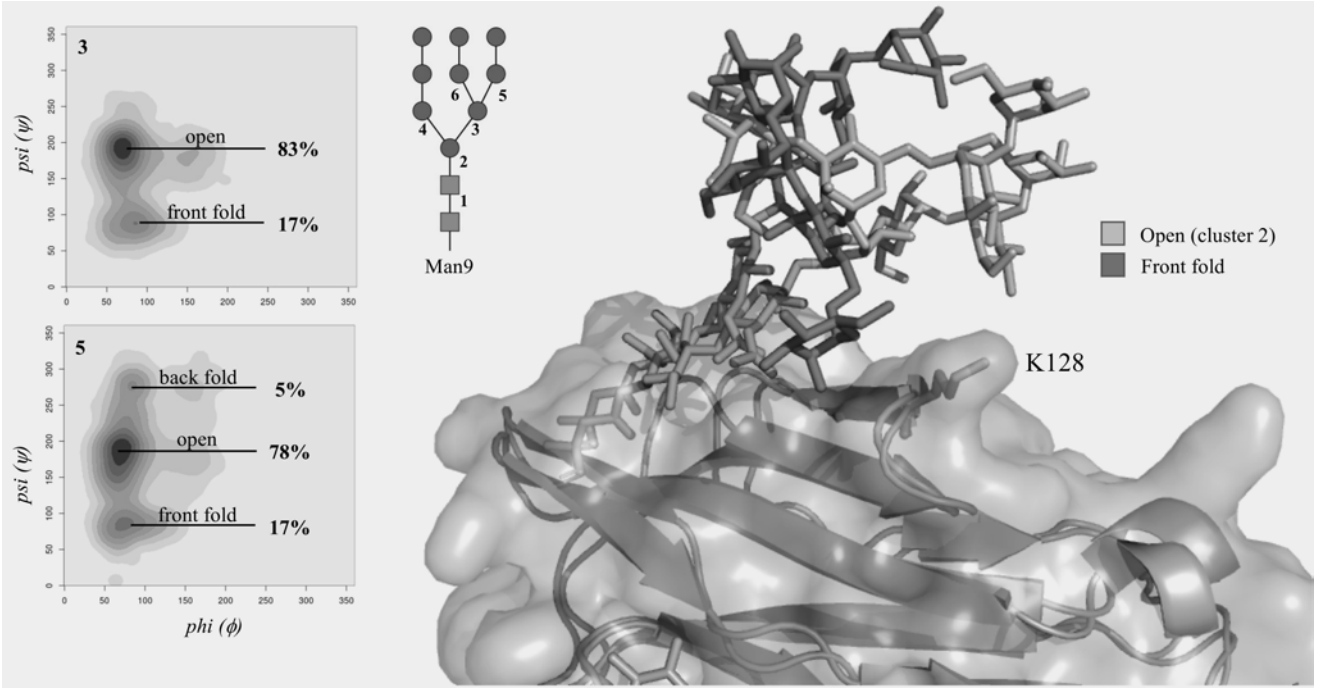

Fig. 1. Conformational analysis of the (1-6) arm and (1-6) branch of the N157-linked Man9 in terms of phi (ϕ) and psi (ψ) torsion angles, obtained from the 2 μs of cumulative MD sampling of the Man9 glycosylated FcγRIIIa. Heat maps are labelled on the top-left corner according to the Man9 numbering in the sketch. The two dominant conformations of the N157-linked Man9 are shown on the right-hand side, with the protein represented by the solvent accessible surface and underlying cartoons in grey and the mannose residues with different shades of green as described in the legend. Heat maps were made with RStudio (www.rstudio.com) and structure rendered with pyMol (www.pymol.org). N-glycan coloured according to the SNFG convention. (adapted to grey-scale).

THIRDï HARMONIC GENERATION MICROSCOPY OF COLLAGEN IN BIOLOGICAL TISSUES STAINED WITH HEMATOXYLIN AND EOSIN

Mykolas Maį iulis[1], Viktoras Maģeika[1], Martynas Riauka[1], Lukas Kontenis[1,2], Danutã Bulotienã[1,3], Vitalijus Karabanovas[1,3,4], Edvardas Ģurauskas[5], Virginijus Barzda[1,6,7]

[1]Laser Research Centre, Faculty of Physics, Vilnius University, Saulãtekio Ave. 10, LTï 10223, Vilnius, Lithuania
[2]Light Conversion, 2B KeramikÔst., LTï 10233, Vilnius, Lithuania
[3]Biomedical Physics Laboratory, National Cancer Institute, P. Baublio st. 3b, LTï 08406, Vilnius, Lithuania
[4]Department of Chemistry and Bioengineering, Vilnius Gediminas Technical University, Saulãtekio Ave. 11, LTï 10223, Vilnius, Lithuania
[5]Department of Pathology, Forensic Medicine and Pharmacology, Faculty of Medicine, Vilnius University, M.K. Į iurlionio st. 21/27, LTï 03101, Vilnius, Lithuania
[6]Department of Physics, University of Toronto, 60 St. Georges st., Toronto, ON M5S 1A7, Canada
[7]Department of Chemical and Physical Sciences, University of Toronto Mississauga, 3359 Mississauga Rd. N., Mississauga L5L 1C6, ON, Canada
mykolas.maciulis@ff.stud.vu.lt

Multimodal nonlinear laserï scanning microscopy is a powerful technique for noninvasive biological imaging [1]. Several nonlinear signals can be generated simultaneously at the focus of a microscope objective, including multiphoton excitation fluorescence, secondï harmonic generation (SHG) and thirdï harmonic generation (THG). Collagen, the main constituent of extracellular matrix in the biological tissue can be visualized with SHG microscopy, which can be used for cancer diagnostics [2]. Changes in the collagen structure are observed in hematoxylinï andï eosinï stained (H&Eï stained) histology sections, which contrast cell nuclei from the cytoplasm and extracellular structures and are considered as the gold standard for histological investigations [3]. Although collagen fibers are visualized with SHG microscopy, in this work THG is used for collagen visualization and characterization. The potential for cancer diagnostics using THG from H&Eï stained samples is also investigated. Fig.1(**a**) visualizes collagen fibrils in SHG, while THG (Fig.1(**b**)) shows endotendineum which wraps individual fascicles. Collagen fibrils are also faintly visible in the THG image. In addition cell nuclei of tendocytes are highlighted in THG. The combined image (Fig.1(**c**)) shows the colocalization between collagen fibrils, endotendineum and tendocytes. Multimodal nonlinear microscopy imaging can be incorporated into the tissue histology investigations without additional modifications of the H&Eï stained histopathology samples. Multimodal imaging can be applied for investigation of structural changes in connective tissue due to various diseases and also is beneficial in observing extracellular matrix and cell nuclei in cancer diagnostics.

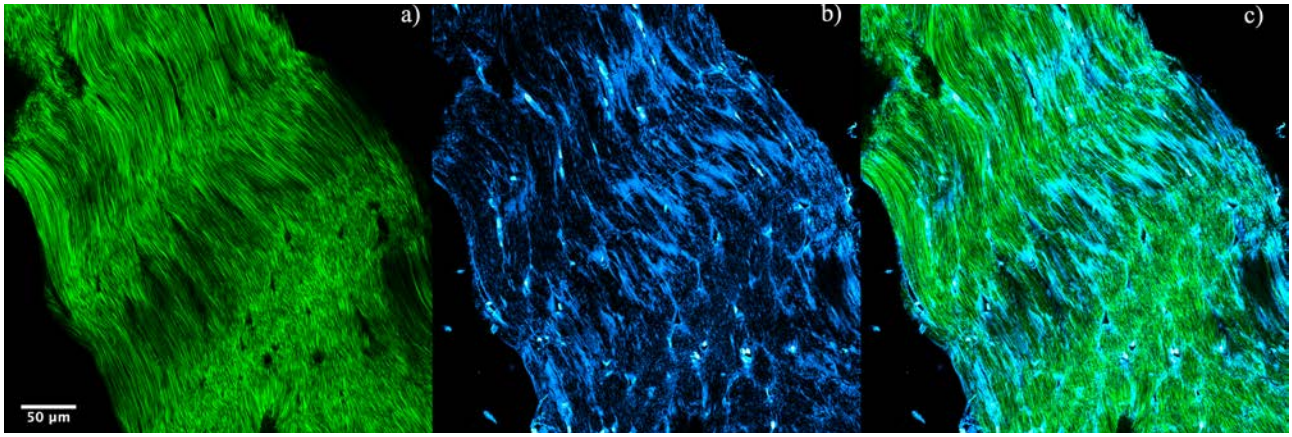

Fig. 1. Multicontrast nonlinear optical microscopy images of rat tail tendon histology section stained with hematoxylin and eosin (H&E staining). **a**) SHG image of collagen tissue, **b**) THG image from the same sample area and **c**) combined image of both.

Acknowledgements: The work was supported by grant No. 1.2.2.-LMT-K-718-02-0016.

[1] R. Carriles, D. N. Schafer, K. E. Sheetz, J. J. Field, R. Cisek, V. Barzda, and J. Squier, ñImaging techniques for harmonic and multi-photon absorption fluorescence microscopy,ò Rev. Sci. Instrum. 80, 081101 (2009).
[2] A. Golaraei, L. Kontenis, R. Cisek, D. Tokarz, S. J. Done, B. C. Wilson, and V. Barzda, ñChanges of collagen ultrastructure in breast cancer tissue determined by second-harmonic generation double Stokes-Mueller polarimetric microscopy,ò Biomed. Opt. Express 7(10), 4054ï 4068 (2016).
[3] J. A. Kiernan, Histological and Histochemical Methods, 3rd ed., Butterworth Heinemann, Woburn, MA (1999).

O12-6

DID NOT PARTICIPATE

MICROMACHINING OF TRANSPARENT BIOCOMPATIBLE POLYMERS APPLIED IN MEDICINE USING BURSTS OF FEMTOSECOND LASER PULSES

Evaldas Kaģukauskas[1], Simas Butkus[1,3], Piotr Tokarski[2], Vytautas Jukna[1], Carlos Vytautas Diamond Manikas[1], Martynas Barkauskas[3] and Valdas Sirutkaitis[1]

[1] Laser Research Center, Faculty of Physics, Vilnius University, Saulãtekio Ave. 10, LT-10223 Vilnius, Lithuania
[2] Msl Med Services Ltd., Rodou 6, Tremithousa, Paphos 8270, Cyprus
[3]Light Conversion, KeramikÔ2b, LT-10233 Vilnius, Lithuania
evaldas.kazukauskas@ff.vu.lt

Biocompatible plastics are used for many different purposes (catheters, artificial heart components, dentistry products, etc. [1]). An important field for the use of biocompatible polymers is the production of vision implants known as intraocular lenses (in short ï IOLs) or custom-shape contact lenses. According to statistics, about 50 % of Americans have developed cataracts by the age 75-79 [2], a condition that is curable by surgically replacing the original eye lens with an artificial lens.

One of the most favorable materials in IOL manufacturing is hydrophilic acrylic ï a soft, biocompatible polymer. Typically, curved surfaces are manufactured by mechanical means such as milling, turning or lathe cutting. Nowadays 2.5D objects/surfaces can also be manufactured by means of laser micromachining, that are more versatile [3]. However, due to the light-matter interaction mechanisms, the surface of the micromachined objects appears rough ~ 1 Õm Ra and cannot reach optical-grade standards. These surfaces may be polished via mechanical methods; however, the process may take up to a few days [4], which makes the process economically challenging, especially when talking about custom-shape lenses. To speed up this process, alternative ways to polish IOLs are on the search.

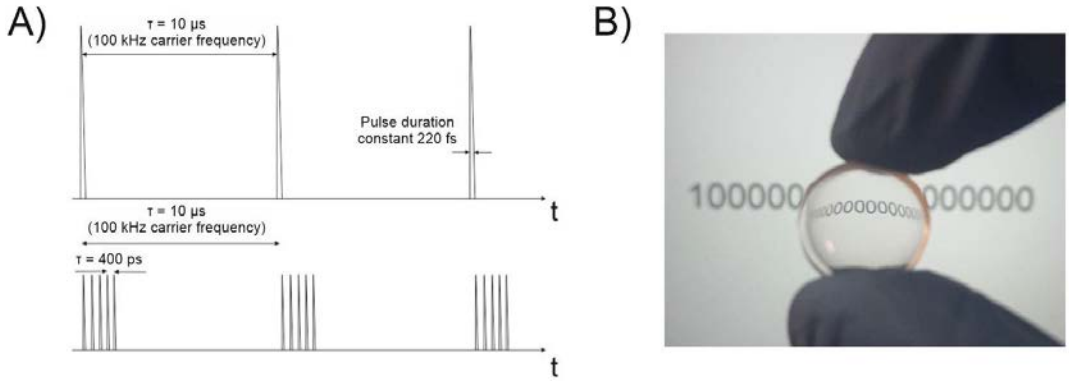

Fig. 1. Femtosecond laser pulses divided into bursts schematic (A); curved surface polished using bursts of femtosecond laser pulses.

The aim of this study is the investigation of the polishing capabilities of rough (0.7 - 3 Õm Ra) hydrophilic acrylic surfaces using bursts of femtosecond laser pulses (laser ñCarbideò), a regime, where single pulses are divided into a sequence of sub-pulses with a time separation of 400 ps. (see Figure 1 (A)). Femtosecond laser pulses were divided into burst packets of 2, 5, 10, 25 sub-pulses, the individual amplitudes were levelled to an error of approximately 10 %. Ablation of the surface was carried out on hydrophilic acrylic (Contamac CONTAFLEX 26% UV-IOL (R)) samples in a two-step process: ablating the desired shape and subsequent polishing using different burst modes. In the first step, number of samples were prepared having different surface roughness values ranging from 0.7 to 3 Õm Ra. In the second step, a series of surface polishing experiments were conducted using bursts of femtosecond laser pulses, while monitoring the temperature of the surface with an IR camera. By changing different laser parameters, it was possible to produce optical-quality surfaces (surface roughness < 20 nm Ra). In addition, it was found, that the resulting Ra roughness of the surface after polishing has a clear correlation with the surface temperature during micromachining. Using the two-step approach, it was possible to produce optical components such as a concave lens from the studied hydrophilic material as shown in Figure 1 (B).

[1] Bauer, S.; Schmuki, P.; von der Mark, K.; Park, J. Engineering biocompatible implant surfaces: Part I: Materials and surfaces. *Prog. Mater. Sci.* **2013**, 58, 261ï326.
[2] Congdon, N. Prevalence of Cataract and Pseudophakia/Aphakia among Adults in the United States. *Arch. Ophthalmol*. **2004**, 122, 487ï494.
[3] Kaģukauskas, E.; Butkus, S.; Tokarski, P.; Jukna, V.; Barkauskas, M.; Sirutkaitis, V. Micromachining of Transparent Biocompatible Polymers Applied in Medicine Using Bursts of Femtosecond Laser Pulses. *Micromachines* **2020**, *11*, 1093.
[4] Valle, M.; Yamada, A.; James, R. Intraocular Lens Tumbling Process Using Coated Beads. U.S. Patent 5,961,370, 5 October 1999.

TOWARDS 50 FS SWIR PULSES BY TRANSIENT STIMULATED RAMAN CHIRPED-PULSE AMPLIFICATION WITH SPECTRUM SYNTHESIS

Vytenis Girdauskas[1], Paulius Mackonis[1], Augustinas Petrulėnas[1], Aleksėj Rodin[1]

[1] Solid State Lasers Laboratory, Department of Laser Technologies, Center for Physical Sciences and Technology, Savanoriu ave. 231, LT-02300 Vilnius, Lithuania
vytenis.girdauskas@ftmc.lt

Expanding the coverage of laser sources spectral range is one of the most urgent scientific problems. Near infrared (NIR) lasers (0.7 – 1.1 μm) are well developed to provide high pulse energy, short pulse duration and high repetition rate. However, the wavelength conversion of ultrashort pulses in short-wave infrared (SWIR) spectral region (> 1.1 μm) with good efficiency has not yet been exhaustively studied. Picosecond and femtosecond pulse width SWIR laser sources are required for a wide range of applications, ranging from spectroscopy, biomedicine to material processing and metrology. In strong field physics, high peak power SWIR laser pulses allow to generate high harmonics and reach attosecond pulse width. In this case, increasing the fundamental wavelength makes it possible to achieve higher photon energy [1]. Also, recent studies have shown that with the increase in the wavelength of the laser source for excitation of THz radiation, the conversion efficiency grows by an one order of magnitude [2].

Stimulated Raman scattering (SRS) is a promising wavelength conversion method that also has advantages for pulse compression and its inherent phase matching in gas, liquid or crystalline media, eliminating the need for parametric crystals. However, stimulated Raman scattering with picosecond and femtosecond laser pulses suffers from lower energy conversion efficiency and nonlinear phenomena caused by the optical Kerr effect. The use of broadband supercontinuum pulses as a seed can improve efficiency and stability of SRS-conversion, maintaining beam quality.

The goal of this study was to investigate transient stimulated Raman chirped-pulse amplification (TSRCPA) and to determine the optimal conditions for broadband spectrum synthesis which allows to achieve a pulse width of 50 fs.

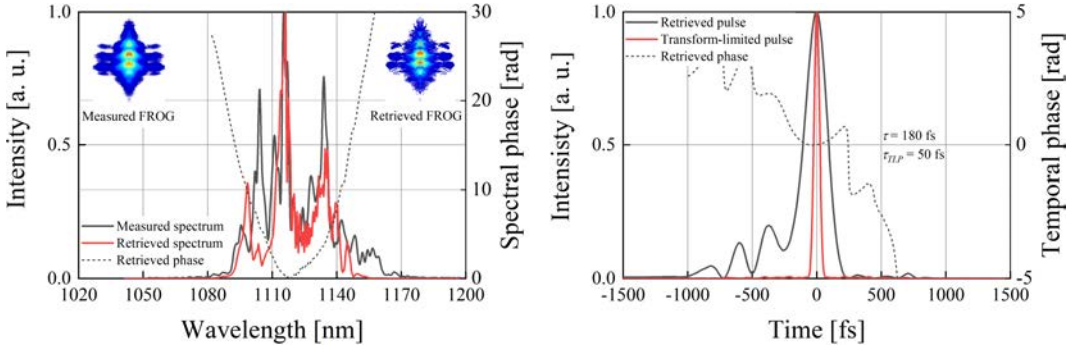

Fig. 1. Left – the measured and retrieved spectrum and spectral phase of the amplified pulse before compression, inset: measured and retrieved FROG traces. Right – retrieved temporal profile of the compressed pulse compared to transform-limited pulse calculated from the spectrum width and retrieved temporal phase.

We report a two-stage TSRCPA system based on KGW crystals seeded with supercontinuum and pumped by 1.2 ps pulses at 1030 nm wavelength [3]. The anisotropic nature of KGW crystal allows several spontaneous Raman scattering modes, which depend on the pump polarization with respect to the crystal axis. This was achieved by rotating KGW crystal about N_p optical axis and controlling pump and seed electric field vectors E parallel to the crystal axes N_g or N_m with Stokes shifts of 767 cm^{-1} and 901 cm^{-1}, respectively. This made it possible to amplify the separate Raman scattering modes and synthesize a common broadband spectrum. In the first amplifier stage, the pump-to-signal conversion efficiency for the 901 cm^{-1} Stokes shift under optimal conditions reached 7 %. The second amplification stage operated in the 768 cm^{-1} Stokes mode and achieved a conversion efficiency of 35 %. Thus, this method of spectrum synthesis made it possible to achieve amplified pulse energy of 460 μJ and expand the spectral bandwidth to 35 nm at a central wavelength of 1120 nm, see 1 fig. left. Amplified pulse bandwidth was about 22 times the pump bandwidth. Eventually, the FROG measurement of the TSRCPA-amplified broadband pulses indicate linear phase modulation, which was partially compensated by N-SF11 prism pair compressor, providing pulse width of up to 180 fs (1 fig. right).

Acknowledgement: This research was partially funded by the European Social Fund under the No 09.3.3.-LMT-K-712-22-0123 Development of Competences of Scientists, other Researchers and Students through Practical Research Activities measure.

[1] B. Dromey, M. Zepf, A. Gopal, K. Lancaster, M.S. Wei, K. Krushelnick, M. Tatarakis, N. Vakakis, S. Moustaizis, R. Kodama, and M. Tampo, High harmonic generation in the relativistic limit, *Nature Phys.* **2**(7), 456–459 (2006).

[2] A.D. Koulouklidis, C. Gollner, V. Shumakova, V.Y. Fedorov, A. Pugžlys, A. Baltuška, and S. Tzortzakis, Observation of extremely efficient terahertz generation from mid-infrared two-color laser filaments, *Nat. Commun.* **11**(1), 1–8 (2020).

[3] P. Mackonis, A. Petrulėnas, A.M. Rodin, V. Girdauskas, and A. Michailovas, Two-stage transient stimulated Raman chirped-pulse amplification in $KGd(WO_4)_2$ with compression to 145 fs, *Opt. Lett.* **45**(24), 6627–6630 (2020).

OPTIMIZATION OF GaInAs/GaAs QUANTUM WELL TECHNOLOGY FOR APPLICATIONS IN NEAR INFRARED VERTICAL-EXTERNAL-CAVITY SURFACE-EMITTING LASERS

Andrea Zelioli[1], Algirdas Jasinskas[2], Ada Gajauskaitā[2], Simona PÎkienā[2], Lukas Joļionis[2], Evelina Dudutienā[2], Bronislovas Ļechaviļius[2] and Renata Butkutā[2, 3]

[1] Department of Physics, University of Modena, Italia
[2] Center for Physical Sciences and Technology, Vilnius, Lithuania
[3] Institute of Photonics and Nanotechnology, Faculty of Physics, Vilnius University, Lithuania
190558@studenti.unimore.it

Today lasers are used in many fields, particularly in optical fiber communication, optical digital recording, material processing, biology and medicine, spectroscopy, imaging, entertainment, and many others. Increasing demand of exceptional investigation conditions studying various materials require unique set of laser parameters - emission wavelength, its tunability, beam quality, operation temperature, optical output power. Herewith, convenient method of laser excitation, power consumption, high-speed modulation and device size become very important factors.

Vertical-external-cavity surface-emitting lasers (VECSEL), also called optically pumped semiconductor lasers or semiconductor disk laser belong to relatively new laser family that combines many of the desirable properties. In comparison to both types of electrically pumped, vertical-cavity surface-emitting lasers (VCSEL) emitting low power circular fundamental transverse mode beam and edge emitting lasers (Fabry-Perot and DFB) reaching high output power but exhibiting asymmetric beam with strong angular divergence, VECSELS are capable to generate high optical power beam keeping high circular quality [1-3].

In this work the behaviour of the emission wavelength was studied in relation to the design parameters of the VECSEL chip.

Modelled VECSEL structure is demonstrated in Fig.1. To obtain lasing it is necessary to design the Bragg mirror, gain region and surface barrier layer (window) depending on the target wavelength of the laser. The gain region is usually composed from quantum well structure calculated to match the laser optical standing wave antinodes as shown in Fig.1 (green curve).

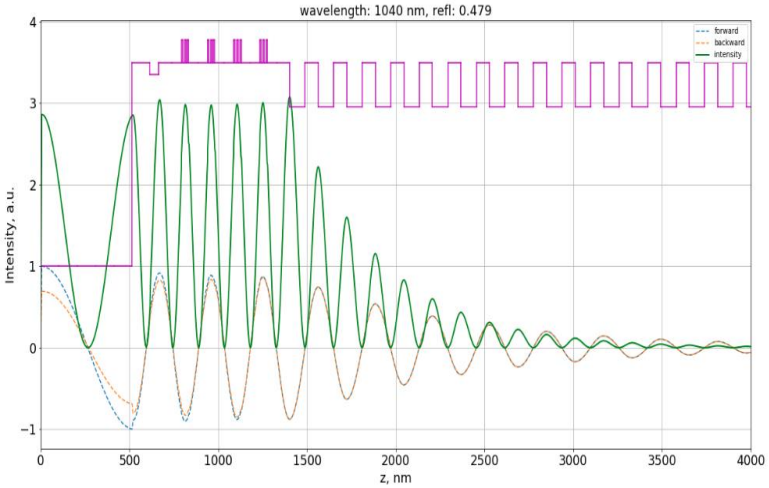

Fig. 1. Energy levels of modelled VECSEL structure.

Multiple InGaAs/GaAs quantum wells (MQWs) and AlAs/GaAs Distributed Bragg reflector (DBR) were used for VECSEL architecture. The separate layers and VECSEL structures were grown using solid-source MBE system (Veeco GENxplor R& D) equipped with standard cells for metallic Al, Ga and unique As design source generating pure arsenic dimers flux. The structure was grown on semi-insulating GaAs substrate oriented in (001) crystalline plane. To balance strain of QW in the laser structure, QW width d and In content was varied. In content in the QW was changed from 5% to 30%, thickness of QW was ranged between 3 nm and 8 nm. The emission wavelength of grown multiple quantum wells and VECSEL structures was measured using photoluminescence spectroscopy at wide temperature range of 300 K - 4K. The quality of DBR in spectral range from 800 nm to 1500 nm was tested using ellipsometer.

After detailed study of In content and QW thickness influence to the optical properties of MQW, the complete chip was fabricated, aiming at the production of a VECSEL demonstrating emission wavelength of 976 nm. The reflectance of DBR was modelled for 25-30 GaAs and AlAs periods to obtain higher than 97% at central DBR wavelength of 976 nm. The number of InGaAs MQWs was optimized to 12. The active area of structure was covered by 165 nm thick-AlAs window and 5 nm GaAs capping layer. The results of Reflectance and Photoluminescence measurements and characterization by Atomic Force Microscopy of grown layers and VECSEL structures will presented.

[1] Mark Kuznetsov, VECSEL Semiconductor Lasers: A Path to High-Power, Quality Beam and UV to IR Wavelength by Design, Semiconductor Disk Lasers. Physics and Technology. Edited by Oleg G. Okhotnikov, 2010, WILEY-VCH Verlag GmbH & Co. KGaA, Weinheim
[2] D. Patil; Semiconductor laser diode: technology and applications, Intech (2012) pp. 217-219.
[3] M. Guina et al., Journal of Physics D: Applied Physics 50 (2017).

O13-4

DID NOT PARTICIPATE

FABRICATION OF THREE-DIMENSIONAL MICROELEMENTS BY TWO-PHOTON LITHOGRAPHY FOR REFRACTIVE INDEX MEASUREMENTS

Diana Gonzalez-Hernandez, Simonas Varapnickas, Mangirdas Malinauskas

Laser Research Center, Faculty of Physics, Vilnius University, Lithuania
laura.gonzalez@ff.stud.vu.lt

Two-photon lithography (TPL) technique has shown the versatility of creation of true three-dimensional (3D) microstructures for optical applications in the recent years. Most of the 3D geometries are a combination of basic shapes such as plane surfaces, curved surfaces, and sharped edges. For this reason, we focused this work in the design of spherical lenses and rectangular prisms which fulfill such conditions. Different approaches have been done for the fabrication of curved surfaces resulting in different surface quality. Writing by subregional slicing [1] and equal-arc slicing [2] methods have shown an improvement in the optical quality of the structures, but the complexity of the implementation limits the fabrication process. The TPL is based on point-by-point process allowing overlapping of voxel during fabrication which determines the lens quality and surface smoothness. We implemented a spiral sphere writing method based in the parametrization in Cartesian representation of the two-dimensional Archimedean spiral in polar coordinates for the writing of concentric shells to form lenses [3].

To optimize the imagining performance of micro-optical elements, detailed knowledge of dispersion is required. Different methods for refractive index characterization have been used, such as interferometry [4], ellipsometry [5], coupler prism m-lines [6], and critical angle by total internal reflection [7]. However, these techniques can be applied only with two-dimensional specimens. We propose a refractive index measurement technique based on the index-matching oils method [8]. The versatility of the proposed method could lead to accurate measurements of refractive index of complex three-dimensional structures and not only two-dimensional flat structures. To perform such measurements, we designed an array of spherical lenses and rectangular prisms with same geometrical characteristics based in the proposed writing method.

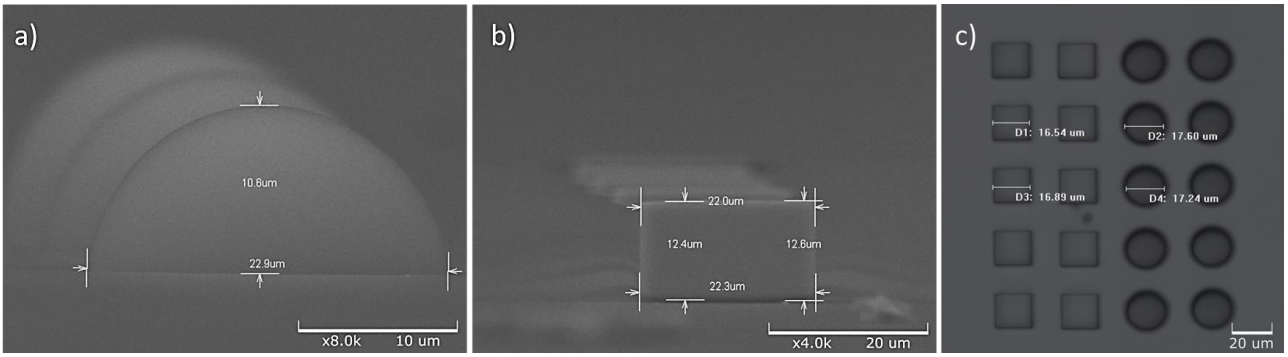

Fig. 1. SEM image of a) 10 um radius spherical lenses and b) rectangular prisms of 12 um height and double length. c) Optical microscope image of array of elements with same geometrical parameters.

We successfully fabricated arrays of elements by TPL system using a 515 nm beam with 80 fs pulse duration 76 MHz repetition rate. Mixture of SZ2080 with 1 weight percent of photoinitiatior was used as prepolymer solution. Using the proposed spiral sphere writing method, we fabricated spherical lenses and linear scanning writing method for layer-by-layer fabrication of rectangular prisms. We achieved high repeatability of structures and error in dimensions below the required for the application of interest.

[1] S. H. Park, S. H. Lee, D. Y. Yang, H. J. Kong, K. S. Lee, Subregional slicing method to increase three-dimensional nanofabrication efficiency in two-photon polymerization, Appl.Phys. Lett. **87**(15), 1ï 3 (2005).
[2] D. Wu, S. Z. Wu, L. G. Niu, Q. D. Chen, R. Wang, J. F. Song, H. H. Fang, H. B. Sun., High numerical aperture microlens arrays of close packing, Appl. Phys. Lett. **97**(3) (2010).
[3] C. H¿ttig, K. Stemmer., The spiral grid: A new approach to discretize the sphere and its application to mantle convection, Geochem. Geophys. Geosyst. **9**(2) (2008).
[4] A. Ţukauskas, I. Matulaitiene, D. Paipulas, G. Niaura, M. Malinauskas, R. Gadonas., Tuning the refractive index in3D direct laser writing lithography: Towards GRIN microoptics, Laser Photonics Rev. **9**(6), 706ï 712 (2015).
[5] Y. Li, S. Park, M. McLamb, M. Lata, S. Schr° che, D. Childers, I. D. Aggarwal, M. K. Poutous, G. Boreman, T. Hofmann., UV to NIR optical properties of IP-Dip, IP-L, and IP-S after two-photon polymerization determined by spectroscopic ellipsometry, Opt. Express **9**(11), 4318 (2019).
[6] S. Monneret, P. Huguet-Chant¹ me, F. Flory., m-Lines technique: Prism coupling measurement and discussion of accuracy for homogeneous waveguides, J. Opt. **2** (3), 188ï 195 (2000).[4]
[7] T. Gissibl, S. Wagner, J. Sykora, M. Schmid, H. Giessen., Refractive index measurements of photo-resists for three-dimensional direct laser writing, Opt. Express **7**(7), 2293 (2017).
[8] R. J. Nussbaumer, M. Halter, T. Tervoort, W. R. Caseri, P. Smith., A simple method for the determination of refractive indices of (rough) transparent solids, J. Mater. Sci **40**(3), 575ï 582 (2005).

NLRP3 INFLAMMASOME ACTIVATION BY VIRAL-LIKE PARTICLES IN MACROPHAGES

Kristina Maġalaitā[1], Asta Luļ iÎ naitā[1], Indrā Dalgādienā[1] Aurelija Ç virblienā[1]

[1] Institute of Biotechnology, Life Sciences Center, Vilnius University, Vilnius, Lithuania
kristina.masalaite@gmail.com

Inflammasomes are intracellular protein complexes and important components of the innate immune system. The best described inflammasome is NLRP3, which contains three major components - nucleotide-binding and oligomerization domain-like receptor, adapter protein apoptosis-associated speck-like protein (ASC) and procaspase-1 [1]. NLRP3 inflammasome activation results in cleavage and activation of inflammatory cytokines, like IL-1ƀ, and inducing inflammatory cell death ï pyroptosis [2]. Activation of NLRP3 inflammasome is associated with various diseases, including asbestosis, gout, Alzheimerõs disease and auto-inflammatory diseases. In our previous research we showed that NLRP3 inflammasome is activated by soluble amyloid-beta protein oligomers and protofibrils [3]. The aim of this study was to extend the latter research and determine whether oligomeric proteins of different structure activate NLRP3 inflammasome in macrophages.

Human monocytic cell line THP-1, differentiated to macrophages were selected as cell culture model for this study. Cells were treated with various viral oligomeric proteins: filaments forming measles and mumps viral proteins [4, 5]; spherical viral-like particles (VLPs) of these polyomaviruses ï Karolinska Institutet polyomavirus (PyV), Merkel cell PyV [6], John Cunningham PyV [7]. MCC950 was used to inhibit NLRP3 inflammasome activation. NLRP3 activation was studied by evaluating cell viability by LDH detection assay, IL-1ƀ and TNF-Ŭ cytokine release by ELISA, active caspase-1 detection using fluorescent probe FLICA, which binds to the activated caspase-1, and ASC speck detection using THP-1 macrophages expressing ASC protein fused to green fluorescent protein.

It was found that filament-like nucleocapsid proteins of measles and mumps viruses did not cause any inflammatory response in macrophages. In contrast spherical VLPs of polyomaviruses triggered cell death, induced IL-1ƀ secretion and ASC speck formation in human cell model indicating NLRP3 inflammasome activation. In addition, it was demonstrated that cathepsins are involved in NLRP3 activation induced by polyomavirus VLPs. To conclude, our results demonstrate that viral proteins can activate inflammasome depending on their structural properties.

Funding:
The study was funded by Research Council of Lithuania (LMTLT), project no. S-SEN-20-11.

[1] Walsh JG, Muruve DA, Power C. Inflammasomes in the CNS. Nat Reviuews Neurosci. 15(2): 84ï 97 (2014).
[2] Elliott EI, Sutterwala FS. Initiation and perpetuation of NLRP3 inflammasome activation and assembly. Immunol Rev. 265: 35ï 52 (2015).
[3] Luļ iÎ naitā A, McManus RM, Jankunec M, R§cz I, Dansokho C, Dalgādienā I, *et al.* Soluble Aƀ oligomers and protofibrils induce NLRP3 inflammasome activation in microglia. J Neurochem. (October 2019): 1ï 12 (2019).
[4] Slibinskas R, Zvirbliene A, Gedvilaite A, Samuel D, Jin L, Beard S, *et al.* Synthesis of mumps virus nucleocapsid protein in yeast Pichia pastoris. J Biotechnol. 103(1): 43ï 49 (2003).
[5] Samuel D, Sasnauskas K, Jin L, Gedvilaite A, Slibinskas R, Beard S, *et al.* Development of a measles specific IgM ELISA for use with serum and oral fluid samples using recombinant measles nucleoprotein produced in Saccharomyces cerevisiae. J Clin Virol. 28(2): 121ï 129 (2003).
[6] Norkiene M, Stonyte J, Ziogiene D, Mazeike E, Sasnauskas K, Gedvilaite A. Production of recombinant VP1-derived virus-like particles from novel human polyomaviruses in yeast. BMC Biotechnol. 15(1): 1ï 14 (2015).
[7] Sasnauskas K, Bulavaite A, Hale A, Jin L, Knowles WA, Gedvilaite A, *et al.* Generation of Recombinant Virus-Like Particles of Human and Non-Human Polyomaviruses in Yeast *Saccharomyces cerevisiae*. Intervirology. 45(4ï 6): 308ï 317 (2002).

INVESTIGATION OF A NEW ORGANIC CONTROL MEASURE AGAINST INVASIVE SLUGS

Mantas Adomaitis[1], Grita Skujienė[1]

[1] Department of Zoology, Institute of Biosciences, Life Sciences Centre, Vilnius University, Lithuania
mantas.adomaitis@gmc.vu.lt

The Spanish slug, *Arion vulgaris* Moquin-Tandon, 1855, is a serious pest in agriculture and private gardens around the world [1]. Saponins, which are secondary metabolites of plants, have previously been shown to have strong molluscicidal effect [2]. The use of saponins-rich plant extracts is gaining importance as are safe (as saponins residues) in agriculture products [3]. However, despite of the proven safety in food, they still do not have a widespread application due to their liquid form and absence of more accurate knowledge of effects on other organisms. White worm, *Enchytraeus albidus* Henle, 1837, is an important model of decomposer organisms in the terrestrial ecosystem [4]. We investigated which doses of saponins are lethal to the slug, *A. vulgaris*, and to the non-target organism, *E. albidus*. An aqueous solution with different concentrations of saponins extract from the bark of the soap tree, *Quillaja saponaria* Mol., was used in repeated treatments. Slugs were tested in filter paper contact tests as they are naturally exposed to soil contact while crawling. Worms were tested in soil contact tests as they live below ground. It was found that lethality of saponins depends on the slugs' age group and environmental temperature. The median lethal concentration (LC_{50}, at 15°C) on adults was 68.5 g/l, and on juveniles, 96.9 g/l. The slugs were significantly more sensitive at 2 and -1°C compared to 15°C. The LC_{50} (at 6°C) on *E. albidus* was 2.7 g/l (or 0.5 g/kg dry weight of soil), far below those in *A. vulgaris* (at 15°C and lower). The LC_{50} for worms at -1°C was also significantly lower than at 6°C (Table 1) [5].

Table 1. Dose-response parameters of *Quillaja* aqueous extract for slugs and worms in g/l (average ± standard error). LC_{50} – median lethal concentration, $\chi 2$ – goodness of fit of probit lines.

Species	Life stage	Temperature (°C)	LC_{50}	χ^2 (df, *P*)
A. vulgaris	Adult	+15	68.52 ± 8.38	15.68 (27, 0.9588)
A. vulgaris	Juvenile	+15	96.94 ± 13.84	16.731 (17, 0.4727)
A. vulgaris	Adult	+2	33.52 ± 7.49	29.077 (30, 0.5135)
A. vulgaris	Adult	-1	18.38 ± 3.64	20.986 (31, 0.9123)
E. albidus	Adult	+6	2.72 ± 0.09	22.792 (29, 0.7857)
E. albidus	Adult	-1	2.07 ± 0.11	51.252 (46, 0.2753)

Therefore, we can conclude: 1) that *Q. saponaria* saponins may be a successful slug control tool used during the colder time of the year, but its concentration should be selected according to the age group of *A. vulgaris*; 2) this measure was more toxic than expected to white worms, therefore, more research should be done with other groups as well.

[1] J. Kozłowski, The distribution, biology, population dynamics and harmfulness of *Arion lusitanicus* Mabille, 1868 (Gastropoda: Pulmonata: Arionidae) in Poland. J. Plant Prot. Res. **47**, 119-230 (2007).
[2] D. González-Cruz, R. San Martín, Molluscicidal effects of saponin-rich plant extracts on the grey field slug, Cienc. Inv. Agr. **40**, 341-349 (2013).
[3] Ö. Güçlü-Üstündağ, G. Mazza, Saponins: properties, applications and processing, Crit. Rev. Food Sci. Nutr. **47**, 231-258 (2007).
[4] C. Erséus, M.-J. Klinth, E. Rota, et al., The popular model annelid *Enchytraeus albidus* is only one species in a complex of seashore white worms (Clitellata, Enchytraeidae), Org. Divers. Evol. **19**, 105-133 (2019).
[5] M. Adomaitis, G. Skujienė, Lethal doses of saponins from *Quillaja saponaria* for invasive slug *Arion vulgaris* and non-target organism *Enchytraeus albidus* (Olygochaeta: Enchytraeidae), Insects **11**, 1-11 (2020).

MOLECULAR BIOMAKERS OF MOUSE TUMOR IMMUNOGENICITY AND PREDICTION OF RESPONSE TO DENDRITIC CELL VACCINES AND ANTI-PD-1 TREATMENT

Karolina Zilionyte[1,2], Ugne Bagdzeviciute[3], Elena Urbstaite[2], Agata Mlynska[1], Emilija Paberale[1], Neringa Dobrovolskiene[1], Vita Pasukoniene[1]

[1] National Cancer Institute, Vilnius, Lithuania
[2] Vilnius University, Vilnius, Lithuania
[3] Vilnius Gediminas Technical University, Vilnius, Lithuania
karolina.zilionyte@nvi.lt

Immunotherapy is a promising cancer treatment that stimulates patient's immune system to fight against tumor. However, the response to cancer immunotherapy is only achieved in a small subset of patients (Fig. 1). Recent studies showed that unequal response to immunotherapy might be governed by tumor immune characteristics. Classification of patients by tumor immune properties in order to individualize immunotherapy is not widely used in the clinics, basically due to the lack of proper molecular markers. The aim of our study was to find two immunologically distinct murine tumor models and molecular markers for their stratification and prediction of response to treatment with dendritic cell vaccines and anti-PD-1.

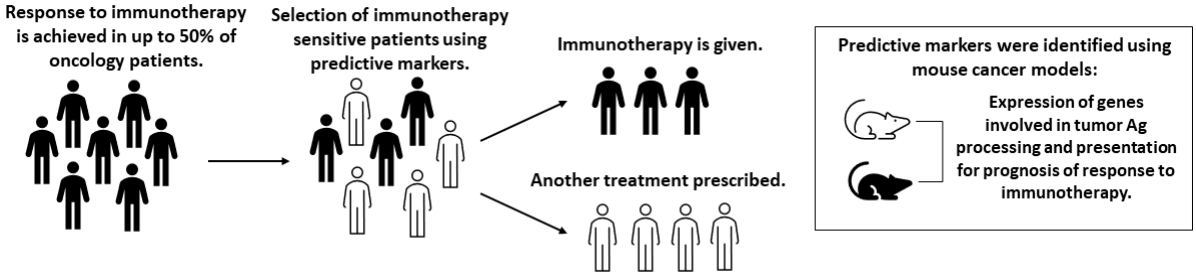

Fig.1. Principal idea of this research.

C57BL/6 syngeneic glioma GL261 and lung carcinoma LLC1 cells were chosen for comprehensive investigation of immunological properties. GL261 and LLC1 cells were assessed by their ability to process and present tumor antigens (Ag) and the general nature of developing anti-tumor immune response. For this reason MHC I and PD-L1 expression was measured on GL261 and LLC1 cells surface. Also in collected primary tumor samples immune cell infiltration, expression of immune-related genes and genes involved in Ag processing and presentation were evaluated. These studies were followed by murine dendritic cell vaccines (DCV) and anti-PD-1 efficacy analysis in the treatment of mice with subcutaneously induced GL261 or LLC1 tumors. DCV were generated from murine bone marrow cells by differentiating with GM-CSF + IL-4 cytokines for 7 days [1] and maturing with LLC1 or GL261 cell lysate and *E.coli* lipopolysaccharide. Mice response to DCV and anti-PD-1 treatment was assessed by tumor size, changes in immune cell infiltration and expression of immune-related genes. All experimental protocols were approved by the local Institutional Animal Care Committee.

Our study showed that GL261 and LLC1 tumors possess different immune properties. The largest differences between these tumors were observed when assessing their ability to process and present tumor Ag. Significant decrease in the expression of genes involved in this process (such as *Tap1, Tap2, Psmb8, Psmb9, Psmb10, Erap1, Irf2*) were observed in LLC1 tumors. Impaired Ag processing and presentation mechanism in LLC1 cells resulted in low tumor immunogenicity, leading to the absence of effective anti-cancer immune response. By contrast in GL261 cells Ag processing and presentation mechanism was not altered, making them immunogenic and resulting in formation of anti-tumor immune reaction. Differences were also seen then treating tumors with DCV or anti-PD-1, there they effectively slowed GL261 development and almost had no effect for LLC1 tumors.

Changes in Ag processing and presentation mechanism might result in tumor insensitivity to dendritic cell vaccines and anti-PD-1 therapy. Therefore, expression evaluation of genes involved in Ag processing and presentation pathway (*Psmb8, Psmb9, Psmb10, Tap1, Tap2, Erap1, Irf2*) might help to stratify primary untreated murine tumors and predict their response to dendritic cell vaccines and anti-PD-1 treatment.

[1] Lutz MB et al. An advanced culture method for generating large quantities of highly pure dendritic cells from mouse bone marrow. J Immunol Methods. 1999 Feb 1;223(1):77-92. doi: 10.1016/s0022-1759(98)00204-x.

NEUROGENIC DIFFERENTIATION OF HUMAN AMNIOTIC FLUID STEM CELLS FROM HEALTHY AND FETUS AFFECTED PREGNANCIES

Aistã Zentelytã, Elizabet Berģanskytã, Giedrã Valiulienã, RÎta Navakauskienã

Department of Molecular Cell Biology, Life Sciences Center, Vilnius University, Lithuania
aiste.zentelyte@bchi.vu.lt

Human amniotic fluid stem cells (AFSC) are a very promising source of stem cells for therapeutic applications. Because of their broad differentiation potential and high proliferation capabilities AFSCs are widely researched. But in order to employ AFSCs in clinical settings, the differences of stem cell properties of cells isolated from healthy and fetus affected pregnancies needs to be elucidated. Our study was focused on addressing metabolic, neurogenic and neurotrophic potential and differences of AFSCs obtained from normal gestations and gestations affected with polyhydramnios.

Stem cells were isolated from amniocentesis samples using two-stage isolation protocol and expanded in monolayer culture *in vitro*. Isolated cells were characterized and showed similar levels of pluripotency gene (*SOX2, NANOG, LIN28A*, etc.) expression and mesenchymal stem cell surface marker (CD44, CD146, CD166) expression, but higher expression levels of CD13, CD73, CD90 and CD105 were detected in AFSCs from healthy pregnancies. Also, stem cells of ñNormalò and ñPathologyò groups were found to be different in terms of oxidative phosphorylation rate, production of ATP and reactive oxygen species. AFSCs from both sources were induced to differentiate towards neurogenic lineage using four differentiation medias composed of commercial supplement N2, neurotrophins (BDNF, NGF) and signaling molecules (cAMP, IBMX, KCl, retinoic acid). Differentiation of AFSCs was confirmed by morphological changes, cytoskeletal reorganization and neural marker expression (Figure 1).

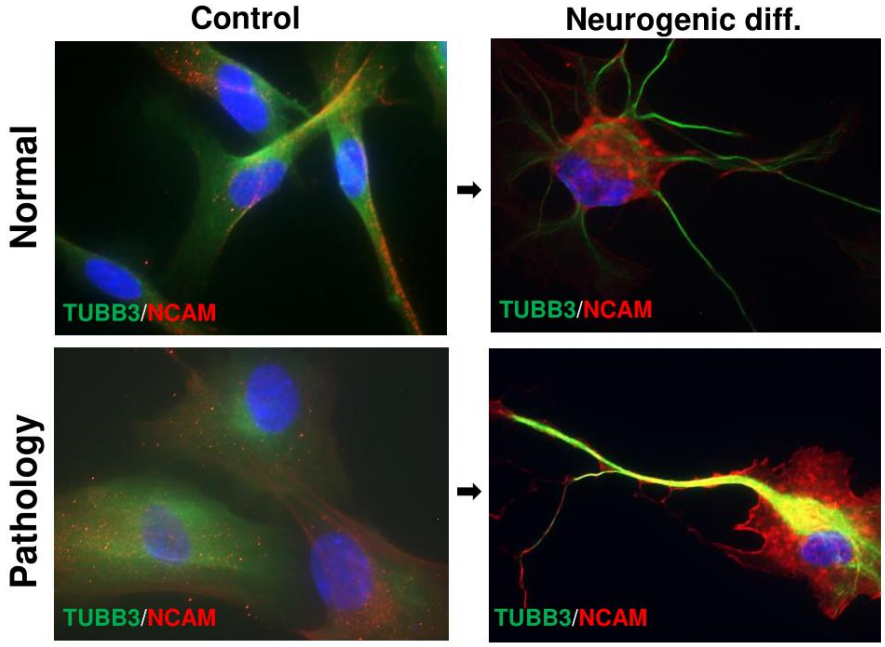

Fig. 1. Immunofluorescence analysis of AFSCs showing positive cells for neural marker TUBB3 protein (green) as well as neural marker NCAM (red). Nuclei were counterstained with DAPI (blue).

Neurogenic differentiation was also confirmed by upregulated expression of differentiation associated genes (*NCAM1, VIM, NeuroD1, SYP, MAP2, GFAP, S100B, NTRK1*, etc.). The secretion levels of neurotrophic factors BDNF and VEGF in differentiated AFSCs were upregulated as well, with higher upregulation ratio in Normal samples. Furthermore, AFSCs from polyhydramnios samples were distinguished by secretion of pro-inflammatory cytokine TNFŭ which secretion levels were significantly downregulated after differentiation.

Overall, our results suggest that AFSCs isolated from healthy pregnancies differentiate towards neurogenic lineage more efficiently compared to AFSCs from polyhydramnios samples. These observations provide new insights into the properties and neurogenic differentiation potential of AFSCs obtained from fetus unaffected and fetus affected gestations, although more detailed studies are required for bringing these cells closer to clinical applications.

SPECIES OF THE GENUS *ANTOCHA* OSTEN SACKEN 1860 (DIPTERA: LIMONIIDAE) IN SICHUAN (CHINA)

Radvilã Markeviļ iÎ tã

Nature Research Centre, Akademijos str. 2, LT-08412 Vilnius, Lithuania
radvile.mark@gmail.com

Genus *Antocha* Osten Sacken, 1860 with three subgenera *Antocha* (s. str.) Osten Sacken 1860, *Proantocha* Alexander, 1919 and *Orimargula* Mik, 1883 includes 158 species, four subspecies [1] and according to Catalogue of the Craneflies of the World this genus is recorded from all zoogeographic regions [2]. The subgenus *Antocha* (s. str.) is the most species-rich subgenus of the genus *Antocha*, with 112 valid species and two subspecies, including 17 species and two subspecies recorded from Sichuan (China). Adults of the genus *Antocha* are small (3 mm) to medium-sized (11 mm) crane flies, which are found near streams or rivers [1]. Wings of these insects are wide with large, nearly right-angled anal angle [1].

The taxonomy of the genus remains unclear; several species are known only from the unique female holotypes and no phylogenetic analysis of *Antocha* has been undertaken. Due to lack of information, it is difficult to identify species of this genus, thus this group of insects is not well known.

This research was carried out in Sichuan province (China). One species was described as new to science (Fig. 1). Insects of the new species have sclerotized and twisted into spiral genital structures ï parameres, which are different in other species [1].

Fig. 1. Adult insect of the genus *Antocha*.

Taxonomy is foundational to Biology. If the scientific name and systematic of any life form is unclear, it will be impossible to repeat an experiment, the results will be incomparable, and hypotheses will be untested. Therefore, scientific works such as this provide foundation for other scientific works.

[1] R. Markeviļ iÎ tã, S. Podenas, A. Saldaitis, R. Bernotienã, A new species of *Antocha* Osten Sacken, 1860 (Diptera: Limoniidae) from Sichuan, China, Zootaxa **4661**, 118-132 (2019).
[2] P. Oosterbroek, Catalogue of the Craneflies of the World (CCW). Available from: http://nlbif.eti.uva.nl/ ccw/index.php

CONICAL THIRD HARMONIC GENERATION FROM FEMTOSECOND LASER INDUCED NANOGRATING IN TRANSPARENT MATERIALS DURING FILAMENTATION AT HIGH REPETITION RATES

Robertas Grigutis[1], Vytautas Jukna[1], Marius Navickas[1], Gintaras Tamoġauskas[1], Kňstutis StaliÎnas[1,2], Audrius Dubietis[1]

[1] Laser Research Center, Vilnius University, Saulãtekio Avenue 10, LT-10223 Vilnius, Lithuania
[2] Instituci· Catalana de Recerca i Estudis Avan-ats (ICREA), Passeig de Llu²s Companys, 23, 08010, Barcelona, Catalonia, Spain
robertas.grigutis@ff.vu.lt

Laser-induced periodic surface structures (LIPSS) are a universal physical phenomenon, which occurs on many materials (metals, semiconductors, dielectrics) within focal spot of the linearly polarized laser radiation [1] and find many applications in plasmonics, photonics and microfluidics [2]. Gradual transition from LIPSS to a polarization-independent low spatial frequency structures, called laser-induced periodic annular surface structures (LIPASS) in the center of the damage crater was observed [3] and more importantly, the formation of nanogratings in the volume of various materials was investigated [4]. More recently, conical third harmonic (TH) generation from in-bulk optical damage was reported and its correlation with extinction of supercontinuum radiation was unveiled [5].

In this Study we demonstrate that filamentation of femtosecond laser pulses at high repetition rate inscribes a nanograting in the volume of transparent nonlinear material, that has a certain spectrum of periods and corresponding lattice vectors, necessary to fullfil the phase-matching condition for conical TH generation. These findings are supported by the measurements of TH cone angles inside of various nonlinear crystals and glasses: YAG, sapphire, YLF, LiF, MgF_2, LiSAF, LiCAF, fused silica and BK-7 glass, performed with an amplified Yb:KGW laser that delivers 180 fs, 1035 nm pulses at 200 kHz repetition rate, see Fig. 1(a). We also investigated LIPSS and LIPASS morphology (Fig. 1(b) and (c) respectively) and the corresponding spectra of nanograting periods retrieved by 2D Fourier transform (Fig. 1(d)). Our results show that conical TH generation occurs as a noncollinear four-wave mixing process, where the TH cone angle is defined by the longitudinal phase-matching set by the material dispersion, while the transverse phase-matching involves the reciprocal lattice vector of nanograting, which is produced by high repetition rate filamentation of femtosecond laser pulses.

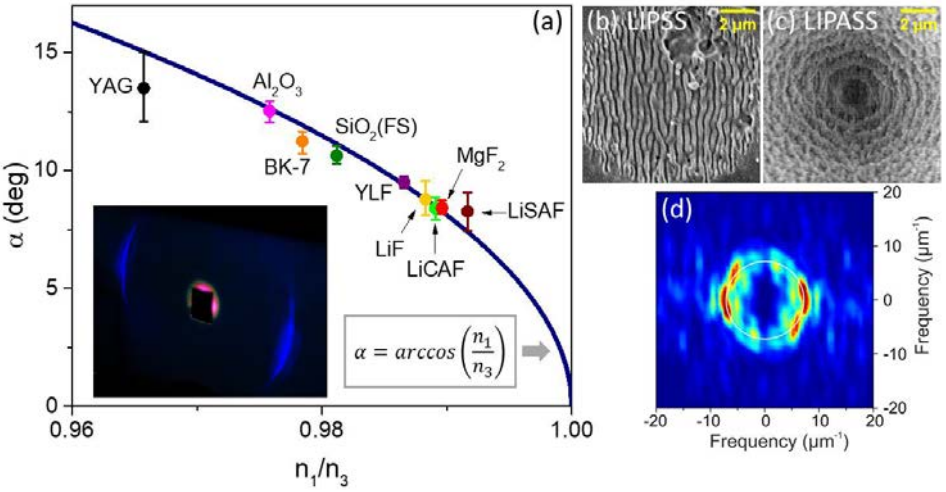

Fig. 1. (a) Measured TH cone angles in various materials. The inset shows a screenshot of conical TH emission in sapphire. (b) SEM image of LIPSS and (c) LIPASS on the surface of sapphire. (d) 2D Fourier transform spectrum of LIPASS, where white circle indicates the nanograting period required to phase-match conical TH generation.

We believe that our study provides a deeper understanding about the nature of conical TH generation and its relation with evolving in-bulk optical damage during femtosecond filamentation and supercontinuum generation in bulk materials at high repetition rates.

[1] J. Bonse, J. Kr¿ger, S. Hº hm, and A. Rosenfeld, "Femtosecond laser induced periodic surface structures", J. Laser Appl. **24**, 042006 (2012).
[2] R. Buividas, M. Mikutis, and S. Juodkazis, "Surface and bulk structuring of materials by ripples with long and short laser pulses: Recent advances", Prog. Quantum Electron. **38**, 119ï 156 (2014).
[3] Y. Liu, Y. Brelet, Z. He, L. Yu, B. Forestier, Y. Deng, H. Jiang, and A. Houard, "Laser-induced periodic annular surface structures on fused silica surface", Appl. Phys. Lett. **102**, 251103 (2013).
[4] A. Rudenko, J.-P. Colombier, S. Hº hm, A. Rosenfeld, J. Kr¿ger, J. Bonse, and T. E. Itina, ñSpontaneous periodic ordering on the surface and in the bulk of dielectrics irradiated by ultrafast laser: a shared electromagnetic originò, Sci. Rep. **7**, 12306 (2017).
[5] R. Grigutis, G. Tamoġauskas, V. Jukna, A. Risos, and A. Dubietis, "Supercontinuum generation and optical damage of sapphire and YAG at high repetition rates", Opt. Lett. **45**, 4507ï 4510 (2020).

AXISYMMETRIC DIFFRACTIVE REFLECTOR FOR BEAM SUPER-COLLIMATION

Indre Meskelaite[1], Darius Gailevicius[1,2], Martynas Peckus[1], Lina Grineviciute[1,3], Ruslan A. Lymarenko[4], Victor B. Taranenko[4], Kestutis Staliunas[1,5,6]

[1] Vilnius University Laser Research Center, 10 Sauletekio avenue, LT- 10223, Vilnius, Lithuania
[2] ñFemtikaò, 15 Sauletekio avenue, LT-10224, Vilnius, Lithuania
[3] Center for Physical Sciences and Technology, 231 Savanoriu avenue, LT-10224, Vilnius, Lithuania
[4] International center ñInstitute of Applied Opticsò NAS of Ukraine, Kudryavskaya Str. 10G, 04053, Kyiv, Ukraine
[5] Instituci· Catalana de Recerca i Estudis Avancats (ICREA), Passeig Llu²s Companys 23, 08010, Barcelona, Spain
[6] Universitat Polit¯cnica de Catalunya (UPC), Rambla Sant Nebridi 22, 08222, Terrassa (Barcelona) Spain
indre.meskelaite@ff.stud.vu.lt

Recently, it has been proposed to use an axisymmetric 3D photonic crystal inside the cavity of a wide aperture microchip laser in order to increase the brightness and the spatial quality of its emission [1]. However, the fabrication of such 3D structures technologically is a very challenging task. Therefore, the idea to combine the properties of 3D photonic crystals [2] and the manufacturing advantages of flat optics by the use of a 2D structure positioned close and parallel to the surface of a mirror has been suggested.

Here we theoretically explain and experimentally prove the far field effects of the axisymmetric diffractive reflector ï a thin transmissive concentric diffraction grating placed at a distance of several micrometers in front of a flat mirror. This configuration provides the effect of super-collimation which is defined by an enhancement of axial components of Gaussian laser beam reflected from such structure. The interpretation of this effect is based on the axisymmetric diffusion of the radiation during the process of diffraction into higher diffraction orders and then back to the zero-order diffraction.

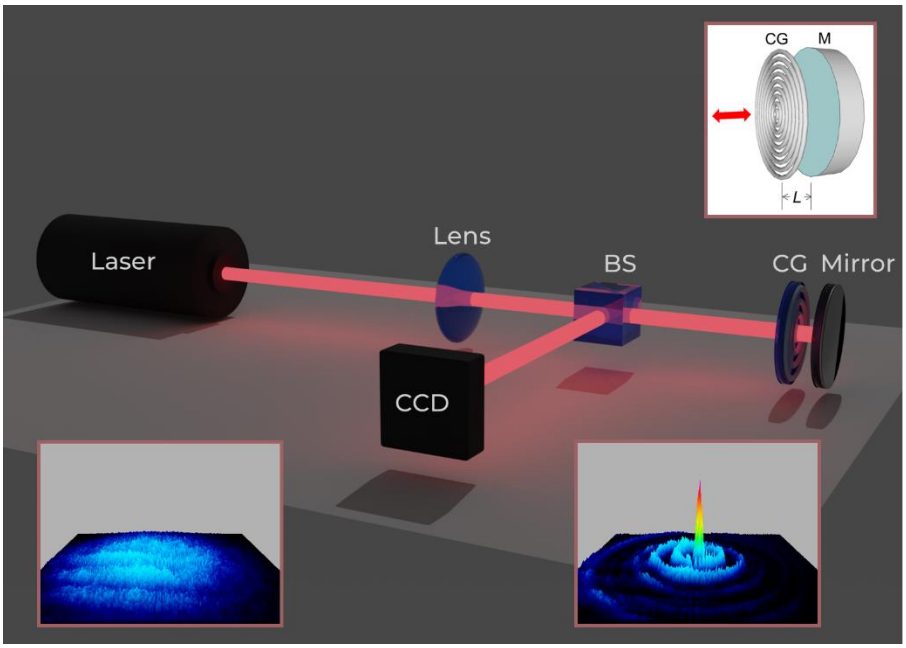

Fig. 1. Experimental scheme with a scheme of axisymmetric diffractive reflector (top right) and measured far field profiles of incident Gaussian (bottom left) and double-diffracted (bottom right) laser beam.

The prototype of the concentric diffraction grating having a quasi-sinusoidal profile and a period of 2 micrometers was fabricated using electron beam lithography. An experimental investigation of the propagation of a diverging Gaussian beam through the grating-mirror tandem (Fig. 1) showed an increase in axial intensity of the reflected beam by up to 7 times. The obtained result qualitatively and quantitatively agrees with the theoretical prediction of the super-collimation effect.

Such axisymmetric diffractive reflectors used as one (or both) cavity mirrors in microlasers could be especially useful for the improvement of the spatial quality of their radiation.

[1] D. Gailevicius, V. Koliadenko, V. Purlys, M. Peckus, V. Taranenko, and K. Staliunas, Photonic Crystal Microchip Laser, Sci. Rep. **6**, 34173 (2016).
[2] V. Purlys, L. Maigyte, D. Galeviļius, M. Peckus, R. Gadonas, and K. Staliunas, Super-collimation by axisymmetric photonic crystals, Appl. Phys. Lett. **104**, 221108 (2014).

HYBRID LIQUID CRYSTAL MICROCAVITY AS A PHOTONIC DEVICE TO CONTROL SYNTHETIC OPTICAL SPIN-ORBIT INTERACTIONS

Sara Piotrowska[1], Mateusz Kr· l[1], Katarzyna RechciŒska[1], Rafağ Mirek[1], Rafağ Mazur[2], Przemysğaw Morawiak[2], Przemysğaw Kula[2], Wiktor Piecek[2], Barbara Piñtka[1], Jacek Szczytko [1,*]

[1] Institute of Experimental Physics, Faculty of Physics, University of Warsaw, Poland
[2] Institute of Applied Physics, Military University of Technology, Warsaw, Poland
[*] Jacek.Szczytko@fuw.edu.pl

Microcavity is an optical resonator, consisting usually of two parallel Distributed Bragg Reflectors (DBR). Such structure allows to trap light in a form of a standing wave. There are some specific electric field distributions called resonator modes, which are obtained due to the condition that the resonator length is an integral multiple of half the wavelength. Photonic modes in microcavities can couple with excitons emerging in a quantum well or different type of emitter (e.g. an organic dye), which leads to weak or strong coupling, both being a source of very interesting phenomena.

By enclosing a nematic liquid crystalline (LC) birefringent medium inside a microcavity (MC), in which LC anisotropy can be controlled by applying an external electric field, we are able to spectrally tune and couple subsequent cavity modes. [1] Recently, we have demonstrated a Rashba-Dresselhaus-like spin orbit coupling (SOC) in such structure, when modes of different parity were brought into a resonance. [2]

In this work, we investigate polarisation-resolved dispersion of spin-orbit coupled modes in a microcavity, that operates in weak coupling regime, with organic dye (pyrromethene-580) incorporated within LC layer. We are allowed to trace cavity modes by detecting photons emitted from the nonresonantly excited sample. We performed angle-resolved tomography to fully map dispersion relation of the cavity modes for all directions of in-plane wave vector of the cavity photons. Polarisation-resolved energy-momentum tomographies for all major regimes in LC MC were included in research: resonance of the modes with opposite parity, when they are coupled by Rashba-Dresselhaus spin-orbit coupling term (Fig. 1) and resonance of the modes of the same parity. Measurements were executed for luminescence and reflectance from the sample.

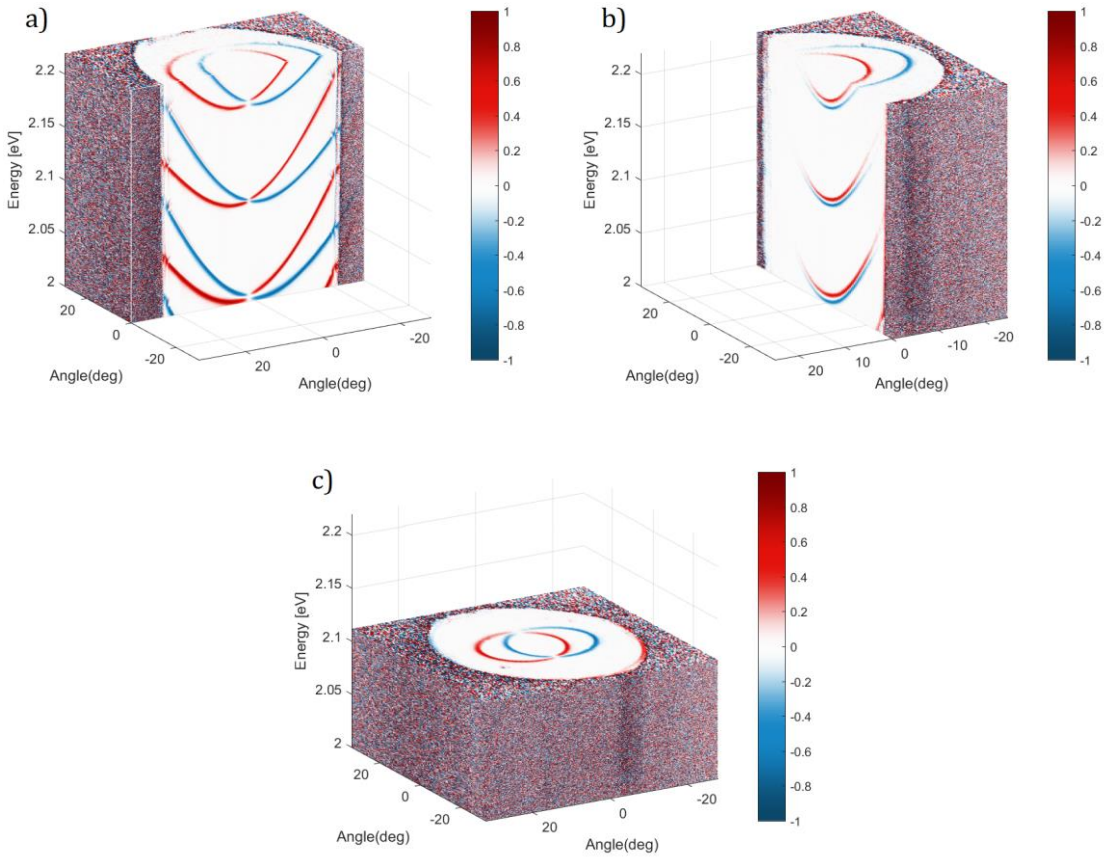

Fig. 1. The third Stokes parameter obtained for the reflectance k-space spectra for the Rashba-Dresselhaus coupling regime sliced with planes at: a) $k_x = 0$, b) $k_y = 0$, c) the energy 2.112 eV.

[1] K. Lekenta et al., Tunable optical spin Hall effect in a liquid crystal microcavity. Light Sci. Appl. **7**, 74 (2018).
[2] K. RechciŒska et al., Engineering spin-orbit synthetic Hamiltonians in liquid-crystal optical cavities. Science **366**, 727 (2019)

DISPERSION ENGINEERING OF WHISPERING GALLERY MODE RESONATORS FOR FREQUENCY COMB GENERATION AND TELECOMMUNICATION APPLICATIONS

Kristians Draguns[1,2], Inga Brice[1], Toms Salgals[2,3], Janis Alnis[1]

[1]Institute of Atomic Physics and Spectroscopy, University of Latvia, 3 Jelgavas Street, 1004, Riga, Latvia
[2]AFFOC Solutions Ltd., 17 Andrejostas street, 1045 Riga, Latvia
[3]Institute of Telecommunications of the Riga Technical University, 12 Azenes Street, 1048, Riga, Latvia
kristians.draguns@lu.lv

Whispering gallery mode resonators (WGMRs) are optical devices with axial simetry, where light is confined within the resonator due to total internal reflection. WGMRs have a typical size of tens to hundreds of micrometers, and experiance strong light-matter interaction due to low losses and high mode density. WGMRs can be used to generate Kerr Frequency combs induced by four wave mixing. The frequency combs are generated at anomalous dispersion and it is desierable to have a flat dispersion profile for best results [1]. Thus it is important to ingeneer the resonator to achieve the dispersion required.

For telecomunication applicattions the desired free spectral range is around 100 GHz, witch translates into a WGMR radius of 332 μm [2]. An interesting geometry is belt type WGMR, where the dispersion profile can be achieved quite flat [3]. The belt resonators are cylindrical structures with an extension with its size characterised by width and height (fig. 1. a).

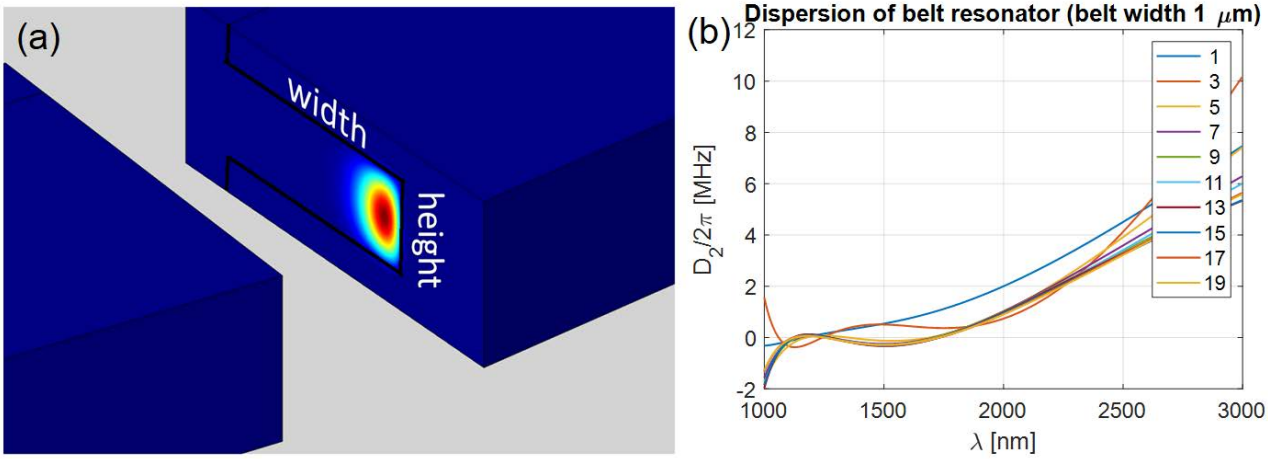

Fig. 1. (a) The electric field distribution inside a belt type fused silica WGMR at 191 THz; (b) calculated second-order dispersion for a belt resonator with the belt width of 1μm and various belt heights shown in the legend in μm.

Computer simulations are made in COMSOL Multiphysics to determine the dispersion. This way we can know at what dimensions we need to make our WGMRs for experiments. For telecommunications the pumping laser should be around 1550 nm ï at the middle of C-band region (1530 nm ï 1565 nm).

[1] S. Fujii, T. Tanabe, Dispersion engineering and measurement of whispering gallery mode microresonator for Kerr frequency comb generation, Nanophotonics 9, 1087ï 1104 (2020).
[2] E.A. Anashkina, M.P. Marisova, A. V. Andrianov, R.A. Akhmedzhanov, R. Murnieks, M.D. Tokman, L. Skladova, I. V. Oladyshkin, T. Salgals, I. Lyashuk, A. Sorokin, S. Spolitis, G. Leuchs, V. Bobrovs, Microsphere-based optical frequency comb generator for 200 GHz spaced WDM data transmission system, Photonics. 7 (2020).
[3] I. S. Grudinin, N. Yu, Dispersion engineering of crystalline resonators via microstructuring, Optica 2(3), 221-224 (2015).

COMPARATIVE NONLINEAR DYNAMICS OF HIGH-POWER FEMTOSECOND LASER PULSES IN KERR MEDIA DEPENDING ON THEIR TOPOLOGICAL CHARGE

Diana Klezovich

Belarusian State University, Physics Faculty, Laser Physics and Spectroscopy Department
diestardom@gmail.com

In present work we compare conditions of spatio-temporal localization of terawatt femtosecond vortex (doughnut) and vortex-less (Gaussian) laser pulsed beams in Kerr media and formation of light bullets. Due to dozens of different applications of light bullets (LB) such as remote sensing of atmosphere, lightning control, high harmonic generation, astronomy, material processing, lithography and so on this activity field draw attention of researchers. As is known, in Kerr media the filamentation makes possible the spatial and temporal compression of pulses. The filament is a self-organized structure formed through the competition of underlying processes such as, for example, diffraction, Kerr nonlinearity, plasma photoinduced via multiphoton absorption or tunnel mechanisms, etc. Under anomalous group velocity dispersion (GVD) one of filamentation regimes may be realized, i.e. LB generation. As shown in experiment [1], the stability of the LB is due to their polychromatic Bessel-like structure consisting of a sharply localized high-intensity core and a weak, delocalized low-intensity periphery, which balances energy losses in the central core.

The system of nonlinear Schrödinger equation for the complex envelope of the electric field and kinetic equation for the electron plasma density is exploited. The Hamiltonian deduced on the base of this equation in approximation of negligible dissipation allowed us to obtain a potential function (Fig. 1). In the frame of two-scale variation approach the system of motion equations for both temporal T(z) and spatial R(z) beam radii was found. The solution of this system allowed to define the stability regions for LB. Solutions of the above equation system have been analyzed in broad spectral range of the anomalous GVD for fused silica and other Kerr solids at different values for topological charge *m* (0,1,2,3,4) and various ratios of input pulse power to critical one for self-focusing $\alpha>10$. Under suggestion that the multi-photon ionization mechanism is dominated, we deduced the expressions for stationary values T_0 and R_0 corresponding to the minimum of the potential function V(R,T) and estimated their values in dependence on medium and radiation parameters. The stability is originated from the complete balance of all underlying processes accompanying the pulsed beam spreading. For vortex beams the following threshold dependence of their possible input power on m is revealed: $\alpha > 2m/0.093$. Only pulsed beams obeying this condition may propagate in vortex LB regime. The Gaussian-type LBs are free of such conditions.

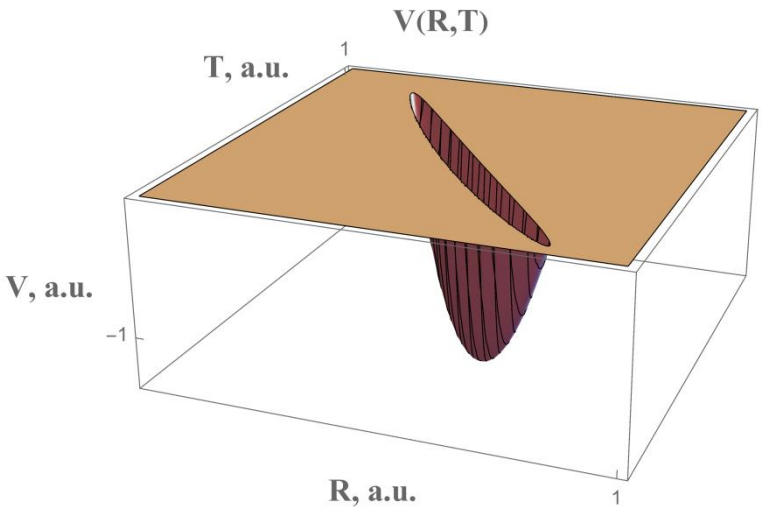

Fig. 1. Potential function V(R, T) for vortex pulsed beam with m=1.

We show for the case of the initial spatial radius and duration of the pulsed beam are detuned from their stationary values R_0 and T_0, the possible scenarios of their behavior under the LB propagation obey the dynamics of two coupled oscillators. So, the LB propagation is accompanied by oscillations of spatial and temporal radii. Furthermore, they may oscillate in phase or in antiphase. The frequency of the "in-phase" oscillations is less than for the antiphase oscillation frequency.

[1] D. Majus, G. Tamošauskas, I. Gražulevičiūtė, et al., Nature of Spatiotemporal Light Bullets in Bulk Kerr Media, Phys. Rev. Lett. **112**, 193901-1-5 (2014).

TERAHERZ WAVE GENERATION IN AIR PLASMA OPTIMISATION USING BICHROMATIC FEMTOSECOND LASER PULSES

Danas Buoģius, Giedrius Balļas, Viktorija Tamulienā

Vilnius University, Laser Research Center, Saulātekio avenue 10, LT-10223 Vilnius, Lithuania
danas.buozius@ff.vu.lt

In the recent years terahertz (THz) wave that represents electromagnetic radiation that ranges in frequency from 0,1 THz to 10 THz has drawn a special attention due to its unique properties [1] and a wide applicability in areas of spectroscopy, biological imaging, detection of hazardous materials, security screening, etc. A high demand for terahertz radiation emitting devices increased the development of new efficient sources. We present a method of THz frequency radiation generation from air plasma induced using bichromatic femtosecond laser pulses. Using this method the order of magnitude of generation efficiency is only 10^{-5} but on the other hand it is impossible to damage our source medium since ambient air is used so laser pump power is not the limiting factor. In this research we focused on optimisation of THz generation efficiency by varying the relative pump pulse timing, pulse energy and polarisations of the pump waves.

In our experiment we used a Ti:Sapphire laser system (Legend elite duo HE+, Coherent Inc.) delivering 43 fs pulses with repetition rate of 1 kHz, central wavelength of 795 nm and maximal pulse energy of 8 mJ. First, the laser beam was split with the help of a thin beam splitter. In one of the two beams a second harmonic (SH) was generated in a BBO crystal, while another laser beam was left as fundamental harmonic (FH). Quarter-wave plates were used on both beams for transforming pump wave polarizations to circular in order to increase THz generation efficiency [2]. SH radiation was filtered out from the FH and passed on to the focusing lens through dielectric mirrors of delay line. Two different lenses were used to focus both pump beams because of their different wavelengths and pulse energies (maximal pulse energies were 0.4 and 1.4 mJ for the SH and FH, respectively). Then both focused beams were concentrically overlapped in time and space using the delay line and a dichroic beam splitter. Then at proper pump pulse energies (up to 0.1 mJ), we have detected THz radiation that is emitted from plasma filament formed in air. THz radiation was filtered out from visible light and pump using silicon filters and then using parabolic mirrors directed to either pyroelectric detector or a microbolometric thermal camera.

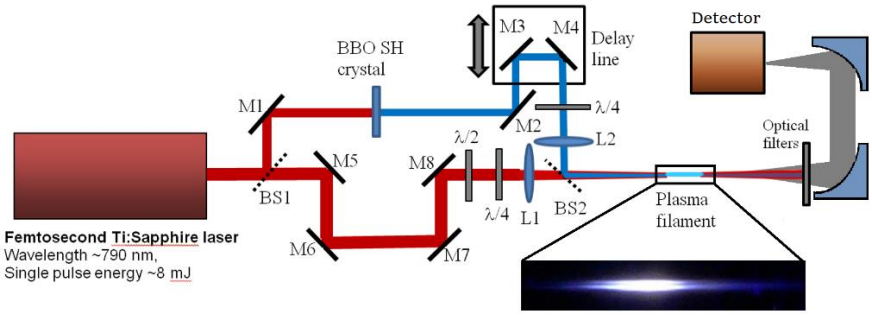

Fig. 1. Experimental setup. M1-M8: dielectric mirrors; L1, L2: focusing lenses; ə/4, ə/2: quarter-wave and half-wave plates; BS1, BS2: beam splitters, SH and FH beams are shown by blue and red-pink colours, respectively.

It was found that increasing power of SH beam decreases the optimal relative delay value of SH pulses with respect to FH pulses. On the other hand, when FH power was increased a similar process occurred but it was much weaker due to lower FH pulse energy. Such dependence of delay values could be explained by the fact that during propagation, trailing part of the pulse is scattered more in the plasma created by the frontal part of the same pulse. Thus, focused pump pulses of the higher energy in air moves faster than these of lower energy. Therefore, the most efficient generation of THz radiation was observed when the relative timing of two pump pulses was adjusted according to the energies of these pulses.

The presented results could be useful in optimizing nonlinear optical processes, such as generation of terahertz radiation [3], as well as parametric four-wave mixing and generation [4], etc., whenever the bichromatic pump beams are used.

[1] Y. S. Lee, Principle of Terahertz Science and Technology (Springer, USA, 2008)
[2] C. Tailliez, A. Stathopulos, S. Skupin, D. Buoģius, I. Babushkin, V. Vaiļaitis, L. Berg® Terahertz pulse generation by two-color laser fields with circular polarization, New J. Phys, . New Journal of Physics. 22. 103038. 10.1088/1367-2630/abb863. (2020)
[3] D. J. Cook and R. M. Hochstrasser, ñIntense terahertz pulses by four-wave rectification in air,ò Opt. Lett. 25, 1210ï 1212 (2000).
[4] E. Gaizauskas, D. Pentaris, T. Efthimiopoulos, and V. Vaicaitis, Probing electronic coherences by combined two- and one-photon excitation in atomic vapors, Opt.Lett. 38, 124 (2013).

INFLUENCE OF pH ON SWELLING PROPERTIES OF ALGINATE HYDROGEL AS A POTENTIAL MATERIAL FOR DRUG DELIVERY SYSTEM

Magdalena B. Ğabowska[1*], Izabela Michalak[2], Jerzy Detyna[1]

[1] Department of Mechanics, Materials and Biomedical Engineering, Faculty of Mechanical Engineering,Wrocğaw University of Science and Technology, Wrocğaw, Poland
[2] Department of Advanced Material Technologies, Faculty of Chemistry, Wrocğaw University of Science and Technology, Wrocğaw, Poland
magdalena.labowska@pwr.edu.pl

Alginate is a naturally occurring polysaccharide obtained from cell walls of brown seaweeds. It consists of repeating ß-D-mannuronic acid (M) and Ű-L-guluronic acid (G) residues linked as homopolymeric blocks or randomly. It is able to form hydrogel in the presence of water. In response to divalent cations (e.g., Ca^{2+}, Ba^{2+}, Fe^{2+}, Mg^{2+} and Al^{3+}) alginate cross-links. The amount of these cations determines the mechanical properties and the maximum water absorption capacity [1].

Alginate hydrogel is often used in the biomedical field, due to its biological activity, biocompatibility with tissues, biodegradability and lack of toxicity. Therefore, this type of hydrogel is excellent for applications in tissue engineering, wound treatment and regenerative medicine [2]. Furthermore, this soft material possesses the ability to undergo hydrolysis depending on pH, time and temperature. The swelling property of hydrogel and osmotic pressure gradient are important factors during the design of drug delivery systems (DDSs) for the controlled release of an active substance. These determinants directly influence the diffusion of drugs from the gel to the surrounding environment [3, 4].

A drug carrier administered orally would encounter various environments during its transit, including stomach, which has acidic conditions (pH about 1-2). Most of the substances are digested at this level. However, if the drug delivery system is desired to bypass the stomach and deliver the drug into the small intestine, where the environment is alkaline, alginate is the best material for this application. Alginate in the acidic environment does not swell. Therefore, to evaluate the effect of different media (aqueous solution with hydrochloric acid at pH 2 and aqueous solution with sodium hydroxide at pH 10) on the swellability of alginate hydrogel a comparative study was carried out [3, 4].

Alginate hydrogel (alginate, Sigma-Aldrich, Saint Louis, USA) was prepared by cross-linking with calcium chloride ($CaCl_2$, Avantor Performance Materials Poland S.A., Gliwice, Poland) at concentrations of 0.1M, 0.5M and 1M, at different times (5 min, 15 min, 30 min and 60 min). The samples were immersed in different solutions (pH 2 and pH 10) at 21,7 °C and their weight was analyzed after a specific time (as shown in Figure 1).

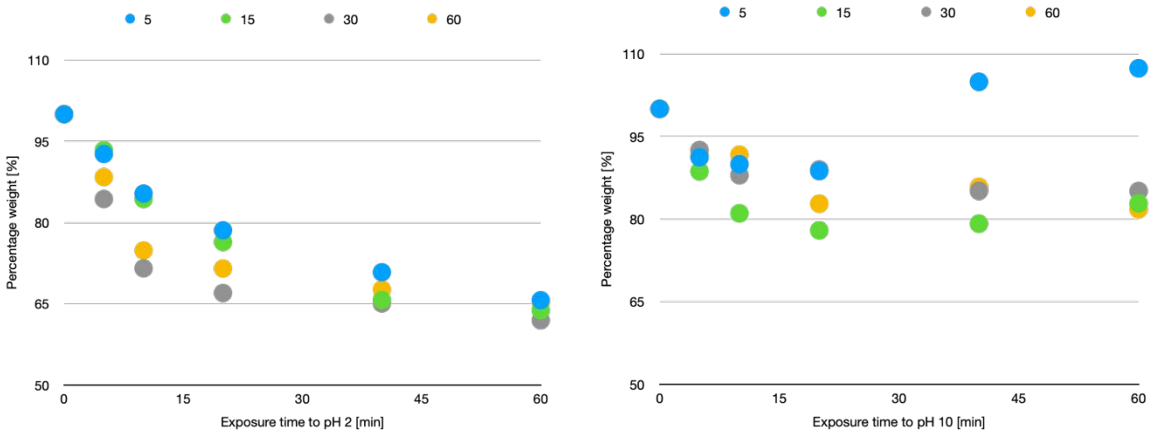

Fig. 1. Correlation of weight changes of 2% alginate hydrogel cross-linked at different time by $CaCl_2$ (0.1M concentration) in relation to soaking time in pH 2 (left) and pH 10 media (right).

The aim of the present work is to compare and select the appropriate concentration of cross-linking agent for alginate as a future drug carrier material. The selection of these parameters (concentration of cross-linker and duration of cross-linking) is important to optimize the active substance release at a specific location in the gastrointestinal tract. Conducted research enables to determine the effect of the cross-linking factor on swelling properties of alginate hydrogel in different pH of media, thereby it would be beneficial in oral DDS design for controlled drug release.

[1] K. Y. Lee, D. J. Mooney, Alginate: Properties and biomedical applications. Progress in Polymer Science 37(1):106-126, 2012.
[2] A. Kaczmarek-Pawelska, Alginate-based hydrogels in regenerative medicine, In book: Alginates - Recent Uses of This Natural Polymer, ed: L. Pereira, Intech Open, 2019.
[3] J-J Chuang, Y-Y Huang, S-H Lo, et al., Effects of pH on the shape of alginate particles and its release behavior. International Journal of Polymer Science 2017(1):1-9, ID 3902704, 2017.
[4] H. H. Tßnnesen, J. Karlsen, Alginate in drug delivery systems. Drug Development and Industrial Pharmacy, 28(6):621-630, 2002.

ANTIFUNGAL ACTIVITY OF FLUCONAZOLE INCORPORATED INTO HYDROGELS MODIFIED WITH NANOHYDROXYAPATITE

Justyna Rewak-Soroczynska[1], Paulina Sobierajska[1], Rafal J. Wiglusz[1]

[1] Institute of Low Temperature and Structure Research, Polish Academy of Sciences, Okolna 2, 50-422 Wroclaw, Poland
j.rewak@intibs.pl

Fungal infections, frequently caused by opportunistic pathogens, are serious medical problem, especially among immunocompromised patients. These afflictions can be divided depending on the site of occurrence hence superficial, cutaneous, subcutaneous and systemic mycoses can be differentiated [1]. Chronic wounds are highly prone to fungal infections and the highest prevalence is reported for *Candida* species (*C. albicans*, *C. glabrata*, *C. tropicalis*) [2].

Fluconazole the member of azole group is one of the most frequently chosen drug for fungal infection treatment. Its activity is based on the inhibition of ergosterol biosynthesis which causes impairments in fungal plasma membranes [3].

The idea of using hydrogels loaded with drugs was reported previously [4]. However hydroxyapatite as a filler and drug carrier is a new approach proposed by our team. Hydrogel can provide gradual drug release towards the infection site and enhance wound healing by moisture retaining. Moreover, hydroxyapatite (Ca (PO) (OH) (HAp)) naturally occurs in human body as a component of teeth and bone tissues is highly bioactive and biocompatible. It is also known for its regenerative properties and wound healing acceleration [5].

The antifungal activity of pure fluconazole was assessed using *C. albicans*, *C. glabrata*, *C. tropicalis*, *Cryptococcus neoformans*, *Cryptococcus gatti*, *Rhodotorula mucilaginosa* and *Rhodotorula rubra* reference and clinical isolates. The biofilm production ability (crystal violet staining) of these strains was tested at 28 and 37°C to select the most appropriate conditions for further experiments. Hydroxyapatite was synthesized by the precipitation method and heat treated at 450°C for 3 hours. Hydrogels (6-anhydro-Ŭ-L-galacto-ɓð D-galactan) were prepared in four different forms: pure hydrogel, hydrogel filled with HAp, hydrogel filled with fluconazole and hydrogel filled with both HAp and fluconazole. All materials were lyophilized and physicochemical characterization was performed to assess their properties. The samples were cut into even pieces and incubated with fungal cultures to evaluate how they influence the growth and biofilm formation (confocal laser microscopy with LIVE/DEAD staining) of selected strains.

Fluconazole-loaded materials almost completely inhibited fungal growth of all tested strains, however living cells were spotted on the surface of all tested materials. It can also be seen that fluconazole additive changed the biofilm morphology increasing the cell aggregation and clusters formation whilst nanohydroxyapatite reversed that effect. That observation suggest the potential antibiofilm activity of HAp which protected from fully grown biofilm formation and suggests its beneficial effect as drug-filled hydrogels additive.

Financial support of the National Science Centre in the course of realization of the Projects ñElaboration and characteristics of biocomposites with anti-virulent and anti-bacterial properties against *Pseudomonas aeruginosa* (no. UMO-2016/21/B/NZ6/01157) and ñPreparation and characterization of biocomposites based on nanoapatites for theranosticsò (no. UMO-2015/19/B/ST5/01330).

[1] Kothavade, R.J.; Kura, M.M.; Valand, A.G.; Panthaki, M.H. *Candida tropicalis: Its prevalence, pathogenicity and increasing resistance to fluconazole*. J. Med. Microbiol. 2010, *59*, 873ï 880, doi:10.1099/jmm.0.013227-0.

[2] Dowd, S.E.; Delton Hanson, J.; Rees, E.; Wolcott, R.D.; Zischau, A.M.; Sun, Y.; White, J.; Smith, D.M.; Kennedy, J.; Jones, C.E. *Survey of fungi and yeast in polymicrobial infections in chronic wounds.* J. Wound Care 2011, *20*, 40ï 47, doi:10.12968/jowc.2011.20.1.40.

[3] Morschhª user, J. *The development of fluconazole resistance in Candida albicans ï an example of microevolution of a fungal pathogen.* J. Microbiol. 2016, *54*, 192ï 201, doi:10.1007/s12275-016-5628-4.

[4] Hamedi, H.; Moradi, S.; Hudson, S.M.; Tonelli, A.E. Chitosan based hydrogels and their applications for drug delivery in wound dressings: A review. *Carbohydr. Polym.* **2018**, *199*, 445ï 460, doi:10.1016/j.carbpol.2018.06.114.

[5] Bruggisser, R. *Bacterial and fungal absorption properties of a hydrogel dressing with a superabsorbent polymer core*. J. Wound Care 2005, *14*, 438ï 442, doi:10.12968/jowc.2005.14.9.26839.

MODULATION SIRT-1 ACTIVITY IN IMMUNE CELLS UNDER OXIDATIVE STRESS: CELL DEATH AND SURVIVAL

Vasyl Velykyi[1], Maria Stupchuk[2], Tatyana Voznesenskaya[2]

[1] Department of Immunology, Taras Shevchenko National University of Kyiv, Ukraine
[2] Department of Immunophysiology, Bogomoletz Institute of Physiology of NASU, Ukraine
vasyl_velykyi_knutsh@outlook.com

Nuclear Sirtuin-1 or SIRT-1 is a member of the family of NAD+ dependent protein deacetylase. Previous studies have showed that SIRT-1 is involved in processes related to programed cell death mechanisms, cell aging, it also can activate tumor suppressor genes, maintain energy metabolic hemostasis, and can reverse innate and adaptive immune tolerance [1,2]. Last researches pointed out perspectives to SIRT-1in application to treat prion-mediated neurodegeneration, cancer, obesity-associated metabolic decreases, cardiac aging and stress [3]. Moreover, it plays role in cellular senescence, inflammatory signaling in response to environmental stress, development and placental cell survival [3].

This research aimed to investigate the role of SIRT-1 in the modulation of immune cell death and survival. We examined biological effects on B- and T-cells death type and autophagy after activation or inhibition of SIRT-1 in vitro under oxidative stress.

For examination effects on cell death and survival, we isolated immune cells from the thymus and inguinal lymph nodes of Albino line mice, adult females weight 18-20 g. B- and T-cells cultivated with 20 μM resveratrol (specific activator of SIRT-1) or 5 mM nicotinamide (unspecific inhibitor of SIRT-1) in RPMI media with 100 μM H_2O_2 (oxidative stress factor) during 1 hour at 27ÁC in the natural atmosphere. Control groups cells cultivated in pure RPMI media for 1 hour at 27ÁC in a natural atmosphere. For detection of live, necrotic and apoptotic cells were used a combination of Propidium iodide and HOECHST dyes solution and fluorescent microscopy imaging (Fig. 1. ϕ pic.) For detection autophagy (Fig.1. B pic.), we used Monodansyl cadaverine dye solution and fluorescent microscopy imaging.

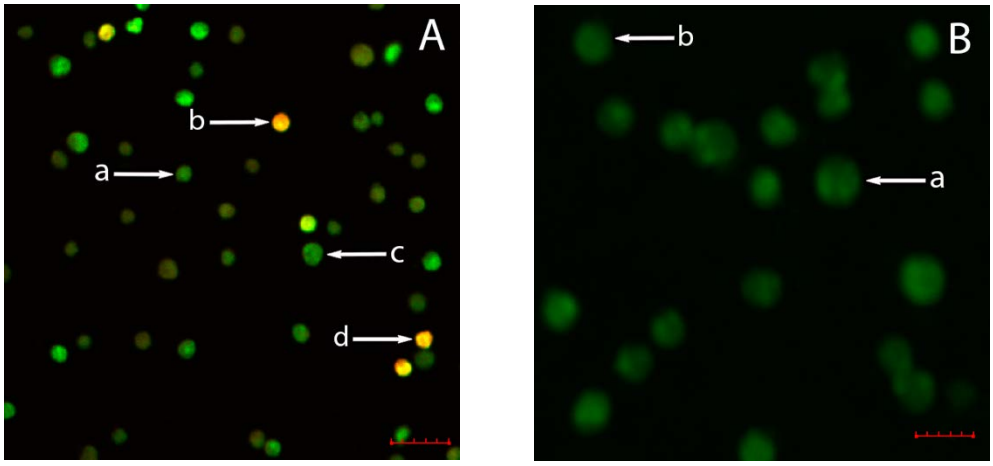

Fig.1. A picture ï confocal imaging of T-cells, Propidium iodide and HOECHST dyes combination, scalebar = 20 μm. a ï living cell, b ï necrotic cell, c ï apoptotic cell, d ï necroptotic cell.; B picture ï confocal imaging of T-cells, Monodansyl cadaverine dye, scalebar = 10 μm. a ï T-cell with autophagy, b ï T-cell without autophagy.

We showed in our research that SIRT-1 activation by resveratrol leads to increasing immune cells resistance to oxidative stress and promotes autophagy. For B-cells survival rate 10,3% increase and for T-cells 13,1% increase. In these groups also was observed increase of autophagy for B-cell up to 8,2% and T-cell up to 9%. Necrosis rate is decreased for B-cell and for T-cell to 14,2% and 11,5% in accordance. Apoptosis rates have a trend to increase for B- and T-cells. Inhibition of SIRT-1 by nicotinamide leads to less survival ability of immune cells and promotes increasing of apoptosis. For B-cells survival rate decreased up to 5,2% and for T-cells decreased up to 6,8%. Apoptosis rate is increased for B-cell and for T-cell to 3,3% and 4,8% in accordance. Necrosis rate for B-cells increases up to 3,5%. Also in this group decrease autophagy rate for B-cell up to 3,7% and T-cell up to 6,2%. We used Studentôs t-test for statistical analysis, $p<0,05$.

Conclusion: SIRT-1 activation increase cell resistance to oxidative stress in immune cells. Using resveratrol leads to increasing immune cells survival and rate of autophagy, at the same time it drives to decreasing necrosis rate. Inhibition of SIRT-1 by nicotinamide leads to less survival ability of immune cells and promotes increasing of apoptosis and decreasing of autophagy.

[1] A. N. Martin, M. Alexander-Miller, B. K. Yoza, et al., Sirtuin1 Targeting Reverses Innate and Adaptive Immune Tolerance in Septic Mice, Journal of Immunology Research, **2018**, 13, (2018).
[2] M. D. Molla, G. Dessie, Y. Akalu, et al., Hepatocellular Expression of SIRT1 and Its Effect on Hepatocellular Carcinoma Progression: A Future Therapeutic Perspective , International Journal of Hepatology, **2020**, 10, (2020).
[3] S. Rahman, R. Islam, Mammalian Sirt1 insights on its biological function, Cell Communication and Signaling **9**, (2011).

EVALUATION OF POLLUTED SOIL-INDUCED OXIDATIVE STRESS USING *VICIA FABA* CHLOROPHYLL MORPHOSES AS A MODEL SYSTEM

Vėjūnė Pukenytė[1], Raimondas Ţiukţta[1,2], Tatjana Ląsnienė[1]

[1]Institute of Biosciences, Life Sciences Centre, Vilnius University, Saulėtekis Ave. 7, LT-10257 Vilnius, Lithuania
[2]Botanical Garden of Vilnius University, Kairėnai Str. 43, LT-10239, Vilnius, Lithuania.
vejune.pukenyte@gmc.stud.vu.lt

Soil pollution is toxic to both the environment and to the organisms that live in it. In Europe the soil is usually mostly polluted by heavy metals [1]. Heavy metals in low concentrations are essential for living organisms, but excessive amounts of them can become genotoxic and cause damage to their DNA [2], thus it is important to study the effect heavy metals have on living organisms.

In this work, the genotoxic effect of soil in closed Vilnius city plants "GrŶtai" and "Rimeda" (GRD) was investigated using the *Vicia faba* chlorophyll morphosis test system under cobalt stress (fig. 1). The heavy metal-induced oxidative stress level was investigated by evaluating the variation in biochemical markers (chlorophylls, carotenoids, proline, hydrogen peroxide, flavanoids, polyphenols, and ascorbic acid), as well as the potential modulating effect of salicylic acid on the amount of these markers in plants. Functional CDDP tags were used to investigate soil genotoxicity.

Research has shown that the soils in the former factories ñGrŶtaiò and ñRimedaò have genotoxic effects on *V. faba* plants by inducing polymorphism in CDDP profiles. It was also found that growing plants in GRD soil contaminated with heavy metals significantly increases the amount of H_2O_2 ($p < 0.05$) and reduces the concentration of antioxidants - free proline ($p < 0.05$) and ascorbic acid ($p < 0.05$) in plant leaves. In addition, Co induces *Vicia faba* chlorophyll morphoses, which are marked by a significant decrease in chlorophyll and carotenoid levels and an increase in lipid peroxidation levels (in all phenotypic groups (unchanged, intermediate and yellow) in $p < 0.05$ compared to control).

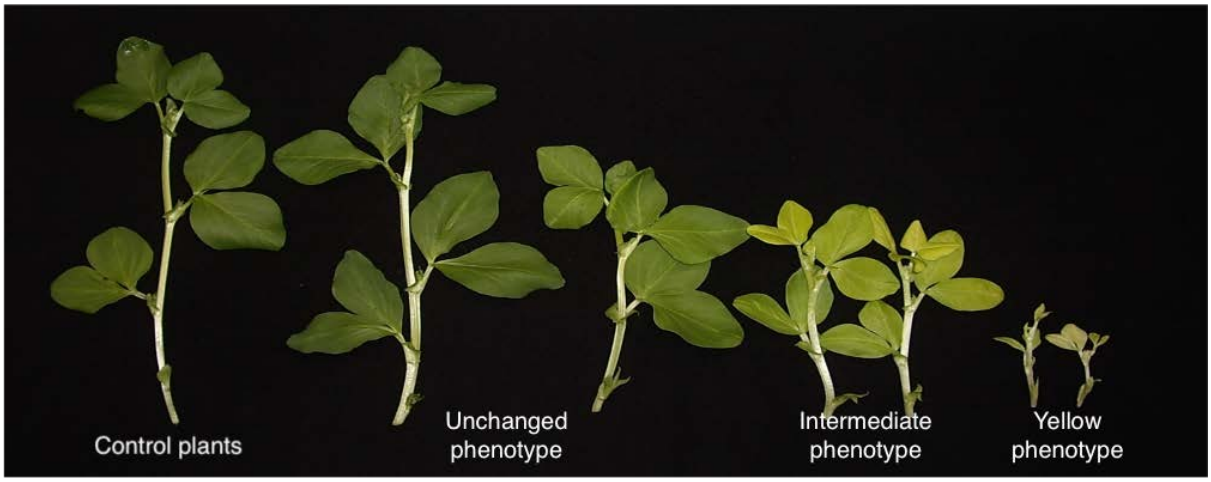

Fig 1. Phenotypes of Co-induced chlorophyll morphoses of *Vicia faba*

[1] ñProgress in management of contaminated sites ð European Environment Agency,ò Jan. 17, 2019. https://www.eea.europa.eu/data-and-maps/indicators/progress-in-management-of-contaminated-sites-3/assessment (accessed on 2021 02 10)
[2] V. Ţlapakauskas, AugalÔekofiziologija. Kaunas: Lututė, 2006.

PRESENCE OF SARS-CoV-2 TRANSCRIPTS IN THE CHOROID PLEXUS OF MS AND NON-MS PATIENTS WITH COVID-19

Vidmante Fuchs[1*], Michael Kutza[2*], Sven Wischnewski[2*], Nikolaus Deigendesch[3], Luc Lutz[1], Laila Kulsvehagen[1], Gerda Ricken[4], Ludwig Kappos[1], Alexandar Tzankov[3], Simon Hametner[4], Stephan Frank[3], Lucas Schirmer[2,5,6*], Anne-Katrin Prº bstel[1*]

[1]Department of Biomedicine, University Hospital and University of Basel, Basel, Switzerland
[2]Department of Neurology, Medical Faculty Mannheim, Heidelberg University, Mannheim, Germany
[3]Institute of Medical Genetics and Pathology, University Hospital Basel, University of Basel, Basel, Switzerland
[4]Department of Neurology, Division of Neuropathology and Neurochemistry, Medical University of Vienna, Vienna, Austria
[5]Mannheim Center for Translational Neuroscience and Institute for Innate Immunoscience, Medical Faculty Mannheim, Heidelberg University, Mannheim, Germany
[6]Interdisciplinary Center for Neurosciences, Heidelberg University, Heidelberg, Germany
[*]These authors contributed equally
Anne-Katrin.Proebstel@usb.ch

Although primarily targeting the respiratory system, coronavirus disease 2019 (COVID-19) also manifests with central nervous system (CNS)-related symptoms in up to 80% of the patients. Little is known not only about SARS-CoV-2 neuropathology, but also about the clinical course of pre-existing CNS autoimmune disease and concurrent SARS-CoV-2-infection. Multiple sclerosis (MS) is the most frequent autoimmune disease of the CNS with inflammatory demyelination and blood-brain barrier (BBB) disruption being typical pathological hallmarks. Whether multiple sclerosis (MS) renders patients more susceptible to CNS involvement during SARS-CoV-2 infection, and the impact of SARS-CoV-2 infection on MS disease activity remain elusive.

Here, we assessed whether an impaired blood-brain barrier in MS facilitates viral CNS entry, and whether COVID-19 infection is associated with MS disease exacerbation. We combined an in-depth histopathological assessment with spatial transcriptomic analysis using multiplex in situ hybridization analysis for SARS-CoV-2 and ACE2 transcripts in autoptic brain tissue of an MS patient, who died from COVID-19-associated respiratory failure, compared to other non-MS COVID-19 cases and inflammatory controls.

Despite a general microglia activation in MS and non-MS COVID-19 brain parenchyma and minor BBB leakage in MS COVID-19 brain, we found neither evidence for active demyelination nor presence of SARS-CoV-2 transcripts in MS lesions. SARS-CoV-2 and ACE2 transcripts were consistently detected in epithelial cells of the choroid plexus (CP) and ependymal cells of the CSF-brain interface in both MS and non-MS COVID-19 cases.

Our findings provide neither evidence for clinical or neuropathological signs of MS disease exacerbation nor presence of viral transcripts in neuronal and glial cells. Notably, presence of viral transcripts in the CP suggests the CP being a key restraint of SARS-CoV-2 entry into the CNS (Fig. 1). Future studies will need to shed light on SARS-CoV-2-associated pathologies in COVID-19 patients with a more active MS course and other autoimmune comorbidities.

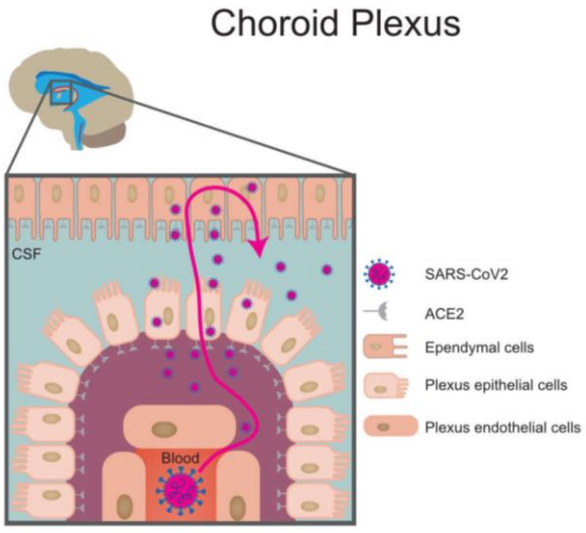

Fig. 1. Anticipated SARS-CoV-2 entry route into the CNS though the choroid plexus, adapted from Fuchs et al. [1].

[1] Fuchs V, Kutza M, Wischnewski S, et al. Presence of SARS-CoV-2 Transcripts in the Choroid Plexus of MS and Non-MS Patients With COVID-19. Neurology - Neuroimmunology Neuroinflammation 2021;8:e957.

THE COMPARISON OF DIFFERENT MODELS FOR INDUCING EXPERIMENTAL PERITONEAL ADHESIONS IN RATS

Anastasiya Kanunnikova[1,2], Natallia Melehavets[1], Artem Goliusov[3], Arina Mamatova[3], Yuliya Prosmytskaya[1], Daniil Lappo[1], Yury Linnik[2]

[1]Chemistry Department, Belarusian State University, Minsk, 220030, Belarus
[2]The Republican Scientific and Practical Center for Pediatric Surgery, Minsk, 220013, Belarus
[3]Belgorod State National Research University, Belgorod, 308015, Russia
a.r.kanunnikova@gmail.com

The formation of postoperative adhesions is a significant clinical problem for the present-day surgery hence there are a diversity of variants how to simulate peritoneal adhesions in a different models which provides reproducible and representative field for new researches. At this moment, investigations in the peritoneal adhesions branch are very exiting field for making an ideal model. Thus the amount of the options how to perform all demands are enormous and even now we have a lot of methods to induce the adhesion formation process in a rat model. However, nothing could be ideal and all the models have some issues, which means that process of invention is still going on [1].

Last year we invent a rat model of postoperative peritoneal adhesions and it shows glorious results even after a year of researches if to compare it with recent models. It shows that our model is stable and durable for time despite other inventions [2]. This year we have analyzed and compared our necrosis model with fixation [2] with three commonly used adhesion models: necrosis model without fixation [3], abrasive model, and dissection model [1].

For developing models in this work, we used 48 male Wistar rats of the same age and mean weight (250-300 g), which were split into five groups of eight rats in each group. Prior to the operation, all rats were quarantined for 3 days in the vivarium and kept in a 12:12-h light-dark cycle with food and water available ad libitum. Then the rats were anesthetized by intramuscular injection of 0.05 ml/kg of Xylazine and 0.5 mg/kg of ñZoletil 50ò, their chest hair were removed by shaving and the skin was scrubbed with ethanol. To access the abdominal cavity a 3-cm laparotomy was performed. In the ñnecrosis with fixationò group, the cecum was delivered and its wall was injured by 1-minute application of a cotton pad soaked in 1N NaOH and then the cecum wall was fixed to the abdominal wall by a non-absorbable suture to localize adhesion sites. In the ñnecrosis without fixationò group, the cecum was delivered and its wall was injured by 1 minute application of a cotton pad soaked in 1N NaOH. After the procedure, the alkaline solution was washed out completely with saline water. In the ñabrasiveò group, the cecum wall was injured by repeating rubbing with the help of the abrasive material. In the ñdissectionò group, dissection of the three peritoneal wall sites (5Ï 2 mm) opposite the cecum were prepared. In the control group, only the 3-cm laparotomy was performed. The wound was closed by two layers of continuous sutures. Prophylactic antibiotic (50 mg/kg Tylosin) was injected once daily for 5 days after the surgery. At day 7 after surgery, the animals were euthanized and the abdominal cavity was opened via a U-shaped incision.

Adhesion formation was evaluated by a macroscopic inspection according to the adhesion rating scale from 0 to 5 proposed by Oncel et al. [4]. Grade 0: no adhesions; grade 1: loose filmy adhesions that can be separated by blunt dissection; grade 2: adhesions requiring <50% of sharp dissection for separation; grade 3: adhesions requiring >50% of sharp dissection for separation; grade 4: serosal injury, grade 5: full-thickness injury.

After the implementation of all procedures, severe grade of adhesion for the ñnecrosis with fixationò group was 2.7 and all the adhesion sites were strictly localized between the cecum and the abdominal wall. In the ñnecrosis without fixationò group all the rats has 2-grade adhesions. In the ñabrasiveò group, three rats had 2-grade adhesions, four rats had no adhesions and one rat died before euthanizing process. In the ñdissectionò group, four rats had 1 grade adhesions, one rat had no adhesions and three rats died before euthanizing process. In the control group, five rats had 1-grade adhesions and three rats had no adhesions. Adhesion sites in all the groups except the ñnecrosis with fixationò group were localized spontaneously between the cecum and the other parts of the abdominal cavity.

From all this data, we can make a derivation that models with abrasion and dissection are not so convenient because they donôt satisfy the demands in reproducibility. Nevertheless, necrosis model without attachment can be used if our main aim are adhesions and not so important were they will be. Also, necrosis model with attachment can be used in some situations too, because despite the huge trauma risk this model is convenient if we want adhesions in determined surface or place. All experiments were carried in compliance with the recommendations of the European Convention on Humane Treatment of Laboratory Animals [5].

[1] Kraemer, B. et al. Standardised models for inducing experimental peritoneal adhesions in female rats / B. Kraemer [et al.] // Biomed Res. Int. ï 2014. ï Vol. 2014 ï P. 1-8.
[2] Pokrovsky, V. et al. The novel experimental rat model of postoperative peritoneal adhesions. Open Readings 2020 63nd International Conference for Students of Physics and Natural Sciences, Vilnius, Lithuania, P. 548
[3] Ozeki, M. et al. Comparison of a chymase inhibitor and hyaluronic acid/carboxymethylcellulose (Seprafilm) in a novel peritoneal adhesion model in rats. PLoS One. 2019. Vol. 14, ¯ 1 ï P. e0211391.
[4] Oncel, M. et al. Comparison of a novel liquid (Adcon-PÈ) and a sodium hyaluronate and carboxymethylcellulose membrane (SeprafilmTM) in postsurgical adhesion formation in a murine model. Dis. Colon Rectum 46, 187ï 191 (2003).
[5] European Convention for the protection of vertebrate animals used for experimental and other scientific purposes. Strasbourg: Europ. Treaty Series, 1986. ¯ 123. P. 48.

ULTRAFAST LOCALIZED SURFACE PLASMON RELAXATION DYNAMICS OF PLASMONIC METAL NANOPARTICLES BY MEANS OF TRANSIENT ABSORPTION SPECTROSCOPY

Gerda Klimaitã[1], Domantas Peckus[2], Tomas Tamulevicius[1,2], Jaunius Mykolaitis[2], Mindaugas Juodãnas[2], Asta Tamuleviļ ienã[1,2], Algirdas Lazauskas[2], Sigitas Tamuleviļ ius[1,2]

[1]Department of Physics, Kaunas University of Technology, StudentÔSt. 50, LT-51368 Kaunas, Lithuania
[2]Institute of Materials Science, Kaunas University of Technology, K. Barġausko St. 59, LT-51423 Kaunas, Lithuania
gerda.klimaite@ktu.edu

Recently, noble metal nanoparticles (NPs) have been very interesting for the scientific community because of their electroptical properties that appear because of localized surface plasmon resonance (LSPR) [1]. Due to their LSPR features plasmonic metal NPs can be used in various electrooptical applications like solar cells, photocatalysis, sensing, medicine and so on [1].

We investigated Ag, Au and Cu NPs in our research because these nanoparticles have well defined LSPR properties and shows great promises for future electrooptical applications [1]. Most metal NPs were synthesized chemically so far but with the development of ultra-short pulse lasers, new methods of synthesis of NPs have emerged like laser ablation in liquids (LAL). The important advantage of LAL is a simple and fast synthesis process. To evaluate the sizes, structural and optical properties of NPs prepared by the LAL method their properties should be explored in detail. The methods like scanning electron microscopy, X-ray diffraction, linear and nonlinear optical measurements can give valuable information about features of these NPs. In our research, we were focusing on the ultrafast LSPR relaxation dynamics of NPs synthesized from three plasmonic metal targets by the LAL technique.

The dynamic plasmonic properties of noble metal nanoparticles were explored by ultrafast transient absorption spectroscopy (TAS) method exploiting Yb:KGW femtosecond laser and nonlinear parametric amplifier. The properties of ultrafast LSPR relaxation dynamics in plasmonic NPs prepared by the LAL method were compared with the ones prepared by chemical synthesis [2]. The TAS measurements results of Ag, Au and Cu NPs are shown in Fig. 1. The sizes and shapes of investigated plasmonic metal NPs were measured with SEM and calculated with ImageJ software (Fig. 2).

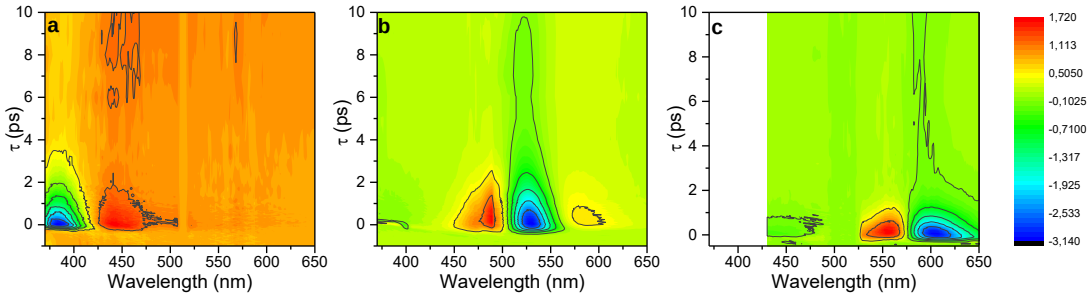

Fig. 1. Transient absorption spectroscopy data contour plots of Ag NPs (**a**), Au NPs (**b**) and Cu NPs (**c**).

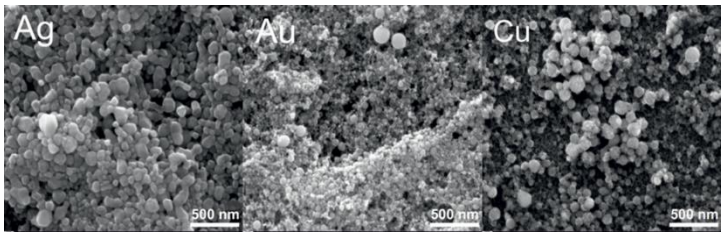

Fig. 2. Ag, Au, Cu NPs SEM images.

he TAS results display that the dynamic properties LSPR of LAL NPs are quite similar to NPs prepared by the wet chemical synthesis method suggesting that their quality is also comparable [2]. Although, the relaxation dynamics of NPs prepared by wet chemistry and LAL is quite similar the sizes distribution is much lower for NPs prepared by wet chemistry methods (Fig. 2) [2]. The preliminary results indicate that the LAL synthesis of NPs could be a perspective method for the preparation of high-quality plasmonic NPs for various electrooptical applications.

Acknowledgements: This research was funded by the European Social Fund under the No. 09.3.3-LMT-K-712 ñDevelopment of Competences of Scientists, other Researchers and Students through Practical Research Activitiesò measure, grant No. 09.3.3-LMT-K-712-22-0212.

[1] G. V. Hartland, Optical Studies of Dynamics in Noble Metal Nanostructures, Chem. Rev. **111**, 3858ï 3887 (2011).
[2] D. Peckus et al., Hot Electron Emission Can Lead to Damping of Optomechanical Modes in Coreī Shell Ag@TiO2 NanocubesJ. Phys. Chem. C, **121**, 24159-24167 (2017).

ZnO TETRAPODS MORPHOLOGY AND STRUCTURE INFLUENCE ON ELECTROCHEMICAL PROPERTIES

Ieva Stagaitytė[1], Andrius Vitkauskas[1], Agnė Gulbinaitė[1,2*], Simas Ramanauskas[2]

[1] Department of Physical and Inorganic Chemistry, Faculty of Chemical Technology, Kaunas University of Technology, Radvilenu plentas 19, Kaunas LT-50254

[2] Department of Physics, Faculty of Mathematics and Natural Sciences, Kaunas University of Technology, StudentÛst. 50, LT-51368, Kaunas, Lithuania

*agne.sulciute@ktu.lt

In the last decade interest in ZnO markedly recur and increase. This outstanding popularity is due to ZnO multi-functionality, suitable for various applications [1]. Depending on the method of synthesis, the structure and morphology can be greatly modified, resulting in changes in physical and chemical properties.

Our aim was to investigate ZnO morphology (size, shape, porosity) on electrochemical properties.

Experimental approach. Tetrapods were synthesized using combustion method [2] and separated by centrifugation into 2 size fractions (large tetrapods – 1000 RPM, named LT; small tetrapods – 3000 RPM, named ST).

Electrochemical properties (active surface area A, electron transfer rate ΔE_p) were evaluated using cyclic voltammetry measurements of 100 µm $K_4[Fe(CN)_6]$ dissolved in 0.1 M KCl solution. Working electrode (WE): glass substrate →100 nm Au, → ZnO tetrapods. Ag/AgCl reference electrode (RE) of 2 mm in diameter and and Pt counter electrode (CE) of 0.5 mm in diameter **Figure 1**.

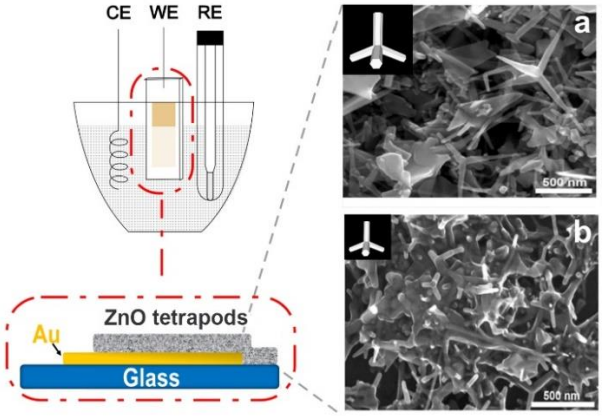

Fig. 1. Simplified version of experimental set-up for electrochemical measurements: a – 1000 RPM large tetrapods (LT); b – 3000 RPM small tetrapods (ST);

Techniques used: resistance measurement, Scanning and Transmission electron microscopies (SEM and TEM), X-ray powder diffraction (XRD), UV-Vis spectroscopy.

Structure and morphology. It was noted both LT and ST tetrapods form a typical tetrapod structure consisting of 4 connected nanorods:

- small tetrapods (ST) diameter 5 nm, length 50 nm;
- large tetrapods (LT) diameter 20 nm, length 150 nm;

Moreover, it was found that nanorods (legs) are well-defined interference fringes corresponding to ZnO $(10\bar{1}0)$ planes.

Electrochemical properties. It was distinguished that the electrochemical reactions of ZnO nanostructures are influenced by two simultaneous mechanisms:

- ZnO nanostructures under different potential;
- ferricyanide on the ZnO electrode.

It was concluded that due to the one-dimensional leg arrangement tetrapods showed great electrochemical properties. The effect is more pronounced for longer leg tetrapods (LTs), leading to peak separation ΔE_p, approaching the theoretical value. Though, LT that has the biggest active surface (0.095 cm^2) and its practical ΔE_p value of 61.7 mV, which is close to the theoretical 59 mV.

These results are significant for the upcoming ZnO tetrapods applications in electrochemistry, where the morphology influence on the properties should be considered [3].

[1] A. Moezzi, A.M. McDonagh, M.B. Cortie,, Zinc oxide particles: Synthesis, properties and applications, Chemical Engineering Journal, **22**, 185-186 (2012).

[2] S. Rackauskas, O. Klimova, H. Jiang, et.al., The Journal of Physical Chemistry C, 2015, **28**, 16366-16373 (2015.)

[3] A. Sulciute, K. Nishimura, E. Gilshtein, et.al.,The Journal of Physical Chemistry C, **2**, 1472-1482 (2021)

APPLICATION OF MAGNETIC GOLD-COATED NANOPARTICLES FOR THE DETERMINATION OF HUMAN GROWTH HORMONE

Ema BaliÎ naitä[1], Almira Ramanaviļ ienä[1]

[1] NanoTechnas ï Center of Nanotechnology and Materials Science, Faculty of Chemistry and Geosciences, Vilnius University, Lithuania
ema.baliunaite@chgf.stud.vu.lt

In recent years, gold nanoparticles were used in a variety of fields, including catalysis, electronics, photonics, as well as nanomedicine, and chemical and biological sensing. Their wide range of applications comes from their unique optical, electromagnetic, and conductive properties, in addition to their good biocompatibility and ease of functionalization and modification with biomolecules. The use of magnetic gold-coated nanoparticles (M-AuNPs) is advantageous because of the combined above-mentioned gold nanoparticle properties, along with the ability to use magnets to control the particlesô position in space. This property is especially useful for the collection of particles after each step of modification [1-3].

Human growth hormone (hGH), also known as somatotropin, is a peptide hormone which is secreted by the anterior pituitary gland. hGH is essential for normal human growth and development, and is involved in such biological processes as lactation, somatogenesis, and activation of microphages. An imbalance of hGH causes various diseases, thus sensitive determination of the hormone is essential [4].

The main aim of this study was to develop an immunoassay for the determination of hGH using M-AuNPs. Synthetized M-AuNPs were characterized spectroscopically and using transmission electron microscopy. In this work, monoclonal antibodies against human growth hormone (m-anti-hGH) were covalently immobilized onto the surface of M-AuNPs using a self-assembled monolayer. After m-anti-hGH interaction with hGH, polyclonal antibodies against human growth hormone labelled with biotin (p-anti-hGH-B) and streptavidin-labelled horseradish peroxidase (S-HRP) were added. Then a mixture of 3,3N5,5N-tetramethylbenzidine (TMB) and hydrogen peroxide as a substrate for the enzymatic reaction was added, and the absorbance of solution after the addition of sulfuric acid was registered.

Acknowledgements

This project has received funding from European Social Fund (project No 09.3.3.-LMT-K-712-22-0171) under grant agreement with the Research Council of Lithuania (LMTLT).

[1] Y. Li, H. Schluesener, & S. Xu, Gold nanoparticle-based biosensors, Gold Bulletin **43**(1), 29ï 41 (2010).
[2] J. Lee, H. Cho, H. Choi et al., Application of Gold Nanoparticle to Plasmonic Biosensors, International Journal of Molecular Sciences **19**(7), 2021 (2018).
[3] L. Wang, H. Park, S. Lim et al., Core@shell nanomaterials: gold-coated magnetic oxide nanoparticles, Journal of Materials Chemistry **18**(23), 2629ï 2635 (2008).
[4] A. Kausaite-Minkstimiene, A. Ramanavicius, J. Ruksnaite et al., A surface plasmon resonance immunosensor for human growth hormone based on fragmented antibodies, Analytical Methods **5**(18), 4757ï 4763 (2013).

DEPOSITION OF THIN FILMS ON STRUCTURED SURFACES

Julianija Nikitina[1,2], Tomas Tolenis[1], Darius Gailevičius[2,3], Kęstutis Staliūnas[2,4,5], Lina Grinevičiūtė[1,2]

[1] Center for Physical Sciences and Technology, Savanorių ave. 231, LT-02300 Vilnius, Lithuania
[2] Laser Research Center, Vilnius University, Saulėtekio Ave. 10, Vilnius LT-10223, Lithuania
[3] Femtika LTD, Saulėtekio Ave. 15, LT-10224, Vilnius, Lithuania
[4] ICREA, Passeig Lluís Companys 23, 08010, Barcelona, Spain
[5] UPC, Rambla Sant Nebridi 22, 08222, Terrassa (Barcelona), Spain

julianija.nikitina@ff.vu.lt

Miniaturisation of laser systems along with still holding high requirements for optical elements, raises demand for novel elements, with 2D or even 3D spatial refractive index modulation, as photonic crystals [1]. Possibilities of state-of-the-art fabrication technologies of such structures are limited due to restricted control over the formation at nanoscale. An alternative fabrication method is based on the deposition of multilayer optical coatings on modulated surfaces employing physical vapor deposition (PVD) technologies. Deposition of multilayer interference coating creates the modulation of the effective refractive index modulation in vertical direction, while pre-structured substrate surface introduces modulation in horizontal direction as well (fig. 1 A). In order to fabricate thin film based periodic structure, precise control of layers deposition is required, which leads to investigating the possibilities of conventional physical vapour deposition technologies to form such nanostructured elements.

This work presents primary experimental and theoretical results of conformal deposition of multilayer structure and formation of periodically organized microstructures on modulated surfaces. Experimental part was performed employing energetically diverse PVD technologies based on sputtering and evaporation processes. Energetic thin film deposition technology as Ion Beam Sputtering (IBS) is well-established and stands out for its highly controlled, densely packed optical coatings fabrication. On the other hand, deposition of low-energy particles potentially may help to form periodically organized microstructures with controlled porosity. In such case evaporation of thin film together with GLancing Angle Deposition (GLAD) method is required. GLAD allows to form the so called sculptured thin films by directing vapor flux towards the substrate at oblique angle. In case of periodic grating several variables appear: structured substrate relative orientation during the deposition process and the angle subtended between the substrate normal and the incident vapour flux. Considering many variables, it is important to evaluate the dependence of final structure on these values. Primary numerical simulations were performed employing NAno SCAle Modeling (NASCAM) software based on kinetic Monte Carlo algorithm [2]. This software does not take into account the vibrational movement of atoms, hence allows to investigate time evolution of relatively large systems containing millions of atoms. As both experimental and simulation results showed, film growth mode heavily depends on energy of incoming flux as well as on substrate orientation. As a result, main arising problems have been identified as modulation extinction after several layers (Fig. 1 B) and cracks formation (Fig. 1 C).

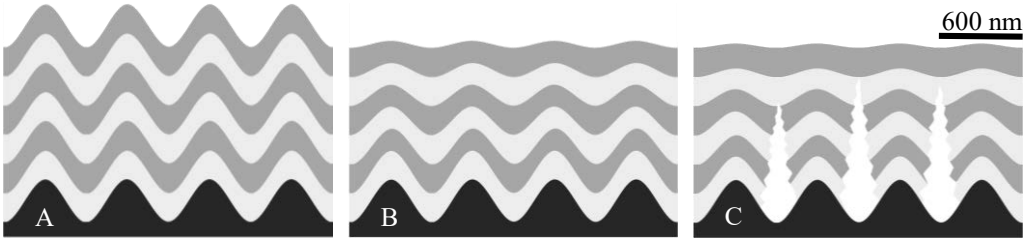

Fig. 1 Schematic representation of (A) an ideal conformally deposited multi-layer coating on periodically corrugated surface; (B) Planarization of surface modulation with increase of deposited coating thickness; (C) Planarization effect along with cracks formation.

The aim of this research is to evaluate the growth mechanism of multilayer optical coatings on modulated surfaces and compare theoretical results with experimental measurements. Experimental part was performed with different PVD technologies, as IBS and electron beam evaporation with GLAD method. The possibility to control the coating formation in both ways: conformally cover modulated surface and periodic microstructure deposition, will be presented during the conference.

[1] L. Grinevičiūtė, C. Babayigit, D. Gailevičius, E. Bor, M. Turduev, V. Purlys, T. Tolenis, H. Kurt, and K. Staliūnas. "Angular filtering by Bragg photonic microstructures fabricated by physical vapour deposition." Appl Surf Sci., 481, pp. 353 – 359 (2019)
[2] Moskovkin, P., & Lucas, S. Computer simulations of the early-stage growth of Ge clusters at elevated temperatures on patterned Si substrate using the kinetic Monte Carlo method. Thin solid films, 536, 313 – 317 (2013)

THE EVALUATION OF KINETIC OPTICAL REDUCING SUGAR SENSOR BASED ON GOLD NANOPARTICLE FORMATION

Benediktas Brasiunas[1], Anton Popov[1], Almira Ramanaviciene[1]

[1] NanoTechnas ï Center of Nanotechnology and Materials Science, Institute of Chemistry, Faculty of Chemistry and Geosciences, Vilnius University, Naugarduko st. 24, LT-03225, Vilnius, Lithuania.
benediktas.brasiunas@chgf.vu.lt

Reducing sugars are found in abundance in the food that we eat every day. Since overconsumption of sugars can be related to various diseases such as diabetes, obesity, heart disease, and various other disorders, the monitoring of reducing sugar levels in food and other mediums is an important task [1]. As such, sugar detection methods are being constantly improved seeking simpler, cheaper, and more accurate detection. Currently nanomaterials play and important role for reducing sugar detection acting as analytical signal providers or being used for analytical signal amplification, for example, in order to improve electron transfer kinetics, increasing sensitivity, reproducibility, and stability of the sensors [2]. Gold based nanomaterials (AuNP) are the most well-known, understood, and used optically active nanomaterials. Regarding their unique physical and optical properties AuNPs have been extensively employed in different analytical systems to strengthen existing signals, or as a separate signal in itself [2, 3]. For example, the formation of AuNPs, induced by reducing sugars, can be used as an analytical signal [4]. Sensors that use the formation of nanomaterials as signals can have unique analytical parameters since the analytical signal is governed by nanomaterial synthesis kinetics allowing for sophisticated analysis of similar analyte mixtures. Due to AuNP optical properties simple detection methods such as UV-vis spectroscopy can be employed to monitor AuNPs formation resulting in a fast and non-destructive detection.

In this work the formation of AuNP resulting from an oxidation-reduction reaction of $HAuCl_4$ in the presence of reducing sugars was used for the development of an optical sensor. Optimal oxidation-reduction reaction conditions were determined. The developed analytical system was evaluated with model samples of glucose, fructose, galactose, lactose, and mannose as well as reducing sugar mixtures. The impact of AuNP formation kinetics on the analytical parameters was established. Additionally, the developed system was tested with real samples.

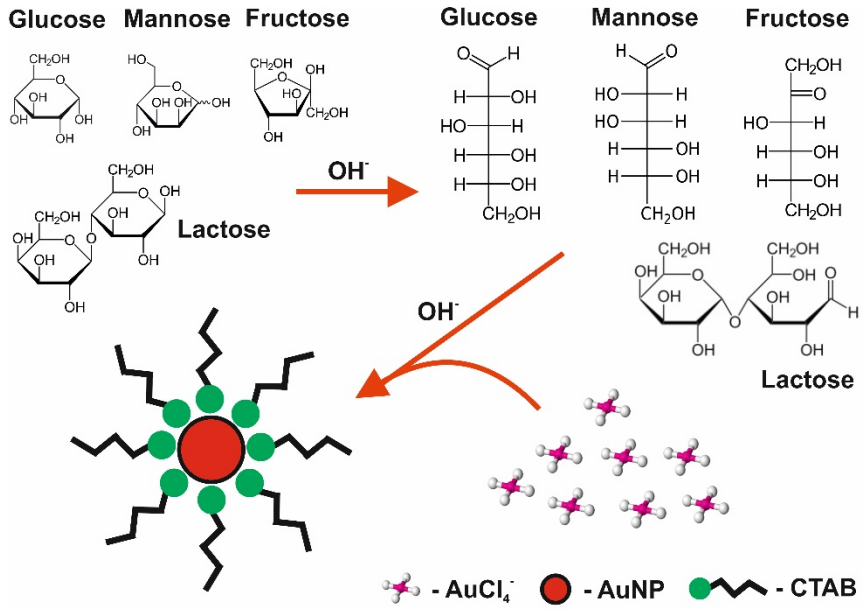

Fig. 1. Oxidation-reduction reaction and gold nanoparticle synthesis scheme.

[1] G. A. Bray, S. J. Nielsen, B. M. Popkin, Consumption of high-fructose corn syrup in beverages may play a role in the epidemic of obesity, Am. J. Clin. Nutr. **79(4)**, 537-543 (2004).

[2] A. Ramanavicius, N. German, A. Ramanaviciene, Evaluation of electron transfer in electrochemical system based on immobilized gold nanoparticles and glucose oxidase, Electrochem. Soc. **164(4),** G45--G49 (2017).

[3] A. Ramanaviciene, J. Voronovic, A. Popov et. al., Investigation of biocatalytic enlargement of gold nanoparticles using dynamic light scattering and atomic force microscopy, Colloids Surf. A Physicochem. Eng. Asp. **510**, 183ï 189 (2016).

[4] B. Brasiunas, A. Popov, A. Ramanavicius, A. Ramanaviciene, Gold nanoparticle based colorimetric sensing strategy for the determination of reducing sugars, Food Chemistry, 129238, (In Press) (2021).

LEAD HALIDE PEROVSKITE NANO- AND MICROLASERS FOR GAS SENSING APPLICATIONS

Anatoly Pushkarev

Department of Physics and Engineering, ITMO University, Russia
anatoly.pushkarev@metalab.ifmo.ru

Over the last 5 years, lead halide perovskite nano- and microstructures have emerged as promising laser medium exhibiting low generation threshold and high quality factor (Q) modes. Among these lasers, external cavity-free single-crystal nanowires and microplates are the most available. They possess high optical gain, well-shaped reflective end facets, and can be grown by cost-effective and large-scale wet chemical approaches at moderate temperature (50-80 °C). One of the possible applications for such lasers could be optical sensing of volatile substances: various organic solvents and hydrogen halides. However, detecting of volatile organic molecules at low concentrations cannot be realized for isolated perovskite nanowire or microplate laser on an ordinary substrate since optical eigenmodes in high refractive index perovskite ($n \approx 2.3$) do not interact effectively with the surrounding low refractive index medium. To address this issue, a perovskite laser needs to be coupled with a whispering gallery mode (WGM) polymer cavity [1] or should be deposited on a nanoporous substrate capable of changing its refractive index owing to the gas sorption process. On the contrary, detecting hydrogen halides vapors with perovskite lasers does not require the change of the refractive index of the surrounding medium because the vapor modifies the surficial chemical composition of the perovskite resonator due to halide exchange reaction [2, 3]. As a result, the change in the complex refractive index for the surface could invoke a small spectral shift of laser modes.

Herein we report on $CsPbBr_3$ nanowires and microplates deposited on a nanostructured indium tin oxide (ITO) substrate (Fig. 1) consisting of ITO whiskers and similar substrate consisting of ITO/Al_2O_3 whiskers by using a simple wet chemical approach. Perovskite crystals were synthesized on an amorphous SiO_2/Al_2O_3 substrate with island-like surface morphology. Thereafter, they were suspended in non-polar solvent via ultrasonication and deposited on the nanostructured substrates. The obtained perovskite cavities show room-temperature laser generation and high-Q laser modes owing to low refractive index ($n \approx 1.15$) of the substrates. Optical sensing of acetone and hydrogen iodide vapors at different concentrations is discussed.

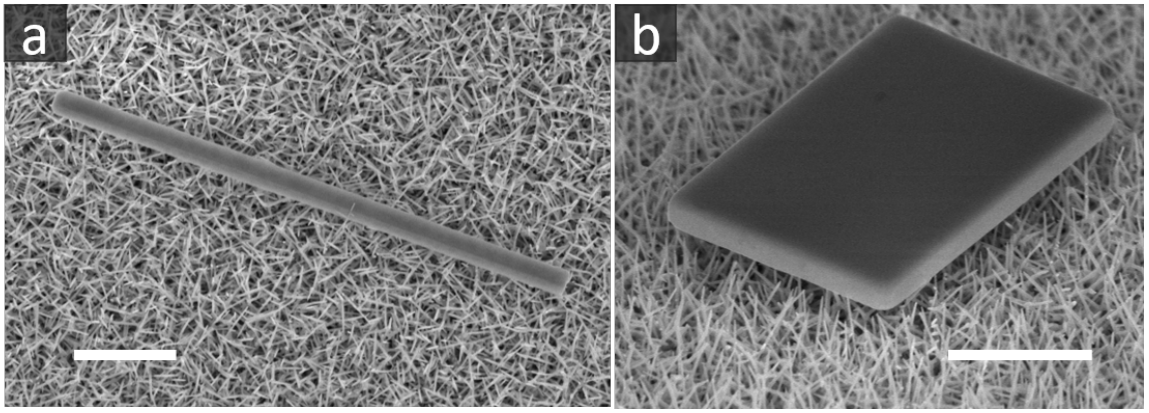

Fig. 1. (a,b) SEM images of $CsPbBr_3$ nanowire and microplate on nanostructured ITO substrate (scale bars are 1 μm).

Acknowledgement: Russian Science Foundation (grant no. 20-73-10183)

[1] J. Zhao, Y. Yan, C. Wei et al., Switchable Single-Mode Perovskite Microlasers Modulated by Responsive Organic Microdisks, Nano Letters **18**, 1241–1245 (2018).

[2] T. Liashenko, E. Cherotchenko, A. Pushkarev et al., Electronic structure of CsPbBr3xClx perovskites: synthesis, experimental characterization, and DFT simulations, Physical Chemistry Chemical Physics **21**, 18930-18938 (2019).

[3] D. Markina, E. Tiguntseva, A. Pushkarev et al.,, Photophysical properties of halide perovskite CsPb(Br1-xIx)3 thin films and nanowires, Journal of Luminescence **2020**, 116985 (2020).

N-DOPED REDUCED GRAPHENE OXIDE AS ELECTRODE MATERIAL FOR HYDROGEN PEROXIDE ELECTROCHEMICAL SENSOR

Justina Gaidukevič [1], Rasa Pauliukaitė[1]

[1] Department of Nanoengineering, Center for Physical Sciences and Technology, Savanoriu Ave. 231, LT-02300 Vilnius, Lithuania
justina.gaidukevic@ftmc.lt

Hydrogen peroxide is the most stable and abundant reactive oxygen species in an organism and present in many biological processes [1]. It is a general enzymatic product of oxidases and a substrate of peroxidases, which are important in biological processes and biosensors. H_2O_2 is also an essential mediator in food, pharmaceutical, clinical, industrial, and environmental analysis [2]. Quantitative detection of H_2O_2 has important scientific significance for understanding intracellular signal transduction and realizing the normal function of cells. The development of low cost, high-speed, uncomplicated, highly selective, and sensitive H_2O_2 sensors are essential.

After discovering the existence of graphene by A. Geim and K. Novoselov, this new material is one of the most celebrated discoveries presently in the field of material science [3]. Several unique properties of graphene make it a capable contender to be used as a sensor. The conjugated structure of graphene can facilitate the electron transfer between the bioreceptor and transducer, which can generate high signal sensitivity for electrochemical sensors. The incorporation of graphene and its related nanomaterials in (bio)sensor technologies have shown great promise due to its high surface area (2630 $m^2 g^{-1}$), electron mobility at room temperature (up to 200000 $cm^2 V^{-1} s^{-1}$), chemical stability and its capacity to immobilize a variety of different biomolecules. Moreover, chemical doping of graphene-based materials is an easy and effective method to modify materials intrinsically, tailor electronic properties, manipulate surface chemistry, and produce local changes to the elemental composition of host materials [3].

The aim of this work was to produce N-doped reduced graphene oxide (rGO) and to investigate its sensitivity in the non-enzymatic detection of hydrogen peroxide.

GO was prepared from natural graphite using the synthesis protocol reported by Yan et al. [4]. In a typical experiment, graphite powder was treated with concentrated H_2SO_4, $K_2S_2O_8$, and P_2O_5. The obtained pre-oxidized graphite was subjected to oxidation by Hummersômethod using $NaNO_3$, H_2SO_4, and $KMnO_4$ [5]. The thermally rGO was produced from GO using a thermal shock method. The dried GO powder was quickly inserted into a preheated tubular furnace at a temperature of about 800 ÁC in Ar atmosphere. To introduce N-functionalities, the rGO surface was modified with gaseous ammonia at 950ÁC for 8 h or with melamine at 700 ÁC for 1 h [6, 7]. The obtained materials were characterized by different methods (elemental analysis, BET measurement, SEM investigations, Raman spectroscopy). Electrochemical measurements, in particular, cyclic voltammetry and electrochemical impedance spectroscopy were used to evaluate the obtained samples sensitivity toward hydrogen peroxide detection.

The results demonstrated that after the reduction of GO, a characteristic morphology of rGO and N-doped rGO occurs independent on the functionalization protocol. Moreover, it was observed, that various nitrogen species including pyridinic-N, pyrrolic-N and quaternary-N were detected in the N-doped rGO. BET measurement results prove that all prepared samples were meso- and macroporous in nature. In addition, after the ammonia-treatment at high temperatures, both BET surface area and pore volume of the samples increased compared to the pristine GO and rGO. Finally, the conducted electrochemical measurements highlighted that N-doped rGO could be a promising electrode material for the detection of hydrogen peroxide.

ACKNOWLEDGMENTS. This project has received funding from European Social Fund (project No 09.3.3-LMT-K-712-19-0050) under grant agreement with the Research Council of Lithuania (LMTLT).

[1] V. Kumar, R.K. Gupta, R.K. Gundampati, D.K. Singh, S. Mohan, S.H. Hasan, M. Malviya, Enhanced electron transfer mediated detection of hydrogen peroxide using a silver nanoparticleï reduced graphene oxideï polyaniline fabricated electrochemical sensor, RSC Advances **8,** 619-631 (2018).

[2] H. Shamkhalichenar, J.-W. Choi, Reviewð Non-Enzymatic Hydrogen Peroxide Electrochemical Sensors Based on Reduced Graphene Oxide, Journal of The Electrochemical Society **167**, 037531 (2020).

[3] W. Yu, L. Sisi, Y. Haiyan, L. Jie, Progress in the functional modification of graphene/graphene oxide: a review, RSC Advances **10**, 15328-15345 (2020).

[4] X. Yan, J. Chen, J. Yang, Q. Xue, P. Miele, Fabrication of Free-Standing, Electrochemically Active, and Biocompatible Graphene Oxideī Polyaniline and Grapheneī Polyaniline Hybrid Papers, App. Mater. **9**, 2521–2529 (2010).

[5] W. S. Hummers, R. E. Offeman, Preparation of Graphitic Oxide, J. Am. Chem. Soc., **80,** 1339 (1958).

[6] J. Long, X. Xie, J. Xu, Q. Gu, L. Chen, X. Wang, Nitrogen-Doped Graphene Nanosheets as Metal-Free Catalysts for Aerobic Selective Oxidation of Benzylic Alcohols, ACS Catalysis **2**, 622-631 (2012).

[7] Z.-H. Sheng, L. Shao, J.-J. Chen, W.-J. Bao, F.-B. Wang, X.-H. Xia, Catalyst-Free Synthesis of Nitrogen-Doped Graphene via Thermal Annealing Graphite Oxide with Melamine and Its Excellent Electrocatalysis, ACS Nano **5**, 4350-4358 (2011).

AMORPHOUS DIAMOND-LIKE CARBON AS A MATRIX FOR NANOCOMPOSITE PLASMONIC LIGHT ABSORBING ANTI-REFLECTIVE COATINGS

Paulius Dolmantas[1,2*], Augrinã Jurkeviļ iÎ tã[1,2], Asta Tamuleviļ ienã[1,2], Andrius Vasiliauskas[2], Ġarî nas Meġkinis[2], Tomas Tamuleviļ ius[1,2]

[1] Institute of Materials Science of Kaunas University of Technology, K. Barġausko St. 59, LT-51423 Kaunas, Lithuania
[2] Department of Physics, Kaunas University of Technology, StudentÔ St. 50, LT-51368 Kaunas, Lithuania
Paulius.Dolmantas@ktu.edu

Advances in understanding and applications of plasmonics has led to beginning of development of unconventional anti-reflective coatings (ARCs) in which absorbing layers are also used. Here, the reduction of reflectance originates not only from phase contrast and destructive interference like in multilayer ARCs, but also due to high extinction in coating material (hence, absorbing ARCs). Using plasmonic scattering by nanoparticles, the reflectivity could be reduced significantly [1]. Such structures could be far thinner than conventional multilayer ARCs. Amorphous diamond-like carbon (DLC) is an attractive material to use as matrix for Ag nanoparticles. This is primarily due to high hardness, chemical inertness, and low friction coefficient [2].

In the present work, we investigated a series of ultra-thin DLC:Ag films of thicknesses ranging from 50 to 300 nm and containing different amounts of silver. Nanocomposite films were deposited using custom build DC reactive magnetron sputtering system in acetylene gas atmosphere. Raman analysis, SEM, EDX, ablation threshold and UV-vis spectral characterizations were carried out. An important characteristic of DLC matrix is its sp^3/sp^2 bonding representing the diamond and graphite phase content in the films. As seen from Fig. 1. most samples fall into nc-graphite to a-C (amorphous carbon) or a-C to ta-C (tetrahedral a-C) category. Samples with low Ag content (< 10 at.%) show high sp^3/sp^2 bond ratio compared to samples with high Ag content (> 10 at.%). Fig. 2. Shows reflectance and absorbance spectra of DLC:Ag with 2.9 at.% Ag.

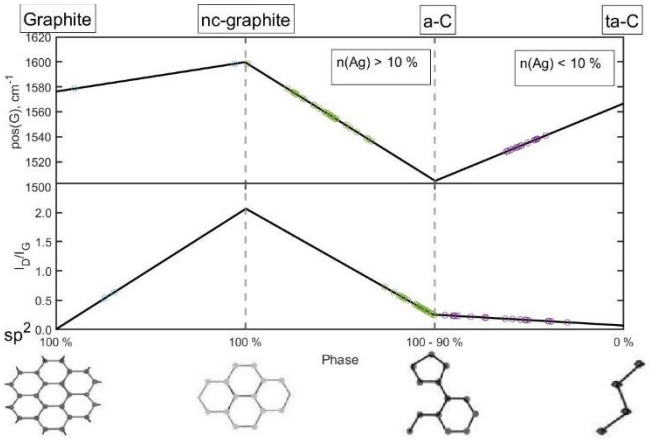

Fig. 1. Classification of deposited DLC:Ag nanocomposite films according to Ferrari three-stage model [3]

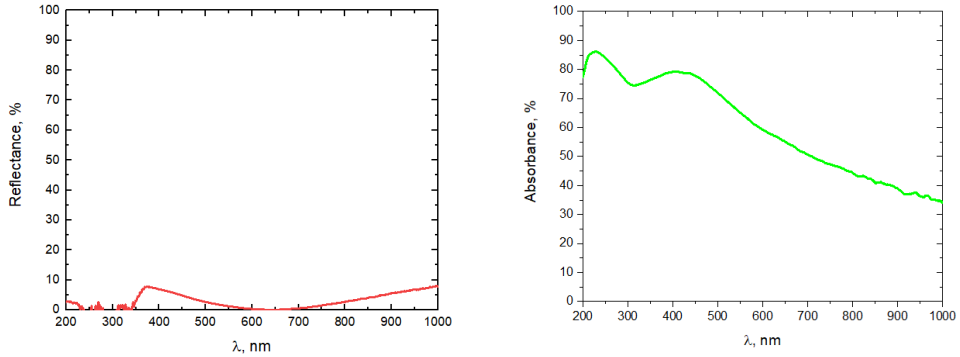

Fig. 2. Reflectance spectrum of DLC:Ag film on crystalline Si substrate (a) and absorbance spectra of identical film on fused silica substrate (b)

[1] M. K. Hedayati and M. Elbahri, ñAntireflective coatings: Conventional stacking layers and ultrathin plasmonic metasurfaces, a mini-review,ò *Materials (Basel).*, vol. 9, no. 6, 2016, doi: 10.3390/ma9060497.
[2] B. Mednikarov *et al.*, ñOptical properties of diamond-like carbon and nanocrystalline diamond films,ò *J. Optoelectron. Adv. Mater.*, vol. 7.
[3] J. Robertson, ñDiamond-like amorphous carbon,ò *Mater. Sci. Eng. R Reports*, vol. 37, no. 4ï 6, pp. 129ï 281, May 2002, doi:10.1016/S0927-796X(02)00005-0.

EVALUATION OF ANTIBODIES IMMOBILIZATION ON GOLD-COATED MAGNETIC NANOPARTICLES

Eimantas Bucmys[1], Viktorija Lisyte[1], Anton Popov[1]

[1] Nanotechnas ï Center of Nanotechnology and Materials Science, Faculty of Chemistry and Geosciences, Vilnius University, Lithuania

eimantas.bucmys@chgf.stud.vu.lt

Gold-coated magnetic nanoparticles (mAuNP) functionalized with antibodies are an interesting area of research. mAuNP application in bioanalysis allows to improve the analytical characteristics of immunosensors under development. Their magnetic properties are useful for separation of the analyte from a complex matrix using a magnetic field [1]. The gold layer provides biocompatibility, unique optical properties, and allows to use various methods for immobilization of antibodies on the surface of particles [2]. The orientation and loading density of immobilized antibodies has a significant influence on the analytical performance of the immunosensor, wherein antigen-binding capacity correlates with the number of accessible Fab domains [3]. Therefore, there is an ongoing effort in search of an optimal immobilization protocol. In this work, different methods of antibody immobilization were evaluated. Already existing information about mAuNP and their modification with antibodies was systematized and optimal methods were selected. To achieve this, surface plasmons resonance (SPR) spectroscopy, which is highly sensitive and reliable for the study of biomolecule interactions was used. Additionally, using a modified Bradford assay [4] and UV-vis spectroscopy the amount of immobilized antibodies was evaluated.

The main aim of this study was to apply different analytical methods for the evaluation of the loading density and orientation of antibodies immobilized onto the surface of mAuNP. Horseradish peroxidase (HRP) and antibodies against HRP were used for the design of the model system. The number of antibodies immobilized on the surface of mAuNPs was determined using the reaction between HRP, H_2O_2, and 3,3',5,5'-tetramethylbenzidine (TMB), which results in a change of solution color. The concentration of antibodies that were not immobilized was determined using a modified Bradford assay. SPR measurements were used for the evaluation of the interaction of the immobilized antibodies with HRP.

Acknowledgements

This project has received funding from European Social Fund (project No. 09.3.3-LMT-K712-22-0168) under grant agreement with the Research Council of Lithuania (LMTLT).

1. Leong, S. S., Ahmad, Z., Low, S. C., Camacho, J., Faraudo, J., & Lim, J., Unified View of Magnetic Nanoparticle Separation under Magnetophoresis. *Langmuir*, *36*(28), 8033ï 8055 (2020).
2. Li, Y., Schluesener, H. J., & Xu, S., Gold nanoparticle-based biosensors. Gold Bulletin, 43(1), 29ï 41 (2010).
3. Ruiz, G., Tripathi, K., Okyem, S., & Driskell, J. D., pH Impacts the Orientation of Antibody Adsorbed onto Gold Nanoparticles. Bioconjugate Chemistry, 30(4), 1182ï 1191 (2019).
4. Tripathi, K., & Driskell, J. D., Quantifying Bound and Active Antibodies Conjugated to Gold Nanoparticles: A Comprehensive and Robust Approach To Evaluate Immobilization Chemistry. *ACS Omega*, *3*(7), 8253ï 8259 (2018).

THE TEMPERATURE INFLUENCE ON ULTRA-HIGH MOLECULAR WEIGHT POLYETHYLENE STRUCTURAL PROPERTIES

Laurynas Tumėnas[1], Skirmantas Norkus[2,3], Brigita Abakevičienė[1,4]

[1] Department of Physics, Kaunas University of Technology, StudentÔstr. 50, LT-51368 Kaunas, Lithuania
[2] Ortho Baltic, Taikos ave. 131A, LT-51124 Kaunas, Lithuania
[3] Center for Physical Sciences and Technology, Saulėtekio ave. 3, LT-10257 Vilnius, Lithuania
[4] Institute of Materials Science, Kaunas University of Technology, K. Barėausko str. 59, LT-51368 Kaunas, Lithuania
laurynas.tumenas@ktu.edu

Medical devices such as implants must be biocompatible, harmless to living organisms, must not cause allergic reactions and do not change their properties over time [1]. One such substance is ultra-high molecular weight polyethylene (UHMWPE) which, like other orthopedic implant materials are characterized by high biocompatibility, low coefficient of friction, and chemical resistance [2]. According to ISO standard 19227 ÄImplants for surgery ï Cleanliness of orthopedic implants ï General requirementsñ one of the main requirements to ensure proper osseointegration of surgical implants and reduce all possible risks of infection is a washing/cleaning process, but cleaning methods must not interact with materials and damage or otherwise affect their properties and structure [3].

In this study, medical grade UHMWPE was used. To determine the structure of UHMWPE polymer after the sterilization at different temperatures, the structural properties of the material were analyzed. The chemical bonds of samples were identified by Fourier transform infrared spectroscopy (FT-IR), thermal material properties were characterized by different scanning calorimetry (DSC) study, and the structure of the material was analyzed by X-ray diffraction analysis (XRD).

The results of the DSC study support the reliability of the XRD and FT-IR results, whereas the DSC results showed that the UHMWPE polymer structure is only affected at 142 ŒC (melting temperature). Therefore, we can say that the thermal exposure of the samples at both 60 ŒC and 100 ŒC does not affect material physical, chemical, structural, and thermal properties.

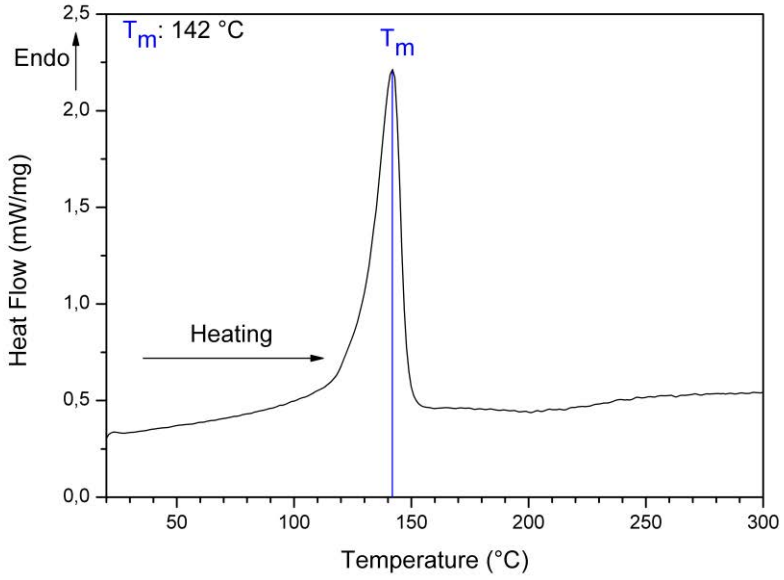

Fig. 1. Different scanning calorimetry heating curve.

[1] D. Mizeras, A. V. Valiulis, A. Ċeġok, and J. Griġkevičius, ñImplantÔir audiniÔregeneracijos karkasÔmedġiagÔanalizã,ò 2015.
[2] N. A. Patil, J. Njuguna, and B. Kandasubramanian, ñUHMWPE for biomedical applications: Performance and functionalization,ò *Eur. Polym. J.*, vol. 125, no. October 2019, 2020, doi: 10.1016/j.eurpolymj.2020.109529.
[3] ñINTERNATIONAL STANDARD Implants for surgery ð Cleanliness of orthopedic implants ð General requirements,ò vol. 2018.

DEVELOPMENT OF ELASTIC PEDOT:PSS-BASED ELECTROCHROMIC COMPOSITES FOR STRETCHABLE ELECTRONICS APPLICATIONS

Juzef Kucinski[1], Mindaugas Gicevicius[2], Lina Mikoliunaite[1]

[1] Department of Physical Chemistry, Faculty of Chemistry and Geosciences, Vilnius University, Lithuania
[2] Department of Physics, University of Cambridge, United Kingdom
Juzef.kucinski@gmail.com

Stretchable electronics refer to electronic devices and materials that have high elasticity, stretchability, and deformability. Unlike their conventional counterparts, stretchable electronics devices can usually be elongated by at least 10% without noticeable loss in conductivity and other functional properties [1]. Development of stretchable and elastic electrochromic materials can be used as a proof-of-concept technology for wearable displays. For example, small screens made from thousands of pixels built by stacking several layers, can display text or even images. Furthermore, by combining different electrochromic materials of red, green, and blue colors it is possible to make multicolor display [2].

The aim of this research was to develop a stretchable electrochromic composite based on elastomer material and conducting polymer poly(3,4-ethylenedioxythiophene) polystyrene sulfonate (PEDOT:PSS) and investigate its functional properties. Electrochromic stretchable films were prepared by mixing conducting polymer PEDOT:PSS with aqueous elastomer dispersion to obtain a homogenous composite. Functional elastomeric films were formed by solution casting in a mold filled with fixed amount of a mixture and dried at 60°C. Dilution by deionized water was used to achieve thickness control. All electrochemical measurements were performed in a custom made three electrode system where Ag/AgCl and platinum wire were used as reference and counter electrodes, respectively, while electrochromic stretchable films fixed on a glass substrate were used as working electrodes.

To evaluate electrochromic properties of the obtained composited chronoamperometric measurements were performed. The duration of a single switching cycle was 60 seconds, and the electrochemical potential was switched between -2 V and +1 V *vs* Ag/AgCl. During chronoamperometric test transmittance (T%) at maximum absorption wavelength 590 nm was recorded. Using acquired data absolute difference between neighboring peak values was calculated to obtain ϕT%.

The optimization of chemical composition, thickness of the films, applied electrochemical potential and pulse duration (Fig. 1.), and temperature treatment were carried out to achieve the greatest change in optical transmittance. Stretchability, Young's modulus, and thickness of the EM were estimated based on theoretical calculations.

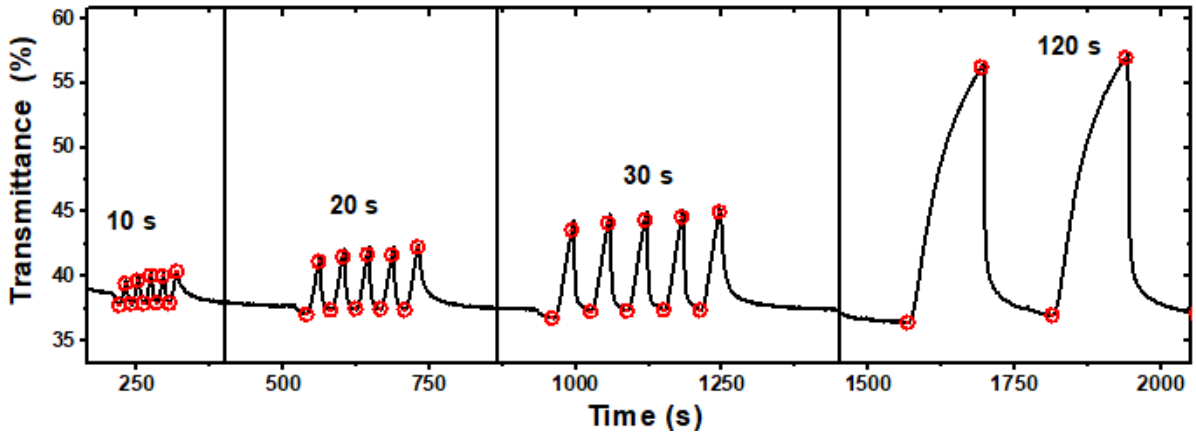

Fig. 1. Change in transmittance at 590 nm of PEDOT:PSS-based stretchable electrochromic composite under different electrochemical pulse durations.

[1] D.Y. Kim, M.J. Kim, et al., Stretchable and reflective displays: materials, technologies and strategies, Nano Converg. 6 (2019).
[2] R.J. Mortimer, A.L. Dyer, et al., Electrochromic organic and polymeric materials for display applications, Displays. 27 (2006) 2ï 18.

ADSORPTION OF DICLOFENAC FROM AQUEOUS MEDIUM ON CHEMICALLY MODIFIED STARCH

Paulina Andriunaite[1], Vesta Navikaite-Snipaitiene[1], Ramune Rutkaite[1]

[1] Department of Polymer Chemistry and Technology, Kaunas University of Technology, Kaunas, Lithuania
paulina.andriunaite@ktu.edu

Diclofenac is an anti-inflammatory drug with the highest acute toxicity among the non-steroidal anti-inflammatory drugs. Due to its extensive consumption, diclofenac has been detected in the samples of surface water such as rivers as well as wastewater treatment plants. Hence, the use of traditional mechanical and biological wastewater treatment technologies results in insufficient removal of this type of contaminant [1]. The aim of this work was to study the adsorption of diclofenac from water on cross-linked cationic starch.

Cross-linked cationic starch (CLCS) microgranular sorbent was obtained by the means of chemical modification of potato starch. CLCS was obtained by cross-linking potato starch with 0.1 mol/AGU (anhydroglucoside unit) of epichlorohydrin and cationization with 2,3-epoxypropyltrimethyammonium chloride by varying molar ratios of reagents. The starch derivatives with the degree of substitution of quaternary ammonium groups of 0.21 and 0.33 were synthesized. Sorbents granules were characterized by scanning electron microscopy, Fourier-transform infrared spectroscopy and thermogravimetric analysis.

The adsorption of diclofenac onto CLCS microgranules was investigated by employing the equilibrium adsorption method. The obtained isotherms of diclofenac adsorption on CLCS at 20 ÁC and diclofenac removal efficiency from water diagram are presented in Fig. 1A and Fig. 1B, respectively.

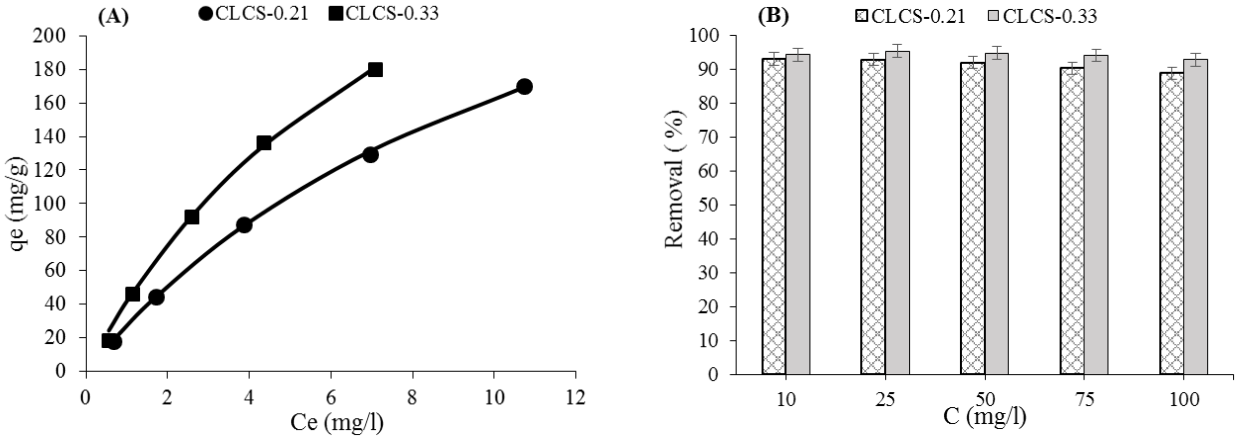

Fig. 1. Adsorption isotherms of diclofenac on CLCS at 20 ÁC (A) and removal efficiency of diclofenac from water (B)

The Langmuir, Freundlich and Dubininï Radushkevich adsorption models were used to describe the adsorption isotherms. According to the Langmuir adsorption model, the diclofenac molecules were adsorbed on the active centers i.e. quaternary ammonium groups of CLCS. The Langmuir sorption capacities were 406 and 365 mg/g when diclofenac was adsorbed onto CLCS-0.33 and CLCS-0.21, respectively (Table 1). The values of Freundlich constant n_F and Dubininï Radushkevich adsorption energy E_{DR} indicated that conditions for diclofenac adsorption onto CLCS were unfavorable and the ion-exchange mechanism was predominant during adsorption.

Table 1. Adsorption model parameters for adsorption of diclofenac onto CLCS at 20 ÁC

Sorbent	Langmuir model		Freundlich model		Dubinin-Radushkevich model	
	Q_L (mg/g)	R^2	n_F	R^2	E_{DR} (kJ/mol)	R^2
CLCS-0.33	406	0.9972	1.33	0.9938	10.0	0.9968
CLCS-0.21	365	0.9970	1.36	0.9947	9.1	0.9975

As can be seen from Fig 1B the removal of diclofenac varied from 93 to 94 % and 89 to 93 % when using different concentrations of CLCS-0.33 and CLCS-0.21 sorbents, respectively. The obtained results confirmed that CLCS is promising sorbent for the removal of pharmaceuticals contaminants containing anionic groups from aqueous medium.

Acknowledgment. This research was supported by the Research, Development and Innovation Fund of Kaunas University of Technology (project grant No. PP-91D/19).

[1] De Franco, M. A. E. et al., Diclofenac Removal from Water by Adsorption Using Activated Carbon in Batch Mode and Fixed-Bed Column: Isotherms, Thermodynamic Study and Breakthrough Curves Modeling: Journal Cleaner Production **181**, 145-154 (2018)

GRANULATION OF INDUSTRIAL WASTE AND ANALYSIS OF THE OBTAINED GRANULES

Kristina Buneviļ ienā[1], Meda Pagvenskaitā[1,2],

[1] Institute of Agriculture, Lithuanian Research Centre for Agriculture and Forestry, Lithuania
[2] Faculty of Medicine, Kaunas University of Applied Sciences, Lithuania
meda.pa9746@go.kauko.lt

Biofuel ash (BA) and lime kiln dust (LKD) are industrial waste. BA is a complex and heterogeneous mixture of inorganic crystalline and amorphous minerals with organic matter [1]. BA usually contains mainly K, P, Ca and Mg, which are essential macroelements for plant growth [2]. Ash processing (granulation) uses similar methods, which are also used to produce mineral fertilizers. Granulation is the transformation of fine powdered materials into granular ones in interaction with the liquid phase. Granular materials are those with a particle diameter >0.5 mm. The granules of fertilizer products must be mechanically strong so that they can be easily transported and spread in the fields but at the same time capable of easily decomposing in the soil. Various synthetic or natural materials can be used as binders in the granulation process, including LKD [3]. At humidity, BA reacts with LKD to form compounds with binding properties.

In this study, biofuel ash granules were produced: BAG30, BAG50 and BAG70 containing 30, 50 and 70% ash. The other part consisted of lime kiln dust, 70, 50 and 30%, respectively. LKD and BP were weighed and mixed thoroughly using a homemade ribbon blade agitator. While agitating the mixture, a small amount of water (~ 12%) was added to the dry materials until small aggregates started to form a paste. The paste was granulated using a disc pelletizer. After granulation, the granules were dried at room temperature in a laboratory fume hood for 24 hours [4].

The samples were ground, sieved, extracted with *aqua regia* according to LST EN ISO 13650:2006. Atomic Absorption Spectroscopy (AAS) was used to find the concentration of Ca and Mg, flame photometer (FP) of K, UV-VIS spectrophotometer of P and inductively coupled plasma mass spectrometry (ICP-MS) of heavy metals [4]. The X-ray diffraction (XRD) data were collected with a DRON-6 powder X-ray diffractometer with Bragg-Brentano geometry using Ni-filtered CuKŬ radiation [5]. The particle size distribution was determined using the digital electromagnetic sieve shaker Filtra Vibracion FTL-0200 and the strength of the granules was determined using strength granule measurer IPG-1M in the measuring range between 5 to 200 N [4].

The analysis of chemical and physicochemical quality indicators of ash granules revealed that these substances consist mainly of chemical compounds containing Ca^{2+} ions (Fig.1).

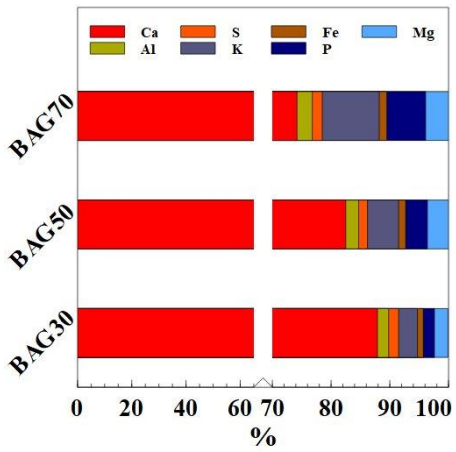

Fig. 1. Chemical composition of the major nutrients in granules.

The strength of the granules correlates with the amount of ash added to the mixture, i. e. the strength increases with increasing ash content in the granule, which weakens the release of nutrients from the granule. The strongest BAG were in the mixture with 70% ash. Higher-strength granules are easier to transport, less physically vulnerable, but have a negative aspect - they stay on the soil surface longer and do not release nutrients, so the most optimal BAG have the lowest ash content in the mixture, i. e. 30%.

[1] S. V. Vassilev, D. Baxter, L. K. Andersen, C. G. Vassileva, An overview of the composition and application of biomass ash. Part 1. Phase-mineral and chemical composition and classification, Fuel 105 (2013) 40ï 76, https://doi.org/10.1016/j.fuel.2012.09.041.
[2] M. Freire, H. Lopes, L. A. C. Tarelho, Critical aspects of biomass ashes utilization in soils: Composition, leachability, PAH and PCDD/F, Waste Manag. 46 (2015) 304ï 315, https://doi.org/10.1016/j.wasman.2015.08.036.
[3] A. Arulrajah, A. Mohammadinia, A. DôAmico, S. Horpibulsuk, Cement kiln dust and fly ash blends as an alternative binder for the stabilization of demolition aggregates, Constr. Build. Mater. 145 (2017) 218ï 225, https://doi.org/10.1016/j.conbuildmat.2017.04.007.
[4] K. Buneviciene, D. Drapanauskaite, R. Mazeika, V. Tilvikiene, J. Baltrusaitis, Granulated biofuel ash as a sustainable source of plant nutrients, Waste Manag. Res. (2020) , https://doi.org/10.1177/0734242X20948952.
[5] K. Baltakys, A. Iljina, A. Bankauskaite, Thermal properties and application of silica gel waste contaminated with F- ions for C-S-H synthesis, J. Therm. Anal. Calorim. (2015) 145ï 154, https://doi.org/10.1007/s10973-015-4663-4.

HEATING BEHAVIOUR INVESTIGATION OF AG/PA BASED KNITTED FABRICS

Md. Reazuddin Repon[1*], Daiva Mikuļ ionienã[2]

[1, 2] Department of Production Engineering, Faculty of Mechanical Engineering and Design, Kaunas University of Technology, Lithuania
reazmbstu.te@gmail.com

Textiles featured with electronic function are becoming one of the major growth sectors in the multidimensional application area. Based on interactive technology, the wearable electronic textiles form a new market segment resulting from the miniaturization of electronics, and innovation for both electronic and textile industries [1, 2]. Electro-conductive textiles can be used in heating purpose particularly in medical application [3]. The aim of this work was to investigate heating behavior of fabricated knitted fabrics designed for orthopedic support. Temperature feasibility was explored based on volume of conductive yarn used in the knitting pattern. The effect of yarn linear density on the thermal behavior used in the structure was also considered and compared.

A flat double needle-bed knitting machine was used to knit Ag coated polyamide yarn with elastomeric inlay-yarn in this study. The fluke 561 HVACPro infrared thermometer and FLIR DM285 thermal imager were used to measure the surface temperature and thermal imaging of the specimens. Two copper plates of accurate dimension, electrode plates were placed on the opposite edges of the specimen and connected with DC power. The applied voltage was progressively increased and observed the corresponding values of current across the fabric were noted from ammeter. Six specimens were manufactured depending on the amount of conductive yarn used in the knitting structure and two variants of linear density of Ag coated yarn.

The surface temperature was measured at different time intervals at fixed voltage applied. The generated temperature showed that the temperature rise was found to be related to the time and applied voltage. Results confirmed that the selected electro-conductive fabric heats up quickly at first two minutes and then very slowly. Finally, this rising is leveled off at a particular temperature. Depending on the knitting structure and the amount of conductive yarn used, the thermal behavior of specimens was varied at specific voltage [4].

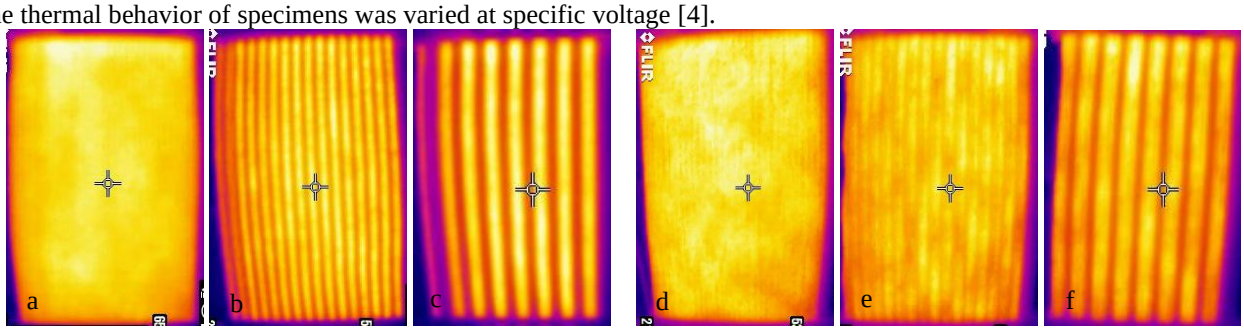

(a-c) Fabrics knitted with 66 tex (12 filaments) yarn (d-f) Fabrics knitted with 235 tex (34 filaments) yarn

Fig. 1. Thermal images of knitted specimens fabricated depending on conductive yarn amount and linear density used in knitting pattern.

The influence of the conductive yarn distribution in the knitting pattern is clearly exhibited in Figure 1, where yellow color indicates the highest temperature (40-45ÁC) while the blue color, accordingly, the lowest temperature (26ÁC).

[1] M. O'Mahony, S. E. Braddock-Clarke, *Techno textiles 2: revolutionary fabrics for fashion and design* (Thames and Hudson, London, 2005).
[2] C. R. Cork, *Conductive fibres for electronic textiles: an overview*, *Electronic Textiles* (Woodhead Publishing, London, 2015).
[3] M. Stoppa, C. Alessandro, Wearable electronics and smart textiles: a critical review, Sensors, **14,** 11957-11992 (2014)
[4] M.R. Repon, D. Mikuļ ionienã, I. Baltina et al., Ag Coated PA-Based Electro-Conductive Knitted Fabrics for Heat Generation in Compression Supports. *Autex Research Journal*, *1*(ahead-of-print, 2021).

PECULIARITIES OF POTATO, CORN AND WHEAT STARCHES CROSS-LINKING

Karolina Almonaityte, Joana Bendoraitiene, Greta Cizauskaite, Diana Masiulionyte, Dovile Liudvinaviciute, Ramune Rutkaite

Department of Polymer Chemistry and Technology, Kaunas University of Technology, Lithuania
karolina.almonaityte@ktu.lt

Starch is a natural carbohydrate based polymer, which is widely available from various natural sources including potato, wheat and corn. The granules occur in all shapes and sizes, i.e. spheres, ellipsoids, polygons, platelets and irregular tubules. Their diameter is ranging from around 0.1 to 200 micrometres depending on botanical origin [1]. Cross-linking occurs when intermolecular bridges are introduced between polysaccharide macromolecules. Cross-linked starches are resistant to high temperature, low pH, and higher shear, and the viscosity and textural properties are changed compared to native starch e.g. the hydrogen bonds in cross-linked granular starch are stronger and preventing swelling of the granules during pasting. The purpose of this work was to evaluate the starch cross-linking with epichlorohydrin process, taking into account the botanical origin, granule size and suspension concentration of starch in order to optimize and predict the cross-linking process.

Potato, wheat or corn starch was mixed with a sodium hydroxide solution and crosslinking agent epichlorohydrin (EPI) at the molar ratio of the AGU : EPI : NaOH : H_2O was 1 : (0.0005ï 0.01) : (0.0025ï 0.012) : 10. The reaction mixture was maintained at the temperature of 45ÁC for 24 h and pH 10.

As the size of the granules is of great importance in starch modification reactions, the particles were first characterized by scanning electron microscopy (SEM) (see Fig. 1) and laser diffraction techniques.

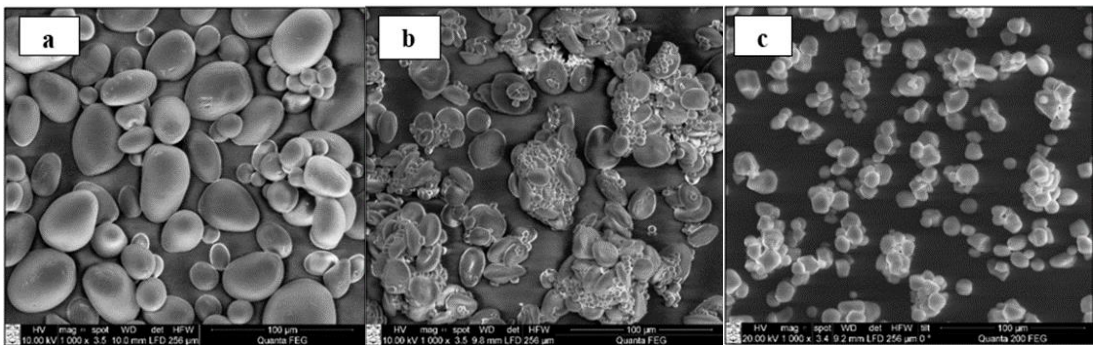

Fig. 1. Scanning electron microscopy (SEM) images of starch granules: a ï potato; b ï wheat; c ï corn. Magnification x1000.

As it is known from literature data [2], starch molecules are highly soluble in 1 M KOH aqueous solution, therefore this solvent was used to investigate synthesized cross-linked starch derivatives. By increasing EPI concentration in the modification mixture, the solubility of the obtained samples decreased due to the formed cross-links between macromolecules. It has been observed that even very small amounts of cross-linking agent have reduced the solubility of native starch by 15-30 %, implying that not only grafting reactions but also cross-linking of macromolecules is taking place. The viscosity changes of the suspensions of starch derivatives were determined by using viscoamylography technique. The lower viscosity was characteristic of the suspensions of wheat and corn starches composed of small granules, meanwhile, the peak viscosities of the slurries of potato starch-based samples composed of large granules were much higher. By selecting tailored starches and amounts of cross-linking agent, the materials with perfect thickening properties can be obtained. Meanwhile, cross-linked starches obtained by using 0.01 mol of cross-linking agent per 1 mol of starch do not form gels during pasting and remain in water in the form of microparticles. Therefore, such derivatives could be also potentially used as sorbents.

[1] S. Perez, E. Bertoft, The molecular structures of starch components andtheir contribution to the architecture of starchgranules: A comprehensive review. Starch, **62**, 389ï 420 (2010)

[2] Kim, H.-S., Huber, R.K.C.. Alkaline Dissolution of Starch Facilitated by Microwave Heating for Analysis by Size - Exclusion Chromatography. J. Agric. Food Chem. **54**, 9664-9669, (2006)

SPECTROSCOPIC CHARACTERISATION OF BODIPY-BASED NEW FLUORESCENT VISCOSITY SENSORS

Rugilė Žilėnaitė[1,2], Karolina Maleckaitė[2], Jelena Dodonova[1], Sigitas Tumkevičius[1], Aurimas Vyžniauskas[2]

[1] Institute of Chemistry, Faculty of Chemistry and Geosciences, Vilnius University, Naugarduko str. 24, Vilnius, Lithuania

[2] Center for Physical Sciences and Technology, Sauletekio av. 3, Vilnius, Lithuania

rugile.zilenaite@chgf.stud.vu.lt

Viscosity and temperature play a major role on microscopic levels in biosystems. These parameters can determine diffusion rate and processes inside cells. Changes in a cell can happen during natural processes, as well as during the development of diseases or pathologies [1,2]. Fluorescent molecular rotors (FMRs) are the group of organic fluorophores, the luminescence of which is sensitive to mediumôs physical properties, such as viscosity or temperature. After FMR excitation intramolecular rotation occurs. Fluorescence intensity depends on the time molecule spends in the excited state before the rotation. Intramolecular rotation is fast in low viscosity solvents, which leads to an increased nonradiative relaxation. In contrast, in high viscosity solvents rotation is slow and a fluorescence intensity increases. Besides the fluorescence intensity, a quantum efficiency and a decay time also increases [3].

Boron-dipyrromethene (BODIPY) based FMRs are widely used as viscosity sensors. In between them, BODIPY-C_{10} and other its derivatives are the most popular molecular rotors. Their main advantages are mono-exponential decay and relatively high molar extinction coefficient [4]. However, their main drawback is absorption and fluorescence wavelengths. The most of the BODIPY based probes emit photons in a green spectral region, although while working with biological tissues red or near-infrared light is more desirable [5].

The main focus of this research was to shift an emission spectra to longer wavelengths by increasing conjugated system. Absorption and fluorescence emission spectra, as well as fluorescence decays have been recorded to characterize spectroscopic properties of the samples. Dependences on solvents polarity, viscosity, and temperature were measured.

The obtained results show that extending the conjugated system results in a bathochromic shift of fluorescence spectra (Fig. 1, B). Measurements showed that BP-OME can be applied for sensing polarity instead of viscosity. BP-ME-NO showed approximately 4 times longer fluorescence decay time in viscous non-polar castor oil solvent in contrast to non-viscous non-polar toluene solvent. Therefore, it could be used as a viscosity sensor.

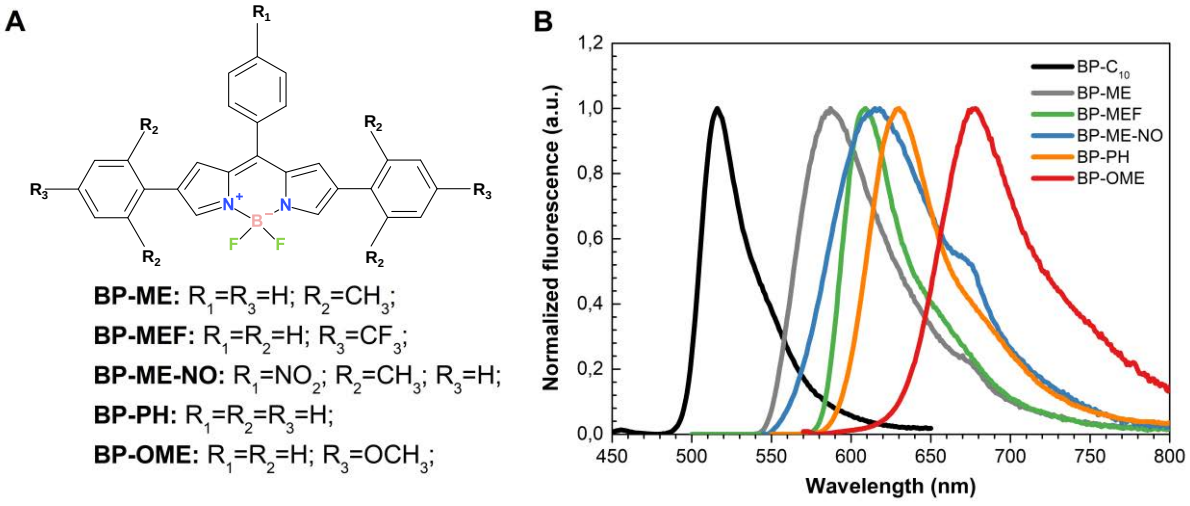

Fig. 1. (A) The molecular structure of examined FMRs. (B) Fluorescence spectra of BP-ME (grey), BP-MEF (green), BP-MEF-NO (blue), BP-PH (orange), BP-OME (red). BP-C_{10} (black) fluorescence spectra is used as a reference.

[1] M. Shinitzky, Membrane fluidity in malignancy Adversative and recuperative, BBA - Rev. Cancer. 738 (1984) 251ï 261.

[2] O. Nadiv, M. Shinitzky, H. Manu, D. Hecht, C.T. Roberts, D. LeRoith, Y. Zick, Elevated protein tyrosine phosphatase activity and increased membrane viscosity are associated with impaired activation of the insulin receptor kinase in old rats, Biochem. J. 298 (1994) 443ï 450.

[3] A. Vyžniauskas, M.K. Kuimova, A twisted tale: Measuring viscosity and temperature of microenvironments using molecular rotors, Int. Rev. Phys. Chem. 37 (2018) 259ï 285.

[4] S. Toliautas, J. Dodonova, A. Žvirblis, I. Ļiplys, A. Polita, A. Devižis, S. Tumkevičius, J. Ūulskus, A. Vyžniauskas, Enhancing the Viscosity-Sensitive Range of a BODIPY Molecular Rotor by Two Orders of Magnitude, Chem.-Eur. J. 25 (2019) 10342ï 10349.

[5] S.-C. Lee, J. Heo, H.C. Woo, J.-A. Lee, Y.H. Seo, C.-L. Lee, S. Kim, O.-P. Kwon, Fluorescent Molecular Rotors for Viscosity Sensors, Chem.-Eur. J. 24 (2018) 13706ï 13718.

ENCAPSULATION OF ANTHOCYANINS AND CINNAMALDEHYDE IN STARCH OCTENYLSUCCINATE

Zygimantas Augys[1], Vesta Navikaite-Snipaitiene[1]

[1] Department of Polymer Chemistry and Technology, Kaunas University of Technology, Kaunas, Lithuania
zygimantas.augys@ktu.edu

The anthocyanins and essential oils are derived from plants and are denoted by antioxidant, antibacterial, anti-cancer and anti-inflammatory properties. They are widely used in cosmetics, pharmaceuticals and food industry because of their active properties. However, anthocyanins are unstable compounds. In order to increase their stability, anthocyanins are immobilized into various carriers which not only protect their molecules from physical and chemical factors, but also maintain their activity [1, 2]. The aim of this work is to encapsulate anthocyanins and cinnamaldehyde in hydrophobically modified starch by using spray drying method.

In this study anthocyanins (AC) from bilberry extract *(Vaccinium myrtillus L.)* and cinnamaldehyde (CA) were encapsulated in starch octenylsuccinate (OSAS) by using spray drying method. Firstly, aqueous emulsion containing 20 % of starch octenylsuccinate, 0.05 % anthocyanins and 5 % cinnamaldehyde was prepared. The droplet size of emulsion (271±5 nm) was measured and antioxidant activity (78±4 %) was determined. The dry capsules of starch octenylsuccinate with entrapped active compounds were obtained by spray drying the emulsion with *Nano Spray Dryer B-90* (Buchi). The obtained OSAS-AC-CA capsules (Fig. 1 C) were characterized by using scanning electron microscopy (SEM) and Fourier transform infrared spectroscopy studies.

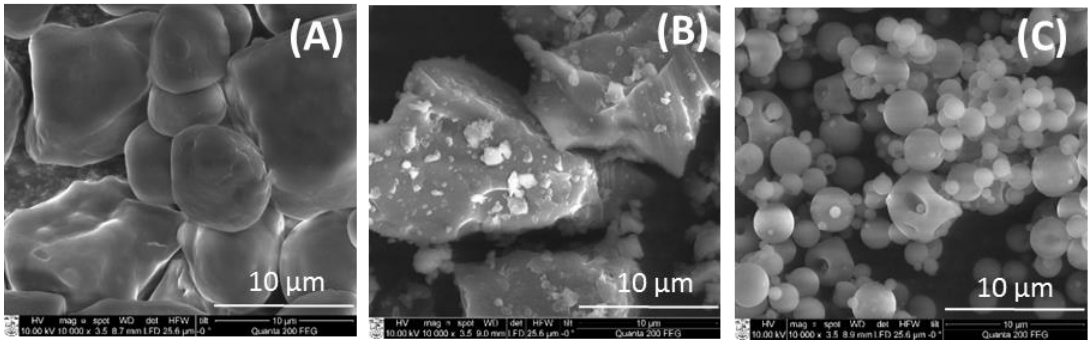

Fig. 1. SEM micrographs of OSAS (A), anthocyanins (B) powders and OSAS-AC-CA capsules (C). The magnification is ×10000

The tablets containing various amounts of OSAS-AC-CA capsules and microcrystalline cellulose were prepared and their antioxidant activity was examined (Fig. 2). The antioxidant efficiency varied from 23±1 to 90±5 % depending on OSAS-AC-CA content in the tablet. Consequently, OSAS-AC-CA capsules could be potentially used as antioxidant component in food supplements.

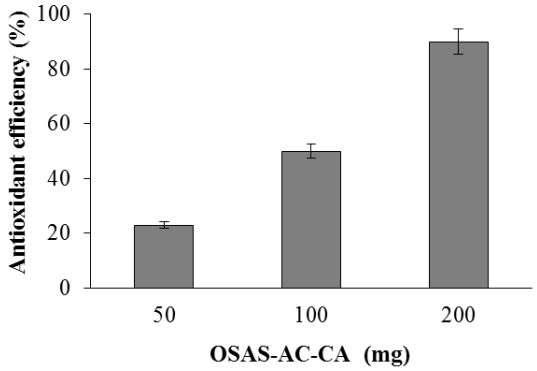

Fig. 2. Dependence of tablet antioxidant efficacy on the amount of OSAS-AC-CA capsules in the tablet. Total weight of the tablet was equal to 500 mg

[1] Tarone A.G. et al., Anthocyanins: New techniques and challenges in microencapsulation: Food Research International **133,** 109092 (2020)
[2] Sharifi-Rad, J. et al., Biological Activities of Essential Oils: From Plant Chemoecology to Traditional Healing Systems: Molecules **22(1)**, 70 (2017)

INVESTIGATION OF PHOTOANODIC PROCESSES ON WO_3 ELECTRODE IN DIFFERENT ELECTROLYTES

Maliha Parvin, Milda Petruleviļienā, Irena Savickaja, Benjaminas Ġebeka, Arnas Naujokaitis, Vidas Pakġtas, Renata Karpicz, Jurga Juodkazytā

Center for Physical Sciences and Technology, Saulātekio av. 3, Vilnius 10257, Lithuania
maliha.parvin@ftmc.lt

Tungsten (VI) oxide (WO_3) is an n-type semiconductor which has been attracting much attention as photoanode for photoelectrochemical (PEC) water splitting as well as degradation of pollutants. WO_3 is attractive due to its relatively low cost, chemical stability and ability to absorb visible light (band gap is 2.5 - 2.8 eV) [1][2]. It is well-known that the product of photoanodic reaction in the case of WO_3 photoanodes depends largely on the composition of the electrolyte used. Valuable oxidizing reagents such as hypochlorite and persulfate can be produced photoelectrochemically on WO_3 photoelectrode in chloride and sulfate solutions, respectively. In this study we compared the efficiency of the photoanodic processes taking place on WO_3 electrode surface in 0.5 M H_2SO_4, 0.5 M NaCl and 0.5 M Na_2SO_4 electrolytes.

WO_3 photoanodes were synthesized using sol-gel method and $Na_2WO_4{\cdot}2H_2O$ as precursor. Five different reductants ï methanol, ethanol, propanol, isopropanol and butanol were used to deposit WO_3 layers on conducting glass (FTO) substrate. The coatings were annealed at 400ºC for 2 h in air atmosphere. The crystallographic structure and surface morphology of the calcined WO_3 films was characterized by X-ray diffraction and scanning electron microscopy (SEM) techniques. Optical properties of the films were analyzed by means of photoluminescence spectroscopy. Photoelectrochemical behaviour of the samples was investigated using cyclic voltammetry, chronoamperometry under chopped illumination, electrochemical impedance spectroscopy. Photoelectrolysis experiments were performed in two electrode cell with Pt cathode. Iodometric and chromatometric titration methods were used to determine the amounts of photoelectrochemically produced ClO^- and $S_2O_8^{2-}$, respectively, in order to evaluate faradaic efficiency (FE) of photoanodic reactions.

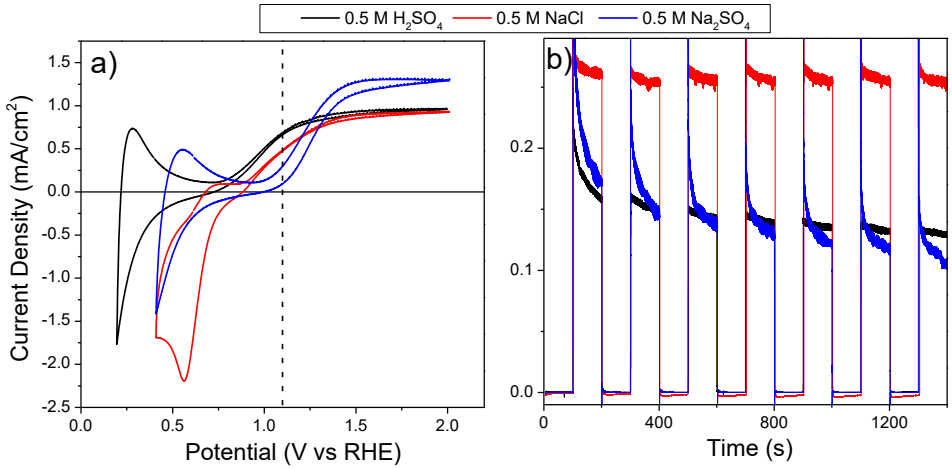

Fig. 1. a) Cyclic voltammograms of WO_3 photoanode prepared using methanol as reductant in 0.5 M H_2SO_4, 0.5 M NaCl and 0.5 M Na_2SO_4 electrolytes under illumination (~100 mW cm^{-2}), potential scan rate 50 mV s^{-1}, b) chronoamperograms of the same electrode obtained at ~1.1 V vs RHE under chopped illumination.

SEM investigations revealed significant differences in morphology of the films prepared using different reductants. The highest PEC activity was observed for the coatings obtained using methanol, isopropanol or butanol. Comparison of photoelectrochemical response of WO_3 photoanode prepared using methanol in different electrolytes under potentiodynamic conditions (Fig.1a) shows that highest photocurrent is observed in 0.5 M Na_2SO_4. However, stationary photocurrentī time profiles (Fig. 1b) obtained at ~ 1.1 V (RHE), i.e. in the E range preceding the photocurrent saturation, where it is limited by photon absorption, revealed that the highest and most stable photocurrent is observed in 0.5 M NaCl solution. This was true for all investigated WO_3 samples irrespective of the synthesis conditions and surface morphology. Average FE of PEC generation of hypochlorite and persulfate species was ~73%, ~45% and ~74% in 0.5 M NaCl, 0.5 M H_2SO_4, and 0.5 M Na_2SO_4 electrolytes, respectively. The findings of the study imply that photo-oxidation of $Cl^ī$ ions on WO_3 photoelectrodes is the most facile process among the photoanodic reactions studied.

[1] K. Sayama, Production of high-value-added chemicals on oxide semiconductor photoanodes under visible light for solar chemical-conversion processes, *ACS Energy Lett.*, **3**, 1093ï 1101 (2018).

[2] J. C. Hill and K. S. Choi, Effect of electrolytes on the selectivity and stability of n-type WO_3 photoelectrodes for use in solar water oxidation, *J. Phys. Chem. C*, **116**, 7612ï 7620 (2012).

METAL IONS SENSING FOR BIOLOGICAL APPLICATIONS BASED ON ORGANIC SEMICONDUCTORS

Lukas Barzdėnas[1], Rokas Skaisgiris[1], Dace Cirule[2], Maris Turks[2], Saulius Juršėnas[1]

[1]Institute of Photonics and Nanotechnology, Faculty of Physics, Vilnius University, Lithuania
[2]Institute of Technology of Organic Chemistry, Faculty of Materials Science and Applied Chemistry, Riga Technical University, Latvia
lukas.barzdenas@gmail.com

Metal ions have vital importance for living organisms. Ions plays important role in life cycle of cell starting with reproduction and ending with programmed cell death (apoptosis). Moreover, metal ions are responsible for enzyme production and generally controls all chemical reactions that are happening in living cell. Naturally, high concentration as well as low concentration of metal ions in living organism can have negative impact. One of many metal ions which has both negative and positive effect on living organism is silver (Ag^{+}). Small concentrations of silver ions have antibacterial properties that can kill pathogenic bacteria, however, high concentration can even lead to liver cirrhosis [1]. Other metal ions such as Zn^{+2}, Cu^{+2} and Ca^{+2} can accumulate in human body and cause neurodegenerative diseases (e.g. Wilson disease) [2].

Thus, it is important to detect and monitor metal ions in living organisms for that purpose metal ion detectors are being developed. Fluorescence detectors gets a great deal of attention because they exhibit high sensitivity, low production cost and short response time. One of many kinds of organic fluorescence detectors are purin-based organic compounds[3].

In this work we researched photophysical properties of purin-based donor-acceptor molecule, its interaction with different metal ions in different protic solvents. The investigated compound (DaC-60) comprises of 2,6-bis-(1,2,3-triazol-1-yl)purine acceptor and two asymmetrically located 4-methoxyphenyl donors.

The results revealed that in methanol solution organic molecule reacted with Zn^{+2}, Ca^{+2}, Ag^{+} ir Fe^{+2} ions producing new fluorescence emission peak at 409 nm wavelength. Similar effect was observed in ethanol, however, only with Ag^{+} ions. During complexation new peak in fluorescence spectrum with shorter wavelength gradually grows while old one diminishes. Though the exact cause of this shift is debatable, a photoinduced electron transfer between donor branches is supposed [4].

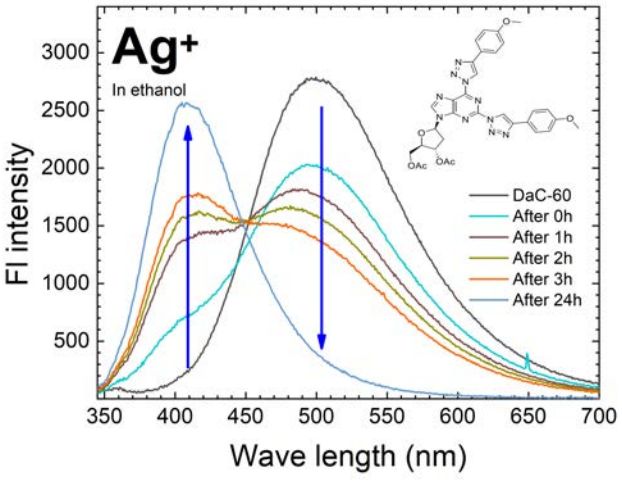

Fig. 1. Fluorescence spectrum of DaC-60 with silver ions in ethanol showing how complexation changes spectrum over time.

Furthermore, during our research we noticed that complexation was not an immediate process, therefore, time dependant measurements (up to 24h after introduction of metal ions) were carried out (Fig. 1). It was shown that the concentration of metal ions and viscosity of solvent plays an important role in complexation suggesting it is a diffusion-induced process.

Overall this compound can be used to detect Ag^{+} and Zn^{+2} ions in methanol and ethanol solutions.

[1] J. Jia, F. Li, H. Zhou, Y. Bai, S. Liu, Y. Jiang, G. Jiang, B. Yan, Oral exposure to silver nanoparticles or silver ions may aggravate fatty liver disease in overweight mice, Environmental Science Technology **51**(16), 9334–9343, pMID: 28723108 (2017).

[2] P. Dusek, T. Litwin, A. Czlonkowska, Wilson disease and other neurodegenerations wi-th metal accumulations, Neurologic Clinics **33**(1), 175–204, movement Disorders (2015)

[3] H. Xu, W. Chen, W. Zhang, L. Ju, H. Lu, A selective purine-based fluorescent chemosensor for the “naked-eye” detection of zinc ions (Zn 2+): applications in live cell imaging and test strips, New Journal of Chemistry **44**(35), 15195–15201 (2020),.

[4] J. Jovaisaite, D. Cīrule, A. Jeminejs, I. Novosjolova, M. Turks, P. Baronas, R. Komskis,S. Tumkevicius, G. Jonusauskas, S. Jursenas, Proof of principle of a purine d–a–d ligand ba-sed ratiometric chemical sensor harnessing complexation induced intermolecular pet, Phys.Chem. Chem. Phys.**22**, 26502–26508 (2020).

COMPLEX FORMATION BETWEEN ANTHOCYANINS AND SODIUM ALGINATES USING ADSORPTION PROCESS AND INVESTIGATION OF PROPERTIES OF FORMED COMPLEXES

Dovilã Liudvinaviļ iÎ tã, Karolina Almonaitytã, Joana Bendoraitienã, Ramunã Rutkaitã

Department of Polymer Chemistry and Technology, Kaunas University of Technology, Radvilenu Rd. 19, Kaunas, Lithuania

dovile.liudvinaviciute@ktu.lt

Anthocyanins (ANC) are natural polyphenolic compounds that show biological activity. These compounds are strong antioxidants and also feature anti-inflammatory and antimicrobial properties [1, 2], so they can be used in such areas as pharmaceuticals, food industry and active packaging. However, anthocyanins are highly unstable compounds as they are sensitive to changes in temperature, pH of the medium, oxidative stress and light [3]. By immobilization of anthocyanins in sodium alginate (ALG), their stability can be increased, and their biological activity can be prolonged. Under suitable conditions, it is possible to obtain biologically active complexes consisting of compounds of exclusively natural origin, without the use of any organic solvents or high temperatures.

The aim of present work was to obtain the complexes of ANC and ALG of two different types by using adsorption method, as well as to assess antioxidant activity of prepared complexes.

Sodium alginate of two types, named as ALG1 and ALG2, with a M/G ratio in the interval of 0.9ï 1.1 and 1.5ï 1.6, respectively, was chosen to form ionic complexes with ANC extracted from wild bilberry *(Vaccinium myrtillus)* by adsorption process. For the formation of the complexes the desired amount of ALG powder was added to a desired amount of aqueous ANC solution and stirred for 90 min at room temperature. The insoluble part of ANC-ALG complex was eliminated by centrifugation and then freeze-dried. The residual concentration of ANC was determined and the amount of adsorbed ANC on ALG1 or ALG2 (expressed as grams of ANC per gram of ALG) was calculated. ANC-ALG1 and ANC-ALG2 complexes having 0.1 g/g and 0.11 g/g of adsorbed ANC were obtained.

Equilibrium adsorption studies showed that during ANC adsorption on ALG powder chemisorption took place and ANC were adsorbed on ALG due to electrostatic interaction between the flavylium cation of ANC and the carboxylate groups of ALG (see Fig. 1).

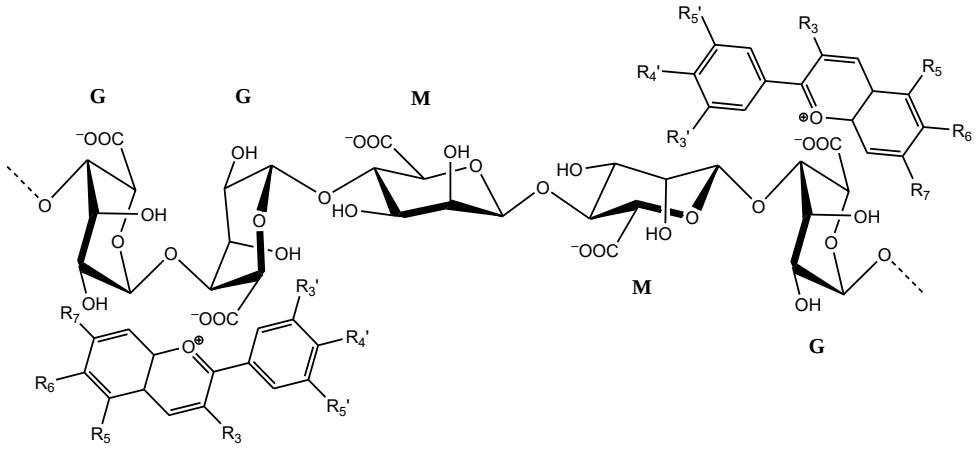

Fig. 1. Formation of ionic complex between carboxylate groups of ALG and flavylium cation of ANC

SEM imaging showed that after adsorption the size and shape of ALG1 and ALG2 changed. The surface of ANC-ALG complexes was rougher and the particles themselves were much flatter compared to respective ALG.

ANC-ALG1 (0.1 g/g) and ANC-ALG2 (0.11 g/g) complexes as well as ANC extract, ALG1 and ALG2 powder was evaluated by a modified ABTS method. ANC extract scavenged $ABTS^{\bullet+}$ instantly within the first few minutes of the experiment. Neither ALG1 nor ALG2 alone showed any antioxidant activity. Meanwhile, ANC-ALG1 (0.1 g/g) and ANC-ALG2 (0.11 g/g) complexes scavenged $ABTS^{\bullet+}$ gradually, which resulted in prolonged antioxidant activity.

[1] T. Tsuda, M. Watanabe, K. Ohshima et al., Antioxidative activity of the anthocyanin pigments cyanidin 3-O-beta-d-glucoside and cyaniding, Journal of Agricultural and Food Chemistry **42** (11), 2407-2410 (1994).

[2] A. Valenza, C. Bonfanti, M. E. Pasini et al., Anthocyanins function as anti-inflammatory agents in a Drosophila model for adipose tissue macrophage infiltration, BioMed Research International **2018**, 6413172 (2018).

[3] P. Wesche-Ebeling and A. Argaiz-Jamet, *Stabilization mechanisms for anthocyanin the case for copolymerization reactions* (In Engineering and food for the 21st century, CRC Press, Boca Raton, 2002)

ORGANIC DYES WITH FUNCTIONAL AMMONIUM GROUPS FOR THE 2D PEROVSKITES

Vilius Samuolis, Vytautas Getautis, Artiom Magomedov

Department of Organic Chemistry, Kaunas University of Technology, Lithuania
vilius.samuolis@ktu.edu

Interest and studies into perovskite solar cells have been rapidly growing during the past few years. Hybrid perovskite can be a more efficient light absorber than commonly used silicon-based absorbers and might supplant them in the future. To achieve this goal, knowledge, and understanding in this field of study must be gained. In particular, our research focuses on the synthesis and investigation of the substances that would fit into the spacing layer of the 2D perovskites (2DPKs), as well as further characterization of the resulting hybrid material.

The crystal structure of the bulk perovskites is usually referred to as 3D. In the typical organic/inorganic perovskite, such as methylammonium lead triiodide, small organic cations with functional ammonium groups are filling the space between inorganic cations. To make it 2D, larger organic cations must be inserted into the 3D lattice. As the result, each inorganic perovskites sheet becomes separated from one another by the so-called spacing layer (Fig. 1). [1]

The majority of the 2DPKs crystal structures can be classified into two major classes: Ruddlesden-Popper and Dion-Jacobson. The exact crystal phase depends on organic cations that are used in the spacing layer. Monocations form the Ruddlesden-Popper phase, while dications form the Dion-Jacobson phase. Due to the absence of the interface between two separate organic molecules it is expected, that 2DPKs with Dion-Jacobson phase space will have better electrical properties, in comparison to that of with the Ruddlesden-Popper phase. [2]

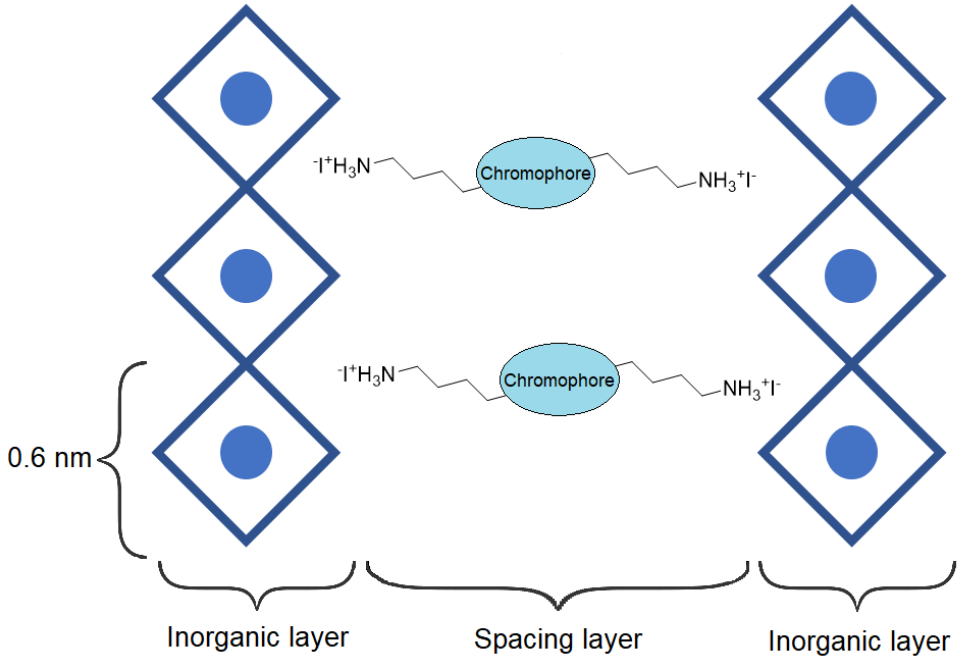

Fig. 1. 2DPK with larger organic dications in the spacing layer.

For this work, several commercially available organic chromophores have been selected for further modification, based on the width of the molecules and their optical properties. The cross-section of the chromophore should not exceed 0.6 nm, otherwise, it might be not possible to form a crystalline structure.

All synthesis in this work will be carried out in a few simple steps, i.e. chromophore reaction with N-(4-bromobutyl)phthalimide, followed by Gabriel synthesis, and finally treating the intermediate compound with hydrogen iodide.

During the further stages of this research, it is expected not only to synthesize and investigate new organic dications but also to find an easier and cheaper way to synthesis them, rather than to look for specific synthesis paths. This would allow us to broaden the explored space of materials and further advance this field.

[1] J.-C. Blancon, J. Evan, C. C. Stoumpos, M. G. Kanatzidis, A. D.Mohite. Semiconductor physics of organic-inorganic 2D halide perovskites, Nature Nanotechnology **15**, 969-985 (2020).

[2] D. Ghosh, D. Acharya, L. Pedesseau, C. Katan, J. Evan, S. Tretiak, A. J. Neukirch. Charge carrier dynamics in two dimensional hybrid perovskites: Dion-Jacobson vs. Ruddlesden-Popper phases. Journal of Materials Chemistry A, **8**, 22009-220222 (2020).

MULTIPLE FANO RESONANCES IN A MIRRORED ARRAY OF SPLIT-RING RESONATORS

Andrius Kamarauskas[1], Gediminas Ġlekas[1], Dalius Seliuta[1], Ģilvinas Kancleris[1]

[1] Department of Physical Technologies, Center for Physical Sciences and Technology, Lithuania
andrius.kamarauskas@ftmc.lt

Recently metasurfaces are gaining steady attention from the research community. This happens mostly due to the perspective to create a new type of flat materials fitting specific properties of different applications. One of the possible realizations of these hopes might be metasurfaces demonstrating high Q factor Fano resonances [1], which are now being widely investigated.

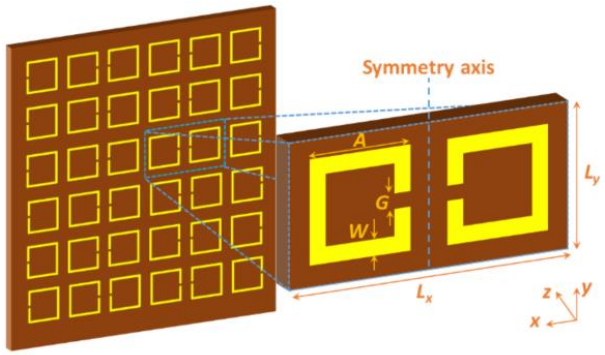

Fig. 1. Schematics of the mirrored array of SRRs and enlarged single unit cell. The thickness of the substrate is 125 ε m, its dielectric constant ($\mathring{U}$= 2.2), dimensions of resonators A = 500 ε m, $W = G$ = 50 ε m.

Recently high Q factor Fano resonance was discovered in a metasurface made from a mirrored array of split-ring resonators (SRRs) [2]. The view of the investigated metasurface is shown in Fig. 1. It can be seen that it is made from a simple planar array of split-ring resonators every second column of which is rotated by 180°. In such a way, a period of the array in the *x*-direction is increased twice, whereas the period in the *y*-direction remains the same. As shown in [2], discovered resonance demonstrates high Q factor and appears due to the direct interaction of plasmonic mode with lattice mode. Therefore, when the period of the array is increased, the resonance shifts to a lower frequency. In the present paper, we numerically investigate mirrored SRRs deposited on a thicker substrate and find multiple Fano resonances.

We investigate the structure shown in Fig. 1. The incident wave falls perpendicularly to the surface of SRR array, and the electric field is parallel to the *y* axis. The unit cell shown in the figure is modeled with periodic boundary conditions at the lateral edges. The thickness of the substrate is changed in a range from 0 to 1.2 mm. Transmittance spectra are calculated using custom made program.

Calculated transmittance spectra are shown in Fig. 2. For sake of clarity, the spectra are intentionally shifted in the vertical axis. The first minimum around 90 GHz (mode n = 1) appearing in the spectrum is attributed to the first plasmonic mode excited in SRRs. It is worth mentioning that due to the asymmetric orientation of the electric field in respect of the gap of SRRs, only the odd modes in the metasurface are excited. It is seen that with increasing the thickness of the substrate the frequency of mode n = 1 shifts to the lower frequency because of the increase of the effective dielectric constant of the structure. The plasmonic mode n = 3 is responsible for the second wide minimum in the transmittance spectrum at d = 0 around 280 GHz. It is seen that with increasing the thickness of the substrate the Fano type resonance appears at this frequency. As already mentioned, it appears due to the interaction of wide plasmonic mode with narrow lattice mode excited in the periodic structure [2]. Further increase of the thickness of the substrate leads to the double and even triple Fano resonances, which clearly manifests itself in the transmittance spectra (to Fig. 2).

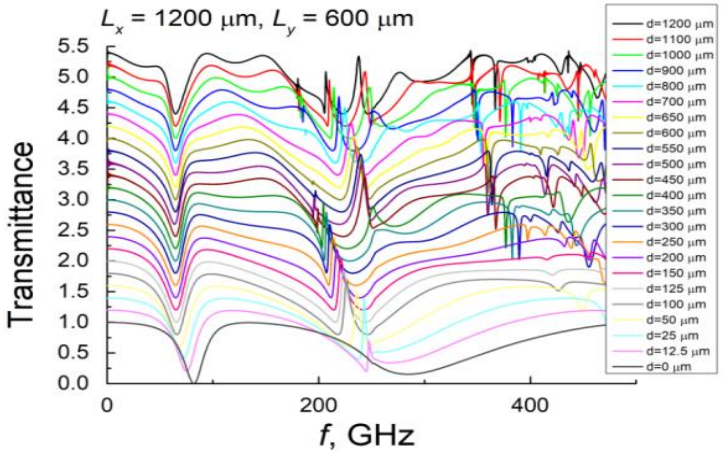

Fig. 2. Calculated transmittance spectra of metasurface composed of a mirrored array of split-ring resonators on a different thickness of the substrate ($\mathring{U}$= 2.2). Substrate thickness is denoted in the figure. Spectra are shifted in the ordinate axis

Our investigations demonstrate that excitation of the dielectric waveguide modes in the substrate is essential in the case of thick substrates. Multiple modes interact with the plasmonic mode n = 3, and this is responsible for the appearance of the multiple Fano resonances in the metasurface composed of a mirrored array of SRRs. We believe that this phenomenon might find application in sensing devices. An experimental investigation is under preparation.

[1] W. Wang1, L.Zheng, et al., Applied Physics, Express Express High Q-factor multiple Fano resonances for high-sensitivity sensing in all-dielectric nano cylinder dimer metamaterials. **Vol. 12,** No 7, pp. 075002-1/5 (2019). doi 10.7567/1882-0786/ab206a;

[2] D. Seliuta, et al., Optics Letters, Fano resonance arising due to direct interaction of plasmonic and lattice modes in a mirrored array of split ring resonators **Vol. 44,** No 4, pp. 759-762 (2019). doi: 10.1364/OL.44.000759;

CONSTRUCTION OF A PULSED MAGNET FOR CLOSED CYCLE HELIUM GAS CRYOCOOLER

JorÎnas Dobilas[1], Voitech Stankevic[2]

[1]Faculty of Physics, Vilnius University, Lithuania
[2]Department of Functional Materials and Electronics, State Research Institute Center for Physical Sciences and Technology, Lithuania
jorunas.dobilas@ff.stud.vu.lt

For measuring of magnetic properties of different materials in a wide range of temperatures (20 ï 300 K) and magnetic fields (up to 5 T), the controllable cryostat and magnetic field generator are needed. It was shown in Ref. [1], that for investigation of magnetic and electric properties of thin manganite films a closed cycle helium gas cryocooler (temperature range 20 ï 300 K) and an electromagnet with a maximum amplitude of 0.8 T were used. For high-field magnetoresistance investigations the compact pulsed magnetic field generator (*B* up to 25 T, pulse duration 1 ms) based on capacitor bank discharge through the coil was designed [2]. However, the temperature in this generator could be changed only in the range of 80ï 300 K. Therefore, the design of pulsed magnetic field generator combined with the closed cycle helium gas cryocooler is an actual task. Moreover, the duration of magnetic pulse should be sufficiently long to avoid the transition processes and to measure the low-field magnetoresistance effects which take place in magnetic field range 0 ï 100 mT.

The main task of this work is to find optimal structure of magnetic coil for generation of a long ~100 ms pulse with amplitudes up to 5 T using a 5.4 mF capacitor charged to 2 000 V, and to investigate how magnetic field depends on the structure of this coil. A special rectangular-shaped wire 1.75×0.5 mm was chosen. To simulate the coil parameters the COMSOL Multiphysics program was used. The first step was to find optimal structure of the coil. During simulations it was found, that increasing the number of windings more than 30, or number of layers more than 13, does not significantly increase the magnitude of the magnetic field. Considering this, the optimal relation between number of windings N_1 and number of layers N_2 was found: 2:1. Fig. 1 presents simulation data plotted in a 3D graph. The left graph shows almost all possible coil structures that fit our needs. For optimal scenario, the smallest possible voltage was used. The figure on the right presents magnetic flux density distribution of the coil model consisting of 30 windings and 50 layers, when capacitor was charged up to 970 V. In this case the maximum *B*=2.7 T in the center of the coil was achieved. The real coil was constructed with N_2:N_1= 46:23 and tested with the cryocooler. It was found that the magnetic field of 5 T could be achieved with a little higher voltage than simulated (1900 V). The pulse length was shorter as predicted: 60 ms. After testing the coil with a manganite sample placed in the cryostat, we found that the pulse amplitude and duration fully satisfies requirements for the magnetoresistance investigation in the intermediate (up to 5 T) magnetic fields in the temperature range (20-300) K.

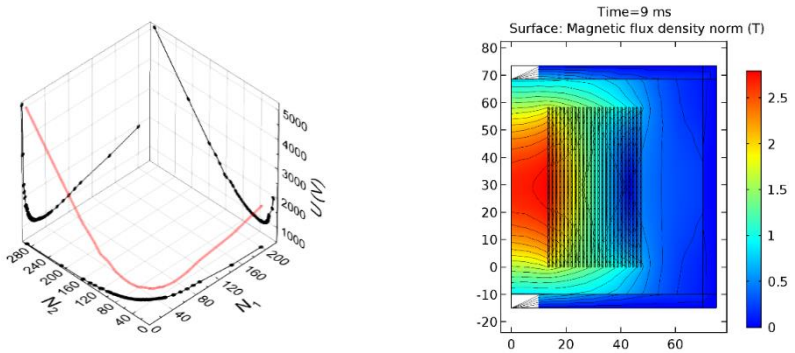

Fig. 1. 3D graph of magnetic coil structures (left). N_1 is number of windings, N_2 ï number of layers, U(V) ï voltage of charged capacitor. The sets of parameters above the lines represent a coil structure which could be used to achieve the tasks. The right figure presents magnetic flux density distribution of the coil model, when N_1=30, N_2=50, U(V)=970 V.

[1] N. Ţurauskienã, S. Balevičius et al., B-Scalar Sensor Using CMR Effect in Thin Polycrystalline Manganite Films. IEEE Trans. Plasma Sci. **39**, 411-416 (2011).
[2] A. Grainys, J. Novickij, T. Stankevič, V. Stankevič, V. Novickij, N. Zurauskiene, Single Pulse Calibration of Magnetic Field Sensors Using Mobile 43 kJ Facility, Meas. Sci. Rev. **15**, 244ï 247 (2015).

TUNING THE EMISSION IN CARBAZOLE - BIPYRIDINE MOLECULAR SYSTEMS FOR TADF APPLICATIONS

Mindaugas Janu̇gauskas[1], Povilas Adomā̃nas[2], Ona Adomā̃nienā̃[2], Regimantas Komskis[1], Saulius Jurg̃ā̃nas[1]

[1] Institute of Photonics and Nanotechnology, Vilnius University
[2] Faculty of Chemistry, Vilnius University
mindaugas.janusauskas@ff.vu.lt

The most efficient organic light emitting diodes (OLEDs), demonstrating high external quantum efficiency (EQE) of up to 30%, are based on a thermally activated delayed fluorescence (TADF) mechanism, where non-emissive triplet states are converted into emissive singlet states by a process of reverse intersystem crossing. The main drawback of TADF emitters is poor control of the emission spectral position, followed by a lack of efficient emitters in the blue and red region of the visible spectrum. The emission spectrum is directly related to the nature of charge transfer in the molecular geometry, therefore it is necessary to be able to control the properties of fluorescence spectrum to achieve desirable OLED emission. Additionally, the control of transition oscillator strength in the molecule is crucial to maintain a high efficiency of the TADF process.

In this research we demonstrate the ability to control emission properties of special class of TADF emitters, constructed from donor ï acceptor carbazole and bipyridine moieties by changing the number of donoric carbazole fragments and their linkage position in a molecular backbone. By using theoretical DFT modeling and absorption - emission spectroscopy methods, we evaluated the distribution of locally excited (LE) and charge transfer (CT) state population in carbazole ï bipyridine derivatives, which directly determines an overall emission spectra and transition oscillator strength.

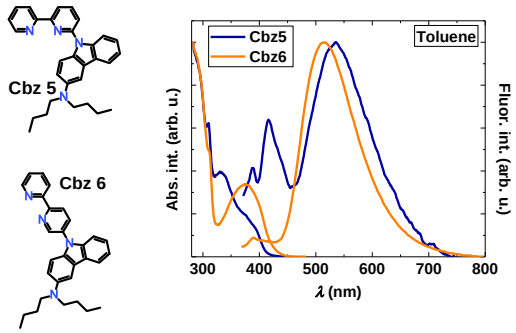

Fig 1. Absorption and emission of Cbz5 and Cbz6

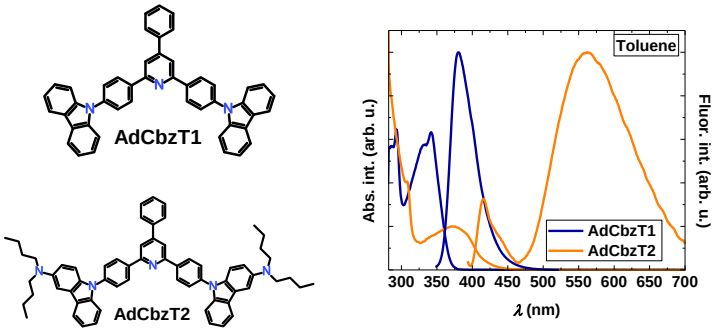

Fig 2. Absorption and emission of AdCbzT1 and AdCbzT2

In the first part of the research, the carbazole - bipyridine molecular system was analyzed by changing the linkage position of the bipyridine acceptor (Cbz5 and Cbz6) (Fig. 1). In the ground state, the molecules exhibit similarly twisted geometry. During optical excitation HOMO level is localized on the carbazole moiety and the LUMO level - at the bipyridine moiety for both molecules and regardless of the connection position, the lowest singulet state is of the CT nature. However, we can observe that the different position of the bipyridine linkage results in a different overlap of the electron wave function between HOMO and LUMO levels. Consequently, the oscillator strength is up to 100 times higher in the indirectly linked Cbz5 molecule. The results of the theoretical modeling are directly reflected in the absorption and emission spectra of these molecules (Fig. 1). The absorption (peaking at 375 nm) and emission (peaking at 520 nm) in directly linked carbazole ï bipyridine system is solely dominated by CT transition, expressed by structureless bands. Meanwhile, indirectly linked carbazole ï bipyridine Cbz5 system exhibits a well expressed locally excited state transition in absorption and emission spectra with characteristic peaks at 350 nm and 420 nm respectively (Fig. 1).

In the second part of the research, we analyzed the bicarbazole - pyridine molecular system by introducing two donor carbazole fragments into the pyridine acceptor (AdCbzT1) and further enhancing the donor properties of carbazole with alkylamine substituents (AdCbzT2). Similarly for both molecules, HOMO is localized on the carbazole moiety and LUMO is on the pyridine. In the ground state, the molecules also exhibit a differently twisted geometry, and the donor carbazole fragments are twisted by 30Á(AdCbzT1) and 70Á(AdCbzT2) relative to the pyridine acceptor (Fig. 1), which determines different components of the LE and CT states in the absorption and emission spectra (Fig. 2). The less twisted geometry of AdCbzT1 results in a more localized absorption spectrum (absorption peak at 330 nm) compared to AdCbzT2 (absorption peak at 380 nm). In the emission spectra, the distribution of LE and CT states differs radically. The introduction of donor alkylamine substituents into the carbazole fragments results in two-wave emission, with excitation relaxation predominating from the CT states (peak position at 560 nm). Part of the excitation relaxation from the LE states (peak position at 420 nm) is also observed.

HIGHLY EFFICIENT EMISSION OF CHARGE TRANSFER STATES IN CARBAZOLE - PYRIDINE MOLECULAR SYSTEMS FOR TADF APPLICATIONS

Milita Uģgirytā[1], Povilas Adomānas[2], Ona Adomānienā[2], Regimantas Komskis[1], Saulius Jurģānas[1]

[1] Institute of Photonics and Nanotechnology, Vilnius University
[2] Faculty of Chemistry, Vilnius University
milita.uzgiryte@ff.vu.lt

Most efficient organic light emitting diodes (OLEDôs) are based on thermally activated delayed fluorescence (TADF) process, when dark triplet states are harvested to emissive singlet states. This process allows to achieve up to 100% of internal quantum efficiency of the emitter. However, TADF process is dipole forbidden and is partially determined by low fluorescence quantum yield of charge transfer states (CT) as a consequence of weak oscillator strength of the transition. Thus, an overall fluorescence lifetime is substantially extended and OLED suffers from quantum efficiency roll-off.

Here, we present a highly efficient carbazole - pyridine CT emitters and demonstrate the possibility to control a fluorescence quantum yield via different content of CT states in an overall excited state relaxation by chemically modifying donoric properties of carbazole and acceptoric properties of pyridine. The charge transfer via molecular backbone was controlled by introducing methoxy groups to carbazole and nitrile substituents to pyridine ring. CT sate population was analyzed by steady state absorption and fluorescence spectroscopy techniques.

Absorption band of model donor ï acceptor carbazole ï pyridine (M5) molecules is in the ultraviolet wavelength range at 250-361 nm (Fig 1). Absorption spectrum has a clear vibronic structure, which indicates a domination of locally excited (LE) states. The fluorescence emission is in 338 ï 466 nm, with a small Stokes shift. A highly expressed LE relaxation enables a very high quantum yield ï 100 %. However, with no prominent CT state emission, the TADF process is inefficient.

Drastic changes in absorption and emission properties are observed when donoric property of carbazole is enhanced by methoxy substituents and pyridine acceptor is modified with nitrile fragments (Fig. 2.). A three-wave absorption band is observed in ultraviolet range, peaking at 300 nm, 356 nm and 409 nm, which indicates two locally excited states (LE) and expressed CT state. Accordingly, fluorescence spectra is redshifted, in range of 457 ï 742 nm, with enhanced CT state emission. Thus, a quantum yield decreases by half to 40 %. However, the overall CT content is high, and the lifetime of overall emission is substantially extended.

When acceptoric property of pyridine ring is reduced with a phenyl ring (Fig. 3), the compound demonstrates an expressed vibronic series of LE states, in ultraviolet wavelength range of 250 ï 376 nm. The fluorescence is observed in 360 ï 550 nm range, with a red shoulder, originating from small part of CT state relaxation. Quantum yield is high ï 79 %. Thus, a CT state relaxation pathway for efficient TADF process, maintaining highly efficient fluorescence is achieved.

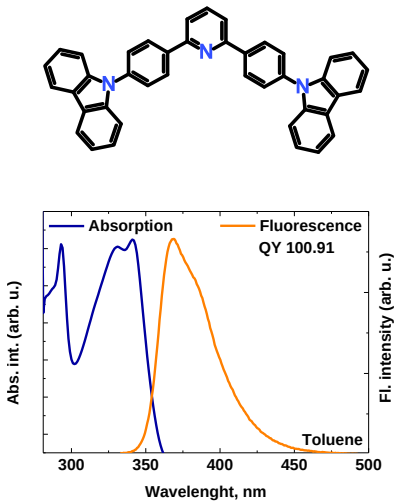

Fig. 1. Absorption and fluorescence spectra of model carbazole ï pyridine molecular system. Fluorescence quantum yield in toluene is also indicated.

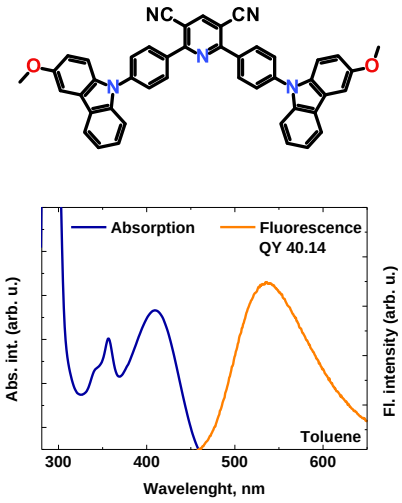

Fig. 2. Absorption and fluorescence spectra of carbazole ï pyridine molecular system, substituted with methoxy and nitrile fragments. Fluorescence quantum yield in toluene is also indicated.

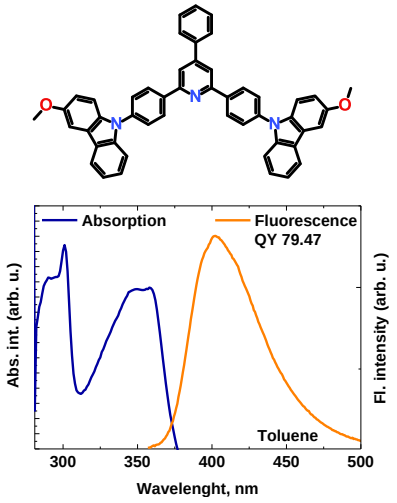

Fig. 3. Absorption and fluorescence spectra of carbazole ï pyridine molecular system, substituted with methoxy and phenyl fragments. Fluorescence quantum yield in toluene is also indicated.

STIMULATED GREEN EMISSION IN LEAD BROMIDE PEROVSKITES

Samanta Lipkevi̧ iÎ tā̄[1], Dģiugas Litvinas[1], Regimantas Komskis[1], Saulius Jurģā̄nas[1]

[1]Institute of Photonics and Nanotechnology, Vilnius University, Lithuania
samanta.lipkeviciute@ff.stud.vu.lt

Laser emitters play an important role in modern science; however, large dimensions, complex manufacturing technologies and low efficiency reduces the availability of such devices. Metal halide perovskites are an emerging class of semiconductors holding promising potential in further advancing the laser technology which might overcome these problems with their easy production and small dimensions. However, perovskite materials exhibit high thresholds for amplified spontaneous emission (ASE). More importantly, the ASE spectra peak position highly depends on the composite of perovskite structure, and a research on the influence of different anions and cations in perovskite lattice to the spectroscopic characteristics of ASE is tremendous. In this study, we focus on a lead bromide perovskite family with mixed organic methylammonium and inorganic cesium anions - $Cs_xMA_{1-x}PbBr_3$ ($MA^+ = CH_3\text{-}NH_2^+$). We selectively substitute cesium anion with different molar parts of methylammonium in $Cs_xMA_{1-x}PbBr_3$ lattice and investigate spectroscopic characteristics of ASE by employing time-resolved photoluminescence (TRPL) spectroscopy.

$Cs_xMA_{1-x}PbBr_3$ perovskite layers were deposited from a solution on cleaned glass substrates via spin coating method. Molar ratios of cesium and methylammonium in the perovskite solution were mixed in the interval x = [0,25;1] by altering the masses of dry precursors cesium bromide (CsBr) and methylammonium bromide (MABr). These two precursors together with lead bromide ($PbBr_2$) were dissolved in dimethylsufoxide (DMSO). Perovskite layers were passivated with a layer of polymethylmethacrylate (PMMA) polymer from oxygen and water vapor to prevent degradation. By changing the angular velocity of the spin coating process, perovskite layers for an efficient ASE were optimized as thinner and smoother layers were acquired with higher velocities.

Spectral composition of sample emission was thoroughly investigated using time resolved photoluminescence (TRPL) spectroscopy at a different excitation fluence (Fig. 1). At a small optical excitation fluence, a photoluminescence peak starts emerging as a consequence of spontaneous emission in $Cs_{0.25}MA_{0.75}PbBr_3$ sample at 530 nm and at 525 nm in single cation $CsPbBr_3$ sample. At a high optical excitation, all perovskite layers demonstrate dual band emission, with additional band emerging at 550 nm in $Cs_{0.25}MA_{0.75}PbBr_3$ and at 535 nm in $CsPbBr_3$ layers. We associate additional emission bands with an ASE process, as a growth of intensity of aforementioned band is quadratic. Ultrafast fluorescence decay confirms the nature second photoluminescence band as an ASE. We were able to achieve a satisfactory threshold for ASE below 10 ÕJ/cm^2 of optical excitation fluence. A tendency of amplified spontaneous emission peak shifting toward ǿgreenerǿ (550 nm) wavelengths when the molar part of methylammonium in the perovskite is increased was observed.

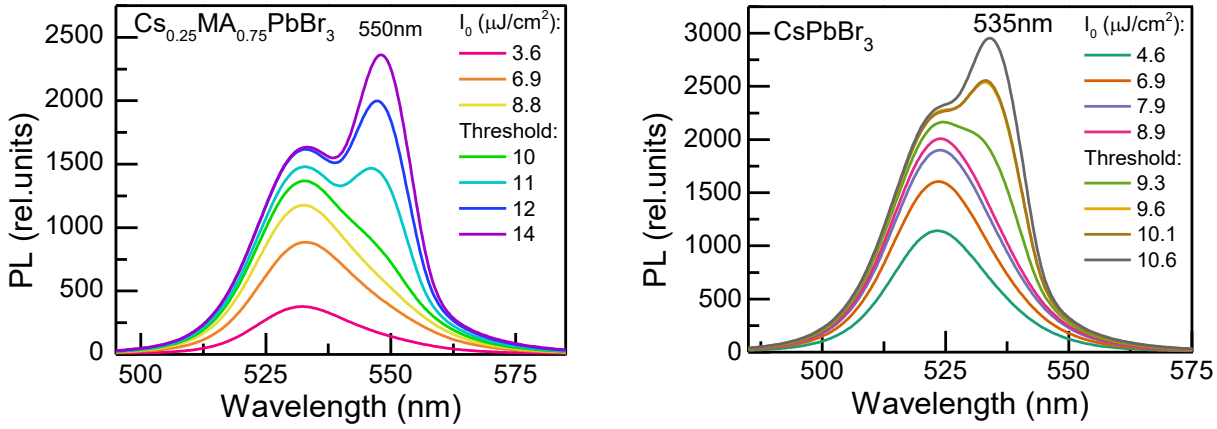

Fig. 1. TRPL measurement results for two perovskite samples at a different excitation fluence I_0. From left to right: $Cs_{0.25}MA_{0.75}PbBr_3$ sample integrated spectra; $CsPbBr_3$ sample integrated spectra.

The main results of this study: thinner and smoother perovskite layers obtained with a higher angular velocity of the spin coater are more suitable for efficient stimulated emission generation. Moreover, the spectral position of the peak of amplified spontaneous emission can be easily controlled by changing the composition of $Cs_xMA_{1-x}PbBr_3$; decreasing molar part of methylammonium leads to amplified spontaneous emission peak shift from 550 nm to 535 nm.

SUBSTANTIAL TADF OLED PERFORMANCE IMPROVEMENT BY SIMPLE EMITTER STRUCTURE MODIFICATION

Dovydas Banevičius[1], Gediminas Kreiza[1], Domantas Berenis[1], Tomas Javorskis[2], Edvinas Orentas[2], Saulius Antanas Jurgėnas[1], Karolis Kazlauskas[1]

[1] Institute of Photonics and Nanotechnology, Vilnius University, Lithuania
[2] Department of Organic Chemistry, Vilnius University, Lithuania
dovydas.banevicius@ff.vu.lt

Thermally activated delayed fluorescence (TADF) compounds have received great attention for their potential to utilize both singlet and triplet excitons in OLEDs formed during charge carrier injection. [1] Rational material design has enabled TADF OLED devices with up to 100% internal quantum efficiencies mainly due to an efficient reverse intersystem crossing (RISC) that allows conversion of dark triplet excitons into emissive singlet states. [2] While RISC is usually a slow process, TADF-OLEDs suffer from early efficiency roll-off associated with high long-lived triplet exciton population. Therefore, TADF emitters with large rISC rate facilitating triplet up-conversion are required. [3]

In this work, by introducing a subtle modification to two carbazolyls containing isophthalonitrile-based TADF emitter, we demonstrate a huge impact on its TADF properties. To be more precise, the increased dihedral angle between D and A units is found to significantly reduce ΔE_{ST}, resulting in substantial boost of RISC rate and shortening of TADF lifetime. We fabricated vacuum and solution processed TADF-OLEDs employing 7% isophthalonitrile-doped emissive layer. Devices exhibited blue to sky-blue emission, external quantum efficiency (EQE) of up to 23.8% and high brightness (up to 95000 cd/m^2). Most importantly, due to the large rISC rates, TADF OLEDs demonstrated extremely low efficiency roll-off. OLEDs based on modified compound (**DMeCzIPN**) exhibited significant performance improvement of two times in terms of EQE. **Fig. 1** shows chemical structures of unmodified **DCzIPN** and modified **DMeCzIPN** compounds and the EQE characteristics of the produced devices together with their electroluminescence (EL) spectra. The obtained results demonstrate the potential of isophthalonitrile-based TADF emitters for high-brightness OLED applications.

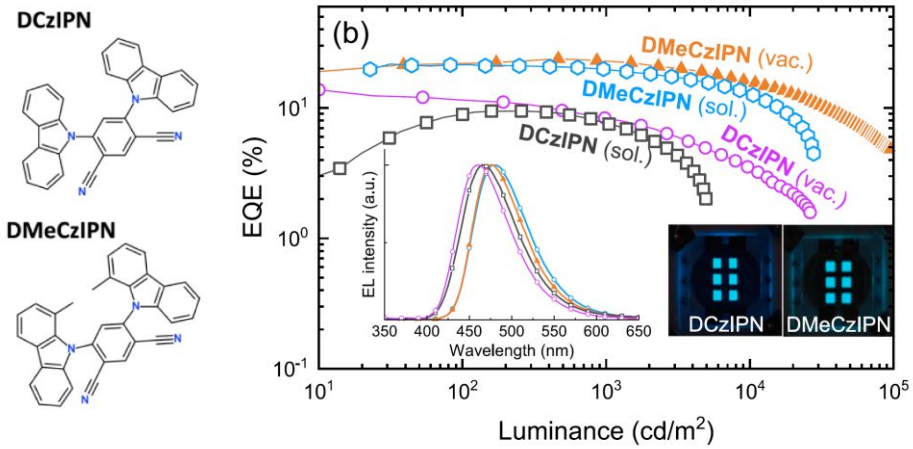

Fig. 1. Chemical structures of investigated compounds and the EQE characteristics of the TADF-OLEDs fabricated employing these isophthalonitrile-based emitters, and EL spectra together with pictures of these devices.

[1] Yang, Z. Mao, Z. Xie, Y. Zhang, S. Liu, J. Zhao, J. Xu, Z. Chi, M.P. Aldred, Recent advances in organic thermally activated delayed fluorescence materials, Chem. Soc. Rev. **46**, 915-1016 (2017).
[2] H. Uoyama, K. Goushi, K. Shizu, H. Nomura, and C. Adachi, Highly efficient organic light-emitting diodes from delayed fluorescence, Nature **492**, 234 (2012).
[3] M. K. Etherington, J. Gibson, H. F. Higginbotham, et al., Revealing the spin-vibronic coupling mechanism of thermally activated delayed fluorescence, Nat. Commun. **7**, 13680 (2016).

TESTING OF CMR-B-SCALAR SENSORS USING MICROSECONDS DURATION HIGH PULSED MAGNETIC FIELDS

Modestas Ļeikauskas[1], Voitech Stankeviļ[1,2]

[1] Department of Functional Materials and Electronics, Center for Physical Sciences and Technology, Saulētekio ave. 3, LT-10257 Vilnius, Lithuania

[2] Faculty of Electronics, Vilnius Gediminas Technical University, Naugarduko 41, LT-03227, Vilnius, Lithuania

modestas.ceikauskas@ftmc.lt

During the last decades, it was demonstrated that magnetic field sensors based on nanostructured lanthanum manganite films exhibiting the colossal magnetoresistance (CMR) phenomenon could be used for high pulsed magnetic field measurement in very small volumes (10^{-2} mm^3) [1]. These sensors are capable of measuring the magnetic field magnitude independent of the magnetic field direction (CMR-B-scalar sensors) [2]. They were used for the measurement of magnetic field distribution [3] and diffusion processes in railguns [4]. It was showed that they are a suitable instrument for measuring the field with high resolution in both time and space. In all these experiments the pulse duration of magnetic field was 1-100 milliseconds.

However, in some processes the significantly shorter magnetic pulses with high amplitude should be measurement. Magnetic Pulse Welding (MPW) is one of this process. The MPW is a collision welding process, which uses a high velocity impact to join two metals that are accelerated by short (about 20 ï 30 ες) strong (~10 T) magnetic field. The measurement of the intensity and dynamics of the magnetic field at different positions during the electromagnetic forming or welding process is not only required for the calculation of the magnetic pressure, which influences the acceleration, but can also provide additional information about the processes that take place during the MPW. Therefore, the magnetic field sensors, which are capable to measure these fields, should be designed and tested.

Short pulsed high magnetic field generation system for electromagnetic welding and forming was designed for testing the CMR-B-scalar sensors. It consisted of capacitor bank, spark-gap switch and a Bitter coil. A 50 ÕF capacitor charged up to 9 kV was discharged throughout 5 winding Bitter coil and the magnetic pulse of about 25 Õs with amplitude of 5 T was generated inside the coil. The tested sensor was positioned inside of the coil (or in the field shaper) and the output signal was recorded by a measuring module. It was found that this kind of sensor is easy installed to the measuring position, because due to diminished anisotropy the CMR-B-scalar sensor does not require an exact orientation with respect to the magnetic field direction. Moreover, it is very small and thus can be applied for measuring the magnetic field locally. In addition, the measurement module of the system has a sufficient time resolution to measure fast magnetic field changes. However, some problems concerning the ñloopò effect (induced parasitic signal due to electromotive forces) and electromagnetic noises should be resolved to obtain output signal of sensor with higher accuracy. The possibility to use these sensors for the measurement of magnetic field dynamics during magnetic pulse forming of metal tube will be demonstrated.

---

[1] N. Ģurauskienā, S. Balevičius et al., B-Scalar Sensor Using CMR Effect in Thin Polycrystalline Manganite Films. IEEE Trans. Plasma Sci. **39**, 411-416 (2011).

[2] T. Stankeviļ, L. Mediģauskas et al., Pulsed magnetic field measurement system based on colossal magnetoresistance-B-scalar sensors for railgun investigation. Rev. Sci. Instrum., **85**, 044704 (2014).

[3] O. Liebfried, M. Schneider et al., Measurement of the magnetic field distribution in railguns using CMR-B-scalar sensors. Acta. Phys. Pol. A, **115**, 1125ï 1127 (2009).

[4] T. L. Haran, R. B. Hoffman, S. E. Lane, Diagnostic capabilities for electromagnetic railguns. IEEE Trans. Plasma Sci., **41**, 1526 ï 1532 (2013).

INVESTIGATION OF OPTICAL PROPERTIES OF $CaAlBO_3F_2$ GLASSY MATRIX DOPED WITH EUROPIUM AND SAMARIUM IONS

Agata Jarocka[1], Dominika WNś[1], Jakub Pğachta[2], Tomasz K. Pietrzak[1]

[1]Faculty of Physics, Warsaw University of Technology, Koszykowa 75, 00-662 Warsaw, Poland
[2]Institute of Physics, Polish Academy of Sciences, Lotnik· w 32/46, 02-668 Warsaw, Poland
agata.jarocka.dokt@pw.edu.pl

Rare earth elements (REE) are widely used in today's technology ï for example, in lasers based on REE-doped crystals or glasses. REE the most frequently used in lasers are lanthanides. This is due to a large variety of their *4f* configurations, which leads to a wide range of fluorescent states and wavelengths [1]. Telecommunication technologies have also benefited from the use of those elements. Oxidized and ceramic glasses doped with REE found their application in WDM technology (Wavelength Division Multiplexing), and thus a series of optical amplifiers based on REE were created. Furthermore, those elements introduced into phosphors help adjust white LED's light to the range of human vision. Therefore, they gained worldwide interest.

The atomic structure of lanthanides (group that includes considered Sm, Eu) is characterized by unfilled *4f* shell and external shells that screen *4f* shell from the influence from outside. This feature is responsible for remarkable optical properties of lanthanides. Optical spectra of those elements exhibit sharp lines characteristic for transition within the *4f* shell, known as forbidden transitions. In real terms it means that they may occur, but with low probability, according to Judd-Ofelt Theory. Aforementioned screening of *4f* shell by outer shells results in protection of optically active electrons from the influence of crystal field and as a result, REE ionôs spectrum in a solid can be similar to that of a free ion spectrum [2].

The research carried out very recently in our group has shown that it is possible to prepare REE-doped glassy materials with that are characterized by strong radial transitions [3]. Therefore, it is worth to investigate different glassy matrices in order to find those of the best mechanical and chemical resistance. In our studies, $CaAlBO_3F_2$ glassy matrices doped with 1 wt% Eu_2O_3 and Sm_2O_3 were successfully prepared by a melt-quenching method. Substrates were melted for 15 min at 1300 ÁC.

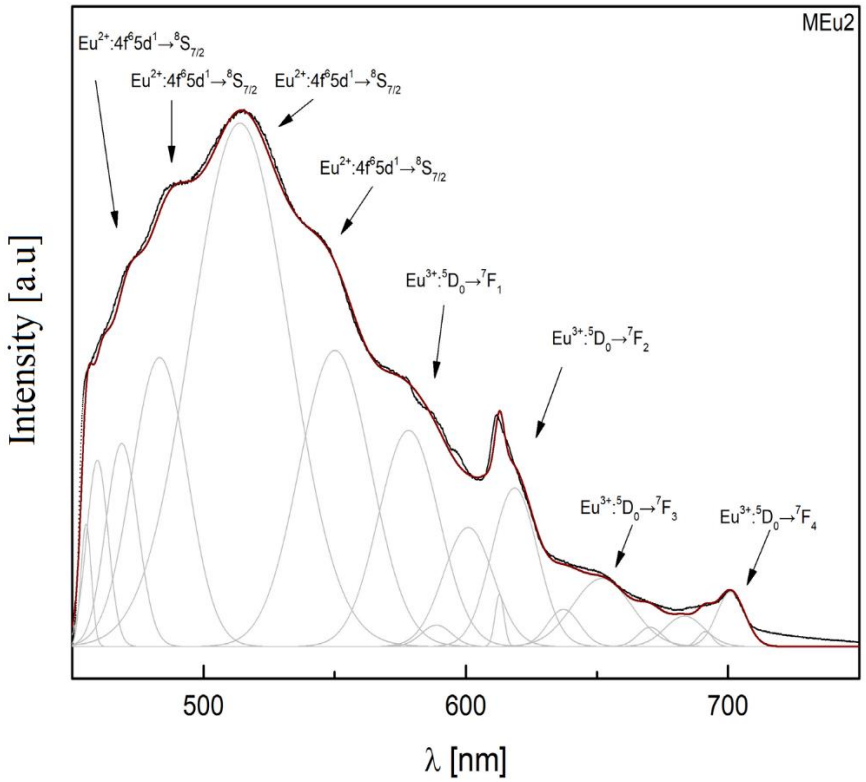

Fig. 1. Photoluminescence spectrum for sample $CaAlBO_3F_2$ doped with europium ions, excited with 325 nm laser.

[1] M. C. Gon-alves, L. F. Santos, R. M. Almeida: *Rare-earth-doped transparent glass ceramics.* Competes Rendus Chimie, 5 (2002) 845ï 854.
[2] B. M. Walsh: *Advances in Spectroscopy for Lasers and Sensing. Judd-ofelt theory: principles and practices*. [red.] Baldassare Di Bartolo, Ottavio Forte. Erice Italy, Springer, 2005
[3] T.K. Pietrzak, A. Goğbiewska, J. Pğachta, M. Jarczewski, J. Ryl, M. Wasiucionek, J.E. Garbarczyk: *Photoluminescence of partially reduced Eu^{2+}/Eu^{3+} active centers in a NaFï Al_2O_3ï P_2O_5 glassy matrix with tunable smooth spectra.* Journal of Luminescence, 208 (2019) 322ï 326.

P1-30

DID NOT PARTICIPATE

CARBAZOLE - PYRIMIDINE MOLECULAR SYSTEMS FOR TADF APPLICATIONS

Justina Savickytė[1], Povilas Adomėnas[2], Ona Adomėnienė[2], Regimantas Komskis[1], Saulius Juršėnas[1]

[1] Institute of Photonics and Nanotechnology, Vilnius University
[2] Faculty of Chemistry, Vilnius University
justina.savickyte@ff.vu.lt

Currently, the most efficient organic light emitting diodes (OLEDs) are fabricated using a thermally activated delayed fluorescence (TADF) emitters, where dark triplet states are turned to radiative states using the reverse intersystem crossing process. The internal quantum efficiency in such emitters can be up to 100%. However, the application of such emitters in OLED devices is limited by the long emission lifetime and the wide emission band. Also there is a lack of efficient emitters in the 400 nm - 500 nm range.

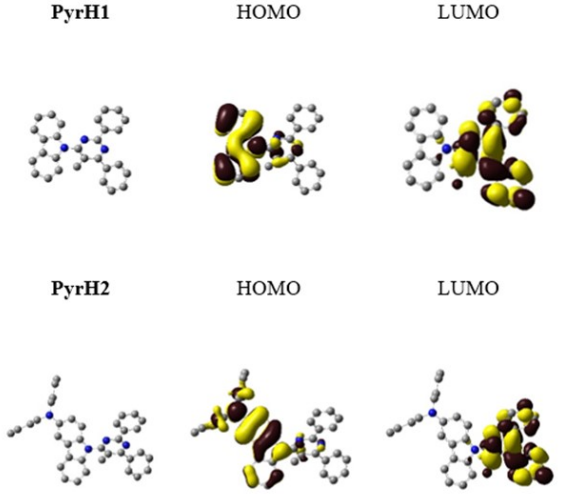

Fig 1. Optimized molecular geometry of donor - acceptor carbazole - pyrimidine systems, distribution of HOMO and LUMO orbitals.

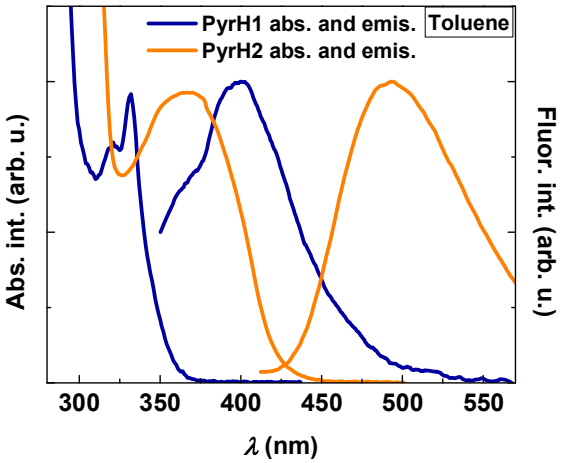

Fig 2. Absorption and fluorescence spectra of donor - acceptor carbazole - pyrimidine systems (top) and fluorescence lifetime characteristics (bottom).

In this research we focus on carbazole – pyrimidine molecular system to evaluate the properties of charge transfer and TADF in a single molecule by employing a subtle modification of a molecular backbone. We investigate the donor - acceptor carbazole - pyrimidine molecular system, where the donoric properties of carbazole were further enhanced by an alkylamine moiety. By using various steady state spectroscopy techniques and computational modeling, we investigated the distribution of excited states and evaluated the possibility of TADF process. Carbazole - pyrimidine molecules exhibited a twisted molecular geometry, where the carbazole moiety is rotated at an angle of 52 degrees relative to the pyrimidine ring. The highest occupied molecular orbital (HOMO) is localized on the carbazole moiety and the lowest unoccupied molecular orbital is located on the acceptor pyrimidine moiety (Fig. 1). In the PyrH1 compound, the lowest singlet excitation is the charge transfer state (CT), with an extremely low transition oscillator strength ($f = 0.05$). The energy gap between the singlet and triplet levels is quite high - 260 meV. Meanwhile, in the PyrH2 compound, part of the HOMO is distributed at the introduced alkylamine moiety. This results singlet excitation energy decrease (from 3.44 eV to 2.66 eV) and an even lower oscillator strength ($f = 0.012$). On the other hand, the energy difference between the lowest singlet and triplet excitations is as low as 66 meV, which is a crucial requirement for an efficient TADF process.

Carbazole - pyrimidine molecular system PyrH1 demonstrated absorption in the ultraviolet wavelength range (from 280 nm to 360 nm), with a pronounced vibronic structure associated with locally excited state from the donoric carbazole moiety (Fig. 2). The fluorescence at 400 nm and with somewhat expressed vibronic series was also observed. After enhancing the donoric properties of carbazole with an alkylamine moiety in the PyrH2 compound, the absorption band redshifts significantly, peaking at 375 nm. The fluorescence peak exhibits redshift to 500 nm, followed by a large Stokes shift (150 nm). Interestingly, both absorption and emission bands are structureless and in combination with a large Stokes shift indicates enhanced charge transfer (CT) character (Fig. 2).

The existence of TADF process was observed in PyrH2 compound. An exponential fluorescence decay with the time constant of 10.02 ns was observed. After removal of oxygen, the decay time constant was enhanced up to 1.4 times (time constant – 14.28 ns), indicating expressed TADF process.

COMPARISON OF SOLID-PHASE EXTRACTION SORBENTS FOR THE DETERMINATION OF SEDATIVE-HYPNOTICS DRUGS IN BIOLOGICAL SPECIMENS

Nerijus Karlonas

The State Forensic Medicine Service, Toxicology Laboratory, Didlaukio 86E, LT-08303 Vilnius, Lithuania
nerijuskarlonas@yahoo.com

Sedative-hypnotics drugs represent a pharmacologically diverse group of compounds, such as benzodiazepines, barbiturates, and other newest agents (e.g. zaleplon and zopiclone), that are used clinically [1]. Currently, there is no scientifically precise or universally accepted classification scheme for these drugs. Sedative-hypnotics drugs are often prescribed in primary care for insomnia.

Zaleplon and zopiclone are sedative-hypnotic drugs, which are used to induce sleep in the short-term treatment of insomnia. These newest medications are less safe than other benzodiazepines and have a tendency to induce physical dependence [1,2]. Currently, these drugs are the most commonly prescribed sedative-hypnotics agents in the United States of America and the European Union.

Although these drugs are widely prescribed for patients the certain side-effects were identified. It should be noted an adverse cognitive (such as, memory loss) and psychomotor (such as, road traffic crashes) effects, daytime fatigue, addiction, and excess of mortalities with no significant difference from the side-effects of typical benzodiazepines [2-5]. However, with increased use of zaleplon or zopiclone drugs, reports of misuse and possible dependence began to appear in the literature, particularly considering people with a history of drugs and/or narcotics misuse and comorbid psychiatric illness [1,2,4]. For this reason, it is essential to develop a fast and sensitive method for the determination of both analytes in biological matrices.

When developing a fast gas chromatography with negative-ion chemical ionization mass spectrometry (GC/NICI-MS) method matrix effects are a major issue. The effect of co-eluting compounds arising from the matrix (blood, urine) can result in a signal enhancement or suppression [6,7]. During method development, much attention should be paid to diminish matrix effects as much as possible.

The main aim of my study was to develop a new sensitive and specific method based on a fast GC/NICI-MS using solid-phase extraction (SPE) for the quantification of zaleplon and zopiclone at trace level in low-volume blood and urine samples. To the best of my knowledge, this method has been used for the first time for the optimization of sample preparation at different pH values (pH 1.0 - 10.0). Comparison of two SPE sorbents for the determination of both analytes in blood and urine were investigated. The analytes were well retained on Oasis MCX and Oasis HLB sorbents, also sufficient extraction efficiency was achieved at pH 9.0. For further study, a hydrophilic-lipophilic (polymeric) sorbent Oasis HLB was selected due to the polarity of sorbent surface and its large surface area (830 $m^2 g^{-1}$) in order to achieve efficient extraction of the analytes in a single step. The surface area is one of the most important factors for extracting the analytes from blood or urine samples by SPE. Special attention was paid to the selection of washing and eluting solvent in the SPE procedure, resulting in very pure and free from moisture extract, which can successfully be applied for gas chromatography-mass spectrometry. Different solvents or mixtures of solvents for elution of the adsorbed analytes, washing step-eliminating interferences in the sorbent were tested.

The developed method provides significant advantages in comparison with other previously published methods [6,8-10]. It shows higher sensitivity (the limit of detection $\leq$ 0.60 ng mL^{-1} and the limit of quantification $\leq$ 2.00 ng mL^{-1}) in blood and urine samples. The mean extraction efficiency was higher than 90.1 % for zaleplon and 82.9 % for zopiclone. The precision for zaleplon and zopiclone was between 3.04 – 10.58 % and 4.08 – 9.52 %, respectively. Whereas the accuracy (Bias value) was in the range from -5.73 to 6.00 % and from -7.00 to 6.32 % for zaleplon and zopiclone, respectively. The results have shown that the developed method is accurate, selective, precise, very fast with excellent recovery, low limits of detection and quantification. Finally, it was demonstrated that this method is applicable for the determination of trace concentrations of zaleplon and zopiclone in whole blood and urine samples. The developed method can be applied in routine toxicological analysis during the investigation of both clinical and forensic cases.

Acknowledgment: This research was supported by the State Forensic Medicine Service, Lithuania

The author has declared no conflict of interest

[1] A. C. Moffat, M. D. Osselton. Clarke's analysis of drugs and poisons, fourth ed., Pharmaceutical Press, London, UK, pp. 2257-2259 (2011).
[2] J. Brandt, C. Leong. Drugs in R&D **17**(4), 493-507 (2017).
[3] H. F. Fang, T. Y. Lee, K. C. Hui, et al. Journal of Cancer **10**(10), 2288-2298 (2019).
[4] M. Enomoto, S. Kitamura, H. Tachimori, M. Takeshima, K. Mishima. General Hospital Psychiatry **62**(1), 49-55 (2020).
[5] G. Nigam, M. Camacho, M. Riaz. Annals of Thoracic Medicine **14**(1), 49-55 (2019).
[6] N. Karlonas, A. Ramanavicius, A. Ramanaviciene. Journal of Separation Science **37**(5), 551-557 (2014).
[7] N. Karlonas, A. Padarauskas, A. Ramanavicius, A. Ramanaviciene. Journal of Separation Science **36**(8), 1437-1445 (2013).
[8] M. A. Tonon, P. S. Bonato. Bioanalysis **4**(3), 291-304 (2012).
[9] D. Xu, L. Sun, J. Wang, Y. Zhao, L. Zhang. International Journal of Clinical and Experimental Medicine **12**(11), 13135-13146 (2019).
[10] K. W. Simonsen, S. Hermansson, A. Steentoft, K. Linnet. Journal of Analytical Toxicology **34**(6), 332-341 (2010).

FORMATION OF SOLID SOLUTION IN XANTHONE DERIVATIVE SYSTEMS EXHIBITING LUMINESCENCE PROPERTIES

Kristaps Sargūns[a*], Aleksejs Karziņins[a], Kaspars Leduskrasts[b], Agris Bērziņš[a], Toms Rekis[a]

[a] Faculty of Chemistry, University of Latvia, Jelgavas iela 1, Riga, Latvia
[b] Latvian Institute of Organic Synthesis, Aizkraukles iela 21, Riga, Latvia
kristaps.sarsuns@lu.lv

Solid solutions (SS) are multicomponent phases for which the component ratios can be varied in continuum. These phases consist of different molecular constituents randomly occupying crystallographic sites [1]. The changes in composition are often accompanied by a continuous change in some physical and/or chemical properties (e.g., density, solubility, stability, and more complex properties such as non-linear optical properties, solid-state luminescence and phosphorescence properties) [1, 2].

Several xanthone (XANT) derivatives (Figure 1) were selected as model compounds because of their physico-chemical properties and chemically similar structures, in which the different atom (X and R) may not significantly affect the dominant intermolecular interactions [2].

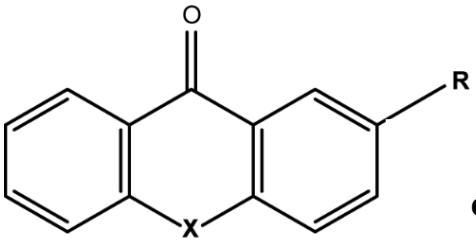

X = **O** (XANT) or **S** (TXANT)
R = **H** (XANT and TXANT),
Cl (TXANT-Cl) or **I** (TXANT-I)

Figure 1. Molecular structure of xanthone derivatives.

The binary systems of xanthone derivatives (XANT : TXANT and TXANT-Cl : TXANT-I) have been explored showing that four different solid solutions (formed based on parent structures of xanthone derivatives, respectively) can be formed. The obtained crystalline phases were characterized using powder X-ray diffraction (PXRD) and differential scanning calorimetry (DSC) methods in order to construct respective phase diagrams. Furthermore, photoluminescence spectra of all crystalline phases in powder form were recorded to see how they change with respect to those of the pure substances known from the literature [3].

Acknowledgements

This work has been supported by the Latvian Council of Science, project "Crystal engineering of pharmaceutical multicomponent phases for more efficient crystalline phase design", project No. lzp-2018/1-0312 and University of Latvia foundation through "Mikrotīklsō doctoral scholarship in the field of natural and medical sciences.

[1] Lusi, M. Engineering Crystal Properties through Solid Solutions. *Crystal Growth & Design*, **2018**, *18(6)*, 3704-3712.

[2] Sargūns, K., Bērziņš, A., Rekis, T. Solid Solutions in Xanthone – Thioxanthone Binary system: How well are Similar Molecules Discriminated in the Solid State? *Crystal Growth & Design*, **2020**, *20(12)*, 7997-8004.

[3] Wen, Y., Liu, H., Zhang, S., Gao, Y., Yan, Y., Yang, B. One-Dimensional "-" Stacking Induces Highly Efficient Pure Organic Room-Temperature Phosphorescence and Ternary-Emission Single-Molecule White Light. *J. Mater. Chem. C*, **2019**, *7*, 12502-12508.

NAPHTHYRIDINE AND CARBAZOLE DERIVATIVES AS ELECTROACTIVE MATERIALS

Lukas Dvylys, Rasa Keruckiene, Juozas Vidas Grazulevicius

Department of Polymer Chemistry and Technology, Kaunas University of Technology, Lithuania
lukas.dvylys@ktu.edu

High-performance organic light-emitting diodes (OLEDs) have been a subject of extensive research both in academia and in industry for the last two decades [1]. Pure organic thermally activated delayed fluorescence (TADF) materials have attracted world-wide attention in academic and industrial communities due to their high exciton utilization efficiency and low cost [2]. Organic materials which possess TADF characteristics are highly promising owing to their small singlet-triplet energy difference (ΔE_{ST}), which facilitates efficient reverse intersystem crossing (RISC). Due to the strong spinï orbit coupling effect in the phosphorescent materials, the optical radiation attenuation of the triplet excitons become possible, and the internal quantum efficiency of organic electroluminescence based on the phosphorescent materials can theoretically reach 100%. To design a novel TADF molecule, two principles should be followed. Firstly, the overlap between the highest occupied molecular orbital (HOMO) and lowest unoccupied molecular orbital (LUMO) should be separated by introducing large twist angles or steric hinderance to obtain a small ΔE_{ST}. Secondly, the HOMO and LUMO need to have partial overlap to guarantee high photoluminescence quantum yield (PLQY) [3].

In this work two naphthyridine and carbazole compounds with different alkyl substituents have been synthesized, where naphthyridine acts as an electron acceptor and carbazole ï as an electron donor. Their thermal, photophysical and electrochemical properties will be reported.

[1] T. Yeh, J. Lee, L. Chen, T. Chatterjee, W. Hung, and K. Wong, New naphthyridine-based bipolar host materials for thermally activated delayed fluorescent organic light-emitting diodes, Organic Electronics 70 (2019) 55ï 62.
[2] X. Zhou, H. Yang, Z. Chen, S. Gong, Z. Lu, and C. Yang, Naphthyridine-based emitters simultaneously exhibiting thermally activated delayed fluorescence and aggregation-induced emission for highly efficient non-doped fluorescent OLEDs, J. Mater. Chem. C, 2019, 7, 6607.
[3] C. Chen, H. Lu, Y. Wang, M. Li, Y. Shen, and C. F. Chen, Naphthyridine-based thermally activated delayed fluorescence emitters for multi-color organic light-emitting diodes with low efficiency roll-off, J. Mater. Chem. C, 2019, 7, 4673.

INVESTIGATION OF MICROPLASTIC CONTAMINATION IN WASTEWATER SAMPLES

Sonata Pleskytė[1], Ieva Uogintė[2]

[1] Department of Chemistry, Vilnius University, Lithuania
[2] Department of Environmental Science, Center For Physical Sciences And Technology, Lithuania
sonata.pleskyte@chgf.stud.vu.lt

The contamination of marine and freshwater ecosystems with plastic, and especially with microplastic (MP), is a global ecological problem of increasing scientific concern. Plastics are used in a wide variety of items and have displaced other important materials such as metal, glass, and wood. Microplastics are formed from polyesters, polyvinylidene chloride, polycarbonates, and many other organic polymers for use in a huge and growing range of applications. The biggest amount of plastic was applied at packaging, building, construction, and automotive industry (Fig. 1) [1]. Every year more than 8 million tons of plastic, including microplastic, is dumped into our freshwater systems, rivers, seas, and oceans [2].

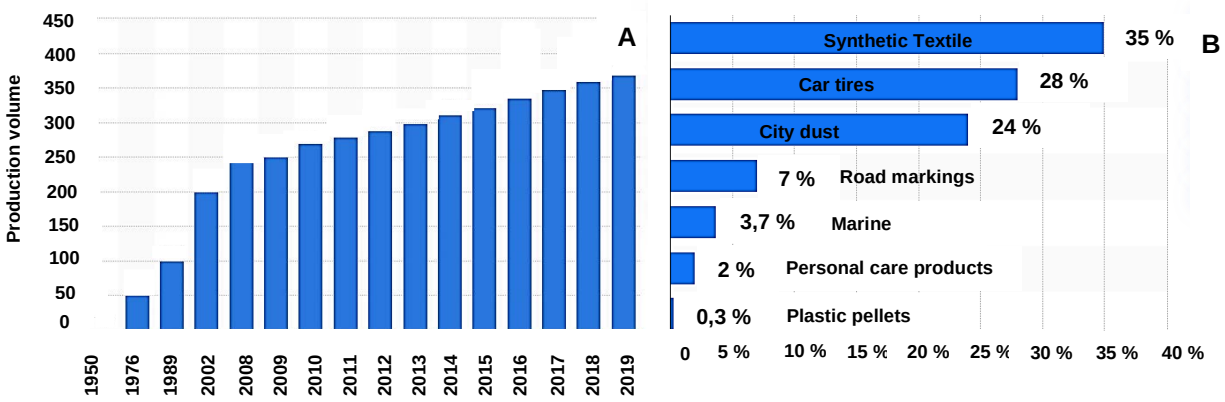

Fig. 1. A - Annual global plastic production (in million metric tons) 1950 ï 2019. **B -** Distribution of ocean microplastics sources worldwide as of 2018 [2].

Wastewater Treatment Plants (WWTPs) are one of the biggest sources of microplastics to the water circulation systems [3, 4]. Primary microplastics include household, industrial products such as cosmetics, personal care products, cleaners, and many other daily use item [5]. Secondary microplastics are released from large plastic parts because of mechanical effects, UV radiation or microbiological degradation. The size of the microplastic is less than 5 mm. Newest research have showed that WWTPs could remove 55-99 % of microplastic particles, but despite that fact, WWTPs is still one of the main MP source [6].

The principal aims of this study: 1) to investigate microplastic contamination in wastewater samples; 2) to present the methods applied for MP analysis including sampling, processing, identification, characterization, and quantification; 3) to evaluate the abundance of microplastic.

In this research, more than 30 wastewater samples were investigated and the presence of microplastic was confirmed. MPs were identified and characterized by the microscopic and spectroscopic analysis methods. Shape, color, and size of particles were described. This investigation let us identify what type of microplastic is mostly found in wastewater contamination. The results indicated the necessity for novel actions to decrease microplastic amount in wastewater. Research of microplastic properties could be the first step in improving our aquatic ecosystem and finding the new innovate methods for removing this pollution source.

Acknowledgement: This research is funded by the European Social Fund under the No 09.3.3-LMT-K-712 ñDevelopment of Competences of Scientists, other Researchers and Students through Practical Research Activitiesò measure. (grant No. 09.3.3-LMT-K-712-19-0112).

[1] PlasticsEurope 2018. Plastics ï the Facts, *Plastics ï the Facts 2018*: 38.
[2] Garside M. 2020. Global plastic production 1950-2019, *Statista* [interactive], [seen: 2021-01-17]. Internet access: https://www.statista.com/statistics/282732/global-production-of-plastics-since-1950/.
[3] Kalį²kov§ G., Aliį B., Skalar T., Bundschuh M., Gotvajn A.Ç. 2017. Wastewater treatment plant effluents as sourc of cosmetic polyethylene microbeads to freshwater, *Chemosphere* 188: 25ï 31. DOI: 10.1016/j.chemosphere.2017.08.131
[4] Hidayaturrahman H., Lee T.G. 2019. A study on characteristics of microplastic in wastewater of South Korea: Identification, quantification, and fate of microplastics during treatment process, *Marine Pollution Bulletin* 146 (May): 696ï 702. DOI: 10.1016/j.marpolbul.2019.06.071.
[5] Casta¶eda R.A., Avlijas S., Anouk Simard M., Ricciardi A. 2014. Microplastic pollution in st. lawrence river sediments, *Canadian Journal of Fisheries and Aquatic Sciences* 71(12): 1767ï 1771. DOI: 10.1139/cjfas-2014-0281.
[6] Akarsu C., Kumbur H., Gº kdaĵ K., Kādeyĸ A.E., Sanchez-Vidal A. 2020. Microplastics composition and load from three wastewater treatment plants discharging into Mersin Bay, north eastern Mediterranean Sea, Marine Pollution Bulletin 150 (September 2019). DOI: 10.1016/j.marpolbul.2019.110776.

INVESTIGATION OF POSSIBILITIES TO CONTROL THE POLYMORPH OBTAINED IN CRYSTALLIZATION OF 3-HYDROXYBENZOIC ACID

Zane Čerpakovska[a*], Kristaps Saršūns[a], Agris Bērziņš[a]

[a] Faculty of Chemistry, University of Latvia, Jelgavas iela 1, Riga, Latvia
zane.cerpakovska@lu.lv

Polymorphism is the ability of a substance to exist in a number of crystalline modifications and can affect many aspects of drug development in pharmacy [1]. A concomitant polymorphism is an important phenomenon in which kinetics and thermodynamics are linked or it is explained how one compound can grow simultaneously to form different polymorphs [2]. The concomitant crystallization, however, is not desirable, because the obtained product is not a pure phase but a mixture in which each polymorph has its own properties [3]. Therefore, in this study we investigated the crystallization of 3-hydroxybenzoic acid (3OHBA, Figure 1), an intermediate in pharmacy, existing in a form of 2 well characterized polymorphs often reported to crystallize concomitantly [4].

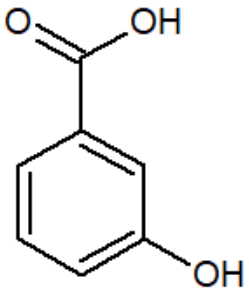

Figure 1. Molecular structure of 3-hydroxybenzoic acid

Crystallization using several different techniques such as evaporative, additive controlled, vapour diffusion and cooling crystallization were performed. Using the first tree of the named techniques solid products were obtained within a week or even several months, while using the last - within a couple of days. 3OHBA with the addition of PEG 6000 does not form a new crystalline phase, but it was observed that by increasing the amount of this additive increased the possibility to obtain a mixture of 3OHBA polymorphs. It was not always possible to find regularities that could explain the connection between the polymorph obtained in the crystallization and the properties of the solvent or the crystallization conditions.

[1] Chen, J., Sarma, B., Evans, J. M. B., Myerson, A. S. Pharmaceutical Crystallization. *Crystal Growth & Design*, **2011**, *11(4)*, 887–895.

[2] Tang, W., Sima, A. D., Gong, J., Wang, J., Li, T. Kinetic Difference between Concomitant Polymorphism and Solvent-mediated Phase Transformation: A Case of Tolfenamic Acid. *Crystal Growth & Design*, **2020**, *20(3)*, 1779-1788.

[3] Raza, K., Kumar, P., Ratan, S., Malik, R., Arora, S. Polymorphism: The Phenomenon Affecting the Performance of Drugs. *SOJ Pharmacy & Pharmaceutical Sciences*, **2014**, *1(2)*, 10.

[4] Nordström, F. L., Rasmuson, Å. C. Polymorphism and thermodynamics of m-hydroxybenzoic acid. *European Journal of Pharmaceutical Sciences*, **2006**, *28(5)*, 377–384.

PREPARATION OF A NOVEL STATIONARY PHASE FOR ION EXCHANGE SEPARATION IN LIQUID CHROMATOGRAPHY

Huda Alghamdi[1], Anna M. Hogan[1], Jeremy D. Glennon[1]

[1] Innovative Chromatography Group, Irish Separation Science Cluster (ISSC)
School of Chemistry, and the Analytical & Biological Chemistry Research Facility (ABCRF),
University College Cork, Ireland.
113220126@umail.ucc.ie

Ion exchange mode high performance liquid chromatography (HPLC) has numerous applications in the pharmaceutical industry. It is used for drug stabilization and used as aids for tablet disintegration. Commercially available polymeric resins ion exchangers exhibit a comparatively high ion-exchange capacity and show a high chemical stability [1]. However, they have many drawbacks, including a swelling nature in organic solvents and a limited pressure stability. While silica-based ion exchangers have many advantages such as a high surface area, a high mechanical strength resulting in high efficiency, and the absence of the swelling problem [2]. However, the silica-based ones possess much lower ion exchange capacity than that of the polymeric resins. Therefore, the surface of the silica was modified via two processes to developed silica based stationary phase coated polymer. In this study, a novel cation exchange stationary phase was designed and synthesized via functionalization of the silica (3 µm, fully porous) by quaternary amino group and coating with Nafion. The material was confirmed and evaluated by elemental analysis, thermogravimetric analysis, Brunauer-Emmet-Teller (BET) analysis, infrared spectroscopy and scanning electron microscopy with Energy Dispersive X-ray detector. The characterizations demonstrated the successful of functionalization of the silica and coating with Nafion. This stationary phase, suitably prepared, exhibited excellent cation exchange separation [3] of N, N, N-trimethyl phenyl ammonium chloride (TMPAC) using HPLC (Fig. 1).

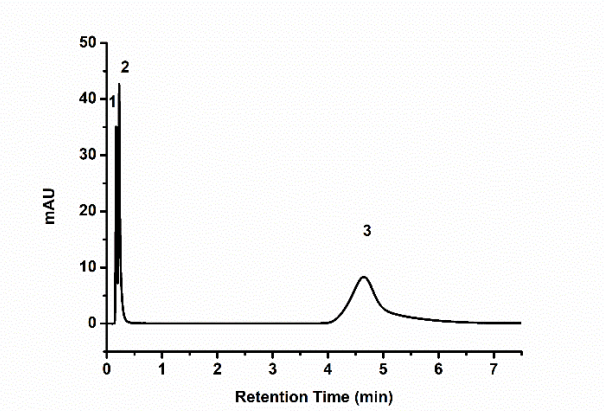

Fig. 1. Cation exchange selectivity for the stationary phase. Test solutes: 1. Toluene (15 mM) 2. Uracil (1 mM) 3. TMPAC (90 mM). Mobile phase: 90:10 v/v ACN: 30 mM ammonium acetate pH 6.7, flow rate: 0.5 mL/min, temperature 30 °C, injection volume: 0.2 µL, wavelength 254 nm.

[1] O. Vyviurska et al., Comparison of commercial organic polymer-based and silica-based monolithic columns using mixtures of analytes differing in size and chemistry, Journal of separation science **41** (7), 1558-1566 (2018).
[2] D. Zhou et al., Preparation and evaluation of a reversed-phase/hydrophilic interaction/ion-exchange mixed-mode chromatographic stationary phase functionalized with dopamine-based dendrimers, Journal of Chromatography A **1571**, 165-175 (2018).
[3] B. Buszewski etal., Multi-Parametric Characterization of Amino Acid- and Peptide-Silica Stationary Phases, Chromatographia **82** (1), 153-166 (2019).

LONG TERM SUBMICRON AEROSOL CHEMICAL CHARACTERIZATION IN RŪGŠTELIŠKIS (LITHUANIA) RURAL ENVIRONMENT

Touqeer Gill[1], Julija Pauraitė[1], Steigvilė Byčenkienė[1] and Kristina Plauškaitė[1]

[1] Center for Physical Sciences and Technology, Vilnius, Lithuania
touqeer.gill@ftmc.lt

Characterization of the chemical components of atmospheric submicron aerosols is important, because of their adverse human health effects and significant influence on the Earth's climate system. Therefore, it is crucial to deepen the knowledge of aerosols chemical composition and pathways of formation.

Aerosol main chemical components were investigated in Rūgšteliškis (Lithuania) rural environment by operating Aerosol Chemical Speciation Monitor (ACSM). The analysis of 5 years (2013, 2014, 2016, 2018 and 2019) data series was performed for 3 seasons (spring, summer and autumn). Time series and diurnal trends of organic aerosols (OA) and inorganic aerosols (IA) were analysed. OA were exhibiting higher contribution 60-80% to total submicron particular matter (PM_1) whereas, IA were showing lower contribution 20-40% (NO_3 = 3-12%, SO_4 = 4-20%, NH_4 = 3-21% and Chl = 0.2-0.4%) over all seasons. During summer of 2013, 2016 and 2018 OA had a higher contribution to PM_1 compared to spring and autumn. Meantime in 2014 and 2019 the highest contribution of OA was observed over the spring.

Diurnal trends of OA and IA were assessed in order to characterise possible day and night aerosol chemistry and sources (Fig 1). Higher mass concentration of OA was observed in morning hours (5-7 h) and lower mass concentration during daytime (13-19 h) (Fig 1A). Similar trend was observed for NO_3 mass concentration, which reached maximum between 5-7 h and minimum between 15-20 h (Fig 1B). This diurnal pattern could indicate nocturnal chemistry. SO_4 and NH_4 had lower mass concentration during daytime (10-19 h and 13-23 h, respectively) and higher mass concentration during night time (1-6 h and 1-10 h, respectively) (Fig 1C, D). Formation of SO_4 aerosol was possibly carried out during day time by the oxidation of gaseous precursor SO_2 followed by particle formation through nucleation and condensation processes. Therefore, significantly higher SO_4 concentration was observed during the daytime. Neutralization of HNO_3 and H_2SO_4 with NH_3 likely formed ammonium derived aerosol in the form of NH_4NO_3 and $(NH_4)_2SO_4$ [1]. In addition, submicron aerosol particles acidity (H^+_{Aer}) and stoichiometric neutralization ratio were calculated and analysed [2]. The results of this study could provide a better understanding regarding atmospheric chemistry on local and global scale.

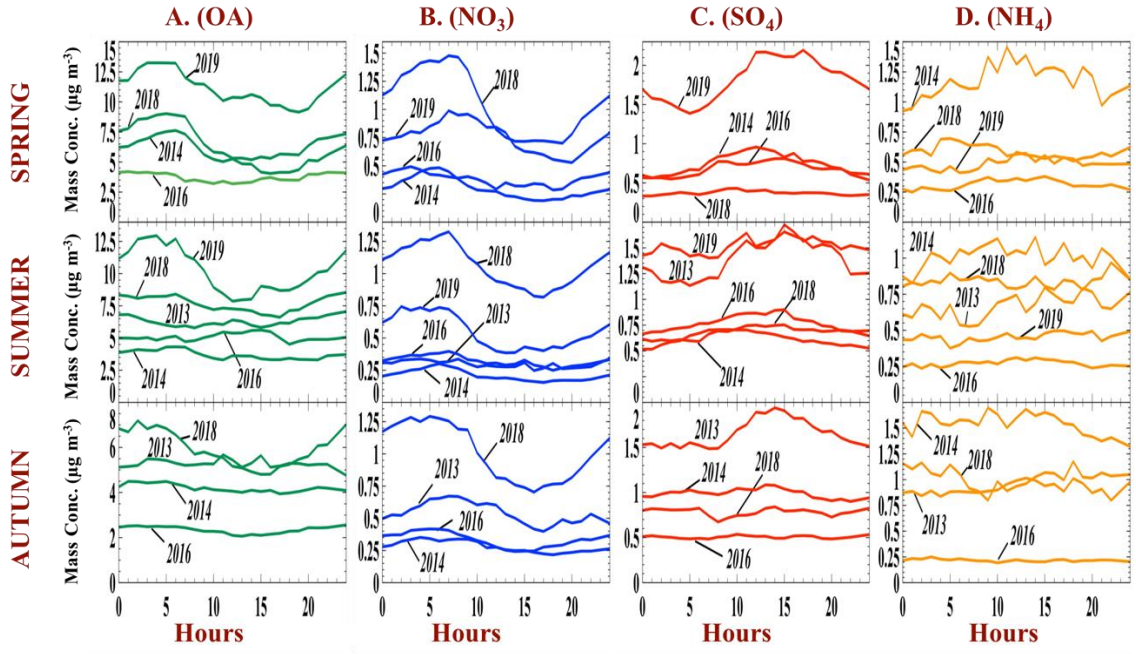

Fig. 1. 5 years diurnal trend of (A) OA, (B) NO_3, (C) SO_4 and (D) NH_4 for 3 seasons (spring, summer and autumn).

[1] A. I. Calvo, C. Alves, A. Castro, V. Pont, A. M. Vicente, and R. Fraile, "Research on aerosol sources and chemical composition : Past , current and emerging issues," vol. 121, pp. 1–28, 2013.

[2] D. R. Worsnop and M. Canagaratna, "A Case Study of Urban Particle Acidity and Its Influence on Secondary Organic Aerosol," pp. 3213–3219, 2007.

SYNTHESIS OF HYDRAZIDE HYDRAZONES WITH LUMINESCENT PROPERTIES

Lena Marciniak[1], Justyna Anna Adamczyk[2], Adam Marek Pieczonka[2], Michał Rachwalski[2]

[1] The Bio-Med-Chem Doctoral School of the University of Lodz and Lodz Institutes of the Polish Academy of Sciences
[2] Department of Organic and Applied Chemistry, Faculty of Chemistry, University of Lodz, Institute of Catalysis and Organic Synthesis
lena.marciniak@edu.uni.lodz.pl

In recent years, organic semiconductors have become an attractive research object in the field of organic electronics. Small-molecule organic compounds are the materials used in this area to produce organic light emitting diodes (OLEDs). OLED technology uses the unique properties of selected compounds, such as structure and luminescence. The appropriate structure of molecules enables the suitable flow of electrons in thin layers of OLEDs.

A group of compounds, hydrazide hydrazones, previously untested in terms of their use in the creation of conductive materials, was tested. The emission of these organic compounds in the solution is much weaker than in the solid, which indicates the presence of the emission effect induced by molecular aggregation. Hydrazide hydrazones, carboxylic acid hydrazide derivatives, including salicylic acid also have an appropriate structure that allows both luminescence and the formation of thin layers of solid. Salicylic acid derivatives have hydroxyl groups in their structure. Thanks to them, it is very easy to create hydrogen bonds between molecules, which have a significant impact on the self-organization of molecules in the layers [1].

The aim of the research was to synthesize new, fluorescent organic compounds with an appropriate chemical structure, enabling the production of thin films by solution methods. An additional goal was to study the morphology of the obtained layers in order to assess the quality of thin films in the context of their use in the creation of potential devices. The chemical compounds obtained during the research were hydrazide hydrazones (Fig. 1.), derivatives of salicylic acid. They show fluorescence due to the presence of the AIE (Aggregation-Induced Emission) effect [2].

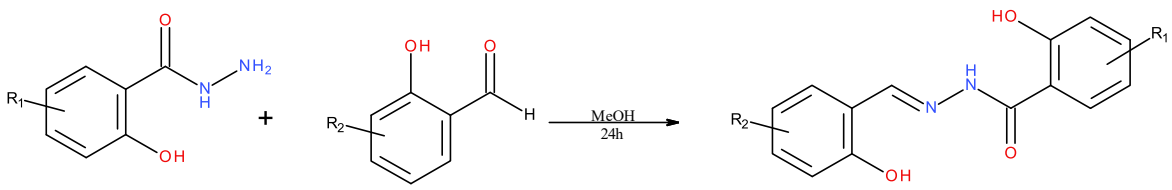

Fig. 1. General scheme of hydrazide hydrazone synthesis.

[1] A. Pieczonka et al., Synthesis and evaluation of antimicrobial activity of hydrazones derived from 3-oxido-1H-imidazole-4-carbohydrazides, European Journal of Medicinal Chemistry **64**, 389 (2013).
[2] J. Adamczyk et al., Photophysical properties of novel fluorescent thin solid layers based on the Aggregation Induced Emission of alkoxy-substituted salicylaldehyde azines, Journal of Luminescence **229**, 117668 (2021).

THE EFFICIENCY OF ZnO NANOPOWDERS MODIFIED BY GRINDING AND DOPING WITH Mg(II) IONS IN THE PHOTOCATALYTIC DEGRADATION OF CIPROFLOXACIN

Duġica JovanoviĹ [1], Tamara IvetiĹ [2], Nina FinĻur[1]

[1] Department of Chemistry, Biochemistry and Environmental Protection, Faculty of Sciences, University of Novi Sad, Serbia
[2] Department of Physics, Faculty of Sciences, University of Novi Sad, Serbia
dh.dusica.jovanovic@student.pmf.uns.ac.rs

The uncontrollable usage of antibiotics has led to their increased concentrations in the environment. Antibiotics are omnipresent in the surface and groundwater, soil, sediments, aquatic plants and animals. Because of their biodegradation resistance, antibiotics can accumulate in the environment and cause the development of antibiotic resistance or can have other detrimental effects [1,2].

The desire to remove various antibiotics present in the environment, using environmentally friendly processes, is one of the current topics. Advanced oxidation processes (AOPs) are chemical oxidative methods based on the production of the hydroxyl radicals ($^{\bullet}OH$) as an extremely reactive oxygen species. AOPs are used for treating a variety of organic compounds by oxidizing them to less harmful intermediate species, or completely mineralizing them to CO_2, H_2O, and inorganic ions [1,3]. Semiconductor photocatalysis, as an AOP, involves the activation of a semiconductor (such as ZnO) by artificial or natural radiation in order to degrade organic pollutants [1].

Ciprofloxacin (Fig. 1) is a fluoroquinolone antibiotic commonly used both in human and veterinary medicine for treating bacterial infectious diseases [4].

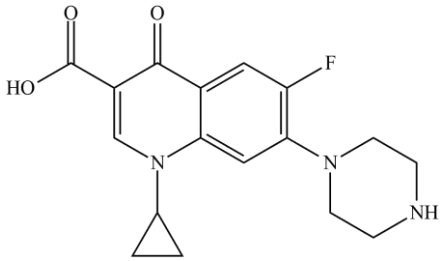

Fig.1. The structural formula of the antibiotic ciprofloxacin.

The conducted research examined the efficiency of photocatalytic degradation of ciprofloxacin in the presence of ZnO nanopowders as a photocatalyst, using simulated sunlight. ZnO nanopowders were modified by different grinding time and doping with various content of Mg(II) ions.

Obtained results showed that modified ZnO nanopowders did not display higher efficiency than commercial ZnO. However, compared with the direct photolysis results, a positive effect of their presence was still observed.

[1] V. Homem, L. Santos, Degradation and removal methods of antibiotics from aqueous matrices ҁ A review, J. Environ. Manage. **92**, 2304ҁ2347 (2011).
[2] R. Gothwal, T. Shashidhar, Antibiotic pollution in the environment: a review, Clean (Weinh) **43**, 479ҁ489 (2014).
[3] R. Hernandez, M. Zappi, et al., Comparing the performance of various advanced oxidation processes for treatment of acetone contaminated water, J. Hazard. Mater. **92**, 33ï 50 (2002).
[4] Z. Vyb²ralov§, M. Nobilis, et al., High-performance liquid chromatographic determination of ciprofloxacin in plasma samples, J. Pharm. Biomed. Anal. **37**, 851ҁ858 (2005).

DEVELOPMENT OF GLUCOSE BIOSENSOR: IMMOBILIZATION OF GLUCOSE OXIDASE ON DENDRITIC GOLD NANOSTRUCTURES

Laura Sakalauskiene[1], Anton Popov[1], Asta Kausaite-Minkstimiene[1], Almira Ramanaviciene[1]

[1]NanoTechnas–Center of Nanotechnology and Materials Science, Faculty of Chemistry and Geosciences, Vilnius University, Lithuania
laura.sakalauskiene@chgf.vu.lt

Among all biosensors present on the market, glucose biosensors account for more than 85% [1]. In recent years, numerous studies have been conducted to improve biosensors measuring glucose in the blood using different nanostructures [2,3]. Gold nanostructures located on the surface of the electrode increase the conductivity, improve the electron transfer, and biosensor analytical characteristics such as sensitivity, selectivity and stability [4]. The proper immobilization of the enzyme on the electrode surface is one of the most important factors affecting the performance of the biosensors. Different methods could be used for enzyme immobilization on the electrode surface, namely, covalent attachment or cross-linking with bifunctional reagents, non-covalent adsorption, physical entrapment, and bio-conjugation [1].

In this work, dendritic gold nanostructures (AuNS) were electrochemically formed on the surface of a graphite rod (GR) electrode. Different glucose oxidase (GOx) immobilization on the surface of GR/AuNS electrode methods were used: adsorption and covalent immobilization through a self-assembled monolayer (SAM) without and with cross-linking (Fig. 1). The impact of enzyme immobilization method on the performance of glucose biosensor was tested using potentiostat/galvanostat PGSTAT 30/Autolab (EcoChemie, Netherlands) with GPES 4.9 using three-electrode system. Glucose biosensor based on working electrode modified by GOx covalently immobilized on AuNS through 11-mercaptoundecanoic acid (GR/AuNS/SAM/GOx) and additionally cross-linked with glutaraldehyde (Fig. 1A) possesses higher sensitivity, repeatability, and better stability.

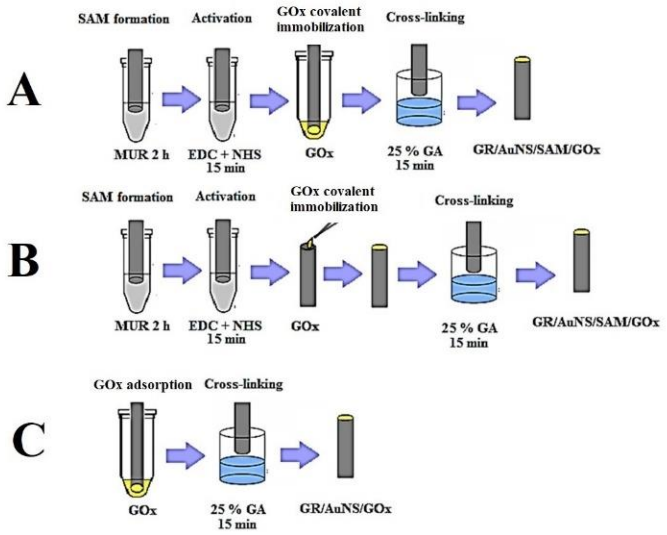

Fig. 1 Schematic illustration of glucose oxidase immobilization on GR electrodes modified with dendritic gold nanostructures: **A** ï covalent immobilization – GR/AuNS/SAM electrode is immersed in the GOx solution, **B** ï covalent immobilization ï GOx solution is poured onto the surface of the GR/AuNS/SAM electrode, **C** ï adsorption on the GR/AuNS electrode.

Acknowledgment

This research was funded by a grant (No. S-LU-20-11) from the Research Council of Lithuania.

[1] J. Lovic, S. Stevanovic, N.D. Nikolic, S. Petrovic, D. Vukovic, N. Prlainovic, D. Mijin and M. A. Ivic, Glucose sensing using glucose oxidase-glutaraldehyde-cysteine modified gold electrode, Int. J. Electrochem. Sci. **12**, 5806ï 5817, (2017).
[2] V. Scognamiglio, Nanotechnology in glucose monitoring: Advances and challenges in the last 10 years, Biosens. Bioelectron. **47**, 12ï 25, (2013).
[3] N. German, A. Ramanavicius, J. Voronovic, Y. Oztekin, and A. Ramanaviciene, The effect of colloidal solutions of gold nanoparticles on the performance of a glucose oxidase modified carbon electrode, Microchim. Acta **172**, 185ï 191, (2011).
[4] A. Galal, N. F. Atta, and E. H. El-Ads, Probing cysteine self-assembled monolayers over gold nanoparticles - Towards selective electrochemical sensors, Talanta **93**, 264ï 273, (2012).

ELECTROCHEMICAL SYNTHESIS OF TIO_2 PEO-COATINGS ON THE ALUMINUM SURFACE

Veronika S. Karpushenkova[1], Hanna M. Maltanava[2]

[1] Department of Chemistry, Belarusian State University, Belarus
[2] The Research Institute for Physical Chemical Problems of the Belarusian State University, Belarus
karpushenkova.v.s@gmail.com

Titanium dioxide (TiO_2) coatings are multifunctional because they combine good chemical inertness, thermal stability, non-toxicity, as well as bactericidal and photocatalytic properties [1]. The plasma electrolytic oxidation method (PEO) allows direct growth of photoactive TiO2 layers with good mechanical adhesion and electrical contact with the substrate. The prospects of such layers are clearly demonstrated in the work [2]. Several authors recently reported that PEO TiO_2 films outperform TiO_2 nanotube arrays, exhibiting a quantum yield of over 90% when converting photons to electrons [3]. It is equally important to obtain such coatings not only on the titanium surface but also on more accessible materials, such as aluminum.

In this work, the PEO method for the deposition of TiO_2 films on an aluminum substrate (99,9%) in an aqueous solution of 0,05 M (17,7 wt.%) potassium titanium oxide oxalate dihydrate ($K_2[TiO(C_2O_4)_2]\cdot 2H_2O$) was used. Potassium titanium oxide oxalate dihydrate was used as a precursor for the formation of titanium dioxide during oxidation [4]. An aluminum anode and a titanium cathode were immersed in a water-cooled electrochemical cell and were connected to a direct current source. The synthesis time for the PEO coatings was 5 min. Two types of spark discharges have been identified: 280 V – a homogeneous minor yellow sparkling is observed on the surface (I oxidation mode); 330 V – the number of sparks decreases and at the same time they become much larger and acquire an orange-yellow color (II oxidation mode). The appearance (a), phase composition (b), and morphology (c) of the obtained PEO coatings are shown in Fig. 1.

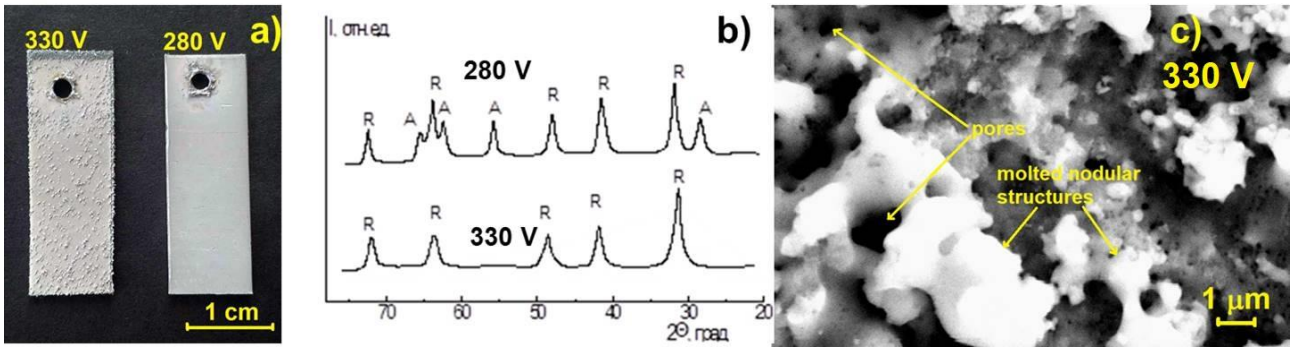

Fig. 1. Surface appearance (a), XRD patterns (b), and surface morphology of obtained TiO_2 coatings on the aluminum substrate (c).

It was found that with an increase in the oxidation voltage from 280 V to 330 V (when the oxidation mode changes from I to II), the thickness of the coating increases (from 25 ± 3 μm to 40 ± 5 μm) and its roughness also increases (see Fig.1a). The color of both obtained coatings is white. XRD analysis (X-ray diffractometer HZG-4A) showed that the main phase in each sample of titanium dioxide is rutile, especially for the coating obtained at 330 V, and anatase is present in insignificant amounts for the coating obtained at 280 V (Fig.1b). A typical morphology of a PEO TiO_2 coating is shown in Fig. 1c (the image was obtained using a scanning electron microscope (SEM) LEO-1455 VP). SEM shows the structure typical for PEO - coatings: the presence of pores and molted nodular structures. The higher the oxidation voltage (330 V) is, the larger the molted nodular structure sizes are and the worse the adhesion to the substrate is observed. To obtain denser coatings with good adhesion to the surface, it is preferable to carry out the synthesis at a lower sparking voltage mode (280 V).

It was found that the method of plasma electrolytic oxidation can be used to obtain titanium dioxide coatings on the aluminum surface. It is shown that, if the synthesis conditions are varied, it is possible to obtain oxide coatings with a different thickness and morphology. In the future, it is planned to obtain a series of TiO_2 coatings for subsequent study of their composition and photocatalytic activity.

[1] H. Ishizaki et al., Electrochemical Fabrication of Titanium Oxide Film from an Aqueous Solution Containing Titanium Ion and Hydroxylamine, ECS Transactions **41**, 111-117 (2011).
[2] S. Franz et al., Degradation of Carbamazepine by Photo(electro)catalysis on Nanostructured TiO_2 Meshes: Transformation Products and Reaction Pathways, Catalysts **10**, 169 (2020).
[3] S. Franz et al., Photoactive TiO_2 coatings obtained by plasma electrolytic oxidation in refrigerated electrolytes. Applied Surface Science **385**, 498–505 (2016).
[4] Ulasevich S.A. et al., Deposition of hydroxyapatite-incorporated TiO_2 coating on titanium using plasma electrolytic oxidation coupled with electrophoretic deposition, RSC Advances **6**, 62540–62544 (2016).

P1-43

DID NOT PARTICIPATE

SYNTHESIS OF BENZENESULFONAMIDE-BEARING β,γ-AMINO ACID DERIVATIVES AS HUMAN CARBONIC ANHYDRASE INHIBITORS

Benas Balandis[1], Vaida Paketurytė[2], Tomas Šinkūnas[2], Daumantas Matulis[2], Asta Zubrienė[2], Vytautas Mickevičius[1]

[1] Department of Organic Chemistry, Kaunas University of Technology, Lithuania
[2]Department of Biothermodynamics and Drug Design, Institute of Biotechnology, Life Sciences Center, Vilnius University, Lithuania
benas.balandis@ktu.edu

Reversible hydration of CO_2 to protons and bicarbonate is catalyzed by twelve alpha carbonic anhydrase (CA) isozymes found in human body. This is an essential reaction for the respiration and transport of CO_2 between tissues, in pH regulation and homeostasis [1]. Increased expression levels of several CA isozymes are associated with some diseases. Currently CAs are established therapeutic targets of cancer (CA IX and CA XII), glaucoma (CA II, CA IV, CA XII) and obesity (CA VA and CA VB). Recently, most of the research focused on designing and developing of inhibitors against CA IX that show potential for treating solid tumors [2].

Compounds **2a,b** were synthesized by nucleophilic ring-opening reactions of pyrrolidones **1a,b** by heating them under reflux in an excess of hydrazine monohydrate. Subsequently, β,γ-amino acid derivatives **2a,b** were used as the precursors for the synthesis of a series of hydrazone derivatives (Fig. 1). Reactions between compounds **2a,b** and ketones (acetone, ethyl methyl ketone and acetophenone) provided corresponding hydrazones **3a,b**–**5a,b**.

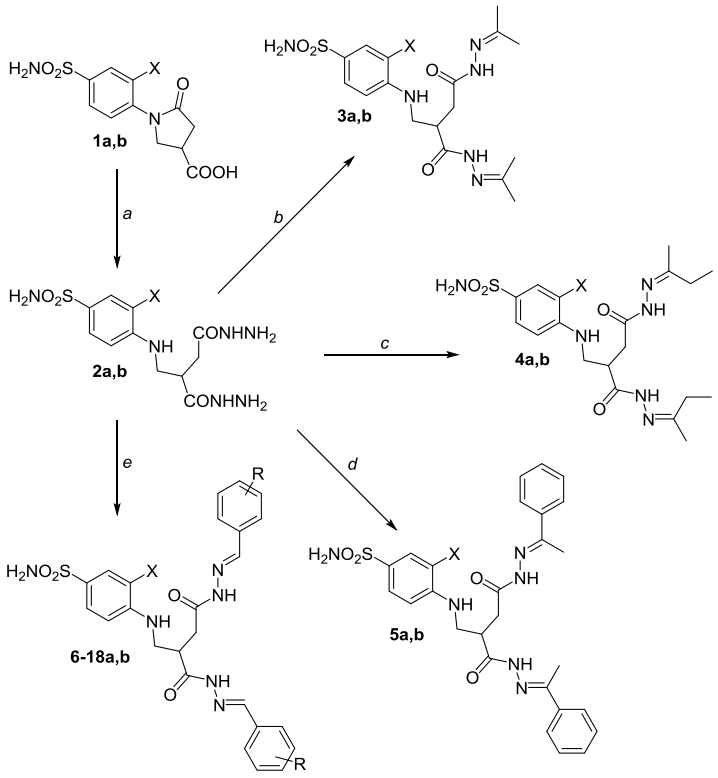

a: X = H; **b: X =** Cl;
6: R = H; **7:** R = 2-OH; **8:** R = 3-OH; **9:** R = 4-OH; **10:** R = 2-Cl; **11:** R = 3-Cl; **12:** R = 4-Cl;
13: R = 4-F; **14:** R = 4-OCH_3; **15:** R = 2-NO_2; **16:** R = 3-NO_2; **17:** R = 4-NO_2; **18:** R = 4-COOH;

Reaction conditions: (a) $N_2H_4 \cdot H_2O$, reflux, 4 h; (b) acetone, reflux, 2 h; (c) methyl ethyl ketone, propan-2-ol, reflux, 3 h; (d) acetophenone, propan-2-ol, reflux, 2 h; (e) corresponding aldehyde, propan-2-ol, reflux, 1-2 h;

Fig. 1. Synthesis of β,γ-amino acid derivatives

Whereas reactions of compounds **2a,b** with corresponding aromatic aldehydes yielded hydrazones **6a,b**–**18a,b** (Fig. 1). The structures of all synthesized compounds have been confirmed by the data of ^{1}H and ^{13}C NMR, FT-IR spectroscopy as well as mass spectrometry data.

Compound binding to human CA isoforms was measured by fluorescent thermal shift assay. The compounds bound CAs with submicromolar affinity.

[1] Aggarwal, M., Boone, C. D., et al., R. Structural annotation of human carbonic anhydrases. J. Enzyme Inhib. Med. Chem. **28**, 267–277 (2013).
[2] R. G. Gieling, K. J. Williams, Carbonic Anhydrase IX as an Imaging and Therapeutic Target for Tumors and Metastases. Bioorg. Med. Chem. **21**, 1470–1476 (2019).

GREEN APPROACH IN THE SYNTHESIS OF PYRAZOLES

Daria Łuczak[1], Adam Marek Pieczonka[1]

[1] Department of Organic and Applied Chemistry, Faculty of Chemistry, University of Łódź,
Tamka 12, 91-403 Łódź, Poland
daria.luczak@op.pl

Green chemistry is a concept that encourages the thoughtful design and execution of chemical processes to reduce the use and generation of harmful substances. Organic solvents used in chemical synthesis are a major threat to the environment. The green approach to synthesis proposes the elimination of organic solvents. One of the reaction environments can be lemon juice. Lemons are among the world's most popular citrus fruits. Lemons contain many plant compounds, minerals and essential oils additionally they are a great source of vitamin C and fiber. Lemon juice can be used in various fields: medical, cosmetic, food, chemical, etc.

Pyrazoles are an interesting class of five-membered heterocyclic compounds which show diverse activities (biological activities, ligands in cross-coupling reactions and optical sensors) [1]. Among them tetraarylpyrazoles exhibit luminescence properties [2]. There are several methods for the synthesis of pyrazoles, such as: reaction of chalcones and hydrazines, coupling of hydrazine, aldehyde and ethyl acetoacetate but these reactions are often performed at elevated temperature in organic solvents, and in the presence of different harmful catalysts [3].

Reactions using lemon juice as medium are eco-frendly. In our research we used lemon juice as a medium in the synthesis of N-acyl substituted 3,5-dimetylpyrazoles with luminescent properties (Fig. 1). Different aromatic carbohydrazides were transformed into expected pyrazole derivatives with high yields. Pyrazoles with large aromatic substituents have luminescent properties in solution as well as in the solid state.

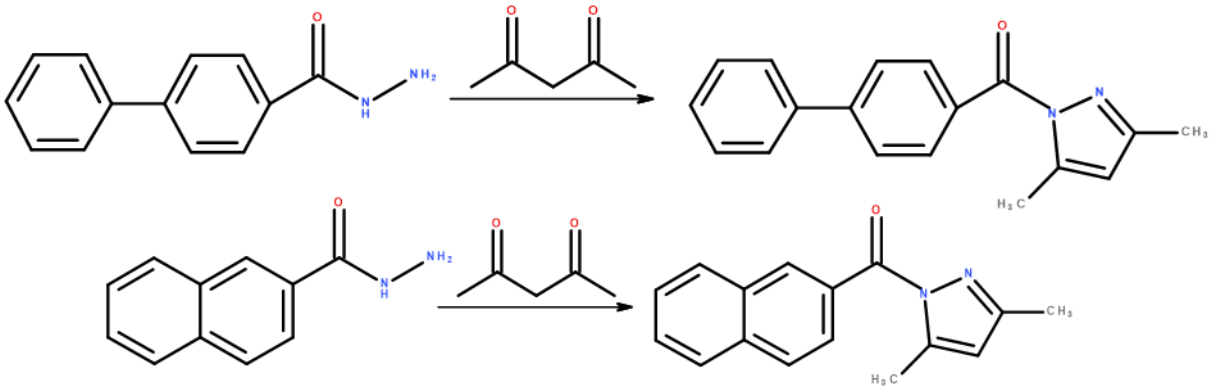

Fig. 1. General procedures for systhesis of pyrazole derivatives.

[1] B. R. Vaddula, R. S. Varma, J. Leazer, Mising with microwaves: solvent-free and catalyst-free synthesis of pyrazoles and diazepines, Tetrahedron Letters 54, 1538-1541 (2013).
[2] S. Mukherjee, P. S. Salini, A. Srinivasan, S. Peruncheralathan, AIEE phenomenon: tetraarys vs. triaryl pyrazoles, Chem. Commun 51, 17148 (2015).
[3] V. Milovanović, Z. D. Petrović, S. Novakowić, G. A. Bogdanović, D/ Simijonović, V. P. Petrović, Structural characterization of benzoyl-1H-pyrazole derivatives obtained in lemon juice medium: Experimental and theoretical approach, Journal of Molecular Structure 1195, 85-94 (2019).

SUGAR ORGANOCATALYSTS WITH UREA FRAGMENT

Karolina Koselak[1], Stanisław Porwański[1], Anna Zawisza[1]

[1] Faculty of Chemistry, Department of Organic and Applied Chemistry, University of Lodz, Poland
karolina.koselak@chemia.uni.lodz.pl

In asymmetric reactions the most important element is the appropriate reaction promoter that allows to receive planned products in an enantioselective approach. Following closely the literature reports of the last decade, we observe an increasing interest in organocatalysts or chiral ligands. An important group are sugar derivatives and structures with urea fragment. Such structures are main research trend in our team. During our work we obtained a large library of organocatalysts containing both mono and disaccharide rings. Our organocatalysts were were tested in many asymmetric reactions such as: aza-Henry, Michael and others [1,2].

My research is a continuation of the work of the team from the Unit of Catalysis and Organic Synthesis at the Department of Organic and Applied Chemistry of the University of Lodz. The catalysts mentioned above are obtained as a result of the Staudinger-aza-Wittig reaction from the corresponding sugar azide and nitrogen nucleophile in the presence of triphenylphosphine and CO_2 [3].

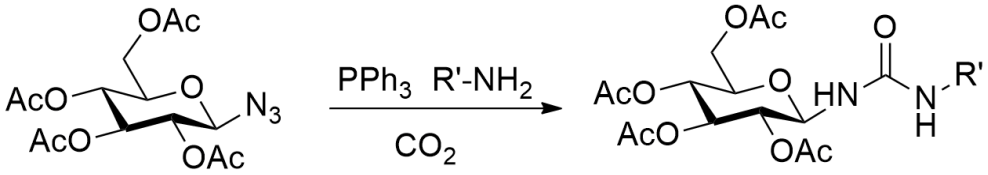

Fig. 1. Staudinger-aza-Wittig reaction.

Their effectiveness in selected asymmetric reactions varied in terms of yield and enantiomeric excess and ranged from average to very good.

[1] S. Porwański, New ureas containing glycosyl and diphenylphosphinyl scaffolds: synthesis and the first attempts to use them in asymmetric synthesis, Carbohydrate Research **394**, 7-12 (2014).
[2] J. Robak, B. Kryczka, B. świerczyńska et all., New sugar-derived bifunctional chiral ureas as highly effective organocatalysts in asymmetric aza-Henry reaction, Carbohydrate Research **404**, 83-86 (2015).
[3] J. Kovacs, I. Pinter, A. Messmer, G. Toth, Unprotected sugar phosphinimines: A facile route to cyclic carbamates of amino sugars, Carbohydrate Research **141**, 57 (1985).

MODELLING ^{17}O NMR SPECTRA OF TAUTOMERIC FORMS OF CITRININ

Gyginta Einorytė[1], Kęstutis Aidas[1]

[1]Institute of Chemical Physics, Faculty of Physics, Vilnius University, Lithuania
zyginta.einoryte@ff.stud.vu.lt

Citrinin is a mycotoxin which causes contamination of food with various toxic effects. Two tautomeric forms of citrinin exist – *para* or *ortho* quinone methide (analogous to a quinone but having one of the carboxylic oxygens replaced with a carbon) (Fig. 1). Citrinin is synthesized as a secondary metabolite by several fungal strains of *Penicillium*, *Aspergillus* and *Monascus* genera and is often found along with another nephrotoxic compound, ochratoxin A. As many other mycotoxins, citrinin is considered a perspective antimicrobial, antitumor and even neuroprotective agent due to its toxicity. Citrinin is known for having toxic effects on the heart, kidneys, liver, reproductive system. Oxidative stress and modified antioxidative enzymatic defences (e.g., glutathione) are thought to be two major causes of citrinin's mediated toxic effects but the precise mechanism of its action is yet to be discovered [1]. More detailed understanding of citrinin's distribution between two tautomeric forms would help in dissecting the possible mechanism of its action.

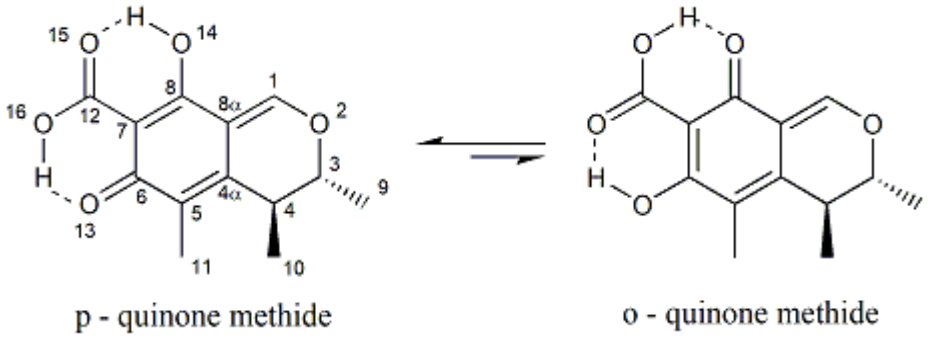

Fig. 1. Tautomeric forms of citrinin

The main goal of this study is to model the ^{17}O NMR spectrum of citrinin in the dichloromethane (DCM) solution in order to compare it to an experimental spectrum from previous studies [2]. The measured ^{17}O NMR spectrum of citrinin is interesting as its qualitative shape is not consistent with citrinin's tautomeric distribution implied by the ^{1}H and ^{13}C NMR spectra measured in the same study. In addition, the ^{17}O NMR signals from oxygen atoms 13 and 14 exhibit additional peaks, almost doublets, which is intriguing because the interconversion between two tautomers should occur at a high rate so that only single peak should be seen in the spectrum [2]. Our computational approach allows evaluating the ^{17}O NMR spectrum of both individual tautomers. Thus, the comparison between theoretical tautomer-averaged spectrum and the experimental spectrum allows us to estimate the populations of each tautomer of citrinin in DCM solution.

Molecular dynamics (MD) simulations were executed for *para*- and *ortho*-citrinin in DCM using an all-atom OPLS force field. The standard Coulomb plus 12-6-type Lennard-Jones potential was used, and atomic point charges were derived by fitting to the quantum mechanical electrostatic potential according to the CHelpG scheme. NMR shielding constants were calculated for isolated molecular species of citrinin. To account for solvation, the hybrid quantum mechanics/molecular mechanics (QM/MM) calculations were considered. These calculations were performed for a set of molecular solute-solvent snapshots extracted from the MD trajectory for each tautomer.

In this study, it was shown that the calculated ^{17}O NMR spectrum of citrinin, constructed using experimental *para*- to *ortho*- tautomeric ratio, corresponds qualitatively to the experimental spectrum. An optimized tautomeric ratio was calculated by comparing modelled and experimental NMR spectra. The optimized ratio improved modelled spectrum's quantitative correspondence to the experimental one and agreed well with the value of the experimental ratio. Furthermore, it was established that citrinin's diolic tautomer's existence is hardly plausible and its effect on the ^{17}O NMR spectrum of citrinin is negligible. On the other hand, forming of citrinin's cyclic dimers could positively affect the computed spectrum's quantitative correspondence to experimental data. Lastly, it was checked whether water existing in the citrinin NMR sample could have affected the ^{17}O NMR spectrum.

[1] J. W. G. de Oliveira Filho, et al. A comprehensive review on biological properties of citrinin. Food Chem. Toxicol. 110, 130–141 (2017).
[2] R. Poupko, Z. Luz, Carbon-13 NMR of Citrinin in the Solid State and in Solutions. Journal of Physical Chemistry A - J PHYS CHEM A 101, (1997).

ASYMMETRIC BETTI REACTION - SEARCHING FOR NEW LIGANDS

Martyna Malinowska, Anna Zawisza, Stanisław Leśniak

Department of Organic and Applied Chemistry, University of Lodz, Poland
martyna.malinowska@chemia.uni.lodz.pl

The Betti reaction is a special case of the aza-Friedel-Crafts reaction - one of the most useful method to create a carbon – carbon bond. The substrates used in the reaction are derivatives of imines and naphthol, which leads to 1-(α-aminoalkyl)-2-naphthols, called Betti bases [1]. Stereocontrolled variant of Betti reaction (Fig. 1) using chiral ligands and catalysts is an effective method leading to compounds with high application potential, commonly found in many biologically active compounds [2]. So far dinuclear zinc complexes [3] and bifunctional cinchona-derived organocatalysts [4] were successfully used in this reaction. Due to the promising biological and catalytic properties, synthesis of variously substituted derivatives of Betti bases become an interesting research problem for scientists from around the world. Based on previous literature, it can be concluded that there are only one example of biological studies on enantiomerically pure Betti base, where the inhibitory properties of botulinum neurotoxin A have been tested [5].

My poster will present the results that I obtained using new ligands in the Betti reaction.

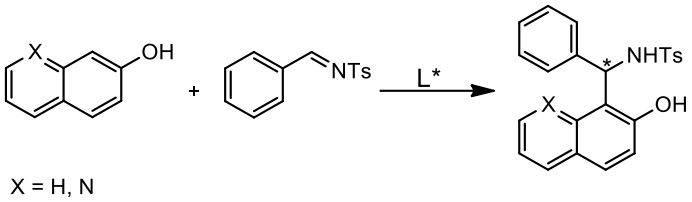

Fig. 1. Stereocontrolled Betti reaction.

[1] C. Cardellicchio, M. A. M. Capozzi, F. Naso, The Betti base: the awakening of a sleeping beauty, Tetrahedron: Asymmetry **21**, 507-517 (2010).
[2] H. Sasai et al., Enantio- and Diastereoselective Betti/aza-Michael Sequence: Single Operated Preparation of Chiral 1,3-Disubstituted Isoindolines, Organic Letters **19**, 5426-5429 (2017).
[3] X.-P. Hui et al., Asymmetric Aza-Friedel-Crafts Reaction of 2-Naphthol with Tosylimines Catalyzed by a Dinuclear Zinc Complex, Synlett **5**, 765-768 (2010).
[4] a) P. Chauhan, S. S. Chimni, Asymmetric Organocatalytic Aza Friedelï Crafts Reaction of Naphthols with N Sulfonyl Imines, European Journal of Organic Chemistry **9**, 1636-1640 (2011).
b) G. Liu, S. Zhang, H. Li, T. Zhang, W. Wang, Organocatalytic Enantioselective Friedel-Crafts Reaction of 1-Naphthols with Aldimines, Org. Lett. **13**, 828-831 (2011).
[5] L. A. Smith et al., Separation of Betti Reaction Product Enantiomers: Absolute Configuration and Inhibition of Botulinum Neurotoxin A, Med. Chem. Lett. **2**, 396-401 (2011).

HYDROGEN PRODUCTION FROM WATER SPLITTING USING PEROVSKITE NANOPARTICLES

Aldona Balį iÎ naitã, Dovydas Vdovinskis, Loreta Tamaġauskaitã-TamaġiÎ naitã, Eugenijus Norkus

Department of Catalysis, Center for Physical Sciences and Technology, Saulãtekio Ave. 3, LT-10257, Vilnius, Lithuania
aldona.balciunaite@ftmc.lt

In recent decades the use of fuel has grown drastically, which leads to the unavoidable truth that one day our planet will eventually run out of fossil fuels. This raises an important task to find an alternative to fossil fuels and to start using renewable energy or different fuels. One of the most commonly used renewable energy sources is fuel cells that directly convert the chemical reaction energy into electricity. Hydrogen, which can be produced from water, is applicable in such fuel cells.

In this work, the production of hydrogen from water splitting reaction is analyzed using different perovskite nanoparticles, which were prepared by a rapid microwave heating method. All syntheses of four different catalysts consist of $Co(NO_3)_2$*$6H_2O$ and $FeSO_4$*$7H_2O$ reagents with two of them being dissolved in water and the other two in ethylene glycol. Also, N-doped carbon material was added in those reaction mixtures with different dissolvents. The synthesis was carried out at a temperature of 150 ŰC for 30 min. The morphology and composition of synthesized nanoparticles were examined using Scanning Electron Microscopy (SEM), X-Ray Diffraction (XRD), and Inductively Coupled Plasma Optical Emission Spectroscopy (ICP-OES). The electroactivity of synthesized catalysts for the hydrogen evolution reaction (HER) was examined using cyclic voltammetry and linear sweep voltammetry at different temperatures in a KOH electrolyte. It was found that the $FeCoO_3$ and $FeCoO_3$/C exhibit an electroactivity for a hydrogen evolution due to the increase in current starting at about 1.4 V potential. The increase in temperature results in higher electroactivity of hydrogen evolution.

THE SPECTRAL PROPERTIES OF BORON-CONTAINING DYES AT LOW TEMPERATURES

Oleksandr Navozenko[1*], Valeriy Yashchuk[1], Mykhaylo Losytskyy[1], Yuriy Slominskii[2], Dalius Gudeika[3]

[1]Faculty of Physics, Taras Shevchenko National University of Kyiv, 64/13 Volodymyrs'ka Str., 01601 Kyiv; [2]Department of Colour and Structure of Organic Compounds, Institute of Organic Chemistry, National Academy of Sciences of Ukraine, Ukraine; [3]Department of Polymer Chemistry and Technology, Lithuania RadvilãnÔplentas 19, LT-50254, Kaunas Lithuania

a.navozenko@ukr.net

Much attention is being paid to the study of solid organic materials for the fabrication of high effective fluorescent materials [1]. In our previous investigations, the properties of thin composite films fabricated on the basis of the boron-containing dyes were studied [2]. Most important role in composite material efficiency belongs to the dopant molecules. Essential characteristic of the materials is functionality temperature. Therefore, the influnce of the temperature on the fluorescence spectra of dyes molecules was investigated.

In order to spectrally characterize the synthesized boron-containing substances and to further confirm the electron-vibrational nature of the bands in their fluorescence spectra, we have recorded absorption, fluorescence excitation and fluorescence emission spectra of the compounds solutions in acetonitrile at liquid nitrogen temperature (77 K) and compared them to those at room temperature (293 K).

Comparing the fluorescence spectra of solutions at 293 K and 77 K, the significant changes in the shape of the bands of the dye spectra has been found. At room temperature, the fluorescence spectra of dyes I and II possess two bands, while the dyes III and IV manifest only one band; at the same time, all the dyes possess two bands in the absorption spectra. The fluorescence intensity of the bands in the spectra increases significantly under lower temperature, which can be explained by the restriction of the dye molecules motion in the rigid medium. At the same time, the fluorescence spectra for these dyes are symmetric in comparison with the absorption spectra, and the fluorescence excitation spectra are similar to the absorption spectra. Fluorescence excitation anisotropy spectra were recorded for interpretation of the changes in the absorption and fluorescence spectra under liquid nitrogen temperature. These spectra also point to the electron-vibrational nature of the recorded bands in the fluorescence spectra. Phosphorescence of these dyes was also investigated.

Acknowledgement:This project has received funding from the Research Council of Lithuania (LMTLT), agreement No [S-LU-20-3].

[1] J. Li, J. Lin, Y. Huang et al., Organic fluorescent dyes supported on activated boron nitride: A promising blue light excited phosphors for high-performance white light-emitting diodes, Sci. Rep.**5** (2015).

[2] O.M. Navozenko, V.M. Yashchuk, Yu. P. Piryatinski et al., Ukr. J. Phys. **65**, N 3, 196-204 (2020).

SINGLE-PARTICLE MOTION IN A WOBBLING NUCLEUS - A CASE-STUDY FOR ODD-MASS ISOTOPES

Robert Poenaru[1,2] , Apolodor Aristotel Raduta[2,3]

[1] Doctoral School of Physics, University of Bucharest, Bucharest, Romania
[2] Department of Theoretical Physics, Horia-Hulubei National Institute of Nuclear Physics and Engineering, Bucharest-Magurele, Romania
[3] Academy of Romanian Scientists, Bucharest, Romania
robert.poenaru@protonmail.ch

The wobbling phenomenon in nuclei, which implies a precession of the total angular momentum combined with an oscillation of its projection onto the rotation axis, is analyzed within the Particle Rotor Model for odd-mass nuclei. Triaxial nuclei are objects with all three moments of inertia associated with the principal axes different in magnitude, making it possible for rotation to occur around all three axes. This results in a rich rotational spectrum with a collective character. Interpretation of the wobbling motion in odd-mass nuclei is usually done through a particle-rotor coupling, where an even-even triaxial is coupled to an odd-j nucleon which is said to be moving in a deformed quadrupole mean-field generated by the core itself. The strength of that potential is crucial in the description of the wobbling spectrum of a nucleus. In the present work, an analysis of the potential strength that characterizes the coupling between the core and the odd-nucleon is made, with the help of a deformed Nilsson potential in the total Hamiltonian of the system. A study of the coupling term is performed for different isotopes in which wobbling motion is known to occur.

EXTREMELY HEAVY RAIN AND VERY STRONG SQUALLS OVER LITHUANIA IN 1961-2020 PERIOD: ANALYSIS AND CLIMATOLOGY

Izolda Marcinonienă

Faculty of Chemistry and Geosciences, Vilnius University
izolda.marcinoniene@chgf.vu.lt

A brief overview of severe weather phenomena such as very heavy rain and very strong squalls over Lithuania in the last 60 years (1961ï 2020) is presented. Synoptic and climatological analyses of 218 cases with rain (Ó50 mm/12 h) and 38 cases of strong squalls (wind speed Ó28 m/s) from April to September (for squalls) and to November (for rain) were examined. All data used for research are taken from Lithuanian Hydrometeorological Service (LHMS) archives.

Extremely heavy rain and powerful squalls mainly develop in warm season. The synoptic situation favourable these severe weather phenomena to occur is formed usually by influence of the North Atlantic Ocean, Mediterranean Sea and Black Sea. Firstly, the Atlantic opens paths for wet and mild airmass, which merges with dry and warm continental airmass and due to big temperature and humidity contrasts creates instability in the whole column of the atmosphere over the country. Atmospheric convection becomes especially active when a warm upper ridge over the northern part of Ukraine, or western part of Russia, is replaced by cold trough moving from W/NW Europe or Scandinavia and pushing the heat eastward (Fig. 1).

As a result, it was determined that 1/3 of heavy rain cases formed by passage of cold airmass: cold or secondary cold fronts (17 % of cases) and cold wavy atmospheric fronts (15 % of cases). Respectively, synoptical situation leading to the development of squalls in Lithuania is following: S/SE troughs from Scandinavian cyclones (39 %) and cold waving fronts (16 %).

Secondly, the results of analysis of the southern-southeastern flow at 500 hPa height from Mediterranean and Black Sea show that tropical airmass dominate in 27 % of cases with heavy rain and 16 % of cases with squalls, warm and occluded atmospheric fronts prevail in 23 % of rainy cases.

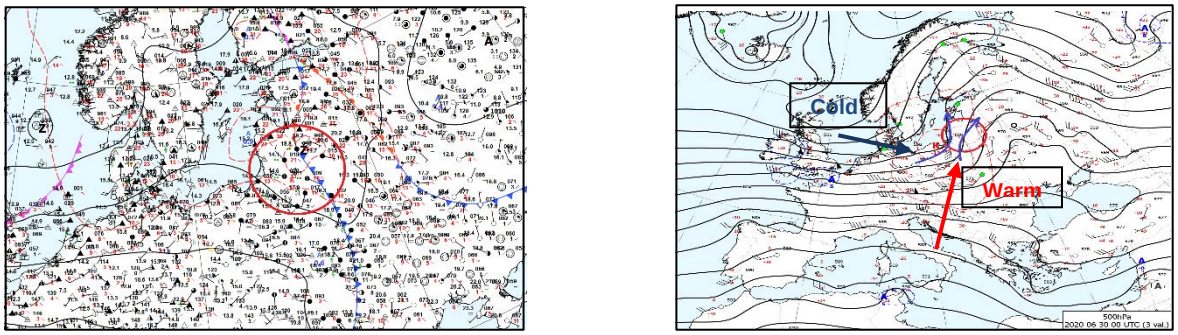

a) b)

Fig. 1. Severe weather case at 00 UTC on 30th of June, 2020: synoptic analysis (a); flow and divergence at 500 hPa geopotencial height (b)

Short range heavy rain (<3 h) and squalls associated with lines of convergence in tropical airmass and are predominant at day and evening; long lasting rain (11ï 12 h) associated with warm and occluded fronts are more often at night and morning.

Rain with 50ï 65 mm is prevailing (74 % of places with rain), squalls with wind gusts 28ï 32 m/s predominate in 86 % of all registered places with squalls.

In fact, on an average 4 heavy rain events per year, and 1 squall per 2 years registered in Lithuania. Considering to squalls locality, the real number of occurences is higher: it is to be supposed near to 2ï 4 very strong squalls per year.

The areas of distribution of both phenomena in Lithuania are different: heavy rain is more often phenomenon in the NW regions, strong squalls ï in the SW and NE parts. It is hard to avoid subjectivity in squalls observations. Obviously, it is a good correlation between density of population and number of squalls ï the more people use technics (mobile phones, cameras etc.), the more events they report to LHMS or media.

Increasing of intensity of extreme weather phenomena is one of the features of climate change impact in the Baltic region. To provide more clarity, mean annual temperature and precipitation anomalies and trends as symptoms of climate change are presented in the poster.

THEORETICAL ANALYSIS OF THE CONFORMATIONS AND IR SPECTRA OF THE HYDROGEN TRIOXIDE (HOOOH) DIMERS

Darya Kisurina[1], Ulyana Hatkevich[1], Danyil Voloshchuk[1], Zlata Lepenkova[1], George Pitsevich[1], Valdas Sablinskas[2]

[1]Belarusian State University, Minsk, Belarus
[2]Vilnius University, Vilnius, Lithuania
kisurinadasha@gmail.com

Hydrogen trioxide (HOOOH) molecule plays an important role in different atmospheric phenomena [1-3] as well as in functioning of biological systems [4,5]. However, the establishment of its spectral and structural characteristics is largely hampered by the ability of this molecule to form associates. To date, practically nothing is known about the spectral and structural characteristics of clusters of the hydrogen trioxide molecule, including its simplest associate, a dimer. Therefore, we made efforts to search for the conformational diversity of dimers of hydrogen trioxide molecules, as well as their spectral characteristics. We optimized the geometry of the dimers starting from different initial points using B3LYP/cc-pVTZ level of theory. At least four equilibrium geometries of the dimers were found. The configurations of three of the found conformers belong to the point symmetry groups C_2, C_i, and C_S. The fourth conformer is characterized by the absence of symmetry elements. We will denote the corresponding conformers of the hydrogen trioxide molecule dimer as follows: D_2, D_i, D_S and D_1. Equilibrium configurations of these conformers are represented on Fig.1,2.

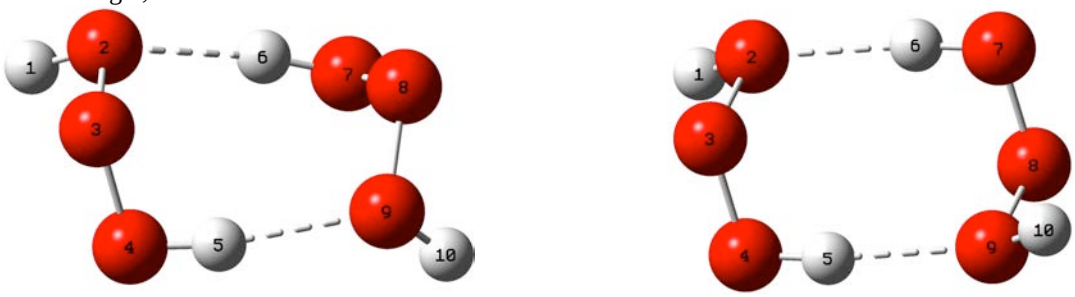

Fig. 1. Equilibrium configurations of the D_2 (left) and D_i (right) conformers of the dimers of the hydrogen trioxide molecules.

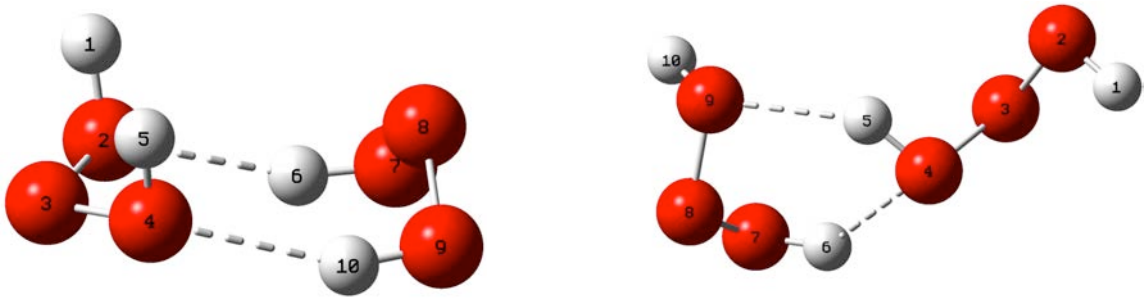

Fig. 2. Equilibrium configurations of the D_S (left) and D_1 (right) conformers of the dimers of the hydrogen trioxide molecules.

As one can see the conformers D_2, D_i and D_1 are ñmadeò from trans- conformers of the hydrogen trioxide molecules. The conformer D_S is ñmadeò from cis- conformers of the hydrogen trioxide molecules. All conformers form a double hydrogen bond. It is known that the trans-conformer of the hydrogen trioxide molecule is energetically preferable to the cis-conformer [6]. Presumably, due to this fact, conformer D_S turnes out to be energetically least preferable in comparison with other conformers. The D_i conformer has the lowest energy. IR spectra of all conformers were calculated at B3LYP/cc-pVTZ level of theory in harmonic and anharmonic approximations.

[1] D. Cannon, T. Tuttle, J. Koller, B. Plesniļar, Comp.Theor.Chem. 1010 (2013) 19
[2] C. Murray, E.L. Derro, T.D. Sechler, M. Lester, Acc.Chem.Res. 42 (2009) 419
[3] W. Zheng, D. Jewitt, R. Kaiser, Phys.Chem.Chem.Phys. 9 (2007) 2556
[4] P. Wentworth Jr., L. Jones, A. Wentworth, X. Zhu, N. Larsen, I. Wilson, X. Xu, Science 293 (2001) 1806
[5] X. Zhu, P. Wentworth Jr., A. Wentworth, A. Eschenmoser, N. Larsen, Proc.Natl.Acad.Sci. USA 101 (2004) 2247
[6] G. Pitsevich, A. Malevich, U. Sapeshka, Chem.Phys., 530 (2020) 110633

THE TRANSITION FROM NON EQUIDISTANT TO EQUIDISTANT GRID FOR THE TORSION COORDINATE OF THE CH_3 GROUP WHEN CALCULATING MULTIDIMENSIONAL POTENTIAL ENERGY SURFACES

Anton Serko[1], Pavel Peretruhin[1], Alex Malevich[1], George Pitsevich[1], Dmitry Shender[1], Darya Kisuryna[1], Vitas Balevicius[2]

[1]Belarusian State University, Minsk, Belarus
[2]Vilnius University, Vilnius, Lithuania
kisurinadasha@gmail.com

Potential energy surface is an important characteristic of molecules and clusters. To be able to take into account symmetry properties of considered molecules it is important to calculate energy values at the nodes of the multidimentional equidistant grid. Usually there is no problem with this aspect with valence and bending coordinates. However, this problem arises every time when one of the tops on internal rotation axis contains more than one atom. One of such tops is CH_3 (methyl) group and dimethyl peroxide molecule (as example, see Fig.1) contains two of these tops.

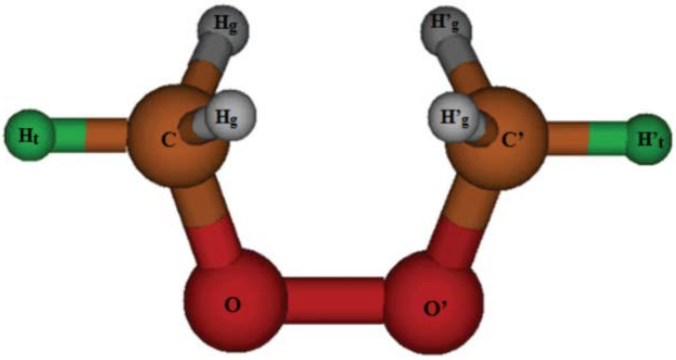

Fig.1. Not equilibrium configuration of the dimethyl peroxide molecule.

It is clear that the internal rotation of the CH_3 groups in dimethyl peroxide molecule around C-O bonds is one dimensional vibrational task. Since carbon atoms are connected with three hydrogen atoms, torsional coordinates γ_1 and γ_2 must be determined as the average of the sum of three dihedral angles:

$$\gamma_1 = \left(\angle H_t COO' + \angle H_g^1 COO' + \angle H_g^2 COO'\right) : 3 \qquad (1)$$

It is well known that CH_3 group loses its C_{3V} local symmetry. It means that the dihedral angles $\angle H_t CH_g O$ are not equal to 120^0 and can change during internal rotation. One can see that the value of $\gamma_1 = 60°$ can be obtained by many different ways (see (1)). Thus, that several values of potential energy and kinematic coefficients will correspond to one value of the torsion angle. To avoid this problem only one dihedral angle (for example $\angle H_t COO'$) is frozen while the values of two other dihedral angles are determined during optimization process. However, the resulting value of the torsional coordinate will slightly differ from the desired one.

In this work, we introduced two methods of the transition from non equidistant to equidistant grid for the torsion coordinate of the CH_3 group when calculating multidimensional potential energy surfaces. The first one is based on interpolation by cubic splines. While the second one is based on solving a system of linear equations using least squares methods. Results of both methods are compared.

HYDROXYL AND METHYL GROUPS TUNNELING PROBABILITY IN THE $HOOCH_3$ MOLECULE CALCULATED AT MP2/cc-pVQZ LEVEL OF THEORY TAKING INTO ACCOUNT ZPVE

Uladzimir Lazicki[1], Egor Molokanov[1], Alex Malevich[1], George Pitsevich[1], Olga Soroka[1], Aleksandr Shastin[1], Darya Kisuryna[1], Vitas Balevicius[2]

[1]Belarusian State University, Minsk, Belarus
[2]Vilnius University, Vilnius, Lithuania
kisurinadasha@gmail.com

Earlier we have reported our data on torsional IR spectrum of the methyl hydroperoxide ($HOOCH_3$) molecule calculated at MP2/cc-pVQZ level of theory [1]. The method used for calculation is described in [2-6]. This molecule (see Fig.1) has two internal tops: the hydroxyl group (OH) which can rotate around the O-O bond and the methyl group (CH_3) which can rotate around the C-O bond.

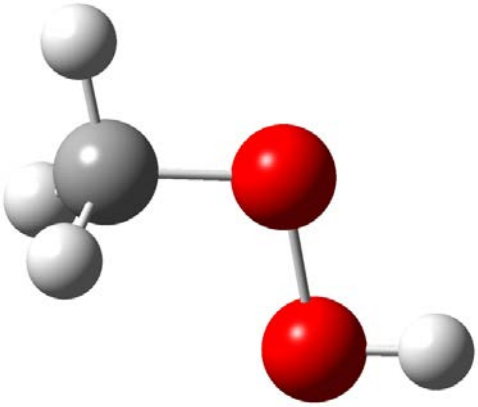

Fig. 1. The equilibrium structure of the methyl hydroperoxide molecule.

According to [1] calculated value of the hydroxyl group tunneling frequency of the methyl hydroperoxide molecule in the ground state is equal to 19.23 cm^{-1}. However, the experimental value of the hydroxyl group tunneling frequency according to [7] is equal to 14.97 cm^{-1}. We assumed that this disagreement between theory and experiment in the hydroxyl group tunneling frequency of the methyl hydroperoxide molecule occurs due to the failure to take into account zero point vibrational energy (ZPVE). Since authors of the [8] have took into account ZPVE of the methyl hydroperoxide molecule in the harmonic approximation, we decided to calculate this energy in anharmonic approximation. Because calculation of the IR spectrum in anharmonic approximation takes a lot of time we carried out this work using MP2/cc-pVTZ level of theory. After ZPVE was calculated it was added to 2D potential energy surface and this total energy was used to calculate tunneling frequency for the hydroxyl group. In this case, it turned out to be equal to 13.03 cm^{-1}. One can see that this result is much closer to the experimental one.

[1] Uladzimir Lazicki, Torsional spectrum of the Methyl Hydroperoxide molecule calculated at MP2/cc-pVQZ / Uladzimir Lazicki, Zlata Lepenkova, Darya Kisuryna , Alex Malevich , George Pitsevich , Vitas Balevicius // Open Readings 2020: 63nd Scientific Conference for Students of Physics and Natural Sciences: programme and abstracts/ Vilnius University; ï Vilnius, 2020. ï P.300
[2] G. Pitsevich, A. Malevich, V. Sapeshko, J.Mol.Spectr., 360 (2019) 31-38.
[3] G. Pitsevich, A. Malevich, V. Sapeshko, Chem.Phys., 530 (2020) 110633.
[4] G. Pitsevich, A. Malevich, F. Markovich U. Sapeshka, Mol.Phys., 118 (2020) e1746425
[5] G. Pitsevich, A. Malevich, D. Kisuryna, A. Vasilevsky, A. Vasilevich, U. Sapeshka, A. Kamnev, Spectrochim. Acta, Part A, 239 (2020) 118209.
[6] G. Pitsevich, A. Malevich, D. Kisuryna, A. Ostyakov, U. Sapeshka, J.Phys.Chem., A, 124 (2020) 8733-8743.
[7] M. Tyblewski, T.-K. Ha, R. Meyer, A. Bauder, C. Blom, J.Chem.Phys., 97 (1992) 6168-6180.
[8] S. Dalbouha, M. Senent, N. Komiha, J.Chem.Phys., 142 (2015) 074304.

REFRACTIVE INDEX SENSOR FOR LIQUIDS BASED ON DIFFRACTION EFFICIENCY MEASUREMENT

Tomas Klinavičius[1], Mindaugas Juodėnas[1], Andrius Čiutautas[1,2], Tomas Tamulevičius[1,2]

[1] Institute of Materials Science, Kaunas University of Technology, Lithuania
[2] Department of Physics, Kaunas University of Technology, Lithuania
tomas.klinavicius@ktu.edu

The refractive index of a material is a dimensionless quantity that defines a ratio of phase velocity of light in a vacuum and that material [1]. Refractive index sensors of liquids are important for chemical analysis, and there are many different constructions of these sensors proposed [2-4]. However, these solutions tend to not be aimed at small samples of liquid.

In this work, we propose a design and working principle for a microfluidic refractive index sensor based on diffraction efficiency measurement. It works by measuring the changes of diffraction efficiency at some wavelength before and after liquid intake, as the change of the diffraction grating superstrate influences its diffraction efficiency. The change in diffraction efficiency is related to the refractive index of liquids by using the Rigorous Coupled Wave Analysis method [5] to model a diffraction grating under different conditions (refractive indexes of superstrate). Typical situation of diffraction efficiency dependence on grating height for different superstrates is depicted in Fig. 1.

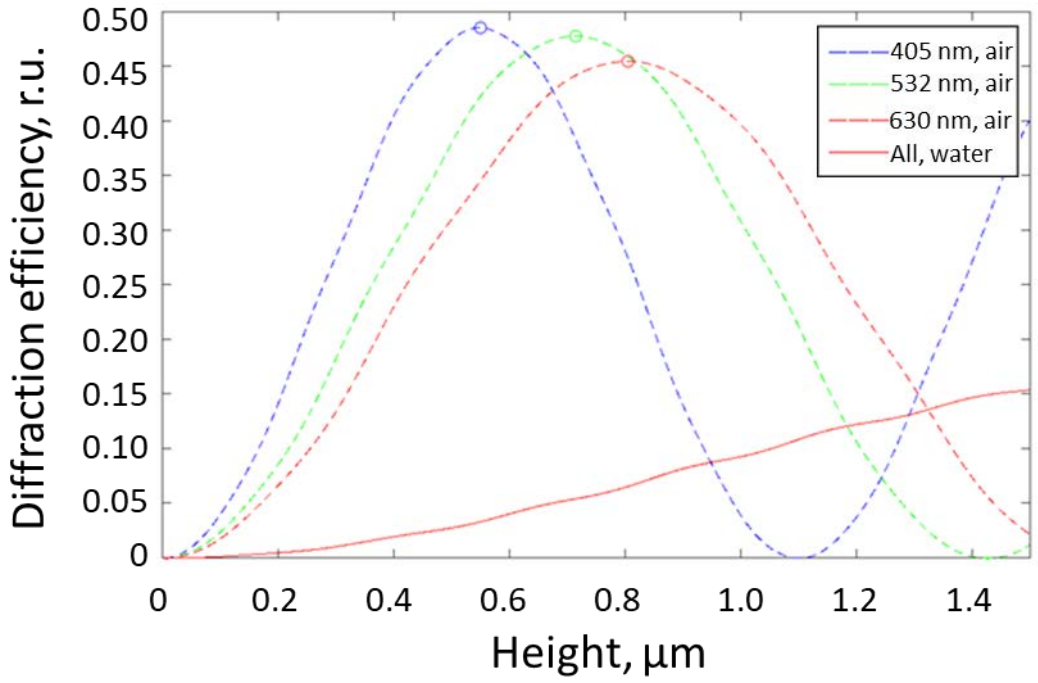

Fig. 1. Concept of sensor working principle – light transmission changes from high (microfluidic filled with air) to low (microfluidic filled with water) at a certain grating height. In case of water, efficiencies of all wavelengths were identical

[1] E. Hetch, Optics, Pearson, ISBN 978-0-321-18878-6, (2016).
[2] T. Tamulevičius, et al. Refractive index sensor based on the diamond like carbon diffraction grating, Thin Solid Films **519**, 4082-4086 (2011).
[3] T. Tamulevičius, et al. Numerical and experimental analysis of optical response of sub-wavelength period structure in carbonaceous film for refractive index sensing, Optics Express **22**, 27462-27475 (2014).
[4] R. Selvas-Aguilar, et al., Noncontact Optical Fiber Sensor for Measuring the Refractive Index of Liquids, Journal of Sensors **2016**, 1-6 (2016).
[5] M. G. Moharam, e al., Stable implementation of the rigorous coupled-wave analysis for surface-relief gratings: enhanced transmittance matrix approach, Journal of the Optical Society of America A **12**, 1077-1086 (1995).

IDENTIFICATION OF NUMBER, FREQUENCY, AND POWER OF SOURCES OF ELECTROMAGNETIC RADIATION IN THE HUMAN LIVING AREA

Zoya Tsoy, Artūras Jukna

Photovoltaic Technologies Laboratory, Department of Physics, Vilnius Gediminas Technical University, Lithuania
zoya.tsoy@stud.vilniustech.lt

Current electronic devices and systems developed for remote communication (*e.g.* wireless/radio communication, electric power transfer, smartphones, tablets, and laptops, *etc*.) become sources of electromagnetic pollution. Although the harm to living organisms caused by electromagnetic pollution is still open to question, the electromagnetic pollution classified as potentially carcinogenic. The sources of extremely low frequency electromagnetic fields (< 300 Hz), intermediate electric fields (300 Hz – 100 kHz), radio frequency electric field (100 kHz – 300 GHz) are classified as sources of the electromagnetic pollution that influence living organisms making harm to their reproductive system [1], memory performance [2], oxidative stress [3], blood parameters and myocardium [4] *etc*. For these reasons, it is very important to understand the impact of electromagnetic pollution on living organisms, stay safe and protected from the potentially harmful effects and/or to leave as soon as possible unsafe of high power radiation environment.

The effect of electronic device's radiation on living organisms increases with increasing frequency [5] and decreasing distance to the source of radiation since the most efficient absorption of the radiant by radiation strongly absorbing bodies happens to be at λ-depth (here λ is the wavelength of the electromagnetic wave). Therefore, the most dangerous for living organisms are radiation sources that come into direct contact with their body (*e.g*. smartphones, wireless headphones, Bluetooth devices) or appear to be located nearby (*e.g.* Wi-Fi routers, computer screens, microwave ovens, etc.) [6]. However, living in urban areas quite often we have no enough information about radiation sources (*i.e.* their exact location and radiation power) and therefore getting exposed to radiated electromagnetic waves.

We propose a method for detection of a location of an "unknown" radiation source of GHz frequency signals and demonstrate that it works well in the case of human living room if the source of radiation is located outside the living area. The radiation source (blue triangle in Fig. 1) set to radiate signals of fixed frequency ranging from 0 to 6 GHz. The power of radiation we measured by a detector (yellow circle) through moving it from one fixed position (blue circles) to another when the signals receiving antenna of the detector is located at different heights from the laboratory ground ranging from 0.4 m to 1.2 m. (Fig.1).

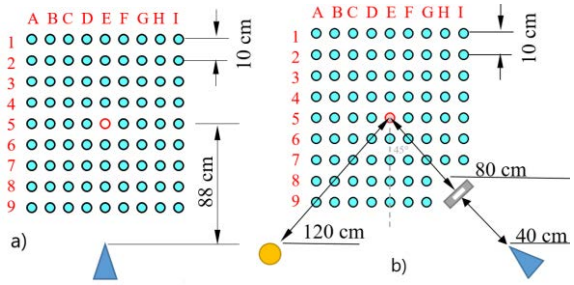

Fig. 1. The 0° (a) and 45° (b) setups we used for identification of the objects (located in a coordinate E5) reflected radiation power from the radiation source (blue triangle imitating an "unknown" source, radiating fixed frequency in the range of 0-6 GHz). For radiation power detection, we used an 8GHz detector, and for the radiation beam adjustments a diaphragm shown by grey rectangular shown in (b).

The experimentally measured radiation power verified through results of our calculations of the power rate using inverse distance square law helped us to recognize the presence of the "unknown" source of radiation, to determine its exact position (distance, height) in a room, and to estimate the magnitude of radiated power at various fixed positions in the room. The precision of the method depends on the signal-to-noise ratio and magnitude of the signals reflected from random surfaces of laboratory stuff and reaches the maximal value at the highest signal-to-noise ratio in the case when both the signals radiating antenna and the detector are located in an echo-free chamber.

[1] M. Saygin, O. Ozmen, O. Erol, *et al.* The impact of electromagnetic radiation (2.45 GHz, Wi-Fi) on the female reproductive system: The role of vitamin C. Toxicology and Industrial Health **34**,620-630 (2018).
[2] M. Foerster, A. Thielens, W. Joseph, M. Eeftens, M. Röösli. A Prospective Cohort Study of Adolescents' Memory Performance and Individual Brain Dose of Microwave Radiation from Wireless Communication. Environ Health Perspectives **126**, 077007 (2018).
[3] S. Santini, V. Cordone, S. Falone, M. Mijit, C. Tatone, F. Amicarelli, G. Di Emidio. Role of Mitochondria in the Oxidative Stress Induced by Electromagnetic Fields: Focus on Reproductive Systems. Oxidative medicine and cellular longevity **2018**, 5076271 (2018).
[4] V.P. Kalanjati, K.E. Purwantari, L. Prasetiowati. Aluminium foil dampened the adverse effect of 2100 MHz mobile phone-induced radiation on the blood parameters and myocardium in rats. Environmental Science and Pollution Research **26**, 11686-11689 (2019).
[5] L. Vinoth Kumar, E. Manikanta, Ch. Leela, and P. Prem Kiran. 2016. Effect of laser intensity on radio frequency emissions from laser induced breakdown of atmospheric air. J. Appl. Phys. **119**, 214904 (2016).
[6] K.K. Kesari, S. Kumar, J. Behari. Pathophysiology of microwave radiation: effect on rat brain. Applied Biochemistry and Biotechnology **166**, 379–388 (2012).

CHARACTERIZATION AND SPECTRAL PROPERTIES OF THERMOGRAPHIC PHOSPHORS FOR OPTICAL THERMOMETRY APPLICATIONS

Anastasija Supranovič[1], Akvilė Zabiliūtė-Karaliūnė[1], Artūras Katelnikovas[2], Pranciškus Vitta[1]

[1]Vilnius University, Faculty of Physics, Institute of Photonics and Nanotechnology, Saulėtekio al. 3, LT-10257 Vilnius, Lithuania

[2] Institute of Chemistry, Faculty of Chemistry and Geosciences, Vilnius University, Naugarduko 24, LT-03225 Vilnius, Lithuania

anastasija.supranovic@ff.stud.vu.lt

Measurement of the surface temperature is a crucial factor in many industrial processes and their optimization. To fulfill the strict requirements and yield accurate temperature measurements, many kinds of sensing devices have been employed, e.g. thermocouples or infrared thermometer. Surface contact temperature sensors, like thermocouple, can sometimes result in poorly characterized results, as a consequence, non-contact thermometers are more preferred for temperature sensing.[1] Although IR thermometer provides the non-contact measurements, its signal may be affected by the background radiation. A revolutionary alternative to the above approaches is phosphor thermometry that implies observation of change in radiation intensity of luminescent phosphor materials in respect to the variations of temperature.[1] Optical temperature sensing relies on the temperature dependent properties of rear-Earth luminescent materials, i.e. phosphors that emit visible, IR or UV radiation upon excitation. The temperature variation is reflected by the change in fluorescence intensity.[1, 2] Studies of phosphor thermometer technology are well documented.

In this study, the spectral properties of two synthesized phosphors prepared by a high temperature solid state reaction [3] - $Lu_3Al_5O_{12}$: 0.5%Ce^{3+} (LuAG) and $Eu_2Mo_4O_{15}$ (EMO) - were analyzed and their applicability for optical thermometry was investigated. The samples of each phosphor were prepared by mixing 15 wt% with silicone and letting them to solidify in 2 mm deep molds as shown in Fig. 1(a).

Data collection was performed with a standard technique involving the use of integrating sphere and measurement of phosphors spectra in A, B and C configurations. The spectral properties such as Photoluminescence (PL), PL efficiency, and PL dependence on the temperature were measured. PL quantum efficiency was determined in line with the analysis described by de Mello (1997). [4] Excitation sources used for LuAG were 450 nm and 468 nm, while in EMO case, a 463 nm source was included. The results have shown that EMO is strongly dependent on the ambient temperature, whereas LuAG was found to be more stable with the changes in temperature.

During the presentation, results of temperature dependence of LuAG and EMO PL spectra as well as fluorescence intensity ration for temperature determination will be demonstrated.

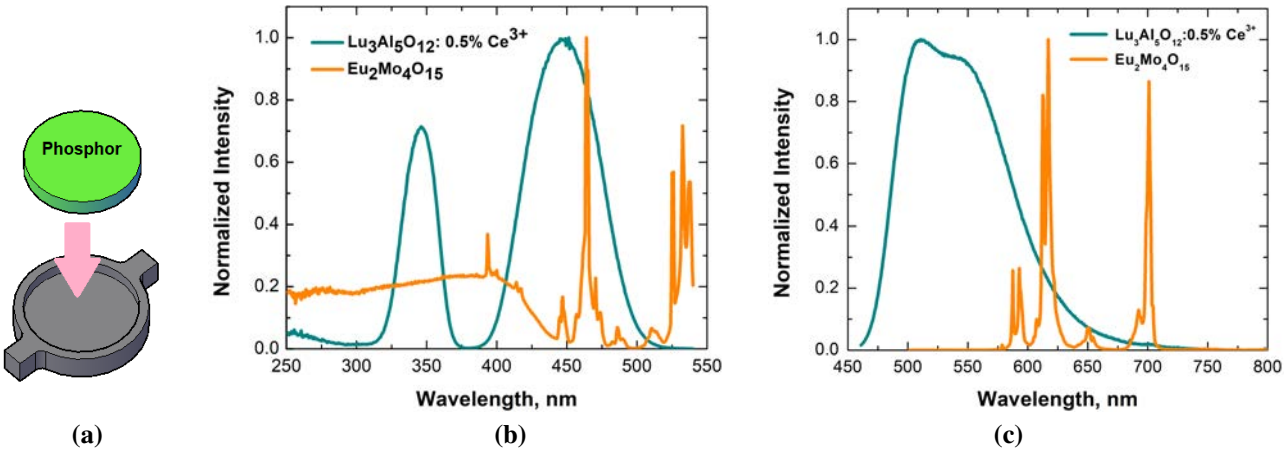

(a) **(b)** **(c)**

Fig. 1. Methodology and experimental results: figure (a) is an illustration of used mold for sample production, (b) and (c) are excitation and photoluminescence spectra of both $Lu_3Al_5O_{12}$: 0.5%Ce^{3+} and $Eu_2Mo_4O_{15}$, respectively.

[1] X. Wang, Q. Liu, C.-S. Liu, Y. Bu, Optical temperature sensing of rare-earth ion doped phosphors, RSC Adv **105**, 86219–86236 (2015).

[2] Y. Zhao, X.Wang, Y. Zhang, Y. Li, Optical temperature sensing of up-conversion luminescent materials: Fundamentals and progress. J. Alloy. Compd. **817**, (2020) 152691.

[3] M. Janulevicius, J. Grigorjevaite, G. Merkininkaite, S. Sakirzanovas, A. Katelnikovas, Luminescence and luminescence quenching of $Eu_2Mo_4O_{15}$, J. Lumin. **179**, 35-39 (2016).

[4] J. C. de Mello, H. F. Wittmann, R. H. Friend, An Improved Experimental Determination of External Photoluminescence Quantum Efficiency, Adv. Mater. **9**, 230-232 (1997).

STUDY OF SAM WITH IMIDAZOLE FUNCTIONAL GROUP BY SURFACE AND SHELL-ISOLATED NANOPARTICLE ENHANCED RAMAN SPECTROSCOPY

Domantas Dunajevas[1], Agnã Zdaniauskienã[2], Martynas Talaikis[2], Rita Sadzeviļienã[2], Gediminas Niaura[2]

[1] Institute of Chemical Physics, Faculty of Physics, Vilnius University, Lithuania
[2] Department of Organic Chemistry, Center for Physical Sciences and Technology, Lithuania
domantas.dunajevas@ff.stud.vu.lt

Histidine is an amino acid with a unique structure that allows it to take part in various molecular interactions. The focus is on the side chain of histidine ï the imidazole ring, which coordinates many metal ions. Because histidine interacts in multiple ways with other amino acids and metal ions [1], further research is required to better understand the role of histidine in protein interactions.

One of the most informative and nonï destructive methods used to determine the structure and properties of materials on a molecular scale is surface-enhanced Raman spectroscopy (SERS) [2]. Unfortunately, the method has some downsides ï only a small number of metals are SERS active, and a metal substrate must be nanostructured, which renders the method useless for systems on smooth surfaces. In 2010 a new method of enhancing Raman signal was introduced, which suggested using Au or Ag nanoparticles with a thin inert shell [3]. The method of shell-isolated nanoparticle-enhanced Raman spectroscopy (SHINERS) suitable with any substrate, and the thin shell does not allow the SERS-active cores to interact with each other and with the probed molecules.

The main aim of this study was to identify the molecular structure of the selfï assembled monolayer (SAM) formed from N-(2-(1H-imidazol-4-yl)ethyl)-6-mercaptohexanamide (IMHA) in an aqueous solution applying SERS and SHINERS methods. For the SERS method, the SAM was adsorbed on a roughened Au electrode, while for the SHINERS method ï on a smooth Au electrode. Moreover, SHINERS method employing $Ag@SiO_2$ nanoparticles.

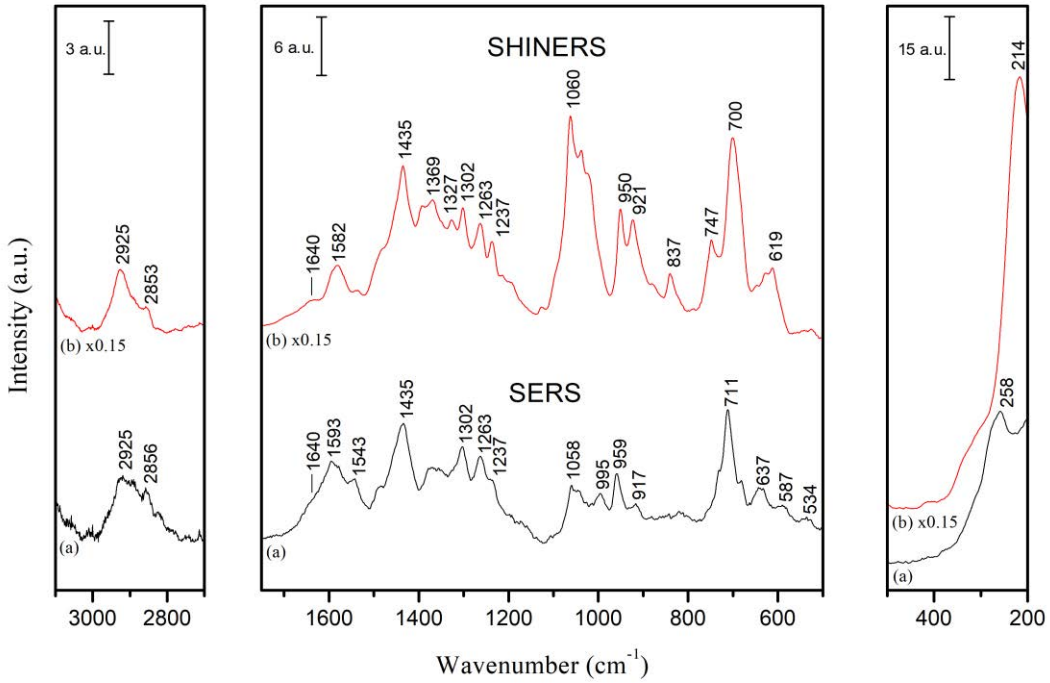

Fig. 1. SERS spectra of IMHA adsorbed on on a roughened Au electrode (a) and SHINERS spectra of IMHA adsorbed on a smooth Au electrode in an aqueous solution solution (b). Excitation wavelength is 785 nm.

During this study, it was found that the symmetric stretching vibration of methylene groups is at slightly lower wavenumbers in the SHINERS spectrum (2853 cm^{-1}) compared with the SERS spectrum. This result is remarkably related to a higher level of ordering for SAM prepared on smooth Au substrate.

[1] S. M. Liao, Q. S. Du, J. Z. Meng, Z. W. Pang, and R. B. Huang, The multiple roles of histidine in protein interactions, Chemistry Central Journal **7**, 9ï 11 (2013).
[2] G. Niaura, Paviršiumi sustiprinta Ramano spektroskopija, *Paviršiaus optinã spektroskopija*, 113ï 150 (2008).
[3] J. F. Li et al., Shell-isolated nanoparticle-enhanced Raman spectroscopy, Nature **464**, 392ï 395 (2010).

STUDY OF PATHOGENIC BACTERIA AND FUNGI BY MEANS OF FTIR ATR SPECTROSCOPY

Gerda MickÎ naitã[1], Aida Kamarauskienã[2], Justinas Ļeponkus[1], Eglã Lastauskienã[2], Rimantã Bandzeviļ iÎ tã[1]

[1]Chemical Physics Institute, Faculty of Physics, Vilnius University, Saulãtekio Av. 3, LT-10257 Vilnius, Lithuania
[2]Institute of Biosciences, Life Sciences Center, Vilnius University, Saulãtekio Av. 7, LT-10257 Vilnius, Lithuania
gerda.mickunaite@ff.vu.lt

Pathogenic microorganisms such as bacteria or fungi, can cause infectious diseases. Currently, medications are usually prescribed to cure patients of infectious diseases. Antibiotics are used for the treatment of bacterial infections and antifungals for the yeast caused infections. It is known that bacteria can develop antibiotic resistance while fungi are not sensitive for the treatment by antibiotics and vice versa. In mixed infections, only one domain of pathological microorganism (eukaryote or procaryote) can be killed while allowing another to spread even faster. For this reason, it is important to identify the species of microorganisms early to accurately prescribe the treatment. In the case of fungal infections, it is important to identify the type of the cell death: apoptosis or necrosis. It is known that during necrotic way of cell death the ROS, damaged proteins, toxins and etc are released to the surrounding environment and can cause secondary inflammation. Therefore, apoptotic pathway is not causing the inflammatory effect, opposite, the compounds released from the apoptotic cell can be used by the host epithelium cells for the regeneration. Currently, the identification of bacteria and fungi can take up to three days and the accuracy of the identification ranges from 40 % to 100 %, while using FTIR ATR spectroscopy, identification can be carried out quickly and more accurately [1-2].

In this work, the method of an attenuated total reflection of infrared radiation (ATR IR) spectroscopy was applied for the analysis. ATR IR absorption spectra of 95 samples of different bacteria (32 samples, 9 different species) and fungi (63 samples, 3 different species) were analysed. The main differences between bacteria and fungi ATR IR absorption spectra were observed in the 1800 cm^{-1} ï 750 cm^{-1} region. In order to determine how accurately bacteria and fungi ATR IR absorption spectra can be identified, hierarchical cluster analysis (HCA) was performed. HCA was performed using Ward Algorithm, selecting the 1800 cm^{-1} ï 750 cm^{-1} spectral region. ATR IR absorption spectra of fungi and bacteria were separated into two clusters with 100 % accuracy.

In order to determine *Candida lusitaniae* fungi death mechanisms HCA was performed. HCA was performed using Ward Algorithm, selecting the 1724 cm^{-1} ï 1535 cm^{-1} spectral region. This spectral region was selected because the shift of Amide I spectral band at 1637 cm^{-1} was observed in the ATR IR absorption spectra of damaged by thermal shock *C. lusitaniae* fungi. HCA showed that ATR IR absorption spectra of undamaged, damaged by thermal shock and UV radiation *C. lusitaniae* can be grouped into different clusters with 100 % accuracy (Fig. 1.).

Spectral differences between ATR IR absorption spectra of different strains of *Geobacillus* sp. were observed in the 1183 cm^{-1} ï 930 cm^{-1} spectral range where the intensity of the spectral bands at 1277 cm^{-1} (proteins), 1382 cm^{-1} (carbohydrates), 1398 cm^{-1} (fatty and amino acids), 1440 cm^{-1} (lipids), 1453 cm^{-1} (alkanes and acyclic compounds) differ. HCA was performed for the ATR IR absorption spectra using Ward Algorithm, selecting the 1174 cm^{-1} ï 1164 cm^{-1} spectral region. ATR IR absorption spectra of *Geobacillus* sp. 612 and *Geobacillus* sp. 95 were separated into two clusters with 100 % accuracy.

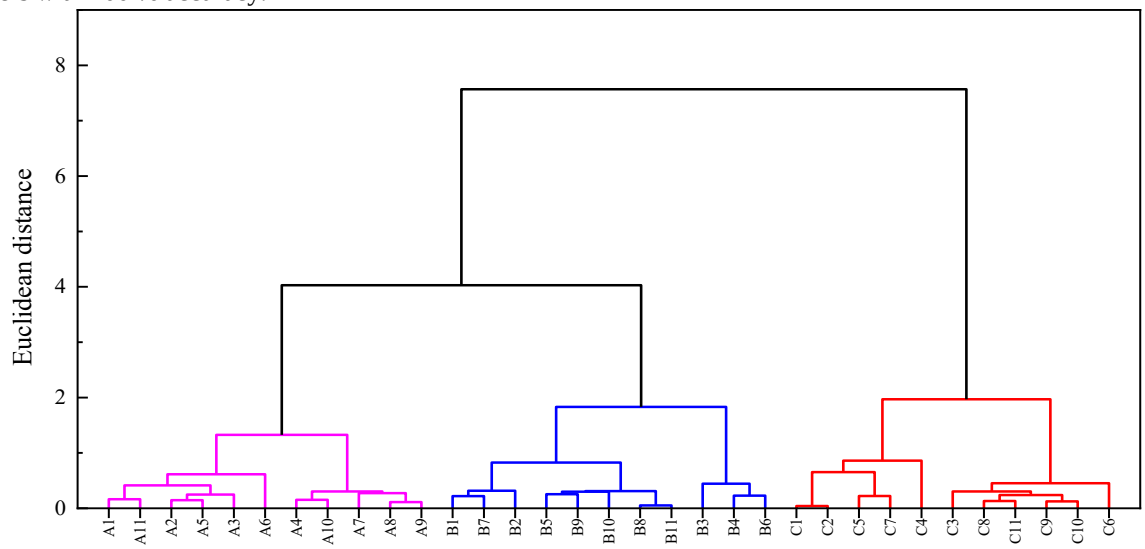

Fig. 1. HCA of ATR IR absorption spectra of undamaged, damaged by thermal shock and UV radiation *C. lusitaniae* fungi. Letter A refers to ATR IR spectra of undamaged, B ï damaged by UV radiation, C ï damaged by thermal shock *C. lusitaniae* fungi. The number following the letter indicates the sample number.

[1] M. Pigğowski, Int. J. Environ. Res. Public health **16**, 477 (2019)
[2] M. Harz et al., Cytometry **75A**, 104-113 (2009)

SPECTROSCOPIC ELLIPSOMETRY INVESTIGATION OF UNIFORMITY OF DIAMOND-LIKE CARBON AND SILVER NANOCOMPOSITE THIN FILM

Auġrinã Jurkeviļ iÎ tã[1,2,3*], Paulius Dolmantas[1,2], Tomas Tamuleviļ ius[1,2], Juris Prikulis[3]

[1] Institute of Materials Science of Kaunas University of Technology, K. Barġausko st. 59, LT-51423, Kaunas, Lithuania
[2] Department of Physics, Faculty of Mathematics and Natural Sciences, Kaunas University of Technology, StudentÔst. 50, LT-51368, Kaunas, Lithuania
[3]Institute of Chemical Physics, University of Latvia, Jelgavas st. 1, LV-1004, Riga, Latvia
*ausrine.jurkeviciute@ktu.lt

For many applications, uniformity of thin films is among the most desired properties. The thin film must have the same properties in the large area. For plasmonic applications (e.g. optical sensors), optical properties of thin film should not change within the whole film. In nanocomposite materials, optical properties depend on layer thickness, optical constant of constituent materials, concentrations of constituent materials, nanoparticles size distributions, etc. All this has to vary as little as possible.

In this work, diamond-like carbon nanocomposite with silver nanoparticles (DLC:Ag) on silicon substrate was investigated. Sample was prepared in unbalanced magnetron sputtering system in direct current mode with silver target in place. The current was 0.1 A, the voltage was 366 V, the pressure was 7.8 Ĭ 10^{-3} mbar, argon flow rate was 80 sccm, acetylene flow rate was 17.5 sccm, growth time was 1132 s. To the naked eye, the sample appeared quite uniform, except around the edges. Thorough analysis of uniformity was carried out employing GES5-E (Semilab) rotating compensator spectroscopic ellipsometer in the reflection mode. Incidence angle was set to 75Áand the spectra was recorded by CCD detector from 250 nm to 950 nm. The surface of the sample was scanned at 22 positions in one line, with 0.5 mm distance between each position. Resulting ellipsometric parameters spectra are depicted in Fig. 1.

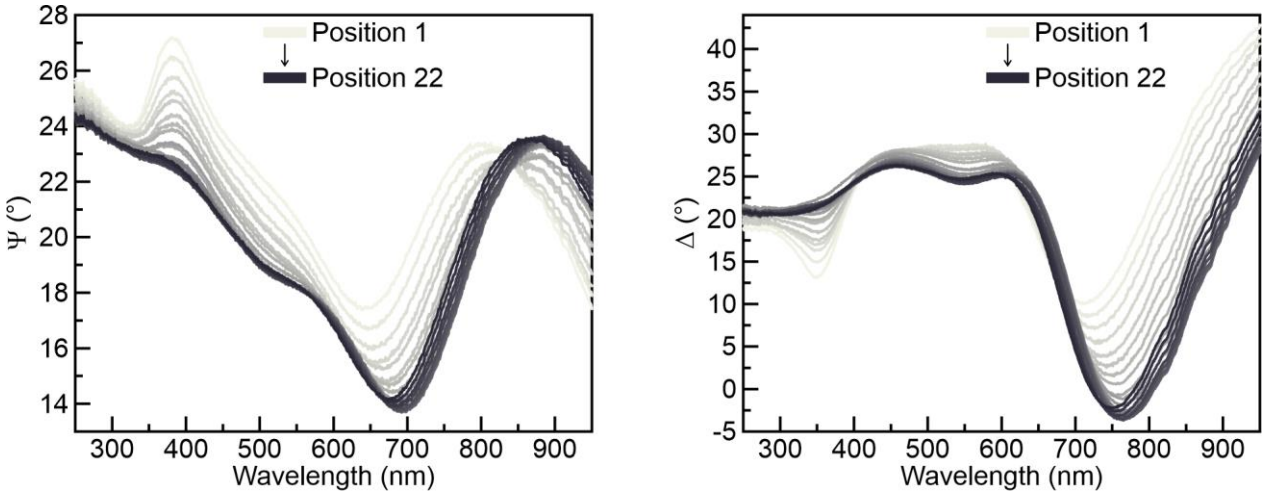

Fig. 1. Ellipsometric parameters Ɋ (left) and ɷ (right) dependence on the position on DLC:Ag sample. Distance between each position is 0.5 mm.

As it can be seen from Fig. 1, the ellipsometric parameters Ɋ and ɷ already indicate the differences in the thin film. The peak at around 380 nm in Ɋ spectra as well as the minima at around 350 nm in ɷ spectra become smaller and eventually completely disappear, when going from the top part of the sample to the bottom. The minima point of extrema at 650 nm in Ɋ spectra and at 720 nm in ɷ spectra shift towards longer wavelengths with the change of the position. This indicates the gradual change of the thin film properties. This could imply that the sample was slightly tilted during the deposition. Further analysis (modelling of ellipsometric data at every position) will reveal the actual reason for these differences: it could either be thickness, refractive index and extinction coefficient, or silver content non-uniformity.

DETECTION OF MALIGNANT HUMAN BLADDER TISSUE BY MEANS OF FIBER BASED ATR IR SPECTROSCOPY

Rimantė Bandzevičiūtė[1], Gediminas Platkevičius[2], Justinas Čeponkus[1], Gerda Mickūnaitė[1], Albertas Čekauskas[2], Arūnas Čelvys[2], Valdas Šablinskas[1]

[1] Institute of Chemical Physics, Faculty of Physics, Vilnius University, Saulėtekio Av. 3, LT-10257 Vilnius, Lithuania
[2] Institute of Clinical Medicine, Faculty of Medicine, Vilnius University, Santariškių Str. 2, LT-08661, Vilnius, Lithuania
rimante.bandzeviciute@ff.vu.lt

Bladder cancer is one of ten most frequently diagnosed cancer types worldwide [1]. Depending on tumor type and stage, conventional treatment of bladder cancer includes surgical operation combined with medication or radiation therapy [2]. The most frequent type of bladder cancer is urothelial carcinoma which requires surgical approach at the presentation in most of the cases. During the surgery, it is important to ensure the complete removal of the whole tumor in order to reduce the risk of recurrence of the disease. The gold standard method for tissue identification is histological examination of the removed tissue. The disadvantage of this method is that the specific sample preparation is required, also, this procedure is time consuming. Therefore, new diagnostic techniques are required. The intraoperative diagnostic technique should give fast and reliable results for precise determination of the tissue area which has to be removed and not to prolong the time of surgery to reduce the risk of complications.

During tumor formation, the metabolism of cells changes, therefore, it affects the chemical composition of the tissue. Vibrational spectroscopy is sensitive method for the qualitative and quantitative chemical analysis, thus chemical changes of the tissue should be observable in the vibrational spectra. In this study fiber based attenuated total reflection infrared (ATR IR) spectroscopy was applied for the tissue examination. Spectra could be measured within few minutes without almost any special sample preparation. Application of fiber probe enables to do measurements *in situ* or *in vivo* conditions, that is important during the surgery.

During the study, samples of normal and tumorous human bladder tissue of 49 patients were examined, including cases of urothelial carcinoma, nonspecific cystitis and papillary urothelial neoplasm of low malignant potential. The technique was applied for the tissues removed after the surgery. The ATR IR absorption spectra of normal and tumorous tissue are represented in Fig. 1. The decreased intensity of spectral bands of collagen located at 1339 cm^{-1}, 1205 cm^{-1} and 1033 cm^{-1} is observed in the ATR IR absorption spectra of urothelial carcinoma tissue. It is related to the decreased amount of collagen in the tissue. The bladder is elastic organ that can dilate when the bladder is full and shrink when it is emptied, collagen provides the elasticity. During the process of tumor development, tissue loses its function, therefore, it could lead to decreased levels of collagen. Also, the increased intensity of the spectral bands located at 1155 cm^{-1} and 1026 cm^{-1} is observed, it is related to increased levels of glycogen. An increased amount of glycogen in the cytosol is a characteristic feature for some types of cancer. Glycogen is accumulated and used as the source of energy since cancerous cells due to high proliferation rate need more energy than normal ones.

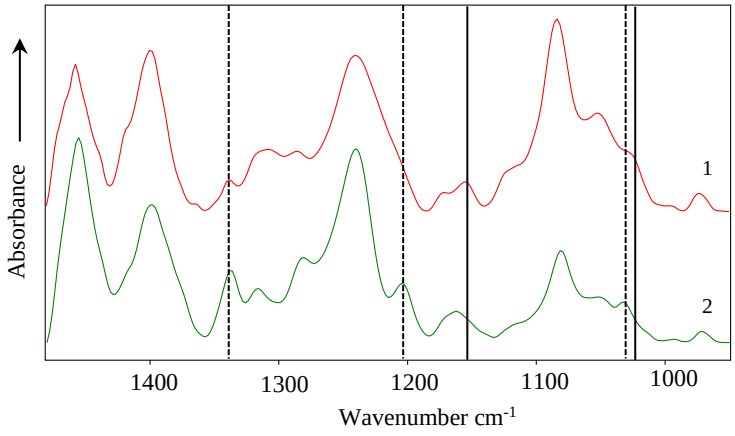

Fig. 1. ATR IR absorption spectra of cancerous (urothelial carcinoma) (1) and normal (2) bladder tissues. Dashed lines indicate spectral bands assigned to collagen, solid lines ï assigned to glycogen.

[1] K. Saginala, A. Barsouk, J. S. Aluru, P. Rawla, S. A. Padala, A. Barsouk, Epidemiology of Bladder Cancer, Med Sci (Basel) **8** (2020)
[2] S. Sharma, P. Ksheersagar, P. Sharma, Diagnosis and treatment of bladder cancer, Am Fam Physician **80**, 717-23 (2009)

P2-13

DID NOT PARTICIPATE

LIBRARY OF RED PIGMENT RAMAN SPECTRA AND PIGMENT IDENTIFICATION IN PAINTED WORKS OF ART

Morta Stadulytė, Rasa Platakytė, Justinas Ļeponkus

Institute of Chemical Physics, Faculty of Physics, Vilnius University, Vilnius
morta.stadulyte@ff.stud.vu.lt

Nowadays there are plenty of old art works which require restoration or historical identification. Before restoring paintings or other art works it is important to know what materials were used while creating them [1]. Knowing what type of materials (including binders, extenders, fillers etc.) were used is also crucial in authentication of the artwork and the determination of paintingôs authorship, place and time of creation. Many methods have been employed to identify the chemical composition of the materials used in works of art but Raman spectroscopy is one of the fastest and most highly specific, and therefore suitable for this type of analysis. There is also a possibility to use Raman spectroscopy *in situ* which would help identify pigments and other paint components in an even faster and more efficient way. The main purpose of this work was to estimate the suitability of Raman scattering spectroscopy method for identification of commonly used red pigments in artworks and create a library of said pigments which could be used while analyzing real paintings and frescoes.

Different standard red pigment samples from Vilnius Pranas Gudynas restoration center were measured. During the study of these pigments, near infrared laser (1064 nm) was employed in order to reduce the risk of fluorescence. The one complication that often arose while measuring different samples was the need to adjust laser power and scanning time in order to obtain spectra with best signal to noise ratio and avoid sample heating and damage. Raman spectroscopy was used to identify specific bands of over ten red pigments. In addition, the spectra proved useful while following degradation of a pigment. In figure 1, two spectra of the same pigment (red lead) from different sources (Kremer standard pigment and Soviet pigment) are presented. It is possible to observe that the latter pigment has degraded from Pb_3O_4 to PbO from the relative intensities of the spectral bands in the 320-280 cm^{-1} and 160-130 cm^{-1} regions [2].

Some samples of original and restored frescoes from Vilnius University *Littera* bookstore were measured as well. The red pigment used in one of the frescoes and materials used in different plaster layers under the frescoes were identified as hematite, calcium carbonate and silicon dioxide.

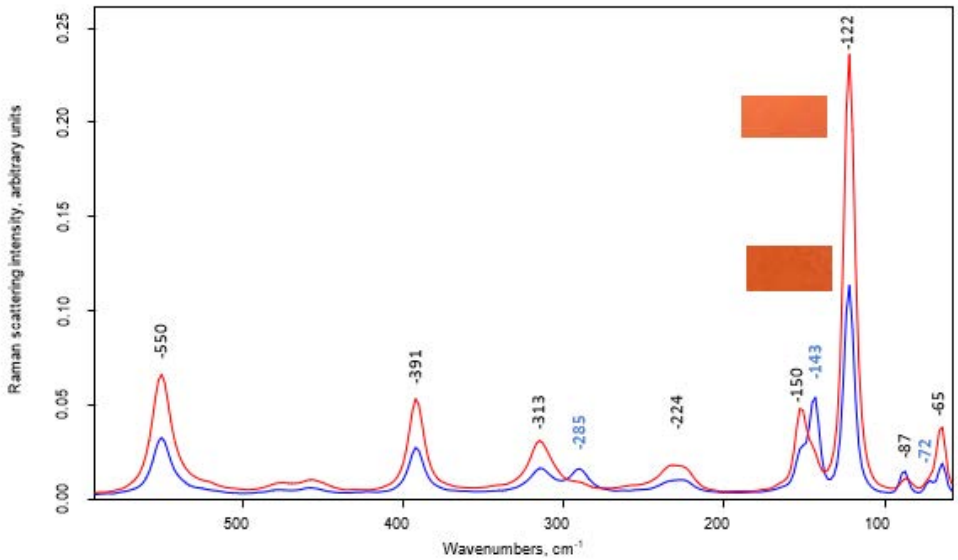

Fig. 1. Red lead pigment Raman spectra (5 mW, 4 cm^{-1}, 300 scans, 1064 nm). Red line shows red lead pigment from Kremer standard pigments, blue line represents red lead pigment from soviet times.

[1] *Invaluable* ancient arts shop paper *The Science Behind the Restoration of a Painting* (2019).
[2] Burgio, Lucia; Clark, Robin J. H.; Firth, Steven. *Raman spectroscopy as a means for the identification of plattnerite (PbO2), of lead pigments and of their degradation products* (2001).

RELATIONSHIP OF SPATIAL AND KINETIC CATHODOLUMINESCENCE PROPERTIES IN NONPOLAR InGaN QUANTUM WELLS

Ģivilė Ļerģkutė, Ģydrĩnas Podlipskas, Gintautas Tamulaitis

Institute of Photonics and Nanotechnology, Vilnius University, Lithuania
zivile.cerskute@ff.stud.vu.lt

The quantum efficiency of extensively used polar InGaN is deteriorated by the spatial separation of electrons and holes in the quantum well due to the built-in electric field. The field is absent in semi-polar and non-polar InGaN quantum wells, thus these types of InGaN receive an increasing attention. Two strongly overlapping bands are observed in the luminescence spectra of non-polar and semi-polar InGaN. Further research is needed to reveal the origin of these bands.

In this work, m-plane InGaN quantum wells have been studied using time-resolved cathodoluminescence (CL) spectroscopy. *Attolight* CL spectrometer *Chronos* has been exploited. The sample was excited with electron beam and the CL spectra were recorded with a CCD camera, whereas CL kinetics was registered with a streak camera.

In time-integrated CL mode, two InGaN-related strongly overlapping bands with peaks at 428 nm and 450 nm have been observed (see Fig. 1a). The band peaked at 362 nm is attributed to GaN which is expected from the capping layer. It was revealed that the increase in excitation intensity results in a faster increase in CL intensity for the band peaked at 428 nm than that for the band peaked at 450 nm. The spatial distribution of time-integrated CL intensity is inhomogeneous with high-intensity spots of ~200 nm in diameter. It was also observed that the spatial distribution of the peak wavelength showed that the band peaked at 428 nm dominates the CL throughout the entire sample surface at high excitation intensity. Meanwhile at low excitation intensity, competition among the two bands is observed from site to site.

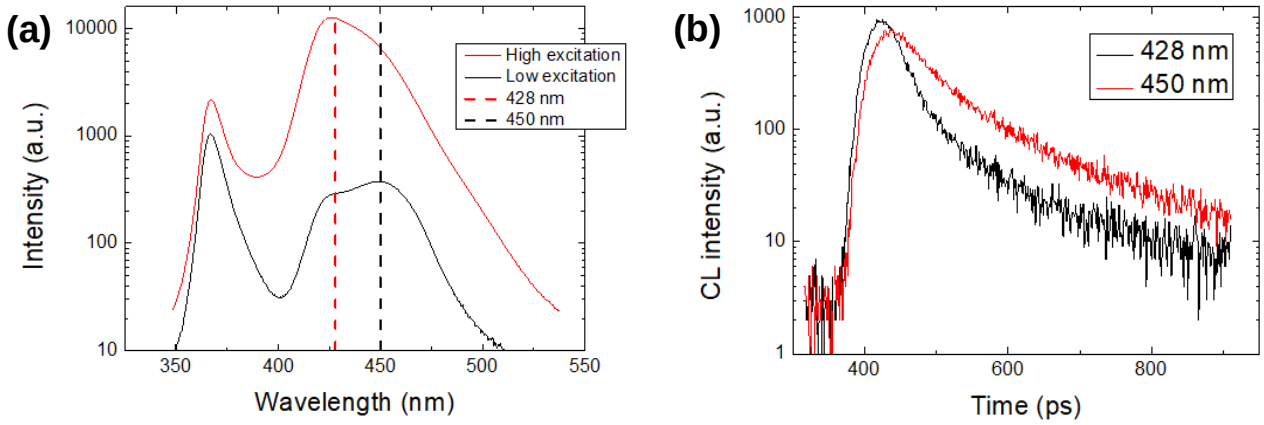

Fig. 1. InGaN CL spectra at high (red line) and low (black) excitation intensity (a) and kinetics of CL at 428 nm (black line) and 450 nm (red) bands measured within a bright spot (b).

Using excitation in pulsed mode, the CL time evolution has been measured in different spots on the sample surface that have different CL intensity. In all the spots, the CL decay contains two components, fast and slow. CL intensity decay in one of the measured spots is shown in Fig. 1b. The decay time of the fast component of the band peaked at 428 nm is equal to 26 Ñ2 ps, whereas it is almost twice as long (50 Ñ6 ps) for the 450 nm band. The carrier lifetime of the slow component is the same for both bands within the limits of error. A strong positive correlation between the CL intensity and the decay time of the fast component is observed. The exact origin of double-peak emission is discussed.

RAMAN SPECTROSCOPY ANALYSIS OF FS LASER INDUCED STRUCTURAL DAMAGE ON SODA LIME AND ALUMINOSILICATE GLASSES

Kasparas Dryģas[1], Laura Tauraitā[1], Antanas Urbas[1,2], Sergejus Orlovas[1]

[1] Center of Physical Sciences and Technology, Coherent Optics Laboratory, Lithuania
[2] Altechna R&D Ltd, Lithuania
kasparasdryzas@gmail.com

Selective etching is an important process in electronic and medicinal instrument manufacturing. However, it is a time-consuming process thus reducing manufacturing speed.

It is known that chemical etching rate (using potassium hydroxide KOH) of corona-charge treated domain of the soda-lime glass substrate is 1.6 times higher than that of normal glass [1]. Furthermore, it was observed that chemical etching rate (using potassium hydroxide KOH) of fs laser induced damage areas of soda-lime glass is up to 100 times higher [2].

The purpose of this study is to analyse structural changes of soda-lime and more complex aluminosilicate (ñGorilla3ò) glasses when affected by fs laser pulses. Soda-lime glass is composed of silicon dioxide (SiO_2), sodium carbonate (Na_2CO_3), calcium oxide (CaO) and aluminosilicate glass of additional aluminium oxide (Al_2O_3) and magnesium oxide (MgO) compounds. The structural network is formed by silicon and oxygen compounds in the shape of tetrahedrons, also known as Q species. Q species are connected by bridging oxygen atoms (Fig. 1). Alkali and alkaline earth elements work as network modifiers, consequently changing physical and chemical properties of the glass (Fig. 2). In this case aluminium in aluminosilicate glass works as glass former and aluminium tetrahedrons forming eing structures could be observed (Fig. 2).

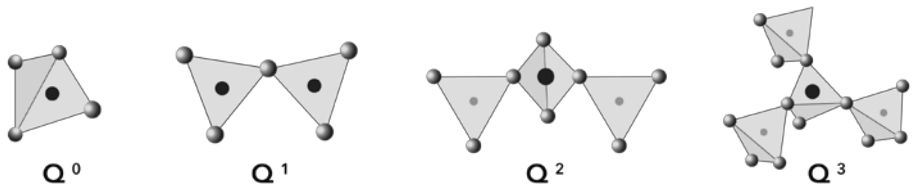

Fig. 1. Visualisation of Q group compounds

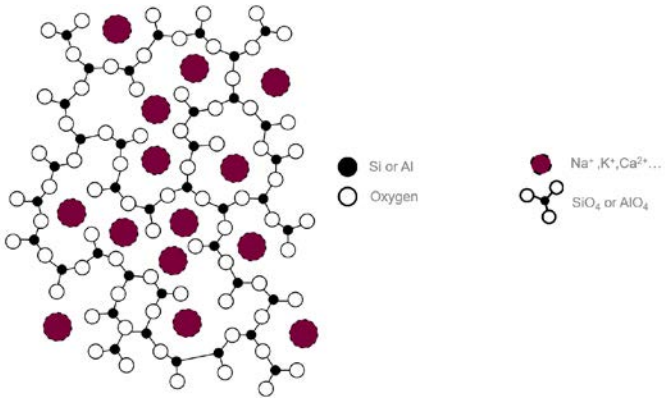

Fig. 2. Visualisation of aluminosilicate glass structure

In this study, soda-lime and aluminosilicate glasses samples were affected by a 1030 nm wavelength Bessel beam. Damaged samples were analysed with Raman spectroscopy. This method was chosen because Raman shift values of Q species compounds are precisely known and do not depend on alkali metal compounds in the glass structure [3]. In this research, Raman spectroscopy was done with a 532 nm wavelength excitation beam. By analysing the measured spectra, structural differences between damaged and normal glass can be determined. Analysis of the Raman spectra showed there was a noticeable difference in the quantity of Q species compounds in the damaged glass compared to normal glass.

[1] Daisuke Sakai et al 2013 Jpn. J. Appl. Phys. 52 036701
[2] Bellouard Yves et al 2004 Fabrication of high-aspect ratio, micro-fluidic channels and tunnels using femtosecond laser pulses and chemical etching. Optics Express, 12(10)
[3] G.S. Henderson, H.W. Nesbitt, G.M. Bancroft, Some Interesting Observations on Oxygen Environments in Silicate Glasses with Implications for the Fitting of the High Frequency Raman Envelope (Cargese, France, 2017).

DISTRIBUTION OF 241AM ACTIVITY CONCENTRATIONS IN THE BALTIC SEA SEDIMENTS

Romanenko Vitaliy[1], Lujanienā Galina[1], Ġemļuk Sergej[1], Jonas Maģeika[2], Ezhova Elena[3], Garnaga-Budrā Galina[4]

[1] SRI Center for Physical Sciences and Technology, Lithuania
[2] SRI Nature Research Centre, Vilnius, Lithuania
[3]P.P. Shirshov Institute of Oceanology RAS, Moscow, Russia
[4]Environmental Protection Agency, Klaipāda, Lithuania
Vitaliy.romanenko@ftmc.lt

The Baltic Sea has been contaminated with anthropogenic radionuclides over a long history of nuclear energy use. Nowadays, the Baltic Sea continues to be contaminated with anthropogenic radionuclides due to the inflow of radionuclides from rivers with a total catchment area of about 2Ā10^6 km^2. For example, the Vistula River brings about 1.6 GBq/y of ^{241}Pu with its waters [1]. Moreover, the ingrown activity concentrations of ^{241}Am are the result of ongoing radioactive decay of ^{241}Pu. The activity of ^{241}Pu in the Baltic Sea due to global fallout and the Chernobyl NPP accident are estimated at 39TBq (data [2] are corrected for 2021). The increase in the activity concentrations of ^{241}Am will reach a maximum of 4.1TBq in ~ 47 years.

Particle-reactive radionuclides have over the years been a useful tool for studying the redistribution of various pollutants in the marine environment. It is known that many toxic organic substances, particularly chlorine-containing ones, easily bind sediments and are transported from land to the marine environment by rivers and coastal waters. Knowledge about the sources of radionuclides and understanding of their behavior are essential for their application in tracer studies. Thį aim of this study is to expand knowledge about the distribution of ^{241}Am and ^{137}Cs in bottom sediments of the Baltic Sea for their future applications in tracer studies.

The bottom sediment samples (Fig. 1) were taken by the Environmental Protection Agency (Klaipāda, Lithuania) and by P.P. Shirshov Institute of Oceanology RAS (Moscow, Russia). Sampling depths was ranged from 43 to 120 m. A Van Veen Grab Sampler was used for taking samples.

Sediment samples were ashed at 550ŒC, then digested using strong acids. Am was extracted with TOPO/cyclohexane, followed by radiochemical purification with TRU and TEVA resins (100-150 mm). 243Am was used as a yield indicator in the separation procedure (AEA Technology UK, Isotrak, QSA Amersham international, ATP10020). The purified Am was electroplated onto stainless steel disks. The alpha-spectrometry system with passivated implanted planar silicon (PIPS) detectors, 450 mm^2 active area (AMETEK, Oak Ridge, Tenn, USA) was used for the detection. The activities of the gamma emitters were measured by HPGe detectors (resolution 1.8 keV (FWHM) at 1.33 MeV and efficiency 42%).

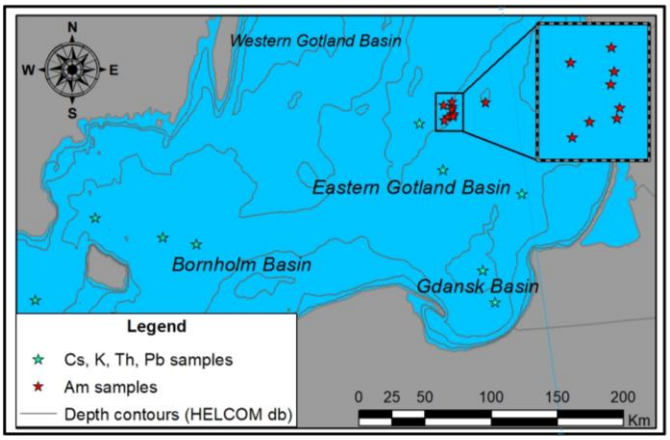

Fig. 1. The sampling area

The data obtained during this study showed that in the bottom sediments of the Gotland Deep, ^{241}Am is distributed unevenly in the range of 0.065-0.231 Bq / m^3. According to preliminary data, there was a general trend for the ^{241}Am activity to increase with depth. The activity concentrations of ^{137}Cs, ^{214}Pb and ^{40}K in studied samples ranged from 62 to 220 Bq/kg, from 30.1 to 80.2 Bq/kg and from 827 to 1093 Bq/kg, respectively. The obtained results will be used to study sediment transport in the Baltic Sea.

[1] D. I. StrumiŒska-Parulska, Vertical distribution of 241Pu in the southern Baltic Sea sediments, (Mar. Pollut. Bull., vol. 89, no. 1ï2, pp. 12ï15, Dec. 2014).
[2] E. Holm, ñPlutonium in the Baltic Sea,ò (Appl. Radiat. Isot., vol. 46, no. 11, pp. 1225ï1229, Nov. 1995).

PMMA WGM MICRO RESONATOR MODE FAMILY ANALYSIS USING SPOT INTENSITY CHANGES FROM IMAGE PROCESSING.

Roberts Berkis[1], Inga Brice[1], Kristians Draguns[1], Aigars Atvars[1], Pauls Kristaps Reinis[1], KÜrlis Grundsteins[1], Janis Alnis[1]

[1] University of Latvia , Institute of atomic physics and spectroscopy, Quantum optics laboratory
Roberts.berkis@lu.lv

The whispering gallery modes (WGM) micro resonators are based on ellipsoidal objects, which can be made from optically transparent materials, that can enable optical wave circulating inside the ellipse using total internal reflection. If there is a monochromatic light source with constant intensity to the ellipse, constructive interference may be observed [1, 2]. Poly methyl methacrylate acrylic (PMMA) WGM micro resonators are commercially available with typical optical quality factor of 10^3-10^4 [3]. These could limit problems with WGM micro resonator expensive manufacturing. Because of advances in high resolution image processing, read-outs using spectroscopy (single photo detector) could be replaced with image processing. Image processing (4.5Õm/px) allows to split elliptical WGM micro resonator in regions and analyze separate sectors of the ellipse [4], which can used as a representation of surface irregularity [5] interaction with higher order special mode groups.

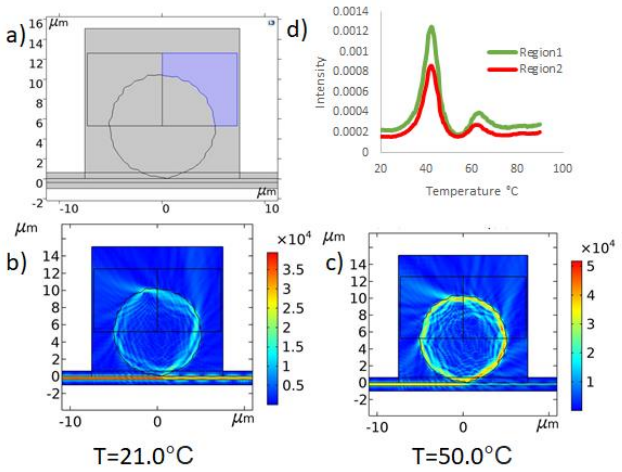

Fig. 1. COMSOL 2D geometry with 10Õm diameter PMMA WGM micro resonator with randomly deformed surface coupled to 0.4 Õm diameter tapered fiber waist region and the selected region at which the average light intensity is being measured. b) Electric field distribution on 10 Õm diameter PMMA WGM micro resonator, which is coupled to 0.4 Õm diameter tapered fiber waist regions with 760nm light propagating inside the fiber at 21^{0}C. c) Electric field distribution on 10 Õm PMMA WGM micro resonator, which is coupled to 0.4 Õm tapered fiber waist regions with 760nm light propagating inside the fiber at 50^{0}C. d) Average intensity distribution at different temperatures for two separate regions of WGM PMMA micro resonator.

In the present work new type of image processing for micro-resonators were developed, to analyze intensity distribution in separate regions for PMMA WGM micro-resonators in diameter range of 40-85 Õm, that were coupled with tapered fiber waist region and fixed wavelength laser (760nm). Temperature was changed from 20-80 ^{0}C which effect the PMMA refractive index (Ŭ), for 760nm dn/dT = -1.32×10^{-4} (^{0}C^{-1}) and thermal expansion (ϭ) which is 2.60×10^{-4} (^{0}C^{-1}). Combining the following physical changes, total changes (Ŭ+ ϭ), WGM PMMA micro-resonator mode mapping was obtained. The following work offers new type of intensity processing methods for measuring applications using PMMA WGM micro resonators and interaction from higher order optical modes and surface deformations on micro resonator surface.

This research was funded by the Latvian Council of Science project No. lzp-2018/1-0510 and ERDF 1.1.1.5/19/A/003 grants.

[1] Y. Zheng, Z. Wu, P. Ping Shum, Z. Xu, G. Keiser, G. Humbert, H. Zhang, S. Zeng, and X. Quyen Dinh, Sensing and Lasing Applications of Whispering Gallery Mode Microresonators, Opto-Electronic Adv. **1**, 18001501 (2018).
[2] M. R. Foreman, J. D. Swaim, and F. Vollmer, Whispering Gallery Mode Sensors: Erratum, Adv. Opt. Photonics **7**, 632 (2015).
[3] R. Berkis, J. Alnis, A. Atvars, I. Brice, K. Draguns, and K. Grundsteins, Quality Factor Measurements for PMMA WGM Microsphere Resonators Using Fixed Wavelength Laser and Temperature Changes, Proc. 2019 IEEE 9th Int. Conf. Nanomater. Appl. Prop. N. 2019 **9** (2019).
[4] A. B. Petermann, T. Hildebrandt, U. Morgner, B. W. Roth, and M. Meinhardt-Wollweber, Polymer Based Whispering Gallery Mode Humidity Sensor, Sensors (Switzerland) **18**, 1 (2018).
[5] R. Popov, G. K. Shankara, C. von Bojnicic-Kninski, P. Barua, D. Mattes, F. Breitling, and A. Nesterov-Mueller, Stochastic Deposition of Amino Acids into Microcavities via Microparticles, Sci. Rep. **9**, 1 (2019).

HOLDER FOR IMPEDANCE SPECTROSCOPY MEASUREMENTS OF MIXED CONDUCTORS IN INERT GAS ATMOSPHERE

Mateusz J. Samsel, Tomasz K. Pietrzak, Maciej Nowagiel

Faculty of Physics, Warsaw University of Technology, Koszykowa 75, 00-662 Warsaw, Poland
mateusz.samsel.stud@pw.edu.pl

Thermal nanocrystallisation of glasses is a method of obtaining highly conductive nanomaterials by means of appropriately selected heat treatment. Experiments carried out at our faculty have shown that this method can lead to a huge increase in electrical conductivity of selected glassy analogues of cathode materials for lithium-ion batteries, even by 9-10 orders of magnitude [1, 2]. Recent studies of the glassy analogues of cathode materials for sodium batteries from NASICON family [3] and alluaudites [4] did not confirm this observation. It is believed that sodium ion conductors may react differently to the heating in air than lithium conductors. Hence the need to investigate the change of conductivity of these materials during thermal nanocrystallization.

During this work we adapted existing systems to measure impedance as a function of temperature , in the flow of inert gas (argon). We constructed the hermetic measuring holder with a gas inlet and then carried out impedance measurements as a function of temperature. The schematic of the holder is shown in Fig. 1. Test measurements were performed to check the effect of an inert atmosphere on the nanocrystallization process of the materials. Those measurements also confirmed that the designed device works properly. The obtained Arrhenius curves (which show how conductivity of studied sample depends on temperature) were compared with the same curves obtained for samples which were nanocrystallized in air.

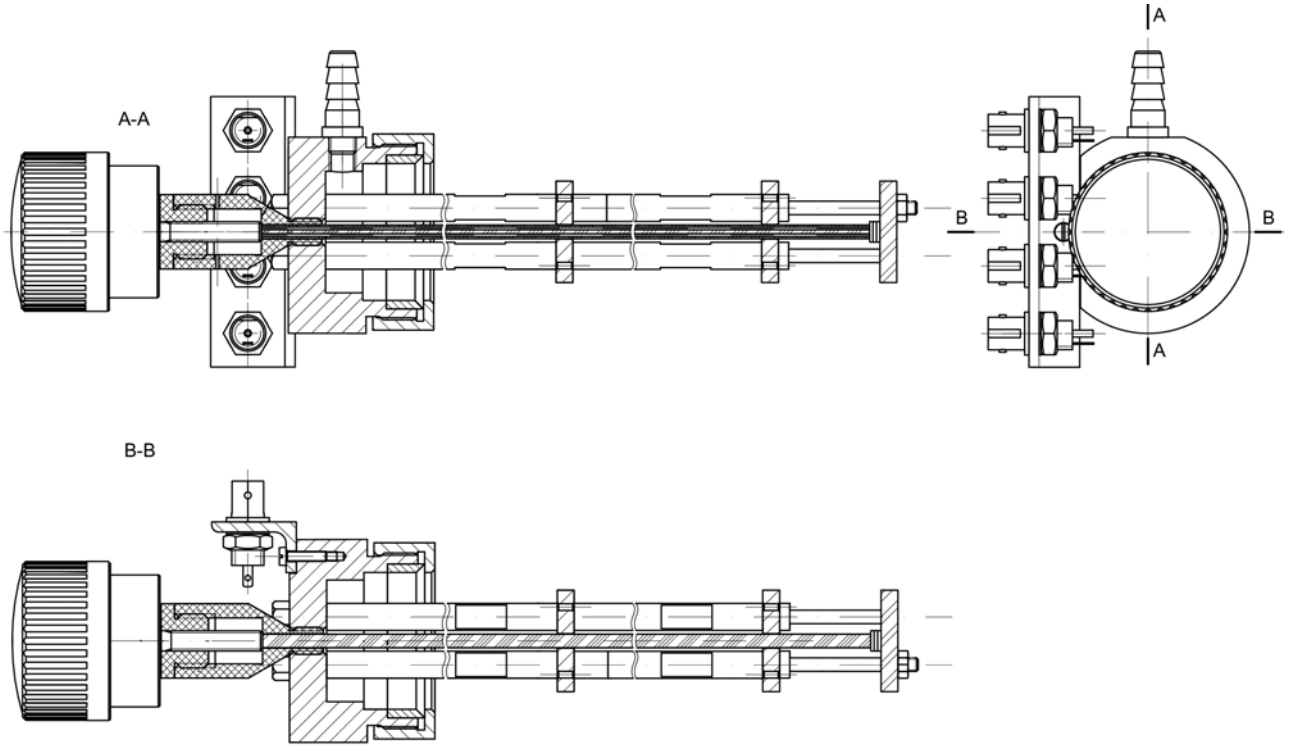

Fig. 1. The designed impedance measurement holder.

[1] T.K. Pietrzak, M. Wasiucionek, P.P. Michalski, A. Kaleta, J.E. Garbarczyk: Highly conductive cathode materials for Li-ion batteries prepared by thermal nanocrystallization of selected oxide glasses. Materials Science and Engineering B 213 (2016) 140-147.

[2] J.E. Frackiewicz, T.K. Pietrzak, M. Wasiucionek, J.E. Garbarczyk: Synthesis and Characterization of Highly-Conducting Nanocrystallized $Li(Fe_{1-x}Mn_x)_{0.88}V_{0.08}PO_4$ Cathode Materials (x = 0.25, 0.5, 0.75). ECS Transactions 80 (2017) 325-330.

[3] T.K. Pietrzak, P.E. Kruk-Fura, P.J. Mikołajczuk, J.E. Garbarczyk: Syntheses and nanocrystallization of NaF—M_2O_3—P_2O_5 NASICON-like phosphate glasses (M = V, Ti, Fe). International Journal of Applied Glass Science 11 (2020) 87-96.

[4] A.E. Chamryga, M. Nowagiel, T.K. Pietrzak: Syntheses and nanocrystallization of Na_2O-M_2O_3-P_2O_5 alluaudite-like phosphate glasses (M = V, Fe, Mn). Journal of Non-Crystalline Solids 526 (2019) 119721.

ENHANCED DETECTION OF UV-INDUCED FREE-CARRIERS BY MULTIPLE PROBE BEAM PASSES INSIDE A CO-DOPED GAGG CRYSTAL

Mohammad Nour Alsamsam[1], Kazimieras Nomeika[2], Žydrūnas Podlipskas[2], Jonas Jurkevičius[2], Ramūnas Aleksiejūnas[2]

[1] Faculty of Physics, Vilnius University, Lithuania
[2]Institute of Photonics and Nanotechnology, Faculty of Physics, Vilnius University, Lithuania
nour.alsamsam@ff.stud.vu.lt

In this work, we have investigated the advantages of increasing the 1064nm CW[1] probe interaction length in a $Gd_3Al_2Ga_3O_{12}$ (GAGG:Ce,Mg) crystal by multiple internal reflections off two gold-coated parallel faces with entry/exit 0.75mm windows (Fig. 1). Modelling of such geometry enabled a more comprehensive experimental approach in terms of achieved results and time consumption by acquiring incidence angles of interest. Signal enhancement thus is achieved by maximizing free carrier absorption of the probe beam through increasing the path travelled inside the sample. A 266nm pulsed pump of 4.2μJ inducing 1.6×10^{15}cm^{-3} free carriers – two orders of magnitude lower than the previous results – in a cubic GAGG sample ($5 \times 5 \times 5$mm^3) yielded a 1% signal change using an InGaAs detector. Higher energy pulses of 0.29mJ showed a signal change up to 65%.

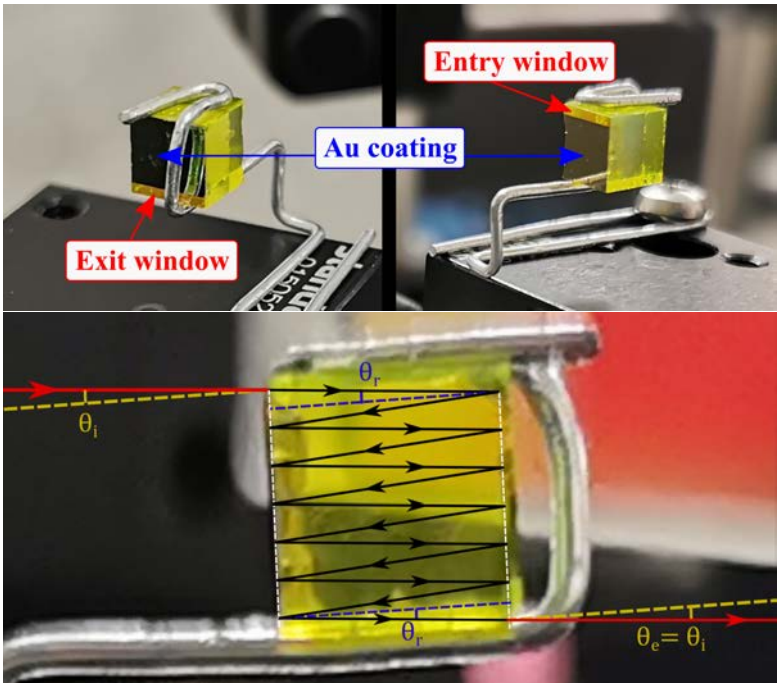

Fig. 1. (Top Right) Entry window, (Top Left) Exit window, (Bottom) Multiple reflections of the probe inside a cubic sample.

[1]Continuous Wave.

METAL GRATING DEPOSITION, CHARACTERIZATION AND IMPACT ON OPTICAL RESPONSE OF GaAs/AlGaAs NANOSTRUCTURES

Dominykas Dumbrė[1], Vytautas Jakštas[2], Vladislovas Čižas[2], Mindaugas Karaliūnas[1,2]

[1]Faculty of Physics, Vilnius University, Saulėtekio Ave. 9 III bld., 10222 Vilnius, Lithuania
[2]Center for Physical Sciences and Technology, Saulėtekio Ave. 3, 10257 Vilnius, Lithuania
dominykas.dumbre@ff.stud.vu.lt

Metal grating (MG) is a critical technique to study the optical properties of quantum structures in epitaxially grown samples [1]. It allows to change the direction of electric field of incident electromagnetic wave that it can couple with the confined electrons in the quantum system. As a result, one can optically measure the electronic structure of the quantum levels in simple experiment geometry [2]. In this work, the MG were deposited on the AlGaAs/GaAs samples and THz range optical response of the samples with MGs are studied. Two samples were used in the experiment. One consists of epitaxially grown AlGaAs on GaAs substrate, the other contains a superlattice of 35 pairs of GaAs/AlGaAs layers on GaAs substrate with GaAs/AlAs buffer.

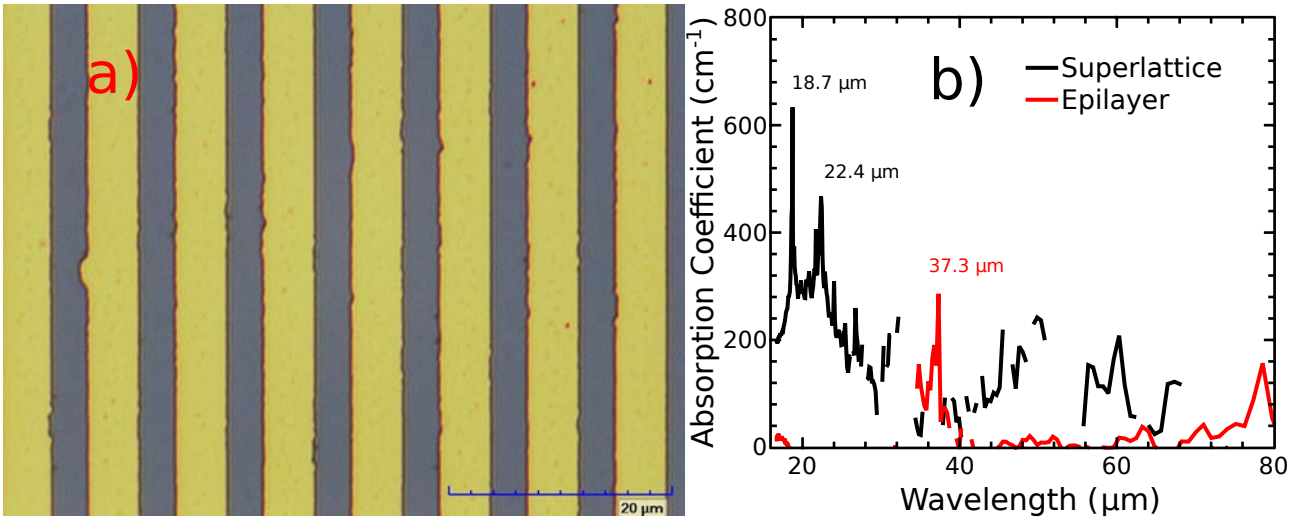

Fig. 1. Image of the MG on the sample surface under the optical microscope. Absorption spectrum of the AlGaAs/GaAs sample with MG in respect to GaAs spectrum (as reference). The red arrows indicate the measured resonance absorption peaks and blue arrows indicate the expected position of the resonance peaks defined by the grating period.

The MG was fabricated using photolithography and thin metal film sputtering techniques. First, the surface of the samples was rinsed using acetone, isopropanol and deionized water. Next, the samples were covered with photoresist and a Mask Aligner SUSS MA/BA6 Gen 4 was used to form the negative photoresist pattern by exposing the samples to UV light through the mask. Then, metalization of 20 nm/180 nm Ti/Au were deposited in vacuum by a E-Beam TFDS-870 equipment. Finally, the samples were immersed in the DMSO to remove remaining photoresist and washed in deionized water. The optical absorption spectra were measured using Fourier transform spectrometer Nicolet 8700 (Thermo Fisher Scientific, U.S.A.).

Fig. 1a shows the MG on the sample surface under the optical microscope. One can see perfectly aligned metal stripes although the edges of the stripes are slightly uneven. The filling factor of the grating is around 0.6 and the period of the grating is 8 μm. The measured optical absorption coefficient spectrum reveals the strong resonance absorption lines at 18.7 μm and 22.4 μm for superlattice sample, as one can see in Fig. 1b. The reference sample with AlGaAs epilayer shows the single absorption resonance line at 37.3 μm

For conclusions, the high-quality MGs were fabricated using photolithography and thin metal film sputtering. The absorption coefficient spectra of the samples show well defined resonance lines. The peaks of superlattice sample at 16 THz and 13.4 THz frequencies may tentatively be attributed to THz radiation coupling with the electrons in the quantum system, whereas the peak of AlGaAs epilayer sample at 8 THz – to the THz radiation coupling with the phonons system.

[1] J. Ulrich, R. Zobl, K. Unterrainer, G. Strasser, E. Gornik, K. D. Maranowski, and A. C. Gossard, Temperature dependence of far-infrared electroluminescence in parabolic quantum wells, Appl. Phys. Lett. **74** 21, 3158-3160 (1999).
[2] M. Karaliūnas, J. Pagalys, V. Jakštas, R. Norkus, A. Urbanowicz, J. Devenson, R. Butkutė, A. Udal, and G. Valušis, Spectral properties of incoherent terahertz torch based on parabolic Ga(As,Bi)/AlGaAs quantum wells, Proc. of SPIE **11124**, 1112409 (2019)

OBSTRUCTIVE SLEEP APNEA PREVENTING AND TREATING BED

Sundar Arumugam Krishnan Nagarajan, Shalini Murugesan

Department of Mechanical Engineering and Design, Kaunas university of technology, Lithuania
sundar.arumugam@ktu.edu

Sleep Apnea is a serious sleep disorder in which breathing starts and stops impulsively. There are many forms of sleep apnea: Obstructive Sleep Apnea, Central sleep apnea and Complex sleep apnea. Obstructive Sleep Apnea disorder involves trouble in breathing during sleep accompanied with loud snoring. In such cases, if any equipment is there, which can awake the person from sleep during breathlessness. So that patient can feel comfortable. In the present project an obstructive sleep apnea preventing and treating bed is developed.

The main motive of this project is to provide an alternative method to surgical treatments. In surgical methods, doctors used to remove the tongue base with the help of laser treatment. This will create discomfort to the patients. Present project is totally a non-invasive approach, which will never cause any discomfort to the patients. The project comprises of pulse oximeter, servomotor, suspension bed interfaced to the Raspberry PI 3 microcontroller [1]. It is programmed using python. Pulse oximeter detects the pulse rate and oxygen saturation level of the patients. Servomotor is attached under the patientôs bed. Pulse oximeter is inserted to the fingertip of the patient. Normal oxygen saturation level is 90 to 95%. When the oxygen saturation level decreases below 90%, the pulse oximeter sends the signal to the servomotor to tilt the bed at three different angles namely 20, 40, 60 degrees. This tilting of bed brings the oxygen saturation level back to normal and thus prevents breathlessness in patients. In addition to this, Raspberry pi 3 micro controller with the help of GSM module sends an alert message in the form of SMS to the doctorôs mobile phone [2]. Thereby, this prevents the patients from obstructive sleep apnea.

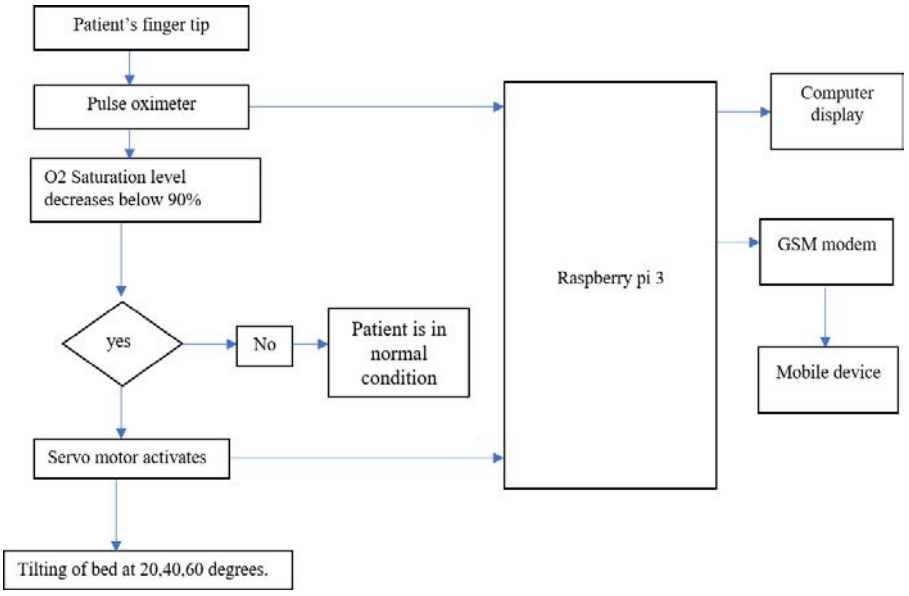

figure 1: Block diagram of Obstructive Sleep Apnea bed

This project has discussed the development of preventing and treating bed. The objectives were to develop necessary hardware, software to measure oxygen saturation level and prevent sleep apnea if saturation level falls outside of threshold limits and send an alert message to doctor via SMS.

[1] J. Ko, C. Lu, M. B. Srivastava, J. A. Stankovic, A. Terzis, and Welsh. (2010),ñWireless Sensor Networks for Healthcare,ò vol. 98, no. 11, pp. 1947ï 1960, Nov 2010.

[2] S. M. R. Islam, D. Kwak, M. H. Kabir, M. Hossain, and K. S. Kwak.(2015),ñThe Internet of Things for Health Care: A Comprehensive Survey,ò vol. 3, pp.678-708.

ANALYSIS OF INKS AND WRITTEN TEXTS USING SURFACE ENHANCED RAMAN SPECTROSCOPY

Daina Afanovaitā[1], Martynas Veliļka[1]

[1]Institute of Chemical Physics, Faculty of Physics, Vilnius University, Lithuania
daina.afanovaitā@ff.stud.vu.lt

Even with evolving technology, document forgery continues to be a major problem, causing damage to not only individuals, but also organizations, banks, and even the economy of whole countries [1]. Forgery during forensic analysis is determined by determining the contents of the document in question, specifically the chemical composition of the constituents, and comparing the differences between sections in the document [2].

The method of analysis is chosen depending on the case and its importance or urgency. Nowadays optical methods are most commonly used for investiagtion as these methods are non-destructive, fast, and easily interpreted. Raman scattering is an optical method usually used for chemical analysis in the authentication of written texts. This method allows the identification of the chemical composition of used ink and in some cases analysis of its degradation. Such information can be used to determine the time when the document was created [4]. However, the ink in written documents is difficult to analyse since fluorescence is a characteristic of some of the dyes used in the constituents of ink. Also, the amount of material in the ink is usually too small to produce a strong Raman signal what results in fluorescence overshadowing it. This problem can be solved using surface-enhanced Raman scattering spectroscopy. It is a method in which the use of noble metal nanoparticles enhances weak Raman signal and in addition quenches the fluorescence. This way the resulting spectra of studied inks allow identification and discrimination of inks made by various companies.

This work aimed to study inks from various companies using different types of nanoparticle solutions used for the enhancement of Raman signal. Analyzing the effects on Raman signal enhancement of different colloidal solutions allows the determination of the most practical way in differentiating various inks and different color variations (Fig. 1). The signal enhancement strongly depends on the nanoparticlesó size, shape, and concentration of the colloidal solution. The mixture of dyes used in the making of inks can be very similar in the products of various companies, with the only differences being the concentration of certain materials, hence the method of analysis of ink must be precise.

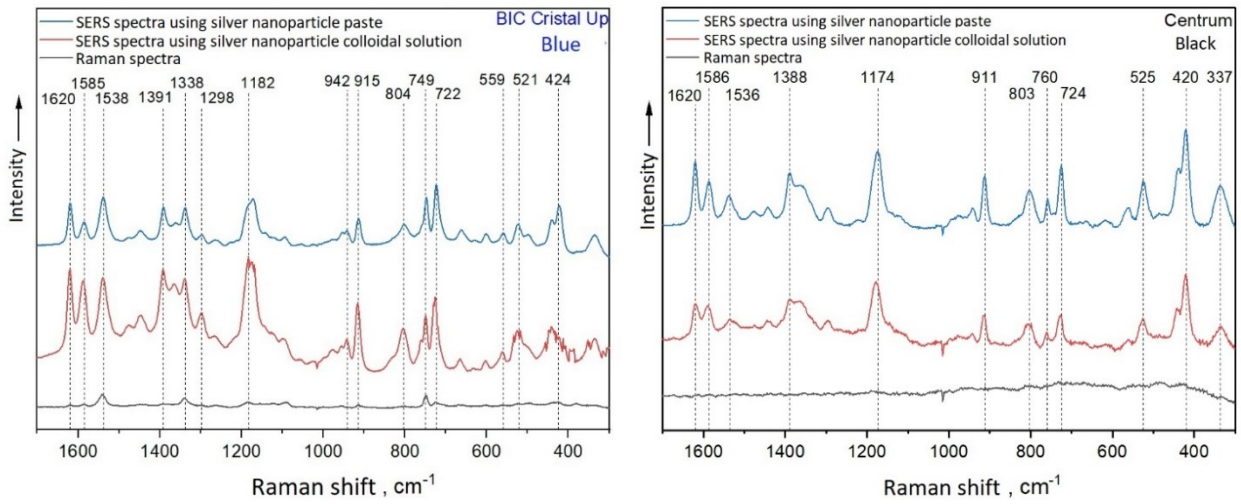

Fig. 1. Surface-enhanced Raman scattering spectra of blue (left) and black (right) inks collected using silver nanoparticle paste and colloidal solution.

[1] S. Baechler, Document Fraud: Will Your Identity Be Secure in the Twenty-first Century?, European Journal on Criminal Policy and Research, 26(3), 379ï 398 (2020).
[2] A. Braz, M. LËopez-LËopez, C. GarcËia-Ruiz, Raman spectroscopy for forensic analysis of inks in questioned documents, Forensic Science International, 232(3), 206ï 212 (2013).
[3] M. Calcerrada, C. Garc²a-Ruiz, Analysis of questioned documents: A review, Analytica Chimica Acta, 853(1), 143ï 166 (2015).

THE CHOOSE OF OPTIMAL CONDITIONS FOR THE DEVELOPMENT OF GLUCOSE BIOLOGICAL SENSOR BASED ON INSOLUBLE ELECTRON TRANSFER MEDIATOR

Erika Putincevaite[1], Natalija German[2]

[1] Department of Chemistry and Bioengineering, Faculty of Fundamental Sciences, Vilnius Gediminas Technical University Vilnius Tech, Sauletekio ave.11, LT-10223, Vilnius, Lithuania
[2] Division of Immunology, State Research Institute Center for Innovative Medicine, SantariskiÔg. 5, LT-08406, Vilnius, Lithuania
erika.putincevaite@stud.vgtu.lt

Biological sensors falls within the interdisciplinary field, which is one of the most active research areas in analytical chemistry [1]. Various cells, bacteria, antibodies, antigens, enzymes and multicellular living organisms are used to develop specific and selective biosensors [1,2]. Last decade the combination of enzymatic biosensors and electrochemical methods due their selectivity became very popular and found the application for diagnostic and monitoring in different area of industry, medicine and pharmacology [3]. About 85 % of the total biosensors market are glucose biosensors [4]. Electrochemical enzyme biosensors based on glucose oxidase play a significant role from simple, easy-to-use blood glucose tests until continuous glucose monitoring [1,2]. Various metal nanoderivatives, such as nanoparticles and nanostructures, are used to increase the electrode surface area and improve the electrical conductivity [4,5,6]. Biosensors with immobilized enzymes and metal nanoderivatives are characterized by high selectivity, sensitivity, rapidity, reversibility, reproducibility, practical application and well catalytic activities [4,5].

The aim of the research was to select optimal conditions for the development of glucose biosensor based on insoluble mediator – 1,10-phenanthroline-5,6-dione and various types of gold and platinum nanoderivatives. For this purpose, graphite electrode was used as working electrode, chronoamperometry and cyclic voltammetry – as electrochemical methods for the registration of analytical signal and the evaluation of the electrochemical process reversibility. It was investigated that electrochemically synthesized gold and platinum nanostructures in a combination with glucose oxidase offered some advantages (the facilitation of indirect electron transfer, higher surface area and the positive effect on the analytical signals) for the design of glucose biosensors. It was investigated that such compound as chitosan mixed with glucose oxidase and immobilized on the covered by gold or platinum nanoderivatives surface of graphite electrode does not have significant effect to the sensitivity of glucose biosensor. It was detected that more suitable is biosensor immobilized by one layer of each compounds in the presence of platinum due the high analytical signals and good repeatability. The optimal immobilization solution for platinum nanostructures formation and their covered conditions were investigated, then the basic analytical characteristics were evaluated. Furthermore, the developed biosensor also offers the possibility of using ultramicroelectrode designing for in vivo measurements.

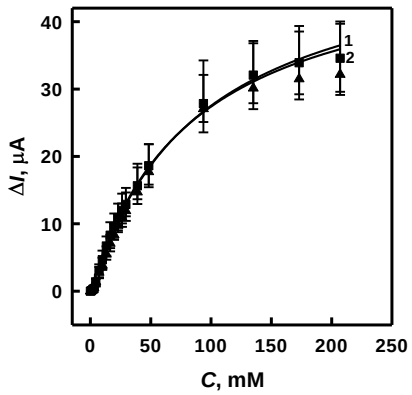

Fig.1. Calibration plots of glucose biosensors using chronoamperometry (1) and cyclic voltammetry (2) methods for the immobilization of platinum nanostructures on the surface of graphite rod electrode.

[1] G. Rebollar-Perez, J. Campos-Teran, N. Ornelas-Soto, A. Mendez-Albores, E. Torres, Biosensors based on oxidative enzymes for detection of environmental pollutants, Biocatalysis **1**, 118-129 (2015).
[2] Q. Liu, H. Li, Q. Zhao, R. Zhu, Y. Yang, Q. Jia, B. Bian, L. Zhuo, Glucose-sensitive colorimetric sensor based on peroxidase mimics activity of porphyrin-Fe_3O_4 nanocomposites, Materials Science and Engineering C **41**, 142-151 (2014).
[3] J. Lai, Y. Yi, P. Zhu, J. Shen, K. Wu, L. Zhang, J. Liu, Polyaniline-based glucose biosensor: A review, Journal of Electroanalytical Chemistry **782**, 138-153 (2016).
[4] J. Wang, Electrochemical glucose biosensors, Chemical Reviews **108**, 814-825 (2008).
[5] N. German, A. Ramanavicius, A. Ramanaviciene, Amperometric glucose biosensor based on electrochemically deposited gold nanoparticles covered by polypyrrole, Electroanalysis **29**, 1267-1277 (2017).
[6] N. German, A. Kausaite-Minkstimiene, A. Ramanavicius, T. Semashko, R. Mikhailova, A. Ramanaviciene, The use of different glucose oxidases for the development of an amperometric reagentless glucose biosensor based on gold nanoparticles covered by polypyrrole, Electrochimica Acta **169**, 326-333 (2015).

THE ENZYME-ASSISTED SYNTHESIS OF POLYMERIC NANOCOMPOSITES AND THEIR INVESTIGATIONS

Rugile Chmieliauskaite[1], Natalija German[2]

[1] Department of Chemistry and Bioengineering, Faculty of Fundamental Sciences, Vilnius Gediminas Technical University Vilnius Tech, Sauletekio ave.11, LT-10223, Vilnius, Lithuania
[2] Division of Immunology, State Research Institute Center for Innovative Medicine, SantariskiÔg. 5, LT-08406, Vilnius, Lithuania
rugile.chmieliauskaite@stud.vgtu.lt

Last decades the interest of nano- and biotechnologyõs application in the diagnostics and the monitoring of compounds increased rapidly [1,2]. Electrochemical enzymatic biosensors are the most popular and widely used in clinical analysis, pharmaceuticals, food processing industries and environmental monitoring due to their specificity and sensitivity in complex systems [2]. Diabetes mellitus – the most common endocrine disorder of carbohydrate metabolism and is considered a chronic disease caused by improper regulation of glucose in the blood [2,3]. Usually high sensitivity and selectivity, the rapidity and the reversibility, the application and the excellent catalytic activities are characterized for electrochemical biosensors immobilized by enzyme and polymers [2,4,5].

The main aim of this research was to synthesize polymeric nanocompositions (PNC) with embedded glucose oxidase and to develop glucose biosensors immobilized by such PNC with following addition of enzyme. To achieve electron transfer between the solution and graphite rod electrode soluble mediator – phenazine methosulfate (PMS) was used. It was predicted that formed by enzyme-assisted polymerization polyaniline and polypyrrole nanocomposites are able to facilitate indirect electron transfer and has the positive effect on the sensitivity and selectivity of developed system [2,4,5]. The most suitable immobilization method by PNC and the kind of polymer were chosen in order to improve analytical characteristics of glucose biosensor during research. Cyclic voltammetry was used to investigate the reversibility of electrochemical reaction and the suitability of developed glucose biosensor. Meanwhile, another electrochemical method such as chronoamperometry was used for the investigations of analytical characteristics and the stability of the developed system. It was evaluated, that the addition of PMS is necessary, because in the absence of mediator no electron transfer is able. Although the presence of polypyrrole nancomposites on the surface of working electrode enhanced the glucose analytical signal the most, however the lower limit of detection was obtained in the presence of polyaniline nanocompositions. Enzyme-assisted PNC could be apply in the construction of electrochemical glucose biosensors and could be use in different diagnostic applications.

Fig.1. Formed by enzyme-assisted polymerization polyaniline (on the left) and polypyrrole (on the right) solutions.

[1] F. Wang, S. Hu, Electrochemical sensors based on metal and semiconductor nanoparticles, Microchim Acta **165**, 1-22 (2009).
[2] J. Lai, Y. Yi, P. Zhu, J. Shen, K. Wu, L. Zhang, J. Liu, Polyaniline-based glucose biosensor: A review, Journal of Electroanalytical Chemistry **782** 138-153 (2016).
[3] E-H. Yoo, S.-Y. Lee, Glucose biosensors: An overview of use in clinical practice, Sensors **10**: 4558-4576 (2010).
[4] N. German, A. Ramanaviciene, A. Ramanavicius, Formation and electrochemical evaluation of polyaniline and polypyrrole nanocomposites based on glucose oxidase and gold-nanostructures, Polymers **12**, 3026 (2020).
[5] N. German, A. Ramanavicius, A. Ramanaviciene, Amperometric glucose biosensor based on electrochemically deposited gold nanoparticles covered by polypyrrole, Electroanalysis **29** 1267-1277 (2017).

EFFECT OF BETULINIC ACID IN THE POLYMERIC SHELL OF ENCAPSULATED QUANTUM DOTS ON THEIR INTERACTION WITH CELLS

Aliaksandra Radchanka[1], Varvara Hrybouskaya[2], Tatiana Terpinskaya[3]

[1] Institute for Physical Chemical Research, Belarusian State University, Belarus
[2] Belarusian State University, Chemistry Department, Belarus
[3] Institute of Physiology of the National Academy of Sciences of Belarus, Minsk, Belarus
aleksandraradchenko10@gmail.com

Betulinic acid is one of the most studied compounds from the class of pentacyclic triterpenoids with high biological activity. Betulinic acid has an antiproliferative and proapoptotic effects on malignant cells, therefore, it is under consideration as a basis for highly active antitumor agents. However, low solubility and poor bioavailability negatively affect clinical efficacy and limit the use of such compounds, that is why it needs to develop strategies for delivery to cells such chemicals. A promising approach to solve this problem is conjugation of these compounds with nanocarriers [1, 2]. Based on this, it is of interest to study the effect of biologically active compounds in the composition of nanoparticles on the interaction of the resulting hybrid nanostructures with cells.

The aim of this work was to study the process of binding of QDs ï betulinic acid conjugates to tumor cells and to determine how this compound in the QDsôshell affects interaction with cells. For this experiment we used fluorescent semiconductor nanoparticles (quantum dots ï QDs) and QDs conjugated with betulinic acid derivative.

Experiments were carried out with CdSe/ZnS core-shell QDs encapsulated with an amphiphilic polymer based on poly(maleic anhydride). The polymer charge was tuned by introducing a controlled amount of quaternary ammonium groups into the polymer. Weakly positive and strongly positive charge of the QDs inverstigated was chosen based on our previous studies [3]. Bethulinic acid was conjugated to polymeric shell of QDs by standard carbodiimide protocol. The conjugates were characterized by ɕ-potential of +9 and +20 mV. Reference QDs (without biomolecules in the shell) had ɕ-potential +4 and +15 mV, respectively. The hydrodynamic size of all particles was in the range from 15 to 22 nm; thus, the size effect between the reference QDs and the conjugates was not considered.

The results from flow cytometry shows that the QDs ï betulinic acid conjugates of +9 mV ɕ-potential (QDs_Bet1) bind to cells better than the reference ones (+4 mV, QDs1). The study of QDs ï betulinic acid conjugates of +20 mV ɕ-potential revealed the opposite effect such that the reference QDs bind to cells more effective than ones with bethulinic acid in the shell.

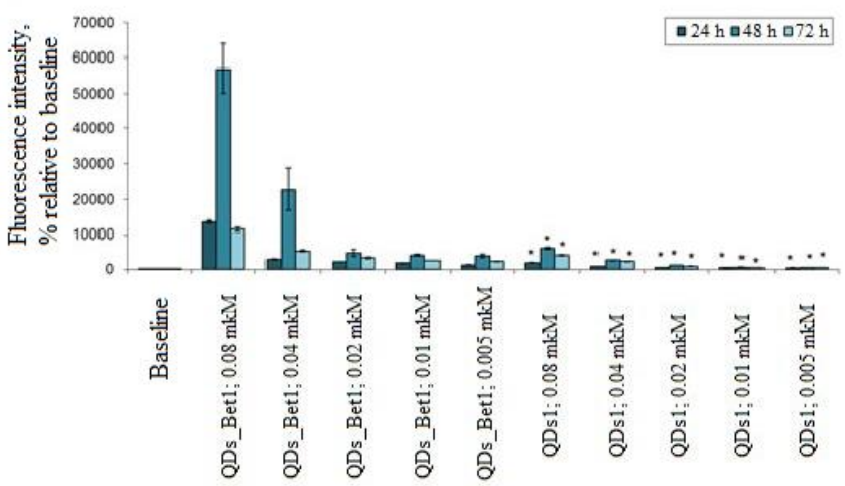

Fig. 1. Results of flow cytometry for interaction between QDs_Bet1 and QDs1 and C6 glioma cells; * $p < 0.05$ comparing QDs_Bet1 with QDs1

The conjugation of QDs with betulinic acid derivative changes the intensity of the interaction of nanoparticles with cells. The direction of changes in the interaction ñnanoparticle ï cellò depends on the value of surface charge of QDs: conjugates with ɕ-potential close to neutral bind to cells more intensively, and conjugates with a high positive ɕ-potential ï less intensely than the initial nanoparticles. The extent of the observed effects depends on the concentration of nanoparticles.

[1] A. Saneja et al., Therapeutic applications of betulinic acid nanoformulations, Ann N Y Acad Sci. **1**, 5-18 (2018)
[2] O. A. Vorobĉeva, et al., Betulin derivatives: biological activity and increasing solubility, Chemistry of plant raw materials **4**, 407 ï 430 (2019)
[3] E. Petrova et al., Luminescent quantum dots encapsulated by zwitterionic amphiphilic polymer: surface charge-dependent interaction with cells, Journal of the Belarusian State University. Chemistry **1**, 3-13 (2018)

RESEARCH AND DEVELOPMENT OF INNOVATIVE FUNCTIONAL NANOMEMBRANES IN BIOENGINEERING

Urtė Ciganė[1], Arvydas Palevičius[1]

[1] Department of Mechanical Engineering, Faculty of Mechanical Engineering and Design, Kaunas University of Technology, Lithuania
urte.cigane@ktu.lt

Nanomembranes receive much attention due to their special properties [1, 2]. Nanomembrane is a structure with a thickness of 1-100 nm, while other dimensions can be the size of nano/micro/macro scale [3]. Mechanical strength is one of the key parameters that determine the application of nanomembrane in various fields [4].

However, many nanomembranes cannot be used in bioengineering because many nanomembranes do not have sufficient mechanical strength and biocompatibility [5]. It is known that mechanical strength depends on the porosity of the material. According to the porosity of nanomembranes, mechanical strength decreases exponentially with increasing porosity [6]. Moreover, the biocompatibility and toxicity of nanomembranes have not yet been fully investigated. It is important that nanomembranes would be similar to natural materials. It means that nanomembrane should be made of biocompatible materials, have well-ordered pores, and have the required mechanical strength. For example, many inorganic nanomembranes have good mechanical properties because their pores are well ordered, while the advantages of organic nanomembranes are relatively low cost and good biocompatibility [7].

A widely used electrochemical fabrication method is anodizing [8]. Anodizing can be used to develop an innovative nanomembrane. The main advantages of anodizing are an ordered pore structure, the ability to control the pore diameter, and relatively low production costs [9].

An analysis of the scientific literature has shown that there is a lot of research, but the best innovative functional nanomembranes have not yet been developed. It is therefore necessary to develop new technologies and expand the possibilities of nanomembranes applications. The innovative functional nanomembrane will be developed in several stages. Firstly, a new anodic aluminum oxide (AAO) membrane fabrication technology with controlled nanopore arrays will be developed. Then, the created geometry will be transferred to a biomaterial that could be applied in bioengineering.

In the revealed case, there becomes a real possibility to create an innovative nanomembrane with the required mechanical strength and biocompatibility. The developed nanomembrane can be used not only in medical care for human health but also in areas such as biosensors used to detect biological/chemical threats or microchips used to test the toxicity of experimental drugs.

[1] Q. Guo, Z. Di, M. G. Lagally et al., Strain engineering and mechanical assembly of silicon/germanium nanomembranes, Materials Science and Engineering: R: Reports **128**, 1-31 (2018).
[2] F. Ma, B. Xu, S. Wu et al., Thermal-controlled releasing and assembling of functional nanomembranes through polymer pyrolysis, Nanotechnology **30**, 354001 (2019).
[3] G. Huang, Y. Mei, Assembly and Self-Assembly of Nanomembrane Materials-From 2D to 3D, Small **14**, 1-23 (2018).
[4] B. B. Sharma, A. Parashar, Mechanical strength of a nanoporous bicrystalline h-BN nanomembrane in a water submerged state, Physical Chemistry Chemical Physics **22**, 20453 (2020).
[5] C. R. Buhr, N. Wiesmann, R. C. Tanner et al., The Chorioallantoic Membrane Assay in Nanotoxicological Research-An Alternative for In Vivo Experimentation, Nanomaterials **10**, 2328 (2020).
[6] P. N. Christy, S. K. Basha, V. S. Kumari et al., Biopolymeric nanocomposite scaffolds for bone tissue engineering applications-A review, Journal of Drug Delivery Science and Technology **55**, 101452 (2020).
[7] S. Adiga, C. Jin, L. Curtiss et al., Nanoporous membranes for medical and biological applications, WIREs Nanomedicine and nanobiotechnology **1**, 568-581 (2009).
[8] G. Absalan, S. Barzegar, M. Moradi et al., Fabricating Al_2O_3-nanopores array by an ultrahigh voltage two-step anodization technique: Investigating the effect of voltage rate and Al foil thickness on geometry and ordering of the array, Materials Chemistry and Physics **199**, 265-271 (2017).
[9] Y. Patel, G. Janugas, A. Paleviius et al., Development of Nanoporous AAO Membrane for Nano Filtration Using the Acoustophoresis Method, Sensors **20**, 3833 (2020).

TOWARDS SPECTROSCOPIC ELLIPSOMETRY BASED BIOSENSOR: EVALUATION OF HUMAN SERUM ALBUMIN ADSORPTION TO POROUS ALUMINIUM OXIDE

Vincentas Maciulis[1], Silvija Juciute[2], Uldis Malinovskis[3], Donats Erts[3], Arunas Ramanavicius[1,2], Almira Ramanaviciene[2], Saulius Balevicius[1], Ieva Plikusiene[1,2]

[1]Laboratory of Nanotechnology, State Research Institute Centre for Physical Sciences and Technology, Sauletekio ave. 3, Vilnius, Lithuania;
[2] Institute of Chemistry, Faculty of Chemistry and Geosciences, Vilnius University, Naugarduko 24, Vilnius Lithuania;
[3]Institute of Chemical Physics, University of Latvia, LV-1586 Riga, Latvia;
vincentas.maciulis@ftmc.lt

Investigating protein adsorption and desorption from nanoporous materials is an important task due to the wide application of nanostructured materials in protein separation, purification, and biosensor development. Nanoporous material ability to adsorb large molecules within the pores, comes from the pore size and is significantly dependent on the hydrophobic or hydrophilic properties of the material. Biosensors based on nanomaterial coatings attract significant attention, especially those that are highly sensitive to a specific protein or molecule [1]. Nanoporous metal oxide coatings can be used in the development of such biosensors due to the physical and chemical properties that they possess.

Porous anodic aluminium oxide (pAAO) coating, which is formed by electrochemical anodization of aluminium in an acidic electrolyte, is one of the typical self-organised fine structures with nanohole arrays. The pore diameter can be changed by varying the concentration and composition of the acidic electrolyte as well as the voltage of anodization [2]. pAAO exhibits such properties as biocompatibility, highly ordered self-assembled honeycomb pore structure, high mechanical and thermal stability, and chemical resistance. Various biosensing platforms based on porous aluminium oxide have been applied in optical and electrochemical biosensors [3].

Spectroscopic ellipsometry (SE) can be successfully used for optical biosensing because it requires no labelling and the light used for the measurement does not affect or destroy the samples. Furthermore, this method makes it possible to perform simultaneous measurement of both s and p polarisation, thus obtaining a better agreement between the experiment and model data [4].

In this work, the investigation of human serum albumin (HSA) adsorption on the pAAO coating was analysed using SE method. The thickness of the formed pAAO layer determined from SE results was 322.75 Ñ0.12 nm. The estimated radius of the nanopores was 39 Ñ5 nm and the distance between nanopores was 107 Ñ6 nm. The obtained results showed that the protein concentration inside the nanochannels was several hundred times higher than in the buffer solution; the initial phase of the adsorption process was slow (3.23 mgIcm^{-3} Imin^{-1}) in comparison with the protein desorption rate (21.2 mgIcm^{-3} Imin^{-1}) by means of pAAO layer washing; conventional washing with PBS solution and deionized water does not completely remove HSA molecules from pAAO pores and, therefore, the HSA concentration inside nanopores after 16 h of washing still remains almost 100 times higher than that present in PBS solution.

Acknowledgement:

This work is part of a project that has received funding from the European Unionôs Horizon 2020 research and innovation program under the grant agreement No. 778157 CanBioSe.

[1] V. Maciulis *et al.*, ñPorous aluminium oxide coating for the development of spectroscopic ellipsometry based biosensor: Evaluation of human serum albumin adsorption,ò *Coatings*, vol. 10, no. 11, pp. 1ï10, 2020, doi: 10.3390/coatings10111018.

[2] H. Masuda and M. Satoh, ñFabrication of gold nanodot array using anodic porous alumina as an evaporation mask,ò *Japanese J. Appl. Physics, Part 2 Lett.*, vol. 35, no. 1 B, 1996, doi: 10.1143/jjap.35.l126.

[3] F. S. H. Krismastuti, H. Bayat, N. H. Voelcker, and H. Schº nherr, ñReal Time Monitoring of Layer-by-Layer Polyelectrolyte Deposition and Bacterial Enzyme Detection in Nanoporous Anodized Aluminum Oxide,ò *Anal. Chem.*, vol. 87, no. 7, pp. 3856ï3863, 2015, doi: 10.1021/ac504626m.

[4] A. Hans, ñEllipsometry on thin organic layers of biological interest¡ characterization and applications,ò *Thin Solid Films*, vol. 377ï378, pp. 48ï56, 2000, doi: 10.1016/S0040-6090(00)01385-7.

ZNO NANOPARTICLES FOR ANTI-REFLECTIVE APPLICATIONS

Paulius Laurikėnas[2], Mindaugas Ilickas[1, 2] Tomas Tamulevičius[1, 2], Simas Ramanauskas[1, 2]

[1]Institute of Materials Science, Kaunas University of Technology, Lithuania;
[2]Department of Physics, Kaunas University of Technology, Lithuania.
paulius.laurikenas@ktu.edu

ZnO nanoparticles have attracted great interest due to their exceptional properties such as defect-induced ferromagnetism, UV sensing and reversible transition from hydrophobicity to hydrophilicity [1] [2]. ZnO nanotetrapods, synthesized by combustion methods [3] are one of various morphologies of ZnO which are used for optoelectronical and photovoltaic applications to reduce the reflection of light from surface. These type of coatings are called anti-reflective [4].

In this work, a simple method of spraying was used to deposit anti-reflective coating of ZnO nanoparticles on glass substrate. The thickness of coating was measured by custom UV transmittance meter. Reflectance, transmittance and other optical properties were investigated by special optical setup, which includes spectrometer. Multifunctional nature of ZnO nanoparticle anti-reflection coatings was observed: such coatings are more neutral to light polarization and reflect less incident light. Moreover, characteristic of UV blocking was observed in reflectance and transmittance near the edge of UVA (~400nm).

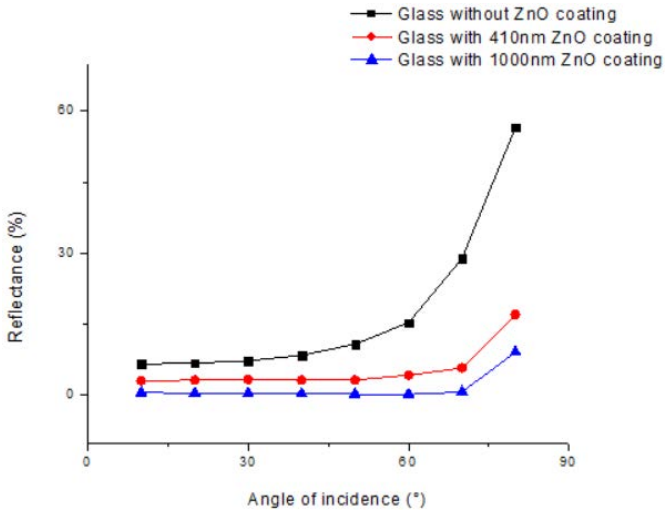

Fig. 1. Light reflection dependence on angle of incidence (ə = 632.8nm).

[1] Y. K. Mishra and R. Adelung, ñZnO tetrapod materials for functional applications,ò *Mater. Today*, vol. 21, no. 6, pp. 631ï 651, 2018, doi: 10.1016/j.mattod.2017.11.003.

[2] X. Feng, L. Feng, M. Jin, J. Zhai, L. Jiang, and D. Zhu, ñReversible Super-hydrophobicity to Super-hydrophilicity Transition of Aligned ZnO Nanorod Films,ò *J. Am. Chem. Soc.*, vol. 126, no. 1, pp. 62ï 63, 2004, doi: 10.1021/ja038636o.

[3] S. Rackauskas *et al.*, ñA novel method for continuous synthesis of ZnO tetrapods,ò *J. Phys. Chem. C*, vol. 119, no. 28, pp. 16366ï 16373, 2015, doi: 10.1021/acs.jpcc.5b03702.

[4] H. K. Raut, V. A. Ganesh, A. S. Nair, and S. Ramakrishna, ñAnti-reflective coatings: A critical, in-depth review,ò *Energy Environ. Sci.*, vol. 4, no. 10, pp. 3779ï 3804, 2011, doi: 10.1039/c1ee01297e.

CONTROL OF THE STAINLESS STEEL WETTABILITY VIA VARYING FEMTOSECOND LASER PARAMETERS USED FOR IMPOSING LASER-INDUCED PERIODIC SURFACE STRUCTURES

Mantas Mikalkevičius[1], Mindaugas Juodėnas[1], Tomas Tamulevičius[1,2]
Asta Tamulevičienė[1,2]

[1]Institute of Materials Science of Kaunas University of Technology, K. Baršausko Str. 59, LT-51423, Kaunas, Lithuania
[2]Department of Physics of Kaunas University of Technology, Studentų Str. 50, LT-51368, Kaunas, Lithuania
mantas.mikalkevicius@ktu.lt

Wettability is a very important surface property for range of tools, implants and devices operating in a watery environment. Processing of solids near their ablation threshold by high intensity polarized laser irradiation may lead to the development of regular nanoscale structures known as Laser-induced Periodic Surface Structures (LIPSS). Applying LIPSS to a surface can lead to numerous applications of surface functionalization including but not limited to improved wetting performance [1], antibacterial activity [2], low optical reflectance [3]. On top of that, wettability can be controlled by varying laser parameters around required LIPSS developing conditions. This has a huge impact on process optimization and structuring time, which is very important for large scale manufacturing. It was reported that wettability properties of the LIPSS structures is prone for aging become even more hydrophobic after exposure to atmosphere [4].

In this work, the fundamental harmonic (1030 nm) of a linearly polarized Yb:KGW femtosecond laser beam was scanned employing a galvoscanner and a f-theta lens over the surface of a stainless steel mirror while varying the pulse energy, pulse density, and laser spot overlap. Two pulse energy density values were used 223 and 447 mJ/cm^2 as well as pulse densities of 1000 and 2000 pulses per millimeter while the pulse repetition rate was kept at 200 kHz. The wettability of the surfaces was evaluated using the sessile drop method where 1 Õl volume droplets of water were dispensed on the pristine and differently treated surfaces. Optical microscope images of the laser-treated samples are depicted in Fig. 1.

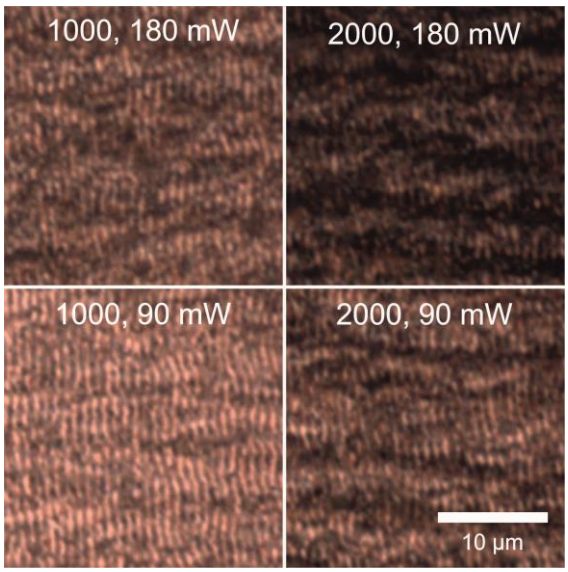

Fig. 1. Optical microscope micrographs of stainless steel surface after the laser treatment. Numbers indicate pulse density and average laser power used for treatment. Scale bar 10 εm.

Laser treatment varying energy density enabled control of the wetting angle for water in a wide range spanning from 97Áto 131Áfor deionized water. The contact angle was increased by 87Ácompared to pristine surface. The highest water contact angle values were obtained after 14 days of laser processing. Faster processing is obtained using 1000 pulses per millimeter with the price of 18Ásmaller water contact angle.

[1] Van Driel, H. M., Sipe, J. E., and Young, J. F., Laser-induced periodic surface structure on solids: a universal phenomenon, Physical Review Letters 49(26), 1955ï 1958 (1982). https://doi.org/10.1103/PhysRevLett.49.1955
[2] Lutey, A. H., Gemini, L., Romoli, L., Lazzini, G., Fuso, F., Faucon, M., and Kling, R., Towards laser-textured antibacterial surfaces, Scientific Reports 8(1), 1ï 10 (2018). https://doi.org/10.1038/s41598-018-28454-2
[3] A. Dostovalov, K. Bronnikov, A. Kuchmizhak, Hierarchical anti-reflective laser-induced periodic surface structures (LIPSSs) on amorphous Si films for sensing applications, Nannoscale 12(25), 2020, DOI: 10.1039/D0NR02182B
[4] Varlamova, O., Hoefner, K., Ratzke, M. et al. Modification of surface properties of solids by femtosecond LIPSS writing: comparative studies on silicon and stainless steel. Appl. Phys. A 123, 725 (2017). https://doi.org/10.1007/s00339-017-1362-y

EFFECT OF SUBSTRATE NATURE ON CELL MORPHOLOGY OF THIN ANODIC ALUMINA FILMS FORMED IN THE SULFURIC ACID SOLUTION

Katsiaryna Charniakova[1], Arunas Jagminas[1], Igor Vrublevsky[2]

[1] Department of Electrochemical Material Science, Center for Physocal Science and Thecnology, Lithuania
[2] Department of Micro- and Nanoelectronics, Belarusian State University of Informatics and Radioelectronics, Belarus
katsiaryna.charniakova@ftmc.lt

Surface morphology of the porous anodic alumina film is determined by both a pore diameter (d_{pore}) and an interpore distance (D_{inter}). In [1], it was shown that for porous anodic alumina the dependance of D_{inter} on anodizing voltage (U_a) was linear, however, the dependance of d_{pore} on U_a was non-linear. The main parameters that affect the surface morphology of the films are anodizing voltage and electrolyte temperature. In addition, the morphology of porous anodic alumina films can be also influenced by non-electrochemical parameters such as nature of substrate. Therefore, in this work we aimed to study and analyze the effect of electrolyte temperature and anodizing voltage on cell morphology of thin films of sulfuric acid anodic alumina formed on different substrates. For that, thin aluminum films of about 100 nm thick were obtained by deposition of aluminum on the silicon substrate with a thin silicon dioxide film (SiO_2/Si wafers), on glass-ceramic and glass substrates through thermal evaporation in a vacuum and on polished aluminum substrates (0.6 mm thick) and then anodized in two-electrode cell (Pt was a counter electrode) in a 1.8 M aqueous solution of sulfuric acid at constant voltage in the range of 12ï 20 V.

The data obtained demonstrated d_{pore} depended on the thermal conductivity of the substrate in the voltage range of 12ï 14 V. Depending on the substrate type, d_{pore} increased in the following order: glass > glass ceramic > SiO_2/Si > aluminum. It was found that the anodizing voltage of 16 V was a turning point for anodic films obtained in sulfuric acid after which the slope of the plots for d_{pore} vs. U_a and D_{inter} vs. U_a changed (Fig. 1). This was explained by the process of oxygen evolution. It was shown that when the anode potential reaches values exceeding the equilibrium potential of oxygen electrode, oxidation of water molecules begins with the release of oxygen from the solution. We assumed that the oxygen evolution reaction on aluminum oxide surface at the pore bottom at U_a > 16 V results in an increase in acid concentration in the solution and, consequently, in higher electrolyte chemical activity and increase in the dissolution rate of the oxide layer of pore walls.

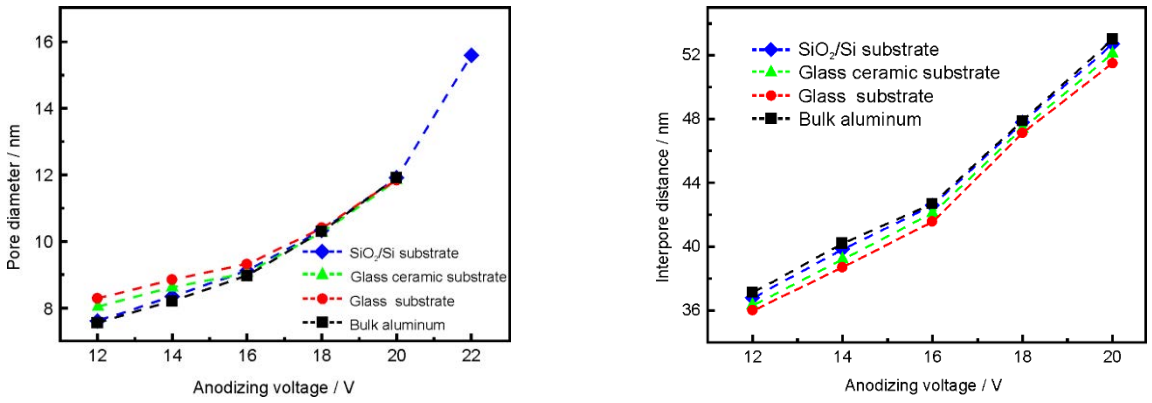

(a) (b)

Fig. 1. Evolution of pore diameter (a) and interpore distance (b) as a function of the anodizing voltage for porous anodic alumina films formed on aluminum substrate, SiO_2/Si substrate, glass ceramic substrate and glass in a 1.8 M sulfuric acid.

[1] W. Lee, S.J. Park, Porous anodic aluminum oxide: anodization and templated synthesis of functional nanostructures, Chem. Rev. **114** 7487ï 7556 (2014).

SYNTHESIS OF GOLDï SILVER NANOPARTICLES USING NANOSECOND LASER AND THIN METALLIC FILMS

Vita Petrikaitã, Evaldas Stankeviļius

Department of Laser Technologies, Center of Physical Sciences and Technology, Lithuania
vita.petrikaite@ftmc.lt

Gold and silver nanoparticles are applied in a variety of technologies, including advanced catalysts, SERS, and components of optical and electronic devices whose properties depend on plasmonic vibrations. Gold and silver nanoparticles have intense colors, high surface area to volume ratio, high electrical conductivity, chemical stability, catalytic functions, etc.[1] The optical properties of metal nanoparticles depend on the localized surface plasmon resonance (LSPR).

The choice of the method for the synthesis of precious metal nanoparticles is no less important as it determines the morphology, stability, and physicochemical properties [2]. The main problem encountered during synthesis is the uniform and repetitive deposition of nanoparticles. The use of a laser helps to solve this problem. Unlike traditional methods, this process does not require chemical reagents and deposition of nanoparticles in solution. Thermal heating of a thin metal coating with a nanosecond pulsed laser can be performed immediately on the desired surface. This method has the advantages of accuracy, easy laser parameters control, a low impact on the surrounding areas, and the surface itself. With this method, nanoparticles can be deposited directly and fairly evenly on various substrates and can be easily replicated.

Here, the generation of gold and silver nanoparticles on a glass surface from the metal films using a nanosecond laser and the investigation of the morphology and plasmonic properties of the particles will be presented. Also, the difference between the generated nanoparticle size, dispersion, and optical properties of different metals will be compared and analyzed.

[1] Y. C. Yeh, B. Creran, V. M. Rotello, Gold nanoparticles: preparation, properties, and applications in bionanotechnology, Nanoscale 4(6), 1871ï 1880 (2012).

[2] V. Pareek, A. Bhargava, R. Gupta , N. Jain, J. Panwar, Synthesis and Applications of Noble Metal Nanoparticles: A Review, Advanced Science, Engineering and Medicine (9), 527ï 544 (2017).

DEVELOPMENT OF NANOCOMPOSITES BASED ON CLAY, GRAPHENE OXIDE AND MAGNETITE/MAGHEMITE

Raman Novikau[1], Galina Lujanienė[1*], Vidas Pakštas[2], Martynas Talaikis[3], Audrius Drabavičius[2*], Arnas Naujokaitis[2*]

[1] Department of Environmental Research, Center for Physical Sciences and Technology, Lithuania
[2]Department of Characterisation of Materials Structure, Center for Physical Sciences and Technology, Lithuania
[3]Department of Organic Chemistry, Center for Physical Sciences and Technology, Lithuania
raman.novikau@ftmc.lt

The dynamically developing industrial sector, as one of the significant anthropogenic factors, is a source of a huge number of pollutants – organic, inorganic and biological, which negatively affect ecological integrity [1]. Despite the huge variety of methods suitable for removing pollutants from various wastes, there is still a shortage of highly efficient, eco-friendly materials. Adsorption methods have great potential for applications in the field of environmental protection [2, 3]. Therefore, it is promising to search for cost-efficient and biocompatible adsorbents possessing high adsorption capacity.

Currently, one of the most prospective adsorbents is clay minerals, which are not inferior in efficiency to commercial adsorbents, and in some cases even surpass them. Clays are being actively modified in order to increase their efficiency and selectivity towards specific pollutants. Another advantage of using clays is their possible combining with other potential adsorbents, that can increase the effectiveness of the composite due to a synergistic effect, while the most important is the ability of clays to minimize the toxic effect of other components in the composite, for example, graphene oxide [4], as well as various other modifiers [5].

The main challenges in this research area are possible additional pollution after the use of these adsorbents, the toxicity aspect of modified clays that are not fully understood, and that the data obtained *in vitro* and *in vivo* are contradictory.

The aim of this study was to develop composites of Clay-Graphene Oxide (GO)-Magnetite (MG)/Maghemite (MGH).

The first step of preparation of composites includes synthesis of all components. GO was obtained by the Hammers method, MG/MGH by a co-precipitation reaction of ferrous and ferric ions. Triassic clay (Šaltiškiai in North Lithuania) was used in this study. The clay was treated with 0.5 M HCl solution while for synthesis both treated and untreated clays were used. The synthesis of the composite included dispersing GO and MG/MGH in an ultrasonic bath for 2 h, followed by the addition to acid-treated (ATC) or untreated clay (UTC) to the solution, keeping the mixture under constant stirring in a flow of argon for 1.5 hours, at 60 °C. Then this mixture is centrifuged, the resulting composite is taken and dried in vacuum for 24 hours.

Thus, four composites were obtained based on acid-treated and untreated clay with different weight ratio (%) - ATC (43.48)-GO (13.04)-MG/MGH (43.48); ATC (66.67)-GO (16.67)-MG/MGH (27.78); UTC (43.48)-GO (13.04)-MG/MGH (43.48); UTC (66.67)-GO (16.67)-MG/MGH (27.78). These composites were characterized using X-ray diffraction analysis (XRD), X-ray fluorescence analysis (XRF), scanning electron microscope (SEM), transmission electron microscope (TEM) and FTIR spectroscopy (FTIR). The obtained composites were applied to remove heavy metals from aqueous solutions. Preliminary results of studying the adsorption of copper on composites showed the adsorption efficiency from 90 to 99%.

[1] M. Hill, Understanding Environmental Pollution (4th ed.) (Cambridge: Cambridge University Press, 2020).
[2] B. Mu, A. Wang, Adsorption of dyes onto palygorskite and its composites: a review. Journal of Environmental Chemical Engineering **4**, 1274-1294 (2016).
[3] H. Han, M. Rafiq et al., A critical review of clay-based composites with enhanced adsorption performance for metal and organic pollutants, Journal of hazardous materials **369**, 780-796 (2019).
[4] M. Kryuchkova, R. Fakhrullin, Kaolin alleviates graphene oxide toxicity, Environmental Science & Technology Letters **5**, 295-300 (2018).
[5] K. Kansara, A. Kumar et al., Combination of humic acid and clay reduce the ecotoxic effect of TiO_2 NPs: A combined physico-chemical and genetic study using zebrafish embryo, Science of the Total Environment **698**, 134133 (2020).

P2-34

DID NOT PARTICIPATE

THE IMPACT OF GOLD NANOPARTICLE SIZE ON SPECTROPHOTOMETRIC DETECTION OF HEPARIN

Ernesta Lubinaite[1]*, Benediktas Brasiunas[1], Anton Popov[1], Asta Kausaite-Minkstimiene[1], Jonas Labutis[1], Almira Ramanaviciene[1]

NanoTechnas ï Center of Nanotechnology and Materials Science, Institute of Chemistry, Faculty of Chemistry and Geosciences, Naugarduko str. 24, Vilnius, Lithuania
ernesta.lubinaite@chgf.stud.vu.lt

Heparin is a pharmaceutical drug that is used to prevent the formation of blood clots [1]. Since diseases that can affect the circulatory system are widespread nowadays, it is important to effectively monitor blood coagulation, especially during surgery. Methods that are currently used for heparin detection have a few drawbacks. Firstly, these methods are not specific for heparin and there are loads of analytical interferences. Secondly, they are time consuming [2]. These drawbacks led to a need for a new analytical system that is specific for heparin. Since it is a highly negatively charged polysaccharide, heparin can be easily adapted to the analytical system where negatively charged colloidal gold nanoparticle (GNP) solution is used resulting in aggregation [3].

In this work, we compared how the difference in GNPs size (13 nm and 3.5 nm) affect analytical parameters such as sensitivity and reproducibility of the system used for heparin detection. The system itself relies on the coagulation of negatively charged colloidal GNP solution in the presence of positively charged polymer poly-L-lysine (PLL). Stable GNP solution is red due to the local surface plasmon resonance (LSPR) and the peak is registered at a wavelength of 520 nm. The addition of PLL to GNP solution results in nanoparticle aggregation. Visible color change can be observed after the aggregation with GNP solution turning blue and LSPR peak shifting to a wavelength of 650 nm. On the other hand, heparin stabilizes GNP solution by preventing the PPL induced aggregation, resulting in a GNP solution of specific color based on heparin concentration allowing for the creation of a heparin sensor (Fig. 1).

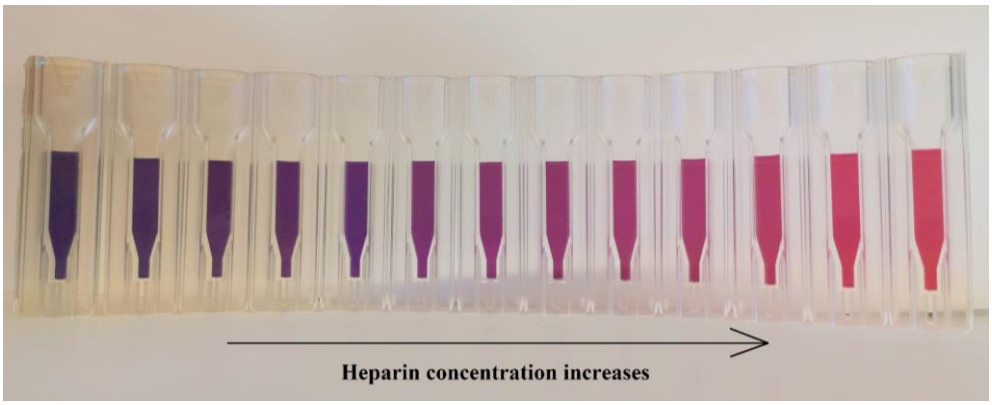

Fig. 1. The color change of GNP solutions increasing concentration of heparin.

[1] P. E. Makris, ñLow molecular weight heparin,ò *Arch. Hell. Med.*, vol. 16, no. 4, pp. 329ï 332, 1999.
[2] M. A. Smythe, J. Priziola, P. P. Dobesh, D. Wirth, A. Cuker, and A. K. Wittkowsky, ñGuidance for the practical management of the heparin anticoagulants in the treatment of venous thromboembolism,ò *J. Thromb. Thrombolysis*, vol. 41, no. 1, pp. 165ï 186, 2016.
[3] X. Ma, X. Kou, Y. Xu, D. Yang, and P. Miao, ñColorimetric sensing strategy for heparin assay based on PDDA-induced aggregation of gold nanoparticles,ò *Nanoscale Adv.*, vol. 1, no. 2, pp. 486ï 489, 2019.

UPCONVERTING NANOPARTICLES - SYNTHESIS AND CHARACTERIZATION

Aleksandra Wosztyl[1,3], Krzysztof Fronc[1], Bożena Sikora[1], Tomasz Wojciechowski[1], Roman Minikayev[1], Wojciech Paszkowicz[1], Kamil Sobczak[2], Przemysław Kowalik[1], Katarzyna Łysiak[3], Danek Elbaum[1], Jacek Szczytko[3], Izabela Kamińska[1]

[1]Institute of Physics, Polish Academy of Sciences, aleja Lotników 32/46, Warsaw, Poland
[2]Faculty of Chemistry, Biological and Chemical Research Centre, University of Warsaw, Żwirki i Wigury 101, Warsaw, Poland
[3]Faculty of Physics, University of Warsaw, Ludwika Pasteura 5, Warsaw, Poland
a.wosztyl@student.uw.edu.pl

Nowadays one of the most challenging issues in medical sciences is the early detection of cancer. There are thousands of chemical and biological methods, but more and more popular become using also physical methods, such as quantum effects from novel nanomaterials. One of the widely explore fields, which shows potential applications in medical sciences, is the upconvertion phenomena. The main goal was to obtain gadolinium oxide nanoparticles doped with selected metals to investigate energy transfer between erbium (Er^{3+}) and ytterbium (Yb^{3+}) ions and enhance of the efficiency of upconvertion by doping structures with magnesium ions (Mg^{2+}).

The examined nanoparticles were synthesized by a homogeneous precipitation method for 2 hours at a temperature of 85°C. The crystal structure arrangement was obtained by calcining at a temperature of 990°C for 3 hours. Additionally, nanoparticles were characterized with several methods. The atomic composition of the nanoparticles was analyzed via energy-dispersive X-ray spectroscopy (EDS). The size were determined by scanning electron microscopy (SEM) and transmission electron microscopy (TEM). The crystal structure was characterized by X-ray diffraction (XRD). Optical properties were investigated by using photoluminescence measurements. Finally, nanoparticles were incubated with mouse mammary carcinoma (4T1) cells for 24h to examine their suitability for use in biology as luminescent markers.

As result of research, nanoparticles show luminescence in green emission region - maxima occur at a wavelength of 565 nm ($^4S_{3/2}$ => $^4I_{15/2}$, $^2H_{11/2}$ => $^4I_{15/2}$) – and in red emission region - maxima occur at a wavelength of 663 nm ($^4F_{9/2}$ => $^4I_{15/2}$). The optical properties were examined by excitation with a semiconductor laser with a wavelength of 980 nm (continuous wave). An increase in the effectiveness of the upconvertion process was observed - an 8-fold increase in red luminescence efficiency was obtained for nanoparticles doped with 2.5% Mg^{2+} compared with non-doped nanoparticles (Gd_2O_3: 1% Er^{3+},18% Yb^{3+}). The measurements were carried out at a laser power density of 12 $W \cdot cm^{-2}$. The nanoparticles were dissolved in a dimethyl sulfoxide solution. The nanoparticles diameter was 380 nm, 282 nm, and 260 nm (before calcining). The diameters of the obtained nanoparticles - are 302 ± 37 nm and 278 + 36 nm (after a calcining) respectively. Obtained upconverting nanostructures show beneficial properties, which make them appropriate material to be used in bioimaging.

INVESTIGATION OF INGAN/GAN QUANTUM WELLS PHOTOLUMINESCENCE AND SURFACE TOPOGRAPHY

Gytis Babaitis[1], Darius Dobrovolskas[1]

[1]Institute of Photonics and Nanotechnology, Faculty of Physics, Vilnius University, Lithuania
gytis.babaitis@ff.stud.vu.lt

InGaN is a direct bandgap semiconductor material made with a mix of GaN and InN. By varying the amount of indium present in the alloy, we can change the bandgap of the material (usually from 0.69 eV to 3.4 eV)[1]. In this research we investigated the effects of the indium percentage difference in the InGaN multiple quantum wells (MQW) grown using metal organic chemical vapor deposition (MOCVD) method by Cheyenne Lynsky's team at University of California, Santa Barbara.

We studied four InGaN MQW samples having varying amounts of In (9 %, 12 %, 17 %, 20 %). They were excited with a 405 nm wavelength laser diode through a high numerical aperture (NA = 0.55) objective. Three measuring techniques were used. Confocal microscope – for the photoluminescence (PL) spatial distribution, atomic force microscope (AFM) – for the topography and using scanning near – field optical microscope (SNOM) technique enabled us to link the surface topography of the samples and its effects on the photoluminescence. Indium percentage and subsequent PL spectrum peaks were: 12 % - 431 nm, 17 % - 485 nm, 20 % - 535 nm (Figure 1). All samples showed highly inhomogeneous spatial distribution of PL intensity and peak position. Statistical analysis of PL maps revealed a positive correlation between PL intensity and peak position, i.e. PL intensity is more intense in areas that emit at longer wavelengths. This is due to carrier localization in the areas of higher indium content. The topography analysis revealed that surface roughness increases with average indium content in the samples. Moreover, SNOM measurements showed that PL intensity drops in the lower parts of the surface. We showed that the topography of the samples correlates with the photoluminescence intensity.

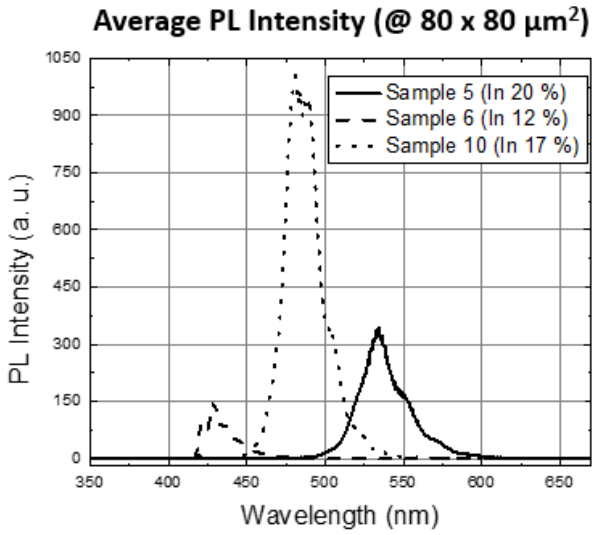

Fig. 1. Spatially averaged PL spectra of InGaN MQW

[1] G. Linti, "The Group 13 Metals Aluminium, Gallium, Indium and Thallium. Chemical Patterns and Peculiarities. Edited by Simon Aldridge and Anthony J. Downs.," Angew. Chemie Int. Ed., vol. 50, no. 49, pp. 11569–11569, Dec. 2011, doi: 10.1002/anie.201105633.

P2-38

DID NOT PARTICIPATE

DEVELOPMENT OF A POROUS SILICON BASED GUIDE MODE RESONATOR AS A TEMPLATE FOR SERS-APPLICATION

Nadzeya Khinevich [1*], Juodãnas Mindaugas[1], Tomas Tamuleviļius[1,2], Sigitas Tamuleviļius[1,2]

[1] Institute of Materials Science of Kaunas University of Technology, Kaunas, Lithuania
[2] Department of Physics, Kaunas University of Technology, Kaunas, Lithuania
nadzeya.khinevich@ktu.edu

Surface enhanced Raman scattering (SERS) spectroscopy is well-known as an efficient method of molecules detection. Rough metallic surfaces or closely packed metallic nanoparticles arrays are the main attributes used to achieve Raman signal enhancement [1]. The signal enhancement is observed when the studied molecule is found next to the metal surface that is characterized by strong electromagnetic field appearing under the external excitation. This effect is known as Localized Surface Plasmon Resonance (LSPR).

The promising use of a guide mode resonator (GMR) for additional amplification of SERS-signal has been shown in recent reports [2]. The GMR is regarded as a diffraction grating with subwavelength dimensions on a dielectric template. The excitation wave tends to travel along the surface interacting with the material and followed by transmitting or reflecting processes. The rise in SERS-activity of GMR/metallic nanostructures is observed due to strong coupling between these two structures and can be controlled by tailoring the height and periodicity of the loaded dielectric grating.

Nanostructured silicon is considered to be an efficient substrate for SERS-active sensors development. Porous silicon (PS) is one of the silicon nanostructures types, that is widely used as a template for deposition of varying metallic forms such as silver and gold nanoparticles, dendrites, quasi-continuous films [3], etc. Furthermore, it is reported that PS can take part in Raman signal enhancement while being measured [4], which raises interest in its use as a substrate for SERS-active sensors fabrication.

In our work we propose a new approach of amplification of the already strong local field that appears between silver nanoparticles located at several nanometers from each other, using porous silicon periodic structures as the GMR for SERS-application. According to this approach the nanostructure of GMR/porous silicon/ silver nanoparticles has been fabricated in several steps. At first, the periodic gratings have been formed on a silicon wafer by direct laser interference patterning using Femto-lab workstation equipped with Yb:KGW femtosecond laser Pharos. The wavelengths of 515 nm and 40 kHz frequency were set in the second harmonic oscillator. The laser power and values of pulses were ranging from 16 mW to 160 mW and from 1000 pulses to 25000, respectively for searching the surface of the silicon grating close to the flat one in order to avoid additional light scattering by irregularities. Then, the fabricated GMR has been porosified by electrochemical etching in aqueous-based electrolyte including 10% hydrofluoric acid at current density 140 mA/cm^2. And finally, the silver nanoparticles have been deposited on GMR/porous silicon by immersion deposition from 3 mM silver salt solution for an hour.

The morphology and optical properties of the nanostructures produced have been studied. The application of the structure to SERS-spectroscopy have been investigated, using Rhodamine 6G as a target molecule and laser wavelength 532 nm. It has been established that GMR/PS/silver nanoparticles system exhibits higher SERS-activity in comparison with PS/silver nanoparticles structure.

The experimental results are supported by the modelling results enabling us to offer way of production of SERS-active porous silicon based substrates. We demonstrate that the most effective sensor with properties individually selected for the used laser wavelength in the SERS-measurements may be produced by varying the pitch of GMR, porosity of silicon and shape of nanoparticles.

[1] M. Fan, G.F.S. Andrade, A.G. Brolo, A review on the fabrication of substrates for surface enhanced Raman spectroscopy and their applications in analytical chemistry, Analytica Chimica Acta. **693**, 7ï 25 (2011).
[2] Y. Shen, X. Cheng, G. Li, Q. Zhu, Z. Chi, J. Wang, C. Jin, Highly sensitive and uniform surface-enhanced Raman spectroscopy from grating-integrated plasmonic nanograss, Nanoscale Horizons **1**, 290ï 297 (2016).
[3] H. V. Bandarenka, K. V. Girel, S.A. Zavatski, A. Panarin, S.N. Terekhov, Progress in the development of SERS-active substrates based on metal-coated porous silicon, Materials. **11**, 1ï 20 (2018).
[4] I.A. Khodasevich, K. V. Girel, H. V. Bandarenka, V.P. Bondarenko, S.N. Terekhov, A.Y. Panarin, Formation Regularities of Plasmonic Silver Nanostructures on Porous Silicon for Effective Surface-Enhanced Raman Scattering, Nanoscale Research Letters. **11**, (2016).

EFFECTS OF GRAPHENE OXIDE NANOSTRUCTURES AND METAL MIXTURES ON *LEPIDIUM SATIVUM*

Mindaugas Kazlauskas[1], Danguolė Montvydienė[1], Živilė Jurgelėnė[1], Sergej Šemčuk[2], Kęstutis Jokšas[1,3], Nijolė Kazlauskienė[1]

[1] Nature Research Centre, Vilnius, Lithuania
[2] SRI Center for Physical Sciences and Technology, Vilnius, Lithuania
[3] Vilnius University, Faculty of Chemistry and Geosciences, Vilnius, Lithuania
mindaugas.kazlauskas@gamtc.lt

Graphene nanomaterials (GMs), such as graphene oxide (GO) due to unique structure and properties have been widely used in various fields [1]. Thus, the rapid increase in production and application, probably will lead to the inevitable release of GMs into water and soil environments with increment of potential health and ecosystem risks [2]. There are only some works on the ability of GO to adsorb heavy metals from aqueous solutions [3]. However, so far, only a few studies have been conducted regarding the effects of GO on plants. Also, the information related to the ability of GO to reduce the toxicity of heavy metals on plants by adsorption is still limited.

Therefore, the aim of the study was to examine the phytotoxicity of GO using garden-cress (*Lepidium sativum* L.) as a test-organism and to evaluate the ability of GO to modify the uptake of metals by plants exposed to metal mixture.

The metal ion mixture (MIX) (Ni(II) 0.034 mg/L, Zn(II) 0.1 mg/L, Cr(III) 0.01 mg/L and Cu(II) 0.01 mg/L) was prepared according to the maximum-permissible-concentrations (MPC) accepted for the inland waters in the European Union. The mixtures MIX20, MIX40 and MIX80 were prepared by increasing the MPC of every single metal ion by 20, 40 and 80 times, respectively. The GO concentrations (1, 20, 40, and 80 mg/L) were chosen in accordance with the previous study [4] concerning the ability of GO to adsorb heavy metals. In addition, the phytotoxicity of mixtures where GO was combined with MIX was evaluated.

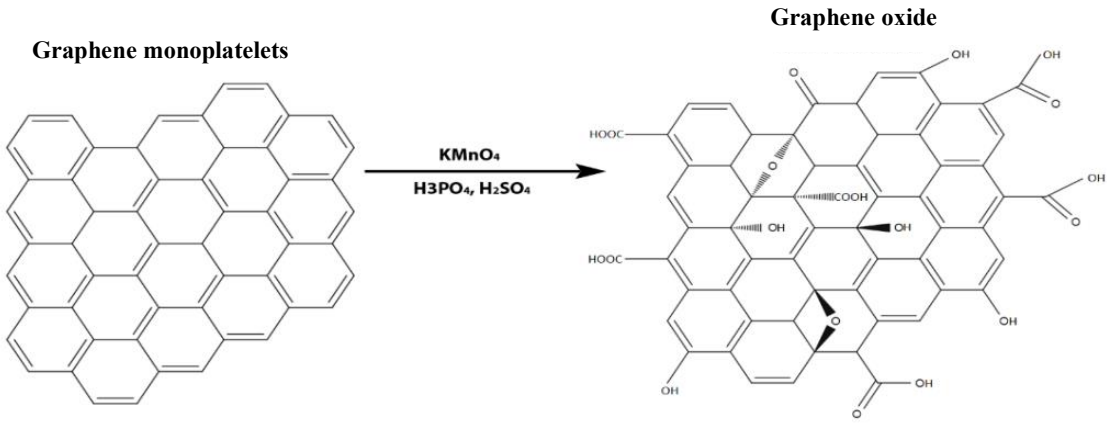

Fig. 1. Scheme of graphene oxide synthesis [4].

Obtained data showed that tested concentrations of MIX, GO and MIX+GO in the most cases did not affect seed germination, root growth and biomass of roots as well as above-ground parts of plants but influenced photosynthesis, increased the production of carotenoids and H_2O_2 with further activation of lipid peroxidation. In addition, statistical analysis showed that in some cases the effect of metals on plants exposed to combined exposure to GO and MIX decreased. This study revealed that GO are promising and advanced adsorbents of metals.

This work was funded by the Research Council of Lithuania, Project No. S-MIP-20-22.

[1] S. Azizighannad & S. Mitra, Stepwise Reduction of Graphene Oxide (GO) and it's Effects on Chemical and Colloidal Properties, Scientific reports **8**:10083 (2018).
[2] K. He et al., Stability, transport and ecosystem effects of graphene in water and soil environments, Nanoscale **17**(9): 5370-5388 (2017).
[3] C. A. Guerrero-Fajardo et al., Preparation and Characterization of Graphene Oxide for Pb(II) and Zn(II) Ions Adsorption from Aqueous Solution: Experimental, Thermodynamic and Kinetic Study, Nanomaterials **10**(6), 1022 (2020).
[4] S. Šemčuk, *Application of graphene oxide based nanocomposites and Šaltiškiai clay for radionuclides removal from contaminated solutions. Summary of doctoral dissertation* (Vilnius University Publishing, Lithuania, 2018).

GRAPHENE OXIDE / CHITOSAN / COPPER NANOCOMPOSITES FOR ANTIBACTERIAL STUDIES

Edith Flora Joel[1], Galina Lujaniene[1], Sandra Stanionytã[1], Loreta Levinskaitã[2]

[1]SRI Centre of Physical Sciences and Technology, Lithuania
[2] SRI Nature Research Centre, Vilnius, Lithuania
edith.joel@ftmc.lt

A genetic mutation in bacterial strains causing resistance to clinical drugs and biocides can be fixed by creating antibacterial nanocomposites. The progress associated with metal nanocomposites demonstrates their growth potential in the control of bacterial infections and the demand to prevent biofilm formation. Copper and its oxides, as well as platinum nanoparticles, possess antibacterial properties. Graphene Oxide-Chitosan nanocomposites are suitable for the creation of antibacterial materials [1]. The combined characteristics of a high surface-to-volume ratio of Graphene Oxide (GO) [2] and the natural antibacterial properties of Chitosan (CTS) [3] act as effective means to increase the effectiveness of antimicrobial materials. Copper [4] and Platinum nanoparticles prohibit further bacterial proliferation [5]. The addition of Platinum and Copper nanoparticles in combination with a biopolymer such as GO/CTS offers a promising approach to obtain a necessary material through research and comparison with other existing ones. Moreover, GO/CTS nanocomposites have a wide range of antibacterial characteristics and are used to improve the antiseptic properties of metal nanoparticles. This work aimed to synthesize nanoparticles of Cu, CuO, Cu_2O, Pt and their Graphene Oxide-Chitosan composites, as well as to test their antimicrobial activity.

Nanoparticles of Cu, CuO, Cu_2O and Pt were prepared by chemical reduction from $CuSO_4.5H_2O$ and used to synthesize composites of GO/CTS/Pt/Cu, GO/CTS/Pt/CuO and GO/CTS/Pt/Cu_2O. GO/CTS/Pt/Cu, GO/CTS/Pt/CuO, GO/CTS/Pt/Cu_2O composites were synthesized for the first time. Characterization of obtained materials was performed using X-Ray Diffraction (XRD). *E.coli* (Escherichia coli) ATCC 25922 was used to test the antibacterial effect of the materials. The 24-hour culture was suspended in sterile saline and standardized to turbidity of 108 CFU / ml using a spectrophotometer at 600 nm. 100 Õl of the suspension was applied to Petri dishes containing Mueller-Hinton agar. The test materials (100 Õg) were placed on inoculated plates and incubated for 24 h at 35 ÁC. The experiment was carried out in triplicate. Evaluation of the bactericidal effect was carried out by measuring the diameter of the zone of inhibition formed around the material and then calculating the mean as well as the standard deviation. Preliminary results of antibacterial tests indicated higher activity against E. Coli for Cu, CuO and Cu_2O nanoparticles as well as for the GO/ CTS/Pt/Cu_2O composite. Considering the potential applications in food packaging, medical devices, textiles and pharmaceuticals and water treatment will have usage from copper based nano composites.

[1] H. Yuan Long-Yue;Park, Soo-Jin;, A review: synthesis and applications of graphene/chitosan nanocomposites, Carbon Lett., vol. 17, no. 1, pp. 1117, 2016.
2] S. Ye et al., Antiviral Activity of Graphene Oxide: How Sharp Edged Structure and Charge Matter, ACS Appl. Mater. & interfaces, vol. 7, no. 38, Sep. 2015.
[3] H. Lim, N. Huang, and C. Loo, Facile preparation of graphene-based chitosan films: Enhanced thermal, mechanical and antibacterial properties, Journal of Non-Crystalline Solids, vol. 358, no. 3. Elsevier, pp. 525530, 01-Feb-2012.
[4] U. Bogdanovi, V. Lazi, V. Vodnik, M. Budimir, Z. Markovi, and S. Dimitrijevi, Copper nanoparticles with high antimicrobial activity, vol. undefined, no. undefined.
[5] K. B. A. Ahmed, T. Raman, and V. Anbazhagan, Platinum nanoparticles inhibit bacteria proliferation and rescue zebrafish from bacterial infection, RSC Adv., vol. 6, no. 50, pp. 4441544424, May 2016.

P2-42

DID NOT PARTICIPATE

SPINEL TYPE $ZnCo_2O_4$ COATINGS FORMATION AND ELECTROCHEMICAL PERFORMANCE

Monika Puzerytė, Augra Simanaitienė, Nerita Ąmuidzinavičienė, Simona Ostachavičiūtė, Dovilė Sinkevičiūtė, Agnė Gulbinienė*

Department of Physical and Inorganic Chemistry, Faculty of Chemical Technology, Kaunas University of Technology, Radvilenu plentas 19, Kaunas LT-50254
*agne.sulciute@ktu.lt

Photoelectrochemical (PEC) water splitting has been widely considered as one of the most promising technologies in clean, green, and renewable energy production [1]. Moreover, numerous studies suggest that various transition metal oxides are the most promising candidates as photoanodes for PEC materials, especially when used in conjunction.

Our aim was to synthesize p-n heterostructure of spinel type $ZnCo_2O_4$ coatings, investigate the influence of morphology on its photoelectrochemical properties, and test them as prospective materials to catalyze oxygen evolving reaction (OER).

Spinel type $ZnCo_2O_4$ coatings were synthesized using two-step process (Fig.1):

- chemical precipitation (Zn:Co ratio 1:2 and 1:1) and thermal decomposition at 500 for 2 h,
- spin-coating technique (the rotation speed of 1000 and 1200 RPM)

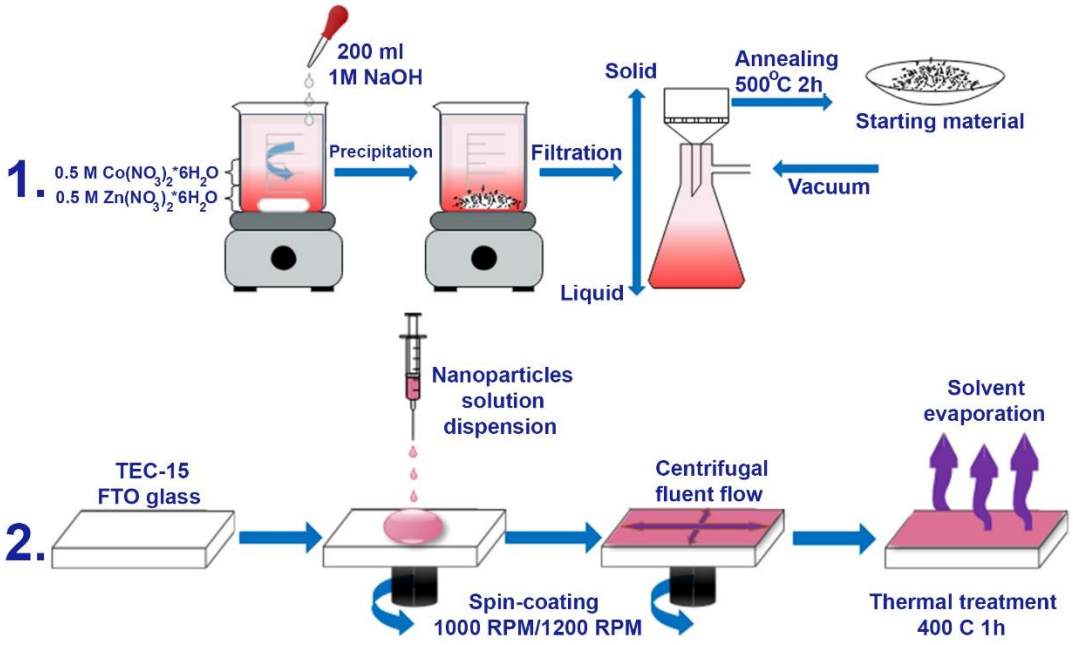

Fig. 1. Simplified version of two-step synthesis process

Composition, structure and morphology were investigated using various techniques such as: scanning electron microscopy (SEM), adsorption / desorption measurements, X-ray energy dispersion spectroscopy (EDS), X-ray diffraction (XRD), N_2 adsorption / desorption measurements and specific surface area calculations were used. Galvanostatic charge-discharge measurement and linear sweep voltammetry were used in order to investigate photoelectrochemical properties and coatings capacitance.

Ratio change from 1:1 of Zn:Co to 1:2 led to formation of different structure, morphology and properties:

- The obtained Zn:Co 1:1 coatings were more rough, granular and thicker (662 nm); with pore size 18.32 nm and 0.55 cm^3/g volume, as well as 57.92 m^2/g specific surface area and active surface area A=0.14 cm^2 at E=0.85 V vs. Ag,AgCl|KCl(sat). These coatings demonstrated the incident- to photon efficiency (IPCE) of 22.4 % and the applied bias photon-to-current (ABPE) 3.18%;
- Zn:Co 1:2 coatings formed uniform, 442 nm thick , vertically, horizontally aligned porous lamellar sturcture; pore size 17.97 nm and 0.14 cm^3/g volume, 24.41 m^2/g specific surface area; active surface area A=0.26 cm^2 , at E=0.85 V vs. Ag,AgCl|KCl(sat) IPCE 37%; ABPE 5.91%.

Due to great photoelectrochemical performance, we anticipate that the comprehensive analysis of such p-n heterostructure $ZnCo_2O_4$ will be important for future applications in OER.

[1] Q.Zhao, Z.Yan, C.Chen, J.Chen, Spinels: Controlled Preparation, Oxygen Reduction/Evolution Reaction Application, and Beyond, Chemical Reviews, **15**, 10121-10211 (2017).

DEPOSITION METHOD INFLUENCE ON MORPHOLOGY AND PHOTOELECTROCHEMICAL PROPERTIES OF ZnO FILMS

Jovita Grigonytã, Simona Ostachaviļ iÎ tã, Dovilã Sinkeviļ iÎ tã, Nerita Ģmuidzinaviļ ienã, Algirdas Ġulļ ius, Agnã Ġulļ iÎ tã*

Department of Physical and Inorganic Chemistry, Faculty of Chemical Technology, Kaunas University of Technology, Radvilenu plentas 19, Kaunas LT-50254
*agne.sulciute@ktu.lt

Zinc oxide is an important semiconducting material which is widely used in catalysis, photovoltaics, and pigment industry [1]. The application of ZnO nanoparticles depends on their structure and morphology, which can be varied by changing film formation methods.

The aim of this work is to compare properties of ZnO coatings deposited on AISI 304 stainless steel by electrochemical deposition (ECD) and electrophoretic deposition (EPD). Electrochemical measurements were performed by a computer controlled Autolab PGSTAT12 (Ecochemie, The Netherlands) potentiostat/galvanostat using a standard three electrode cell (volume 100 mL). All the potentials are referred to the Ag, $AgCl|KCl_{(sat)}$ reference electrode. The surface morphology and the composition of ZnO powder were investigated with a Quanta FEG 200 (FEI) high resolution scanning electron microscope (SEM) that was equipped with a Bruker XFlash® 4030 detector (Bruker AXS) for high resolution energy dispersive X-ray spectroscopy (EDX). X-ray powder diffraction (XRD) data were collected with a DRON-6 (Bourevestnik Inc., Russia) powder diffractometer equipped with Braggï Brentano geometry and using Ni-filtered CuKŬradiation and a graphite monochromator. The photoelectrochemical activity of the prepared electrodes was investigated by employing photovoltammetry measurement methods. A photoelectrochemical quartz cell was employed. A General Electric F8W/BLB lamp (λ_{max}=366 nm, power density 1.8 mWĀm$^{ï 2}$) was placed at a distance of 2 cm from the ZnO electrode and was used as an UV radiation source [2].

Electrochemically deposited zinc oxide coatings were produced using slightly acidic zinc (II) acetate solution under galvanostatic conditions - the current density was 1.0 mAĀm$^{ï 2}$ and duration time - 10 min. Homogeneous suspension (2 g of the ZnO powder dispersed in 100 mL of methanol) was used for the electrophoretic deposition of ZnO coatings and the potential of 30 V was applied for 20 minutes. In order to achieve better adhesion of ZnO particles on stainless steel deposited by ECD and EPD were annealed at 400 ÁC for 1 h in the atmospheric air.

XRD pattern of ECD and EPD ZnO films showed diffraction peaks at 2θ equal to 31.78Á 34.44Áand 36.24Á which correspond to the well-crystallized wurtzite type ZnO (PDF 04-004-4120). However, the surface of ZnO coatings prepared by ECD and EPD differs. SEM images revealed that ECD ZnO film surface is granular composed of grains with diameter of 30−110 nm, whereas films prepared by EPD is flower-like structure mainly composed of rods.

Photoelectrochemical behavior of the ZnO electrode was determined from the current-potential curves obtained in 0.1 M Na_2SO_4 solutions both in the dark and under UV irradiation. Significant anodic current increase under UV irradiation shows n-type semiconducting properties. The calculated values of incident photon-to-current efficiency (IPCE) and applied bias photon-to-current conversion efficiency (η) for the 0.6 V potential are shown in **Figure 1.** Electrochemically deposited ZnO films on stainless steel showed the best performance as a photoelectrode in 0.1 M Na_2SO_4 electrolyte.

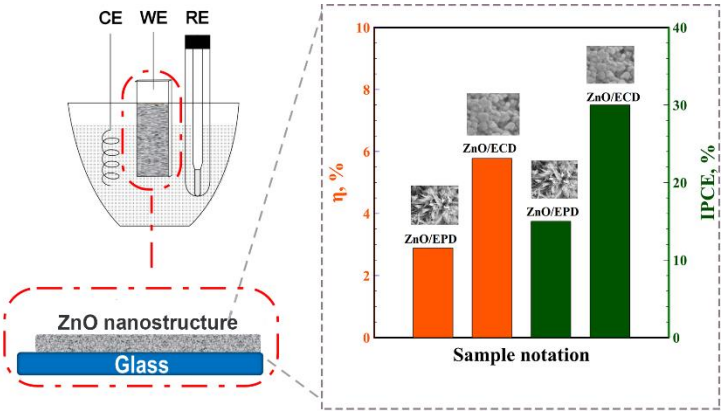

Fig. 1. The incident photon-to-current efficiency (IPCE) and applied bias photon- to-current conversion efficiency (η) values for ZnO films in 0.1 M Na2SO4 electrolyte

[1] A. Moezzi, A.M. McDonagh, M.B. Cortie, Chem. Eng. J., Zinc oxide particles: Synthesis, properties and applications, Chemical Engineering Journal, **22**, 185-186 (2012).

[2] E.M.P Steinmiller, K.S. Choi, Photochemical deposition of cobalt-based oxygen evolving catalyst on a semiconductor photoanode for solar oxygen production, Proceedings of the National Academy of Sciences, **49**, 20633-20636 (2009).

STAR CLUSTERS IN THE ANDROMEDA GALAXY

Eimantas Kriščiūnas[1], Vladas Vansevičius[1]

[1]Vilnius University Observatory, Saulėtekio av. 3, LT-10257 Vilnius, Lithuania
eimantas.krisciunas@ff.stud.vu.lt

The Panchromatic Hubble Andromeda Treasury (PHAT) survey is a *Hubble Space Telescope (HST)* multi-cycle program which obtained images of one third of the Andromeda (M31) disk in six passbands, ranging from near-ultraviolet to near-infrared wavelengths. High spatial resolution of *HST* has allowed users to identify hundreds of new clusters that were previously inaccessible with existing ground-based surveys. All of the detected clusters were sorted out into three catalogues: star cluster, galaxy, and ancillary [1].

The aim of this study is to perform an aperture photometry of the M31 star clusters in a colour-consistent way. For this purpose, we analysed the sample of 1471 cluster. New centre coordinates, apertures, and background levels are determined. We use a two-aperture approach: "total" and "colour" apertures in order to perform cluster photometry. The "colour" aperture is used to obtain an accurate cluster colour indices by avoiding bright field stars, the "total" aperture measures a total cluster magnitude. In Fig.1 "total" aperture sizes are compared with ones applied in [1]. Negative values indicate that we reduced aperture in order to exclude contaminating stars; positive values show that we increased aperture for star clusters in dense regions, globular clusters, and stellar associations. New centre coordinates are determined for 90% of star clusters. Our study demonstrates that by applying a new method of cluster photometry, we improve photometric accuracy of the Andromeda star cluster measurements.

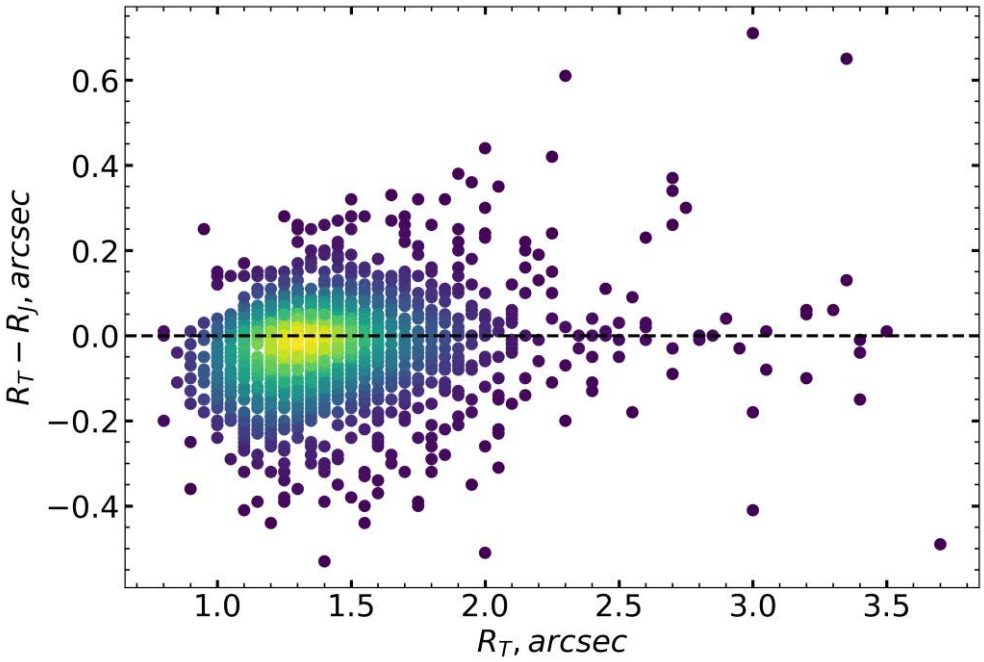

Fig. 1. Differences of aperture size selected in this study ($\boldsymbol{R_T}$) and in [1] ($\boldsymbol{R_J}$) vs. aperture size selected in this study. Total number of objects – 1468. Three clusters were discarded, since they are double clusters.

[1] L. C. Johnson, A. C. Seth, J. J. Dalcanton et al., PHAT stellar cluster survey II. Andromeda Project cluster catalog, The Astrophysical Journal, 802:127 (22pp), 2015.

MODELLING CIRCUMSTELLAR MOLECULAR LINE VARIABILITY IN IRC +10216

Karlis Pukitis[1], Miroslaw Schmidt[2], Ryszard Szczerba[2], Jinhua He[3,4]

[1] Laser Center, Faculty of Physics, Mathematics and Optometry, University of Latvia, Latvia
[2] Nicolaus Copernicus Astronomical Center, Poland
[3] Chinese Academy of Sciences South America Center for Astrophysics, Chile
[4] Yunnan Observatories, Chinese Academy of Sciences, China
karlis.pukitis@lu.lv

IRC +10216 (CW Leo) is a red giant carbon star in the asymptotic giant branch (AGB) phase of evolution. The star changes brightness with period of 630 days and is losing its outer layers due to the stellar wind driven by the radiation pressure on dust grains. Intense mass loss of $2 \cdot 10^{-5}$ $M_\odot$/yr has created an extended nebula around the star - circumstellar envelope (CSE), expanding with the velocity of 14.5 km/s in which over 80 molecules have been detected. Relatively small distance to CW Leo (130 pc) and high brightness in the infrared are the main reasons why it is regarded as the archetypal C-rich AGB star.

Molecular emission lines are a powerful tool for studying various physical and chemical processes in the CSE. Most poorly understood region of the CSE is the innermost part close to the stellar surface, which is probed by the high energy rotational and rovibrational lines in the submillimeter and infrared light.

The star shows periodic variability in all photometric bands. Recently, millimeter line variability for IRC +10216 was revealed by HSO (Herschel Space Observatory) HIFI instrument spectra [1] and has attracted increasing interest since then. Variability of the highly excited molecular lines has a potential to probe how mass loss rate is dependent on the pulsation phase.

In this study we explore possibility for variation of SiO emission lines observed by Herschel/HIFI and try to model SiO and SiS line variation observed with Atacama Large Millimeter/submillimeter Array (ALMA) in IRC +10216. For our analysis we use approach presented in the analysis of ammonia lines for the same star [2]. For the numerical solution of the multilevel radiative transfer in spherically symmetric expanding envelope we use code MOLEXCSE [2].

For the analysis of the sensitivity of the periodically varying radiation field on the excitation of SiO we have chosen rotational transitions in the ground vibrational state (v=0) ranging from J=12-11 (520.881 GHz) to J=23-22 (997.297 GHz). Calculations were performed at three different pulsation phases (minimum, mean and maximum brightness) by changing stellar and dust radiation fields. In result, only minuscule changes in line intensities are observed and it is seen that variation is more pronounced in lower J transitions. Observed and computed profiles for J=12-11 line is shown in Fig. 1. Due to high levels of noise in HIFI spectra, it is not possible to test whether modelled variations in line intensity match observations. Observations of ^{30}SiO J=6-5 line with ALMA [3][4] show 10% variation in line intensity. Approximately, only half of the variation amplitude seems to be reproduced by our calculations.

For SiS we model v=0, v=1 and v=2 J=14-13 lines. Observations of these lines show significant (even 25%) variation in intensity over time. Our calculations suggest that the contribution of the variation from the radiation is definitely insufficient to explain observations. Also, the formation of the line shape is poorly understood.

In summary, for SiO lines in the spectral range of HIFI no noticeable variation is expected. The main cause for SiO line variability might be the changes in radiation field due to stellar pulsation, however this is not the case for SiS. Discrepancies between observed and calculated profiles suggest that our model of the CSE needs to be improved.

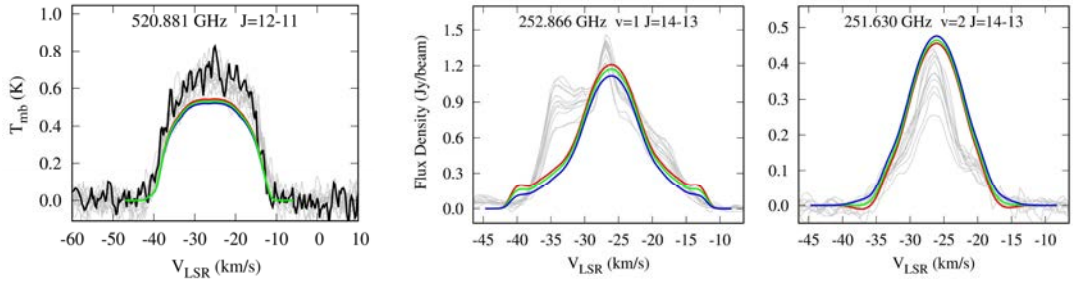

Fig. 1. Left: observed and modelled SiO v=0, J=12-11 line for IRC +10216. Black and grey lines – HSO HIFI observations for different epochs, blue, green and red – our calculation corresponding to minimum, mean and maximum brightness phases, respectively. Right: the same for SiS v=1, J=14-13 and v=2, J=14-13 profiles with grey lines depicting ALMA observations.

[1] J. Cernicharo et al., Discovery of Time Variation of the Intensity of Molecular Lines in IRC+10216 in the Submillimeter and Far-Infrared Domains, The Astrophysical Journal Letters, **796**, 21 (2014).
[2] M. R. Schmidt et al., Herschel/HIFI observations of the circumstellar ammonia lines in IRC+10216, Astronomy & Astrophysics **592**, 131 (2016).
[3] J. H. He, Dinh-V-Trung, and T. I. Hasegawa, Monitor Variability of Millimeter Lines in IRC+10216, The Astrophysical Journal **845**, 38 (2017).
[4] J. H. He et al., ALMA Monitoring of Millimeter Line Variation in IRC +10216. I. Overview of Millimeter Variability, The Astrophysical Journal **883**, 165 (2019)

ABUNDANCE OF ZIRCONIUM IN THE ATMOSPHERES OF RED GIANTS IN GALACTIC GLOBULAR CLUSTER 47 TUC

Edgaras Kolomiecas[1], Vidas Dobrovolskas[1], ArÎnas Kuļinskas[1]

[1] Institute of Theoretical Physics and Astronomy, Faculty of Physics, Vilnius University, Lithuania
edgaras.kolomiecas@ff.vu.lt

It has been long held that Galactic globular clusters (GGCs) are homogeneous objects consisting of stars that have the same age and chemical composition. However, research done during the past decade has shown that stars in the GGCs do not share the same chemical composition and may have formed during different star formation episodes (see, e.g., [1]). This suggests that GGCs may consist of two (or more) generations of stars, with the second generation born from the material enriched by the ejecta of first-generation stars, with the most plausible candidates being fast-rotating massive stars [2] and asymptotic giant branch (AGB) stars [3], the so-called polluters. Unfortunately, our current knowledge about the GGCs does not allow us to discriminate between the possible pollution scenarios.

In order to determine which polluters were most likely to enrich the intracluster medium during the early stages of GGC formation, one may look at the abundances of *s*-process elements. Since the light (peak around Sr, Y, Zr) and heavy (peak around Ba, La) *s*-process elements are produced in different types of objects, correlations between abundances of light/heavy *s*-process elements and those of light elements (N, Na) may allow us to put tighter constraints on the possible polluters. One earlier study has suggested a tentative existence of a correlation between the abundances of Na and Ba in the globular cluster 47 Tuc (note that Ba is a heavy *s*-process element and is synthesized during the main *s*-process, which mostly takes place in low-mass AGB stars) [4]. To check if such a correlation may also exist in the case of Zr, which is a light *s*-process element and is synthesized during the weak *s*-process, we determined Zr abundance in 283 RGB stars in 47 Tuc. Importantly, the studies of Zr abundance in the GGCs have been very scarce until now and the results were inconclusive, i.e., not only for this but also for other GGCs.

Abundance analysis was based on the archival spectra of RGB stars in 47 Tuc that were obtained with GIRAFFE spectrograph mounted on the VLT UT2 telescope (ESO, Chile). Three spectral lines of neutral Zr were used, with their central wavelengths located at 612.7475 nm, 613.4585 nm and 614.3252 nm. Line equivalent widths were measured using IRAF package, by fitting Gaussian profiles to the observed spectral lines. Stellar model atmospheres were computed using the ATLAS9 code and were further employed to derive 1D LTE Zr abundances with the WIDTH9 package.

The mean Zr to Fe abundance ratio that we obtained in a sample of 283 RGB stars in 47 Tuc is [Zr/Fe] = +0.37 Ñ 0.09 (the error is standard deviation due to star-to-star abundance variation). This is so far the largest sample of RGB stars analyzed in this cluster for Zr abundance. Analysis of Zr and Na abundances shows a weak, but statistically significant correlation (Fig. 1). Taken together with the [Ba/Fe] ratios determined by [4], our results suggest that in this GGC both elements were synthesized in massive AGB stars.

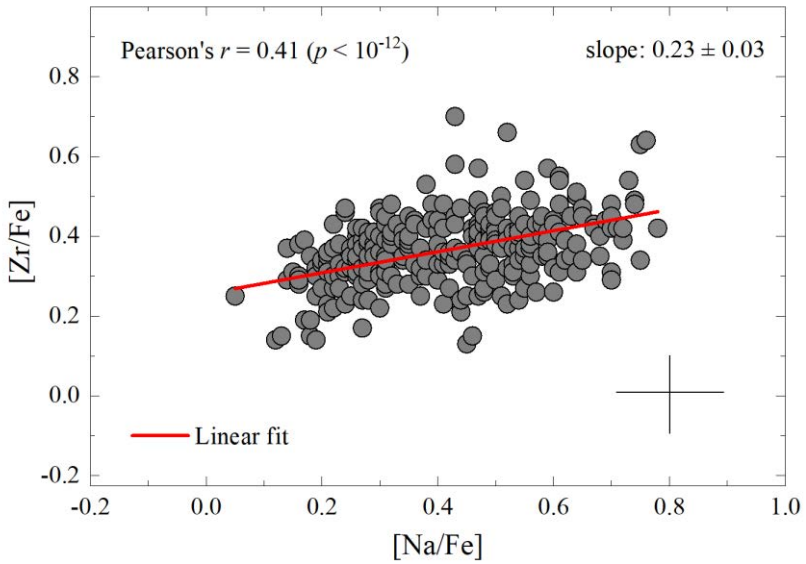

Fig. 1. Abundance of Zr in the RGB stars of 47 Tuc plotted against the sodium-to-iron abundance ratio.

[1] Bastian, N. & Lardo, C. 2018, ARA&A, 56, 83.
[2] Krause, M., Charbonnel, C., Decressin, T., Meynet, G., & Prantzos, N. 2013, A&A, 552, A121.
[3] Ventura P., D'Antona F., Mazzitelli I., Gratton, R., 2001, ApJ, 550, L65.
[4] Gratton, R. G., Lucatello, S., Sollima, A., Carretta, E., Bragaglia, A., Momany, Y., DôOrazi, V., Cassisi, S., Pietrinferni, A., & Salaris, M. 2013, A&A, 549, A41.

CHARACTERIZATION OF THE VARIABLE STAR EPIC 246257206 DISCOVERED WITH OBSERVATIONS OF THE K2-C12-FOV TAKEN BY THE KEPLER SPACE TELESCOPE

Jorge Pérez González[1], Enrique Díez Alonso [2], Faustino García[3]

[1]Department of Physics and Astronomy, University College London, UK
[2]Instituto de Ciencias y Tecnologías Espaciales de Asturias, University of Oviedo, Spain
[3]Observatorio La Vara, Spain
jorper.gonzalez@gmail.com

Variable stars are stars of variable brightness. This means that their brightness doesn't remain constant throughout time. Eclipsing variables are binary stars where two stars orbit periodically around their common center of mass [1]. When one of them is situated in front of the other relative to the observer, the total brightness of the system decreases. These brightness variations depend only on geometric factors. There are three types of eclipsing variables: EA (well defined eclipses with constant brightness outside the eclipses), EB (well defined eclipses with brightness variations outside the eclipses) and EW (the eclipses are not noticeable).

Throughout this investigation an unregistered variable star has been found through observations taken by the Kepler Space Telescope. With this data, and with data from other land and space observatories its period, amplitude and distance to the Earth was calculated in order to find out the cause of variability of the star and to register it in the Variable Star Index. Besides the Kepler Space Telescope, observations from the Minor Planet Center (MPC) L94 observatory, MPC J38 observatory, the PanSTARRS telescope in Hawaii and the European Space Agency's Gaia space observatory have been used. Photometric observations were taken from the Kepler Space Telescope, from the Minor Planet Center (MPC) L94 observatory and from the MPC J38 observatory. Astrometric observations were taken from the Gaia space telescope. The PanSTARRS telescope was used to validate Kepler's K2 data.

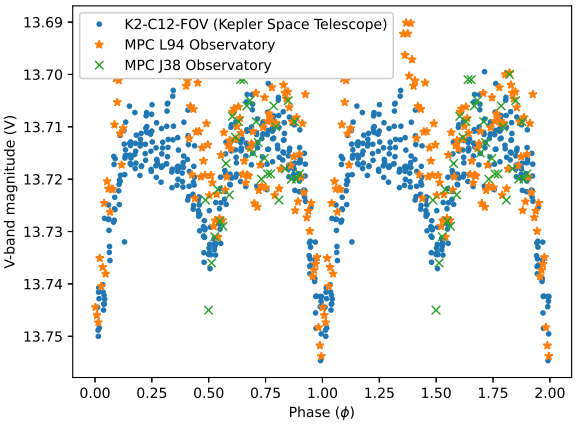

Fig. 1. EPIC 246257206 phased lightcurve. The amplitude of the light curve is 0.05 magnitudes and the period is 0.2198 ± 0.0004 days.

The star found is EPIC 246257206. Analyzing the photometric data using the Lomb-Scargle periodogram, the period 0.2198 ± 0.0004 days was obtained. Analyzing its phased light curve, shown in figure (**??**) and the value of the period, it can be concluded that the star is an EA type eclipsing variable. Using the parallax method and the observations taken by GAIA, it has been calculated that the EA variable star EPIC 246257206 is 7.0832 ± 0.0002 light years away from Earth.

The most peculiar aspect of the star is its amplitude, of only 0,5 magnitudes (astronomical unit referring to the brightness of the star). This is probably due to the fact that the eclipses produced are *grazing eclipses*: in the plane that both stars are observed, they are not overlapping totally but partially. This, therefore reduces the total brightness change of the system. To confirm this, spectroscopic observations of the system are suggested. With these type of observations, joint with the already conducted photometric observations, the system could be modeled and its orbit can be calculated. With this information, it is possible to figure out the nature of the eclipses. Its small amplitude also suggests the possibility of a third body in the system that also blocks part of the light. To confirm this an investigation searching for transit-timing variation is also recommended.

In summary, to characterize the EPIC 246257206 star, its distance to the Earth, its amplitude and its period had to be determined. These values allowed to conclude that the star EPIC 246257206, located at $(7,0832 \pm 0,0002) \cdot 10^2$ light years away from the Earth, presents a variability of 0,05 magnitudes periodically every 0,2198 ± 0,0004 days due to the eclipses formed by the two stars that constitute the binary system. This can be viewed at its webpage at the International Star Index site: https://www.aavso.org/vsx/index.php?view=detail.top&oid=1540324.

[1] D. Gonzalez. *Curvas de luz y modelos de las estrellas binarias eclipsantes*. (2003). http://www.grupoastronomicosilos.org/variables/analisis_binarias_eclipsantes.html [Accessed 7. Feb. 2020.]

COMPARISON OF DIFFERENT DEUTERATED DIPALMITOYL PHOSPHATIDYLCHOLINE MONOLAYERS USING SUM-FREQUENCY GENERATION SPECTROSCOPY

Edvinas Navakauskas[1] and Simona Strazdaitė[1]

[1]Center of Physical Sciences and Technology, Department of Organic Chemistry, Saulėtekis ave. 3, LT-10257 Vilnius
Edvinas.Navakauskas@ftmc.lt

The key component of a cell membrane is phospholipids, consisting of two hydrophobic tail groups and a hydrophilic head group linked together via the ester group. A phospholipid monolayer is often used experimentally to mimic the outer leaflet of the cell membrane in order to investigate the peptide-lipid interaction at the lipid-water interfaces. The disruption of phospholipid monolayer can be evaluated by probing certain vibrations: from the C-H region, the changes in lateral packing order as well as the conformation of the hydrocarbon chains, can be determined [1]; the carbonyl group region has a strong dependence on packing of the lipid alkyl chains and headgroups as well as the hydration state of the headgroups [2]; and the phosphate group region is the most sensitive to the changes in the hydration [3].

However, in a multi-component system, which consists of, e.g., lipids, cholesterol and protein mixture, the C-H region produces an overall band profile that reflects the weighted contributions of all components in the mixture. Therefore, information concerning individual components is lost. The method that circumvents this problem relies on the isotopic substitution of ^{2}H for ^{1}H in the phospholipids [1,2], which results in a shift of the C-D stretching modes to lower frequencies. Nevertheless, there is still a lack of studies that show, how the monolayerôs formation, stability, and characteristics are affected by various lipidôs deuteration levels. For this purpose we used vibrational sum-frequency generation (VSFG) spectroscopy technique that enables detection of a single monolayer formed at water surface.

This paper seeks to understand and compare the major differences between monolayers made of non-deuterated 1,2-dipalmitoyl-sn-glycerol-3-phosphocholine (DPPC), choline group deuterated (DPPC-d13), alkyl group deuterated (DPPC-d62), and both groups deuterated (DPPC-d75) lipids. In order to observe changes in monolayersô formation, stability, and hydration, different phase monolayers were formed on the D_2O and H_2O surfaces. We found that monolayer made of DPPC-d62 are stable for up to 8 days. At high surface pressures (~30 mN/m) only vibrations of the methyl group were registered in the CH region for all studied monolayers, which implied that alkyl chains adopted an all-trans conformation. The carbonyl ester group acts similar for all monolayers, upon increasing the amount of lipid on the surface, the strength of dipole-dipole interaction between the carbonyl groups increases. Meanwhile, the deuteration of the lipidôs choline group has the strongest impact on the vibrations of the phosphate group. The absence of a PO_2^- vibrational band for monolayers formed of DPPC-d13 and DPPC-d75 leads to the conclusion that deuteration of the choline group impacts the orientation of the lipidôs headgroup in respect to surface normal. Moreover, we used calcium chloride to evaluate the interaction between phospholipid monolayer and ions, which play a major role in many biological processes. We observed frequency shifts of PO_2^- and C=O vibrational bands induced by increased dehydration of the monolayer and additional interaction with Ca^{2+} ion, which in the case of carbonyl group also affect the strength of dipole-dipole interaction.

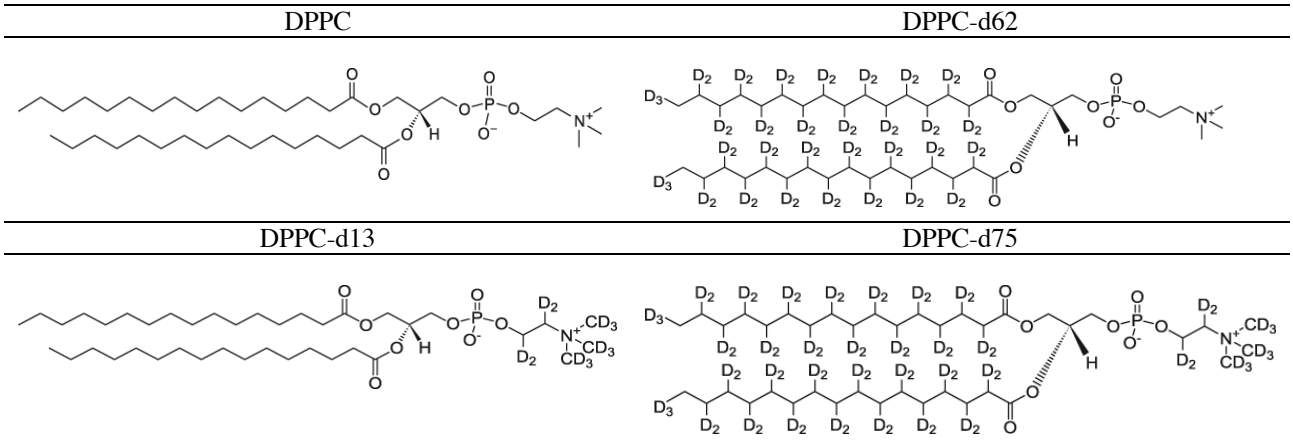

Figure 1. Molecular structure of DPPC (1,2-dipalmitoyl-sn- glycero-3-phosphocholine) with different levels of deuteration

[1] D. D. Baldyga, R. A. Dluhy, On the use of deuterated phospholipids for infrared spectroscopic studies of monomolecular films: a thermodynamic analysis of single and binary component phospholipid monolayer, Chemistry and Physics of Lipids **96**, 81-97 (1998).
[2] H. H. Mantsch, R. N. McElhaney, Phospholipid Phase Transitions in Model and Biological Membranes as Studied by Infrared Spectroscopy. Chemistry and Physics of Lipids 57, 213ī 226 (1991).
[3] G. Ma, H. C. Allen, DPPC Langmuir Monolayer at the Air-Water Interface: Probing the Tail and Head Groups by Vibrational Sum Frequency Generation spectroscopy, Langmuir 22, 5341-5349 (2006).
[4] R. Mendelsohn, S. Sunder, H. Bernstein, Deuterated fatty acids as Raman spectroscopic probes of membrane stuctures. Biochimica et Biophysica Acta **443**, 613-617 (1976).
[5] R. Mendelsohn, C. Koch, Deuterated phospholipids as Raman spectroscopic probes of membrane structure: Phase diagrams of the dipalmitoyl phosphatidylcholine (and its d_{62} derivative)-dipalmitoyl phosphatidylethanolamine system, Biochimica et Biophysica Acta **598**, 260-271 (1980).

PLASMA-INDUCED MODIFICATION OF ZnO-BASED CATALYSTS DOPED WITH Ag PLASMON NANOPARTICLES FOR PHOTODEGRADATION OF PHARMACOLOGICAL WASTE

Aliaksandr Miadzvetski, Valery Plakhodzka, Anastasiya Shcherbovich, Natalie Savastenko

International Sakharov Environmental Institute, Belarusian State University, Republic of Belarus
aleksander.medvedskiy@gmail.com

Water purification from pollutants containing various organic substances and their compounds, including medical waste (MW), is one of the main problems facing the world community. According to the World Health Organization, 15% of MW are considered hazardous materials that can be toxic, infectious or radioactive, and harm human health and the environment [1]. Existing methods have serious drawbacks, which makes it necessary to develop new solutions.

Heterogeneous photocatalysis using nanocatalysts is considered as a promising method for cleaning aqueous media from waste from the pharmaceutical industry, but the effectiveness of known photocatalysts is insufficient for use in industrial applications. In previous studies, it was shown that plasma treatment and impregnation of a ZnO-based catalyst with silver nanoparticles leads to an increase in its activity [2].

In this paper, photocatalysts were executed, which were impregnated with silver nanoparticles during the synthesis process. Such an injection mechanism should lead to a change in the morphology of the catalysts and an increase in their activity [2].

ZnO nanoparticles were prepared by dropwise addition of 25 mL of NaOH 0.4 mol/L into 25 mL of $ZnSO_4$ 0.2 mol/L at an approximate addition rate of 5 mL/min. After stirring with a magnetic stirrer SOLOR SCUID IKAMAG WHITE (IKA, Germany) at a speed of 150 rpm for 60 min, the solution was kept at 60°C for 2 h. Ag-ZnO composite nanoparticles were prepared by adding 6 mL of ascorbic acid 0.01 mol/L and 13 mL of $AgNO_3$ 0.01 mol/L into the solution of NaOH and $ZnSO_4$, while stirring under the same condition as in the first experiment, and again the solution was kept at 70°C for 2 h. The catalysts synthesized by this method should have a size equal to 50-60 nm [3].

The photocatalytic activity of the obtained catalysts was researched in a model decomposition reaction of caffeine simulating pharmacological waste under the action of ultraviolet radiation in aqueous suspensions of synthesized samples. During the experiments for the preparation of the suspension, a 40 mg catalyst was mixed with 20 ml of an aqueous solution of caffeine sodium benzoate with a concentration of 300 mg/l. The mortars are prepared based on distilled water.

The selected concentration of caffeine for the model reaction is in the range of concentrations contained in wastewater. Suspensions of catalysts in aqueous solutions of model substances were exposed to UV radiation. As a source of ultraviolet radiation, a mercury-quartz lamp DRT-240 (power 240 W) was used. During the irradiation, the change in the concentration of caffeine in the solution was monitored using a SOLAR PB 2201 spectrophotometer (SOLAR, Belarus). The irradiation was carried out under constant stirring of the suspension in a magnetic stirrer SOLOR SCUID IKAMAG WHITE (IKA, Germany) at a speed of 200 rpm.

The reaction rate constant was determined by the slope of the graph of the dependence of the logarithm of the concentration of the decomposed substance on time. The relative concentration of the model substance C_r was determined by measuring the optical density at the absorption maximum:

$$C_r = \frac{C(t)}{C_0} \cdot 100\% = \frac{A_t}{A_0} \cdot 100\%, \quad (1)$$

where C_0 is the initial concentration of the model substance, C(t) is the concentration of model substances after irradiation of the UV radiation at time t, A_0 and A_t the optical density of the solution of the model substance in the absorption maximum (λ=452 nm) before irradiation and at time t after the start of irradiation of the samples, respectively.

To compare the photocatalytic activity of different samples, it was assumed that the photodegradation reaction can be described by a first-order equation, therefore, the kinetic equation has the form:

$$\frac{dc}{dt} = -kC \quad (2)$$

Here C – the concentration of the decomposed substance, k- the reaction constant. The solution of equation (2) can be represented as follows:

$$C(t) = C_0 e^{-kt} \quad (3)$$

Thus, by constructing a time dependence $ln\frac{C(t)}{C_0}$, the values of the reaction rate constant can be easily found on the graph.

$$ln\frac{C(t)}{C_0} = -kt \quad (4)$$

The activity of the synthesized samples was compared with the activity of commercially available ZnO (ECOS-1, Russia) with a particle size ranges from 100 nm to 1 μm [2].

This research was partially financially supported by the State Research Program “Convergence. Microworld, Plasma, Universe. 9490- 8.1GPNI/6758192.NIR 8.”.

[1] *World Health Organization*, electronic resource, accessed 25 January 2021, <https://www.who.int/news-room/fact-sheets/detail/health-care waste>.
[2] Savastenko, N., et. al (2020). Effect of silver nanoparticles impregnation on efficiency of plasma treated ZnO-based photocatalysts. High Temperature Material Processes: An International Quarterly of High-Technology Plasma Processes. 24. 10.1615/HighTempMatProc.2020033434.
[3] Tran Thi, et. al. (2019). *Journal of Chemistry, 2019, 1–13.* doi:10.1155/2019/2979517

DEVELOPMENT OF CHITOSAN SPONGE MODIFIED WITH CARBON NANOTUBES FOR PHENOL ADSORPTION

Daniele Costa da Silva Alves[1,2], Luiz Ant¹ nio de Almeida Pinto[2], Tito Roberto SantôAnna Cadaval Junior[2], Carmel Bernadette Breslin[1*]

[1]Department of Chemistry, Maynooth University, Maynooth, Co. Kildare, Ireland
[2]School of Chemistry and Food, Federal University of Rio Grande, Rio Grande, RS, Brazil
daniele.costadasilvaalves.2021@mumail.ie

Phenol is widely found in effluents generated by several chemical industries and it is considered one of the priority contaminants due to its high toxicity at low concentrations. This makes it necessary to remove phenol from industrial effluents before it is discharged into the environment. The emergence of nanotechnology has enabled the design of new and promising adsorbent materials [1]. In particular, carbon nanotubes (CNTs) have proved to be a promising solution for water purification through the adsorption operation, as they have an excellent adsorption affinity for various organic pollutants [2]. However, it is difficult to remove and separate CNTs from water after the adsorption operation. In order to overcome this barrier, an interesting alternative is the development of hybrid CNTs adsorbents. The biopolymer chitosan is attracting considerable interest as a matrix for CNTs, due to the presence of hydroxyl groups (-OH) and primary amines ($-NH_2$) that act as active adsorption sites, making it an efficient adsorbent [3]. Therefore, a sponge composed of chitosan/CNT was developed, characterized by scanning electron microscopy (SEM) and applied to phenol adsorption in aqueous solution. The kinetic behavior was evaluated using different stirring rates (50, 100 and 150 rpm). The results show that the adsorbents presented a rough and irregular surface, as shown in Fig. 1, which indicates good accessibility of phenol on the surface of the adsorbent. According to Table 1, the pseudo-second-order (PSO) was more adequate than pseudo-first-order (PFO) kinetic model to represent the adsorption phenomenon at all rotations, and the maximum adsorption capacity was 228.7 mg g^{-1} at 150 rpm. Therefore, this study demonstrated the development of a promising adsorbent with high adsorption capacity, low cost and interesting mechanical properties for the removal of phenol from aqueous solution.

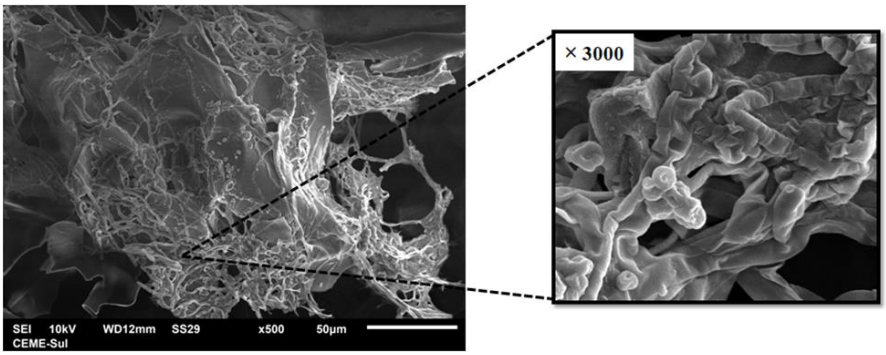

Fig. 1. SEM image of chitosan/CNT sponge.

Table 1. Kinetic parameters for phenol adsorption onto chitosan/CNT sponge in different stirring rates.

Stirring rate (rpm)	50	100	150
PFO			
q_1 (mg g^{-1})	162.8	196.6	210.6
k_1 (min^{-1})	0.102	0.140	0.167
R_I^2	0.987	0.982	0.987
ARE (%)	5.5	5.7	4.1
PSO			
q_2 (mg g^{-1})	184.5	216.1	228.7
k_2 (g mg^{-1} min^{-1})	0.0007	0.0009	0.0010
R_I^2	0.993	0.994	0.993
ARE (%)	4.7	2.5	2.6

[1] D. Alves, J. Gon-alves, B. Coseglio et al., Adsorption of phenol onto chitosan hydrogel scaffold modified with carbon nanotubes, Journal of Environmental Chemical Engineering **7**, 103460 (2019).
[2] D. Rawtani, N. Khatri, S. Tyagi et al., Nanotechnology-based recent approaches for sensing and remediation of pesticides, Journal of Environmental Management **206**, 749-762 (2018).
[3] G. Dotto, L. Pinto, Adsorption of food dyes onto chitosan؛ Optimization process and kinetic. Carbohydr Polymer **84**, 231-238 (2011).

THE USE OF MACHINE LEARNING IN ORTHOTROPIC MATERIALS CLASSIFICATION VIA MODAL ANALYSIS

Mohamed Abdelkader[1,2,3]

[1]Department of Mechanics and Materials Engineering, Vilnius Gediminas Technical University, Vilnius, Lithuania
[2]Department of preparation and analysis of nanostructures, Institute for Nanomaterials, Advanced Technologies and Innovation, Technical University of Liberec, Liberec, Czech Republic
[3]Department of Nanoengineering, State research institute Center for Physical Sciences and Technology SavanoriÛave. 231, LT-02300 Vilnius, Lithuania
mohamed.fawzy@ftmc.lt

Modal analysis is a powerful tool to ensure the safety of materials and one of the non-destructive materials characterization methods, the study shows applying machine learning to have a classification scheme of materials. The concept of classification through the study is validated for isotropic and orthotropic materials reaching up to a 100% accuracy when deploying the machine learning approach with the created interrelation variables between the mode number and the associated frequency, ANSYS was used to simulated modal analysis. This study shows a new classification method depending only on the knowledge of resonance frequency only of the material.

The study demonstrates the ability to classify the engineering materials including isotropic and orthotropic materials by applying ML (Machine Learning) algorithms on the modal analysis results, the proposed ML approaches could reach an accuracy of 100% when interrelations are created between the inputs to the ML algorithms (the combined linear regression approach in this study). Keras model wasnû suitable for this study as it showed 50% accuracy when compared to the ML approaches. The study validates the classification applicability based on the resonance frequencies information only which broadens the horizons of further applications like a device that can classify the materials based on their modal analysis. Potential future studies can study other DL (Deep Learning) approaches and the deployment of neural networks that can achieve promising classification studies. Further extensions and relations can be established for detailed materials properties identification through deploying the concept of ML and DL into the field of mechanical engineering which proves the modern concept of science integration. The results of this study can boost the non-destructive materials characterizations in general and analysis methods not just the explored modal analysis example as ML and DL deal mainly with data regardless of the acquiring method.

.

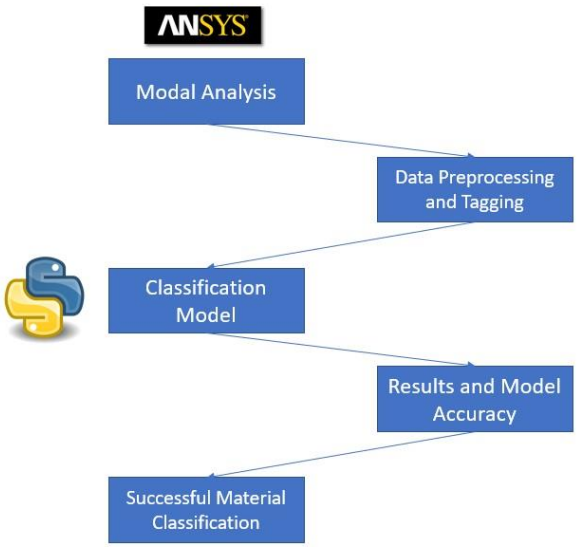

Fig. 1. Overall summary and procedures of using ML and DL in engineering materials classification

SYNTHESIS AND INVESTIGATION OF FUNCTIONAL PROPERTIES OF ZINC OXIDE NANOPOWDERS

Mindaugas Ilickas[1,2], Simas Raļkauskas[1,2], and Brigita Abakeviļienã[1,2]

[1] Department of Physics, Kaunas University of Technology, Lithuania
[2] Institute of Materials Science, Kaunas University of Technology, Lithuania
mindaugas.ilickas@ktu.edu

The work focuses on the synthesis of zinc oxide (ZnO) nanoparticles and the study of the functional properties of these particles. ZnO has a unique combination of optical, piezoelectric, magnetic, and sensory properties (this is an important aspect in the development of various sensors). The ability of ZnO to absorb ultraviolet light (10-400 nm) is applied in the production of solar cells coatings and ultraviolet sensors [1]. By illuminating the surface of the ZnO coating with ultraviolet light, it is possible to create free vacancies of the oxygen atom, which changes the internal properties of the material, such as increasing the n-type conductivity and wetting the material. Zinc oxide is an inorganic compound found in the form of a white powder, almost insoluble in water. ZnO is a relatively soft material with a Mohs hardness of ~ 4.5 [2]. High heat capacity and conductivity and high melting point are particularly important in ceramics [3]. ZnO has a wide range of functional properties when applied in optoelectronics, spintronics, and piezoelectric transducers. ZnO is a semiconductor, from the point of view of nano- and microstructures it is a very extraordinary material with a wide band gap ï E = 3.37 eV [4]. This material is physically very strong, its Jungôs modulus reaches 150 GPa and is relatively stable up to high temperatures (1800 ºC). ZnO has a relatively high nuclear binding energy (60 meV), so ZnO shows potential for ultraviolet (UV) optoelectronics applications [5]. This unique tetrapod structure consists of four hexagonal rods, also called ñlegsò, which are connected to each other through the central core at an angle of 105 Áto 110 Á[5].

The synthesis of ZnO structures is performed by continuous synthesis (combustion) process [6]. UV-Vis spectral analysis, scanning electron microscopy (SEM) and X-ray diffraction (XRD) methods were used in this work. Based on ultraviolet - visible light spectrometry and scanning electron microscopy, zinc oxide particles of different shapes - tetrapods, nanoparticles, and various 1D and 3D nanostructures - were formed during the synthesis. UV-Vis spectrometry showed that as the colour of the flame in the burner changed from bluish to greenish, the particle size increased (58-64 nm) and the particle size decreased (63-52 nm) with increasing centrifugation speed in the range of 1000 - 10000 rpm. This shows the potential of ZnO nanoparticles for application in optoelectronic devices.

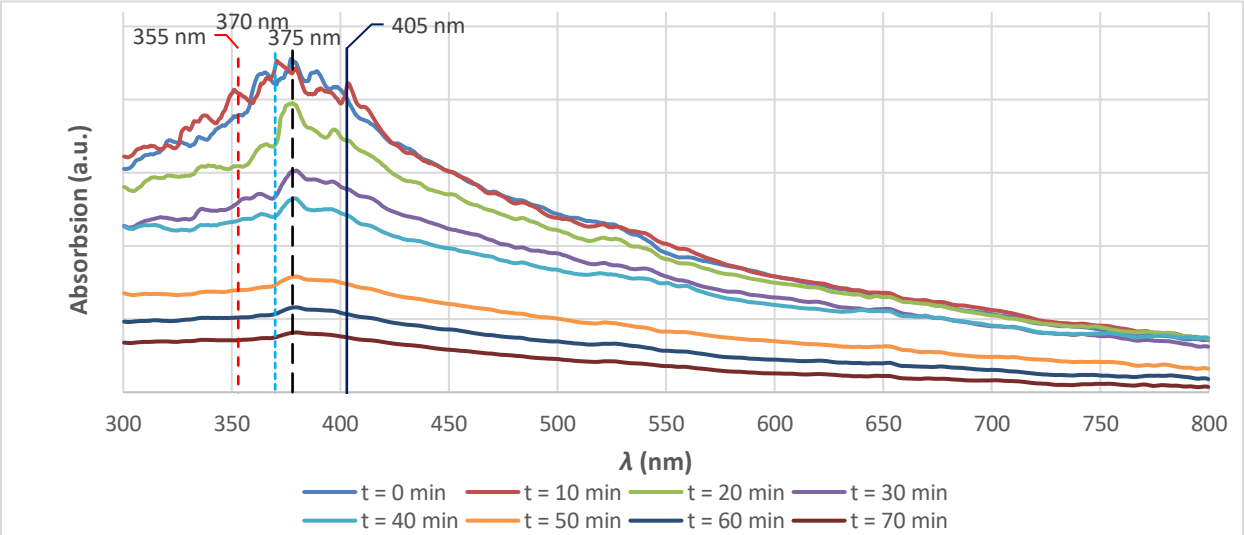

Fig. 1. UV-Vis absorption spectras of various ZnO structures. The red dashed line (ɔ= 355 nm) corresponds to nanoparticles, the blue dotted line (ɔ= 370 nm) corresponds to nanowires, the black dashed line (ɔ= 375 nm) corresponds to tetrapods, and the blue dashed line (ɔ= 405 nm) is due to light shift to the blue region that results from the quantum core-shell ZnO closure.

This research is funded by the European Regional Development Fund according to the supported activity ñAttracting scientists from abroad to carry out researchò, project No. 01.2.2-LMT-K-718-02-0011.

[1] Jacobs, Christopher B et al. UV-activated ZnO films on a flexible substrate for room temperature O_2 and H_2O sensing. *Scientific Reports*, **7(1)**, 6053, 2017.
[2] A. Hern§ndez Battez et al. CuO, ZrO_2 and ZnO nanoparticles as antiwear additive in oil lubricants. Elsevier,**265(3-4),** 422ï 428, 2008.
[3] J. Das, et al. Raman and XPS studies of pure ZnO ceramics. *Physica B: Condensed Matter* **405(10)**, 2492ï 2497, 2010.
[4] V. A., Coleman, and C. Jagadish. Basic Properties and Applications of ZnO. Zinc Oxide Bulk, *Thin Films and Nanostructures*, 1ï 20, 2006.
[5] Y. Mishra, et al. ZnO tetrapod materials for functional applications. *Materials Today* **21(6)**, 631ï 651, 2018.
[6] S. Rackauskas, et al. A Novel Method for Continuous Synthesis of ZnO Tetrapods. *The Journal of Physical Chemistry C*, **119(28)**, 16366ï 16373, 2015.

STEGANOGRAPHIC INTEGRATION OF COMMUNICATION SCHEMES IN MAPS

Avtushko Kirill Valentinovich, Sadov Vasily Sergeevich

Department of Intelligent System, Faculty of Radiophysics and Computer Technologies, Belarusian State University, Republic of Belarus
rct.avtushko@bsu.by

According to the UN Department of Economic and Social Affairs for 2018, urban populations across Europe are growing, while rural populations are falling. The problem of urbanization is growing. Today, when building, modernizing or researching a land plot, it is necessary to obtain a variety of plans, diagrams, and drawings. Some of these plans are classified information, such as the system of water supply routes. To simplify the handling of all diagrams and maps, you can steganograph the location of engineering communications diagrams into cartographic materials. That will reduce the amount of stored data, but at the same time preserve the secrecy of information.

The initial containers for embedding information in this work are satellite images in the GeoTIFF format. The scheme of conditional engineering communications is a specialized topographic and geodetic plan. When describing utility networks in the topographic and geodesic plan, both underground and ground networks are taken into account, their brief characteristics, control points are removed. The explanatory part contains information about these control points and additional information: coordinates and heights of points of reference and alignment networks for the area of tracks, coordinates of the start point of tracks and end point of tracks, the tops of their turning angles, and the length of straight sections

Control point information is stored in a text file (.txt) and has the following format: point order / north latitude coordinate / east longitude coordinate / distance from previous point / altitude / azimuth from previous point. The embedding uses information about five control points, the start (S) and end (E) points. Example of information used:

S / 54.050177 / 27.879798 / 0/184/0; E / 54.051580 / 27.885816 / 16.2 / 188 / 86.783; 1 / 54.051401 / 27.882033 / 198.81 / 183 / 47.714; 2 / 54.052225 / 27.883631 / 137.96 / 182 / 47.318; 3 / 54.052518 / 27.884187 / 47.72 / 182 / 51.436; 4 / 54.051712 / 27.885086 / 104.28 / 186 / 145.096; 5 / 54.051587 / 27.885560 / 36.94 / 187 / 115.258

Fig. 1.The original container (top left), the original container with a superimposed communication scheme (top right), the filled stegano container (bottom).

To implement the embedding of a text file into the container under investigation, we will use a ready-made software solution for steganography Image Spyer G2. The author's implementation of the LSB algorithm is used for embedding. Hiding message bits occurs in the last significant bits of the container [1]. This embedding is difficult for human vision [2, 3]. In addition to the fact that the image itself is difficult to suspect in the presence of any third-party information in it, the program protects the embedded file with one of 40 strong cryptoalgorithms. The use of cryptoalgorithms not only provides an additional line of protection, but also represents the embedded information as statistical noise, which provides protection against statistical attacks on the container [4].

Files were embedded with information about 5 different corner points and 100,000. To evaluate the results, we used a pixel-by-pixel comparison of containers, as well as an assessment by the PSNR criterion. Note that average PSNR values for a good quality empty container are in the 35-45 dB range. For 100,000 corner points, there were 1274 pixel differences, and the PSNR level reached 38 dB, which is typical for a good quality empty container [3].

Based on the data obtained, it can be concluded that it is advisable to embed communication schemes into cartographic materials. At the same time, small distortions of the original container are achieved while storing even a large sample of corner points.

[1] Digital steganography. V.G. Gribunin, I. N. Okov, I. V. Turintsev. - M .: SOLON PRESS, 2009 - 272s.
[3] Computer technologies and data analysis: materials of the II Intern. scientific-practical Conf., Minsk, April 23-24, 2020 / editorial board: V. V. Skakun (editor-in-chief) [and others]. - Minsk: BSU, 2020.S 208 - 211
[2] Zaitsev V.M., Gulai V.A., Dubovik A.V .: Collection of scientific papers "Intelligent, sensory and mechatronic systems - 2020" .: BNTU, Minsk - 2020. ч 43-44.
[4] Sadov V.S. Computer steganography: lecture notes: BSU, 2010. P. 232.

INNOVATIVE TECHNOLOGIES FOR THE FORMATION OF MICROSTRUCTURES IN FUNCTIONAL MATERIALS

Justas Ciganas[1], Giedrius Janu̇gas[1]

[1] Department of Mechanical Engineering, Faculty of Mechanical Engineering and Design, Kaunas University of Technology, Lithuania
justas.ciganas@ktu.lt

Microstructures are structures where the main dimension is micro-meter scale [1]. The formation of microstructures has many technical challenges. In order to obtain the high quality microstructures, it is necessary to define and select the appropriate forming method and materials. Moreover, it is necessary to determine and use optimal production characteristics [2].

There are four main production methods: photolithography, stamping, material removal, and deposition [3]. These four production methods groups are commonly used in microstructures formation research. In addition to these, other manufacturing methods such as 3D printing or wet stamping stand out by their innovative formatting methods [4].

Materials also affect the quality of microstructures. There are four groups of materials widely used and studied in research: silicon, polymers, metals, and glass [5]. There are also various metal oxides or carbides, but they are rarely used in the production of microstructures. Silicon is the most commonly used material to make microstructures. It has semiconductor properties and good mechanical properties, which allows these materials to be used in devices such as micropumps, pressure sensors or accelerometers [6]. Polymers are dielectrics with the least mechanical strength and low melting point. Due to ongoing research, the list of various polymeric materials used in microsystems is constantly updated [7]. Metals have good mechanical properties, electrical conductivity, and high melting point. They are most commonly used for microsystem contact formation [8]. Glass stands out from other materials due to its particularly good optical properties. Glass is also characterized by high thermal and mechanical resistance [9].

However, the choice of the right material and production method does not guarantee the desired quality of the microstructure. Certain phenomena during the production of microstructures are very complex and need to be controlled and investigated. Therefore, it is necessary to develop a new adaptive technology that allow the accurate, fast and inexpensive formation of microstructures in various functional materials.

[1] W. Nawrot, K. Malecha, Additive manufacturing revolution in ceramic microsystems, Microelectronics International **37**, 79-85 (2020).
[2] O. Spahn, M. Seethambal, *MOEMS: Micro-Opto-Electro-Mechanical Systems* (ISBN: 9780819450210, 2005).
[3] Y. C. Kim, J. H. Kang, Microfluidic biomechanical device for compressive cell stimulation and lysis, Sensors and Actuators B: Chemical **128**, 108-116 (2007).
[4] V. A. Camarena-Ch§vez, R. Castro-Beltr§n, O. M. Medina-C§zares, Implementation and assessment of a low-cost 3D laser platform controlled by open software for printing polymeric micro-structures, Journal of Micromechanics and Microengineering, **30**, 3 (2020).
[5] L. Mou, X. Jiang, Materials for Microfluidic Immunoassays: A Review, Advanced Healthcare Materials **6**, 28322517 (2017).
[6] J. G. Jung, K. Lee, Effect of rapid thermal annealing on bulk micro-defects and plastic deformation in silicon during high temperature processing, Materials Science in Semiconductor Processing **85**, 83-89 (2018).
[7] P. M®® J. Giboz, Micro injection molding of thermoplastic polymers: Proposal of a constitutive law as function of the aspect ratios, Journal of Applied Polymer Science **135**, 4 (2017).
[8] H. Kargar-Pishbijari, S. J. Hosseinipour, A novel method for manufacturing microchannels of metallic bipolar plate fuel cell by the hot metal gas forming process, Journal of Manufacturing Processes **55**, 268-275 (2020).
[9] N. Van Toan, M. Toda, Investigation of Processes for Glass Micromachining, Micromachines **7,** 51 (2016).

IMPROVEMENT OF FLAME RETARDANCY AND EVALUATION OF PHYSICAL PROPERTIES OF JUTE FABRIC USING COMBINED CHEMICAL

Mohaiminul Quayum[1*], Md. Reazuddin Repon[1, 2]

[1] Department of Production Engineering, Faculty of Mechanical Engineering and Design, Kaunas University of Technology, Studentu 56, LT-51424, Kaunas, Lithuania

[2]ZR Research Institute for Advanced Materials, Sherpur-2100, Bangladesh

*Email: mohaiminul.quayum@ktu.edu

Development of protective cloth particularly flame-retardant apparel is a big challenge for textile industries nowadays [1]. Usually, inherent flame retardant is more expensive, so making natural fiber as a flame-retardant material is cheap and ecofriendly alternatives. Jute is a natural fiber as well as biodegradable material has taken more attention to develop flame-retardant clothing [2,3]. Chemisorption of combined flame retardant including borax and DAP, borax and Thio-urea, DAP and Thio-urea with different concentrations were conducted on untreated and hydrogen peroxide treated tabby weave jute fabric in padding- dry cure method in this study. The flammability, weight gain (%), breaking load percentages and wash durability of the treated specimens were investigated and compared the outcomes to optimize the chemical concentration. This study exhibits higher improvement of flame-retardancy with the increase of chemical concentrations for both untreated and hydrogen peroxide treated jute fabric. Weight gain percentage is increased for both the specimen but especially borax and Thio-urea combined chemical shows the higher result. In contrast, breaking load percentage is decreased for hydrogen peroxide treated jute fabric with the comparison of untreated jute fabric. Results revealed that borax and DAP combination chemical with 6% concentration shows the better wash durability for hydrogen peroxide treated jute fabric though wash durability decrease for all combination. Moreover, borax and diammonium phosphate (DAP) showed the better performance for all experiment. All samples developed in this study can be used for flame-retardant materials.

Fig.1. Jute a) plant, b) fibre, c) yarn and d) fabric

[1] A R Horrocks and S C Anand, *Handbook of Technical Textiles*, (Woodhead Publishing Ltd, Cambridge, UK, 2000).

[2] Papaspyrides, C. D., Pavlidou, S., & Vouyiouka, S. N. Development of advanced textile materials: Natural fibre composites, anti-microbial, and flame-retardant fabrics. Proceedings of the Institution of Mechanical Engineers, Part L: Journal of Materials: Design and Applications, 223(2), 91ï 102 (2009).

[3] A.K. Samanta, K. Bhattacharya, Simultaneous dyeing and fire-retardant finishing of jute fabric using an acid dye and selective F-R finishing chemicals. Textiles Light Indus, Sci. Technol.41501, 2304-9421(2015).

INVESTIGATION OF $Na_4Fe_3(PO_4)_2(P_2O_7)$ AS CATHODE FOR AQUEOUS Na-ION BATTERIES

Gintarã Pleļ kaitytã[1], Jurgis Pilipaviļ ius[1], Jurga Juodkazytã[1], Linas Vilļ iauskas[1]

[1] Center for Physical Sciences and Technology (FTMC), Saulãtekio al. 3, LT-10257 Vilnius, Lithuania
gintare.pleckaityte@ftmc.lt

Aqueous Na-ion batteries have received particular attention of researchers as one of the main alternatives to Li-ion batteries for sustainable grid-scale energy storage. The use of aqueous electrolytes instead of organics ensures the safety, low price and environmental friendliness of such systems. Exploration and development of suitable positive and negative electrode materials are critically important for high-performance of Na-ion batteries. A great variety of polyanionic or mixed-polyanion compounds have been investigated as cathodes for such batteries. However almost all of them still face different challenges such as poor stability, low energy density or voltage [1]. Among different Fe-based phosphates ($Na_2FeP_2O_7$, $Na_3Fe_2(PO_4)_3$ and etc.), the mixed-polyanionic $Na_4Fe_3(PO_4)_2(P_2O_7)$ represents a more attractive option since it possesses the highest discharge voltage (3.1 V vs Na^+/Na), favorable theoretical capacity (129 mAh g^{-1}) and suitable 3D structure with low volume change during sodium insertion [2, 3].

In this work, we prepared pure phase $Na_4Fe_3(PO_4)_2(P_2O_7)$ via solid-state and sol-gel synthesis methods using different Fe-based precursors ($Fe(CH_3COO)_2$, FeC_2O_4 $2H_2O$ and $C_4H_2FeO_4$). The structure and morphology of prepared materials were characterized by X-ray diffraction (Fig. 1), scanning electron microscopy and thermogravimetric analysis. The electrochemical properties of prepared electrodes were investigated by cyclic voltammetry, charge/discharge galvanostatic cycling and impedance spectroscopy.

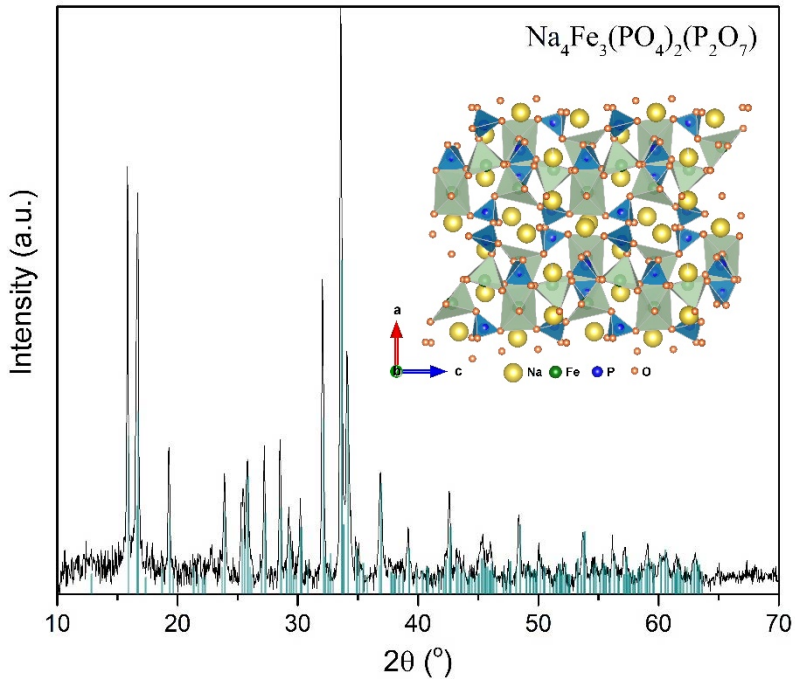

Fig. 1. X-ray diffraction pattern of $Na_4Fe_3(PO_4)_2(P_2O_7)$ synthesized via sol-gel method.

Acknowledgements:
This project has received funding from the European Regional Development Fund (Project No. 01.2.2-LMT-K-718-02-0005) under grant agreement with the Research Council of Lithuania (LMTLT).

[1] Y. Fang, Z. Chen, L. Xiao et al., Recent Progress in Iron-Based Electrode Materials for Grid-Scale Sodium-Ion Batteries, Small, 14 (2018)
[2] M. Chen, W. Hua, J. Xiao et al., NASICON-type air-stable and all-climate cathode for sodium-ion batteries with low cost and high-power density, Nature communications, 10, 1480 (2019).
[3] X. Wang, S. Roy, Q. Shi et al., Progress in and application prospects of advanced and cost-effective iron (Fe)-based cathode materials for sodium-ion batteries, Journal of Material Chemistry A, 9, 1938-1969 (2021).

SYNTHESYS AND PROPERTIES OF METHOXYPHENYL OR METHYLTHIOPHENYL SUBSTITUTED CARBAZOLE DERIVATES AS HOLE-TRANSPORTING MATERIALS

Eduardas Peļiulis, JÎratā Simokaitienā, Juozas Vidas Graǵuleviļius

Department of Polymer Chemistry and Technology, Kaunas University of Technology, Kaunas, Lithuania
eduardas.peciulis@ktu.lt

Enormous effort worldwide is being put into making organic semiconductors, which could be distinguished with the most advantageous charge-transport stability and processability properties. In the synthesis of organic hole-transporting materials (HTMs) toxic inorganic compounds such as gallium, cadmium are not used. In addition, organic HTMs can be more cost-efficient in comparison with their inorganic counterparts. Therefore, it is important to continue the development of HTMs to increase the overall performance of devices of organic optoelectronics and contribute to the development of renewable power sources.

Recently, many researchers are involved in the synthesis and studies of organic HTMs for perovskite solar cells (PSC). The requirements raised for organic HTMs intended for PSC are: high hole drift mobilities, low ionization potentials, glass forming properties, morphological stability of molecular glasses, good solubility in organic solvents, good processability and reproducibility of the characteristics. HTMs in PSC is crucial for high open circuit voltage and high power conversion efficiency.

Electron rich heterocyclic systems such as carbazoles are widely utilized in the synthesis of HTMs [1]. In this work, to decrease ionization potential, electron-donating p-dimethoxydiphenylamine and p-dimethylthiodiphenylamine groups are introduced into the molecular structures of HTMs. Carbazole derivatives were chosen for the synthesis due to their excellent physical and chemical properties, such as high stability, diverse possibilities of functionalization and appropriate photovoltaic characteristics. The compounds were synthesized using different synthesis methods, primarily Ullman coupling and Buchwald-Hartwig methods.

In this presentation physical, thermal, optical and electrochemical properties of the synthesized derivates will be presented. The properties of methoxyphenyl or methylthiophenyl substituted carbazole derivatives will be compared.

This project has received funding from the Research Council of Lithuania (LMTLT), agreement No S-MIP-20-42.

[1] L. Gao, T. H. Schloemer, F. Zhang, X. Chen, C. Xiao, K. Zhu, A. Sellinger. *Carbazole-Based Hole-Transport Materials for High-Efficiency and Stable Perovskite Solar Cells.* ACS Appl. Energy Mater. 3 (5), 4492-4498 (2020)

TADF BEHAVIOUR OF CARBAZOLE AND PHENOTHIAZINE SUBSTITUTED PYRIDINES TOWARDS OLED APLICATIONS

Karolis Leitonas[1], Dmytro Volyniuk[1], Viktorija Andruleviciene[1], Pavel Arsenyan,[2] Brigita Vigante,[2] Juozas Vidas Grazulevicius[1]

[1]Department of Polymer Chemistry and Technology, Kaunas University of Technology, K. Barsausko g. 59, LT- 51423, Kaunas, Lithuania

[2]Latvian Institute of Organic Synthesis, Aizkraukles 21, LV-1006, Riga, Latvia.

karolis.leitonas@ktu.edu

Organic compounds exhibiting thermally activated delayed fluorescence (TADF) in recent years have attracted significant interest in the field of organic optoelectronics. [1] Organic light emitting diodes (OLEDs) can reach 100% internal quantum efficiency (IQE) when TADF compounds are used as emitters due to harvesting of triplet excitons through the reverse intersystem crossing (RISC). Since the first publication on application of TADF materials in OLEDs, multiple-donor approach is widely used in the design of efficient TADF emitters. [2] High external quantum efficiency (EQEs) of TADF based OLEDs is directly related to emissive triplet harvesting via T_1 Ÿ S_1 RISC process in purely organic compounds with small singlet-triplet energy splitting (ϕE_{ST}) and high photoluminescence quantum yields (PLQYs) in the solid state. [3] Some multiple-donor-acceptor TADF emitters with small ϕE_{ST} and high PLQYs in the solid-state were previously developed and showed efficient and relatively stable electroluminescence. [4]

Here we report on a pair of multiple donor substituted dicyanopyridines with three donors of one-type (carbazole) or of two types (carbazole and phenothiazine) in their molecular structures. [5] The compounds were characterized by efficient conventional green and dual orange TADF which results from recombination of one or two intramolecular charge transfer states, respectively. OLEDs based on the phenothiazine and carbazole containing emitter exhibiting dual TADF (Fig. 1) showed low device life-times and low maximum external efficiency of 3.1 (for the non-doped device) and of 5 % (for the doped device). OLEDs based on the carbazolyl multiple substituted dicyanopyridine exhibiting normal TADF showed relatively high device life-times and high maximum external efficiency of 8.1 (for non-doped device) and of 25 % (for doped one). Such device stability and efficiency effects are partly related to ultra-long emission decay (up to milliseconds) which can enhance probability of exciton-exciton and exciton-polaron annihilations under electrical excitation.

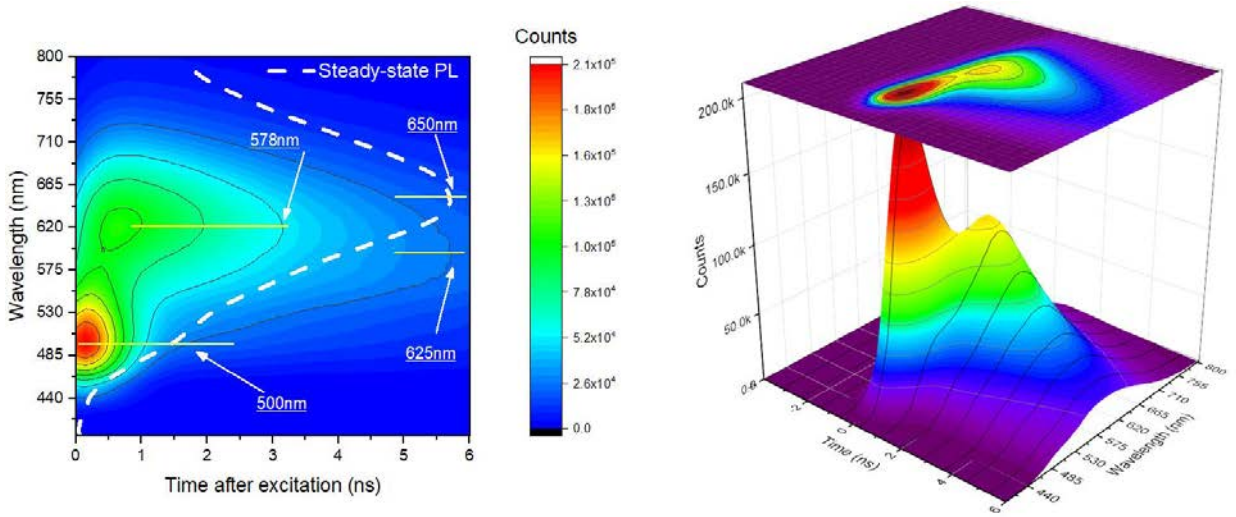

Fig. 1. Steady-state (dashed white line) and time-resolved (recorded in 0-5 ns range after excitation) emission spectra of carbazole and phenothiazine donors containing dicyanopyridine: Contour plot (left) and 3D plot (right) of 10^{-4} mg/ml toluene solution.

Acknowledgement: This work was supported by the project of scientific co-operation program between Latvia, Lithuania and Taiwan ñPolymeric Emitters with Controllable Thermally Activated Delayed Fluorescence for Solution-processable OLEDsò (grant No. S-LLT-19-4).

[1] Y. Liu, C. Li, Z. Ren, S. Yan, M. R. Bryce, Nat. Rev. Mater. 18020 (2018) 1-20.
[2] H. Uoyama, K. Goushi, K. Shizu, H. Nomura, C. Adachi, *Nature* 2012, **492**, 234ï 238
[3] K. Sato, K. Shizu, K. Yoshimura, A. Kawada, H. Miyazaki, C. Adachi, *Phys. Rev. Lett.*, 2013, **110**, 247401.
[4] S. K. Jeon, H. L. Lee, K. S. Yook, J. Y. Lee *Adv. Mater.* 2019, **31**, 1803524
[5] P. Arsenyan. B. Vigante, K. Leitonas, D. Volyniuk, V. Andruleviciene, L. Skhirtladze, S. Belyakov, J. V. Grazulevicius, *J. Mater. Chem. C*, 2021 (*Accepted*)

REAL-TIME PHOTORHEOMETRY STUDY OF DUAL PHOTOCURING KINETICS OF BIO-BASED MONOMERS

Greta Motiekaityte*, Aukse Navaruckiene, Jolita Ostrauskaite

Department of Polymer Chemistry and Technology, Kaunas University of Technology, Radvilenu Rd. 19, LT-50254 Kaunas, Lithuania
greta.motiekaityte@ktu.edu

A dual-curing process is defined as a combination of two curing reactions taking place simultaneously or sequentially. It is a method to combine two otherwise distinct polymer networks. The resulting interpenetrating polymer network exhibits superior properties compared to its individual parts [1]. In this study, a combination of two simultaneous and sequential photopolymerization processes was investigated. Photoinitiated polymerization have the advantages of rapid cure, low energy consumption, high efficiency, low volatile organic compound emission, and the large number of applications in not only conventional areas such as coatings, inks, and adhesives, but also in high-tech domains, such as microelectronics, optoelectronics, laser imaging, stereolithography, and nanotechnology [2]. The replacement of petroleum-based materials by materials derived from renewable resources in such technologies would give the ecological and economic benefits.

In this work, two processes of free radical and cationic photocross-linking of biobased monomers carried out simultaneously and sequentially were investigated by the real-time photorheometry. This method provides the wide range information on typical rheological properties such as viscosity and storage modulus Gó, loss modulus Gò, loss factor tanŭ, and complex viscosity ḍ* while a material is irradiated with UV/VIS light. It enables to track the occurrence of structural phenomena, such as gelation and vitrification, indicating the moment, when the structural changes have started [3].

The dual photocuring of various acrylated and epoxidized vanillin and glycerol-based monomers was investigated in this study. Several free radical and cationic photoinitiators were used. The influence of the initial reaction mixture composition to the photocuring kinetics, rheological properties, rigidity and shrinkage of the resulting cross-linked polymers was investigated.

It was determined that the highest values of storage modulus Gó and thus the highest rigidity were achieved using sequential dual photocuring process. The gel point of the most dual photo-curing systems was higher than that of pure acrylates but lower than that of pure diglycidyl ethers. The shrinkage of the samples of the most dual photocuring systems was lower than that of the pure acrylate samples but higher than that of pure diglycidyl ether samples.

Acknowledgement. This research was funded by the Research Council of Lithuania (project no. S-MIP-20-17).

[1] O. Konuray, X. Fernandez-Francos, X. Ramis, A. Serra, State of art in dual-curing acrylate systems, Polymers **10**, 178 (2018).
[2] Y. Yagci, S. Jockusch; N.J. Turro, Photoinitiated Polymerization: Advances, Challenges, and Opportunities, Macromolecules **43**, 6245-6260 (2010).
[3] L.E. Schmidt; D. Schmª h; Y. Leterrier; J.E. M¬nson, Time-intensity transformation and internal stress in UV-curable hyperbranched acrylates, Rheol. Acta **46**, 693-701 (2007).

THE CONTROL OF THERMAL BEHAVIOR COIR MIXED GLASS FIBER SPUR GEAR DURING MESHING PROCESS (HAND-LAYUP METHOD)

Sandesh Mysore Sathyaraj[1], Harsha Dyanesh[2,] Veeraraghavan Rajagopalan[3*]

[1] Department of Electrical and Electronics Engineering,, Kaunas University of Technology, Lithaunia
[2,3] Department of Mechanical Engineering and Design, Kaunas University of Technology, Lithaunia
Sandesh.mysore@ktu.edu, veeraraghavan.rajagopalan@ktu.edu, harsha.nelavai@ktu.edu.

The present work describes the development and mechanical characterization of new polymer composites consisting of reinforcement of E-glass fiber, epoxy resin, and hardener, natural fiber (coir fiber). The mechanical properties of the newly developed composites are characterized. In order to find the significant influence of natural fiber (coir) on the mechanical characteristics of glass fiber reinforcement composites, experiments such as hardness test, tensile test, compression test, impact test were carried out. A significant class of materials available to mankind are composites. In material science, metallurgy, chemistry, solid mechanics and engineering applications, studies of such composites play a very important role. Due to its benefits, such as low cost, noise control, low weight and ease of processing, the E-glass fiber1 reinforced polymer composite is more widely used in the automotive industry and other industrial applications. Cheap and environmentally friendly materials are natural fibers [1]. Composites are a new development in the field of material science. Aircraft industries today need material at low cost, less weight, but should have high strength to increase the efficiency of aircraft and even in the automotive industry. The above solutions are only composite materials. Natural fiber composites can also be very cost-effective material for application in construction and construction areas, storage devices, furniture, electronic devices, interior parts of cars and railway coaches, etc. This paper provides the manufacture and investigation of hemp and bagasse fiber reinforced with epoxy hybrid composite mechanical properties. The production is performed by hand-layup technique with random orientation of hemp and bagasse fibers in this method. Here, a flexural test is performed according to ASTM standards by changing the volume fraction of the fibers to 10 percent & 20 percent composite laminates and tested for its mechanical properties such as tensile. And the hardness test is also carried out for both the laminate volume fractions [2].

(a) (b) (c)

Fig. 1. (a) Glass Fiber (b) Coir Fiber (c) Spur Gear

A single spur gear is typically selected to have a ratio range of between 1:1 and 1:6 with a pitch line velocity up to 25 m/s. The spur gear has an operating efficiency of 98-99 percent. To have the maximum number of teeth, consistent with an acceptable safety margin in strength and wear, a gear pair should be chosen. On a gear with a normal pressure angle of 20 degrees, the minimum number of teeth is 18. The final composition is produced from 60 percent fiber composition as a better strength compared to 40 percent composition and the final manufacture of gear is made from 60 percent epoxy composition as a better strength. Epoxy resins are pre-polymers of relatively low molecular weight capable of being processed under a variety of conditions. These have two significant advantages over unsaturated polyester resins: first, they can be partially cured and stored in that state, and second, during cure, they exhibit low shrinkage. [2]. Approximately 45 percent of the total amount of epoxy resins produced is used in protective coatings, while the rest is used in structural applications such as laminates and composites, tooling, molding, casting, construction, adhesives, etc. The strength/weight ratios of glass fiber composites are higher than those of most other materials and are phenomenal in their impact resistance. They also have good electrical properties, moisture and outdoor weather resistance, and heat and chemical resistance. Such properties are combined with ease of manufacturing.

---

[1]Sandhya Rani Borukati, International Conference of Trends in Information, Management, Engineering and Sciences (ICTIMES) Volume 5, Special Issue 02, Feb.-2018, ñDesign and characterization of E-Glass Fiber Reinforced Composite Material with use of Coir Fiberñ

[2] Yashas Gowda, T.G.; Sanjay, M.R.; Subrahmanya Bhat, K.; Madhu, P.; Senthamaraikannan, P.; Yogesha, B. SSPolymer matrix-natural fiber composites: An overview. Cogent. Eng. 2018, 5, 1446667. [CrossRef]

PRODUCTION OF VARIOUS SIZE ORGANIC PHOTOVOLTAIC CELLS WITH P3HT:PC61BM AS AN ACTIVE LAYER

Dominik Suwala, Grzegorz Wryk,
Aleksandra Szymanska[1], Krzysztof Domanski,
Alicja Kalucka, Ola Bednarczyk, Dana Binczuk
Wojciech Mech, Adam Wincukiewicz, Maciej Krajewski,
Joanna Sitnicka, Krzysztof P. Korona, Maria Kaminska

Faculty of Physics, University of Warsaw, Pasteura 5 st. 02-093, Warsaw
[1] a.szymanska40@student.uw.edu.pl

Developing effective renewable energy sources is essential due to the world's efforts for carbon-neutrality. Organic photovoltaics (OPV) provide unique possibilities. They are much cheaper than silicon cells and moreover, can be deposited on flexible substrates, which opens the potential for new niches such as wearable electronics and building incorporated panels.

Although promising, OPV suffers from relatively low efficiencies (c.a. $5-7\%$) which is currently the main obstacle in the way for commercialization. The two major reasons behind this behavior are short exciton diffusion lengths and very low carrier mobility in an active layer.

Here, we present organic solar cell structures with P3HT:PC61BM mixture in weight ratio 1:0.6 as an active layer. P3HT (Poly(3-hexylthiophene-2,5-diyl)) is a conductive polymer with absorption edge in the visible region working as an electron donor. PC61BM is a C_{60} fullerene derivative working as an acceptor. During research, we focus on the optimization of the deposition parameters, i.e. the active layer annealing temperature, spin coating rotation speed and used solvents. Also, to test our method at a larger scale we prepare the cells onto indium-tin oxide substrates with two, substantially different sizes: 3 cm^2 and 25 cm^2.

As the result, we present absorption spectra of the P3HT and PC61BM. Regarding solar cells, I-V characteristics, photocurrent and external quantum efficiency measurements will be discussed.

VANILLIN ACRYLATE-BASED POLYMERS: INFLUENCE OF RESIN COMPOSITION TO PHOTOCURING KINETICS AND PROPERTIES OF THE RESULTING POLYMERS

Aukse Navaruckiene[1], Danguole Bridziuviene[2], Vita Raudoniene[2], Jolita Ostrauskaite[1]

[1] Department of Polymer Chemistry and Technology, Kaunas University of Technology, Radvilenu Rd. 19, LT-50254 Kaunas, Lithuania.
[2] Biodeterioration Research Laboratory, Nature Research Center, Akademijos Str. 2, LT-08412 Vilnius, Lithuania.
aukse.navaruckiene@ktu.lt

Additive manufacturing is getting popular in the manufacturing companies, because it is a cheap and fast way to produce new products in complex shapes [1]. Additive manufacturing provides such benefits as lower material loss, reduced product weight and possibility to print spare parts without using fixtures or molds [2,3].

In this study, cross-linked polymers were obtained by photopolymerization of vanillin diacrylate and vanillin dimethacrylate with 1 or 0.5 mol.% of 1.3-benzenedithiol, using phenylbis(2,4,6-trimethylbenzoyl)phosphine oxide (BAPO) as photoinitiator. Photorheometry was used to monitor the evolution of photocross-linking process. The UV/Vis real-time photorheometry curing tests were performed on a MCR302 rheometer from Anton Paar equipped with the plate/plate measuring system. Dependencies of storage modulus Gô, loss modulus Gò, loss factor tanŭ, and complex viscosity ɖ* of pure vanillin diacrylate-based resin with 3 mol.% of BAPO on irradiation time is presented in Figure 1. It was determined that the addition of solvent into the resin slowed down the photocuring process and less rigid polymers were obtained. The addition of thiol increased the photocuring rate but reduced the rigidity of the resulting polymers.

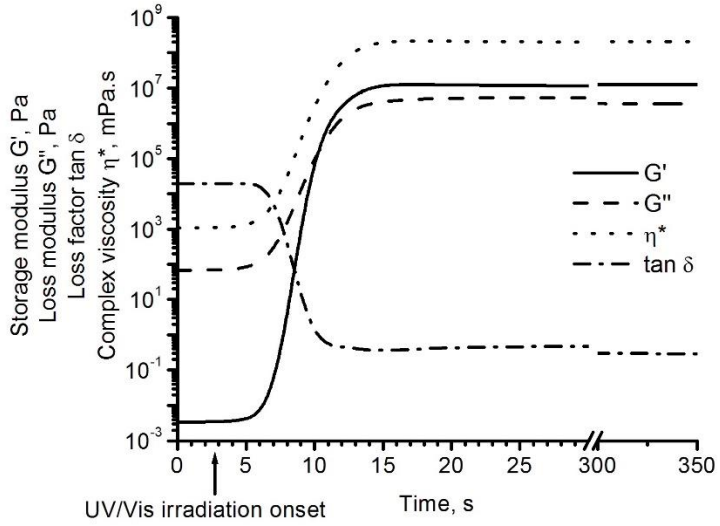

Fig. 1. Dependencies of storage modulus Gô, loss modulus Gò, loss factor tanŭ, and complex viscosity ɖ* of pure vanillin diacrylate-based resin with 3 mol.% of BAPO on irradiation time, at 25 ÁC.

Vanillin-based polymers showed significant antibacterial activity against *Escherichia coli* and *Staphulococcus aureus* in direct contact and on medium. Toxicity to microscopic fungus *Aspergillus niger* and *Aspergillus terreus* was less pronounced.

Acknowledgement. This research was funded by the EU ERDF, through the INTERREG BSR Programme, (ECOLABNET project #R077), the European Social Fund under the measure no. 09.3.3-LMT-K712 ñDevelopment of Competences of Scientists, other Researchers and Students through Practical Research Activitiesò, and the Research Council of Lithuania (project no. S-MIP-20-17).

[1] M. K. Niaki, S. A. Torabi, F. Nonino, Why manufacturers adopt additive manufacturing technologies: The role of sustainability, J. Clean. Prod. **222**, 381-392 (2019).
[2] D. Bº ckin, A.-M. Tillman, Environmental assessment of additive manufacturing in the automotive industry, J. Clean. Prod. **226**, 977-987 (2019).
[3] A. Chergui, K. Hadj-Hamou, F. Vignat, Production scheduling and nesting in additive manufacturing, Comput. Ind. Eng. **126**, 292-301 (2018).

SYNTHESIS AND INVESTIGATION OF TRIDECYL METHACRYLATE-BASED PHOTOCROSS-LINKED POLYMERS

Justinas Jaras*, Aukse Navaruckiene, Jolita Ostrauskaite

Department of Polymer Chemistry and Technology, Kaunas University of Technology, Radvilenu Rd. 19, LT-50254 Kaunas, Lithuania
justinas.jaras@ktu.edu

In recent years, natural oils have become the center of attraction for their potential use as starting materials for the preparation of polymers. The use of photoinitiated polymerization is continuously growing in industry as reflected by the large number of applications in not only conventional areas such as coatings, inks, and adhesives but also in high-tech domains, such as optoelectronics, laser imaging, stereolithography, and nanotechnology [1]. The use of materials derived from renewable raw materials for the production of polymers exhibiting properties similar to those of conventional petroleum-derived polymers and able to decompose into harmless substances after use and release into the environment is of increased interest of both research and industry. Among all renewable resources, natural vegetable oils are considered to be one of the most important classes of renewable sources because of the wide variety of possibilities for chemical transformation, universal availability, and low price [2]. Tridecyl methacrylate was chosen as a biobased monomer derived from natural oil in this study.

The aim of this work was to investigate the influence of the amount of the cross-linking agent dipentaerythritol pentaacrylate to the photopolymerization kinetics of tridecyl methacrylate and properties of the resulting polymers. 2,2ڍ Dimethoxyڍ2ڍphenylacetophenone was used as photoinitiator. Chemical structure of the used compounds is presented in Figure 1.

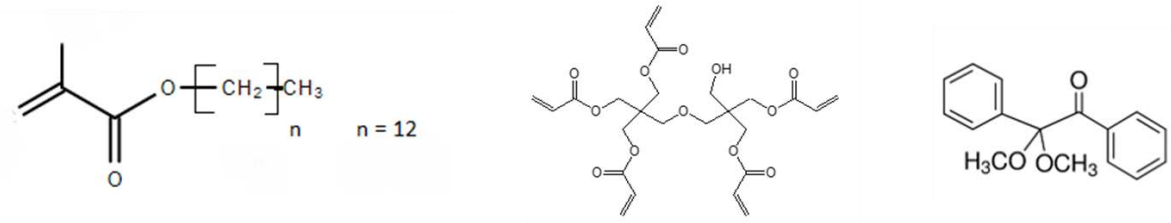

Fig. 1. Chemical structure of tridecyl methacrylate (a), dipentaerythritol pentaacrylate (b), and 2,2ڍdimethoxyڍ2ڍ phenylacetophenone (c)

Photocross-linking kinetics was monitored by the real-time photorheometry which provides the wide range information on typical rheological properties such as viscosity and shear modulus while a material is irradiated with UV/VIS light. The chemical structure of the cross-linked polymers was confirmed by FT-IR spectroscopy. The yield of the insoluble fraction of the cross-linked polymers was determined after Soxhlet extraction with acetone for 24 h. Mechanical characteristics were determined by tensile/bending/compressive tests. Thermal properties were investigated by differential scanning calorimetry and thermogravimetric analysis.

It was determined that the rheological, thermal, mechanical properties, and swelling of the synthesyzed polymers in polar and nonpolar solvents strongly depended on the amount of the cross-linking agent fragments in the polymer and the density of the network.

Acknowledgement. This research was funded by the EU ERDF, through the INTERREG BSR Programme, (ECOLABNET project #R077) and the Research Council of Lithuania (project no. S-MIP-20-17).

[1] Y. Yagci, S. Jockusch; N.J. Turro, Photoinitiated Polymerization: Advances, Challenges, and Opportunities, Macromolecules **43**, 6245-6260 (2010).
[2] C. Zhang, T.F. Garrison, S.A. Madbouly, M.R. Kessler, , Prog. Polym. Sci. **71**, 91-143 (2017).

HELICITY INDUCED SPIN-ORBIT COUPLING FOR ULTRAFAST ISC IN ALKYNE BRIDGED BIFLUORENES

Eglė Tankelevičiūtė[1], Paulius Baronas[1], Regimantas Komskis[1], Povilas Adomėnas[2], Ona Adomėnienė[2], and Saulius Juršėnas[1]

[1] Institute of Photonics and Nanotechnology, Vilnius University, Vilnius, Lithuania
[2] Fine Synthesis, Ltd., Kalvarijų g. 201E, LT-08311, Vilnius, Lithuania
egle.tankeleviciute@ff.stud.vu.lt

Compounds with strong spin-orbit coupling (SOC) and fast intersystem crossing (ISC) are important for organic light emitting diodes and photosensitizers used for photo-dynamic therapy [1]. However, achieving a high ISC rate usually requires heavy atoms, such as Pt or Ru, thus making materials of this kind not cost-efficient. Here, we propose a concept to enhance SOC in carbon-only structures by taking advantage of helical molecular orbitals (Hel-MOs). Intersystem crossing dynamics in bifluorenes were investigated by means of pump-probe measurements, which indicated that minor modifications of the molecule (extended alkyne bridge) cause considerable photophysical differences (Fig. 1). Furthermore, theoretical calculations were performed to confirm the helical shape of the MO in the dialkyne bridge unit. Formation of helical molecular orbitals results in enhanced SOC leading to an increased ICS rate.

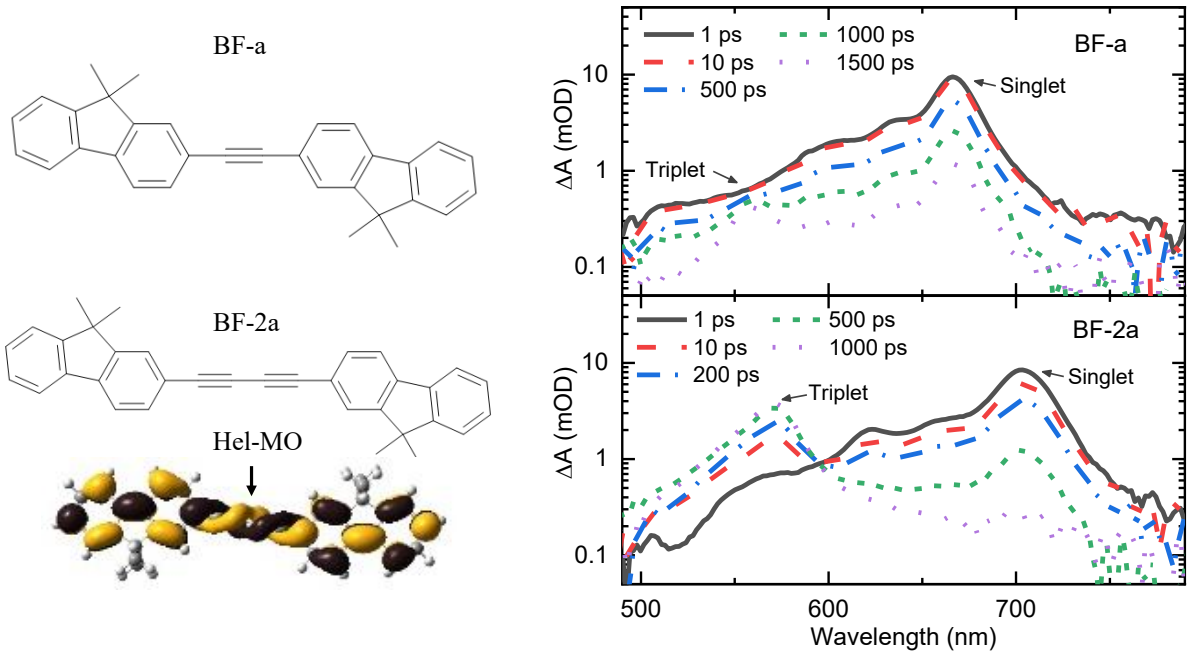

Fig. 1. Bifluorene molecules and their transient absorption spectra

[1] D. Sasikumar, A. T. John, J. Sunny, M. Hariharan, Chem. Soc. Rev. 2020, 49, 6122.

DEVELOPMENT OF MEDICAL PLANT DRYING METHOD BASED ON THE CONTROL OF RELATIVE HUMIDITY

Mykyta Kovalenko[1], Daniela Senkeviļ[1], Karolina Lapkauskaitā[1],Andrius Dzedzickis[1], Vytautas Buļinskas[1]

[1] Department of Mechatronics, Robotics and Digital Manufacturing, Vilnius Gediminas Technical University
mykyta.kovalenko@vilniustech.lt

Drying is one of the most popular and essential operations in the post-harvesting processing of medical plants or food products. During drying, the moisture from inside the product moves towards its surface, where it transforms to a gaseous state (water vapor) and then transfers to the surrounding air in terms of heat or mass transfer [1]. Contemporary food industry mostly uses drying methods that apply heat to induce the phase change of water from liquid to gaseous state [1, 2]. However, dehydration at high temperatures may influence the appearance, structure, and biochemical compound of dried specimen [3].

Our suggested method of drying does not involve the use of heat for dehumidification of drying air ï the process initially occurs at room temperature. An operating principle of a created system is based on the dependence of relative humidity (RH) of air from its temperature. The air from the drying chamber is blown through a heatsink which is in thermal contact with a cold surface of a thermoelectric cooler (TEC). An immediate decrease of airflow temperature at this moment increases its RH; water vapor in the air reaches saturation point, and contributes to the formation of condensate, that should be collected and removed.

The workability of a proposed method was tested using computational fluid dynamics (CFD) software. The simulation was performed at following initial parameters: temperature of the air is 20,05 ÁC, RH is 65%, the air pressure is 101325 Pa, heatsink temperature is -2,15 ÁC, the volume of a drying chamber is 0,096 m^3, total simulation time was 10 min with a step-up of 1 min. The simulation results in the form of cut plots presented at Figure 1.

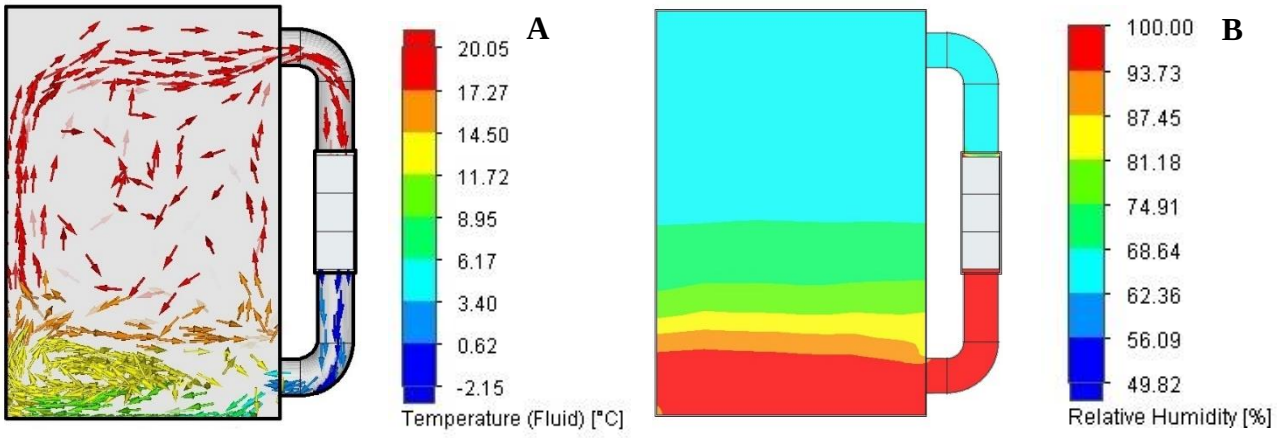

Fig. 1. Parameters of drying air in a chamber: A ï temperature change; B ï relative humidity change.

Correlation of RH and temperature plots (Fig. 1) demonstrates that the RH of air immediately reaches its maximum value when it passes through a cold heatsink and stays at that level until temperature increases to approximately 11 ÁC. Later, it gradually decreases as temperature rises. It means that the plant sample to be dried should be located in an optimal position between a minimal RH and maximal temperature zone.

Additionally, it is essential to note that RH change in the air stream, passing through the cold heatsink affects its temperature. Change of the heatsink temperature, required to induce moisture condensation ï the dewpoint, could cause a decrease of the drying system efficiency. Higher temperature slows down the condensation process, too low temperature may lead to ice formation on the heatsink. Maintenance of highest system efficiency requires precise control of the heatsink temperature and its setpoint adjustments according to other system parameters. Definition of the optimal ratios between parameters affecting systems efficiency will become the main aim for further research.

Acknowledgement

This project has received funding from the European Social Fund (project No 09.3.3.-LMT-K-712-22-0295) under a grant agreement with the Research Council of Lithuania (LMTLT).

[1] Kerr, W. L. (2013). Food Drying and Evaporation Processing Operations. In *Handbook of Farm, Dairy and Food Machinery Engineering: Second Edition*. https://doi.org/10.1016/B978-0-12-385881-8.00012-4

[2] Sabarez, H. T. (2015). Modelling of drying processes for food materials. In *Modeling Food Processing Operations*. https://doi.org/10.1016/B978-1-78242-284-6.00004-0

[3] M¿ller, J., & Heindl, A. (2007). Drying of Medicinal Plants. In *Medicinal and Aromatic Plants*. https://doi.org/10.1007/1-4020-5449-1_17

PROCESS PARAMETER INFLUENCE ON SURFACE ROUGHNESS OF ADDITIVELY MANUFACTURED STAINLESS STEEL PARTS

Ada Steponaviļ iÎ tā, Karolis Stravinskas, Augra Selskienā, Genrik Mordas

Department of Laser Technologies, Center for Physical Sciences and Technology, Lithuania
ada.steponaviciute@ftmc.lt

Additive manufacturing (AM) is a manufacturing technology used for 3D object production which opens a pathway to fabricate complex parts due to the high geometrical flexibility of the technology [1]. Direct Metal Laser Sintering (DMLS) is one of the most widely applied metal AM technologies, where, in a layer-by-layer fashion, bulk parts are created by selective sintering and consolidation of thin powder layers using a laser beam [2]. DMLS can be used for part fabrication using different metals and their alloys. Although iron and its alloys have been used in conventional manufacturing for a long time and the most advantages and disadvantages of these materials are well known, using them in additive manufacturing to achieve high quality still can be problematic. In DMLS, the main challenge is to understand the influence of energy density on porosity, microstructure and mechanical properties of a manufactured part.

In this study, test specimens were produced from 17-4PH stainless steel using different sets of build parameters on the EOSINT M280 machine in order to determine the influence of different process parameters and specimen positioning on specimen surface quality. A stylus profiler was used in the study to determine the relation between specimen positioning on the build platform during the printing process and the surface roughness of printed objects. To better understand what causes different surface roughness in specimens produced with various volumetric energy density values, cross-sectional microstructure of the manufactured specimens was investigated using scanning electron microscopy (SEM) and optical microscopy and defects visible in cross-sections were evaluated with help of image processing software.

Results have shown that the best surface quality can be achieved when the energy density values during the manufacturing process are from 48 to 65 J/mm^3. However, only applying certain energy density is not sufficient and surface quality differs depending on the surfaceôs positioning on the building platform.

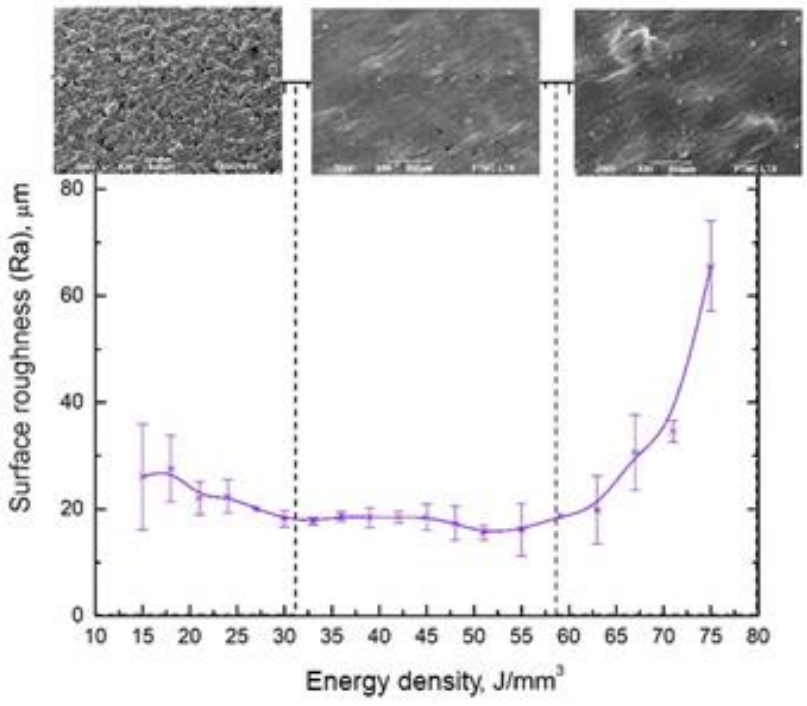

Fig. 1. Influence of volumetric energy density on specimen surface roughness

[1] L. Hitzler, M. Merkel et al., A Review of Metal Fabricated with Laser- and Powder-Bed Based Additive Manufacturing Techniques: Process, Nomenclature, Materials, Achievable Properties, and its Utilization in the Medical Sector, Advanced Engineering Materials Volume 20, Issue 5 (2018).
[2] B. Song, S. Dong et al., Microstructure and tensile properties of iron parts fabricated by selective laser melting, Optics & Laser Technology 56, 451-460 (2014).

EXPERIMENTAL RESEARCH OF FORCE/PRESSURE SENSOR STATIC AND DYNAMIC ACCURACY AND REPEATABILITY

Nikita Edgar Sitiajev[1], Vaiva Trečiokaitė[1], Ernestas Šutinys[1]

[1] Department of Mechatronic, Robotics and Digital Manufacturing, Vilnius Gediminas Technical University, Vilnius
nikita-edgar.sitiajev@stud.vgtu.lt

The progress observed in 'soft robotics' brought some promising research in flexible tactile, pressure and force sensors, which can be based on polymeric composite materials. Therefore, in this paper, we intend to evaluate the characteristics of a force-sensitive material – polyethene-carbon composite (Velostat®) by implementing this material into the design of the flexible tactile sensor [1].

Velostat® is a composite polymer material consisting of carbon-impregnated polyethene. Entrapped carbon powder turns initially dielectric polyethene into electrically conducting composite material which belongs to the group of piezoresistive materials. Simply speaking by applying force or pressure on this material, its resistance is changed.

The main problem is an insufficiency of research of Velostat®, in order to successfully predict its reaction to particular mechanical irritation and therefore implement it as a reliable sensor in a mechatronic system.

During the research, the velostat® film was placed between two conductive copper electrodes which allowed to measure the resistance of the material in respect of time and evaluate sensors' dynamic response.

Dynamic load acting on the sensor's upper surface was created using a motor carrying an eccentric load (Fig. 1.). By changing the mass and adjusting the loading fixture offset from motor shaft different magnitude mechanical loads were exerted. The loading frequency was controlled by the stepper motor's varying rotation speed.

From the Fig. 1 you can observe a velostat® film (1) being place between two conductive strips (2), to connect it to measuring device, placed between a lower (3) and upper (4) plates to hold it in place. The upper plate is represented transparent, in order to show the interconnection between the elements. The upper plate is firmly connected to the motor (5), which is going to create an eccentric load for force-sensitive material. On the shaft of the motor a pulley (6) with slots is mounted, in order to allow attachment and adjustment of different weights making testing device more versatile also an accelerometer (7) is joined with the upper plate to monitor the magnitude of excited force and create a closed-loop system.

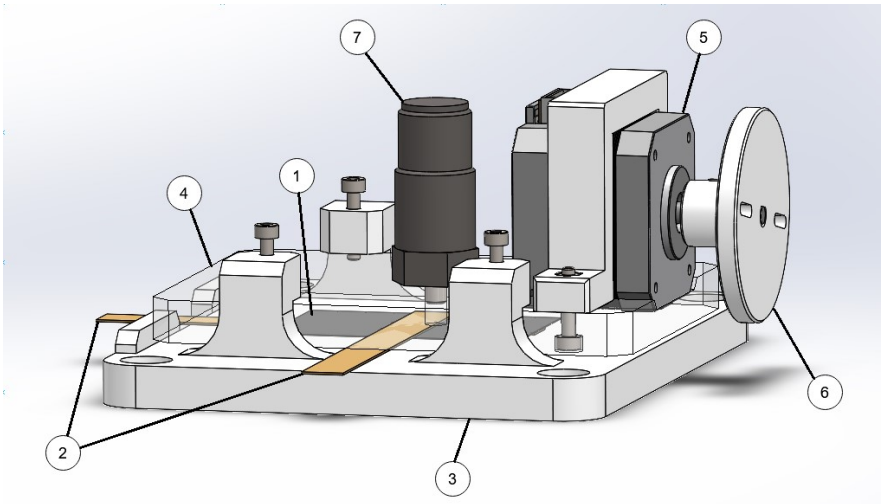

Fig. 1. Testing device scheme: 1 - Velostat® film, 2 - conductive strip, 3 – bottom plate, 4 – upeer plate, 5 – electric motor, 6 – pulley, 7 - accelerometer

When the experiment is carried out, data is obtained and saved on the memory device. Correlation between frequency and amplitude of applied dynamic load and change in resistance of velostat® defines how precisely sensor can react to varying load. Obtained data allows defining the sensor's main dynamic characteristics such as response time and bandwidth.

After result evaluation, precise velostat® reaction is established, promoting the further implementation of force-sensitive material into "soft robotics" applications.

Acknowledgement

This project has received funding from the European Social Fund (project No 09.3.3.-LMT-K-712-22-0328) under a grant agreement with the Research Council of Lithuania (LMTLT).

[1] A. Dzedzickis, E. Sutinys, V. Bucinskas, U. Samukaite-Bubniene, B. Jakstys, A. Ramanavicius, I. Morkvenaite-Vilkonciene, Polyethylene-Carbon Composite (Velostat®) Based Tactile Sensor, *Polymers* **2020**, *12*(12), 2905 (2020).

OPTICALLY 3D PRINTED SCAFFOLDS: BIOCOMPATIBILITY EVALUATION AND IMPROVEMENT

Jurga Jeršovaitė[1,*], Edvinas Skliutas[1], Giedrė Grigalevičiūtė [1],
Daiva Baltriukienė [2], Mangirdas Malinauskas[1]

[1]Laser Research Center, Faculty of Physics, Vilnius University, Vilnius LT-10223, Lithuania
[2]Life Sciences Center, Institute of Biochemistry, Vilnius University, Vilnius LT-10257, Lithuania
jurga.jersovaite@ff.stud.vu.lt

The manipulation of biological tissues, including their growth or regeneration is a very promising field. However, most of the current researches are *in vivo* or based on the biological tissue or organ sample donations that in most cases causes a discomfort for the patient. Therefore the development of micro/nano bioscaffolds is a successful alternative for the manipulation and growth of the biological samples *in vitro*.

In this study we analyse two types of commercial stereolithography 3D printers: Ember (Autodesk) and Asiga PICO 2 UV DLP and their abilities for printing bioscaffolds. The concept is based on the articles by Grigalevičiūtė [1] and Hart [2]. The authors of these articles present studies of the biocompatibility of printed structures with cells in the case of various widely used resins. It is also well known that bio-based resin can be used in 3D printing [3, 4] so there is a possibility to print any wanted biocompatible 3D geometry with a resolution of a few nanometers and this leads to accurate organs engineering. Methods for increasing biocompatibility in the following ways are also discussed: treatment with IPA (isopropyl alcohol), UV, thermal baking, autoclaving and coating with another material. All these steps are shown in Fig. 1

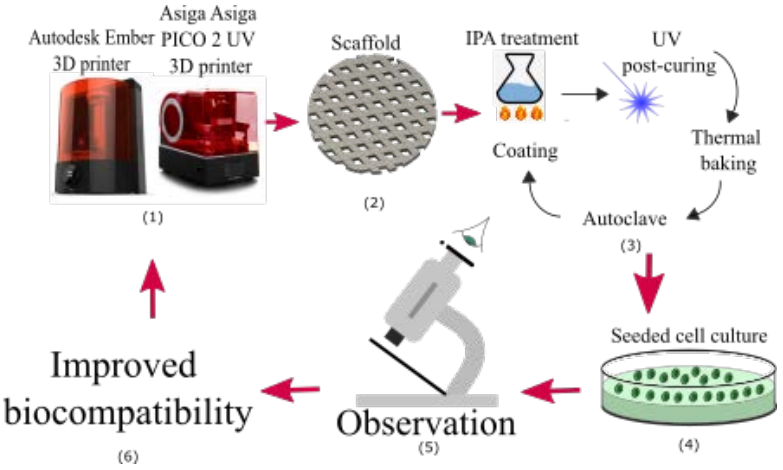

Fig. 1. Iteration steps of the proposed experiment: (1) Asiga PICO 2 UV digital light processing (DLP) 3D printer and Ember (Autodesk) 3D printer. (2) Scaffold, that can be printed from many commercial and bio-based resins. (3) Scaffold post-processing stages. (4) Samples, seeded with adult-organism derived stem cells and tested for biocompatibility (cell adhesion (integration), cell proliferation and differentiation capabilities). (5) Discussion of the results and conclusions. Knowing what went wrong and witch parts of the experiment succeeded, we repeat the experiment again with new ideas

Based on the results obtained in previously mentioned articles it can be seen that Formlabs Clear and Flexible resins showed the best biocompatibility results. Taking into account the results obtained by Grigalevičiūtė, it is promising to achieve even better compatibility by changing the geometrical parameters of the scaffold (pore size, shape and porosity). Since cells die mostly in the middle of the scaffolds due to the pure leaching of monomers, changing of their geometry (making it with a higher resolution or creating a different geometric structures in the middle compared to the edges of the scaffold) might lead to even more biocompatible scaffolds. Various post-processing methods have also shown that the use of PDMS coating alone has greatly increased a biocompatibility. It would also be useful to try coating with other materials or even with several of them.

[1] Grigaleviciute, G.; Baltriukiene, D.; Bukelskiene, V.; Malinauskas, M. Biocompatibility Evaluation and Enhancement of Elastomeric Coatings Made Using Table-Top Optical 3D Printer. *Coatings* **2020**, 10, 254. https://doi.org/10.3390/coatings10030254
[2] Hart, C.; Didier, C.M.; Sommerhage, F.; Rajaraman, S. Biocompatibility of Blank, Post-Processed and Coated 3D Printed Resin Structures with Electrogenic Cells. *Biosensors* **2020**, 10, 152. https://doi.org/10.3390/bios10110152
[3] Skliutas, E., Lebedevaite, M., Kasetaite, S. et al. A Bio-Based Resin for a Multi-Scale Optical 3D Printing. *Sci. Rep.* **10**, 9758 (2020).https://doi.org/10.1038/s41598-020-66618-1
[4] Navaruckiene, A.; Skliutas, E.; Kasetaite, S.; Rekštytė, S.; Raudoniene, V.; Bridziuviene, D.; Malinauskas, M.; Ostrauskaite, J. Vanillin Acrylate-Based Resins for Optical 3D Printing. *Polymers* **2020**, 12, 397. https://doi.org/10.3390/polym12020397

INFLUENCE OF FIBER CONTENT ON THE BENDING STIFFNESS OF FUNCTIONAL TEXTILES

Norina Asfand, Virginija Daukantienă

Department of Production Engineering, Kaunas University of Technology, Lithuania
norina.asfand@ktu.edu

Knitted fabrics are preferred for clothing due to their outstanding comfort. Knitted fabrics featuring with the antistatic properties are increasingly used for smart textile applications due to their flexible nature [1]. Nowadays knitted fabrics are also widely used for composite materials applied in automotive engineering, in civil engineering, etc. [2]. Mechanical properties of knitted fabrics are highly important when choosing mostly suitable one for a particular application.

1Ǐ 1 rib knitted fabrics were developed by using the yarns of four different blend ratios of cotton fibers and antistatic fibers made from polyester containing carbon particles. Fibers blend ratios in the used yarns were these: 90 % cotton/10 % antistatic polyester, 80 % cotton/20 % antistatic polyester, 70 % cotton/30 % antistatic polyester, and 65 % cotton / 35 % antistatic polyester. A fully automatic flat knitting machine MATSUYA-M100 with 14 gauge was used for sample development. Thickness of all the investigated fabrics ranged within the limits of 1.87–1.90 mm, wale density – 14.6–15.8 cm^{-1}, and course density – 10.6–11.6 cm^{-1}. These structure characteristics were determined according to the standards LST ISO 5084 and LST EN 14971, respectively. Area density *w* of the tested fabrics was determined according to the standard LST EN 12127. The area densities of the investigated textiles were 598 g/m^2 for MR1 fabric, 578 g/m^2 for MR2 fabric, 566 g/m^2 for MR3 fabric, and 511 g/m^2 for MR4 fabric. Bending lengths *L* of 50×150 mm rectangular specimens cut from the investigated knitted fabrics were measured applying a cantilever method with the FAST-2 bending meter. Fabric bending stiffness *B* was calculated by using Eq. (1):

$$B = w \cdot c^3 \cdot 9.81 \cdot 10^{-6} \quad (1)$$

where *B* ï bending stiffness, ε Nm; *w* ï area density, g/m^2; *c* ï half of bending length *L* of the tested specimen, mm.

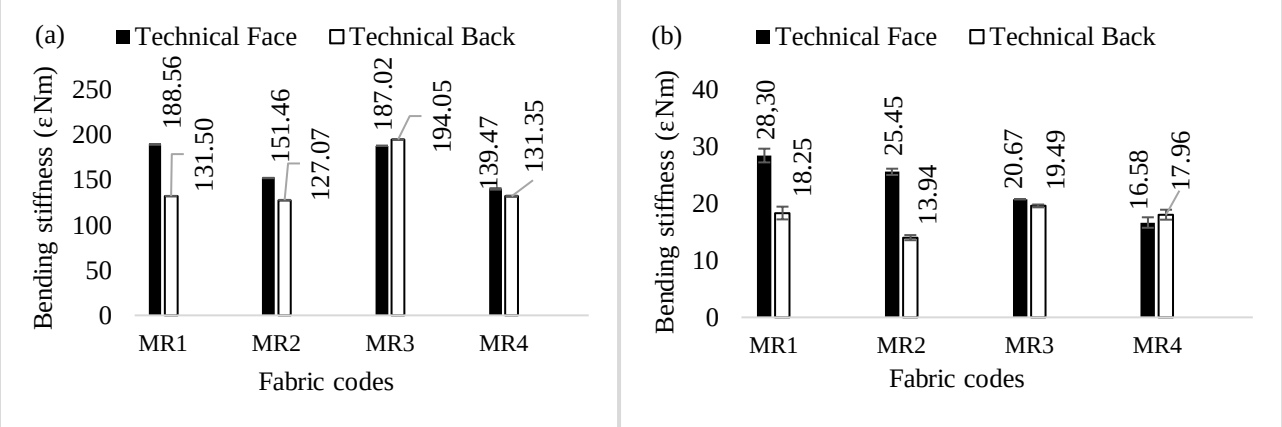

Fig. 1. Bending stiffness of 1Ǐ 1 rib knitted fabrics in wale direction (a) and course direction (b).

Bending stiffness of 1Ǐ 1 rib knitted fabrics was found significantly higher in fabric wale direction (Fig. 1, a) than in course direction (Fig. 1, b), supposedly, due to the higher fabric density in wale direction influencing its higher capability to withstand the stress. A decreasing tendency of the bending stiffness of the investigated 1Ǐ 1 rib knitted fabrics was related with the decrease in their area densities [3] as well as with the increase in the antistatic polyester percentage in fabric structure, especially for MR3 and MR4 knitted fabrics [4].

When summarizing up the research results, it can be seen that the bending stiffness of knitted fabric is highly dependent on the fabric direction. Area density of the investigated knitted fabrics makes significant influence as well. Higher percentage of the antistatic polyester fibers in fabric structure influences its lower stiffness.

[1] G. M. N. Islam, A. Ali, and S. Collie, Textile sensors for wearable applications: a comprehensive review, Cellulose **27**, 6103ï 6131 (2020).
[2] R. Hessami, A. A. Yazdi, and A. Mazidi, Investigation of tensile and flexural behavior of biaxial and rib 1Ǐ 1 weft-knitted composite using experimental tests and multi-scale finite element modeling, Journal of Composite Materials **53**, 3201ï 3215 (2019).
[3] G. S¿le, Investigation of bending and drape properties of woven fabrics and the effects of fabric constructional parameters and warp tension on these properties, Textile Research Journal **82**, 810ï 819 (2012).
[4] A. Telli and N. ¥ zdil, Effect of recycled PET fibers on the performance properties of knitted fabrics, Journal of Engineered Fibers and Fabrics **10**, 47ï 60 (2015).

P3-21

DID NOT PARTICIPATE

3D PRINTED HYDROXYAPATITE ï PROPERTIES AND APPLICATIONS AS SCAFFOLD MATERIAL FOR BONE REGENERATION

Skirmantas Norkus[1,3], Osvaldas Grubys[2,3], Simona Raugalaitã[2,3], Brigita Abakeviļienã[2], RamÎnas Valiokas[1]

[1] Center for Physical Sciences and Technology, Saulãtekio ave. 3, LT-10257, Vilnius, Lithuania
[2] Department of Physics, Kaunas University of Technology, StudentÔstr. 50, LT-51368, Kaunas, Lithuania
[3]Ortho Baltic, Taikos ave. 131A, LT-51124, Kaunas, Lithuania
skirmantas.norkus@ftmc.lt

Recently bone grafts have been increasingly used around the world. Bone grafting frequency is indeed the second most frequent tissue transplantation worldwide, coming right after blood transfusion [1]. Over two million surgical surgeries are performed per year to treat bone tissue defects [1-2]. Bone tissue defects larger than 4-6 cm are critical and should be treated with bone grafts [2]. Critical-sized defects can be congenital or formed due to trauma, tumours, infections, and diseases such as osteoporosis, necrosis, or bone atrophy [1]. Four main types of bone grafting are used to treat bone tissue defects: autologous, allogeneic, xenogeneic, alloplastic. Autologous bone is currently considered the ñgoldò standard for treating bone tissue defects [1,3]. However, more and more attention is paid to alloplastic bone graft materials, as the use of these bone grafts could simplify operations and avoid the most common complications [1,3]. The major advantages of alloplastic materials include their high abundance relative to natural materials, no risk of disease transmission and the very low antigenicity. They can be made available in both resorbable and non-resorbable forms, and can be customized with varying levels of porosity and pore sizes [4].

The main objective of this study was to print hydroxyapatite (HA) scaffolds of complex geometry that could potentially be used to fill bone defects. One of the world's latest 3D ceramic printing technologies LMC (*Lithography-based ceramic manufacture)* was used for printing hydroxyapatite scaffold. Using this technology, the production of printed hydroxyapatite scaffold essentially consists of two main parts: 3D printing and heat treatment. The geometry of the printed HA experimental specimens (see Fig. 1), scaffold porosity, scaffold pore size, and material density fluctuations were analysed using industrial computed tomography (ÕCT). In order to analyse the structural properties of HA samples, studies were performed using X-ray diffraction (XRD) analysis and Fourier transform infrared spectroscopy (FT-IR) analysis. The surface topography and roughness of HA samples were analysed using optical profilometry.

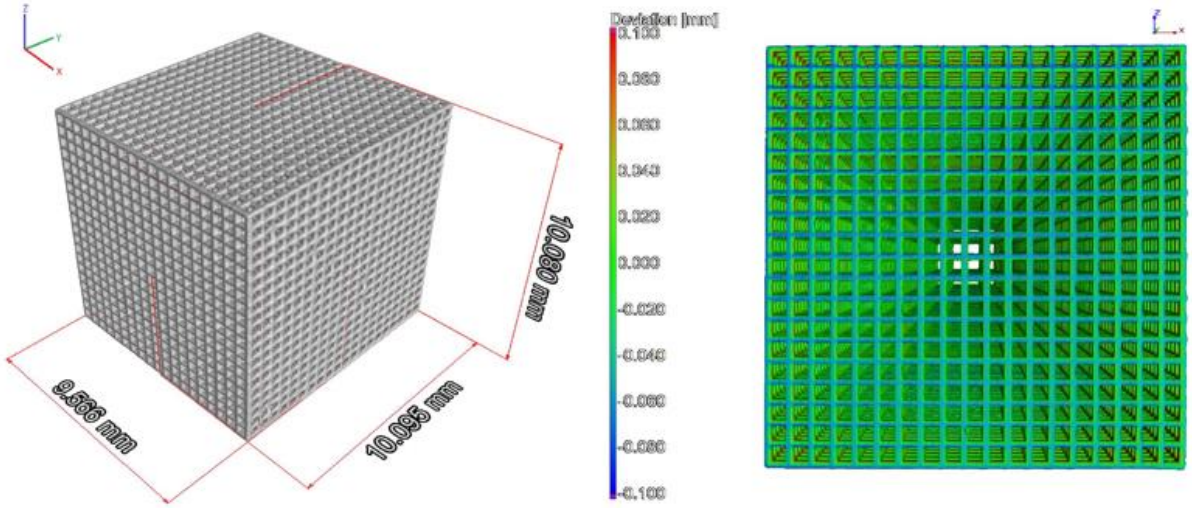

Fig. 1. Micro computed tomography (ÕCT) measurements. The colours map shows the deviation of the printed HA scaffold from the designed STL model.

Based on the analysis of the results and comparison of the obtained results with the values found in the scientific literature as well as the requirements for bone grafts in medicine, it can be stated that printed HA scaffolds have a great potential to be used as synthetic bone grafts in the near future.

[1] Campana, V., Milano, G., Pagano, E., Barba, M., Cicione, C., Salonna, G., é Logroscino, G. (2014). Bone substitutes in orthopaedic surgery: from basic science to clinical practice. Journal of Materials Science: Materials in Medicine, 25(10), 2445ï 2461. doi:10.1007/s10856-014-5240-2

[2] Hixon, K. R., Eberlin, C. T., Kadakia, P. U., McBride-Gagyi, S. H., Jain, E., & Sell, S. A. (2016). A comparison of cryogel scaffolds to identify an appropriate structure for promoting bone regeneration. Biomedical Physics & Engineering Express, 2(3), 035014. doi:10.1088/2057-1976/2/3/035014

[3] Henkel, J., Woodruff, M. A., Epari, D. R., Steck, R., Glatt, V., Dickinson, I. C., é Hutmacher, D. W. (2013). Bone Regeneration Based on Tissue Engineering Conceptions ð A 21st Century Perspective. Bone Research, 1(3), 216ï 248. doi:10.4248/br201303002

[4] Sheikh, Z., Sima, C., & Glogauer, M. (2015). Bone Replacement Materials and Techniques Used for Achieving Vertical Alveolar Bone Augmentation. Materials, 8(6), 2953ï 2993. doi:10.3390/ma8062953

RECOMBINATION OF CHARGE CARRIERS IN BULK HETEROJUNCTION SOLAR CELLS

Romualdas Jonas Ļepas[1], Lukas Kukulas[1], Gytis Juġka[1], Kristijonas Geneviļ ius[1]

[1] Institute of Chemical Physics, Vilnius University, Lithuania
romualdas.cepas@ff.vu.lt

Organic solar cells (OSCs) have attracted a wide spread attention in the past decades due to their unique advantages of light weight, flexibility and solution processability, which enables low cost and a potential for large area fabrication. A major and unsolved problem with organic bulk heterojunction (BHJ) devices remains the optimization of the network morphology. In general, increasing the structural order of the BHJ is desirable as it improves charge carrier mobility and extraction.

Low mobility organic materials exhibit Langevin type recombination, but in bulk-heterojunctions reduced Langevin recombination is observed [1], because of the nanomorphology of the interpenetrating network of donor and acceptor materials. Reduced recombination is strongly responsible high performance of solar cell and charge that can be extracted from the device (Fig.1(a)). Usage of proper processing solvents and additives, such as 1.8-diiodiooctane (DIO) is a known method to further enhance device efficiency [2]. Although, the most popular processing combination of chlorobenzene (CB) solvent and DIO is known to reduce overall number of ordered aggregates in the sample[3], but increasing thickness of bulk heterojunction can lead to the changes of the morphology. As such, these structures can have different morphologies, so different charge carrier mobilities and recombination rates.

One of the main methods used to determine the bimolecular recombination rate in such materials is time-of-flight (TOF)[1] technique, but it does not allow to determine how bimolecular recombination varies with carrier concentration. This drawback can be removed by using extraction of injected charge carriers by linearly increasing voltage technique (i-CELIV)[4,5], where the total recombination losses in the bulk can be determined. The goal of this work was to determine bimolecular recombination dependency on bulk heterojunction thickness with and without solvent additive DIO and to compare recombination data with that extracted from i-CELIV and establish dependency on carrier concentration.

Using i-CELIV we determined that samples processed with DIO show strong carrier recombination with increasing layer thickness, while omitting the additive seems to have no effect while varying the thickness of the sample, DIO in combination with CB causes morphological changes with increasing sample thickness. It was also determined that poly(3-hexylthiophen-2,5-diyl) (P3HT) : [6,6]-phenyl-C61-butyric acid methyl ester (PCBM) 1:1 ratio bulk heterojunction has a 2D Langevin recombination mechanism as bulk recombination rate follows $\upsilon \sim n^{\frac{3}{2}}$ (Fig.1(b)). Additional measurements done by time-of-flight (TOF) technique shows clear link between reduced Langevin recombination and υ recombination rate.

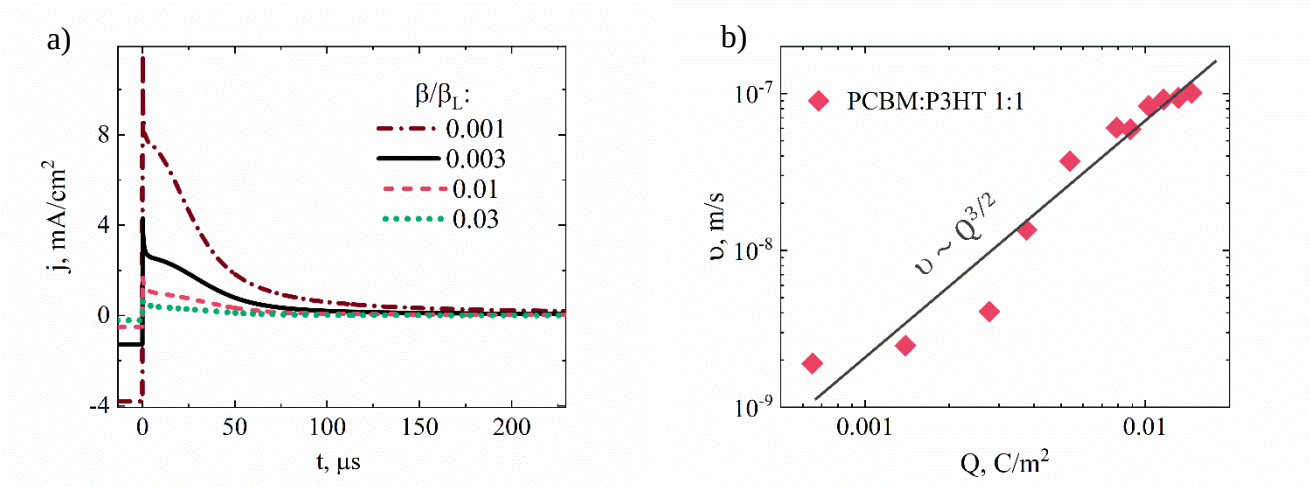

Fig. 1 (a) Simulated i-CELIV current transients in bulk-heterojunction (P3HT:PCBM 1:1) for different recombination rates and (b) bulk recombination rate dependency on extracted charge.

[1] Pivrikas, A. *et al.* Bimolecular recombination coefficient as a sensitive testing parameter for low-mobility solar-cell materials. *Phys. Rev. Lett.* **94**, (2005).
[2] Arca, F., Loch, M. & Lugli, P. Enhancing efficiency of organic bulkheterojunction solar cells by using 1,8-diiodooctane as processing additive. *IEEE J. Photovoltaics* **4**, 1560ï 1565 (2014).
[3] Guo, S. *et al.* Influence of solvent and solvent additive on the morphology of PTB7 films probed via X-ray scattering. *J. Phys. Chem. B* **118**, 344ï 350 (2014).
[4] J. Vaġgãla, K. Geneviļ ius, G. Juġka, i-CELIV technique for investigation of charge carriers transport properties, Chemical Physics **478**, 126-129 (2016).
[5] G. Juġka, K. Geneviļ ius, Investigation of recombination in organic heterostructures by i-CELIV, Applied Physics Letters **113**, 123301 (2018).

IMPROVING DISPLACEMENT ESTIMATION BY MEMS ACCELEROMETER USING DEEP Q-LEARNING ALGORITHM

Algirdas Petronis[1], Tomas Januģkeviļius[1], Kňstutis Dumbrava[1], Karolina Lapkauskaitā[1], Andrius Dzedzickis[1], Vytautas Buļinskas[1]

[1] Department of Mechatronics, Robotics and Digital Manufacturing, Vilnius Gediminas Technical University
algirdas.petronis@vilniustech.lt

Precise estimation of movement trajectories using cheap MEMS accelerometers could have a wide range of applications, such as simplified industrial robot control, drone navigation, etc. Cheap accelerometers, however, have significant errors in acceleration measurements. These compound to extremely large deviations when calculating displacements which result in estimated trajectories becoming completely different from the real ones. Traditional filtering techniques ranging from simple threshold filter to more complex Kalman filter can be used to improve the measurement accuracy with varying levels of success. For this application, however, these filters either make the whole system insensitive or require dedicated tuning of filter parameters for each trajectory measurement case.

Applying machine learning (ML) algorithms for improving both accuracy and consistency of trajectories estimated based on accelerometer data is a promising area of research. There already are studies confirming that both LSTM-based ML algorithm [1] and ML-Kalman filter combinations [2, 3] offer improved performance compared to traditional filtering methods. To supplement that research, this work explores the application of deep q-learning algorithm to improve displacement accuracy evaluation based on accelerometer data.

The method involves training the algorithm on ideal displacement data and the displacement datasets calculated from raw acceleration data. The algorithm outputs corrected displacement value for each datapoint. To smooth out the displacement curve, approximating filter is applied. One of preliminary results of this research is given in (Fig. 1), which shows displacement curves of moving a MPU6050 accelerometer in a straight line along one axis at constant velocity for 0.4 m. distance.

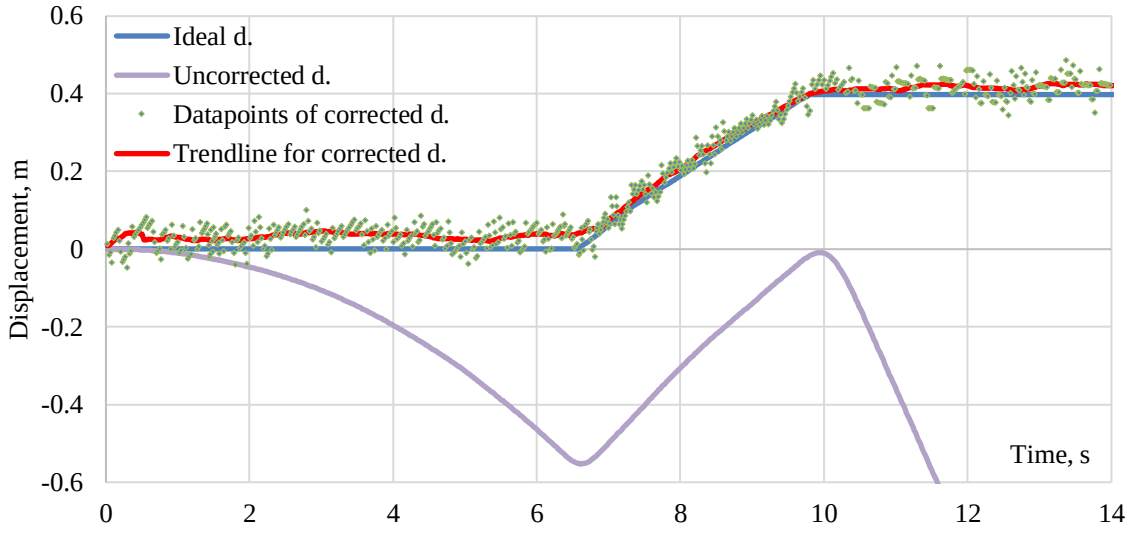

Fig. 1. Comparison of uncorrected and corrected displacements to the ideal displacement case.

There is a complete mismatch between the uncorrected displacement (calculated from raw acceleration data) and the one that was performed in reality (ideal case). Meanwhile, the displacement corrected by a deep q-learning algorithm and then passed through an averaging filter (shown as trendline in Fig. 1) matches the ideal case closely. The average deviation from the ideal case is around 5%, while maximum deviation is around 18%, which is a significant accuracy improvement for such type of accelerometer. However, while the results are promising, further research is required to make the technique applicable in practise: the algorithm needs to be made less reliant on ideal displacement data, while its performance for motion in complex trajectories needs to be investigated.

Acknowledgement

This project has received funding from the European Social Fund (project No 09.3.3.-LMT-K-712-22-0344) under a grant agreement with the Research Council of Lithuania (LMTLT).

[1] Lima, J., Uchiyama, H. and Taniguchi, R., 2019. End-to-End Learning Framework for IMU-Based 6-DOF Odometry. Sensors, 19(17), p.3777.
[2] Silva do Monte Lima, J., Uchiyama, H. and Taniguchi, R., 2019. End-to-End Learning Framework for IMU-Based 6-DOF Odometry. Sensors, 19(17), p.3777.
[3] Ullah, I., Fayaz, M. and Kim, D., 2019. Improving Accuracy of the Kalman Filter Algorithm in Dynamic Conditions Using ANN-Based Learning Module. Symmetry, 11(1), p.94.

CELIV TECHNIQUE FOR INVESTIGATION OF PHOTO-GENERATED CHARGE CARRIERS MOBILITY IN THIN FILMS

Egidijus Kamarauskas[1], Romualdas Jonas Ļepas[1], Kristijonas Geneviļius[1]

[1] Institute of Chemical Physics, Faculty of Physics, Vilnius University
egidijus.kamarauskas@ff.vu.lt

In nowadays, due to cheap synthesis and simple deposition techniques organic materials are promising low cost alternatives for classical inorganic materials. In addition, organic materials can be used in the production of flexible devices. Most promising areas of application are light emitting diodes, field effect transistors, detectors and solar cells. The efficiency or (and) speed of operation of transistors, light emitting diodes, solar cells or other electronic devices is determined by the charge carriers mobility ε.

Usually the charge carrier mobility ε in organic materials is measured by time-of-flight (TOF) technique, application of which in thin layers could be challenging. The time constant *RC* of the system with thin layer is usually higher than transit time of the carriers, what complicates the analysis of the current transient in the case of dispersive transport. Another problem, of application of TOF in thin films, is volume photo-generation of charge carriers, this makes hard to distinguish the sign of charge carriers.

In this work we propose a modified photo-CELIV [1] (extraction of the photo-generated charge carriers by linearly increasing voltage) method for investigation of the charge carrier transport in thin organic films on dielectric layer. In order to distinguish sign of the charge carriers we apply offset voltage before photo excitation ï one type of carriers are pushed towards the insulator, another type is extracted from the sample (Fig. 1a). After some delay time we apply triangle voltage pulse and extract the charge carriers located near insulator interface (Fig. 1b). For the analysis of extraction currents and estimation of mobility we use same approach as in the case of injection CELIV (i-CELIV)[2].

This method allows to obtain more accurate mobility values in very thin organic layers, as well as to study a dependency of mobility on time, in the case of dispersive transport. Demonstration of the modified CELIV technique was done with the layers of PTAA polymer on the top of PVA insulator. Obtained results were compared with TOF results in thick layer of PTAA.

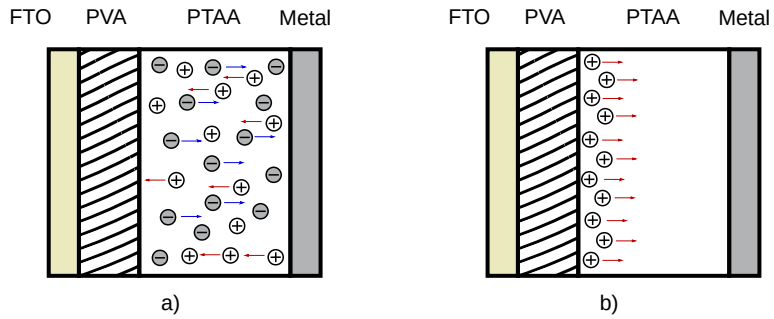

Fig. 1. a) - Charge carrier separation under applied voltage offset, b) - extraction of the charge carriers from insulator-semiconductor interface by triangle voltage pulse.

[1] Juģka, G. ; Nekraģas, N. ; Geneviļius, K. ; Stuchlik, J. ; Koļka, J. Relaxation of photoexited charge carrier concentration and mobility in εc-Si:H., Thin Solid Films, **451ï 452**, 290ï 293 (2004)

[2] Vaģgāla, Julius ; Genevicius, Kristijonas ; Juģka, Gytis. I-CELIV technique for investigation of charge carriers transport properties, Chemical Physics, **478**, 126-129 (2016)

THE INFLUENCE OF GRAPHENE SURFACE TREATMENT ON REMOTE EPITAXY OF GALLIUM NITRIDE

Dominykas Augulis[1], Kazimieras Badokas[1], Arūnas Kadys[1], Simonas Strumskis[1], Ilja Ignatjev[1,2], Giedrius Juška[1], Jūras Mickevičius[1] and Tadas Malinauskas[1]

[1]Institute of Photonics and Nanotechnology, Vilnius University, Vilnius LT-10257, Lithuania
[2]Center for Physical Sciences and Technology, Vilnius LT-10257, Lithuania
dominykas.augulis@ff.stud.vu.lt

Gallium nitride (GaN) is a widely used material in many optoelectronic applications due to its direct band gap, high breakdown voltage and high electron mobility. However, GaN growth on foreign substrates deteriorates its crystalline quality due to the lattice constant and thermal expansion differences. The solution to this problem would be the use of native substrates. Yet, bulk GaN substrates are relatively pricy and come in limited size. To tackle these problems, graphene interlayers could be used [1]. In the process called remote epitaxy, GaN formation is governed by its interaction with the GaN substrate through monolayer graphene. The seeding effect of the substrate enables high quality GaN growth, while weak van der Waals interaction facilitates subsequent layer release and the reuse of an expensive substrate. In addition, this growth method enables production of flexible GaN films, which can be used for novel applications. It is essential to examine interlayers quality and thickness. It was shown that graphene surface treatment has an impact on subsequent GaN formation [2].

In this work, metalorganic chemical vapour deposition (MOCVD) was used to grow GaN epilayers on the single-layer graphene covered GaN/sapphire templates (see schematics in Figure 1). Commercially available, transfer-ready monolayer graphene with PMMA support was wet-transferred to partially cover the templates prior to the MOCVD growth. The quality of graphene was evaluated by Raman shift. Particular attention to the graphene treatment temperature prior GaN deposition was given. GaN layers of different thickness were grown and investigated using XRD, AFM and PL techniques.

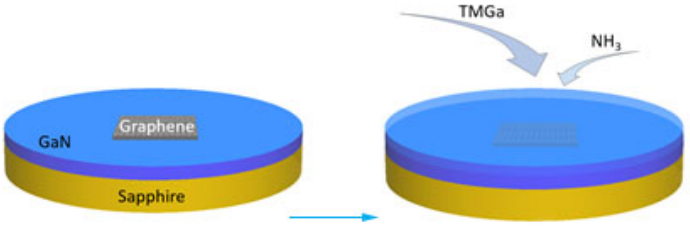

Fig. 1. Schematic representation of GaN epilayers growth process on the single-layer graphene covered GaN/sapphire template.

X-ray diffraction scan of (1 0 $\bar{1}$ 0) plane GaN revealed crystalline quality improvement over the GaN template. The crystalline quality improvement is presented in the Figure 2.

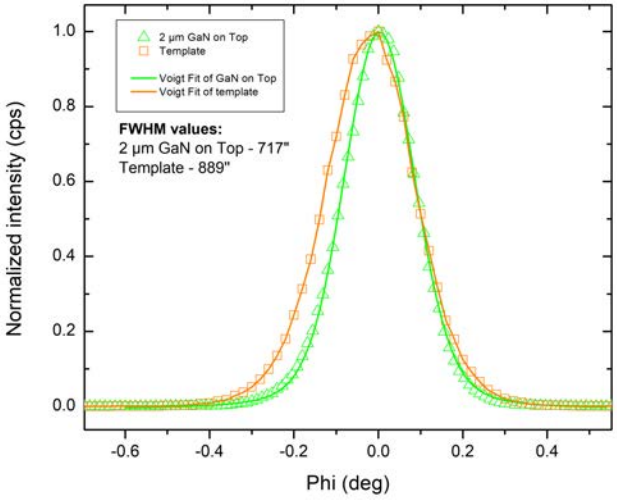

Fig. 2. XRD in-plane ϕ scans of GaN template and grown GaN. FWHM of both measurements are calculated in order to evaluate crystaline quality improvement.

[1] Kim, J., Bayram, C., Park, H., Cheng, C. W., Dimitrakopoulos, C., Ott, J. A., … Sadana, D. K. (2014). Principle of direct van der Waals epitaxy of single-crystalline films on epitaxial graphene. Nature Communications, 5, 1–7. https://doi.org/10.1038/ncomms5836

[2] Journot, T., Okuno, H., Mollard, N., Michon, A., Dagher, R., Gergaud, P., … Hyot, B. (2019). Remote epitaxy using graphene enables growth of stress-free GaN. Nanotechnology, 30(50), 505603. https://doi.org/10.1088/1361-6528/ab4501

INVESTIGATION OF THE STRUCTURE AND OPTICAL PROPERTIES OF DIAMOND LIKE CARBON THIN FILMS

Julija Jokšaitė[1], Andrius Vasiliauskas[2], Aušrinė Jurkevičiūtė[2], Asta Tamulevičienė[1,2]

[1] Department of Physics, Kaunas University of Technology, Lithuania
[2] Institute of Materials Science, Kaunas University of Technology, Lithuania
julija.joksaite@ktu.edu

Diamond like carbon (DLC) films can have different properties depending on their atomic structure. The ratio between sp^2 and sp^3 bond hybridizations determines what kind of properties prevail in the film. High content of sp^3 hybridization leads to properties similar to diamond, while greater amount of sp^2 hybridized bonds leads to more graphitic material [1]. Atomic structure is influenced by the deposition conditions, therefore allowing to control properties of the films. This makes DLC thin films to possess great potential for applications in a variety of technological fields including wear resistance [2], medicine, optics [3] and particle accelerators [4]. An important application of DLC films in particle accelerators is related to the ability to reduce secondary electron yield. It was already shown in [4] that DLC films deposited with PECVD are characterized by secondary electron yield (SEY) coefficient of 1.5.

The objective of this research was to investigate optical properties and structure of an amorphous hydrogen-free carbon (a-C) films synthesized using different deposition methods (unbalanced magnetron sputtering (MS), high power impulse magnetron sputtering (HiPIMS) and conditions (bias voltage, deposition temperature, impulse power). Our previous research has shown that DLC films created by MS from graphite target had lower SEY coefficient in ca range of ~1-1.33 and we found direct correlation between SEY and Tauc gap and B parameter. Tauc optical band gap and B parameter of the films was determined from optical measurements (transmittance and reflectance) employing UV-VIS spectroscopy (Avantes system, 192-1100 nm, resolution – 1.4 nm). The absorption coefficient was calculated considering the thickness of the films determined with spectroscopic ellipsometer (GES5-E (Semilab)). Structure of the films was analysed with Raman scattering spectrometer inVia (Renishaw). The excitation beam from a diode laser of 532 nm wavelength was focused on the sample using a 50× objective (NA=0.75). Laser power at the sample surface was 3.5 mW.

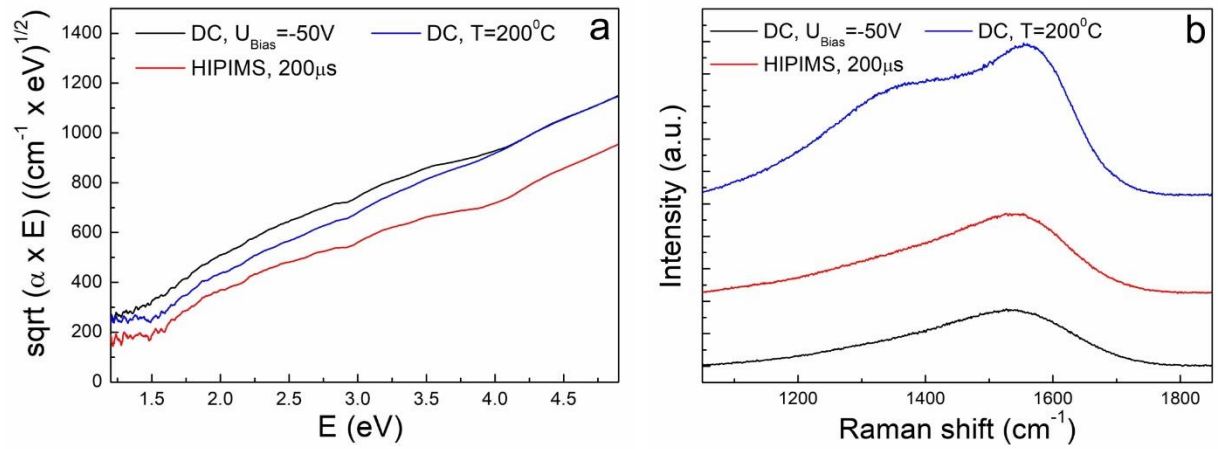

Fig. 1. (a) Tauc plots and (b) Raman scattering spectra of the films deposited employing different deposition conditions

The analysis of optical properties revealed that the optical band gap (Tauc gap determined from the graphs in Fig.1, a) varied in a range from 0.23 eV till 1,08 eV depending on the deposition conditions. We should emphasize that the widest bandgap was determined for the films deposited using HiPIMS and its value strongly depend on the pulse duration (band gap decreases with increase of pulse duration). Analysis of Raman spectra (Fig. 1, b) revealed similar tendency for HiPIMS deposited films, where the FWHM of G peak increased indicating higher sp^3 content in the film.

[1] J. Robertson, "Diamond-like amorphous carbon," Mater. Sci. Eng. R Reports, vol. 37, no. 4–6, pp. 129–281, 2002
[2] A. Tyagi, R. S. Walia, Q. Murtaza, S. M. Pandey, P. K. Tyagi, and B. Bajaj, "A critical review of diamond like carbon coating for wear resistance applications," International Journal of Refractory Metals and Hard Materials, vol. 78. 2019,
[3] R. Hauert, K. Thorwarth, and G. Thorwarth, "An overview on diamond-like carbon coatings in medical applications," Surf. Coatings Technol., vol. 233, 2013
[4] Zhang, Yuxin & Wang, Yong & Ge, X & Bo, Zhang & Wei, W & Wang, S & Zhu, B & Shao, J & Li, W. (2019). Research On Secondary Electron Emission Characteristics of Diamond-Like Carbon Thin Films. Journal of Physics: Conference Series. 1350. 012177. 10.1088/1742-6596/1350/1/012177.

ARSENIC DETECTION BY COBALT GOLD ELECTRODES IN AQUEOUS MEDIA

Kristina RadinoviĹ [1], Jadranka MilikiĹ [1*], Aldona BalĻiĮ naitã[2], Zita Sukackienã[2], Loreta TamaġauskaitÃ-TamaġiĮ naitã[2] and Biljana ĠljukiĹ [1]

[1] Faculty of Physical Chemistry, University of Belgrade, Studentski trg 12-16, 11158 Belgrade, Serbia
[2] Department of Catalysis, Center for Physical Sciences and Technology, SaulÃtekio Ave. 3, LT-10257, Vilnius, Lithuania
*jadranka@ffh.bg.ac.rs

Drinking arsenic-polluted water causes serious health problems including irregular heartbeat, atherosclerosis and skin cancer [1]. Arsenic in natural waters usually exists in arsenite (As(III)) and arsenate (As(V)) as inorganic forms. It can also exist as organic dimethylarsinic and monomethylarsonic acids. Still, arsenite is more toxic than arsenate, the same as inorganic arsenic being more toxic than the organic arsenic forms [2]. Arsenic presence in aqueous media can be detected by several analytical methods such as atomic absorptions spectroscopy, inductively coupled plasma ï atomic emission spectrometry, inductively coupled plasma ï mass spectrometry, etc. [3]. These analysis are typically long and require expensive equipment; thus, electrochemical methods could be a good replacement as cheap, fast and easy methods for arsenic detection.

Herein, three different cobalt gold (CoAu) electrodes were prepared by electroless deposition of Co on Cu surface, followed by Au nanoparticles deposition on the prepared surfaces by galvanic displacement using three different deposition times (30, 60 and 300 s). Au loading was determined by energy-dispersive X-ray spectroscopy analysis and it was found to be 5.8, 7.1 and 15.3 Õg cmï 2 for CoAu(30s), CoAu(60s) and CoAu(300s), respectively.

Next, these electrodes were tested in 1 mM $NaAsO_2$ in $NaHCO_3$ + Na_2CO_3 buffer by anodic stripping voltammetry (ASV). Arsenic determination by ASV method proceeds in two steps where As(III) is reduced to As(0) as the adsorbed form on the electrode surface and then oxidized to As(III) form that diffuses into the solution, scheme 1.

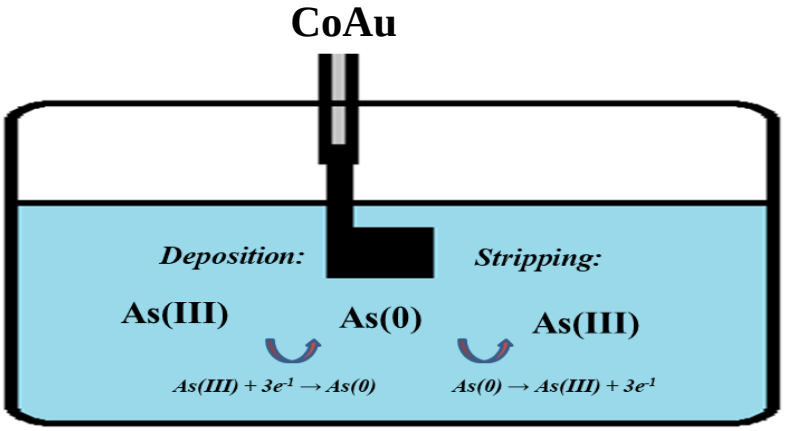

Scheme 1. Schematic representation of arsenic ions sensing at CoAu electrodes by anodic stripping voltammetry.

Cyclic voltammogram (CV) of CoAu(30s) electrode revealed its activity for detection of As(III) in aqueous media. Namely, CoAu gave a well-defined peak corresposning to As electrooxidation. The peak current density amounted to1.73 mA cm^{-2} at -0.4 V, compared to only 0.15 mA cm^{-2} at the same potential in the absence of As ions in the solution. The influence of experimental conditions on arsenic detection was tested by recording CVs at different deposition potential (E_d) and different deposition time (t_d) and subsequently these parameters optimised.

Arsenic determination was also tested in a real water sample that was diluted with $NaHCO_3$ + Na_2CO_3 buffer (sample: buffer 75:25 vol.% ratio). CoAu(30s) electrode shows a well-defined arsenic oxidation peak in the real sample.

Within this work, CoAu(30s) electrode, prepared bysimple and fast method and containing only 5.8 Õg cmï 2 of Au showed good activity for arsenic detection in aqueous media, in buffer as well as in a real sample. Thus, this electrode could be a potentially good sensor for arsenic detection in aqueous media.

Acknowledgements: This research was financially supported by the Ministry of Education, Science and Technological Development of the Republic of Serbia (Contract number: 451-03-68/2020-14/200146).

[1] Y.G. Zhu, P.N. Williams, A.A. Meharg, Exposure to inorganic arsenic from rice: A global health issue?, Environmental Pollution **154,** 169ï 171 (2008).
[2] A. Giacomino, O. Abollino, M. Lazzara, M. Malandrino, E. Mentasti, Determination of As(III) by anodic stripping voltammetry using a lateral gold electrode: Experimental conditions, electron transfer and monitoring of electrode surface, Talanta **83**, 1428ï 1435 (2011).
[3] M. Yang, Z. Guo, L.N. Li, et al. Electrochemical determination of arsenic(III) with ultra-high anti-interference performance using Au-Cu bimetallic nanoparticles, Sensors and Actuators, B: Chemical. **231**, 70ï 78 (2016).

LASER ADDITIVE MANUFACTURING OF CRYSTALLINE 3D NANOSTRUCTURES

Greta Merkininkaitė[1,2], Edvinas Aleksandravičius[3], Mangirdas Malinauskas[3], Darius Gailevičius[2,3], Simas Šakirzanovas[1,4]

[1]Faculty of Chemistry and Geosciences, Vilnius University, Naugarduko str. 24, Vilnius LT-03225, Lithuania
[2]Femtika, Saulėtekio Ave. 15, Vilnius LT-10224, Lithuania
[3]Laser Research Center, Physics Faculty, Vilnius University, Saulėtekio Ave. 10, Vilnius LT-10223, Lithuania
[4]Department of Chemical Engineering and Technology, Center for Physics Sciences and Technology, Saulėtekio Ave. 3, Vilnius LT-10257, Lithuania
greta.merkininkaite@chgf.vu.lt

Ceramics play an important role in today's science and industry as it can withstand immense thermal, mechanical, chemical and other hazards. While 3D ceramic structures can be made in multitude of ways, optical 3D printing with subsequent heat treatment was proven to be one of the best methods combining simplicity of photolithography with freedom to choose any required 3D architecture.

In this work we disclose an advanced method for transforming silicon and zirconium metalorganic 3D nano-structures, prepared via sol-gel and laser multi-photon lithography, into a pure inorganic material. Such approach brings breakthrough for extremely small feature size (spatial resolution up to 60 nm) inorganic 3D structures [1]. In order to characterize the printed and heat treated 3D nano/micro structures the single-crystal diffraction technique was used. The phase purity of obtained structures are tunable, ranging from amorphous glass to ordered polycrystalline phases.

With a variable synthesis procedure of the initial resist and a post-heat treatment a range of inorganic phases for the 3D structures were achieved: amorphous glass, cristobalite, t-ZrO_2, m-ZrO_2, $ZrSiO_4$ (Fig. 1).

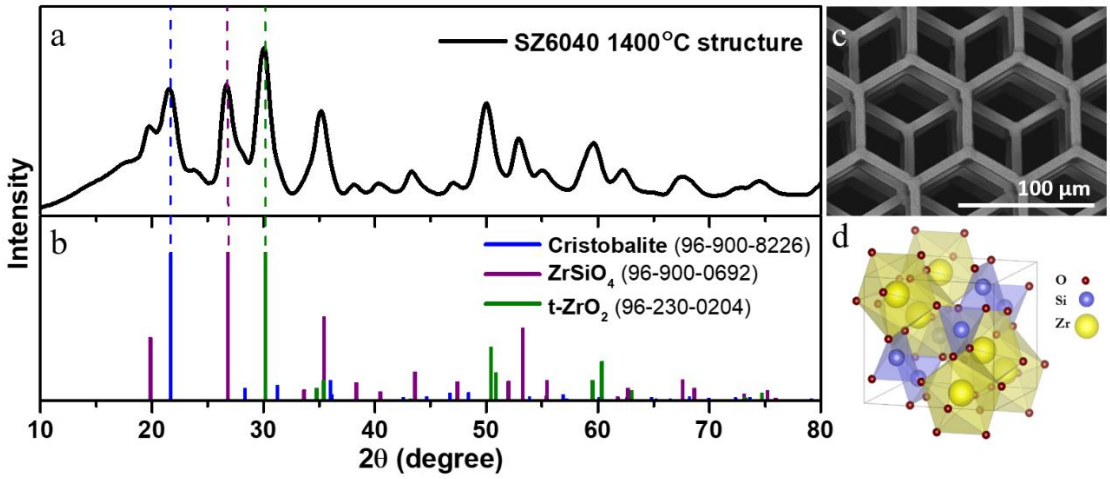

Fig. 1. (a) X-ray diffraction (XRD) analysis of the SZ6040 material heat-treated at 1400 ÁC for one hour in air at an ambient pressure; (b) reference patterns; (c) SEM image of SZ6040 material heat-treated at 1400 ÁC for one hour in air at an ambient pressure; (d) lattice structure of the $ZrSiO_4$.

Overall, results show multi-photon lithography and thermal post-processing as a powerful tandem for creating ultra-resilient multifunctional 3D micro-/nano-scale ceramic crystalline structures.

[1] Merkininkaite, G.; Aleksandravicius, E.; Malinauskas, M.; Gailevicius, D.; Sakirzanovas, S. Laser Additive Manufacturing of Si/ZrO2 Tunable Crystalline Phase 3D Nanostructures. Preprints 2020, 2020120707 (doi: 10.20944/preprints202012.0707.v1).

OPTIMIZATION OF ANODE PREPARATION PROCESS FOR AQUEOUS NA-ION BATTERIES

Nadeġda Traġkina[1], Jurgis Pilipaviļius[1], Milda Petruleviļienã[1], Jurga Juodkazytã[1], Linas Vilļiauskas[1]

[1] Center for Physical Sciences and Technology (FTMC), Saulãtekio al. 3, LT-10257 Vilnius, Lithuania
nadezda.traskina@ftmc.lt

In recent years, environmental concerns have shifted the scientific attention towards the development of novel renewable and clean energy storage devices. The most investigated and developed technology, lithium ion batteries (LIBs), despite their high energy and power densities, suffer from lithiumôs high cost and lack of environmental benignity. [1] Consequently, sodium ion batteries, especially their aqueous variations, have emerged as an appealing alternative to LIBs owing to sodiumôs high abundance in nature and elimination of highly toxic and flammable organic electrolytes. [2] Aqueous sodium ion batteries with good capacity and cycle life characteristics are a combination of precisely selected electrode composition and morphology, electrolyte chemistry and comprehensive cell design. Electrode morphology can be tailored by varying the shape and size of both active material (AM) and conductive additive (CA) particles, the binding polymer properties as well as the ratio of abovementioned materials. Simultaneously, electrode morphology depends on the preparation process, which conventionally includes mixing AM, CA, polymer and solvent, casting of as-prepared slurries onto the current collectors and subsequent drying. [3] Despite being generally overlooked, a suitable mixing sequence and active material dispersion homogeneity play a crucial role in the preparation and properties of high-performance electrodes. [4]

The aim of this work is to investigate the dependency of electrode morphology on mixing conditions and establish a reliable slurry preparation procedure for the future studies. The electrodes were prepared by varying the duration of mixing, bead size used in ball mill during the dry pre-mixing of AM with CA and the mixing of final slurry. The morphology of prepared electrodes was characterized by Scanning Electron Microscopy (SEM). The electrochemical properties of $NaTi_2(PO_4)_3$ based prepared electrodes were investigated by charge/discharge galvanostatic cycling in three-electrode bottom mount flat sample beaker cells. The results (Fig. 1) imply that introducing a dry pre-mixing stage is highly beneficial for both electrode homogeneity, tap density and electrochemical properties.

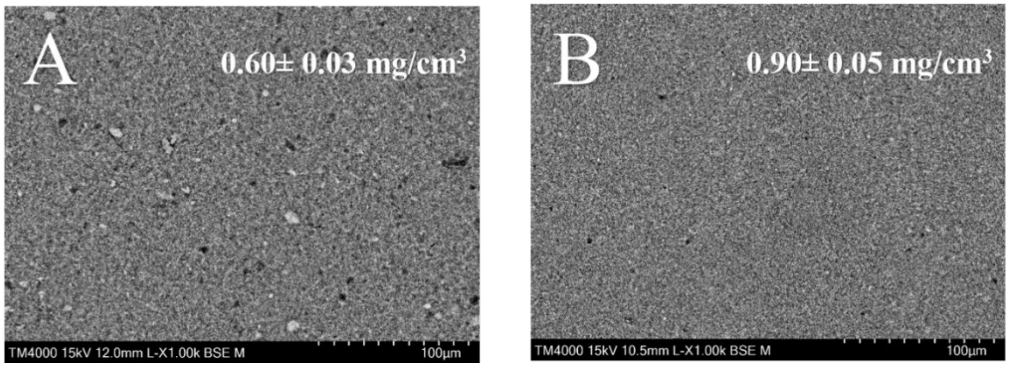

Fig. 1. SEM image of A) $NaTi_2(PO_4)_3$ based electrode prepared by single-step mixing; B) $NaTi_2(PO_4)_3$ based electrode prepared by introducing dry AM + CA pre-mixing.

Acknowledgements:
This project has received funding from the European Regional Development Fund (Project No. 01.2.2-LMT-K-718-02-0005) under grant agreement with the Research Council of Lithuania (LMTLT).

[1] Wu, M., et al., NASICON-Structured NaTi2(PO4)3 for Sustainable Energy Storage. Nano-Micro Letters **11**, 44 (2019).
[2] Bin, D., et al., Progress in Aqueous Rechargeable Sodium-Ion Batteries. Advanced Energy Materials, **8,** 1703008 (2018).
[3] Kraytsberg, A. and Y. Ein-Eli, Conveying Advanced Li-ion Battery Materials into Practice The Impact of Electrode Slurry Preparation Skills. Advanced Energy Materials, **6**, 1600655 (2016).
[4] Liu, Z., V. Battaglia, and P.P. Mukherjee, Mesoscale elucidation of the influence of mixing sequence in electrode processing. Langmuir, **30**, 15102-13 (2014).

SELECTIVE LASER ï MATERIAL POWDER MELTING

Karolis Stravinskas, Genrik Mordas, Alireza Shahidi, Romuald Petkeviļ

Department of Laser Technologies, Center for Physical Sciences and Technology, Lithuania
karolis.stravinskas@ftmc.lt

Selective laser melting (SLM) technology is an additive manufacturing technique, which allows producing metal parts with low consumption of the metal material. The SLM manufactured parts have good mechanical properties and can be applied in many different fields such as mechanical engineering, automotive, aerospace, etc. The main properties of a part manufactured by SLM technology depend on the attributes of a single track and single layer characteristics. In SLM processes, powder is usually fed by layers into a platform, where a focused laser beam heats a spot on the substrate to form a melt pool, spot solidifies quickly after the laser beam moves away.

In this study selective laser melting technology will be applied with different powder materials and gasses. A layer of material powder is deposited on a square-shaped steel substrate. Laser beam is attached to a CNC machine where it can move by different coordinates. It is possible to set different laser scanning speed values. Laser beam attacks the substrate in a gas pumped chamber and melts a track. After the track is melted the results are evaluated by using SEM and optical microscopy.

The study results consist of a thorough analysis of the single laser melted powder material parameters such as laser power, scanning speed, thickness of a layer, working conditions (temperature of the base, used gases).

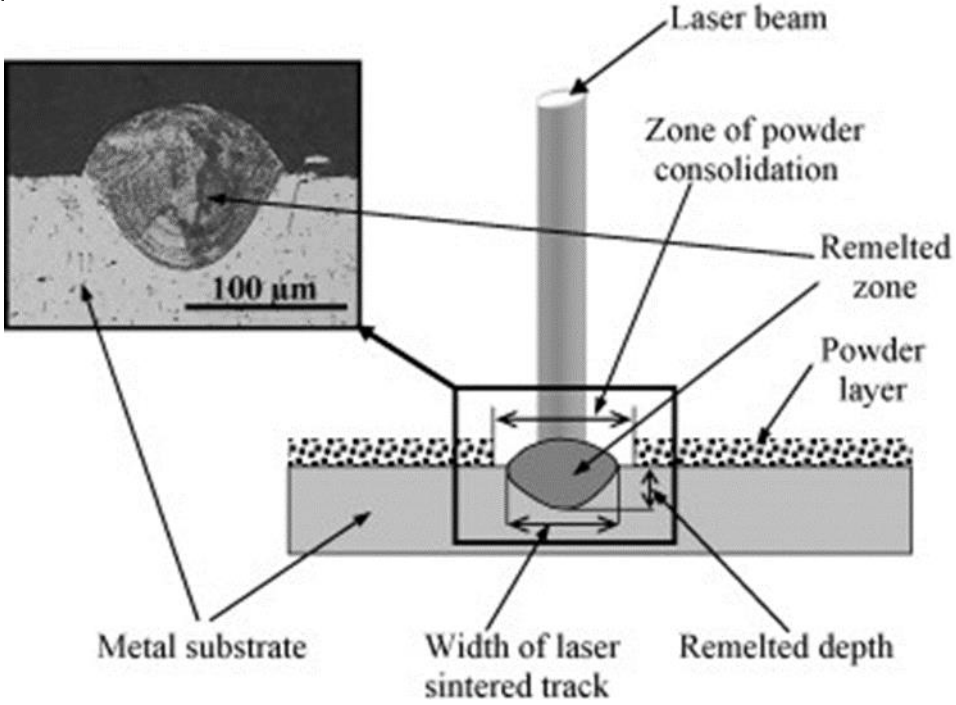

Fig. 1. Selective laser melting single track [1].

[1] I. Yadroitsev, I. Smurovet., Selective laser melting technology: from the single laser melted track stability to 3D parts of complex shape, Physics Procedia 5 (2010) 551ï 560.

XPS STUDIES OF VANADIUM-DOPED LITHIUM-MANGANESE-BORATE GLASSES AND NANOCOMPOSITES

Agata Jarocka[1], Przemysław P. Michalski[1], Jacek Ryl[2], Tomasz K. Pietrzak[1], Marek Wasiucionek[1]

[1]Faculty of Physics, Warsaw University of Technology, Koszykowa 75, 00-662 Warsaw, Poland
[2]Faculty of Chemistry, Gdańsk University of Technology, Narutowicza 11/12, 80-233 Gdańsk, Poland
agata.jarocka.dokt@pw.edu.pl

Growing demand on good quality storage systems is an extremely important global concern, e.g., for renewable energy sources ï solar or wind power ï when need for electricity is not that high and excess energy has to be stored. Hence comes the need for constant development of new solutions. Furthermore, similar but smaller systems are also a crucial part of every electric car. All of this has irrefutable influence on ecology and pollution reduction.

Nowadays, rapid technology development in the field of portable devices needs adjusting those devicesôbatteries in a way that their efficiency will improve. There is growing need for smaller, lighter and more efficient cell phones or personal computers and therefore also for batteries exhibiting improved properties. One of the factors that has significant influence on cellsô parameters is the electrical conductivity of their cathode material. Therefore, scientists conduct researches on materials that potentially can be used as cathodes and search for ways to improve their conductivities.

An interesting method to improve this property is thermal nanocrystallisation of glasses developed in Solid State Ionic Division, Faculty of Physics, Warsaw University of Technology. Lithium manganese borate has found high interest in nowadays research on cathode materials for Li-ion batteries mostly due to its high theoretical gravimetric capacity of 222 mAh/g [1], which is even greater than for the widely studied phosphates. However, our research on this compound showed that final electrical conductivity after nanocrystallisation was still not sufficient enough. Basing on the studies [2] on vanadium-doped $LiFePO_4$ compound and on conclusion that even small amount of vanadium can significantly improve electrical and electrochemical properties of material, we attempted to dope aforementioned $LiMnBO_3$ with vanadium.

Glassy $LiMn_{0.925}V_{0.05}BO_3$ was successfully synthesized with use of melt-quenching process. Then, the samples were nanocrystallised in different temperatures and characterized [3]. In this work, mainly XPS (X-ray photoelectron spectroscopy) studies (Fig. 1) will be presented in order to demonstrate changes in Mn^{2+}/Mn^{3+} ions relative ratio before and after nanocrystallisation.

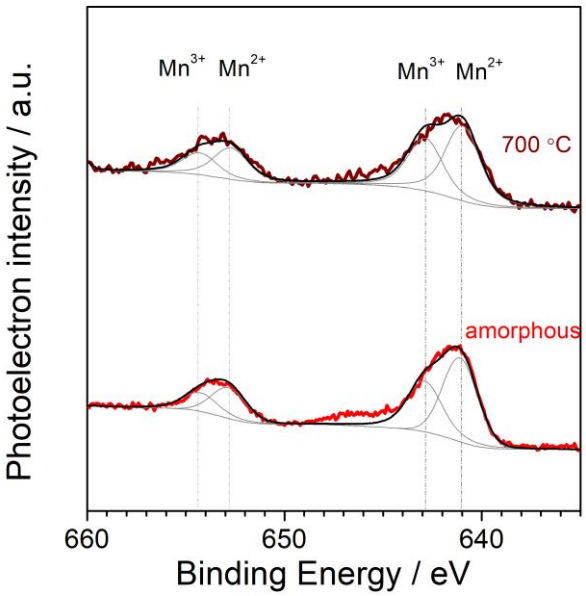

Fig. 1. High-resolution XPS spectra glassy sample and the sample crystallised at 700 ÁC. Fitted profiles ascribed to presence of Mn^{2+} and Mn^{3+} ions are shown as grey lines above the background.

[1] V. Legagneur, Y. An, A. Mosbah, R. Portal, A. Le Gal La Salle, A. Verbaere, D. Guyomard, Y. Piffard. Solid State Ionics 139 (2001) 37ï46.
[2] F. Omenya, N.A. Chernova, S. Upreti, P.Y. Zavalij, K.-W. Nam, X.-Q. Yang, M.S. Whittingham, Chemistry of Materials 23 (2011) 4733-4740.
[3] A. Jarocka, P.P. Michalski, J. Ryl, M. Wasiucionek, J. E. Garbarczyk, T.K. Pietrzak, Ionics (2019). https://doi.org/10.1007/s11581-019-03229-5

CHARACTERIZATION OF TENSILE PROPERTIES OF KNITTED UNI-DIRECTIONAL THERMOPLASTIC PREPREG COMPOSITES

Sikander Abbas Basra[1*], Zeeshan Azam[1], Norina Asfand[2]

[1]National Textile University, Department of Knitting, Pakistan
[2]Kaunas University of Technology, Department of Production Engineering, Lithuania
Email: Basra.ntu@gmail.com

Composites materials and products have got much importance from the last few decades due to their lightweight, high strength, and high modulus [1]. In this study, we investigated the mechanical properties of knitted unidirectional thermoplastic composite prepregs. Knitted prepregs were fabricated by using thermoplastic yarns (high-density polyethylene and polypropylene) and high-performance yarns (Kevlar, Basalt, and Carbon) in a double jersey inlay structure. This was a new approach to combine the reinforcing fiber with resin forming thermoplastic fiber during the knitting operation. The structures were stacked further in three stacking sequences at different angles (0/0/0/0, 0/90/0/90, 0/90/90/0), and hot compression was used to convert them into composite prepregs by melting the thermoplastic yarns. Specimen code (Inlay Yarn, Main Yarn, Plies Direction) are given as KH1(Kevlar, HDPE, 0/0/0/0), KH2 (Kevlar, HDPE, 0/90/0/90), KH3 (Kevlar, HDPE, 0/90/90/0), KP1 (Kevlar, PP, 0/0/0/0), KP2 (Kevlar, PP, 0/90/0/90), KP3 (Kevlar, PP, 0/90/90/0), BH1 (Basalt, HDPE, 0/0/0/0), BH2 (Basalt, HDPE, 0/90/0/90), BH3 (Basalt, HDPE, 0/90/90/0), BP1 (Basalt, PP, 0/0/0/0), BP2 (Basalt, PP, 0/90/0/90), BP3 (Basalt, PP, 0/90/90/0), CH1 (Carbon, HDPE, 0/0/0/0), CH2 (Carbon, HDPE, 0/90/0/90), CH3 (Carbon, HDPE, 0/90/90/0), CP1 (Carbon, PP, 0/0/0/0), CP2 (Carbon, PP, 0/90/0/90), and CP3, (Carbon, PP, 0/90/90/0).

The tensile strength and modulus were investigated according to the standard test method of ASTMD3039. Results in Fig. 1 showed that high modulus was observed in all materials when plies were stacked in the same direction i.e. 1st direction of stacking and specimen were tested in a parallel direction to yarns. As previously reported that strength of knitted thermoplastic composites is influenced mainly by orientation and as well as breakages of reinforcing components [2]. But least modulus was observed in the same specimen when tested in cross direction as there was no breakage of reinforcement yarns [3]. Because in cross direction there was the strength of only thermoplastic material i.e. resin. But materials strength was in parallel direction and as all yarns were in that direction. From the second and third direction of stacking more strength was observed in all materials in the second direction i.e. [0/90/0/90] but the difference is not much significant. As the uniform transfer of load to resin in alternative plies second stacking sequence had higher strength than the third stacking sequence. In the third stacking sequence group of two plies are stacked which causes to concentrate force [4].

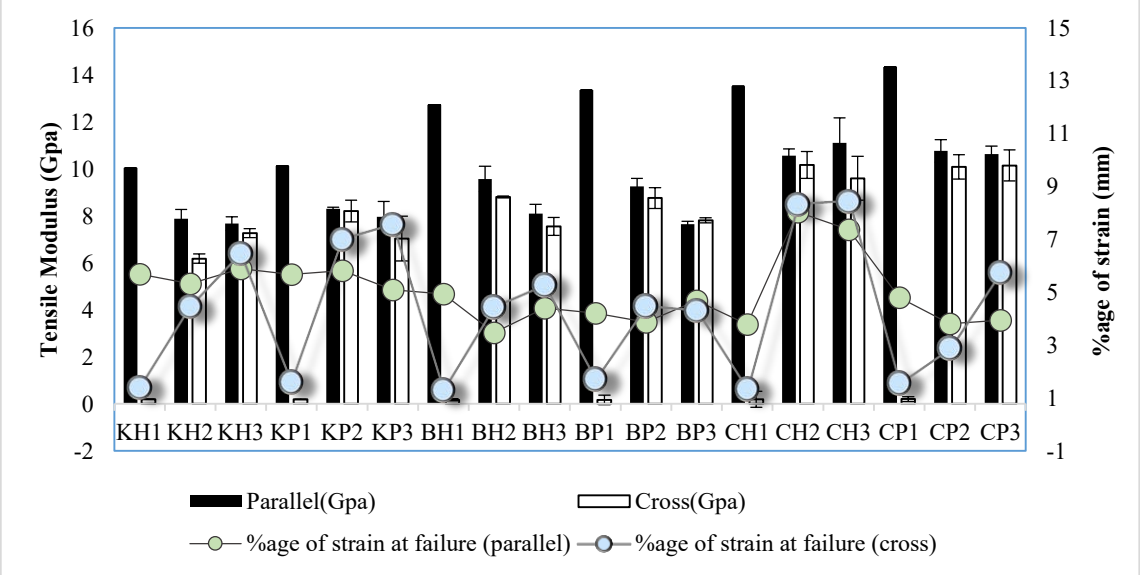

Fig. 1. Tensile modulus and percentage of strain in cross and parallel direction

[1] A. Siddique *et al.*, Mode I fracture toughness of fiber-reinforced polymer composites: A review, Journal of Industrial Textiles **2999** (2019).
[2] M. Abounaim, O. Diestel, G. offmann, and C. Cherif, High performance thermoplastic composite from flat knitted multi-layer textile preform using hybrid yarn, Composite Science and Technology **71 4** , 511-519 (2011).
[3] M. H. Ameer, Y. Nawab, Z. Ali, A. Imad, and S. Ahmad, Development and characterization of jute/polypropylene composite by using comingled nonwoven structures, Jouranal of Textile Institute **11011**, 1652-1659 (2019).
[4] S. Van Hoa, M. Duc Hoang, and J. Simpson, Manufacturing procedure to make flat thermoplastic composite laminates by automated fibre placement and their mechanical properties, Journal of Thermoplastic Composite Materials **3012**, 1693-1712, (2017).

VISUAL ACUITY EXAMINATION AT HOME DURING COVID-19

Kristine Kalnica-Dorosenko[1, 2], Aiga Svede[1]

[1] Department of Optometry and Vision Science, University of Latvia, Latvia
[2]Eye Diseases Clinic, Childrenós Clinical University Hospital, Latvia
kristinekalnica@gmail.com

In total, we receive more than 80 % of our information about the environment through our vision. Evaluating a personôs visual acuity is one of the main clinical steps to detect and correct refractive errors, or when evaluating the progression of visual anomalies or pathologies. Early detection of vision problems and rapid treatment prescribe better results. Recent studies in 2019 report that the use of telemedicine framework increased to accommodate for patients who required remote eye care due to the Severe Acute Respiratory Syndrome Coronavirus 2 (COVID19), which infected the globe in 2019 [1]. It is often not possible to examine patients remotely, so telemedicine is no substitute for face-to-face specialist consultations. Ophthalmology and optometry are one of the specialties well suited for telemedicine consultations, and acute problems in ophthalmology are an area where telemedicine can complement existing specialized services [2, 3]. There are currently many available tools for testing visual acuity at home, one of which is the Freiburg Visual Acuity & Contrast Test (FrACT) test. The test shows good reliability when compared to the golden standard ETDRS chart, or the Snellen chart [4, 5]. The purpose of this paper was to analyze the effectiveness of the FrACT test for testing visual acuity at home together with vision care specialist. The study involved 80 participants (5-86 years old, mean age 28 Ñ 14 years), 44 females (55 %) and 36 males (45 %). Visual acuity was assessed using a specialized FrACT computer test at both distance (3 m) and near (1 m) with and without optical glasses. No additional equipment is required without a computer, monitor and keyboard. The computerized FrACT test can be calibrated to the size and resolution of the monitor used. Before the visual acuity test using the Zoom video call app or WhatsApp, the participant had to contact a vision specialist to explain the process of the visual acuity test, the settings, the test parameters and monitor the quality of the visual acuity test, provide necessary advice, answers to patients' questions, results, next steps.The results have shown that the specialized computer program FrACT is a good tool to be used at home to check visual acuity and whether it is normal, as well as to monitor visual acuity improvement by performing various types of visual therapy (amblyopia treatment, medication treatment, etc.). Participants who did not pass the vision test were referred to a vision specialist for an advanced vision examination.In conclusion, during COVID-19, it was possible to check visual acuity remotely, from the comfort of home, using various tools, specifically the specialized computer program FrACT. They make life easier for the patient because they do not have to spend time visiting a vision specialist, checking whether their vision is normal (together with the vision specialist online), and the work of the vision specialist because it is possible to monitor the patient and/or the results of the therapy.

[1] L.J. Caffery, M. Taylor, G. Gole et al., Models of care in tele-ophthalmology: a scoping review, J Telemed Telecare **25**, 106-122 (2019).
[2] I. Tan, L.P. Dobson, S. Muir et al., Real-time teleophthalmology versus face-to-face consultation: A systematic review, J Telemed Telecare 23(7), 629-638 (2017).
[3] S.E. Bartnik, S.P. Copeland, A.J. Aicken et a., Optometry facilitated teleophthalmology: an audit of the first year in Western Australia, Clin Exp Optom **101**, 700-703 (2018).
[4] M.Bach, The Freiburg Visual Acuity Test-Variability unchanged by post-hoc re-analysis, Graefeôs Arch Clin Exp Ophthalmol **245**, 965-971 (2007).
[5] J.K. Jolly, J.M. Gray, A.P. Salvetti et al., A randomized crossover study to assess the usability of two new vision tests in patients with low vision, Optom Vis Sci **96(6)**, 443-452 (2019).

P3-35

DID NOT PARTICIPATE

GADOLINIUM LOADED ORGANIC DETECTOR FOR THE DARKSIDE EXPERIMENT

Anna Marini[1], Bianca Bottino[2]

[1] Department of Physics, University of Genova, Italy
[2] National Institute of Nuclear Physics, University of Genova, Italy
anna.marini@ge.infn.it

The DarkSide project - located at the Gran Sasso National Laboratories - aims to directly detect dark matter particles, using a liquid argon detector. One of the key features in the DarkSide-20k experiment is a neutron veto detector, used to reject the background signals caused by neutron interactions. The veto detector will consist of a gadolinium loaded polymethyl methacrylate (PMMA) shell, surrounded by liquid argon. Neutrons capture on the gadolinium which emits multiple gamma rays that interact in liquid argon, producing scintillation light. This light is then detected with dedicated photosensors.

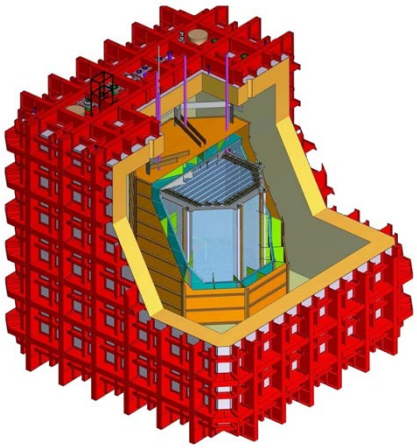

Fig. 1: The DarkSide-20k cryostat containing the veto system and the argon TPC.

In this context my work is focused on an R&D project to make a uniform gadolinium oxide nano- particle dispersion in a PMMA matrix, starting from the liquid monomer (MMA). Since gadolinium oxide is not mixable in MMA, but the nano grains tend to aggregate and to deposit during the polymerisation - thus causing inhomogeneity in the final product - a functionalization study of the oxide grains with a suitable surfactant is required, in order to create a coating that minimizes the grains clusterisation.

CENTERED METAL POWDER FLOW FOR PRECISION LASER METAL POWDER DEPOSITION

Romuald Petkevil [1], Sergejus Borodinas[2], Genrik Mordas[1]

[1]Department of Laser Technologies, Center for Physical Sciences and Technology, Vilnius, Lithuania
[2]Faculty of Civil Engineering, Vilnius Gediminas Technical University, Vilnius, Lithuania
romuald.petkevic@ftmc.lt

Since 1980, the development of additive production has begun. In recent years, several additive manufacturing technologies have been developed based on the creation of 3d objects using sequential layering processes. In such processes, the layers form a homogeneous structure by consistently coating 3d objects with properly prepared materials that can sometimes be modified during the process. This creates opportunities for the production of new unexplored structured materials.

One such technology is laser metal deposition technology (LMD) [1]. This additive manufacturing method, which generates 3D structures through the interaction of a laser beam, 3d objects and a gas powder stream. Most LMD systems use coaxial powder nozzles that form a conical powder flow. The position of the focal plan of such a powder flow affects the size, efficiency, and regularity of the sediment pathways [2,3].

To reduce the influence of the powder flow on the process, a new nozzle was developed to change the geometry from conical to cylindrical.

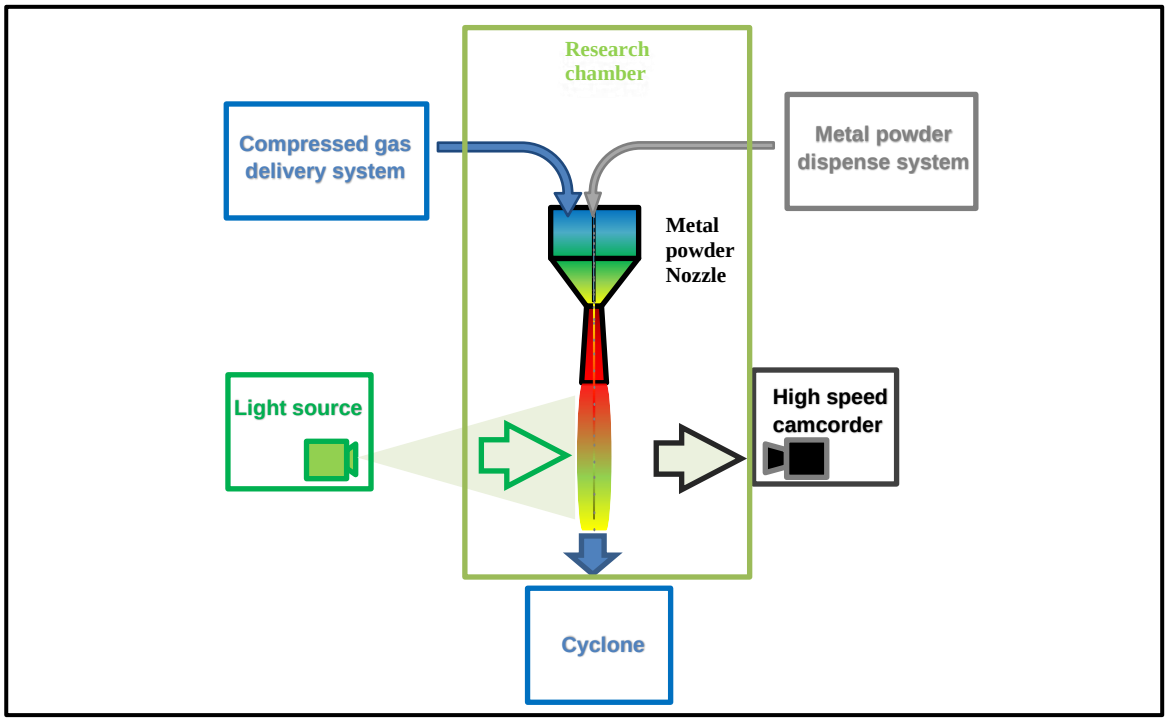

Fig. 1 Measurement setup of the metal powder nozzle.

In order to control the process and increase its reliability and re-use in industry, it is necessary to know the exact characteristics of the metal powder nozzle.

In this study, we will investigate the fiber distribution of nozzle particles using different gas pressure values. The measurement setup is illustrated in Fig. 1. The results of the experiment will be determined using a fast video camera, pressure measurements, weighting methods to analyze gas and particle velocity, powder flow diameter, focal plan position, and density.

[1] Lei Yan, Yitao Chen, Frank Liou., *Additive manufacturing of functionally graded metallic materials using laser metal deposition* (Additive Manufacturing 31 2020).

[2] Zoe Jardon, Patrick Guillaume, Julien Ertveldt, Michael Hinderdael, Galid Arroud, *Offline powder-gas nozzle jet characterization for coaxial laser based Directed Energy Deposition* (Conference on Photonic Technologies [LANE 2020] on September 7-10, 2020).

[3] Simone Donadelloa, Maurizio Mottaa, Ali Gokhan Demira, Barbara Previtali., *Monitoring of laser metal deposition height by means of coaxial laser triangulation* (Optics and Lasers in Engineering, Volume 112, January 2019, Pages 136-144).

P3-38

DID NOT PARTICIPATE

OPTICAL AND ELECTROLUMINESCENCE PROPERTIES OF SOLUTION PROCESSIBLE IR(PPY)3 DERIVATIVES WITH ADDED TRIPHENYLMETHANE GROUPS

Natalija Tetervenoka[1], Kaspars Traskovskis[2], Aivars Vembris[1]

[1] Institute of Solid State Physics, University of Latvia, Latvia
[2] Riga Technical University, Faculty of Materials Science and Applied Chemistry, Latvia
natalie@cfi.lu.lv

It is now considered that organic light emitting diodes (OLEDs) are the most appropriate technological solution for high quality displays [1].

One of the most investigated compounds applicable for wet processing is Ir(ppy)3 (tris(2-phenylpyridine)iridium) [2] due to its exceptional thermal and chemical stability and high photoluminescence quantum yield (ū PL) of near 1.0. If it is vacuum deposited, ū PL retains near a unity, in contrast, if it is solution processed, aggregation of Ir(ppy)3 occurs, which leads to phase separation between emitter and host material [3], as a consequence ï efficiency of OLED decreases. To overcome this condition it has been determined that adding to Ir(ppy)3 bulky groups with purely isolating or charge transport functionality provides physical barrier that suppress the tendency of aggregate formation and helps to keep a large distance between emitter molecules.

In this study Ir(ppy)3 and its structural analogues with gradually increasing number of attached passive isolating groups were investigated. The molecular composition of these compounds consists of Ir(ppy)3 core and one (1TPY), two (2TPY) or three (3TPY) attached bulky triphenylmethane groups (TR). Absorption and emission spectra of all compounds did not show significant deviations among compounds, which means that adding TR groups does not greatly affect the electronic configuration of Ir(ppy)3 core.

Onwards series of corresponding OLEDs with solution-processed emissive layer containing electron deficient, hole deficient or balanced host material were created and analyzed.

The best outcome in terms of turn on voltage, current and power efficiencies and maximal brightness were achieved using balanced host material.

Compounds investigated in this study can be used as emitters in solution-processible OLEDs, but further studies are required.

[1] Chen, H.W., Lee, J.H., Lin, B.Y., Chen, S. and Wu, S.T., 2018. Liquid crystal display and organic light-emitting diode display: present status and future perspectives. Light: Science & Applications, 7(3), pp.17168-17168.

[2] Baldo, M., Lamansky, S., Burrows, P., Thompson, M. and Forrest, S., 1999. Very high-efficiency green organic light-emitting devices based on electrophosphorescence. Applied Physics Letters, 75(1), pp.4-6.

[3] Kim, Y.T., Seol, J.B., Kim, Y.H., Ahn, H.J. and Park, C.G., 2017. Correlation of Controllable Aggregation with Light-Emitting Property in Polymer Blend Optoelectronic Devices. small, 13(14), p.1602874.

LASER-ASSISTED SELECTIVE FABRICATION OF COPPER TRACES ON POLYMERS BY ELECTROPLATING

Vitalij Fiodorov[1], Karolis Ratautas[1], Zenius Mockus[2]

[1] Department of Laser Technologies, Center for Physical Sciences and Technology, Lithuania
[2] Department of Chemical Engineering and Technology, Center for Physical Sciences and Technology, Lithuania
vitalij.fiodorov@ftmc.lt

The paper reports a facile and low-cost laser-assisted method for selective deposition of copper traces on polymer surfaces. The technique uses a laser for selective polymer surface modification. The electrical conductivity of some polymers could be increased due to laser irradiation. Kapton PI film was used in our experiment. Samples were patterned using a picosecond laser at 1064 nm wavelength. The experiments were performed using average powers ranging from 4 to 8.5 W in 0.5 W increments, pulse repetition rates from 10 to 100 kHz and a constant scan rate of 100 mm/s. The sheet resistance was measured using the four-probe method, and it was reduced to < 50 Ý per square after laser patterning. Afterwards, the modified surface was metal deposited by electroplating.

The main advantage of the method is that direct electroplating on polymers allows very fast, selective and low-cost metal deposition process to compare with other deposition methods, like PVD coating, painting with conductive ink, etc. Selective deposition of copper on polymers could be used in flexible electronic devices. This technology shows a huge potential in many fields: consumable electronics, automotive, medicine, etc. The aim of this research is to find the optimal laser patterning and copper plating parameters for high quality, recurrent fabrication of copper traces on polymer.

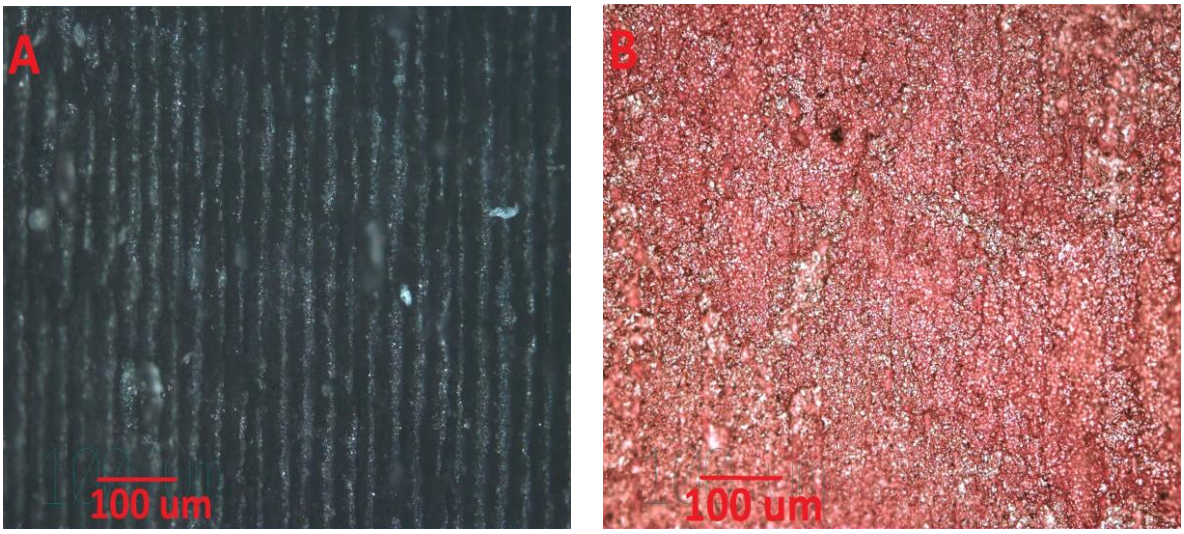

Fig. 1. Polymer Kapton PI film after laser patterning (A) and after electroplating process (B).

WIRELESS COMMUNICATION IN THE INTERNET OF THINGS

Arsenii Kovalenko

Department of Radiophysics and Biomedical Electronics and Computer Systems, V. N. Karazin Kharkiv National University, Ukraine
arsenkiy002@gmail.com

Recently, the Internet of Things has become one of the most common trends in the development of data network transmission technologies. Modern companies such as Vodafone, Huawei, Ring and others are actively introducing the latest means of wireless communication in the Internet of Things technology. In this regard, the study of wireless communications is of interest for researchers. This is proved by the research of Yang Yu, Chen Wenzhou, Weijianhui [1; 2; 3]. The purpose of my report is to provide an overview of wireless communication types and reveal their advantages and disadvantages of each.

The Internet of Things uses both wired and wireless communications. The Wired ones are more reliable, while the wireless ones have more prospects in this area. Therefore, I paid more attention to wireless communication. There are two main types of wireless communication. Short-range wireless communications include Bluetooth Wi-Fi ZigBee and Z-Wave. Sigfox, LoRa and NB-IoT belong to the second type of long range wide area communication. Bluetooth is a large capacity communication technology. It was invented as an alternative to wired technology. Bluetooth enables data exchange over short distances among devices and personal area networks. It uses the radio waves in the ISM band from 2.4 to 2.485 GHz with a transmission rate up to 1 Mbps [1]. Bluetooth has a short transmission distance of 10 cm to 10 m, which limits its use. At the same time, there are Bluetooth devices, which have a transmission distance of up to 100 m with a high power level. Bluetooth is widely used in applications. Its usage can be found in mobile phones, headphones, home appliances and smart wearables. Low power consumption, high reliability and high speed are the advantages of Bluetooth. But it is not suitable for multi-point deployment. The next wireless technology, which is widely known in the world, is Wi-Fi. The peculiarity of Wi-Fi is that it allows electrical devices to connect to a wireless local area. It most commonly uses the 2.4 G UHF or 5G SHF ISM radio bands [1]. Wi-Fi can be either password protected or an open network. Most of the devices such as computer, mobile phone, printer and others in our house can be connected with WLAN via Wi-Fi. Wi-Fi has the highest transmission speed among short-distance technologies. It has also wide coverage. Along with this, it has also disadvantages such as low transmission security, weak stability and high energy consumption [2]. ZigBee specializes in the internet of things. It is a low-power consumption LAN protocol based on IEEE802.15.4[1]. ZigBee is widely used in the industrial area and smart homes. It is easy to use, inexpensive and possesses high reliability. For instance, ZigBee base station costs less than 200 dollars while cellular base station costs hundreds of thousands dollars to build. It also transmits data from other network nodes. ZigBee has a wide range of applications to IoT such as smart home terminals and others. Thereby, ZigBee is a low-power consumption communication technology. It has a low complexity and low speed. Transmission distances can reach hundreds of meters. But this technology in smart parking is weakened by vehicles. Z-Wave is very similar to ZigBee. The main advantages of the Z-Wave are low price, low energy consumption and high reliability. Z-Wave can be used in light control, status checking and measurements. For instance, metering, home appliance control, access control, fire detection etc. Its transmission distance is from 30m to 100m. It features a simple network structure, low power consumption and high reliability. The main disadvantage of Z-Wave is low rates and closed standards [3].

There are only three main technologies for long-range wireless communication called Low Power Wide Area. LPWA technologies include Sigfox, LoRa and NB-IoT. The main aim of Sigfox is building a private wireless IoT network, which requires a low power consumption and low costs. Sigfox can maintain stable data connection without high power consumption. It also uses ultra-narrowband technology and has transmission speed up to 100 bps [4]. The Sigfox uses license-free Sub-Ghz radio waves. It works in the ISM band 868 MHz in Europe and 915 MHz in the USA. LoRa also uses Sub-GHz frequency bands in its turn to achieve a wider range by means of higher frequencies and low-power consumption. It is based on spread spectrum technology. It avoids the tradeoff between transmission range and low-power consumption and provides users with a simple system. Narrow Band IoT is built on cellular networks and uses a bandwidth of about 180 kHz. It can be deployed on GSM, UMTS and also on LTE networks. Thereby, it reduces its cost. NB-IoT technologies provide wide coverage, multiple connections, low costs, low power consumption, low speed and excellent architecture. It can be used in smart parking, remote metering, smart agriculture and more [4].

Thus, it can be concluded, that there is a large number of communication technologies. The article outlined the advantages and disadvantages of each of them. In the Internet of Things, you can combine the use of technologies, depending on what task was set.

[1] Yang Yu, Liping Zheng, et al., Technology of short-distance wireless communication and its application based on equipment support, AIP Conference Proceedings **1955,** 040135 (2018)**.**

[2] Chen Wenzhou, Research and application of Wi-Fi technology, Data Communication, **2**, 14-17 (2008).

[3] Weijianhui, A brief analysis of main technologies and applications of short-range wireless communication, Science & Technology Information, **04**, 5-97 (2016).

[4] M. Pointl, H.-D. Fuchs, Assessing the Potential of LPWAN Communication Technologies for Near Real-Time Leak Detection in Water Distribution Systems, SENSORS, **21**, 1 (2021).

GAZE PARAMETERS WHEN VIEWING IMAGES ON THE MULTI-PLANE VOLUMETRIC DISPLAY

Linda Krauze, Vita Konosonoka, Kristiana Zizlane, Tatjana Pladere, Gunta Krumina

Department of Optometry and Vision Science, Faculty of Physics, Mathematics and Optometry, University of Latvia, Latvia
linda.krauze@lu.lv

As the demand for three-dimensional image displays keeps growing continuously, so does the requirement for the objective evaluation of user experience. Multi-plane volumetric display is a new technology developed to visualize complex information in the form of spatial images in the volume of the optical element [1]. Visual information is perceived through a series of saccadic eye movements that are interrupted by visual fixations [2]. Most of fixations land on the certain objects that draw our visual attention [3]. Therefore, the evaluation of eye movements can provide useful insights about the quality of user experience for the novel displays.

To assess how individuals react on the third dimension of image provided by the multi-plane architecture of optical element, participants performed a visual search task on the multi-plane volumetric display. The study included target-absent trials to elucidate how observing three-dimensional and flat images affects eye movements. Search elements were displayed at four field eccentricities (2, 4, 6, and 8 degrees) in a random order. In target-present trials, the target was presented per one plane closer to the participant in comparison to other elements. The task was to determine which of the four circles was displayed closer to the observer. In each trial, the image was displayed for two seconds, and at the end of this time, participants had to submit the response about the location of the target or report whether the target was absent. The viewing distance to the screen was 65 cm.

The results have shown that the performance accuracy is the highest in the target-present trials. However, more errors have been made in the target-absent trials. Evaluation of eye movements has revealed that if the three-dimensional effect is noticed immediately, the gaze is more often directed to the location of the target in comparison to other elements in the scene. On the other hand, when the spatial effect is not observed or it is more difficult to be noticed, the distribution of eye movements changes considerably. Specifically, similar amount of time is devoted to viewing each element.

To sum up, the obtained results indicate that it is easier to distinguish the three-dimensional images than the flat images on the multi-plane volumetric display if the viewing time and head movements are limited. To facilitate the comparison of displayed information in depth, the elements should be close to each other, because otherwise the three-dimensional images presented on sequential planes might be viewed and perceived as the two-dimensional ones, as shown by the results at higher field eccentricities. Thus, the distribution of eye movement parameters clearly shows whether a person has noticed the three-dimensional image effect. Therefore, the method base on the evaluation of eye movements can be further developed for the reliable assessment of user experience for the three-dimensional visualization systems.

This work is a part of the research project supported by LightSpace Technologies (ñEvaluation of volumetric displayõs 3D image effect on human visual systemò, project No. ZD2019/20807). It is also supported by the European Regional Development Fund (ñDevelopment of a compact, high- brightness laser image projection system for application in volumetric 3D displaysò, project No. 1.1.1.1/18/A/179).

[1] Osmanis, K., Valters, G., Zabels, R., Gertners, U., Osmanis, I., Kalnins, L., Kandere, U., Ozols, A., Advanced multiplanar volumetric 3d display. *Proceedings of SPIE*, 10555, Article No. 1055510, 1-13 (2018).

[2] Findlay, J. & Walker, R., Human saccadic eye movements. *Scholarpedia*, 7(7), 5095 (2012).

[3] Rayner, K., Eye movements and attention in reading, scene perception, and visual search. *The Quarterly Journal of Experimental Psychology*, 62(8), 1457-1506 (2009).

IMPROVEMENT OF HEARING PROTHESES AND AIDS BY USING CAD/CAE TECHNIQUES

Shalini Murugesan[1], Sundar Arumugam Krishnan Nagarajan[1],
Virginija Gyliene[1], Valdas Eidukynas[1], Giedrius Gylys[2]

[1] Department of Mechanical Engineering and Design, Kaunas university of technology, Lithuania
[2] Department of ORL, Hospital of Lithuanian university of health sciences, Lithuania
shalini.murugesan@ktu.edu

Nowadays, the higher humanôs longevity provides new challenges how to maintain hearing loss, due to the ageing. Despite that, the hearing loss may result from genetic causes, complications at birth, certain infectious diseases, chronic ear infections, the use of drugs and even the exposure to excessive noise.

One cause of hearing loss is the none-transmission of the sound vibration in the middle ear due to the failure in the ossicular chain. In this case, an ossiculoplasty can be done, and the prosthesis will be placed to recreate the initial mechanism of the hearing, by reconstructing ossicular chain. In the case of conductive hearing loss, the conventional hearing aid does not work and the usage of hearing aid, which is composed from the implant and prothesis, becomes inevitable.

Concerning the reconstruction of ossicular chain, the selection of the type of protheses depends on the clinical situation and of the amount of damage. For example, Yuang [1] summarized ossicular damage in the patients with atelectasis and found that for 72% of cases in posterior retraction pocket only incus was eroded. As it was found in previous research [2] Ăworking ñ, but injured incus (Fig. 1) must be replaced and appropriate prothesis must be selected. Finally, for the reconstruction of the ossicular chain, a large variety of protheses (different materials and shapes) have been proposed. So, here the CAD/CAE systems are applied to differentiate the behavior of prothesis, according to the shape and used material.

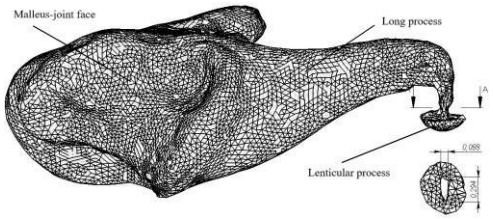

Fig. 1. The smoothed numerical model of human incus with injured long process [1]

Bone anchored hearing aids (BAHA) are surgically implanted by drilling a special fixation hole in slow speed in order not to overheat the bone, what finally could impact the conduction of sound from the processor. Detailed BAHA implant is presented in Fig.2., which was modelled to study implantôs fixation.

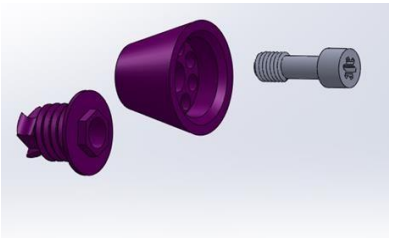

Fig. 2. Bone anchored hearing aid: implant

SolidWorks software was used for the conception of the numerical 3D models and CAE analysis.

[1] M.W. Yung, Retraction of the pars tensa long-term results of surgical treatment, Clin. Otolaryngol. Al-lied Sci. 22(4): 323-326.1997.
[2] V. Gyliene et al. Characterization of mechanical behaviour of healthy and injured human incus by eigenfrequency evaluation , Proceedings of the Institution of Mechanical Engineers, Part H: Journal of Engineering in Medicine, 234(3), 265ï 272. 2020.

CARBAZOLE-BASED MONOLAYERS FOR PEROVSKITE SOLAR CELLS

Aida Drevilkauskaitā[1], Amran Al-Ashouri[2], Steve Albrecht[2], Vytautas Getautis[1], Artiom Magomedov[1]

[1]Department of Organic Chemistry, Kaunas University of Technology, Lithuania
[2]Young Investigator Group Perovskite Tandem Solar Cells, Helmholtz-Zentrum Berlin, 12489 Berlin, Germany
aida.drevilkauskaite@ktu.edu

Perovskite solar cells (PSCs) have reached a major interest over the last decade, due to their rapidly growing efficiency. PSC is a type of solar cells, based on an organic-inorganic light-absorbing material, called perovskite. PSC can be used as a single-junction solar cell, or in tandem, in a combination with commercial technologies (e.g. Silicon, CIGS). In the latter case, perovskite converts higher energy photons from visible light and ultraviolet regions, meaning they can make higher efficiency tandem with lower energy photon absorber material solar cells.

While light-absorbing material is usually regarded as the most important component of the solar cell, there are also other layers, that are important to ensure the highest efficiency. The perovskite material is usually sandwiched between two so-called transport layers (electron-transporting layer and hole-transporting layer), that are ensuring high selectivity for the respective carriers. After the absorption, the hole-electron pair is formed and the negatively charged electron and positively charged hole are moving in opposite directions through transporting layers. One of the mentioned layers, the hole-selective, is often described as the weakest link of the solar cell. [1]

There are several parameters, that are of the highest importance for the hole-transporting material (HTM). One of them is the ability of the HTM to pass large amounts of carriers while maintaining high selectivity. In traditional HTMs, such as Spiro-OMeTAD, this is usually achieved by the use of oxidative dopants. However, it is leading to the decreased overall stability of the solar cells, therefore it is important to search for alternative materials and/or technologies.

Recently, self-assembled monolayers were used as hole-transporting dopant-free materials in PSCs. [2] The monolayers solve the doping-related issues, which are leading to stability problems. Moreover, they have some additional advantages, such as simplicity of the layer formation process, and the high flexibility to change layer properties by changing molecule structure. While traditional HTM layers are formed by spin-coating, self-assembled molecules can form layers by simple and scalable dipping method. Furthermore, if the perovskite solar cell is formed as a tandem on top of silicon solar cells, the self-assembled molecules can easily create a layer on a rough silicon surface, as well as provide minimal parasitic absorption, because of the small thickness.

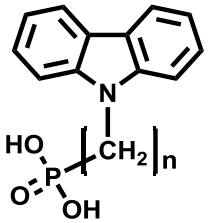

Fig. 1. The general structure of the carbazole-based phosphonic acids **nPACz** (n=2, 3, 4, 5, 6).

As a part of the structure-properties relationship investigation, a series of new carbazole derivatives were synthesized. In brief, in the first stage 9*H*-carbazole was alkylated with dibromoalkanes. Afterward, the intermediate compounds were transformed into phosphonic acid ethyl esters, by the use of the triethyl phosphite. In the final step, esters were cleaved with bromotrimethylsilane and methanol, to give the final compounds **nPACz**. The structures of synthesized materials were confirmed by ^{1}H and ^{13}C NMR spectroscopy. To determine electrical properties, materials were tested in photovoltaic devices. Preliminary results of the measurements have shown that the power conversion value decreases with increasing aliphatic chain length. Further investigations will be performed, for more detailed characterization.

[1] A.K. Jena, A. Kulkarni, T. Miyasaka Halide Perovskite Photovoltaics: Background, Status, and Future Prospects. Chemical Reviews, ACS 119(5), 3036ï 3103 (2019) https://doi.org/10.1021/acs.chemrev.8b00539

[2] A. Al-Ashouri, A. Magomedov, M. RoÇ, et al. Conformal monolayer contacts with lossless interfaces for perovskite single junction and monolithic tandem solar cells. Energy & Environmental Science, 12(11), 3356ï 3369. (2019) https://doi.org/10.1039/c9ee02268f

INVESTIGATION OF CHROMIUM THIN FILMS FOR OPTICAL APPLICATIONS

Kazimieras Baltrusaitis[1], Anna Sytchkova[2], Remigijus Juġkānas[1], Vitalija Jasulaitienā[1], Rimantas Simniġkis[1], Viktoras Vaiļikauskas, Alexandr Belosludtsev[1]

[1] Center for Physical Sciences and Technology, SavanoriÔave. 231, Vilnius 02300, Lithuania
[2] Optical Coatings Group, ENEA, Via Anguillarese 301, Roma 00060, Italy
Corespondance: Kazimieras.Baltrusaitis@ftmc.lt, Alexandr.Belosludtsev@ftmc.lt

Ultrathin metal are of a high interest due to their unique properties. Due to small thickness of nanometre scale they stay semi-transparent in a wide wavelength range. They are used in many field, for example, optoelectronics, optics, engineering, electronics, decoration and plasmonic. Chromium (Cr) metal thin films are attractive due to their mechanical, electrical and optical properties. Cr films play an essential role in many applications and can be used as decorative plating, transparent electrode, spacer layer, adhesive layer, light absorbing layer, optical beam splitters, spatial light modulator and tunable filter.

In our research, we have made a detailed study of Cr ultrathin films. Films with various thickness were deposited using magnetron sputtering. The films were investigated by various techniques in order to get better understanding of observed dependencies. A film thickness was varied from several nanometers to several tens of nanometrs. Such coatings, for example, might be used in optoelectronics and plasmonics.

It was evaluated that films have only chromium cubic phase. The elemental composition analysis confirmed the purity of the films.

Sheet resistance significantly decreased with the film thickness increased from 3 nm (1000 q/sq) to 12 nm (55 q/sq), afterward, with further thickness increase up to 57nm sheet resistance decreased to 19 q/sq. These values are comparable with the ITO values.

Optical constants of ultrathin Cr films were evaluated from ellipsometry are and compared with spectrophotomic measurements. These constants might be used for further modeling of multilayer coatings.

This project has received funding from European Social Fund (project No 09.3.3-LMT-K-712-19- 0203) under grant agreement with the Research Council of Lithuania (LMTLT).

CARRIER TRANSPORT PROCESSES IN MIXED CATION LEAD HALIDE PEROVSKITE MATERIALS

Vaiva Soriūtė[1], Patrik Ščajev[1]

[1] Institute of Photonics and Nanotechnology, Vilnius University, Sauletekio al. 3, LT 10257, Vilnius, Lithuania
vaiva.soriute@gmail.com

Hybrid organic–inorganic perovskites are very promising materials for various optoelectronic applications since during one decade solar cells, LEDs, lasers [1], transistors [2] and photodetectors [3] were created using these compounds. Perovskites have many desirable properties such as solution processibility at low temperatures, high carrier mobility and a tunable bandgap. The energy bandgap tunability can be achieved by mixing cations or exchanging anions and it allows us to manufacture perovskites with different emission and absorption wavelengths which is very useful while finetuning designs of LEDs or tandem solar cells. Therefore, mixed cation perovskites require further research to determine optimal composition with the best optoelectronic parameters.

The main goal of this work was to study perovskite samples $FA_xMA_yCs_{(1-x-y)}PbHA_3$ (FA – phenylammonium, MA – methylammonium, HA – halide ions) of different chemical composition where ratio of cations was gradually changed. Carrier dynamics was investigated using light-induced transient grating (LITG) technique. From these measurements important photoelectric parameters such as diffusion coefficient and recombination lifetime were obtained.

Pulsed laser irradiation at 351 nm wavelength was used to excite the samples. Spatially modulated excitation caused the creation of transient grating. This grating decayed with time due to diffusion and recombination processes and it was monitored by the probe beam of 1053 nm which was delayed by an optical delay line. Photoelectric properties were investigated within the wide range of excess carrier density by employing an optical attenuator to control the excitation energy fluence. Diffraction efficiency (η) decays, measured at different grating periods Λ, allowed us to extract carrier lifetime (τ_R) and diffusion coefficient (D).

Carrier lifetime dependence on the excess carrier density in $MA_xCs_{(1-x)}PbBr_3$ samples can be seen in fig. 1 (a). τ_R decreases with growing excess carrier density (ΔN_{av}) due to Auger recombination. Furthermore, increasing part of cesium in compound decreases carrier lifetime which can be explained by poorer crystal ideality and deceasing symmetry.

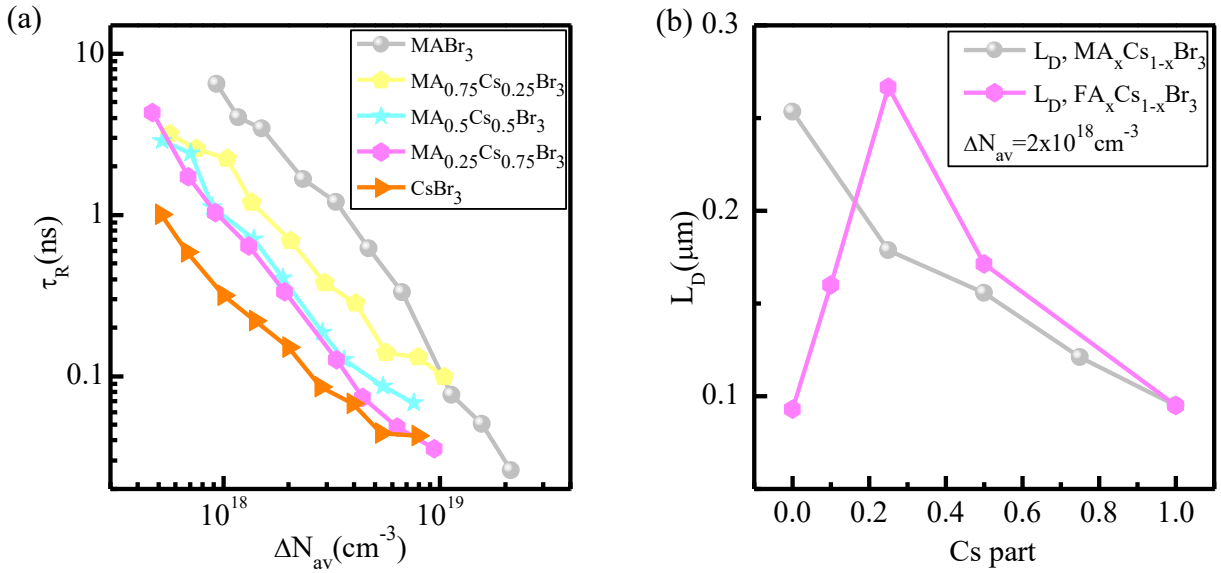

Fig. 1. (a) Carrier lifetime dependence on the excess carrier density ΔN_{av} in $MA_xCs_{(1-x)}PbBr_3$ samples, (b) diffusion length dependence on the Cs part in perovskite compounds.

In fig. 1 (b) diffusion length dependence on Cs part in the compound is shown. It is evident that diffusion length decreases with more Cs and is attributed to decreasing crystal ideality. However diffusion length varies in the interval of $0{,}1 \div 0{,}3\ \mu m$ which is comparable to thickness of the layers. This fact allows us to conclude that such perovskites are suitable for optoelectronic applications where charge carriers have to diffuse from the active layer.

This research was funded by the European Social Fund (Project No. 09.3.3-LMT-K-712-22-0217).

[1] J.R. Harwell *et. al.,* Green Perovskite Distributed Feedback Laser. Scientific Reports 7, 11727 (2017)
[2] T. Matsushima *et al.,* N-Channel Field-effect Transistors with an Organic-Inorganic Layered Perovskite Semiconductor. Appl. Phys. Lett. 109, 253301 (2016).
[3] S. Tong *et al.,* Fully-Printed, Flexible Cesium-Doped Triple Cation Perovskite Photodetector. Applied Materials Today Volume 15, 389-397 (2019)

THIN PEROVSKITE La:$BaSnO_3$ FILMS - TOWARDS NOVEL OPTOELECTRONIC MATERIALS

Miglė Sančiauskaitė[1], Tomas Murauskas[1], Valentina Plaušinaitienė[1], Virgaudas Kubilius[1]

[1] Department of Inorganic Chemistry, Vilnius University, Lithuania
migle.stanciauskaite@chgf.stud.vu.lt

Wide bandgap semiconductor La-doped $BaSnO_3$ (LBSO) has attracted increasing attention due to its outstanding electron mobility reaching 320 $cm^2V^{-1}s^{-1}$ at room temperature [1]. Many researchers have developed LBSO epitaxial films. However, the obtainable carrier mobility is much lower in thin films compared to single crystals. Worse electrical performance has been attributed to the formation of the structural defects and nonstoichiometry. Thin film electrical properties (mainly carrier mobility) were demonstrated to depend on film morphology, structure and lattice mismatch between the substrate and the film. The composition-dependent properties to-date are not fully investigated. Therefore, in this work thin La-doped $BaSnO_3$ films were deposited using pulsed injection metal organic chemical vapor deposition (PI-MOCVD) method on different substrates using different stoichiometric ratios of Sn/Ba. This method allowed easy compositional control of thin films and to investigate composition-dependent thin LBSO film properties.

Thin films were characterized using investigated using X-ray diffraction, X-ray photoelectron spectroscopy and scanning electron microscopy. La-doped film carrier mobility and carrier concentration were determined using Hall measurements. Surface morphology, microstructure and electrical properties of LBSO films were highly dependent on the selected substrate and film composition. Here we report thin film electron mobility, surface morphology and elemental core-shell electron spectroscopy dependence on thin film nonstoichiometry and successful optimization of the deposition process to achieve highly desirable electrical and structural properties.

---

[1] William Shepherd et al., Accurate control of stoichiometry and doping in barium stannate perovskite oxide nanoparticles, Chemical Communications **55** (79) 11880-11883, (2019).

P3-48

DID NOT PARTICIPATE

P3-49

DID NOT PARTICIPATE

FLUCTUATION CONDUCTIVITY IN $YBa_2Cu_3O_{7-\delta}$ SINGLE CRYSTALS UNDER ELECTRON IRRADIATION

Eugene V. Petrenko[1], Lyudmila V. Omelchenko[1], Andrei L. Solovjov[1]

[1] B.Verkin Institute for Low Temperature Physics and Engineering of NAS of Ukraine,
47 Nauky Ave., Kharkiv, 61103, Ukraine
petrenko@ilt.kharkov.ua

The phenomenon of superconductivity in high-temperature superconductors (HTSC's or cuprates) can be understood by studying HTSC's properties in the normal state, which are well known to be very peculiar. The most intriguing property is a pseudogap (PG) observed mostly in oxygen deficient cuprates below any representative temperature $T^* >> T_c$ [1]. At present, it is believed that the proper understanding of PG physics has to offer the possibility to decipher the basic pairing mechanism in the HTSC's which still remains uncertain.

The effect of 2.5 MeV electron irradiation on the temperature dependences of the resistivity ρ(T) of an optimally doped $YBa_2Cu_3O_{7-\delta}$ single crystal has been studied. Here we show that with an increase in dose φ, the value of ρ(300K) increases linearly, while T_c decreases linearly. The value of ρ(100K) increases nonlinearly, demonstrating a feature for $\varphi = 4.3 \cdot 10^{18}$ e/cm^2, which is also observed on the number of other dose dependent parameters. Regardless of the irradiation dose, in the temperature range from T_c up to T_{01}, the excess conductivity σ′(T) obeys the classical fluctuation theories of Aslamazov - Larkin (3D-AL) and Maki-Thompson (2D-MT), demonstrating 3D-2D crossover with increasing temperature. The crossover temperature T_0 makes it possible to determine the coherence length along the c-axis, $\xi_c(0)$, which increases by ~ 2.6 times under irradiation. Furthermore, the range of superconducting fluctuations above T_c also noticeably increases. At φ = 0, a "classical" pseudogap dependence Δ*(T) is observed with a maximum at T_{pair} ~ 120 K and a clear minimum at $T = T_{01}$ [2]. It was determined for the first time that at $\varphi = 4.3 \cdot 10^{18}$ e/cm^2 the shape of Δ*(T) changes strongly and becomes the same as in optimally doped $YBa_2Cu_3O_{7-\delta}$ single crystals with defects, which is accompanied by a sharp decrease in T_{pair} and the pseudogap opening temperature T*, while at $T_c(\varphi)$ there are no singularities. With an increase in the irradiation dose up to $\varphi = 8.8 \cdot 10^{18}$ e/cm^2, the shape of Δ*(T) is restored and becomes the same as in well-structured $YBa_2Cu_3O_{7-\delta}$ films. Moreover, in this case, T_{pair} and T* increase noticeably.

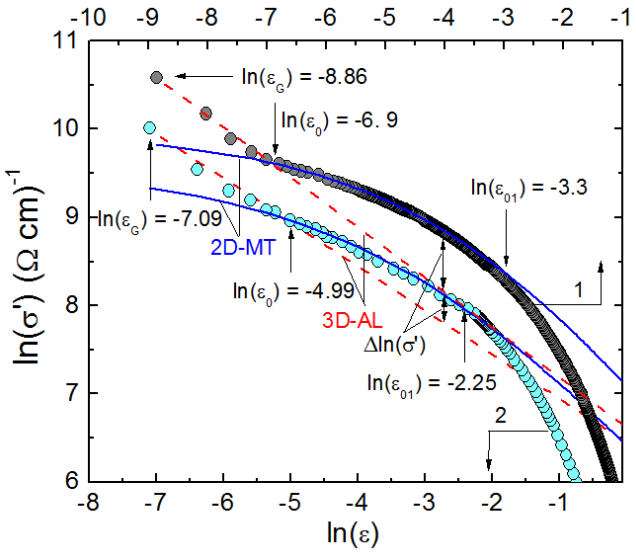

Fig. 1. Dependences of lnσ ′ on lnε of the $YBa_2Cu_3O_{6.94}$ single crystal at φ = 0 (curve 1) and $\varphi = 8.8 \times 10^{18}$e/cm^2 (curve 2) in comparison with fluctuation theories: 3D-AL (red dashed lines) and 2D-MT (solid blue curves). ln(ε_G) determines the Ginzburg temperature T_G, ln(ε_0) determines the crossover temperature T_0, and ln(ε_{01}) determines T_{01}, which limits the region of the SC fluctuations from above. The X-axis scales have been shifted for readability.

[1] A. L. Solovjov, V. M. Dmitriev, Low Temp. Phys. 35, 169 (2009).
[2] A. L. Solovjov, et al. Scientific Reports 9, 9274 (2019).

FABRICATION OF COMPOSITE HELMET USING BANANA FIBER AND FLY ASH

Sandesh Mysore Sathyaraj[1], Veeraraghavan Rajagopalan[2], Harsha Dyanesh[3*]

[1] Department of Electrical and Electronics Engineering,, Kaunas University of Technology, Lithaunia
[2,3] Department of Mechanical Engineering and Design, Kaunas University of Technology, Lithaunia
Sandesh.mysore@ktu.edu, veeraraghavan.rajagopalan@ktu.edu, harsha.nelavai@ktu.edu.

For the manufacture of construction helmets, natural fiber particle reinforced materials such as sisal, banana and jute reinforced polymer composite materials with epoxy resin were used. Impact strength and compression strength values are identified. The components of helmet production are checked. From the point of view of development, both the thermoplastic and natural fiber composite shell manufacturing techniques are provided with specific mention of the advantages and disadvantages for each form. Natural fiber has many advantages such as light weight, biodegradability, high strength, smaller elongation, quality of fire resistance, quality of moisture absorption and promising me These fibers are growing towards eco-friendly manufacturing, and the current review addresses research in the field of epoxy-based natural fiber composites and mechanical property analysis. Mechanical properties of the composite material have been studied in this paper by considering various parameters such as fiber content, fiber geometry, volume fraction, fiber size, epoxy resin properties, and fiber orientation, etc.[1]. It was found that when the liner's foaming ratio and shell-thickness were varied, it indicated that there is an optimal combination where the shell part fails without the liner bottoming, enhancing a helmet's ability to absorb shock. As the glass fiber concentration increased from 5, 10, 20, 30 wt percent in the manufactured ABS, the tensile strength was improved, the tensile module was improved but the strain value was decreased. Increasing glass fiber concentration also shows better bonding between ABS and SGFF [2].

Fig. 1. Banana Fiber.

The fibers obtained are washed and dried with water. Then the segregation is gently dispersed with patiently seated hands. Pineapple fibers and banana fibers are pounded with a hammer after retting the husks. Ripped from the husks, these fibers are separated from the comb. After drying at the room temperature, both the fibers were combed with a cotton carding frame for several times further separate the fibers into individual state. After that, both fibers are weighed for the correct weight and length [3]. The Composite Helmet uses banana fibre and fly ash to complete this work plan and investigation. In this ongoing world the fibre fortified composite materials are orchestrated using natural fiber as fortifications along with grid, which have pulled in the consideration of analysts because of their low thickness with high explicit mechanical qualities, accommodation, and inexhaustibility. The new work aims to advance the current safety helmet manufacturing strategy and the materials used to have improved mechanical properties in order to enhance the similarity between the strands and the structure.

[1]B.Murali, D.Chandramohan., ñFabrication of Industrial Safety Helmet by using Hybrid Composite Materialsò, Journal of Middle East Applied Science and Technology (JMEAST), pp. 584-587, 2014.
[2]"Effects of the Mechanical Properties of the Shell and Liner on the Shock Absorption of Helmets" Yusuke Miyazaki, Sadayuki Ujihashi, Tomohiko Jin, Shinichirou Akiyama and Ko Cheol Woong. Tokyo Institute of Technology, Tokyo, Japan.
[3]Seviaryna, I. Bueno, H.G.Maeva, E. Tjong, J., "Characterization of natural fibre-reinforced composites with advanced ultrasonic techniques," Ultrasonicôs Symposium (IUS), 2014 IEEE International, vol., no., pp.1428, 1431, 3-6 Sept. 2014.

DESCRIBING THE WOBBLING MOTION IN ^{163}LU THROUGH A SEMI-CLASSICAL APPROACH

Robert Poenaru[1,2]

[1] Doctoral School of Physics, University of Bucharest, Bucharest, Romania
[2] Department of Theoretical Physics, Horia-Hulubei National Institute of Nuclear Physics and Engineering, Bucharest-Magurele, Romania
robert.poenaru@protonmail.ch

Triaxial nuclei behave uniquely due to their anisotropy in both the mass and charge distributions. One clear fingerprint of nuclear triaxiality - Wobbling Motion - is the phenomenon in which the total angular momentum of the nucleus precesses and wobbles around its rotational axis, resulting in a rich rotational spectrum with a phononic character and thus making the final nuclear motion behave similarly to a harmonic oscillator. A lot of effort was made for developing theoretical models that describe wobbling motion in both even-even and even-odd nuclei. Considered the best wobbler to date, ^{163}Lu has four triaxial strongly deformed bands up to high spins which are established as having a wobbling nature. A successful description of the excitation energies for all four bands using a semi-classical approach is made within the current formalism. Indeed, by starting from a quantal Hamiltonian specific to the Particle-Rotor-Model, a Time-Dependent Variational Principle is applied to obtain a set of classical equations of motion. Analysis of the nuclear motion in this isotope is also made with the use of a classical energy function which is studied in terms of its stability region. As such, conditions when nuclear wobbling motion is stable/unstable arise. Interpretation of obtained results helps to establish certain features of the current work.

RENORMALIZING THE NEUTRINO MIXING MATRIX IN THE GRIMUS-NEUFELD MODEL

Simonas Draukšas[1], Thomas Gajdosik[1]

[1]Institute of Theoretical Physics and Astronomy, Vilnius University, Lithuania
simonas.drauksas@ff.vu.lt

The Grimus-Neufeld model [1] is an extension of the Standard Model (SM) of particle physics providing a mechanism of neutrino mass generation. The addition of neutrino masses to the SM also introduces mixing between neutrinos and there is a corresponding mixing matrix, known as the Pontecorvo–Maki–Nakagawa–Sakata (PMNS) matrix [2, 3]. This matrix has to be measured, however, to connect theory and experiment, it is needed to take care of ultraviolet (UV) divergences arising already in 1-loop calculations. With the procedure of renormalization it is possible to absorb all the UV divergences by adding counterterms to the Lagrangian of the theory. The PMNS matrix is no exception and one has to define a corresponding counterterm to ensure the finiteness of physical quantities. However, there is freedom in choosing a renormalization scheme and a few options are already available in literature [4, 5, 6]. One of the available schemes is gauge dependent, a feature one usually tries to avoid, while the other is slightly unconventional.

In this work we define a new scheme of fermion mixing renormalization and as an example we use the Grimus-Neufeld model. The new renormalization scheme provides explicitly gauge independent counterterms for the mixing matrix while mostly keeping in tact the usual definitions of renormalization constants. We have already checked some properties of the new scheme by explicit calculation in the Grimus-Neufeld model, but there still are outstanding tasks, for example, checking whether all of the UV divergences are correctly subtracted in the $Wl\nu$-vertex.

[1] W. Grimus and H. Neufeld. Radiative neutrino masses in an SU(2) × U(1) model. *Nuclear Physics, Section B*, 325(1):18–32, oct 1989.
[2] Ziro Maki, Masami Nakagawa, and Shoichi Sakata. Remarks on the Unified Model of Elementary Particles. *Progress of Theoretical Physics*, 28(5):870–880, 11 1962.
[3] Bruno Pontecorvo. Inverse beta processes and nonconservation of lepton charge. *Sov. Phys. JETP*, 7:172–173, 1958.
[4] Ansgar Denner and Thomas Sack. Renormalization of the quark mixing matrix. *Nuclear Physics, Section B*, 347(1-2):203–216, 1990.
[5] Bernd A. Kniehl and Alberto Sirlin. Simple on-shell renormalization framework for the Cabibbo-Kobayashi-Maskawa matrix. *Physical Review D - Particles, Fields, Gravitation and Cosmology*, 74(11), 2006.
[6] Bernd A. Kniehl and Alberto Sirlin. Novel formulations of CKM matrix renormalization. *AIP Conference Proceedings*, 1182:327–330, 2009.

HEAVY GAUGE BOSON W' SEARCH IN MUON CHANNEL USING MADMINER PACKAGE

Simas Jankauskas[1], Ugnė Šilingaitė[1], Simonas Draukšas[1]

[1]Institute of Theoretical Physics and Astrophysics, Vilnius Unitersity, Vilnius (Lithuania)
simas.jankauskas@ff.stud.vu.lt, ugne.silingaite@ff.stud.vu.lt

As the field of elementary particle physics is evolving, it is becoming complicated to perform analyses with usual methods due to increasing amounts of data and rising complexity of interesting processes, thus there is the need of other analysis techniques, such as machine learning. Due to the Neural Networks' ability to recognize relationships in vast amounts of data they can be used in various analyses which contain difficult data structures. `MadMiner` [1] is a new tool which provides machine learning techniques to efficiently approximate arbitrary ratios of likelihood functions. `MadMiner` streamlines the steps involved in elementary physics data analysis. It also provides interfaces to `MadGraph5_aMC` [2] for the generation of events, to `Pythia8` [3] for parton showering and to `Delphes3` [4] for the detector simulation, therefore the tool is able to support any physics process and model.

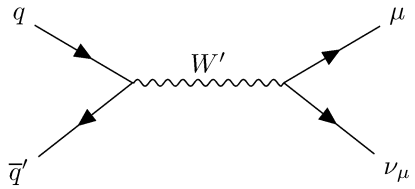

Fig. 1. $W' \to \mu + \nu_\mu$ channel Feynman diagram

In this work we investigate the parameter space by searching for the mass of the heavy gauge boson W' [5], which is predicted in various extensions of the Standard Model (SM), including the Sequential Standard Model (SSM) [6] which we use in our work. The search is performed in the muon channel (Fig. 1) using `MadMiner`. To achieve that, we train neural network models on the generated data at Leading Order (LO) and use them to estimate the likelihood ratio. The ratio of Likelihood functions, in our case the ratio of SSM to the SM, is used to determine the likeliness of one model over the other. Using generated test signals we evaluate the accuracy of the pre-trained Neural Network models' ability to maximize the likelihood.

[1] J. Brehmer, F. Kling, I. Espejo, and K. Cranmer, MadMiner: Machine learning-based inference for particle physics, (2020).
[2] J. Alwall, R. Frederix, S. Frixione, V. Hirschi, F. Maltoni, O. Mattelaer, H.-S. Shao, T. Stelzer, P. Torrielli, M. Zaro, The automated computation of tree-level and next-to-leading order differential cross sections, and their matching to parton shower simulations, Journal of High Energy Physics, vol. 2014, (2014).
[3] T. Sjöstrand, S. Mrenna, P. Skands, A brief introduction to Pythia 8.1, Computer Physics Communications, vol. 178, 852–867 (2008).
[4] J. de Favereau, C. Delaere, P. Demin, A. Giammanco, V. Lemaître, A. Mertens, and M. Sel-vaggi, Delphes 3: a modular framework for fast simulation of a generic collider experiment, Journal of High Energy Physics, vol. 2014 (2014).
[5] V. Khachatryan, A. Sirunyan, A. Tumasyan, W. Adam, E. Asilar, T. Bergauer, J. Brands-tetter, E. Brondolin, M. Dragicevic, J. Erö et al., Search for heavy gauge W' bosons in events with an energetic lepton and large missing transverse momentum at sqrt(s)=13 TeV, Physics Letters B, vol. 770, 278–301 (2017).
[6] G. Altarelli, B. Mele, and M. Ruiz-Altaba, Searching for new heavy vector bosons in pp colliders, Z. Phys. C45, 109 (1989).

ANALYSIS OF Z BOSON DECAY TO NEUTRINOS USING LHC

Domantas Čiapas, Aurelijus Rinkevičius

Faculty of Physics, Vilnius University, Vilnius, Lithuania
domantas.ciapas@ff.stud.vu.lt

Current detectors used in particle accelerators are not able to detect neutrinos. Due to this, studying processes with neutrinos in high energy physics experiments is not as trivial as processes with detectable objects. A deeper understanding of neutrino processes is necessary for pushing the limits of the Standard Model of particle physics. The aim of this research is to evaluate the decay of the Z boson, one of the weak-interaction mediating particles, to neutrinos.

To get the events with Z boson decay to neutrinos, the process $pp \to \ell\bar{\ell}\nu\bar{\nu}$ is generated with MG5_aMC@NLO (MadGraph) [1] event generator to simulate proton–proton collisions in a collider. The process is dominated by lowest order diagrams. Of these, one is the signal process, out of five major backgrounds the two are mostly negligible (cross sections are tiny). Using the event information provided by the event generator, it is possible to split the events into signal and background. The use of physically observable quantities (like invariant mass, p_{T}, etc.) is necessary for analysis of real processes seen in nature. For unaltered data, the signal cannot be isolated, due to the background processes being more frequent. Cuts on the data are made around Z boson mass to help isolate the signal. Fully isolating the signal from background processes both from reducible and irreducible backgrounds is the ultimate aim of this research.

This research is one of the few attempts to directly study neutrino processes in collider-based experiments. Findings gathered from this or similar experiments can lead to a validation of the Standard Model in the lepton sector, possibly opening a door for Beyond the Standard Model physics.

[1] J. Alwall, M. Herquet, F. Maltoni, O. Mattelaer and T. Stelzer, "MadGraph 5 : Going Beyond," JHEP **06** (2011), 128 doi:10.1007/JHEP06(2011)128 [arXiv:1106.0522 [hep-ph]].

APPROXIMATION OF BURST DURATIONôS PDFS OF BIRTH-DEATH PROCESSES

Ignas Kazakevičius[1], Vygintas Gontis[2]

[1] Institute of Theoretical Physics and Astronomy, Vilnius University, Lithuania
[2] Institute of Theoretical Physics and Astronomy, Vilnius University, Lithuania
ignas.kazakevicius93@gmail.com

Indicator of long-range memory is considered to be a power-law power spectral density in the low frequency domain [1]. However, many different stochastic processes may have this long-range memory property. In order to identify different stochastic processes and solve previously mentioned problem we are focusing on the analysis of the stochastic processes burst and inter-burst durationôs probability density functions (PDF) which can be used to determine whether a particular complex process retains the characteristics of a long-range memory in cases of different inter-burst durationôs threshold limits [2].

To generate time series we used the stochastic differential equation (SDE) asymptotically describing agent-based Kirman Birth-Death process. We performed the numerical calculation of burst and inter-burst durationôs PDFôs dependence on the threshold value of the process. It was shown that such PDFs generated by respective SDE in general case cannot be described by analytical approximation proposed for transformations of Bessel process. However, it was shown that analytical approximation derived in this work can be used to describe the bursts PDF of Bessel process and in specific cases could be used to approximate more complex processes than Bessel process such as agent-based Birth-Death process [3].

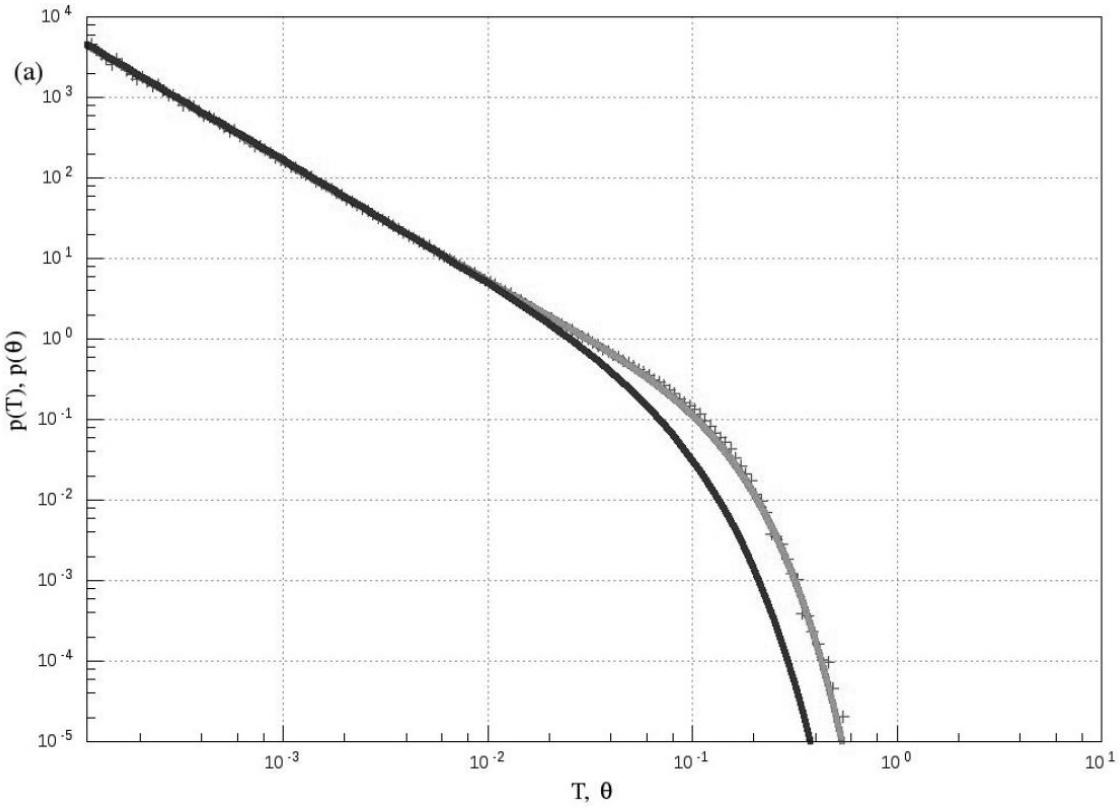

Fig. 1. Burst durationôs PDFs: a) PDF calculated by solving SDE numerically (crosses), b) analytical PDF approximation [4] (black lines), c) Analytical PDF approximation in a newer work (gray lines) [3].

[1] [28] Beran J., Feng Y., Ghosh S., Kulik R. Longï Memory Processes probabilistic Properties and Statistical Methods, Spingerï Verlag Berlin Heidelberg, 2013, DOI: 10.1007/978-3-642-35512-7.
[2] V. Gontis, A. Kononovičius, Spurious Memory in Non-Equilibrium Stochastic Models of Imitative Behavior, Entropy, 19 (8), 2017, p. 387, 2017, DOI: 10.3390/e19080387.
[3] Kazakevičius I., First Passage Time of Birth-Death processes, Master Thesis, Vilnius University, 2019.
[4] Kononovičius A., Gontis V. Approximation of the First Passage Time Distribution for the Birthï Death Processes, Journal of Statistical Mechanics 2019: 073402 (2019).

ANALYSIS OF THE TOTAL RADIATION POWER OF THE SECONDï HARMONIC GENERATION FROM A LINEAR STRUCTURE OF LONG CYLINDRICAL DIELECTRIC PARTICLES

Valery Kapshai, Anton Talkachov, Anton Shamyna

Department of Physics and Information Technologies, F. Scorina Gomel State University, Republic of Belarus
anton.talkachov@gmail.com

The phenomenon of second-harmonic generation (SHG) has been widely applied to study interfaces of dielectrics. The paper focuses on analysis of signal generated from the lateral surfaces of long dielectric cylinders coated with an optically nonlinear substance and ordered in a linear structure (Fig. 1a).

As previously shown in paper [1], second-harmonic radiation is predominantly concentrated in a plane perpendicular to the cylinder axis in the case of normal incidence of a plane electromagnetic wave on the lateral surface of long cylindrical particle coated with a nonlinear layer. Therefore, generation occurs only in the *Oxy* plane.

Let us calculate SHG from the linear structure of long cylinders using the principle of superposition and taking into account the phase shift. The second-order nonlinear dielectric susceptibility tensor for an elementary part of a surface can be represented in the form

$$\Gamma^{(2)}_{ijk} = \Gamma^{(2)}_1 n_i n_j n_k + \Gamma^{(2)}_2 n_i \delta_{jk} + \Gamma^{(2)}_3 \left(n_j \delta_{ik} + n_k \delta_{ij} \right) + \Gamma^{(2)}_4 n_m \left(n_k \varepsilon_{ijm} + n_j \varepsilon_{ikm} \right), \qquad i, j, k = x, y, z, \tag{1}$$

where n_i are the components of unit normal vector **n** to the surface, δ_{ij} and ε_{ijk} are Kronecker and Levi-Civita symbols, respectively. Let the anisotropy type $\Gamma^{(2)}_i$ means the values of components of the tensor $\Gamma^{(2)}_{ijk}$ are $\Gamma^{(2)}_i = 1$, $\Gamma^{(2)}_j\big|_{j \neq i} = 0$.

Let us consider SHG from the structure of N cylinders with radius of their bases a ($k_x a$ = 0.1) and distances between their axes d at normal incidence of a plane polarized wave (with the polarization plane *Oxy* and the direction along *Ox* axis) (Fig. 1a). Let us analyze the dependence of the SHG power on the distance d. Figures 1b and 1c show the dependences of the ratio of the SHG power from the structure of N cylinders (W_N) to a similar value for one cylinder (W_1) on the distance between cylinder axes. All curves tend to a value $W_N/W_1 = N$. An increase in distance between cylinder axes leads to decrease in variations around this level. All dependences are almost periodic; however, the distances between the peaks are non constant and vary in range $k_x d \in [6.2; 6.5]$.

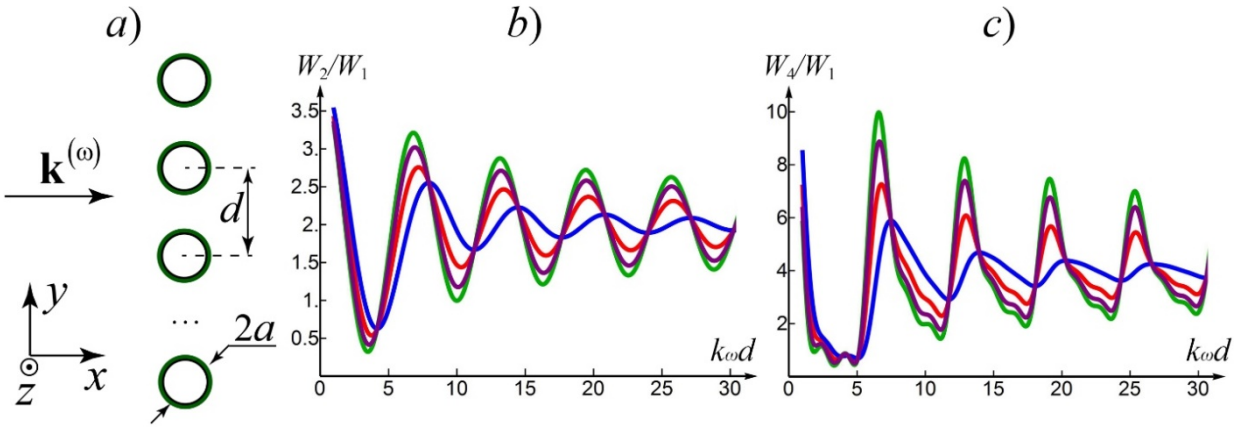

Fig. 1. a) Scheme of the problem of the SHG from the linear structure of cylindrical particles.
b), c) Dependences of the ratio of the SHG power from the structure of N cylinders to the similar value for one cylinder.
In b) and c) panels, red, green, blue and purple curves correspond to the anisotropy types $\Gamma^{(2)}_{1-4}$.

For the anisotropy types $\Gamma^{(2)}_{1,2,4}$ the curves have similar shapes with close positions of maximums and minimums. Whereas, there is a faster attenuation and entirely different position of extrema for type of the anisotropy $\Gamma^{(2)}_3$. At this distances between cylinder axes, the ratios W_N/W_1 for all anisotropy types are equal (all curves cross). As the number of particles in the structure increases, the maxima become sharper, the number of local minima increases and positions of the maxima shift to lower values of $k_x d$ for the anisotropy types $\Gamma^{(2)}_{1,2,4}$.

This work was supported by Belarusian Republican Foundation for Fundamental Research (project No. F20Mï 011).

[1] A. A. Shamyna, V. N. Kapshai, Second-Harmonic Generation from a Thin Cylindrical Layer. I. An Analytical Solution, Opt. Spectrosc. **126**, 645-652 (2019).

NONLINEAR RESPONSE THEORY IN ULTRA-THIN ELECTRON LAYERS

Mario Graml[1], Dominik Kreil[2], Helga M. Böhm[2]

[1]ZONA, Johannes Kepler Universität, A 4040 Linz, Austria
[2]Institut für Theoretische Physik, Johannes Kepler Universität, A 4040 Linz, Austria
mario.graml@jku.at

Perturbational response theory is one of the most successfully used tools in physics, its linear version being the standard procedure to fruitfully treat complex systems. Ongoing advances in laser power combined with increasing accuracy in material design drive the need to go beyond linearity. Here we present a general formalism for the arbitrary order response functions of any observable in Fermi systems and derive a closed form for the non-interacting case. As novel technological devices for radio- and electrical signals operating outside the linear regime, e.g. as detectors, mixers, or multipliers for terahertz waves, are often based on very thin nano-structures. The two dimensional uniform electron gas (2Deg) was chosen to test our theory. We verify our expressions by confirming the results reported by Lee [1] for the quadratic order Lindhard function and newly derive the cubic density response, which can be cast into a notably lucid form.

Interactions are then accounted for using the random phase approximation (RPA). This self-consistent mean field approach is quite accurate in experimentally studied 2Degs [2]. We extend the linear RPA up to third order in the perturbation aiming at an analysis of the collective modes, the sheet plasmons. In the harmonic co-linear case we further accomplished to extend the relations of Mikhailov [3] to hold for more general input signals. Compared to the linear case, a much richer particle-hole excitation spectrum gives rise to stronger Landau damping, significantly reducing the live-time of the collective modes, manifest in the electron-energy-loss-scattering function and in good agreement with the experiment of Nagao et. al [4].

So far, the spin degree of freedom was not treated explicitly. Work to investigate partially polarized systems [5] is in progress, aiming at a better understanding of the polarized electron sheets applicable in spintronics.

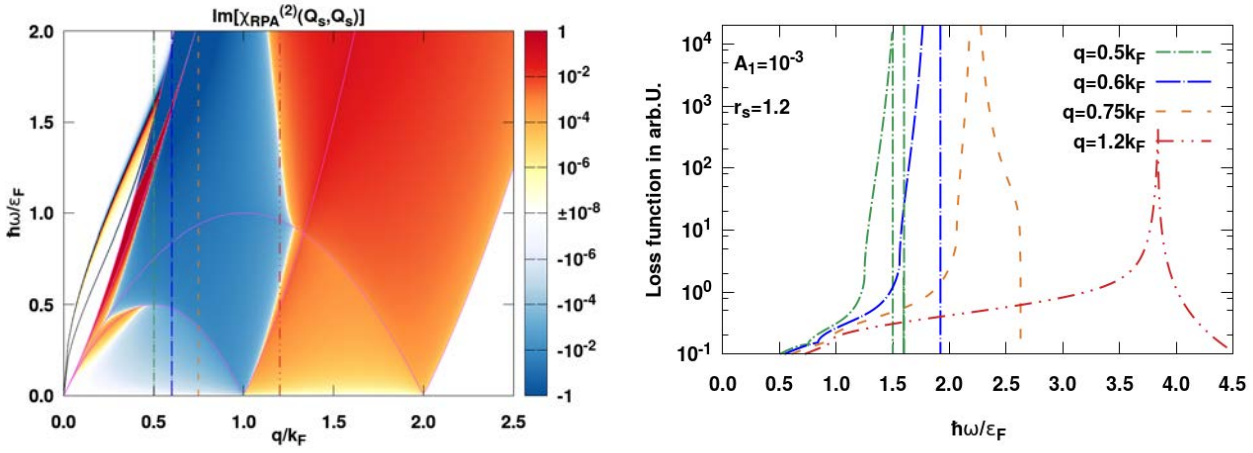

Fig. 1. **(left):** 2nd order interacting response function $\chi^{(2)}_{\mathrm{RPA}}$ for a harmonic perturbation. In comparison to the first order, the second order shows two distinct and overlapping particle-hole bands (PHB), bounded with solid magenta lines. The two appearing collective modes are undamped in a wide region of wave-vectors q and enters the PHB at approx. 0.6 and $0.7k_{\mathrm{F}}$, respectively. Additional four specific cuts at $q_{\mathrm{s}}/k_{\mathrm{F}} \in \{0.5, 0.6, 0.75, 1.2\}$ are marked. **(right):** The electron–energy–loss function within quadratic response theory for the marked wavelengths q with Wigner-Seitz radius $r_{\mathrm{s}} = 1.2$ and input field strength A_1. The weight and energy of the mode depends significant on q. After entering the PHB, the collective mode becomes damped quite rapidly. (k_{F}, ε_{F} denote the Fermi wave-vector and energy, respectivly)

Mario Graml is grateful for partial support through the European Union's Horizon 2020 research and innovation program under grant agreement No. 899598 (PHEMTROMICS).

[1] C.J. Lee. Quadratic density response function of a two dimensional electron gas. Results in Physics, 5:184–195, 2015.
[2] Pavel Arturovich Gusikhin, Vyacheslav Mikhailovich Murav'ev, and Igor Vladimirovich Kukushkin. Observation of plasma waves with anomalously weak damping in a two-dimensional electron system. JETP letters, 100(10):648–651, 2015.
[3] S. A. Mikhailov. Nonlinear electromagnetic response of a uniform electron gas. Phys. Rev. Lett., 113:027405, Jul 2014.
[4] T. Nagao, T. Hildebrandt, M. Henzler, and S. Hasegawa. Dispersion and damping of a two-dimensional plasmon in a metallic surface-state band. Phys. Rev. Lett., 86:5747–5750, Jun 2001.
[5] Dominik Kreil, Raphael Hobbiger, Juergen T Drachta, and Helga M Boehm. Excitations in a spin-polarized two-dimensional electron gas. Physical Review B, 92(20):205426, 2015.

Z BOSON DECAY CLASSIFICATION USING ARTIFICIAL INTELLIGENCE WITH LHC

Dominykas Orlovas, Aurelijus Rinkevičius

Faculty of Physics, Vilnius University, Vilnius, Lithuania
dominykas.orlovas@ff.stud.vu.lt

In particle physics, even with massive amount of data collected by the current detectors, some particles are elusive. Such are neutrinos. Neutrinos, while common, only couple weakly to all known matter. This means that interactions are very rare, even in the presence of dense detectors.

A way to look for them, without a direct detection, is through momentum balance. In a beam all particles are roughly going along the beam axis, with very little if any transverse momentum. This means that the full transverse momentum of a collision is zero. If this is not the case, there are missing particles in the detector. These could likely be neutrinos.

This work analyzes Z boson decays into a pair of neutrinos (Z -> *νν*). Since there is no pure Z boson source, the biggest machine ever built, the LHC (Large Hadron Collider), serves as the best all-purpose source. LHC provides protons at initial state. While pp -> *νν* is a possible and a very likely process, it is difficult to detect. When the outcome is completely undetectable how can you be sure the process even happened. Therefore, some detectable particles are needed in the final state. Leptons are clean and easily detectable detector objects that can simplify the neutrino hunt. For that reason, the initial state containing a pair of charged leptons in addition to neutrinos is chosen i.e., the process pp -> *llνν*.

Now the problem comes in distinguishing the Z boson decays from the rest of the processes with the same initial and final states. This is achieved through the use of artificial intelligence. To be specific a neural network based classifier. This classifier was constructed using TensorFlow [1] and Keras [2]. But an untrained neural network is useless. To apply it to any real data it needs to be trained first. Training data is generated using a simulation software, in particular, Madgraph [3]. A good candidate process with *llνν* final states is pp -> ZZ -> *llνν*, here we can take advantage of the invariant mass of the lepton pairs that should be around the Z boson mass, as is seen in Fig. 1. Other processes (with *llνν* final states) include W bosons and their subsequent decays, which are around 10 times more likely, but the clear peak seen in Fig. 1 allows us to cut the data in such a way that the event counts are very similar. A classifier can then be trained to further discriminate the underlying processes.

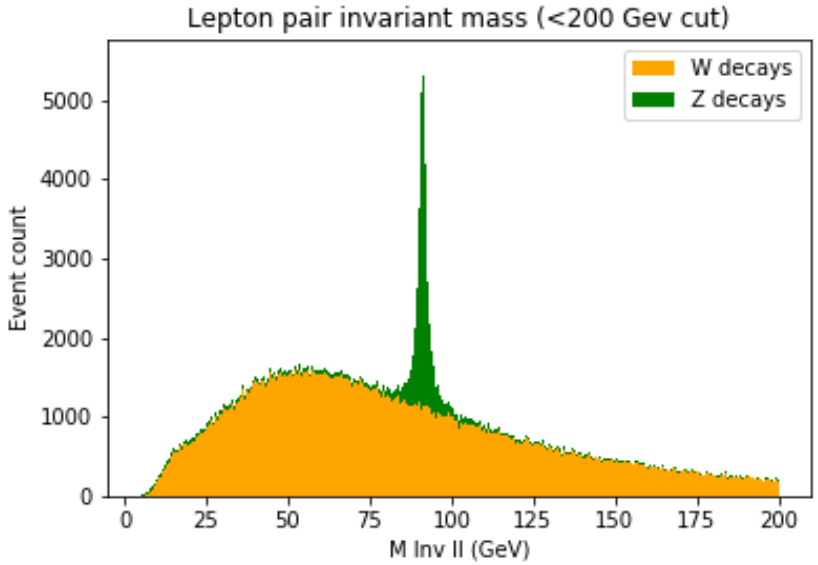

Figure 1 Lepton-pair invariant mass distribution for *llνν* events

[1] Mart²n Abadi and others. TensorFlow: Large-scale machine learning on heterogeneous systems, 2015. Software available from tensorflow.org. Chollet, F., & others. (2015).
[2] Chollet, F., & others. (2015). Keras. https://keras.io.
[3] J. Alwall et al, "The automated computation of tree-level and next-to-leading order differential cross sections, and their matching to parton shower simulations", arXiv:1405.0301 [hep-ph]

COMPARISON OF NEUTRON FLUX IN EU DEMO DIVERTOR PLASMA-FACING COMPONENTS USING WCLL AND HCPB BREEDING BLANKET MODELS

Simona Breidokaite[1], Gediminas Stankunas[1],

[1]Laboratory of Nuclear Installation Safety, Lithuanian Energy Institute, Lithuania
simona,breidokaite@lei.lt

The primary purpose of the plasma-facing component (PFC) is power exhaust and removal of impurity particles. The plasma-facing component consists of three layers and a support [1]. The first and third layers are made of tungsten alloy. The second layer is a mixture of Tungsten, CuCrZr, water, and a support is made of Eurofer alloy. This paper considers two different breeder blanket models of DEMO reactor: Water-Cooled Lithium Lead (WCLL) and Helium Cooled Pebble Bed (HCPB) and the same specified DEMO neutron source. Even though both models have the same divertor configuration, the neutron flux is slightly different.

MCNP6 code [2] and Joint Evaluated Fission and Fusion (JEFF 3.2) [3] nuclear data library were used for neutron flux calculations. MCNP6 is widely recognized and used for fusion neutronic applications. Neutrons are divided into 709 energy groups from 10^{-5} eV to 1000 MeV.

The statistical error of Monte Carlo calculation results for divertor PFC cells was less than 10% with 10^9 particle histories. In energy region from 0.166 $*10^{-4}$ eV up to 5.75 $*10^{-4}$ eV and in 3.47 MeV up to 15.6 MeV HCPB has 1.2 times more neutron than WCLL. While in region 5.75 $*$ 10^{-4} eV - 3.47 MeV showed more neutrons in energy groups by factor 1.5 on average. However, in remaining groups there were no neutrons identified.

[1] S. Noce et.al., Nuclear analyses for the design of the ITER-like plasma facing components vertical targets of the DEMO divertor, Fusion Engineering and Design, Volume 155, 2020, [2] M. A. Green, *High Efficiency Silicon Solar Cells* (Trans. Tech. Publications, Switzerland, 1987)
[2] C.J. Werner (editor), "MCNP Users Manual - Code Version 6.2", LA-UR-17-29981 (2017)
[3] OECD Nuclear Energy Agency, JEFF-3.2 Evaluated Data Library (2014). http://www.oecd-nea.org/dbforms/data/eva/evatapes/jeff_32/

REGIONAL OVERESTIMATION OF SUMMER TEMPERATURES DUE TO REGIONAL CLIMATE MODELS DEFICIENCIES IN SPAIN

Jos®Carlos Lozano Garc²a[1]

[1] Department of Physics of Ice, Climate and Earth; Niels Bohr Institute, University of Copenhagen, Denmark
knv118@alumni.ku.dk

The Iberian Peninsula has been experiencing new temperature records in the last few decades making some parts of this region less and less habitable, especially during summer. To simulate present-day climate conditions accurately and to determine better estimates of extreme temperatures over the southwestern part of Europe, high-resolution regional climate models (RCMs) have been applied. However, it is unknown to which degree state-of-the-art RCMs may tend to overestimate regional amplification of global warming, especially during the warmest months (Christensen et al. 2008[1]; Boberg and Christensen, 2012[2]).

Studies have revealed that RCMs have systematic temperature dependence of biases increasing with temperature. The warmer the month is, the stronger the tendency is. The project aims to analyse potential non-stationary biases between climate simulations (EURO-CORDEX project) and observational datasets over the Iberian Peninsula (Herrera et al., 2015[3]). Such an analysis has not been done with the current high-resolution RCMs or relying on a high-resolution observational dataset before. In addition, the analysis will be extended to also address monthly means of daily maximum and minimum temperatures, which has not been addressed before. A bias correction method could be then be proposed to mend some of the model deficiencies.

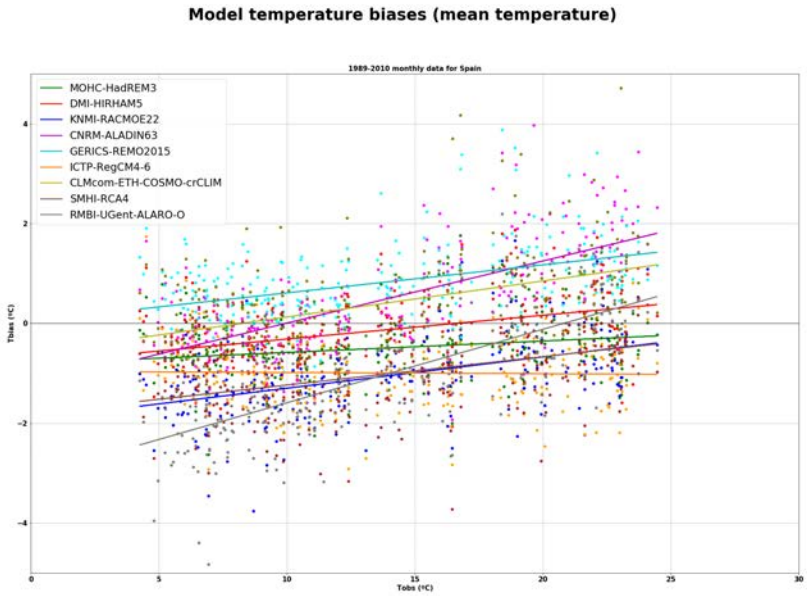

Fig. 1. Model temperature biases covering the period 1989-2010. RCMs from EURO-CORDEX project and observational gridded dataset from CSIC.

[1] Christensen, J. H., Boberg F., Christensen, O.B. & Lucas-Picher, P., 2008. On the need for bias correction of regional climate change projections of temperature and precipitation.
[2] Boberg, F., Christensen, J.H., 2012. Overestimation of Mediterranean summer temperature projections due to model deficiencies.
[3] Herrera, S., Fern§ndez, J., and Guti®rrez, J. M., 2015. Update of the Spain02 gridded observational dataset for EURO-CORDEX evaluation: assessing the effect of the interpolation methodology.

STUDY OF ELECTRICAL CHARACTERISTICS OF SiGe AND CdZnTe MATERIALS APPLICABLE TO RADIATION DETECTION

Laimonas Deveikis, Tomas Čeponis, Eugenijus Gaubas

Institute of Photonics and Nanotechnology, Vilnius University, Saulėtekio av. 3, LT-10257, Vilnius, Lithuania
laimonas.deveikis@tmi.vu.lt

SiGe material based devices are capable to operate in the radiation harsh environment and it had been demonstrated that SiGe alloys are prospective for fabrication of γ-ray detectors [1]. Cadmium zinc telluride (CZT) is a promising material for the room-temperature X- and γ -ray detectors due to high average atomic number providing high stopping power as well as rather large band-gap which determines large resistivity, small leakage-current, and good energy resolution [2]. Generation of the undesirable point defects is inevitable during crystal growth and operation of detector in radiation harsh environment. The dopants, native impurities and radiation induced defects usually act either as recombination, trapping or carrier emission centres and contribute to the decrease of charge collection efficiency by reducing carrier lifetime. The role of point defects is also important in charge compensation processes. Therefore, the analysis of defects is important in prediction of the optical and electrical characteristics of the SiGe and CZT materials. In this work, study of pristine, 5.5 MeV electron and 1.6 MeV proton irradiated $Si_{1-x}Ge_x$ structures, containing 1% and 5% of Ge, and two sets of CZT samples, exhibiting good and unacceptable performance of radiation detection, have been performed by combining techniques of the microwave probed photoconductivity (MW-PC) and pulsed barrier evaluation by linearly increasing voltage (BELIV).

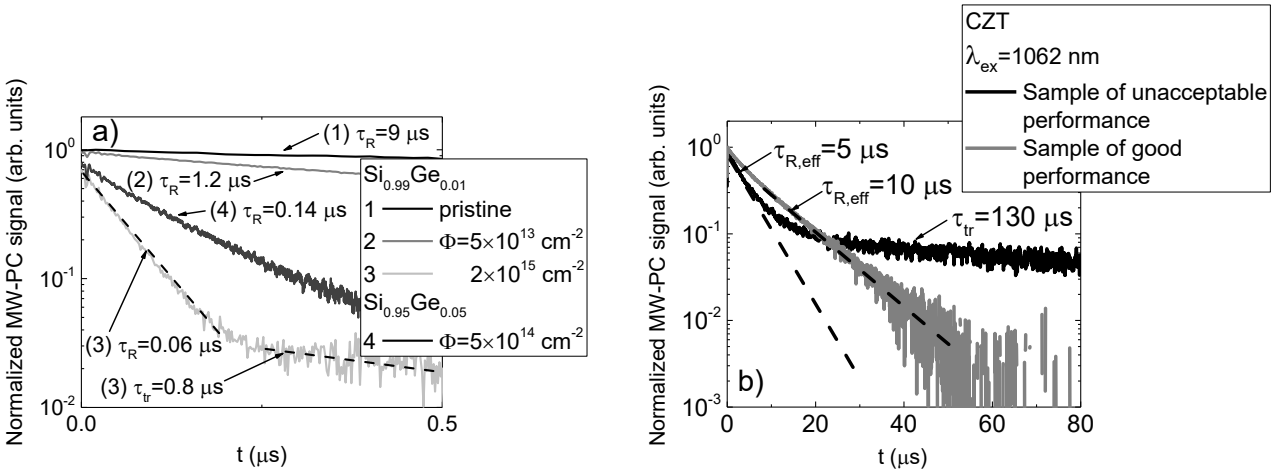

Fig. 1. The MW-PC transients normalized to a peak of the MW-PC response using bulk excitation (1062 nm wavelength) by 400 ps laser pulses: **a)** transients recorded on $Si_{1-x}Ge_x$ diodes irradiated with different fluences of 5.5 MeV electrons; **b)** transients recorded on CZT samples, exhibiting unacceptable and good performance of radiation detection.

It has been revealed that in SiGe material both carrier recombination and trapping lifetimes decrease near-reciprocally (Fig. 1a) relative to the density of radiation defects acting as carrier capture and thermal emission centres, with predominance of point radiation defects. It has been hypothesized that the single-type deep centres are involved in both carrier photo-generation and thermal emission processes. Activity of point defects can be modified by anneal procedures, and sensor functionality can be recovered (at least, partially).

The main difference between the examined CZT diodes appeared through carrier trapping effect, observable only for diodes exhibiting unacceptable performance of radiation detection (Fig. 1b). The rather long instantaneous trapping lifetime of τ_{tr} = 130 μs showed the trapping coefficient to be of the order K_{tr} = 27. The concentration of trapping centres has been estimated to be > 3×10^{14} cm^{-3} for the shallowest thermal emission centres. These trapping centre concentrations exceed dopant density by several orders of magnitude. The trapping centres in CZT material might be associated with Te_{Cd} as well as $V_{Cd}^{0/-}$ point defects and Te inclusions.

[1] I. Yonenaga, *Si_x-Ge_{1-x} bulk crystals* (Reference Module in Materials Science and Materials Engineering, Netherlands, 2016).
[2] T.E. Schlesinger, J.E. Toney et al., Cadmium zinc telluride and its use as a nuclear radiation detector material, Mater. Sci. Eng. R Rep. **32**, 103 (2001).

CHALCOGENIDE-PEROVSKITES FOR MULTIJUNCTION SOLAR CELL APPLICATION

Rokas Kondrotas[1*], ArÎnas Krotkus[1], Saulius Tumėnas[1], Bronislovas Cechavicius[1], Maarja Grossberg[2], Marit Kauk-Kuusik[2], Xiaofeng Li[2]

[1] Center for Physical Sciences and Technology, SavanoriÛAve. 231, Vilnius, 02300, Lithuania
[2] Department of Materials and Environmental Technology, Tallinn University of Technology, Ehitajate tee 5, 19086 Tallinn, Estonia
rokas.kondrotas@ftmc.lt

On theoretical level, multijunction solar cells have a potential to achieve over 60% power conversion efficiency. In practice, device with 47% efficiency has been fabricated based on III-V material and five-junction structure. However, extremely high cost of such multijunction devices inhibit their wide-spread application. In the recent years due to the unprecedent development of perovskite technology, two-junction solar cells comprising perovskite and well-established Si has demonstrated very promising results reaching 29% in 2020 [1], and opening the technological path for ultra-high and low-cost solar cells. To improve such tandem device further, adding additional junction with absorption edge at 0.7 eV can potentially add 5% of absolute efficiency.

In this work, we study underexplored class of materials for potential application in multijunction devices as bottom sub-cell (Figure 1). The selected compounds are from the chalcogenide-perovskite material group, containing earth-abundant chemical elements and compatible with low-cost synthesis methods are predicted to have low band gap (< 0.0 eV) [2]. Chalcogenide-perovskites have a general compound formula ABX_3, where in our study A=Ca, Sr, Sn; B=Ti, Zr, Sn; X=S,Se. Samples were synthesized via solid state reaction (Figure 1 inset) and characterized by x-ray diffraction method to study chalcogenide-perovskite thermodynamic stability and crystal structure.

We found that many chalcogenide-perovskites are not stable and do not form under normal (without transport agent or catalysis) conditions. In contrast to halogen and oxide perovskites, the structure of chalcogenide-perovskites cannot be predicted according to the tolerance factor (*t*), i.e., when *t* is close to unity, adopted structure is not cubic. This shows that atomic bonding in chalcogenide-perovskites is more covalent than ionic in nature and therefore usually adopt one of the following lower symmetry crystal structure: needle-like (prototype NH_4CdCl_3), hexagonal (prototype $BaNiO_3$) or distorted perovskite (prototype $GdFeO_3$).

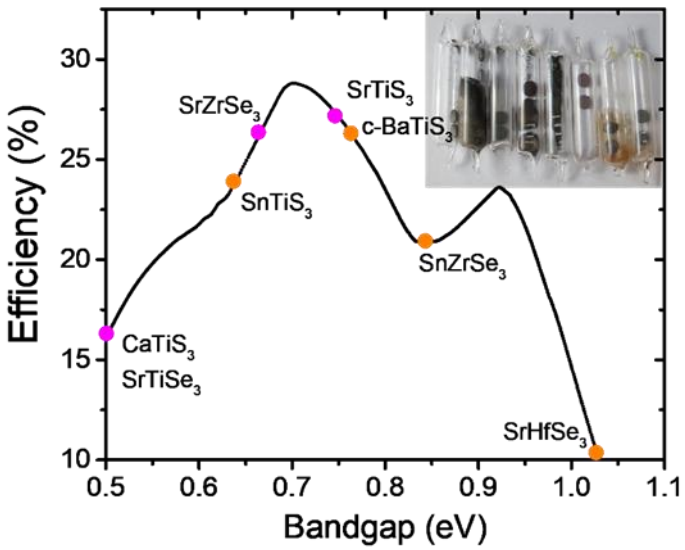

Fig. 1. Power conversion efficiency versus the band gap within Shockleyï Queisser theory under 1.5 AM. Solar radiation with cutoff at 1100 nm. Potential efficiency of chalcogenide-perovskite solar cells based on their band gap.

Among studied compounds, we found that $SrTiS_3$ is stable under ambient conditions, crystalizes into hexagonal (prototype $BaNiO_3$) and non-stoichiometric ($Sr_{1.2}Ti_{0.8}S_3$) structure and with a bang gap at around 0.65 eV. On the other hand, there also other potential chalcogenide-perovskites where chemical composition can be fine-tuned by cationic or anionic substitution to achieve optimal 0.7 eV band gap.

[1] A. Al-Ashouri, E. Kº hnen, B. Li et al. Monolithic perovskite/silicon tandem solar cell with >29% efficiency by enhanced hole extraction, Science **370**, 6522 (2020).
[2] Y.Y. Sun, M. L. Agiorgousis, P. Zhang et al., Chalcogenide Perovskites for Photovoltaics, Nano letters, **15**(1), 581-585

INVESTIGATION OF TWO LUMINESCENCE BANDS IN NONPOLAR InGaN/GaN MULTIPLE QUANTUM WELLS SPECTRA

Elena ValkiÎ naitä, JÎ ras Mickeviļ ius

[1] Institute of Photonics and Nanotechnology, Faculty of Physics, Vilnius University, Lithuania
elena.valkiunaite@ff.vu.stud.lt

Nowadays, InGaN light emitting diodes (LEDs) are widely used for application in solid-state lighting and large area displays. The commercial devices are mostly grown on polar c-plane substrates, however, the optical properties of InGaN quantum wells (QWs) in such devices are strongly affected by the internal electric field along the polar growth direction [1]. Nonpolar (a- or m-plane) InGaN/GaN multiple quantum wells (MQWs) attract attention due to the absence of polarization-related electric field, which should improve the optical performance, and capability to emit highly polarised light [2].

In this work, we present the photoluminescence study of nonpolar InGaN/GaN MQWs with the main focus on the dynamics of double-band structure. We have studied seven (m-plane) InGaN/GaN samples with different indium content or QW width. Samples were grown on sapphire substrates using metalorganic chemical vapor deposition (MOCVD). Measurements were performed under the excitation power density varied from 3.6 W/cm^2 to 13.4 MW/cm^2 in wide temperature range of 8 - 300 K.

The typical double-band PL spectrum of the nonpolar InGaN/GaN samples can be clearly observed at low excitation (3.6 W/m^2) when the lower-energy band dominates (see Fig. 1). As the excitation power density is increased, the higher-energy band grows faster, and the clear separation between the two peaks disappears. Meanwhile, at the highest excitation, the higher energy band0 dominates. Similar behaviour of the two bands is also observed at lower temperatures of 8 K and 150 K. Multiple peaks were also observed in the PL spectra of previously studied polar InGaN/GaN samples.

The nature of the two PL bands is not yet well understood and several interpretations are under consideration: the emission from narrow sidewall MQWs in V-pits [3] or by the slowly decaying tail of the density of states due to potential fluctuations [4]. The observed blue shift of the peaks is attributed to the quantum Stark effect and the filling of the localized states [5]. The simple estimation of quantized energy levels in the InGaN QWs (indicated by the shaded region in Fig. 1) allowed us to attribute the higher-energy PL band to the transitions between the lowest levels. The lower-energy band is then assigned to the recombination of localized carriers.

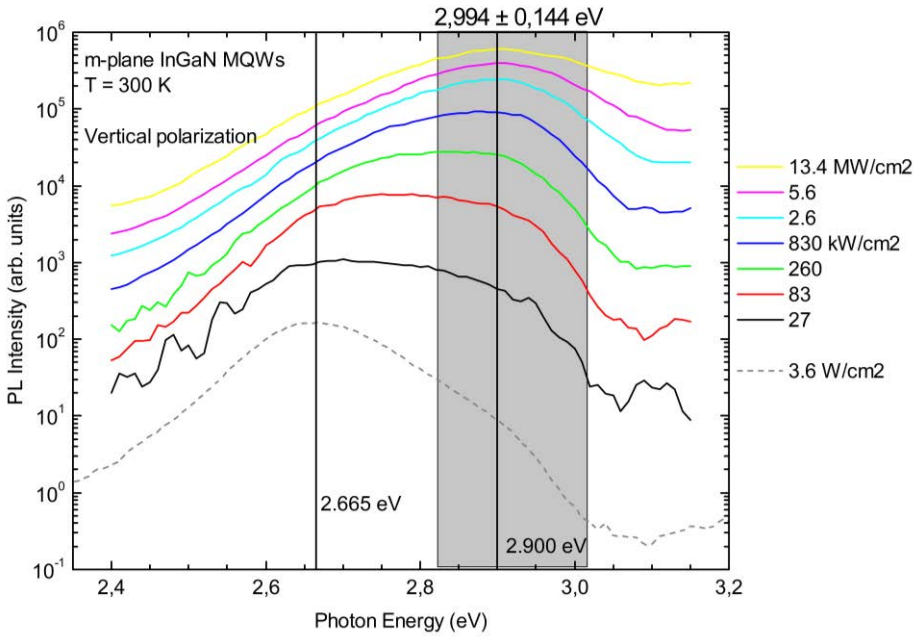

Fig. 1. Luminescence bands of the sample (vertical polarization) dependence on the excitation power density at 300K temperature.

[1] Keller, S. et al. Recent progress in metal-organic chemical vapor deposition of (0001ľ) N-polar group-III nitrides. Semiconductor Science and Technology 29, 113001 (2014)
[2] Tang, F. et al. Microstructural dependency of optical properties of m -plane InGaN multiple quantum wells grown on 2Ámisoriented bulk GaN substrates. Appl. Phys. Lett. 107, 082104 (2015).
[3] Chang, C. Y., Li, H., Shih, Y. T. & Lu, T. C. Manipulation of nanoscale V-pits to optimize internal quantum efficiency of InGaN multiple quantum wells. Appl. Phys. Lett. 106, 091104 (2015).
[4] Sakai, S., Yamaguchi, A. A., Kurihara, K. & Nagao, S. Possible origin of double-peak emission in InGaN quantum wells on m-plane free-standing GaN substrates. in Japanese Journal of Applied Physics 55, 05FG08 (2016).
[5] Li, J., Li, S. & Kang, J. Quantized level transitions and modification in InGaN/GaN multiple quantum wells. Appl. Phys. Lett. 92, 101929 (2008).

MICROSCOPIC LUMINESCENCE PROPERTIES OF VARIOUS POLARITY InGaN QUANTUM STRUCTURES

Mariamija Nikitina

Institute of Photonics and Nanotechnology, Vilnius University, Lithuania
mariamija.nikitina@ff.stud.vu.lt

Non-polar and semi-polar Group-III nitrides are of great interest due to their potentially high quantum efficiency. Photonic devices based on nitride quantum wells (QWs) with reduced or even eliminated internal electric fields demonstrate better quality, specifically better radiation efficiency, charge transport, optical gain; however, spatial variations of light emission still significantly affect the performance of such devices [1]. Therefore, there is a need to investigate in more detail the microscopic-scale optical properties of non-polar quantum structures and their relations with structural quality and growth conditions.

This work is dedicated to investigation of the spatial uniformity of luminescence of InGaN multiple quantum wells grown on different crystallographic planes by Metal Organic Chemical Vapour Deposition (MOCVD) technology. In order to determine InGaN luminescence properties and their correlations with structural defects, Scanning Electron Microscopy (SEM) as well as both spatial- and time- resolved cathodoluminescence (CL) characterization were employed. SEM allows to evaluate defects density at different sample areas, while CL analysis is convenient in order to get an insight into materials properties as bandgap and carrier dynamics with high spatial and temporal resolutions.

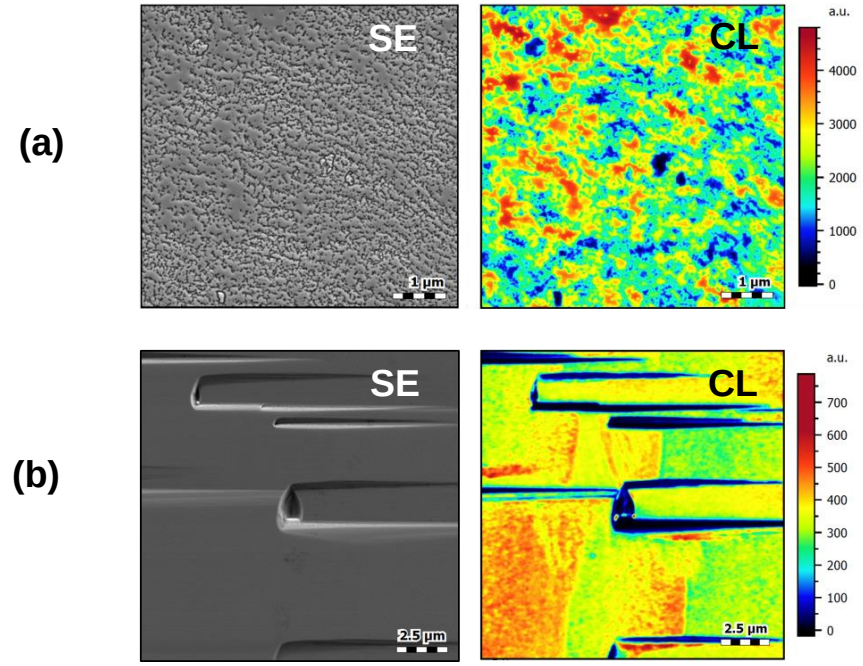

Fig. 1. SE image and the CL intensity distribution at the same area in *c*-plane InGaN MQWs (a); same-area SE image and the CL intensity distribution in *m*-plane InGaN MQWs (b).

The measurements revealed that the spatial distribution of CL intensity is inhomogeneous and correlates with surface topography in both polar and non-polar structures (fig.1). In *c*-plane InGaN quantum wells the luminescence properties are strongly affected by high density of *v*-pits (~10^{10} cm^{-2}) and trench defects. Moreover, the CL decay time shows positive correlation with the emission intensity. In case of *m*-plane sample, the comparison of Secondary Electron (SE) image and CL intensity distribution indicates that scattered step bunches were formed, possibly due to substrate imperfections. In such defects, quantum structures of other than *m*-plane polarity occur, which leads to inhomogeneous Indium distribution and spatial variation in the light emission. Furthermore, the CL decay time in *m*-plane structure did not show such a pronounced correlation with the emission intensity as in polar InGaN.

[1] M. MonOvGriOn, ϕ. RGshidi, Gnd D. Feezell, ñϕ DecGde of NonpolGr Gnd SemipolGr III Nitrides: ϕ Review of Successes Gnd ChGllenges,ò *Phys. stGtus solidi*, vol. 216, no. 1, Dec. 2018.

TEMPERATURE-DEPENDENT PHOTOLUMINESCENCE OF ROCKSALT $Zn_{1-x}Mg_xO$ EPILAYERS

Monika Jokubauskaitã[1], Evelina Dudutienã[1], RamÎnas Nedzinskas[1], Liuwen Chang[2], Mitch Chou[3]

[1]Center for Physical Sciences and Technology, Vilnius, Lithuania
[2]Department of Materials and Optoelectronic Science, National Sun Yet-Sen University, Kaohsiung, Taiwan, ROC
[3]Center of Crystal Research, National Sun Yat-sen University, Kaohsiung, Taiwan
monika.jokubauskaite@ftmc.lt

In thermodynamic equilibrium, the crystal structures of zinc oxide (ZnO) and magnesium oxide (MgO) are hexagonal wurtzite (wz) and cubic rocksalt (rs), respectively. In a ternary compound of ZnMgO both Zn and Mg can be substituted by each other up to ~40% without losing structural stability [1]. ZnMgO solid alloy with a higly-tunable bandgap (from 3.3 eV to 7.8 eV) thus has a great potential for applications of optoelectronics in the deep-ultraviolet spectral region [2]. However, (due to rs-wz phase transformation) it is difficult to grow purely either wurtzite or rocksalt $Zn_{1-x}Mg_xO$ epilayers exhibiting the bandgap energies in the region between 4.3ï 5.4 eV [3]. Nevertheless, it was recently reported that the use of MgO (100) substrate provides ZnO solubility up to 85% sustaining single-phase rocksalt crystal structure. Also, MgO (100) substrate allows for a significantly smaller lattice-mismatch, enhancement of surface roughness and therefore higher optical quality, compared to conventionally used sapphire or Si substrates [4].

This work presents detailed temperature- and excitation- dependent photoluminescence (PL) investigation of rs-ZnMgO epilayers grown on (100) MgO substrate by plasma-assisted molecular beam epitaxy [5]. A set of samples investigated contain six rs-$Zn_{1-x}Mg_xO$ structures with different MgO content of x = 0.15 (sample S22), 0.2 (S18), 0.29 (S20), 0.52 (S16), 0.66 (S6) and 0.76 (S14). PL technique was used to explore interband excitonic and defect related optical transitions in 3-300 K temperature range (see Fig. 1, a). Moreover, activation energies derived from PL measurements provided in-sight into thermal quenching of luminescence processes. Additionally, thermal annealing effect on luminescent properties of $Zn_{0.71}Mg_{0.29}O$ structure (S20) were investigated. It can be observed for the S20 structure (see Fig. 1, b) that thermal annealing (performed at 580 °C and 700 °C temperatures) favors in better optical yield, owing to the reduced density of threading dislocations in these highly-strained rs-ZnMgO thin films [5].

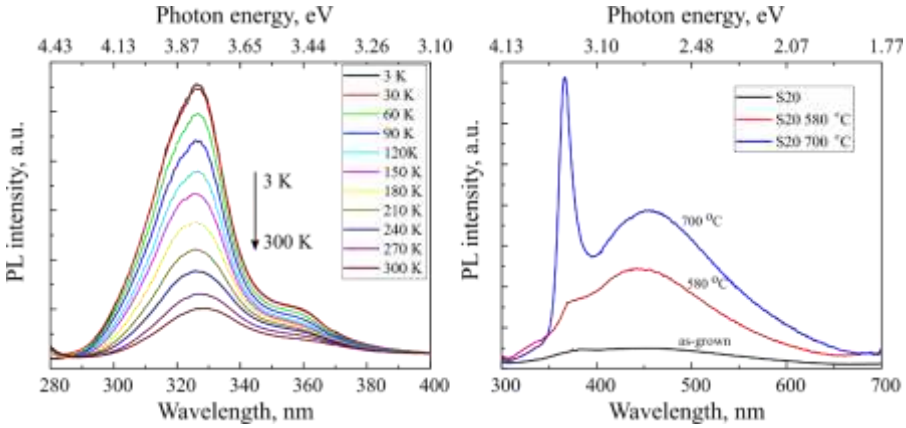

Fig. 1. (a) Temperature-dependent PL spectra of rs-$Zn_{0.24}Mg_{0.76}O$ (sample S14) layer; (b) Room temperature PL spectra of as-grown and annealed $Zn_{0.71}Mg_{0.29}O$ (S20) structures.

Acknowledgments
This work is funded by Taiwan-Latvia-Lithuania Cooperation project No. S-MERA. NET-19-3 òZnMgO materials with tunable band gap for solar-blind UV sensorsò

[1] I. Takeuchi et al., Monolithic multichannel ultraviolet detector arrays and continuous phase evolution in $Mg_xZn_{1ï x}O$ composition spreads. Journal of Applied Physics **94**(11), 7336-7340 (2003).
[2] Gruber, Th, et al. "ZnMgO epilayers and ZnOï ZnMgO quantum wells for optoelectronic applications in the blue and UV spectral region." Applied physics letters **84**(26), 5359-5361 (2004).
[3] H. Tanaka et al., Fabrication of wide-bandgap $Mg_xZn_{1ï x}O$ quasi-ternary alloys by molecular-beam epitaxy, Applied Physics Letters, **86**(19), 192911 (2005).
[4] L. K. Wang et al., Epitaxial growth of high quality cubic MgZnO films on MgO substrate, Journal of crystal growth **312**(7), 875-877 (2010).
[5] M. C. Wen et al., Epitaxial growth of rocksalt $Zn_{1ï x}Mg_xO$ on MgO (100) substrate by molecular beam epitaxy, Journal of Crystal Growth **477**, 169-173 (2017).

TCAD SIMULATIONS OF P-TYPE Si AND $Si_{1-x}Ge_x$ LOW GAIN AVALANCHE DETECTOR CHARACTERISTICS

Kornelijus PÎkas, Tomas Ļeponis, Eugenijus Gaubas

Vilnius University, Faculty of Physics, Institute of Photonics and Nanotechnology
kornelijus.pukas@tmi.vu.lt

Siliconï germanium ($Si_{1-x}Ge_x$) based devices are promising materials for operating in harsh radiation environments. Enhanced radiation tolerance siliconï germanium-based pixel detectors are capable of operating for applications in future Large Hadron Collider (LHC) [1]. Nevertheless, it is difficult to grow bulk SiGe single-crystals with intermediate Ge content due to differences in the physical properties of silicon and germanium. It has been determined that $Si_{1-x}Ge_x$ single-crystals can only be obtained for containing either $0 < x < 0.1$ or $0.85 < x < 1$ of Ge when using the Czochralski technique. For the other *x* range of Ge content this alloy usually becomes a polycrystalline material. The radiation induced deep carrier traps determine the changes of semiconductor particle detector characteristics. Impurities, such as carbon or oxygen, are also important in formation of radiation-induced deep traps. It was revealed that the carbonï oxygen metastable complexes (C_iO_i*) were transformed into the stable-state complexes (C_iO_i) under 125ęC annealing for 15 min of the irradiated $Si_{1-x}Ge_x$ detectors [2].

In this work, simulations of electrical characteristics of the Low Gain Avalanche Diodes (LGAD) made of both p−type silicon and silicon-germanium $Si_{1-x}Ge_x$ with different Ge content materials were performed by Technology of Computer-Aided Design (TCAD) means. The functionality of the LGAD devices has been validated by digital experiments performed using TCAD algorithms and the Drift-Diffusion (DD) approach. Simulations have been carried out employing a Sentaurus Device software platform. Conventional p-type LGAD consists of $N^+PP^-P^+$ layers with p-well formed by deep diffusion of boron (B) during formation of the p-layer. The parameters of traps in silicon and silicon-germanium were borrowed from literature data. The structure of both material diodes were designed using the identical dimensions, the same concentrations of dopants and the same origin of traps in order to compare the characteristics of Si and SiGe LGADs. Ge content has been varied in the range from 1% to 10%.

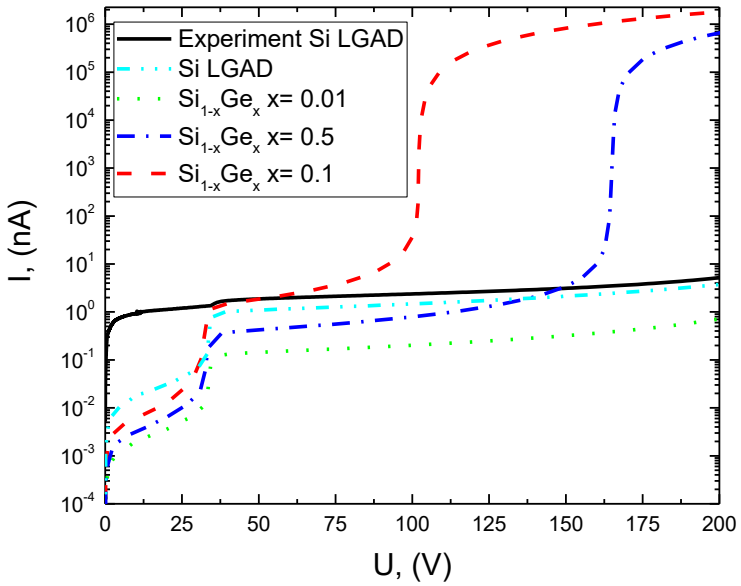

Fig. 1. Comparison of the simulated I-V characteristics of Si and different *x* $Si_{1-x}Ge_x$ p-type LGADs.

The simulations revealed the lower values of dark current in $Si_{1-x}Ge_x$ LGAD structure containing 1% Ge content compared with pure Si LGAD structure. However, the higher concentrations of Ge in the SiGe LGAD structures caused the higher dark current values compared with the pure silicon LGAD. LGAD structures containing traps exhibit the higher dark current values in I-V characteristics for both Si and SiGe trap-less structures. The current pulses in Si LGAD response transients showed the elongation of the carrier extraction durations with enhancement of the trap concentration. This could be caused by carrier trapping effect due to deep emission centers.

[1] High Luminosity LHC Project. Available online: https://hilumilhc.web.cern.ch/ (accessed on11 November 2020).
[2] T. Ļeponis, S. Lastovskii, E. Gaubas et al., Study of Radiation-Induced Defects in p-Type $Si_{1-x}Ge_x$ Diodes before and after Annealing, Materials **13**, 5684 (2020).

PHOTOLUMINESCENCE STUDIES OF GaN EPITAXIAL LAYERS

Aleksandra Širvinskytė[1], Jūras Mickevičius[1]

[1] Institute of Photonics and Nanotechnology, Vilnius University, Vilnius, Lithuania
aleksandra.sirvinskyte@ff.stud.vu.lt

GaN and related alloys are materials widely used for applications in optical and electronic devices, such as light-emitting diodes (LEDs), laser diodes (LDs), and high-electron mobility transistors (HEMTs). GaN has been the most intensively studied in III-nitride materials due to relatively simpler growth technology, while the recombination processes are not obscured by the carrier localization. However, there are still challenges in understanding and modelling the radiative and nonradiative mechanisms, which play a key role in emission efficiency, efficiency droop in GaN-based LEDs [1] and threshold current of LDs. In this study, the recombination dynamics in GaN films were analysed by using excitation-dependent photoluminescence (PL) measurements.

The GaN epitaxial layers under study were grown on sapphire substrate by metalorganic chemical vapor deposition (MOCVD). Samples exhibiting different background carrier concentrations and carrier lifetimes were studied. The 4th harmonic (266 nm) of a nanosecond YAG:Nd laser radiation was used to excite the samples in a wide range of excitation power densities from 100 W/cm^2 up to 10 MW/cm^2. Luminescence signal was registered by ICCD camera. All measurements were performed at room temperature.

The typical behavior of GaN PL spectra at different excitation power densities is presented in Fig. 1(a) for one sample. Similar spectra families were obtained for all samples under study. The integrated PL intensity dependence on excitation power density is shown as dots in Fig. 1(b) and reveals rapid PL intensity increase at low excitations, and saturation of PL intensity at the highest excitation power densities. To analyze the recombination processes in GaN in more detail, numerical modeling of the excitation-dependent PL intensity was carried out using the model described by Brandt et al. [2] and performed by using Python 3.8 programming language. Modeling results were compared to the experimentally obtained results. Good fit was obtained in high excitation region. The disagreement at low excitations indicates either the inadequate choice of parameters or the importance of ignored recombination mechanisms, and requires further analysis.

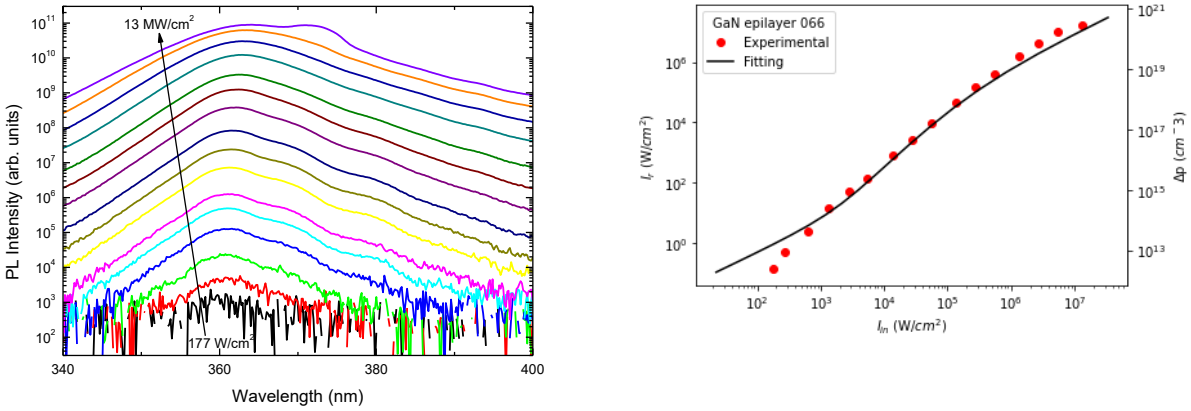

Fig. 1. (a) PL spectra of GaN sample 066 at different excitation power densities (177 W/cm^2 – 13 MW/cm^2). (b) Excitation dependence of integrated PL intensity (dots) and modeling results (line) of GaN sample 066.

[1] Piprek, J. Efficiency models for GaN-based light-emitting diodes: Status and challenges. *Materials* **13**, 1–18 (2020).
[2] Brandt, O., Yang, H. & Ploog, K. H. Impact of recombination centers on the spontaneous emission of semiconductors under steady-state and transient conditions. *Phys. Rev. B - Condens. Matter Mater. Phys.* **54**, R5215–R5218 (1996).

MODELING OF P-N JUNCTION OF III GROUP NITRIDE BY FINITE DIFFERENCE METHOD

Kristupas Razas, Tomas Grinys

Institute of Photonics and Nanotechnology, Vilnius University
kristupas.razas@ff.vu.lt

This work aims at detailed examination and modeling of p-n junction of III group nitrides.

We analyzed experimental IV curves of planar structure prepared by metal original chemical vapor deposition (MOCVD) equipment. The equivalent scheme consisting of a diode, and two resistances connected in parallel and series way was applied to fit the IV curves.

It was assumed the current in p-n junction diode is due to two components: space-charge region(scr) recombination/generation and quasi-neutral region (qnr) recombination/generation.

The modeling of p-n junction was performed by finite difference method. The equations of Poisson's, current-density, continuity including equations describing radiative and nonradiative recombination of charge carriers were applied in the model. The band diagram, carrier density and IV curve was extracted from model.

We compared the theoretical IV curve to the experimental one. The received data will be useful for the further optimization of device structure.

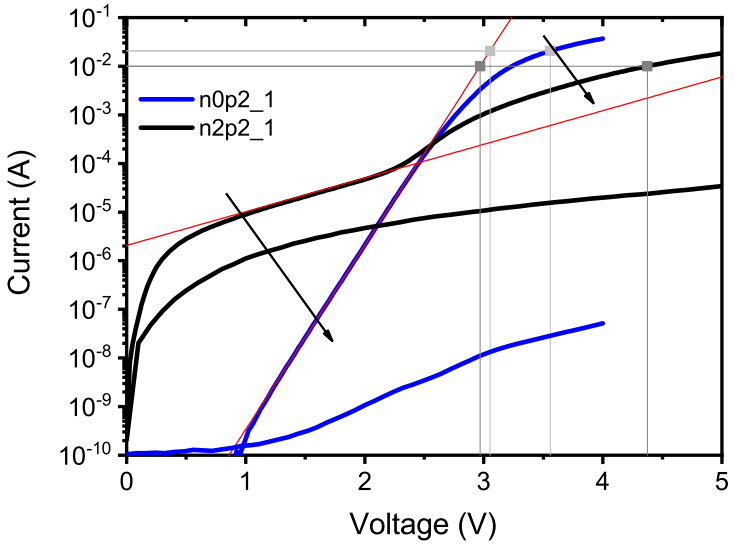

Fig. 1. Experimental IV curves. Arrows show the direction of increase resistance in low current and high current range respectively.

HOT CARRIER EVIDENCE IN A SOLAR CELL

Jonas Gradauskas[1,2], Steponas Ašmontas[1], Algirdas Sužiedėlis[1], Aldis Šilėnas[1], Aurimas Čerškus[1,2], Ovidijus Žalys[1], Oleksandr Masalskyi[2]

[1] Center for Physical sciences and Technology, Lithuania
[2] Vilnius Gediminas Technical University, Lithuania
oleksandr.masalskyi@vgtu.lt

The Shockley-Queisser theory puts limits on conversion efficiency of a single-junction solar cell [1]. It assumes that only photons having energy close to a semiconductor forbidden energy gap are used effectively in the formation of an electrical output signal. Lower energy photons are not absorbed at all, while the residual extra energy of the higher energy photons is reckoned in only through the process of carrier thermalization.

Our investigation is initiated by our confidence that photons having energy larger than the band gap as well as photons having energy smaller than the forbidden energy gap need to be accounted through the hot carrier phenomena participating in the photoresponse formation before the lattice heating.

GaAs p-n-junction was illuminated with 25 ns-long laser pulses of 1.06 μm wavelength. Short enough pulse and the wavelength opened a way to reveal that the induced photoresponse consists of three components. The first one, U_G, is an electron-hole pair generation caused component resulting from the multiphoton absorption [2]. The second one, U_{HC}, follows the laser pulse shape and has opposite polarity, it is caused by the heating of free carriers. The third one, U_T, has the same polarity as U_{HC} but is much slower and is caused by the heating of a p-n junction.

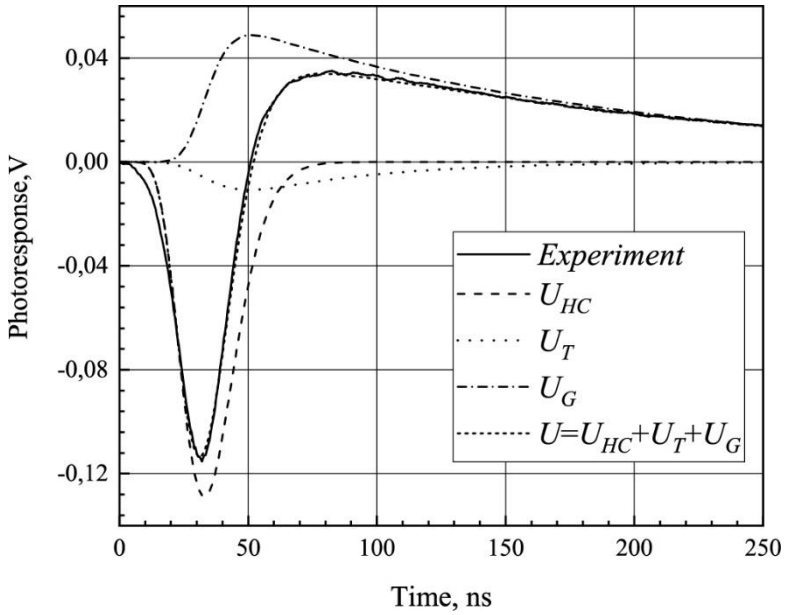

Fig. 1. Experimental photoresponse across GaAs p-n junction and modelled its components.

In addition to the experimental evidence of the hot carrier photoresponse, we propose a theoretical model of separation of the photoresponse components which gives good agreement with the experimental [3]. The model enables to reveal contribution of each component to the net magnitude of the photoresponse and opens the possibility to find the way of reducing the negative impact of hot carrier phenomena to the conversion efficiency of a solar cell.

[1] W. Shockley and H. J. Queisser, Detailed balance limit of efficiency of p–n junction solar cells, J. Appl. Phys. **32**, 510-519 (1961).

[2] W. C. Hurlbut, Y.-S. Lee, K. L. Vodopyanov et al., Multiphoton absorption and nonlinear refraction of GaAs in the mid-infrared, Opt. Lett. **32**, 668-670 (2007).

[3] J. Gradauskas, S. Ašmontas, A. Sužiedėlis et al., Unfolding hot carrier impact in photovoltage across a p-n junction, Appl. Sci. **10**, 1-8 (2020).

TRIPLET EXCITON DIFFUSION IN PHOTON UPCONVERTING RUBRENE FILMS

Manvydas Dapkeviļius[1], Edvinas Radiunas[1], Saulius Jurgėnas[1], Steponas Raigys[1], Karolis Kazlauskas[1]

[1]Institute of Photonics and Nanotechnology, Vilnius University, Lithuania
manvydas.dapkevicius@ff.vu.lt

Photon upconversion (UC) through triplet-triplet annihilation is a phenomenon that finds many possible applications e.g. to increase solar cell efficiency,[1] to activate proteins inside organic tissue,[2] to enhance bio-imaging capability [3] and many others [4]. Rubrene is an excellent choice for near infrared to visible light UC, since it features low triplet energy and efficient photoluminescence (PL), which allows reaching UC quantum yield (UCQY) up to 5.6% in toluene solution [5]. However, solid-state UC rubrene systems show drastically reduced UCQY efficiency [6]. Although all the factors limiting UCQY are still unclear, the aggregation induced PL quenching and inefficient triplet exciton diffusion are the most likely ones. Reduced concentration of the annihilator may prevent quenching, however, it would also restrict exciton diffusion and hence lower the probability for triplet excitons to encounter. Therefore, the determination of diffusion length (L_D) of triplet excitons and evaluation of its influence on UC performance is of crucial importance.

In this work, triplet exciton diffusion in polystyrene (PS) films containing rubrene as an annihilator, palladium phthalocyanine (PdPc) as a triplet exciton sensitizer and tetraphenyldibenzoperiflanthene (DBP) as emitter was investigated. The films were prepared by spin coating under N_2 environment and encapsulated to protect films from ambient air during photophysical characterization. Triplet exciton diffusion was determined from the PL quenching efficiency in the rubrene/PS/PdPc and rubrene/PS/PdPc/DBP films with randomly distributed quenchers. Stern-Volmer analysis were applied to analyze excited state relaxation dynamics (Figure 1) of UC films with increasing quencher concentration (0.0 ï 0.3 wt%) for the evaluation of L_D.

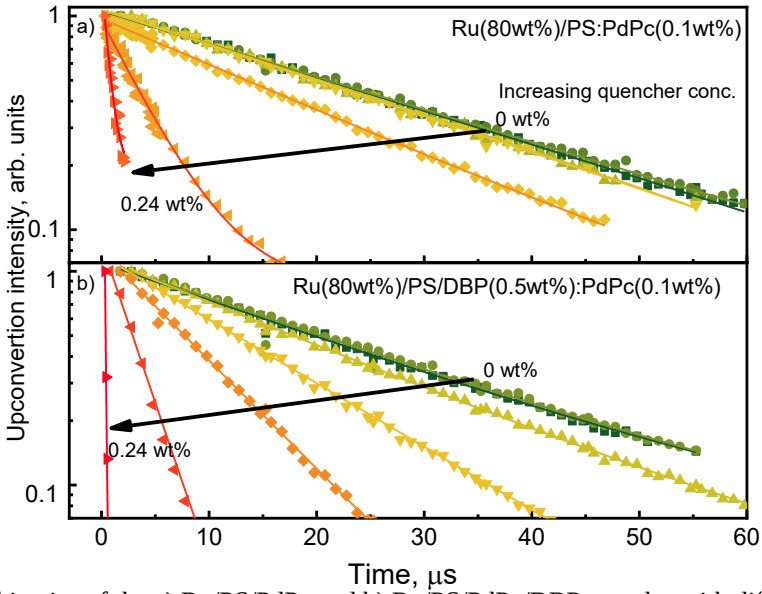

Fig. 1. UC kinetics of the a) Ru/PS/PdPc and b) Ru/PS/PdPc/DBP samples with different chloranil quencher concentration.

The obtained results revealed that triplet exciton diffusion length in both rubrene/PS/PdPc and rubrene/PS/PdPc/DBP films is ~22 nm. It was found that estimated L_D is close to the average distance between sensitizer molecules suggesting that UC performance in rubrene UC films, to some extent, is triplet exciton diffusion limited process.

[1] A. Nattestad, Y.-Y. Cheng, R.-W. MacQueen, et al., Dye-sensitized solar cell with integrated tripletï triplet annihilation upconversion system, J. Phys. Chem. Lett. **4**, 2073-2078 (2013).
[2] S.-H.-C. Askes, M.-S. Meijer, T. Bouwens, et al., Red light activation of Ru(II) polypyridyl prodrugs via triplet-triplet annihilation upconversion: feasibility in air and through meat, Molecules **21**, 1460 (2016).
[3] F. Liu, T. Yang, W. Feng, et al., Blue-emissive upconversion nanoparticles for low-power-excited bioimaging in vivo, J. Am. Chem. Soc. **134**, 5390-5397 (2012).
[4] J. Zhou, Q. Liu, W. Feng, et al., Upconversion luminescent materials: advances and applications, Chem. Rev. **115**, 395-465 (2014).
[5] E. Radiunas, S. Raigys, S. Jurgėnas, et al., Understanding the limitations of NIR-to-visible photon upconversion in phthalocyanine-sensitized rubrene systems, J. Mat. Chem. **8**, 5525-5534 (2020).
[6] E. Radiunas, M. Dapkeviļius, S. Raigys, et al., Impact of t-butyl substitution in a rubrene emitter for solid state NIR-to-visible photon upconversion, Phys. Chem. Chem. Phys. **22**, 7392-7403 (2020).

HYPERSPECTRAL IMAGING TECHNOLOGY WITH A SMARTPHONE AND MULTICOLOUR FLASH

Lukas Matulis and Pranciğkus Vitta

Institute of Photonics and Nanotechnology, Faculty of Physics, Vilnius University,
Saulãtekio av. 3, Vilnius, Lithuania
lukas.matulis@ff.stud.vu.lt

International research data shows that due to the counterfeiting of products in 2017, global producer losses reached 1.2 trillion dollars and up to 1.82 trillion in 2020. This forecast covers the full range of products from pharmaceuticals to watches and consumer products. Currently, available security (anticounterfeiting) technologies have limited efficiency or are extremely sophisticated and expensive. Therefore, we propose a novel approach helping the manufacturers and users to protect themselves against counterfeit goods on the market by employing hyperspectral imaging technology based on a smartphone and multicolour (5-10 colours) flash. Dedicated software (application) synchronizes the operation of the camera and flash and shoot the same image under different lighting conditions. Superposition of narrow spectra illumination and camera sensor response functions results in an increased spectral resolution of the resulting image stack. Furthermore, as it is intended to include UV and IR illumination, this will extend the effective wavelength range and include fluorescence -up and -down conversion spectra of dedicated security ink and/or conventional polygraphy. Such a technique would be incomparably simpler and cheaper than analytical laboratory equipment and would allow the authentication to be brought closer to the end-user.

For the experimental trials, a smartphone Samsung Galaxy Note 10 Lite, capable to take photos in RAW format (.DNG), was used. Image J Fiji software was used to perform spectral image analysis, calibration and initial analysis. Sample colour prints printed by different commercial printers were analysed by recording diffuse reflectance. Sample reflectance spectra are presented in Fig. 1., and one can see that the different printers, performing ñthe sameò colour result in different reflectance spectra which is almost indistinguishable by the naked eye but can be detected by hyperspectral imaging device.

We conclude that almost any consumer-grade camera can be transformed into the hyperspectral imaging device by adding smart multicolour flash. Such a system could have a vast applicability and anticounterfeiting is just one of the application areas.

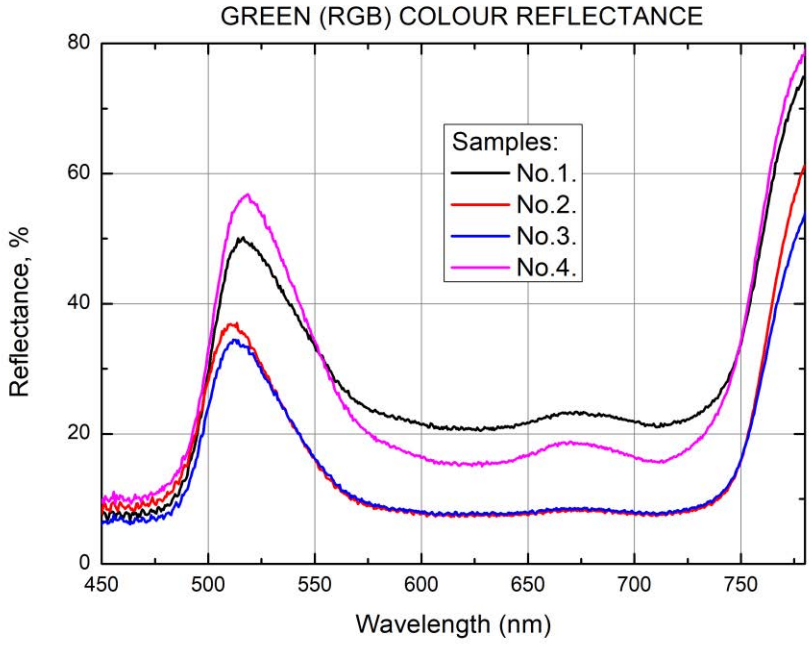

Fig.1. The reflectance of ñPure Greenò colour samples printed by different printers on different paper.

P4-23

DID NOT PARTICIPATE

OPTOELECTRONIC PROPERTIES OF GERMANIUM-TIN LAYER

Vaiva Soriūtė[1], Patrik Ščajev[1], Pavels Onufrijevs[2], Arturs Medvids[2], Hung-Hsiang Cheng[3]

[1] Institute of Photonics and Nanotechnology, Vilnius University, Sauletekio al. 3, LT 10257, Vilnius, Lithuania
[2] Institute of Technical Physics, Faculty of Materials Science and Applied Chemistry, Riga Technical University, P. Valdena 3/7, Riga, LV-1048, Latvia
[3] Center for Condensed Matter Sciences and Graduate Institute of Electronic Engineering, National Taiwan University, Roosevlet Road No 1, Section 4, Taipei 10617, Taiwan
vaiva.soriute@gmail.com

Silicon has been dominating the market of electronic and photonic devices for several decades [1]. However, mid-IR photodetectors and lasers have been recently gaining more attention due to their applicability in military, medicine and night vision and those devices require Si emission to be shifted to mid-IR. Germanium-tin (GeSn) alloy is a highly promising material for such purposes since it is compatible with silicon technology, direct energy bandgap can be achieved in this material when Sn content reaches 6-8% and GeSn absorption and emission can be shifted to mid-IR by increasing Sn content in the alloy [2]. Because of these desirable properties GeSn photodetectors, LEDs, lasers and various transistors such as MOSFETs and TFETs were created [3]. However, not all GeSn properties are well known and understood and therefore they require further research.

In this work carrier lifetime, diffusion coefficient and diffusion length in $Ge_{0.95}Sn_{0.05}$ epilayer grown on Si substrate were studied. These important optoelectronic parameters were determined using light induced transient grating technique. The sample was excited by pulsed laser irradiation at 527 nm wavelength which created transient grating in the layer. It caused the probe beam (1053 nm) to diffract and by using an optical delay line diffraction efficiency (η) decays were obtained. They were measured at three different grating periods Λ (Fig. 1 (a)). This allowed us to determine carrier lifetime (τ_R) and diffusion coefficient (D) using Eq. (1), while diffusion length was later calculated from these parameters. Nitrogen cryostat was used to obtain temperature dependence.

$$\frac{1}{\tau} = \frac{1}{\tau_R} + \frac{1}{\tau_D} = \frac{1}{\tau_R} + \frac{4\pi^2 D}{\Lambda^2} \quad (1)$$

In Fig. 1 (b) it can be seen that diffusion coefficient decreases with temperature. It is attributed to increased phonon and defect scattering. Weak excitation dependences of the parameters are related to saturated trap regime. Also, the value of diffusion coefficient is lower than that of pure germanium $D_a = 68\ \frac{cm^2}{s}$ which indicates that incorporating Sn causes worse material quality.

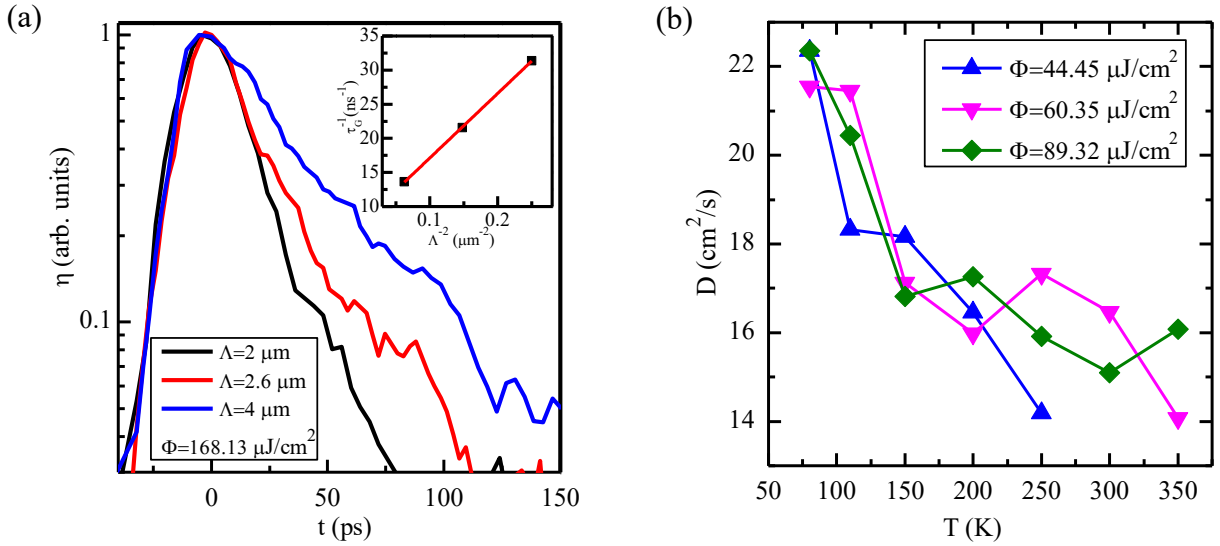

Fig. 1. (a) LITG transients measured at three different grating periods Λ, inset shows angular plot $^1/_\tau \sim {}^1/_{\Lambda^2}$. (b) Diffusion coefficient D temperature dependence [4].

[1] V. Narayanan, M. M. Frank, A. A. Demkov, Thin Films on Silicon: Electronic and Photonic Applications, Series "Materials and Energy" (World Scientific Publishing, Singapore, 2016), Vol. 8.
[2] S. Wirths *et. al.,* Si–Ge–Sn Alloys: From Growth to Applications. Progress in Crystal Growth and Characterization of Materials 62(1), 1-39 (2016).
[3] J. Zheng *et al.,* Recent Progress in GeSn Growth and GeSn-based Photonic Devices. J. Semicond. 39, 061006 (2018)
[4] P. Ščajev *et al.,* Temperature Dependent Carrier Lifetime, Diffusion Coefficient, and Diffusion Length in Ge0.95Sn0.05 Epilayer. Journal of Applied Physics 128, 115701 (2020)

OPTICAL FREQUENCY CONVERSION TO VISIBLE AND NEAR-IR RANGES USING PHOTONIC CRYSTAL FIBERS

Gustas Liaugminas[1], Julijanas Çeludeviļius[1], Kňstutis Regelskis[1]

[1] Department of Laser Technology, Center for Physical Sciences and Technology, Lithuania
gustas.liaugminas@ftmc.lt

Near-IR and visible range fiber lasers find many applications in biomedicine and atmosphere monitoring [1, 2]. However, wavelengths that can be generated from these laser sources are often limited by amplifying medium which is chosen. Degenerate four-wave mixing allows to convert optical frequency of two pump photons into two photons of different wavelength in a third-order non-linearity medium. For this to happen energy conservation and phase-matching conditions should be satisfied [3]. Phase-matching conditions can be met while operating near zero-dispersion wavelength but can be hardly satisfied in ordinary fused silica fibers. In photonic crystal fibers (PCF), on the other hand, dispersion curve can be tailored by designing specific hole structure around the fiber core thus allowing different phase-matching scenarios for different pump wavelengths and extending available wavelength range.

In this work we used a pulsed fiber laser as our pump source to produce 200 ps duration, 1038 nm wavelength pulses at 100 kHz repetition rate . Pulses from the fiber laser are then amplified in two fiber amplifier stages and a final Yb-doped large-mode-area polarization-maintaining fiber amplifier stage to achieve sufficient peak power for frequency conversion. Amplified pulses were coupled to PCF under test using standard aspheric lenses.

In this experiment we used two different commercially available photonic crystal fibers (SC-5.0-1040 and LMA 8), both having different dispersion curves, therefore, different phase-matched wavelengths for the same pump. For SC-5.0-1040 fiber, two waves were observed: signal at 993 nm (with maximum average power of 1,266 mW and 16,54% conversion efficiency) and idler at 1087 nm (with maximum average power of 0,866 mW and 15,74% conversion efficiency). For LMA 8 fiber, signal wave at 648 nm (maximum average power 260 mW, and 31% conversion efficiency) was observed but idler, expected at 2759 nm, could not be detected due to limitation of spectrum analyzer. All of the generated wavelengths for both PCFôs accurately match the wavelengths calculated from phase matching relations using specified dispersion characteristics of the fibers.

Results from this experiment show potential for photonic crystal fibers to be used for optical frequency conversion in applications where no laser medium is available but a specific wavelength is required. These results will be used in further development of all-fiber ultrashort pulse laser system operating in a broad wavelength range.

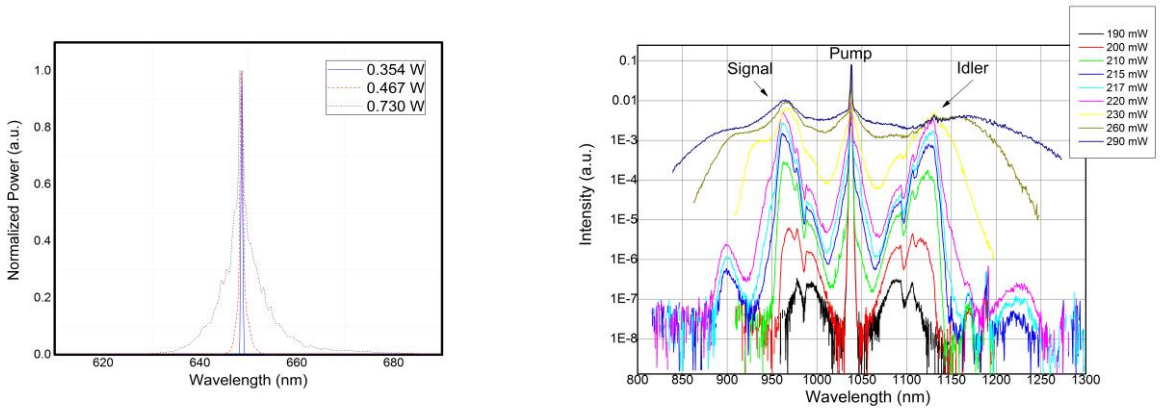

Fig. 1. Spectrums of four-wave mixing products for different photonic crystal fibers: signal wave in LMA 8 (left), signal, pump and idler waves in SC-5.0-1040 (right)

[1] T. Gottschall, T. Meyer, M. Schmitt, J. Popp, J. Limpert, and A. T¿nnermann, Four-wave-mixing-based optical parametric oscillator delivering energetic, tunable, chirped femtosecond pulses for non-linear biomedical applications, Opt. Express **23** (18), 23968ï 23977 (2015)[2] A. Fried, Tunable infrared laser instruments for airborne atmospheric studies, Appl. Phys. B, vol. **92**, no. 3, 409ï 417 (2008)
[3] G. P. Agrawal, *Nonlinear Fiber Optics* (Academic, 2001)

P4-26

DID NOT PARTICIPATE

HIGH REPETITION RATE LASER-INDUCED PERIODIC STRUCTURES IN TRANSPARENT DIELECTRIC MATERIALS

Marius Navickas[1], Robertas Grigutis[1], Gintaras Tamošauskas[1], Vytautas Jukna[1], Audrius Dubietis[1]

[1]Laser Research Center, Vilnius University, Saulėtekio av. 10, LT-10223, Vilnius, Lithuania
marius.navickas@ff.vu.lt

Irradiation of transparent materials with femtosecond laser pulses at high repetition rate induces so called self-organized quasiperiodic nanostructures at its surface [1]. In addition, this type of material modification depends on the exposure time or a number of accumulated laser pulses. Low exposure time produces quasiperiodic structures, the so-called nano-ripples. By further increasing the exposure time, the formation of microgrooves can be observed. In this case, the nanostructures reminds the cornflake-like structures with quasiperiodic ordering. In the sequel, the higher exposure time is responsible for the formation of another type modification – laser induced periodic annular surface structures (LIPASS), containing the damage crater in the center and superimposed periodic rings around [2]. Note that such transition is universal, observed in many dielectric bulk materials and can be applied in a broad range of applications including plasmonics, photonics and microfluidics [3].

In this work we investigate the laser-induced periodic nanotructures at high repetition rate of femtosecond laser pulses in sapphire, YAG, MgF_2 and fused silica. The experiments were performed using Yb:KGW laser (Pharos, Light Conversion), with 180 fs FWHM pulse duration, operating at 1035 nm central wavelength and repetition rate of 200 kHz. To investigate laser induced structural changes we used PrismaSEM scanning electron microscope (SEM). Fig. 1 (a) shows SEM image of LIPASS on sapphire surface irradiated by 10^4 consecutive pulses and Fig. 1 (b) represents its frequency spectrum retrieved by 2D Fourier transform. The experimental results revealed that the formation of nanostructures in bulk materials is a universal process producing exposure time dependent periods of the structures as presented in Fig. 1 (c). By using the low number of pulses, high spatial frequencies are dominant, while the low spatial frequencies are obtained by irradiating with high number of pulses. In addition, such a behaviour can be observed in many other materials such as alkali metal-fluorides and fused silica. Furthermore, femtosecond laser pulses produces very similar structures in materials volume [4]. Such a phenomenon is accompanied by the appearance of the conical third harmonic (TH) indicating the multipulse optical damage [5]. Note that TH generation can be understood in the frame of four-wave mixing process, requiring to fulfill the transverse phase matching (PM) condition. Also, we show that such condition can be satisfied via reciprocal lattice vector involving the nanograting period. Indeed, the two-dimensional Fourier transform of the SEM image yields a broad distribution of nanograting periods, including the required period to satisfy the transverse the PM condition.

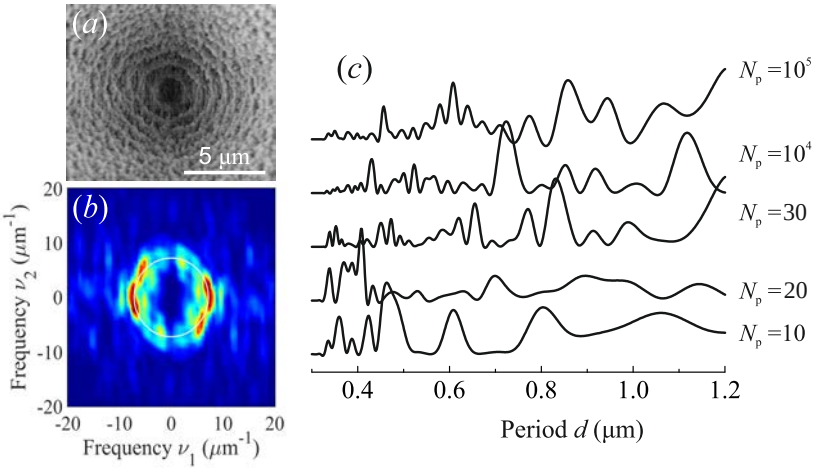

Fig. 1. (a) SEM image of LIPASS in sapphire, produced with 10^4 pulses at 200 kHz repetition rate, (b) Fourier transform of the SEM image and (c) period spectra of produced nanostructures with different number of pulses. The white circle in (b) marks the spatial frequencies required to fulfill the transverse phase matching condition for TH generation. Here $d = 2\pi/\nu_s$, where ν_s is a spatial frequency.

[1] M. J. Bonse, J. Krüger, S. Höhm et al., Femtosecond laser induced periodic surface structures, Journal of laser applications **24**, 1–5 (2012).
[2] Y. Liu, Y. Brelet, Z. He et al., Laser-induced periodic annular surface structures on fused silica surface, Applied physics letters **102**, 1–4 (2013).
[3] R. Buividas, M. Mikutis, S. Juodkazis et al., Surface and bulk structuring of materials by ripples with long and short laser pulses: Recent advances, Progress in quantum electronics **38**, 119–156 (2014).
[4] A. Rudenko, J.-P. Colombier, S. Höhm et al., Spontaneous periodic ordering on the surface and in the bulk of dielectrics irradiated by ultrafast laser: a shared electromagnetic origin, Science reports **7**, 1–14 (2017).
[5] R. Grigutis, G. Tamošauskas, V. Jukna et al., Supercontinuum generation and optical damage of sapphire and YAG at high repetition rates, Optics letters **45**, 4507–4510 (2020).

LASER MICRO-MACHINING OF TRANSPARENT MATERIAL WITH BESSEL BEAMS GENERATED BY SPATIALLY DISPLACED AXICONS

Ernestas Nacius[1,2], Benas Stanionis[1,2], Pavel Gotovski[1,3], Orestas Ulčinas[1,2], Sergej Orlov[1], Vytautas Jukna[1,4]

[1]Center for Physical Sciences and Technology, Coherent Optics laboratory, Saulėtekio Avenue 3, Vilnius, Lithuania, 10257

[2]Workshop of Photonics, Mokslininku str., 6A, Vilnius, Lithuania, 08412

[3]Faculty of Electronics, Vilnius Gediminas Technical University, Naugarduko str. 41, LT-03227 Vilnius, Lithuania

[4]Laser Research Center, Vilnius University, Saulėtekio Avenue 10, LT-10223 Vilnius, Lithuania

ernestas.nacius@ftmc.lt

Bessel-Gauss beams have attracted much attention in laser micro-fabrication of transparent materials due to elongated focal zone and that is very attractive in various laser micro-machining applications where high width/depth ratio is needed. Compared to the Gaussian beam, the Bessel-Gauss beam is much more efficient in single shot micro-channel fabrication [1] or in cutting of various glasses up to a few millimeters thick [2]. Most commonly adapted Bessel-Gauss shaping element in lab is an axicon - a conical lens with sharp tip at the center. Despite the straightforwardness of axicon applicability, the element must have close to perfect shape quality, because any irregularities of its surface and especially a rounded tip greatly reduces the quality of the generated beam by inducing unwanted axial intensity modulations along the focal zone [3]. Some alternative beam shaping methods have emerged to substitute refractive axicons to increase the overall quality of the beam or create more complex patterns - from diffractive optical elements (DOEs), spatial light modulators to complex sub-wavelength metasurfaces [4, 5]. Freedom of choosing Bessel-Gauss beam generation method allows to fit in various specific beam shaping applications, thus the only limiting factors of element price or optical damage thresholds remain. Another type beam shaping element can be created by implementing birefringent nanogratings inscribed in bulk of fused silica [6]. Direct laser written nanogratings can have controllable retardance and orientation (fast axis) enabling to manufacture custom flat optical elements, usually named after geometric phase optical elements (GPOEs).

In this work we use geometric phase optical elements to create custom displaced phase axicons that form modified Bessel-Gauss beams (manufactured by Workshop of Photonics). With numerical simulation and experimental work, we present practical applications of the generated beams in transparent material laser micro-fabrication. Physical phase displacement allows to create new and fanciful patterns of Bessel-Gauss beams, varying from single elongated peak to multi-peaked intensity patterns. Taking advantage of high optical damage threshold of geometric phase optical elements, we demonstrate thin glass processing with high-peak power ultra-short pulse laser.

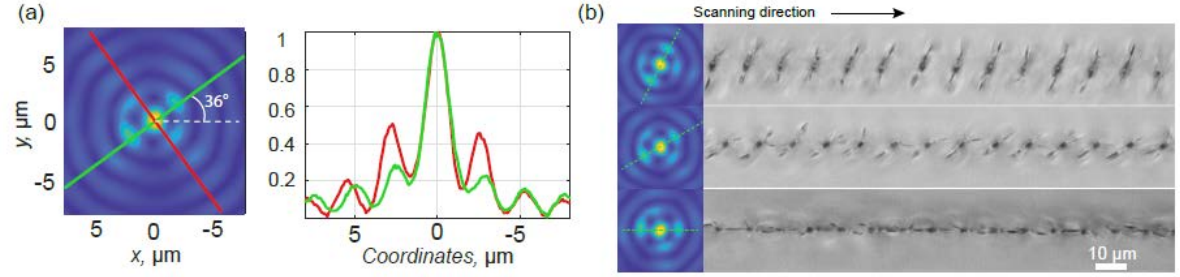

Fig. 1. (a) Intensity distribution of modified Bessel-Gauss beam, produced by geometric phase optical element. Red and green lines represent intensity profiles. (b) Images by optical microscope of dependence of volume micro-crack orientation on rotation of the intensity profile of the beam, pulses with energy of 240 µJ and 4 ps duration were used.

[1] J. Baltrukonis, O. Ulčinas, S. Orlov, and V. Jukna "Void and micro-crack generation in transparent materials with high-energy first-order vector Bessel beam", J. Opt. Soc. Am. **B37**, 2121–2127 (2020).

[2] R. Meyer, M. Jacquot, R. Giust, J. Safioui, L. Rapp, L. Furfaro, P.-A. Lacourt, J. Dudley and F. Courvoisier "Single shot ultrafast laser processing of high-aspect ratio nanochannels using elliptical Bessel beams", Optics Letters **42** 21 (2017).

[3] O. Brzobohatý, T. Čižmár and P. Zemánek "High quality quasi-Bessel beam generated by round-tip axicon", Opt. Express **16**, 12688–12700 (2008).

[4] A. Vasara, J. Turunen and A. T. Friberg "Realization of general nondiffracting beams with computer-generated holograms", J. Opt. Soc. Am. **A6**, 1748–1754 (1989).

[5] D. Lin, P. Fan, E. Hasman and M. Brongersma "Dielectric gradient metasurface optical elements", Science (New York, N.Y.) **345**, 298–302 (2014).

[6] Y. Shimotsuma, P. G. Kazansky, J. Qiu and K. Hirao "Self-organized nanogratings in glass irradiated by ultrashort light pulses", Phys. Rev. Lett. **91**, 247405 (2003).

Nd:YVO_4 AMPLIFIERS SEEDED WITH Nd:YAP AND Nd:YVO_4 LASER PULSES AT 1.34 Õm FOR NON-INVASIVE BLOOD DIAGNOSTICS

Rycard Lebed and Aleksej M. Rodin

Solid State Lasers Laboratory, Department of Laser Technologies, Center for Physical Sciences and Technology, Savanoriu 231, LT-02300 Vilnius, Lithuania
rycard.lebed@ff.stud.vu.lt

Fast, accurate and inexpensive medical diagnostics is critical to treat and eradicate malaria. The non-invasive, high-speed, and field-deployable photoacoustic method has demonstrated great potential in detecting this dangerous disease. In the blood, pathogens digest hemoglobin to form nanoparticles of hemozoin [1]. High optical absorption of hemozoin made it possible to detect and destroy malaria pathogens using laser radiation. In response to a laser pulse, the vapor nanobubbles are formed around the hemozoin in infected erythrocytes. The acoustic signals of the nanobubbles can be detected by an ultrasonic sensor to diagnose malaria. The clearest acoustic response was achieved at laser wavelength of 672 nm due to the lower absorption of the pigment melanin and hemoglobin compared to hemozoin [2]. At this wavelength, background noise and skin tone dependence are significantly reduced. The lowest threshold for the generation of nanobubbles was achieved at a pulse width of 70 ps [3], which is 4 times lower compared to 14 ns with damage of only < 2% of uninfected erythrocytes compared to 25% for longer pulses due to delocalized photothermal heating. Thus, sub-ns laser pulses at ~0.67 Õm combine the best acoustic response with high safety.

To date, the only viable solution that simultaneously meets the requirements for ~0.67 εm laser wavelength, sub-ns pulse width and output energy is second harmonic generation from Nd-doped laser radiation at 1.34 Õm. A record output of ~0.5 mJ, ~0.7 ns at 100 Hz was recently achieved [4] from Nd:YAP microchip oscillator emitting at 1341 nm, still not satisfying in terms of energy and repetition rate. Although the regenerative Nd:YVO_4 amplifier can effectively scale-up ps pulses at 1342 nm wavelength from the initial nJ energy level and at a repetition rate of 300 kHz [5], the size, reliability, and cost of such laser systems are not suitable. Therefore, we are investigating the feasibility of inexpensive and reliable two- and four-pass Nd:YVO_4 amplifiers using high-brightness pumping laser diodes at 808 nm wavelength. In a two-pass Nd:YVO_4 amplifier at continuous-wave pump power of 4 W, a ~23-fold amplification of picosecond seed pulses from a passively mode-locked fiber laser at a wavelength of 1064 nm with an input power of 1.7 mW and a repetition rate of 29 MHz was achieved (Fig. 1 ï left).

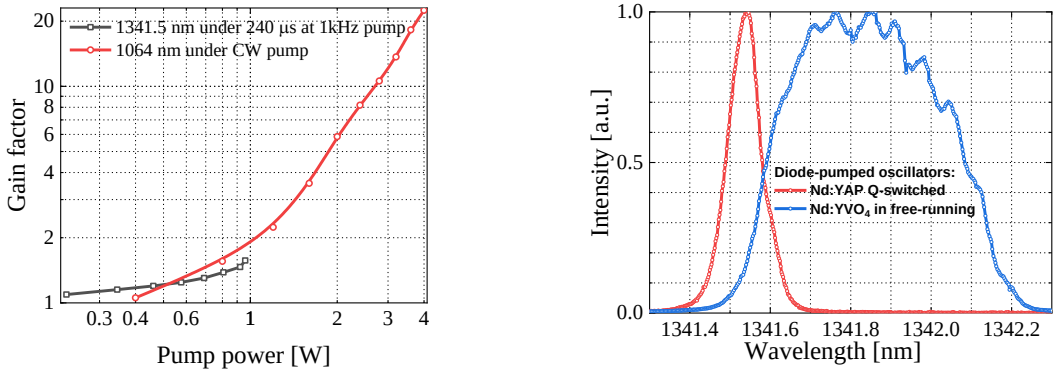

Fig. 1. Gain at 1064 nm and ~1341.5 nm wavelength versus pump power in a double-pass Nd:YVO_4 amplifier ï left. Emission spectra of Q-switched Nd:YAP laser and Nd:YVO_4 oscillator in free-running mode ï right.

It is known that Nd:YVO_4 crystal has a 2 ï 3 times smaller stimulated emission cross section and ~2 times more quantum defect at 1342 nm wavelength compared to the competing transition at 1064 nm. Accordingly, under conditions of pulsed pumping with a duty cycle of 24%, the gain factor of 1.6 ns pulses of Nd:YAP oscillator at a wavelength of ~1341.5 nm (Fig. 1 ï left) with an average power of ~100 mW at a repetition rate of 1 kHz doesnôt reach even up to 2. However, such a limited gain is also explained by the unsatisfactory overlap of the emission spectra from Q-switched Nd:YAP oscillator (Fig. 1 ï right) and the gain bandwidth of Nd:YVO_4 amplifier. Therefore, further results of the investigation of multi-pass Nd:YVO_4 amplifier, seeded with a short-cavity passively Q-switched Nd:YVO_4 oscillator, are discussed.

Acknowledgement: This research was partially funded by the European Social Fund under the No 09.3.3.-LMT-K-712-22-0105 Development of Competences of Students through Practical Research Activities measure.

[1] E.Y. Lukianova-Hleb, K.M. Campbell, P.E. Constantinou, Hemozoin-generated vapor nanobubbles for transdermal reagent-and needle-free detection of malaria, *Proceedings of the National Academy of Sciences*, **111**(3), 900ï 905 (2014).
[2] C. Cai, K.A. Carey, D.A. Nedosekin, Y.A. Menyaev, In vivo photoacoustic flow cytometry for early malaria diagnosis, *Cytometry Part A*, 89(6), 531ï 542, (2016).
[3] E.Y. Lukianova-Hleb ir D.O. Lapotko, Malaria theranostics using hemozoin-generated vapor nanobubbles, *Theranostics*, **4**(7), 761ï 769 (2014).
[4] K. Georgiev, D.N. Georgieva, A. Trifonov, and I. Buchvarov, Sub-ns, high energy, passively Q-switched laser at 1.3 Õm, *ASSL Laser Congress*, paper JTh2A.12 (2020).
[5] A.M. Rodin, M. Grishin, A. Michailovas, Picosecond laser with 11 W output power at 1342 nm based on composite multiple doping level Nd:YVO_4 crystal, *Optics and Laser Technology*, **76**, 46ï 52 (2016).

UV-VISIBLE LIGHT GENERATION IN PHOTONIC CRYSTAL FIBER PUMPED BY IR 110 FS PUMP PULSES

Miglã Kulieġaitã, JokÎbas Pimpã, Vygandas Jarutis, Julius Vengelis

Laser Research Center, Faculty of Physics, Vilnius University, Lithuania
migle.kuliesaite@ff.vu.lt

Photonic crystal fibers (PCFs) are different from conventional optical fibers, because PCFs have a periodic microstructure region inside them where light is propagating [1]. Solid core PCFs are perfect nonlinear media, in which it is possible for nonlinear processes to occur due to third order nonlinearity [2]. Third order susceptibility $\chi^{(3)}$ is related to optical Kerr effect, which leads to several nonlinear processes such as pulse self-phase modulation, cross-phase modulation, four-wave mixing or even stimulated Raman scattering, which results in pulse spectral broadening [3].

In this study we present experimental results of our investigation of UV ï VIS light generation in photonic crystal fiber pumped by IR 110 fs pump pulses. The pump source for UV ï VIS light generation was Yb:KGW laser ñFlintò oscillator generating 1028 nm wavelength with repetition rate of 75.2 MHz and 110 fs duration pulses. A beam splitter, which transmits 35% of energy and reflects 65% of energy, was used to divide the radiation into two beams. The beam with more energy was used as a reference pulse for cross-correlation frequency-resolved optical gating (XFROG) measurements and the other beams with less energy was used for the generation UV ï VIS light in PCF. Polarization maintaining solid core PCF with high nonlinear coefficient and zero dispersion wavelength of 1040 nm was used. PCF length was 2.6 cm and core diameter - 4.3 Õm. XFROG measurements were performed by non-colinearly focusing reference radiation and light from PCF into 300 Õm thickness BBO crystal, which was cut at ű=0Áand ď=30Áfor type II phase matching. By changing delay of reference pulse sum frequency radiation spectrum was measured and a joint representation of delay time and spectrum was obtained XFROG spectrograms.

In this report it is shown, that when IR pump pulse of 110 fs duration and central wavelength of 1028 nm is seeded into PCF, pulse spectrum broadens from 900 to 1200 nm, which can be seen from retrieved XFROG trace (Fig. 1). A small pulse broadening is caused due to short PCF length (2.6 cm) and such spectrum broadening can be explained based on nonlinear process such as self ï phase modulation. Furthermore, spectrum measured at PCF output showed that alongside of pulse spectrum broadening in IR range, a generation of weak UV-VIS wavelength range was also observed. The bandwidth of such spectral range was from 350 to 500 nm and several oscillations were observed (Fig. 1), which might be explained by interference of UV-VIS light generated at different PCF segments.

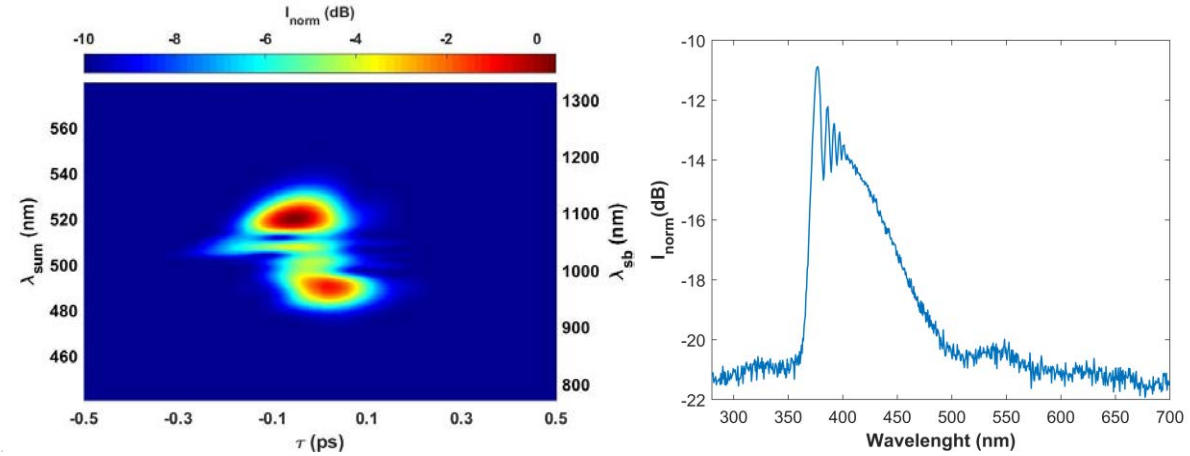

Fig. 1. Left ï measured XFROG trace of radiation form PCF. Right ï measured spectrum of UV-VIS light at PCF output.

[1] R. Buczynski, Photonic Crystal Fibers, Acta Phys. Pol. A. **106**(2), 141ï 167(2004).
[2] P. S. J. Russell, Photonic-Crystal Fibers, J.Lightwave Technol. **24**(12), 4729ï 4749 (2006).
[3] R. W. Boyd, Nonlinear Optics Third Edition (Academic Press, New York 2008).

P4-31

DID NOT PARTICIPATE

ATOMIC LAYER DEPOSITION OF SIO_2 USING OXYGEN PLASMA AND OZONE

Mantas Drazdys[1], Darija Astrauskytã[1], Vitalija Jasulaitienã[2], Ramutis Drazdys[1]

[1]Microoptical components laboratory, Center for Physical Sciences and Technology, Lithuania
[2]Department of Characterisation of Materials Structure, Center for Physical Sciences and Technology, Lithuania
mantas.drazdys@ftmc.lt

The main requirements for optical coatings are low scattering losses and low absorption. Additionally, films must be deposited with precise thickness control as well as thickness uniformity. There are well known physical vapour deposition (PVD) techniques used in manufacturing optical coatings. However, due to development of laser industry, optical components are becoming increasingly complex. Examples of complex optics are photonic crystals, lenses, microoptics etc. Traditional PVD techniques are not able to achieve high-performance optical coatings on these complex substrates.

Atomic layer deposition (ALD) is a branch of chemical vapour deposition (CVD) techniques and is a promising chemical coating technology. In ALD, when depositing dielectric films, substrates are cyclically exposed to gaseous precursors which react in a self-limiting manner. This cyclic process prevents precursors from reacting in gas phase, thus the reaction is limited to the surface. The surface-controlled ALD reactions allow to control film thickness within a sub-nanometer range [1].

Optical coating design is a sequence of layers with high and low refractive indices. To manufacture simple coatings using ALD, Al_2O_3 could be used as a low refractive index material because thermal deposition of Al_2O_3 is well known and does not require a complex reactor design [2]. However, a more precise and complex optical coating design may require a higher refractive index contrast between the two layers. Silicon dioxide (SiO_2) is one of the most widely used materials in manufacturing of optical coatings owing to its low refractive index and large band gap. Unfortunately, it has been shown that the deposition SiO_2 using thermal process, where oxidant is water, is not sufficient [3]. Therefore, ozone and oxygen plasma were started to be used as oxidants [4].

In this work we studied SiO_2 thin films deposited by ALD using tris(dimethylamino)silane and O_3 or oxygen plasma as oxidant. We analysed transmission spectra in the spectral range of 190 ï 980 nm of thin films deposited using different ALD process technological parameters (Fig. 1).

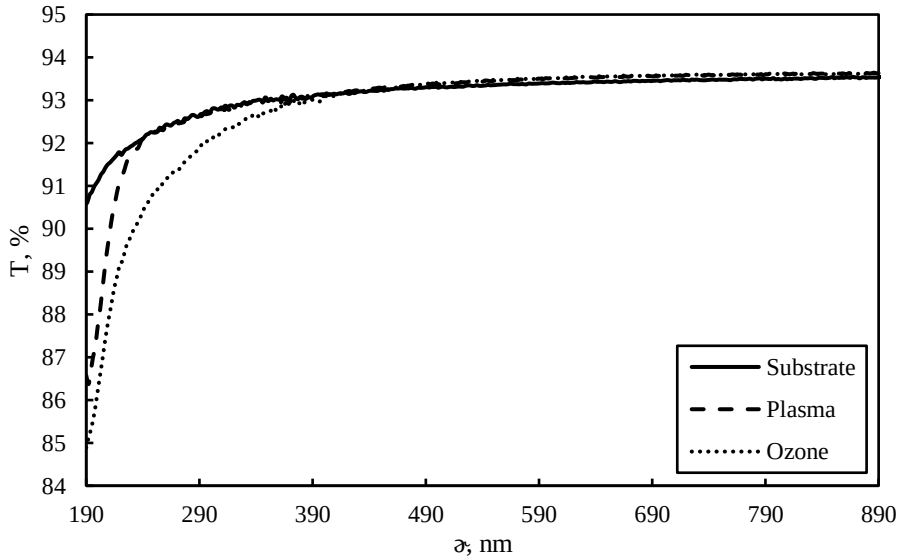

Fig. 1. Transmission spectra of SiO_2.

We observed different levels optical losses in UV range which were higher compared to bare fused silica substrate. To find out possible causes of absorption the investigation of chemical composition and appropriate stoichiometry of thin films using X-ray photoelectron spectroscopy (XPS) was made.

[1] S. M. George, Atomic Layer Deposition: An Overview, Chem. Rev. **110**, 111-131 (2010).
[2] D. Riihel[a] et al., Introduction atomic layer epitaxy for the deposition of optical thin films, Thin Solid Films **289**, 250-255 (1996).
[3] B. B. Burton et al., SiO_2 Atomic Layer Deposition Using Tris(dimethylamino)silane and Hydrogen Peroxide Studied by in Situ Transmission FTIR Spectroscopy, J. Phys. Chem. **113**, 8249-8257 (2009).
[4] K. Pfeiffer et al., Comparative study of ALD SiO_2 thin films for optical applications, Opt. Mater. Express **6**, 660-670 (2016).

COMPARISON OF FIRST-ORDER SELECTIVE DIFFRACTION EFFICIENCIES OF VOLUME BRAGG GRATINGS IN THREE DIFFERENT TYPES OF GLASS

Justas Kudirka[1], Erminas Kozlovskis[1], Antanas Urbas[1,2]

[1] Center of Physical Sciences and Technology, Industrial Laboratory for Photonic Technologies, Lithuania
[2] Workshop of Photonics, Mokslininku st., 6A, Vilnius, Lithuania, 08412
justas.kudirka@gmail.com

Transparent dielectric material modification with ultrafast laser pulses has seen enormous interest and implementation in both scientific and industrial communities. Formation of well-defined homogenous regions of modified refractive index is possible by keeping the intensity of femtosecond laser pulses slightly above the given materialôs damage threshold [1]. This method allows us to fabricate many structures in a number of wide band-gap transparent materials, which expanded the choice of glasses suitable for volume Bragg grating (VBG) fabrication since photosensitive materials are no longer required. VBGs are phase gratings that exhibit outstanding angle and wavelength selectivity [2].

The diffraction efficiency of VBGs at Bragg condition is determined by the product of refractive index modulation (RIM) and grating thickness. Moreover, the value of RIM is determined by the structure of the investigated material and laser parameters [3]. In order to obtain the most cost-effective VBG, we fabricated VBGs with the same thickness but different RIM, which is achieved by varying the laser fluence. In this work, we compared the first-order selective diffraction efficiency of volume Bragg gratings obtained by direct laser writing (DLW) using Gauss-Bessel beam in three different types of glass: silica, borosilicate, and gorilla glass.

In this work, we first theoretically calculated the maximum diffraction efficiency for each type of glass using Kogelnikôs coupled wave theory [4]. Then we used DLW to fabricate multiple VBGs with different laser fluence in all given samples. Finally, we compared first-order selective diffraction efficiencies of VBGs in different glasses using a CCD camera, which allowed us to capture the intensity profile of the diffracted beam.

[1] F. He, H. Sun et al., Rapid fabrication of optical volume gratingsin Foturan glass by femtosecond laser micromachining, Applied Physics **A97.4**, 853ï 857 (2009)
[2] M. Mikutis, T. Kudrius et al., High 90% efficiency Bragg gratings formed in fused silica by femtosecond Gauss-Bessel laser beams, Optical Materials Express **3.11**, 1862-1871 (2013)
[3] D. Paipulas, M. Mikutis et al., Volumetric modifications in fused silica using Gaussian and Bessel femtosecond laser beams, Proc SPIE **8786** (2013)
[4] H Kogelnik, Coupled Wave Theory for Thick Hologram Gratings, Bell System Technical Journal **48.9**, 2909ï 2947 (1969)

SUPERCONTINUUM GENERATION IN CaF_2 CRYSTAL PUMPED BY HIGH REPETITION RATE GREEN FEMTOSECOND LASER PULSES

Vaida Marčiulionytė, Vytautas Jukna, Gintaras Tamošauskas, Audrius Dubietis

Laser Research Center, Faculty of Physics, Vilnius University, Lithuania
vaida.marciulionyte@ff.stud.vu.lt

Supercontinuum (SC) generation is an effect produced by filamentation of ultrashort laser pulses in transparent dielectric media and resulting in broad spectra with high spatial and temporal coherence [1]. SC generation in the ultraviolet (UV) spectral range is highly demanded in ultrafast time-resolved spectroscopy. However, UV SC generation is still a complicated task due to the scarcity of suitable nonlinear materials. Spectral broadening in alkali metal fluorides (BaF_2, CaF_2, MgF_2, LiF, LiSAF) produces spectra with the largest blue shifts. As a rule, CaF_2 crystal is widely considered to be the preferred material for UV SC generation due to its properties: large bandgap of 10 eV, wide transparency in the UV (short-wavelength absorption edge at 120 nm) and low chromatic dispersion [2]. However, under standard (tight focusing, thin crystal) experimental conditions for SC generation CaF_2 (and other fluorides) undergoes rapid color center formation as well as heat accumulation even at relatively low (1 kHz) pulse repetition rate. This eventually leads to optical damage and results in SC spectrum narrowing within seconds. To produce stable SC generation for longer periods of time, CaF_2 crystal has to be continuously translated or rotated with respect to the pump beam [3]. This complicates experimental setup and calls for optimisation of experimental settings for SC generation in the UV by proper choice of pump wavelength and focusing geometry.

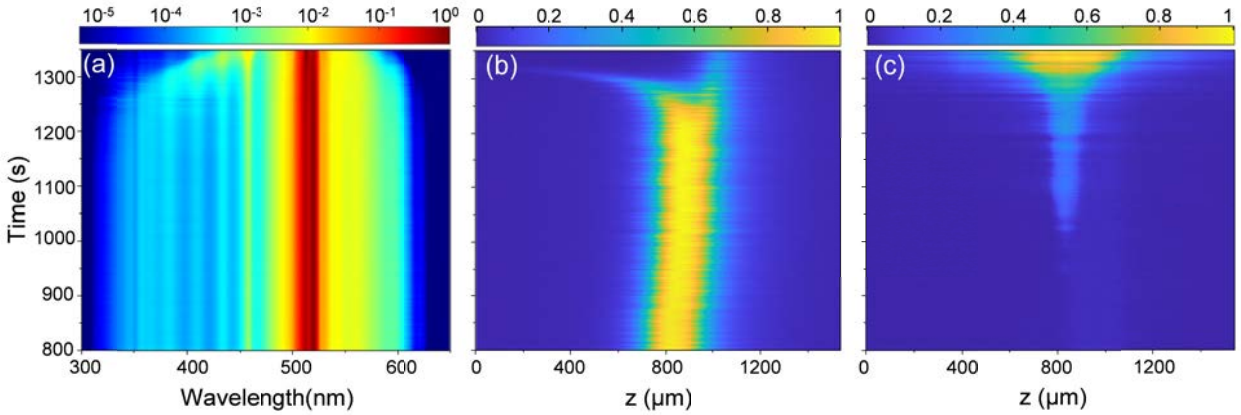

Fig. 1 The time evolutions of (a) supercontinuum spectrum, (b) filament-induced luminescence trace and (c) intensity of scattered light in a thick (25 mm) CaF_2 slab measured with loosely focused (NA = 0.0044) 180 fs, 515 nm pulses at 10 kHz repetition rate.

In this study, we investigate SC generation in an untranslated thick (25 mm) CaF_2 crystal using loosely (NA = 0.0044) focused 515 nm pulses provided by the second harmonic of Yb:KGW laser having a pulse duration of 180 fs and a central wavelength of 1035 nm at a repetition rate of 10 kHz. SC generation in thin (5 mm) CaF_2 crystal in tight (NA = 0.0117) focusing conditions was measured for a comparison.

We demonstrate that the blue-shifts (at ~300 nm) of SC spectra do not depend on focusing condition. However, almost no red-shifted spectral broadening was observed using tight focusing conditions, while symmetric spectral broadening (up to 635 nm) was observed with loosely focused pump beam. This observation is explained by enhanced self-steepening of the leading pulse front [4]. Experiments show that SC spectrum shrinks rapidly (in a few seconds) under tight focusing conditions in a thin CaF_2 sample, whereas damage-free SC generation for 20 min was observed in an untranslated thick crystal using loose focusing conditions (Fig. 1 (a)). We also recorded the dynamics of the filament-induced luminescence trace and light scattering (Figs. 1(b) and 1(c)), which demonstrate a correlation between shrinking of SC spectrum, filament break up and occurrence of strong scattering due to evolving optical damage. The longevity of SC spectrum is explained as a result of dynamic balance between the rate of color centers formation and decay.

[1] A. Dubietis, G. Tamošauskas, R.Šuminas, V. Jukna, and A. Couarion, Ultrafast supercontinuum generation in bulk condensed media, Lith. J. Phys. **57**, 133-157 (2017).
[2] E. Riedle, M. Bradler, M. Wenninger, C. F. Sailer and I. Pugliesi, Electronic transient spectroscopy from the deep UV to the NIR: unambiguous disentanglement of complex processes, Faraday Discuss. **163**, 139-158 (2013).
[3] J. Wang, Y. Zhang, H. Shen, Y. Jiang, and Z. Wang, Spectral stability of supercontinuum generation in condensed mediums, Opt. Eng. **56**, 076107 (2017).
[4] V. Jukna, J. Galinis, G. Tamošauskas, D. Majus, A. Dubietis, Infrared extension of femtosecond supercontinuum generated by filamentation in solid-state media, Appl.Phys.B **116**, 477-483 (2014).

MULTI-PLATE CONTINUUM GENERATORS FOR FEW CYCLE PULSE FORMATION

RamÎnas Logminas[1], ArÎnas Varanaviļius[1]

[1]Laser Research Center, Vilnius University, Lithuania
ramunas.logminas@gmail.com

A straight way into generating ultra-short optical pulses ï is a supercontinuum generation followed by broad-banded pulse temporal compression. There are variety of ways for pulse spectrum broadening techniques, however, recently a lot of attention was dedicated to, so called, multi-plate continuum generator setup. The idea behind it is simply divide a bulk medium into thinner fractions (order of parts of millimeter) and place them at certain distances along the focused pulse propagation direction [1]. It allows to get significantly higher pulses energies at the continuum generator output, compared to traditional methods (even more than a thousand times!). Moreover, the supercontinuum pulses from multiplate setups can be compressed to virtually transformation limited pulse [2].

Dividing bulk medium into thinner plates allows to bypass unwanted nonlinear optical effects that distorts pulse spatio-temporal properties (for example, multiple filamentation). This is avoided because required intensity for such effects inside a bulk medium is reached outside plates, where intensity requirements for same phenomena are way higher.

Several nonlinear optical effects contribute to pulse broadening. However, only two (or maybe even one, depends on generator setup) has considerably larger contributions: self-phase modulation and pulse splitting. While self-phase modulation slowly but consistently broadens pulse spectrum, pulse splitting does it instantaneously and indicates itself with asymmetrical broadening of the spectra and pedestal in shorter wavelength region.

As mentioned, before it depends on multi-plate generator setup whenever pulse splitting will occur or not. If all broadening is done at once ï pulse splitting will occur. However, if firstly pulse passed number of plates before it splits and then it gets compressed it can be guided through the rest of the plates, and pulse splitting (and pedestal in spectra) will not occur. This leads to even better pulse compression in time. To get a detailed information about pulse chirp after it was broadened its convenient to use frequency resolved optical gating (FROG) method. Moreover, at the same time we will also get pulse length.

In our experiment multi-plate setup was pumped with Ti:sapphire laser with a central wavelength being approximately 800 nm. Laser pulse was investigated with FROG and it was figured out that pulse length is ~50 fs. We used pulse energy as high as 0.5 mJ. Plates had different thickness: five ï 0.1 mm and two ï 0.2 mm. The broadened spectrum was approximately from 500 to 1000 nm. The result after all plates was the same whenever first plates were thinner or thicker, however, spectra after same number of plates (1, 2, é etc.) were slightly different.

For any kind of application, the stability of output pulse characteristics is of high importance. The energy measurements during one hour of continuous operation has shown high stability of output radiation with standard deviation of 0.02. The results are presented in Fig.1.

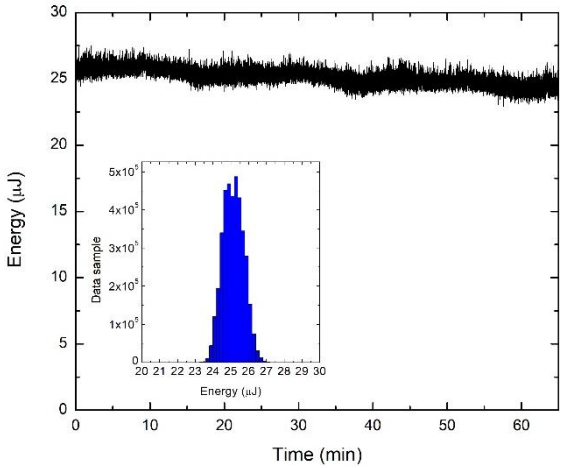

Fig. 1. One hour stability of supercontinuum which was generated in multi-plate system.

After measuring the input energy and output energy we got that our used setup transmittance is ~83%. The energy in the central part of supercontinuum radiation is ~50% of an input energy.

Presentation will include more data on energy, spectral and temporal characteristics, and prospects for compression of pulses from multi-plate setup.

[1] Y.-C. Cheng, C.-H. Lu, Y.-Y. Lin, and A. H. Kung, Supercontinuum generation in a multi-plate medium, Opt. Express **24**, 7224-7231 (2016).
[2] M. Seo, K. Tsendsuren, S. Mitra, M. Kling, and D. Kim, High-contrast, intense single-cycle pulses from an all thin-solid-plate setup, Opt. Lett. **45**, 367-370 (2020).

INVESTIGATION OF IMPURITIES IN LASER MEDIA: CATHODOLUMINESCENCE AND FILAMENT INDUCED LUMINESCENCE COMPARISON

Akvilė Bunkevičiūtė, Balys Momgaudis, Mikas Vengris

Laser Reasearch center, Vilnius University, Saulėtekio Ave. 10, LT-10223 Vilnius, Lithuania
akvile.bunkeviciute@ff.stud.vu.lt

Luminescence is the light emitting process when an electron jumps from excited to a ground state. In undoped laser host material luminescence could be generated in various ways: using optical filaments, photons of light (photoluminescence), accelerated electrons (cothodoluminescence), X-ray beam (X-ray luminescence), etc.

In this work we are using filaments of light in order to induce luminescence and observe the resulting spectrum. This method is more convenient compared to cathodoluminescence or X-ray luminescence because the specimen is excited by laser beam. In this way, we have a system which is easily adjustable, requires no complex optical elements and no vacuum chamber is needed. Besides, it allows to study decay of excited states which is not possible during other experiments. Use of filaments in luminescence spectroscopy could be nondestructive way to examine transparent solid material in order to determine it's quality.

Luminescence was generated by using filaments of light. Its formation is dynamic process which is caused by non-linear matter-light interaction such as self-focusing, self-phase modulation, non-linear absorption, free-electron plasma, etc. In order to observe these processes high intensities are needed. In this experiment these intensities are reached by focusing femtosecond laser pulses into the specimen. The peak intensity of the filament is sufficient to excite impurities and charge carriers in the material. The filament induced luminescence is observed and registered from the side of the filament.

The main purpose of this work is to compare two different methods: filament induced luminescence and cathodoliuminescence. Therefore, spectra were registered in different popular laser media such as YAG, Al_2O_3 and KGW. Specimens were provided by different manufacturers.

Overall, it was shown that characterizing lines of impurities and defects are repeated in both experiments for all specimens (YAG, Al_2O_3 and KGW) provided by different manufacturers. For instance, figure 1 a) shows emission spectra of YAG specimens excited by filament, figure 1 b) shoes spectra of samples which were excited by accelerated electrons. The characteristic peaks differ in intensity, depending on the type of the excitation. Moreover, luminescence decay of these specimens were measured.

Thus, generation of optical filament is suitable way to investigate luminescence in laser host media. On the other hand, luminescence generated by filaments is more suitable method in samples which have intense luminescence. When intensity is low it is better to use cathodoluminescence experiment because light is collected from larger area of the sample's surface.

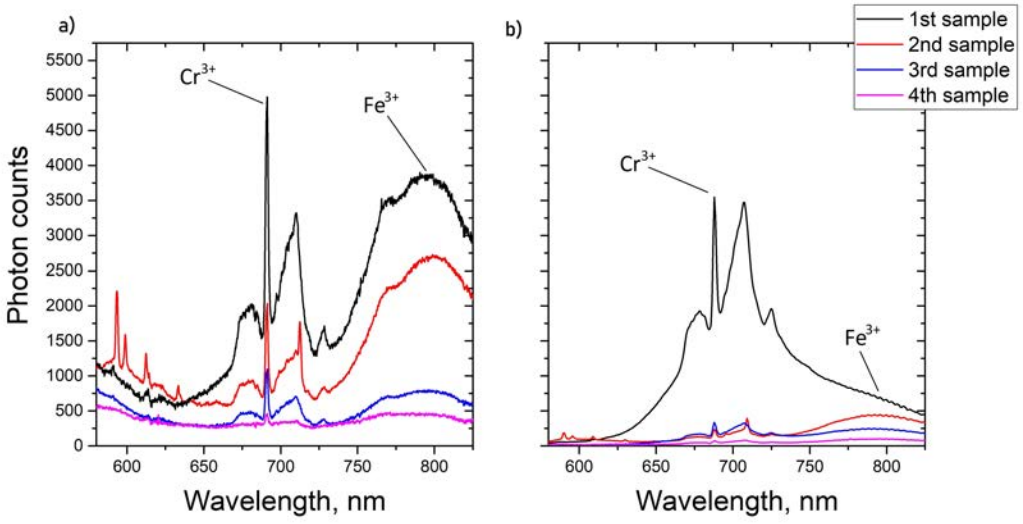

Fig. 1. Filament induced luminescence (a) and cathodolimonescence (b) spectra in YAG samples.

CONSTRUCTION AND INVESTIGATION OF ROD-TYPE FIBER AMPLIFIER SYSTEM FOR FEMTOSECOND YB:KGW OSCILLATOR

Jonas Banys[1], Julius Vengelis[1]

[1]Laser Research Center, Faculty of Physics, Vilnius University, Lithuania
jonas.banys@ff.vu.lt

Finding new methods to obtain higher average powers and shorter pulse durations is an important topic of laser physics research [1]. One of the ways to achieve such parameters of light is amplification of ultrashort pulses with fiber amplifiers. Intensive studies and improvements on Yb-doped fibers has led to the demonstration of many advantageous properties if compared to conventional bulk solid-state systems. Due to their geometry and design, Yb-doped fiber amplifiers feature outstanding thermo-optical properties, large gain bandwidth and high optical pumping efficiency. However, the drawback of amplification of ultrashort pulses in fibers is the long confined propagation length that limits both the power and the energy scaling due to nonlinear pulse distortions [2]. In fiber chirped pulse amplification (FCPA) system pulses are temporally stretched before amplification, to reduce nonlinear effects in the amplifier, and then compressed to ~200 fs [3]. On the other hand, nonlinear amplification methods - parabolic pulse amplification, pre ï chirp managed (PCMA) and gain managed amplification (GMA), clearly denote how fiber nonlinearity can be harnessed, rather than being a limiting factor: amplified pulses have broadened spectrum, exhibit linear chirp and can be effectively compressed to <50 fs [3, 4]. These amplification techniques nowadays are frequently realized by using large mode area (LMA) double cladding photonic crystal rod-type fiber amplifiers in which nonlinear effects are significantly reduced and single mode regime coupled with high optical efficiency enables amplification of ultrashort pulses up to 10 - 100 W of average power [5].

Exactly this type of fiber amplifier is used in this work. Single pass fiber amplifier system was designed and utilized for amplification of femtosecond pulses from Yb:KGW oscillator ñFlintò (ñLight Conversionò). Spatial, temporal and energy characteristics of amplified light was measured. Yb-doped LMA double-clad polarization maintaining photonic crystal rod-type fiber (ñNKT Photonicsò) was used for the amplification.

It was determined that maximum average output power from the amplifier system was 19,5 W when the pump power was 29 W with the seed power of 4 W. Highest core-clad power ratio (CCR) of 0,935 (11,6 dB) was reached at maximum output power, while polarization contrast ratio (PER) of the amplifier was 19,4 dB. Due to self-phase modulation effect, modest spectral broadening of the amplified pulses was observed (Fig. 1): root mean square spectral width increased by 3 ï 4 nm compared to input seed spectrum. Second harmonic FROG measurements showed that amplified pulses broadened in time from 83 fs from the oscillator to 864 fs ï 1,07 ps at the fiber output (Fig. 2). Also, spectral and temporal broadening of pulses depended on seed polarization. In all cases amplified pulses exhibited quadratic temporal phase therefore the pulse chirp was linear and can be effectively compensated down to duration that is shorter than oscillator pulse duration. Required group delay dispersion for dispersion compensation was also calculated. Finally, it was evaluated that, in this case, chirped mirrors are most suitable for optimal compression of amplified pulses. Final amplifier system will be used as a high power and high pulse quality laser system for further nonlinear optics experiments.

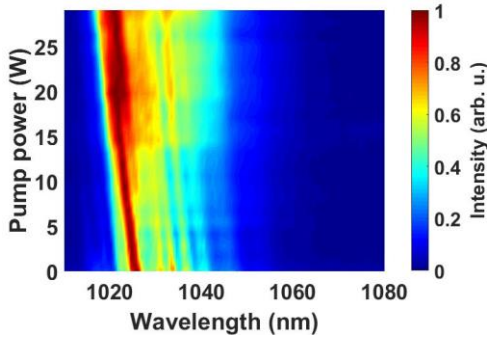

Fig. 1. Spectral evolution of amplified pulses when amplified to 19,5 W output power.

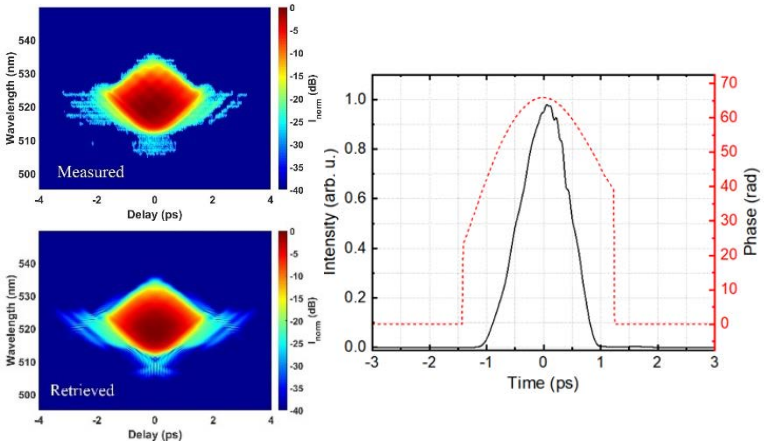

Fig. 2. SHG FROG measured and retrieved traces of amplified pulses and temporal intensity profile at maximum output power.

[1] C. Saraceno, et al., Trends in high-power ultrafast lasers, International Society for Optics and Photonics, Vol. 9835, p. 98350X (2016).
[2] Y. Zaouter, et al., Stretcher-free high energy nonlinear amplification of femtosecond pulses in rod-type fibers, Opt. Lett. **33**(2), 107ï 109 (2008).
[3] P. Sidorenko, W. Fu, F. Wise, Nonlinear ultrafast fiber amplifiers beyond the gain-narrowing limit, Optica, **6**(10), 1328-1333 (2019).
[4] Y. Zhang, et al., High-power pre-chirp managed amplification of circularly polarized pulses using high-dispersion chirped mirrors as a compressor, OSA Continuum, **3**(7), 1988-1998 (2020).
[5] Z. Zhao, B. M. Dunham and F. W. Wise, Generation of 150 W average and 1 MW peak power picosecond pulses from a rod-type fiber master oscillator power amplifier, JOSA B, **31**(1), 33-37 (2014).

INVESTIGATION OF THE DYNAMICS OF OPTICAL DAMAGE USING PUMP-PROBE SPECTROSCOPY

Aivaras Peļiulis, Mikas Vengris

Laser Research Center, Vilnius University, Lithuania
aivaras.peciulis@ff.stud.vu.lt

Any irreversible change of coating, surface or bulk of an optical component, that is induced by exposing material to laser light is called laser induced damage. Laser induced damage threshold (LIDT) defines the fluence of radiation, that optical element can withstand without suffering damage. For various optical components it is usually given as single pulse fluence, but in reality, damage can occur at lower fluences after exposition of many pulses ï this effect, known as accumulation, will be the main focus of presented investigation.

Change of differential absorption spectra of an element after excitation with femtosecond pulses was chosen as indication of irreversible damage. For that, a typical pump-probe spectroscopy measurement was modified to register spectra after each excitation pulse and then calculate the difference from the first pulse to hit the sample:

$$\delta A(\lambda, N) = \Delta A_0 - \Delta A_N, \quad (1)$$

where λ is wavelength, N ï number of pulses and ΔA ï differential absorption. Sequential pulse trains of precisely 100 pulses per each would reach the material and then we simply calculate how many pulses were needed to induce optical damage.

Measurements were performed with $0{,}2mm$ thickness fused silica covering glass. In Fig. 1 (a) a typical set of results is shown. The moment of damage, when δA becomes greater then 0 and grows further (so we donôt confuse it with noises) is clearly distinctive from the graph. Because threshold dependency on pulse count is rather scattered, we can conclude that optical damage is a probabilistic process.

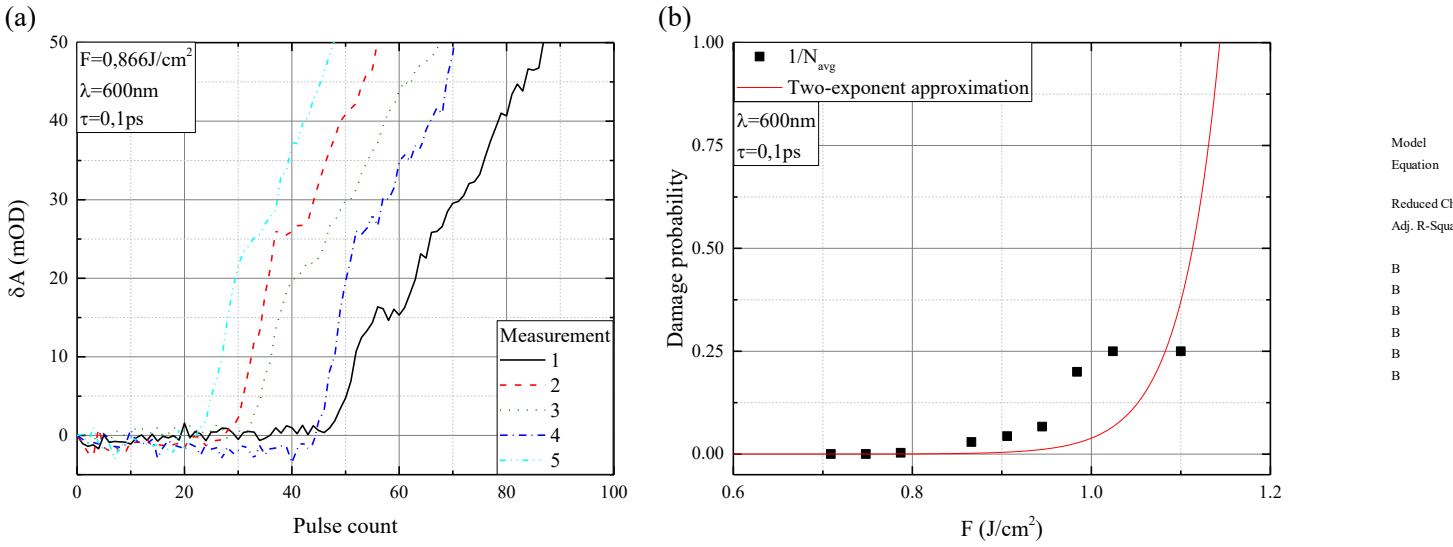

Fig. 1. Difference of differential absorption spectra at $\lambda = 600nm$ dependence on pulse count (a); an inverse of average count of pulses dependence on single pulse fluence and approximation (b).

An inverse of average count of pulses N_{avg} required to induce optical damage can be considered as a probability to damage the sample with the very first pulse. In Fig. 1 (b) that probabilityôs dependence on fluence is plotted and results are approximated with two-exponent function. This implies that there are two stages of damage probability and at higher fluences it is more dependent on density of surfaces defects, that can act as damage precursors, rather than properties of material itself. The approximation also allows to evaluate at what minimal fluence a certain sample would definitely be damaged (probability is equal to 1) ï in our case it was $F_{min} = 1{,}143J/cm^2$.

NUMERICALLY PROCESSED INTERFEROMETRIC NONLINEAR REFRACTIVE INDEX MEASUREMENTS AT 3240nm

Gaudenis Jansonas[1], Rimantas Budriîˆ nas[1,2], Arîˆ nas Varanaviļ ius[1]

[1] Laser Research Center, Vilnius University, Lithuania
[2] Light Conversion, Vilnius, Lithuania
gaudenisjansonas@yahoo.com

Nonlinear refractive index (n_2) describes how the refractive index of a medium depends on the intensity of light. This parameter is responsible for many phenomena of nonlinear optics and in modeling such phenomena it is important to know the most precise value of n_2. Popular methods for measuring n_2, like Z-scan [1], are based on the assumption that laser beam and pulse profiles are Gaussian. In practice this is sometimes difficult to fulfill, especially in the mid-infrared (MIR) wavelength range between 2ε m and 20ε m, where there is a shortage of information about n_2. Therefore, n_2 measurements, with included real spatial and temporal intensity distributions, are of great importance.

We measured n_2 by using an interferometer to detect a total on-axis nonlinear phase shift (B) acquired in a sample and including measured spatial and temporal intensity distributions by numerically simulating the experiment. A simplified optical scheme of the measurement is shown in Fig. 1. For 3240nm light generation we used a label-free optical parametric amplifier (OPA), pumped by a femtosecond Yb:KGW laser ñPharosò. From the interference pattern we obtain a surface of spatial phase difference between two interfering waves by using Fourier transform method [2]. To avoid the effects of linear wavefront distortions we obtain a change of B (ΔB) from a change of two phase surfaces at different pulse energies. Here ΔB was found by fitting spatial intensity distribution of a beam at the sample to a phase difference surface.

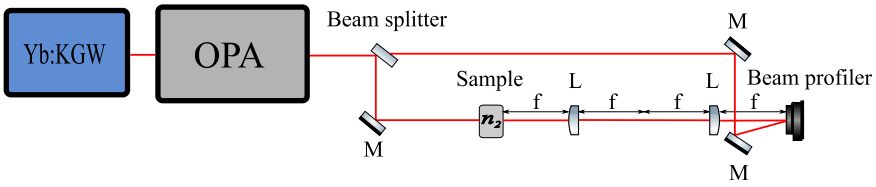

Fig. 1. Simplified optical scheme of the measurement. Here L ï converging lens, f ï focal length of a lens, M - mirror.

First we successfully [3] measured n_2 of fused silica ($2.74 \cdot 10^{-16}\mathrm{cm}^2/\mathrm{W}$) at 1030nm. Then we proceeded to measure ZnSe, GaSe, AGS (using ordinary (o) and extraordinary (e) polarized light) and SBN samples at 3240nm. The results are shown in Fig. 2. The values of ΔB were obtained at different pulse energy changes ΔE. Obtained ΔB values were corrected according to the measured pulse shape and the n_2 was found from linearly fitted experimental data with a fixed intercept value of zero. Some of our results were similar to the ones given in the scientific literature [4] [5].

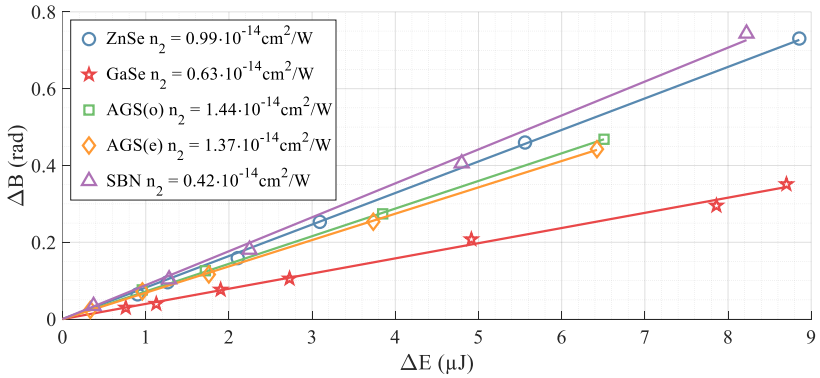

Fig. 2. Obtained ΔB of different materials and their n_2. Dots ï experimental points, line ï linear fit.

In conclusion, we prepared a method to include real temporal and spatial intensity distributions of light in n_2 measurements and successfully measured some popular IR materials at 3240nm. This method could be used to further measure n_2 in the MIR, where such measurements are needed.

[1] M. Sheik-bahae, A. A. Said, and E. W. Van Stryland, High-sensitivity, single-beam n2 measurements, Opt. Lett. **14**, 955-957 (1989).
[2] M. Takeda, H. Ina and S. Kobayashi, Fourier-transform method of fringe-pattern analysis for computer-based topography and interferometry, J. Opt. Soc. Am. **72**, 156-160 (1982).
[3] D. Milam, Review and assessment of measured values of the nonlinear refractive-index coefficient of fused silica, Appl. Opt. **37**, 546-550 (1998).
[4] T. R. Ensley and K. B. Neal, Ultrafast nonlinear refraction measurements of infrared transmitting materials in the mid-wave infrared. Optics express **27**, 37940-37951 (2019).
[5] W. Li et al., Measurements of nonlinear refraction in the mid-infrared materials ZnGeP 2 and AgGaS 2, Applied Physics B **123**, 82 (2017).

LABEL-FREE IMAGING OF BIOLOGICAL TISSUE USING WIDEFIELD SECOND-HARMONIC GENERATION MICROSCOPY

Danielius Samsonas[1,2], Lukas Kontenis[1,2], Mikas Vengris[1,2]

[1]Faculty of Physics, Vilnius University, Vilnius, Lithuania
[2]Light Conversion, Vilnius, Lithuania
danielius.samsonas@ff.vu.lt

Second-harmonic generation (SHG) microscopy is a nonlinear imaging technique based on the frequency-doubling of photons interacting with non-centrosymmetric structures. It enables label-free *in vivo* and *in situ* visualization of non-centrosymmetric biopolymers such as collagen in most structural tissues and myosin filaments in the sarcomeres of striated muscles. Structural label-free nonlinear imaging emerges as a successful tool for faster biomedical diagnostics, while quantitative polarimetric imaging opens up new ways for more detailed tissue characterization.

The SHG process requires hight intensity coherent light. For this reason, imaging is commonly performed by raster-scanning a tightly focused femtosecond oscillator beam and acquiring the image pixel-by-pixel using a single-element photodetector. The frame rate is thus limited by the laser scanning speed. Increasing availability of robust, affordable, high-power, femtosecond lasers operating at MHz rates has stimulated the advancement of widefield SHG microscopy. Widefield microscopy does not require scanning and therefore enables real-time imaging of large samples [1]. A high frame rate is achievable because a large imaging area is exposed to short high intensity laser pulses and the image is obtained as a single frame using a camera. It should be noted that laser parameters need to be carefully optimised because high intensity laser radiation eventually damages the sample. The signal level can also be increased by using a higher repetition rate, leading to higher average power, which eventually causes photobleaching [2].

The purpose of this work was to develop a widefield microscope and to demonstrate its performance by imaging label-free biological samples. A *PHAROS* high-repetition-rate amplified laser system was used for evaluation of the developed widefield microscope by imaging label-free rat skeletal muscle tissue (Biomax RAT901a). The laser parameters at the sample were: 1 W average power, 100 kHz repetition rate, 680 μm beam diameter ($1/e^2$), energy density of 5.5 μJ/cm^2 and a peak intensity of 19 GW/cm^2 using 290 fs pulses. We were able to produce 410 μm × 485 μm images with sub-micron resolution and with no observable damage to the sample. The image in figure 1(a,b) exhibits a periodic structure of the sarcomere anisotropic A-bands, which are clearly distinguishable from the dark isotropic I-bands due to SHG signal from myosin nanomotors. Figure 1(c) shows the SHG intensity profile of 20 sarcomeres along a myofibril, with the average sarcomere length of approximately 1 μm.

The work shows that widefield SHG microscopy provides sub-micron resolution over a large imaging area. The setup will be used to optimize novel high-repetition-rate amplified laser sources for nonlinear microscopy.

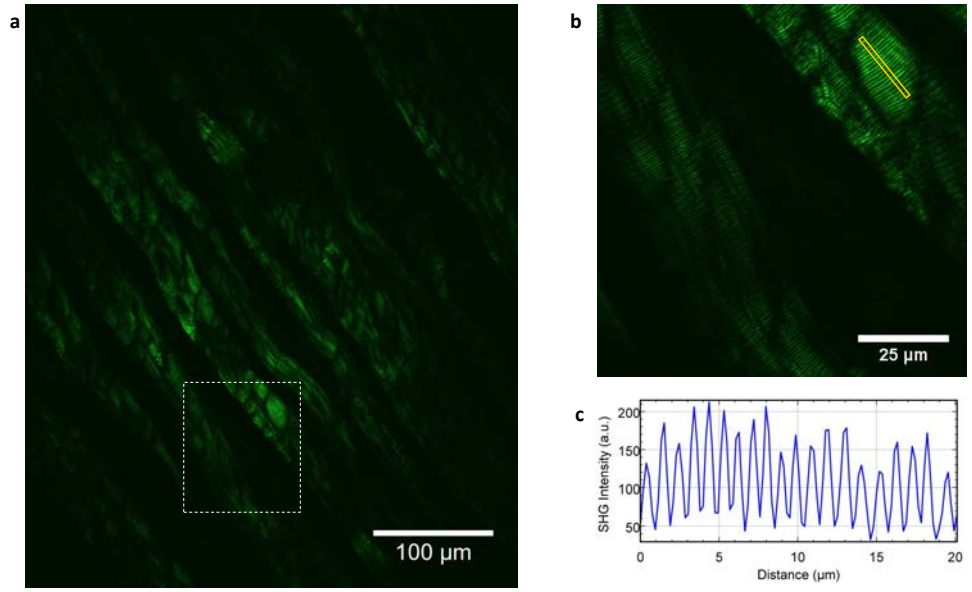

Fig. 1. Widefield SHG image of a fixed label-free rat skeletal muscle. (a) The entire 410 μm × 485 μm image area. (b) 100 μm × 100 μm cropped image area, indicated in (a) by the dashed line. (c) SHG intensity profile along the myofibrilis in the yellow rectangle.

[1] H. Zhao, R. Cisek, A. Karunendiran, D. Tokarz, B. A. Stewart, and V. Barzda, "Live imaging of contracting muscles with wide-field second harmonic generation microscopy using a high power laser," Biomedical Optics Express, vol. 10, no. 10, p. 5130, 2019.

[2] C. Macias-Romero, V. Zubkovs, S. Wang, and S. Roke, "Wide-field medium-repetition-rate multiphoton microscopy reduces photodamage of living cells," Biomedical Optics Express, vol. 7, no. 4, p. 1458, 2016.

INVESTIGATION OF OPTIMIZATION AND MANUFACTURE POTENTIAL FOR SCULPTURED THIN FILM BASED ACHROMATIC WAVEPLATES

Emanuelis Lazauskas, Lina Grinevičiūtė, Gabija Petrauskaitė, Lukas Ramalis and Tomas Tolenis

Center for Physical Sciences and Technology, Lithuania
emanuelis.lazauskas@ftmc.lt

Sculptured thin film technology allows to produce nanostructured coatings featuring various properties, like certain porosity and anisotropy [1]. By optimizing these and other parameters, one can obtain coatings with different optical characteristics, which can be adapted for optical element realization. Furthermore, these coatings possess excellent resistivity to laser irradiation when silica material is used and can be deposited directly onto microlaser system components [2]. Therefore, this technology is a potential research area for microlaser component manufacture.

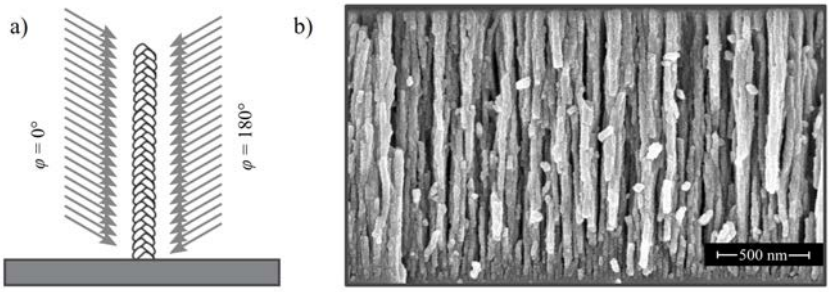

Fig. 1. (a) Illustration of serial bideposition technique involving rapid 180° substrate turns. (b) Cross-sectional SEM image of SiO_2 sculptured thin film.

In this work, however, the scope of investigation was limited to achromatic waveplates. Thus, the main objective was to examine the optimization and manufacture potential for sculptured thin film based achromatic waveplates. The problem was approached by utilizing anisotropic properties of serially bideposited (see Fig. 1) orthogonally birefringent SiO_2 multilayer structures (see Fig. 2). Due to the existence of unique Kramers-Kronig relations for transmission amplitude coefficient τ [3], different transmittance T band-gaps for S and P polarised radiation result in corresponding phase shift differences, which allow to compensate for natural dispersion (see Fig. 2). Taking full advantage of this mechanism, achromatic waveplate designs were optimized employing Dlib global optimization C++ library routines [4].

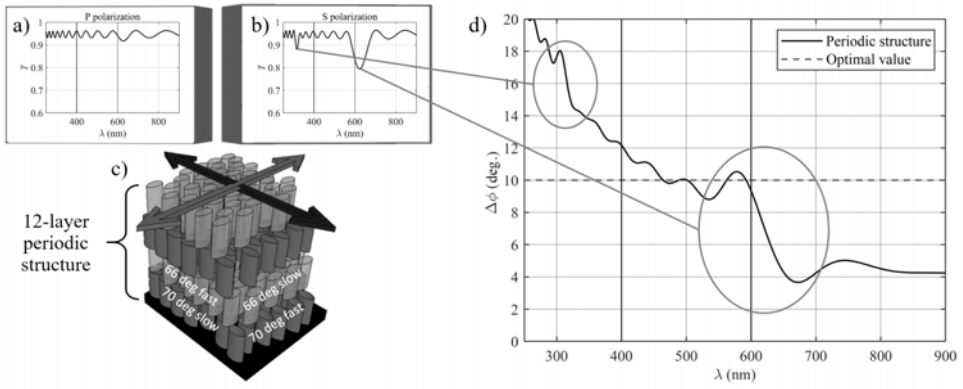

Fig. 2. Differential phase compensation mechanism. (a) and (b) Transmittance spectra for P and S polarised radiation. (c) Example of orthogonally birefringent periodic structure. (d) Phase difference spectrum.

The main source of error in manufactured waveplate optical and phase characteristics was determined to be caused by inaccurately chosen birefringence values and deposited layer thickness errors, which reached 7,5%. Nevertheless, the examination of a more robustly designed waveplate allows to conclude that with accurately chosen birefringence values a functioning achromatic waveplate can be successfully manufactured.

[1] K. M. M. Hawkeye, *Glancing angle deposition of thin films: engineering the nanoscale* (John Wiley & Sons, 2014).
[2] L. Grinevičiūtė, M. Andrulevičius, A. Melninkaitis et al., Highly Resistant Zero-Order Waveplates Based on All-Silica Multilayer Coatings, physica status solidi (a) **214**, 1700764 (2017).
[3] B. Gralak, M. Lequime, M. Zerrad et al., Phase retrieval of reflection and transmission coefficients from Kramers–Kronig relations, JOSA A **32**, 456–462 (2015).
[4] D. E. King, Dlib-ml: A machine learning toolkit, The Journal of Machine Learning Research **10**, 456–462 (2015).

INVESTIGATION OF RELATION BETWEEN OPTICAL RESISTIVITY AND STORING CONDITIONS OF POROUS SILICA BASED MULTILAYER COATINGS

Ugnã Norkutã*, Lukas Ramalis, Rytis Buzelis and Tomas Tolenis

Center for physical sciences and technology, SavanoriÛave. 231, LT-02300 Vilnius, Lithuania
*ugne.norkute@ftmc.lt

Optical coatings are used to direct and control laser-generated radiation. At present, there are increasing demands on high performance coatings, featuring stability of their optical parameters and the highest possible resistance to laser radiation. Sculptured thin films may be used to form coatings with a high laser-induced damage threshold (LIDT). Such coatings have a porous nanostructure and are formed by rotating the substrate at an oblique angle in terms of vapor flux. However, porosity causes the coating to absorb water and other harmful particles from the environment, thus insolation of the coating or all element must be implemented [1].

The aim of this study was to investigate the dependence of the optical resistance of nanostructured silicon oxide-based Bragg mirrors on sample storage conditions. The structures of the multilayer coating (50 layers) were formed using electron beam evaporation technology at zero-degree angle (dense, high refractive index layer) and seventy-degree angle (porous, low refractive index layer). To determine the environmental impact of porous coatings, three samples were placed in an oxygen environment (by injecting O_2 gas into a plastic bag), others three in a dry air environment: in a glass desiccator in which the coatings were held with silica gel to maintain moisture as low as possible. Subsequently, one coating was removed from the initial environments each week and spectral and laser resistance measurements were performed.

LIDT test 1-on-1 measurements were made using ND: YAG laser pulses with parameters: ɔ = 355 nm, Ű 3 ns, spot diameter 70 Õm. The obtained results show that the LIDT of the sculptural coatings kept in dry air for three weeks is larger and reaches 51.5 J/cm^2 (see Fig. 1) while a coating stored in the oxygen environment for the same period of time - 11.5 J/cm^2.

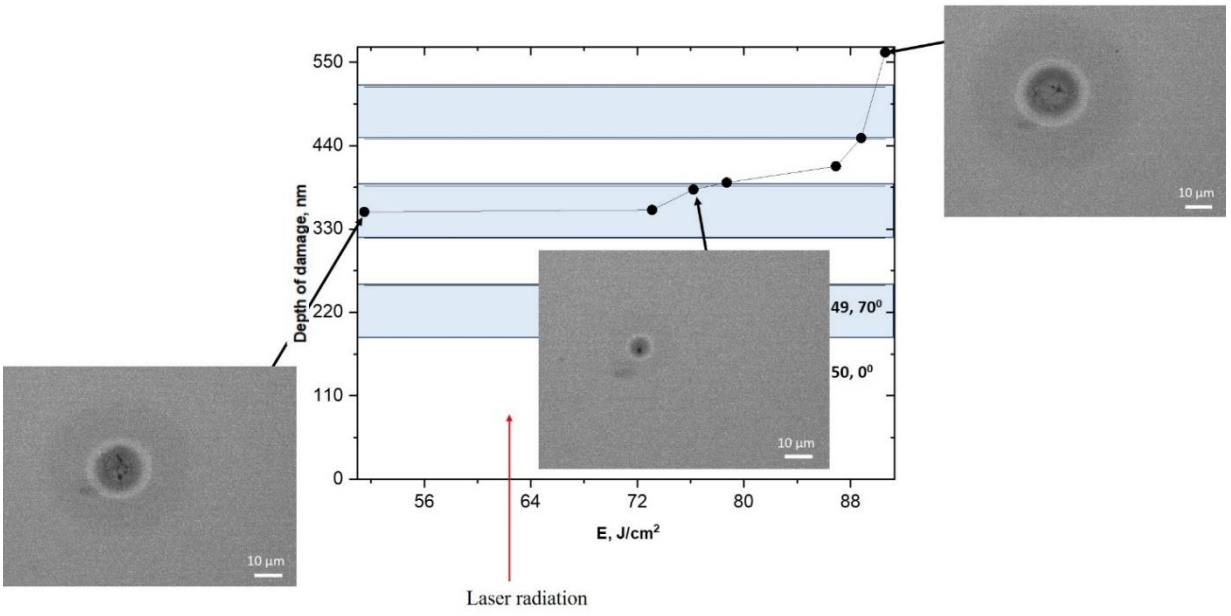

Fig. 1. The dependence of the damage crater depth in the sculptural coating. Sample kept in dry air for three weeks.

Thus, a sculptural coating stored in a dry air environment is more resistant to laser radiation and resistance remains constant, because the coatings stored in an only oxygen environment have the oxygen vacancyôs, which caused damage by nanosecond pulses [2]. This research showed that a dry air environment is better place to store porous silica based multilayer coatings than an only oxygen environment.

[1] D. N. Nguyen, Femtosecond pulse damage thresholds of dielectric coatings in vacuum. Opt. Express 19, 5690-5697 (2011).
[2] S. Papernov. et al, Optical properties of oxygen vacancies in HfO_2 thin films studied by absorption and luminescence spectroscopy, Opt. Express 26, 17608-17623 (2018).

CRYSTALLIZATION BEHAVIOR OF TITANIUM OXIDE THIN FILMS DEPOSITED BY PLASMA ENHANCED AND OZONE-BASED ATOMIC LAYER DEPOSITION

Darija Astrauskytã[1], Mantas Drazdys[1], Ramutis Drazdys[1]

[1] Microoptical components laboratory, Center for Physical Sciences and Technology, SavanoriÔav. 231, Vilnius LT-02300, Lithuania
darija.astrauskyte@ftmc.lt

Optical coatings are a multilayer dielectric high and low refractive index materials thin film structures. They are widely used for dielectric mirrors, antireflective coatings, polarizers, filters etc., that are necessary components in laser system. The laser induced damage threshold of an optical coating depends on the quality of the thin film. Essential characteristics of materials involve surface and optical quality. In order to reach high optical quality, the losses of absorption and scattering should be small as possible [1]. To achieve high quality parameters of the amorphous thin films optimization of coating process parameters should be established. One of the widely used high refractive index materials for the production of optical coatings is titanium oxide TiO_2 or its suboxides Ti_2O_5 and Ti_2O_7.

The research was made on titanium oxide thin films grown by atomic layer deposition (ALD) technique. Tetrakis(dimethylamino)titanium was used as precursor and ozone or oxygen plasma were used as reactants. The thin films coating processes were carried out at two different temperatures - 65 ÁC and 150 ÁC. The refractive indices, roughness and growth rates of manufactured titanium oxide monolayers were determined. Morphology, film thickness and optical properties changes after annealing at 250 ÁC, 500 ÁC and 750 ÁC were investigated. The surface properties of the samples were characterized using atomic force microscopy (AFM). Growth per cycle and film thickness were calculated from transmittance spectra and quartz crystal microbalance measurements. Optical properties were evaluated from the transmittance and reflectance spectra.

Titanium oxide monolayers morphology and optical properties depend on the process technological parameters and annealing temperature. It was found that thermal annealing at temperatures in the range of 500-750 ÁC enhance the formation of crystal grains and crystallites density depends on the annealing temperature. The film roughness increases to more than 10 nm only after annealing at 750 ÁC temperature (Fig. 1). Before the annealing all samples surface was smooth in all deposition conditions. A tendency to rise of titanium oxide thin films refractive index at higher deposition temperatures obtained in this study is similar to previously reported investigations [2, 3].

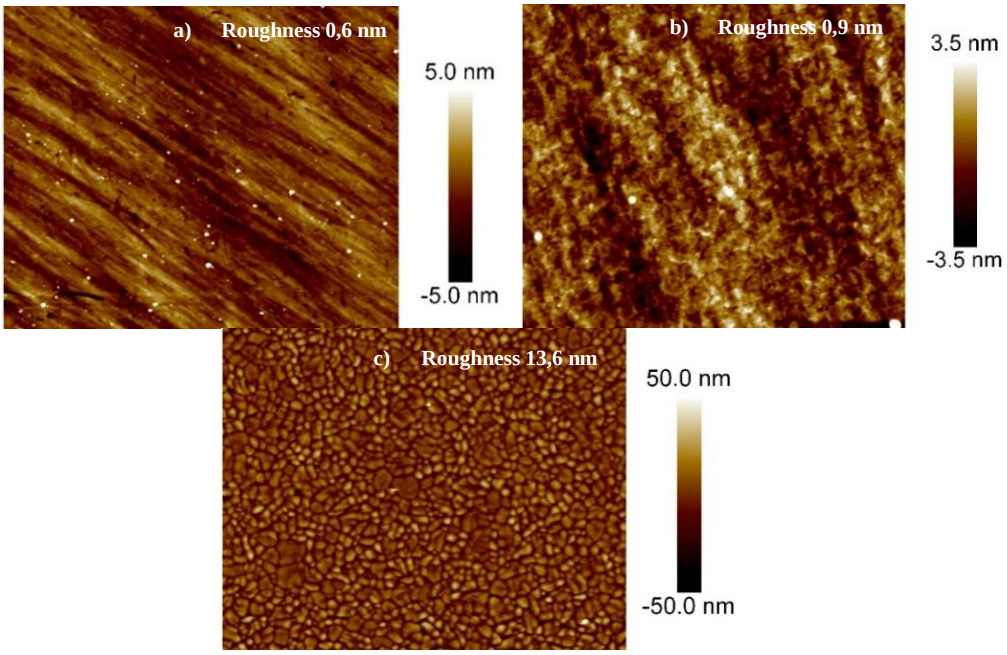

Fig. 1. TiO_2 monolayers AFM scanograms a) ï 250 ÁC, b) ï 500 ÁC, c) ï 750 ÁC (Picture size 10 Ĭ 10 ε m).

[1] X. Bi, H. A. Lopez, P. Narasimha, et al., High rate deposition for the formation of high quality optical coatings, US patent (2014).
[2] S. Ratzsch, E. B. Kley, A. T¿nnermann, A. Szeghalmi, Influence of the oxygen plasma parameters on the atomic layer deposition of titanium dioxide, Nanotechnology 26, 24003 (2014).
[3] A. Szeghalmi, M. Helgert, R. Brunner, F. Heyroth, U. Gº sele, M. Knez, Atomic layer deposition of Al_2O_3 and TiO_2 multilayers for applications as bandpass filters and antireflection coatings, Applied Optics 48, 1727 (2009).

PASSIVATION OF $FA_{0.95}Cs_{0.05}PbI_3$ PEROVSKITE WITH (PHENYLENE)DI(ETHYLAMMONIUM) ORTO-, META-, PARA- CATIONS IMPROVES CHARGE CARRIER EXTRACTION

Simonas Driukas[1], Gabrielė Kavaliauskaitė[1], Raminta Skačkauskaitė[2], Kasparas Rakštys[2], Marius Franckevičius[1], Vidmantas Gulbinas[1]

[1] Center of Physical Sciences and Technology, Department of Molecular Compound Physics, Saulėtekio av. 3, LT-10257 Vilnius, Lithuania

[2] Department of Organic Chemistry, Kaunas University of Technology, Radvilėnų pl. 19, LT-50254 Kaunas, Lithuania

simonas.driukas@ftmc.lt

During the last decade, the development of perovskite solar cells has flourished, as efficiencies as high as 25% were reached [1]. This indicates a potential and cheaper substitute for conventional silicon-based solar cells. However, one of the main problems preventing wide perovskite usage is their instability in ambient atmospheric conditions.

Recently a way of passivating the perovskite surface with thin layers of more stable two-dimensional perovskite was suggested. This increases the stability of the active perovskite layer and passivates surface defects but may compromise charge carrier extraction [2]. In this study, we studied the relationship between the structure of two-dimensional perovskite organic cation and charge carrier extraction through the passivating layer.

The conventional lead halide perovskite used in best performing solar cells crystallizes in cubic $APbX_3$ structure, where A is an organic cation and X the halogen atom. While this cubic perovskite structure exhibits superior optoelectronic properties compared to two-dimensional ones, the high concentration of surface defects due to organic cation and halogen vacancies and the solubility of the organic cation in water, hinder the perovskite solar cell performance and stability. By exposing the surface of three-dimensional perovskite to certain hydrophobic organic cations thin layers of two-dimensional perovskite are formed which can both reduce the density of vacancies and increase the water-resistance of the active perovskite layer [2].

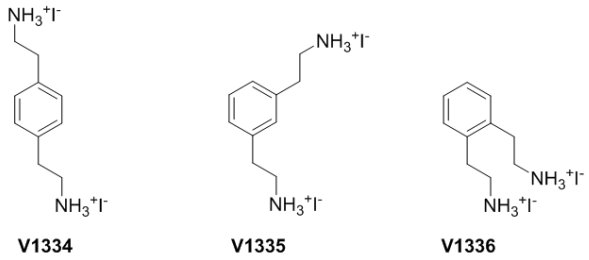

Figure 1. Chemical formula of organic cations used for perovskite passivation.

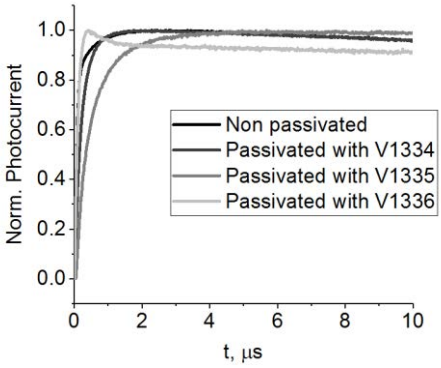

Figure 2. Transient photocurrent of $FA_{0.95}Cs_{0.05}PbI_3$ perovskite solar cells.

Here we present application of three isomers of a a newly synthesized (phenylene)di(ethylammonium) cation (fig. 1) towards the passivation of $FA_{0.95}Cs_{0.05}PbI_3$ perovskite solar cells. After measuring the efficiencies of these devices, we found different values for each isomer. The cell which was passivated with V1335 performed significantly worse than non-passivated or passivated with V1336 which increased the efficiency. To further explore the causes of these differences we performed transient photocurrent and voltage dependent PL decay kinetic measurements. We observed that better-performing devices have faster photocurrent response and PL decay kinetics with applied external voltage than lower efficiency cells. We attribute this difference to a barrier that forms between the perovskite and hole transport layers which increases after passivation with V1335 and decreases with V1336. This suggest that perovskite passivation with o-(phenylene)diethylammonium cation allows improving hole extraction from perovskite to hole transporting material.

[1] https://www.nrel.gov/pv/cell-efficiency.html

[2] *J. Mater. Chem. A*, 2018,6, 2122-2128

CONSTRUCTION AND INVESTIGATION OF SUBNANOSECOND OPG/OPA

Gabrielã Stanionytã, Julius Vengelis

Laser Research Center, Faculty of Physics, Vilnius University, Lithuania
gabriele.stanionyte@ff.stud.vu.lt

The wavelength of laser radiation is usually constant and changing it is extremely hard, which is why, in practice, parametric light generators are used, which allow to continuously change radiation wavelength in a wide spectral range. Currently, the parametric generators are created with ultrashort (less than 100 ps) and long (more than 1 ns) pulse durations, however subnanosecond pulse (less than 1 ns and more than 100 ps) generators have not yet been invented. This is due to certain physical limitations - in the case of subnanosecond pulses, the damage threshold of many nonlinear media is lower than the parametric generation threshold [1-3].

The goal of this research was to construct and investigate an optical parametric generator/amplifier (OPG/OPA) system, which uses 15 mm LBO crystal as a nonlinear medium and Nd:YAG MOPA laser as a seed. Here, 3rd harmonic of laser (355 nm) was used as pump radiation, and fundamental harmonic (1064 nm) ï as pump source for seed radiation. OPG/OPA seed was supercontinuum generated in a photonic crystal fiber (PCF).

The supercontinuum radiation used as OPG/OPA seed extended from 650 nm to 1600 nm at maximum pump pulse energy. The maximal seed energy was measured to be 5 mW over the entire spectrum. We achieved signal wave generation via optical parametric amplification of idler wave. Further on, we measured spectral and energy characteristics of OPG/OPA. Signal wave tunning range was from 456 nm to 670 nm and was limited by idler wave tunning range which depends on seed radiation spectrum extension. Signal wave power was of the order of microwatts over the whole wavelength tuning range due to the fact that during this work, we used a single-pass OPG/OPA configuration. The measured generation threshold was similar for most of the OPG/OPA tunning range.

The results of this work will be used for further development of more effective subnanosecond OPG/OPA systems.

This research is founded by the European Regional Development Fund according to the supported activity óResearch Projects Implemented by World-class Researcher Groupsô under Measure No. 01.2.2-LMT-K-718. Grant No. 01.2.2-LMT-K-718-03-0004.

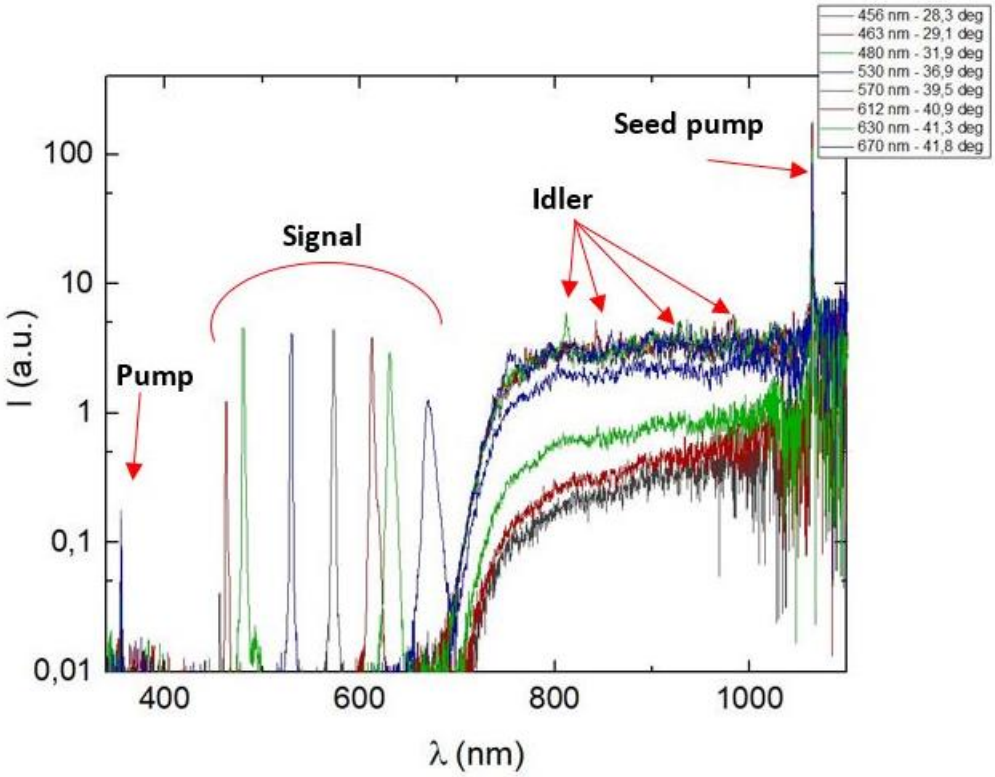

Fig. 1. Spectra of signal wave, pump and seed radiation at different LBO crystal rotation angles.

[1] M. H. Dunn and M. Ebrahimzadeh, Parametric Generation of Tunable Light from Continuous-Wave to Femtosecond Pulses, Science 286, 1513ï 1518 (1999).
[2] A. Dubietis, *Netiesinã optika*, (Publisher Vilnius University, Vilnius 2011).
[3] R. W. Boyd, *Nonlinear Optics* ed. 3 (Academic press, New York 2008).

INCLUSION OF SCULPTURED TOP LAYER IN CHIRPED MIRROR DESIGN FOR REDUCED GROUP DELAY DISPERSION OSCILLATIONS

Simas Melnikas, Lukas Ramalis, Simonas Kiļas, Tomas Tolenis,

Optical Coatings Laboratory, Center for Physical Sciences and Technology, Lithuania
simas.melnikas@ftmc.lt

Chirped mirrors (CMs) are special type of dielectric multilayer coatings intended for stretching or compressing of ultra-short (femtosecond) laser pulses. Various types of CMs were proposed in the past: double CMs (DCMs), back side coated CMs (BASIC), complementary CM pairs, and other [1]. Such effort allowed to compress optical pulses below 2 fs using complementary CM pair approach [1]. All of the mentioned CM configurations were implemented to reduce spectral oscillations of group delay dispersion (GDD) ï the main parameter of CM. Large amplitude GDD oscillations may increase pulse duration, induce additional satellite pulses or distort optical pulse shape.

Most recent approach for reduction of GDD oscillations in CMs is by including a porous sculptured layer (PSL) as a top layer of CM structure [2,3]. Refractive index of PSL may be lower than refractive index of dense material and therefore better optical impedance matching between CM structure and ambient medium (i.e. air) may be achieved. However, optical parameters of such mirrors may be more sensitive to the humidity in the air due to water adsorption within the porous layer. Furthermore, the accuracy of porous layer deposition may be insufficient for CM application. So far, to the best of our knowledge, the CM with PSL with wider bandwidth than half an optical octave ï an approximate bandwidth limit achievable by standard materials [1] ï was never experimentally demonstrated before. In this work we designed and deposited a chirped mirror with over 400 nm (0.67 octave) spectral bandwidth. After deposition we investigated the sensitivity of spectral parameters to deposition errors and humidity changes.

Ion beam sputtering (IBS) technology and glancing angle deposition (GLAD) setup within electron beam evaporation coating plant were used to deposit chirped mirror coating (Fig.1a). 51 layers of Nb_2O_5/SiO_2 materials were deposited using IBS technology. The last (52^{nd}) layer of the coating was deposited with GLAD method (layer consisting of vertical columns was formed) [4]. After deposition, spectral parameters (transmittance coefficient and GDD) were measured at normal conditions (Fig. 1b) and in reduced humidity environment.

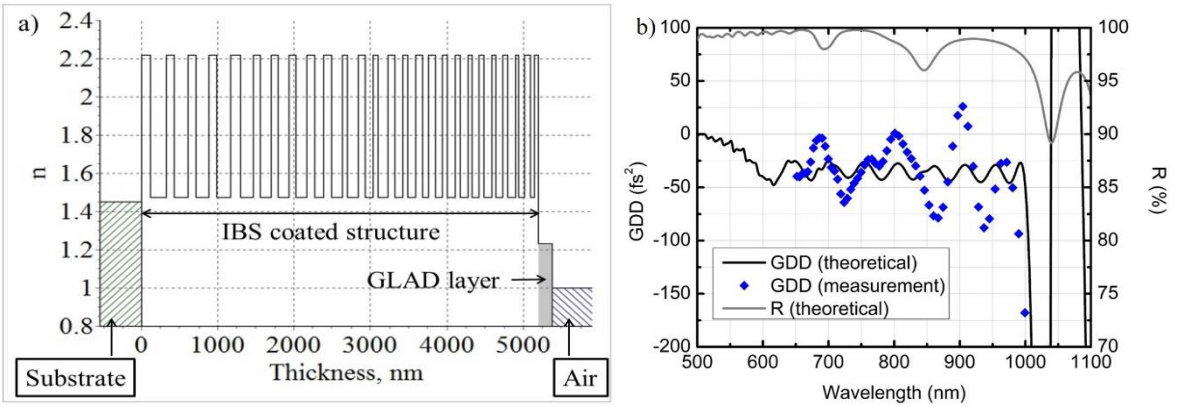

Fig. 1. Refractive index profile of CM multilayer structure: last layer (nå1.23) was deposited using GLAD method (a); spectral parameters of CM: reflectance (R) and GDD (b).

According to the measurements, GDD oscillations do not exceed ī 35Ñ70 fs^2 limits in wavelength range ə=650-1000 nm. Additional analysis showed that this amplitude is approximately 2-3 times smaller than theoretical limit for same bandwidth CM without PSL. Deposition error analysis indicated that the amplitude of GDD oscillations might have been reduced at least by half if IBS deposition errors had been avoided. However, variation of PSL refractive index due to humidity changes by approximately Ñ0.5 % was determined. It may lead to increase of GDD oscillations by Ñ30 fs^2 for theoretical design. Therefore, the GDD oscillations of at least Ñ30 fs^2 are expected even in well optimized and deposited CM with PSL.

[1] V. Pervak, O. Razskazovskaya, *et al.*, Dispersive mirror technology for ultrafast lasers in the range 220ï4500 nm, Adv. Opt. Technol., **3**(1), 55-62 (2014).
[2] J. Liu, Y. Wang, *et al.*, Design, fabrication and application of dispersive mirrors with a SiO2 sculptured layer, Opt. Mater. Express, **8**(4), 836-843 (2018).
[3] P. Ma, A. Szeghalmi, *et al.*, Design and Fabrication of Single, Smooth and Broadband Chirped Mirrors with a Top Nano-Porous Layer, Optical Interference Coatings Conference (OIC) 2019, Santa Ana Pueblo, New Mexico, ThB.3, (2019).
[4] L. Grinevičiūtė, M. Andrulevičius, *et al.*, Highly Resistant Zero-Order Waveplates Based on All-Silica Multilayer Coatings, Phys. Status Solidi A, **214**(12), 1770175 (2017).

LISSAJOUS FIGURES AS DATA PROCESSING METHOD FOR OPTICAL WAVELENGTH SHIFT BASED SENSORS

Pauls Kristaps Reinis[1], Lase Milgrave[1], Kristians Draguns[1], Inga Brice[1], Janis Alnis[1], Aigars Atvars[1]

[1]Quantum Optics laboratory, Institute of Atomic Physics and Spectroscopy, University of Latvia
pauls_kristaps.reinis@lu.lv

In the last decade scientific field researching microscopic optical sensors has rapidly emerged. Optical sensors offer high sensitivity as well as non-invasive sensing methods. There are many possible sensing mechanisms but those based on monitoring wavelength shift, are one of the most common. In this paper we show how Lissajous figures can be used as data processing method and demonstrate this method in action as a part of novel optical humidity sensor.

We used transparent microsphere resonators which due to total internal reflection can trap light inside them, thus constructive interference can occur. This process is also known as whispering gallery modes (WGM). Our optical relative humidity (RH) sensor mainly consisted of liquid glycerol microdroplet acting as microsphere resonator, 760 nm tunable VCSEL laser, detector and oscilloscope. Experiments with glycerol microdroplet showed that clear fundamental modes can be excited **(Fig. 1a)** and glycerol by its nature is great material for humidity sensing as it is hygroscopic, non-toxic, non-irritating, stable, viscose. For every RH level microdroplet has got exact diameter and refractive index. If RH changes in the surrounding environment, resonance conditions for the microdroplet changes and one can observe rapid wavelength shift in the transmission spectrum. In fact, sensitivity of the glycerol microdroplet sensor is so high, that up to 25 resonant peaks crossed the oscilloscope screen for change of 1 % RH. To make use of such properties Lissajous figures were introduced into data processing algorithm. Intensity at points I1(X1) and I2(X2) (**Fig. 1a**) from transmission spectrum was continuously recorded and Lissajous figure could be created in real time (**Fig. 1b)**. When RH conditions changed, resonant modes were shifting to longer wavelengths if RH increased and vice versa. By knowing whether the wavelength of resonant modes increased or decreased and for how much, precise RH change could be determined.

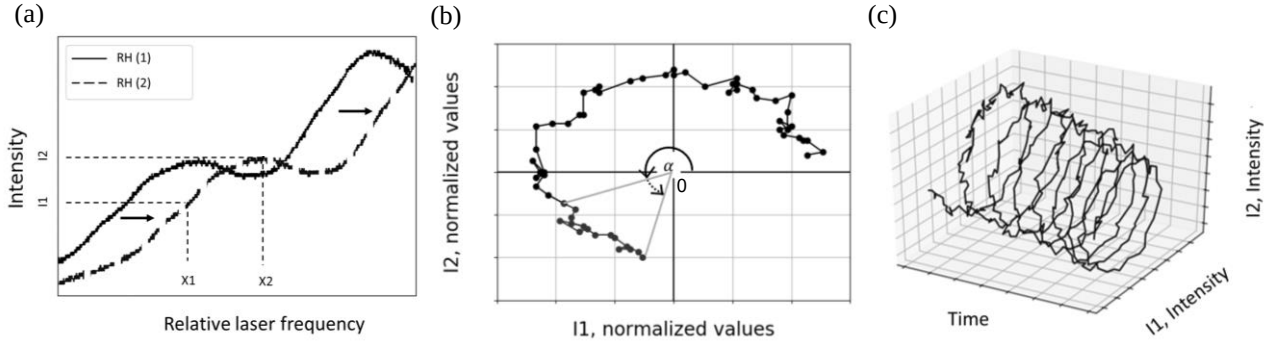

Fig. 1. Main steps of wavelength shift determination. (a) Spectrum from microsphere sensor. Figure shows how resonant modes are shifting and points X1 and X2 from which intensity was recorded. (b) 2D Lissajous figure. I1 and I2 values were normalized so that figure is rotating around the origin point (0,0). (c) Lissajous figure in time domain.

Each point shown in **Fig. 1b** has directly measured coordinates (normalized I1 and I2 values). Using simple trigonometry one can determine what angle Ŭradius vector would have as shown in **Fig. 1b**. A shift of 360Áis equal to wavelength shift of free spectral range. This allows us to measure wavelength shift in real time despite unordinary mode shift where up to 300 modes can cross the oscilloscope screen within an hour.

The data processing method presented in this paper can be useful for optical sensors where one has to deal with high sensitivity and use of tunable lasers. This methodology is also promising for microresonator sensors with lower Q-factors (Q-factor of the resonator used in this work was 10^4). Constructing Lissajous figures as shown in **Fig. 1** require minimal capacity to process data as only 2 data points are needed for each measurement which greatly simplifies the process of measuring wavelength shift. This study discusses the full process of Lissajous figures based data processing and benefits of it.

This research was funded by LZP project Nr. lzp-2018/1-0510 ñOptical whispering gallery mode microresonator sensorsò and ERDF project No.1.1.1.5/19/A/003.

[1] Giorgini, A.; Avino, S.; Malara, P.; De Natale, P.; Gagliardi, G. Fundamental limits in high-Q droplet microresonators, *Scientific Reports* (**2017**).
[2] Brachmann, J.F.S.; Kinder, T.; Dieckmann, K. Calibrating an interferometric laser frequency stabilization to megahertz precision. *Applied Optics* (2012).

ULTRAFAST VOLUMETRIC (3D) HUMAN RETINA IMAGING WITH FOURIER-DOMAIN FULL-FIELD OPTICAL COHERENCE TOMOGRAPHY

[1]Karolis Adomaviļius, [1]Ieva Ģiļkienā, [1,2]Egidijus Auksorius,
[2] Dawid Borycki, [2] SlawomirTomczewski, [2] Maciej Wojtkowski

[1] Center for Physical Sciences and Technology, Department of Optoelectronics, Vilnius
[2] Institute of Physical Chemistry, Polish Academy of Sciences, Warsaw, Poland
karolis.adomavicius@ftmc.lt

Optical coherence tomography (OCT) is an interferometric imaging method ï widely used for retinal imaging ï that can image deep in tissue. Compared to classical OCT systems where a single point detector is used to register the signal, full-field OCT (FF-OCT) systems utilize ultrafast CMOS cameras. Thus, the need to scan sample in both *x* and *y* directions is eliminated by obtainingan entire image at once. Low-speed mechanical scanning of interferometerô s reference arm is replaced by swept source laser to enable registering multispectral interference patterns of the sample [1]. Fourier transformation of such acquired volume along wavelength yields real sample structure. This establishes principles of Fourier-domain (FD) FF-OCT.

We have built a FD-FF-OCT system, shown in Fig. 1, that consisted of a swept source laser (Broadsweeper BS-840-2-HP, Superlum), a Linnik interferometer and an ultrafast camera (Fastcam SA-Z, Photron).Spatial coherence was reduced with a specialized device (not shown in Fig. 1) to remove crosstalk coherent noise in the FF-OCT images.

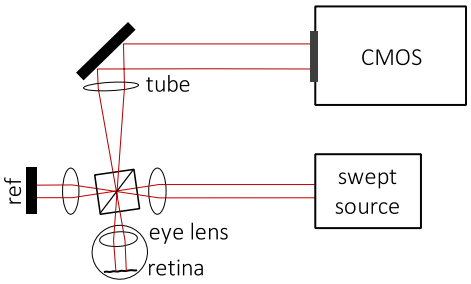

Fig. 1. The principal scheme of Fourier-domain Full-Field Optical Coherence Tomography setup for human eye imaging.

Fig. 2 shows a cross-sectional image of the human retina as acquired *in vivo* in the macular region. The whole volume was acquired in just 8.6 ms.

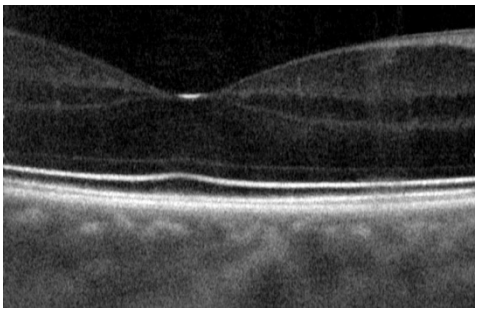

Fig. 2. Axial (XZ) image of the human retina acquired *in vivo*. The image was derived by averaging 7 cross-sectional images in the volume that was acquired in just 8.6 ms.

In conclusion, FD-FF-OCT provides increase of acquisition speed that significantly reduce image distortions induced by the natural eye movement [2].

1.E. Auksorius, D. Borycki, and M. Wojtkowski, "Crosstalk-free volumetric in vivo imaging of a human retina with Fourier-domain full-field optical coherence tomography," Biomedical Optics Express 10, 6390-6407 (2019).
2.E. Auksorius, D. Borycki, P. Stremplewski, K. LiÕewski, S. Tomczewski, P. NiedŸwiedziuk, B. L. Sikorski, and M. Wojtkowski, "In vivo imaging of the human cornea with high-speed and high-resolution Fourier-domain full-field optical coherence tomography", Biomedical Optics Express 11, 2849-2865 (2020).

(IN-SITU) STUDY OF IMMOBILIZED RECEPTOR BINDING KINETICS BY USING PLANAR PHOTONIC-PLASMONIC NANOSTRUCTURES FOR BIOSENSING

Vytautas Gradauskas[1], Justina Anulytė[1], Ernesta Bužavaitė-Vertelienė[1], Ieva Plikusienė[1,2], Zigmas Balevičius[1,3]

[1] State Research Institute Center for Physical Sciences and Technology, Sauletekio ave. 3, LT-10257 Vilnius, Lithuania
[2] Faculty of Chemistry and Geoscience, Vilnius University, Naugarduko str. 24, LT-03225 Vilnius, Lithuania
[3] Faculty of Electronics, Vilnius Gediminas Technical University, Naugarduko str. 41, LT-03227 Vilnius, Lithuania
vytautas.gradauskas@ff.stud.vu.lt

Biosensors based on surface plasmon resonance (SPR) are widely used in biosensing due to the high sensitivity of the SPR. However, various photonic-plasmonic structures are investigated in order to reduce the high losses in the metal, that broadens the width of plasmonic resonance, and as a result, decreasing sensitivity of the sensor. In order to reduce the losses in the metal a modified photonic-plasmonic nanostructure, supporting Tamm plasmon-surface plasmon polaritons (TPP-SPP) [1] mode could be employed for detection of protein interactions on solid-liquid interfaces [2, 3]. Such type of plasmonic mode consists of two different plasmonic excitations: the so called Tamm plasmon-polariton (TPP) and surface plasmon-polariton (SPP). The SPP mode is generated at metal/dielectric interface as the TPP is generated at the PC/metal boundary in the photonic band gap of PC.

In this research a photonic-plasmonic nanostructure consisting of PC (TiO_2/SiO_2) with thin (~40 nm) Au layer was investigated. A total internal reflection ellipsometry (TIRE) method for generation of plasmonic modes were employed. A stem cell factor receptor (SCF-R) and bovine serum albumin (BSA) were used in order to investigate the sensitivity of the plasmonic modes. The kinetics interactions of immobilized SCF-R receptor on the chip surface with genetically engineered ligands was studied. The results showed a higher concentration detection limit on a TPP-SPP mode, rather that of SPR.

[1] E. Bužavaitė-Vertelienė, V. Vertelis and Z. Balevičius, The experimental evidence of a strong coupling regime in the hybrid Tamm plasmon-surface plasmon polariton mode, *Nanophotonics*, 2021. https://doi.org/10.1515/nanoph-2020-0660
[2] E. Buzavaite-Verteliene, I. Plikusiene, T. Tolenis et. al., Hybrid Tamm-surface plasmon polariton mode for highly sensitive detection of protein interactions, *Opt. Express* **28**, 29033-29043 (2020).
[3] Z. Balevičius, Strong coupling between Tamm and surface plasmons for advanced optical biosensing, *Coatings*, **10**(12), 1187 (2020).

P5-1

DID NOT PARTICIPATE

THE GENOTOXIC IMPACT TO PERIPHERAL BLOOD CELLS OF *PERCA FLUVIATILIS* INDUCED BY MULTIPLE STRESSORS. COMET ASSAY AND NUCLEAR ABNORMALITIES ANALYSIS

Gelminą Vanseviļ iĨ tą[1], Milda Stankeviļ iĨ tą[1]

[1] Laboratory of Genotoxicology, Nature Research Centre, Lithuania
vangelmine@gmail.com

Anthropogenic pollution in aquatic systems is damaging living organisms. Furthermore, aquatic animals are constantly exposed to naturally occurring parasitic infections, which may infringe host (i. e. fish) immune system weakening its resistance to various pollutants such as metals. Consequently, this study focuses on genotoxic damage to *Perca fluviatilis* peripheral blood cells induced by naturally occurring stressors (co-infection with *Trichodina sp.* and *Saprolegnia parasitica*) and anthropogenically caused ones (heavy metals). These stressors occurring simultaneously lead to unpredictable genotoxic outcomes in aquatic organisms. Until now, there have been no studies focusing on combined effects of parasitic co-infection and metal mixture exposure, only on genotoxic effects caused by single stressor. Therefore, in this study the analysis of nuclear abnormalities, such as micronucleus (MN), nuclear buds (NB), blebbed nuclei (BL) and comet assay analysis in erythrocytes of peripheral blood cells was performed. The experimental study was designed to recreate realistic interaction conditions concerning multiple stress effects to show possible genotoxicity outcomes. Results indicate that simultaneously co-infected and exposed to pollutants fish tend to get highest genotoxic impact compared to when only one stressor is present. The study also suggests that stressors may affect fish in synergetic manner, strengthening one anotherôs genotoxic impact.

This study was funded by the Research Council of Lithuania through the project P-MIP-21-229.

OPTIMIZATION OF SOL-GEL SYNTHESIS PROCEDURE OF TUNGSTEN (VI) OXIDE COATINGS FOR EFFICIENT PHOTOELECTROCHEMICAL PRODUCTION OF HYPOCHLORITE

Evelina Griniuk[1,2*], Irena Savickaja[2], Arnas Naujokaitis[2], Jurga Juodkazytė[2], Milda Petruleviļienė[2]

[1] Institute of Chemistry, Faculty of Chemistry and Geosciences, Naugarduko str. 24, LT-03225 Vilnius University, Lithuania

[2] Center for Physical Sciences and Technology, Department of chemical engineering and technology Saulėtekio av. 3, LT-10257 Vilnius)

evelina.griniuk@stud.chgf.vu.lt

Photoelectrochemical (PEC) techniques have received a lot of attention because they provide insights into the utilization of solar energy for sustainable production of hydrogen and other chemicals, degradation of organic pollutants, generation of electricity in photofuel cells, etc. A pivotal challenge to realize PEC applications in practice is development of efficient photoelectrode materials [1-3].

Many semiconductor metal oxides, such as TiO_2, WO_3, $BiVO_4$ and α-Fe_2O_3, have been intensely investigated as photoelectrodes due to their high chemical stability in oxidation conditions and reasonably high incident light-to-current conversion efficiencies. Among them, WO_3 is a promising photoanode material for its moderate band gap of 2.5ï 2.7 eV, which allows absorbing ~12% of solar spectrum with a theoretical maximum energy conversion efficiency of ~6.3% [1].

In this work, WO_3 thin films on conductive glass (FTO) substrate were synthesized using sol-gel method and dip-coating technique. Coatings were modified using different amount of polyethylene glycol (PEG) in order to evaluate the influence of this additive on photoelectrochemical response of the layers. The synthesis was carried out at 85ÁC for 180 minutes using different Na_2WO_4 to PEG ratios of (1:1; 1:2, 1:0.5; 1:0.1). Coatings were annealed at 400ÁC for 2 h in air. The composition and surface morphology of the coatings were investigated using X-ray diffraction and scanning electron microscopy (SEM) techniques. Photoelectrochemical response was investigated by cyclic voltammetry in three electrode cell in 0.5 M H_2SO_4 solution in the dark and under light irradiation. Chronoamperometry in two-electrode set-up along with titrimetric analysis were used to evaluate the Faradaic efficiency of photoelectrochemical hypochlorite production with WO_3 photoelectrodes in NaCl solution.

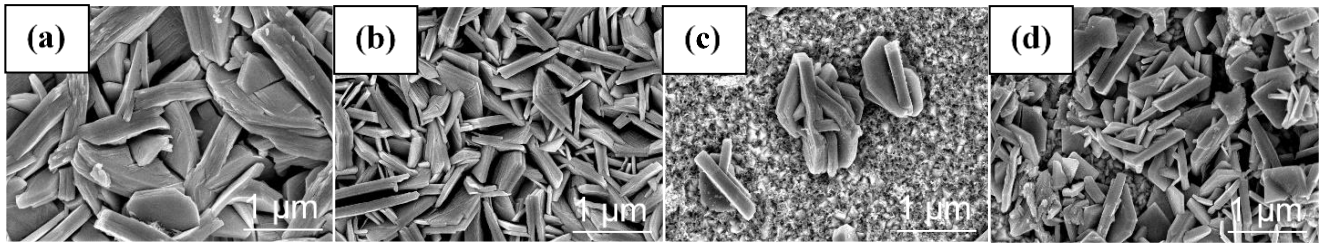

Fig.1. Top view SEM images of WO_3 films synthesized with different Na_2WO_4 to PEG ratios: 1:0.1 (a), 1:0.5 (b), 1:1 (c) and 1:2 (d).

It was found that different amount of PEG used in sol-gel synthesis strongly influences morphology of the WO_3 coatings (Fig. 1). All coatings were photoelectrochemically active, however the highest photocurrent of 0.7 mA cm^{-2} at 1.6 V (Ag/AgCl) was found for the coating synthesized with Na_2WO_4:PEG molar ratio of 1:0.5, which means that these synthesis conditions ensure the most effective generation and transport of photogenerated charge carriers in the oxide layer. Faradaic efficiency of hypochlorite formation ranged between 64 ï 67 %.

Acknowledgment:
This research is funded by the European Social Fund under the No 09.3.3-LMT-K-712-22-0185 ñDevelopment of Competences of Scientists, other Researchers and Students through Practical Research Activitiesò measure.

[1] Q. Zeng, J. Li, J. Bai, X. Li, L. Xia, B. Zhou, Preparation of vertically aligned WO3 nanoplate array films based on peroxotungstate reduction reaction and their excellent photoelectrocatalytic performance, Applied Catalysis B: Environmental **202**, 388-396 (2017)

[2] K. Sayama, Production of High-Value-Added Chemicals on Oxide Semiconductor Photoanodes under Visible Light for Solar Chemical-Conversion Processes, ACS Energy Letters **3 (5)**, 1093-1101 (2018).

[3] W. Yang, R. Ramanujam Prabhakar, J. Tan, S. David Tilley, J. Moon, Strategies for enhancing the photocurrent, photovoltage, and stability of photoelectrodes for photoelectrochemical water splitting, Chemical Society Reviews **48**, 4945ï 5178 (2019).

TROPHIC ECOLOGY OF SMALL MAMMALS IN COMMERCIAL ORCHARDS: INSIGHTS FROM STABLE ISOTOPE STUDIES

Vitalijus Stirkã[1*], Linas Balļiauskas[1], Laima Balļiauskienã[1], Raminta Skipitytã[2], Andrius Garbaras[2]

[1]Nature Research Centre, Lithuania
[2]Center for Physical Sciences and Technology, Lithuania
vitalijus.stirke@gamtc.lt

Foraging strategies in various animal species in recent years are mainly determined by their isotopic niche which is defined by means of stable isotope analysis. According the trophic peculiarities small mammals of the middle latitudes are grouped into herbivores, granivores, omnivores and insectivores. Herbivores (*Microtus* spp.) mainly feed on the green plant material, granivores (*Apodemus* and *Micromys* spp.) on seeds, fruits and/or foods of animal origin, omnivores (*Myodes glareolus*) on both low and high energetic plant resources and animal food, and insectivores (*Sorex* spp.) on foods of animal origin.

In 2018ï 2019 we trapped small mammals in 15 commercial orchards, berry plantations and neighboring control habitats, mainly meadows [1]. In total, 1087 individuals (11 species) were trapped. In the orchards dominant species was common vole (*Microtus arvalis*), 37.9% of all trapped individuals, while in the control habitats dominant was striped field mouse (*Apodemus agrarius*) with the share of 29.0%.

Knowing the trophic ecology of the species that occur in a given location is crucial for understanding the factors that allow their co-existence. Values of the stable isotopes provide trophic-level information that is a time-integrated approximation of assimilated diet. We used hair of the trapped small mammals to investigate ŭ^{13}C and ŭ^{15}N stable isotope signatures. Carbon and nitrogen stable isotope ratios were measured using an elemental analyzer (EA) (Flash EA1112) coupled to an isotope ratio mass spectrometer (IRMS) (Thermo Delta V Advantage) via a ConFlo III interface (EA-IRMS). The accuracy of measurements were better than 0.15 ă for carbon and 0.2 ă for nitrogen isotope ratio.

Species position according ŭ^{15}N values formed one group of all herbivores and the yellow-necked mouse (*Apodemus flavicollis*) and the second of omnivore bank vole *M. glareolus* with the rest of granivore species. ŭ^{15}N values in *Sorex* species exceed all mentioned groups 2ï 3-fold [2]. Compared to natural habitat of the floode meadows [2], distribution of ŭ^{13}C values in commercial orchards was very wide (Fig. 1), especially in harvest mouse (*Micromys minutus*). Most distinct trophic position was characteristic to the commensal house mouse (*Mus musculus*).

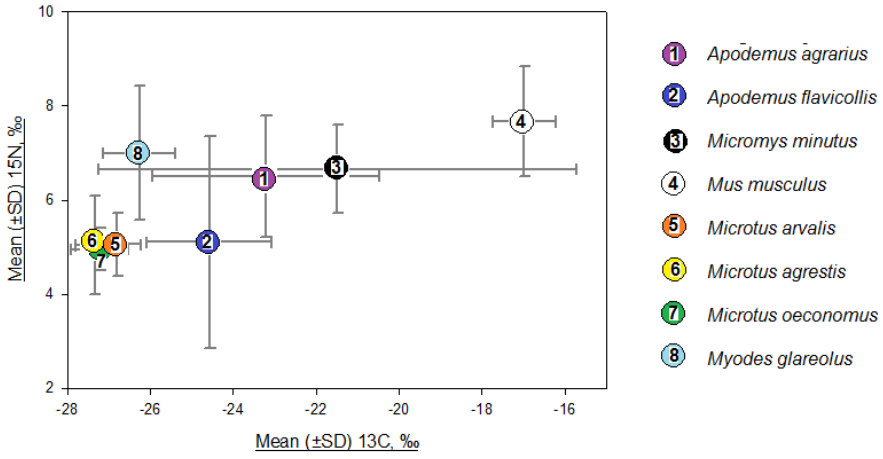

Fig. 1. Differences in the trophic space of granivores (1ï 4), herbivores (5ï 7) and omnivores (8) in commercial orchards.

Concluding, we found that (1) small mammal diet in the orchards did not differ significantly from the surrounding meadows ï this implies also migration of the animals between orchards and meadows; (2) according distribution of ŭ^{15}N and ŭ^{13}C values, dietary niche in the orchards is segregated between small mammal species and groups; and (3) according small mammal community composition and diet, commercial gardens are in between natural and the other agricultural habitats. We presume possible effects of season, intensity of agricultural practices and crop type on the amplitude of the trophic niche of dominant species. Preliminary, the influence of habitat on the isotopic trophic niche is species-dependent and not unidirectional, thus being difficult to make general predictions of species response.

VS, LB and LB were financed by grant MoA Lithuania, No MT-18-3.

[1] Balļiauskas, L., Balļiauskienã, L., Stirkã, V., Mow the grass at the mouse's peril: diversity of small mammals in commercial fruit farms, Animals, **9(6)**, art. no. 334 (2019).
[2] Balļiauskas, L., Skipitytã, R., Balļiauskienã, L., Jasiulionis, M., Resource partitioning confirmed by isotopic signatures allows small mammals to share seasonally flooded meadows, Ecology and Evolution, **9(9)**, 5479-5489 (2019).

ARID1A MUTATIONS IN UTERINE LAVAGE FLUID INDICATES EARLY ENDOMETRIAL AND OVARIAN CANCERS

Ieva Vaicekauskaitơ[1,2], Diana Çilovi ļ [1,2], RÎta Ļiurlienơ[1,], Rasa Sabaliauskaitơ[1,], Sonata Jarmalaitơ[1]

[1] National Cancer Institute, Vilnius, Lithuania
[2] Institute of Biosciences, Vilnius University, Vilnius, Lithuania
ieva.vaicekauskaite@nvi.lt

Introduction. Endometrial cancer (EC) is the most common oncogynecological malignancy worldwide, while ovarian cancer (OC) is the deadliest malignancy[1]. The high incidence and mortality rates are attributed to lack of specific symptoms or effective screening techniques resulting in late diagnosis. OC is mostly diagnosed at stages III or IV, when the 5-year survival rates are only 3-19% [2]. However, even when the cancer is detected early, as is often with EC, disease recurrence rate is 10-15% and there is no available genetic biomarkers with a potential to predict the most aggressive cases with a high risk of relapse [3]. Both EC and OC are often characterized by genomic alterations. *ARID1A*, a subunit of SWI/SNF chromatin remodeling complex, is often mutated in both endometriosis-associated OC and EC. *ARID1A* participates in nucleosome repositioning, thus loss of function mutations in this tumor suppressor gene could lead to global impact on transcription and gene expression [4]. Although currently biopsies are regarded as the gold standard for diagnosis, staging and genetic analysis that may suggest targeted treatment, they are invasive and not suitable for long-term disease monitoring [5]. Both OC and EC shed cells into uterine cavity, which can be sampled non-invasively by uterine lavage, a simple sampling technique that can be performed in a gynecologistôoffice [6]. Sequencing of uterine lavage fluid from EC patients has been shown to detect mutations in up to 100% of malignancies, proving that uterine lavage could be useful in gynecological cancer diagnosis [7].

The Aim of this study was to use targeted sequencing to asses *ARID1A* mutations in OC and EC patientôs uterine lavage fluid and tissue samples and determine *ARID1A* SNP association with clinical features.

Methods. 34 uterine lavage and 21 tissue samples from 54 patients (24 high grade serous ovarian cancer, 8 non-serous ovarian cancer, 11 endometrial cancer and 11 patients with benign conditions) were analyzed by targeted next generation sequencing using Ion AmpliSeqÊ On-Demand Panel targeting *ARID1A* mutations. Pathogenicity of uncertain significance mutations were predicted using online database VarSome [8].

Results. 14 *ARID1A* SNPs were detected in 26% (14/54) patients. 64% (9/14) of these were determined to be pathogenic and the rest were of uncertain significance. *ARID1A* mutations were primarily detected in early stage (pT1, G1) endometrioid EC and mucinous OC, 8/9 pathogenic SNPs were detected in non-serous malignancies. 43% (3/7) mutations were detected in both tissue and uterine lavage samples.

In conclusion, *ARID1A* mutations in uterine lavage samples could be a useful tool to non-invasively detect early stage gynecological malignancies.

[1] F. Bray, J. Ferlay, I. Soerjomataram et al., Global cancer statistics 2018: GLOBOCAN estimates of incidence and mortality worldwide for 36 cancers in 185 countries, CA. Cancer J. Clin. **68**, 394-424 (2018).
[2] H. J. Whitwell, J . Worthington, O. Blyuss et al., Improved early detection of ovarian cancer using longitudinal multimarker models, Br. J. Cancer **122**, 847-856 (2020).
[3] P. Morice, A. Leary, C. Creutzberg, N. Abu-Rustum, E. Darai, Endometrial cancer, The Lancet **387**, 1094-1108 (2016).
[4] T. Takeda, K. Banno, R. Okawa, et al., *ARID1A* gene mutation in ovarian and endometrial cancers (Review), Oncol. Rep. **35**, 607-613 (2016).
[5] Q. Chen, Z. H. Zhang, S. Wang, J. H. Lang, Circulating cell-free DNA or circulating tumor dna in the management of ovarian and endometrial cancer, Onco. Targets. Ther. **12**, 11517-11530 (2019).
[6] J. A. Martignetti, D. Pandya, N. Nagarsheth et al., Detection of endometrial precancer by a targeted gynecologic cancer liquid biopsy, Cold Spring Harb. Mol. Case Stud. **4**, 1-11 (2018).
[7] N. Nair, O. Camacho-Vanegas, D. Rykunov et al., Genomic Analysis of Uterine Lavage Fluid Detects Early Endometrial Cancers and Reveals a Prevalent Landscape of Driver Mutations in Women without Histopathologic Evidence of Cancer: A Prospective Cross-Sectional Study, PLoS Med. **13**, 1-26 (2016).
[8] C. Kopanos, V. Tsiolkas, A. Kouris et al., VarSome: the human genomic variant search engine, Bioinformatics **35**, 1978-1980 (2018).

HIGH AFFINITY BINDING INHIBITORS OF PROTOZOAN PARASITE HSP90

Marius Gedgaudas[1], Aurelija Mickevi ī tė[1], Algirdas Bruk ė tus[2], Daumantas Matulis[1], Egidijus Kazlauskas[1]

[1] Department of Biothermodynamics and Drug Design, Institute of Biotechnology, Vilnius University, Lithuania
[2] Department of Organic Chemistry, Faculty of Chemistry,Vilnius University, Lithuania
marius.gedgaudas@gmc.vu.lt

Parasitic protozoan diseases remain a huge burden worldwide afflicting millions of people. A few notable diseases include malaria, leishmaniasis, toxoplasmosis. These three diseases alone account for over a million deaths every year. Even with current advances in medicine these diseases remain problematic: parasites develop resistance against current drugs, available therapeutics cause severe side affects and for some of the diseases there is no treatment at all.

We are investigating ligands, small organic molecules, that could target an essential protozoan parasite protein ï heat shock protein 90 (Hsp90). Hsp90 is an molecular chaperone found in most eukaryotic cells. Healthy human cells have been shown to tolerate partial Hsp90 inhibition, whereas protozoan parasites rely heavily on their Hsp90 to adapt to stressful conditions when infecting the host. Hsp90 inhibition can disrupt the parasiteõs life cycle [1]. This makes Hsp90 an attractive drug target against these diseases.

Here we present binding characteristics of a series of thiadiazole-based ligands (fig. 1) of human and protozoan N-domain Hsp90.

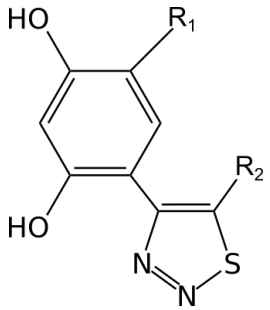

Fig. 1. Thiadiazole-based inhibitor.

[1] Banumathy, Gowrishankar, et al. "Heat shock protein 90 function is essential for *Plasmodium falciparum* growth in human erythrocytes." Journal of Biological Chemistry 278.20 (2003).

PREDICTION OF CANCER CELL VIABILITY AND COMPROMISED MEMBRANE INTEGRITY AFTER PULSED ELECTRIC FIELD TREATMENT USING LUMINESCENCE

Veronika Malyġko[1], Vitalij Novickij[1], Auksã Zinkeviļienã[2], Jurij Novickij[1], Julita Kulbacka[3], Nina Rembialkowska[3], Irutã Girkontaitã[2]

[1] Faculty of Electronics, Vilnius Gediminas Technical University, Vilnius, Lithuania
[2] State Research Institute Centre for Innovative Medicine, Department of Immunology, Vilnius, Lithuania
[3] Department of Molecular and Cellular Biology, Wroclaw Medical University, Wroclaw, Poland
veronika.malysko@vilniustech.lt

Electroporation phenomena is a highly effective method in different fields of application, including cancer treatment [1]. This method is based on pulsed electric fields (PEF) and pore formation in cell membrane consequently causing the increase in cell membrane permeability [2]. The combination of electroporation with drugs, which is known as electrochemotherapy, is the highly effective method in cancer treatment [3]. Although the outcome depending on pulse parameters, and physical factors may vary. Hence the occurrence the permeabilization rate *in vitro* is quite frequently evaluated using fluorescent markers such as propidium iodide (PI), while the viability is checked after 24 hours or days using metabolic activity test or clonogenic assay. In this work, an alternative way for detection of the electroporation efficacy and drop of cell viability following PEF treatment is proposed. This method is based on oxidation of D-luciferin sodium salt utilized to assay the luciferase gene expression in stably transfected bioluminescent mice Sp2/0 myeloma cells.

A 0ï3 kV, 60 A pulsed power generator (VGTU, Lithuania) was used in the study. Cells were treated in electroporation cuvette with 1 mm gap aluminum electrodes (Biorad, Hercules, USA). Pulses in the range of 1ï2.5 kV/cm 0.1ï100 ɛs were generated. Cell permeabilization efficiency was evaluated using propidium iodide (PI, Sigma-Aldrich) and flow cytometry, while viability was estimated using alamarBlueÊ cell viability reagent (Thermo Fisher Scientific, USA) after 24 h. Alternatively, the Sp2/0 transfected cells (Luciferase-pcDNA3 plasmid, Adgene #18964) were treated by PEF and later transferred into the white 96-well plates. Subsequently, D-Luciferin (Promega, USA) was added to the cells, then analyzed concentration was 150 ɛg/ml. Synergy 2 microplate reader and Gen5 software (BioTek, USA) were used for SP2/0 cells luminescence evaluation.

It was shown that the bioluminescence signal was scaling in a dose dependent manner following the same tendency as permeabilization curves obtained using conventional toolkits. At the same time, it also provided a real-time feedback on cell viability since only viable cells luminesce. It was also shown that the extent of permeabilization and thus, the oxidation of D-luciferin is not the same for microsecond and sub-microsecond pulses, while bioluminescence still can be implemented as an effective method for analysis of electroporation phenomena *in vitro*.

This work was supported by grant Nr. S-MIP-19-22 from Research Council of Lithuania. The study was also partly supported by PL NCN Grant SONATA BIS 6 (2016/22/E/NZ5/00671; PI: J. Kulbacka).

[1] T. Kotnik, L. Rems, M. Terek, D. Miklavļiļ, Membrane Electroporation and Electropermeabilization: Mechanisms and Models, Annu. Rev. Biophys. (2019).
[2] D. Miklavļiļ, G. Serġa, E. Brecelj, J. Gehl, D. Soden, G. Bianchi, P. Ruggieri, C.R. Rossi, L.G. Campana, T. Jarm, Electrochemotherapy: Technological advancements for efficient electroporation-based treatment of internal tumors, Med. Biol. Eng. Comput. (2012).
[3] M. Cemazar, G. Sersa, Recent Advances in Electrochemotherapy, Bioelectricity. (2019).

REPRODUCTIVE CHARACTERISTICS OF CRIMEAN TATAR WOMEN ACCORDING TO THEIR SUB-ETHNIC GROUPS

Nataliya Kozak, Lubov Atramentova

Department of genetic and cytology, V. N. Karazin Kharkiv National University, Ukraine
kozaknatali93@gmail.com

Information about genetic processes in local populations plays an important role in understanding many socio-demographic and medical problems. Studies conducted in economically developed countries show that about half of the human gene pool does not reproduce in the next generation due to the death of embryos, stillbirths, neonatal mortality and mortality before the reproductive age, celibacy and sterile marriages [1, 2]. The reproductive behavior of women mainly depends on cultural traditions and differs among representatives of different ethnic groups. As of 2013, in the Autonomous Republic of Crimea, the proportion of Crimean Tatars, whose cultural traditions were based on the Muslim religion, increased in connection with repatriation [3]. The ethnic group of Crimean Tatars is subdivided into three sub-ethnic groups: southern coastal, steppe and mountain-foothill [4]. The purpose of this research is to study the reproductive behavior of Crimean Tatar women, considering their sub-ethnic division.

The data were collected in 2013 in the women's clinic of the Crimean Republican institution "Medical Center for Serving Deported Peoples" (Simferopol). Anonymous survey of women in the post-reproductive age (from 45 to 90 years) was carried out. The questionnaire included questions about the woman's year of birth, her nationality, considering the sub-ethnos, as well as the nationality of her parents. The number of pregnancies and their outcomes were studied as well: medical and spontaneous abortions, ectopic pregnancies, the number of stillbirths and live births.

The distribution of the number of pregnancies and their outcomes in women during the reproductive period indicates statistically significant differences between sub-ethnic groups in terms of the number of pregnancies and medical abortions. In average, a Crimean Tatar woman had 3.6 pregnancies during the reproductive period (4.0 for representatives of the steppe and southern sub-ethnic groups, 2.6 for representatives of the mountain-foothills, $p < 0.05$). Also, one Crimean Tatar woman on average had less than one medical abortion (1.0 in the southern and steppe, 0.65 in the mountain-foothills, $p < 0.05$); 0.3 spontaneous abortions, 0.04 ectopic pregnancies, 2.7 births, 0.1 stillbirths, and 2.6 live births.

Comparison of reproductive indicators in Crimean Tatars and Slavs (Ukrainian and Russian) living in the city of Eupatoria (Autonomous Republic of Crimea) [5] revealed statistically significant differences. Thus, the gene pool of the Crimean Tatar ethnos is reproduced more fully (97 %) than the gene pool of the Slavs (95 %). Slavic women resorted to artificial termination of pregnancy almost twice more often (83 %) than Tatars (45 %). Ectopic pregnancies were noted only by 0.5 % of Tatar women, which is 14 times less frequent than Slavic women (7 %). The percentage of artificially interrupted pregnancies among Tatars is almost 2.5 times less than among Slavs (24 and 58 %, respectively). As a result, the fraction of implemented zygotes in Tartars is twice as high as in Slavs (69 % and 33 %). In terms of the number of pregnancies, Slavs are almost one and a half times larger than Crimean Tatars (5.3 and 3.6, respectively), but despite the greater number of pregnancies, Slavs give birth to fewer children number than Crimean Tatars (on average, 1.8 and 2,7 children respectively). If interethnic differences in the rates of natural increase persist, the ethnic and confessional composition of the Crimean population and its gene pool may change.

The study of the reproductive behavior of Crimean Tatar women of different sub-ethnic groups revealed statistically significant differences in the number of pregnancies and medical abortions. The Crimean Tatar population of the Autonomous Republic of Crimea is characterized by expanded reproduction, in contrast to the narrowed one among the Slavic part of the population.

The authors are grateful to L.A. Mustafayeva for assistance in collecting of factual material.

[1] O.L. Kurbatova, Demographic genetics of urban population (abstract. dis. Sc.D. Moskow, 2014).
[2] Ed. by Ju.P. Altuhov, *Dynamics of population gene pools under anthropogenic pressures.* (Moskow, Nauka, 2004).
[3] State Statistics Committee of Ukraine. All-Ukrainian population census 2001. Russian version. Results. Nationality and mother tongue (2003), [Electronic resource] http://2001.ukrcensus.gov.ua/rus/results/ .
[4] Ed. by E. Chyrbakova. *Essays on the history and culture of the Crimean Tatars* (Simferopol, Crimeauchpedgiz, 2005).
[5] L.A. Atramentova, I.P. Meshcheryakova, O.V. Filiptsova, Reproductive characteristics and the Crowôs index in different populations of Evpatoria, Genetika 49 ¯ 12, 1398ï 1406 (2013).

THE EFFECT OF NAPHTHYLACETIC ACID ON CREEPING GLOXINIA

Gabija Çalpytã

Vytautas Magnus University Agriculture Academy, Faculty of Agronomy, Institute of Agricultural and Food Sciences
Lithuania
gabija.zalpyte@stud.vdu.lt

Creeping gloxinia is a tender climbing plant with bright pink flowers, that originated in Mexico [1]. These plants can be propagated using seeds or cuttings [2]. Creeping gloxinia varieties can be only propagated using cuttings, otherwise they would lose qualities that are characteristic to specific variety. Growth regulators are required to grow plants effectively using cuttings. Auxins are mostly responsible for plant root growth [3] and affect shoot growth [4]. Because of that most attention in this experiment was dedicated to these plant hormones, especially naphthylacetic acid (NAA).

The aim of this study is to determine the effects of different concentrations of naphthylacetic acid on creeping gloxinia plant root and shoot growth.

'Queen Letizia' and 'Queen Morta' cuttings were cut from 4-year old mother plants and were dipped for 2 seconds into four different concentrations of concentrated spirituous (50%) naphthylacetic acid solution and planted into pots filled with peat moss. Used cuttings were 5-7 cm tall of first year shoots. The measurements were carried out twice every 4 weeks.

The results can be seen in Table 1. All the cuttings rooted when the naphthylacetic acid concentration was 0,4%. By increasing the concentration of naphthylacetic acid the number of newly formed roots also increases, and most roots formed after using 0,3 and 0,4% concentration of naphthylacetic acid solution. While the longest roots formed in those cuttings which were dipped in a 0,3% concentration of naphthylacetic acid solution, but after raising the concentration to 0,4% the newly formed roots were shorter.

Significant difference of the length of newly formed shoots can be seen between varieties. While the new shoots of 'Queen Letizia' were measured between 8,8 cm and 17,7 cm, new shoots of 'Queen Morta' reached the length of 22,2 cm to 46,1 cm. Compared to control significantly longer shoots of 'Queen Letizia' were after using 0,2% naphthylacetic acid solution, while significantly longer shoots of 'Queen Morta' compared to control were after using 0,3% NAA concentration.

Table 1. The effect of naphthylacetic acid on root and shoot growth of creeping gloxinia

No.	Treatments	'Queen Letizia'				'Queen Morta'			
		Rooted cuttings, %	Number of roots, pcs.	Root lenght, cm	Lenght of new shoots, cm	Rooted cuttings, %	Number of roots, pcs.	Root lenght, cm	Lenght of new shoots, cm
1.	Control	85,2 abc	2,7 a	3,4 a	8,8 a	81,5 a	2,2 a	4,2 abc	22,2 a
2.	0,1 % NAA	77,8 a	4,9 b	3,6 ab	14,8 abc	77,8 a	4,0 b	4,0 a	34,2 abc
3.	0,2 % NAA	81,5 a	5,5 c	3,9 bcd	17,7 c	96,3 bc	4,4 bc	4,5 abc	33,5 abc
4.	0,3 % NAA	92,6 abc	7,2 d	4,3 d	14,1 abc	92,6 bc	5,2 cde	5,6 c	46,1 c
5.	0,4 % NAA	100,0 c	7,5 d	4,1cd	14,5 abc	100,0 c	6,1e	4,3 abc	39,0 bc

Note: different letters show considerable differences between treatments ($P < 0,05$).

In conclusion we can see that higher concentrations (0,3 -0,4 %) had significantly bigger impact on the rooting and number of roots of creeping gloxinia, however in 0,4 % naphthylacetic acid concentration newly formed roots were shorter. 'Queen Letizia' cuttings grew the longest shoots after using 0,2 % naphthylacetic acid concentration solution, while the longest new shots in 'Queen Morta' cuttings grew after using 0,3% naphthylacetic acid concentration.

[1] J. Paxton. Paxton's magazine of botany, and register of flowering plants, vol. 2, p. 27 (1836).
[2] S. DapkÎnienã, S. Glioþeris. Skiauteruþiø (*Lophospermum* D. Don) morfologiniø dekoratyviøjø savybiø apibÎdinimo apraðas. Akademija, p. 4-8 (2015).
[3] S. Paque; D. Weijers. Q&A: Auxin: the plant molecule that influences almost anything. BMC Biology, vol. 14, **67** (2016).
[4] E. Jakienã, V. Venskutonis. Augimo reguliatoriai augalininkystãje. Akademija, p. 11-20 (2008).

ACCLIMATION EFFECT ON SALMONIDS (*ONCORHYNCHUS MYKISS* AND *SALMO SALAR*) SWIMMING BEHAVIOUR: DETERMINATION OF APPROPRIATE ACCLIMATION PERIOD

Tomas Makaras[1,2], Milda Stankeviļiūtė[2]

[1] Vilnius University, Life Sciences Center, Saulėtekio Ave. 7, 10257 Vilnius, Lithuania
[2] Nature Research Centre, Akademijos Str. 2, 08412, Vilnius, Lithuania
Makaras.tomas@gmail.com

So far, no standards for acclimation guidelines have been established for acceptable acclimation periods prior to behavioural testing with fish. The acclimation period taken by fish to recover from stress after transference to new experimental conditions may play a crucial role in deepening the understanding of behavioural characteristics of the test species, especially in short-term toxicity testing [1,2].

In the present study, we investigated the effect of acclimation period (4 h) on swimming behaviour (locomotor activity) of rainbow trout (*Oncorhynchus mykiss*) and Atlantic salmon (*Salmo salar*). Specifically, we explored fish behavioural patterns based on specific endpoints (average, maximum and angular velocity) during the acclimation period and determined the acclimation period suitable for the test fish species. We expected that after transference to their new experimental conditions, fish individuals would experience stress followed by a period of exploration and increased intensity of fish locomotor activity before settling to more stable (baseline) activity levels.

The locomotor activity of *O. mykiss* and *S. salar* significantly varied during the 4-h-acclimation period (Fig. 1). Based on the tested endpoints, the locomotor activity of both species significantly decreased over time. According to average and angular velocity endpoints, the locomotor activity of *O. mykiss* significantly decreased ($p < 0.004$) during 3–4 h of acclimation. A similar behavioural tendency to *O. mykiss* was observed in the assessed endpoints of *S. salar* locomotor activity. According to average velocity a significant decrease ($p < 0.001$) in locomotor activity was determined during 3–4 h, while changes in angular velocity data were established much earlier, i.e. during 2 h of acclimation. However, no significant behavioural differences between test species was found. These results revealed that in order to adjust fish activity to more stable baseline levels, acclimation of *O. mykiss* and *S. salar* should last at least for 2 h.

Since behavioural testing is not clearly standardized and experimental setup may depend on the purpose of the study, acclimation period setup in toxicity testing remains an important issue across studies. In cases of inappropriate duration of fish acclimation (e.g. duration is too short), the observed behaviour in fish may not reflect the actual impact of toxicants due to the interference of effects caused by stressors (e.g. new environment or toxicants) leading to high behavioural variability of fish. The results of this study revealed that the appropriate acclimation period on salmonid species is important in managing fish stress before the onset of behavioural observations. We consider it important to the acclimation period suitable for specific fish species before starting actual toxicity experiments.

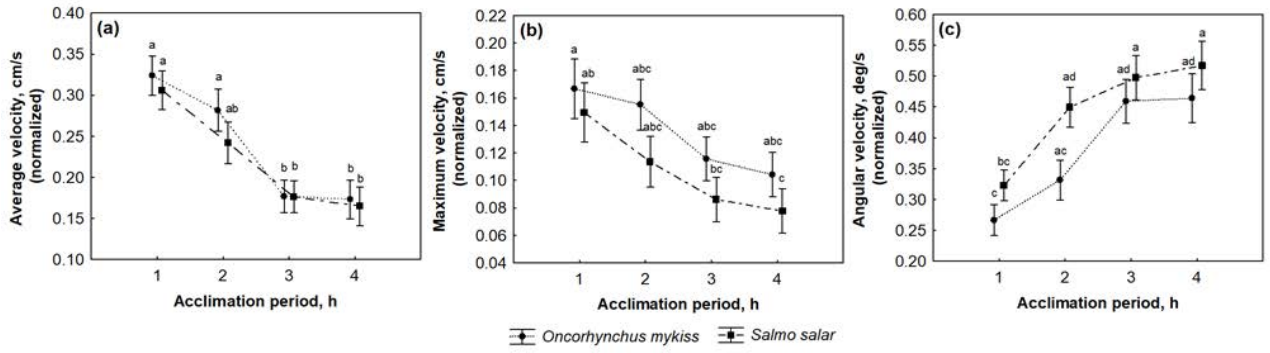

Fig. 1. Comparison of average velocity (cm/s) (a), maximum velocity (cm/s) (b) and angular velocity (deg/s) (c) (mean ÑSEM, n = 24) of *O. mykiss* and *S. salar* during a total 4-h acclimation. Letters indicate the groups that differ significantly at level $p < 0.05$.

This research was supported by the research infrastructure Vilnius University, Life Sciences Center and Open Access Centre for Nature Research at the initiative of the Open R&D Lithuania network. This research was funded by the European Social Fund under the measure No 09.3.3-LMT-K-712 ñDevelopment of Competences of Scientists, other Researchers and Students through Practical Research Activitiesò.

[1] S. D. Melvin, M. A. Petit, J. P. Duvignacq, J. P. Sumpter, Towards improved behavioural testing in aquatic toxicology: Acclimation and observation times are important factors when designing behavioural tests with fish, Chemosphere **180**, 430-436 (2017).
[2] S. J. OõNeill, J. E. Williamson, L. Tosseto, C. Brown, Effects of acclimatisation on behavioural repeatability in two behaviour assays of the guppy *Poecilia reticulate*, Behavioral Ecology and Sociobiology **72**, 166 (2018).

THE INFLUENCE OF NANOSECOND ELECTROPORATION ON THE DEVELOPMENT OF ANTIBODIES AGAINST TUMOR CELLS

Eivina Radzevičiūtė[1], Austėja Balevičiūtė[1], Augustinas Želvys[1],Vitalij Novickij[2], Karolina Žilionytė[3], Irutė Girkontaitė[1]

[1]State Research Institute Centre for Innovative Medicine, Department of Immunology, Vilnius, Lithuania
[2]Institute of High Magnetic Fields and Department of Electrical Engineering, Vilnius Gediminas Technical University, Vilnius, Lithuania
[3]National Cancer Institute, laboratory of Immunology, Vilnius, Lithuania
eivina.radzeviciute@gmail.com

Oncological diseases are one of the most common causes of death worldwide. According to the World Health Organization, over 18 million new cases of various cancers were recorded in 2018 [1]. The limited range of solutions for fighting oncological diseases encourages searching for alternative, more effective anticancer treatment strategies. One of the novel therapeutic approaches uses electroporation (EP) in combination with chemotherapeutics, calcium ions or other drugs. Pulsed electric fields (PEF) create nanoscale aqueous membrane pores, facilitating rapid intracellular, usually impermeable drug molecule delivery [2].

In this study tumors in C57BL/6J and BALB/c mice were induced by subcutaneously injecting LLC1 and SP2/0 cells respectively. When tumors reached 100 mm^3, treatment was applied as described below. For C57BL/6J carcinoma tumor ablation, bleomycin electrochemotherapy (ECT) was used with four different conditions of high-frequency nanosecond EP*[1] in comparison with ESOPE*[2] procedure. BALB/c mice tumors were ablated with calcium electroporation (CaEP) (4.5 kV/cm x 600ns x 500 /1 MHz) with or without dendritic cells vaccine (DCV) (Fig.1). Mice survival and development of antibodies (Ab) against tumor cells were assessed during the experiment.

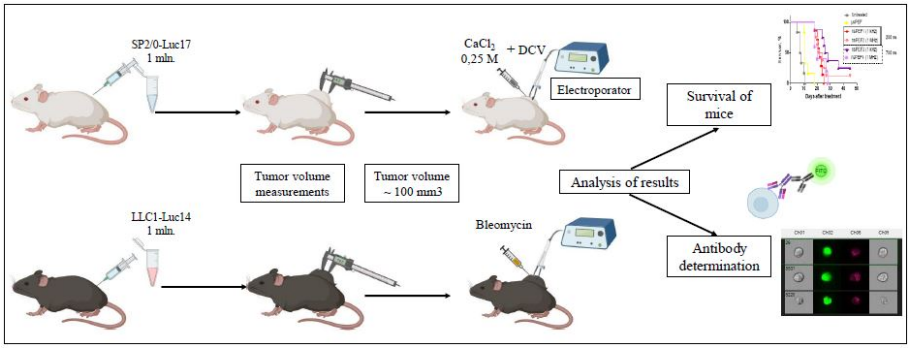

Fig. 1. Experimental scheme.

We showed that CaEP and ECT of tumors prolonged the lifespan of BALB/c and C57BL/6J mice. Tumor–bearing untreated BALB/c mice median survival was 8 days while CaEP and CaEP + DCV-treated mice median survival was 32 and 30 days, respectively. Untreated C57BL/6J tumor–bearing mice median survival was 7.5 days, whereas EP-treated mice median survival was approximately 2-3 times longer (nsPEF1 – 11 days; nsPEF2 – 22 days, nsPEF3 – 22.56 days, nsPEF4 – 27 days, and ESOPE-treated – 20 days).

Tumor-bearing untreated BALB/c mice did not develop Ab to SP2/0 tumor cells. The lifespan of untreated mice was up to 11 days. Probably, the Ab did not develop due to the rapid growth of tumors, resulting in reduced mice lifespan. Anti-Sp2/0 Ab in treated BALB/c mice were assessed at 0, 10, 20 and 30 days after the treatment. The Ab against tumor cells were detected not earlier than 20 days after the treatment. Only 30 days after treatment, CaEP + DCV-treated mice had higher level of Ab compared to only CaEP-treated mice.

We observed that tumor-bearing untreated C57BL/6J mice develop Ab against LLC1 tumor cells 10 days after development of the tumors. However, the levels of Ab in ECT-treated mice were higher. The levels of anti-LLC1 Ab have increased in nsPEF1, nsPEF2, nsPEF3 and nsPEF4-treated mice compared with the untreated and ESOPE-treated mice.

Our study has shown the EP, by itself or in combination with other drugs, to prolong the lifespan of tumor-bearing mice, resulting in increased anti-tumor Ab levels. These results suggest that anti-cancer Ab may be on the frontline in the fight against cancer. Although, further studies need to be done to confirm this hypothesis.

Acknowledgement: The financial support of the Research Council of Lithuania (S-MIP-19-22).

*[1]nsPEF1 (3.5 kV/cm x 200 ns x 200 /1 kHz); nsPEF2 (3.5 kV/cm x 200 ns x 200 /1 MHz); nsPEF3 (3.5 kV/cm x 700 ns x 200 /1 kHz); nsPEF4 (3.5 kV/cm x 700 ns x 200 /1 MHz).

*[2]ESOPE - European standard operating procedures for electrochemotherapy (1.3 kV/cm x 100 μs x 8 /1 Hz).

[1] WHO. (2020). Who Report on Cancer. WHO.
[2] Chen, Y., Moser, M. A. J., Luo, Y., Zhang, W., and Zhang, B. (2019). Chemical Enhancement of Irreversible Electroporation: A Review and Future Suggestions. Technology in Cancer Research and Treatment, 18, 1–13. https://doi.org/10.1177/1533033819874128

ESTABLISHMENT AND CHARACTERIZATION OF A NEW PANCREATIC DUCTAL ADENOCARCINOMA CELL LINE CAPAN-26

Eglã Çalytã[1], Veronika Dedonytã[2], Benediktas Kurlinkus[3], Audrius Ġileikis[3], Peter Schemmer[3,4], Mindaugas Valius[1]

[1]Proteomics Centre, Institute of Biochemistry, Vilnius University Life Sciences Centre, Vilnius, Lithuania
[2]Department of Botany and Genetics, Institute of Biosciences, Vilnius University Life Sciences Centre, Vilnius, Lithuania
[3]Institute of Clinical Medicine, Clinic of Gastroenterology, Nephrology, and Surgery, Faculty of Medicine, Vilnius University, Vilnius, Lithuania
[4]General, Visceral and Transplant Surgery, Department of Surgery, Medical University of Graz, Graz, Austria
egle.zalyte@gf.vu.lt

Cell lines have been used in cancer research for many years. However, an ideal model of cancer must resemble primary tumor as close as possible. Established lines that have been passaged for a long time adapt to an artificial *in vitro* environment and lose their original phenotype due to genetic drift. Also, each cancer patient and each disease is different. If we want to gain a broader knowledge about cancer intertumoral heterogeneity, we are constantly in need of new cancer cell lines. It is especially important for pancreatic cancer, which is one of the most aggressive cancers known. Although pancreatic cancer accounts for only 3% of cases among the leading cancer types in the United States, it places fourth according to the number of deaths. When metastatic pancreatic cancer is diagnosed, the 5-year patient survival decreases about ten-fold in comparison to an early detected disease [1] and, unfortunately, most of the time pancreatic cancer is diagnosed at an advanced stage. Difficulties regarding an early pancreatic cancer detection arise from great genetic and phenotypic diversity in pancreatic tumors, which makes it difficult to develop sensitive and specific biomarkers [2,3]. Here, again, new cell lines that can represent a variety of pancreatic cancer cases become critically important.

In this study we present a novel pancreatic ductal adenocarcinoma cell line Capan-26. This cell line was derived from a primary tumor of a 65-years old female Lithuanian patient with pancreatic ductal adenocarcinoma stage II. To our knowledge, it is the first pancreatic cancer cell line derived from a Lithuanian patient. We characterized the cells functionally and genetically: determined their growth rate, detected expression of pancreatic cancer and stem cell markers (CEACAM6, CA19-9 and CD44, OCT4, ZEB1, respectively), confirmed that cells form colonies in soft agar, analyzed karyotype and found mutations of cancer related genes *KRAS* and *TP53*. Also, we discovered that Capan-26 cell line is sensitive to gemcitabine, drug that is widely used for pancreatic cancer treatment.

In conclusion, we believe that Capan-26 cell line represents an effective tool for preclinical pancreatic cancer studies.

This work was funded by ñHealthy Ageingò programme of the Research Council of Lithuania (LMTLT); agreement No. S-SEN-20-16.

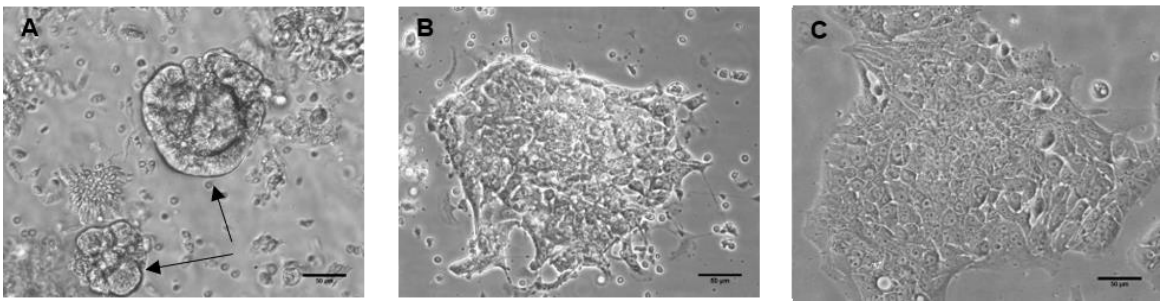

Fig. 1. Process of cancer cell line establishment. A. Day 0 - dissociated tumor tissue. Arrows depict complexes of cancer cells. B. Day 2 - primary cancer cell colony. C. Day 200 - an established cancer cell line. Scale bar - 50 µm.

[1] R.L. Siegel, K.D. Miller, A. Jemal, Cancer statistics, 2020, CA: a cancer journal for clinicians 70(1) (2020) 7-30.
[2] A.K. Witkiewicz, E.A. McMillan, U. Balaji, G. Baek, W.C. Lin, J. Mansour, M. Mollaee, K.U. Wagner, P. Koduru, A. Yopp, M.A. Choti, C.J. Yeo, P. McCue, M.A. White, E.S. Knudsen, Whole-exome sequencing of pancreatic cancer defines genetic diversity and therapeutic targets, Nature communications 6 (2015) 6744.
[3] S. Hasan, R. Jacob, U. Manne, R. Paluri, Advances in pancreatic cancer biomarkers, Oncology reviews 13(1) (2019) 410.

GENOTOXIC AND CYTOTOXIC EFFECTS OF MICROPLASTICS ON *ONCORHYNCHUS MYKISS*: EXPLORATORY DATA ANALYSIS USING MACHINE LEARNING

Agnė Bulaitė[1], Milda Stankevičiūtė[1], Janina Pagusienė[1]

[1] Laboratory of Genotoxicology, Nature Research Centre, Lithuania
bucaite.agne@gmail.com

Plastic production increased dramatically in the last couple of decades making microplastic (MP) a growing problem today. MPs are tiny ubiquitous plastic particles smaller than five millimeters (5 mm) in size and are composed of different polymer types. The presence of this anthropogenic pollutant in aquatic ecosystems concerns researchers worldwide since adverse effects on animal models are not fully understood. The aim of this study was to explore the long-term genotoxic and cytotoxic effects of microplastics on the rainbow trout (*Oncorhynchus mykiss*) larvae. Fish were exposed to polystyrene (PS), polyethylene terephthalate (PET) and polyethylene (PE) MPs. It is important to notice that environmentally relevant concentrations of MP were used. Cytogenetic damage was assessed using erythrocyte nuclear abnormalities assay. The formation of micronuclei (MN), nuclear buds (NB), nuclear buds on filament (NBf), blebbed nuclei (BL) cells were assessed as genotoxicity endpoints, and 8-shaped nuclei, fragmented apoptotic (FA) and bi-nucleated (BN) cells as cytotoxicity endpoints. In addition, bean shaped nuclei, non-nucleated (EN) and vacuolated nuclei (VacNuc) cells were evaluated. Data analysis was performed using R [1] and RStudio [2] software. Correlations between variables were calculated separately in each treatment and control groups. In control group the highest correlation was between MN and BL (Pearson correlation coefficient r = -0.43), in control (with particles) group - between 8-shaped nuclei and EN (Pearson correlation coefficient r = 0.72), in PS group - between MN and 8-shaped nuclei (Pearson correlation coefficient r = 0.67), in PET group - between MN and NB (Pearson correlation coefficient r = 0.57) and in PE group - between MN and 8-shaped nuclei (Pearson correlation coefficient r = 0.82). The investigation of potential relationships between cytogenetic endpoints in rainbow trout using principal component analysis (PCA) yielded two principal components (PCs) which explained 43% of the total variance. Afterwards, PCA was done in each treatment group separately. Contributions of variables were different in different MP exposure groups which could suggest a possibility that MPs of different polymer types could induce nuclear and cellular damage by different mechanisms. Unfortunately, this area of study is not adequately researched. In this analysis, the Hopkins statistic was more than 0.5 (H = 0.712), indicating that the data tends to cluster. For this reason, k-means analysis was performed. Optimal number of clusters was calculated using elbow method (yielded 2 clusters), average silhouette method (yielded 2 clusters) and gap statistic method (with 500 bootstrap samples yielded 1 cluster). k-means clusters were compared with real treatment groups by performing cross-tabulation. Results of this analysis help to generate new hypotheses for future experiments, as further studies of the ecotoxicological impacts of MPs on fish (especially in early stages of development) are required.

Genotoxicity and cytotoxicity studies were funded by the Research Council of Lithuania through the project P-MIP-21-229.

[1] R Core Team (2020). R: A language and environment for statistical computing. R Foundation for Statistical Computing, Vienna, Austria. https://www.R-project.org/. R version 4.0.3

[2] RStudio Team (2020). RStudio: Integrated Development Environment for R. RStudio, PBC, Boston, MA. http://www.rstudio.com/. RStudio version 1.3.1073

DEVELOPMENT OF FLUORESCENCE-BASED TRANSPOSITION ASSAY FOR *SACCHAROMYCES CEREVISIAE*

Gerda Skinderytė[1], Saulius Serva[1], Aleksandras Konovalovas[1]

[1]Department of Biochemistry and Molecular Biology, Vilnius University, Lithuania
gerda.skinderyte@gmail.com

Yeast *Saccharomyces cerevisiae* is one of the best understood eukaryotic model organisms. It is used for research of various biological processes like gene expression, cell cycle, and metabolism, as well as for virus research [1,2]. ScV-LA is a dsRNA yeast virus belonging to *Totiviridae* family. The extracellular phase of this virus is unknown; in addition, virus does not interfere with cell growth [3]. Another endogenous elements of yeast are mobile genetic elements ï transposons. Six families of transposons Ty1-Ty5 and Ty3p belonging to LTR-retrotransposons are found in yeast [4,5]. Transposons can impact the integrity of the genome, alter the expression of adjacent genes, or cause gross chromosomal rearrangements [6]. Basing on transcriptomic and proteomic data, the hypothesis was raised that ScV-LA virus may influence transposition efficiency. In order to assess the influence of ScV-LA on the transposition rate, the classical transposition test was updated by design of new fluorescence-based transposition rate assay, suitable for wild type yeast strains to be addressed.

In this study, the new transposition assay was developed and applied practically. The control experiment demonstrated that *S. cerevisiae* cells expressing GFP can be separated from non-fluorescent cells. The experimental plasmid, containing Ty1 transposon sequence and fluorescent reporter gene, was constructed and used to test transposition efficiency in laboratory yeast strains. Furthermore, suitable method to fix yeast cells prior to flow cytometry was selected and sufficient time of transposition induction was determined. The new transposition assay based on fluorescence will be used to study the interplay between ScV-LA virus and Ty1 transposition in *S. cerevisiae*.

---

[1] D. Petranovic, K. Tyo, G.N. Vemuri, J. Nielsen, Prospects of yeast systems biology for human health: integrating lipid, protein and energy metabolism, FEMS Yeast Research. **10**, 1046ï 1059 (2010).
[2] R.Y. Zhao, Yeast for virus research, Microb Cell. **4**, 311ï 330 (2017).
[3] R.B. Wickner, T. Fujimura, R. Esteban, Viruses and prions of Saccharomyces cerevisiae, Adv Virus Res. **86**, 1ï 36 (2013).
[4] J.M. Kim, S. Vanguri, J.D. Boeke, A. Gabriel, D.F. Voytas, Transposable Elements and Genome Organization: A Comprehensive Survey of Retrotransposons Revealed by the Complete Saccharomyces cerevisiae Genome Sequence, Genome Res. **8**, 464ï 478 (1998).
[5] M. Carr, D. Bensasson, C.M. Bergman, Evolutionary Genomics of Transposable Elements in Saccharomyces cerevisiae, PLoS One. **7** (2012).
[6] G. Bourque, K.H. Burns, M. Gehring, V. Gorbunova, A. Seluanov, M. Hammell, M. Imbeault, Z. Izsv§k, H.L. Levin, T.S. Macfarlan, D.L. Mager, C. Feschotte, Ten things you should know about transposable elements, Genome Biol. **19** (2018).

INVESTIGATION OF ANTICANCER DRUGS INFLUENCE ON BREAST CANCER CELL MODELS

Yuliia Khmelnytska[1,2], Olena Perepelytsina[2], Mykhailo Sydorenko[2]

[1] Educational and Scientific Centre „Institute of Biology and Medicine“. Taras Shevchenko National University of Kyiv, Ukraine

[2] Department of Biotechnical Problems of Diagnostics, Institute for Problems of Cryobiology and Cryomedicine, National Academy of Science of Ukraine, Kyiv, Ukraine.

iuliakhmelnitska@gmail.com

Background. The tumor consists of different malignant cells like ordinary cancer cells and cancer stem cells. It is necessary to use therapeutic agents targeting all heterogeneous tumor cells population for successful treatment. The research aimed to study the mono- and combination therapeutic effects of anticancer drugs such as methotrexate (0.1 and 1 μg/ml) and salinomycin (1-40 μM). Two anticancer drugs with different cytotoxic mechanisms were tested in 2D and 3D culture.

Methods. The cells MCF-7 were cultivated in standard conditions in 2D and 3D culture. MCF-7 spheroids were generated with 2% carboxymethyl cellulose on an orbital shaker (PSU-10i, Biosan, Latvia) at 80 rpm for 3–5 hours at non-adhesive conditions. Monolayer and spheroid cultures were incubated with salinomycin (1-40 μM) and methotrexate (0.1 and 1 μg/ml). MTT-test was used to detect the cytotoxicity effect of antitumor drugs. Expression markers of cancer stem cells (bmi-1, CD44, CD133) and cytokeratin (clone AE1/AE3) were performed by immunochemistry. Morphometric study on 3D culture was carried out using the AxioVision 2ooo (Zeiss) program.

Results. The results demonstrated that the IC50 for Sal was 19 μg/ml, IC50 for Met 67,4 μg/ml, IC50 for Sal+Met 0,1μg/ml – 42.7 μg/ml, IC50 for Sal+Met1μg/ml – 34,5 μg/ml. The IC50 for Sal 1-40 μM + Met 1 μg/ml had twice smaller than the IC50 for Sal and Met separately. The results of immunochemistry showed that after incubation with Met 10 μg/ml expression level of cancer stem cells markers were higher 2-3 times than Sal 4 μM + Met 0,1 μg/ml. The expression of cytokeratin decreased by 25% and 0 % compared to control after combination Sal 40 μM + Met 0.1 and Sal 40 μM + Met 1 μg/ml respectively. The next stage of the work was the study of drugs in a 3D culture. The results of culturing spheroids with (Sal 40μM +Met 1μg/ml; Sal 40μM + Met 0,1 μg/ml) was decreased spheroid size by 82% and 73% in accordance. Cytotoxicity of antitumor drugs on tumor spheroids with Sal 4 μM + Met 1 μg/ml and Sal 4 μM + Met 0,1 μg/ml were reflected in decreasing spheroid volume by 40% and 36%. The decreasing of spheroids size was a dose-dependent tendency from 4μM to 40 μM of Sal.

Conclusion. Our result demonstrated that 2D and 3D cultures were sensitive to mono- and combination therapy. The decrease of size spheroid culture and decrease in live-cell viability after incubation with Sal 4-40 μM + Met 0,1-1 μM is a good marker for synergistic activity. The data showed that Sal + Met hasn’t cytotoxic influence on the cancer stem cell population.

INSIGHT INTO THE HETEROGENEITY OF BREAST CANCER THROUGH NEXT GENERATION SEQUENCING

Justina Gaizevska[1,3], Ausra Stumbryte-Kaminskiene[2], Rasa Sabaliauskaite[1], Sonata Jarmalaite[1,3]

[1] Laboratory of Genetic Diagnostic, National Cancer Institute, Vilnius, Lithuania
[2] Department Biobank, National Cancer Institute, Vilnius, Lithuania
[3] Institute of Biosciences, Vilnius University Life Sciences Center, Vilnius, Lithuania
justina.gaizevska@nvi.lt

Worldwide, breast cancer (BC) is the most commonly diagnosed type of cancer in women and the leading cause of cancer-related death [1]. BC is a heterogeneous disease, which differ biologically among different patients and even within each individual tumor, therefore a major goal of improved classification of BC subtypes, is to stratify patient populations. Advanced in molecular characterization of tumors not only improve classification, but also point directly to molecular mechanisms that lead to different therapeutic responses [2]. Aim of this study was to identify clinicopathological and potential molecular/genetical predictors of breast cancer.

A total of 24 female BC patients form National Cancer Institute were included in this study. Six genes: *TP53*, *CASP8*, *MTHF*, *MDM2*, *MDM4* and *CCR5* were selected based on their mutation frequency and significance for disease development. Next generation sequencing (NGS) technology was applied for genomic profile analysis of BC. All identified mutations were validated by reviewing the results with Integrative Genomics Viewer (IGV). All identified genetic changes were classified as pathological, drug-responsive, benign, and variant of uncertain significance (VUS). Though, ClinVar is the major database used in clinical practice, mutations rated as VUS were additionally checked in other databases.

130 mutations were identified in breast tumor samples (24/24 patients). Non-pathological changes accounted for 77.7% of all detected mutations. Among them, benign gene sequence changes were the most common (62.3%). Pathological/likely pathological mutations accounted for 8.4% of all variants detected. *TP53* had the greatest variety of genetic changes. Two VUS of *TP53* gene were identified as likely pathological by COSMIC and VARSOME databases. *CASP8* and *MTHFR* genes also showed a high frequency of changes, but no pathological mutations were detected. We did not find any associations between presence of pathological changes and clinical-demographic characteristics of patients.

In conclusion, this genetic profiling revealed that *TP53* gene has the greatest variety of mutations and the largest number of pathological variants in BC patients in this study. However, more research is needed to determine connection between genetic changes and clinical manifestations of disease and to use the results in molecular/genetic classification of tumors.

[1] Z. Momenimovahed, H. Salehiniya, Epidemiological characteristics of and risk factors of breast cancer in the world, Breast Cancer (Dove Med Pres) 11, 151-164 (2019).
[2] D. P. Hill, A. Harper et al., Cisplatin-resistant triple-negative breast cancer subtypes: multiple mechanisms of resistance, BMC Cancer 19, 1039 (2019).

REDOX ENZYMES INVOLVED IN *ARABIDOPSIS THALIANA* (L.) HEYNH. SEEDLING RESPONSE TO COLD PLASMA TREATMENT OF SEEDS

Edgaras Tamelis[1,2], Lauryna Ragauskaite[1], Dalia Gelvonauskiene[1], Danas Baniulis[1]

[1] Institute of Horticulture, Lithuanian Research Centre for Agriculture and Forestry, Babtai, Kaunas reg., Lithuania,
[2] Faculty of Natural Sciences, Vytautas Magnus University, Kaunas, Lithuania
E.tamelis@gmail.com

Successful seed germination and seedling establishment are critical steps in agricultural production and in the maintenance of natural ecosystems. Seed treatment with cold plasma (CP), is an emerging eco-agricultural technology that has potential application for enhancement of plant growth and adaptation. In addition to sterilization effect, treatment of seeds with CP has been shown to have effect on a broad spectrum of plant development and physiological processes. Although the body of information on the biological effects of the CP is growing, the complex biological mechanisms involved in the plant response remains vague. The objective of this study was to assess role of reactive oxygen species (ROS) producing and redox balance regulating enzymes in response of the model plant *Arabidopsis thaliana* (L.) Heynh. to the seed treatment with atmospheric pressure dielectric barrier discharge plasma source. Seeds of *A. thaliana* Columbia ecotype wild-type (Col-0) and gene knockout mutant lines of ROS producing enzymes NADPH oxidase *AtRbohB* and *AtRbohF* and enzymes involved in maintenance of the cellular redox balance, *AtAPX1* and *AtCAT2,* were used in the study. Seeds were treated for 1.5 or 3.0 min at 3 mm distance from the CP source at 60-80% air humidity and stored for 7 days at 25 ^{o}C after the treatment. The significant changes in root length was observed for the 2 day old seedlings of Col-0, *AtRbohB, AtRbohF* and *AtCAT2* germinated from the seeds treated for 3 min. *AtRbohF* showed an enhanced (~6 % compared to control) root growth response similar to that of the wild-type genotype, meanwhile the length of roots was reduced for the *AtRbohB* and *AtCAT2* mutants (20 % and 10 %, respectively). In contrast to the effect observed for the roots, 3 min CP treatment had stimulating effect on hypocotyl development of the *AtAPX1* mutant (~7 %). Meanwhile hypocotyls of the *AtRbohF* and *AtCAT2* were shorter compared to control (9 % and 23 %, respectively). Hypocotyls of the Col-0 and *AtRbohB* mutant showed no response to CP treatment. The analysis confirmed that the redox enzymes play essential role in *A. thaliana* seedling phenotype formation in response to CP treatment and the effect could be linked to the role of ROS in seed germination and seedling organ development.

BIOACCUMULATION OF GRAPHENE OXIDE NANOSTRUCTURES IN *SALMO TRUTTA* AT EARLY DEVELOPMENT STAGES

Augustas Morkvėnas[1], Givilė Jurgelėnė[2], Sergej Ġemļiuk[3], Nijolė Kazlauskienė[2], Vitalijus Karabanovas[1,4]

[1] Biomedical Physics Laboratory, National Cancer Institute, Baublio 3b, LT-08406, Vilnius, Lithuania
[2] Nature Research Centre, Akademijos st.-2, LT-08412 Vilnius, Lithuania
[3] SRI Center for Physical Sciences and Technology, SavanoriÛave. 231, LT-02300, Vilnius, Lithuania
[4]Department of Chemistry and Bioengineering, Vilnius Gediminas Technical University, Sauletekio Ave. 11, LT-10223 Vilnius, Lithuania
a.mmorkvenas@gmail.com

Graphene oxide (GO) has the great potential for biomedical applications and environmental protection. The increased use of GO raises their release into the environment. However, the health risks associated with environmental exposure to GO are largely unknown. Due to their unique physiochemical properties, GO and its composites could be applied to wastewater treatment and to adsorptive remediation of environmental pollutants.

The aim of this study is to examine the distribution of GO 40 mg/L in *Salmo trutta* embryos and larvae using confocal fluorescence microscopy. Analysis was based on 3D autofluorescence imaging of test-organisms (Fig. 1. B and E). GO distribution in embryo chorion and external body tissues of larvae was evaluated. For the experiment, *S. trutta* embryos at the eyed-egg stage and 4 day old larvae were obtained from the hatchery (Lithuania). Studies have been carried out with non-protected life-stages accordance with EU Directive 2010/63/EU. The laboratory treatment was carried out in an environmental chamber (Bronson PGC-660, Zaltbommel, The Netherlands) with continuous aeration under static conditions.

The bright field image of control embryos show that the chorion surface is smooth with regularly distributed darker spots (Fig. 1. A). These darker spots are chorion pores that are important for oxygen/carbon dioxide, nutrients and excretion product transport to and from the embryo, respectively. After 4 days of incubation with GO 40 mg/L, in embryos chorion appeared non autofluorescence areas (dark spots), which indicated GO adhesion on surface of chorion (Fig. 1. E). Furthermore, dark spots of GO can be seen directly in some areas of embryos chorion and larvae internal tissues in the bright field image (Fig. 1. D and F). GO could clog the chorion pores and affect embryonic development of fish [1]. The question about non-homogenous GO adhesion on the organism is still open, because their biodistribution have not been fully investigated.

This work was funded by the Research Council of Lithuania, Project No. S-MIP-20-22.

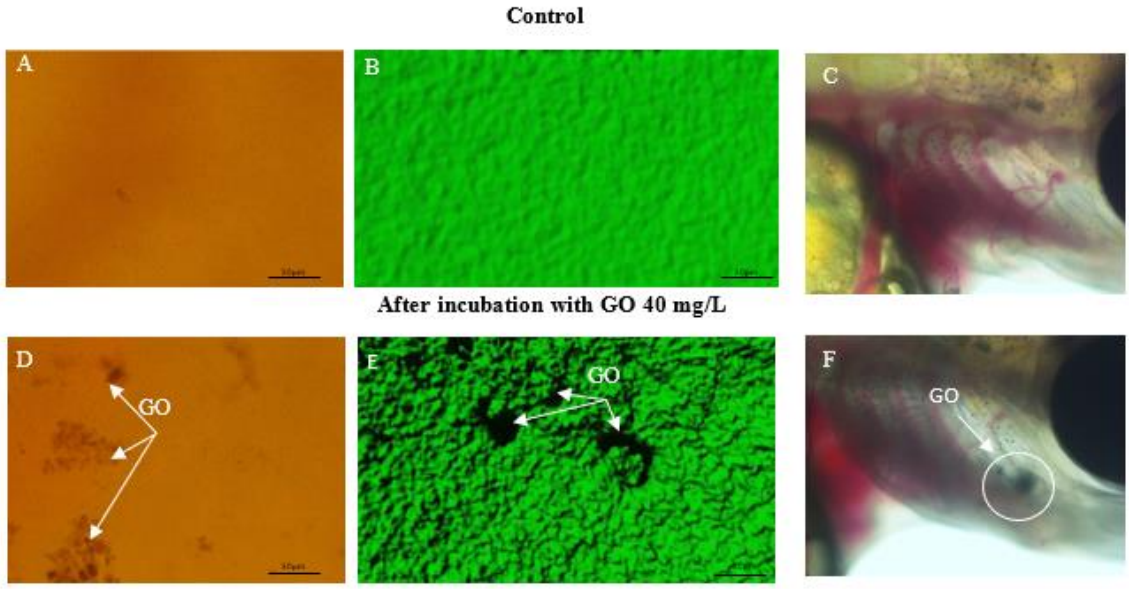

Fig. 1. The bright field (A and D) and 3D reconstruction images (B and E) of *S. trutta* embryos chorion and larvae (C and F) after 4 days of incubation with GO 40 mg/L.

[1] Chen Y., Sun J., Hu X., Zhou Q. 2016. Specific nanotoxicity of graphene oxide during zebrafish embryogenesis. Nanotoxicology **10**(1), 42-52.

GENO- AND CYTOTOXIC RESPONSES IN FLOUNDER (*PLATICHTHYS FLESUS*) FROM THE LITHUANIAN COASTAL ZONE (BALTIC SEA)

Reda Nalivaikienė[1], Virginija Kalcienė[2], Aleksandras Rybakovas[1], Gilvinas Pilkys[1], Giedrė Vilkinskienė[1], Laura Butrimavičienė[1]

[1] Nature Research Centre, Institute of Ecology, Akademijos Str. 2, LT-08412 Vilnius, Lithuania
[2] Vilnius University, Life Sciences Center, Institute of Biosciences, Saulėtekio av. 7, LT-10257 Vilnius, Lithuania
reda.eglinskaite@gamtc.lt

Lithuanian coastal areas of the Baltic Sea are under significant threat of contamination from whole basin of the Nemunas River, Klaipėda port – one of the largest in the region, resorts and oil terminals. Genotoxic contaminants can pose risk to marine organisms and eventually induce changes in whole ecosystem. *In situ* performed environmental monitoring, which is based on cytogenetic assessment, provides data about the current status of target organisms and can be successfully used for the evaluation of impacts caused by accidental spills and/or release of hazardous contaminants in the marine environment. Number of studies performed *in situ* in different areas of the Baltic Sea demonstrates, that *Platichthys flesus* is sensitive and informative bioindicator of genotoxic contamination [1, 2, 3].

The aim of this study was to assess levels of environmental genotoxicity and cytotoxicity in *P. flesus* at three study sites of the coastal zone of Lithuania (Klaipėda-Būtingė area) in summer of 2016 and in 2019. Selected stations were characterized by different pollution. Būtingė station was located at vicinity of the Būtingė oil terminal, Klaipėda station – situated gates of the Klaipėda port and oil terminal and Palanga station – under the influence of the large resort.

The preparation of biological material and evaluation of the geno- (micronuclei and nuclear buds) and cytotoxicity (fragmented-apoptotic and binucleated cells) endpoints were carried out following the earlier described methodology [1].

Assessed frequencies of micronuclei (MN) in fish from Būtingė and Palanga (accordingly 0.36‰ and 0.19‰), were elevated, compare to the data obtained in 2001 (0.2‰ and 0.15‰ respectively), when such study was conducted for the first time. In *P. flesus* specimens collected in Klaipėda station there were measured high (5.5‰) and statistically significant increase of nuclear buds (NB) in comparison to other both stations. Significantly increased levels of micronuclei, nuclear buds and fragmented-apoptotic cells were found in fish and bivalves after the oil spill in the Būtingė terminal in November 2001 and January 2008 [3, 4, 5]. Increased NB frequencies were observed in *P. flesus* from the Gulf of Gdansk and Riga Bay [2, 3]. High levels of NB in erythrocytes were found in fish caught at oil and gas platform zones, aluminum smelter zone, and in mussels after oil spill [4, 5]. Cytotoxic responses between study stations were not statistically significant.

Increased frequencies of geno- and cytotoxicity parameters in *P. flesus* from investigated sites of the Lithuanian costal zones indicates the presence of pollution with genotoxic agents, which might lead to genome instability, formation of cancer, reproductive disorders, abnormal physiological responses, increase risk of developmental and degenerative diseases, hereby affect biodiversity [6]. In order to achieve good environmental status, continuous investigations of the biological effects of environmental pollution in marine coastal ecosystems are essential.

[1] A. Rybakovas, J. Bargielienė, Lang T. Lang, Environmental genotoxicity and cytotoxicity in the offshore zones of the Baltic and the North Seas, Marine Environmental Research, 68:246-256 (2009).
[2] L. Butrimavičienė, J. Bargielienė, J. Greicius Kontautė, M. Stankevičius Kontautė, R. Valskienė, Environmental genotoxicity and risk assessment in the Gulf of Riga (Baltic Sea) using fish, bivalves, and crustaceans, Environmental Science and Pollution Research, 25:24818–24828 (2018).
[3] R. Valskienė, J. Bargielienė, L. Butrimavičienė, J. Pagusienė, W. Grygiel, M. Stankevičius Kontautė, A. Rybakovas, Induction of nuclear abnormalities in herring (*Clupea harengus membras*), flounder (*Platichthys flesus*) and Atlantic cod (*Gadus morhua*) collected from the southern part of the Gotland Basin - the Baltic Sea (2010–2017), Environmental Science and Pollution Research, 26(13):13366-13380 (2019).
[4] J. Bargielienė, L. Andreikėnaitė, G. Garnaga, A. Rybakovas, Genotoxic and cytotoxic effects in bivalve mollusks *Macoma balthica* and *Mytilus edulis* from the Baltic Sea, Ekologija, 54:44-50 (2008).
[5] J. Bargielienė, A. Rybakovas, G. Garnaga, L. Andreikėnaitė, Environmental genotoxicity and cytotoxicity studies in mussels before and after the oil spill in marine oil terminal (Baltic Sea), Environmental Monitoring and Assessment, 184:2067-2078 (2012).
[6] A. Ginebreda, M. Kuzmanovic, H. Guasch, M. L· pez de Alda, J.C. L· pez-Doval et al., Assessment of multi-chemical pollution in aquatic ecosystems using toxic units: Compound prioritization, mixture characterization and relationships with biological descriptors, Science of the Total Environment, 468/469:715-723 (2014).

DENDRITIC CELL VACCINE MODULATION *IN VITRO* WITH CHARACTERISED EPITHELIAL OVARIAN CANCER CELL LINE LYSATE

Eglã Ģymantaitã[1], Jan Aleksander KraŜko[2], Agata Mlynska[2], Emilija Paberalã[2]

[1] Faculty of Medicine, Vilnius University, Lithuania
[2] Immunology Laboratory, National Cancer Institute, Vilnius, Lithuania
egle.zymantaite@mf.stud.vu.lt

Epithelial ovarian carcinoma (EOC) is a highly heterogeneous and aggressive disease that remains the most lethal gynaecological malignancy. EOC is the most frequent ovarian tumour, distinguished by high mortality in late stages when conventional therapies are no longer effective. The role of the immune system is pivotal for efficient control and destruction of cancer cells. Dendritic cells (DCs) serve as orchestrators of the cytotoxic response of the adaptive arm of the immune system and as such is an attractive target or component of cutting edge cell-based immunotherapies against cancer. DC vaccines have shown promising results in ovarian and several other types of cancers such as melanoma, prostate, lung cancer [1]. Some of the most commonly used are DC-based vaccines loaded with allogeneic cancer cell line lysate, which mimics the tumour present in the patient. Lysates developed from different cancer cell line models of the same tumour might, however, have a dissimilar effect on DC maturation and surface protein expression. That is because different cell lines represent distinct variances of the same disease and, therefore, have different protein constitutions. [2,3]. In our study, we undertook the task of creation of a DC-based vaccine with different ovarian cancer cell line lysates and their mixture to find out whether unique EOC cell lysates have an impact on dendritic cell maturation. We characterised four different EOC cell lines: OV7, SKOV3, COV362, A2780; under standardised culture conditions, by performing flow cytometry (FACS) (Fig. 1.) and analysing 23 immune-related genes expression by quantitive real-time PCR (qPCR). Cytokine array was used to evaluate 105 cytokines concentration in produced cancer cell line lysates later used for dendritic cell maturation. We noted that the four ovarian cancer cell lines differ both in stemness- related CD274, CD44, CD105, CD73 marker expression (FACS), and in immune-related gene expression (qPCR). In agreement, the cytokine array revealed that ovarian cancer cell line lysate profiles are highly diverse.

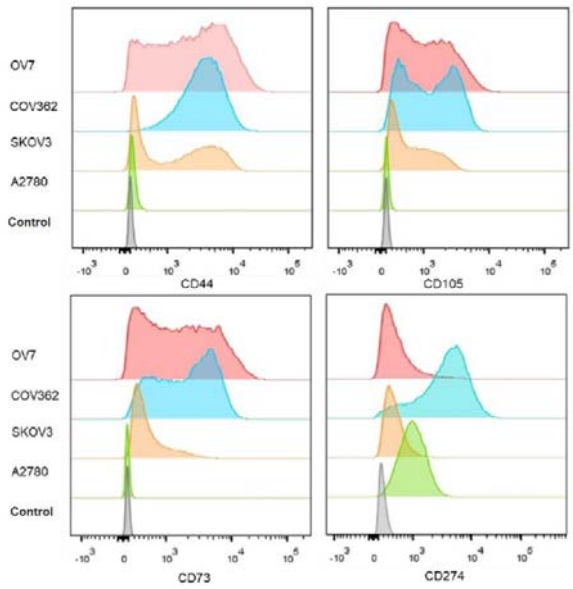

Fig. 1. Different stemness marker expression in 4 different ovarian cancer cell lines.

After cancer cell line characterisation, we successfully produced DCs loaded with different ovarian cancer cell line lysates and their mixture. DC characterisation was performed using FACS, maturation markers: CD11c, CD80, CD83, MHCII were examined. We strongly believe that our findings will lead to development of more potent cell-based immunotherapies for patients suffering from EOC and, possibly, other tumors.

[1] Gardner, Alycia, and Brian Ruffell. ñDendritic Cells and Cancer Immunity.ò Trends in immunology vol. 37,12 (2016): 855-865. doi:10.1016/j.it.2016.09.006

[2] L· pez, Mercedes N et al. ñProlonged survival of dendritic cell-vaccinated melanoma patients correlates with tumor-specific delayed type IV hypersensitivity response and reduction of tumor growth factor beta-expressing T cells.ò Journal of clinical oncology : official journal of the American Society of Clinical Oncology vol. 27,6 (2009): 945-52. doi:10.1200/JCO.2008.18.0794

[3] Flores, Iv§n et al. ñDendritic Cells Loaded with Heat Shock-Conditioned Ovarian Epithelial Carcinoma Cell Lysates Elicit T Cell-Dependent Antitumor Immune Responses *In Vitro*.ò *Journal of immunology research* vol. 2019 9631515. 25 Nov. 2019, doi:10.1155/2019/9631515

EVALUATION OF pH INFLUENCE ON ONION ROOT GROWTH AND GENOTOXICITY INDICES BY *ALLIUM CEPA* ASSAYS

Joelis Verdingas[1], Asta Stapulionytā[1]

[1]Institute of Biosciences, Life Sciences Center, Vilnius University, Lithuania
joelis.verdingas@gmc.stud.vu.lt

Plants are well adapted to grow in a certain range of environmental conditions. One of the most important environmental factors influencing plant growth is the pH of their growth medium. [1] Different plant species and cultivars vary by pH range they can grow without restriction and cytotoxic/genotoxic damage. This research aimed to determine pH range in which common onions (*Allium cepa L.)* can grow without experiencing toxic and genotoxic effects and whether the response of different onion cultivars to varying pH is similar.

pH toxicity was determined using *Allium cepa* root growth inhibition test where onions were grown in an interval of 2 -12 pH for 96 h. ñ*AlephĂ* and *ñSturonĂ* cultivars were used. Mean root length in root bundle and root morphology were evaluated. Hereafter, genotoxicity of pH was assessed analyzing onion root meristemic cells which were grown in pH solution that is equal to EC50 for both acidic and basic mediums 3,5 and 10,5, respectively. Tap water and 10 mg/l MMS solution were used as a negative control (NC) and positive control (PC), accordingly. Cells were evaluated microscopically using anaphase-telophase chromosome aberration assay after 24 h exposure and micronuclei assay after 24h recovery period along with the determination of mitotic and phasic indices. Statistical analysis was done using two-way ANOVA following Tukey post-hoc test.

Root growth was inhibited and root morphology changed in extreme pH solutions. Length of roots was maintained in 4-10 pH interval compared to NC and in 2 and 12 pH solution roots were up to 3-5 times shorter. Through entire 96 h growth period, in 4-10 roots grew at a similar rate, while roots exposed to highest and lowest pH did not grow at all. Different cultivar response to pH was the same in every solution, except in 10 pH. In a genotoxicity assay, most chromosome aberrations were found in water samples (Fig 1b.) but most micronuclei were found in the positive control (Fig. 1d). Mitotic activity was not remarkably increased or inhibited in different pH solutions and did not deviate in direct exposure and after a recovery. (Fig.1a, c) Prophase was the most abundant phase in mitotic cells, but its rate has decreased after the recovery period where relative part of cells in other mitotic phases increased.

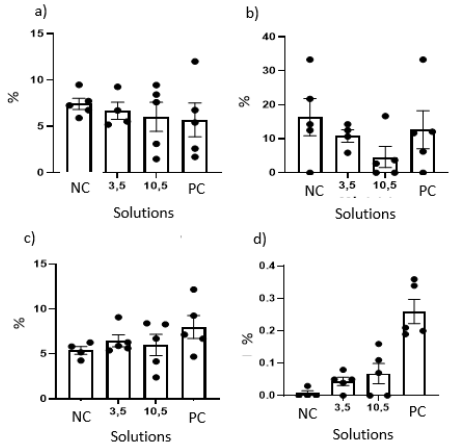

Fig. 1. Genotoxicity assays results a) mitotic index after 24 h exposure b) chromosomic aberrations after 24 h exposure c) mitotic index after 24 h recovery d) micronuclei after 24 h recovery. Black dots represent single samples.

Low and high pH negatively affects onion root growth, probably because intrinsic pH regulation systems are disturbed. [2] Comparison of different cultivars showed almost similar in their response to varying pH. Chromosome aberration rate did not depend on solution pH and genotoxic damage was reversible because there was almost no formation of micronuclei. High frequency of chromosomal aberrations in onions grown in water can be explained by relatively low number of mitotic cells in anaphase - telophase. Cell division activity did not depend on solution pH. Phasic indices changed insignificantly and, during recovery, older cells that were in prophase could proceed further into the cell cycle.

[1] Neina D., The Role of Soil pH in Plant Nutrition and Soil Remediation, Applied and Environmental Soil Science, vol. 2019, 2019
[2] Yan F, Schubert S, Mengel K., Effect of Low Root Medium pH on Net Proton Release, Root Respiration, and Root Growth of Corn (Zea mays L.) and Broad Bean (Vicia faba L.). Plant Physiol. 1992 Jun;99(2):415-21.

INFLUENCE OF THE ISOFORM P85 S6K1 ON THE ACTIVITY OF OTHER ISOFORMS IN CELLS WITH CRISPR-EDITED EXPRESSION OF S6K1.

Mariia Naumova[1,2], Lilia Savinska[1]

[1] Institute of Molecular Biology and Genetics NAS of Ukraine, Ukraine
[2] ESC ñInstitute of Biology and Medicineò Taras Shevchenko National University of Kyiv, Ukraine
maria27nm@gmail.com

S6K1 - kinase 1 of the ribosomal protein S6 functions as one of the key components of the PI3K / mTOR / S6K1 signaling path. This signaling pathway regulates various cellular processes - protein synthesis, cell growth, proliferation, homeostasis and others. It has also been shown that dysregulation of S6K1 is associated with pathologies such as cancer, obesity, aging, and diabetes. So far, the isoforms p85, p70 and p60, which are produced using the first three translation initiation starts, have been described, as well as an alternatively spliced p31 isoform, which is considered as proto-oncogenic.

Earlier, on the MCF-7 cell line, using CRISPR/Cas9 technology, 2 model cell lines were obtained with different expression of the studied isoforms: clone F1 with blocked expression of the p85 isoform (p85- / p70 + / p60 +) and clone F3 where expression of all isoforms was blocked (p85- / p70- / p60-). To study the contribution of the p85 isoform to signaling, mRNA of the full-length S6K1 sequence was transfected into the cells of clone F3, and stable cell line with p85 overexpression was obtained (F3/p85).

To study the activity of isoforms, the following cell treatments were carried out: 24 hours of starvation, 24 hours of serum starvation + 3 hours of restimulation (15% FBS) and 24 hours of starvation + 3 hours of restimulation with rapamycin, an inhibitor of the mTORC1 complex. The following antibodies were used for Western blot analysis: C-terminal polyclonal affinity purified antibodies [Savinska L, 2015], pThr389 S6K1 antibodies (Cell Signaling), pSer 235/236 S6 (Cell Signaling), beta-actin (Sigma).

The results showed that there was no significant change in the F1 clone compared to the wild type. After restimulation, a high level of rapamycin-sensitive phosphorylation of protein S6 is observed. An analysis of the activity of various isoforms showed that the p70 isoform is most responsible for the phosphorylation of the S6 protein.

In clone F3 / p85, in addition to a high level of expression of the p85 form in the presence of serum in the medium, the p60 isoform is also expressed, which probably uses an alternative, third start of translation, whereas neither the level of p70 expression nor its phosphorylation is increased in comparison with clone F3. Both expressed forms, p60 and p85, had a high level of phosphorylation. Importantly, starvation did not decrease the level of Thr389 phosphorylation of all S6K1 and Ser 235/236 isoforms in S6. In this way, overexpression of the p85 isoform may contribute to cell survival, which does not contradict the latest literature data [1].

---

[1] Zhang J, Guo J, Qin X, et al. The p85 isoform of the kinase S6K1 functions as a secreted oncoprotein to facilitate cell migration and tumor growth. Science Signaling. 2018 Mar;11(523).

CIRCULATING MIRNAS AS DIAGNOSTIC BIOMARKERS FOR PERIODONTITIS

Benita Buragaite-Staponkiene[1], Kristina Snipaitiene[1], Adomas Rovas[2], Ruta Matuleviciute[1], Egle Punceviciene[3], Irena Butrimiene[3], Alina Puriene[1,2], Sonata Jarmalaite[1]

[1] Human Genome Research Group, Life Sciences Center, Vilnius University, Vilnius, Lithuania
[2] Vilnius University Hospital Zalgiris Clinic, Vilnius, Lithuania
[3] Vilnius University Hospital Santaros Clinics, Vilnius, Lithuania
benita.buragaite-staponkiene@gmc.stud.vu.lt

Periodontitis (PD) is highly prevalent inflammatory oral disease affecting the supporting tissues of the teeth and leading to connective tissue attachment loss and bone resorption. Besides its negative impact on quality of life, PD is also strongly associated with an increased risk of particular systemic disorders, e.g., respiratory and cardiovascular diseases, rheumatoid arthritis, diabetes, cancer etc. [1-5]. Various mechanisms of PD pathogenesis are epigenetically regulated and microRNAs (miRNAs) are considered as one of the key modulators that influences periodontal homeostasis. This study aimed to reveal PD-associated miRNAs in gingival tissue and bodily fluids, including gingival crevicular fluid (GCF), saliva and plasma, and to evaluate the utility of those miRNAs as minimally- and non-invasive diagnostic markers for PD.

MiRNA expression was profiled in eight gingival tissue samples using microarray platform (Human miRNA Microarrays, 8x60K format). Four significantly differently expressed miRNAs were validated in gingival tissue samples (N=61) and further analyzed in bodily fluid specimens (N=171) by means of quantitative reverse transcription PCR.

A number of miRNAs was found to be significantly upregulated in inflamed gingival tissues as compared to periodontally healthy tissues. After thorough validation, miR-199a-5p, miR-483-5p, miR-3198 and miR-4299 were analyzed in bodily fluids. The level of GCF miR-3198 was significantly higher amongst participants with PD (P=0.019). The level of miR-199a-5p was increased in saliva samples from patients with severe PD (P=0.045), and decreased in plasma samples collected from PD-affected patients (P=0.008), as compared to periodontally healthy participants (P<0.050). A combination of GCF miR-3198 and miR-4299 demonstrated high diagnostic potential (AUC=0.86, P<0.0001) with 68% sensitivity and 96% specificity (Fig. 1).

The results of the current study suggest that PD-specific inflammatory miRNAs in bodily fluids can serve as potential biomarkers of PD that could be applied for minimally- and non-invasive diagnostics of the disease.

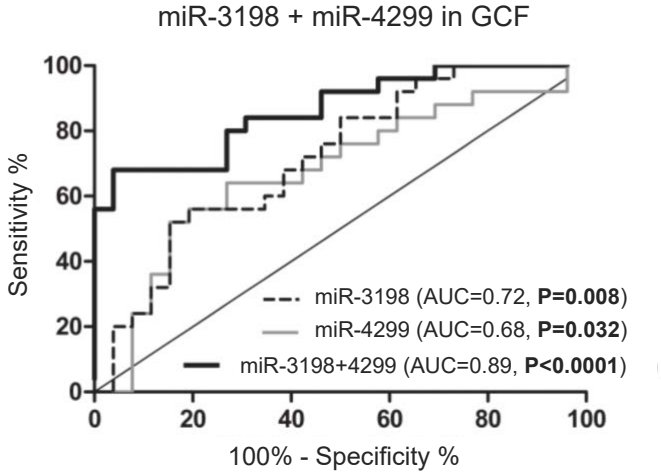

Fig. 1. ROC curve analysis of gingival crevicular fluid (GCF) -derived miR-3198, miR-4299 and a combination of them.

[1] X.T. Zeng, M.L. Tu, D.Y. Liu, et al., Periodontal disease and risk of chronic obstructive pulmonary disease: A meta-analysis of observational studies, PLoS One **7(10)**, e46508 (2012).
[2] A. Blaizot, J.N. Vergnes, S. Nuwwareh et al., Periodontal diseases and cardiovascular events: meta-analysis of observational studies, Int Dent J. **59**, 197ï 209 (2009).
[3] X. Zhao, Z. Liu, D. Shu et al., Association of Periodontitis with Rheumatoid Arthritis and the Effect of Non-Surgical Periodontal Treatment on Disease Activity in Patients with Rheumatoid Arthritis. Med Sci Monit. **24**, 5802-5810 (2018).
[4] M.H. Patel, J.V. Kumar, M.E. Moss, Diabetes and tooth loss: An analysis of data from the national health and nutrition examination survey, 2003-2004. J Am Dent Assoc. **144**, 478ï 485 (2013).
[5] D.C. G¿ven, ¥ . Dizdar, A.C. Akman et al., Evaluation of cancer risk in patients with periodontal diseases. Turk J Med Sci. **49(3)**, 826-831 (2019).

CONSTRUCTION OF SACCHAROMYCES CEREVISIAE DOLICHOL KINASE MUTANTS USING CRISPR-CAS9 SYSTEM AND INVESTIGATION OF THEIR GLYCOSYLATION PROPERTIES

Andrius Burdulis[1], Danguolã Çiogienã[1], Alma Gedvilaitã[1]

[1] Department of Eukaryote Genetic Engineering, Institute of Biotechnology, Life Sciences Center, Vilnius University, Lithuania
andrius.burdulis@gmc.stud.vu.lt

Yeast *Saccharomyces cerevisiae* is a unicellular eukaryote widely used for recombinant protein production and as a model organism for investigation of various cellular processes including protein secretion and glycosylation in lower and higher eukaryotes. Protein glycosylation is an enzymatic oligosaccharide attachment to protein amino acids. Dolichol kinase (DK), encoded by the *SEC59* gene in *S. cerevisiae*, is essential for core steps of protein glycosylation. DK resides in the membrane of endoplasmic reticulum where it phosphorylates dolichol. Synthesized dolichol phosphate is then used as a carrier on which the core oligosaccharide is assembled and transferred on protein in the process of its glycosylation. Such glycoproteins are then further modified in the Golgi apparatus and highly diverse glycoproteins, needed for various cellular functions are produced [1].

Although core steps of protein glycosylation in different yeast species are very similar, some significant functional differences also exist. It was shown that reduced DK activity of temperature-sensitive *S. cerevisiae* DK mutant *sec59-1* results in decreased secretion and glycosylation of both invertase and carboxypeptidase Y (CPY), alterations of cell wall structure and accumulation of hypoglycosylated proteins in its endoplasmic reticulum [2, 3]. *Kluyveromyces lactis* DK mutant WSS also demonstrated protein glycosylation deficiencies but this had fewer effects on yeast cell wall integrity and even improved secretion of some recombinant proteins compared to wild type cells [4].

The aim of this research was to investigate the effect of different DK mutations on protein glycosylation process in yeast *S. cerevisiae*. For introduction of mutations into *SEC59* gene we used components of bacterial adaptive immunity system CRISPR-Cas9 which became one of the most widely used genome editing tools and has been applied to modify yeast genomes as well. Employment of this system allowed to edit the genome of *S. cerevisiae* with the effectiveness close to 100 % and without the use of any selective markers [5]. We introduced mutations, encoding W332G, G407S, G420D, L421S and double G407S and L421S substitutions in DK amino acid sequence, into *SEC59* gene of *S. cerevisiae* and investigated the CPY glycosylation ability as well as sensitivity to tunicamycin and fluorescent Calcofluor white dye (CFW) of all five constructed yeast strains. Our results showed that the degree of CPY glycosylation deficiency correlated with sensitivity of constructed mutants to tunicamycin and temperature and these changes were most pronounced in double DK mutant, similar to *K. lactis* WSS mutant with the corresponding mutations. Nonetheless, the decrease in DK activity in *S. cerevisiae* double mutants, in contrast to *K. lactis* mutants, had impact on yeast cell wall structure, as mutant cells became sensitive to CFW. It is possible, that the decrease in DK activity in *S. cerevisiae*, more strongly than in *K. lactis* affects the cell wall protein composition through changes of lipid metabolism and/or GPI glycosylation.

[1] Aebi M. N-linked protein glycosylation in the ER. *Biochim Biophys Acta - Mol Cell Res.* 2013;1833:2430ï 7.
[2] Orğowski J, Machula K, Janik A, Zdebska E, Palamarczyk G. Dissecting the role of dolichol in cell wall assembly in the yeast mutants impaired in early glycosylation reactions. *Yeast.* 2007;24:239ï 52.
[3] Bernstein M, Kepes F, Schekman R. Sec59 encodes a membrane protein required for core glycosylation in Saccharomyces cerevisiae. *Mol Cell Biol.* 1989;9:1191ï 9.
[4] Çiogienã D, Valaviļ iÎ tã M, Norkienã M, Timinskas A, Gedvilaitã A. Mutations of Kluyveromyces lactis dolichol kinase enhances secretion of recombinant proteins. *FEMS Yeast Res.* 2019;19.
[5] Dicarlo JE, Norville JE, Mali P, Rios X, Aach J, Church GM. Genome engineering in Saccharomyces cerevisiae using CRISPR-Cas systems. *Nucleic Acids Res.* 2013;41:4336ï 43.

INVESTIGATION OF ALUMINUM TOXICITY RESPONSE OF NEWLY CREATED LITHUANIAN BARLEY CULTIVARS

Vilius Mensonas[1], Raimondas Ġukġta[1,2], Violeta Kleizaitā[1]

[1]Institute of Biosciences, Life Sciences Centre, Vilnius University, Saulā̃tekis Ave. 7, LT-10257 Vilnius, Lithuania

[2]Botanical Garden of Vilnius University, Kairā̃nai Str. 43, LT-10239, Vilnius, Lithuania.

vilius.mensonas@gmc.stud.vu.lt

Soil acidity has been and continues to be among the biggest problems for farmers worldwide. With approximately one third of soils in the world [1] and over 20% in Lithuania already being acidic, as well as with increasing global usage of nitrogen fertilizer [2], the problem is expected to be even more accentuated in the future. Urgent solutions are necessary, and along with soil engineering and the creation of responsible fertilization systems, plant genetic engineering and targeted selection appear to be possible answers.

The main issue caused by soil acidity, along with imbalance in micro and macro elements, is the toxicity caused by free Al^{3+} ions. Upon entering roots, aluminum ions can cause permanent damage to cellular functions and in turn hamper the growth of plant roots, thus lowering its survivability. One of the most aluminum-susceptible major crop is barley (*Hordeum vulgare* L.). In this analysis we compare local Lithuanian barley cultivars with international standards, in an attempt to find the most aluminum-resistant genotypes and identify genetic and molecular mechanisms behind this resistance.

To determine barley varieties best suited to acidic environments a host of morphological, biochemical and genetic analyses was employed. Throughout the early seedling growth period in Al stress environments we observed the changing morphology, then, afterwards we measured chemical changes in various plant tissues. Finally, we explored the genetic basis for aluminum toxicity resistance or lack thereof.

Our results show an observable morphological change in aluminum stress groups. From biochemical perspective, Evans blue and Hematoxyline staining assays appeared to be the most indicative of changes induced by Al^{3+} toxicity. Further analyses will incorporate genetic findings, which we hope to correlate with data found in lab experiments as well as obtained in the field. According to our analysis so far, the cultivar ôEmaô appears to be the most resistant.

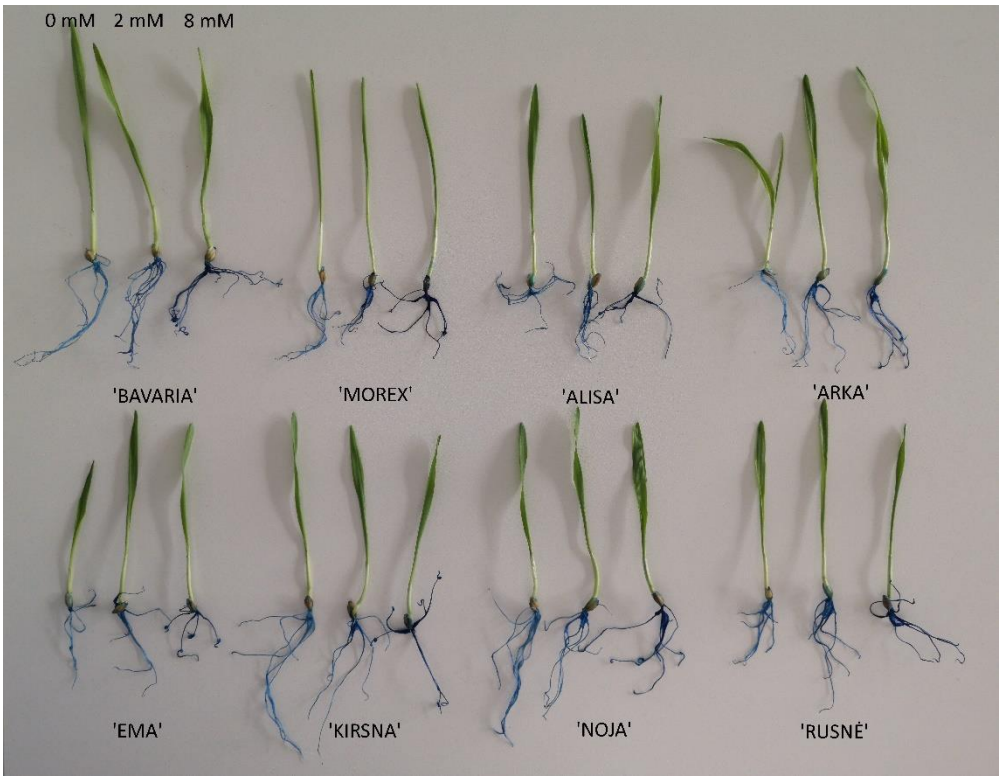

Fig. 1. Individual plant roots of various barley cultivars after Evans Blue test. Three plants in each cultivar represent different levels of Al stress: 0 ï control group versus 2 mM and 8mM $AlCl_3$ treatment groups.

[1] S. K. Behera, S. Kumar et al., 2015. ñSpatial Distribution of Surface Soil Acidity, Electrical Conductivity, Soil Organic Carbon Content and Exchangeable Potassium, Calcium and Magnesium in Some Cropped Acid Soils of India.ò Land Degradation and Development 26 (1): 71ï 79.

[2] S. S. Kalkhoran, et al., 2019. ñSoil Acidity, Lime Application, Nitrogen Fertility, and Greenhouse Gas Emissions: Optimizing Their Joint Economic Management.ò Agricultural Systems 176

ISOLATION AND CHARACTERIZATION OF CELLULASE PRODUCING MICROORGANISMS FROM BIOGAS DIGESTATE

Indrã Juodvirgytã[1], Justina KaziÎnienã [2], Audrius Gegeckas [3]

[1] Department of Biology, Vytautas Magnus University, Lithuania
[2] Institute of Biology and Plant Biotechnology, Vytautas Magnus University, Lithuania
[3] Department of Microbiology and Biotechnology, Vilnius University, Lithuania
juodvirsyteindre@gmail.com

Cellulose is a polymer consisting of ɓ linked D-glucose. Cellulose degradation is a very slow process [1]. Cellulose is mainly degraded by cellulase enzyme which is commonly produced by bacteria and fungi [2]. There are three types of cellulases: endoglucanases, exoglucanases and ɓ-glucosidases. They can be used very widely, for example: paper, textile industries, as detergents in laundry, renewable energy production [3].

In this research microorganisms were isolated from biogas straw digestate. Cellulolytic activity was indicated by clear zones around the colonies on CMC with Congo red agar plates. Sixteen different morphology microorganisms that produce cellulases were isolated. The largest activity zone produced microorganism was named IJ1 and selected for further investigation. Phylogenetic analysis of 16S rRNA sequences showed that IJ1 isolate belongs to *Bacillus* spp. (Fig. 1). Different media and incubation time for biomass along with cellulase production were optimized.

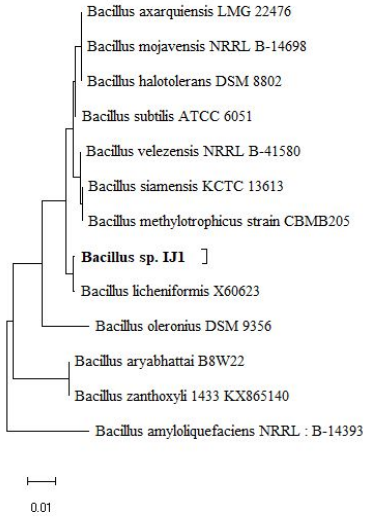

Fig. 1. Neighbour-joining phylogenetic tree of *Bacillus* sp. IJ1 strain and other closely related *Bacillus* species.

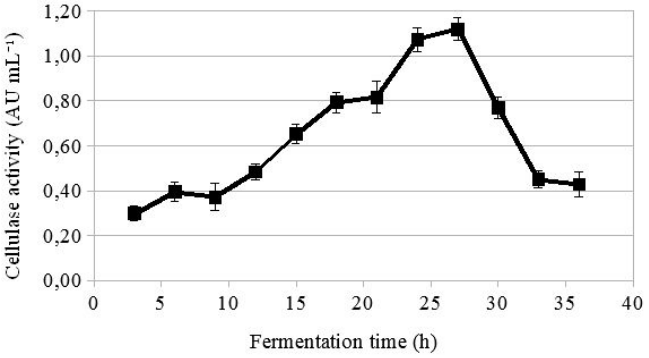

Fig. 2. Cellulase activity over different fermentation time.

Maximum amount of cellulases was reached at 27 hours of fermentation (Fig. 2), produced cellulases were most active in pH 5 and temperature 45 ÁC. Cellulase activity was measured qualitatively - on agar plates, and quantitative - neocuproine method Based on electrophoretic analysis, there is more than one cellulase produced by Bacillus sp. IJ1. The peak of biomass was reached at 24 hours of fermentation.

See you in Vilnius!

[1] Aulitto, Martina, et al. "Bacillus coagulans MA-13: a promising thermophilic and cellulolytic strain for the production of lactic acid from lignocellulosic hydrolysate." *Biotechnology for biofuels* 10.1 (2017): 1-15.
[2] Immanuel, G., et al. "Effect of different growth parameters on endoglucanase enzyme activity by bacteria isolated from coir retting effluents of estuarine environment." *International Journal of Environmental Science & Technology* 3.1 (2006): 25-34.
[3] Sinjaroonsak, Santat, Thanongsak Chaiyaso, and H. Aran. "Optimization of cellulase and xylanase productions by Streptomyces thermocoprophilus TC13W using low cost pretreated oil palm empty fruit bunch." *Waste and Biomass Valorization* (2019): 1-12.

TOXICOLOGICAL EFFECTS OF TIRE FIRE EFFLUENTS: CATALASE AND METALLOTHIONEIN INDUCTION IN RAINBOW TROUT (*Oncorhynchus mykiss*) LARVAE

Lina Anuleviļ iÎ tā[1,2], Gintarā Sauliutā[2], Arvydas Markuckas[1], Çivilā Jurgelānā[2], Milda Stankeviļ iÎ tā[2]

[1]Vilnius University, Life Sciences Center, Saulātekio av. 7, 10223 Vilnius, Lithuania
[2]Nature Research Centre, Akademijos St. 2, LT-08412 Vilnius, Lithuania
lina.anuleviciute@chf.stud.vu.lt

Environmental chemical stressors cause oxidative stress in aquatic organism. The consequences of oxidative damage include modifications of lipids and carbohydrates, protein denaturation, DNA and RNA damage. The aim of the study was to investigate the biomarkers of oxidative stress in the larvae of rainbow trout (*Oncorhynchus mykiss*) after exposure to tire fire effluents. The biochemical status of antioxidant defences of rainbow trout (*O. mykiss*) larvae, which is a valuable model fish for monitoring water pollution, were studied after 4 days exposure to tire fire effluents. In addition, 8 days recovery experiment was carried out. As biochemical biomarkers of toxicity and oxidative stress, metallothioneins (MT) induction and catalase (CAT) activity were analysed. Metallothioneins level was measured by colorimetric reaction using Elman reagent. Catalase activity was assessed by a modified colorimetric reaction. Protein content was determined by the Bradford method. Fish larvae were exposed to tire fire effluents at 100% and 12.5% concentrations. The results showed that tire fire effluents resulted in decreased amount of MT and increased activity of CAT in *O. mykiss* larvae. The data obtained showed that after 8 days of recovery MT amount increased to a control level. Accordingly, CAT activity reached a level of control in all recovery groups. This study highlights the ecotoxicological potential of tire fire accidents to the aquatic biota.

Acknowledgments
This study was funded by the Research Council of Lithuania through the project P-MIP-21-229.

IDENTIFICATION OF CRITICAL GENETIC EVENT OF CLEAR CELL RENAL CELL CARCINOMA BASED ON PLASMA mRNA LEVELS

Augustã Vipartaitã[1], Kristina Çukauskaitã[2], Rasa Sabaliauskaitã[1,2], Sonata Jarmalaitã[1,2]

[1] Institute of Biosciences, Life Science Center, Vilnius University, Vilnius, Lithuania
[2]National Cancer Institute, Vilnius, Lithuania
auguste.vipartaite@gmc.stud.vu.lt

Renal cell carcinoma (RCC) is the most common type of kidney cancer. Most cases of RCC are discovered incidentally and survival is highly dependent upon the stage of disease at diagnosis, with the late-stage metastatic disease having only a 12% 5-year survival rate [1]. RCC is a highly heterogeneous disease. Clear cell renal cell carcinoma (ccRCC) is the most common and particularly challenging histologic RCC subtype [2]. It is classically associated with a loss of the short arm of chromosome 3p which is regarded as the common earliest genetic event, found in >90% ccRCC patients. This genetic change is seemingly arising in childhood or adolescence, even though cancer may not be diagnosed for another 30-50 years. The deleted region encompasses four tumor suppressor genes: *VHL*, *PBRM1*, *BAP1*, and *SETD2* (Fig. 1). Early identification of the disease is highly important because it can impact clinical management. Considering the lack of sufficient non-invasive markers for ccRCC diagnosis, liquid biopsies such as blood plasma could provide an attractive, minimally invasive, and promising method to identify diagnostic biomarkers in ccRCC patients.

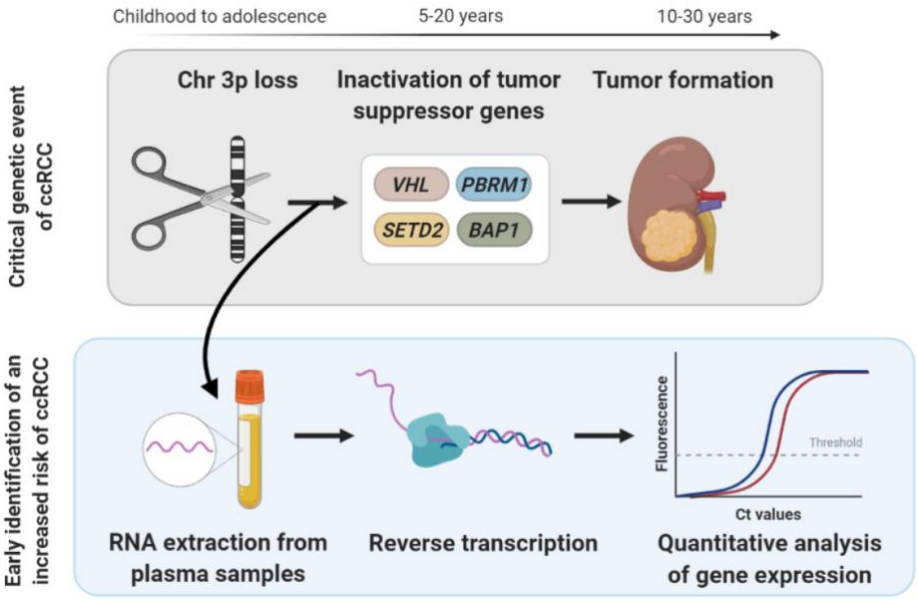

Fig. 1. Schematic representation of ccRCC formation and potential possibility of early disease prediction.

The aim of this study was to determine the changes in the expression of genes *VHL*, *PBRM1*, *SETD2* and *BAP1* in the plasma of patients with ccRCC compared to samples from people with non-malignant tumors in order to adapt them for disease risk assessment and early diagnosis.

In the present study, 9 plasma samples of ccRCC patients and 16 plasma samples from patients with benign kidney tumors were analyzed. Clinical samples were collected during 2019-2021 at National Cancer Institute. Plasma mRNA levels were evaluated using reverse transcription polymerase chain reaction.

The results of our study revealed significant differences in *VHL*, *SETD2*, and *BAP1* mRNA levels comparing plasma samples from patients with ccRCC and benign tumors (all $P < 0.05$). Gene expression analysis revealed that *VHL*, *SETD2*, and *BAP1* plasma mRNA levels in ccRCC samples were significantly lower compared to noncancerous cases. Such differences in gene expression may have occurred before the onset of the disease. Early detection of chromosome 3p loss associated with decreased *VHL*, *PBRM1*, *SETD2*, and *BAP1* expression would help to identify an increased risk of renal cancer and to provide the most appropriate treatment in a timely manner.

In conclusion, detection of *VHL*, *PBRM1*, *SETD2*, and *BAP1* expression changes in plasma samples could help to define the potential of occurring disease and thus guide patient management.

[1] Padala, Sandeep Anand et al. ñEpidemiology of Renal Cell Carcinoma.ò World J. Oncol. vol. 1,3 (2020): 79-87.
[2] Tomaszewski, Jeffrey J et al. ñHeterogeneity and renal mass biopsy: a review of its role and reliability.ò Cancer Biol Med vol. 11,3 (2014): 162-172.

EVALUATION OF CYTOTOXICITY AND GENOTOXICITY OF ZINC OXIDE NANOPARTICLES BY *ALLIUM CEPA* TEST

Dominyka Breimelytã[1], Asta Stapulionytã[1]

[1]Institute of Biosciences, Life Sciences Center, Vilnius University, Lithuania
dominyka.breimelyte@gmc.stud.vu.lt

The nanotechnology industry is growing rapidly, encompassing a wide range of industries from medicine to engineering. Due to their small size, as well as physical and chemical properties, the application of nanoparticles is very versatile e.g. nanoparticles can be used to improve the properties of heat resistance and elasticity of a given material. The increasing use of nanoparticles calls for deeper studies of their genotoxicity. Zinc oxide (ZnO) nanoparticles (NP) were selected for this study because they are a key ingredient in many products such as sunscreens, paints, asphalt, electric diodes and chemical catalysts.

It has been observed in previous research that ZnO nanoparticles can cause oxidative stress when they enter the cell[1]. ZnO NPs cause formation of intercellular reactive oxygen species that are responsible for changes in mitochondrial potential along with swollen mitochondria. Moreover, ZnO NP can adhere to chromosomes involved in the normal process of mitosis, and thus can cause abnormalities that stop normal cell division and the cell cycle. For these reasons, it is important to find out what is the lowest level of concentration can cause detrimental health effects.

To assess the potential toxicity of zinc oxide *Allium cepa* assay was performed. The prepared onions were transferred to selected concentrations of 6 ZnO NP solutions varying from 0.2 to 625 ppm. The effective concentration EC50 was determined from the growth curves by performing a root inhibition test and evaluating these concentrations. The EC50 was obtained at 0.9 ppm with the *ôShakespeareô* cultivar, which indicates the detrimental potency of the substance. In this part of the experiment, a. regression analysis was performed. Root length after 96 hours was regressed on levels of ZnO concentration in the solution. This dependence was assessed as statistically significant, noting that p-value < 0.01.

[1] Ahmed B, Dwivedi S, Abdin MZ, et al. Mitochondrial and Chromosomal Damage Induced by Oxidative Stress in Zn(2+) Ions, ZnO-Bulk and ZnO-NPs treated Allium cepa roots. *Sci Rep*. 2017;7:40685. doi:10.1038/srep40685

GENETIC DIVERSITY ANALYSIS OF *HERACLEUM SOSNOWSKYI* IN VILNIUS CITY AND SURROUDINGS USING ISSR MOLECULAR MARKERS

Raminta Saulãnaitã[1], Jolanta Patamsytã[1*]

[1]Institute of Biosciences, Vilnius University Life Sciences Center, Lithuania
raminta.saulenaite@gmc.stud.vu.lt

Heracleum is common in North and East Europe. There are a few *Heracleum* species such as *Heracleum mantegazzianum, H. sphondylium, H. persicum* and most common in Lithuania *Heracleum sosnowskyi*. These plants, as being an invasive species, damage natural ecosystem, displacing naturally growing species and causing economic damage and endangering human health. Separated juice from the plant that gets on human skin and reacts with sunlight can cause skin burns. Hazardous plant compounds can cause cancer and birth defects in the developing embryo. The aim of the study was to elucidate the polymorphism of Vilnius city samples of *H. sosnowskyi* using ISSR markers.

The plants were collected from six populations: City center, Uģupis, Paģlaiļiai, PerkÎnkiemis, Verkiai and Visoriai in Vilnius city and surroundings in 2019 ï 2020 during early autumn season. DNA was extracted using CTAB method. After that ISSR ï PCR was done with six ISSR primers which were preselected for *H. sosnowskyi*. PCR products were fractionated on a 1.2% agarose gel. Also, statistical data analysis was performed using electrophoresis results as a guide to create binary matrix.

Six populations were examined and determined mean of DNA polymorphism in the populations was found to be 56%. The smallest genetic distance was found between Vilnius city center and Uģupis populations, which were the closest. The largest genetic distance was between Paģlaiļiai and Visoriai populations. A major part of the genetic diversity of *H. sosnowskyi* populations was within populations (61%).

In conclusion, in six populations of *Heracleum sosnowskyi*, the highest polymorphism of ISSR loci was found in the Verkiai population (69.81%) and the lowest in the City center population (45.28%). *H. sosnowskyi* populations of Uģupis, City center and Verkiai were genetically close. Their similarity was 80%.The populations of *H. sosnowskyi* Paģlaiļiai and Visoriai were the most genetically different. Their similarity was 66%. Our results indicate different origin of studied *Heracleum sosnovskyi* populations.

PHOTOMECHANICAL EFFECT INDUCED ON INDRADERMAL TATTOO PIGMENTS WITH PICOSECOND Nd:YAG LASER

Justinas Baleiğis[1], dr. Romualdas Rudys[1].

[1] Department of Biomodels, State Research Institute Centre for Innovative Medicine, Lithuania
Justinas.baleisis@imcentras.lt

A Tattoo is a permanent mark or design made on the body by the introduction of pigment through ruptures in the skin. Currently the tattoos market is growing at a phenomenal rate. This has led in growth of tattoo removal procedure as well. Methods of tattoo removal include dermabrasion, skin grafts or plastic surgery, and laser surgery. The most appealing form is the Q-switched nanosecond domain lasers, that up until recently were the gold standard in the field. Complex and multicolor pigment induced tattoos are a challenge to remove and promising results are seen in the published data regarding the use of shorter ï picosecond domain lasers [1]. The reason behind that being that for picosecond domain pulses a lower fluence is needed during the treatment sessions due to the higher peak power and greater photoacoustic effect, which can offer less side-effects and a better pigment clearance [2].

When stating the term ñtattoo removalò it is necessary to explain, that the ñremovalò is the fragmentation of the targeted particle into smaller fragments. Thermal and stress confined laser-energy deposition in the targeted particle is needed, to generate an internal pressure wave or acoustic wave. Fracture can occur when the tensile force of the acoustic wave exceeds the corresponding limit of the particle. That can be affected by the influence of the used laser pulse length, as with shorter length can be noted an increase of particle fracture. This relationship has its limits when the acoustic wave confinement time is longer than the pulse length [3].

Most commercially available lasers excel at 300-600 ps. In our study, we aimed to investigate the laser-tissue interactions of a picosecond domain Nd:YAG laser, that can generate 150 ps pulses and energies ranging up to 250 mJ and 120 mJ for 1064 and 532 nm wavelength, respectively. Thus, providing insight in shorter pulse efficacy and safety in the use for tattoo pigment fragmentation. The effects of 150 ps ultrashort pulses were not currently described, and the area was absent of in vivo animal studies that could offer great translational value, when interpreting study results from animal to human. For that reason, this study was performed on a in vivo porcine model.

As excessive energy delivered to the superficial skin can lead to blistering, prolonged healing, scurrying and change in pigmentation [4] it is important to optimize the fluence of the laser energy. Impact of different fluencies for side-effect development and pigment fragmentation efficacy were investigated on different color tattoos of known pigment composition. This has been carried out by changing the wavelength, spot size and pulse energy of the laser. The tattoo removal was analyzed using clinical macroscopic examination (siascopy) and histochemistry.

[1] R. Torbeck, L. Schilling, H. Khorasani, J. Dover et al., Evolution of the Picosecond Laser: A Review of Literature. Dermatologic Surg.45(2):183ï 94 (2019).
[2] O. Reiter, L. Atzmony, L. Akerman, A Levi et al., Picosecond lasers for tattoo removal: a systematic review. Lasers Med Sci [Internet];31(7):1397ï 405. Available from: http://dx.doi.org/10.1007/s10103-016-2001-0 (2016).
[3] D.C. Wu, M.P. Goldman, H. Wat et al., A Systematic Review of Picosecond Laser in Dermatology: Evidence and Recommendations. Lasers Surg Med.;(March):1ï 41 (2020).
[4] W. Bª umler. Laser Treatment of Tattoos: Basic Principles. Curr Probl Dermatology ;52:94ï 104 (2017).

ALLELOPATHIC ACTIVITY OF INVASIVE PLANT CANADIAN GOLDENROD (*SOLIDAGO CANADENSIS* L.)

Donata Stancelytė[1], Irena Nedveckytė[1]

[1]Life Sciences Centre, Institute of Biosciences, Center of Ecology and Environment, Vilnius University, Lithuania
donata.stancelyte@gmc.stud.vu.lt

Canadian goldenrod (*Solidago canadensis* L.) is one of the most successful and widespread invasive plant species in the world. Native to North America, it was introduced to Europe as an ornamental plant and rapidly spread throughout almost all of Europe and other parts of the world including China, Japan, Taiwan as well as Australia, New Zealand [1]. As other alien plants, *S. canadensis* causes negative effects on natural ecosystems, which affect biodiversity and native species communities [2].

In 2004 *S. canadensis* among other 17 plant species was listed as invasive to Lithuania. The rapid spread of the plant is determined by several reasons. Firstly, plant has broad climatic tolerance. In addition, it is tolerant to wide range of soil fertility, texture conditions and soil pH. Other important aspect is plant lifecycle and dispersion. *S. canadensis* is a perennial rhizomatous hemicryptophyte and spreads via seeds and underground rhizomes. Plant has relatively long flowering time (from late July to mid-September and sometimes until October) and one sprout of Canadian goldenrod can mature more than 10 000 or even up to 20 000 seeds per season [3]. Seeds are essential for long-distance dispersal and the colonisation of unoccupied sites. However, for the expansion of established populations rhizomatous growth is substantial. Individual clones are long lived (can reach an age of 100 years) and spreads fast with each year.

On the other hand, invasion success of Canadian goldenrod may be determined by its allelopathic compounds. It is known, that allelochemicals can be obtained from varied parts of the plant (leaves, stems, flowers, buds, fruits and roots) and can affect seed germination and root formation, as well as the growth of the whole plant: membrane conductivity, chlorophyll production, photosynthetic activity, etc. The allelopathic effect of the *S. canadensis* on other plants has not been studied very widely. Thus, it is important to identify allelopathic compounds and its role in the spread of invasive species.

The aim of the present study was to determine the activity of leaf/stem extracts of the Canadian goldenrod to seed germination and seedling growth. Under laboratory conditions allelopathic properties of acidic, neutral and alkaline fractions were tested on Lettuce (*Lactuca sativa* L.) and Garden pepper cress (*Lepidium sativum* L.) seeds. Inhibitory allelopathic effect was established. The effect of leaf/stem exudates were the most active at neutral fraction and at tested concentration inhibited lettuce seed germination up to 100 %. Neutral fraction in all relative concentrations (1.0; 0.1; 0.01) has shown highest inhibitory effect. It suppressed growth of *L. sativa* (from 0 to 2.3 mm in comparison to 22.7 mm in control) and *L. sativum* (from 0.5 to 16.8 mm in comparison to 35.3 mm in control) (Fig. 1). Seven potentially allelopathically active compounds have been identified.

a) 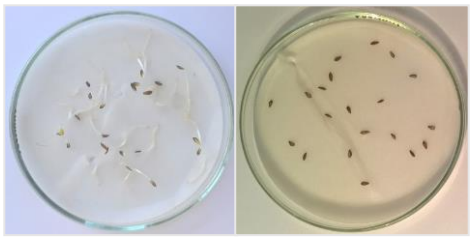 b)

Fig.1. Growth of model objects a) *Lactuca sativa* and b) *Lepidium sativum* in control solution and in neutral leaf/stem extract of Canadian goldenrod

[1] Wang C., Xiao H., Zhao L., Liu J., Wang L., Zhang F., Shi Y., Du D. 2016. The allelopathic effects of invasive plant *Solidago canadensis* on seed germination and growth of *Lactuca sativa* enhanced by different types of acid deposition. Ecotoxicology, 25: 555–562.
[2] Gudžinskas Z., Kazlauskas M., Pilate D., Balalaikins M., Pilats M., Šaulys A., Šaulienė I., Šukienė L. 2014. Lietuvos ir Latvijos pasienio regiono invaziniai organizmai. Vilnius, BMK leidykla. p. 8–16; 52–53.
[3] http://www.am.lt/VI/article.php3?article_id=17545

ANALYSIS OF CIRCULATING MIRNA LEVELS IN BLOOD OF WOMEN DIAGNOSED WITH GESTATIONAL DIABETES

Gabrielė Dzimitraviļ iÎ tė[1], Kristina DaniÎ naitė[1]

[1]Institute of Biosciences, Life Sciences Center, Vilnius University, Vilnius, Lithuania
gabriele.dzimitraviciute@gmc.vu.lt

Gestational diabetes mellitus (GD) is a chronic hyperglycemia diagnosed during the 2nd trimester of pregnancy [1]. Despite the tendency to disappear after delivery, the prevalence of this disease is constantly growing in Lithuania and worldwide and correlates with the type 2 diabetes mellitus (T2D) as GD causes higher risk of T2D for the mother and her child [2, 3]. Therefore, it is important to elucidate molecular biomarkers for the risk evaluation of both GD and T2D development.

As epigenetic alterations show great perspectives as liquid-biopsy biomarkers [4], the aim of this study was to analyze 6 selected microRNAs ï miR-16-5p, miR-27a-3p, miR-152-3p, miR-155-5p, miR-222-3p, and miR-518d-5p ï in whole-blood samples of women diagnosed with GD and to associate them with clinical GD indicators.

In total, 56 women (49 diagnosed with GD and 7 healthy pregnant women) were included in the study and 108 samples were tested. Blood samples were taken at 24ï 28 weeks of gestation (n = 39), at 6ï 12 weeks after delivery (n = 12), and also from the umbilical artery (n = 26) and vein (n = 26). The selected miRNAs were quantified by means of quantitative PCR using TaqMan-based assays after reverse transcription (RT) of all miRNAs.

Higher amounts of miR-16-5p, miR-152-3p, miR-155-5p and miR-222-3p were detected in the blood of GD women after delivery compared to the gestational period (all $p < 0.05$). Also, higher levels of miR-16-5p, miR-27a-3p and miR-152-3p were detected in the blood of GD women after delivery as compared to healthy not pregnant women (all $p < 0.05$; Fig. 1). The miRNA levels did not differ between the GD and non-GD women in blood during gestational period (all $p > 0.05$). MiR-518d-5p was detected only in blood from the umbilical artery. The amount of miR-16-5p in GD women during gestational period was associated with body mass index before pregnancy, while miR-27a-3p and miR-155-5p correlated with plasma glucose levels (all $p > 0.05$). Furthermore, the blood level of miR-155-5p after delivery was associated with womenôs age ($p = 0.017$) and similar tendencies were observed regarding miR-16-5p and miR-222-3p in blood from the umbilical vein.

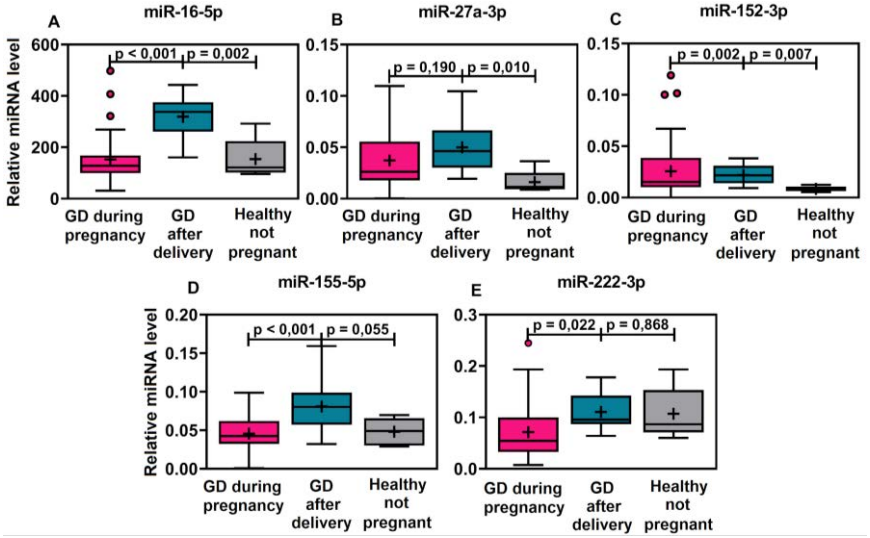

Fig. 1. Comparison of miRNA blood levels among GD women during gestational period, GD women after delivery and healthy not pregnant women. A ï miR-16-5p, B ï miR-27a-3p, C ï miR-152-3p, D ï miR-155-5p, E ï miR-222-3p. The middle line in the box ï median, + ï mean, top and bottom lines of the box ï 75 % and 25 % quartiles (respectively), whiskers ï maximum and minimum values, dots - outliers.

This study showed various associations between the levels of analyzed miRNAs in the blood of GD women and their clinical indicators, indicating their potential for GD and T2D diagnostics and / or prognosis. However, comprehensive studies in larger cohorts are needed to validate these miRNAs as potential GD biomarkers.

[1] R. Ding et al. Integrated transcriptome sequencing analysis reveals role of miR-138-5p/ TBL1X in placenta from gestational diabetes mellitus. Cellular Physiology and Biochemistry. 2018;51(2):630.
[2] J. Rãpgaitã et al. Connection of gestational diabetes and metabolic syndrome among women diagnosed with gestational diabetes more than 15 years ago. Kaunas: Lithuanian University of health sciences. 2017.
[3] S. Dias et al. Molecular Biomarkers for Gestational Diabetes Mellitus. International Journal of Molecular Sciences. 2018;19(10):2926.
[4] C. V. Collares et al. Identifying common and specific microRNAs expressed in peripheral blood mononuclear cell of type 1, type 2, and gestational diabetes mellitus patients. BMC Research Notes. 2013;6:491.

EVALUATING OF TWO ELISA ASSAYS IN KHARKIV OBLAST

Svetlana Ohiienko[1,2], Roman Trokhymchuk[1], Yuliia Ilchenko[2], Nadiia Zolotarova[2]

[1] Research Institute of Biology, V. N. Karazin Kharkiv National University, Ukraine
[2] Limited Liability Company çMEDYCHNYI TSENTR ZDOROVIAè, Ukraine
ohiienko.svetlana@gmail.com

In the modern pandemic situation, the main objective is swift and correct diagnosis of SARS-CoV-2. This is essential issue, especially for epidemiological situations in big cities where virus circulates in huge density of people. It should be noted, that antigenic tests of viral proteins are cheaper and faster than molecular diagnosis. Ukraine as a developing country has several test-systems, which were separated into post-Soviet, and EU-trade countries ones. The aim of this investigation is to compare an in-house system (ELISA Vitrotest SARS-CoV-2) and ELISA kit NovaLisa È SARS-CoV-2. Investigations were carried out on the patients of Kharkiv oblast.

Blood samples positive for COVID-19 were collected from symptomatic patients who came to the emergency room of Medical center çMEDYCHNYI TSENTR ZDOROVIAè. Patients were considered positive according to the results of the quantitative reverse transcription-polymerase chain reaction (RT-qPCR). Blood samples were collected in serum collection tubes (BD Vacutainer SST II advance, BD, Plymouth, UK). We evaluated two commercial ELISA kits: ELISA Vitrotest SARS-CoV-2 (IgG, IgM) (Kyiv, Ukraine, hereafter called ñVitrotestò) and NovaLisaÈ SARS-CoV-2 I (IgG, IgM) (NovaTecÈ, Dietzenbach, Germany, hereafter called ñNovaLisaò). For each ELISA kit, negative and positive controls were assessed and successfully passed. Inconclusive ELISA results were considered as negative for statistical analysis. Significant associations between variables were searched using chi-square test (or Fisherôs exact test to prevent overestimation of statistical significance for small data sets) and determination of agreement rate and Cohenôs Kappa. The significance threshold was set at $p < 0.05$.

Control subjects tested negative for SARS-CoV-2 antibodies with all two systems. Estimated sensitivities varied from 72,5 to 91.5% for IgG detection and from 60,6 to 82.0% for IgM detection. For IgG, Vitrotest and NovaLisa displayed 62ï 70.5% agreement with other systems. Intermethod agreement for IgM determination was between 30 and 72.5%. Comparison of two systems for SARS-CoV-2 IgG and IgM antibodies showed sensitivity and overall concordance.

The obtained results allow using in-house system to detection of coronaviruses infection SARS-CoV-2 correctly.

The authors are grateful to all persons who contribute for collecting material.

NATURAL REPELLENTS FOR MEALWORM (*TENEBRIO MOLITOR* L.) LARVAE

Gabrielã Bumbulytã[1, 2], Vincas BÎ da[1]

[1]The Nature Research Centre, Laboratory of Chemical and Behavioural Ecology, Vilnius
[2]Vilnius University Life Sciences Centre, Vilnius
gabriele.bumbulyte@gmail.com

The use of insects for food has attracted increasing interest in recent years. Insects as mealworms (*Tenebrio molitor* L.) may represent an alternative source of proteins and micronutrients compared to conventional meat sources. It is very important to increase the effectiveness of the collection of insect larvae biomass for the insect breeders. One of the possibilities could be the manipulation of insect larvae behavior using natural repellents. In previous studies we found that mealworm larvae have the strongest repellent effects on *Mentha spicata* L. and *Thymus vulgaris* L. essential oils. Thus, the objective of this work was to determine the effect of essential oils (*M. spicata* and *T. vulgaris*) compounds for mealworms. The behavioural experiment was performed in a Petri dish using behavioural assay. Larva behaviour was recorded and monitored by a computer program ï EthoVision XT 12 (Noldus, the Netherlands). Behavior was recorded for 5 minutes and 10 replications were performed with each the most abundant essential oil compound. Five spots on a Petri dish side were applied with the essential oil chemical compound (2ε l each, 10ε l total). The results showed that the most repellent active compound for the mealworm larvae was carvone, active at concentrations of 10 and 100 mM.

GENE EXPRESSION ANALYSIS OF HISTONE METHYLATION ASSOCIATED GENES IN PROSTATE TUMORS

Greta Meidutė[1], RÎta Maleckaitė[1], Kristina DaniÎnaitė[1].

[1]Human Genome Research Group, Institute of Biosciences, Life Sciences Center, Vilnius University, Vilnius, Lithuania
greta.meidute@gmc.stud.vu.lt

Prostate cancer (PCa) is the most prevalent type of male cancer and the 5th leading cause of death in males with cancer worldwide in 2020 [1]. A large proportion of PCa is latent and does not tend to progress, whereas others are aggressive and significantly affect the lifeôs quality. Therefore, it is of high importance to identify which PCa cases need immediate treatment while others could undergo active surveillance. Prostate-specific antigen (PSA) screening remains as a primary method for PCa diagnostics; however, it lacks specificity for other prostate diseases, such as benign prostate hyperplasia (BPH), and can often lead to false positive results and, in turn, unnecessary treatment. Moreover, it lacks prognostic value [2]. Abnormal changes in gene expression and epigenetic regulation are fundamental in any tumor type and lead to the development and further progression of PCa as well [3]. Altered histone methylation is one of the characteristic features during carcinogenesis, which may be due to altered expression of regulatory genes, like histone lysine methyltransferases (KMTs) and demethylases (KDMs). Therefore, histone methylation regulators might be utilized as effective biomarkers for more accurate diagnostics and characterization of PCa.

The aim of this study was to analyze the expression of *KDM3A*, *KDM5D*, *KMT5A* and *PHF8* (a.k.a. *KDM7B*) genes associated with histone methylation in prostate tumors and control samples as potential biomarkers.

In the present study, 64 PCa, 25 noncancerous prostate tissues (NPT) and 16 BPH samples were analyzed for gene expression. The tissue samples were collected in 2008-2014 during the previous projects. First, total extracted RNA was used for the synthesis of complementary DNA. The latter was used for quantitative gene expression analysis by means of real-time PCR (qPCR).

The results of our study revealed differences in the expression of selected genes associated with histone methylation in PCa as compared to NPT and BPH. The expression of *KDM3A* in tumors and NPT was higher than that in BPH ($p = 0.0082$ and $p = 0.0164$, respectively), but it did not differ between PCa and NPT ($p > 0.0500$; Fig. 1A). *KMT5A* was highly expressed in BPH as compared to both PCa and NPT (both $p < 0.0001$; Fig. 1B), whereas *PHF8* had generally low expression in all samples, nevertheless, it was significantly different between NPT and BPH ($p = 0.0206$; Fig. 1C). No associations were found between *KDM3A*, *KDM5D*, *KMT5A* and *PHF8* expression and patientôs age, prostate mass, serum PSA levels, tumor stage or biochemical disease recurrence (all $p > 0.0500$, not shown).

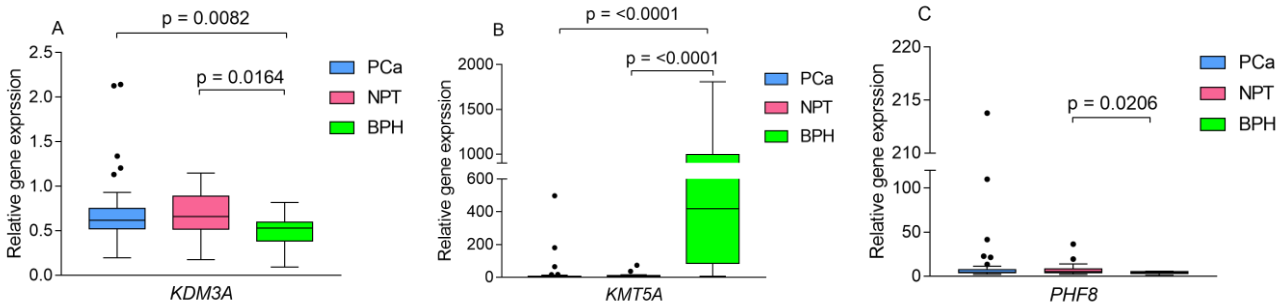

Fig. 1 Relative expression levels of genes *KDM3A* (A), *KMT5A* (B) and *PHF8* (C) in prostate tumors (PCa), noncancerous prostate tissues (NPT) and benign prostatic hyperplasia (BPH) samples

In conclusion, our analysis revealed significant differences in the expression of *KMT5A*, *KDM3A* and *PHF8* genes in prostatic tissues, which suggest their potential utility for improved PCa diagnostics. However, their prognostic value was not determined. Additional investigation in larger independent cohorts is needed for further elucidation of the role of histone methylation regulatory genes in PCa.

[1] Global Cancer Observatory; https://gco.iarc.fr (World Health Organisation, France, 2021).

[2] X. Filella, E. Fern§ndez-Galan, R. Fern§ndez Bonifacio, L. Foj. Emerging biomarkers in the diagnosis of prostate cancer. *Pharmacogenomics and Personalized Medicine*, *11*, 83ï 94 (2018).

[3] S. S. Willard, S. Koochekpour. Regulators of gene expression as biomarkers for prostate cancer. *American Journal of Cancer Research*, *2*(6), 620ï 657 (2012).

EVALUATION OF ANTICANCER ACTIVITY OF KINASE INHIBITORS IN MDA-MB-231 BREAST CANCER CELL LINE

Paulina Ġlimaitā[1], Elias Maccioni[2], Vilma Petrikaitā[1*]

[1] Laboratory of Drug Targets Histopathology, Institute of Cardiology, Lithuanian University of Health Sciences, Lithuania

[2] Department of Life and Environmental Sciences, University of Cagliari, Italy

vilmapetrikaite@gmail.com

Breast cancer is the most common type of diagnosed malignancies and the second leading cause of cancer death in women around the world [4]. Triple-negative breast cancer (TNBC) is characterized by the aggressive nature and lack of targeted therapies, which results in very limited treatment options [5]. Protein kinases are responsible for regulating different cellular functions, such as proliferation, cell cycle, apoptosis, motility, differentiation. Many studies have shown a causal role of protein kinase dysregulations or mutations in different human diseases, including cancer [1]. Over 25 kinase inhibitors are approved as anticancer drugs [2]. One of them is sunitinib, which is used to treat kidney cancer and gastrointestinal stromal tumors [3].

The aim of our study was to evaluate the anticancer activity of new sunitinib analogues on TNBC cell line MDA-MB-231.

Materials and methods. Experiments were performed on human cell line MDA-MB-231. 17 kinase inhibitors, which are sunitinib analogues, have been tested. These analogues were synthesized at the University of Cagliari, Italy, and their synthesis and characterization was published [6]. The effect of kinase inhibitors on cell viability was evaluated by MTT assay after 72 hours of incubation. First, we selected the most active kinase inhibitors that reduced cell viability up to 5% or less. Then the EC50 values of the most active compounds were established and compared to the sunitinib activity. Compound activity on breast cancer cell ability to migrate was examined using single cell tracking assay. This experiment was performed on a special imaging dish with a grid. Cells were seeded at a low concentration in the dish, to get 50-70 cells in total on a grid area. Cell were allowed to attach overnight, and then the solutions with tested compounds in a fresh medium were added. Images of the migrating cells were taken at one-hour intervals for 8 hours by using an inverted microscope. Single cells were tracked and the cell migration distance was measured. Then the average cell migration velocity was calculated.

Results. Kinase inhibitors 1, 6, 7, 8 and 17 were the most active ones. Among tested compounds, the compound 1 possessed the greatest effect on cell viability (EC50 value after 72 h on MDA-MB-231 was 73.61 Ñ 5.77 ε M). Most of the other compounds reduced cancer cell viability at the concentrations ranging from 170 to 600 nM. All tested sunitinib analogues were more active than sunitinib. Also, tested compounds reduced the MDA-MB-231 cell migration. The compound 6, one of the most active ones, inhibited breast cancer cell migration by about 28% compared to the control.

Conclusions. Tested kinase inhibitors possess anticancer activity on triple-negative breast cancer cell line. They reduce the viability and inhibit migration of cells, and may be worthy for further studies.

[1] J. Cicenas, E. Zalyte, A. Bairoch et al., Kinases and Cancer, Cancers, 10(3), 63 (2018).

[2] S. Gross, R. Rahal, N. Stransky et al., Targeting cancer with kinase inhibitors, J Clin Invest., 125(5):1780ï 9 (2015).

[3] Z. Hao, I. Sadek, Sunitinib: the antiangiogenic effects and beyond, OncoTargets Ther. 9:5495ï 505 (2016).

[4] AJ. Redig, SS. McAllister, Breast cancer as a systemic disease: a view of metastasis. J Intern Med, 274(2):113ï 26 (2013).

[5] K. Aysola, A.Desai, C. Welch et al., Triple Negative Breast Cancer ï An Overview, Hereditary Genet., 2013(Suppl 2): 001 (2013).

[6] R. Meleddu, V. Petrikaite, S. Distinto et al., Investigating the Anticancer Activity of Isatin/Dihydropyrazole Hybrids, ACS Medicinal Chemistry Letters, 10, 4, 571ï 576 (2019).

IMPACT OF WATER TRANSPORT ON WATER COURSES WITH *RANUNCULION* VEGETATION ï HABITAT TYPE 3260 OF EUROPEAN IMPORTANCE

Liucija Kamaitytā-Bukelskienā [1], Jurgita Butkuvienā [2,3], Donatas Naugģemys [3]

[1] Laboratory of Flora and Geobotany, Nature Research Centre, Lithuania
[2] Institute of Biosciences, Life Sciences Centre, Vilnius University, Lithuania
[3] Botanical Garden, Vilnius University, Lithuania
liucija.bukelskiene@gamtc.lt

During the period of summer rivers are intensively used for leisure activities such as kayaking. The most noticeable impact of such water transport is a mechanical disturbance of aquatic plants (cut off the flowers and fruits) and their habitats (causing the erosion of riverbed and accumulation of sediments in river onshore). Water courses with *Ranunculion fluitantis* and *Callitricho-Batrachion* vegetation ï habitat type (HT) of European importance 3260 is one of the habitat types that is sensitive to kayaking caused disturbances. It requires special attention, because its sustainability related not only with support of typical environmental conditions (fast course, low temperatures, coarse bottom sediments), but also with the influence of anthropogenic activity. The *Ranunculus* sect. *Batrachium* as a key vegetation component of these habitats are at risk by reason of increasing human activities, environmental pollution, and recreation.

The study investigated the impact of disturbance due to kayaking in 5 Lithuanian rivers of 15 experimental fields and 5 control fields. In each field, the species composition of the plants and their cover (according to the Braun-Blanquet scale) and the total cover of all plants (%) were assessed.

The study showed that kayaking is most intense in the months of July and August when *Ranunculus* species are flowering or producing the achenes. We could also find a negative correlation between the number of kayaks and the abundance of *Ranunculus* plants in our experimental plots. In addition, kayaking moves sediments that accumulate along the river's banks, facilitating the establishment of shade-tolerant plants, like invasive *Elodea canadensis*.

This research is funded by grant no. S-SIT-20-1 from the Research Council of Lithuania.

DETERMINATION OF BIOLOGICALLY ACTIVE COMPOUNDS AND ITS RADICAL SCAVENGING ACTIVITY IN *CANNABIS SATIVA* L. MORPHOLOGICAL PARTS

Ieva Ļalkaitā[1,3], Algimanta Kundrotaitā[2,3], Karolina Barļauskaitā[3]

[1] Kaunas University of Technology, Faculty of Chemical Technology, Department of Polymer Chemistry and Technology, Kaunas, Lithuania
[2]Vytautas Magnus University, Faculty of Natural Sciences, Department of Biology, Kaunas, Lithuania
[3]Lithuanian Research Centre for Agriculture and Forestry, Institute of Agriculture, Lithuania
Ieva.Calkaite@lammc.lt

Fibre hemp (*Cannabis sativa* L.) is the non-THC-producing species, one of the oldest crops cultivated all over the world to produce fibre, food products and biomass which is rich in biologically active compounds [1]. There are many sources about hempseed composition and nutritiousness in various databases, but other parts of this plant (stem, leaves and inflorescences) were not investigated as much. Sample list and vegetation stage investigated in this study presented in table 1. Previous studies did not explore differences in all parts of the plant and how the quantity of polyphenolic compounds and flavonoids change in various vegetation stages. Therefore, experiments, which can help to find out how different density of plants (15 plants per square meter and 80 plants per square meter) influences biologically active compounds accumulation in various parts of the plant, were performed. Industrial hemps from sparse area accumulated slightly higher amount of biologically active compounds than the one which grew up under denser conditions.

Table 1. Samples and industrial hemp vegetation phases at harvesting time [2]

	1st harvest	2nd harvest	3rd harvest	4th harvest	5th harvest	6th harvest
	4th leaf pair	GV point, Change of phyllotaxis on the main stem from opposite to alternate*	Female flower formation*	Beginning of seed maturity*	Leaf desiccation*	Stem desiccation*
Stem	+	+	+	+	+	+
Leaves	+	+	+	+	+	+
Inflorescences	-	-	-	+	+	+

From previous studies it was known that radical scavenging activity directly correlates with number of hydroxyl groups [3] Consequently, it can be assumed that the more phenolic compounds are found in extract the higher radical scavenging activity should be. In this research, this statement has been proven by using slightly modified Brand-Williams, Cuvelier and Berset method (1995). The extracts capability to bleach DPPH free radical solution was estimated using the following formula:

Inhibition (%) = $((A_B-A_E)/A_B)) \times 100$

where A_B – absorption of blank sample, t = 0min, A_E – absorption of tested extract, t = 30min.

All measurements were carried out using spectrophotometric analysis.

[1]D. Fiorini, A. Molle, M. Nabissi, G. Santini, G. Benelli, and F. Maggi, Valorizing industrial hemp (Cannabis sativa L.) by-products: Cannabidiol enrichment in the inflorescence essential oil optimizing sample pre-treatment prior to distillation, Ind. Crops Prod., vol. 128, no. October 2018, pp. 581–589, 2019.
[2]V. Mediavilla, M. Jonquera, I. Schmid-Slembrouck, and A. Soldati, Decimal code for growth stages of hemp, Journal of the International Hemp Association, 1998.
[3]O. P. Sharma and T. K. Bhat, DPPH antioxidant assay revisited, Food Chem., vol. 113, no. 4, pp. 1202–1205, 2009.

POST-EXTRACTION SITE WOUND HEALING USING PLATELET-RICH-FIBRIN IN DOGS

Indre Zakiene[1], Gintare Ziukaite[2], Juozas Grigas[1], Arnoldas Pautienius[1], Judita Zymantiene[1]

[1] Department of Anatomy and Physiology, Lithuanian University of Health Sciences, Lithuania
[2] Small animal clinic, Ltd VetPet LT, Lithuania
indre.zakiene@lsmu.lt

Introduction. Periodontal disease is one of the most common condition in dogs and dental extraction is usually required [1]. Platelet-rich fibrin (PRF) membranes are widely and successfully used in the oral surgery of humans. Platelet-rich-fibrin membrane contains a fibrin matrix with leukocytes, erythrocytes, platelets, B and T lymphocytes, monocytes, stem cells and growth factors which provides better and faster tissue regenerating [2]. Faster wound healing helps to reduce the amount of nonsteroidal anti-inflammatory drugs and makes general comfort for the dog.

Methods. Clinical condition and periodontal disease stage were evaluated in the group of 11 dogs that had no any other chronic disease. The dogs were split in two groups (n1=6; n2=5): the procedure of tooth extraction and use of platelet-rich fibrin (n1=6); and procedure of standard tooth extraction (n2=5).

Procedure of closed dental extraction was made under general anaesthesia. Oral cavity was cleaned with chlorhexidine 0.12% solution. Whole blood sample (5 ml) was collected from saphenous vein into the sterile tube without anticoagulant. WB sample was centrifuged on 2400 rpm, 12 min., 500 g. After separation and compression, PRF membrane was put and fixated in the alveolar wound of the first group dogs (n1). Mucosal flap was created and sutured to close the wound. After the procedure the results of Early Wound Healing Score (EWHS) [3] and Pain Score [4] were evaluated on the first, third and seventh day after the procedure.

Results. The average of EWHS after 3 days was significantly bigger in the group n1=8, $p<0.05$ where platelet-rich fibrin was used, comparing to the group n2=5.8, $p<0.05$ (Fig. 1). The same result, but with a less contrast between groups, was found after 7 days (n1=9.67, n2=9, $p<0.05$). The average of Pain Score in the first group with platelet rich fibrin was smaller comparing to the second group in the 1st (n1=0.83, n2=1.4, $p<0.05$) and 3rd (n1=0.17, n2=0.6, $p<0.05$) days of evaluation. On the 7th day the result was non-significant in both groups.

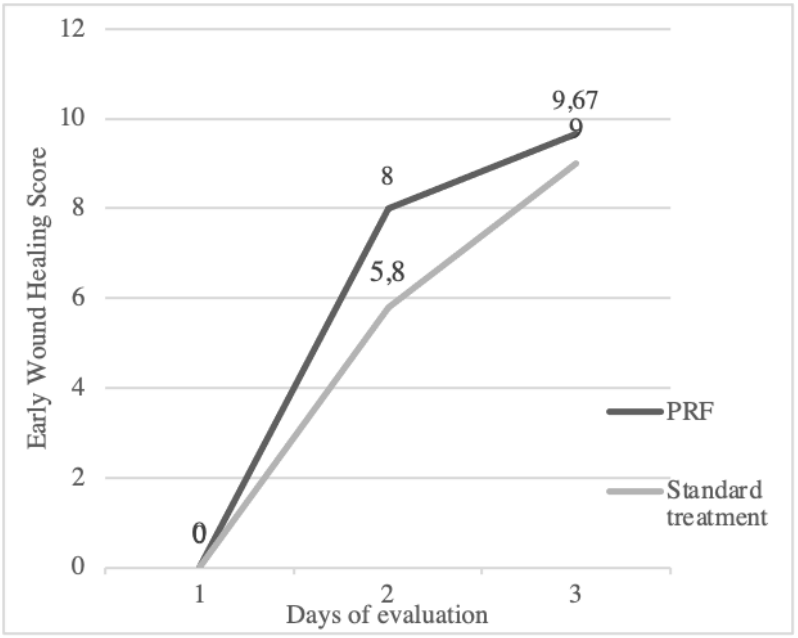

Fig. 1. Comparison of Standard Treatment and PRF treatment of the alveolar wound, Early Wound Healing Score were counted.

Conclusion. PRF may be a useful tool in post-extraction alveolar wound treatment but there is a need of more research about its concept in dogs.

[1] C.E. Harvey. Periodontal disease in dogs. Etiopathogenesis, prevalence, and significance. Vet Clin North Am Small Anim Pract. (1998) 28(5):1111-28.
[2] S. Ghanaati, P. Booms, A. Orlowska, et al. Advanced platelet-rich fibrin: a new concept for cell-based tissue engineering by means of inflammatory cells. J Oral Implantol. (2014) 40(6):679-89.
[3] L. Marini, M.A. Rojas, P. Sahrmann, R. Aghazada, A. Pilloni. Early Wound Healing Score: a system to evaluate the early healing of periodontal soft tissue wounds. J Periodontal Implant Sci. (2018) 48(5):274-283.
[4] P.W. Hellyer, S.R. Uhrig, N.G. Robinson. Canine Acute Pain Scale. Veterinary Medical Center. Canine Acute Pain Scale.

INFLUENCE OF ANTIMICROBIAL PHOTOINACTIVATION ON MONOCULTURAL BACTERIAL BIOFILMS

Laura Jurkaitytė, Ieva Dumčytė, Alisa Gricajeva, Lukas Stasiulionis, Lilija Kalėdienė

Department of Microbiology and Biotechnology, Life Sciences Center, Institute of Biosciences, Vilnius University, Vilnius, Lithuania
laura.jurkaityte@gmc.stud.vu.lt

Most of the bacteria are naturally found living in sessile coordinated functional communities called biofilms. Microbial biofilms are widespread in the environment and form on biotic and abiotic surfaces if constant moisture is present. Adhesion of biofilms to different surfaces is promoted by the extracellular matrix that bacteria are self-embedded in [1]. Compared to floating or planktonic cells, one of the benefits of living in biofilms is the substantially higher resistance to adverse external physical and chemical impact [2].

Biofilms play an important role in human infections and can pose a potential threat to material integrity in confined facilities such as hospitals, food, and other industrial settings. Thus, nowadays, facing the enormously fast development of bacterial resistance to different conventional antimicrobial agents there is a need in a discovery and analysis of new, natural bacterial control methods that would be safe and effective to use, especially against recalcitrant bacterial biofilms [3].

Therefore, this study aimed to investigate a photosensitization-based method known as antimicrobial photoinactivation (API) [4] against monocultural biofilms, as well as planktonic cells (to investigate prevention of biofilm formation) of *Pseudomonas aeruginosa* atcc 27853, *Staphylococcus saprophyticus* AG1 and *Staphylococcus epidermidis* atcc 12228 (only planktonic cells evaluated). For the API, natural photosensitizers (PS) such as riboflavin (RF) and chlorophyllin (Chl) in combination with appropriate photosensitizing visible-light irradiations were used. It was found that RF- and Chl-base API can have bacteriocidic effect against biofilms of the selected bacteria. However, considering actual application of the technology, concentration of selected natural PSs, irradiation doses and other optimization studies should be further performed.

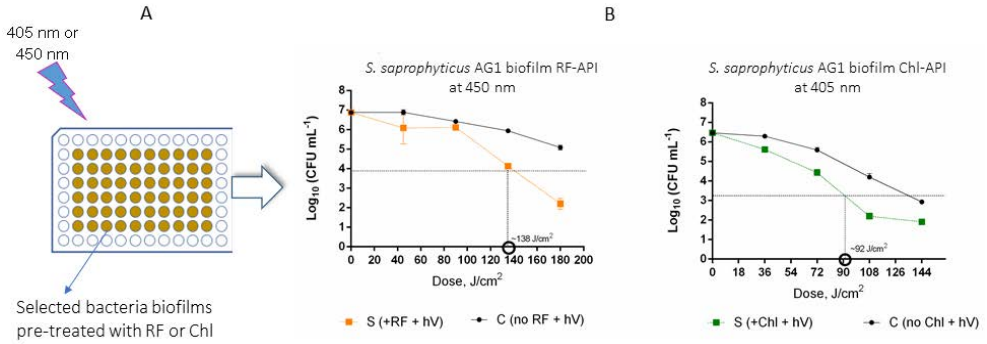

Fig. 1. Simplified scheme of the API method used in this work (A); results of RF- and Chl-based API exemplified by *S. saprophyticus* AG1 (B). A horizontal dashed line in the graphs denotes minimal 3 log reduction (indicating bactericidal effect).

[1] M. Berlanga, R. Guerrero, Living together in biofilms: the microbial cell factory and its biotechnological implications, Microbial Cell Factories **15**, 165 (2016).
[2] H. C. Flemming, J. Wingender, U. Szewzyk et al., Biofilms: an emergent form of bacterial life, Nature Reviews Microbiology **14**, 563ï 575 (2016).
[3] H. Koo, R. N. Allan, R. P. Howlin et al., Targeting microbial biofilms: current and prospective therapeutic strategies, Nature Reviews Microbiology **15**, 740ï 755 (2017).
[4] I. Buchovec, A. Gricajeva, L. Kalėdienė, P. Vitta, Antimicrobial photoinactivation approach based on natural agents for control of bacteria biofilms in spacecraft, International Journal of Molecular Sciences **21**, 6932 (2020).

ANTICANCER ACTIVITY OF SUNITINIB ANALOGUES IN BRAIN CANCER MODELS

Girstautã Dabkeviļ iÎ tã[1], Elias Maccioni[2], Vilma Petrikaitã[1*]

[1]Department of Drug Targets Histopathology, Institute of Cardiology, Lithuanian University of Health Sciences, Lithuania

[2] Department of Life and Environmental Sciences, Cagliari University, Italy

vilma.petrikaite@lsmuni.lt

Glioblastoma (GBM) is the most aggressive type of brain cancer. Median survival time for GBM patients is about 12.1 to 14.6 month [1], and there are still extremely limited opportunities of conventional therapy. Tyrosine kinase inhibitors currently are considered as a perspective targeted therapy for GBM. There are numerous studies linking changes in kinase activity to carcinogenesis and tumor progression. Tyrosine kinase inhibitors generally target the active site of the kinase and thereby prevent the phosphorylation resulting in inhibition of migration and apoptosis of cancer cells [2]. One of them is sunitinib, a multi-targeted agent, approved for the treatment of kidney cancer and gastrointestinal stromal tumours [3]. Moreover, the new chemical compounds are suggested as more effective sunitinib analogues [4]. The aim of our study was to evaluate the effect of new sunitinib analogues on human brain cancer cell viability and migration.

The two human GBM cell lines, U87-MG and A172, and non-malignant human fibroblasts were used to investigate anticancer activity of 17 sunitinib analogues in vitro. The effect of kinase inhibitors on cell viability was evaluated by MTT assay after 72 hours of incubation. Then the most active kinase inhibitors that reduced cell viability up to 5% or less have been selected for further studies. The EC_{50} values of the most active compounds were established and compared to the sunitinib cytotoxicity. Single cell migration assay was performed to examine the effect of selected compounds on U87-MG cell migration. Cells were seeded in the dishes with numbered grids in such way that about 50-70 cells would be on the gridded area. Images of cells were taken every hour for 8 hours by inverted microscope. Coordinates of the cells were established and the travelled distance has been calculated. The single cell distance travelled per hour was defined as the cell velocity. The data were presented as average cell velocity Ñstandard deviation.

The results of MTT assay experiment have shown that compounds 1, 6 and 7 were the most active ones. All three tested compounds had more potent reducing effect on the brain cancer cell viability of A172 cell line compared to U87-MG cell line and non-malignant cells. It should be noted, that compound 6 was the only one that showed a stronger cytotoxic effect on tested cancer cell lines in comparison with non-malignant cells. However, data analysis revealed that compound 1 had the greatest effect on reducing cell viability (EC_{50} values after 72 h on U87-MG, A172 and HF were 82 Ñ6 nM, 72 Ñ6 nM and 82 Ñ6 nM, respectively). All tested sunitinib analogues were more cytotoxic than sunitinib. In migration assay, compound 6 reduced U-87-MG cell migration by 13% more efficiently than sunitinib, and decreased the average cell velocity by 2 times compared to the control. Unexpectedly, compounds 1 and 7 showed an opposite effect on cell migration as cell velocity was increased by 33% and 73%, respectively, compared to the control.

To conclude, compound 6 may be worthy of further studies as it had U87-MG and A172 cancer cell specific cytotoxicity as well as was the most effective kinase inhibitor in U87-MG cell line.

[1] Bahadur S, Sahu AK, Baghel P, Saha S. Current promising treatment strategy for glioblastoma multiform: A review. Oncol Rev [Internet]. 2019 Jul 25 [cited 2020 Oct 11];13(2). Available from: https://www.ncbi.nlm.nih.gov/pmc/articles/PMC6661528/

[2] Tyrosine Kinase Inhibitors in Cancer: Breakthrough and Challenges of Targeted Therapy [Internet]. [cited 2020 Oct 11]. Available from: https://www.ncbi.nlm.nih.gov/pmc/articles/PMC7140093/

[3] Le Tourneau C, Raymond E, Faivre S. Sunitinib: a novel tyrosine kinase inhibitor. A brief review of its therapeutic potential in the treatment of renal carcinoma and gastrointestinal stromal tumors (GIST). Ther Clin Risk Manag. 2007 Jun;3(2):341ï 8.

[4] Meleddu R, Petrikaite V, Distinto S, Arridu A, Angius R, Serusi L, et al. Investigating the Anticancer Activity of Isatin/Dihydropyrazole Hybrids. ACS Med Chem Lett. 2019 Apr 11;10(4):571ï 6.

P5-43

DID NOT PARTICIPATE

P5-44

DID NOT PARTICIPATE

APPLICATION OF A MULTIFUNCTIONAL LASER DIAGNOSTIC COMPLEX “LAKK-M” IN DENTISTRY

Kristina Khudaleeva, Nikolay Abolmasov

Faculty of Orthopedic Dentistry, Smolensk State Medical University, Russia
verazaytseva@yandex.ru

Investigation of microcirculation in the periodontium can be beneficially conducted with certain devices like a multifunctional laser diagnostic complex "LAKK-M" and simultaneously using a number of non-invasive diagnostic methods. The study evaluates the following characteristics:

1) Microhemodynamics (laser Doppler fluometry – LDF method)

The essence of this method is that a low-intensity monochromatic light beam emitted by a laser diode embedded in a Doppler laser flowmeter passes through a flexible light guide and through the tip of the sensor illuminates the tissue under study. In the fabric, the light is scattered by reflecting particles. Part of the light is reflected back and passes through the receiving light guide to the internal photodetector of the device. In accordance with the Doppler effect, only moving particles (mainly red blood cells) lead to a frequency shift. The spectrum of the received signal is processed in the device in accordance with the algorithm obtained by Bonner for this type of reflection, and the flow volume (ml/min/100 g of tissue) is calculated. Thus, the LDF method is based on the measurement of the Doppler component in the spectrum of the reflected laser signal scattered on the shaped blood elements moving in the microvessels.

2) Delivery and consumption of oxygen in the microcirculatory bed (optical tissue oximetry – GRT method)

The method of optical tissue oximetry (GR) estimated delivery and consumption of oxygen in the microvasculature; and the relative volume fraction of erythrocytes (Vr) in the study of ≈ 4-5 mm3 and saturation mixed-blood (that is, arteriole and venules)

3) Saturation of arterial blood with oxygen (pulse oximetry method)

4) Content of oxidative metabolism enzymes (laser fluorescent diagnostics (LPD) method))

The spectrum of reflected radiation of the tissue is recorded when a laser beam probes it with a wavelength corresponding to the wavelength of the maximum absorption of the beam by a certain enzyme, sources with three wavelengths are used to excite the fluorescence of enzymes (nicotinamides, flavins, lipofuscin, porphyrin, etc.): 365 nm, 532 nm and 630 nm. Diagnosis of the main functions of the microcirculatory bed in the form of their comprehensive assessment (LDF + OTO + LPD) is more informative compared to the individual methods mentioned above, since microcirculation is variable and adapts to the specific physiological needs of the tissue. An integrated approach to the study of tissue in vivo allows obtaining complementary data on microdynamics, oxygen consumption and the state of metabolic processes for their analysis and decision-making in dental diagnostics.

PHYSICS IN MEDICINE: DISORDERS OF MICROCIRCULATORY PROCESSES IN THE MUSCLE AND THEIR DIAGNOSIS IN DISEASES OF THE NERVOUS SYSTEM

Derevtsova Anastasia[1], Derevtsova Svetlana[2]

[1]Smolensk State Medical University, Faculty of Pediatrics, Russia
[2]Smolensk State Medical University, Department of Physics, Mathematics and Medical Informatics, Russia
nastyaderevtsova@gmail.com

Currently, there is a problem of cerebral palsy; it is one of the most urgent problems in Pediatric Orthopedics and Neuropathology. In the social context, the problem is significance as well [1]. Due to the combination of underdevelopment and pathology of motor development, disorders of the regulation of muscle tone - such as spasticity, rigidity, dystonia, and hypotension-are particularly significant and complicated [2]. The aim of the treatment of cerebral palsy children with is a possible more complete adaptation, the degree of which largely depends on mental and motor functions, speech development, and intelligence. Adaptation is associated with the choice of an individual rehabilitation scheme for each patient.

In children, motor disorders are primarily determined by a pronounced increase in muscle tone (spasticity) in combination with muscle weakness (paretic). This leads to difficulty or impossibility of voluntary movements. Prolonged muscle spasm in cerebral palsy affects the capillaries and leads to a violation of microcirculation in the muscle.

As a non-medicinal means of restoring normal peripheral blood circulation, we consider effects aimed at relaxing the muscle-tours – massage. Differentiated technique of segmental reflex massage with physical therapy developed by us reduces muscle tone and most intensively contributes to an increase in peripheral blood circulation, the external manifestation of which is arterial hyperemia. Determining the degree of severity of muscle spasticity, we can talk about the qualitative (indirect) state of peripheral blood circulation. Identification the level of muscle tone and correction the strength and duration of massage effects are key elements in management of cerebral palsy patients.

In our study to assess and monitor the functional state of the muscles, we used such device as myotonometer, which is an analog of the myotonometer system of Dr. Sirmai (Hungary). We examined 14 children under the age of 3 years with cerebral palsy (spastic form).

Methods of measurement: 1. Checking the calibration of the device. Firstly,we put the myotonometer with its base on the glass and count the reading of the device on the scale. This reading should be equal to 250 myotons (1 myoton is equal to the deviation of the arrow of the device by 1 division). If the reading of the device is different from 250, then we move the stop flange to get this reading. 2. Place the device with its base on the measured muscle group. With a light force, press the device against the measured area of the body and touch the flange-limiter of this area. 3. Make a reading on the myotonometer scale.

Muscle tone was determined in the center of the abdomen of individual muscles. The rod of the myotonometer was installed strictly perpendicular to the examined muscle. All measurements were performed in the initial lying position (before the massage, after the massage). Experimental data were obtained (significance level $\alpha = 0,05$):

Points for measuring muscle tone	Before the massage (readings in myotonic)		After the massage (readings in myotonic)	
	Experiment roup	Control group	Experiment group	Control group
Mid-biceps	86,77±1,26	83,07±1,42	64,85±1,01	73,14±1,42
Mid-calf muscle	91,23±1,44	94,14±1,69	73,64±1,29	86,14±0,74
Middle of the adductor muscle of the thigh	82,50±1,75	79,21±0,46	66,64±1,10	72,07±0,77

The level of muscle tone is significantly reduced in the experimental group, where an individual massage technique is used with the inclusion of elements of physical therapy. We use a modern method of prevention and treatment – massage, providing the correct, differentiated in time and strength massage effect. Taking into account the severity of cerebral palsy and using a myotonometer, we create a more effective therapeutic result in the conditions of the procedure, by increasing the work on the muscle group that is more prone to spastic reactions. This technique is being implemented in the practice of a massage therapist.

The activities can significantly facilitate the efforts of experts in various fields (doctors, remedial gymnastics trainers, speech therapists, speech pathologists, educators of special institutions, as well as parents) in order to ensure maximal social adaptation of patients and their proper inclusion into the society.

[1] A.A. Brujkov, A.V. Gulin, J.A. Brujkov. The use of non-drug methods in the treatment of cerebral palsy. Bulletin of TSU, vol. 22, issue 6, 2017.

[2] E.V. Semenova, E.V. Klochkova. Rehabilitation of children with cerebral palsy: a review of modern approaches to help rehabilitation centers-Moscow: Lepta Kniga, 2018. - 584 p.

P5-47

DID NOT PARTICIPATE

THE ROLE OF LAPAROSCOPY IN THE MANAGEMENT OF ABDOMINAL TRAUMA

Ugne Imbrasaite[1], Bronius Buckus[2]

[1] Faculty of Medicine, Vilnius University, Lithuania
[2] Clinic of Gastroenterology, Nephro-Urology and Surgery, Faculty of Medicine, Vilnius University, Lithuania
ugne.imbrasaite@mf.stud.vu.lt

Abdominal trauma ï one of the major causes of morbidity and mortality worldwide. It accounts for 9ï 14.9% of all trauma cases [1] and is very common in the case of young people under the age of 40 years [2]. Laparotomy has traditionally been the standard of care for evaluation and treatment of patients with abdominal trauma [2,3]. Laparoscopic surgery has greatly improved surgical outcome in many areas of abdominal surgery. However, there are many controversial opinions about its safety in abdominal trauma surgery. According to several studies, laparoscopy has a high rate of missed injuries (up to 40%) [4ï 6], a perceived inability to visualize all areas of the abdomen [6] and it requires surgeons with adequate experience and proper equipments [4,7].

The aim of our study was to estimate the use of laparoscopy in the evaluation and treatment of patients with abdominal trauma. This was a retrospective 4ï year (2015-2018) study carried out in the Republican Vilnius university hospital. All abdominal trauma patients managed by operative interventions were included. Patients were divided into two groups: laparotomy and laparoscopy, and were compared with each other. A total of 200 trauma patients were evaluated for abdominal injury. Out of these, 115 (57.50%) underwent surgical intervention for abdominal trauma and were thus included in the study: 24 (20.87%) patients in laparoscopy group and 91 (79.13%) - laparotomy. There was no statistically significant difference in demographic criteria between the groups ($p>0.05$). The mean age of patients was 42ï 45 years and the majority of them were males (78.26%). Blunt trauma was sustained by 39 (33.91%) patients and 76 (66.09%) patients sustained penetrating injury ($p>0.05$). Preoperative imaging was performed to all patients from laparoscopy group and 87% - laparotomy group (>50% experienced two imaging methods). False negative results of the imaging techniques accounted for 20-30% of all the results. False positive results were 4 in laparoscopy group and 6 - laparotomy. Multiple, one and no injuries were presented in 4 (16.67%), 16 (66.66%) and 4 (16.67%) patients of laparoscopy group respectively. Nine (37.50%) patients required conversion to laparotomy: 2 patients (22.22%) after blunt trauma and 7 - penetrating injury (77.78%) due to hollow viscus injuries, intensive bleeding and multiple injuries. Laparotomy was therapeutic for 80 patients (87.91%) including 19 (23.75%) patients with multiple injuries and 61 (76.25%) ï single, and was diagnostic for 11 (12.09%) patients. Multiple injuries accounted for 20% of all the cases and the most common injury was the injury of intestines. There was no statistically significant difference in the mean operating time and postoperative complication rates between the groups ($p>0.05$). But the mean length of hospital stay was in shorten laparoscopy group ($p<0.05$). No missed injuries were also reported in the laparoscopy group.

According to this retrospective study, we conclude that laparoscopy could become a safe and effective method of treating patients with abdominal trauma. This method might reduce the frequency of unnecessary laparotomies, including laparotomy-related complications and length of hospital stay. We also present a possible algorithm for the use of laparoscopy in the management of abdominal trauma patients based on our limited study and a review of the literature.

[1] O. V. Ozkan, V. Justin, A. Fingerhut, and S. Uranues, ñLaparoscopy in Abdominal Trauma,ò Curr. Trauma Reports, vol. 2, no. 4, pp. 238ï 246, (2016).
[2] P. K. Sharma, G. Gupta, ñThe role of laparoscopy in abdominal trauma,ò Int J Res Med Sci, no. 5, pp. 1853ï 1861, (2019).
[3] M. June, ñThe Role of Laparoscopy in Abdominal Trauma : A 10-Year Review,ò vol. 114, no. 3, pp. 359ï 368, (2019).
[4] K. H. Lim, B. S. Chung, J. Y. Kim, and S. S. Kim, ñLaparoscopic surgery in abdominal trauma: A single center review of a 7-year experience,ò World J. Emerg. Surg., vol. 10, no. 1, pp. 1ï 7, (2015).
[5] M. Z. Koto, O. Y. Matsevych, and S. R. Motilall, ñThe Role of Laparoscopy in Penetrating Abdominal Trauma: Our Initial Experience,ò J. Laparoendosc. Adv. Surg. Tech., vol. 25, no. 9, pp. 730ï 736, (2015).
[6] P. J. Chestovich, T. D. Browder, S. L. Morrissey, D. R. Fraser, N. K. Ingalls, and J. J. Fildes, ñMinimally invasive is maximally effective: Diagnostic and therapeutic laparoscopy for penetrating abdominal injuries,ò J. Trauma Acute Care Surg., vol. 78, no. 6, pp. 1076ï 1085, (2015).
[7] L. H.-F., C. Y.-D., and C. S.-C., ñValue of diagnostic and therapeutic laparoscopy for patients with blunt abdominal trauma: A 10-year medical center experience,ò PLoS One, vol. 13, no. 2, pp. 1ï 14, (2018).

P5-49

DID NOT PARTICIPATE

COMPARTMENT-SPECIFIC PROTEOME CONSTRAINTS DRIVE CHANGES IN YEAST METABOLISM

Pranas Grigaitis[1], Ibrahim El-Semman[2,7], Angelica Rodrigues Prado[1,3], Manuel Garcia Albornoz[4], Victoria Harman[5], Stephen Holman[5], Johan van Heerden[1], Simon Hubbard[4], Rob Beynon[5], Frank J. Bruggeman[1], Pascale Daran-Lapujade[3], Nikolaus Sonnenschein[2], Jens Nielsen[2,6], and Bas Teusink[1]

[1] Systems Biology Lab, Amsterdam Institute of Molecular and Life Sciences, VU Amsterdam, The Netherlands
[2] Novo Nordisk Foundation Center for Biosustainability, Technical University of Denmark, DK2800 Lyngby, Denmark
[3] Department of Industrial Microbiology, Technical University Delft, Delft, The Netherlands
[4] Division of Evolution and Genomic Sciences, School of Biological Sciences, Faculty of Biology, Medicine and Health, The University of Manchester, Manchester, United Kingdom
[5] Department of Biochemistry, Institute of Integrative Biology, Biosciences Building, University of Liverpool, Liverpool, United Kingdom
[6] Department of Biology and Biological Engineering, Chalmers University of Technology, SE41296 Gothenburg, Sweden
[7] Department of Mathematics, Faculty of Science, Assiut University, Assiut, Egypt (On leave)
p.grigaitis@vu.nl

Metabolism is at the core of cellular functions as it provides energy and building blocks required for cellular maintenance and growth; there is therefore much interest in the driving forces that shape metabolic adaptations. In bacteria, constraints on cellular resources explain allocation of proteins to different cellular processes. In eukaryotes, however, metabolism is distributed into several different compartments. Thus it is unclear which constraints shape cellular metabolism. Here we integrated metabolic fluxes and proteomics data with a genome-scale model of budding yeast *Saccharomyces cerevisiae*, enhanced with detailed, growth rate-dependent, description of protein turnover and associated, compartment-specific, proteome constraints. We find that the Crabtree effect, i.e. the onset of alcoholic fermentation (analogous to the Warburg effect in cancer) is governed by mitochondrial or cytosolic constraints, depending on nutrient availability and quality. These effects are reflected in predictions of condition- and compartment-specific proteome composition, which are in agreement with quantitative proteomics measurements. Our modeling approach provides a powerful platform to study multiple scenarios of compartment-specific yeast metabolism at genome-scale in a fine-grained manner.

MODELING OF CONCENTRATION QUENCHING IN TWO-DIMENSIONAL SYSTEMS

Sandra Barysaitė[1], Andrius Gelzinis[1,2], Jevgenij Chmeliov[1,2], Leonas Valkunas[1,2]

[1]Faculty of Physics, Vilnius University, Vilnius, Lithuania
[2]Department of Molecular Compound Physics, Centre for Physical Sciences and Technology, Vilnius, Lithuania.
sandra.barysaite@ff.stud.vu.lt

The phenomenon of concentration quenching has been investigated throughout the last century, however, its origin is not fully understood to this day. An example of such occurrence has been observed in chlorophyll solutions: at higher concentrations the relative fluorescence intensity becomes dependent on the concentration and starts decreasing [1]. It is important to note that in artificial systems the fluorescence is usually significantly quenched at fluorophore concentrations typical to that of unquenched *in vivo* photosynthetic systems.

In this work, concentration quenching in a two-dimensional system was simulated using approach similar to Ref. [2]. The two-dimensional model was chosen for simplicity, however, its real life equivalent could be an especially thin film or membrane. Molecules, each 1 nm in diameter, were scattered in a 10000 nm^2 area using a uniform distribution. Different concentrations were obtained by changing the number of molecules from 100 to 1000. Randomly chosen molecules acted as traps; excitation, after reaching such molecule, could not escape. The amount of traps used were 1%; 2%; 5%; 10%; 20% of the total number of molecules. At the initial time moment, excitation was distributed equally among all non-trap molecules. Time dependence of the total excitation probability was calculated by solving the system of kinetic equations with energy transfer rates between the molecules being proportional to the inverse sixth power of the distance between the molecules, following the Forster level of description. Obtained results were averaged over different molecule distributions and are shown in Fig. 1.

As expected, we can observe that in larger concentrations quenching is more rapid. A comparison between this model and a dynamic quenching model (where traps are formed when two or more molecules are closer to each other than a certain distance) will be presented.

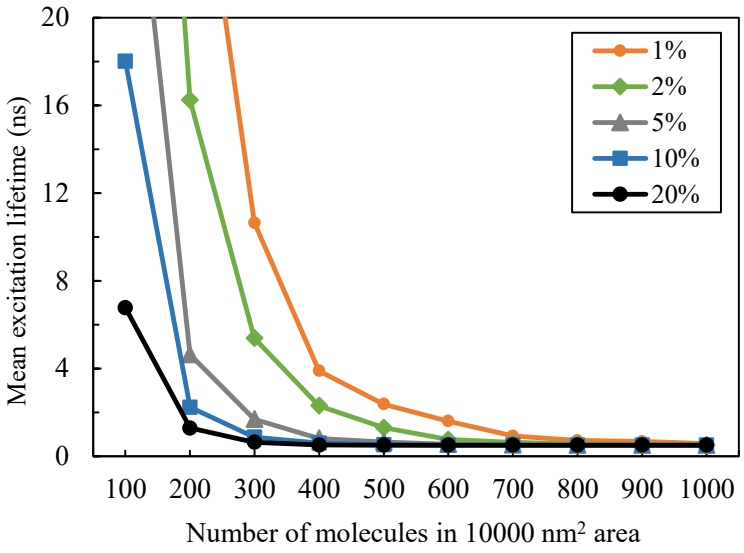

Fig. 1. Dependence of mean excitation lifetime on different molecular concentrations and relative amount of traps.

[1] G. Beddard, G. Porter, Concentration quenching in chlorophyll, *Nature* **260**, 366–367 (1976).
[2] W.-J. Shi, J. Barber, Y. Zhao, Role of Formation of Statistical Aggregates in Chlorophyll Fluorescence Concentration Quenching, *The Journal of Physical Chemistry B* **2013** *117* (15), 3976-3982

SYNTHESIS AND IVESTIGATION OF NEW ORGANIC SEMICONDUCTORS WITH AMIDE AND REACTIVE FUNCTIONAL GROUPS

Elġbieta Poļobut, Tadas Malinauskas

Faculty of Chemical Technology, Kaunas University of Technology, Lithuania
elzbieta.pocobut@ktu.edu

Nowadays fossil fuels remain the most common source of energy. Limited reserves, adverse effect on human health and the environment are demanding more intense research on sustainable and renewable alternatives. Solar energy has the largest potential among all renewable energy sources and it can be transformed into usable electricity by photovoltaic conversion in solar cells [1].

Silicon solar cells have been the dominant driving force in photovoltaic technology for the past several decades due to their well-known mechanism of action, the longevity and reliability during the operation. In addition, silicon is the abundant element in earthôs crust and its nature is environmentally friendly. The efficiency of current thin-film silicon solar cells is about 26%, but this requires the very pure silicon and complex technological processes [2]. For these reasons, the silicon-based solar cell production is still expensive.

Perovskite solar cells (PSCs) can be one of the alternatives to silicon solar cells. PCSs have recently attracted a lot of attention due to their high power conversion efficiency (PCE), inexpensive starting materials, and ease of production. In less than a decade, these photovoltaics have made tremendous progress in effectiveness, rising PCE from 3.8% to 25.5% [3]. Perovskites possess intrinsic properties like wide absorption spectrum, fast charge separation, long transport distance of electrons and holes, long carrier separation lifetime. The PSC consists of an active perovskite layer located between the electron transporting layer (ETL) and the hole transporting layer (HTL). The HTL plays an important role in transporting holes, blocking electrons and protecting the perovskite from external factors, including moisture heat, and oxygen [4]. The main disadvantage of HTL is its conductivity, which can be increased by the addition of dopants. The use of dopants, however, impairs the stability of the perovskite solar cells, so intensive research is conducted to abandon them.

One way to avoid the use of dopants in HTL is to use self-assembling (SAM) positive charge-carrying compounds. Triarylamine-type molecules are considered as very efficient functional units that are widely used as photoconductors and charge carriers [5]. Combining triphenylamine with amide moieties can allow molecules to self-assemble into helical aggregates when exposed to visible light. Meanwhile, presence of the diacetylene functional groups allows formed structure to be fixated with covalent bonds into stable aggregate during the photopolymerization induced by ultraviolet light.

In this work several triphenylamine-based organic semiconductors with amide and reactive functional groups were synthesized as dopant-free SAM HTMs. Their optical, photophysical and thermal properties were investigated.

This research was funded by the European Social Fund under the No 09.3.3-LMT-K-712-22-0026 ñDevelopment of Competences of Scientists, other Researchers and Students through Practical research Activitiesò measure.

[1] A. Bozzola, P. Kowalczewski, M. Liscidini, L. Redorici. Silicon Solar Cells: Towards the Efficiency Limits. *Advances in Physics: X*. 2019, 4, 1, 1548305.

[2] Bhattacharya, S., John, S. Beyond 30% Conversion Efficiency in Silicon Solar Cells: A Numerical Demonstration. *Sci Rep* 9, 12482 (2019).

[3] Li, Z., Dong, J., Liu, C. *et al.* Surface passivation of Perovskite Solar Cells Toward Improved Efficiency and Stability. *Nano-Micro Lett.* 11, 50 (2019).

[4] R. Wang, M. Mujahid, Y. Duan, Z. K. Wang, J. Xue, Y. Yang. A Review of Perovskites Solar Cell stability. *Adv. Funct. Mater*. 2019, 29, 47, 1808843.

[5] Moulin E, Niess F, Maaloum M, Buhler E, Nyrkova I, Giuseppone N. The hierarchical self-assembly of charge nanocarriers: a highly cooperative process promoted by visible light. Angew Chem Int Ed Engl. 2010 Sep 17;49(39):6974-8.

SYNTHESIS AND INVESTIGATION OF *N*-TYPE ORGANIC SEMICONDUCTORS CONTAINING ANCHORING GROUPS

Lauryna Monika Svirskaitã, Tadas Malinauskas

Department of Organic Chemistry, Kaunas University of Technology, RadvilãnÔpl. 19, Lithuania
lauryna.svirskaite@ktu.lt

Compared with traditional forms of electricity production, photovoltaic technology offers us the possibility to produce green and sustainable energy and reducing emission of greenhouse gasses and other toxic or harmful particles. A great deal of effort has been made during the past few years to improve the performance of perovskite solar cells (PSC) by optimizing the device structure, composition and morphology of the perovskite layer, as well as synthesizing and applying more efficient electron (ETM) and hole transporting materials [1]. As a result, PSC conversion efficiency (PCE) reached 25.5 % [2], which makes PSC quite promising photovoltaic technology. However, stability issues remain as a main obstacle, hindering commercialization of PSCs.

For inverted PSCs, fullerenes and their modified derivatives are widely used as ETMs, among which PCBM is the most prevalent one. Unfortunately, limited solubility of non-modified fullerenes in organic solvents hinders their applicability in PSCs, while modified ones are rather expensive [3]. Efficient method to improve the performance and stability of PSC is to coat perovskite with derivatives, able to form self-assembled monolayers (SAM), e.g. ETM SAM. The ionic nature of the perovskite layer capable of interaction with different anchoring groups, by forming coordination or ionic bonds. Therefore, SAMs can form ordered one-atom thick layer with well-defined orientation on the perovskite surface. The layout of directed ETMs molecules maintain constant dipole moment, which influences charge transporting efficiency and the alignment of energy levels at the layers interface. Incorporating particular functional groups, which provide hydrophobicity, into SAM molecular structure, e.g. fluorine atoms, can also improve perovskite resistance to moisture [4].

In this work new n-type semiconductors containing 1,4,5,8,-naphtalenetetracarboxylic diimide (NDI) central fragment along with various anchoring and protective groups were synthesized.

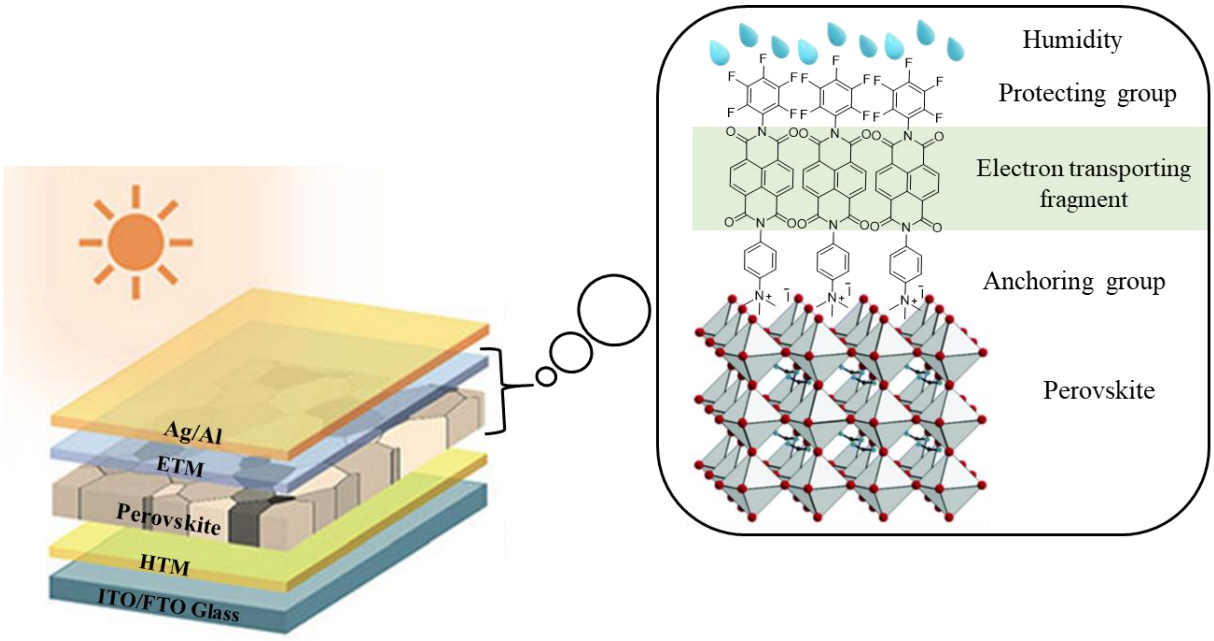

Fig. 1. Perovskite surface modification by NDI SAM

Photoelectrical, optical, thermal properties of the synthesized compounds were investigated and different monolayer forming procedures were tested. SAMs with pentafluorphenyl fragments formed the most hydrophobic layer on the surface of perovskite, which has improved moisture resistance of the perovskite. Additionally, using synthesized ETMs perovskite solar cells were constructed and photovoltaic characteristics of these devices were measured.

[1] Bairu Li, et. al. Anchoring Fullerene onto Perovskite Film via Grafting Pyridine toward Enhanced Electron Transport in High-Efficiency Solar Cells, ACS Appl. Mater. Interfaces 2018, **10**, 32471ī 32482.
[2] Best Research-Cell Efficiency Chart. https://www.nrel.gov/pv/cell-efficiency.html
[3] Chaohua Cui, et. al. Fullerene Derivatives for the Applications as Acceptor and Cathode Buffer Layer Materials for Organic and Perovskite Solar Cells, Adv. Energy Mater. 2017, **7**, 1601251.
[4] Ru Qiao and Lijian Zuo, Self-assembly monolayers boosting organic-inorganic halide perovskite solar cell performance, Journal of Materials Research volume, 2018, 33, 387ī 400.

DEEP EUTECTIC SOLVENTS FOR HEADSPACE GAS CHROMATOGRAPHIC DETERMINATION OF HEXANAL

Birutė Bugelytė, Ingrida Jurkutė, Vida Vičkačkaitė

Department of Analytical and Environmental Chemistry, Vilnius University, Naugarduko St. 24, LT-03225 Vilnius, Lithuania
b.bugelyte@gmail.com

During storage and when subjected to heat, unsaturated fatty acids of edible oils undergo oxidation forming hydroperoxides and secondary volatile oxidation products [1]. Oxidation has a great impact on the quality of food products because of off-flavours, of a decrease in the nutritional properties and especially because of the formation of toxic compounds and can increase propensities to various cardiovascular and metabolic diseases [2]. Thus there is a great interest on fast and simple detection of lipid oxidation. The evaluation of the oxidation level can be based on the quantity of hexanal as it is the main secondary oxidation product of linoleic acid which is one of the principle fatty acids of many edible oils [3].

The most complicated step of the determination of volatile compounds in complex matrices is the separation of analytes from the matrix. Traditional analyte separation methods (liquid extraction, Soxhlet extraction) require a lot of time and labour, moreover, there is a risk to lose the volatile analytes. In recent years, headspace gas chromatography has been used to determine the volatile compounds. To date, traditional extraction solvents have been used in headspace gas chromatography. As a rule, such solvents are rather volatile; therefore, a large amount of solvent vapour enters into the headspace together with the analyte. Because of that the determination sensitivity of the analyte is reduced, a huge solvent peak in the chromatogram can overlap with the peaks of the analyts. The sensitivity is also limited by the fact that the sample can't be heated at a higher temperature than the solvent boiling point.

Hexanal in fat-rich food can be determined by static headspace gas chromatography (SHS-GC). It includes a partial transfer of the volatile compounds into the gaseous phase and subsequently to GC system, meanwhile high molecular weight non-volatile molecules remain in the sample. For SHS extraction a solvent should be used to disperse the matrix and to prepare calibration solutions of hexanal. To promote the transfer of the volatile analyte into the headspace, the sample should be heated. Heating temperature should not reach the boiling point of the solvent, otherwise the vapour pressure becomes too great and leakages can occur or the vial could even burst. In order to increase heating temperature and to drive the equilibrium in favour of the gas phase, nonvolatile solvent should be advantageous.

In this work we suggest to replace traditional headspace gas chromatographic solvents by non-volatile, eco-friendly, biodegradable, inexpensive, easy to prepare deep eutectic solvents (DESs).

Eight hydrophilic and hydrophobic DESs have been synthesized and the influence of the temperature on their headspace gas chromatographic behaviour has been investigated. All the DESs studied were resistant to heating at 80 ^{o}C temperature. Among the solvents studied, DES composed of choline chloride, glucose and water showed the highest hexanal extraction efficiency. Using this solvent, headspace gas chromatographic conditions have been optimized for the determination of hexanal in potato chips. Under optimized conditions quality parameters of the prepared technique have been determined. The suggested technique was applied for the determination of hexanal in fat-rich food.

[1] L. Sghaier, J. Vial, P. Sassiat et al., Analysis of target volatile compounds related to fishy off-flavor in heated rapeseed oil: A comparative study of different headspace techniques, European Journal of Lipid Science and Technology **118**, 906-918 (2016).

[2] N. Gotoh, H. Watanabe, R. Osato et al., New Sight on the Possibility of the Neurotoxic Behavior Affected by the Oxidized Compounds in Fats and Oils, Journal of Oleo Science **54**, 397-405 (2005).

[3] M. H. Azarbad, H. Jeleń, Determination of Hexanal—an Indicator of Lipid Oxidation by Static Headspace Gas Chromatography (SHS-GC) in Fat-Rich Food Matrices, Food Analytical Methods **8**, 1727-1733 (2015).

ASYMMETRIC FRIEDEL-CRAFTS ALKYLATION OF INDOLES CATALYZED BY CHIRAL AZIRIDINE-PHOSPHINES

Aleksandra Buchcic, Anna Zawisza, Stanisław Leśniak, Michał Rachwalski

Department of Organic and Applied Chemistry, Faculty of Chemistry, University of Lodz, Poland
aleksandra.buchcic@edu.uni.lodz.pl

The necessity to develop new methods of production of biologically active compounds makes asymmetric synthesis an interesting and still exploring field of organic chemistry. The majority of species applied in pharmacy could be obtained utilizing this method. Asymmetric synthesis have a lot of advantages, e.g. the presence of byproducts and unwanted enantiomer is very small, so the loss of substrates is slight and the products exhibit high optical purity.

Indole derivatives are key species in human body: this skeleton is present in tryptophan, which is the substrate in melatonin and serotonin synthesis. Both of metioned compounds are responsible for various fuctions in organism, such as circadian rhythm, smooth muscle cramps, body temperature, etc. The drugs acting upon 5-hydroxytryptamine receptors are based on indole skeleton. The commonly used medicines are ondasetron, sumatriptan, indomethacin or alosetron. Among the variety indole-possesing drugs usually being 5-HT antagonists and agonists, anticancer agents could be found, e.g. vincamine or vincristine. [1]

Asymmetric Friedel-Crafts alkylation consitutes one of the most important methods of enantioselective formation of carbon-carbon bond. This reaction is utilized not only in various total syntheses of natural compounds, e.g. aflatoxin B_2 [2], (Ñ)-brasiliquinone B [3], but also in 2- or 3-substituted indoles, indoquinolines and spiorooxindoles [4]. Friedel-Crafts alkylation could be effectively catalyzed by chinchona alkaloids, thiourea derivatives or various copper (II) complexes [5], but there is lack of information about applying phosphines as chiral ligands in this reaction.

Based on chiral phosphinoyl-aziridine skeleton [6], a series of chiral phosphine-aziridines was synthesized with reasonable yields. These compounds were tested in asymmetric Friedel-Crafts alkylation of indole by ß-nitrostyrene in the presence of copper (I) trifluoromethanesulfonate benzene complex (Fig. 1). The products were obtained with good chemical yields and enantioselectives (80-92 %). The influence of ligand structure and aryl substituents in substrates will be discussed in poster presentation.

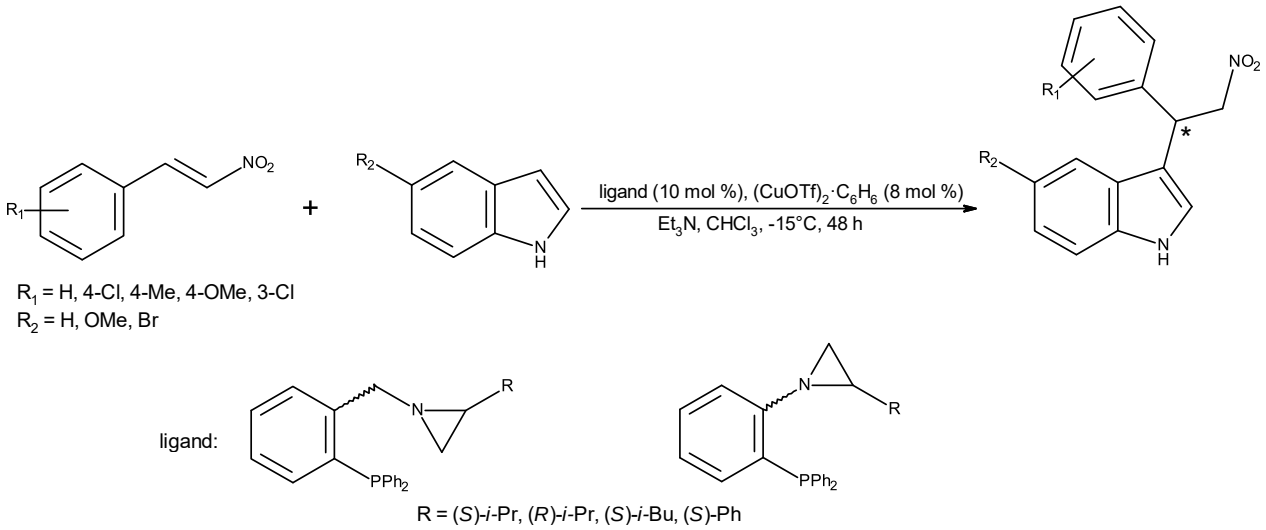

Fig. 1. Asymmetric Friedel-Crafts alkylation catalyzed by chiral phosphine-aziridines.

[1], N. K. Kaushik, N. Kaushik, P. Attri, N. Kumar, C. H. Kim, A. K. Verma, E. H. Choi, Biomedical importance of indoles. Molecules **18**, 6620-6662 (2013).
[2] Z. Wang, L. Zu, Organocatalytic enantioselective direct alkylation of phloroglucinol derivatives: asymmetric total synthesis of (+)-aflatoxin B_2. Chem. Commun. 5171-5174 (2019).
[3] M. L. Patil, H. B. Borate, D. E. Ponde, V. H. Deshpande, Total synthesis of (Ñ)-brasiliquinone B, Tetrahedron **58**, 6615-6620 (2002).
[4] E. Sansinenea, E.F. Martª nez, A. Ortiz, Organocatalytic synthesis of chiral spirooxindoles with quaternary stereogenic centers, Eur. J. Org. Chem. **32**, 5101-5118 (2020).
[5] P. K. Singh, A. Bisai, V.K. Singh, Enantioselective Friedel-Crafts alkylation of indoles with nitroalkanes catalyzed by a bis(oxazoline)-Cu(II)-complex. Tetrahedron Lett. **48**, 1127-1129 (2007).
[6] A. Buchcic, A. Zawisza, S. Leśniak, J. Adamczyk, A. M. Pieczonka, M. Rachwalski, Enantioselective Mannich reaction promoted by chiral phosphinoyl-aziridines. Catalysts **9**, 837-848 (2019).
[7] A. Buchcic, A. Zawisza, S. Leśniak, M. Rachwalski Asymmetric Friedel-Crafts alkylation of indoles catalyzed by chiral aziridine-phosphines, Catalysts **10**, 971-981 (2020).

THE THERMAL DECOMPOSITION OF GRAPHENE OXIDE IN THE PRESENCE OF CARBON SUBOXIDE

RÎta Aukġtakojytã[1], Justina Gaidukeviļ[1], Jurgis Barkauskas[1]

[1] Institute of Chemistry, Faculty of Chemistry and Geosciences, Vilnius University,
Naugarduko 24, LT-03225 Vilnius, Lithuania
ruta.aukstakojyte@chgf.vu.lt

Graphene is an allotrope of carbon that possesses unique thermal, chemical, electrical, optical, physical, and mechanical properties. It has broad application prospects in high-frequency electronics, water purification systems, semiconductor materials, drug carriers, flexible energy storage, and biosensing devices [1]. Nowadays, thermal reduction of graphene oxide (GO) is one of the potential synthesis methods to obtain graphene in a simple, low-cost, high yield, and time-saving way. However, GO is attributed to a class of energetic materials due to its high enthalpy change of thermal decomposition (q_pH). Thus, it could decompose violently if not properly stored and handled, and cause irreversible damage [2]. Furthermore, the mechanism of thermal reduction of GO is complex and not yet fully understood because of the consecutive stages of water evaporation, oxygen-containing functional groups removal, and basal-plane carbon decomposition occurring during the thermal exfoliation [3]. Therefore, it is necessary to focus on the kinetic analysis of GO thermal decomposition for a deeper understanding of the behaviour of the exothermic reduction reaction and ensuring safe manufacturing of graphene.

In this study, we present the impact of carbon suboxide (C_3O_2) on the kinetics of GO thermal decomposition. GO was prepared from natural graphite by the synthesis protocol reported by Yan et al. [4]. In a typical experiment, graphite powder was treated with concentrated H_2SO_4, $K_2S_2O_8$, and P_2O_5. The obtained pre-oxidized graphite was subjected to oxidation by Hummersô method [5]. According to the literature, C_3O_2 could be synthesized by heating the mixture of malonic acid and phosphorus pentoxide [6]. To evaluate the effect of C_3O_2 on the kinetics of GO thermal reduction, the homogenous mixture of GO, malonic acid and phosphorus pentoxide was prepared. It was named GO_MA_P. The prepared samples were analysed by using thermogravimetry (TG) and differential scanning colorimetry (DSC) methods at three different heating rates: 2.5 ÁC min$^{ï 1}$, 5 ÁC min$^{ï 1}$, and 10 ÁC min$^{ï 1}$. The kinetic and thermodynamic parameters of the thermal decomposition reaction of GO and GO_MA_P were determined by using Borchardt-Daniels, Kissinger, and Ozawa models [7].

DSC results revealed that the reduction temperature of GO is reduced (up to 125 °C) by using C_3O_2. Moreover, it was observed that C_3O_2 lowers the enthalpy q_pH and activation energy E_a but does not influence the reaction order n of GO thermal decomposition. The values of E_a for the thermal deposition of GO and GO_MA_P were obtained similar by using all three methods (Kissinger, Ozawa and Borchardt-Daniels). Results obtained by Borchardt-Daniels method showed that the values of E_a increase with increasing the heating rate for both studied samples. The apparent reaction order n for both GO and GO_MA_P equals 0.7. In fact, the mechanism of this process can be modelled including simultaneous zero-order and first-order stages. The zero-order process may originate in the case when the energy consumed in the thermal decomposition reaction comes through the basal graphene plane; then the reaction rate should not depend on the reagent concentration (i.e., the concentration of functional groups). The first-order process may occur in the case when the energy is absorbed directly by a functional group; this time the reaction rate depends only on the concentration of the reagent. The same reaction order for GO and GO_MA_P reduction reveals the same mechanism for both processes.

[1] S. Ren, P. Rong, Q. Yu, Preparations, properties and applications of graphene in functional devices: A concise review, Ceram. Int., **44**, 11940ï 11955 (2018).
[2] Y. Qiu, F. Guo, R. Hurt, I. K¿laots, Explosive thermal reduction of graphene oxide-based materials: Mechanism and safety implications, Carbon, **72**, 215ï 223 (2014).
[3] G.T.T. Le, J. Manyam, P. Opaprakasit, N. Chanlek, N. Grisdanurak, P. Sreearunothai, Divergent mechanisms for thermal reduction of graphene oxide and their highly different ion affinities, Diam. Relat. Mater. **89**, 246ï 256 (2018).
[4] X. Yan, J. Chen, J. Yang, Q. Xue, P. Miele, Fabrication of Free-Standing, Electrochemically Active, and Biocompatible Graphene Oxideī Polyaniline and Grapheneī Polyaniline Hybrid Papers, App. Mater. **9**, 2521–2529 (2010).
[5] W. S. Hummers, R. E. Offeman, Preparation of Graphitic Oxide, J. Am. Chem. Soc., **80,** 1339 (1958).
[6] O. Bortolini, L. Pandolfo, C. Tomaselli, P. Traldi, Ion-molecule chemistry of carbon suboxide in an ion-trap mass spectrometer, Int. J. Mass Spectrom. **190ï 191**, 171ï 179 (1999).
[7] M. V. Alonso, M. Oliet, J.M. P®rez, F. Rodr²guez, J. Echeverr²a, Determination of curing kinetic parameters of lignin-phenol-formaldehyde resol resins by several dynamic differential scanning calorimetry methods, Thermochim. Acta. **419**, 161ï 167 (2004).

MODELING OF SINGLETï SINGLET ANNIHILATION IN ONE-DIMENSIONAL MOLECULAR LATTICE

Gabrielã Rankelytã[1], Jevgenij Chmeliov[1,2]

[1]Institute of Chemical Physics, Faculty of Physics, Vilnius University, Vilnius, Lithuania
[2]Department of Molecular Compound Physics, Centre for Physical Sciences and Technology, Vilnius, Lithuania
gabriele.rankelyte@ff.stud.vu.lt

Singletï singlet annihilation is a common phenomenon in molecular structures. It is often difficult to provide experimental conditions that could prevent annihilation ï the excitation radiation of low intensity must be used, so that at most one light photon per excitation pulse is absorbed per molecular aggregate, generating just a single electronic excitation. Consequently, to increase signal-to-noise ratio, the measurement time must be extended. These experimental conditions may not be suitable for some samples; therefore, it might often be necessary to account for annihilation while analyzing data.

Simple annihilation model can be described by rate equation Eq. 1:

$$\frac{\mathrm{d}n}{\mathrm{d}t} = -\gamma n^2, \tag{1}$$

here $n(t)$ is the mean number of remaining excitations in the system at time t and γ is the rate constant for annihilation. In this model, the size of molecular aggregate, excitation transfer rate across the aggregate, and initial population of excitations are considered very large. In order to include finite transfer rate, γ must be considered as a function of time which at longer times can be approximated by a power law [1]. More precise modelling would also include discrete number of excitations, resulting in the system of Pauli Master equations [2].

To account for both finite transfer rate and discrete number of excitations in annihilation model, we have chosen to use Monte Carlo method. During the modelling process one-dimensional molecular lattice is formed and excitations are randomly distributed in the lattice. At each time step, the excited state has three fates: it can stay in the same position, relax to the ground state, or move to another position with probability to annihilate if that site is already occupied. The fate is decided by generating random numbers. Eventually, number of excitations in the lattice becomes zero, and then the same process is repeated by generating new initial distribution. After 10 000 lattices have been generated, the average kinetics is calculated (Fig. 1). The first model was based on discrete time random walk. The same model is now modified and based on continuous time random walk. This modification reduces the computing time approximately ten times.

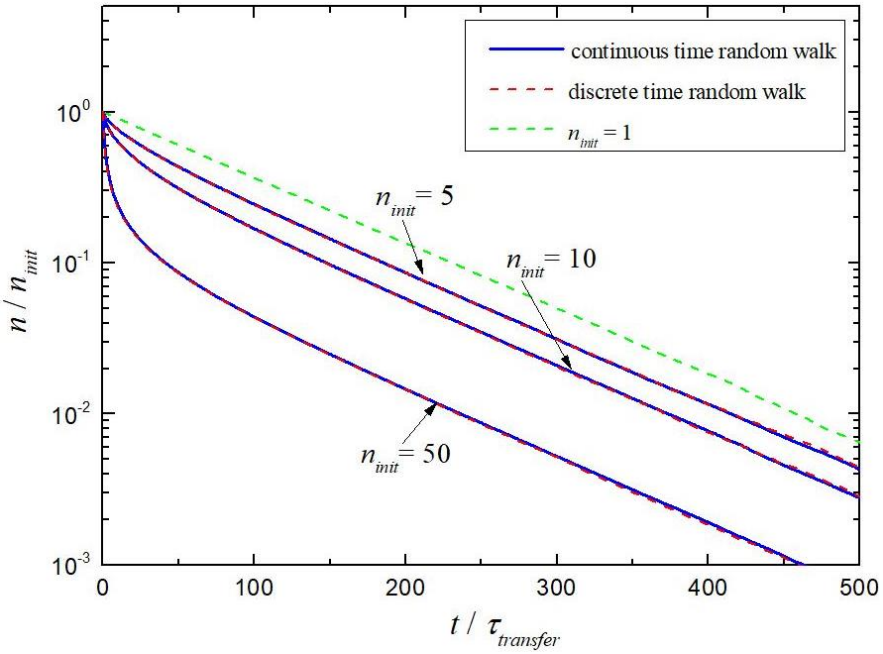

Fig. 1. Excitation population kinetics (n_{init} is the initial population size, molecular lattice size is N = 100 nodes). When one excitation is left in the lattice, quenching becomes exponential due to linear relaxation (relaxation rate is $k_{rel} = 10^{ï\,2}\, k_{\mathrm{transfer}}$).

[1] H. van Amerongen, L. Valkunas, R. van Grondelle, *Photosynthetic Excitons* (World Scientific, Singapore, 2000).
[2] V. Barzda, V. Gulbinas, R. Kananavicius, V. Cervinskas, H. van Amerongen, R. van Grondelle, L Valkunas, Singlet-Singlet Annihilation Kinetics in Aggregates and Trimers of LHCII, Biophys. J. **80**, 2409ï 2421 (2001).

TOTAL INTERNAL REFLECTION ELLIPSOMETRY FOR THE INVESTIGATION OF SARS-CoV-2 NUCLEOCAPSID PROTEIN AND SPECIFIC ANTIBODY BINDING KINETICS

Silvija Juciute[1], Ieva Plikusiene[1,2], Vincentas Maciulis[2], Almira Ramanaviciene[1], Zigmas Balevicius[2], Ernesta Buzavaite-Verteliene[2], Evaldas Ciplys[1], Rimantas Slibinskas[1], Martynas Simanavicius[3], Aurelija Zvirbliene[3], Arunas Ramanavicius[1,2].

[1]Institute of Chemistry, Faculty of Chemistry and Geosciences, Vilnius University, Naugarduko 24, Vilnius, Lithuania;
[2]Laboratory of Nanotechnology, State Research Institute Centre for Physical Sciences and Technology, Sauletekio ave. 3, Vilnius, Lithuania
[3]Institute of Biotechnology, Life Sciences Center, Vilnius University, Sauletekio ave. 7, LT-10257 Vilnius, Lithuania
silvija.juciute@chgf.stud.vu.lt

Severe acute respiratory syndrome coronavirus 2 (SARS-CoV-2) is a virus that causes COVID-19 disease. This illness started global pandemic in late 2019 which is still going. It is extremely important to investigate SARS-CoV-2 proteins structure and their binding mechanisms because this knowledge could help scientists to develop new virus detection and monitoring methods. SARS-CoV-2 virus contains 4 structural proteins: nucleocapsid (N), spike (S), envelope (E) and membrane (M) [1]. N-protein enters host's cell and releases RNA which starts its replication and virus spreads to other cells [2]. Nucleocapsid protein is highly immunogenic and causes strong immune response. Thus, we chose to study N-protein in this investigation.

Various methods can be applied to study kinetics of antigen and specific antibodies binding. In this case, optical methods get special attention. Many of them are nondestructive and label-free which are huge advantages when investigating protein-protein interactions. One of such methods is total internal reflection ellipsometry (TIRE). The real time measurements can be performed and information about protein binding mechanisms can be obtained using TIRE [3].

In this study TIRE was applied for the investigation of SARS-CoV-2 N-protein and polyclonal antibodies against this protein interaction kinetics. The obtained results showed that the two steps binding kinetic model is suitable to describe the immune complex formation. Association and dissociation rate constants, affinity and dissociation constants were evaluated from two-steps binding kinetic model. Calculated thermodynamic properties of such immune complex showed that it has very strict steric requirements. Estimated Gibbs free energy (ΔG_{Form}) was −34 kJ/mol. These findings could be useful for the design of new analytical systems for the determination of specific antibodies formed in the organism after infection, for the development of new SARS-CoV-2 detection methods, and for production of medications that are blocking viral SARS-CoV-2 proteins.

Acknowledgement
This project has received funding from European Social Fund (project No 09.3.3-LMT-K-712-19-0106) under grant agreement with the Research Council of Lithuania (LMTLT).

[1] R. Lu, X. Zhao, J. Li, P. Niu, B. Yang, H. Wu, W. Wang, H. Song, B. Huang, N. Zhu, Y. Bi, X. Ma, F. Zhan, L. Wang, T. Hu, H. Zhou, Z. Hu, W. Zhou, L. Zhao, J. Chen, Y. Meng, J. Wang, Y. Lin, J. Yuan, Z. Xie, J. Ma, W.J. Liu, D. Wang, W. Xu, E.C. Holmes, G.F. Gao, G. Wu, W. Chen, W. Shi, W. Tan, Genomic characterisation and epidemiology of 2019 novel coronavirus: implications for virus origins and receptor binding, Lancet. 395 (2020) 565–574.
[2] K. Narayanan, C.-J. Chen, J. Maeda, S. Makino, Nucleocapsid-Independent Specific Viral RNA Packaging via Viral Envelope Protein and Viral RNA Signal, J. Virol. 77 (2003) 2922–2927.
[3] I. Plikusiene, Z. Balevicius, A. Ramanaviciene, J. Talbot, G. Mickiene, S. Balevicius, A. Stirke, A. Tereshchenko, L. Tamosaitis, G. Zvirblis, A. Ramanavicius, Evaluation of affinity sensor response kinetics towards dimeric ligands linked with spacers of different rigidity: Immobilized recombinant granulocyte colony-stimulating factor based synthetic receptor binding with genetically engineered dimeric analyte d, Biosens. Bioelectron. 156 (2020) 112112.

DEVELOPMENT OF ADD-ON PROTOTYPE FOR GC OVEN COOLING

Audrius Sadaunykas, Audrius Zolumskis, Evaldas Naujalis

Metrology Department, State Research Institute Center for Physical Sciences and Technology
LukiğkiÔstr. 9, LT-01108 Vilnius, Lithuania
audrius.sadaunykas@ftmc.lt

One of the most popular analytical method used around the world is gas chromatography (GC), which is applied for various volatile compounds analysis. Principle of gas chromatography is separation, performed on chromatographic column. GC column is usually a thin silica capillary placed in an oven with precise temperature control. Analytes are being retained by stationary phase in the column and propelled forward by gas flow and temperature increase [1]. Ramping temperature from 40-60 ŰC to even 200-300 ŰC is common in GC applications. This way researchers can control analyte separation and make analysis more efficient. The problem with standard GC ovens is that, they did not evolve significantly since they were started to use in 1970s. It takes a long time to cool down after each run and they commonly cannot be cooled bellow ambient temperature what is a must for some more volatile compound analysis [2]. We aim to solve this problem with in-house designed and built cooling add-on prototype for GC oven.

This prototype scheme showed in Figure 1 is based on evaporating cooling principles [3]. Unit outside the GC houses compressor, condenser and thermal expansion valve. Compressed refrigerant is cooled down in condenser and travels inside the GC through isolated transfer line where it expands inside the evaporator and cools down the GC oven. Then refrigerant is transported back to compressor, where it performs the cycle again. By using this prototype, we have achieved faster cooling of the GC oven. Temperature in the oven decreased from 200 ŰC to 40 ŰC in about 1,5 min. instead of around 8 min normally. That is an improvement of almost 80 %. This kind of increase would speed up routine analysis in the laboratory significantly by reducing GC system equilibration time between injections.

Secondly, we tested the system by measuring lighter gas mixture which mostly contains isobutane and its isomers. Normally we could only start the analysis at 35 ŰC in the GC oven. Starting at this temperature we couldn't see any separation but with application of our cooling add-on, the analysis could be started at -10 ŰC and we registered three separate peaks. This broadens capabilities of GC analysis and it is very beneficial for highly volatile compounds screening.

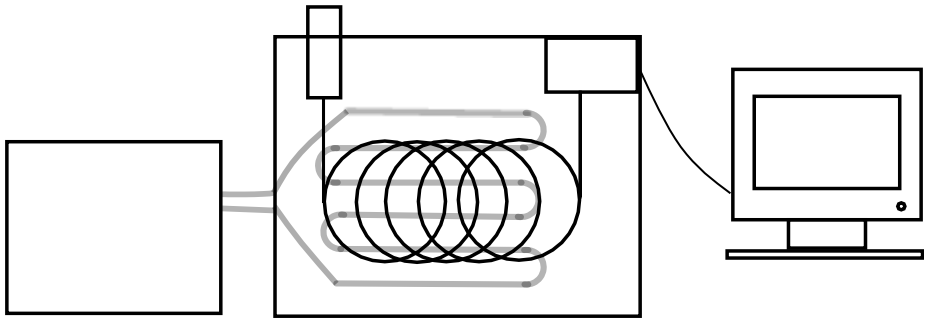

Fig. 1. Gas chromatography systems with oven cooling add-on

These results are just the beginning of our work on this topic and we will continue with improvement of the prototype.

[1] Skoog, Douglas A.; West, Donald M.; James Holler, F.; Crouch, Stanley R., Fundamentals of analytical chemistry, (Ninth ed.). Belmont, CA, (2013)ISBN-13: 978-0495558286
[2] Schomburg G., Practical Limitations of Capillary Gas Chromatography, Journal of High Resolution Chromatography, 2(7), 461-474, (1979).
[3] McDowall, R. Fundamentals of HVAC Systems, Elsevier, San Diego, page 16, (2006)

SYNTHESIS OF ASYMMETRIC NAPHTHALENE DIIMIDE AS A MODEL PHOTOCATALYST FOR MULTICOMPONENT PHOTOREDOX REACTIONS

Ugnã Rimkaitã, Ieva Karpaviļienã, Edvinas Orentas

Vilnius University, Faculty of Chemistry and Geosciences, Naugarduko 24, LT-03225, Vilnius, Lithuania
ugnerimkaite@gmail.com

The importance of photochemistry has grown significantly in recent decades along with the revival of interest in radical processes. One of the most essential field of photochemistry in organic synthesis is development and application of photoredox catalysts. These compounds are promising materials in innovative synthesis due to their ability to generate unique reactive radical species that are difficult or sometimes even impossible to obtain by another chemical methods. Furthermore, activation of reactions, which are catalyzed by organic photoredox catalysts, is based on light ï one of the cheapest energy source ï absorption. This is considerable superiority in compare with reactions that are catalyzed by nowadays widely used expensive and often environmentally damaging transition metal catalyst [1-2]. In our research, we seek to synthesize asymmetric naphthalene diimide (NDI) and explore its possible application for a photo induced intramolecular enamine activation reactions under mild conditions.

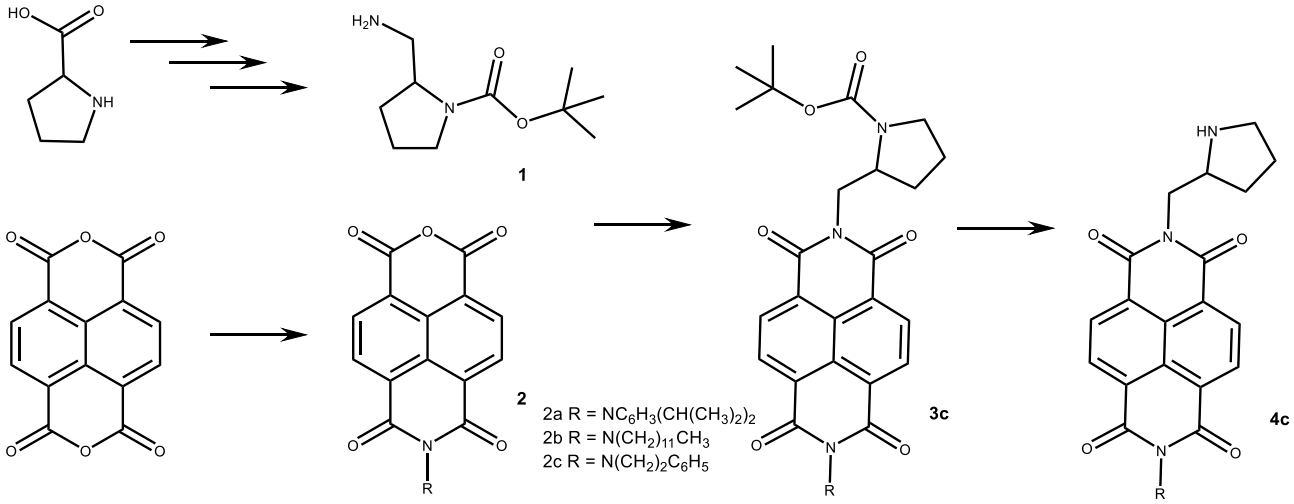

Scheme 1. Synthesis of asymmetric NDI

The synthesis of desired NDI catalyst was started from modification of commercially available L-proline in order to obtain chiral 2-methylpirolidine derivative **1** with protected amine group (Scheme 1). Further, naphthalene intermediate **2** was synthesized and few different methods were used on purpose to increase yield of this step. Condensation reaction of compounds **1** and **2** led to the formation of NDI derivative **3**. Finally, amine deprotection reaction was initiated and model catalyst **4** was obtained.

Acknowledgment: This research is funded by the European Social Fund under the No 09.3.3-LMT-K712-22-0181 ñDevelopment of Competences of Scientists, other Researchers and Students through Practical Research Activitiesò measure

[1] M. K. Bogdos, E. Pinard, J. A. Murrphy, Applications of organocatalyzed visible-light photoredox reactions for medical chemistry, Beilstein Journal of Organic Chemistry **14**, 2035ï 2064 (2018).
[2] N. A. Romero, D. A. Nicewicz, Organic Photoredox Catalysis, Chemical Reviews **116**, 10075ï 10166 (2016).

IN-SITU SHINERS ANALYSIS OF IMIDAZOLE RING TERMINATED MONOLAYER AT ELECTROCHEMICAL INTERFACE

Agnė Zdaniauskienė, Tatjana Charkova, Rita Sadzevičienė, Gediminas Niaura

Department of Organic Chemistry, Center for Physical Sciences and Technology, Lithuania
agne.zdaniauskiene@ftmc.lt

Self-assembled monolayers (SAMs) of functional thiol molecules at a metal surface are widely used to study various functional groups' interactions with solution components or adjacent thiols in the monolayer [1]. Imidazole ring terminated molecules can thus interact with other aromatic residues as well as forming hydrogen bonds with polar and charged residues because they can exist in neutral or positively charged forms within a pH range of 5.0 to 7.0. The introduction of amide functionality in the hydrocarbon chain of adsorbing molecules greatly increases the stability of SAM due to hydrogen bonds forming between the adjacent molecular chains in the monolayer [2]. Interfaces between biologically active molecules and metals are an important issue in biocatalysis, biocompatibility, and biosensors. SAMs at metal surfaces provide a possibility to create stable molecular structures suitable for probing potential-driven molecular structure changes [3].

Surface-enhanced Raman spectroscopy (SERS) is a powerful spectroscopic technique to study molecular structure and interaction mechanisms between a terminal functional group of a monolayer and solution species at metal/electrolyte interfaces. Nonetheless, SERS is limited by SERS-active substrates (mostly Ag, Au, and Cu), and the requirement to use roughened or nanostructured surfaces restrict the applicability of this analysis method. Therefore, Tian et al. suggested a novel SERS technique named ―shell-isolated nanoparticle-enhanced Raman spectroscopy‖ (SHINERS). The method is based on the enhancement of Raman signal by strong electromagnetic field provided by noble metal core nanoparticles surrounded by a few nanometer thick inert silica shell [4].

In this work, SHINERS was applied to determine the potential-induced changes in the molecular structure of N-(2-(1H-imidazol-4-yl)ethyl)-6-mercaptohexanamide (IMHA) at a smooth Au electrode. SHINERS method employing synthesized spherical silver nanoparticles with 85 Ñ 5 nm core size and SiO_2 shell of 3 nm thickness.

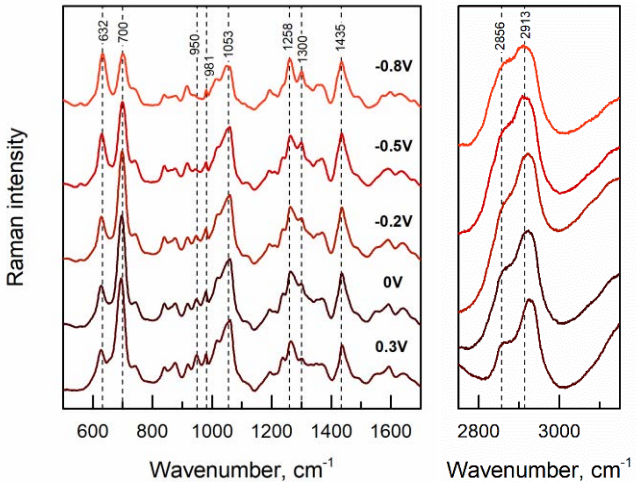

Fig. 1. SHINERS spectra of IMHA adsorbed on a smooth Au electrode at indicated potentials in 0.1 M Na_2SO_4 solution containing 0.01 M phosphate buffer (pH 7). The excitation wavelength is 785 nm.

Spectroscopic evidence for potential-driven conformational changes in the structure of IMHA monolayer was revealed. *In situ* electrochemical SHINERS results show that the intensity of $\nu(C\text{-}S)_T$ mode (697 cm^{-1} at 0.0 V) of trans conformer is high at positive electrode potential value and noticeably decreases as electrode potential shifts to -0.8 V. The integrated intensity of the $\nu(C\text{-}S)_T$ band decreases by a factor of 2.3. The opposite of tendency with corresponding gauche band $\nu(C\text{-}S)_G$ (630 cm^{-1} at 0.0 V), the intensity of this mode increases by a factor of 1.46. These spectroscopic data indicate hydrocarbon chain conformational changes from predominant trans to gauche as electrode potential shifts to the more negative value.

[1] J. C. Love et al., Self-assembled monolayers of thiolates on metals as a form of nanotechnology, Chem. Rev. **105**, 1103-69 (2005).
[2] Z. Kuodis et al., Reflection absorption infrared spectroscopy characterization of SAM formation from 8-mercapto-N-(phenethyl)octanamide thiols with Phe ring and amide groups, Molecules **25**, 5633 (2020).
[3] Vericat, C et al., Self-assembled monolayers of thiolates on metals: A review article on sulfur-metal chemistry and surface structures, RSC Adv. **4**, 27730ï 27754 (2014).
[4] J. F. Li et al., Shell-isolated nanoparticle-enhanced Raman spectroscopy. Nature **464**, 392ī 395 (2010).

NONSYMMETRICAL AZINES WITH AGGREGATION INDUCED EMISSION ENHANCEMENT

Justyna Anna Adamczyk[1], Lena Marciniak[2], Adam Marek Pieczonka[1], MichałRachwalski[1]

[1] Department of Organic and Applied Chemistry, Faculty of Chemistry, University of Lodz, Poland
[2] The Bio-Med-Chem Doctoral School of the University of Lodz and Lodz Institutes of the Polish Academy of Science, Poland
justyna.adamczyk@edu.uni.lodz.pl

Many organic fluorophores show good emission in dilute solutions. However, their emissions will be weakened or completely quenched when they aggregate in solid state or at a high concentration because of the strong ´-´ interactions. This phenomenon is called the aggregation-caused quenching (ACQ) effect. In contrast to conventional fluorophores with ACQ drawbacks, salicylaldehydes derivatives exhibit Aggregation Induced Emission (AIE). AIEgens are almost non-emissive in dilute solution, but become highly emissive in the aggregate state because of restricted intramolecular motion [1-4].

Salicylaldehyde azines are highly stable condensation products with hydrazine which display several advantages such as easy synthesis and product purifications, low costs or high melting points. They exhibit strong aggregation induced emission in aggregate/solid state which were used in various applications such as optoelectronics [5], chemosensors [6, 7] or for bio-imaging [8, 9]. Azines also exhibit keto enol tautomerism upon photoexcitation. Tautomerism in azines is characterized by translocation of a proton with a pre established intramolecular hydrogen bond giving birth to a phototautomer phenomenon, commonly termed as excited state intramolecular proton transfer (ESIPT) [10].

New group of nonsymmetrical salicylaldehyde azine derivatives was prepared and investigated starting from differently substituted salicylaldehydes (Fig.1.).

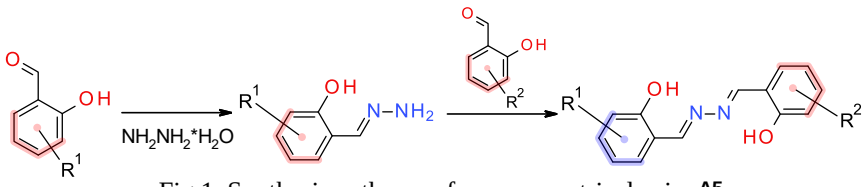

Fig.1. Synthesis pathway of nonsymmetrical azines[A5]

The introduction of two different substituents into the fluorescent core has a significant effect on the physicochemical properties of the obtained compounds.

[1] Y. Hong, J.W.Y. Lam, B.Z. Tang, Aggregation-induced emission, Chemical Society Reviews, 40 (2011) 5361 - 5388.
[2] J. Mei, N.L.C. Leung, R.T.K. Kwok, J.W.Y. Lam, B.Z. Tang, Aggregation-Induced Emission: Together We Shine, United We Soar!, Chemical Reviews, 115 (2015) 11718 - 11940.
[3] J. Mei, Y. Hong, J.W.Y. Lam, A. Qin, Y. Tang, B.Z. Tang, Aggregation-induced emission: The whole is more brilliant than the parts, Advanced Materials, 26 (2014) 5429 - 5479.
[4] S. Kagatikar, D. Sunil, Aggregation-induced emission of azines: An up-to-date review, Journal of Molecular Liquids, 292 (2019).
[5] Z. Wang, F. Zhou, J. Wang, Z. Zhao, A. Qin, Z. Yu, B.Z. Tang, Electronic effect on the optical properties and sensing ability of AIEgens with ESIPT process based on salicylaldehyde azine, Science China Chemistry, 61 (2018) 76 - 87.
[6] X. Ma, J. Cheng, J. Liu, X. Zhou, H. Xiang, Ratiometric fluorescent pH probes based on aggregation-induced emission-active salicylaldehyde azines, New Journal of Chemistry, 39 (2015) 492 - 500.
[7] P.-X. Pei, J.-H. Hu, Y. Chen, Y. Sun, J. Qi, A novel dual-channel chemosensor for CN? using asymmetric double-azine derivatives in aqueous media and its application in bitter almond, Spectrochimica Acta Part A: Molecular and Biomolecular Spectroscopy, 181 (2017) 131 - 136.
[8] M. Gao, C.K.i. Sim, C.W.a.T. Leung, Q. Hu, G. Feng, F. Xu, B.Z.h. Tang, B. Liu, A fluorescent light-up probe with AIE characteristics for specific mitochondrial imaging to identify differentiating brown adipose cells, Chemical communications (Cambridge, England), 50 (2014) 8312 - 8315.
[9] M. Gao, Q. Hu, G. Feng, B.Z. Tang, B. Liu, A fluorescent light-up probe with "aIE + ESIPT" characteristics for specific detection of lysosomal esterase, Journal of Materials Chemistry B, 2 (2014) 3438 - 3442.
[10] S.S. Chourasiya, D. Kathuria, S.S. Nikam, A. Ramakrishnan, S. Khullar, S.K. Mandal, A.K. Chakraborti, P.V. Bharatam, Azine-Hydrazone Tautomerism of Guanylhydrazones: Evidence for the Preference Toward the Azine Tautomer, Journal of Organic Chemistry, 81 (2016) 7574 - 7583.

HYDROTHERMAL SYNTHESIS OF ZINC WHITLOCKITE

Agne Kizalaite, Aleksej Zarkov

Institute of Chemistry, Vilnius University, Lithuania
agne.kizalaite@chgf.vu.lt

Magnesium whitlockite ($Ca_{18}Mg_2H_2(PO_4)_{14}$) is the second most abundant mineral in human body and one of the main components of the human hard tissue, constituting to approximately 20ï 35 wt% [1]. This compound is known for its excellent biocompatibility and osteogenic capability which makes this material a promising candidate for application in bone regeneration [2]. However, synthesis of pure phase whitlockite remains a challenge due to poor thermal stability, high sensitivity to synthesis conditions and large amount of possible intermediate phases.

Incorporation of biologically active ions into the structure of the material can result in superior biological performance of calcium phosphate based materials in addition to expanded clinical applications of the material. To further improve biological properties of whitlockite, as well as design new properties for specific medical fields, other ions instead of Mg could be used for synthesis of the compound. Zn substituted calcium phosphates are characterized by enhanced rate of metabolic processes and antibacterial properties which makes these materials very attractive for usage in medicine [3].

The main goal of the present work was to develop a hydrothermal synthesis method to obtain pure phase and low crystallinity whitlockite powders containing Zn ions. For this purpose synthesis conditions such as temperature, time, pH, concentration and Ca/Zn molar ratio in the initial solution were carefully studied and optimized. Calcium hydrogen phosphate dihydrate and zinc acetate dihydrate were used as starting materials. Synthesized compounds were analyzed by X-ray diffraction (XRD), Fourier-transform infrared spectroscopy (FTIR), scanning electron microscopy (SEM), inductively coupled plasma optical emission spectroscopy (ICP-OES) and Raman spectroscopy.

Acknowledgements

This project has received funding from European Social Fund (project No. 09.3.3-LMT-K-712-19-0069) under grant agreement with the Research Council of Lithuania (LMTLT).

[1] H. Cheng, R. Chabok et al. Synergistic interplay between the two major bone minerals, hydroxyapatite and whitlockite nanoparticles, for osteogenic differentiation of mesenchymal stem cells, Acta Biomaterialia **69**, 342-351 (2018).

[2] H. L. Jang, G. Bin Zheng et al. s, In Vitro and In Vivo Evaluation of Whitlockite Biocompatibility: Comparative Study with Hydroxyapatite and ß-Tricalcium Phosphate, Advanced Healthcare Material **5**, 128ï 136 (2015).

[3] I. V. Fadeeva, M. R. Gafurov et al., Tricalcium Phosphate Ceramics Doped with Silver, Copper, Zinc, and Iron (III) Ions in Concentrations of Less Than 0.5 wt.% for Bone Tissue Regeneration, BioNanoScience **7**, 434ï 438 (2017).

SYNTHESIS AND INVESTIGATION OF LuAG:Pr,B COATINGS ON QUARTZ SUBSTRATE OBTAINED BY SOL-GEL SPIN COATING TECHNIQUE

Greta Inkrataitã[1*], RamÎnas Skaudġius[1]

[1] Institute of Chemistry, Faculty of Chemistry and Geosciences, Vilnius University, Vilnius, Lithuania
greta.inkrataite@chgf.vu.lt

In recent years materials with luminescent properties have become very popular. In addition, these materials are very popular for usage in lamps and other light emitting devices, but nowadays scintillators and their research is becoming a very interesting subject for scientists. Scintillators are the basis for devices, that are used for radioactive contamination detection and measurement, nuclear material monitoring, also they are included in the computer detector composition of the tomography devices. There are various compounds that can be used as scintillators, but one of the most popular are those which have a garnet structure [1]. Amongst others, these can be yttrium or lutetium aluminum garnet, doped with different lanthanides (YAG:Ln; LuAG:Ln). These inorganics compounds have the required optical properties and radiation resistance [2]. The development of new scintillators is important. However, not the materials which are used are important but also their form. The preparation of powder is the simplest, but they are not suitable for the construction of scintillator detectors. Best suited and used for the manufacture of various devices are single crystals. In addition to single crystals, coatings on various pallets or microfibers can be used [3]. Due to the possibility of using different substrates, different methods of coating, materials with different properties can be prepared, which makes this method widely used. Using the sol-gel method we can obtain homogeneous multicomponent coatings at low temperature, leaving the possibility of synthesizing compounds with emission intensity [4].

Improvement of luminescence is essential for getting the fastest scintillators properties. One way to do this is to additionally dope compounds with other elements. Replacing one element with another in the crystal lattice can influence the properties of the materials. The most common goal is to improve key parameters: compound emission intensity, quantum efficiency and decay times. One of the greatest scintillators drawbacks that is being addressed is that decay time is too long. When it is extremely long, then these second signal captured by the materials overlaps with the first, making the results unreliable and provides less data than it could. Scintillators such as and LuAG:Pr doped with boron can solve this problem. If a quick quench of decay time was obtained given result would be more accurate, and this method of synthesizing scintillators could be practically applicable [5, 6].

In this work praseodymium and boron doped LuAG are synthesized on quartz substrates using sol-gel spin coating method. Boron ir expected to improve required luminescent properties, and with the sol-gel method, homogeneous compounds will be synthesized at low temperatures. Phosphor coatings were analyzed by x-ray diffraction (XRD) and scanning electron microscopy (SEM). Of course, emission, excitation spectra and decay times have been investigated as well.

[1] D. S. McGregor, Materials for Gamma-Ray Spectrometers: Inorganic Scintillators, Annual Review of Materials Research, **48**, 254-277 (2018).
[2] A.D. Sontakke, J. Ueda, J. Xu, et. al., A Comparison on Ce3+ Luminescence in Borate Glass and YAG Ceramic: Understanding the Role of Hostõs Characteristics, The Journal of Physical Chemistry C, **120**, 31, 17683 ï 17691 (2016).
[3] S. Rawat, M. Tyagi, P. K. Netrakanti, et. al., Pulse shape discrimination properties of Gd3Ga3Al2O12:Ce,B single crystal in comparison with CsI:Tl, Nuclear Instruments and Methods in Physics Research Section A: Accelerators, Spectrometers, Detectors and Associated Equipment, **840**, 186 ï 191 (2016).
[4] A. Potdevin, G. Chadeyron, D. Boyer, et. al., Solï gel based YAG: Tb3+ or Eu3+ phosphors for application in lighting sources, Journal Of Physics D: Applied Physics, 3251 ï 3260 (2005).
[5] C. Foster, Y. Wu, M. Koschan, et. al., Boron Codoping of Czochralski Grown Lutetium Aluminum Garnet and the Effect on Scintillation Properties, Journal of Crystal Growth, **486**, 126 ï 129 (2018).
[6] H. S. Yoo, W. B. Im, J. H. Kang, D. Y. Jeon, Preparation and photoluminescence properties of YAl3(BO3)4:Tb3+, Bi3+ phosphor under VUV/UV excitation Optical Materials, **31**, 2, 131 ï 135 (2008).

SYNTHESIS AND CHARACTERISTICS OF ORGANIC SEMICONDUCTORS WITH *N*-CARBAZOLYL-BASED CHROMOPHORES

Povilas Luizys[1], Maryte Daskeviciene[1], Kasparas Rakstys[1], Vygintas Jankauskas[2], Egidijus Kamarauskas[2]

[1] Department of Organic Chemistry, Kaunas University of Technology, Lithuania
[2] Institute of Chemical Physics, Vilnius University, Lithuania
povilas.luizys@ktu.lt

With a growing world community's concern of environmental pollution there are increased interest how this can be addressed. One of the main causes of environmental problems is the energy production, which is not easy to solve due to the growing global demand of energy [1]. Therefore, it is not surprising that a great deal of attention is being paid to renewable energy sources, given their environmental friendliness and potential for use. One of the most promising renewable energy source is solar energy, which theoretically could satisfy the energy needs of mankind. Silicon solar cells are currently the most widely used on the market, but due to their high production costs, search of alternatives is underway. One of possible alternative is perovskite solar cells, which just in a last decade have become a subject of great interest in the development of next generation solar cells that have already exceeded 25.5% power conversion efficiency [2]. Perovskite solar cells hold promise for inexpensive raw materials and low device production costs, but perovskite solar cell commercialization is hindered by drawbacks which need to be resolved. One of them is that perovskite is sensitive to moisture, which reduce device stability. It is proposed to solve this problem by covering the perovskite layer with moisture impermeable electron and hole transporting layers. Furthermore, often additives are needed to increase the conductivity of hole transporting material, which may cause the device degradation [3]. Therefore, the search for new suitable organic semiconductors remains highly relevant.

In this work, new hole transporting organic semiconductors with four *N*-carbazolyl chromophores (Fig.1) were synthesized for the use in perovskite solar cells.

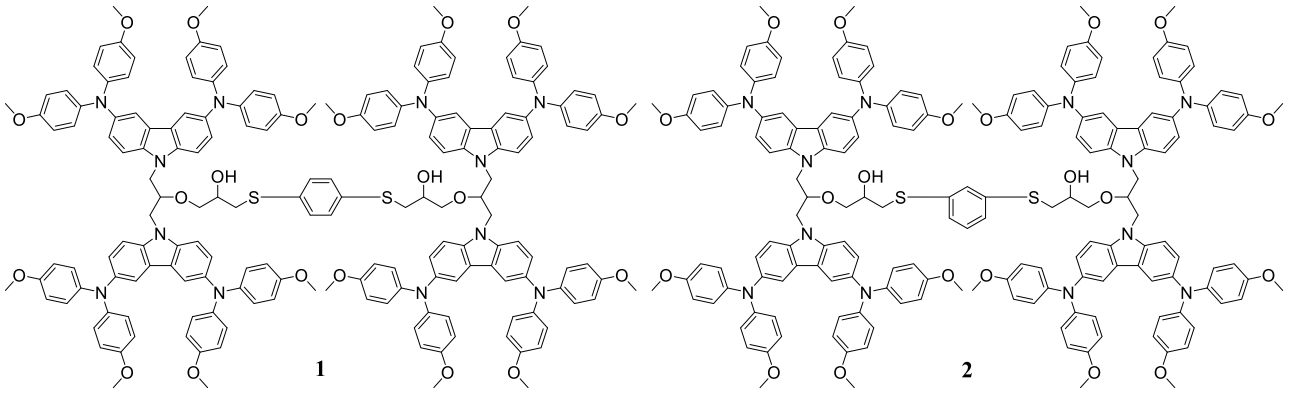

Fig. 1. Structures of synthesized organic semiconductors with four *N*-carbazolyl chromophores.

New hole transporting organic semiconductors were obtained via step-by-step synthesis. Molecular structure of the newly synthesized organic compounds were confirmed by ^{1}H NMR, ^{13}C NMR and IR spectroscopy. Thermogravimetric analysis shows that synthesized molecules are thermally stable at high temperatures. Thermal decomposition of compound **1** starts at 374 ÁC and at 379 ÁC for compound **2**, respectively. Differential scanning calorimetry analysis of target compounds proved that they are molecular glasses and demonstrate stable amorphous state. Glass transition temperature of compound **1** is 116 ÁC and 111 ÁC for compound **2**, respectively. Photoelectron spectroscopy in air method was used to measure ionization potentials of organic semiconductors **1** and **2**. Obtained *Ip* value of molecule **1** is 5.26 eV, while **2** has slightly lower value of 5.16 eV. *Ip* measurements indicate that the HOMO energy level of the synthesized products is compatible with the valence band of the photoactive perovskite layer. Therefore, new organic semiconductors could potentially be used in construction of perovskite solar cells.

[1] Global primary energy consumption by source, https://ourworldindata.org/grapher/global-energy-substitution?time=earliest..latest (accessed 2020-02-02).
[2] Best Research-Cell Efficiency Chart, Photovoltaic Research, NREL, 2021.
[3] X. Zhao and M. Wang, Organic hole-transporting materials for efficient perovskite solar cells, Mater. Today Energy **7**, 208-220 (2018).

STRUCTURAL AND MAGNETIC STUDY OF $YFeO_3$-$GdFeO_3$ SOLID SOLUTIONS

Dovydas Karoblis[1], Aleksej Zarkov[1], Kestutis Mazeika[2], Dalis Baltrunas[2], Gediminas Niaura[3, 4], Aldona Beganskiene[1], Aivaras Kareiva[1]

[1] Institute of Chemistry, Vilnius University, Naugarduko 24, LT-03225 Vilnius, Lithuania
[2] Center for Physical Sciences and Technology, Vilnius LT-02300, Lithuania
[3]Department of Organic Chemistry, Center for Physical Sciences and Technology, Sauletekio Ave. 3, LT-10257, Vilnius, Lithuania
[4]Institute of Chemical Physics, Faculty of Physics, Vilnius University, Sauletekio Ave. 3, LT-10257, Vilnius, Lithuania
Dovydas.karoblis@chgf.vu.lt

Multiferroicity, where two or more kinds of ferroicities coexist in the same phase, have attracted a lot of attention in materials science and condensed matter physics in recent years [1]. This type of compounds can be applied in magnetic field sensing, data recording, as field probes etc. Different material classes, like borates ($GdFe_3(BO_3)_4$) [2], boracites ($Ni_3B_7O_{13}I$) [3] and most notably perovskites are known for possible concurrence of both magnetic and ferroelectric orders. Orthoferrites $RFeO_3$ (where R=rare earth element) are perovskite-type materials with multiferroic properties.

$YFeO_3$ orthoferrite has demonstrated ferroelectric and weak ferromagnetic characteristics at room temperature in bulk and thin film forms [4, 5]. Equivalently, $GdFeO_3$ has showed improper ferroelectric ordering, antiferromagnetism and weak magnetoelectric coupling [6]. It was displayed that different $Y_{1-x}Gd_xFeO_3$ solid solutions compositions can lead to peculiar magnetic properties, with higher Y^{3+} concentration leading to enhanced magnetization values [7].

In this study, $YFeO_3$-$GdFeO_3$ solid solutions were prepared for the first time by sol-gel synthesis. Thermogravimetric analysis was performed in order to determine possible calcination temperature and investigate thermal degradation of different composition precursor gels. X-ray diffraction, Mössbauer and Raman measurements were carried out to assess structural changes. Morphology of prepared samples was investigated with scanning electron microscopy (SEM). Lastly, magnetization studies were employed for all solid solutions.

Acknowledgments
This work was supported by a Research grant BUNACOMP (No. SMIP-19-9) from the Research Council of Lithuania.

[1] K. F. Wang, J. M. Liu, Z. F. Ren, Multiferroicity: the coupling between magnetic and polarization orders, Advances in physics, **58:4**, 321-448 (2009).
[2] A. G. Gavriliuk et al, Structural and electronic transitions in gadolinium iron borate $GdFe_3(BO_3)_4$ at high pressures, Journal of Experimental and Theoretical Physics Letters, **80**, 426-432 (2004).
[3] E. Ascher, H. Schmid, D. Tar, Dielectric properties of boracites and evidence for ferroelectricity, Solid State Communications, **2**, 45-49 (1964).
[4] M. Shang et al., The multiferroic perovskite $YFeO_3$, Applied Physics Letters, **102**, 62903 (2013).
[5] M. Shang et al., The multiferroic epitaxial thin film $YFeO_3$, Materials Letters, **175**, 23–26 (2016).
[6] S. Sahoo et al., Structural, electrical and magnetic characteristics of improper multiferroic: $GdFeO_3$, Materials Research Express. **3**, 1–20 (2016).
[7] X. Yuan, Y. Sun, M. Xu, Effect of Gd substitution on the structure and magnetic properties of $YFeO_3$ ceramics, Journal Solid State Chemistry, **196**, 362–366 (2012).

MODELLING BINARY SYSTEMS OF ACETIC ACID AND DIMETHYL SULFOXIDE: STRUCTURAL ANALYSIS AND ^{1}H NMR SPECTRA

Gyginta Einorytė[1], Greta Majauskaitė[1], Kęstutis Aidas[1]

[1]Institute of Chemical Physics, Faculty of Physics, Vilnius University, Lithuania
zyginta.einoryte@ff.stud.vu.lt

The basis for this study comes from the ^{1}H NMR spectra in binary systems of acetic acid (AA) and dimethyl sulfoxide (DMSO). According to experimental studies [1], the correlation between NMR chemical shift of the acidic proton in acetic acid and the molar part of acid in a AA/DMSO binary system is non-monotonic. When the mole fraction of acetic acid in a binary system increases from 0 to ~0.7, the chemical shift of hydrogen drops around 0.5ppm (from 11.9ppm to 11.4ppm), then rises, reaching around 11.7ppm in pure acetic acid. This phenomenon is caused by the shifting equilibrium between various molecular (hydrogen bond) aggregates formed between acetic acid molecules themselves as well as between acetic acid and DMSO when the molar fraction of the binary mixture is changing. It is nearly impossible to find out the nature of these molecular aggregates in particular their population experimentally, however, these problems can be very effectively dealt with by using advanced molecular modelling techniques such as molecular dynamics (MD) simulations and combined quantum mechanics/molecular mechanics (QM/MM) approaches. These techniques have also been very recently applied to study molecular aggregation in glacial acetic acid [2].

There are two main objectives of this study: carrying out a qualitative and quantitative analysis of molecular aggregates and calculating the chemical shift of the acidic proton in AA/DMSO systems of different composition. Comparison between computational and experimental results allows for a detailed understanding of the reasons of curious concentration dependence of the chemical shift of the acidic proton. A different binary system of acetic acid and a non-polar solvent ï cyclohexane, also displays a non-monotonic fashion [1], but it is caused only by interactions between acetic acid molecules themselves. However, when analysing AA/DMSO systems it is important to also account for interactions between acetic acid and DMSO because of polarity of the solvent.

The analysis of molecular aggregates in a binary system was carried out for three different AA:DMSO mixtures: 1:3, 1:1 and 3:1 (molar ratios). MD simulations were executed using an all-atom OPLS force field and standard Coulomb plus 12-6 type Lennard-Jones potential. Systemôs equilibrium was achieved by allowing systemôs density to converge in NPT simulations, then switching to NVT ensemble, running another equilibration run and completing with 2ns long production run. Atomic point charges were calculated for pure AA and DMSO, according to the CHelpG scheme, and then averaged considering mole fractions of components in each system. NMR shielding constants were calculated for all three AA/DMSO systems using QM/MM calculations. These calculations were performed for a set of molecular configurations captured during MD simulations of a given system. The analysis of hydrogen bonds in different AA/DMSO systems was based on geometric definition of a hydrogen bond which allowed to identify different types of molecular aggregates forming in these systems.

The presentation will include a comparison between experimental and computed ^{1}H NMR spectra of acidic proton of acetic acid and results of the analysis of molecular aggregates in AA/DMSO binary systems.

[1] H. Fujiwara, Studies of hydrogen bonding in carboxylic acid-dimethyl sulfoxide systems by nuclear magnetic resonance dilution shifts, J. Phys. Chem. 78 (1974) 1662ï 1666. https://doi.org/10.1021/j100609a013.

[2] D. Lengvinaite, K. Aidas, L. Kimtys, Molecular aggregation in liquid acetic acid: Insight from molecular dynamics/quantum mechanics modelling of structural and NMR properties, Phys. Chem. Chem. Phys. 21 (2019) 14811ï 14820. https://doi.org/10.1039/c9cp01892a.

COMPARATIVE STUDY OF *in silico* TOOLS TO PREDICT THE ADME PROFILING FOR SELECTED 5,6-OXYGENATED D-HOMO STEROIDS

Milica Ilić [1], Ivana Kuzminac[1], Marija Sakać [1]

[1] University of Novi Sad, Faculty of Sciences, Department of Chemistry, Biochemistry and Environmental Protection, Trg Dositeja Obradovića 3, Novi Sad, Serbia
milica.ilic@dh.uns.ac.rs

ADME (absorption, distribution, metabolism, and excretion) properties affect pharmacological activity of drug candidates. These can be determined from physicochemical properties that can be predicted from the structure of the drug candidate. Determining *in silico* ADME characteristics of newly synthesized compounds can be crucial in the drug discovery process. Multiple web servers and software were developed for this purpose.

In our previous work, we have synthesized a serie of 5,6-oxygenated steroidal D-homo lactones and tested their anticancer properties [1]. Herein, we have selected four of these compounds with the highest cytotoxicity (Fig. 1) and *in silico* tested their ADME properties. In order to determine optimal *in silico* tool for ADME properties calculation, we have compared results obtained from five tools: ChemDraw, Molinspiration [2], SwissADME [3], admetSAR [4], and pkCSM [5]. Besides the number of calculated parameters, we have also taken into account the elapsed time and number of structures that can be submitted simultaneously.

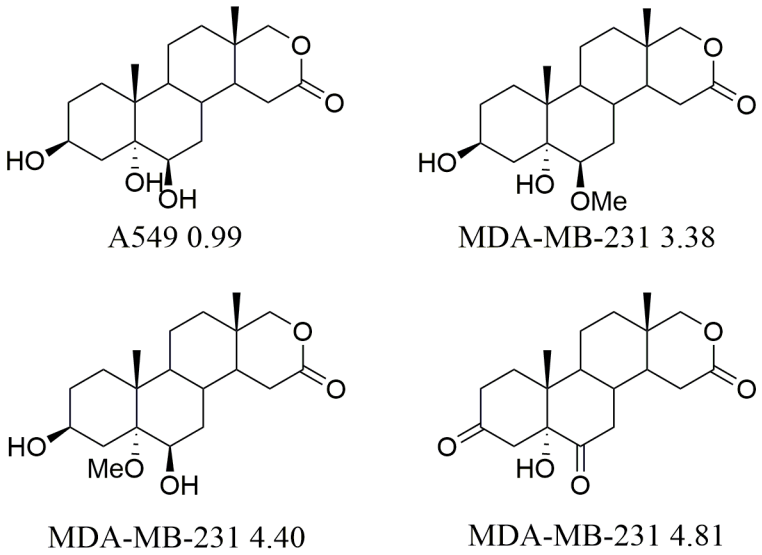

Fig. 1. Structures and most significant cytotoxicity IC_{50} values (ε mol/L) of selected steroidal compounds [1].

[1] I. Z. Kuzminac, D. S. Jakimov et al., Synthesis and anticancer potential of novel 5,6-oxygenated and/or halogenated steroidal D-homo lactones, *Bioorg. Med. Chem.* **30**, 115935 (2021).
[2] www.molinspiration.com (accessed 09.02.2021).
[3] A. Daina, O. Michielin, V. Zoete, SwissADME: a free web tool to evaluate pharmacokinetics, drug-likeness and medicinal chemistry friendliness of small molecules, *Sci Rep.* **7**, 42717 (2017)
[4] H. Yang, C. Lou, et al., admetSAR 2.0: web-service for prediction and optimization of chemical ADMET properties, *Bioinformatics* **35**, 1067ï 1069 (2019).
[5] D. E. V. Pires, T. L. Blundell, D. B. Ascher, pkCSM: predicting small-molecule pharmacokinetic and toxicity properties using graph-based signatures, *J. Med. Chem.* **58**, 4066ï 4072 (2015).

YEAST CELL MODIFICATION WITH PRUSSIAN BLUE

Gabija Kavaliauskaitā[1], Povilas Virbickas[1], Augra Valiî niānā[1], Urtā Samukaitā ï Bubnienā[1]

[1] Department of Physical Chemistry, Faculty of Chemistry and Geosciences, Vilnius University, Lithuania
gabija.kavaliauskaite@chgf.stud.vu.lt

Iron hexacyanoferrate, as well known as Prussian Blue, is an inorganic compound with formula $Fe_4[Fe(CN)_6]_3$. This salt is electrochromic material with specific electrochemical and optical properties [1], which are widely used in formation of electrochemical [1] sensors and biosensors [2,3].

Yeasts are a single-cell fungi [4], which is widely used in baking and as leaveling agent, therefore is very affordable and cheap. Yeast cell is an eukaryotic microorganism and has a cell membrane with enzymes ï oxidoreductases [5]. These enzymes are involved in oxidation ï reduction reactions [5]; during such a reaction, the corresponding iron salts can form Prussian Blue in yeast cell membrane. Yeast cells, modified with Prussian Blue, have a higher electric conductivity. This property could be used in electrochemical analytical system or to form a bioenergetic element.

In this research work yeast (*Saccharomyces cerecisiae*) cells were modified with iron salts, thus, under the action of oxidoreductases, Prussian Blue was formed in a membrane of a yeast cell. After this modification, yeast cells were immobilized on glass/FTO electrode surface by using glutaraldehyde. Further, modified and unmodified yeast cells were photographed using an optical microscope (Fig. 1). Moreover, a difference in electric conductivity of modified and unmodified yeast cells was observed in ferri/ferro system, by using cyclic voltammetry.

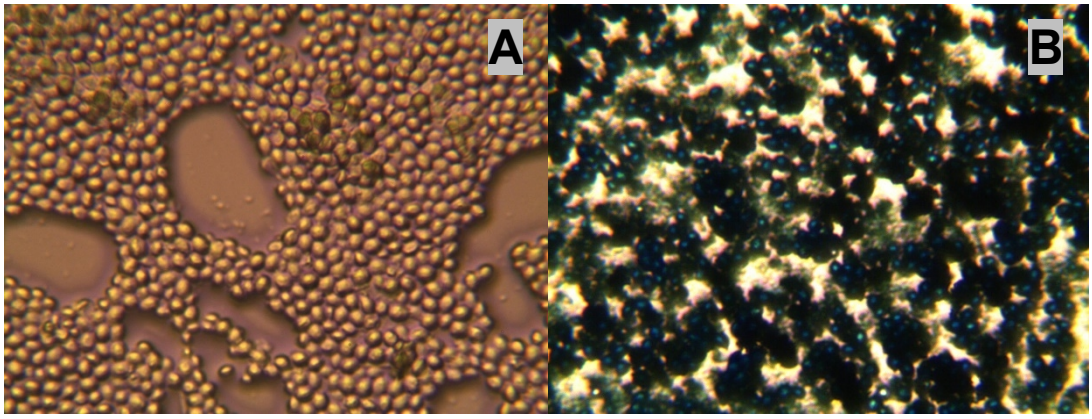

Fig. 1. Yeast cells photographed with optical microscope zoomed in 40 times: A) before modification with iron salts, B) after modification with iron salts.

[1] P. Virbickas, A. Valiî nienā, A. Ramanavicius, Towards electrochromic ammonium ion sensor, Electrochemistry Communications, 94, 41-44 (2018)
[2] P. Virbickas, G.Kavaliauskaitā, A. Valiî nienā, A. Ramanavicius, Prussian White- Based Optical Glucose Biosensor, Journal of Electrochemical Society, 166 (12), B927-B932 (2019)
[3] A. Valiî nienā, P. Virbickas, G. Medivikytā, A. Ramanavi¸ius,Urea Biosensor Based on Electrochromic Properties of Prussian Blue, Electroanalysis, vol. 32 (3), 503-509 (2019)
[4] F. Sherman,Getting started with yeast, Methoods in Enzymology, vol. 350, 3-41 (2002)
[5] H. S. Toogood, J. M. Gardiner, N. S. Scrutton,Biocatalytic reductions and chemical versatility of the old yellow enzyme family of flavoprotein oxidoreductases ChemCatChem, vol. 2, issue 8 (2010)

SYNTHESIS OF BILE ACID PRECURSOR FOR NEW GLUCOCORTICOID DERIVATIVES

Ljubica Brenjo[1], Srđan Bjedov[1]

[1] Department of Chemistry, Biochemistry and Environmental Protection, Faculty of Sciences, University of Novi Sad, Trg D. Obradovića 3, Novi Sad, Serbia
ljubicabrenjo@gmail.com

Inflammation is part of the non-specific immune response that occurs in reaction to harmful stimuli [1], which is recognized by the cardinal signs of heat, redness, swelling, pain and loss of function [2]. Whereas inflammation is beneficial and protective response, excessive or persistent inflammation incites tissue destruction and disease. Anti-inflammatory drugs decrease or neutralize the level of pro-inflammatory mediators and/or inhibit the recruitment and activation of leukocytes [2]. Glucocorticoids (GC) are class of steroid hormones that regulate several immunological functions and are among the most commonly prescribed drugs used for the treatment of inflammatory and immune disorders [3], however their therapeutic use is limited by severe side effects, and there is a need for GC with enhanced therapeutic activities and fewer or less severe side effects. GC mediate their physiological effect through number of mechanisms where the most important are transrepression (TR) and transactivation (TA) [4].

Our goal is the synthesis of a series of compounds that will manifest a different ratio of TR and TA activity and will lead to potential drug candidate. Starting from the deoxycholic acid we have developed a method for synthesis of precursor **1** (Fig. 1), that could be easily functionalized at the position C3 and C11, positions which are crucial for interaction with glucocorticoid receptors. Synthesis of this compound will be presented in detail.

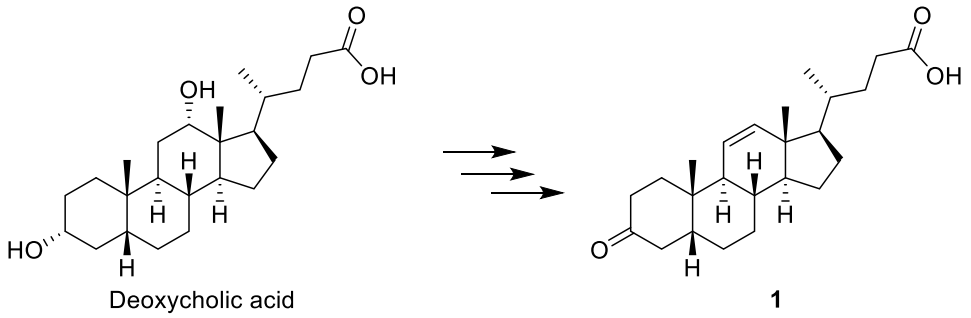

Fig. 1. Multistep synthesis of precursor **1** from deoxycholic acid.

[1] L. Ferrero-Miliani, O. H. Nielsen, P. S. Andersen, S. E. Girardin, Chronic inflammation: importance of NOD2 and NALP3 in interleukin-1β generation, Clin Exp Immunol. **147**, 227-235 (2007).
[2] A. L. Alessandri, L. P. Sousa, C. D. Lucas, A. G. Rossi, V. Pinho, M. M. Teixeira, Resolution of inflammation: Mechanisms and opportunity for drug development, Pharmacology and Therapeutics **139**, 189-212 (2013).
[3] A. Shimba and K. Ikuta, Control of immunity by glucocorticoids in health and disease, Seminars in Immunopathology **42**, 669-680 (2020).
[4] B. M. Vayssière, S. Dupont, A. Choquart, F. Petit, T. Garcia, C. Marchandeau, H. Gronemeyer, M. Resche-Rigon, Synthetic glucocorticoids that dissociate transactivation and AP-1 transrepression exhibit antiinflammatory activity in vivo, Mol Endocrinol. **11**, 1245-1255 (1997).

MICROWAVE-ASSISTED SYNTHESIS OF SILVER NANOPARTICLES WITH POLYOLS

Edita Daublytė[1], Agnė Zdaniauskienė[2], Tatjana Charkova[2]

[1] Life Sciences Center, Vilnius University, Lithuania
[2] Department of Organic Chemistry, Center for Physical Sciences and Technology, Lithuania
editadaublyte@gmail.com

In recent years, silver nanoparticles have been intensely studied for their unique optical, electrical, catalytic, thermal, and other related properties. Precious metal nanoparticles of a certain size, shape, and coatings amplify Raman signals from different analytical targets. This promising method is called shell-isolated nanoparticle-enhanced Raman spectroscopy (SHINERS) [1].

Various reducing and stabilizing agents are used to optimize the properties of synthesized nanoparticles [2]. Polyols are widely used because they help to maintain high temperatures and keep uniform heating. Microwave-assisted synthesis of nanostructures has several advantages over other methods: shorter reaction times, lower energy consumption, higher product yields with narrower size distributions [3]. Consequently, we combined microwave synthesis and chemical reduction to synthesize silver nanoparticles using popular polyols: ethylene glycol (EG), tetraethylene glycol (TEG), pentaethylene glycol (PEG), polyethylene glycol 200 (PEG-200). We aim to compare which agents are most suitable for obtaining stable, monodisperse silver nanoparticles. The nanoparticles meeting our criteria were coated with a silica (SiO_2) shell to avoid direct chemical and electrical contact of the nanoparticles with a gold substrate, analyte, and environment. In this way, silver core-silica shell ($Ag@SiO_2$) nanospheres with a size of 70Ñ5 nm were synthesized (Fig. 1). A self-assembled monolayer of 4-mercaptobenzoic acid (MBA) was formed onto a gold plate and $Ag@SiO_2$ nanoparticles were spread on it to amplify the Raman signal. A clear enhanced SHINERS spectrum of MBA on a smooth gold plate was obtained (Fig. 2).

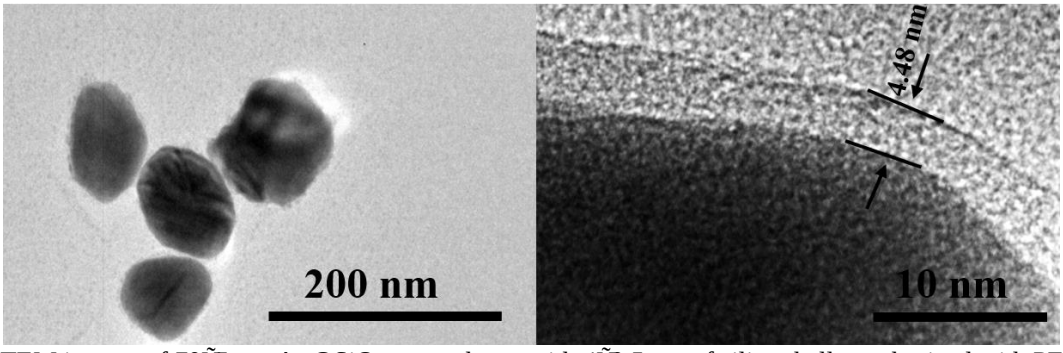

Fig. 1. HR-TEM images of 70Ñ5 nm $Ag@SiO_2$ nanospheres with 4Ñ0.5 nm of silica shell, synthesized with PEG-200.

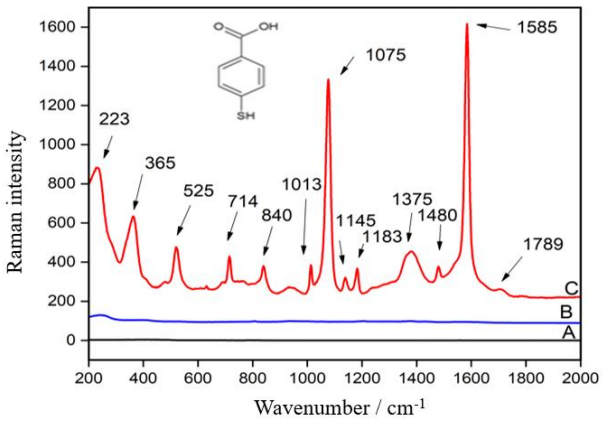

Fig. 2. Raman spectrum of MBA adsorbed on a smooth Au surface without nanoparticles (A ï black), Raman spectrum of $Ag@SiO_2$ nanoparticles, synthesized with PEG-200 (B ï blue) and SHINERS spectrum of MBA with $Ag@SiO_2$ nanoparticles.

[1] J. F. Li, Y. J. Zhang, S. Y. Ding, R. Panneerselvam, Z. Q. Tian, Core-shell nanoparticle-enhanced Raman spectroscopy, J. Chem. Rev. **117**, 5002-5069 (2017).
[2] S. Mukherji, S. Bharti, G. Shukla, S. Mukherji, Synthesis and characterization of size- and shape-controlled silver nanoparticles, Phys. Sci. Rev. **4**, 20170082 (2019).
[3] Y. J. Zhu, F. Chen, Microwave-assisted preparation of inorganic nanostructures in liquid phase, J. Chem. Rev. **114**, 6462-6555 (2014).

SYNTHESIS, CHARACTERIZATION AND APPLICATION OF CHITOSAN-CLAY-BASED NANOCOMPOSITES FOR SORPTION OF METALS/RADIONUCLIDES

Karolina Karaleviļ iÎ tā[1,2], Galina Lujanienā[2], Raman Novikau[2], Vidas Pakġtas[3], Audrius Drabaviļ ius[3], Arnas Naujokaitis[3]

[1] Department of Analytical and Environmental Chemistry, Faculty of Chemistry and Geosciences, Vilnius University, Lithuania
[2] Department of Environmental Research, Center for Physical Sciences and Technology, Lithuania
[3]Department of Characterisation of Materials Structure, Center for Physical Sciences and Technology, Lithuania
karolina.karaleviciute@chgf.stud.vu.lt

Unique properties of chitosan such as biocompatibility, biodegradability, antimicrobial activity and non-toxicity have resulted in an increasing interest of its investigation and widespread application [1]. Chitosan biopolymer is used in various fields: medicine, pharmacy, agriculture, food packaging and cosmetic industry as well as for removal of heavy metals from wastewater [2]. However, chitosan has low water resistance, poor mechanical and thermal properties limiting its usage.

A commonly used way for improving the mechanical and barrier properties of chitosan is to add nanosized reinforcing elements into chitosan chains [3]. The use of clay as an adsorbent is due to the peculiarities of its structure, as well as its economic availability and ubiquity. The trend towards the use of clay has undergone several changes, from its use in its pure form to modifications and combination with other adsorbents. Chitosan-clay nanocomposites have attracted considerable interest because they combine the structure, physical and chemical properties of inorganic and organic materials [4].

The aim of this study was to prepare chitosan ï clay nanocomposites with various clay concentrations, in order to identify and characterize the structure of nanocomposites using X-ray diffraction (XRD), transmission electron microscope (TEM) and scanning electron microscopy (SEM) as well as to apply the synthesized nanocomposites for sorption of metals and radionuclides.

In this research, chitosan powder was dissolved in 100 ml of an aqueous solution of acetic acid (1%, v/v), using a magnetic stirring plate at 90 ÁC and 150 rpm for 1 hours and then cooling the solution to room temperature. Chitosan-clay nanocomposites were obtained by mixing the chitosan with different amounts of clay (0, 5, 10, 15 wt %). The structure morphology and composition of nanocomposites were characterized using X-ray diffraction (XRD), transmission electron microscope (TEM) and scanning electron microscopy (SEM). This investigation let us identify what shapes and size of particles were synthesized. The obtained nanocomposites were applied for the sorption of metals and radionuclides.

[1] Biswas S., Rashid T.U., Debnath T., Haque P. 2020. Application of Chitosan-Clay Biocomposite Beads for Removal of Heavy Metal and Dye from Industrial Effluent,: 1ï 14. DOI: 10.3390/jcs4010016.
[2] Kusmono, Abdurrahim I. 2019. Water sorption, antimicrobial activity, and thermal and mechanical properties of chitosan/clay/glycerol nanocomposite films, *Heliyon* 5(8): e02342. DOI: 10.1016/j.heliyon.2019.e02342.
[3] Neji A.B., Jridi M., kchaou H., Nasri M., Dhouib Sahnoun R. 2020. Preparation, characterization, mechanical and barrier properties investigation of chitosan-kaolinite nanocomposite, Polymer Testing 84(October 2019): 106380. DOI: 10.1016/j.polymertesting.2020.106380.
[4] A Neves M. 2016. Development and Characterization of Chitosan-Nanoclay Composite Films for Enhanced Gas Barrier and Mechanical Properties, Food Science & Nutrition 2(1): 1ï 7. DOI: 10.24966/fsn-1076/100007.

INTERACTION OF COPPER(II) WITH ACIDIFIED SODIUM ORTOTUNGSTATE AQUEOUS SOLUTIONS

Duvanova Ella[1], Radio Serhii[2], Rozantsev Georgiy[1]

[1] Faculty of Chemistry, Biology and Biotechnologies; Vasyl' Stus Donetsk National University, Ukraine
[2] Department for Research, Research Laboratory ñChemistry of Polyoxometalates and Complex Oxide Systemsò Vasyl' Stus Donetsk National University, Ukraine
e.ivantsova@donnu.edu.ua

Copper(II) isopoly tungstates (CuIPTA) have a variety of perspective properties that allows to use them as antiviral and antitumor medicines. Considering this, the search of new synthesis routes, the structure and properties characterization of this compounds are actual research tasks.

The most studied among CuIPTA are paratungstates which contain the $[W_{12}O_{40}(OH)_2]^{10-}$ anion. These compounds are usually synthesized by an exchange reaction from dissolved in water alkali metal paratungstate, or from acidified to the needed acidity ($Z = C(H^+) / C(WO_4^{2-})$) aqueous solutions of orthotungstate anion during self-assembly. The second synthesis route is simpler and faster, because it does not require the synthesis of alkali metal paratungstate B.

At the same time the acidity range where definite isopoly anions dominate are rather wide. And the synthesis can be done in a wide pH range of solution. Thus, an aqueous solution of Cu^{2+} ï WO_4^{2-} ($Z = 1.17$) ï H^+/OH^- ï H_2O was studies by methods of mathematical modeling, which made it possible to determine the most accurate Copper(II) paratungstates B synthesis conditions.

In this regard a pH-potentiometric titration of the Cu^{2+} ï WO_4^{2-} ($Z = 1.17$) ï H_2O system by acid or alkali in $Z = 1.17$ï 1.67 and $Z = 1.17$ï 1.05 acidity ranges respectively with the ε = 0.05; 0.10; 0.15; 0.20; 0.25 (molÂ¯ï 1) ionic strengthes was carried out. The titration results were used for modeling in CLINP 2.1 program which showed that the expected Anderson heteropoly anions were not formed at this acidity range. A model with $[Cu^{2+}, W_{12}O_{40}(OH)_2]^{8-}$, $[Cu^{2+}, HW_{12}O_{40}(OH)_2]^{7-}$, $[Cu^{2+}, H_2W_{12}O_{40}(OH)_2]^{6-}$, $[Cu^{2+}, H_3W_{12}O_{40}(OH)_2]^{5-}$ ion pairs and CF=50.19 ($\sigma^2_{exp.} = 28.70 << \sigma^2_{f,\ \check{U}=0.05} = 54.57$) was chosen to describe the ion state in the system. That explains the preservation of the homogeneity of the system at a sufficiently high content of free Cu^{2+} and WO_4^{2-} ions.

Interactions in the system were investigated by conductivity measurement which can prove the presence of ion pairs between Copper(II) cations and isopoly tungstates anions of the 12th row.

The calculated values of the logarithms of concentration constants of the anions formation at the corresponding values of ionic strength were used to calculate the logarithms of thermodynamic constants lgK^0 by the Pitzer method by extrapolating the dependence $lgK_C = f(\varepsilon)$ to $\varepsilon = 0$ (molÂ¯ï 1).

A new synthesis procedure was developed and a new sodium-copper(II) paratungstate B $Na_2Cu_3(CuOH)_2[W_{12}O_{40}(OH)_2]\cdot 32H_2O$ in acidified to $Z = 1.17$ aqueous solution with ч(Na_2WO_4) = ч(HNO_3) = 0.05 (molÂ¯ï 1) and $C(Cu(NO_3)_2) = 8{,}3333Ł10^{-3}$ (molÂ¯ï 1) was synthesized. The obtained salt was studied by chemical elemental analysis, scanning electron microscopy (SEM) and FT-IR spectroscopy. The study of surface micromorphology showed that salt exists in the form of plates with 240-340 nm grain sizes (Fig. 1). The proposed synthesis procedure can be used to obtain similar salts with cations of other d-metals.

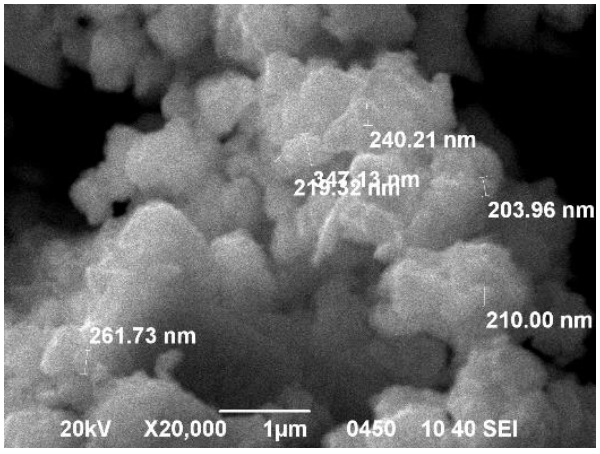

Fig. 1. SEM image of $Na_2Cu_3(CuOH)_2[W_{12}O_{40}(OH)_2]\cdot 32H_2O$ in SEI electron mode (Ť 20,000)

The study was carried out within the Fundamental Research Programme funded by the Ministry of Education and Science of Ukraine (grant ID 0119U100025).

SYNTHESIS AND ANALYSIS OF YTTRIUM ALUMINIUM GARNET DOPED WITH TANTALUM, CALCIUM AND EUROPIUM OR CERIUM

Ruta Juodvalkyte[1], Monika Skruodiene[2], Ramunas Skaudzius[1]

[1] Institute of Chemistry, Faculty of Chemistry and Geosciences Vilnius University, Naugarduko 24, LT-03225, Vilnius, Lithuania

[2] Institute of Solid State Physics, University of Latvia 8 Kengaraga str., LV-1063 Riga, Latvia

rutajjuodvalkyte@gmail.com

The growing need for LEDs and laser development by human society demands environmentally friendly synthesis techniques, safe use and fabrication of low-cost novel multifunctional materials. One of the most suitable ways to solve this demand is the search for novel structure garnets for versatile applications with controllable broad color tuning and improvement of quantum yield, thermal and radiation stability.

Yttrium aluminum garnet ($Y_3Al_5O_{12}$) is a very perspective host matrix for rare-earth (RE) ions. RE doped YAG has interesting optical properties that allows to use it in the optical fields. Moreover, YAG possesses high thermal and chemical stability, and good mechanical properties at high temperatures. These characteristics enable the use of YAG:RE for thermal barrier coatings and high-temperature structural applications [1], [2] [3], [4].

In recent experiments, it was noticed that Ta_2O_5 can help to improve phosphorõs thermal, structural and optical properties. The main aim of this work is to investigate the concentration influence of Ta and Ca ions in doping to $Y_{3-2x}Ca_{2x}Ta_xAl_{4-x}O_{12}$:1% Eu and $Y_{3-2x}Ca_{2x}Ta_xAl_{4-x}O_{12}$:0,5% Ce synthesized by the citric acid sol-gel method.

The samples were prepared using different amounts of Ta and Ca (x=0.01 ï 0.1). All samples were annealed at 1000 ÁC for 4 h in covered crucibles in the air to remove organic components and residual nitrates, then heat treated in 1300 ÁC for 2 h in the air or in a reduction atmosphere.

All synthesized samples were analyzed by the XRD method. The concentration influence of Ta and Ca ions on luminescence properties are discussed in detail. The optimal concentration of these ions is also determined.

Excitation and emission spectra are presented in Fig. 1. and Fig. 2. respectively.

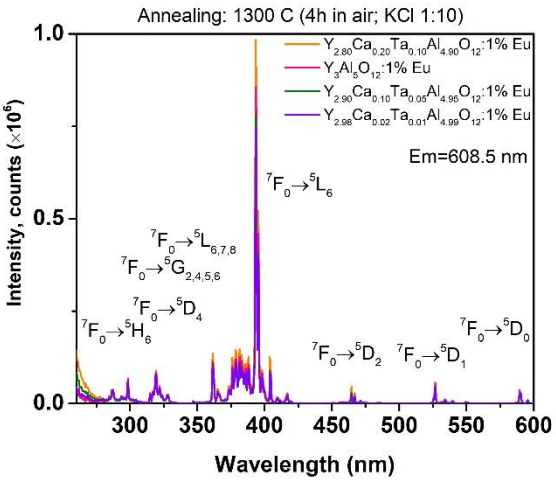

Fig. 1. Excitation spectra of $Y_{3-2x}Ca_{2x}Ta_xAl_{4-x}O_{12}$:1% Eu.

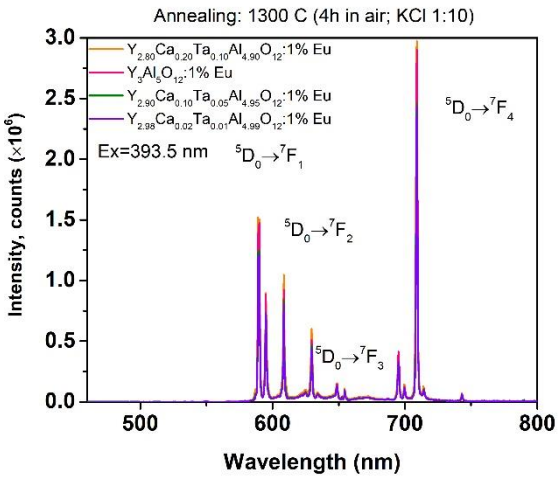

Fig. 2. Emission spectra of $Y_{3-2x}Ca_{2x}Ta_xAl_{4-x}O_{12}$:1% Eu.

[1] Maęzka, M., Bednarkiewicz, A., Mendoza-Mendoza, E., Fuentes, A. F., & Kĩ piC ski, L. (2014). Low-temperature synthesis, phonon and luminescence properties of Eu doped Y3Al5O12 (YAG) nanopowders. Materials Chemistry and Physics, 143(3), 1039ï 1047. https://doi.org/10.1016/j.matchemphys.2013.11.002.

[2] Borlaf, M., Frankowska, M., Kubiak, W. W., & Graule, T. (2018). Strong photoluminescence emission at low dopant amount in YAG:Ce and YAG:Eu phosphors. Materials Research Bulletin, 100(August 2017), 413ï 419. https://doi.org/10.1016/j.materresbull.2018.01.005.

[3] Paula de Sousa, B., Marcondes, L. M., Maestri, S. A., Ramos da Cunha, C., Cassanjes, F. C., & Poirier, G. Y. (2020). Phosphate glasses with high tantalum oxide contents: Thermal, structural and optical properties. Materials Chemistry and Physics, 239(May 2019). https://doi.org/10.1016/j.matchemphys.2019.121996.

[4] Marcondes, L. M., Santagneli, S. H., Manzani, D., Cassanjes, F. C., Batista, G., Mendoza, V. G., Ramos da Cunha, C., Poirier, G. Y., & Nalin, M. (2020). High tantalum oxide content in Eu3+-doped phosphate glass and glass-ceramics for photonic applications. Journal of Alloys and Compounds, 842, 155853. https://doi.org/10.1016/j.jallcom.2020.155853.

SYNTHESIS OF BENZIMIDAZOLE DERIVATIVES AS POTENTIAL INHIBITORS FOR HSP90

Lukas Neverdauskas, Paulina Kaziukonytė, Algirdas Brukštus

Faculty of Chemistry and Geosciences, Department of Organic chemistry, Vilnius University, Lithuania
lukas.neverdauskas@chgf.stud.vu.lt

Heat shock proteins (HSPs) are responsible for the stabilisation of proteins in the cell [1]. Significant member of HSPs is HSP90, which is responsible for 1-2% of total cellular protein when the cell is exposed to stressful conditions such as heat, cold, UV light, etc. [2]. Its function depends on its ability to bind and hydrolyse ATP, resulting in changed complex and folded client protein. However, HSP90 in tumour cells is overexpressed and may cause uncontrolled reproduction of mutated cells. This means that inhibition of this HSP can lead to effective strategy in cancer therapy [1]. Potential structures of inhibitors of the HSP90 are predicted using molecular docking and, according to the 2019 study, 18 HSP90 inhibitors are undergoing clinical trials, at least a third of them with resorcinol moiety [3]. Therefore, we aim to synthesise some benzimidazole derivatives containing resorcinol moiety as potential inhibitors for HSP90.

The synthesis was started from commercially available 1-(2,4-dihydroxyphenyl)ethenone (**1**) (Fig. 1.). 10-step synthesis pathway, including protection of hydroxyl groups by benzylation and reactions such as Wittig reaction and Vilsmeier-Haack reaction, led to successful formation of 2-(2,4-dihydroxy-5-isopropylphenyl)acetic acid (**2**). Synthesis of target benzimidazoles (**3** and **4**) was carried out by heating o-phenylenediamine derivatives with compound **2** in Wood's metal bath with no solvent.

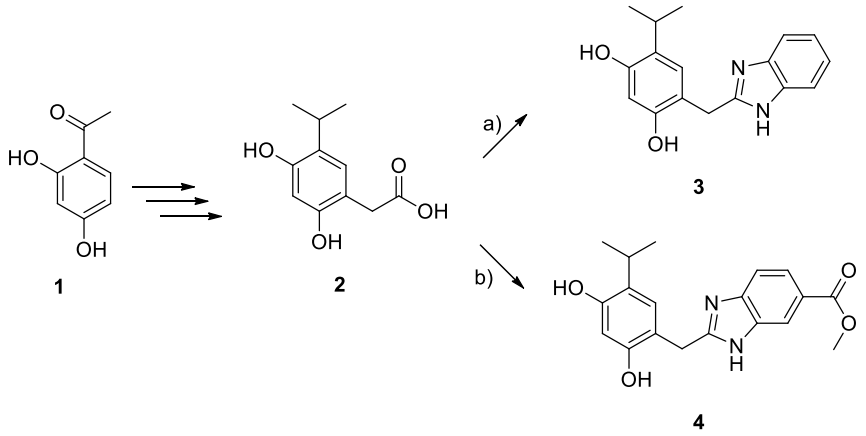

Fig. 1. Synthesis pathway of benzimidazole derivatives from 1-(2,4-dihydroxyphenyl)ethenone. Reagents and conditions: a) benzene-1,2-diamine, 3 h at 145 ÁC; b) methyl 3,4-diaminobenzoate, 3 h at 145 ÁC.

Final products **3** and **4** are yet to be analysed of inhibition properties for HSP90.

[1] M. Abbasi, H. Sadeghi-Aliabadi, M. Amanlou. Prediction of new Hsp90 inhibitors based on 3,4-isoxazolediamide scaffold using QSAR study, molecular docking and molecular dynamic simulation. *DARU, J. Pharm. Sci.* **2017**, 25 (1), 1ï 16.

[2] K. Sidera, E. Patsavoudi. HSP90 Inhibitors: Current Development and Potential in Cancer Therapy. *Recent Pat. Anticancer. Drug Discov.* **2013**, 9 (1), 1ï 20.

[3] Y. Liu, X. Liu, L. Li, R. Dai, M. Shi, H. Xue, Y. Liu, H. Wang. Identification and Structure-Activity Studies of 1,3-Dibenzyl-2-aryl imidazolidines as Novel Hsp90 Inhibitors. *Molecules* **2019**, 24 (11), 1ï 11.

AZIRIDIN-2-YL METHANOLS AS CHIRAL SOLVATING AGENTS FOR CARBOXYLIC ACIDS

Martyna Malinowska, Anna Zawisza, Stanisław Leśniak

Department of Organic and Applied Chemistry, University of Lodz, Poland
martyna.malinowska@chemia.uni.lodz.pl

Chirality plays a significant role in chemistry, biology and pharmacy. For this reason, the development of fast and easy methods to determine the absolute configuration of compounds as well as their enantiomeric purity is of interest to many research groups. Although many methods of analyzing chiral compounds are currently known, such as GC analysis, HPLC, fluorescence spectroscopy, mass spectroscopy, circular dichroism, electrophoresis or NMR spectroscopy, new methods are still being sought that allow rapid analysis without the need to derivatization the analyte [1]. Among these methods, NMR spectroscopy occupies a special place, because using only 1 mg of the appropriate reagent in less than 1 ml of deuterated solvent, we gain an easy and environmentally friendly analytical tool.

This technique requires finding an effective so-called chemical shift reagent that, in combination with the tested sample, gives diastereoisomeric forms that show differences in the chemical shifts of some signals [2]. Therefore, the design and synthesis of new molecules that act as chemical shift reagents is an important and still relevant issue in modern organic synthesis.

My poster will present the ability to chiral recognition Ď-substituted carboxylic acids using synthesized aziridinylcarbinols by measuring the non-equivalence of chemical shifts (qpqpď) the enantiomers of the analyzed carboxylic acids.

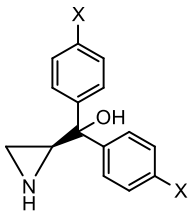

X = H, CH_3, OCH_3, F, CF_3,

Fig. 1. Scope of aziridinylcarbinols used as chiral chemical shift reagents.

[1] M. Malinowska et al., Optically Pure Aziridin-2-yl Methanols as Readily Available ^{1}H NMR Sensors for Enantiodiscrimination of Ď-Racemic Carboxylic Acids Containing Tertiary or Quaternary Stereogenic Centers, *J. Org. Chem*. **85**, 11794ī 11801 (2020).

[2] M. Raban, K. Mislow, The determination of optical purity by nuclear magnetic resonance spectroscopy. II. Compounds which owe their dissymmetry to deuterium substitution, Tetrahedron Letters **33**, 3961-3966 (1966).

STRUCTURE OPTIMIZATION AND TADF PROPERTIES OF NOVEL ACRIDINE-PYRIMIDINE DERIVATIVES

Irina Fiodorova[1*], Tomas Serevičius[2], Rokas Skaisgiris[2], Gediminas Kreiza[2], Dovydas Banevičius[2], Karolis Kazlauskas[2], Saulius Jurgėnas[2], Sigitas Tumkevičius[1]

[1] Department of Organic Chemistry, Faculty of Chemistry and Geosciences, Vilnius University, Naugarduko 24, LT-03225 Vilnius, Lithuania
[2] Institute of Photonics and Nanotechnology, Faculty of Physics, Vilnius University, Sauletekio 3, LT-10257 Vilnius,Lithuania
[*]irina.fiodorova@chgf.vu.lt

Organic lightī emitting diodes (OLEDs) are one of the most promising green technologies for displays and lighting resources owing to their low power consumption and their being ultra-thin, lightweight, and flexible [1]. Thermally activated delayed fluorescent (TADF) emitters consisting of pure organic materials have been developed as a new generation of emitters to harvest all the molecular excitons. The main requirement for efficient TADF is thought to be a negligible energy difference between the lowest singlet and triplet states (æE_{ST}), which often is obtained in the non-flat (hetero)aromatics possessing donor (D) and acceptor (A) fragments [2]. However, a molecular structure, where the D and A units are rotationally flexible, simultaneously brings unwanted consequences, such as distinct emission properties in solution and the solid state [3]. In solid hosts, the rigid surroundings prevent structural relaxation towards the potential minimum, forming a set of molecular geometries with different singletï triplet energies, so called conformational disorder. Consequently, the dispersion of ΔE_{ST} gaps disturbs the single exponential TADF decay profile, typical for the solution state, and leads to the emergence of multiexponential TADF decay with prolonged lifetime, leading to a decreased average rISC rate. The structural inhomogeneity of TADF compounds in solid films may be lowered by the careful enhancement of the structural rigidity of the molecular core. In this connection, on the example of acridine-pyrimidine based compounds we performed an optimization of the molecular structure leading to the minimization of conformational disorder and thus, ensuring the single-exponential TADF decay profile in the solid state, while small singletï triplet gaps were shown to promote rapid rISC.

Synthesis of the target compounds **I-V** (Fig. 1) and some intermediates was accomplished starting from easily accessible halopyrimidine derivatives by a combination of Buchwald-Hartwig, Suzuki-Miyaura palladium-catalyzed cross-coupling and Raney Ni reduction reactions.

The noncontinuously conjugated acridine tends to form two distinct conformers, namely quasi-axial (qa) and quasi-equatorial (qe) [4]. Really, compounds **I, III** were found to show a strong emission of qa conformers. To overcome this problem, a 5-methyl group was introduced into the pyrimidine moiety to enlarge the steric hindrance between the D and A units and prevent the formation of qa conformers. DFT simulations were employed to assess the ground state geometry and the corresponding transition energies of compound **IV**. Single crystal XRD analysis confirmed the DFT-predicted distorted molecular geometry.

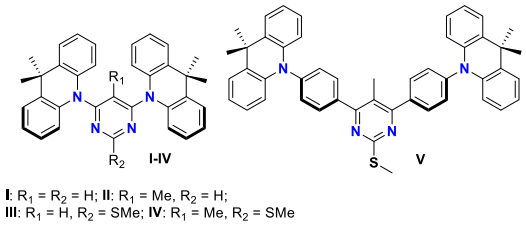

Fig. 1. Structures of acridine-pyrimidine based fluorophores **I-V**

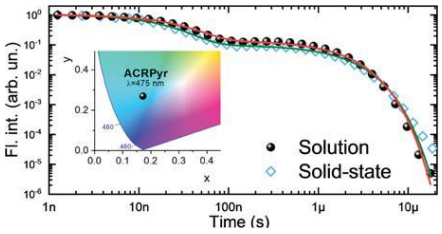

Fig. 2. Fluorescence decay transients of compound **IV** (ACRPyr) in toluene and 3 wt% TSPO1 film.

The enlarged structural rigidity of optimized structure **IV** (ACRPyr) minimized the ΔE_{ST} dispersion, leading to a rapid mono-exponential TADF decay in the solid host with a lifetime of 1.76 μs (Fig. 2). Moreover, a high fluorescence quantum yield of about 0.67 and an exceptional rISC rate of 5.7 x 10^6 s^{-1} were observed for the optimized compound **IV**. The pronounced TADF activity of compound **IV** allowed us to attain efficient sky-blue electroluminescence. The OLED device showed sky-blue electroluminescence (λ = 475 nm) with a turn-on voltage of about 3.5 V, corresponding to CIE 1935 color coordinates of (0.17, 0.27) (Fig. 2). The OLED device yielded a 14.3% EQE with minor roll-off at large luminance.

Our findings, we hope, will foster further advance in the development of TADF compounds.

[1] Oh C.-H., Shin H.-J., Nam W.-J., Ahn B.-C., Cha S.-Y., Yeo S.-D., *SID Int. Symp. Dig. Tech. Pap.*, **2013**, 44, 239ï 242.
[2] Uoyama H., Goushi K., Shizu K., Nomura H., Adachi C., *Nature*, **2012**, 492, 234ï 238.
[3] Serevičius T., Skaisgiris R., Dodonova J., Kazlauskas K., Jursenas S., Tumkevicius S., *Phys. Chem. Chem. Phys.*, **2020**, 22, 265ï 272.
[4] Wang K., Zheng C.-J., Liu W., Liang K., Shi Y.-Z., Tao S.-L., Lee C.-S., Ou X.-M., Zhang X.-H., *Adv. Mater.*, **2017**, 29, 1701476.

THE PPY LAYER THICKNESS CONTROL FOR THE DEVELOPMENT OF THE SENSOR

Raimonda Boguģaitā[1], Vilma Ratautaitā[1], Ernestas Brazys[2], ArÎnas Ramanaviļius[1,2]

[1] Center for Physical Sciences and Technology, Department of Functional Materials and Electronics, Laboratory of Nanotechnology, Sauletekio av. 3, Vilnius LT-10257, Lithuania
[2] Vilnius University, Faculty of Chemistry and Geosciences, Institute of Chemistry, Naugarduko str. 24, LT-03225 Vilnius
raimonda.boguzaite@gmail.com

Molecularly imprinted polymers (MIPs) are encouraging materials that can be used in the recognition process [1,2]. The technique of molecular imprinting enables the construction of selective molecular recognition sites in polymeric matrices that operate on the principle of a lock and key mechanism [3]. The functional monomers initially form a complex with the imprint molecules, and following polymerization, their functional groups are held in position by the highly cross-linked polymeric structure [4]. MIPs exhibits exceptional thermal and chemical stability [5]. In the development of MIPs pyrrole is one of the most used polymers. It is applied because of the simplicity, ability to form thin coatings, stability, and ability to electropolymerize [6].

Furthermore, usually it is necessary to control the thickness of the MIP layer in order to optimize the sensitivity [5]. The thickness can be partially controlled by changing the concentration of the monomer, the number of potential pulses. During the development of uric acid-imprinted polypyrrole-based sensor, MIP preparation was based on a single potential pulse of 1 V vs Ag/AgCl lasting for 10 s. The polymerization mixture consisted of 5 mM uric acid and 50 mM pyrrole solution in PBS [3]. On the other hand, to develop a pyrrole-based CO_2 sensor, pyrrole was polymerized electrochemically on glass/ITO or glass/$ITO_{(TEMS)}$ electrode surface from a solution containing 10 mM of pyrrole and 0.1 M of $LiClO_4$ as an electrolyte. Polymerization was performed in room temperature by 10 potential cycles in the range from ī 0.2 V to +1.0 V vs $Ag/AgCl_{(3M\ KCl)}$ at the sweep rate of 50 mV/s and step potential of 2.44 mV [7]. By choosing a higher polymer concentration and a lower number of potential pulses, or a lower concentration but a higher number of potential pulses, both methods lead to the formation of a sufficiently thin layer that can be adapted to the design of the sensor.

References

[1] O.S. Ahmad, T.S. Bedwell, C. Esen, A. Garcia-cruz, A. Piletsky, L. Le, Molecularly Imprinted Polymers in Electrochemical and Optical Sensors, Trends Biotechnol. 37 (2019) 294ï 309. https://doi.org/10.1016/j.tibtech.2018.08.009.
[2] V. Ratautaite, M. Nesladek, A. Ramanaviciene, I. Baleviciute, A. Ramanavicius, Evaluation of Histamine Imprinted Polypyrrole Deposited on Boron Doped Nanocrystalline Diamond, Electroanalysis. 26 (2014) 2458ï 2464. https://doi.org/https://doi.org/10.1002/elan.201400294.
[3] D. Plausinaitis, L. Sinkevicius, U. Samukaite-bubniene, V. Ratautaite, Evaluation of electrochemical quartz crystal microbalance based sensor modified by uric acid-imprinted polypyrrole, Talanta. 220 (2020) 121414. https://doi.org/10.1016/j.talanta.2020.121414.
[4] K.H. Bin Chena, Chuanjun Liub, Lingpu Gea, Localized surface plasmon resonance gas sensor of Au nano-islands coated with molecularly imprinted polymer_ Influence of polymer thickness on sensitivity and selectivity _ Enhanced Reader.pdf, Sensors Actuators B Chem. (2016). https://doi.org/http://dx.doi.org/10.1016/j.snb.2016.03.117.
[5] R.H. Schmidt, K. Mosbach, K. Haupt, A Simple Method for Spin-Coating Molecularly Imprinted Polymer Films of Controlled Thickness and Porosity, Adv. Mater. 16 (2004) 719ï 722. https://doi.org/https://doi.org/10.1002/adma.200306374.
[6] A. Ramanavicius, Y. Oztekin, A. Ramanaviciene, Electrochemical formation of polypyrrole-based layer for immunosensor design, Sensors Actuators B. Chem. 197 (2014) 237ï 243. https://doi.org/10.1016/j.snb.2014.02.072.
[7] V. Ratautaite, G. Bagdziunas, A. Ramanavicius, A. Ramanaviciene, An Application of Conducting Polymer Polypyrrole for the Design of Electrochromic pH and CO 2 Sensors , J. Electrochem. Soc. 166 (2019) B297ï B303. https://doi.org/10.1149/2.1221904jes.

PHOTOPHYSICAL STUDY OF TIRAPAZAMINE BASED COMPOUNDS

Kamilã Tulaitã[1], Justina Jovaiġaitã[1], Jelena Tamulienã[2], Jonas Ġarlauskas[3], Narimantas Ļ.ānas[3] and Saulius Jurġãnas[1]

[1]Institute of Photonics and Nanotechnology, Faculty of Physics, Vilnius University, Lithuania
[2]Institute of Theoretical Physics and Astronomy, Vilnius University, Lithuania
[3]Institute of Biochemistry, Life Sciences Center, Vilnius University, Lithuania
kamile.tulaite@ff.stud.vu.lt

One of the main cytotoxin class compounds suitable for cancer treatment is tirapazamine (TPZ), which exhibits selective behavior in a hypoxic environment [1]. Tumor hypoxia is still a big challenge in the treatment of cancer as the hypoxic regions are resistant to the effect of radiation therapy and other anticancer drugs [2]. During the treatment stage, TPZ compound can attach oxygen to its molecule and so reduce to a radical that causes DNA double-strand, single-strand breaks and base damage [3]. The use of tirapazamine derivatives in medicine has been widely investigated for several decades. However, the photophysical examination of these compounds remains scarce. In order, to successfully understand their usability, more studies of tirapazamine optical properties need to be performed.

The aim of this study was to investigate the influence of the number of oxygen atoms and different substituents on the photophysical properties of tirapazamine compounds. Here we present a photophysical study of tirapazamine based derivatives, that have no oxygen atoms, one double bonded oxygen atoms at N1 position of tirapazamine core or two double bonded oxygen atoms at N1 and N4 positions. In addition, the substituents at C8 were also altered. Various characterization techniques, such as steady-state absorption and fluorescence and time-resolved fluorescence spectroscopy, were employed. The optical properties of TPZ compounds were tested in polar environment: ethylacetate, acetonitrile and 1 v/v% dimethylsulfoxide (DMSO)/water mixture. Photophysical properties of TPZ compounds are changing dramatically in the presence of one double bonded oxygen atom and can be controlled by the different substituents at C8. Furthermore, another interesting feature is observed as the fluorescence quantum yields tend to increase in solvent of higher polarity. The experiments in DMSO/water mixture also gave promising results as sufficient fluorescence quantum yields were recorded. This may allow using new TPZ derivatives for the applications in biological systems.

[1] M. J. Done and J. M. Brown, Tumor-specific, Schedule-dependent Interaction between Tirapazamine (SR 4233) and Cisplatin, Cancer Res., **53**, 4633ï 4636 (1993).
[2] S. B. Reddy and S. K. Williamson, Tirapazamine: A novel agent targeting hypoxic tumor cells, Expert Opinion on Investigational Drugs, **18**, 77ï 87 (2009) .
[3] G. D. Jones and M. Weinfeld, Dual action of tirapazamine in the induction of DNA strand breaks., Cancer Res., **56**, 1584ï 90 (1996).

INVESTIGATION OF PHOTOCROSS-LINKING KINETICS OF ACRYLATED SOYBEAN OIL WITH DIFFERENT PHOTOINITIATORS AND PROPERTIES OF THE RESULTING POLYMERS

MigleLebedevaite*, JolitaOstrauskaite

Department of Polymer Chemistry and Technology, Kaunas University of Technology, Radvilenu Rd. 19, LT-50254 Kaunas, Lithuania
migle.lebedevaite@ktu.lt

The UV-curing of photopolymerizable systems containing monomer/oligomer, photoinitiator and additives, has found an industrial application mainly in coatings, varnishes, adhesives, and microelectronics [1]. These systems undergo prompt conversion from liquid monomer/oligomer into solid polymer easily by exposure to UV irradiation in the presence of photoinitiators [2]. As the photocross-linking reaction is a rapid process, investigation of the photocuring kinetics of (meth)acrylates determining their reaction propagation and termination mechanisms or understanding the influence of various process parameters (i.e. light intensity, concentration and type of photoinitiator, or temperature) is crucial [3]

Acrylatedepoxidized soybean oil (AESO) is a bio-based material, easily cross-linked via UV-induced free radical polymerization, resulting into a highly dense polymer. It has brought a lot of researcherôs attention as a replacement for synthetic (meth)acrylates in UV-curable coatings, varnishes, and even in optical 3D printing [4]. Even though it has a wide spectrum of applications, the investigation of AESO UV-curing kinetics is still mandatory.

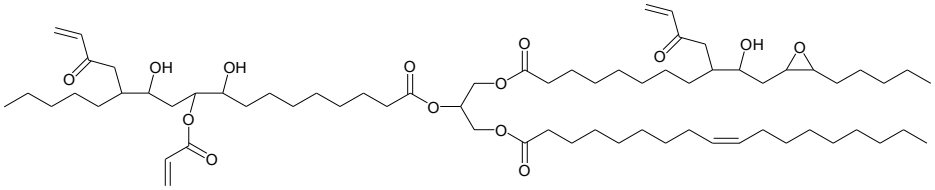

AESO

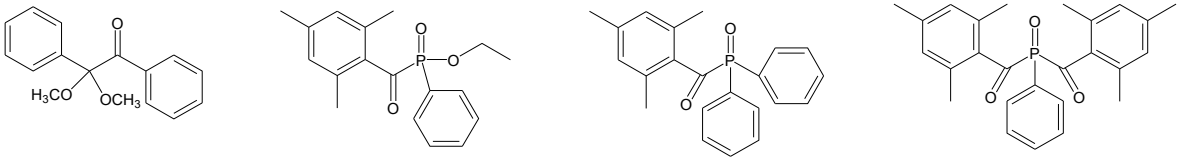

DMPA **TPOL** **TPO** **BAPO**

Fig. 1.Chemical structure of acrylatedepoxidized soybean oil (AESO), 2,2-dimethoxy-2-phenyl acetophenone (DMPA), ethyl (2,4,6-thimethylbenzoyl) phenyl phosphinate (TPOL), diphenyl (2,4,6-trimethylbenzoyl) phosphine oxide (TPO), and phenyl bis(2,4,6-trimethylbenzoyl) phosphone oxide (BAPO)

In this study, a detailed investigation of pure AESO photocross-linking kinetics using four different photoinitiators was performed by real-time photorheometry. The photocross-linking of AESO using the most popular near-UV photoinitiator DMPA and phosphine oxides, BAPO, TPO, and TPOL, was compared (Figure 1). The influence of photoinitiator type and concentration on AESO photocross-linking rate and rheological characteristics was investigated. The photocross-linking kinetics and storage modulus were determined byphotorheometry tests at different temperatures. Thermal and mechanical properties of the synthesized AESO polymers were investigated and compared.

It was determined that hard polymers of AESO were formed using 1, 3 and 5 mol.% of photoinitiators TPOL, BAPO, DMPA, and TPO. Higher amount of photoinitiator influenced the shape of storage modulus Gô curve indicating the faster attainment of the Gô plateau and the formation of more tough polymer.The increment of temperature reduced AESO viscosity and thus caused the more rapid photopolymerization and more vertical Gô curve in the first stage.The higher elastic modulus (E_E) and the lower elongation at break (Ůj of polymer films were observed when higher amount of photoinitiator was used.

Acknowledgments: Financial support from the EU ERDF, through the INTERREG BSR Programme (ECOLABNET project #R077) is gratefully acknowledged.

[1] F. Liu, et al.ñUV curable EA-Si hybrid coatings prepared by combination of radical and cationic photopolymerizationò. Progress in Organic Coatings (2015):85:46-51.
[2] Ligon-Auer, Samuel Clark, et al. "Toughening of photo-curable polymer networks: a review." Polymer Chemistry 7.2 (2016): 257-286.
[3] Lebedevaite, Migle, et al. "Influence of photoinitiator and temperature on photocross-linking kinetics of acrylatedepoxidized soybean oil and properties of resulting polymers." Industrial Crops and Products 161 (2021): 113210.
[4] B. Wu, et al.ñDirect Conversion of McDonaldôs Waste Cooking Oil into a Biodegradable High Resolution 3D Printing Resinò. ACS Sustainable Chemistry & Engineering 8.2 (2019): 1171-1177.

EXAMINATION OF NEW SPIROHYDANTOINS AND THEIR MOLECULAR DESCRIPTORS RELATED TO THEIR BIOACTIVITY AND TOXICITY

Kristina Tot[1], Anita Lazić[2], Tatjana Đaković Sekulić[1]

[1] Department of Chemistry, Biochemistry and Environmental Protection, Faculty of Sciences, University of Novi Sad, Republic of Serbia
[2] Faculty of Technology and Metallurgy, University of Belgrade, Republic of Serbia
kristina.tot@dh.uns.ac.rs

Hydantoin derivates are a well-known class of antiepileptic drugs used in the treatment of epilepsy for decades. Besides anticonvulsive hydantoins shows and other types of activities, such as antiarrhythmic, antimicrobial agents, and skeletal muscle relaxants [1]. Similarly, spirohydantoins represent a pharmacologically activities important class of compounds with a wide range of activities [2].

One of the most important properties closely related to the biological activity is lipophilicity. Lipophilicity refers to the tendency of a compound to partition between a lipophilic organic phase and a polar aqueous phase. In drug development lipophilicity of a compound is represented either as partition coefficient, log *P*, or distribution coefficient, log *D*. Lipophilicity is responsible for pharmacokinetics, and hence important for further development of potentially active compounds [3]. In addition to lipophilicity, adequate bioavailability is one of the crucial properties of drug candidates. Recognition of potentially biologically active compounds can be supported by the use of very simple rules, such as the Lipinski Rule of five [4]. The rule describes molecular properties important for a drug's pharmacokinetics and includes absorption, distribution, metabolism, excretion, and toxicity (ADMET).

The goal of this study was to determine chromatographic lipophilicity parameters of cycloalkylspiro-5-hidantoins using different mobile phase and to find the correlation between retention, log *P* as well as in silico ADMET descriptors of the investigated spirohydantoins. Lipinski rule of five is carrying out to verify if investigated spirohydantoins exhibit good (theoretical) oral bioavailability. To estimate the potential acute toxicity of the investigate spirohydantoin derivatives, their effective concentrations, EC_{50}, on the selected test organisms have been calculated.

The lipophilicity of 21 new spirohydantoin derivatives was determined using reversed-phase thin-layer chromatography on C-18 modified silica gel and a two-component aqueous mobile phase. As a modifier of the mobile phase were used different organic solvents (ethanol, *n*-propanol, *i*-propanol, or *t*-butanol). Also, lipophilicity was calculated by using the relevant software packages. The calculated partition coefficient, log *P*, as a standard measure of lipophilicity are compared with experimentally determined lipophilicity.

[1] M. Meusel, M. Gütschow, Recent developments in hydantoin chemistry, A review, Organic Preparations and Procedures International: The New Journal for Organic Synthesis **36**, 391-443 (2004).
[2] L. K. Abdulrahman, M. M. Al-Mously, M. L. Al-Mosuli, K. K. Al-Azzswii, The biological activity of 5, 5'-Imidazolidine-2,4-Dione derivatives, International Journal of Pharmacy and Pharmaceutical Sciences **5**, 494-504 (2013).
[3] X. Liu, B. Testa, A. Fahr, Lipophilicity and its relationship with passive drug permeation, Pharmaceutical Research **28,** 962–977 (2011).
[4] C. A. Lipinski, Lead- and drug-like compounds: the rule-of-five revolution, Drug Discovery Today Technologies **1,** 337–341(2004).

INDUCTION OF VISCOSITY INCREASE DURING POLYGLYCOL ADDITION TO ISOCYANATES

Paulina Nemaniutė[1]*, Dalia Bražinskienė [1], Svajus Asadauskas [1]

[1] Department of Chemical Engineering and Technology, FTMC, Vilnius, Lithuania
paulina.nemaniute@ftmc.lt

Two-component polyurethane adhesives often require accurate viscosity control for curing. When mixing the components, polyols engage into addition reaction with isocyanates, which increases mol. wt. resulting in higher viscosity and solidification. Multifunctional additives can be employed to assure cross-linking. However, viscosity does not necessarily increase in parallel with polymerization and such discrepancy cannot be easily explained. In this study, an oligomeric ether-ester macro diol (EEMD of 2700 g/mol) was used as a polyol, diluting it with polyethylene glycols (PEG of 200 g/mol or 400 g/mol) for viscosity control. The polyols were mixed with a trifunctional adduct of hexamethylene diisocyanate (HDI3) to initiate the addition reaction and viscosity was monitored, similarly to the previous report [1].

A rotary viscometer Lamy CP-2000 Plus was used with a 1° cone spindle RM100. Beforehand, EEMD was premixed with PEG and heated separately at 50℃ for 15 minutes, as was HDI3. The polyol was mixed with HDI3 at 1+1.4 mol ratio. Within 1 min a 1 mL sample was placed onto a bottom plate of the viscometer, which was preheated to 50°C. The upper spindle was lowered and viscosity was periodically recorded at 100 s^{-1} shear rate. The full rotational (not oscillatory) trajectory was used and the spindle was not removed from the plate until the end of the polymerization test. Three blends were tested: w/o PEG (EEMD at 83.25%+ HDI3 at 16.75% wt/wt), with PEG 200 (at 12.1%+ EEMD at 48.5% + HDI3 at 39.4%) and with PEG 400 (at 22.3% + EEMD at 41.4% + HDI3 at 36.3%). Two runs were performed for each blend, see average values in Fig. 1.

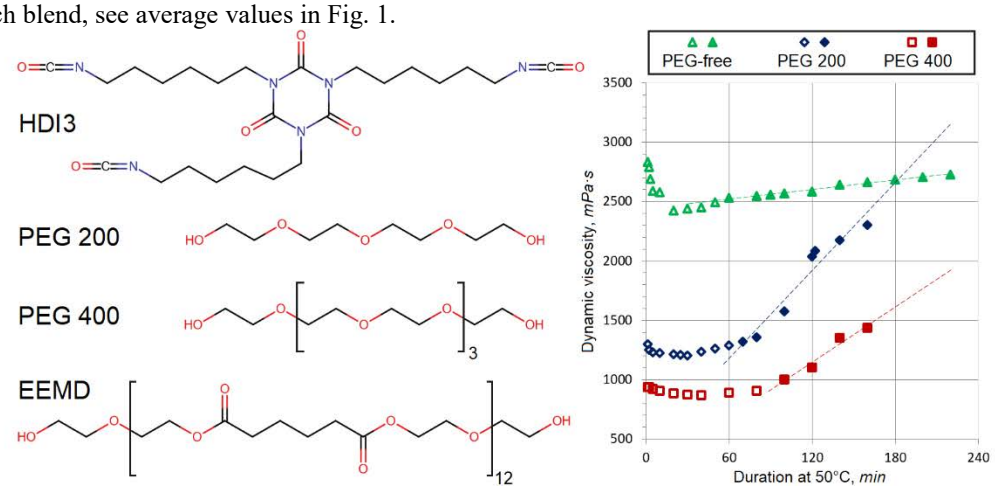

Fig. 1. Left: structures of employed compounds for addition reaction. Right: viscosity change during the reaction between HDI3 and EEMD (with or without PEG); filled symbols denote viscosities, higher than the early values.

Counter-intuitively, all the blends showed some thinning initially. The drop in viscosity was the most evident in the PEG-free blend. On the other hand, this blend was more viscous than the other two. Nevertheless, its polymerization proceeded slower as a result of lower HDI3 concentration and during the later stages viscosity of PEG 200 blend became more similar. The initial viscosity drop was also evident in the blends with PEG. After the drop, viscosity stagnated or was slowly recovering for quite some time. Only well after 1 hr of polymerization viscosities finally exceeded the initial values, which were measured in the beginning of the test. Further viscosity increase approximately followed linear kinetics, with trendline correlations of the average values better than $R^2 = 0.938$.

This suggests that some induction period is present before viscosity begins increasing despite ongoing polymerization. It remains unclear, which factors might cause such induction effect. Inclusion of PEG seems to enhance the effect, because the PEG-free blend simply thinned down initially and began thickening quite soon. Bubble formation or compositional non-homogeneities in the blend are not likely to have a strong effect, since the blends were agitated quite vigorously between the cone and plate of the viscometer when measuring each point.

It might be possible that supramolecular arrangements could yield the observed induction of viscosity increase. However, more diverse formulations, extensive testing and additional analytical techniques might be needed to further elaborate on this hypothesis.

This study was carried out under project TERMINUS, funded by the European Union under Horizon 2020. Call: H2020-NMBP-ST-IND-2018. Grant Agreement: 814400.

[1] S. Mačiulytė, P. Nemaniutė, D. Bražinskienė et al., Influence of ester diluents and chain extension on polyurethane viscosities. Proc. of 22nd Conf. Advanced Materials and Technologies, ISSN 1822-7759, pg 128, Palanga, DOI: 10.5281/zenodo.4064006 (2020).

ISOMORPHOUS SUBSTITUTION AND STABILITY OF SOLID SOLUTIONS IN THE $La_{1-x}Ln_xF_3$, Ln = Ce – Ho SYSTEMS

Yuliia Oleksii[1], Serhii Radio[2], Eugeni Get'man[2]

[1] Faculty of Chemistry, Biology and Biotechnologies; Vasyl' Stus Donetsk National University, Ukraine
[2] Department for Research, Research Laboratory ñChemistry of Polyoxometalates and Complex Oxide Systemsò, Vasyl' Stus Donetsk National University, Ukraine
oleksii.i@donnu.edu.ua

Solid solutions of trifluorides rare-earth elements (REEs) in the form of powders, ceramics, single crystals and nanomaterials are currently being intensively studied since they often surpass the corresponding chlorides and bromides in many properties. They can be used as materials for lasers, scintillators, phosphors, displays, light sources, catalysts, ionic conductors, fibre-optic amplifiers, as well as biological labels, drug delivery agents. It is also known to use trifluorides for microelectronics, analytical chemistry, the technology of separation of elements, regeneration and purification of nuclear fuel.

Using the crystal-chemical approach in the approximation of regular solutions, the mixing energies (interaction parameters) and decomposition temperatures of $La_{1-x}Ln_xF_3$ solid solutions, where Ln = Ceï Ho, are calculated. With an increase in the REE nuclear charge, the calculated mixing energies and critical decomposition temperatures of solid solutions regularly increase from 1.83 to 51.92 kJ/mol and from 110 to 3100 K, respectively, which is due to a decrease in the ionic radii of REEs in the series from Ce to Ho. It is shown that the total value of the mixing energy is determined mainly by the component caused by the difference in the sizes of the substituted structural units. The presented diagram (Fig. 1) for the $La_{1-x}Ln_xF_3$ systems, where Ln = Ceï Ho, makes it possible to estimate not only the thermodynamic stability, instability and metastability of solid solutions in a wide range of compositions and temperatures, but also to predict the limits of substitutions for limited series of solid solutions by a given decay temperature, or their decay temperature at a given substitution limit.

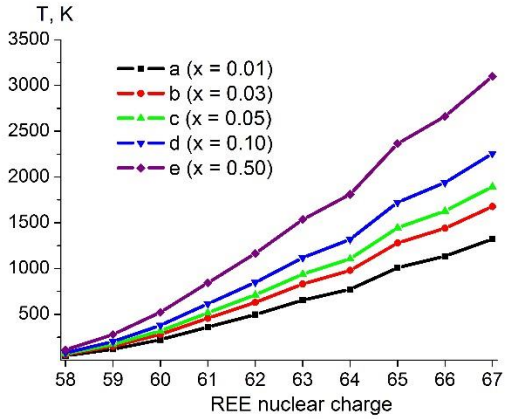

Fig. 1. Dependences of the calculated decomposition temperatures of $La_{1-x}Ln_xF_3$ solid solutions for x = 0.01 (a); x = 0.03 (b); x = 0.05 (c); x = 0.10 (d), and x = 0.50 (e) on the REE nuclear charge (diagram of the thermodynamic stability of solid solutions).

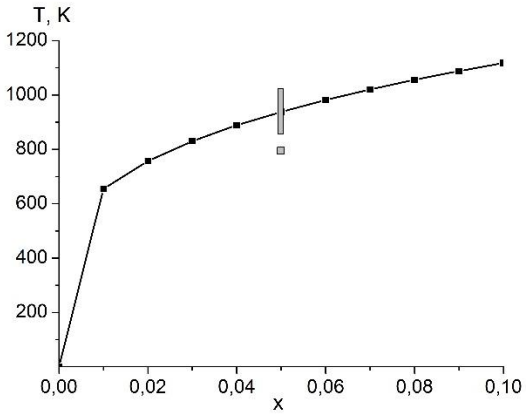

Fig. 2. Dependence of the temperatures (K) of the decomposition of solid solutions of the $La_{1-x}Eu_xF_3$ system on the composition (□) and the synthesis temperature of the solid solution (773K) of the composition $La_{0.95}Eu_{0.05}F_3$ according to the data of [1]. (square). Vertical rectangle ï calculation error.

The calculation results for $La_{1-x}Ce_xF_3$, $La_{1-x}Pr_xF_3$, $La_{1-x}Nd_xF_3$ systems do not contradict the experimental data obtained earlier by instrumental research methods in the sense that continuous series of solid solutions in these systems are in the predicted region of thermodynamic stability. The calculated decomposition temperature of the $La_{0.95}Eu_{0.05}F_3$ solid solution (Fig. 2) is in satisfactory agreement with the experimentally found one [1]. The results of calculations of the mixing energies of the systems under consideration can be used to supplement their phase diagrams in the low-temperature region (to construct a dome of solid solution decomposition).

The study was carried out within the Fundamental Research Programme funded by the Ministry of Education and Science of Ukraine (grants ID 0119U100025, 0120U102059).

[1] T. Grzyb, S. Lis. Photoluminescent properties of $LaF_3:Eu^{3+}$ and $GdF_3:Eu^{3+}$ nanoparticles prepared by co-precipitation method, Journal of Rare Earths **27**, 588ï 592 (2009).

APPLICATION OF STARCH ACETATE FOR REMOVAL OF ALKYL PARABENS FROM AQUEOUS MEDIUM

Karolina Aleknaite, Laura Peciulyte, Deimante Rosliuk, Ramune Rutkaite

Department of Polymer Chemistry and Technology, Kaunas University of Technology, Kaunas, Lithuania
karolina.aleknaite@ktu.edu

Over the past several decades, advancement in societal modernization has led to elevated living standards for human beings and growing self-consciousness in personal care and hygiene. These social evolutions also result in the extensive use of cosmetic and personal care products (CPCPs). The occurrence of CPCP residues in domestic sewage, municipal waste water and waste water treatment systems is inevitable. The monitoring results showed their ambient accumulation exhibiting an increasing trend during the past few years [1]. Among the observed constituents of CPCP residuals, parabens are a group of compounds of concern because of their popularity as additives. Due to their potential toxicity and estrogen-mimicking property, the presence of parabens also poses a potential threat to the stability of microbial communities in a biological treatment system as well as in the ecological environment [2]. Hence, there is a need for search for new ways to additionally eliminate those contaminants.

In this study the synthesized microgranular starch acetate have been tested as a potential sorbent for removal of alkyl parabens from aqueous medium. Starch acetate (SA) microgranules with the degree of substitution of acetyl groups of 0.41 was obtained by reacting potato starch granules with acetic anhydride using aqueous NaOH solution as a catalyst.

The adsorption of alkyl parabens, namely methylparaben (MP), ethylparaben (EP) and propylparaben (PP), on SA microgranules in water has been investigated by employing the equilibrium adsorption method. The adsorption kinetics studies showed that the adsorption equilibrium has been reached within 7 min (Fig. 1A). The obtained isotherms of methyl-, ethyl- and propylparabens on SA at 20 ÁC are presented in Fig. 1B.

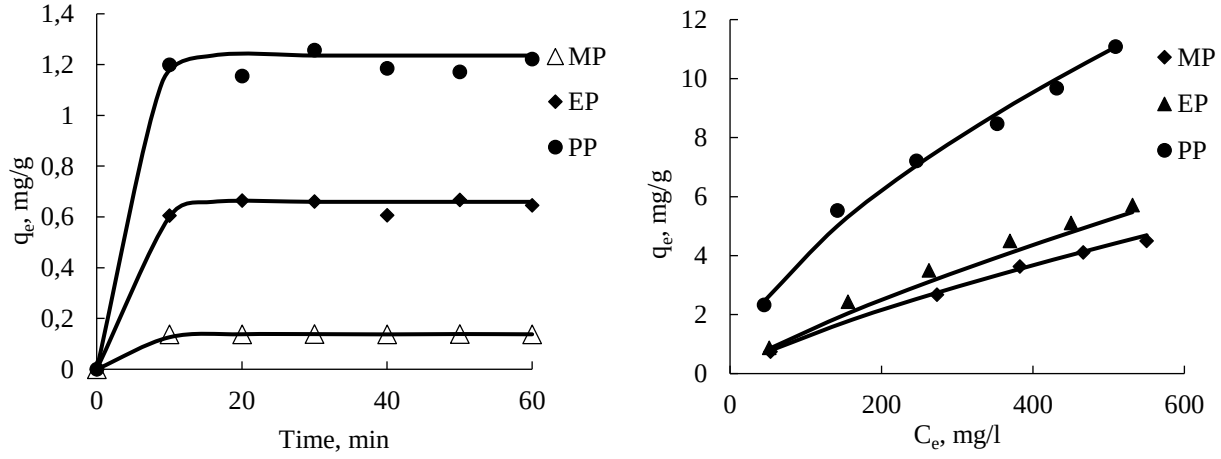

Fig. 1. Adsorption kinetics (A) and isotherms (B) of alkyl parabens on SA at 20 ÁC

Table 1. Adsorption model parameters for adsorption of alkyl parabens on SA at 20 ÁC

Alkyl paraben	Langmuir model		Freundlich model		Dubinin-Radushkevich model	
	Q_L (mg/g)	R^2	n_F	R^2	E_{DR} (kJ/mol)	R^2
MP	10.19	0.965	1.30	0.994	7.2	0.997
EP	13.64	0.992	1.25	0.994	7.1	0.999
PP	16.50	0.969	1.61	0,990	8.2	0.995

The Langmuir, Freundlich and Dubininï Radushkevich adsorption models were used to describe the adsorption isotherms (see Table 1). The adsorption model parameters data revealed that adsorption was mainly due to physical interactions. The values of Langmuir sorption capacity QL increased by increasing the length of alkyl chain in paraben molecule, in the following order: propylparaben > ethylparaben > methylparaben. The obtained results confirmed that SA granules can be promising adsorbent for the removal of parabens from aqueous environments.

[1] Z.R Hopkins, L. Blaney, An aggregate analysis of personal care products in the environment: identifying the distribution of environmentally-relevant concentrations: Environment International 92-93, 301-316 (2016)
[2] C. Haman et al., Occurrence, fate and behavior of parabens in aquatic environments: A review: Water Research 68, 1-11 (2015)

MEASUREMENT OF STORAGE MODULUS IN UNCURED ELASTOMERS USING PLATE-PLATE AND MOVING DIE TECHNIQUES

Audrė Kalinauskaitė [1], Marijus Jurkūnas [1 2], Svajus Asadauskas [1]

[1] Department of Chemical Engineering and Technologies, Center for Physical Sciences and Technology, Lithuania
[2] Faculty of Chemistry and Geoscience, Vilnius University, Lithuania
audre.kalinauskaite@ftmc.lt

Development of new elastomers and their recycling technology is often focused on rheological properties, dynamic moduli in particular [1]. A number of methods can be used for their measurement, primarily highlighting the dependence of storage modulus G' on strain, temperature and other factors. Plate-plate and moving die techniques are often employed. Despite different sample sizes and topography, the techniques exert similar stress onto the elastomer and record the same factors as feedback. This study attempts to compare G', recorded by both techniques on same elastomers. Non-vulcanized Isoprene Rubber (IR) was used to simulate the elastomer with or without squalane (SQ) at 13% wt. as a plasticizer.

Storage modulus G' was measured using the two techniques tuned to operate under similar thermal and mechanical regimes. Plate-plate technique employed a MCR 302 rheometer with Ø 8 mm spindle PP08 (Anton Paar). Temperature sweep was carried out under 0.5% strain at 1 Hz with 5 min preheating for each temperature. Frequency sweeps were taken progressively at 25°C, 100°C and 120°C with 5 min preheating under 0.5% strain, total duration of ~2 h. Load was constant at 1 N. The elastomer samples were pre-cut into Ø 8.5 ± 0.5 mm discs 0.5 ± 0.1 mm thick. Moving die technique employed D-MDR 3000 rheometer (Montech, Germany) with biconical dies per ASTM D6204, guarded by disposable polymer sheets. Strain sweep (0.02 – 90% range, 3 cycles for each angle under 1 Hz) and frequency sweep (0.01 – 50 Hz range, 3 cycles for each frequency under 0.5% strain) were carried concurrently on the same specimen at 25°C, 100°C and 120°C with 5 min preheating and total duration of 2 h per sample. Temperature sweep (25 – 120°C with 5°C step every 1.4 min under 1 Hz and 0.5% strain) was performed on different specimens. In both techniques the attempts were made to avoid bubbles, wrinkles or other imperfections, however perfect adherence to plate surface could not be assured. Built-in software calculated G' whose values were processed from multiple runs using Origin software to derive error bars. The most representative curves are shown in Fig. 1.

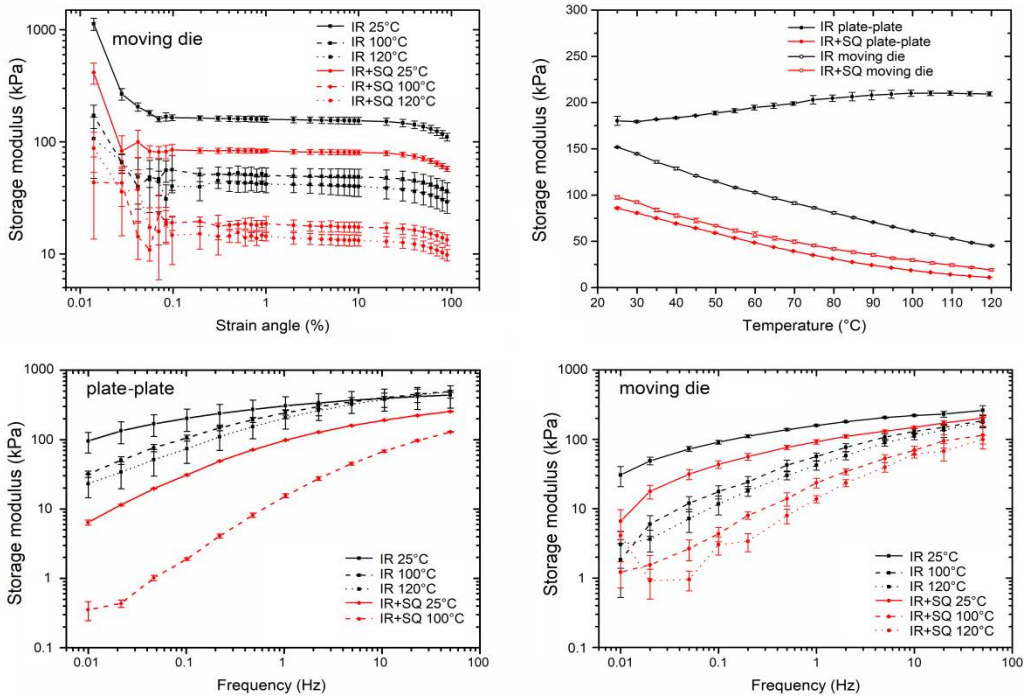

Fig. 1. Variation of storage modulus G' due to increasing strain or temperature (top) or frequency (bottom). Plate-plate (MCR) or moving die (MDR) rheometers were used.

Temperature effects on non-plastified IR appear inexplicably opposite. Despite these and other differences in recorded values, tendencies of G' dependence on frequency and plastification appear similar and match expectations. It can be noted that frequency sweep at 120°C by the plate-plate technique matches results from other researchers quite well [1]. Therefore, both techniques can be instrumental in evaluation of rheological properties of elastomers and composites.

[1] X. Sun, A.I. Isayev, Ultrasound devulcanization: comparison of synthetic isoprene and natural rubbers, J. Materials Sci. **42** (17), 7520-7529 (2007).

SYNTHESIS, CHARACTERIZATION, AND INVESTIGATION OF NITROGEN-DOPED CARBON SUPPORTED MANGANESE-COBALT NANOPARTICLES

Loreta Tamaġauskaitā-Tamaġiî naitā, Eivilā Budrytā, Aldona Balį iî naitā, JÎ ratā Vaiį iî nienā, Eugenijus Norkus

Department of Catalysis, Center for Physical Sciences and Technology, Saulātekio Ave. 3, LT-10257, Vilnius, Lithuania
loreta.tamasauskaite@ftmc.lt

The development and investigation of various materials used in fuel cells, as a renewable energy source, is a major challenge among the scientific community. In this study, nitrogen-doped carbon (N-doped C), which has a graphene-like structure, has been chosen as a support for the deposition of Mn-Co nanoparticles (Mn-CoNPs) using microwave heating method to use them as anode material for direct hydrazine fuel cells (DHFCs), likewise, identify its features as a supercapacitor. For comparison, pure CoNPs/N-doped C and MnNPs/N-doped C catalysts have been synthesized under identical conditions.

The structure, morphology, and composition of nanocomposites have been characterized using Transmission Electron Microscopy (TEM), Raman Spectroscopy, X-ray Photoelectron Spectroscopy (XPS), and Inductively Coupled Plasma Optical Emission Spectroscopy (ICP-OES). Moreover, electrochemical performance has been investigated by cyclic voltammetry (CV) in a 1 M Na_2SO_4 solution at the scan rates of 1, 5, 10, 20, 100, and 150 mV s^{-1}. Cyclic voltammograms on the prepared catalyst have been also recorded in a 0.05 M N_2H_4 + 1 M NaOH solution at a potential scan rate of 10 mV s^{-1}.

It has been determined that Mn-CoNPs/N-doped C, CoNPs/N-doped C, and MnNPs/N-doped C catalysts show an enhanced electrocatalytic activity towards the oxidation of hydrazine in an alkaline medium and it is controlled by the diffusion processes. What is more, it was found that the specific capacitance (C_s) value for the Mn-CoNPs/N-doped C nanocomposite in a 1 M Na_2SO_4 solution was equal to 497.5 F g^{-1} at a scan rate of 1 mV s^{-1} and decreased to 254.4 F g^{-1} at a scan rate of 150 mV s^{-1}. The Mn-CoNPs/N-doped C catalyst preserves 51.1 % of its specific capacitance as the scan rate increases from 1 mV s^{-1} to 150 mV s^{-1}. The obtained results confirmed the good performance of the prepared Mn-CoNPs/N-doped C nanocomposite as the electrode material for supercapacitors application.

INVESTIGATION OF HYDROGEN PEROXIDE REDUCTION ON COPPER-NICKEL FOAMS

Aldona Balčiūnaitė, Titas Stanevičius, Loreta Tamašauskaitė-Tamašiūnaitė, Eugenijus Norkus

Department of Catalysis, Center for Physical Sciences and Technology, Saulėtekio ave. 3, LT-10257, Vilnius, Lithuania
aldona.balciunaite@ftmc.lt

In this study, the copper-nickel (Cu-Ni) foams have been investigated as a catalyst for the reduction of hydrogen peroxide (H_2O_2). The Cu-Ni foams have been prepared using the low-cost electrochemical metal deposition method. Chemical baths contained a constant concentration of Cu^{2+} ions (0.05 M) and different concentrations of Ni^{2+} ions in the range from 0.05 to 0.5 M have been used for the electrodeposition of the Cu-Ni foams on the titanium (Ti) surface. The surface morphology, structure, and composition of the prepared catalysts have been examined using Scanning Electron Microscopy (SEM), X-Ray Diffraction (XRD), and Inductively Coupled Plasma Optical Emission Spectroscopy (ICP-OES). The electroactivity of the prepared catalysts has been evaluated for the reduction reaction of H_2O_2 employing linear sweep voltammetry in a 0.1 KOH electrolyte at a potential scan rate of 50 mV s^{-1}.

It was found that the best electroactivity for the H_2O_2 reduction reaction shows the Cu-Ni foams deposited using a chemical bath contained 0.05 M Cu^{2+} ions and 0.2 M Ni^{2+} ions. Moreover, H_2O_2 reduction current density recorded on the Cu-Ni foams in the O_2-saturated 0.1 M KOH solution containing 5 mM H_2O_2 is ca. 1.3 times higher than that in the O_2-saturated 0.1 M KOH solution without H_2O_2.

Acknowledgment

This research is funded by the European Social Fund under Measure No. 09.3.3-LMT-K-712-19-0138 "Development of Competences of Scientists, other Researchers, and Students through Practical Research Activities".

NITROGEN-DOPED CARBON SUPPORTED WITH GOLD NANOPARTICLES AS AN EFFICIENT CATALYST FOR GLUCOSE ELECTRO-OXIDATION

Daina Upskuvienė[1], Jūratė Vaičiūnienė[1], Ivar Kruusenberg[2], Katlin Kaare[2], Aleksandrs Volperts[3], Galina Dobele[3], Aivars Zurins[3], Loreta Tamašauskaitė-Tamašiūnaitė[1], Eugenijus Norkus[1]

[1]Department of Catalysis, Center for Physical Sciences and Technology, Sauletekio Ave. 3, LT-10257, Vilnius, Lithuania
[2]National Institute of Chemical Physics and Biophysics, Akadeemia Tee 23, 12618, Tallinn, Estonia
[3]Latvian State Institute of Wood Chemistry, Dzerbenes Street 27, Riga LV-1006, Latvia
Saulėtekio Ave. 3, LT-10257, Vilnius, Lithuania
e-mail.: daina.upskuviene@ftmc.lt

This study is focused on the preparation of gold nanoparticles (AuNPs) supported carbon (C) and nitrogen-doped activated carbon (N-doped C) nanocomposites and their application for the electro-oxidation of glucose. The AuNPs/N-doped C nanocomposite has been prepared by a two-step process. At first, activated wood-based carbon has been prepared from alder charcoal and doped with nitrogen by pyrolyzing samples at a temperature of 800 ÁC in the presence of dicyandiamide (DCDA). Further, the AuNPs have been deposited on the obtained N-doped activated carbon material or carbon using glucose and ascorbic acid as reducing agents. The prepared nanocomposites have been characterized by scanning electron microscopy (SEM), energy-dispersive spectroscopy (EDS), X-ray powder diffraction (XRD), Raman and X-ray photoelectron spectroscopy (XPS). The electrocatalytic activity of the nanocomposites for glucose electro-oxidation has been investigated in alkaline media using cyclic voltammetry.

It has been determined that the AuNPs/N-doped C and AuNPs/C nanocomposites had a higher catalytic activity for the electro-oxidation of glucose than the pure Au or carbon and N-doped carbon alone, indicating the synergistic effect of AuNPs and N-doped carbon or carbon. Moreover, the highest activity shows the AuNPs supported N-doped carbon as compared with that of AuNPs supported carbon.

ASSESSMENT OF THE IGNALINA NUCLEAR POWER PLANT INFLUENCE ON RADIOCARBON CONCENTRATION IN LAKE DRUKSIAI

Laurynas Butkus[1], RÎ ta Barisevi ļ iÎ tā[1], Justina Ġapolaitā[1], Ģilvinas Eġerinskis[1], Evaldas Maceika[1], Algirdas Pabedinskas[1], Andrius Garbaras[1], Vidmantas Remeikis[1]

[1] State Research Institute Center for Physical Sciences and Technology, Vilnius, Lithuania
laurynas.butkus@ftmc.lt

Radiocarbon (^{14}C) is a long-lived carbon isotope that has a half-life of 5730 Ñ 40 years. Nuclear power plants are one of the main producers of anthropogenic radiocarbon. Anthropogenic radiocarbon can be released into the environment in gaseous forms, with liquid releases or with spent nuclear fuel. Despite this pollution is not significant in the sense of population exposure doses, but it is a significant ^{14}C increase above background effect that allows the use it as an anthropogenic contamination tracer to study the dissemination, accumulation, and dynamics redistribution processes of the pollutant in ecosystem [1].

The lake sediment and fish scale samples were collected from the Druksiai lake. The lake water was used to cool the reactors of the Ignalina nuclear power plant (INPP). ABA (acid-base-acid) chemical pretreatment procedure was used to extract humin (HM) and humic acid (HA) fractions from the sediments (from two different lake sediment columns). Radiocarbon measurements in these samples were performed using the accelerator mass spectrometer (AMS).

^{14}C measurements in humin and humic acid fraction have shown that atmosphere-lake CO_2 exchange accounted for about 22% carbon in bottom sediments. During the 1983-1998 period, ^{14}C-enriched dissolved inorganic carbon (DIC) was continuously released into Lake Druksiai. During that time, an average of about 0.24 GBq of radiocarbon was released per year. Measurements of radiocarbon concentrations in fish (both benthic and pelagic) confirm that the ^{14}C contamination was in dissolved inorganic form.

Around 2000, ^{14}C-enriched DIC (2.3 GBq radiocarbon) was released into Lake Druksiai from Ignalina NPP. Furthermore, organic compounds were additionally released in the same year. These compounds were not ^{14}C-enriched but affected the interaction between humic and humic acids. After 11 years after the end of the INPP operation, the concentration of radiocarbon in the bottom sediments is higher than in the atmosphere.

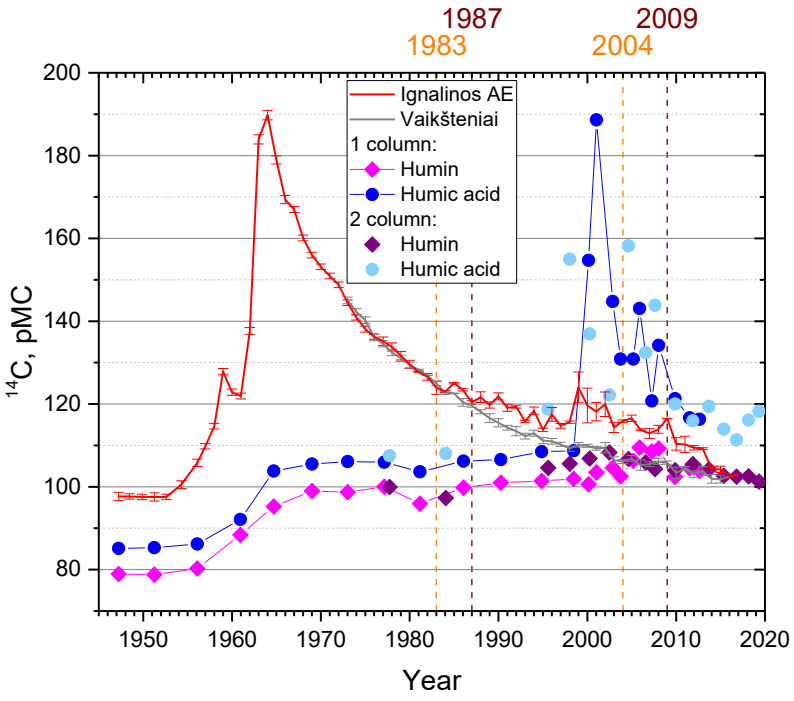

Fig. 1. Temporal ^{14}C variations in Lake Druksiai

[1] R. Barisevi ļ iÎ tā et al., Tracing Carbon Isotope Variations in Lake Sediments Caused by Environmental Factors During the Past Century: A Case Study of Lake Tapeliai, Lithuania, Radiocarbon 61(4), 885ï 903 (2019).

INFLUENCE OF PEAT EXTRACT ON THE PROPERTIES OF LIQUID FERTILIZERS

Goda Gudinskaitā, Danguolā Jakimaviļ iÎ tā, Rasa Ġlinkġienā

Faculty of Chemical Technology, Kaunas University of Technology, Lithuania
goda.gudinskaite5@gmail.com

Dolomite is a carbonate-grade mineral that contains calcium and magnesium. The color of this mineral can vary from white to brown depending on the number of impurities. Powdered dolomite is easily decomposed by mineral acids while carbon dioxide is released. Although dolomite-bearing rocks are found all over the world, the most famous quarries are in the Midwestern United States, Canada, Switzerland, Spain, and Mexico [1]. Large dolomite quarries are also exploited in northern Lithuania. Dolomite is used as a thermal insulation material, also in agriculture as a liming material, electrical engineering, ceramics, paint, glass and building materials industry. This mineral can also be used as a source of calcium magnesium in the production of fertilizers by decomposing it with various concentrations of nitric acid.

Based on previous research in our department, different concentrations (35, 40, 45 %) of nitric acid were used in this work for the decomposition of dolomite. Decomposition was performed at room temperature at 20ï 25 ŰC. Excess of 20 % and 40 % nitric acid was compared to the stoichiometric amount and used. It was found that the reaction is faster and decomposition takes 50 minutes, when 140 % acid is used. During the decomposition, the temperature increased to 40ï 50 ŰC and not only CO_2 gas but also brown NO_2 gas was released too. In this way, in the production of liquid fertilizers, it is necessary to provide for the purification of the different gases in the technological line. During the decomposition for 50 minutes, the highest concentration of CaO and MgO was obtained when 45 % nitric acid was used in the dolomite decomposition process.

Solutions after the decomposition are very acidic, so neutralization needs to be performed. 25 % ammonia water was chosen for this process. Liquid nitrogen calcium magnesium fertilizer solutions of different pH values were prepared for neutralization using different amounts of ammonia water. The produced fertilizers contained ~10 % N, ~6 % CaO and ~4 % MgO. The physical properties of the prepared fertilizer solutions, which are important for the development of the liquid fertilizer production technology, are given in the table.

Table. Physico chemical properties of aqueous solutions of calcium magnesium and ammonium nitrates

Sample No.	Ammonia water quantity, %	Crystallization temperature, ŰC	pH	Density, g/cm^3	Viscosity, mm/s^2	Electrical conductivity, mS/cm^3
1	11.6	-30	4.15	1.364	2.395	138.4
2	11.8	-32	4.50	1.364	2.390	137.8
3	12.9	-30	5.10	1.360	2.282	135.8

In order to increase the nitrogen concentration in the fertilizer, and after evaluating the solubility data of multicomponent systems available in the literature, additional nitrogen-increasing substances such as urea was added. These substances increased the nitrogen concentration in liquid fertilizers, but do not increase their crystallization temperature, which is one of the most important positive properties of liquid fertilizers. After decomposition of dolomite with nitric acid, neutralization of solutions and addition of urea, the nitrogen concentration increased to 22 %.

To produce the most efficient liquid fertilizers, a peat extract additive was added to the solutions, which acts as a bioactive substance, activates the processes taking place in the soil and improves the uptake of nutrients in plants [2]. UAB ñKlasmann-Deilmannò Ġlutā peat and potassium hydroxide were used to obtain the extract. Up to 20 % of the obtained extract was added to the liquid fertilizer. In the laboratory test, it was found that the addition of peat extract to liquid nitrogen calcium magnesium fertilizers reduced the nitrogen concentration from ~22 % to ~16 %, and the addition of the extract did not affect the calcium and magnesium concentration. The pH value of liquid fertilizers with peat extract increases and varies between 5.5 and 7.0, the density increases from 1.265ï 1.270 g/cm^3 to 1.332ï 1.335 g/cm^3 and the viscosity increases from 0.55ï 0.75 mm/s^2 to 0.65ï 0.84 mm/s^2. The crystallization temperature of liquid nitrogen calcium magnesium fertilizers with peat extract varies in the range of -12.5 ï -15 ŰC. All the specified physical properties comply with the requirements for liquid fertilizers.

In conclusion, a solution of the decomposition of dolomite with 45 % nitric acid, neutralized with 25 % ammonia water and with the addition of 38 % urea can produce liquid nitrogen calcium magnesium fertilizers containing 21.5 % N, 3.8 % K_2O, 3.6 % CaO and 2.5 % MgO with a crystallization temperature of 3 ÁC. Addition of 20 % peat extract can be used to produce bioactive liquid nitrogen calcium magnesium fertilizers containing 15.1 % N, 3.8 % K_2O, 3.6 % CaO and 2.5 % MgO with a crystallization temperature of -15 ÁC.

[1] Warner, John. Dolomite: occurrence, evolution, and economically important associations. Earth-Science Reviews (2000).
[2] Dziadek, K. Basic chemical composition and bioactive compounds content in selected cultivars of buckwheat whole seeds, dehulled seeds and hulls. J. Cereal Sci. 69, 1-8 p. (2016).

OPTICAL AND REDOX PROPERTIES OF POLYMETHINE DYES

Hanna Maltanava[1], Nikita Belko[2], Michael Samtsov[2], Sergey Poznyak[1*]

[1] Research Institute for Physical Chemical Problems, Belarusian State University, Belarus
[2] A. N. Sevchenko Institute of Applied Physical Problems, Belarusian State University, Belarus
poznyak@bsu.by

Polymethine dyes (PD) have become important for many biomedical applications, including photodynamic therapy of cancer [1]. Among a great number of polymethine dyes, indotricarbocyanine dyes attract special interest due to long-wavelength absorption possessing a high penetration depth into the majority of biological tissues. To increase the water solubility and specificity of accumulation in tumor, indotricarbocyanine dyes can be modified with biocompatible compounds, such as polyethylene glycols [1]. Some features of the photochemical transformations of indotricarbocyanine dyes can be investigated using the combination of cyclic voltammetry and optical spectroscopy to reveal the parameters for optimal performance of dyes in model and physiological media. Herein, we studied the optical and redox properties of different indotricarbocyanine dyes by optical spectroscopy and cyclic voltammetry.

Symmetric cationic indotricarbocyanine dyes (PD1−4) were synthesized and purified as previously described [2]. The concentration of dyes in acetonitrile solutions was 0.14 mM (PD1), 0.25 mM (PD2, PD3) and 0.2 mM (PD4). The redox activity of the indotricarbocyanine dyes was examined by cyclic voltammetry (CV) using an Autolab PGSTAT 302N potentiostat in a standard three-electrode cell. Pt disc electrode (diameter - 0.4 mm) and Pt wire were used as the working and the counter electrodes, respectively. An Ag/Ag+ (0.01 M $AgBF_4$) electrode (+0.32 V relative to the SCE) served as the reference electrode. UV-vis spectra were acquired on a SOLAR PV 1251 spectrophotometer.

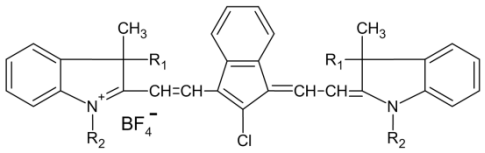

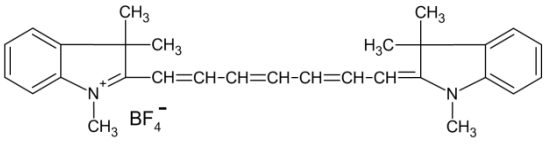

PD1 (R_1=CH_3,R_2=C_3H_6COOH); **PD4**
PD2 (R_1=CH_3, R_2=$C_3H_6COOPEG_{300}$); **PD3** (R_1=C_2H_5, R_2=CH_3)

Fig.1. Structural formulas of the studied indotricarbocyanine dyes.

Figure 2a demonstrates the absorption spectra of indotricarbocyanine dyes in acetonitrile containing a supporting electrolyte (0.1 M tetrabutylammonium tetrafluoroborate ($TBABF_4$)). The absorption maxima of the long-wavelength band of dyes are at 713 (PD1 and PD2), 705 (PD3), and 739 nm (PD4). Figure 2b shows typical CV curves recorded for the dyes in the range from –0.5 to 1.1 V (sweep rate - 0.2 V/s). The pronounced wave is observed at anodic polarization. Moreover, maximum of this wave (E_{ox}) as well as reversibility of the electrooxidation depend significantly on the structure of the dye. The dyes PD1−3, characterized by the same structure of the polymethine chain, but different groups bound to nitrogen atoms of heterocycle, have similar E_{ox} values ranging from 0.88 to 0.91 V. Moreover, the dyes PD2 and PD3 demonstrate a relatively high reversibility of the oxidation process. The electrooxidation of the PD1 is only partially reversible: the reduction wave on the reverse scan is much smaller in magnitude than the oxidation wave. At the same time, the PD4 exhibits completely irreversible oxidation process with E_{ox} = 0.55 V.

Fig. 2. Absorption spectra (a) and CV curves (b) of indotricarbocyanine dyes in acetonitrile containing 0.1 M $TBABF_4$. The curve number corresponds to the dye number in Fig.1.

Based on the literature data [2], it can be assumed that the electrooxidation of cyanine dyes PD1−4 in the potential range of 0.4 – 1.1 V is associated with the formation of radical dication. The stability of radical dications, as measured by their anodic CV response, is markedly dependent on the structure of the dye. The radical dications of PD4, which has no substituents in the polymethine chain, undergo rapid dimerization through the even carbon atoms of the polymethine chain, which explains the irreversibility of the oxidation reaction of this dye. The appearance of a substituent (aromatic ring) in the polymethine chain in the case of PD1−3 dyes creates steric hindrance for the dimerization reaction of the resulting radical dications, which significantly increases their lifetime and, accordingly, the reversibility of the electrooxidation process.

[1] A. A. Lugovski, M. P. Samtsov, K. N. Kaplevsky et al., Novel indotricarbocyanine dyes covalently bonded to polyethylene glycol for theranostics, J. Photochem. Photobiol. A: Chem. **316**, 31-36 (2016).
[2] R. L. Parton, J. R. Lenhard, Dimerization reaction of cyanine radical dications, J. Org. Chem. **55**, 49-57 (1990).

P6-42

DID NOT PARTICIPATE

FABRICATION OF PHOSPHOR IN GLASS MATRIX MATERIALS UTILIZING NOVEL LOW MELTING TEMPERATURE PHOSPHATE GLASSES

Mantas Norkus[1], Gediminas Niaura[2,3], RamÎ nas Skaudģius[1*]

[1] Faculty of Chemistry and Geosciences Institute of Chemistry, Vilnius University, Naugarduko st. 24, LT-03225 Vilnius, Lithuania
[2] Department of Organic Chemistry, Center for Physical Sciences and Technology (FTMC), Saulãtekio Ave. 3, LT-10257, Vilnius, Lithuania
[3] Institute of Chemical Physics, Faculty of Physics, Vilnius University, Saulãtekio Ave. 3, LT-10257, Vilnius, Lithuania
mantas.norkus@chgf.vu.lt

Incandescent light sources have mostly been shifted out of their application areas with the commercialization of LED lighting solutions, especially with the rise of white LEDs [1]. One of the most common ways of easily realising such a device is to combine yellow phosphor (YAG:Ce^{3+}) dispersed in silicone or other organic resin and blue emitting InGaN chips. This kind of technology has its limitations: in application areas where high brightness of LEDs are required arises a need to use high current densities which in turn makes the junction between blue LED and yellow phosphor dramatically increase in temperature, which has an impact on the longevity of the phosphor composite. At high temperatures the thermal aging of the silicone resin is sped up, which leads to luminous efficiency degradation and constant color shift thus leading to reduction in long-term reliability [2,3]. In order to improve thermal characteristics and extend LEDs operating temperature range several solutions have been proposed in recent literature, such as, the usage of various inorganic glasses both as matrices and as composite materials for phosphors, crystallizing phosphors directly in molten glass precursors or synthesizing transparent ceramic phosphor plates [4].

In this work phosphate glasses with different compositions were synthesized and established as host materials for Eu^{3+} ions. The glass precursors and luminescent materials were ground and mixed together, melted in a muffle furnace. The molten mixture was poured into premade brass molds and heated again at lower temperatures to relieve internal stress (named melt-quenching technique). The obtained samples were polished and characterized by x-ray diffractometry, scanning electron microscopy, Raman spectroscopy, photoluminescence measurements and inductively coupled plasma optical emission spectrometry.

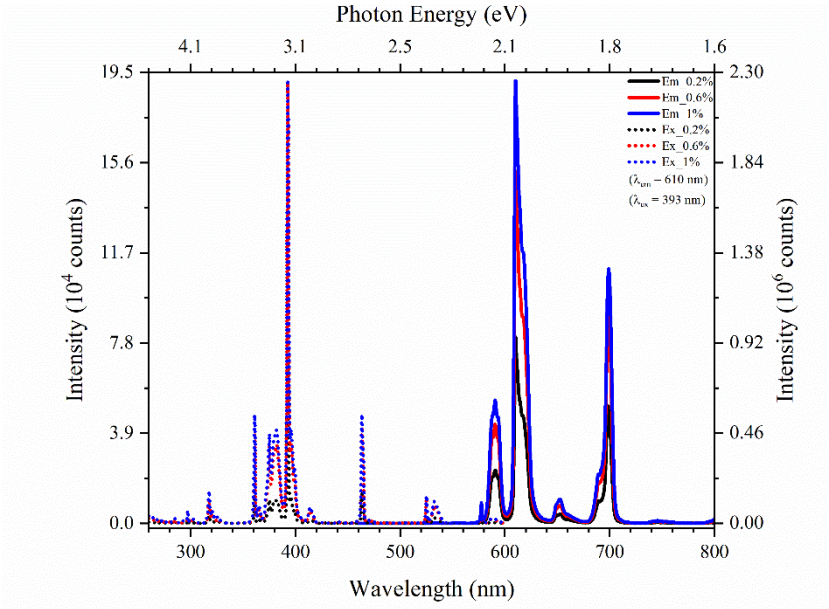

Figure 1. Emission and excitation spectra of phosphate glasses with different mol% of Eu^{3+}

[1] S. Nakamura, M. Senoh, S.I. Nagahama et al., InGaN-Based Multi-Quantum-Well-Structure Laser Diodes, Japanese Journal of Applied Physics, **35**, L74-L76, (1996).
[2] J. J. Wierer, J. Y. Tsao, D. S. Sizov, Comparison between blue lasers and light-emitting diodes for future solid-state lighting, Laser & Photonics Reviews, **7**, 963-993, (2013).
[3] M.H. Chang, D. Das, P. V. Varde, M. Pecht, Light emitting diodes reliability review, Microelectronics Reliability, **52**, 762-782, (2012).
[4] H. Lin, T. Hu, Y. Cheng et al. Glass Ceramic Phosphors: Towards Long-Lifetime High-Power White Light-Emitting-Diode Applications-A Review, Laser & Photonics Reviews, **12**, 1700344 (2018).

A MICROWAVE-FACILITATED SYNTHESIS OF MAGNETIC Fe_3O_4 NANOPARTICLES

Gytaute Sirgedaite[1], Lina Mikoliunaite[1, 2]

[1] Department of Physical Chemistry, Institute of Chemistry, Faculty of Chemistry and Geosciences, Vilnius University, Lithuania

[2] Department of Organic Chemistry, Center for Physical Sciences and Technology, Lithuania

gytaute.sirgedaite@chgf.stud.vu.lt

Over the last two decades, magnetic nanoparticles have gained popularity due to their thermophysical properties, which can be applied in various disciplines - biology, medicine, chemistry, physics. There are many applications of nanoparticles and they are making progress in many fields of science: drug delivery, therapeutic agents for cancer treatment, magnetic resonance imaging, biological sensors, catalysts, magnetic recording media [1].

Magnetic nanoparticles are obtained from oxides of iron, cobalt, or nickel, which have special properties, such as surface and volume ratios, and high magnetic moments. Iron oxide nanoparticles are selected for magnetic studies due to their easy availability and superparamagnetic properties [2], [3]. The size of the nanoparticles ranges from 10 nm to 100 nm. The shape and size of nanoparticles are important parameters for synthesis and application because a large surface area increases reactivity, ion transfer, or contact. Besides, physical properties such as shape, composition, charge, and solubility can unpredictably change nanoparticles behaviour. It is therefore important to discover methods to obtain desired size, shape, and properties of magnetic nanoparticles [1].

Magnetic nanoparticles are synthesized using three different preparation routes a) biological methods, b) physical methods, and c) chemical methods. Physical methods are easy to perform, however, control of the particle size is difficult. Biological methods assuring low cost, high yield, reproducibility, but time-consuming. Chemical synthesis methods are mainly used due to low production cost and high productivity. Chemical synthesis route involves electrochemical method, sol-gel method, hydrothermal method, chemical co-precipitation, microemulsion, solvothermal method, microwave method. Comparing these techniques, each of them has advantages and disadvantages, depending on size, structure, time, yield, reproducibility. In all these techniques, aqueous medium is the most efficient pathway to obtain iron magnetic nanoparticles. It has been demonstrated that the particle size, as well as the polydispersity of the nanoparticles, could be tailored by changing factors such as Fe^{2+}/Fe^{3+} ratio, base (NaOH, ammonium hydroxide), and ionic strength. Other factors as mixing rate, temperature, agitation, pH, and reactants ratio influence nanoparticles size as well [4].

In this work, we present a comparison of iron oxide nanoparticles synthesized by microwave technique. Different synthesis time, temperature was investigated as well as reduction agent. Obtained nanoparticles were investigated using X-Ray Spectroscopy, Transmission Electron Microscopy and Raman Spectroscopy.

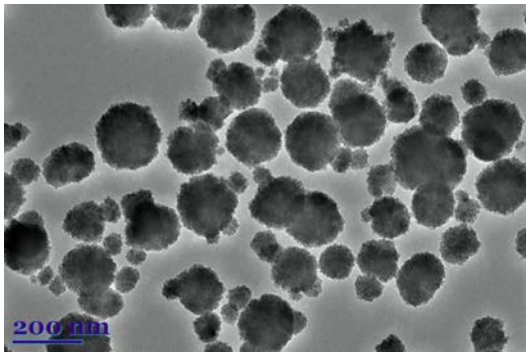

Fig. 1. TEM image of magnetic iron oxide nanoparticles synthesized using microwave synthesis reactor.

Acknowledgement

This research is funded by the European Social Fund under the No 09.3.3-LMT-K-712 ñDevelopment of Competences of Scientists, other Researchers and Students through Practical Research Activitiesò measure.

[1] A. S. Teja, P.Y. Koh, Synthesis, properties, and applications of magnetic iron oxide nanoparticles. Progress in Crystal Growth and Characterization of Materials, **55**(1-2), 22-45 (2009).

[2] V. Chaudhary, R. Chaudhary, *Magnetic Nanoparticles: Synthesis, Functionalization, and Applications. Encyclopedia of Nanoscience and Nanotechnology*, (Valencia: American Scientific Publishers, 2018).

[3] D. Xiao, et al., Preparation and highlighted applications of magnetic microparticles and nanoparticles: a review on recent advances. Microchimica Acta, **183**(10), 2655ï 2675 (2016).

[4] A. Ali, et al., Synthesis, characterization, applications, and challenges of iron oxide nanoparticles. Nanotechnology, Science and Apllications, **9**, 49ï 67 (2016).

P6-45

DID NOT PARTICIPATE

FLUORENE-BASED ENAMINES AS LOW-COST AND DOPANT-FREE HOLE TRANSPORTING MATERIALS FOR HIGH PERFORMANCE AND STABLE PEROVSKITE SOLAR CELLS

Sarune Daskeviciute[1], Cristina Momblona[2], Kasparas Rakstys[1], Albertus Adrian Sutanto[2], Maryte Daskeviciene[1], Vygintas Jankauskas[3], Alytis Gruoodis[3], Giedre Bubniene[1], Vytautas Getautis[1], Mohammad Khaja Nazeeruddin[2]

[1] Department of Organic Chemistry, Kaunas University of Technology, Lithuania
[2] Group for Molecular Engineering of Functional Material, Institute of Chemical Sciences and Engineering, £cole Polytechnique F®d®rale de Lausanne, Switzerland
[3]Institute of Chemical Physics, Vilnius University, Lithuania
sarune.daskeviciute@ktu.lt

The power conversion efficiency of perovskite solar cells is approaching the Shockleyï Queisser limit, and therefore this technology is next to the commercialization stage [1]. Inexpensive and stable hole transporting materials are highly desirable for the successful scale-up. Most high performing devices generally employ expensive hole conductors that are synthesized via cross-coupling reactions which require expensive catalysts, inert reaction conditions and time-consuming sophisticated product purification [2]. In a quest to employ cost-effective chemistry to combine the building blocks, we explore enamine-based small molecules that can be synthesized in a simple condensation reaction from commercially available materials leading to an estimated material cost of a few euros per gram.

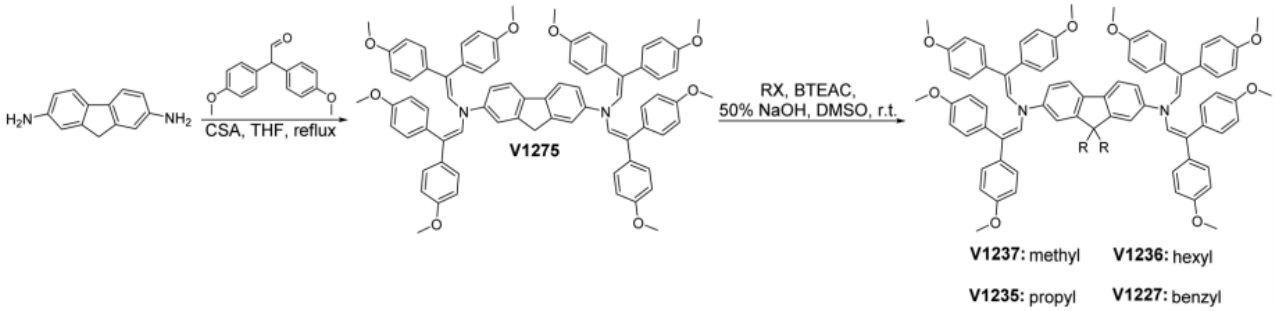

Fig. 1. Straightforward reaction scheme of fluorene enamine HTMs and their molecular structures.

The synthesized fluorene-based enamines exhibit a very high hole mobility up to 3.3 Ĭ 10^{-4} cm^2 V^1 s^1 and enable the fabrication of perovskite solar cells with a maximum power conversion efficiency of 19.3% in a doped configuration and 17.1% without doping. In addition, both PSC systems demonstrate superior long-term stability compared to spiro-OMeTAD.

	HTM	V_{OC} (mV)	J_{SC} (mA cm^{-2})	FF	PCE (%)	R_S (Ω)	HTM thickness (nm)
Doped-HTM	**V1275**	1077	23.24 (23.11)	0.77	19.3	5.9	~150
	V1237	1090	22.97 (22.74)	0.76	19.2	6.2	~150
	V1235	1089	22.86 (22.85)	0.77	19.2	5.1	~150
	V1236	1094	22.95 (22.94)	0.76	19.1	5.2	~150
	V1227	1024	22.32 (21.82)	0.55	12.6	26.0	~120
	Spiro-OMeTAD	1115	22.97 (21.86)	0.77	19.7	5.7	~260
Dopant-free HTM	**V1275**	1033	22.95 (22.81)	0.72	17.1	22.2	~70
	V1237	1038	22.98 (22.93)	0.71	16.9	22.9	~70
	V1235	1029	23.09 (22.81)	0.70	16.6	24.5	~70
	V1236	1022	23.02 (22.88)	0.69	16.2	25.2	~70
	Spiro-OMeTAD[58]	972	22.83	0.47	10.4		

Table 1. Photovoltaic parameters, series resistance, and thickness of the fluorene-based enamine HTMs extracted from the best-performing devices.

This work shows that hole transporting materials prepared via a simple condensation protocol have the potential to compete in terms of performance with materials obtained via expensive cross-coupling methods at a fraction of their cost and deliver exceptional stability of the final device.

[1] NREL, *Photovoltaic Research: Best Research Cell Efficiency Chart*, https://www.nrel.gov/pv/cell-efficiency.html, accessed 28 April 2020.
[2] T. P. I. Saragi, T. Spehr, A. Siebert, T. Fuhrmann-Lieker and J. Salbeck, *Chem. Rev.*, 2007, 107, 1011ï 1065.

P6-47

DID NOT PARTICIPATE

MODELING OF ELECTROCHEMICAL-BASED IMMUNOSENSORS FOR THE DETECTION OF SPECIFIC ANTIBODIES

Maryia Drobysh[1], Viktorija Liustrovaite[2], Alma Rucinskiene[3], Martynas Simanavicius[4], Aurelija Zvirbliene[4], Rimantas Slibinskas[4], Ieva Plikusiene[1,2], Evaldas Ciplys[4], Arunas Ramanavicius[1,2]

[1]Department of Functional Materials and Electronics, State Research Institute Center for Physical Sciences and Technology, Lithuania
[2]Department of Physical Chemistry, Faculty of Chemistry and Geosciences, Vilnius University, Lithuania
[3]Department of Electrochemical Materials Science, State Research Institute Center for Physical Sciences and Technology, Lithuania
[4]Institute of Biotechnology, Life Sciences Center, Vilnius University, Lithuania
maryia.drobysh@ftmc.lt

For the purpose to handle the ongoing pandemic of the coronavirus disease 2019 (COVID-19) rapid, specific, sensitive, and simple diagnosis methods are required. The causative agent of the COVID-19 is severe acute respiratory syndrome coronavirus 2 (SARS-CoV-2), whose RNA, structural proteins, or antibodies against it can act as target biomolecules for the detection of infection in a patient sample. Biosensors are widely used for the identifications of informational biomolecules, namely, nucleic acids [1] and proteins. The latter type includes immunosensors, which work principal is the detection of antigen-antibody coupling [2]. One of the most common types of immunosensors are based on electrochemistry, because of their affordability and simplicity without loss in accuracy and sensitivity.

Our study aimed to investigate the possibility to develop a novel method for viral disease diagnosis employing a common electrochemical technique. In our work, we used electrochemical impedance spectroscopy (EIS) as a powerful tool for observing the interaction between an immobilized virus antigen and antiviral antibodies at the modified working electrode surface. Immobilization of the antigen and formation of the antigen-antibody complex affected ion diffusion and electrical capacitance, thus influencing on electrochemical impedance of electrodes [3]. To immobilize the virus antigen on the working surface a self-assembled monolayer (SAM) was used, as an effective reusable tool for stable covalent binding of biomolecules to the different solid surfaces [4]. SAM modification was applied to the working gold electrode being part of an electrochemical cell that also included the platinum counter electrode and the reference [$Ag/AgCl/KCl_{sat}$] electrode.

Our experiments showed correspondences between impedimetric signals and stepwise modifications of electrode surface. We achieved a reproducible trend of significant increasing electrical impedance, i.e. electron-transfer resistance, on the key stage of antibody coupling. That fact indicates an increase in the layer thickness on the working surface and thereby testifies to the registered interaction. Hence, our outcome gives us the reason to suggest EIS-based immunosensor as an effective, rapid, easy to use, and to interpret detection tool. It is also worth noting that our experiment will serve as the basis for our further research in the field of electrochemical biosensors for the diagnosis of viral diseases in particular COVID-19.

---

[1] A. Ramanaviciene, A. Ramanavicius, Pulsed amperometric detection of DNA with an ssDNA/polypyrrole-modified electrode, Analytical and Bioanalytical Chemistry **379**, 287-293 (2004).
[2] A. Ramanaviciene, N. German, et.al., Comparative study of surface plasmon resonance, electrochemical and electroassisted chemiluminescence methods based immunosensor for the determination of antibodies against human growth hormone, Biosensors Bioelectronics **36(1)**, 48-55 (2012).
[3] A. Ramanavicius, A. Finkelsteinas, et.al., Electrochemical impedance spectroscopy of polypyrrole based electrochemical immunosensor, Bioelectrochemistry **79(1)**, 11-16 (2010).
[4] A. Ramanaviciene, A. Kausaite-Minkstimiene, et.al., Comparative study of random and oriented antibody immobilization techniques on the binding capacity of immunosensor, Analytical Chemistry **82(15)**, 6401-6408 (2010).

THE EFFECT OF STABILIZING AGENTS IN SOL-GEL SYNTHESIS OF $BiVO_4$ COATINGS

Donatas Plėškys[1], Irena Savickaja[2], Vidas Pakštas[2], Arnas Naujokaitis[2], Jurga Juodkazytė[2], Milda Petruleviļienė[2]

[1] Institute of Chemistry, Faculty of Chemistry and Geosciences, Naugarduko str. 24, LT-03225 Vilnius University, Lithuania

[2] Center for Physical Sciences and Technology, Department of chemical engineering and technology Saulėtekio av. 3, LT-10257 Vilnius)

e-mail: donatas.pleskys@chgf.stud.vu.lt

Recently, photoelectrochemical (PEC) sensing techniques have attracted substantial research interest in the area of detection of biomolecules. Compared to conventional electrochemical methods, the PEC sensor has high sensitivity and a low background signal, which can be ascribed to its separate excitation source and detection signals [1]. Efficiency of PEC systems strongly depends on photoanodes, which convert the energy of visible light into chemical energy. Among the various photoelectrodes studied for PEC applications, monoclinic bismuth vanadate ($BiVO_4$) is considered to be a promising material owing to its moderate band gap (2.4 eV) and appropriate band-edge positions, which allow it to absorb as much as 11% of the solar spectrum. Nevertheless, the photocatalytic activity of bare $BiVO_4$ is still not ideal for practical applications because of its excessive charge recombination, poor charge transport, and slow oxidation kinetics [2].

In our work citric acid, urea and polyethylene glycol (PEG) were used as stabilizing agents for formation of $BiVO_4$ thin films in sol-gel approach. Organic additives serve as complexing agents of Bi^{3+} ion, therefore different morphology and photoelectrochemical properties of $BiVO_4$ coatings are obtained. Ratio of citric acid and PEG to $BiVO_4$ was chosen to be 2:1, however ratio of urea to $BiVO_4$ was 0.5:1, because at higher amounts of urea formation of precipitates occurred. After dip-coating of $BiVO_4$ on conducting glass (FTO) substrate all samples were annealed at 450ÁC for 2h. Crystallinity and morphology of coatings were evaluated using X-ray diffraction (XRD) and scanning electron microscopy (SEM) analysis. Photoelectrochemical response of obtained coatings were analyzed using cyclic voltammetry in three electrode cell in 0.5M Na_2SO_4 solution in the dark and under illumination (Fig. 1). Photoelectrochemical oxidation of glucose was studied in three electrode cell in sodium borate buffer (pH=9) with 5-35mM of glucose.

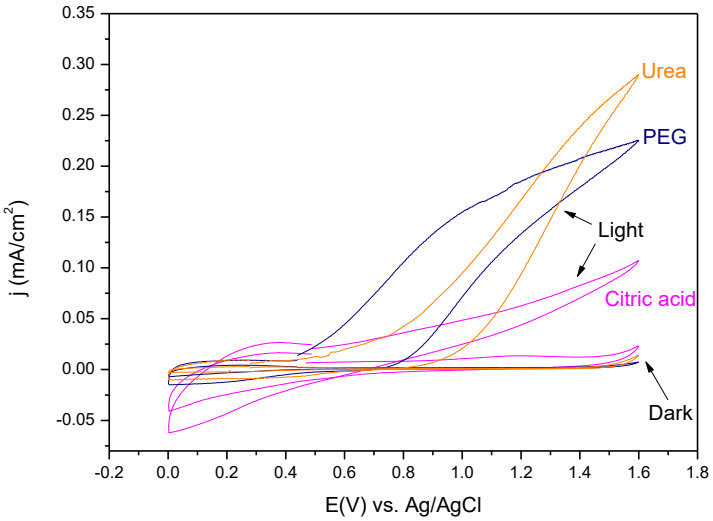

Fig. 1. Cyclic voltammograms of BiVO4 electrodes in 0.5 M Na_2SO_4 solution; potential scan rate 50 mV/s, intensity of illumination ~ 100 mW cm^{-2}

Obtained results revealed, that different stabilizing agents strongly influence morphology and PEC activity of the coatings. The highest photocurrent was obtained for coating synthesized with urea (Fig. 1). Photoelectrochemical oxidation of glucose showed the linear enhancement of photocurrent with increased concentration of glucose in the range of 5 ~ 35 mM. Obtained sensitivity of $BiVO_4$ for glucose detection will be evaluated and presented.

[1] S. Wang, S. Li, W.Wang et al. A non-enzymatic photoelectrochemical glucose sensor based on BiVO4 electrode under visible light, Sensors and Actuators B: Chemical, **291**, 34-41 (2019).

[2] L. Xia, J. Li, J. Bai et al. BiVO4 Photoanode with Exposed (040) Facets for Enhanced Photoelectrochemical Performance, Nano-micro Letters **11**, 1-10 (2018).

MODIFICATION OF $BiVO_4$ AND INVESTIGATION OF PHOTOELECTROCHEMICAL ACTIVITY

Laura Michailova[1,2*], Irena Savickaja[2], Gintarã Pleļ kaitytã[2], Arnas Naujokaitis[2], Vidas Pakġtas[2], Milda Petruleviļ ienã[2], Jurga Juodkazytã[2], Rimantas Ramanauskas[2]

[1] Institute of Chemistry, Faculty of Chemistry and Geosciences, Naugarduko str. 24, LT-03225 Vilnius University, Lithuania

[2] Center for Physical Sciences and Technology, Department of chemical engineering and technology Saulãtekio av. 3, LT-10257 Vilnius)

e-mail: laura.michailova@chgf.stud.vu.lt

Overuse of fossil fuels has resulted in serious environmental problems, and global energy shortages have become an increasingly urgent issue. Consequently, clean and renewable energy sources such as solar energy have become an attractive way to address this energy crisis. Photoelectrochemical (PEC) water splitting and organic pollutant degradation driven by visible light have attracted worldwide attention as promising applications of solar energy. However, a key technical problem faced in PEC application is the development of suitable photoelectrodes, which play an important role in the PEC conversion of solar energy to chemical energy[1].

Over the last two decades, bismuth vanadate ($BiVO_4$) has attracted much attention as one of the most efficient, robust and inexpensive metal oxide photoanodes. Photoactive c-$BiVO_4$ with 2.4 eV band gap energy can absorb UV and visible light up to 520 nm [2]. Particle size, porosity and morphology of bismuth vanadate can be controlled with the help of structure directing agents used in the synthesis.

In this work sol-gel approach and dip-coating technique was applied to synthesize bismuth vanadate coatings using different amounts of polyethylene glycol (PEG) (1% and 3%) as a structure directing agent. It was investigated how different $BiVO_4$:PEG ratios influence the morphology and photoelectrochemical response of the thin films. Composition and morphology of the coatings were analyzed by means of XRD and SEM techniques. TG-DSC analysis was used to analyse the thermal decomposition of the precursor solution mixture. Photoelectrochemical activity of $BiVO_4$ films was investigated using cyclic voltammetry in three electrode cell in 0.5 M NaCl solution in the dark and under illumination.

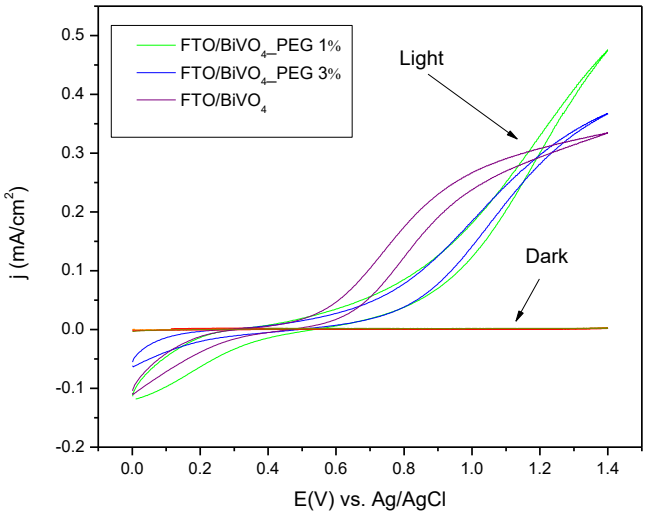

Fig. 1. Cyclic voltammograms of unmodified and PEG-modified $BiVO_4$ electrodes in 0.5 M NaCl solution; potential scan rate 50 mV/s, intensity of illumination ~ 100 mW cm^{-2}

It was found that morphology of coatings strongly depends on amount of PEG used in the synthesis. Results of cyclic voltammetry (Fig. 1) revealed differences in photoelectrochemical performance of the samples.

Acknowledgment:
This research is funded by the European Social Fund under the No 09.3.3-LMT-K-712-22-0286 ñDevelopment of Competences of Scientists, other Researchers and Students through Practical Research Activitiesò measure.

[1] M. Fakhrul, R. Samsudina, R. Bashirib, Tailoring the morphological structure of BiVO4 photocatalyst for enhanced photoelectrochemical solar hydrogen production from natural lake water, Journal of the Taiwan Institute of Chemical Engineers **93** 582ï 589 (2018)

[2] L. Guo, J. Li, N. Lei, Q. Son et al., Morphological evolution and enhanced photoelectrochemical performance of V^{4+} self-doped, [010] oriented BiVO4 for water splitting, Journal of Colloid and Interface Science **534**, 37ï 46 (2019)

NEW BIPOLAR HOSTS FOR HIGH EFFICIENCY OLEDS

Simas Macionis[1], Dalius Gudeika[1], Dmytro Volyniuk[1], Oleksandr Bezvikonnyi[1], Jiun Haw Lee[2], Pei-Hsi Lee[2], Chia-Hsun Chen[2], Tien-Lung Chiu[3], Juozas V. Grazulevicius[1]

[1] Department of Polymer Chemistry and Technology, Kaunas University of Technology, Radvilenu pl. 19, LT-50254, Kaunas, Lithuania, [2] Graduate Institute of Photonics and Optoelectronics, National Taiwan University, 1, Section 4, Roosevelt Road, Taipei 10617, Taiwan, [3] Department of Electrical Engineering, Yuan Ze University, 135 Yuan-Tung Road, Taoyuan 32003, Taiwan
simas.macionis@ktu.edu

Organic light-emitting diodes (OLEDs) nowadays represent one of the most promising and dominant technology in the market of displays and illumination equipment. OLEDs are superior to competitive technologies with respect of mechanical flexibility, low response time, quality of image, transparency, low mass and wide range of working temperatures [1,2]. In this work blue phosphorescent organic light-emitting diodes (PhOLEDs) with maximum external quantum efficiency from 22.7 to 30.5% were fabricated using new bipolar derivatives of benzimidazole linked through phenyl spacer with the different number of *tert*-butyl substituted carbazoles, as hosts. Applicability of the newly synthesized compounds as hosts for blue PhOLEDs was justified by their high triplet levels (2.94-2.98 eV), bipolar transporting properties with charge mobilities up to 2.34×10^{-3} cm^2/Vs at electric field of 2.7×10^5 V/cm, and high ionization potentials (5.63-5.81 eV).

[1] N. Savage, Tomorrowôs industries: from OLEDs to nanomaterials, Nature **576,** (7786):S20-S22, (2019).
[2] K. Leo, Efficient and flexible solution, Nat. Photon, **5**, 716 (2011).

THE APPLICATIONS OF PRUSSIAN BLUE IN pH SENSING

Povilas Virbickas[1], Aug÷ra ValiÎnien÷[1], Gabija Kavaliauskait÷[1], Gerda Çi¿i¿Înait÷[1]

[1] Faculty of Chemistry and Geosciences, Vilnius University, Lithuania
povilas.virbickas@chgf.vu.lt

Sensing of pH is often applied as a signal transduction way in biosensors, whereas chemical reactions catalyzed by some enzymes (e.g. glucose oxidase, urease, etc.) are accompanied with the change in pH of local environment [1, 2]. Moreover, pH sensing can be used to determine several physiological and pathological conditions for health care purpose, e.g. higher than normal pH of sweat can be related to the dehydration and/or cystic fibrosis [3]. Therefore, creation of reliable and accurate ways of pH sensing is important in the development of biosensors and other healthcare devices.

Prussian blue (PB) is an inorganic pigment widely applied in formation of sensors and biosensors [4]. Even though PB is most commonly used in (bio)sensors due to its selectivity to hydrogen peroxide [4, 5], PB also could be applied in sensing systems due to its optical [6, 7] and electrochemical [8, 9] sensitivity to the changes in pH of solution. Furthermore, optical sensitivity of PB to changes in pH have been successfully applied in construction of biosensor for urea [6].

In this study comparison between optical and electrochemical ways of pH sensing with PB layers is presented and differences between preparation of PB coatings for optical and electrochemical sensing of pH are discussed. The stability of PB layers during measurements of pH and the influence of composition of analysis solution on the performance of optical and electrochemical measurements of pH are also considered in this study.

The main difference between structures of PB, which are required for optical and electrochemical measurements of pH, is based on amount of Fe^{2+} ion in the crystal lattice of PB. In optical measurements of pH ñinsolubleò form of PB ($Fe^{3+}{}_4[Fe^{2+}(CN)_6]_3$) is used [6, 7]. The optical sensitivity of ñinsolubleò PB to the change in pH is based on reversible hydrolysis of PB (Eq. (1)), which occurs due to increase in OH^- ion concentration in solution [6, 7]. This reversible hydrolysis of pH causes a decrease in absorption of PB, thus, pH of solution can be determined from absorption spectrum of PB. This pH-induced change in absorption of PB layer can be possibly applied in construction of naked-eye sensing devices, which are very convenient for unqualified users. However, PB-based optical sensing of pH has some limitations ï when pH value of solution is higher than 9 an ñinsolubleò form of PB over goes irreversible hydrolysis caused by destruction of $Fe^{3+}[Fe^{2+}(CN)_6]^-$ ion (Eq. (2)). Therefore, optical PB-based sensors of pH can be utilized in analysis of sample with pH value up to 9. Nevertheless, during the PB-based optical analysis of pH high concentrations of K^+ ion should be avoided, since K^+ can induce spontaneous transformation of the ñinsolubleò PB into the ñsolubleò form.

$$Fe^{3+}{}_4[Fe^{2+}(CN)_6]_3 + 3H_2O \rightleftharpoons Fe(OH)_3 + 3Fe^{3+}[Fe^{2+}(CN)_6]^- + 3H^+ \quad (1)$$

$$3Fe^{3+}[Fe^{2+}(CN)_6]^- + 3OH^- \text{ Ÿ } Fe(OH)_3 + 3[Fe^{2+}(CN)_6]^{4-} \quad (2)$$

Even though PB has not been involved in formation of the electrochemical pH sensor yet, PB exhibits the dependency of charge transfer through PB film on pH [8, 9], which can be observed during the measurement of electrochemical impedance spectroscopy and cyclic voltammetry. This relation between pH and charge transfer resistance of PB is explained [8, 9] by the role of hydrogen ion in charge transport through the PB film ï it is postulated that hydrogen ion is involved in electron-hopping between neighboring active positions in the PB [8, 9]. Therefore, the PB-coated electrode could be possibly used as an electrochemical pH sensor. Moreover, ñsolubleò form of PB ($K^+Fe^{3+}[Fe^{2+}(CN)_6]$) is suitable for observation of pH impact on charge transport through the PB [8, 9]. The ability to use ñsolubleò PB makes the electrochemical measurement of pH more accurate, since ñsolubleò PB exhibits better electrochemical stability and it is able to undergo multiple redox transitions [8, 9]. Moreover, ñsolubleò form of PB is considered to be more stable in alkaline conditions ï during our recent investigation ñsolubleò form of PB appeared to be stable in pH values up to 11 [1]. Therefore, electrochemical sensing of pH with PB seems to be promising tool in the development of biosensors and other healthcare devices.

[1] A. ValiÎnien÷, P. Virbickas, G. Medvikyt÷, A. Ramanavi¸ius. Urea Biosensor Based on Electrochromic Properties of Prussian Blue. Electroanalysis **32**, 503ï 509 (2020).
[2] A. A. Karyakin, O. A. Bobrova, L. V. Lukachova, E. E. Karyakina. Potentiometric biosensors based on polyaniline semiconductor films. Sensors and Actuators B **33**, 34ï 38 (1996).
[3] E. Scarpa, V. M. Mastronardi, F. Guido et al. Wearable piezoelectric mass sensor based on pH sensitive hydrogels for sweat pH monitoring, Scientific Reports **10**, 10854 (2020).
[4] Y. Matos-Peralta, M. Antuch. Reviewð Prussian Blue and Its Analogs as Appealing Materials for Electrochemical Sensing and Biosensing. Journal of the Electrochemical Society **176**, 037510 (2020).
[5] A. A. Karyakin. Advances of Prussian blue and its analogues in (bio)sensors. Current Opinion in Electrochemistry **5**, 92ï 98 (2017).
[6] R. Koncki, T. Lenarczuk, A. Radomska, S. Glab. Optical biosensors based on Prussian Blue films. Analyst **126**, 1080ï 1085 (2001).
[7] R. Koncki, O. S. Wolfbeis. Composite Films of Prussian Blue and N-Substituted Polypyrroles: Fabrication and Application to Optical Determination of pH. Analytical Chemistry **70**, 2544ï 2550 (1998).
[8] J. J.Garc²a-Jare¶o, J.Navarro-Laboulais, F.Vicente. Charge transport in prussian blue films deposited on ito electrodes. Electrochimica Acta **41**, 835ï 841 (1996).
[9] J. J. Garc²a-Jare¶o, A. Sanmat²as, J. Navarro-Laboulais, F. Vicente. The role of potassium and hydrogen ions in the Prussian Blue ⇆ Everitt÷s Salt process. Electrochimica Acta **44**, 395ï 405 (1998).

CHLOROPHYLL a IMMOBILIZATION INTO TETHERED BILAYER LIPID MEMBRANE

Viktorija Liustrovaite[1], Ausra Valiuniene[1], Gintaras Valincius[2], Arunas Ramanavicius[1, 3]

[1]Department of Physical Chemistry, Faculty of Chemistry and Geosciences, Vilnius University, Vilnius, Lithuania
[2]Centre for Natural Sciences, Vilnius University, Vilnius, Lithuania
[3]Laboratory of Nanotechnology, State Research Institute Center for Physical Sciences and Technology, Vilnius, Lithuania
viktorija.liustrovaite@chgf.stud.vu.lt

Chlorophyll (Chl-a) is a special ´-´-conjugated structure situated around its macrocyclic skeleton, and the variety of side groups around it allows all photosynthetic species to serve as a major photoactive and structural part [1]. Chl-a has been created by evolution to interact with light and is responsible for absorbing the sun photons and converting their energy into chemical bond energy in a shape that is open to nearly all life forms [2]. It is believed that chlorophyll is in the cell plasma membrane, which means that the area between the cell outer and inner medium is divided, and its nature and arrangement are providing a shape to the cell [3]. The tethered bilayer lipid membrane (tBLM) is a complex system that can be used as an experimental platform for fundamental studies of the structure and function of the bio membrane. In this work, one of such models, tBLM on the gold surface are formed by using the fusion of vesicles [4]. This immobilized membrane alteration enables different biosensors to be produced by adding lipid components such as DOPC (1,2-dioleoyl-sn-glycero-3-phosphatidylcholine) and cholesterol [5], having stability which can be modified by adding molecules such as chlorophyll a (Chl-a).

The aim of this study is to create phospholipid bilayer model with immobilized Chl-a. The investigation is performed with electrochemical impedance spectroscopy (EIS) to measure dielectric capacity and conductivity changes. Fluorescence microscopy (FM) is used to estimate the morphology of the membranes. The goal of this research is to explore the effectiveness of incorporating the photoactive compound Chl-a into the tethered bilayer lipid membrane in order to build a platform that could be used in the future for the development of photosensitive surface structures based on tBLM that could theoretically be used for the development of new biomimetic artificial leaves and biosensors.

---

[1] J. M. Anderson, A. Melis, Localization of different photosystems in separate regions of chloroplast membranes (photosynthesis/chloroplast structure/chloroplast function/reaction center/membrane differentiation), Proceedings of the National Academy of Sciences, **80(3)**, 745-749 (1983).
[2] B. Krª utler, S. Hº rtensteiner, Chlorophyll catabolites and the biochemistry of chlorophyll breakdown, Chlorophylls and Bacteriochlorophylls, 237-260 (2007).
[3] M. E. El-Khouly, E. El-Mohsnawy, S. Fukuzumi, Solar energy conversion: From natural to artificial photosynthesis, Journal of Photochemistry and Photobiology C: Photochemistry Reviews, **31**, 36-83 (2017).
[4] A. ValiÎ nienã, I. Gabriunaite, M. Poderyte, A. Ramanavicius, Electroporation of a hybrid bilayer membrane by scanning electrochemical microscope, Bioelectrochemistry, **136**, 107617 (2020).
[5] G. Valincius, M. Mickevicius, Tethered phospholipid bilayer membranes: An interpretation of the electrochemical impedance response, Advances in Planar Lipid Bilayers and Liposomes, **21**, 27-61 (2015).

STUDY OF FORMATION OF TIN SULFIDE LAYERS ON POLYAMIDE SHEET

Joana Sinkeviļ iÎ tā[1], Remigijus Ivanauskas, Ingrida Ancutienā, Algimantas Ivanauskas

[1] Department of Physical and Inorganic Chemistry, Kaunas University of Technology, Lithuania,
joana.sinkeviciute@ktu.edu

Inorganicï organic composites are a quickly developing group of materials with a tremendous range of highly tunable structural, physical and chemical properties. High compositional variability of these materials allows incorporating variety of inorganic compounds. Of particular interest are composite materials with group IVï VI group binary chalcogenides, which possess unique physical properties of tremendous importance to modern science and technology. Among them, tin sulphide (SnS) has attracted the attention of many researchers because of its higher absorption coefficients (>10^4 $cm^{i\,1}$) and the energy gap of ~1.3 eV [1]. It is made the composites with layer of SnS potential applicability in the field of solar energy conversion strategies [2]. In addition, SnS has great potential for use in memory switching devices, holographic recording systems and as an anode material for lithium batteries [3]. In this work for formation of tin sulphide layer on polyamide PA 6 sheets sorption/diffusion method in two stages was used.

Polyamide sheets attributed to the semi-hydrophilic polymer. Therefore, there is capable to absorb ions of various electrolytes from aqueous solutions. This fact allows sulfur anions with a low oxidation state to be introduced into PA sheets. Further treatment of sulfurized PA sheets with metal salts water solution leads to the formation of metal sulfide layers on the surface and matrix of the polymer sheets.

The aim of this study was to select the most suitable compounds for polymer sheet saturation with anions of low oxidation state sulfur as well as formed tin sulfide layers on polymer. Firstly, the pieces of boiled polyamide sheets (Tecamid 6, 500 μm thickness, Germany) 15×60 mm in size were treated in a thermostatic vessel for one hours in solution of sulfurization agent. As sulfurization agents we used the solutions of higher polythionic acids, $H_2S_nO_6$ (n = 5÷33) and their potassium salts ($K_2S_nO_6$). In the second stage the pieces of sulfurized PA sheets were treated with a solution of divalent tin precursor solution.

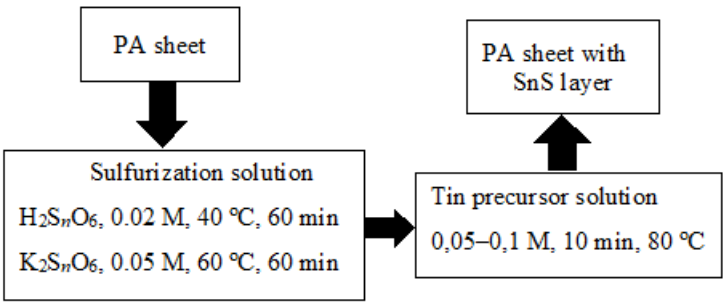

Fig. 1. Schematics of tin sulfide layer formation procedure.

Structural and elemental composition of the obtained layers were investigated by atomic absorption spectroscopy (AAS) and X-ray diffraction (XRD) analysis.

Acknowledgements.
This research is funded by the European Social Fund under the No 09.3.3-LMT-K-712-22-0252 ñDevelopment of Competences of Scientists, other Researchers and Students through Practical Research Activitiesò measure.

[1] M.G. Sousa, A.F. da Cunha, P.A. Fernandes, Annealing of RF-magnetron sputtered SnS_2 precursors as a new route for single phase SnS thin films, Journal of Alloys and Compounds **592**, 80-85 (2014).
[2] V.E. Gonz§lez-Flores, R. Neendoor et. al., Thin film solar cells of chemically deposited SnS of cubic and orthorhombic structures, Thin Solid Films **672**, 62-65 (2019).
[3] B. Purusottam Reddya, M. Chandra Sekhara et.al, Solution-based spin-coated tin sulfide thin films for photovoltaic and supercapacitor applications, Materials Research Bulletin **103**, 13ï 18 (2018).

VARIATIONS OF RARE EARTH ELEMENTS IN THE BOTTOM AND FLY WOOD ASH

Megija Neimane[1], VitŪijs Lazarenko[1], MŪris BŪrtiÁģ[1], Arturs Vǫksna[1], Dagnija LazdiÁa[2], Kristaps Makovskis[2], Ilze KŪrkliÁa[2], Andis LazdiÁģ[2]

[1]University of Latvia, Faculty of Chemistry, Jelgava street 1, Riga, Latvia
[2]Latvian State Forest Research Institute ñSilavaò, Riga street 111, Salaspils, Latvia
megijaneimanee@gmail.com

Wood ash is biomass obtained by the combustion of wood products (wood chips, logs, etc.). Burning wood products produces about 6-10% ash from the total weight of wood. Wood ash contains a high amount of macro- and micro-elements. However, several studies show that wood ash also contains rare earth elements. Wood ash is produced in large quantities through the combustion of wood for energy and heat production. For example, factories (for energy production) and boiler houses (for heat production) use wood products as fuel.

Nowadays, several applications have been found for the use of wood ash. In several European Union countries, wood ash is used in road construction and asphalting works. However, the most common application of wood ash is as a fertilizer for agricultural and forest soil. The high content of macro- and micro- elements in the wood ash ensures plants with the necessary nutrients and reduces soil acidity. The use of wood ash can create biocycle, increase the amount of renewable energy, reduce the number of landfill sites and CO_2 emissions.

Wood ash dived into two main types ï bottom ash and fly ash. Bottom ash is a coarsest and granulated ash fraction with particle size 0.4-4.7 mm that contains impurities (stones, sands, etc.) and most of the wood ash mass consists of silicon (~57 %) and calcium (~19 %). Fly ash is the finest fraction with particle size 12-250 ε m which contains inorganic compounds and a small amount of unburned carbon.

The aim of this research was to evaluate rare earth element content in the bottom and fly wood ash. Both types of wood ash samples were collected from boiler houses from different parts of Latvia in 2014. Wood ash samples were extracted in 5 mL of concentrated HNO_3 by using a shaker (5 hours, 190 rpm). The resulting solution was diluted with deionized water and filtered (Whatman 541) to get rid of undissolved particles. The rare earth element content was determined by ICP - MS (Agilent 8900 ICP-QQQ) analysis method. The pH and electrical conductivity were also determined in the extract in the water.

Obtained results show that wood ash is a highly basic material (pH > 12). The electrical conductivity of bottom ash is higher than fly ash. The content of rare earth elements shows the diversity of the contents between the bottom and fly wood ash.

AB INITIO CALCULATIONS OF $Na_{1+2x}Mn_xTi_{2-x}(PO_4)_3$ (x = 0.0; 1.0) RAMAN SPECTRA

Nojus Radzevičius[1], Linas Vilčiauskas[1,2]

[1] Institute of Chemistry, Faculty of Chemistry and Geosciences, Vilnius University, Lithuania
[2] Center for Physical Sciences and Technology (FTMC), Saulėtekio al. 3, LT-10257, Lithuania
Nojus.Radzevicius@chgf.stud.vu.lt

The search for new battery electrode materials is becoming one of the most active areas of research in modern chemistry and materials science. NASICON-structured phosphate framework compounds with general formula $Na_xMe_2(PO_4)_3$, where Me is usually a transition metal, started to emerge as some of the most potent solid electrolyte and electrode materials for the upcoming generation of Na-ion batteries. [1] They show superior thermal and electrochemical stability, low-cost and environmental sustainability. However, the complete understanding of factors governing their properties and limitations is still lacking.

Density Functional Theory (DFT) calculations have become a standard tool for calculating the electronic structure and molecular properties of, in principle, any chemical system. They not only help to obtain physical parameters but also proved to be extremely helpful in elucidating chemical properties, analyzing spectroscopic data, guiding materials synthesis etc. Raman spectroscopy is a versatile tool to not only investigate the vibrational properties but also relate them to other material properties, identify phases and their formation signatures. [2]

In this study, we perform hybrid DFT calculations, compute their Raman spectra and compare results to experiments of $Na_{1+2x}Mn_xTi_{2-x}(PO_4)_3$ (x = 0.0; 1.0) compounds. The calculations results show good agreement with the available experimental data (see Fig. 1) and indicate that Raman spectroscopy is a capable technique for investigating phase formation in this and similar systems and that DFT calculations are indispensable for helping to interpret the spectroscopic data.

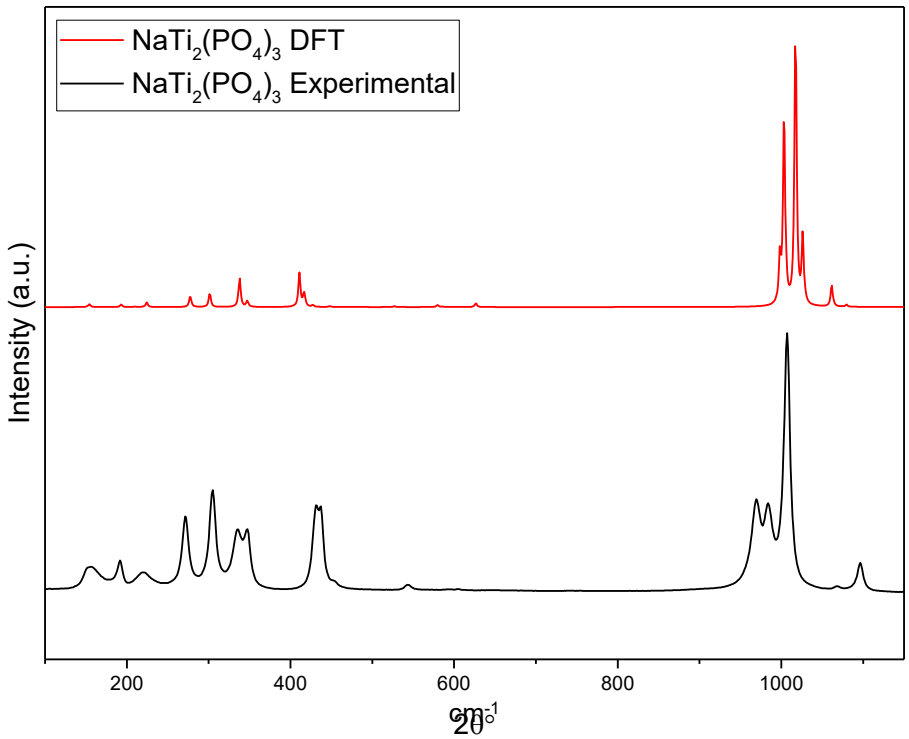

Fig. 1. Comparison of DFT calculated and experimental Raman spectra for $Na_{1+2x}Mn_xTi_{2-x}(PO_4)_3$ (x = 0.0).

[1] H. Gao, J. B. Goodenough, Angew. Chem. Int. Ed. **55**, 12768-12772 (2016).
[2] D. Gryaznov, S. K. Stauffer, E. A. Kotomin, L. Vilčiauskas, Phys. Chem. Chem. Phys. **22**, 11861-11870 (2020).

SYNTHESIS AND CHARACTERIZATION OF DIBENZOTHIOPHENE DERIVATIVES AS THERMALLY ACTIVATED DELAYED FLUORESCENCE EMITTERS

Tomas Janeliunas[1], Malek Mahmoudi[1], Melika Ghasemi[1], Dalius Gudeika[1], Dmytro Volyniuk[1], Juozas Vidas Grazulevicius

[1] Department of Polymer Chemistry and Technology, Kaunas University of Technology, Lithuania
tomas.janeliunas@ktu.edu

Thermally activated delayed fluorescence materials have emerged as the most promising candidates for constructing high-performance organic light-emitting-diodes (OLEDs) due to their efficient harvest of both singlet and triplet excitons through the reverse intersystem crossing (RISC) process [1,2]. In this work organic semiconductors with differently substituted donor-acceptor molecular structure were synthesized and investigated by different experimental methods. The molecular structures were certified through ^{1}H and ^{13}C NMR spectroscopies, mass spectrometry. The following characterizations of new compounds were mainly performed 1) photophysical measurements, 2) evaluation of thermal properties, 3) energy level measurements, 4) charge transport characterization. Upon such examinations it was concluded that, their neat films emit cyan/green fluorescence with PLQY of 7.7% in the best case. Their 5% weight loss temperature exceeded of 300 ^{o}C. Ionization potentials of the studied compounds were in the range of 5.5-5.62 eV. The studied compounds were characterized by hole-transporting properties reaching 10^{-3} cm^2/Vs at high electric fields in the best cases. According provided characterizations, selected compounds may be used as hole-transporting materials in OLEDs.

[1] H. Uoyama, K. Goushi, K. Shizu et al., Highly efficient organic light-emitting diodes from delayed fluorescence, Nature, **492**, 234ï 238 (2012)
[2] K. Goushi, K. Yoshida, K. C. Adachi et al., Organic light-emitting diodes employing efficient reverse intersystem crossing for triplet-to-singlet state conversion, Nat. Photonics **6**, 253ï 258 (2012)

1,8-NAPHTHALIMIDE DERIVATIVES EXHIBITING THERMALLY ACTIVATED DELAYED FLUORESCENCE

Naveen Masimukku[1], Dalius Gudeika[1], Oleksandr Bezvikonnyi[1], Dmytro Volyniuk[1], Juozas Vidas Grazulevicius[1]

[1] Kaunas University of Technology, Department of Polymer Chemistry and technology
Radvilenu plentas 19, LT-50254, Kaunas, Lithuania
naveen.masimukku@ktu.edu

Organic materials exhibiting thermally activated delayed fluorescence (TADF) have attracted much attention due to their enhanced efficiency in organic light emitting diodes (OLEDs) which is possible due to harvesting triplet excitons [1]. Red emitting materials are always the short slab among the materials exhibiting emission of three-primary colours, due to the anabatic internal conversion (IC) coefficient managed by the energy gap law [2]. Red phosphor materials are widely used in the industry at present owing to the 100% exciton utilization efficiency (EUE). The introduction of precious metals, such as Ir, Pt, etc., increase the costs and phosphorescent emitters are not eco-friendly [3]. OLEDs based on metal-free TADF materials can also achieve 100% internal quantum efficiency by reverse intersystem crossing (RISC) process of triplet excitons. High photoluminescence (PL) quantum yield (PLQY) and small energy splitting (φE_{st}) between the first excited singlet state (S_1) and excited triplet state (T_1) are crucial factors for high-performance TADF materials [3]. New efficient orange-red TADF emitters are highly demanded to fill in the gap. The slow development of efficient orange-to-red TADF emitters is associated with the numerous strict molecular design considerations and corresponding difficulties. Naphthalimide acceptor-donor molecular design is suitable for the development of orange-red TADF emitters.

In this work we synthesized four emitters, which were obtained by the reactions of diphenylamine phenyl boronic acid and vinyl phenyl diphenylamine with 6,7-dibromo2-(2,6-dimethylphenyl)-1H-benzo[de]isoquinoline-1,3(2H)-dione and 5,8-dibromo-2-(2,6-dimethylphenyl)-1H-benzo[de]isoquinoline-1,3(2H)-dione. The yields of the compounds ranged from 52 to 70%. Glass transition temperatures of the synthesized glass-forming compounds were observed in the range of 132-156 ÁC. Ionization potential values of the compounds ranged from 5.38 to 5.69 eV (Fig. 1a) The PL spectra of THF solutions and films showed single peaks located at wavelengths varying from 600 to 650 nm (Fig. 1b). The positive solvatochromism indicates the intramolecular charge transfer character of the emission. The PL decay curves showed the presence of a long-lived emission components which were almost not influenced by the interaction with oxygen. The emission of the compounds underwent aggregation caused quenching. PLQY values of their dilute solutions ranged from 43 to 75% while those of the solid films ranged from 1 to 25%.

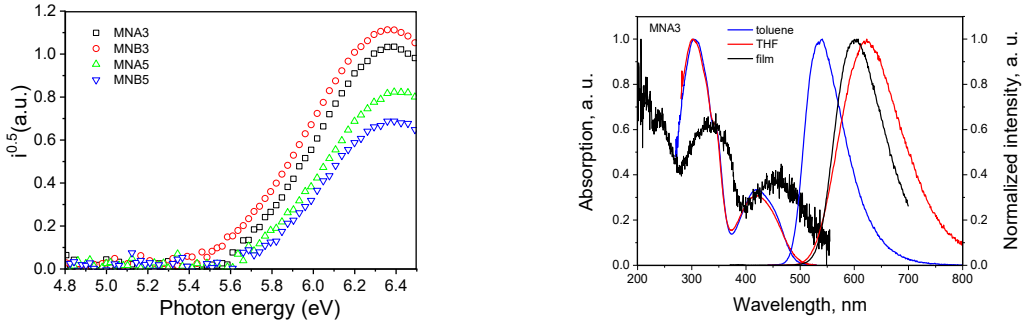

(a) (b)

Fig. 1. (a) Photoelectron emission spectra of the solid samples of compounds, (b) fluorescence spectra of naphthalimide-based derivatives.

[1] T. J. Penfold, F. B. Dias, A. B. Monkman, The theory of thermally activated delayed fluoroscence for organic emitting diodes, Chem. Commun **58**, 3925 (2018).
[2] T. Miwa, S. Kubo, K. Shizu et al., Blue organic light-emitting diodes realizing external quantum efficiency over 25% using thermally activated delayed fluorescence emitters, Nature **7**, 1-2 (2017).
[3] H. Li, T. Yang, J. Wang et al., Highly Efficient Orange-Red Thermally Activated Delayed Fluorescence Compounds Comprising Dual Dicyano-Substituted Pyrazine/Quinoxaline Acceptors, ChemPlusChem **86**, 95ï 102 (2021).

SYNTHESIS OF NOVEL 2-[(2,6-DICHLORO-4-SULFAMOYLPHENYL)AMINO]ACETIC ACID DERIVATIVES

Liucija Urbelytė, Birutė Grybaitė, Vytautas Mickevičius

Department of Organic Chemistry, Kaunas University of Technology, Kaunas, Lithuania
birute.grybaite@ktu.edu

Targeted therapy is currently a very important area of anticancer chemotherapy and is becoming one of the main way in the fight against oncogenesis. Benzenesulfonamides based compounds are effective in inhibiting tumor cell growth in vitro and in vivo. The antitumor activity of these inhibitors explains inhibition of carbonic anhydrases IX and carbonic anhydrases XII. Derivatives of benzenesulfonamides strongly inhibit the formation of metastases by the highly aggressive 4T1 mammary tumor cells and human breast carcinoma [1]. Human carbonic anhydrases (CA) are metalloenzymes that catalyze the hydration of carbon dioxide into bicarbonate. There are twelve catalytically active human CA isoforms involved in many crucial physiological processes. All benzenesulfonamide-based inhibitors are characterized by a sulfonamide head group, able to bind the Zn^{2+} ion in a pocket of the CA active site [2]. Also benzenesulfonamides with aromatic or heterocyclic moiety in their structure show promising inhibition activity against the species Schistosoma mansoni is endemic in Africa, where it causes intestinal schistosomiasis [3].

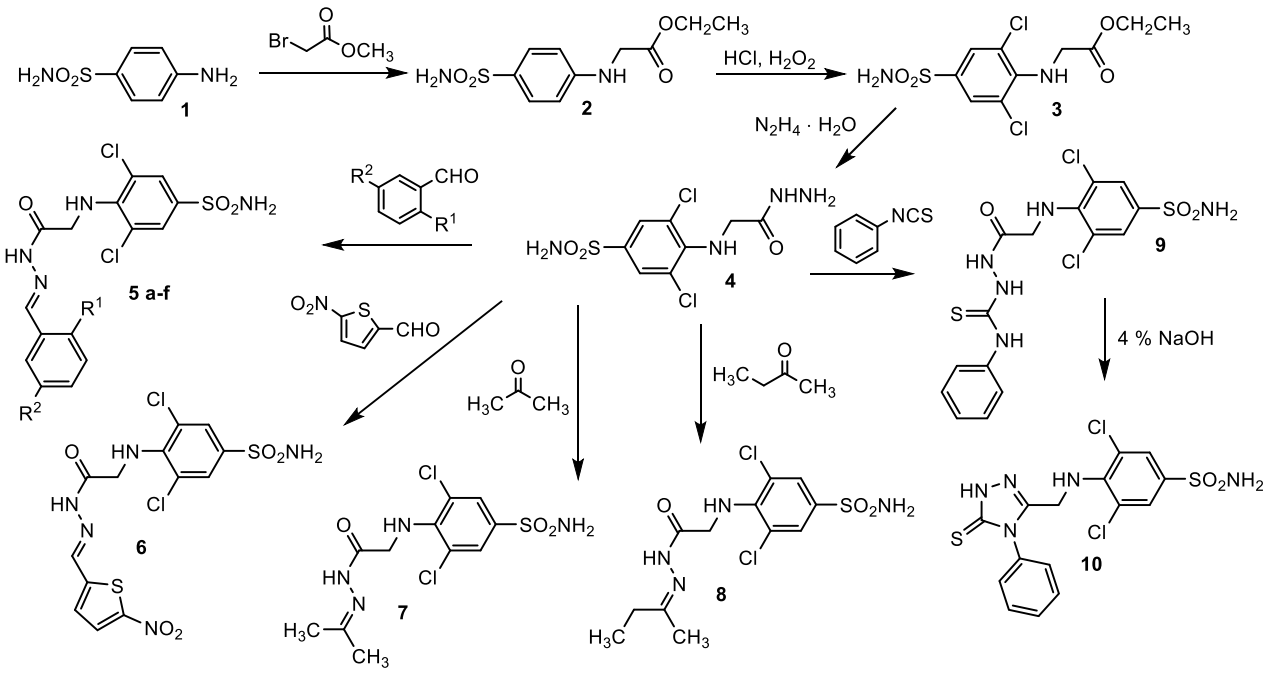

a-f: **a** R^1, R^2=H; **b** R^1=Cl, R^2=H; **c** R^1=OH, R^2=H; **d** R^1= OCH_3, R^2=H; **e** R^1=NO_2, R^2=H; **f** R^1=Cl, R^2=NO_2

Fig. 1. Synthesis of substituted benzenesulfonamides **2-10**

The aim of this work was to synthesize new benzenesulfonamides that can have biological activity. (Fig. 1). For this purpose, compound **1** first was alkylated with methyl bromoacetate in ethanol to give ester **2**. Ethyl 2-[(2,6-dichloro-4-sulfamoylphenyl)amino]acetate **(3)** was synthesized by treating **2** with HCl in the presence of hydrogen peroxide. Then the obtained ester **3** was converted to the hydrazide **4**. Hydrazones **5aï f, 6** were prepared by the reaction of corresponding hydrazide **4** and heterocyclic or aromatic aldehydes in 2-propanol. The reaction with acetone or ethyl methyl ketone in the presence of a catalytic amount of acetic acid provided hydrazones **7, 8**. *N*-phenylhydrazinecarbothioamide **9** was synthesized by the interaction of the hydrazide **4** with phenylisothiocianate in methanol. This compound was used for the synthesis of 1,2,4-triazole **10**.

All of the synthesized compounds were characterized by ^1H and ^{13}C NMR, elemental analysis and some representative compounds were characterized by mass spectrometry analysis.

[1] P. A Colinas, Novel sulfonamide compounds for inhibition of metastatic tumor growth, Expert Opinion on Therapeutic Patents **23**, 761ï 763 (2013).

[2] I. Vaģkevičienė, V. Paketurytė, A. Zubrienė at el., N-Sulfamoylphenyl- and N-sulfamoylphenyl-N-thiazolyl-b-alanines and their derivatives as inhibitors of human carbonic anhydrases, Bioorganic Chemistry **75**, 16ï 29 (2017).

[3] A. Angeli, M. Pinteala, S. S. Maier at el., Sulfonamide Inhibition Studies of an Ü-Carbonic Anhydrase from Schistosoma mansoni, a Platyhelminth Parasite Responsible for Schistosomiasis, International Journal of Molecular Sciences **21**, 1842 (2020).

INSPECTION OF THE MORPHOTROPIC PHASE BOURANDY IN SAMARIUM SUBSTITUTED $BiFeO_3$

Andrius Pakalniškis[1], Ramūnas Skaudžius[1], Tomas Murauskas[1], Siarhei I. Latushka[2], Denis Alikin[3], Algirdas Selskis[4], Dmitry Karpinsky[2], Aivaras Kareiva[1]

[1]Institute of Chemistry, Vilnius University, Naugarduko 24, LT-03225 Vilnius, Lithuania
[2]Scientific-Practical Materials Research Centre of NAS of Belarus, 220072 Minsk, Belarus
[3]School of Natural Sciences and Mathematics, Ural Federal University, Russia
[4]Center for Physical Sciences and Technology, LT-02300 Vilnius, Lithuania
andrius.pakalniskis@chgf.vu.lt

The term morphotropic phase boundary (MPB) usually refers to a concertation region where different crystal structures with a low energy barrier can coexist [1]. The most common and well understood MPB exists between the polar rhombohedral (R3m) and tetragonal (P4mm) structures in lead zirconate titanate [2]. While such transitions are not allowed by symmetry rules, recently it has been explained that they are mediated by a formation by transitionary monoclinic phase. This phase coexistence region has attracted a lot of attention from scientists as it has been discovered that such compounds show large sensitivity to external stimuli. However, while currently dominant piezoelectric materials with MPB (PZT, PMN-BT) are extremely efficient they contain lead which is highly toxic. Due to this drawback and overall shift towards green and sustainable chemistry, which was partly induced by anti Pb legislations, a search for a greener alternative is ongoing.

Over the last couple of decades many different compounds were analyzed in search of a possible alternative. $BiFeO_3$, a lead free multiferroic compound with perovskite type structure, was found to have a polar to non-polar morphotropic phase boundary upon doping with RE ions (La ï Lu) [3]. The undoped compound is characterized by polar active rhombohedral structure described by R3c space group as well as magnetically active sublattice formed by iron ions which makes it to be room temperature multiferroic with Currie temperature of ~1100 K and Neel temperature of 643 K [1]. There are some drawbacks specific for the initial compound, viz. bismuth ferrite is characterized by a large leakage current as well as difficulties in preparation of single phase materials. Doping of the initial compound with rare earth ions has shown to at least partly solves these problems as well causes a polar (R3c) to non-polar (Pnma) structural transition, with an intermediate PbZrO3-like anti-polar (Pbam) phase [1]. While the concentration range of MPB varies depending on the type of RE ion, the stabilization of the anti-polar phase has only been possible with RE ions up to Sm within the MPB which is very narrow among similar oxide systems ~1% [4]. Moreover, correct determination of morphotropic phase boundary is quite difficult because it is strongly dependent on preparation technique and post synthesis treatment [3]. It should be noted, that structural characterization of MPB region performed based on X-Ray diffraction analysis and microscopic measurements such as Raman or IR spectroscopy can give different results as compared to local measurements such as TEM or PFM, which poses a great problem for further scientific research [5].

Hence the main aim of this work was to investigate the morphotropic phase boundary region in Sm-doped $BiFeO_3$ compounds prepared by ethylene glycol assisted sol-gel technique, viz. to itemize the structural phase transition from the polar rhombohedral to the anti-polar orthorhombic followed by the non-polar orthorhombic phase driven by the dopant content using both local scale and microscopic measurement techniques. The obtained results highlight the differences specific for the MPB assuming the data obtained by microscopic measurements as compared to local scale structural results.

Acknowledgements. This work was supported by the European Unionôs Horizon 2020 research and innovation programme under the Marie Skłodowska-Curie grant agreement No. 778070.

[1] J. Walker, H. Simons, D.O. Alikin, et.all., Dual strain mechanisms in a lead-free morphotropic phase boundary ferroelectric, Scientific Reports **6,** 1ï 8 (2016).
[2] F. Zheng, J. Chen, X. Li, M. Shen, Morphotropic phase boundary (MPB) effect in Pb $(Zr,Ti)O_3$ rhombohedral/tetragonal multilayered films, Materials Letters, Mater. Lett. **60,** 2733ï 2737 (2006).
[3] T. Rojac, A. Bencan, B. Malic, et.all., $BiFeO_3$ Ceramics: Processing, Electrical, and Electromechanical Properties, Journal of the American Ceramic Society **97** 1993ï 2011 (2014).
[4] D. V. Karpinsky, A. Pakalniškis, G. Niaura, et.all., Evolution of the crystal structure and magnetic properties of Sm-doped $BiFeO_3$ ceramics across the phase boundary region, Ceramics International **47**, 5399-5406, (2021).
[5] S. Bhattacharyya, J.R. Jinschek, H. Cao, et.all., Direct high-resolution transmission electron microscopy observation of tetragonal nanotwins within the monoclinic MC phase of Pb $(Mg_{13}Nb_{23})O_3$-0.35$PbTiO_3$ crystals, Applied Physics Letters **92** (2008).

ELECTROCHEMICALLY ACTIVE SURFACE AREA MEASUREMENT OF HONEYCOMB-LIKE COPPER FOAM ELECTRODE

Birutã Serapinienã, Jurga Juodkazytã, Laima Gudaviļ iÎ tã, Algirdas Selskis, Rimantas Ramanauskas

Center for Physical Sciences and Technology, Saulãtekio al. 3, LT-10257 Vilnius, Lithuania
birute.serapiniene@ftmc.lt

The main goal of Paris Agreement is to reduce worldwide temperature by reducing greenhouse gas emissions [1]. CO_2 electrochemical reduction is one of possible solutions of this problem. In addition, this reaction is of major interest, due to the possibility of synthesizing useful products for the chemical industry from a practically inexhaustible carbon source. There have been many attempts to develop suitable catalysts. Among them metallic Cu has been demonstrated to be promising for selective CO_2 reduction to HCOOH, CO or, more importantly, to CH_4, C_2H_4 and C_2H_6 with relatively high efficiency [2]. However, the smooth polycrystalline and single crystal Cu electrode surface has low catalytic activity. It is expected that the electrocatalytic activity and the selectivity of Cu electrodes can be improved by modifying the surface. The nanostructuring can provide different surface morphologies with more active sites for CO_2 electroreduction and help controlling the product selectivity.

Three-dimensional (3D) porous metal foam has a wide spread interest as its open porous structure is very suitable for electrode, which requires a large specific surface area for electrochemical reaction. The production method of metal foams involves a metal electrodeposition process which is accompanied by hydrogen evolution. Copper foams with highly open porous walls have been successfully sculptured using the gas evolving in an electrochemical deposition process in a diluted acidic sulphate solution. The pore sizes and wall structures of the foams are tunable by adjusting the deposition conditions [3].

Efficiency of the catalysts and reduction product selectivity depends on electrochemically active surface area of the electrode. The aim of this research was to find easy, fast and reliable method for the measurement of real electrochemically active surface area of Cu honeycomb-like structure electrodes. Cu 3D porous metal foam was produced by electrodeposition on Cu electrode in a 0.5 M $CuSO_4$ + 2.5 M H_2SO_4 electrolyte, at 3 A/cm^2 current density for 20 s. The surface morphology of the obtained structures was evaluated from SEM analysis. Some of the Cu foam SEM images are presented in Fig. 1.

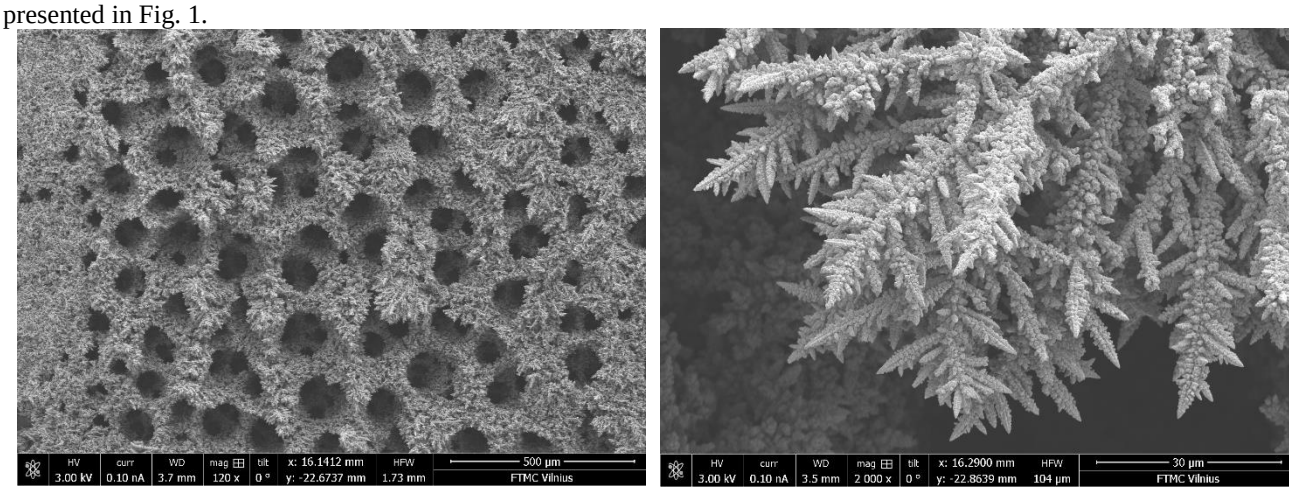

Fig. 1. SEM images of Cu honeycomb-like structure electrodeposited in 0.5 M $CuSO_4$, 2.5 M H_2SO_4 electrolyte.

Several electrochemical methods are available for active surface area determination, which are based on the measurement of charge associated with the deposition or removal of chemisorbed monolayer of species. Therefore, the real electrochemically active surface area of Cu honeycomb-like electrodes was assessed by the Cu oxidation-reduction method (Cu_2O monolayer formation), underpotential deposition (UPD) of Pb monolayer method and double layer capacitance method. Advantages and disadvantages of the mentioned methods are discussed.

[1] https://unfccc.int/process-and-meetings/the-paris-agreement/the-paris-agreement
[2] Xie, H., Wang, T., Liang, J., Li, Q., & Sun, S. Cu-based nanocatalysts for electrochemical reduction of CO2. Nano Today, 21, 41ï 54. (2018)
[3] Shin, H. C., & Liu, M. Copper foam structures with highly porous nanostructured walls. Chemistry of Materials, 16(25), 5460ï 5464. (2004).

MACROMOLECULAR DIKETOPYRROLOPYRROLE AS THE ANNIHILATOR IN UPCONVERTING ORGANIC FILMS

Barbara Chatinovska[1], Augustina JozeliÎnaitã[1], Edvinas Radiunas[2], Lukas Naimoviļius[2], Karolis Kazlauskas[2], Edvinas Orentas[1]

[1] Department of Organic Chemistry, Faculty of Chemistry and Geosciences, Vilnius University, Lithuania
[2] Institute of Photonics and Nanotechnology, Faculty of Physics, Vilnius University, Lithuania
barbara.chatinovska@chgf.stud.vu.lt

Triplet fusion (TF) upconversion is a process allowing the conversion of two or more low ï energy photons to one high ï energy photon. Light upconverting systems have great implications in many fields, such as photovoltaics, photocatalysis or bioimaging. Despite a large demand, the choice of efficient organic materials is rather limiting, especially for the most practically relevant NIR to visible upconversion [1-2]. TF upconversion requires two types of molecules, a sensitizer and an annihilator, the latter often being the limiting component. To extend the collection of possible emitters and to gain fundamental insights into upconversion process itself our team sought to develop new derivatives of diketopyrrolopyrrole (DPP), a commonly used dye in organic optoelectronics.

DPP has been widely explored in the field of organic photovoltaics because of its excellent optical properties, such as strong absorption in the visible range and high fluorescence quantum yield [3]. In order to apply DPPs in upconversion devices, their high aggregation propensity, detrimental to fluorescence, has to be attenuated by structural design. To this end we have designed, synthesized and evaluated new alkyl chain strapped sterically hindered DPP derivative **1** (Fig. 1). The successful modulation of aggregation process is expected to provide a working material not only for solution but also for more difficult to achieve upconversion in films.

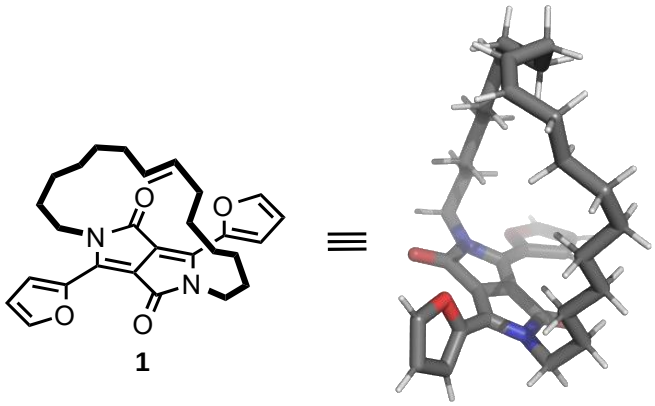

Fig. 1. Chemical structure of macrocyclic DPP derivative.

[1] J. Zhou, Q. Liu, W. Feng et al., Upconversion luminescent materials: advances and applications, Chemical Reviews 115, 395-465 (2015).
[2] S. Wen, J. Zhou, J. Schuck et al., Future and challenges for hybrid upconversion nanosystems, Nature Photonics 13, 828-838 (2019).
[3] A. B. Pun, L. M. Campos, D. N. Congreve., Tunable Emission from Triplet Fusion Upconversion in Diketopyrrolopyrroles, J. Am. Chem. Soc. 141, 9, 3777-3781 (2019).

Acknowledgements: This project has received funding from the European Regional Development Fund (Project No. 09.3.3-LMT-K712-22-0191) under grant agreement with the Research Council of Lithuania (LMTLT)

CORRELATION BETWEEN PYRIDINE AND FURFURYL ALCOHOL INGESTION AND THEIR PRESENCE IN BREATH

Adri§n Vicent-Claramunt, Evaldas Naujalis

Metrology Department, State Research Institute Center for Physical Sciences and Technology
Lukiğkiô str. 9, LT-01108 Vilnius, Lithuania.
adrian.vicent@ftmc.lt

Furfuryl alcohol (FFA) and Pyridine (Py) are, among many other compounds, food contaminants produced mainly in thermally processed food such as coffee, juices, alcoholic beverages or baked food [1,2]. Those compounds, which are considered toxic and potential carcinogenic [3], are not present in healthy humans but can be found in high concentration in breath after coffee consumption. Coffee is one of the most popular drinks and widely consumed all around the world. In 2019/2020, around 10 million tons of coffee were consumed worldwide [4]. The aim of this work is to identify and quantify Py and FFA after ingestion by using breath analysis. And compare it with the actual amount ingested by analysing the brewed coffee samples.

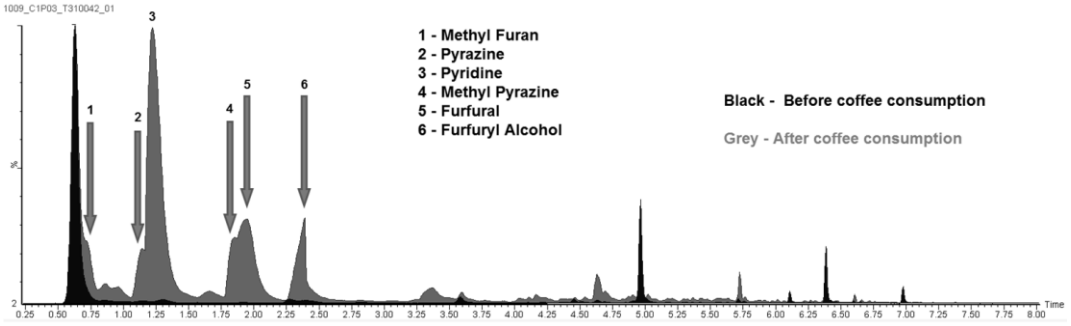

Fig.1: Chromatogram from breath sample, before and after coffee consumption. Column DB-5MS (30x0.25x0.25). Magnet Scan 50-200m/z. Temp. range: 40 to 280 ŒC

Brewed coffee samples were prepared using CafeRomatica (Nivona) coffee machine. A 10 ml aliquot of the brewed was collected to be analysed by HPLC to stablish the quantity of Py and FFA present in the sample. In order to quantify the analytes, standard addition method was employed. Breath samples from volunteers were collected before and after the consumption of the brewed coffee in order to determine the concentration detected in it. Samples were collected using self-designed LDPE plastics bags for sampling. Calibration of pyridine and furfuryl alcohol was also obtained filling the bags with the standard solutions. All the samples were analysed using Thermal Desorption coupled to Gas Chromatography Mass Spectrometer (TD/GC-MS).

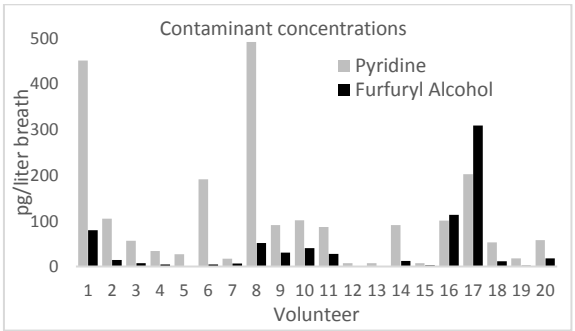

Fig.2: Concentrations of Py and FFA found in breath after coffee consumption.

Different levels of contaminants were quantified from volunteersô samples (Fig.2). There seems to be not clear relation between the quantity of both compounds ingested and their presence in breath. Many factors, like time to drink the coffee, time after collection of the sample, eating or drinking something else while consuming the coffee, if the coffee is diluted afterwards or consumed with milk, or even the body assimilation could influence the correlation. However, breath VOCs collection can be used for the detection of food contaminants after consumption even at very low concentrations.

[1] A.N. Gloess, C. Yeretzian, R. Knochenmuss, M. Groessl / International Journal of Mass Spectrometry Volume 424, January 2018, Pag 49-57.
[2] F. Cincotta et al. / LWT - Food Science and Technology 118 (2020) 108718.
[3] A. O. Okaru and D. W. Lachenmeier / Toxics 2017, 5, 9.
[4] International Coffee Organization (www.ico.org).

A RRDE STUDY OF MN-BASED CATHODE MATERIAL DEGRADATION IN AQUEOUS NA-ION BATTERIES

Davit Tediashvili,[1,2] Linas Vilį iauskas[2]

[1] Institute of Chemistry, Faculty of Chemistry and Geosciences, Vilnius University, Lithuania
[2] Center for Physical Sciences and Technology, Sauletekio al. 3, LT-10257 Vilnius, Lithuania
Davit.Tediashvili@ftmc.lt

Rechargeable lithium-ion batteries with organic electrolytes are widely used as commercial energy storage devices. They have many attractive properties, such as high efficiency, energy density and stability. However, as the energy storage demand increases, growing prices on scarce lithium resources also increase, making lithium-ion batteries less attractive. On the other hand, sodium is the sixth most abundant element in earthôs crust. Another big issue of commercial batteries remains the usage of organic solvents, which increase production cost and raise safety concerns. This problem is solved by replacing organic solvents with aqueous electrolytes. Traditionally, the use of aqueous electrolytes in batteries was limited by narrow potential window of operation, beyond which water decomposes. However, recently developed water-in-salt electrolytes can expand this potential window [1], making aqueous electrolytes a viable alternative. However, the problem of electrode material stability during operation needs to be solved to fully utilize this technology.

With general formula of $Na_3M_2(PO4)_3$, NASICON-structured materials are exceptional due to their unique framework structure providing fast Na-ion transport. They can offer high theoretical capacity and operating voltage, however, might suffer from poor cycling performance especially in aqueous electrolytes [2].

Here, we present a rotating ring-disc electrode (RRDE) study of the $Na_3MnTi(PO_4)_3$ degradation in aqueous electrolyte. A similar study was carried out on $LiMn_2O_4$, and showed that material degradation takes place in fully charged or fully discharged state [3]. In the case of $Na_3MnTi(PO_4)_3$, the results show that degradation occurs only during the discharge phase (0.7 V vs. Ag/AgCl) or reduction of Mn^{4+}, suggesting that it is driven by chemical dissolution of Mn^{2+} formed in aqueous media. The degradation of $Na_3V_2(PO_4)_2F_3$ (NVPF) was also studied with the same technique. Overall, the understanding of degradation mechanisms of electrode materials is crucial for their mitigation and RRDE is simple and useful tool for this task.

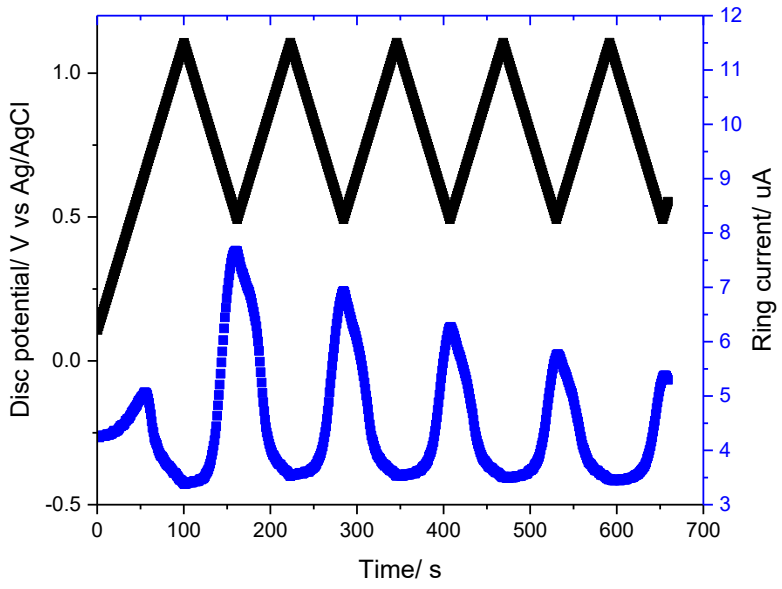

Figure 1. Applied potential on a disc (black) and current response on Pt ring (blue) during RRDE experiment on NMTP.

Acknowledgements:

This project has received funding from the European Regional Development Fund (Project No. 01.2.2-LMT-K-718-02-0005) under grant agreement with the Research Council of Lithuania (LMTLT)

[1] L. Suo et al., ñWater-in-saltò electrolyte enables high-voltage aqueous lithium-ion chemistries, Science **350**, 938-943 (2015)
[2] D. Bin et al., Progress in Aqueous Rechargeable Sodium-Ion Batteries, Advanced Energy Materials **8** (17), 1-31 (2018)
[3] L Wang et al., Study of Mn Dissolution from $LiMn_2O_2$ Spinel Electrodes Using Rotating Ring-Disk Collection Experiments, Journal of Electrochemical Society, **150** (7), 905-911 (2003)

SYNTHESIS OF Cu-CONTAINING CALCIUM PHOSPHATE WITH WHITLOCKITE STRUCTURE THROUGH THE LOW-TEMPERATURE DISSOLUTION-PRECIPITATION PROCESS

Diana Griesiute, Agne Kizalaite, Hanna Klipan, Aleksej Zarkov

Institute of Chemistry, Vilnius University, Naugarduko g. 24, LT-03225, Vilnius, Lithuania
diana.griesiute@chgf.vu.lt

Calcium phosphates (CaPs) are the main inorganic constituents of human hard tissues. There are a lot of CaP phases, which have different physical properties and application. Human hard tissues mostly consist of calcium hydroxyapatite (HAp) which is the most stable CaP phase around neutral pH [1]. The second most abundant CaP phase is whitlockite. Magnesium whitlockite is a member of CaPs family, where some calcium ions are substituted by smaller magnesium ions. Chemical formula of magnesium whitlockite is $Ca_{18}Mg_2(HPO_4)_2(PO_4)_{12}$ [2]. Unfortunately, the preparation of phase-pure whitlockite remains very challenging and the obtained synthesis products often contain impurities. Nevertheless, this material is a promising candidate in orthopedic surgery because it is biocompatible and possesses excellent osteogenic properties. Whitlockite phase is more stable than HAp in acidic solution so it is beneficial in bone mineralization [1].

Doping of CaPs with other ions may result in the appearance of new physical and biological properties, which can be used in wider application area. Copper is an essential trace element, necessary for mammalian life and it plays a crucial role in the cross-linking of collagen and bone elastin [3]. It is important for metabolism processes because it acts like cofactor for many enzymes [4]. Copper exhibits antibacterial properties and limited cytotoxicity, due to these reasons it is a promising candidate for doping into CaPs matrices. Cu-substituted CaPs are well known for their antibacterial, angiogenic and osteogenic properties [5].

The main goal of this work was to synthesize single phase whitlockite powders. Copper whitlockite powders were synthesized by dissolution-precipitation method under hydrothermal conditions using calcium hydrogen phosphate dihydrate ($CaHPO_4$I$2H_2O$) and copper nitrate trihydrate ($Cu(NO_3)_2$I$3H_2O$) as starting materials. The crystallinity, crystal structure and structural changes were evaluated by powder X-ray diffraction (XRD), Fourier-transform infrared (FTIR) and Raman spectroscopies. Scanning electron microscopy (SEM) was used for the characterization of morphological features of products. Chemical composition of synthesized powders was analyzed by inductively coupled plasma optical emission spectrometry (ICP-OES).

The results of XRD, FTIR and Raman spectroscopies confirmed that synthesized CaP has whitlockite structure. It was demonstrated that optimal reaction temperature is 200°C, at this temperature was synthesized single phase whitlockite powders. Optimal pH range was determined to be from 6.4 to 6.6. Neighboring crystal phases were obtained at lower temperatures and higher/lower pH of the reaction medium. Also, it was found, that optimal reaction time is about 3 hours. Thermal stability studies revealed that copper-containing whitlockite is thermally unstable and decomposes after a heat treatment.

Acknowledgements

This research was funded by the European Social Fund under the No. 09.3.3-LMT-K-712 ñDevelopment of Competences of Scientists, other Researchers and Students through Practical Research Activitiesò measure (grant No. 09.3.3.-LMT-K-712-22-0053).

[1] H. L. Jang, H. K. Lee, K. Jin, H. Y. Ahn, H. E. Lee, & K. T. Nam, Phase transformation from hydroxyapatite to the secondary bone mineral, whitlockite. *Journal of Materials Chemistry B*, **3** (2015) 1342ï 1349. https://doi.org/10.1039/c4tb01793e.

[2] H. Cheng, R. Chabok, X. Guan, A. Chawla, Y. Li, A. Khademhosseini, & H. L. Jang, Synergistic interplay between the two major bone minerals, hydroxyapatite and whitlockite nanoparticles, for osteogenic differentiation of mesenchymal stem cells. Acta Biomaterialia, 69 (2018) 342ï 351. https://doi.org/10.1016/j.actbio.2018.01.016. [1] H. L. Jang, H. K. Lee, K. Jin, H. Y. Ahn, H. E. Lee, & K. T. Nam, Phase transformation from hydroxyapatite to the secondary bone mineral, whitlockite. *Journal of Materials Chemistry B*, **3** (2015) 1342ï 1349. https://doi.org/10.1039/c4tb01793e.

[3] S. Gomes, C. Vichery, S. Descamps, H. Martinez, A. Kaur, A. Jacobs, J. M. Nedelec, & G. Renaudin, Cu-doping of calcium phosphate bioceramics: From mechanism to the control of cytotoxicity. Acta Biomaterialia, 65 (2018) 462ï 474. https://doi.org/10.1016/j.actbio.2017.10.028.

[4] M. Bost, S. Houdart, M. Oberli, E. Kalonji, J. F. Huneau, & I. Margaritis, Dietary copper and human health: Current evidence and unresolved issues. Journal of Trace Elements in Medicine and Biology, 35 (2016) 107ï 115. https://doi.org/10.1016/j.jtemb.2016.02.006.

[5] A. Jacobs, G. Renaudin, C. Forestier, J. M. Nedelec, & S. Descamps, Biological properties of copper-doped biomaterials for orthopedic applications: A review of antibacterial, angiogenic and osteogenic aspects. Acta Biomaterialia, 117 (2020) 21ï 39. https://doi.org/10.1016/j.actbio.2020.09.044.

SYNTHESIS AND CRYSTAL STRUCTURES OF SAMARIUM(III)ï CONTAINING HETEROPOLY SALTS WITH PEACOCKï WEAKLEY TYPE ANION $Na_{9-x}H_x[Sm(W_5O_{18})_2]\cdot nH_2O$

Oleksandra Mariichak[1,2], Georgii Rozantsev[1], Serhii Radio[2]

[1] Faculty of Chemistry, Biology and Biotechnologies; Vasyl' Stus Donetsk National University, Ukraine
[2] Department for Research, Research Laboratory ñChemistry of Polyoxometalates and Complex Oxide Systemsò, Vasyl' Stus Donetsk National University, Ukraine
radio@donnu.edu.ua

To determine the critical acidity for obtaining of lanthanide(III)-containing heteropoly salts with Peacockï Weakley type anion $[Ln(W_5O_{18})_2]^{9-}$ (Ln = lanthanide) a new procedure for the synthesis of sodium heteropoly decatungstosamarates(III) from $Sm(NO_3)_3$ ï Na_2WO_4 ï HNO_3 ï H_2O solutions with the ratio з(Sm) : з(W) = 1:10, which acidified up to $Z = з(HNO_3)/з(Na_2WO_4) = 0.90$ï 1.20 (Mariichak O.Yu., *et al.* Patent of Ukraine No. 121322, 2017), was used. The formation of heteropoly anions by self-assembly process corresponds to the equation:

$$Sm^{3+} + 10\ WO_4^{2-} + (8+n)\ H^+ = n[Sm(W_5O_{18})_2]^{(9-n)-} + 4\ H_2O.$$

The synthesized crystalline salts of $Na_8H[Sm(W_5O_{18})_2]\cdot 38.25H_2O$ (Z = 0.90) and $Na_7H_2[Sm(W_5O_{18})_2]\cdot 24.75H_2O$ (Z = 1.00) were characterized by Single Crystal X-ray analysis (Fig. 1), FT-IR spectroscopy and elemental analysis.

The main crystallographic data for $Na_8H[Sm(W_5O_{18})_2]\cdot 38.25H_2O$ are: triclinic, Pï 1, *a* = 12.894(4) ¡ , *b* = 13.112(4) ¡ , *c* = 20.885(6) ¡ , Ŭ= 76.99(3)Á ß = 84.05(3)Á ɔ = 77.42(3)Á V = 3352.2(18) ¡ ^{3}, Z = 2; and for $Na_7H_2[Sm(W_5O_{18})_2]\cdot 24.75H_2O$ are: triclinic, Pï 1, *a* = 12.5506(4) ¡ , *b* = 12.9656(2) ¡ , *c* = 18.9744(8) ¡ , *Ŭ*= 96.461(2)Á *ß* = 100.389(3)Á ɔ = 102.472(2)Á V = 2928.23(17) ¡ ^{3}, Z = 2.

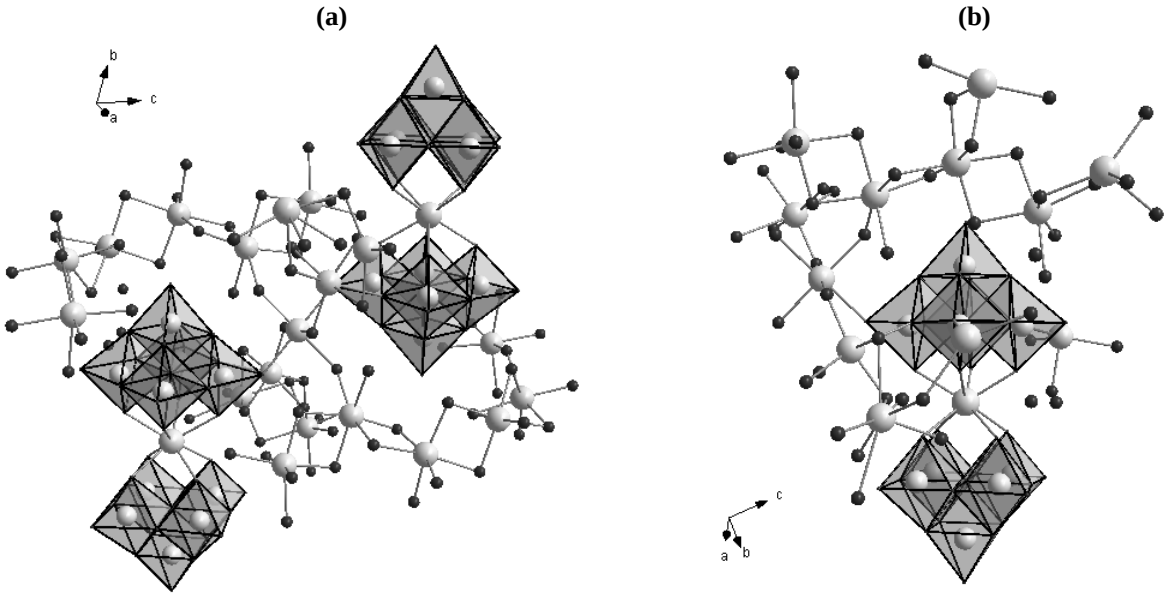

Fig. 1. Crystal structures of $Na_8H[Sm(W_5O_{18})_2]\cdot 38.25H_2O$ (a), and $Na_7H_2[Sm(W_5O_{18})_2]\cdot 24.75H_2O$ (b).

Amorphous precipitates which isolated from solutions with Z = 1.10 and 1.20, were investigated by FT-IR spectroscopy. The results of the study showed the presence of Peacockï Weakley type anion in the salt obtained at Z = 1.10, and heptatungstate anion $[W_7O_{24}]^{6-}$ ï at Z = 1.20. Thus, Z = 1.10 is the critical acidity, which allows to obtain salts with heteropoly decatungstosamarate(III) anion.

The obtained X-ray diffraction data supplement the results of structural studies of two Sm(III)-containing polyoxotungstates with Peacockï Weakley type anion described in the literature: $Na_6H_3[Sm(W_5O_{18})_2]\cdot 28H_2O$ [1] and $K_3Na_4H_2[Sm(W_5O_{18})_2]\cdot 22H_2O$ [2]. From the analysis of the comparison of structural parameters of compounds it can be concluded that changes in the composition of the cationic sublattice and the presence of different numbers of coordinated and uncoordinated water molecules have almost no effect on the values of bond lengths and valence angles in the heteropoly anion.

The study was carried out within the Fundamental Research Programme funded by the Ministry of Education and Science of Ukraine (grants ID 0119U100025, 0120U102059).

[1] T. Ozeki, T. Yamase, Hexasodium Trihydrogen Decatungstosamarate Octacosahydrate, Acta Cryst. **C50**, 327ï 330 (1994).
[2] T. Ozeki, T. Yamase, Effect of lanthanide contraction on the structures of the decatungstolanthanoate anions in $K_3Na_4H_2[LnW_{10}O_{36}]\cdot nH_2O$ (Ln = Pr, Nd, Sm, Gd, Tb, Dy) crystals, Acta Cryst. **B50**, 128ï 134 (1994).

DETERMINATION OF COMPOUNDS STRUCTURES FORMED DURING ELECTROPHILIC CYCLIZATION REACTIONS OF BENZIMIDAZOL-2-YL ALKYNES USING NMR

Indrė Misiūnaitė, Karolis Žigas, Ieva Karpavičienė

Faculty of Chemistry and Geosciences, Vilnius University, Naugarduko g. 24, LT-03225, Vilnius, Lithuania
Indre.Misiunaite@gmail.com

Identification of compounds in proteomics [1], metabolomics [2] and scientific laboratories is very important in organic chemistry. There are many analytical techniques that allow such studies to be performed, for example, chromatography, mass spectroscopy or quantification of the absorption of radiation [3]. However, these methods do not allow the structure of compounds to be determined. Nuclear magnetic resonance (NMR) spectroscopy and X-ray crystallography can solve this problem. Crystallography, however, has a number of limitations. The most significant is the need of single crystals. Therefore, NMR spectroscopy is used more widely. This method is nondestructive, easily quantifiable and very informative. One-dimensional (1-D) spectra (e.g. ^{1}H, ^{13}C, ^{15}N, ^{31}P) provide information about the presence of different atoms in a molecule, while two-dimensional (2-D) spectra help to determine how they are connected. The major 2-D NMR experiments can be divided in two categories: homonuclear and heteronuclear [4]. The homonuclear 2-D NMR experiments are the correlation spectroscopy (COSY) and the total correlation spectroscopy (TOCSY). In the heteronuclear experiment category, there are the heteronuclear single quantum correlation experiment (HSQC) and heteronuclear multiple bond correlation (HMBC). By combining these methods, the structure of the compound can be easily determined. Keeping this in mind we determined the structures by 2-D NMR spectroscopy of the formed compounds in the electrophilic cyclization reactions of benzimidazol-2-yl alkynes.

The electrophile induced alkynes cyclization reactions can proceed through *endo-dig* or *exo-dig* cyclization modes, depending on the chain length, the substitution pattern on the chain, and the electrophile employed. In our research we have several groups of starting materials (**Fig. 1**). After NMR spectra analysis, it was found that in reactions with iodine 2-((3-aryl prop-2-yn-1-yl)thio)-*1H*-benzo[d]imidazoles **1a-d** formed 6-*endo-dig* **2a-d** and 2-((2-prop-2-yn-1-yl)thio)-*1H*-benzo[d]imidazoles **1e** formed 5-*exo-dig* cyclization products **3e** respectively. Hence, after 2-D NMR analysis of the cyclization reactions of both starting materials **4** and **5** spectra data showed that only seven-membered heterocyclic frameworks were formed *via* a 7-*endo-dig* ring-closing pathway. The main proof of formed products was obtained using HMBC spectra. For example, the HMBC spectrum of compound **7a** showed only the interaction of the $–CH_2$ group (3H) with the carbon to which the electrophile was attached (10C). Because HMBC spectra show $^{1}H–^{13}C$ interaction through 2-3 bonds R-group hydrogen (8H) did not show interaction with the carbon 10C. If this interaction was visible, it would mean that hydrogens 8H are distant through 3 bonds from 10C and the 6-*exo-dig* cyclization product was formed. More details about 2-D NMR analysis and spectra will be discussed in presentation.

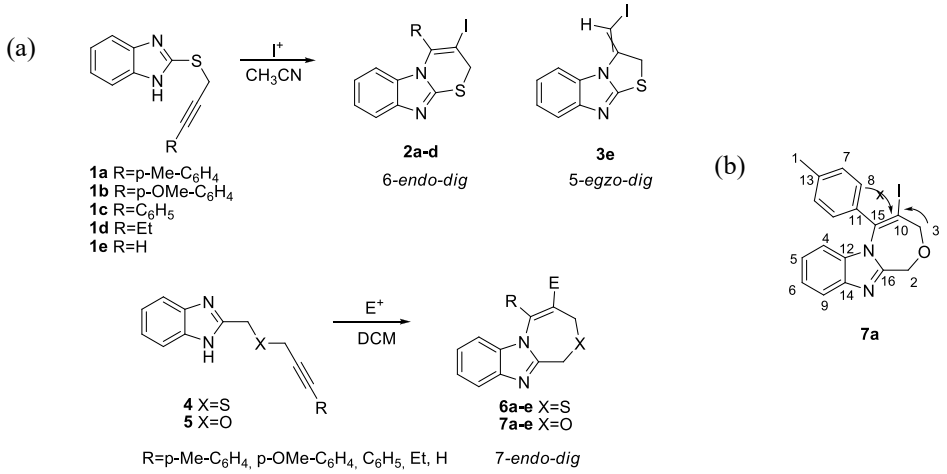

Fig.1. (a) General scheme of reactions, (b) 4-iodo-5-(p-tolyl)-*1H*,*3H*-benz[4,5]imidazo[2,1-c][1,4]oksazepine **7a**

[1] J. Shin, W. Lee, W. Lee, Expert Rev., *Proteomics*,**5**(4), 589-601, (2008).
[2] A. H. Emwas, R. Roy, R. T. McKay, L. Tenori,E. Saccenti, G. A.N. Gowda, D. Raftery, F. Alahmari,L. Jaremko, M. Jaremko,D. S. Wishart, *Metabolites*,**9**, 123, (2019).
[3] Th. E. Crowley, *Purification and characterization of secondary metabolites*, **Chapter 7**, 67-78, (2020).
[4] J.H. Simpson, Organic structure determination using 2-D NMR spectroscopy**, Chapter 6**, 123-168, (2012).

INVESTIGATION OF ELECTROPORATION EFFECTS BY MEDIATED AMPEROMETRY AT YEAST MODIFIED ELECTRODES

Sabina Pavliukovič[1], Povilas Šimonis[1], Rasa Garjonytė[2], Arūnas Stirkė[1]

[1] Laboratory of Bioelectrics, [2] Laboratory of Spektroelectrochemistry,
State Research Institute, Center for Physical Sciences and Technology,
Saulėtekio al. 3, Vilnius, Lithuania
sabina.pavliukovic@gmc.stud.vu.lt

Budding yeast (*Saccharomyces cerevisiae*) is one of the most well-studied and understood eukaryotic organisms. Yeast cells could be used for whole-cell bioprocesses such as biocatalysis and recombinant protein fermentation, but natural barrier functions of the cell wall and cell membrane often retards entry of substrates and release of products [1]. One of the possible techniques which could be used to improve permeability for target molecules is pulsed electric field (PEF), yet there is still a lack of sufficient data related to the effects of PEF on yeast cells especially in combination with whole-cell bioprocesses.

In this study we modified electrodes with whole yeast cells to detect electroporation effects. For the analysis, PEF-treated cells were immobilized on carbon paste electrodes which were then immersed into solution with potassium ferricyanide or menadione acting as mediators and producing measurable currents through oxidizing at electrode surface. Menadione-mediated amperometry was used for measurement of redox activity inside the yeast cells [2], while ferricyanide currents from amperometric sensor for lactic acid reflected membrane permeability (Fig 1.) [3]. Viability of cells was evaluated by counting colony-forming units. Leakage of intracellular compounds was evaluated by measuring fluorescence of supernatant or staining it with Ellman's reagent. Cells were exposed to single square shaped electric field pulses with pulse duration τ = 300 µs and electric field strengths (E) up to 16 kV/cm.

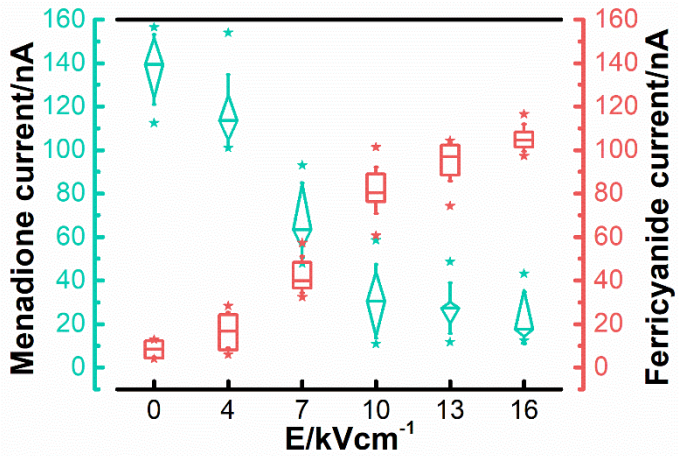

Fig. 1. Effect of electric field strength on current responses of yeast-modified electrode. Teal diamonds: 67 µM menadione at an operating potential 0.3 V in phosphate buffer at pH 6.5. Pink squares: 0.2 mM lactic acid at yeast-modified electrodes at an operating potential 0.3 V in phosphate buffer at pH 7.3 containing 0.5 mM mediator $K_3[Fe(CN)_6]$.

We showed that after exposure to PEF, permeability of cell membrane/wall increased while viability decreased. Yeast-modified electrode responses to lactic acid and menadione were dependent on PEF exposure. Currents obtained from amperometric biosensor with treated cells increased from 9 ± 4 nA (E = 0 kV/cm) up to 103 ± 10 nA (E = 16 kV/cm). PEF treated yeast cells also showed lower redox activity which decreased (from 138 ± 15 nA to 23 ± 12 nA) with raise in electric field strength (0 kV/cm up to 16 kV/cm). Decrease of menadione-mediated current showed similar pattern with viability. Viability of yeast cells decreased (from 100 % up to ~ 2%) with raise in electric field strength (E = 10 kV/cm). We conclude that amperometric measurements can be effectively used for investigation of various cellular responses after PEF treatment.

[1] Chen, R., "Permeability issues in whole-cell bioprocesses and cellular membrane engineering" Applied Microbiology and Biotechnology 74, 730-738 (2007).
[2] R. Garjonyte, V. Melvydas, and A. Malinauskas, "Mediated amperometry reveals different modes of yeast responses to sugars", Bioelectrochemistry 107, 45–49 (2016).
[3] R. Garjonyte, V. Melvydas, and A. Malinauskas, "Effect of yeast pretreatment on the characteristics of yeast-modi fi ed electrodes as mediated amperometric biosensors for lactic acid", Bioelectrochemistry 74, 188–194 (2008).

HPLC METHOD DEVELOPMENT AND VALIDATION FOR MAIN CANNABINOIDS DETERMINATION IN HEMP BIOMASS AND OIL

Miglã Bartkutã[1], Audrius Sadaunykas[2], Evaldas Naujalis[2*]

[1]Department of Analytical and Environmental Chemistry, Faculty of Chemistry and Geosciences, Vilnius University, Lithuania

[2] Metrology Department, State Research Institute Center for Physical Sciences and Technology, Lithuania

migle.bartkute@chgf.stud.vu.lt

The main purpose of this work was to develop and validate a method for detection and quantification of cannabinoids in different hemp samples. Nowadays a lot of attention has been paid to the plant called *Cannabis sativa* and the main reason for this interest is its therapeutic effect. *Cannabis sativa* has more than 500 compounds from which the major role of activity performs compounds known as cannabinoids [1]. Phytocannabinoids possess a lot of different activities such as analgesic, anti-inflammatory, antimimetic and anticancer effects, and that is why these compounds has such a big interest [2].

The fact that the cannabis plant has a lot of different compounds makes it a complex matrix and it requires an accurate and reliable method for determination of cannabinoids. One of the main methods which have been mainly used in the most of research works dealing with the analysis of cannabinoids is a high performance liquid chromatography (HPLC) [3]. This method suggest fast and reliable determination and quantification of the main cannabinoids in different cannabis matrices. Consequently our main focus was on the development and validation of efficient and accurate HPLC method. We developed the analytical method, which in 11 minutes allows to determine a broad spectrum of cannabinoids in different hemp samples (Fig. 1). The method was validated for the hemp biomass and hemp oil showing good sensitivity ï LOD for hemp biomass 0,0005 % - 0,018 %, for oil 0,001 % - 0,036 %, LOQ for hemp biomass 0,002 % - 0,055 % and for hemp oil 0,003 % - 0,110 %.

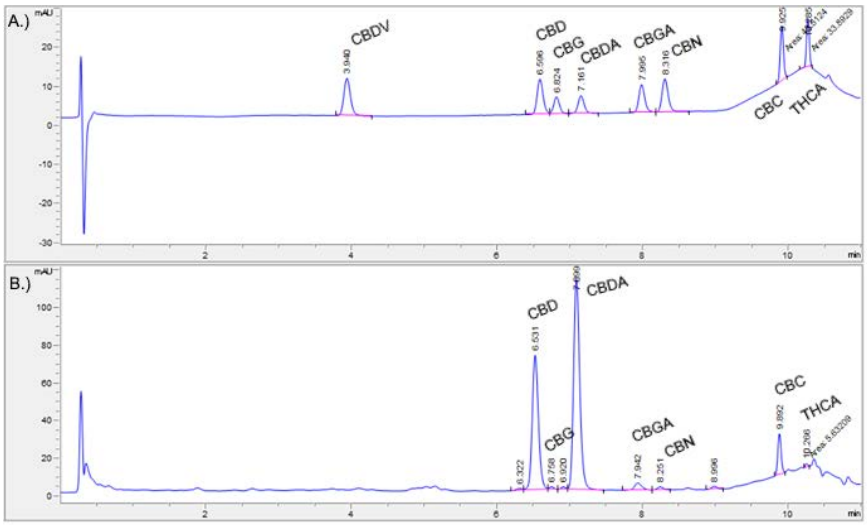

Fig. 1. Chromatograms of 8 cannabinoids analytes: (A) 10 ppm standard solution in methanol and (B) sample of dried hemp biomass. HPLC method parameters: column Agilent Poroshell EC-C18, 3,0 x 60 mm, 2,7 ε m; mobile phase: water and methanol with 0,1% formic acid; flow 1 mL/min; detection at 228 nm.

This method was successfully applied for the detection and quantification of 8 cannabinoids analytes in different real samples available in a local market. The concentrations were compared to the specified by the manufacturers.

[1] O.Aizpurua-Olaizola, J.Omar, P.Navarro et al., Identification and quantification of cannabinoids in *Cannabis sativa L.* plants by high performance liquid chromatography-mass spectrometry, *Anal Bioanal Chem* 406, 7549-7560 (2014).

[2] F. Grotenhermen, K. Muller-Vahl, The therapeutic potential of cannabis and cannabinoids, *Dtsch Arzbtebl Int* 109(29-30), 495-501 (2012).

[3] S. Zivovinovic, R. Alder, M. D. Allenspach et al., Determination of cannabinoids in *Cannabis sativa L.* samples for recreational, medical, and forensic purposes by reversed-phase liquid chromatography-ultraviolet detection, *J Anal Sci Technol* 9, 27 (2018).

NEW FLUORENE CLASS SEMICONDUCTORS AS HOLE TRANSPORTING MATERIALS FOR PEROVSKITE SOLAR CELLS

Aistė Jegorovė[1], Marytė Daškevičienė[1], Vygintas Jankauskas[2], Egidijus Kamarauskas[2], Vytautas Getautis[1]

[1] Department of Organic Chemistry, Kaunas University of Technology, Lithuania
[2] Institute of Chemical Physics, Vilnius University, Lithuania
aiste.ilciukaite@ktu.lt

Nowadays, people cannot imagine their life without everyday appliances. Most of these devices require electricity to operate. One of the most popular ways to extract energy is from non-renewable energy sources. Scientists have been looking for alternative ways to generate energy from renewable sources, such as wind energy, geothermal energy, solar energy, hydropower etc. The Sun is known to be the most powerful source of energy. Solar cells are devices that convert absorbed light into electricity and silicon solar cells are currently the most commonly used technology to do that. However, it has its own drawbacks and other high efficiency solar cell technologies have been developed. The efficiency of perovskite solar cells has increased significantly over the last decade [1]. In addition, their production requires cheap raw materials. Perovskite Solar cells are among the most efficient third-generation cells however, there are several obstacles that need to be addressed in order for it to see a widespread use. One of them is that Perovskite layer is unstable. And the other problem is the use of expensive charge-transporting semiconductors such as Spiro-OMeTAD or fullerene derivatives to obtain efficient devices [2]. Therefore, there is a vigorous search for cheaper and simpler methods for the synthesis of organic semiconductors. Fluorene class derivatives are known to be promising as positive charge carriers [3]. Carbazole class compounds have also attracted the attention of scientist due to their plain synthesis and simple purification methods [4].

The aim of this project is to synthesize inexpensive materials, containing carbazolyl- and fluorenyl-chromophores, that would be obtained by a simple synthetic methods and would be suitable as hole-transporting semiconductors for perovskite solar cells.

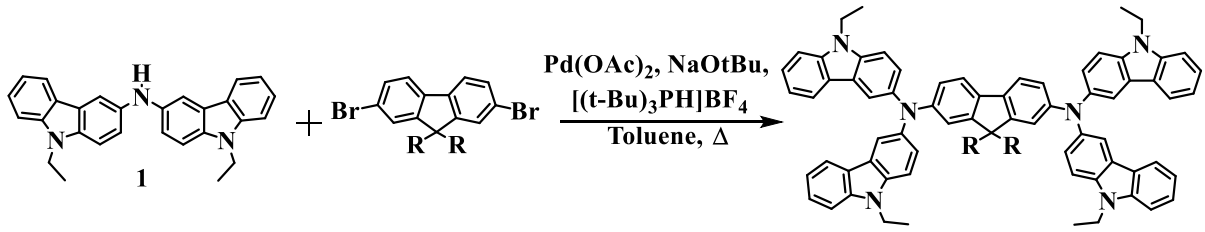

V1257: R= $-CH_3$;
V1258: R= $-CH_2CH_2CH_3$;
V1269: R= $-CH_2CH(CH_2CH_3)CH_2(CH_2)_2CH_3$.

Fig. 1. Synthesis of new fluorene derivatives.

All target compounds are amorphous and has thermal stability greater than 400 °C. The length of alkyl chain affects thermal stability and glass transition temperatures. T_d decreases when there are longer alkyl chains in fluorene „central“ fragment except with ethylhexyl substitutes. The obtained data shows that jonization potencial increases with the lenght of alkylchain and it is near up to 5 eV. The charge carrier mobility is in range of $1.8 \cdot 10^{-4} – 7.8 \cdot 10^{-4}$ $cm^2/V \cdot s$ in strong fields.

[1] https://www.nrel.gov/pv/cell-efficiency.html
[2] T. P. I. Saragi, T.Spehr et al. Spiro Compounds for Organic Optoelectronics, Chem. Rev. **107**, 1011- 1065 (2007).
[3] N. J. Jeon et al. A fluorene-terminated hole-transporting material for highly efficient and stable perovskite solar cells, Nature Energy **3(8)**, 682–689 (2018).
[4] A. Singh et al. Bis(diphenylamine)-tethered carbazolyl anthracene derivatives as hole-transporting materials for stable and high-performance perovskite solar cells, ACS Appl. Energy Mater., **3, 11**, 10752–10764 (2020).

2014-2020 Operational Programme for the European Union Funds Investments in Lithuania

DATE SEED: A GREAT SOURCE OF BIOACTIVE COMPOUNDS WITH ANTIOXIDANT POTENTIAL

Yasmina Halabi[1], Chaimae Nasri[1], Hicham Harhar[1], Abdelkebir Bellaouchou[1], Mohamed Tabyaoui[1]

[1] Department of Chemistry, University Mohammed V, Morocco
halabiyasmina@yahoo.fr

The date palm (Phoenix dactylifera L.) is a popular fruit among Middle Eastern countries. Indeed, it is a staple food for millions of people in these countries. Besides, Date palm plays an important economic, social and ecological role for people living in arid and semi-arid areas. Date seeds, also known as pits or seeds, are waste products from date processing and packaging plants. Therefore, seeds contain many precious substances such as carbohydrates, vegetable oil, dietary fiber, bioactive polyphenols, and natural antioxidants. The latter can be used in many applications such as the formulation of food supplements, cosmetics, or alternative medicine[1]. In south Moroccan folklore, date seeds are frequently used for making non-caffeinated coffee or for making eyeliner kohl and hair coloring by ladies. They can also be used as an alternate feed ingredient for cattle to increase their weight[2]. Phytochemical profiling indicates the presence of some important compounds such as polyphenols, flavonoids, tannins, carotenoids, saponins, terpenes, anthocyanins, and leucoanthocyanins with a lack of tannins gallic and cardiac glycosides[3]. Likewise, date seed oil contains 38.71-50.08% of saturated fatty acid and 48.89-60.77% of unsaturated fatty acid with lauric and oleic as the main ones, respectively. The quantitative analysis of date seed extract showed a high amount of phenolics, flavonoids, and tannins content. It also contains an important amount of alkaloids and saponins. The inhibitory activity by DPPH, ABTS, and FRAP of date seed extract shows that Moroccan date palm seeds have a high antioxidant potential. It can be considered as a great source of natural antioxidants and bioactive compounds having a decent biological process, therapeutic, medicinal, and purposeful values.

[1] A. M. Adeosun, S. O. Oni, O. M. Ighodaro, O. H. Durosinlorun, and O. M. Oyedele, "Phytochemical, minerals and free radical scavenging profiles of Phoenix dactilyfera L. seed extract," *J. Taibah Univ. Med. Sci.*, vol. 11, no. 1, pp. 1–6, 2016, doi: 10.1016/j.jtumed.2015.11.006.

[2] S. B. Al-Suwaiegh, "Effect of feeding date pits on milk production, composition and blood parameters of lactating ardi goats," *Asian-Australasian J. Anim. Sci.*, vol. 29, no. 4, pp. 509–515, Apr. 2016, doi: 10.5713/ajas.15.0012.

[3] P. Tepal, "Phytochemical screening, total flavonoid and phenolic content assays of various solvent extracts of tepal of Musa paradisiaca," *Malaysian J. Anal. Sci.*, vol. 20, no. 5, pp. 1181–1190, 2016.

EVALUATION OF THE POLYMER FILMS DEGRADATION IN VITRO

Yuliya Prosmytskaya[1], Anastasiya Kanunnikova[1,2]

[1]Chemistry Department, Belarusian State University, Minsk, 220030, Belarus
[2]The Republican Scientific and Practical Center for Pediatric Surgery, Minsk, 220013, Belarus
prosmjulia47@gmail.com

The environmental situation in the world is one of the most important problems of our time. Huge mountains of unutilized plastic continue to pollute the atmosphere of our planet, its water and soil. In this regard, the creation of biodegradable materials is very relevant. Biodegradable polymers are designed to degrade upon disposal by the action of living organisms. They can be used in various fields: heavy and light industry, food industry, as well as medicine. The field of using depends on different properties that polymer material have. For instance, biodegradable material for medical use must posses a number of specific properties: do not cause a local inflammatory reaction, do not have a toxic and allergic effect on the body, do not have a carcinogenic effect, do not provoke the development of infection and maintain functional properties during the intended service life.

The time period during which the material decomposes under the influence of various factors directly depends on the composition of the polymer. The aim of our study was to correlate the data on the degradation time of composite polymer films with its composition.

In this work, different kinds of polymer films based on the natural polysaccharides blends were prepared for studying their degradation. Carboxymethyl cellulose (CMC) posess outstanding characteristics, including good biocompatibility, high thermal stability, and good affinity with body tissue, for which reason CMC-based material can be widely used [1]. Polyvinyl alcohol (PVA) is biocompatible, nontoxic, and relatively inert in body fluids. Such favourable properties have gained wide interest in its use for biomedical applications such as contact lenses, linings in artificial heart, and polymeric scaffolds for tissue engineering [2]. Sodium alginate (SA) can improve the residency stability of hydrophilic polymers in the body because of the embedding of hydrophilic polymers in the alginate network structure [3]. Alginate dressings in the dry form absorb wound fluid to re-gel, and the films then can supply water to a dry wound, maintaining a physiologically moist microenvironment and minimizing bacterial infection at the wound site during surgical operations. Alginate can be selectively ionically cross-linked with calcium ions to maximize its performance as a film. In addition, we used glycerol in different concentrations as the plasticizing agent in all samples.

To study the degradation process we choose medium of the PBS (phosphate buffered saline, pH = 7,4). It is a balanced salt solution used for a variety of cell culture applications, such as washing cells before dissociation, transporting cells or tissue, diluting cells for counting, and preparing reagents. It was prepared according to the method described in the source [3].

Prepared membranes were cut into 20×20 mm pieces, then placed in a test tube containing 30 ml of pH 7.4 phosphate-buffered saline for the study of degradation in vitro. The tubes were immersed in a 37 °C and observed for 16 weeks. At predetermined time intervals, the PBS was collected and replaced with a fresh one. The assessment was carried out according to the following marks: the beginning of destruction, complete decomposition of the film into pieces, complete dissolving.

During the experiment, the following results were obtained: the optimal concentration of the calcium chloride solution for crosslinking the alginate was selected in order to obtain a film with a established dissolution time For comparison, when the film is cross-linked with a 2% solution of calcium chloride, the destruction of the film begins on the second day, while without it, the film completely dissolves in 15 minutes. However, due to the interaction of phosphate anions and calcium cations, turbidity is formed due to the appearance of insoluble calcium phosphates and calcium hydrophosphates. An increase in the alginate content also extends the degradation time of the film compared to a single-component composition. The film with a mass content of 50% alginate disintegrated into segments in 3 days, while the 30% alginate film began to degrade on 2 days. The addition of PVA extends the degradation time, but all samples didn't dissolve during the all time of experiment. An important factor is the content of glycerol in the film sample: excess or lack of it negatively affects the process of degradation. For comparison, after treating the film with a 5% glycerol solution for 15, 30, and 90 seconds, destruction began on the 2nd, 7th, and 2nd day, respectively.

During the experiment, it can be concluded that the best compositions based on CMC and alginate completely dissolve within 3 weeks, therefore, they can be used for effective prevention of peritoneal adhesions. PVA-based films have shown themselves to be quite resistant to the external environment. They can be offered for use as the same packaging materials for products for which a long shelf life is important.

[1] Polymer materials for prevention of postoperative adhesion / J. Li [et al.] // Acta Biomater. – 2017. – Vol. 61 – P. 21-40.
[2] Tracking the urinary excretion of high molar mass poly(vinyl alcohol) / A. Besheer [et al.] // J. Biomed. Mater. Res. - Part B Appl. Biomater. – 2007. – Vol. 82, № 2 – P. 383-389.
[3] Hyaluronic acid/mildly crosslinked alginate hydrogel as an injectable tissue adhesion barrier / S.Y. Na [et al.] // J. Mater. Sci. Mater. Med. – 2012. – Vol. 23, № 9 – P. 2303-2313.
[4] Interaction of chitosan with cefotaxime / R. H. Mudarisova [et al.] // Journal of Applied Chemistry. – 2006. – Vol. 79, № 7. – P. 1210–1212

DEVELOPMENT OF A VOLTAMMETRIC METHOD FOR THE DETERMINATION OF CU (II) IONS IN AQUEOUS SAMPLES USING NOVEL AZO-AZOMETHINE COMPOUNDS AS COMPLEXING AGENTS

Artem Bezfamilnyi[1], Stela Georgieva[1*], Anton Georgiev[2]

[1]University of Chemical Technology and Metallurgy, Department of Analytical Chemistry, 1756 Sofia, Bulgaria
[2]University of Chemical Technology and Metallurgy, Department of Organic Chemistry, 1756 Sofia, Bulgaria
st.georgieva@uctm.edu

The compounds and their derivatives containing the azo component N = N are increasingly used in various fields of life and practice. They are used as indicators, dyes, optical sensors and recording devices in holographic environments, in photodynamic therapy, in molecular motors and in other photonic devices, and some of their metal complexes as drugs. Unfortunately, the literature has no enough information for azo-azomethine derivatives application for the determination of metal ions in samples with different matrix compositions. The mention above gives us the reason for developing a sensitive and selective method for the determination of heavy metals in aqueous samples. Therefore, the present abstract describes the development of a voltammetric method for the determination of Cu (II) ions in surface water samples using novel N-phthalimide azo-azomethine compounds as ligands. The assays were performed in a three-electrode cell with a voltammeter (Metrohm 797 VA, with 797 VA stand) on a HMDE-working electrode against Ag / AgCl, KCl (3.00 mol l^{-1}) as a reference electrode. The results showed that the proposed method allows selective determination of Cu (II) with detection limits: 0.230 ng ml^{-1} and determination: 0.423 ng ml^{-1}. The method is sensitive with a coefficient of analytical function: $5x10^6$ μA.ml mol^{-1}. The precision of the determinations estimated by the relative standard deviation is Sr = 0.8%.

Acknowledgments: Financial support from Bulgarian National Scientific Fund project КП-06-ОПР 03/3 of the Ministry of Education and Science, Bulgaria is gratefully acknowledged.

3D METALLIC COPPER-NICKEL FOAMS AS CATALYSTS FOR THE ELECTROOXIDATION OF SODIUM BOROHYDRIDE

Gana Linlienã, Aldona Balinaitã, Loreta Tamagauskaitã-Tamagiinaitã, Eugenijus Norkus

Department of Catalysis, Center for Physical Sciences and Technology, Saulãtekio ave. 3, LT-10257, Vilnius, Lithuania
zana.cinciene@ftmc.lt

The search for novel efficient catalysts for fuel cells is industrially vital. This work aims to form efficient nanostructured catalysts by electroplating 3D metallic copper-nickel (Cu-Ni) foams with the further decoration of them with gold nanoparticles (AuNPs) for the electrooxidation for sodium borohydride ($NaBH_4$). Cu-Ni foams have been electroplated on the titanium (Ti) surface electrolytes contained 0.5 M Ni^{2+} ions and Cu^{2+} ions concentrations in the range from 0.01 to 0.02 M. AuNPs have been deposited on the Cu-Ni/Ti electrodes by their immersion into a 1 mM $HAuCl_4$ solution at 25 ÜC for 1 min. The morphology and composition of synthesized catalysts were examined using Scanning Electron Microscopy (SEM), X-Ray Diffraction (XRD), and Inductively Coupled Plasma Optical Emission Spectroscopy (ICP-OES).

It was found that the prepared 3D metallic Cu-Ni foams and those decorated with AuNPs show good electrochemical stability in an alkaline $NaBH_4$ solution for a long time in a potential range from -1.2 to 0.6 V at an electrode potential scan rate of 10 mV s^{-1}. Moreover, decoration of Cu-Ni foams with AuNPs results in enhancement of electrocatalytic activity for the electrooxidation of $NaBH_4$ as compared with that at pure Cu-Ni foams.

Acknowledgments

This research is funded by the European Social Fund under Measure No. 09.3.3-LMT-K-712-19-0138 ódevelopment of Competences of Scientists, other Researchers and Students through Practical Re-search Activitiesô

METHODS FOR THE DETERMINATION OF COVALENT BONDS IN SMALL MOLECULE CRYSTALS

Eglã Ġidlauskaitã[1], Andrius Merkys[2]

[1] Department of Mathematical Computer Science, Vilnius University, Lithuania
[2] Department of Proteinï DNA Interaction, Institute of Biotechnology, Vilnius University, Lithuania
egle.sidlauskaite@mif.stud.vu.lt

Crystallography allows to determine the exact position of the atoms that constitute crystal structures [1]. Crystal structure determination methods however are unable to capture chemical bonding. In practice, two atoms are considered to be connected by a chemical bond if calculated distance between them is smaller or equal to the sum of their covalent radii. This distance is called covalent bond length.

Covalent radii tables that are often used to determine chemical bonds between atoms are created by statistically analysing lengths of observed chemical bonds. The most popular covalent radii tables [2] are derived from data from Cambridge Structural Database [3] which is not an open-access database, therefore restricts usage and spread of its data and derived results. This issue motivates research for a suitable method for determination of covalent bonds which would allow covalent radii tables to be calculated based on data from an open-access database, e.g. Crystallography Open Database [4].

Van der Waals gap is an interval which separates covalent bond lengths from distances between atoms affected by Van der Waals forces. In this interval distances between atoms are not observed. Thus, Van der Waals gap corresponds to the lowest density region in the dataset [5]. In order to identify the lowest density region, Gaussian distribution mixture model can be applied to the distribution of distances between atoms (Fig. 1).

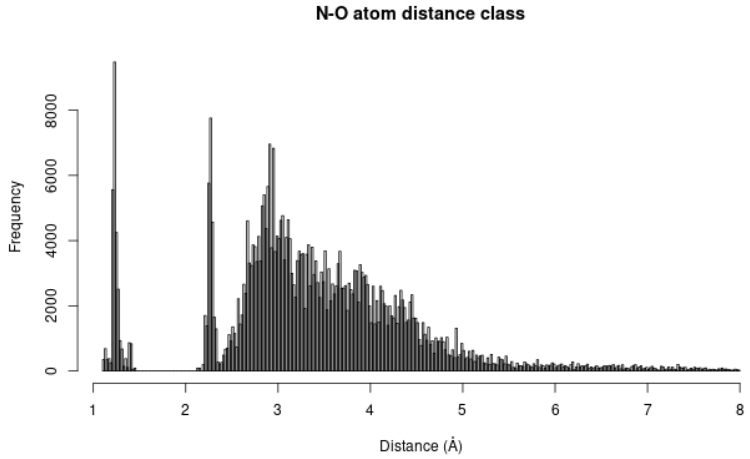

Fig. 1. Van der Waals gap (1.5ï 2) observed in histogram of distances between nitrogen and oxygen atoms.

Distribution of distances between atoms can be approximated by a two component Gaussian mixture model, with first component representing covalent bonds peak and second component representing Van der Waals peak. Lowest density region of the model is determined using simplex method. This process is complicated by random distribution (observed on the right side (>2.3) of Fig. 1). In order to reduce the impact of random distribution three methods were analysed: replacement of the initialisation vector, removal of small-proportioned model components and removal of observations exceeding Van der Waals interaction length.

During the research, methodology for automated determination of lowest density regions was developed. The most effective method was determined to be the removal of small-proportioned model components, resulting in model with two components selected as best in almost 50% of the cases. Removal of observations exceeding Van der Waals interaction length has also demonstrated positive results which incites further analysis on methods to reduce the impact of random distribution on parameters of mixture model components.

[1] Graġulis, S., Merkys, A., Vaitkus, A. & Okuliþ-Kazarinas, M. *Computing stoichiometric molecular composition from crystal structures*. Journal of Applied Crystallography, 48(1), 85-91. (2015) doi: 10.1107/s1600576714025904

[2] Cordero, B., G· mez, V., Platero-Prats, A. E., Rev®s, M., Echeverr²a, J., Cremades, E., Barrag§n, F. & Alvarez, S. *Covalent radii revisited*. Dalton Trans. (21), 2832ï 2838. (2008) doi: 10.1039/b801115j

[3] Groom, C. R., Bruno, I. J., Lightfoot, M. P. & Ward, S. C. *The Cambridge Structural Database*. Acta Cryst. (B72), 171-179. (2016) doi: 10.1107/S2052520616003954

[4] Graġulis, S., Daġkeviþ, A., Merkys, A., Chateigner, D., Lutterotti, L., Quir· s, M., Serebryanaya, N. R., Moeck, P., Downs, R. T. & LeBail, A. *Crystallography Open Database (COD): an open-access collection of crystal structures and platform for world-wide collaboration*. Nucleic Acids Research (40), D420-D427. (2012) doi: 10.1093/nar/gkr900

[5] Alvarez, S. *A cartography of the van der Waals territories.* Dalton Trans. (42): 8617-8636. (2013) doi: 10.1039/C3DT50599E

CHARACTERISATION OF LOW MOLECULAR WEIGHT BIOMARKERS OF INFLAMMATION AND CANCER

Giedrė Karzaitė[1,2], Mahboubeh Eskandari[1], Tautgirdas Ruzgas[1]

[1]Malmö University, Department of Biomedical Sciences, Per Albin Hanssons 35, SE-214 32 Malmö, Sweden
[2]Vytautas Magnus university, Department of Biological, Vileikos str. 8-802, LT-44404, Kaunas, Lithuania
giedre.karzaite@gmail.com

Increased amino acid catabolism is essential for tumor growth and immune regulation in cancer. This is especially true for the kynurenine metabolites of tryptophan, which exert diverse biological effects and have been investigated as markers of tumor progression and therapeutic effect. The kynurenine pathway has been associated mostly with immune tolerance and tumor escape [1]. Approximately 95% of the free L-Trp in the body is metabolised down the Kyn pathway, generating several biologically active metabolites, including kynurenine (Kyn), kynurenic acid, 3-hydroxykynurenine (3-HK), 3-hydroxyanthranilic acid (3-HAA) [2].

In this research the main tasks were to review low molecular weight (LMW) biomarkers of inflammation and cancer, which are derivatives of amino acids, e.g., derivatives of histidine, tryptophan, arginine, etc; to evaluate methods enabling transdermal detection of amino-acid derived LMW biomarkers of inflammation and cancer; to experimentally assess the relevance of some of these methods for detection of skin inflammation and cancer, e.g., skin penetration assays and cell culture methods.

Our results showed that the 3-HKYN and 3-HAA are relatively stable in the pH range 5.5-7.4. If we are going to make extraction of these compounds from skin at basic solutions we might need to study stability at pH 10 and higher. It is possible to measure penetration of these compounds through skin after lipid extraction from skin using electrochemical methods. Detection limits by electrochemistry are 1 μM or higher.

[1] Clara R. O., Assmann N., Moreno A. C. R., Coimbra J. B. 2015. Melanocytes are more responsive to IFN-γ and produce higher amounts of kynurenine than melanoma cells. *Biol. Chem*. Vol. 397. No. 1. P. 85–90.
[2] Yeung A. W.S., Terentis A. C., King N. J.C., Thomas S. R. 2015. Role of indoleamine 2,3-dioxygenase in health and disease. *Clinical Science.* Vol. 129. No. 7. P. 601–672.

THE EFFECT OF STORAGE TIME ON THE LOADING EFFICIENCY OF NISIN-LOADED ULVAN PARTICLES

Edita Kodyte[1*], Ruta Gruskiene[1], Jolanta Sereikaite[1]

[1] Department of Chemistry and Bioengineering, Vilnius Gediminas Technical University, Lithuania
edita.kody@gmail.com

Nisin, which is produced by the lactic acid bacteria, *Lactococcus lactis* subsp. *lactis*, is a small 3510 Da cationic peptide composed of 34 amino acid residues. It is a broad-spectrum antimicrobial agent against Gram-positive bacteria. Nisin is widely used in the food sector for improving food safety, for example, dairy and canned food products [1]. However, nisin antimicrobial efficacy is influenced by many factors, i.e. interactions with food components or conditions used for food production. To ensure nisin stability, nisin is coating with the wall materials, e.g. proteins, polysaccharides, or lipids [2]. In this work, for particles preparation ulvan was used. Ulvan is a water-soluble anionic sulphated polysaccharide, which is derived from green algae, *Ulvales*. Ulvan polysaccharide is inexpensive, biocompatible, biodegradable, and nontoxic [3]. Due to numerous advantages, ulvan can be used as a coating material that forms complexes with an oppositely charged molecule.

The aim of this work was to prepare nisin-loaded ulvan particles using the complexation method and observe the effect of storage time on the loading efficiency. Nisin-loaded ulvan particles at a different pH range of 4.0-7.0 were prepared and stored at 4 ÁC. The final concentration of ulvan was 0.4 mg/mL, and the nisin concentration was in the range of 0.1-1 mg/mL. The loading efficiency was determined by the capillary zone electrophoresis method using 7100 Capillary Electrophoresis unit (Agilent Technologies).

The loading efficiency was evaluated after two and four weeks and was compared with the initial loading efficiency. It didnôt change at all pH values with nisin concentration up to 0.3 mg/mL. The loading efficiency has decreased very slightly over time when nisin concentration was in the range from 0.4 to 1 mg/mL.

Acknowledgements:

We thank Professor Vassilios Roussis from the National and Kapodistrian University of Athens for the gift of the ulvan sample used in this study.

This research was funded by the European Social Fund under the No 09.3.3-LMT-K-712 ñDevelopment of Competences of Scientists, Other Researchers and Students through Practical Research Activitiesò measure. Grant No 09.3.3.-LMT-K-712-22-0040.

[1] L. J. de Arauz, A. F. Jozala, P. G. Mazzola, T. C. V. Penna. Nisin biotechnological production and application: a review. Trends in Food Science &Technology, 20(3-4), 146-154 (2009).

[2] I. Khan, D. H. Oh. Integration of nisin into nanoparticles for application in foods. Innovative Food Science & Emerging Technologies, 34, 376-384 (2016).

[3] L. A. Tziveleka, E. Ioannou, V. Roussis, Ulvan, a bioactive marine sulphated polysaccharide as a key constituent of hybrid biomaterials: A review, Carbohydrate Polymers **218**, 355-370 (2019).

IDENTIFYING INSULIN FIBRIL CONFORMATIONAL DIFFERENCES BY THIOFLAVIN-T BINDING CHARACTERISTICS

Mantas Ziaunys[1], Andrius Sakalauskas[1], Vytautas Smirnovas[1]

[1] Institute of Biotechnology, Life Sciences Center, Vilnius University, Lithuania
mantas.ziaunys@gmail.com

Amyloidogenic protein aggregation into insoluble fibrillar aggregates is linked to several amyloidoses, including neurodegenerative Alzheimer's and Parkinsonôs diseases [1]. Despite many years and countless studies, there are still very few effective anti-amyloid drugs available and most potential compounds fail to pass all clinical trials. One of the main reasons for these failures is the complex nature of amyloid aggregates. It is known that the same protein molecule may form fibrils with distinct conformational and morphological characteristics. Each of these fibril types also possess specific self-replication tendencies and may respond differently to potential anti-amyloid compounds. In many cases, fibril identification is done by employing atomic force microscopy, where results are highly dependent on sample deposition techniques, as well as infrared spectroscopy, which requires relatively high concentrations of the protein sample. In recent years it has been observed that distinct protein fibrils have specific amyloidophilic dye binding [2] characteristics (affinity, fluorescence intensity), which could potentialy be used to identify unique amyloid aggregates.

In order to examine whether an amyloid-specific dye ï thioflavin-T [3] could be used to differentiate between conformationally-different fibrils, insulin was aggregated into four distinct fibril types, under four environmental conditions. Human recombinant insulin powder was dissolved in four types of solutions (1. 20% acetic acid, containing 100 mM NaCl; 2. 100 mM sodium phosphate buffer (pH 2.0); 3. 100 mM sodium phosphate buffer (pH 2.4), containing 100 mM NaCl; 4. PBS (pH 7.4)) and incubated at 60ÁC. After fibrils were formed, they were initially examined by atomic force microscopy and Fourier-transform infrared spectroscopy, to verify morphological and structural differences. Afterwards, the samples were mixed with a range of thioflavin-T concentrations and their absorbance, as well as excitation-emission matrices were scanned.

The results show that each type of aggregate has unique bound-dye fluorescence properties, such as maximum excitation and emission wavelengths, as well as fluorescence quantum yield. Considering that such a dye-based examination requires minimal amounts of fibrils and is relatively quick to perform, it may be used as an alternative method to identify amyloid fibril conformation differences.

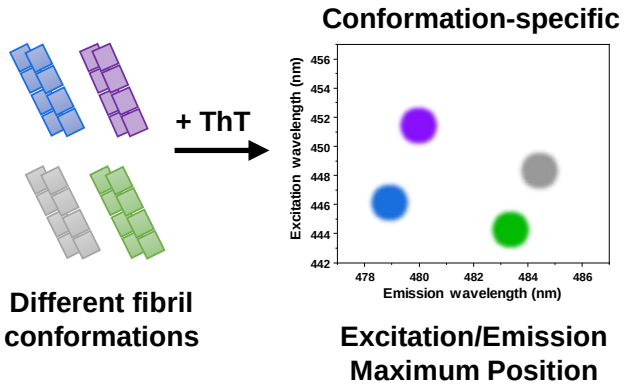

Fig. 1. Different insulin fibril conformations have specific ThT binding and fluorescence characteristics.

[1] Knowles, Tuomas P. J., et al. ñThe Amyloid State and Its Association with Protein Misfolding Diseases.ò Nature Reviews Molecular Cell Biology, vol. 15, no. 6, 2014.
[2] Krebs, M. R. H., et al. ñThe Binding of Thioflavin-T to Amyloid Fibrils: Localisation and Implications.ò Journal of Structural Biology, vol. 149, no. 1, 2005.
[3] Xue, Christine, et al. ñThioflavin T as an Amyloid Dye: Fibril Quantification, Optimal Concentration and Effect on Aggregation.ò Royal Society Open Science, vol. 4, no. 1, 2017.

S-SUBSTITUTED 5-(2-((4-ETHOXYPHENYL)AMINO)ETHYL)-4-PHENYL-2,4-DIHYDRO-3*H*-1,2,4-TRIAZOLE-3-THIONE DERIVATIVES AS POTENTIAL ANTIOXIDANT AGENTS

Aida Ġermukġnytā[1], Ingrida Tumosienā[1], Kristina Kantminienā[2]

[1] Department of Organic Chemistry, Kaunas University of Technology, Radvilā nÔpl. 19, LT-50254 Kaunas, Lithuania
[2] Department of Physical and Inorganic Chemistry, Kaunas University of Technology, Radvilā nÔpl. 19, LT-50254 Kaunas, Lithuania
aida.sermuksnyte@ktu.edu

1,2,4-Triazole derivatives are promising chemical scaffolds in medicinal chemistry due to their vast biological activity and extensive structural modification capability. 1,2,4-Triazole moiety has been incorporated into a structure of many drugs, including the ones with antiviral (ribavirin), antimigraine (rizatriptan) and antifungal (fluconazole, itraconazole, and voriconazole) activities. Well-known drugs, triazolam, alprazolam, estazolam, contain the 1,2,4-triazole cycle as well [[1]]. 1,2,4-Triazole-3-thione derivatives possess a broad spectrum of potential biological activity including antimicrobial, antioxidant, anticancer, anti-tubercular, anticonvulsant, fungicidal, antiepileptic, and anti-inflammatory ones [[2]].

A series of novel *S*-substituted 4-phenyl-2,4-dihydro-*3H*-1,2,4-triazole-3-thione derivatives were synthesized from 3-[(4-ethoxyphenyl)amino]propanehydrazide (Scheme 1). First, propanehydrazide **1** was treated with phenyl isothiocyanate in methanol to give a corresponding thiosemicarbazide **2**, which subsequently underwent cyclization under alkaline conditions to provide 5-(2-((4-ethoxyphenyl)amino)ethyl)-4-phenyl-2,4-dihydro-*3H*-1,2,4-triazole-3-thione (**3**) [[3], [4]]. Reactions of the latter with a series of acetophenone derivatives afforded the target compounds **4-9** [[5]]. Structures of the synthesized compounds were confirmed by IR, ^{1}H, ^{13}C NMR spectroscopy and mass spectrometry data.

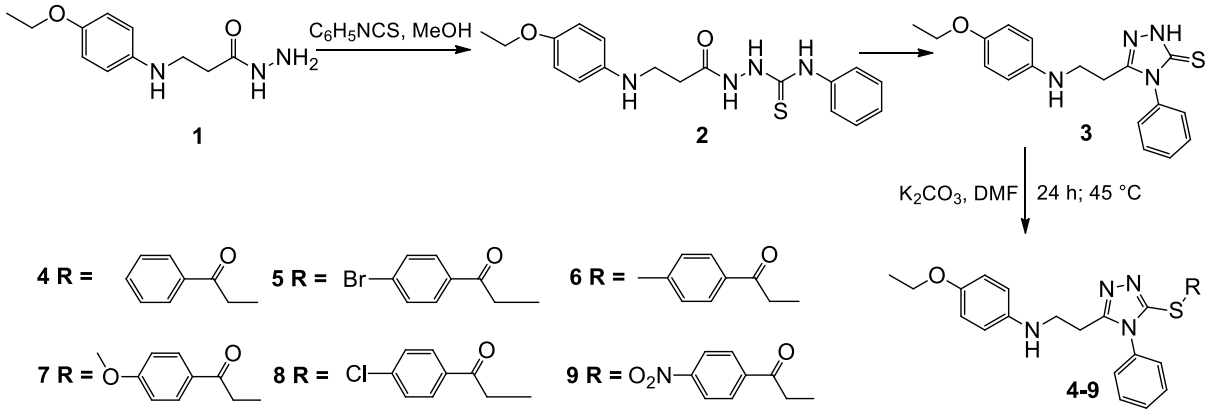

Scheme 1. Synthesis of compounds **2**ï **9**.

Antioxidant activity of the synthesized compounds **3-9** was screened by DPPH (2,2-diphenyl-1-picrylhydrazyl) radical scavenging assay and FRAP (ferric reducing antioxidant power) assay. 2-((5-(2-((4-Ethoxyphenyl) amino)ethyl)-4-phenyl-4*H*-1,2,4-triazol-3-yl)thio)-1-(4-nitrophenyl) ethan-1-one (**9**) has been identified as a promissing antioxidant agent possessing antioxidant activity 1.6 times higher than that of a well-known antioxidant ascorbic acid as determined by DPPH radical scavenging assay and 1.1. times higher according to FRAP assay. Compound **8** bearing Cl substituent in its molecule has shown higher antioxidant activity than that of vitamin C as detected by both methods as well.

[1] ķ.G. K¿-¿kg¿zel, P. ¢ākla-S¿zg¿n, Recent advances bioactive 1,2,4-triazole-3-thiones, European Journal of Medicinal Chemistry **97**, 830-870 (2015).
[2] A.A. Aly, A.A. Hassan, M.M. Makhlouf, et al., Chemistry and Biological Activities of 1,2,4-Triazolethiones -Antiviral and Anti-Infective Drugs, Molecules **25**, 3036 (2020).
[3] Tumosienā, K. Kantminienā, A. Pavilonis, et al., Synthesis of azole derivatives from 3-phenylaminopropanohydrazide and evaluation of their antimicrobial efficacy, Heterocycles **78**, 59-70 (2009).
[4] Tumosienā, I. Jonuġkienā, K. Kantminienā, et al., The synthesis of azole derivatives from 3-[(4-methylphenyl)amino]propanehydrazide and its *N*-phenylcarbamoyl derivatives, and their antibacterial activity, Monatshefte f¿r Chemie/Chemical Monthly **143**, 1441-1450 (2012).
[5] I. Tumosienā, I. Jonuġkienā, K. Kantminienā, et al., The synthesis of *S*-substituted derivatives of 3-[2-[(4-methylphenyl)amino]ethyl]-4-phenyl-4,5-dihydro-1*H*-1,2,4-triazole-5-thiones and their antioxidative activity, Monatshefte f¿r Chemie/Chemical Monthly **145**, 319-327 (2014).

ISOLATION OF PHOSPHATE SOLUBILIZING MICROORGANISM AND INDUSTRIAL FERMENTATION PROCESS OPTIMIZATION

Raimonda Maģylytã[1*], Justina KaziÎnienã[2], Eglã Lastauskienã[1], Audrius Gegeckas[1]

[1] Department of Microbiology and Biotechnology, Vilnius University, Lithuania
[2] Institute of Biology and Plant Biotechnology, Vytautas Magnus University, Lithuania
raimonda.mazylyte@gmail.com

Phosphorus is one of the most necessary macronutrients that are indispensable for plant development and growth. In plant cells, phosphorus plays an important role in the energy and nutrient metabolism, in the fission and reproduction stages of cells, promotes vitality and resistance to disease [1]. Phosphate solubilizing bacteria (PSB) has ability to convert insoluble soil phosphate forms into a bioavailable form through solubilization and mineralization processes and making it available to plants as biofertilizers. In this study a phosphate solubilizing microorganism was isolated from the soil sample of Lithuania agricultural field using Pikovskayaôs (PVK) agar and National Botanical Research Instituteôs phosphate growth medium with bromothymol blue (NBRIP-BMB) containing $Ca_3(PO_4)_2$ as the insoluble tricalcium phosphate (TCP) [2].

Based on 16Ss rRNA gene sequence analysis and phenotypic and molecular characteristics, the strain was identified as *Bacillus* sp. MVY-004. The culture nutrient medium and fermentation process growth conditions were optimized: molasses was used as a carbon source; yeast extract powder was used as a organic source; $NH_4H_2PO_4$ was used as a nitrogen source; the culture temperature was 30Ñ0.5 ÁC; the initial value of pH was 7.0Ñ0.5; the partial pressure of oxygen (pO_2) was 60Ñ2.0; the mixer revolutions per minute (RPM) was 25-850; and the incubation and fermentation time was 48-50 hours. Bacterial suspensions analysis using Liquid Chromatography Time-of-Flight Mass Spectrometry (LS-TOF/MS) showed that *Bacillus* sp. MVY-004 was produced organic acids as: citric, succinic, 2-ketogluconic, gluconic, malic, lactic, oxalic acids.

Sample No.	Concentration, Õg/mL (average from triplicates ÑSD)						
	Citric acid*	Succinic acid**	2-ketogluconic acid*	Gluconic acid*	Malic acid**	Lactic acid***	Oxalic acid***
1.	13.5Ñ0.6	257.0Ñ3.0	68.0Ñ2.0	287.0Ñ13.0	232.0Ñ7.0	419.0Ñ3.0	34.0Ñ2.0

*concentration calculated using citric acid calibration curve
**concentration calculated using succinic acid calibration curve
***concentration calculated using oxalic acid calibration curve

Fig. 1. Organic acids detection using LC-TOF/MS

Furthermore, the experiment showed that *Bacillus* sp. MVY-004 can produced phytohormones as: indole-3-acetic (IAA), jasmonic (JA) and gibberellic (GA_3) acids. Phosphate solubilizing bacteria (PSB) *Bacillus* sp. MVY-004 synthesizes and exports phytohormones which are called plant growth regulators (PGRs). PGRs are organic substances that influence physiological processes of plants at extremely low concentrations [3].

Sample No.	Concentration, Õg/mL (average from triplicates ÑSD)		
	Indole-3-acetic acid*	Jasmonic acid**	Gibberellic acid***
1.	1.370Ñ0.020	0.173Ñ0.009	0.800Ñ0.060

*concentration calculated using indole-3-acetic acid calibration curve
**concentration calculated using jasmonic acid calibration curve
***concentration calculated using gibberellic acid calibration curve

Fig. 2. Phytohormones detection using LC-TOF/MS

The use of PSB in agriculture is gaining importance and is becoming a permanent part of cropping systems throughout the world. It is not only environment-friendly but also cost-effective, reliable, and durable. Efficient phosphate solubilization by *Bacillus* sp. MVY-004 demonstrated the strong application potential and have probable use for future agricultural and biotechnological application.

[1] F. Wang, M. Deng, J. Xu et al., Molecular mechanisms of phosphate transport and signaling in higher plants, Seminars in Cell and Developmental Biology 74, 114-122 (2017).
[2] M. R. Sarikhani, B. Khoshru, and R. Greiner, Isolation and identification of temperature tolerant phosphate solubilizing bacteria as a potential microbial fertilizer, World Journal of Microbiology and Biotechnology 35, 126 (2019).
[3] D. Egamberdieva, S. J. Wirth, A. A. Alqarawi et al., Phytohormones and Beneficial Microbes: Essential Components for Plants to Balance Stress and Fitness, Frontiers in Microbiology, 8: 2104 (2017).

ANTIOXIDANT ACTIVITY IN *TRIFOLIUM PRATENSE* L. BLOSSOMS USING DIFFERENT EXTRACTION METHODS

Jurga Andrãja Kazlauskaitã[1,2], Jurga Bernatonienã[1,2]

[1] Department of Drug Technology and Social Pharmacy, Lithuanian University of Health Sciences, Lithuania
[2] Institute of Pharmaceutical Technologies, Medical Academy, Lithuanian University of Health Sciences, Lithuania
jurga.andreja.kazlauskaite@stud.lsmu.lt

Red clover (*Trifolium pratense* L.) is a perennial legume is a rich source of isoflavones, which are reported to have beneficial health effects [1]. Moreover, it contains significant amounts of phenolic compounds which are known for their potential bio-active antioxidant properties and radical scavenging capacity [2].

The aim of this study was to investigate the antioxidant activity of *Trifolium pratense* L. blossoms extracted using different extraction methods.

Ultrasound assisted extraction was performed using 1 Ñ 0.001 g of dried and milled flower heads and 30 mL of 50 % ethanol. Temperature during extraction ï 40 and 60 ÁC. Ultrasound power 250 W and extraction time 10 and 30 min [3]. Thermal processing was performed after sonication placing extract in a heating mantle under a reflux condenser for one hour. Heat-reflux extraction was done using 1 Ñ 0.001 g of dried and milled flower that was mixed with 30 mL of 50% ethanol in a 250 mL round bottom flask and refluxed in the sand bath at 100 ÁC for 1 hour. Maceration [4] results was used as control. The antioxidant activity of extracts has been evaluated using 2,2-diphenyl-1-picrylhydrazyl (DPPH) [5] and 2,2Ñazino-bis(3-ethylbenzthiazoline-6-sulfonic acid) (ABTS) [6] radical scavenging methods. All experiments were performed in triplicate.

Spectrophotometric analysis showed that the antioxidant activity differed significantly between differently prepared extracts. Highest radical scavenging capacity in both antioxidant activity methods were determined in sample UT4 (88.23% and 40.29% ABTS and DPPH results respectively), that was prepared using ultrasound (30 min; 60 ÁC). Using ultrasound, the increase in antioxidant activity was observed by extending the duration of the ultrasonic treatment from 10 to 30 minutes. The lowest antioxidant activity was found in M sample, that was prepared using maceration and used as control (57.82% and 13.59% ABTS and DPPH results respectively). Comparing ABTS and DPPH methods, DPPH showed almost 2-3 times lower antioxidant activity in extracts, but DPPH is a more stable radical and the results of the extracts are more repetitive.

Acknowledgements

The authors would like to thank Open Access Centre for the Advanced Pharmaceutical and Health Technologies (Lithuanian university of Health Sciences) and for the opportunity to use modern infrastructure and perform this research. The authors declare no conflicts of interest.

This work was supported by the Research council of Lithuania (grant no. 09.3.3-ESFA-V-711-01-0001).

[1] T. Sabudak and N. Guler, ñ*Trifolium* L. - A review on its phytochemical and pharmacological profile,ò *Phyther. Res.*, 439ï 446, **2009**, doi:10.1002/ptr.2709.
[2] A. Tava, Ğ. Pecio, R. Lo Scalzo, A. Stochmal, and L. Pecetti, ñPhenolic Content and Antioxidant Activity in Trifolium Germplasm from Different Environments,ò *Molecules*, 298, **2019**, doi: 10.3390/molecules24020298.
[3] Y. Sun, Z. Liu, and J. Wang, ñUltrasound-assisted extraction of five isoflavones from Iris tectorum Maxim,ò *Sep. Purif. Technol.*, 49ï 54, **2011**, doi: 10.1016/j.seppur.2011.01.017.
[4] A. Krª hmer, G. Gudi, N. Weiher, M. Gierus, W. Sch¿ tze, and H. Schulz, ñCharacterization and quantification of secondary metabolite profiles in leaves of red and white clover species by NIR and ATR-IR spectroscopy,ò *Vib. Spectrosc.*, **2013**, doi: 10.1016/j.vibspec.2013.05.012.
[5] A. Wojdyğ, J. OszmiaŒski, and R. Czemerys, ñAntioxidant activity and phenolic compounds in 32 selected herbs,ò *Food Chem.*, 940ï 949, **2007**, doi: 10.1016/j.foodchem.2007.04.038.
[6] A. P. Tiveron, P. S. Melo, K. B. Bergamaschi, T. M. F. S. Vieira, M. A. B. Regitano-dôArce, and S. M. Alencar, ñAntioxidant Activity of Brazilian Vegetables and Its Relation with Phenolic Composition,ò *Int. J. Mol. Sci.*, 8943ï 8957, **2012**, doi: 10.3390/ijms13078943.

ANTIOXIDANT ACTIVITY OF NUTMEG ESSENTIAL OIL (PURE, WITH MAGNESIUM ALUMINOMETASILICATE AS EXCIPIENT AND THEIR MIXTURE IN A RATIO OF 1:1)

Inga Matulytė[1,2], Akvilė Mataraitė[3], Jurga Bernatonienė[1,2]

[1] Department of Drug Technology and Social Pharmacy, Lithuanian University of Health Sciences, Lithuania
[2] Institute of Pharmaceutical Technologies, Lithuanian University of Health Sciences, Lithuania
[3] Faculty of Medicine, Lithuanian University of Health Sciences, Lithuania
inga.matulyte@lsmu.lt

Nutmeg essential oil is colorless to pale-yellow with a specific odor [1]. It has antimicrobial, antiseptic, antiparasitic, anti-inflammatory, and antioxidant effects [2,3]. Chemical compounds, existing in essential oil, can bind free radicals and protect the live organism from negative influence [4]. The aim of this study was to compare the antioxidant activity of nutmeg essential oil prepared in different conditions.

The dried seeds of nutmeg (*Myristica fragrans*) were from Grenada. Hydrodistillation lasted 4 hours and was carried out by using Clevenger type apparatus, nutmeg and distilled water ratio was 1:20 in a round bottom flask. Magnesium aluminometasilicate (1% of water amount) was used as excipient in modified hydrodistillation. Antioxidant activity was evaluated by using 2,2-diphenyl-1-picrylhydrazyl (DPPH, Sigma Aldrich, USA). A total of 1 mL of ethanolic DPPH solution (0.1 mM) was placed in a spectrophotometer cuvette and 100ÕL of ethanolic essential oil solutions (5% and 10%) were added. All samples (pure essential oil, essential oil with excipient prepared by hydrodistillation, and a mix of these solutions in a ratio of 1:1) were incubated in the dark for 30 minutes and absorbance was measured at 515 nm (UV Spectrophotometer UV-1800 (Shimadzu, Kyoto, Japan)). The results are presented as mean ÑSD.

Antioxidant activity of pure nutmeg essential oil was 53.85Ñ0.10% and 72.14Ñ0.63%. Essential oilôs with excipient antioxidant activity was 6.43% and 5.53% lower than pure essential oilôs (5% and 10% essential oil concentration, respectively). Antioxidant activity of 5% concentration of the essential oil mix was 1.21 and 1.29 times higher than that of pure essential oil and essential oil with excipient, respectively. Essential oil mix (10%) had an approximately 11.57Ñ3.17% higher activity than the individual nutmeg essential oil solutions. The used mix of nutmeg essential oil solutions had a significantly higher antioxidant activity than the separate essential oils.

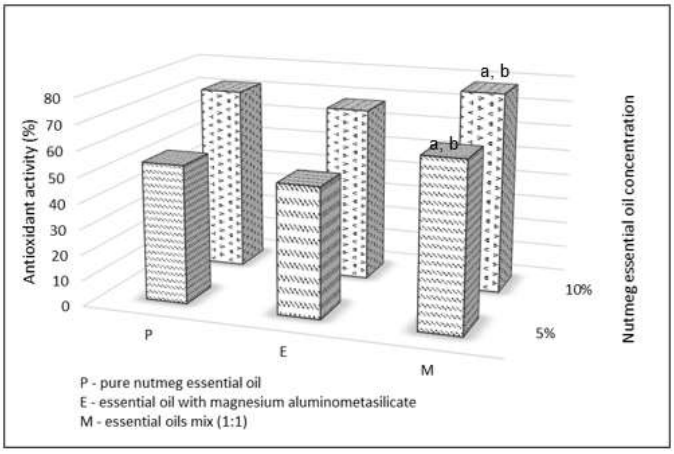

Fig. 1. Nutmeg essential oil antioxidant activity. a - $p<0.05$ versus pure essential oil, b - $p<0.05$ versus essential oil with excipient. *All samplesôstandard deviation of antioxidant activity is less than 0.78% and was not marked in the figure.

The excipient decreased the antioxidant activity of nutmeg essential oil but the mix of pure essential oil and essential oil with magnesium aluminometasilicate had a higher antioxidant activity than the separate essential oils. Two essential oil solutions work synergistically and the mixtureôs antioxidant activity is higher.

[1] Djilani, A.; Dicko, A. The Therapeutic Benefits of Essential Oils. *Nutr. Well-Being Heal.* **2012**, No. February 2012. https://doi.org/10.5772/25344.
[2] Baser, K. H.; Bunchbauer, G. *Handbook of Essential Oils: Science, Technology, and Applications*; CRC Press NW, 2010.
[3] Muchtaridi; Subarnas, A.; Apriyantono, A.; Mustarichie, R. Identification of Compounds in the Essential Oil of Nutmeg Seeds (Myristica Fragrans Houtt.) That Inhibit Locomotor Activity in Mice. *Int. J. Mol. Sci.* **2010**, *11* (11), 4771ï 4781. https://doi.org/10.3390/ijms11114771.
[4] Amorati, R.; Valgimigli, L. Methods to Measure the Antioxidant Activity of Phytochemicals and Plant Extracts. *J. Agric. Food Chem.* **2018**, *66* (13), 3324ï 3329. https://doi.org/10.1021/acs.jafc.8b01079.

DEVELOPMENT OF CONTROLLED GENE EXPRESSION SYSTEM FOR *(PARA)GEOBACILLUS* SPP. BACTERIA

Aistė Kairytė[1], Inga Matijošytė[2], Arnoldas Kaunietis[1]

[1]Department of Microbiology and Biotechnology, Institute of Biosciences, Life Sciences Center, Vilnius University, Saulėtekio ave. 7, LT-10257 Vilnius, Lithuania
[2]Sector of Applied Biocatalysis, Institute of Biotechnology, Life Sciences Center, Vilnius University, Saulėtekio ave. 7, LT-10257 Vilnius, Lithuania
aiste.kairyte@gmc.stud.vu.lt

Thermostable enzymes, such as cellulases, xylanases, proteases, pectinases, etc. have wide biotechnological and industrial applications. Most of these proteins are currently produced in mesophilic bacteria using heterologous gene expression systems due to a lack of versatile expression system for thermophilic bacteria. This often leads to different post-translational modifications or incorrect folding and, thus, protein properties are affected. These obstacles could be overcome if thermostable proteins were produced by thermophilic bacteria. Until now most attempts were unsuccessful due to a lack of genetic tools necessary for thermophilic expression, including thermostable reporter proteins, selection markers, plasmid vectors and others. However, these genetic tools are being rapidly developed which allows further successful attempts to construct an expression system for thermophilic bacteria.

The aim of our work is to create a regulated gene expression system for *(Para)Geobacillus* spp. bacteria. *(Para)Geobacillus* are thermophiles that usually have higher reaction rates at elevated temperatures and often are susceptible to genetic modifications, which makes them a suitable host for thermophilic expression.

To achieve this, pMSN4-GFP vector was developed. It was constructed by inserting genes of geobacillin I two component induction regulation system (*geoR, geoK*), promoter (^{P}*geoA*), reporter protein (sfGFP) and terminator (^{P}*geoT*) into pNW33N plasmid. sfGFP was inserted between ^{P}geoA promoter and ^{P}geoT terminator. Its expression is regulated by adding subinhibitory amount of geobacillin I. Added geobacillin I binds to a histidine-protein kinase (GeoK) which is then autophosphorylated. Subsequently, phosphate group is transfered to a response regulator (GeoR) which in turn leads to an activation of ^{P}geoA promoter. Finally, activated ^{P}geoA induces the expression of sfGFP or another protein in its place. Geobacillin I two component induction regulation system and sfGFP were chosen because of their stability at higher temperatures (55 ÁC).

pMSN4-GFP vector was later successfully inserted into *Parageobacillus thermoglucosidasius* DSM 2542 electrocompetent cells by electroporation method. Geobacillin I produced by *Geobacillus thermodenitrificans* DSM 465 was used for pMSN4-GFP expression system induction. However, sfGFP fluorescence was not detected. Therefore, we will use recombinant geobacillin I which was synthesized in *E. coli* [1] for further induction efficiency assessment.

[1] Garg, N., Tang, W., Goto, Y., Nair, S. K., & Van Der Donk, W. A., Lantibiotics from Geobacillus thermodenitrificans. *Proceedings of the National Academy of Sciences of the United States of America*, *109* (14), 5241ï 5246 (2012)

HETEROLOGOUS EXPRESSION OF NOVEL BACTERIOCIN FROM THERMOPHILIC BACTERIA

Akvilã Vilpiġauskaitã[1], Saulã Ulinauskaitã[1], Algirdas Kaupinis[2], Mindaugas Valius[2], Arnoldas Kaunietis[1]

[1]Department of Microbiology and Biotechnology, Institute of Biosciences, Life Sciences Canter, Vilnius University, Saulãtekio ave.7, Vilnius, Lithuania
[2]Proteomics Centre, Institute of Biochemistry, Life Sciences Canter, Vilnius University, Saulãtekio ave.7, Vilnius, Lithuania
akvile.vilpisauskaite@gmc.stud.vu.lt

Bacteriocins are a heterogeneous group of ribosomally synthesised antimicrobial peptides with the ability to kill closely related (narrow spectrum), or a diverse range of (broad spectrum), microorganisms [1]. They are classified into three major classes based on their structural and physicochemical properties: class I bacteriocins, class II bacteriocins, and class III bacteriocins. These antibacterials inhibit the growth of target organisms by functioning primarily on the cell envelope and by affecting gene expression and protein production within cells. These molecules have antimicrobial activity against pathogenic and deteriorating bacteria, which justifies their biotechnological potential. The use of bacteriocins has been reported for the following: food preservation, diverse therapeutic purposes such as treatment of peptic ulcer, spermicidal agent, and woman care, anticancerous agent, veterinary use, skincare, and oral care, and also for plant growth promotion in agriculture among others [2].

The genus *Geobacillus* comprises bacteria that are Gram-positive, thermophilic spore-formers, which are found in a variety of environments from hot-springs, cool soils, to food manufacturing plants, including dairy manufacturing plants [3]. *Geobacillus* has historically been associated with spoilage of canned food. However, in recent years it has become the subject of much attention due its biotechnological potential. One aspect of this genus that has not been fully explored or realized is its use as a source of novel forms of the ribosomally synthesized antimicrobial peptides known as bacteriocins [4]. Bacteriocins from thermophilic bacteria have the potential to be used in various industries that maintain higher temperatures, since thermophilic bacteria proteins are usually thermostable.

Geobacillus stearothermophilus 15, isolated from oilfield located in Lithuania, produces two bacteriocins geobacillin 26 (Geo26) and geobacillin 19 (Geo19). Since Geo26 have already been purified, heterologously expressed in *Escherichia coli* and characterized, the aim of our study is to clone, perform heterologous expression of recombinant novel Geo19 bacteriocin in *E.coli* and to characterize it. This bacteriocin can be assigned to class II, it has similarity to already characterized bacteriocin SDP. Native Geo19 is active against thermophilic bacteria, which often survive high temperatures during heat treatment of food and could therefore be widely applied in the food industry.

[1] Paula M OõConnor, Ta²s M Kuniyoshi, Ricardo PS Oliveira, Colin Hill, Reynolds Paul Ross, Paul D Cotter, Antimicrobials for food and feed; a bacteriocin perspective, Current Opinion in Biotechnology, 160-167 (2020).
[2] Abebe Worku Negash, Berhanu Andualem Tsehai, Current Applications of Bacteriocin,
Review Article (2020).
[3] Burgess, S.A., Flint, S.H., Lindsay, D. et al. Insights into the Geobacillus stearothermophilus species based on phylogenomic principles. BMC Microbiol 17, 140 (2017).
[4] Kevin Egan, Des Field, R. Paul Ross, Paul D. Cotter, Colin Hill, In silico Prediction and Exploration of Potential Bacteriocin Gene Clusters Within the Bacterial Genus Geobacillus. Frontiers in Microbiology 9 (2018).

IDENTIFICATION AND CHARACTERIZATION OF L- AND D-LACTIC ACID-INDUCIBLE SYSTEMS FOR TRANSCRIPTION FACTOR-BASED BIOSENSOR DEVELOPMENT

Ernesta Augustinienã[1], Naglis Malys[1]

[1] Bioprocess Research Centre, Faculty of Chemical Technology, Kaunas University of Technology, RadvilãnÔpl. 19, Kaunas, Lithuania
ernesta.augustiniene@ktu.lt

Lactic acid is an important platform chemical used in food, agriculture, cosmetic, pharmaceutical, and chemical industries. In addition, optically pure forms of this acid (L- and D- stereoisomers) are essential for the production of polylactic acid, a biodegradable polymer that has potential to replace traditional petroleum-based plastics and reduce environmental pollution. Naturally, lactic acid, as a primary fermentation product, is produced by a number of microorganisms including lactic acid bacteria (*L. lactis*, *L. paracasei*, *E. hirae*), *Bacillus* species (*B. coagulans*, *B. subtilis*), and filamentous fungi (*R. oryzae*). However, in order to achieve technologically and economically sustainable production, the complex selection for best producing bacterial strains and multifactorial process optimization are often required. Fortunately, high-throughput technologies based on whole-cell genetically encoded biosensors show great potential to facilitate and drive the multifaceted screening process.

Recent studies have shown that transcription factor (TF)-based biosensors can be used for real-time monitoring of extracellular and intracellular metabolite concentrations, high-throughput screening of vast mutant libraries, dynamic pathway control, and adaptive laboratory evolution [1, 2]. The design of the biosensor is based on two essential components: sensing and reporting units. The sensory module consists of TF-promoter pair that is in an inducible gene expression system and responds to the corresponding ligand molecule. Reporting unit typically consists of the fluorescent protein and is coupled to the sensing unit, so that changes in the sensory block change the output [3].

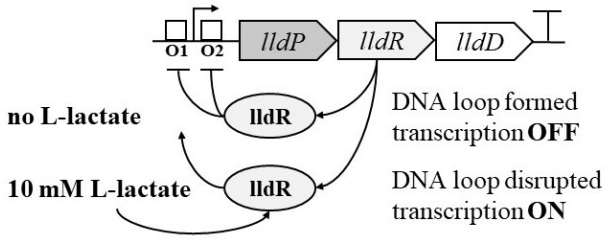

Fig. 1. Gene clusters in *Escherichia coli* MG1655 encoding the enzymes required for Lï lactic acid catabolism [4].

A few lactic acid-inducible gene expression systems have been reported previously in various microorganisms, including *Ec*LldR/P_{lldP} (*E. coli* MG1655) [4], *Cg*LldR/P_{lldP}, (*Corynebacterium glutamicum* ATCC 13032) [5], *Pa*LldR/P_{lldP} (*Pseudomonas aeruginosa* XMG) [6], *Bc*LutR/P_{lutA} (*Bacillus subtilis* 168) [7], *Dv*LurR/P_{por} (*Desulfovibrio vulgaris* Hildenborough) [8], and *Aw*LctA/P_{lctB} (*Acetobacterium woodii* DSM 1030) [9]. The basic regulation mechanism of L-lactic acid-inducible gene expression system from *E. coli* is presented in Figure 1. This system controls, an *lldPRD* operon, responsible for aerobic L-lactate metabolism. We identify and characterize L- and D-lactic acid-inducible systems that can potentially be used for developing transcription factor-based biosensors. Our data show that the *Ec*LldR/P_{lldP} inducible system is specific to the L-lactic acid and can be used to achieve up to 25-fold induction of gene expression using micromolar inducer concentrations.

[1] Hossain, G. S. et al., Genetic biosensor design for natural product biosynthesis in microorganisms, Trends in Biotechnology **38**(7), 797-810 (2020).
[2] Mitchler, M. M., Garcia, J. M., Montero, N. E. & Williams, G. J., Transcription factor-based biosensors: a molecular-guided approach for natural product engineering, Current Opinion in Biotechnology **69**, 172-181 (2021).
[3] Hanko, E., Minton, N. & Malys, N., Design, cloning and characterization of transcription factor-based inducible gene expression systems, Methods in Enzymology **621**, 153-169 (2019).
[4] Aguilera, L. et al., Dual role of LldR in regulation of the *lldPRD* operon, involved in L-lactate metabolism in *Escherichia coli*, Journal of Bacteriology **180**(8), 2997ï 3005 (2008).
[5] Gao, Y.-G.et al., Structural and functional characterization of the LldR from *Corynebacterium glutamicum*: a transcriptional repressor involved in L-lactate and sugar utilization, Nucleic Acids Research **36**(22), 7110ï 7123 (2008).
[6] Gao, C. et al., Lactate utilization is regulated by the FadR-type regulator LldR in *Pseudomonas aeruginosa*, Journal of Bacteriology **194**(10), 2687-2692 (2012).
[7] Chiu, K.-C., Lin, C.-J. & Shaw, G.-C., Transcriptional regulation of the L-lactate permease gene *lutP* by the LutR repressor of *Bacillus subtilis* RO-NN-1, Microbiology **160**, 2178ï 2189 (2014).
[8] Rajeev, L. et al., LurR is a regulator of the central lactate oxidation pathway in sulfate-reducing *Desulfovibrio species*, PLoS ONE **14**(4), e0214960 (2019).
[9] Schoelmerich, M. C. et al., Regulation of lactate metabolism in the acetogenic bacterium *Acetobacterium woodii*, Environmental Microbiology **20**(12), 4587ï 4595 (2018).

CHANGES IN THE TOTAL MICROBIAL COUNT AND ANTIBACTERIAL ACTIVITY OF KOMBUCHA PREPARED WITH HERBAL TEAS

Milda Bulotaitã, Vilma Kaġkonienã, RÎta Mickienã, Audrius Marugka

Instrumental Analysis Open Access Centre, Faculty of Natural Sciences, Vytautas Magnus University, Vileikos 8, LT-44404 Kaunas, Lithuania
mildabulotaitee@gmail.com

Kombucha is a fermented *Camellia sinensis* L. black tea drink with a sweet and sour taste. This fermented drink has recently attracted the attention of researchers due to its variable and unique composition. Kombucha is so unique because of the symbiotic culture of bacteria and yeast (SCOBY) which affects the properties of the drink. According to research, kombucha culture abounds in acetic acid (*Acetobacteraceae*), lactic acid bacteria, and osmophilic yeast [1,2]. The microbiological profile of a kombucha culture may depend on the raw material used and the fermentation conditions [2,3].

The aim of this study was to evaluate the changes of total count of microorganisms and antibacterial activity of four different medicinal plants and their mixes water infusions after 7, 14 and 21 days of fermentation with kombucha culture.

In this research fermentation was performed using the local kombucha culture purchased at local supermarket. All experiments were done with sugared drinks from nettle (*Urtica dioica* L.), lemon balm (*Melissa officinalis* L.), fireweed (*Chamaenerion angustifolium* L.), rose hips (*Rosa canina* L.) and their mixes. Kombucha prepared from Ceylon tea from Sri Lanka was used for comparison. Kombucha was prepared in the same conditions and fermentation was performed for 21 days in a dark room at 20Ñ1 ÁC. Compact Dry test plates were used for total bacteria and yeast count. Antimicrobial activity was determined against gram-positive *Bacillus mojavensis* and *Bacillus megaterium*, gram-negative *Azotobacter vinelandii* using agar well diffusion method [4].

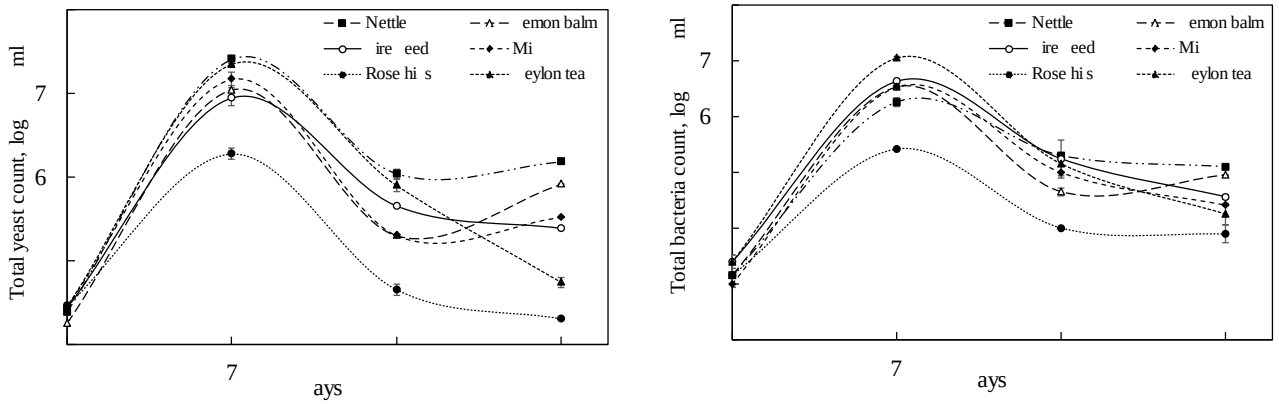

Fig. 1. Total count of yeast (left) and bacteria (right) (SNNÒ6.67%, n=3).

The highest counts of yeast and bacteria were found in the nettle tea kombucha and Ceylon tea kombucha, after 7 days of fermentation, 7.41Ñ0.01 log CFU/ml and 7.05Ñ0.02 log CFU/ml, respectively (Fig. 1). The lowest total counts of yeast and bacteria were found in rose hips kombucha, after 21 days of fermentation, 4.30Ñ0.01 log CFU/ml and 3.89Ñ0.16 log CFU/ml, respectively (Fig. 1). The prepared drinks did not show any antibacterial activity against tested bacteria before and after 7 days of kombucha fermentation, while after 14 days, minimal antibacterial activity was noticed against *Azotobacter vinelandii*. The inhibition zone radius increased up to 0.3-2.3 mm in all fermented drinks after 21 days of fermentation. The widest zone of inhibition against *Bacillus mojavensis* and *Azotobacter vinelandii* was in *Melissa officinalis* L. kombucha and against *Bacillus megaterium* was in herbals mix kombucha. This study showed that herbal teas are a suitable medium for the growth of a kombucha culture and the duration of fermentation has an effect on antibacterial activity.

Acknowledgements: Financial support from Research Council of Lithuania project No. 09.3.3-LMT-K-712-22-0104 is acknowledged.

[1] M. Coton, A. Pawtowski, B. Taminiau et al., Unraveling microbial ecology of industrial-scale Kombucha fermentations by metabarcoding and culture-based methods, FEMS Microbiology Ecology, 2017, Vol. 93, Iss. 5.
[2] F. de Filippis, A. D. Troise, P. Vitaglione et al., Different temperatures select distinctive acetic acid bacteria species and promotes organic acids production during Kombucha tea fermentation, Food Microbiology, 2018, Vol. 73, p. 11ï 16.
[3] O. N. Reva, I. E. Zaets, L. P. Ovcharenko et al., Metabarcoding of the Kombucha microbial community grown in different microenvironments. AMB Express, 2015, Vol. 5, Iss. 35.
[4] C. Valgas, S.M. De Souza, E.F.A. Sm@nia et al., Screening methods to determine antibacterial activity of natural products, Brazilian Journal of Microbiology, 2007, Iss. 38, p. 369ï 380.

SCREENING OF PURIFICATION METHODS FOR ANTIMICROBIAL PEPTIDE FROM *PEDIOCOCCUS ACIDILACTICI* JEM-1

Kamilė Šimelytė[1], Augustė Rastenienė[1], Ramunė Stanevičienė[2], Elena Servienė[2], Jolanta Sereikaitė[1*]

[1] Vilnius Gediminas Technical University, Lithuania
[2] Nature Research Centre, Lithuania
kamile.simelyte@stud.vgtu.lt

Nowadays, a healthy lifestyle is rapidly gaining popularity around the world. People promote not only an active leisure, sports, but also tend to pay more attention to a healthy nutrition. Customers want to consume food without chemical preservatives. Lactic acid bacteria which secrete bacteriocins are extensively studied since bacteriocins such as pediocins could replace chemical preservatives. Bacteriocins as bioconservants could be used to prolong the shelf life of foods and prevent the growth of microorganisms. Moreover, bacteriocins could be also an appealing alternative to antibiotics [1]. The use of those antimicrobial peptides is still limited due to the challenging procedures of purification and low yields [2].

Previously, we purified pediocin from *Pediococcus acidilactici* JEM-1 based on the adsorption method of pediocin on the cells and the following desorption. The yield of purification was low. About 1.6 μg of partially purified pediocin was obtained from 250 mL of *Pediococcus acidilactici* JEM-1 cultivation medium. The molecular mass of peptide was about 4.4 kDa as judged by Tricine-SDS polyacrylamide gel-electrophoresis. The chosen purification step is not effective and does not meet the expectations. To obtain higher yield of pediocin, the experiments are continued for choosing one-step purification method using ion-exchange chromatography.

[1] M. Papagianni, S. Anastasiadou, Pediocins: The bacteriocins of *Pediococci*. Sources, production, properties and application, Microbial Cell Factories, **8** (3), 1-16 (2009).
[2] J. M. Rodríguez, M. I. Martínez, J. Kok, Pediocin PA-1, a wide-spectrum bacteriocin from lactic acid bacteria, Critical Reviews in Food Science and Nutrition, **42** (2), 91-121 (2002).

ISOLATION AND SCREENING OF DIAZOTROPHIC MICROORGANISMS WHICH ARE SIGNIFICANT FOR SUSTAINABLE AGRICULTURE

Justina KaziÎnienã [1], Raimonda Maģylytã [2], Audrius Gegeckas [3]

[1] Institute of Biology and Plant Biotechnology, Vytautas Magnus University, Lithuania
[2] Department of Microbiology and Biotechnology, Vilnius University, Lithuania
justina.smel@gmail.com

Microbial biostimulants containing nitrogen fixing microorganisms are perspective products which helps to reduce amounts of mineral nitrogen fertilizer on agriculture and the negative impact on the environment an human caused by the misuse of chemical fertilizers [1][2]. It is huge importance to select right microorganisms for microbial biostimulants production, microorganisms need to have positive effect on plants and should easy be applying on an industrial scale [3].

All thirteen isolates were screened by using different nitrogen free media. Phylogenetic analysis of 16 rRNA sequences showed that isolates belong for five different genus *Bacillus* spp., *Paenibacillus* spp., *Ensifer* spp., *Rhizobium* spp. and *Lelliottia* spp. The most intensive growth on nitrogen free media were showed two isolates S1 and S7 which both are members of *Paenibacillus* spp. (Fig. 1A).

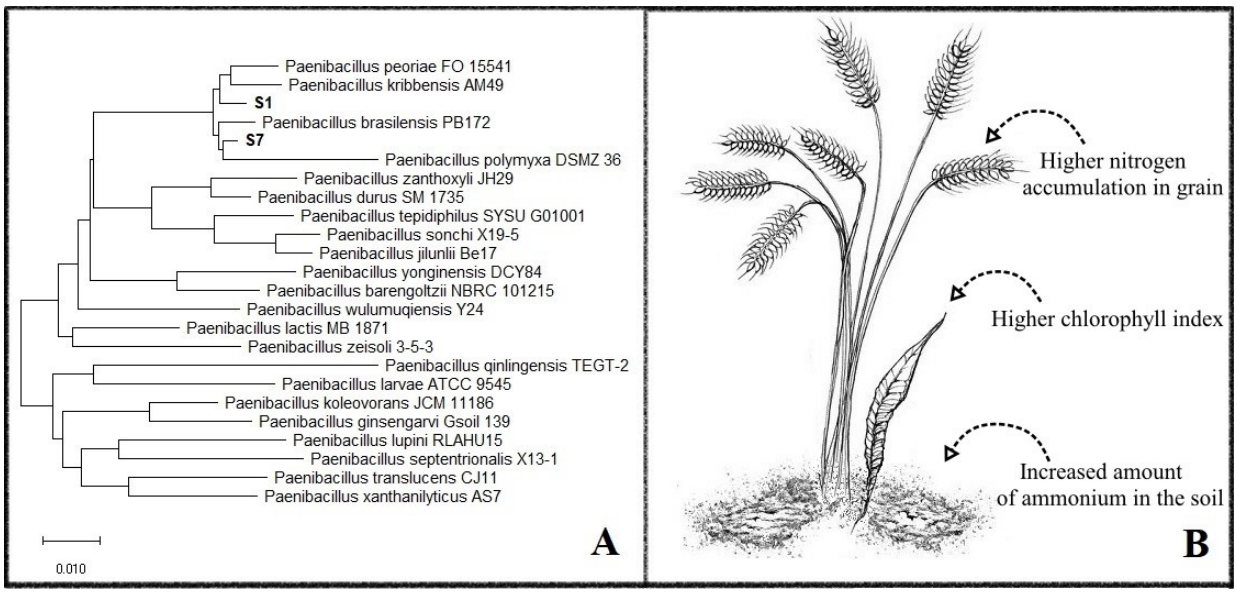

Fig.1. Isolates phylogenetic tree and their effect on spring wheat development. **A.** The phylogenetic relationships of *Paenibacillus* sp. S1 and *Paenibacillus* sp. S7 within the genus of *Paenibacillus* spp. investigated using 16S rRNA gene sequence analysis. **B.** Spring wheat development after *Paenibacillus* sp. S7 application.

The impact of *Paenibacillus* sp. S1 and *Paenibacillus* sp. S7 isolates on the development and growth of spring wheat was analyzed. Isolate *Paenibacillus* sp. S7 was found to significantly increase the amount of ammonium in the soil, furthermore, positive effect on chlorophyll index and nitrogen accumulation in grain were determined (Fig. 1B). The most suitable nitrogen and carbon sources were founded for biomass production of *Paenibacillus* sp. S7.

See you in Vilnius!

[1] A. Beneduzi, A. Ambrosini, and L. M. P. Passaglia, ñPlant growth-promoting rhizobacteria (PGPR): Their potential as antagonists and biocontrol agents,ò *Genetics and Molecular Biology*. 2012, doi: 10.1590/S1415-47572012000600020.
[2] Z. A. Siddiqui, ñPGPR: Prospective biocontrol agents of plant pathogens,ò in *PGPR: Biocontrol and Biofertilization*, 2006.
[3] S. Savci, ñInvestigation of Effect of Chemical Fertilizers on Environment,ò *APCBEE Procedia*, 2012, doi: 10.1016/j.apcbee.2012.03.047.

PRODUCTION OF RECOMBINANT MOUSE CARBONIC ANHYDRASE XIV PROTEIN

Tautvydas Kojis, Aurelija Mickeviļ iÎ tā, Lina Baranauskienā.

Department of Biothermodynamics and Drug Design, Institute of Biotechnology, Life Sciences Center, Vilnius University, Vilnius, Lithuania

tautvydas.kojis@chgf.stud.vu.lt

Carbonic anhydrases (CA) are enzymes that catalyse reversible hydration of carbon dioxide ($CO_2 + H_2O \rightleftharpoons HCO_3^- + H^+$). CAs are metalloproteins ï most of them contain zinc in their active centre. Multiple CA isoenzymes are widely expressed in different mammalian tissues, as they participate in pH regulation, CO_2 and HCO_3^- transport, gluconeogenesis, lipogenesis, and other processes [1]. Different CA isozymes are recognized as drug targets for management of fluid secretion and pH change linked diseases. Mouse carbonic anhydrase XIV (Car XIV) is orthologous to human CA XIV protein, and is mostly expressed in brain, heart, and kidney tissues [2].

The aim of this study is to produce functionally active recombinant Car XIV protein. We constructed recombinant plasmid using vector pET-15b. This vector introduces N-terminal His_6-tag to target protein to make purification of the protein more effective by using immobilized metal affinity chromatography. To confirm the DNA sequence of insert, plasmid was sequenced.

After careful selection of protein expression conditions, we obtained optimal expression of Car XIV in *Escherichia coli* Origami B (DE3) strain cultured in LB medium at 37ÁC until OD_{600}=0,5-0,6 and then induced with 0,5 mM IPTG and 0,5 mM $ZnCl_2$andincubated at 16ÁC overnight. We used two-step affinity chromatography for Car XIV purification: immobilized metal affinity chromatography followed by purification using p-aminomethylbenzenesulfonamide-agarose. Expression and purity of Car XIV protein has been confirmed using SDS-PAGE (fig. 1 A).

Protein functional activity was confirmed according to its binding to CA-specific small molecule compounds, bearing unsubstituted sulfonamide group, using fluorescent thermal shift assay (FTSA). Unfolding of recombinant Car XIV protein exhibited single transition curves, typical for single domain globular proteins. Binding of small molecule ligands was confirmed by increased melting temperature of protein-ligand complex in a concentration-dependent manner (fig. 1B).

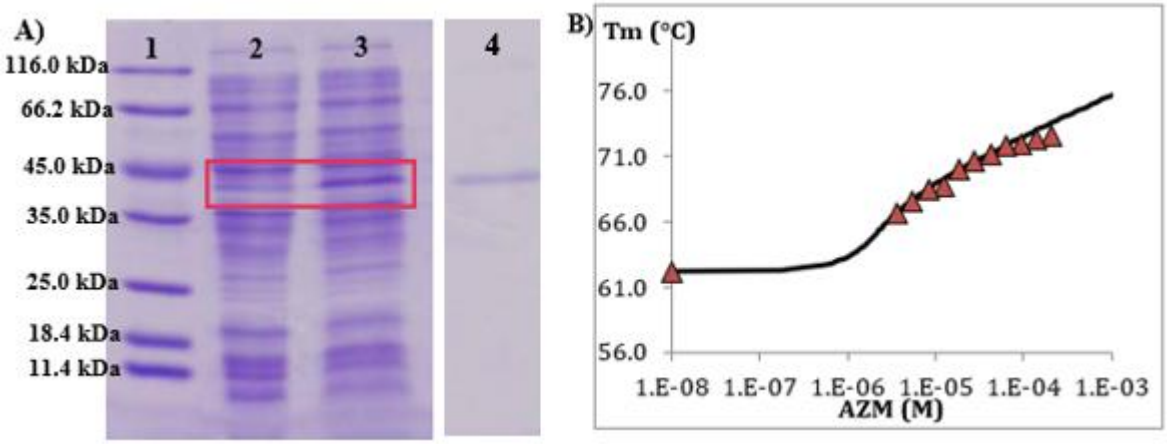

Figure 1. Car XIV expression, purity, and functional activity. (A) SDS-PAGE of Car XIV protein expression and purity: lane 1 ï MW markers, 2 ï bacterial lysate before induction, 3 ï bacterial lysate after induction; 4 ï purified Car XIV (B)FTSA results of Car XIV binding to acetazolamide ï symbols correspond to experimental data, and line presents fitting usingK_d determination model [3].

[1] Whittingtons, D. A., et.al,Expression, Assay, and Structure of the Extracellular Domain of Murine Carbonic Anhydrase XIV: implications for selective inhibition of membrane-associated isozymes. 2003, J. Biol. Chem., 279(8).

[2] NCBI gene database ï Search results.https://www.ncbi.nlm.nih.gov/gene/23831

[3] Cimmperman, P., et.al, A Quantitative Model of Thermal Stabilization and Destabilization of Proteins by Ligands.2008, Biophysical Journal, 95(7), 3222ï 3231

ANTIMICROBIAL EFFECT OF GEOBACILLIN 26 BY ATOMIC FORCE MICROSCOPY

Mantã Rakauskaitã[1,2*], Arnoldas Kaunietis[1], Marija Jankunec[2]

[1]Institute of Biosciences, Life Sciences Center, Vilnius University, Vilnius, Lithuania
[2]Institute of Biochemistry, Life Sciences Center, Vilnius University, Vilnius, Lithuania
*mante.rakauskaite@gmc.stud.vu.lt

In the worldwide fight against bacterial resistance, there is a need for a novel family of antimicrobial drugs. Antimicrobial peptides (AMPs) are promising candidates to replace antibiotics. Still, the majority of them have an unclear mechanism of action. Atomic force microscopy (AFM) is a surface-sensitive technique and aims to study the physical properties of living biological cells under physiologically relevant conditions without the destruction of the sample. However, the studies involving live bacteria limits the necessity to attach a specimen to the substrate. Therefore, the existing protocol needs to be adapted. Here we present a protocol to immobilize Gram-positive bacterial cell membranes.

This study focuses on the antimicrobial effect of heat-labile Geobacillin 26 peptide against Gram-positive bacteria. The bacteria are attached to the substrate via crosslinking with glutaraldehyde. Time-resolved AFM images revealed no changes in the topography of the affected cell wall. This result is in line with recent studies, Geobacillin 26 was named as not a cell wall degrading enzyme [1]. However, the differences in cell volume of affected bacteria from a control group showed the leakage of inside fluids. That indicates the loss of membrane integrity. But the mode of action of Geobacilin 26 remains unclear. For this purpose, before and after the impact of Geobacillin 26, bacteria were evaluated by force spectroscopy (Fig.1). The technique where subtle changes in cell wall elasticity are detected.

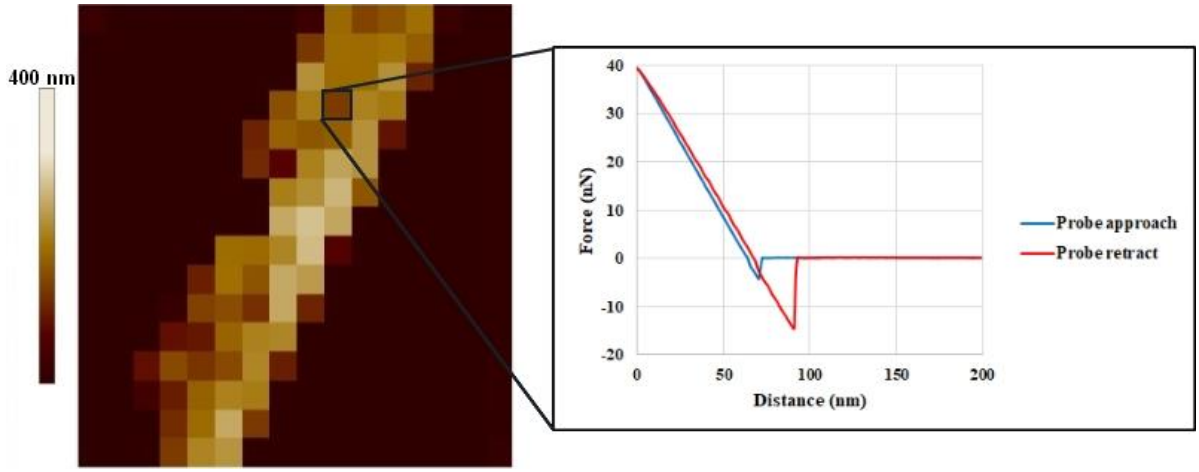

Fig. 1. Force spectroscopy analysis of bacteria control group.

[1] Vaiļikauskaitã M., Ger M., Valius M., Maneikis A., Lastauskienã E., Kalãdienã L., Kaunietis A. Geobacilin 26 ï high molecular weight bacteriocin from a thermophilic bacterium. International Journal of Biological Macromolecules 2019 (141): 333-344.

IN SILICO ANALYSIS OF CUTINASE FROM *STREPTOMYCES SCABIEI* 87.22

Agnė Savickaitė[1], Renata Gudiukaitė[1]

[1] Institute of Biosciences, Life Sciences Center, Vilnius University, Saulėtekis ave. 7, LT-10257 Vilnius, Lithuania
agne.savickaite@gmc.stud.vu.lt

Cutinases are hydrolytic enzymes that catalyze hydrolysis, synthesis, or transesterification reactions of ester bonds, which makes them attractive to the industrial sector [1]. One of the most promising applications of such enzymes is degradation of polymers (plastics), such as PCL (polycaprolactones) and PET (polyethylene terephthalate). These polymers are widely used in various industrial sectors (pharmaceuticals, food industry, agriculture) [2]. Thus, recycling and, most importantly, the reuse of plastic waste is a serious global problem. Nevertheless, the amount of research related to the analysis of the structure-function relationship of microbial cutinases and the perspectives of their application is limited. There are only a few publications about the isolation, purification and characterization of these enzymes [3]. In known genomes, open-reading frames that encode cutinases are difficult to identify, which makes the analysis of these enzymes even more complicated. Moreover, cutinases themselves are often classified as lipases, esterases, or other hydrolytic enzymes. Thus, there is a lack of fundamental knowledge about these bacterial enzymes.

During earlier studies, a synthetic *Streptomyces scabiei* 87.22 cutinase was created. Some authors describe this enzyme as suberinase [4], others ï as cutinase [5], whereas in UniProt database it is called secreted esterase. Since the primary enzyme under the study was a cutinase with an N-terminal signal sequence, it is important to evaluate its effect on enzyme yield and activity. In the case of lipolytic enzymes, the N-terminal signal sequence has been shown not only to lead to differences in protein yield but also in properties [6]. In this study, *in silico* analysis of *S. scabiei* 87.22 cutinase was performed. First of all, N-terminal signal sequence was predicted using SignalP-5.0 Server. Then the structure of cutinase without signal sequence (Fig. 1) and ligand binding sites were predicted with I-TASSER. Based on I-TASSER analysis results and other studies [5] catalytic amino acids were also identified. Moreover, *S. scabiei* 87.22 cutinase gene was aligned using Nucleotide Blast, sequences with the most similarity were chosen and conserved regions were analyzed.

The results obtained during this study would undoubtedly contribute to filling the lack of fundamental information about bacterial cutinases. Therefore, in the future it would be useful to apply mutagenesis strategies for conserved cutinase regions and this way provide more insight to the structure-function relationship.

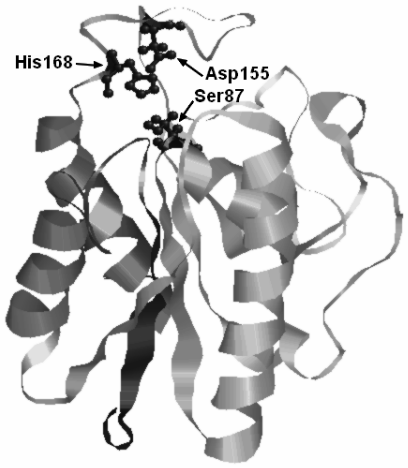

Fig. 1. Structure of *S. scabiei* 87.22 cutinase without N-terminal signal sequence. Catalytic amino acids are marked in black.

Acknowledgment. This research was funded by the European Social Fund under the No 09.3.3-LMT-K-712 ñDevelopment of Competences of Scientists, other Researchers and Students through Practical Research Activitiesò measure, Grant No. 09.3.3-LMT-K-712-22-0074.

[1] K. Al-Tammar, O. Omar, A. M. Abdul Murad et al., Expression and characterization of a cutinase (AnCUT2) from *Aspergillus niger*, Open Life Sciences 11, 29-38 (2016)
[2] A. Banerjee, K. Chatterjee, G. Madras, Enzymatic degradation of polymers: a brief review, Materials Science and Technology 30, 567ï 573 (2014)
[3] S. Chen, X. Tong, R. W. Woodard et al., Identification and characterization of bacterial cutinase, The Journal of Biological Chemistry 283, 25854ï 25862 (2008)
[4] D. Komeil, A.-M. Simao-Beaunoir, C. Beaulieu, Detection of potential suberinase-encoding genes in *Streptomyces scabiei* strains and other actinobacteria, Canadian Journal of Microbiology 59, 294ï 303 (2013)
[5] R. Jabloune, M. Khalil, B. Moussa et al., Enzymatic degradation of *p*-nitrophenyl esters, polyethylene terephthalate, cutin, and suberin by Sub1, a suberinase encoded by the plant pathogen *Streptomyces scabies*, Microbes and Environments 35 (2020)
[6] R. Gudiukaitė, A. Gegeckas, D. Kazlauskas et al., Influence of N- and/or C-terminal regions on activity, expression, characteristics and structure of lipase from *Geobacillus* sp. 95, Extremophiles 18, 131ï 145 (2014)

THE ANTIOXIDANT ACTIVITY OF NISIN-LOADED PECTIN-CHITOOLIGOSACCHARIDES PARTICLES

Jolita Pachaleva[1], Ruta Gruskiene[1], Alma Bockuviene[2], Jolanta Sereikaite[1*]

[1]Department of Chemistry and Bioengineering, Vilnius Gediminas Technical University, Vilnius, Lithuania
[2] Department of Polymer Chemistry, Vilnius University, Vilnius, Lithuania
jolita.pachaleva@stud.vgtu.lt

Today food supply and demand are growing, and the preservation takes an important place in the food industry. Synthetic antibacterial food additives have an impact on the quality and commercial appearance of the food products. Many efforts have been focused on natural food preservatives and their use in the food industry. Nisin is one of the most known natural food preservatives used for dairy products, generally recognized as safe (GRAS), and has a number E234. Nisin is a small 3510 Da peptide produced by *Lactococcus lactis* [1].

The antimicrobial activity of bacteriocin can decrease due to proteolytic degradation or the interaction with food components. Nisin application for food preservation becomes limited. Nisin encapsulation into various biopolymers can protect the bacteriocin from external interactions and provide additional features. Antioxidant activity is a valuable property of food additives. Oxidation in foods modifies proteins, lipids, and carbohydrates. Free radicals, reactive oxygen species (ROS) harm cellular systems and cause diseases. Antioxidants preventing taste changes of food due to oxidation, lengthen the shelf life of products and have a positive effect on human health [2]. Biopolymers pectin and chitooligosaccharides are commonly used materials for encapsulation systems. These substances are simple in use, biodegradable, have high loading capacity and antioxidant activity properties [3][4].

This study is aimed to evaluate the antioxidant activity of nisin-loaded particles. For nisin-loading, three different types of anionic pectin biopolymer, i.e. high methoxy pectin (HMP), low methoxy pectin (LMP) and pectic acid (PecA) were used. The complexation process between nisin and pectin was performed at pH5. Prepared complexes were additionally coated using 0.025 and 0.3 mg/ml of chitooligosaccharides. The final concentration of nisin and pectin was 0.1 mg/ml and 0.2 mg/ml, respectively.

The antioxidant activity of nisin loaded nanoparticles was evaluated by 2,2-diphenyl-1-picrylhydrazyl (DPPH) free radical method (Fig. 1).

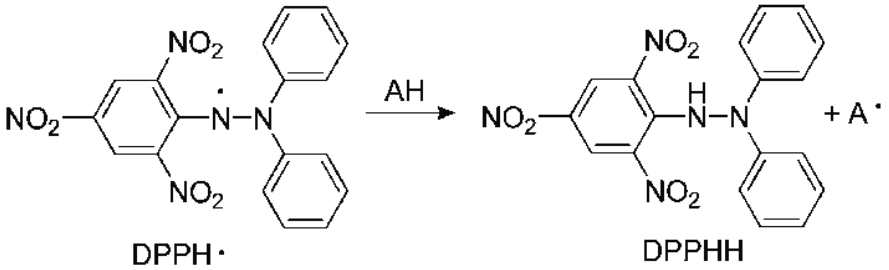

Fig. 1. Reaction of DPPH with antioxidants [5]

The reaction was performed at the different temperatures of 20ÁC, 25ÁC, and 37ÁC for 24 hours. All types of particles showed antioxidant activity. It was found that the temperature had no significant effect on the antioxidant activity of the nisin loaded particles. The maximum value of antioxidant activity of particles was reached when chitooligosacharides concentration was 0.3 mg/ml. The nisin-loaded particles with antioxidant activity could be used for the preservation and quality improvement of food products.

Acknowledgements: This research was funded by the European Social Fund under the No 09.3.3-LMT-K-712**.** ñDevelopment of Competences of Scientists, Other Researchers and Students through Practical Research Activitiesò measure. Grant No 09.3.3-LMT-K-712-22-0039.

[1] L. J. de Arauz, A. F. Jozala, P. G. Mazzola, T. C. V. Penna. Nisin biotechnological production and application: a review. Trends in Food Science & Technology, 20(3-4), 146-154 (2009).
[2] J. W Finley, A.N. Kong, k.J.Hintze, E.H. Jeffery, L.L Ji. & X. G.Lei, Antioxidants in Foods: State of the Science Important to the Food Industry. Journal of Agricultural and Food Chemistry, 59(13), 6837ï 6846. (2011)
[3] D. Sun, X. Chen, C. Zhu, Physicochemical properties and antioxidant activity of pectin from hawthorn wine pomace: A comparison of different extraction methods, International Journal of Biological Macromolecules, Volume 158, 2020, Pages 1239-1247. (2020)
[4] D.H. Ngo., & S.K. Kim. Antioxidant Effects of Chitin, Chitosan, and Their Derivatives. Advances in Food and Nutrition Research, 15ï 31. (2014)
[5] M. Massaro, S. Riela,, S. Guernelli, P. F. Parisi, G. Lazzara, A. Baschieri, L. Valgimigli, R.Amorati.. A synergic nanoantioxidant based on covalently modified halloysiteï trolox nanotubes with intra-lumen loaded quercetin. J. Mater. Chem. B. 4. (2016)

ELECTROPORATION ASSISTED IMPROVEMENT OF FREEZING TOLERANCE IN YEAST CELLS

Elvyra Gumbinaitė[1], Povilas Ġimonis[1], Augra Linkevičiūtė[2], Arūnas Stirkė[1]

[1] Laboratory of Bioelectrics, [2] Laboratory of Materials analysis,
State Research Institute, Center for Physical Sciences and Technology, Lithuania
elvyra.gumbinaite@gmc.stud.vu.lt

Preservation of yeast cell viability is essential in research and the food industry. In research it is important to maintain strains possessing useful traits for long periods of time. Meanwhile, in the food industry viability is required for efficient fermentation of food products like frozen dough [1]. Preservation is often achieved by freezing, which can cause formation of ice crystals and the removal of water from within the cells [2]. Cryoprotectants like trehalose, which naturally occurs in yeast, are used to inhibit these freezing injuries. Multiple studies show that tolerance to freezing is strongly related to the concentration of intracellular trehalose [3-5]. Cryoprotectants have benefits both extracellularly and intracellularly, but only few cryoprotectants could enter the cells straight from the media. One of the techniques that could improve yeast cells permeability to cryoprotectants by weakening membrane barriers is exposure to pulsed electric fields (PEF).

In this study we investigated electric field induced effects by analyzing yeast cell viability. In order to find optimal treatment conditions for the introduction of cryoprotectant, cell suspension was exposed to pulses with different electric field strengths (E Ò8 kV/cm). Before exposure to electric fields yeast cells were washed twice with electroporation buffer and resuspended in electroporation buffer supplemented with D-(+)-Trehalose dihydrate or sorbitol. The yeast cell suspension was exposed to a single electric field pulse and thereafter soaked in the trehalose solution for up to 60 min before freezing. For evaluating freezing effects on yeast cells we kept cell suspension at -20 ºC from 4 to 40 days (Fig. 1). Viability of cells was evaluated by counting colony-forming units. As a control, PEF untreated suspension was used. In order to validate whether PEF treatment improved the introduction of trehalose into yeast cells, we evaluated its concentration in yeast cells (Õg of trehalose/mg of dry yeast mass). Extracts from yeast cell lysates were analyzed via chromatography.

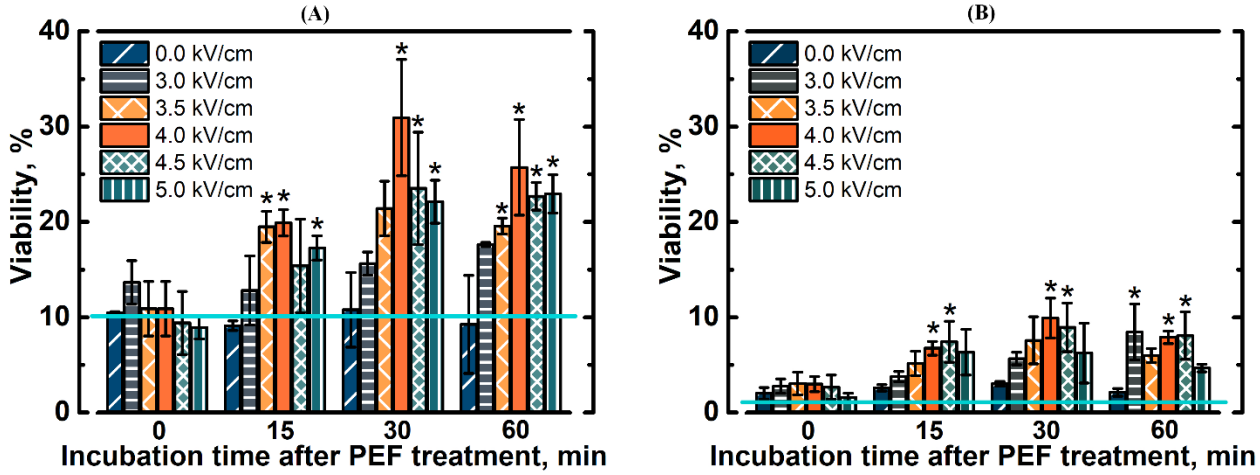

Fig. 1. Viability of yeast cells after exposure to single electric field pulse and subsequent freezing for (A) 4 days or (B) 40 days at ī 20 ºC. Teal line represents viability of yeast cells without soaking in trehalose and pulsed electric field (PEF) treatment. Asterisks (*) indicate significant difference ($p < 0.05$) in the viability when compared to PEF-untreated cells with the same soaking time.

We showed that the PEF pretreatment could improve the freezing tolerance of yeast cells thus resulting in higher viability of up to 3 times. Pretreatment in trehalose solution also resulted in higher concentration of intracellular trehalose (by up to 60%) when compared to PEF untreated cells. The optimal electric field strength in the case of single square shaped pulse with duration of 150 Õs was 4 kV/cm. Soaking time had an effect on the viability after thawing only for PEF-treated cells. The optimal soaking time after PEF treatment in trehalose solution was 30 min. Investigation of intracellular trehalose contents confirmed that its concentration increased with rise in strength of the electric field.

The prospect of our research is to develop a new freezing technology suitable for yeasts and other cells by increasing their resistance to freezing injuries without manipulating the genetic background.

[1] Luo, W.; Sun, D.W.; Zhu, Z.; Wang, Q.J. Improving freeze tolerance of yeast and dough properties for enhancing frozen dough qualityð A review of effective methods. Trends Food Sci. Technol. 2018, 72, 25ï 33.
[2] Dalvi-Isfahan, M.; Jha, P.K.; Tavakoli, J.; Daraei-Garmakhany, A.; Xanthakis, E.; Le-Bail, A. Review on identification, underlying mechanisms and evaluation of freezing damage. J. Food Eng. 2019, 255, 50ï 60.
[3] Coutinho, C.; Bernardes, E.; Fø8lix, D.; Panek, A.D. Trehalose as cryoprotectant for preservation of yeast strains. J. Biotechnol. 1988, 7, 23ï 32.
[4] Gelinas, P.; Fiset, G.; Willemot, C.; Goulet, J. Lipid content and cryotolerance of bakersô yeast in frozen doughs. Appl. Environ. Microbiol. 1991, 57, 463ï 468.
[5] Sun, X.; Zhang, C.Y.; Wu, M.Y.; Fan, Z.H.; Liu, S.N.; Zhu, W.B.; Xiao, D.G. MAL62 overexpression and NTH1 deletion enhance the freezing tolerance and fermentation capacity of the bakerôs yeast in lean dough. Microb. Cell Fact. 2016, 15, 1ï 8.

SLA 3D PRINTING APPLICATION FOR FAST ELECTROCHEMICAL DEVICE PROTOTYPING

Martynas Raila[1,2], Eivydas Andriukonis[1,2], Arĩnas Ramanaviļius[1,2]

[1] Institute of Chemistry, Faculty of Chemistry and Geosciences, Vilnius University, Lithuania
[2] Department of Functional Materials and Electronics, State research institute Center for Physical Sciences and Technology, Lithuania
martynas.raila@chf.stud.vu.lt

Stereolithography (SLA) is a technology commonly used for high resolution desktop 3D printing. SLA is an additive manufacturing process during which the models are produced by illuminating layer after layer of liquid plastic precursor with ultraviolet light. The light initiates a polymerization reaction in the precursor, causing it to solidify. The potential field of applications for SLA is wide, ranging from prototyping industrial parts to bioengineering.

During our research, we used SLA 3D printing to construct an electrochemical flow cell prototype. The cell was optimized and verified to be a suitable device for electroanalysis of live cell suspensions.

The construction of the electrochemical cell is as follows: two main parts produced from plastic resin are connected by a stainless steel tube, which also acts as an auxiliary electrode (counter electrode, CE) in the cell; a platinum working electrode and a Ag/AgCl reference electrode are inserted into specially designed holes in one of the plastic parts; the printed parts have holes at both ends, which have in-built threads for easy and fast connection of rubber tubes and are used to supply the analyzed solution into the electrochemical cell. The flow of the fluid is initiated by a peristaltic pump connected to one of the tubes.

Optimization of the prototype was carried out by measuring the electric signal at different flow speeds, by determining the optimal connecting order of the flow cell components and by finding the correct mediator to be used in the cell.

The prototype of the electrochemical cell was used to analyze a suspension of *Saccharomyces cerevisiae* cells, which was run through the electrochemical cell in a closed circle and the change of electric current in time was measured with a stable potential applied to the working electrode. A few samples of yeast cells modified by electrically conductive polymer polypyrrole (Ppy) inside their walls were also tested in this prototype. The electrochemical cell was able to measure the different electric signals produced depending on the concentration of the yeast cells and on the concentration of Ppy in the cell walls. These results suggest that an improved version of the prototype may potentially be applicable for industrial uses, such as monitoring in biofuel cells.

ELECTROCHEMICAL INVESTIGATION OF ADSORBED CYCLODEXTRINS ON ITO ELECTRODE FOR POTENTIAL HYSTAMINE SENSING

Delianas Palinauskas, Gintautas BagdģiÎnas

Institute of Biochemistry, Department of Bioanalysis, Life Sciences Centre, Vilnius University, Sauletekio av. 7, LT-10223, Vilnius, Lithuania
delianas.palinauskas@chgf.vu.lt

Electrochemical sensing has received much attention and is employed in the detection of biomolecules due to its cheap and portable instruments, low cost and rapid analysis, high sensitivity and selectivity. The selection and development of effect materials for modifying electrodes are key factors to improve the sensitivity and selectivity of electrochemical sensing. These effect materials are so-called hostï guest supramolecular recognition systems. One family of candidates for effect materials as a host-guest interaction-based supramolecular recognition systems are class of cyclic oligosaccharides, namely cyclodextrins (CDs). Most well-known CDs consist of 6 to 8 joined together D-(+)-glucopyranose subunits and are called α-, β-, ɔ-CDs, accordingly. One important structural feature of these compounds is their conical shape with hydrophobic cavity and hydrophilic exterior. Due to this structural feature, CDs are capable of forming host-guest complexes by the means of hydrophobic interactions.

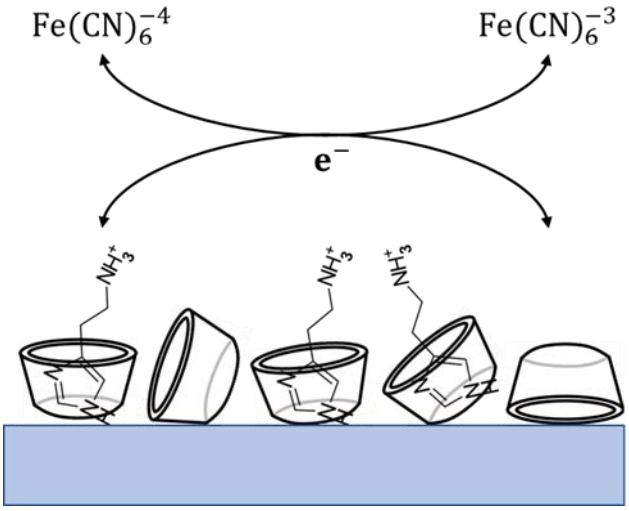

Fig. 1. Scheme of charge transfer from/to redox probe through self-assembled monolayer on ITO electrode consisting of adsorbed β- or ɔ-CD molecules and their 1:1 inclusion complex with hystamine under physiological pH conditions (7.4)

On the other hand, hystamine is important biomolecule that control physiological function of the gut and is involved in processes of our central nervous system as a neurotransmitter [4]. Therefore, the analysis of hystamine in biosamples is of great clinical and pharmaceutical importance. One example of electrochemical determination of hystamine concentration in gut involves usage of molecularly imprinted polymers as a supramolecular effect material [5]. Here, we present investigation of the self-assembled β- and ɔ-CD monolayers on ITO (Indium Tin Oxide) electrode as possible supramolecular platform for determination of hystamine concentration (Fig. 1). In this work, faradaic electrochemical impedance spectroscopy detection of histamine as an enhanced analyte was applied. According to equivalent-circuit modelling, the molecular recognition of histamine by the CDs cavity increases the resistive component of the electrodeī solution interface while capacitive effects are negligible. Moreover, this sensor enables the quantification of histamine in a broad concentration range from 10 nM to 1 ε M.

Acknowledgements: This ñSupramolecular recognition-based sensors for electrodetection of biomoleculesò project has received funding from the Research Council of Lithuania (LMTLT), agreement no. S-MIP-20-45.

[1] G. BagdģiÎnas, D.Palinauskas, Poly(9H-carbazole) as a Organic Semiconductor for Enzymatic and Non-Enzymatic Glucose Sensors, Biosensors, 10, 104 (2020).
[2] G.T.Williams et al., Advances in applied supramolecular technologies, Chem. Soc. Rev., 10, 1039 (2021).
[3] G.Zhu, Y. Yi, J.Chen, Recent advances for cyclodextrin-based materials in electrochemical sensing, TrAC Trends in Analytical Chemistry, 80, 232ï 241 (2016).
[4] Nieto-Alamilla et al., The Histamine H3 Receptor: Structure, Pharmacology, and Function, Molecular Pharmacology, 90(5), 649.
[5] P.Wagner et al., Electropolymerized Receptor Coatings for the Quantitative Detection of Histamine with a Catheter-Based, Diagnostic Sensor, ACS Sens., 6(1), 100.

STUDY OF THE INTERACTION OF MISFOLDED PROTEINS WITH MEMBRANE MODEL SYSTEMS

Evelina Jankaitytė[1], Zigmantas Toleikis[2], Vytautas Smirnovas[2], Gintaras Valinį ius[1], Rima Budvytytė[1]

[1] Institute of Biochemistry, Life Sciences Center, Vilnius University, Vilnius, Lithuania
[2] Institute of Biotechnology, Life Sciences Center, Vilnius University, Vilnius, Lithuania
evelina.jankaityte@gmc.vu.lt

Protein misfolding is a common cellular event that can occur throughout the lifetime of a cell. The accumulation of misfolded proteins in the brain is a hallmark of several neurodegenerative diseases. For example, beta-amyloid is associated with Alzheimerôs disease. In the Alzheimer's brain, abnormal levels of this naturally occurring protein clump together to form plaques that accumulate between neurons and disrupt cell functions [1]. S100A9 protein has amyloid-like properties and can be found in extracellular senile plaques together with beta-amyloid. S100A9 is involved in aggregates formation and inflammatory processes associated with neurodegeneration [2]. In this work the interaction of S100A9 and beta-amyloid with membrane model systems was studied. Tethered bilayer lipid membranes (tBLM) and liposomes were used as simplified membrane models for these studies. The aim of this work was to form tethered bilayer lipid membranes [3] and unilamellar liposomes with encapsulated fluorescent calcein and use them to study interaction with misfolded proteins.

Atomic force microscopy (AFM) and dynamic light scattering (DLS) methods were used for characterisation of S100A9 and beta-amyloid (Fig. 1). By employing electrochemical impedance spectroscopy and fluorescence spectroscopy, we investigate interaction of phospholipid bilayer with S100A9 and beta-amyloid depending on their oligomerization state.

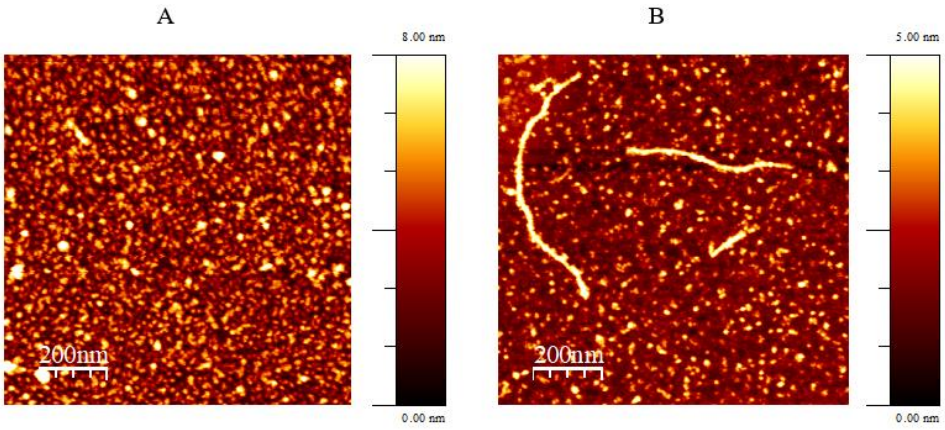

Fig. 1. AFM topographic images of ß-amyloid (1-42) oligomers (A) and fibrils (B).

[1] L§zaro DF, Bellucci A, Brundin P, Outeiro TF. Editorial: Protein Misfolding and Spreading Pathology in Neurodegenerative Diseases. Frontiers in Molecular Neuroscience. 2020; 12:312.
[2] Wang C, Klechikov AG, Gharibyan AL, Wª rmlª nder SKTS, Jarvet J, Zhao L, Xueen J, Shankar SK, Olofsson A, Brannstrom T, Mu Y, Graslund A, Morozova-Roche LA. The role of pro-inflammatory S100A9 in Alzheimerôs disease amyloid-neuroinflammatory cascade. Acta Neuropathologica. 2013; 127(4):507ï 22.
[3] Budvytytė R, Valinį ius G, Niaura G, Voiciuk V, Mickeviį ius M, Chapman H, Goh HZ, Shekhar P, Heinrich F, Shenoy S, Losche M, Vanderah DJ. Structure and Properties of Tethered Bilayer Lipid Membranes with Unsaturated Anchor Molecules. Langmuir. 2013; 29(27):8645ï 56.

HARNESSING THE DIVERSITY OF CAS9 ORTHOLOGS FOR GENOME EDITING

Tomas Urbaitis[1,3], Giedrius Gasiunas[1], Joshua K. Young[2], Monika Jasnauskaite[1], Mantvyda Grusyte[1], Sushmitha Paulraj[2], Jennifer L. Curcuru[4], Megumu Mabuchi[4], Ryan T. Fuchs[4], Ezra Schildkraut[4], G. Brett Robb[4] and Virginijus Siksnys[1,3]

[1] CasZyme, Vilnius, LT-10257, Lithuania
[2] Department of Molecular Engineering, Corteva AgriscienceÊ Agriculture Division of DowDuPontÊ , Johnston, IA 50131, USA
[3] Institute of Biotechnology, Vilnius University, Vilnius, LT-10257, Lithuania
[4] New England Biolabs, Ipswich, MA 01938, USA
tomas.urbaitis@gmc.vu.lt

The Cas9 protein from CRISPR (Clustered Regularly Interspaced Palindromic Repeats)-Cas (CRISPR Associated) bacterial defense systems has been adopted as a robust and multifaceted genome editing tool. The Cas9 RNA guided DNA endonuclease can be directed to cleave, nick or bind a specific site in the chromosomal DNA just by changing the guide RNA sequence. Cas9-based tools have been used to edit genomic DNA, modulate gene expression, visualize genomic loci in cells and deaminate nucleotide bases. However, for Cas9 to bind a given target, a short nucleotide sequence motif, termed PAM, is required. This PAM constraint as well as insufficient specificity are major obstacles for Cas9 genome editing. Thus, analysis of natural Cas9 orthologs could offer an increased diversity of PAM sequences and biochemical properties which may be beneficial to genome editing applications.

Cas9 nucleases are abundant in microbes. To explore this large uncharacterized diversity of Cas9 orthologs, we established a phylogeny-guided bioinformatic selection approach and developed biochemical screens based on cell-free recombinant protein expression and interrogation of plasmid libraries containing randomized PAM sequences for the rapid characterization of novel Cas9 proteins and identification of PAM requirements. Guide RNAs for each Cas9 ortholog were designed *in silico* by identifying putative tracrRNA (trans-activating CRISPR RNA) coding regions in respective native loci. The examined set revealed nucleases that exhibit a wide range of distinctive T-, A-, C- and G-rich PAM preferences, ranging from two to more than four nucleotides, as well as generate staggered-end breaks or require longer spacers to function robustly. Our results indicate that the natural diversity of Cas9 orthologs provides a source of various PAM recognition sequences and other potentially desirable properties that may be used to expand the genome editing toolbox.

SYNTHESIS AND INVESTIGATION OF OLIGOMERIZED AROMATIC AMINE FOR LACCASE ACTIVITY ASSAY

Justinas Babinskas[1], Jerica Sabotiļ[2], Inga Matijoģytė[1]

[1] Sector of Applied Biocatalysis, Institute of Biotechnology, Life Sciences Center, Vilnius University, Lithuania
[2]Department of Biotechnology, Joģef Stefan Institute, Slovenia
justinas.babinskas@gmc.vu.lt

Laccases are multi-copper oxidases (EC 1.10.3.2), containing T1, T2 and T3 copper sites. The catalytic mechanism consists of several stages: i) the transfer of one electron and proton from the substrate to T1 Cu (oxidation); ii) the transfer of one electron from T1 to T2/T3 Cu cluster; iii) the T2/T3 cluster reduces one oxygen molecule to two water molecules, by using four electrons and protons. The reaction by product is water, thus this enzyme has high potential for industrial application [1]. Their natural substrates are aromatic compounds containing at least one hydroxyl, thiol, primary or secondary amine functional group.

Thought the years of investigating various laccases, a lot of information has already been accumulated: redox potentials, enzyme sources, reorganization energies, catalytic mechanism, etc. However, tangible application of laccases is hindered by the unresolved drawbacks such as poor stability, commercial unavailability, lack of efficient expression systems, low immobilization yields, etc.

One of the shortcomings for discovering laccases with new and/or novel features is a lack of substrates suitable for high-throughput screening and functional analysis. Currently, the most common compounds used for laccase functional analysis are 2,2'-azino-bis(3-ethylbenzothiazoline-6-sulphonic acid) under the trivial name ABTS and 4-[[2-[(3,5-dimethoxy-4-oxocyclohexa-2,5-dien-1-ylidene)methyl]hydrazinyl]methylidene]-2,6-dimethoxycyclohexa-2,5-dien-1-one known as syringaldazine [2,3]. Spectrophotometric activity assays with these substrates give acceptable results, but these compounds have poor stability, low specificity and are rather expensive.

By our investigation, we present a new substrate for laccase activity screening on high-throughput agar-plates. This compound was synthesized using relevantly low priced aromatic diamine ï N,N-dimethyl-p-phenylenediamine dihydrochloride. The latter substrate was tested on substrate-agar plates with commercially available laccase Novozym 51003 from *Aspergillus oryzea* (**Fig. 1**) and with the collection of wild fungi protein extracts provided by Joģef Stefan Institute (**Fig. 2**). The results in more detail will be presented during the poster session.

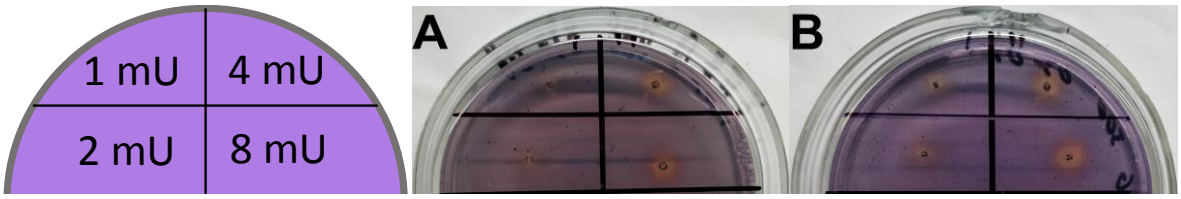

Fig. 1. The amount of laccase enzymatic activity units used for reaction on substrate-agar plate with different concentrations of the substrate: **A** ï 400 ε M; **B** ï 500 ε M.

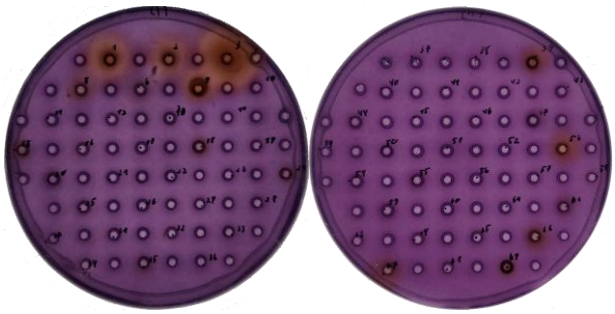

Fig. 2. The results of screening for laccase activity with the collection of wild fungi protein extracts on agar plates with 830 ε M substrate.

[1] Jones S. M., Solomon E. I. Electron transfer and reaction mechanism of laccases. *Cellular and Molecular Life Sciences* **72**, 869-883 (2014).
[2] Call H. P, M¿cke I. History, overview and applications of mediated lignolytic systems, especially laccase-mediator-systems (LignozymÈ-process). *Journal of Biotechnology* **53**, 163-202 (1997).
[3] Lucas M. F. *et al*. Simulating substrate recognition and oxidation in laccases: from description to design. *Journal of Chemical Theory and Computation* **13**, 1462-1467 (2017).

HYDROGEL BASED MICRO AG/AGCL REFERENCE ELECTRODES. QUICK PROTOTYPING OF REFERENCE ELECTRODES

Eivydas Andriukonis[1,2], Marius Butkevicius[3]

[1]Faculty of Chemistry and Geosciences, Department of Physical Chemistry, Vilnius University, Vilnius, Lithuania.
[2]Laboratory of Nanotechnology, Center for Physical Sciences and Technology, Vilnius, Lithuania.
[3]Institute of Biochemistry, Life Sciences Center, Vilnius University, Vilnius, Lithuania.
eivydas.andriukonis@ftmc.lt

Electrochemical measurements are based on the control or observation of potential at the working electrode, for that purpose an electrode of constant potential is needed. Reference electrode (RE) has a fixed potential and this potential does not change as current flows through it. One of the most popular RE is Ag/AgCl electrode. Ag/AgCl RE is often used for electrochemical measurements due to simplicity, inexpensive design, and nontoxic components. These RE are commercially available in various shapes, sizes, junctions and other parameters. However when developing an electrochemical device prototypes there can rise necessity to make unconventional shape or size RE.

Here we explore applicability of RE membrane preparation from polyacrylamide hydrogel. During experimenting we observed almost excellent electrochemical performance of ñin houseò made RE compared with several commercially available ones. The electrode potential difference was 40 mV versus the calomel electrode and 7 mV versus the commercial Ag/AgCl electrode. On the other hand polyacrylamide membranes have porous micro/nano structure with varying pore sizes, which was observed with scanning electron microscopy. Observed porous structure does not permit leakage of inner chloride ions, as chloride flux was evaluated. Permeability to chloride ions doesnôt make polyacrylamide hydrogel an ideal membrane in long term experiments. Though as membranes are quickly and easily prepared it is ideal candidate for quick electrochemical system designing and testing even possible application in disposable one time use devices.

ACTION POTENTIAL PROPAGATION VELOCITY IN *NITELLOPSIS OBTUSA*

Egle Plukaite[1], Vilmantas Pupkis[1], Indre Lapeikaite[1], Vilma Kisnieriene[1*]

[1] Department of Neurobiology and Biophysics, Vilnius University, Vilnius, Lithuania
egle.plukaite@gmc.stud.vu.lt

Electrical impulses in plants can code and transfer information about various environmental changes and condition an appropriate response [1]. Generation of these impulses in plant cells heavily depends on the plasma membrane selective permeability to particular ions and their gradient on both sides of the membrane. Usually, Ca^{2+} concentration in the cytosol is kept low, whereas its increase causes the depolarization of the membrane potential and initiates action potential generation [2]. However, not much is known about the transmission characteristics of these impulses such as their propagation velocity and the compounds potentially affecting them.

We used an extracellular recording system [3] by placing an oblong cylinder-shaped *Nitellopsis obtusa* giant internodal cell along a chamber with electrically isolated compartments and fixing two potential-difference-recording electrode pairs. Knowing the exact distance between these pairs and measuring the time a potential took to propagate from one pair to another (qpt, see Fig. 1), velocity of an action potential propagation can be evaluated. Experiments were performed using two types of stimuli in 10 min. intervals ï electrical and of a low temperature solution, and two types of medium ï artificial pond water (APW) and a solution of Ca^{2+} channel blocker verapamil (0.1 mM) ï a compound that might affect the impulse propagation velocity.

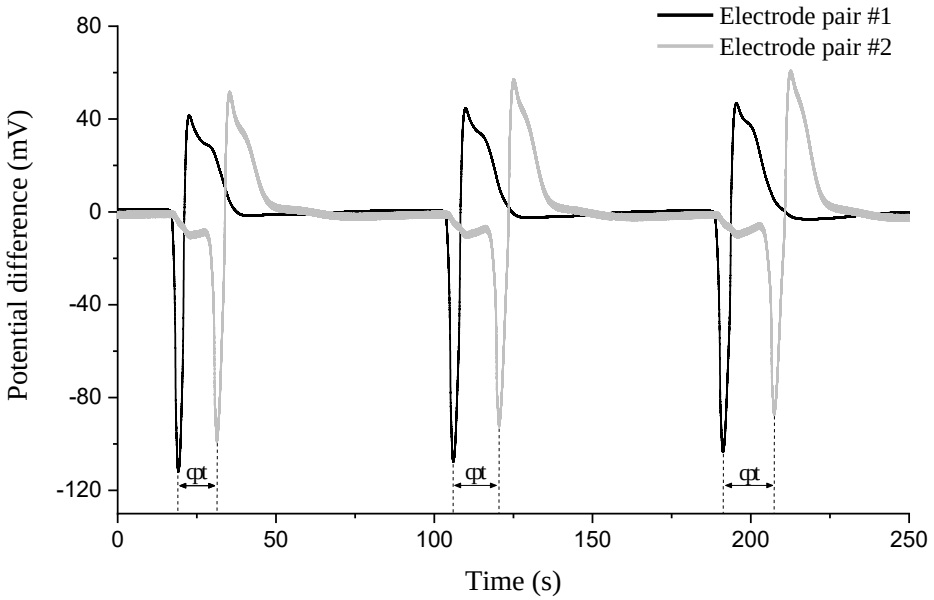

Fig. 1. Propagation of three spontaneous action potentials registered by two electrode pairs. qpt ï the time a potential took to propagate from the first electrode pair to the second one.

Results showed the dynamics of action potential propagation velocity in time: in control solution, regardless of stimulus modality, the very first stimulated potential propagated with the greatest velocity and with each given stimulus it decreased until the value steadied. 0.1 mM verapamil solution evoked a sequence of spontaneous potentials even before the stimulus could be provided. After the spontaneous activity ceased, we observed that the first stimulated action potential propagated the slowest with the velocity similar to the steadied one in the control group. Verapamil did not affect the action potential propagation velocity, but rather provoked spontaneous potentials and led the cell to death. The mortality of cells exposed to 0.1 mM verapamil proved to be of a 100%.

Hence, the action potential in plant cells propagates regardless of whether it is stimulated or spontaneous. The velocity of stimulated action potential propagation depends on if and how many times it has been recently evoked.

[1] J. Fromm, S. Lautner, *Electrical Signals and Their Physiological Significance in Plants*. Plant, Cell & Environment; Plant Cell Environ (2007, March)

[2] V. Kisnieriene, I. Lapeikaite, V. Pupkis, *Electrical signalling in Nitellopsis obtusa: Potential biomarkers of biologically active compounds*. Functional Plant Biology: FPB, 45(2), 132ï 142 (2018)

[3] V. Pupkis, R. Buisas, I. Lapeikaite, V. Kisnieriene, *Using Plant Cells of Nitellopsis obtusa for Biophysical Education*. The Biophysicist (2020)

APPLICATION OF SCANNING ELECTROCHEMICAL IMPEDANCE MICROSCOPE FOR INVESTIGATION OF ELECTROPORATION PROCESS

Margarita Poderyte, Ausra Valiuniene, Inga Gabriunaite

Faculty of Chemistry and Geosciences, Vilnius University, Naugarduko str. 24, Vilnius, Lithuania
margarita.poderyte@chgf.stud.vu.lt

Scanning electrochemical impedance microscopy is an informative research method that can be used to study processes that take place in living cells without damaging them. This test method is a combination of two separate methods - scanning electrochemical microscopy and electrochemical impedance spectroscopy [1]. With the help of a scanning electrochemical microscope, immobilized cells can be examined at various heights from their surface and horizontal scans can be performed to detect individual cells or their higher concentration on the surface [2]. Electrochemical impedance spectroscopy equipment allows monitoring of fast-moving processes in an electrochemical system. This combined test method can be applied not only to cells but also to biological sensors, corrosion, various surfaces and their defects [3].

The plasma membrane is a complex biological system responsible for vital cellular functions. Membranes have selective permeability that can be modified. One of the modification methods is electroporation - a physical method in which cells are exposed to a strong electrical pulse (about 1 kV cm-1), which results in the formation of temporary or permanent pores in the phospholipid layer [4].

The aim of these studies is to develop a controlled model of the electroporation phenomenon and apply it to the study of biological systems using the method of scanning electrochemical microscopy (SECM). To avoid undesired damage to the biological system under study, experiments are performed by selecting the optimal distance between the ultramicroelectrode (UME) and the surface of sample and giving a relatively low potential (form 1 to 2 V) between the UME and the reference electrode using a three-electrode system. The experiments are performed with two types of samples: (i) live yeast cells immobilized on a Petri dish and (ii) a phospholipid bilayer membrane formed on a solid surface.

The scheme of the electroporation process is visualized in figure 1. Using SECM feedback mode, the ultramicroelectrode is approached to the sample. Then the electroporation process is being proceeded. Impedance spectroscopy is used to evaluate electrochemical changes of live yeast cells before and after electroporation. Using SECM scanning mode, surface changes are visualized after the electroporation. It was determined that a pore has been formed exactly below the working electrode.

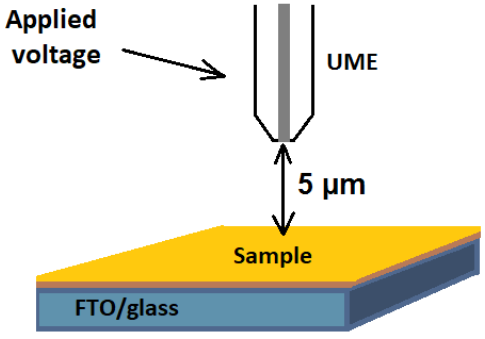

Fig. 1. Scheme of electroporation process using SECM.

Electroporation is already being used in various fields, such as medicine, gene engineering, or the food industry. Although the process is highly applicable, it is still random and incomplete controllable [5]. So, the goal of these studies is to develop a targeted electroporation process model, with good efficiency and easy performance.

This project has received funding from the European Social Fund (project number [09.3.3.-LMT-K-712-22-0045] under a grant agreement with the Research Council of Lithuania (LMTLT).

[1] Morkvenaite ï Vilkonciene, I., ValiÎnienã, A., Petroniene, J., Ramanavicius, A. Hybrid system based on fast Fourier transform electrochemical impedance spectroscopy combined with scanning electrochemical microscopy, Electrochemistry Communications 83, 110ï 112, (2017).
[2] Sun, P., Laforge, F. O., Mirkin, M. V. Scanning electrochemical microscopy in the 21st century, Phys. Chem. Chem. Phys. 9, 802ï 823, (2007).
[3] Daniel, M, Micro- and Nanopatterning Using Scanning Electrochemical Microscopy. Scanning Electrochemical Microscopy, Second Edition, 489ï 524, (2012).
[4] R. Stampfli, Reversible electrical breakdown of the excitable membrane of a Ranvier node. Ann. Acad. Brasil. Ciens. 30, 57ï 63 (1958).
[5] A. Valiuniene, I. Gabriunaite, M. Poderyte, A. Ramanavicius. Electroporation of a hybrid bilayer membrane by scanning electrochemical microscope. Bioelectrochemistry (2020).

TOWARD TO AN ENZYMATIC BIOFUEL CELL POWERED BY GLUCOSE

Algimantas Kaminskas[1*], Asta Kausaite-Minkstimiene[1]

[1] NanoTechnas–Center of Nanotechnology and Materials Science, Faculty of Chemistry and Geosciences, Vilnius University, Lithuania
algimantas.kaminskas@chgf.stud.vu.lt

To replace energy production from fossil fuel or nuclear energy, researchers have put a lot of effort into developing fuel cells (FCs) - electrochemical devices that convert chemical energy into electrical energy by oxidizing fuel at the anode and reducing oxidant at the cathode using noble metal catalysts and supplying electrical energy until sufficient fuel and oxidant are available [1]. Biological fuel cells (biofuel cells, BFCs) are devices capable of directly transform chemical energy to electrical energy via electrochemical reactions involving biochemical pathways. These devices have received considerable attention in the last few decades due to their potential use as alternative energy sources and the advantages over conventional fuel cells. BFCs use enzymes as catalysts, alone or within an organism, and tend operate under mild conditions. Therefore, they are an attractive alternative when it is not possible to use high temperatures or where harsh reaction conditions are undesirable. Enzymatic fuel cells (EBFCs) are the sub-class of FCs relying on purified redox enzymes to achieve electrocatalytic reactions [2]. EBFCs are very attractive due to high specificity of enzymes to their respective substrate, high catalytic activity at mild conditions and variety of enzymes. Moreover, enzymes immobilized on the electrode surface allow membrane-less configuration of FCs, opening up possibility of developing miniature EBFCs [3]. Researchers have focused on development of EBFCs that could supply energy using fuel oxidation, such as blood glucose, at the anode, and reduction of O_2 or H_2O_2, which is formed during enzymatic oxidation of glucose, at the cathode [4]. Glucose and O_2 are an ideal source of fuel and oxidizer because they are readily available in all organic tissues and can be constantly replenished in biological fluids during metabolism, [5]. EBFCs that use enzymatic reactions on both electrodes have also been researched and published over the past decade. It is likely that in the future, miniature membrane-less EBFCs will supply energy to implantable medical devices and will also be used as self-powered biosensors, which, using an analyte as a fuel, are able to supply themselves with energy, and at the same time determine the amount of analyte [6]. However, for this EBFCs must to produce enough energy and have a long lifetime. Therefore, the development of high-performance EBFC is still promising.

The aim of this work was to develop a biocathode for a glucose powered EBFC. The proposed biocathode was based on a graphite rod electrode with an electrochemically coated layer with electrocatalytic properties for H_2O_2 reduction and a layer of a conjugated polymer with carboxyl functional groups. Carboxylic groups allowed covalent immobilization of an enzyme that catalysed the reaction between glucose and dissolved O_2 and produced H_2O_2, which was electrocatalytically reduced on the biocathode surface and caused an increase in the reduction current. The basic scheme of the biocathode and the principle of operation are shown in Fig. 1.

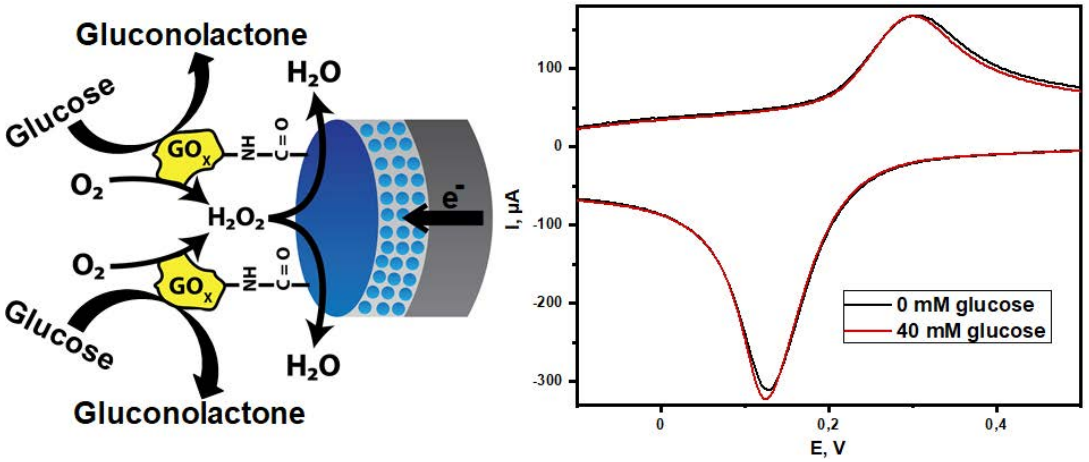

Fig. 1. The basic scheme of the biocathode and the principle of operation

Acknowledgment
This research was funded by a grant (No. S-LU-20-11) from the Research Council of Lithuania.

[1] D. Leech, P. Kavanagh, W. Schuhmann, Enzymatic fuel cells: Recent progress, Electrochimica Acta **84**, 223-234 (2012).
[2] A. L. Goff, M. Holzinger, S. Cosnier, Recent progress in oxygen-reducing laccase biocathodes for enzymatic biofuel cells, Cellular and Molecular Life Sciences **72**, 941-952 (2015).
[3] A. Heller, Miniature biofuel cells, Physical Chemistry Chemical Physics **6**, 209-216 (2004).
[4] M. Rasmussen, S. Abdellaoui, S. D.Minteer, Enzymatic biofuel cells: 30 years of critical advancements, Biosensors and Bioelectronics **76**, 91-102 (2016).
[5] S. Xu, S. D. Minteer, Enzymatic biofuel cell for oxidation of glucose to CO_2, ACS Catalysis **2**, 91-94 (2012).
[6] M. Zhou, J. Wang, Biofuel cells for self-powered electrochemical biosensing and logic biosensing: a review, Electroanalysis **24**, 197-209 (2012).

ACTION POTENTIALS OF PLANTS: EFFECTS OF CHLORIDE CHANNELSô INHIBITION

Benas Kuģmarskis, Vilmantas Pupkis, Vilma Kisnierienã, Indrã Lapeikaitã

Department of Neurobiology and Biophysics, Institute of Biosciences, Life Sciences Center, Vilnius University, Lithuania
benas.kuzmarskis@gmc.stud.vu.lt

In plant cells, action potentials (AP) begin with an increase of cytoplasmic Ca^{2+} concentration, consequently the Cl^- efflux via specific ion channels is activated ï this causes the depolarization of cell membrane. It is difficult to distinguish Ca^{2+} influx from Cl^- efflux because they carry unidirectional current. To date the characteristics and standardized assessment of influx of Ca^{2+} have not been described. Thus, we used ethacrynic acid (EA) to block Cl^- channels in giant Characeaen cells. The effect of 1 mM EA solution on *Nitellopsis obtusa* electrophysiological parameters were tested using intracellular glass microelectrode and two pair current/voltage clamp methods.

For the first time, in addition to the decrease of Cl^- efflux current upon exposure to EA, the alterations of AP parameters were described. AP peak from the usual positive values was reduced to negative ones, thus AP amplitude was also decreased by 30%, while the excitation threshold was not altered at all. Furthermore, depolarization of the membrane resting potential with increased specific resistance and a surprisingly extended duration of repolarization phase was observed upon exposure to EA ï thus implicating interference with other ion transport systems.

Summarizing current/voltage clamp results we affirm that in plant cells AP amplitude is dependent on Cl^- efflux. We conclude that the action potential excitation threshold does not depend on chloride channelsôactivity.

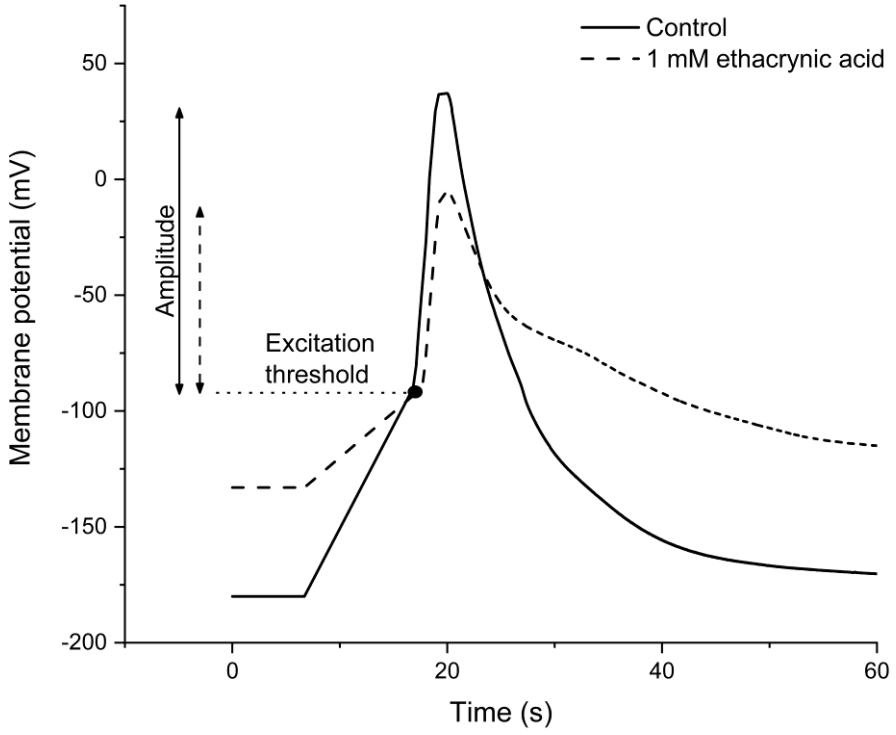

Fig. 1. Average action potentials of *Nitellopsis obtusa* in standard conditions and after exposure to 1 mM ethacrynic acid (n=7).

STUDY OF THE INTERACTION OF HSP70 WITH UNILAMELLAR VESICLES

Akvilė Milašiutė, Rima Budvytytė, Gintaras Valinčius

Institute of Biochemistry, Life Sciences Center, Vilnius University, Lithuania
akvile.milasiute@gmc.stud.vu.lt

Cells produce a various heat shock proteins in response to stress. 70-kDa heat shock protein (Hsp70) is one of the best known heat shock proteins. Hsp70 participates in folding and assembly of newly synthesized proteins, refolding of misfolded and aggregated protiens. Hsp70 expresion is increased during stress conditions, and their function is vital for the recovery of cells after the insult [1]. Hsp70 is mainly localized in subcellular compartments, for example, cytosol, endoplasmic reticulum and mitochondria. In addition, Hsp70 is detected in extracellular space where this protein appear to play a different function from their chaperone activity [2].

Extracellular Hsp70 do not contain a consensus signal for their secretion via classical ER-Golgi compartment. Therefore, they are likely export by an alternative mechanism but the exact Hsp70 translocation mechanism across the plasma membrane remain to be elucidates.

The aim of this work was to investigate Hsp70 interaction with various compositions unilamellar vesicles. In this study, Hsp70 was added to DOPC, DOPC/Chol (60:40) and DOPC/DOPE/Chol/DOPS (20:30:20:30) vesicles solutions and the change in fluorescence intensity due to calceine release from vesicles was detected. Results show that the incubation time of Hsp70 and unilamellar vesicles was 10 min. The smallest Hsp70 concentration which disturbs the integrity of membrane was 0,25 nM. Furthermore, fluorescence intensity of calcein release was about 1.5 times bigger at higher (>2nM) Hsp70 concentrations and vesicles contained negatively charged phospholipids (Fig. 1)

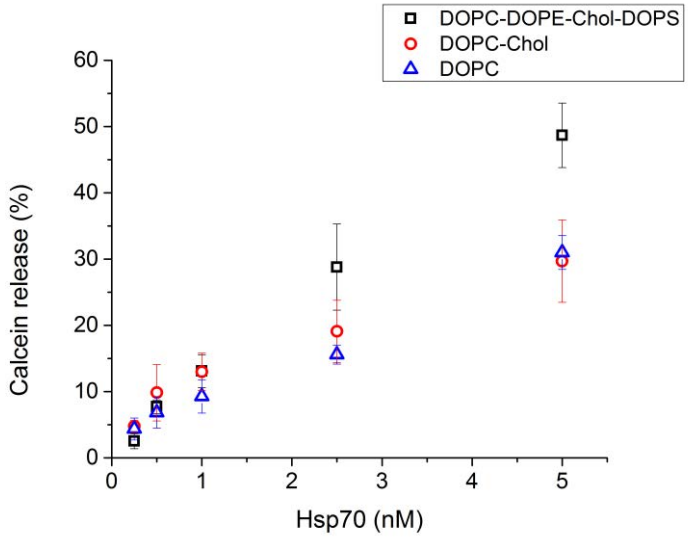

Fig. 1. Hsp70 interaction with unilamellar vesicles. Calsein release from vesicles was similar at lower Hsp70 concentrations (<1 nM). At higher (>2 nM) Hsp70 concentrations, calsein release was 1.5 times bigger in case of negatively charged vesicles. Incubation time – 10 min.

[1] F.U. Hartl, M. Hayer-Hartl, Converging concepts of protein folding in vitro and in vivo, Nat Structural Mol Biol **16**, 574-581 (2009).
[2] A. De Maio, Extracellular heat shock proteins, cellular export vesicles and the Stress Observation System: a form of communication during injury, infection, and cell damage, Cell Stress Chaperones **16**, 235-249 (2011).

INVESTIGATION OF YEAST CELL WALL BARRIER FUNCTIONS AFTER PEF TREATMENT

ArÎnas Stirkã[1], Raimonda CeliesiÎtã-Germanienã[1], Aurelijus Zimkus[2], Nerija Çurauskienã[1], Povilas Ġimonis[1], Aldas Dervinis[1], ArÎnas Ramanaviļius[1, 3], Saulius Baleviļius[1], Klaudija Maļiîtã[1], Justina Kriovaitã[1]

[1] Center for Physical Sciences and Technology, [2] Department of Biochemistry and Biophysics, Life Sciences Center, [3]Department of Physical Chemistry, Faculty of Chemistry and Geosciences, Vilnius University

justina.kriovaite@gmc.stud.vu.lt

Saccharomyces cerevisiae is one of the most analysed eukaryotic organisms because of their high potential of use in industry and daily basis, moreover, it is simple organism to investigate. Natural barriers of the yeast cells which is the cell wall and plasma membrane often limits transport and access of molecules or substrates to as well as from the cell. In this study the absorption of the tetraphenylphosphonium (TPP^+) ion by the yeast cells was studied to investigate resealing process of the yeast cell depending on experimental conditions.

In this research pulsed electric field (PEF) regime was adapted to investigate electrical permeabilization of the yeast cell without causing any damage to the cells, i.e. most of the cells can recover to their non-permeabilized state. These studies were performed by applying two different methods. One method was based on the research of the TPP^+ ion absorption kinetics with the use of potentiometric ion selective electrode, which provides data about the yeast cell wall permeabilization. The other method was based on fluorescent dye assessment that demonstrated the permeabilized state of the cell membrane. Results were analysed by applying the mathematical model. Experiments have displayed firm connection between the yeast cell plasma membrane and the cell wall resealing process after PEF impact. It was determined that the main barrier for the uptake of TPP^+ is the cell wall. Preliminary data regarding yeast cell barrier functions in different pH buffers, strengths of PEF and durations of electric impulses will be provided.

CHARACTERIZATION OF VIRUS-LIKE PARTICLES OF *TORULASPORA DELBRUECKII* VIRUS TDV-1 PRODUCED IN *SACCHAROMYCES CEREVISIAE*

Ona Bartininkaitė[1], Aleksandras Konovalovas[1], Justas Lazutka[2], Elena Servienė[3], Saulius Serva[1]

[1]Institute of Biosciences, Life Sciences Center, Vilnius University, Lithuania
[2]Institute of Biotechnology, Life Sciences Center, Vilnius University, Lithuania
[3]Laboratory of Genetics, Institute of Botany, Nature Research Center, Vilnius, Lithuania
ona.bartininkaite@gmc.stud.vu.lt

Yeasts are widely used model microorganism for virus research. In addition, some yeasts own double-stranded RNA viruses that are considered as non-infectious since no naturally occurring extracellular route of transmission has been determined [1]. Yeasts are also an attractive platform to synthesize virus-like particles (VLPs) due to numerous advantages such as capability for post-translational modifications, high yield of recombinant protein and simple cultivation procedure. The majority of virus-like particles were biosynthesized in *S. cerevisiae* expression systems followed by *P. pastoris* and *H. polymorpha*. In the past several years, significant changes occurred in virus-like particle biosynthesis strategies including multilayered VLPs or VLPs produced of more than one type of structural protein [2].

In previous work, the dsRNA virus TdV-1 of the *Partitiviridae* virus family was identified in nonconventional yeast *Torulaspora delbrueckii*. The partitiviruses are typically isolated from filamentous fungi, protozoan and plant hosts [3]. The *Partitiviridae* virus forms non-enveloped particles in the range of 25 nm to 43 nm in diameter. Therefore, TdV-1 is the first virus to be discovered in non-filamentous fungi, belonging to the *Partitiviridae* family. This study aimed to characterize the properties of the capsid protein encoded by TdV-1 virus.

To produce TdV-1 capsid protein, yeast expression plasmids encoding recombinant TdV-1 capsid protein were constructed and protein biosynthesis in *S. cerevisiae* has been performed. Protein analysis confirmed that TdV-1 recombinant capsid protein biosynthesis occurs in *S. cerevisiae*. According to transmission electron microscopy (TEM) analysis, the recombinant TdV-1 capsid protein is capable to form virus-like particles of 30 nm in diameter. To evaluate TdV-1 virus-like particle assembly capabilities, capsid protein was fused with the fluorescent protein mCherry and biosynthesis of modified recombinant capsid protein was performed in *S. cerevisiae*. Microscopy analysis of TEM demonstrated that modified TdV-1 capsid protein is able to assemble into VLPs, thus mCherry fluorophore does not interfere with VLPs assembly. To identify TdV-1 recombinant capsid protein C-terminus localization in VLP, it was labeled with 6xHis affinity tag and immobilized metal affinity chromatography purification was carried out. Protein fraction profile analysis suggested that C-terminus of TdV-1 capsid protein is located on the inner surface of VLP.

[1] R. B. Wickner et al., Viruses and Prions of Saccharomyces cerevisiae, Advances in Virus Research 86, 1ï 36 (2013).
[2] H. J. Kim et al., Yeast as an expression system for producing virus-like particles: what factors do we need to consider?, Letters in Applied Microbiology 64, 111-123 (2016).
[3] E. J. Vainio et al., ICTV virus taxonomy profile: Partitiviridae, Journal of General Virology 99, 17-18 (2018).

ANTIOXIDANT ACTIVITY AND RESISTANCE TO LOW PH OF STRAINS BELONGING TO LACTOBACILLUS AND BIFIDOBACTERIUM GENERA

Jolita Jagelaviciute, Dalia Cizeikiene

Department of Food Science and Technology, Kaunas University of Technology, Lithuania
jolita.jagelaviciute@ktu.lt

Probiotics have been defined by The Food Agricultural Organization/World Health Organization (FAO/WHO) as ñlive microorganisms which when administered in adequate amounts confer a health benefit on the hostò [1]. Probiotic bacteria not only have to be safe but also have to survive in the gastrointestinal tract conditions and possess beneficial properties [1]. Food supplemented with probiotics is preferable for consumers than supplementation with capsules, tablets and other drug forms. Food has buffering properties and may maintain the survival of probiotic bacteria during passage through the gut [2]. Moreover, strains with strong functional properties including antioxidant and antimicrobial activity would be desirable for developing novel functional food supplemented with probiotic microorganisms. However, due to different probiotic bacteria properties, one of the most essential factors are the selection of the proper cultures [3]. The evaluation of potential probiotic bacteria for probiotic properties with the potential application for functional products as supplements is growing nowadays [4,5].

The aim of this study was to evaluate probiotic characteristics *in vitro* such as resistance to low pH and bile salts and antioxidant activity of commercially available strains belonging to *Lactobacillus* and *Bifidobacterium* genera.

The *in vitro* resistance of 9 *Lactobacillus* and 5 *Bifidobacterium* spp. to low pH and bile salts were investigated. Most of tested bacteria were able to tolerate pH 3 for 4 h, while in pH 2 for 4 h survived 8 of 14 strains. *Bifidobacterium pseudolongum* DSM 20099, *Bifidobacterium animalis* DSM 20105 showed resistance to pH 2 for 4 h. The antioxidant activity of probiotic bacteria intact cell and intracellular cell-free extract was determined by 1-diphenyl-2-picrylhydrazyl (DPPH) and 2-azinobis-(3-ethylbenzothiazoline-6-sulfonic acid) diammonium salt (ABTS) radical scavenging assays. The results showed that antioxidant activity varied among the different strain of tested probiotics. Intact cells and cell-free extracts of *L. reuteri* DSM 20015 and *L. paracasei* subsp. *paracasei* DSM 4905 exhibited the highest DPPH radical scavenging activity, while the highest ABTS radical scavenging activity was exhibited by intact cells and intracellular cell-free extract of *B. longum* subsp. *infantis* DSM 20088. However, these strains were sensitive to low pH. Results suggest that probiotic bacteria which survive in low pH could be suitable candidates for food production, while other strains should be protected with specific vehicle.

[1] World Health Organisation (WHO) and Food and Agriculture Organization of United Nations (FAO) Probiotics in food: health and nutritional properties and guidelines for evaluation. FAO food and nutrition paper, ISSN 0254-4725 (2006).
[2] Rad A. Homayoni, E. Vaghef Mehrabany, B. Alipoor, L. Vaghef Mehrabany, The comparison of food and supplement as probiotic delivery vehicles. Crit Rev Food Sci Nutr 56:896ï 909 (2016).
[3] A. Terpou, A. Papadaki, IK. Lappa, et al., Probiotics in food systems: significance and emerging strategies towards improved viability and delivery of enhanced beneficial value. Nutrients 11(7):1591 (2019).
[4] G. Mulaw, T. Sisay Tessema, D. Muleta, A. Tesfaye, In vitro evaluation of probiotic properties of lactic acid bacteria isolated from some traditionally fermented ethiopian food products. Int J Microbiol, (2019)
[5] X. Wei, Y. Zhang, H. Zhou, F. Tian, Y. Ni., Antimicrobial activities and in vitro properties of cold-adapted Lactobacillus strains isolated from the intestinal tract of cold water fishes of high latitude water areas in Xinjiang, China. BMC Microbiol 19(1):247(2019)

BAKERôS YEAST-BASED QUINONES-MEDIATED MICROBIAL FUEL CELL

Katazyna Blazevic[1], Juste Rozene[1], Vakare Guoba Sataite[1], Inga Morkvenaite-Vilkonciene[1]

[1] Department of Mechatronics, Robotics, and Digital Manufacturing, Vilnius Gediminas Technical University, Vilnius, Lithuania
katazyna.blazevic@vilniustech.lt

Recently, to ensure the efficiency of various alternative energy sources to stop the greenhouse effect and utilize renewable organic materials, the focus is on biofuel cells [1]. Microbial fuel cell (MFC) bioelectrochemical devices available to directly transform chemical energy to electrical energy via a series of electrochemical reactions catalyzed by microorganisms. In the design of a microbial fuel cell, it is essential to choose not only the anode, redox mediators but also the microorganisms. Usually, few different yeast strains are used as biocatalysts in MFC with or without external mediators [2]. One of the most popular eukaryotic organisms is simple and easy to cultivate bakerôs yeast *(Saccharomyces cerevisiae).* They are resistant to environmental influences and can metabolize a wide range of substrates [3].

In this research, we used three electrodes system: quinones-mediated graphite rod as the working electrode, Ag/AgCl/KCl (3M) as a reference electrode, and platinum as the counter electrode. Cyclic voltammetry (CV) was applied for the electrochemical measurements. The changes in current density can be seen.

To improve charge transfer from the yeast cells to the electrode, we used two lipophilic mediators: i) 9,10-phenantrenequinone (PQ) and ii) 2-methyl-1,4-naphthoquinone (menadione, MD). Bakerôs yeast solution was sequentially changed by adding it in the same measurement cell. The result is shown in Figure 1.

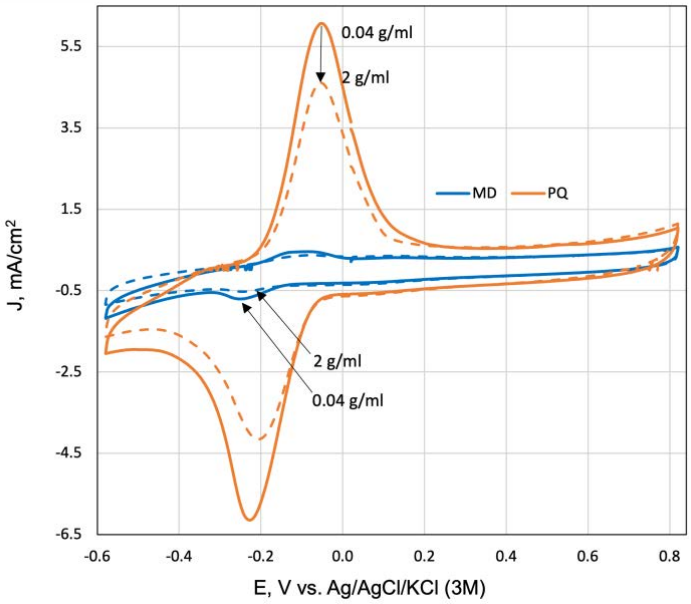

Fig. 1. Cyclic voltammograms with PQ and MD mediators at different bakerôs yeast concentration.

The current density decreased whit, increasing bakerôs yeast solution concentrations while using both MD and PQ mediators. While the yeast concentration was increased 50 times, the current density decreased by 1.3 mA/cm^2 with immobilized PQ and by 0.2 mA/cm^2 with MD. It means that it is unnecessary to use a high concentration of yeast in the biofuel cell to generate more electricity. To improve the efficiency of the MFC in the future, we need to consider modifying other components.

Acknowledgement. This project has received funding from European Social Fund (project No 09.3.3.-LMT-K-712-22-0325) under grant agreement with the Research Council of Lithuania (LMTLT).

[1] F. Davis and S. P. J. Higson, ñBiofuel cells-Recent advances and applications,ò *Biosens. Bioelectron.*, 2007.

[2] J. Rozene, I. Morkvenaite-Vilkonciene, I. Bruzaite, A. Dzedzickis, and A. Ramanavicius, ñYeast-based microbial biofuel cell mediated by 9, 10-phenantrenequinone,ò *Electrochim. Acta*, p. 137918, 2021.

[3] G. Silveira, M. Ikegaki, and J. M. Schneedorf, ñA low-cost yeast-based biofuel cell: an educational green approach,ò *Green Chem. Lett. Rev.*, vol. 10, no. 1, pp. 32ï 41, 2017.

SACCHAROMYCETALES AND THEIR ALLIES IN BIOLOGICAL VERSATILITY

Kristupas Paulius, Aleksandras Konovalovas, Saulius Serva

Department of Biochemistry and Molecular Biology, Institute of Biosciences, Life Sciences Center, Vilnius University, Vilnius, Lithuania
kristupas.paulius@chgf.stud.vu.lt

The sheer knowledge about yeasts ï unicellular organisms, their conserved biology and most vital processes allow us to have sufficient contextual foundations for broadening the perspective in their evolutionary behavior. Yeastôs adaptation to environment is driven, among others, by specific biocidic, or killer phenomenon ï the main ambition of this research. Our goal was to analyze the processes derived from yeasts in their relationship with double-stranded RNA (dsRNA) viruses. The scientific literature is mostly limited to the findings specifically in *Saccharomyces sensu stricto*, although we decided to dwell deeper into other yeasts from the wild origin as well.

We investigated 28 niches of various flora through different geographic zones of Lithuania, consisting of unique fruit-trees, oaks, fungi, and few other surroundings. 240 unique strains of yeasts were thoroughly inspected for morphology, growth, and signs of possessing a viral genome. Out of analyzed yeast strains, about third possessed dsRNAs, and half of them demonstrated some sort of killer activity, uncovered by RNA gel electrophoresis and cultivation on selective media. However, each of the killer phenotype was unique in its manifestation ï we found silent, progressive, and weak killers, three classifications of the same phenomenon. These findings provide us with new prospects of potential research on natural processes occurring in different niches.

SYNTHESIS OF METAL-OXIDE NANOPARTICLES FROM MACROALGAL EXTRACTS

Katarzyna Dziergowska[1], Izabela Michalak[1]

[1] Wrocğaw University of Science and Technology, Faculty of Chemistry, Department of Advanced Material Technologies, 50-372 Wrocğaw, Poland
katarzyna.dziergowska@pwr.edu.pl

The aim of this paper is to present a novel biological method of metal-oxide nanoparticles (NPs) synthesis with the use of macroalgal extract and to analyze parameters, which can have an influence on this synthesis. As an example, ZnO and CuO NPs were biosynthesized with the use of extract obtained from green macroalga ï *Cladophora glomerata*. Macroalgae can be used for synthesis of many different metal-based nanoparticles due to the presence of bioactive compounds such as polysaccharides, pigments, proteins and antioxidants, which act as biocompatible reductants [1,4].

NPs can be synthesized in three ways: physical, chemical and biological. Nowadays, biological methods are more and more often examined, because they are environment friendly and low in toxicity [1]. Currently, among biological methods, very popular is biosynthesis with the use of plant extracts (mostly made from leaves), bacteria, fungi and microalgae [2]. However, lately methods based on macroalgal extracts are increasing in popularity [3]. Fig. 1 compares the number of publications on different reducing agents used in NPs biosynthesis over the past 20 years.

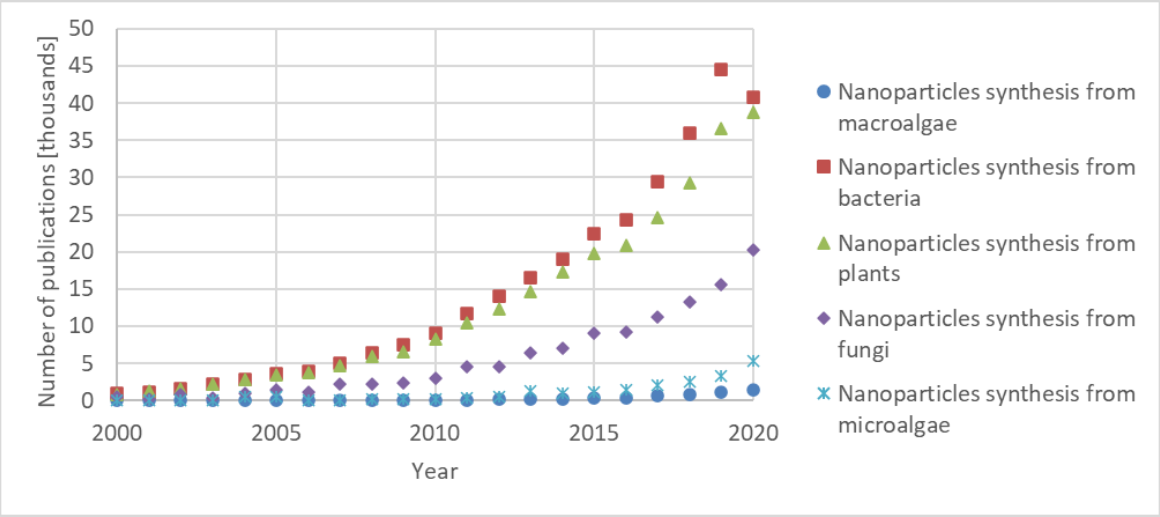

Fig. 1. Popularity of different reducing agents for NPs biosynthesis over the past 20 years (based on Google Scholar, accessed on 10th February 2021).

In the present study, different biosynthesis methods of ZnO and CuO NPs with the use of macroalga extract were compared. Algal extract was obtained by ultrasound assisted extraction with water or ethanol. The solvent used for extraction has an influence on later NPs biosynthesis. It was found out that many parameters influenced the efficiency of nanoparticles biosynthesis, among them were: type of salt used (inorganic ï nitrate/sulfate or organic ï acetate), salt concentration, salt to extract ratio, pH, temperature, time of incubation.

The highest yield of NPs biosynthesis has been obtained for the use of organic salts, salt concentration higher than 0.1 M, pH 12, organic solvent (ethanol) and temperature higher than room temperature. Further investigation is needed to find the optimal temperature, salt to extract ratio, time of incubation and if the use of ultrasounds or microwave radiation can improve the process.

[1] L. Pourakbar, S. Siavash Moghaddam, J. Popoviĺ-Djordjeviĺ, Synthesis of metal/metal oxide nanoparticles by green methods and their applications. In: S. Hayat, J. Pichtel, M. Faizan, Q. Fariduddin (Eds.) Sustainable Agriculture Reviews **41**. Nanotechnology for Plant Growth and Development. Springer Nature Switzerland AG, **4**, 63-81 (2020).
[2] A. Saravanan, P. Senthil Kumar, S. Karishma, et al., A review on biosynthesis of metal nanoparticles and its environmental applications, Chemosphere **264**, 128580 (2021).
[3] S. Roy, A Review: Green synthesis of nanoparticles from seaweeds and its some applications, Austin Journal of Nanomedicine & Nanotechnology **7** (1), ISSN 2381-8956 (2019).
[4] P. Khanna, A. Kaur, D. Goyal, Algae-based metallic nanoparticles: Synthesis, characterization and applications, Journal of Microbiological Methods **163**, 105656 (2019).

Acknowledgments
This work was financed in the framework of project entitled ñEco-friendly technologies for the management of seaweed biomass for products useful for sustainable agriculture and biosorbents used for the removal of heavy metal ions from the environmentò (No 2019/33/B/NZ9/01844) attributed by The National Science Centre in Poland.

STUDY OF THE INTERACTION OF S100A9 PROTEIN WITH LIPID MEMBRANES

Rimgailã Tamulytã[1], Evelina Jankaitytã[1], Zigmantas Toleikis[2], Marija Jankunec[1]

[1]Institute of Biochemistry, Life Sciences Center, Vilnius University, Vilnius, Lithuania
[2]Institute of Biotechnology, Life Sciences Center, Vilnius University, Vilnius, Lithuania
rimgaile.tamulyte@gmc.stud.vu.lt

Amyloid plaque formation and neuroinflammatory processes are the main features of Alzheimerôs disease pathology. S100A9 is pro-inflammatory, calcium-binding protein, belonging to the S100 family [1]. S100A9 protein levels are increased in many inflammatory disorders, including Alzheimerôs disease [2]. In Alzheimerôs disease, S100A9 serves as a junction between amyloid and neuroinflammatory cascades [3]. Due to its amyloidogenicity, together with ß-amyloid S100A9 forms neurotoxic amyloid plaques [3], which results in neuronal death and memory impairment. Similar to ß-amyloid, *in vitro* S100A9 forms cytotoxic fibrillar and annular structures [3]. However, the exact mechanism of the interaction of S100A9 with lipid membranes is still unknown.

The aim of this work is to investigate the mechanisms of S100A9 protein aggregation and interaction with lipid bilayer. We used the solid supported membrane and unilamellar vesicles models to mimic the fundamental chemical and physical properties of a cell membrane. To visualize the protein-membrane interaction and to determine the nanomechanical properties of lipid bilayer, we used atomic force microscopy (AFM). AFM is non-destructive and high-resolution imaging tool. AFM not only provides information on the morphology but also on physical properties of the sample. We demonstrate that protein S100A9 induce local thinning of the membrane composed of brain total lipid extract (TLE) (Fig. 1).

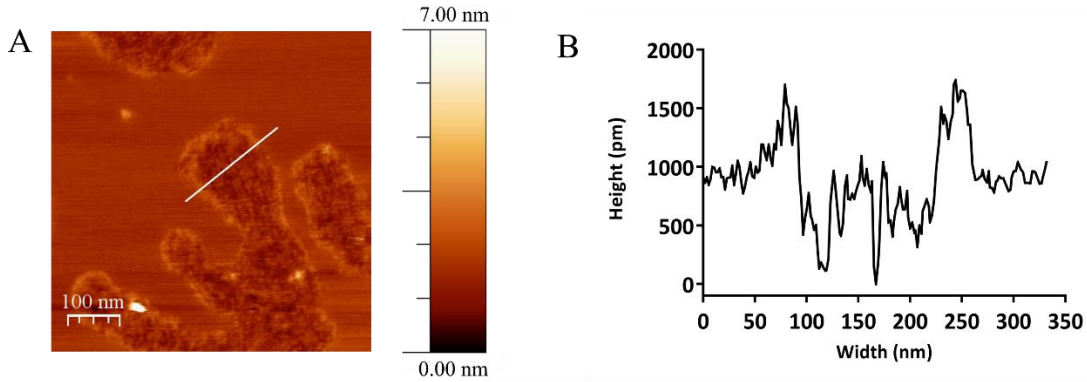

Figure 1. AFM observation of S100A9 disruption on solid supported membrane. (A) AFM topography image showing the local thinning of a TLE membrane. (B) Height profile along the line in the AFM image.

[1] C. Wang, I.A. Iashchishyn, J. Pansieri et al., S100A9-Driven Amyloid-Neuroinflammatory Cascade in Traumatic Brain Injury as a Precursor State for Alzheimerôs Disease. *Sci Rep* **8**, 12836 (2018).
[2] K.A. Chang, H.J. Kim, Y.H. Suh. The role of S100a9 in the pathogenesis of Alzheimer's disease: the therapeutic effects of S100a9 knockdown or knockout. Neurodegenerative Dis. **10**, 27-9 (2012).
[3] C. Wang, A.G. Klechikov, A.L. Gharibyan et al., The role of pro-inflammatory S100A9 in Alzheimer's disease amyloid-neuroinflammatory cascade. Acta Neuropathol. **127**, 507-22. (2014).

APPLICATION OF ENZYMATIC AND BACTERIAL HYDROLYSIS FOR INCREASE OF THE BIOLOGICAL ACTIVITY OF RAW PLANT MATERIAL

Auġrinã Venckaitytã, Vilma Kaġkonienã, RÎta Mickienã, Audrius Maruġka

Instrumental Analysis Open Access Centre, Vytautas Magnus University, Lithuania
ausrine.venckaityte@stud.vdu.lt

Synthetic antioxidants and antimicrobials can cause many unwanted side effects that attract the interest of food producers and consumers in their search for ingredients of natural origin. The evaluation of natural products as safe and effective antimicrobials is one of the scientific strategies to lessen the threat of drug-resistant pathogens. In recent years, the interest in natural plant raw materials is being intensified, as they have created an impressive number of modern medicines [1]. Bee pollen, *Salvia hispanica* L. (chia) and *Anethum graveolens* L. (dill) seeds may be among the plant raw materials that can be further investigated, as these plant products contain high levels of phenolic compounds and flavonoids, as well as have significant antimicrobial, anti-inflammatory or other positive effects on human health.

Research on bee pollen included the determination of their detailed composition, especially regarding biologically active compounds, such as quercetin, naringenin, kaempferol, isorhamnetin, as well as rutin and 3-O-glucosides [2]. In addition to this, bee pollen helps to overcome metabolic problems and reduces the activity of harmful bacteria [3]. Nevertheless, *Salvia hispanica* seeds can be very important for health due to containing high percentage of fatty acids, which are also significant for antioxidant and antimicrobial activity [4]. Moreover, *Anethum graveolens* contains significant bioactive compounds too, such as phenolic acids (vanillic, caffeic, ferulic and others) [5].

On the other hand, it is known that these raw plant materials are surrounded by a wall which may prevent the human body from absorbing the biologically valuable substances. Therefore, it is very important to perform studies of extracts treated and non-treated with enzymatic and bacterial hydrolysis. Such studies will help to reveal whether the bioavailability of products can be increased. The aim of this work is to study the plant products of interest, to find out the composition and properties of their compounds. Also, to compare the effects of enzymatic and bacterial hydrolysis treatments on increasing the bioavailability of bee pollen, dill seeds, and chia seeds to the human digestive system. According to our data, the combined enzymatic and bacterial hydrolysis has not been applied to any product.

[1] Tabart, J., Franck, T., Kevers, C., Pincemail, J., Serteyn, D., Defraigne, J. O., & Dommes, J., Antioxidant and anti-inflammatory activities of *Ribes nigrum* extracts. Food Chemistry **131**, 1116ï 1122 (2012).

[2] Zhang, Y., Yang, F., Jamali, M. & Peng, Z., Antioxidant Enzyme Activities and Lipid Oxidation in Rape (*Brassica campestris* L.) Bee Pollen Added to Salami during Processing. Molecules **21**, 1ï 13 (2016).

[3] Zuluaga Dom²nguez, C., Castro Mercado, L., & Cecilia Quicaz§n, M., Effect of enzymatic hydrolysis on structural characteristics and bioactive composition of bee pollen. Journal of Food Processing and Preservation **43**, 3ï 11 (2019).

[4] Mohd Ali, N., Yeap, S. K., Ho, W. Y., Beh, B. K., Tan, S. W., & Tan, S. G., The Promising Future of Chia, *Salvia hispanica* L. *Journal of* Biomedicine and Biotechnology **1**, 1ï 9 (2012).

[5] Orhan, I., Senol, F. S., Ozturk, N., Celik, S. A., Pulur, A., & Kan, Y., Phytochemical contents and enzyme inhibitory and antioxidant properties of *Anethum graveolens* L. (dill) samples cultivated under organic and conventional agricultural conditions. Food and Chemical Toxicology **59**, 96ï 103 (2013).

THE PHOTOSTABILITY OF CdSe/ZnS-COOH QUANTUM DOTS IN AQUEOUS AND BIOLOGICAL MEDIA

Emilija Januġkaitã[1], Osvaldas Vilutis[1], Agnã Kalnaitytã [1,2]

[1] Biophotonics Group of Laser Research Centre, Vilnius University, Saulãtekio ave. 9, III bld., LT ï 10222, Vilnius, Lithuania
[2] Institute of Ecology, Nature of Research Centre, Akademijos str. 2, LT-08412, Vilnius, Lithuania
emilija.januskaite@ff.stud.vu.lt

Quantum Dots (QDs) are fluorescent semiconductors, 1-100 nm in size, with unique optical and electrical properties [1]. Moreover, due to sensitivity of QDs spectral properties to environment, it is advantageous to use QDs as biosensors [2]. Also, as QDs already are used in many areas, it is possible that they may leak into the waterways and enter the food chain [3]. So, it is important to analyze the QDs photostability in aqueous or biological media to understand how different conditions effect their fate in the environment.

In this study, measuring an optical density and fluorescence of CdSe/ZnS-COOH QDs (625nm Invitrogen) in various aqueous and biological media under different light condition and temperature was assessed the photostability of QDs spectral properties. The samples of QDs with 4nM concentration were prepared in distilled, deep well, and lake waters, in MWC medium for growing algae, and with unicellular freshwater green *Scenedesmus sp.* and *Chlorella sp.* algae cells. After preparation of samples, they were kept at different conditions: in dark at +4 temperature, also in dark and under continuous white light (Osram Dulux Star, 11W/827) at about +20 temperature. The samples with algae cells were prepared with irradiated (violet light diode, 404 nm, 30mW/cm^2, 120 min) QDs in deep well water (DWW) and kept in indirect sunlight.

Despite that, hour after the preparation of QDs samples, the photoluminescence (PL) intensity of QDs in deep well water was greatest compared of QDs samples in other studied media. During the period of 16 days, the PL intensity was the least stable in DWW, regardless of storing conditions (Fig. 1(a)). The QDs held under the white light had decreased PL intensity and shifted the peak of spectra to the red side of wavelength after a day compared with samples kept in the dark, where these spectral changes appeared later. This gives an indication that light might accelerate the aggregation of ODs. Regarding the fact that light had the strongest initial effect on spectral properties of QDs in lake water (the furthest shift of PL spectra to the red side) they were more stable under the continuous light than in dark over the time of experiment.

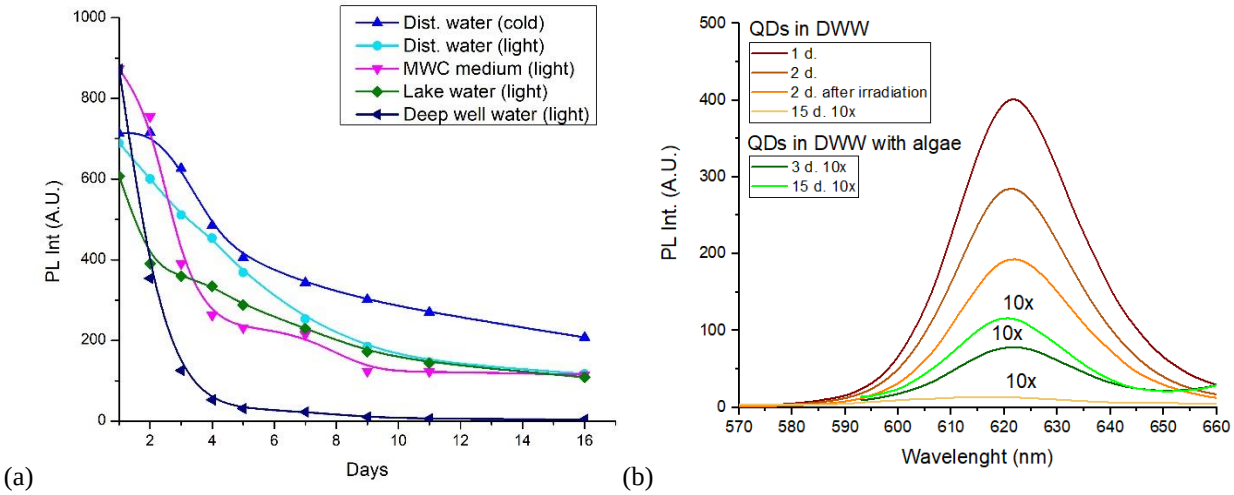

Fig. 1. (a) The PL intensity (at spectrum peak about 621nm) of QDs samples in different media exposed to continuous white light and the QDs in distilled water stored in dark at +4 temperature during 16 days; (b) the PL intensity of QDs in deep well water with and without algae cells. Excitation wavelength 405nm.

The PL intensity of QDs samples in deep well water after irradiation by violet light with 216 J/cm^2 dose decreased most likely due to the partial disintegration of QDs coating, and kept decreasing during 15 days (Fig. 1(b)). The PL intensity of these QDs increased after addition of algae cells compared to the PL intensity immediately after irradiation. It seems that substances with algae cells had a partial restoring effect on the QDs coating, which was affected by the light.

This work was funded by the Research Council of Lithuania, Project No. S-MIP-20-22.

[1] P. A. Keane, H. Ruiz-Garcia et al. Advanced Imaging Technologies, Retina, 133-150 (2013).
[2] R. H. Pierce, X. Gao. Applications of Quantum Dots in Bioimaging and Bioassay (2019)
[3] H. E. Elzorkany, M. A Farghali et al., Ecotoxicology impact of silica-coated CdSe/ZnS quantum dots internalized in Chlamydomonas reinhardtii algal cells, Science of The Total Environment (2019)

CONSTRUCTION OF TYPE III-A CRISPR-CAS EFFECTOR COMPLEX FOR TRANSPORTATION INTO THE ZEBRAFISH NUCLEUS

Danas Klimavičius[1], Dalia Smalakyte[1], Abhishek Pateria[2], Matthias Bochtler[2,3], Gintautas Tamulaitis[1]

[1] Institute of Biotechnology, Life Sciences Center, Vilnius University, Saulėtekio av. 7, 10257 Vilnius, Lithuania
[2] International Institute of Molecular and Cell Biology, Trojdena 4, 02-109 Warsaw, Poland
[3]Institute of Biochemistry and Biophysics PAS, Pawinskiego 5a, 02-106 Warsaw, Poland
klimaviciusdanas@gmail.com

RNA knockdown is a powerful experimental technique to study gene function and it is commonly mediated through RNA interference. However, some organisms such as zebrafish cannot tolerate the additional load on their interfering RNA machinery [1]. Our group proposed that type III-A CRISPR-Cas effector complex Csm from *Streptococcus thermophilus* (StCsm) could be used for RNA knockdown as a programmable ribonuclease in this model organism. We demonstrated greater than 50% efficiency of StCsm in RNA knockdown and hence provided a proof of principle of programmable mRNA degradation by StCsm in eukaryotes [2].

Recently it was shown that type I CRISPR-Cas effector complex Cascade, which is of similar size to Csm, could be successfully transported into the nucleus by attaching the nucleus localization sequence (NLS) [3]. Since DNA transcription occurs in the nucleus, synthesized transcripts could be cleaved immediately before transporting them into the cytoplasm. In order to further improve transcript degradation efficiency we decided to deliver StCsm into the nucleus of a cell. In this study we present construction of StCsm variants optimized for transportation into zebrafish nucleus.

[1] Liu W., Wang Y., Sun Y., Wang Y., Wang Y., Chen S., Zhu Z. (2005) Efficient RNA interference in zebrafish embryos using siRNA synthesized with SP6 RNA polymerase. *Development Growth and Differentiation*, 47(5), p. 323ï 331

[2] Fricke T., Smalakyte D., Lapinski M., Pateria A., Weige C., Pastor M., Kolano A., Winata C., Siksnys V., Tamulaitis G., Bochtler M. (2020) Targeted RNA knockdown by Type III-A CRISPR-Cas Complex in Zebrafish. *The CRISPR Journal*, 3(4), p. 299-313

[3] Dolan A., Hou Z., Xiao Y., Gramelspacher M., Heo J., Howden S., Freddolino P., Ke A., Zhang Y. (2019) Introducing a Spectrum of Long-Range Genomic Deletions in Human Embryonic Stem Cells Using Type I CRISPR-Cas. *Molecular Cell*, 74(5), p. 936-950.

APPLICATION OF MARCUS THEORY TO ANALYSIS OF GLUCOSE OXIDASE CATALYZED REDUCTION REACTION

Marius Butkevičius[1], Audrius Laurynėnas[1]

[1]Department of Bioanalysis, Institute of Biochemistry, Life Sciences Center, Vilnius University, Vilnius, Lithuania
marius.butkevicius@gmc.vu.lt

Oxidoreductases are enzymes that catalyze oxidation and reduction reactions in biochemical processes. They participate in glycolysis, citric acid cycle, oxidative phosphorylation, amino acid metabolism and in other vital biochemical transformations. Many of these reactions are interesting both from theoretical and practical perspectives. In industry, oxidoreductases are used as catalysts for synthesis of valuable products, biodegradation of pollutants, fabrication of biofuel cells and biosensors. Therefore, a better theoretical understanding of processes such as electron transfer (ET) catalysis of oxidoreductases provide routes for practical implementations.

Here we used glucose oxidase from *Aspergillus niger* (GOx) as a model enzyme to study ET between the active center of enzyme and a set of artificial electron acceptors. GOx catalysis cycle involves two separate reactions. In the first reaction, β-D-glucose is oxidized to D-glucono-δ-lactone. In the second reaction, molecular oxygen, the natural second substrate of the enzyme, is reduced to hydrogen peroxide. According to the literature, the rate of this reaction is limited by ET [1, 2]. In addition, GOx can reduce a wide range of artificial electron acceptors, and in this study we investigated which process is the rate-limiting of reduction of these compounds.

According to Marcus theory [3], when the reaction rate is ET-limited, then a parabolic relationship between natural logarithm of the reaction rate and free Gibbs energy exists [4,5]. However, this relationship is expected to hold only for a series of homologous substrates. A more generalized version of Marcus theory predicts a parabolic relationship between free energy of activation and free energy of a reaction (Fig. 1. B), without any assumptions about similarity of substrates. We measured these thermodynamic parameters for GOx catalyzed reduction reactions of 12 non-homologous artificial electron acceptors (Fig. 1. A, blue dots) and found a completely different relation than it is predicted by assuming ET as a reduction rate-limiting step. These observations could be explained by consecutive electron and proton transfer mechanism. In the case of this study, the reduction rate constants measured consist of both electron and proton transfer rate parameters. If ET is very fast, then the reaction rate is limited by proton transfer rate, and vice versa, if ET is slow, the reaction rate is limited by ET rate.

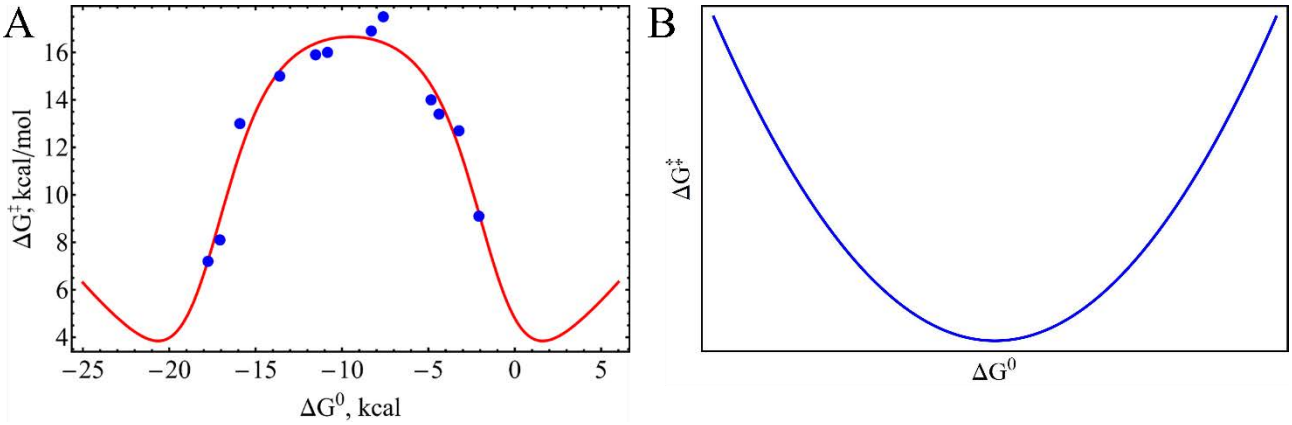

Fig. 1. A – The dependency of reaction activation energy on free Gibbs energy of substrates. Blue dots – experimental result, red line – mathematical model. B – Theoretical dependency of reaction activation energy on free Gibbs energy of substrates

[1] Roth, J. P., & Klinman, J. P. Catalysis of electron transfer during activation of O2 by the flavoprotein glucose oxidase. Proc. Natl. Acad. Sci. U.S.A, 100(1), 62-67 (2003)

[2] Roth, J. P., Wincek, R., Nodet, G., Edmondson, D. E., McIntire, W. S., & Klinman, J. P. Oxygen isotope effects on electron transfer to O2 probed using chemically modified flavins bound to glucose oxidase. J. Am. Chem. Soc, 126(46), 15120-15131 (2004)

[3] Marcus R A. On the theory of oxidation-reduction reactions involving electron transfer. I. J Chem Phys. 24(5), 966-978 (1956)

[4] Tetianec, L. & Kulys, J. Kinetics of N-substituted phenothiazines and N-substituted phenoxazines oxidation catalyzed by fungal laccases. Cent. Eur. J. Biol. 4, 62–67 (2009).

[5] Tsuruoka, N., Sadakane, T., Hayashi, R. & Tsujimura, S. Bimolecular rate constants for FAD-dependent glucose dehydrogenase from Aspergillus terreus and organic electron acceptors, Int. J. Mol. Sci. 18, (2017).

PREPARATION OF IMMOBILIZED MICROBIAL LIPOLYTIC ENZYMES APPLICABLE FOR THE SYNTHESIS OF FLAVOR ESTERS

Gintarė Povilaitytė, Lilija Kalėdienė, Alisa Gricajeva

Department of Microbiology and Biotechnology, Life Sciences Center, Institute of Biosciences, Vilnius University, Vilnius, Lithuania
gintare.povilaityte@gmc.stud.vu.lt

At present, enzymes are the key players in different industrial processes with microbial lipolytic enzymes being one of the most widely used in biocatalysis, both at academic and industrial levels. However, for the industrial implementations, especially in organic synthesis, immobilized enzymes are preferred over their soluble forms because of their reusability, greater activity, specificity, stability, resistance to inhibitors and in some cases even purity [1]. Immobilized preparations are more suitable for the biocatalysis in organic media. Immobilization may improve enzymes rigidity which can lead to higher stability in organic media and, therefore, such enzyme preparation maintains not only high residual activity, but also can exhibit improved thermostability and substrate specificity [2]. Unfortunately, ready-to-use immobilized preparations of lipolytic enzymes suitable for the synthesis of the desired compounds do not always exist and/or usually have a high cost. Therefore, in the present study, we aimed to find effective way of immobilization of different lipolytic enzymes for the use in organic media. So far, two enzymes were selected for the study: a novel recombinant Lip4 carboxylesterase from *S. saprophyticus* AG1 and a chimeric lipolytic enzyme (made of *Theromyces lanuginosus* lipase and *Fusarium oxysporum* phospholipase A1) Lecitase Ultra (Novozymes). The former enzyme-coding gene (*lip4*) was cloned and expressed in *E. coli* C41 (DE3) and purified using affinity chromatography. Lip4 and Lecitase Ultra were immobilized utilizing adsorption immobilization on octylsepharose (OS). Adsorption immobilization was chosen since lipolytic enzymes have a hydrophobic lid domain and this unique structural feature can be used to "lock" the enzyme in active form by immobilization on hydrophobic supports, which mimic the hydrophobic substrates of enzymes [3] (Fig. 1). Immobilization of Lip4 and Lecitase Ultra on OS have shown that compared to free enzymes, both Lip4 and Lecitase Ultra possessed higher activities indicating their hyperactivation upon immobilization. However, for the further synthesis of valuable flavor esters (2-phenylethylbutanoate and 2-phenylethylpropanoate) immobilization requires further studies in selecting the optimal conditions for each enzyme.

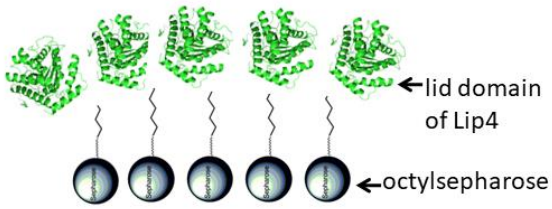

Fig. 1. Schematic representation of how lid-having lipolytic enzymes can be "locked" on the surface of the hydrophobic OS resulting in the hyperactivation of the enzyme. Model of recombinant Lip4 was used for the visualization.

[1] O. Barbosa, C. Oritz, Á. Berenguer-Murcia et al., Strategies for the one-step immobilization-purification of enzymes as industrial biocatalysts, Biotechnology Advances **33**, 435–456 (2015).
[3] G.M. Borelli, D. Tronno, Recombinant Lipases and phospholipases and their use in as biocatalysts for industrial applications, International Journal of Molecular Sciences **16**, 20774-20840 (2015).
[4] A. Gricajeva, S. Kazlauskas, L. Kalėdienė et al., Analysis of *Aspergillus* sp. lipase immobilization for the application in organyc synthesis. International Journal of Biological Macromolecules **108**, 1165-1175 (2018).

EFFECTS OF COLD PLASMAON THE AMOUNT OF STEVIOL GLYCOSIDES IN *STEVIA REBAUDIANA* BERTONI LEAVES

Tomas Mockaitis[1], Vida Mildaģienã[1], Rasa ÇÎkienã[1]

[1]Faculty of Natural Sciences, Vytautas Magnus University, Vileikos str. 8, LT-44404 Kaunas, Lithuania, tomas.mockaitis@vdu.lt

Stevia rebaudiana Bert. (Bertoni) has attracted the attention of scientists and industry in recent years for its properties, natural and low-calorie sweeteners, steviol glycosides (SGs), which are an alternative to sugar. The main SGs are stevioside (Stev) and rebaudioside A (RebA). They compose up to 40 % of the dry weight of the leaf and are 300 times sweeter than sucrose, also they are thermostable making them favorable in the food industry [1, 2]. RebA has better water solubility and a milder taste, closer to sucrose, than Stev. Seed treatment by cold plasma (CP) is an environmentally friendly method used to improve various plant properties and stimulate secondary metabolites synthesis [3].

The aim of this study was to determine the effect of cold plasma (CP) seed treatment (2, 5, or 7 min) on Stev and RebA accumulation in stevia leaves at different growth weeks (8, 12, 14 and 20). Other biochemical traits such as amount of total phenolics, total flavonoids and antiradical scavenging activity were also determined.

The largest change in SGs concentration at week 8 was induced by CP 2 min and reached 141 mg/g, as compared to 103 mg/g in control. At week 12 and 14, the largest increase in SGs concentration was observed in CP 5 min group. At week 12, it increased from 123 mg/g in control to 161 mg/g, and at week 14 it was 331 mg/g as compared to 220 mg/g in control. At week 20, the SGs concentration decreased to 150 mg/g and CP had no effect. The amount of SGs in the leaves inversely correlated with the scavenging activity and the total amount of phenolics and flavonoids. It can be concluded that the effect of cold plasma had a positive effect on the accumulation of steviol glycosides at least until week 14 of vegetation.

[1] Bergs, D., Burghoff, B., Joehnck, M., Martin, G., & Schembecker, G. (2012). Fast and isocratic HPLC-method for steviol glycosides analysis from Stevia rebaudiana leaves. Journal f¿r verbraucherschutz und lebensmittelsicherheit, 7(2), 147-154. doi: 10.1007/s00003-012-0760-5

[2] Jeppesen, P.B., Gregersen, S., Alstrup, K.K., & Hermansen, K. (2002). Stevioside induces antihyperglycaemic, insulinotropic and glucagonostatic effects in vivo: studies in the diabetic Goto-Kakizaki (GK) rats. Phytomedicine, 9(1), 9ï 14. doi:10.1152/ajpendo.00331.2005

[3] Jiang, J. F., He, X., Li, L., Li, J. G., Shao, H. L., Xu, Q. L., Ye, H. R. & Dong, Y. H. (2014). Effect of cold plasma treatment on seed germination and growth of wheat. Plasma science technology, 16(2), 54ï 58.

POLARIMETRIC NONLINEAR MICROSCOPY WITH TEXTURE ANALYSIS FOR COLON CANCER DIAGNOSTICS

Viktoras Maģeika[1], Mykolas Maļiulis[1], Martynas Riauka[1], Lukas Kontenis[1,2], Edvardas Ģurauskas[3], Virginijus Barzda[1,4,5]

[1]Faculty of Physics, Laser Research Centre, Vilnius University, 10 Saulãtekio Ave., LT- 10222, Vilnius, Lithuania
[2]Light Conversion, 2B Keramiku st., LT-10233, Vilnius, Lithuania
[3]Department of Pathology, Forensic Medicine and Pharmacology, Faculty of Medicine, Vilnius University, M.K. Ciurlionio St 21/27, LT-03101, Vilnius, Lithuania
[4]Department of Physics, University of Toronto, 60 St. Georges st., Toronto, ON M5S 1A7, Canada
[5]Department of Chemical and Physical Sciences, University of Toronto Mississauga, 3359 Mississauga Rd. N., Mississauga L5L 1C6, ON, Canada
viktoras.mazeika@ff.vu.lt

Nonlinear microscopy methods, such as multiphoton excitation fluorescence (MPEF), second-harmonic generation (SHG), and third-harmonic generation (THG) microscopies, have been successfully applied for histopathology imaging [1]. SHG microscopy is particularly interesting because of its capability for label-free imaging of non-centrosymmetric structures, such as collagen fibers in the extracellular matrix. As collagen structure is known to undergo changes during carcinogenesis [2], SHG microscopy can be a useful tool for investigating the resulting structural differences. Texture analysis can be performed on the acquired images via the gray-level co-occurrence matrix (GLCM), which contains the numbers of occurrences of neighboring pixels having particular values. GLCM can be used to calculate several statistical parameters describing the image, such as contrast, correlation, and entropy. In addition to SHG intensity images, GLCM can also be used to analyze maps of various polarimetric parameters, for example, SHG circular dichroism (SHG-CD) and achiral susceptibility ratio R. Such maps can be obtained by performing polarimetric measurements, as polarization of the generated SH depends on polarization of incident light and on sample characteristics [3]. Use of GLCM for cancer diagnostics has been investigated in multiple studies, and in some cases it was even shown to differentiate between different stages of cancer [3, 4].

In this work, SHG polarimetric microscopy is used to investigate collagen structure in normal and cancerous human colon histological samples. GLCM is employed to analyze the obtained maps of polarimetric parameters. Resulting textural data is used to compare normal and cancerous colon tissue.

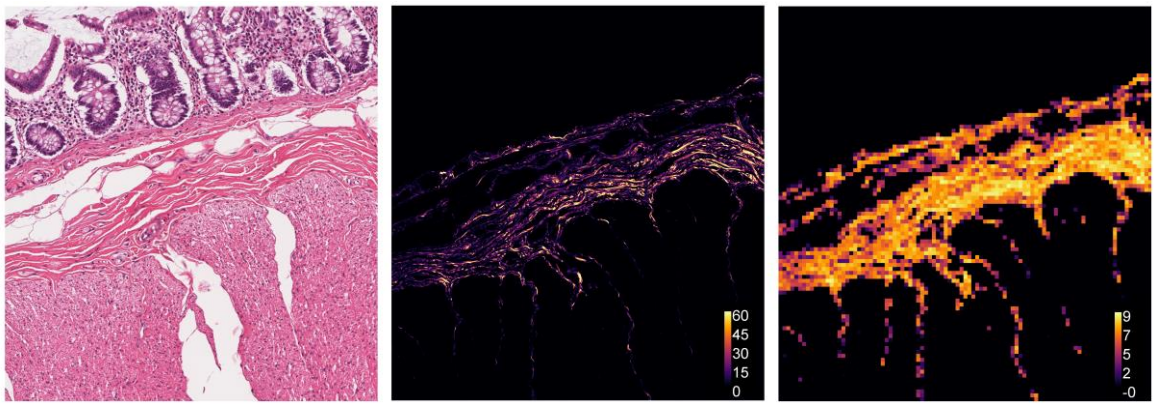

Fig. 1. Polarimetric SHG microscopy and texture analysis of normal colon tissue. H&E stained histological slide (left), SHG intensity image (middle) and an SHG intensity entropy map (right). Size of images: 800 Ĭ 800 ɛm.

[1] A. Tuer et al., ñNonlinear multicontrast microscopy of hematoxylin-and-eosin-stained histological sections,ò J. Biomed. Opt. **15(2)**, 026018 (2010).
[2] C. C. Le et al., ĂFunctional Interplay Between Collagen Network and Cell Behavior Within Tumor Microenvironment in Colorectal Cancer,ñ *Front. Oncol.* **10**, 527 (2020).
[3] A. Golaraei et al., ñPolarimetric second-harmonic generation microscopy of the hierarchical structure of collagen in stage I-III non-small cell lung carcinoma,ò *Biomed. Opt. Express*, **11**, 1851-1863 (2020).
[4] N. Fujima et al., ñThe utility of MRI histogram and texture analysis for the prediction of histological diagnosis in head and neck malignancies,ò *Cancer Imaging* **19**, 5 (2019).

PHYTOCHEMICAL ANALYSIS OF *ARTEMISIA DUBIA* WALL. SECONDARY METABOLITES AND ITS SOLID PELLET CALORIFIC VALUE

Vilmantas Pedišius[1], Audrius Maruška[1], Irena Vaškevičienė[2]

[1]Instrumental Analysis Open access center, Vytautas Magnus university, Vileikos g. 8, LT-44404, Kaunas, Lithuania
[2]Heat Equipment Research and Testing Laboratory, Lithuanian Energy Insitute, Breslaujos g. 3, LT-44403 Kaunas, Lithuania
vilmantas.pedisius@vdu.lt

Secondary metabolites exert significant pharmacological and toxicological effects and their efficient antioxidant activity has lead these compounds being used as nutraceuticals [1]. *Artemisia dubia* Wall. exhibits many of these natural compounds, such as flavonoids, phenolics and alkaloids. Aside from the pharmacological aspect, the plant is also a prosperous energetic plant, obtaining significant heating value and large growth rate, yearly reaching up to 11,10 t/ha [2]. The aim of the research is to investigate *A. dubia* Wall. methanol/water extraction fractions phytochemical properties and the solid phase residue heating value before and after the extraction. In the research *A. dubia* Wall. was harvested from 3 different areas on 2018 July 27 and dried for lower enzymatic activity. The areas differed one from each other by different level of nitrogen fertilizers: no fertilization, N90 and N180. Extraction was performed using distilled water and 3 concentrations of methanol: 50%, 75 % and 100 %. Phytochemical capabilities were measured using spectrophotometric analysis methods according to Stankevičius et al. (2011) to evaluate the total amount of phenolic compounds using Folin-Ciocalteu reagent and the total amount of flavonoids using AlCl3 reagent. Antioxidant activity was evaluated using DPPH reagent. The lower calorific value (LHV) of the dry basis for the solutions was measured by an IKA C5000 calorimeter in accordance with the LST EN ISO 18125:2017 adiabatic method for automated bomb calorimetry. Extraction influence on *A. dubia* Wall. calorific value and comparison of increasing polarity solvent effect on total phenolic content, flavonoid content and antioxidant activity has yet not been published.

Acknowledgements: This project has received funding from the Research Council of Lithuania (LMTLT), grant No. 09.3.3-LMT-K-712-22.

[1] G. Velu, V. Palanichamy, and A. P. Rajan, Phytochemical and Pharmacological Importance of Plant Secondary Metabolites in Modern Medicine, Bioorganic Phase Nat. Food An Overv., 135–156 (2018).
[2] J. Slepetys, Z. Kadziuliene, L. Sarunaite, V. Tilvikiene, and Kryzeviciene Aldona, Biomass Potential Of Plants Grown For Bioenergy Production, Renew. Energy Energy Effic. Proc. Int. Sci., 64–72 (2012).
[3] M. Stankevičius, I. Akuåeca, I. Jákobsone, and A. Maruška, Comparative analysis of radical scavenging and antioxidant activity of phenolic compounds present in everyday use spice plants by means of spectrophotometric and chromatographic methods, J. Sep. Sci., vol. 34, no. 11, 1261–1267, (2011).

COLLAGEN ULTRASTRUCTURE CHANGES IN LENTIGINOUS MELANOMA CHARACTERIZED BY SECOND-HARMONIC GENERATION MICROSCOPY

Martynas Riauka[1], Viktoras Mazeika[1], Mykolas Maciulis[1],
Edvardas Zurauskas[2], Lukas Kontenis[1,3] and Virginijus Barzda[1,4]

[1] Laser Research Centre, Faculty of Physics, Vilnius University, Sauletekis Avenue 3, LT-10222, Vilnius, Lithuania
[2] Department of Pathology, Forensic Medicine and Pharmacology, Faculty of Medicine, Vilnius University, M.K. Ciurlionio St 21/27, LT-03101, Vilnius, Lithuania
[3] Light Conversion, Keramiku st 2B, LT-10234, Vilnius, Lithuania
[4] Department of Physics, Department of Chemical and Physical Sciences, University of Toronto, 3359 Mississauga Rd North, Mississauga, L5L 1C6, Canada
martynas.riauka@ff.vu.lt

Development and spread of cancer are known to cause changes in the structure of extracellular matrix (ECM). A substantial portion of ECM is comprised of collagen, which is a noncentrosymmetric structure. Due to this, it is known to produce second-harmonic generation (SHG) signals. Furthermore, the SHG signals, produced in collagen, are strongly dependent on the angle between the collagen fibers and the incoming light polarization, hence the structural changes of collagen can be studied using polarimetric second-harmonic generation microscopy [1].

A reduced polarimetric SHG microscopy techniques, namely linear polarization-in, polarization-out (PIPO) microscopy, is applied for skin tissue imaging. In PIPO case, for each orientation of linearly polarized incoming laser radiation a set of linearly polarized states of outgoing second harmonic signal is measured [2].

In this work, PIPO technique was applied to obtain the intensity, achiral susceptibility ratio *R* and collagen fiber orientation angle distributions in pT1b stage lentiginous melanoma histological sections. The parameter distributions were extracted by performing a pixel by pixel fitting procedure of the intensity variations in the image using the SHG intensity equation for the PIPO case [2]. The same sample contained normal (intersection between healthy epidermis and dermis) and cancerous tissue (intersection between tumor tissue and dermis), therefore these parameters were used to investigate the structural differences between the two cases.

PIPO data analysis revealed the differences in collagen fiber orientations as well as increase in *R* ratio and decrease in SHG intensity in cancerous tissues, which suggests a modified collagen structure. Therefore, the differences in the polarimetric parameters of collagen can be applied for melanoma research and diagnostics.

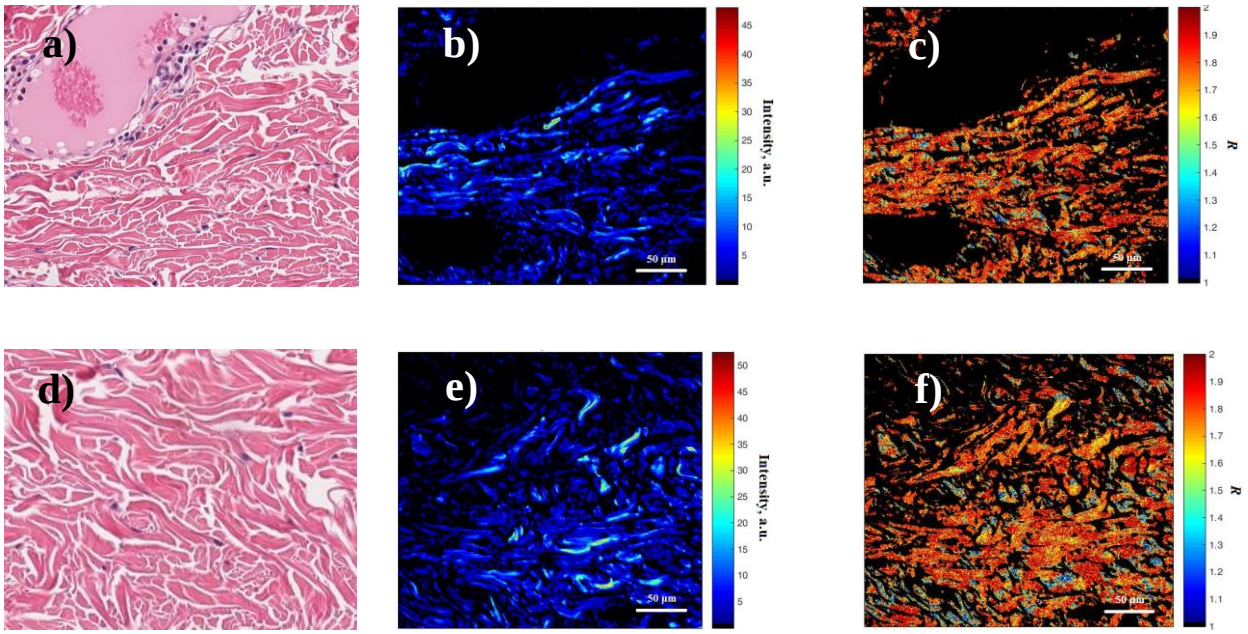

Fig. 1. Nonlinear microscopy of melanoma in H&E histopathology samples. H&E stained cancerous (a) and normal (d) tissues with corresponding SHG intensity and R ratio distribution maps in cancerous (b, c) and normal (e, f) tissues.

Acknowledgements: The work was supported by grant No. 1.2.2.-LMT-K-718-02-0016.

[1] Masood Samim, Serguei Krouglov, and Virginijus Barzda, "Double Stokes Mueller polarimetry of second-harmonic generation in ordered molecular structures," J. Opt. Soc. Am. B 32, 451-461 (2015).
[2] A. Golaraei, Polarimetric second-harmonic generation microscopy for histopathology. PhD thesis, University of Toronto, 2018.

INVESTIGATIONS OF BIOLOGICAL EFFECTS OF GRAPHENE OXIDE NANOSTRUCTURES ON BROWN TROUT (*SALMO TRUTTA*)

Gytis Martuseviļius[1, 2], Gintarã Sauliutã[1], Janina Paģusienã[1], Çivilã Jurgelãnã[1], Sergej Ġemļuk[3], Milda Stankeviļiî tã[1]

[1] Nature Research Centre, Akademijos St. 2, LT-08412 Vilnius, Lithuania
[2]Vilnius University, Life Sciences Center, Department of Biochemistry and Molecular Biology, Saulãtekio av. 7, 10223 Vilnius, Lithuania
[3]SRI Center for Physical Sciences and Technology, SavanoriÔav. 231, LT-02300 Vilnius, Lithuania
gytis.martusevicius@gmc.stud.vu.lt.

Graphene oxide (GO) nanoparticles are useful and promising material for graphene-based applications in electronic, optics, chemistry, energy storage, and biology. Recently developed methods for preparation of graphene oxide derivatives open the new attractive application areas in green technologies including energy storage and utilizing nuclear wastes [1]. Extensive application of GO increases its probability to enter the environment. GO belong to the class of carbon nanomaterials, which have the ability to cross cellular barriers, interact with many of cellular components, including the plasma membrane, cytoplasmic organelles and nucleus [2]. For these reasons GO may cause toxic effects on aquatic invertebrates and fish (*in vitro* and *in vivo*) [3].

The aim of this study was to determine genotoxicity responses (nuclear abnormalities assay) and metallothioneins (MT) level in *Salmo trutta* larvae exposed to graphene oxide nanostructures (GON), metal mixture (MIX), and GON+MIX. Toxicity of metal mixture (MIX) at 40-fold (40ŷ) increased maximum-permissible-concentrations (MPC) set for EU inland waters to *S. trutta* larvae were evaluated using the whole-mixture approach. Induction of micronuclei (MN), nuclear buds (NB), nuclear buds on filament (NBf), bi-nucleated erythrocytes with nucleoplasmic bridges (BNb) and blebbed nuclei (BL) cells were assessed as genotoxicity endpoints. The total genotoxicity (ƐGentox) level was assessed as the sum of frequencies of the analysed genotoxicity (MN+NB+NBf+BNb+BL) endpoints. Metallothioneins induction was measured by colorimetric reaction using Elman reagent.

Results showed that after exposure to GON40ŷ, the amount of MT in *S. trutta* larvae increased, as well after the exposure to GON40ŷ+MIX40ŷ, but was not statistically significant. Exposure to MIX40ŷ resulted in 100% mortality of fish larvae. The genotoxicity assay showed that the highest frequencies of analysed endpoints were found in GON40ŷ+MIX40ŷ exposed larvae. *S. trutta* larvae exposure to GON40ŷ+MIX40ŷ resulted in a significant elevation of MN, NB and ƐGentox frequencies compare to control and GON40ŷ exposure groups. GON40ŷ induced significant MN and ƐGentox formation compare to control group; and MN, NB and ×Gentox levels compared to GON40ŷ+MIX40ŷ group. This research highlights the genotoxic and cytotoxic potential of GON in early stages of *S. trutta*. The results of the MT analysis may indicate the potential of GON to bind heavy metals in *S. trutta* larvae.

Acknowledgments
This work was funded by the Research Council of Lithuania, Project No. S-MIP-20-22.

[1] A. T. Dideikin, A. Y. Vul, Graphene Oxide and Derivatives: The Place in Graphene Family, Frontiers in Physics **6**, 149 (2019).
[2] A. K. Dasmahapatra, T. P. S. Dasari, P. B. Tchounwou, Graphene-Based Nanomaterials Toxicity in Fish. Rev Environ Contam Toxicol **247**, 1ï 58 (2019).
[3] N. Malhotra, O. B. Villaflores, G. Audira, P. Siregar, J-S. Lee, T-R. Ger, C-D Hsiao, Toxicity studies on graphene-based nanomaterials in aquatic organisms: current understanding, Molecules **25 (16)**, 3618 (2020).

IMPACT OF RED CLOVER SEED COLOR ON GERMINATION, MORPHOMETRY, AND ROOT NODULATION AFTER SEED TREATMENT WITH COLD PLASMA AND ELECTROMAGNETIC FIELD

Anatolii Ivankov[1], Rasa Çukienã[1], Zita Nauļienã[1], Laima Degutyte-Fomins[1], Irina Filatova[2], Veronika Lyushkevich[2], Vida Mildaģienã[1]*

[1] Faculty of Natural Sciences, Vytautas Magnus University, Lithuania
[2] B. I. Stepanov Institute of Physics, National Academy of Sciences, Belarus
anatolii.ivankov@vdu.lt

It has been shown by numerous studies [1-3] that exposure of plants to environmental stress can increase seed germination and promote morphometrical changes in plants. This study aimed to evaluate the effects of seed coat color on the seed germination of red clover (*Trifolium pratense L.),* seedling development, and the amount of flavonoids and root nodulation induced by electromagnetic field (EMF) and cold plasma (CP). The experiments were performed on seeds of red clover cultivar ćSadÎnaiâ. Before sowing, red clover seeds of different seed colors (yellow and dark purple) were treated with two types of physical stressors: CP for 5 and 7 minutes (CP5 and CP7) and EMF for 10 minutes (EMF10). The effect of treatment on seed germination was estimated by *in vitro* germination test. The kinetic parameters of germination were determined: Vi - the final germination percentage, Me - the median germination time, Qu ï quartile deviation, uniformity germination in seed population. The morphometric changes, changes in the amount of flavonoids, and the number of root nodules for the cultivar that was growing in the substrate for 5 weeks were measured.

The results have shown that the effect of seed treatment with CP and EMF on the germination kinetics, seedling development of red clover seeds significantly depends on the color of the seeds. Control seeds of both colors showed Viå100%, therefore, treatment of seeds with stressors could not have a positive effect on this indicator. However, CP5 reduced Vi of yellow seeds by 17%. Nonetheless, the stress-induced changes in the Me index were different for yellow and dark purple seeds. Stress treatment did not have a significant effect on Me index for yellow seeds, but the treatment of purple seeds with CP5, CP7 reduced Me by 24% and 56%, respectively. Treatment with EMF10 did not affect the germination rate of either yellow or purple seeds.

EMF10 seed treatment had positive effect (16%) on the height of the aboveground part of seedling grown from the yellow seeds and the length of their roots. None of the other stressors had a significant effect on these parameters. EMF10 promoted aboveground part weight gain by 30%, although it did not have a reliable effect on root weight. CP7 had a negative effect on root weight, which decreased by 50%. The EMF10 and CP5 exposure did not cause such a significant difference. Stressor treatment did not change the number of seedling leaves, but CP5 and EMF10 increased the number of nodules by 6.6 and 11.6 times, respectively. The height of the aboveground part of the control group of seedlings grown from the purple seeds was 20%, the weight was 29% higher, these parameters for the seedlings of the CP7 group were as much as 28% and 40% higher compared to the seedlings growing from the respective groups. Treatment of purple seeds with CP5 reduced the height of the aboveground part of seedlings by 20%. Stress treatment of purple seeds had no reliable effect on root length, the number of leaves, and the number of nodules.

Seed treatment with CP and EMF induced changes in the amount of flavonoids (except luteolin) in root exudates. Particularly strong was effect of CP7 - the amount of hesperetin, quercetin, 7-hydroxyphlavone, daidzein increased 2-3 times. The obtained results confirm the hypothesis that the changes in red clover nodulation activity caused by seed treatment stressors may be due to an active interaction with rhizobacteria due to the changed chemical composition of root exudates.

The study showed that pre-sowing treatment of red clover seeds with cold plasma and an electromagnetic field can induce seed coat color-dependent changes in germination, morphometrical parameters, nodulation, and the amount of flavonoids.

[1] Stariļ, P., Vogel-Mikuģ, K., Mozetiļ, M. & Junkar, I. Effects of Nonthermal Plasma on Morphology, Genetics and Physiology of Seeds: A Review. *Plants* **9**, 1736 (2020).
[2] Ģvubov§, R. *et al.* Evaluation of the Impact of Cold Atmospheric Pressure Plasma on Soybean Seed Germination. *Plants* **10**, 177 (2021).
[3] Mildaziene, V. *et al.* Seed treatment with cold plasma and electromagnetic field induces changes in red clover root growth dynamics, flavonoid exudation, and activates nodulation. *Plasma Process. Polym.* (2020).

ANALYSIS OF SECONDARY METABOLITES OF MEDICAL PLANTS *Levandula* L. AND *Helichrysum* L.

Karolina Lankaitã, RÎta Mickienã, Vilma Kaġkonienã, Audrius Sigitas Maruġka

Faculty of Natural Sciences, Instrumental Analysis Open Access Centre, Vytautas Magnus University, Vileikos str. 8, LT44404, Kaunas, Lithuania
karolina80808@gmail.com

Lavender (*Lavandula angustifolia*) essential oil is one of the most popular and can be considered one of the best-selling essential oils for anxiety, stress and depression. International organizations such as the World Health Organization (WHO), the European Scientific Cooperative for Phytotherapy (ESCOP) or the European Medicines Agency (EMA) validate the properties of this medicinal plant, such as anxiety and stress relief [1]. Also, interest in *Helichrysum* L. essential oil is growing rapidly. *Helichrysum* L. essential oil has been shown to have anti-inflammatory properties in recent decades. In addition, several studies have shown that secondary metabolites of *Helichrysum* L. act as a free radical scavenger that can restore cellular redox balance and slow tumor cell growth and can be used in cancer therapy [3].

Essential oils are made up of larger aromatic and volatile compounds found naturally in all parts of the plant. Like medicines, cosmetics and food preservatives they are widely used in different countries. Today, 3,000 essential oil types are known, and there are about 300 commercial types [5]. Demand for essential oils is growing, due to their various therapeutic properties. *Helichrysum* L. and *Levandula* L. essential oils are widely used all over the world (in cosmetics, aromatherapy, perfumery, pharmacy, etc.), therefore, this natural composition of products is very important nowadays, as natural treatments are becoming more and more popular.

One of the most common ways to obtain essential oils is steam distillation or hydrodistillation. This method is used when, in the presence of a high content of essential oils in the raw material, exposure to water vapor and distillation temperature, the essential oils do not change their compositional properties. Also, steam distillation is based on the properties of essential oils (volatility, immiscibility with water) [6].

Gas chromatography of essential oil samples, one of the test methods, was chosen because selective test methods are very important for determining the composition of essential oils. Gas chromatography - mass spectrometry (GC / MS) is one of the most important methods for the determination of purity [2].

GC - MS analysis was used for *Helichrysum italicum* essential oil. The study showed 67 constituents in the essential oil, accounting for 99.24% of the total oil. Essential oil is characterized by the predominance of oxygen-containing sesquiterpenes and oxygen-containing monoterpenes. The main constituents of the essential oil are Ŭ-cedrene, Ŭ-curcumin, geranyl acetate, limonene, neroli, neryl acetate and Ŭ-pinene [3].

GC - MS analysis was used to determine the chemical composition of lavender oil. As expected, the main components were linalool and linalyl acetate, accounting for 32.75% and 43.13% of the essential oil, respectively [4].

According to the analysis of the literature, the volatile compounds of *Helichrysum italicum* essential oils are based on terpenes: nerilacetate, Ŭ-Pinene, neroli, ɓ-caryophyllene, bisabolene, azulene, and the dominant compounds derived from *Levandula angustifolia* in essential oils are linalool and linalyl acetate.

[1] Lopez V., Nielsen B., Solas M., Ram²rez M.J., Jª ger A.K., (2017). Exploring Pharmacological Mechanisms of Lavender (Lavandula angustifolia) Essential Oil on Central Nervous System Targets. Department of Pharmacy, Faculty of Health Sciences, Universidad San Jorge, Zaragoza, Spain.
[2] Buckle J., (2003). Clinical Aromatherapy: Essential Oils in Practice. Second Edition. Page 72-74.
[3] Gismondi a., Marco G., Canini A., (2020). Helichrysum italicum (Roth) G. Don essential oil: Composition and potential antineoplastic effect. South African Journal of Botany Volume 133, Pages 222-226.
[4] D'Auria F. D., Tecca M., Strippoli V., SalvatoreG., Battinelli L., Mazzanti G., (2005). Antifungal activity of Lavandula angustifolia essential oil against Candida albicans yeast and mycelial form. Medical Mycology, Volume 43, Issue 5, Pages 391ï 396.
[5] Bhavaniramya S., Vishnupriya S., SalehAl-Aboodyb M., Vijayakumar R., Baskaran D., (2019). Role of essential oils in food safety: Antimicrobial and antioxidant applications. Grain & Oil Science and Technology, Volume 2, Issue 2, Pages 49-55.
[6] Handa S., Swamiet S., (2008). Extraction Technologies for Mesicinal and Aromatic Plants. International center for sience and high technology. Page 44.

ANALYSIS OF THE BIOCONSOLIDATION POTENTIAL OF *STAPHYLOCOCCUS* SP. H6

Laurynas Vaģkeviļius[1], Vilius MalÎnaviļius[1], Marija Jankunec[2], Renata Gudiukaitā[1]

[1] Vilnius University, Center of Life sciences, Institute of Biosciences, Vilnius, Lithuania
[2] Vilnius University, Center of Life sciences, Institute of Biochemistry, Vilnius, Lithuania
laurynas.vaskevicius@gmc.stud.vu.lt

Microbially induced calcite precipitation (MICP) for soil bioconsolidation is a relatively recently developed safe, effective and eco-friendly technique to improve the general properties of soils and solve several of the most common geoenvironmental problems, i.e. erosion, pollution and CO_2 sequestration. This process utilizes the metabolic pathways of bacteria to form calcites ($CaCO_3$) that bind soil particles together, leading to increased soil strength and stiffness because of this physical connection. The precipitation of carbonates via urea hydrolysis by ureolytic bacteria is the most straightforward and easily controlled mechanism of MICP with potential to produce large amounts of carbonates in a short period of time[1].

This study presents the analysis of *Staphylococcus* sp. H6 as a perspective biological tool to perform bioconsolidation of sand via MICP due to its high ureolytic activity. To our knowledge, we also present the first reported atomic force microscopy (AFM) analysis of an initial growth and precipitation of calcite on bacterial surface.

We conducted the analysis of *Staphylococcus* sp. H6 surface topography changes after treatment with cementation mixture using AFM. The obtained results indicated that the topology of *Staphylococcus* sp. H6 culture already changes after 1 hourõs incubation with the cementation mixture (Fig. 1). It was observed that topographical changes begin forming from one pole of the cells (Fig. 1b, Fig. 1c, Fig. 1e), however this can be due to cell immobilization in the monolayer. It was hypothesized that amorphous $CaCO_3$ precipitates were forming on the cells.

To test small-scale sand bioconsolidation, urease activity dependence on growth rate of *Staphylococcus* sp. H6 was first investigated. The small scale pilot studies of *Staphylococcus* sp. H6 application in bioconsolidation indicated that after exposure of sand with *Staphylococcus* sp. H6 culture solid sand column structures, or in some cases only platelets were formed. The structures obtained by using 0.5/1 M urea and 0.5/1 M $CaCl_2$ displayed hardiness against H_2O and can serve to clog pores in the soil and reduce soil permeability.

This report highlights a soil abundant *Staphylococcus* culture as a promising microorganism for MICP. *Staphylococcus* sp. H6 demonstrated attractive characteristics for CaCO3 precipitation and for sand particle bioconsolidation.

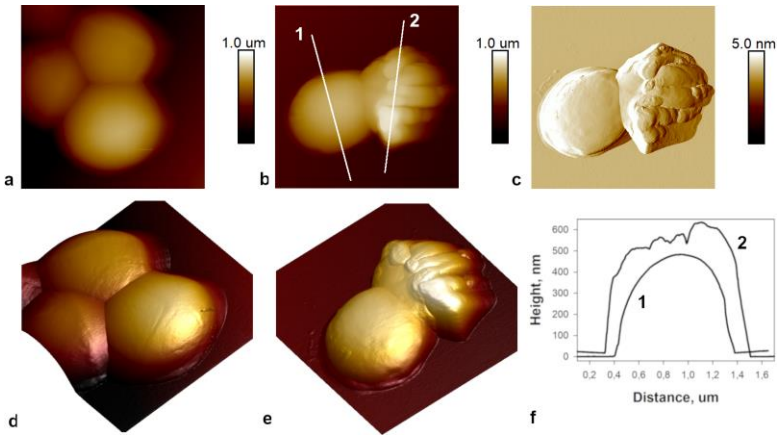

Fig. 1. Changes in bacterial morphology after 1h incubation with cementation solution. 2D and 3D AFM topography images of *Staphylococcus* sp. H6 cells not-affected (a, d) and affected (b, e) with cementation mixture; c) Amplitude signal to show the topography (b) data in more detail; f) section analysis of line 1 and 2 presented in (b). Scan size 2 ε m x 2 ε m.

[1] Anbu, P., Kang, C.-H., Shin, Y.-J. & So, J.-S. Formations of calcium carbonate minerals by bacteria and its multiple applications. Springerplus 5, (2016).

P8-26

DID NOT PARTICIPATE

CONCENTRATION QUENCHING OF ZINC-PHTHALOCYANINE IN SOLUTIONS

Justė Tamošiūnaitė[1,2], Simona Streckaitė[2]

[1] Life Sciences Centre, Vilnius University, Vilnius, Lithuania
[2] Department of Molecular Compound Physics, Centre for Physical Sciences and Technology, Vilnius, Lithuania
juste.tamosiunaite@gmc.stud.vu.lt

Concentration quenching, or aggregation-induced quenching, occurs when the fluorescence quantum yield of fluorophores is significantly reduced upon increase of fluorophore concentration. This phenomenon is encountered in many systems [1]. From biological point of view, a particularly interesting case is quenching in chlorophyll solutions, which has been examined from the middle of previous century to this day [2,3].

In this work, we experimentally examine concentration quenching of Zinc 2,9,16,23-tetra-tert-butyl-29H,31H-phthalocyanine (TB-ZnPC). While phthalocyanine molecules are interesting in their own right [4], their similarity to chlorophyll makes them excellent model systems. It is often argued that formation of H-aggregates is responsible for fluorescence quenching. In Fig. 1a we present the fluorescence spectra of TB-ZnPC in ethanol for a few concentrations. The relative increase of the longer wavelength transition upon increasing concentration demonstrates formation of aggregates for TB-ZnPC molecules. The monomer transition demonstrates redshift upon increasing concentration, also consistent with aggregate formation. Meanwhile, in Fig. 1b the fluorescence decay kinetics are shown and only a minimal dependence upon concentration can be observed. This suggests that no simple relation exists between the mean excitation lifetime and the quantum yield which will be discussed in the presentation.

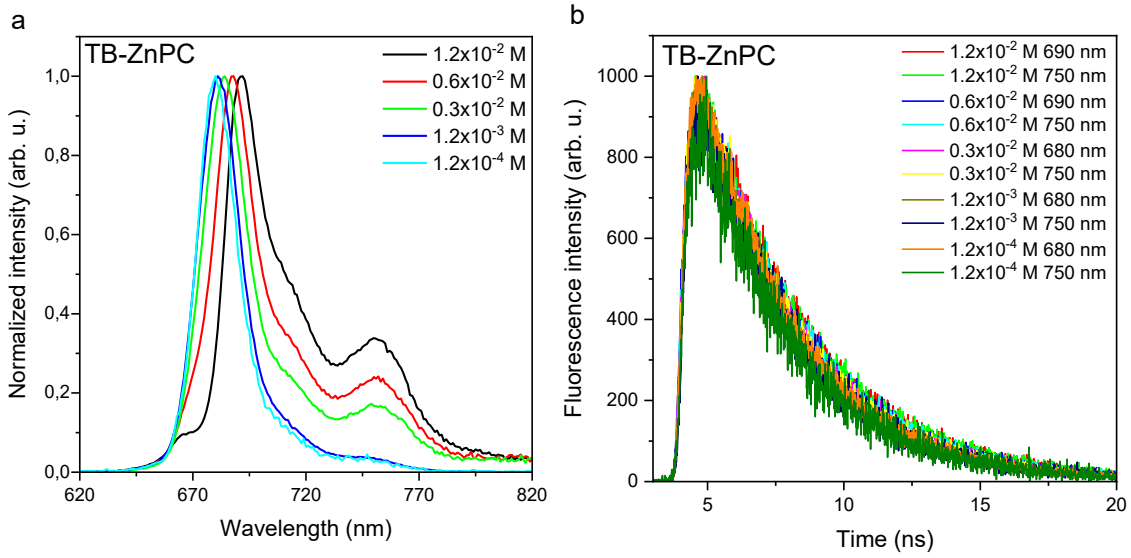

Fig. 1. a) Normalized fluorescence spectra of TB-ZnPC in ethanol at several different concentrations. b) Fluorescence kinetics of the main bands of fluorescence spectra in panel a.

[1] A. I. Burshtein, Concentration of noncoherent excitation in solutions, Sov. Phys. Usp. **27**, 579-606 (1984).
[2] W. F. Watson, R. Livingston, Self-Quenching and Sensitization of Fluorescence of Chlorophyll Solutions, J. Chem. Phys. **18**, 802-809, 1954.
[3] W.-J, Shi, J. Barber, Y. Zhao, Role of Formation of Statistical Aggregates in Chlorophyll Fluorescence Concentration Quenching, J. Phys. Chem. B **117**, 3976-3982 (2013).
[4] J. Mack, N. Kobayashi, Low Symmetry Phthalocyanines and Their Analagoues, Chem. Rev. **111**, 281-321, 2011.

P8-28

DID NOT PARTICIPATE

THE POTENTIAL OF *BACILLUS PSEUDOFIRMUS* AS HEALING AGENT OF BIOLOGICAL SELF-HEALING CONCRETE IN NORTH EUROPE REGION

Augusta Jankutā[1,2], Simona Guobuģaitā[1,2], Ronaldas Jakubovskis[2], Viktor Gribniak[2], Jaunius Urbonaviļius[1]

[1]Department of Chemistry and Bioengineering, Vilnius Gediminas Technical University, Vilnius, Lithuania
[2]Laboratory of Innovative Building Structures, Vilnius Gediminas Technical University, Vilnius, Lithuania
augusta.jankute@vilniustech.lt

Concrete is the most widely used building material in the world. However, cracks inevitably open up in concrete structures. Microbiologically induced calcite precipitation (MICP) can be used to fill cracks arising in concrete. For the formation of biological self-healing concrete specific alkaliphilic spore-forming bacteria, which can survive extreme pH values and harsh conditions in concrete matrix, and mineral precursor compounds such as calcium lactate are needed. In this study, the viability of *Bacillus pseudofirmus* in sub-zero temperatures and in a concrete matrix containing several types of cement with different metal ion concentrations was investigated.

An expanded clay (EC) was used as a carrier for two-component self-healing agent consisting of *Bacillus pseudofirmus* spores and calcium lactate. After 72 days of incubation of EC particles at temperatures below 0 ÁC (-20 ÁC), the number of viable spores remained almost constant (~10^7 CFU/g of EC) compared to control specimens stored at the room temperature. That indicates that *B. pseudofirmus* has a potential to be used in biological self-healing concrete for the Northern Europe region with high number of freeze-thaw cycles. The concrete mix was obtained by mixing EC, cement, sand and water. Out of four cement types commonly used in Lithuania, the best survival rate was obtained in a concrete mix using white CEM I cement. The number of viable *B. pseudofirmus* spores after three days of concrete curing varied from 2.34 Ĭ 10^3 to 6.59 Ĭ 10^4 CFU/g of concrete [1]. These results demonstrate that additional coating of EC aggregates is needed to improve the viability of bacteria in the concrete.

[1] Jakubovkis, R.; Jankutā, A.; Urbonaviļius, J.; Gribniak, V. 2020. Analysis of mechanical performance and durability of self-healing biological concrete. *Construction and Building Materials*, 260, Paper ID: 119822, 1-15.

THE ROLE OF TRPV4 CATION CHANNELS IN SMOOTH MUSCLE CONTRACTILE ACTIVITY IN RATS WITH PARKINSON`S DISEASE

Anastasiia Tsymbaliuk[1], Viktoriia Stetska[1], Taisa Dovbynchuk[1], Oleksandr Gorbach[2], Ganna Tolstanova[3], Alexander Zholos[1]

[1]ESC "Institute of Biology and Medicine" Taras Shevchenko National University of Kyiv,
[2] National Cancer Institute, Kyiv, Ukraine
[3]Institute of High Technologies Taras Shevchenko National University of Kyiv,
64/13, Volodymyrska Street, Kyiv, 01601, Ukraine
inastuska48@gmail.com

Constipation and motility dysfunction are the most common non-motor gastrointestinal (GI) symptoms in Parkinson`s disease (PD) patients [1]. Transient receptor potential vanilloid-type 4 (TRPV4) are expressed in the intestine and can control GI motility [2]. But the specific role of this channels in PD remains largely unknown.

The aim of the study was to test the action of transient receptor potential vanilloid-type 4 selective agonist GSK1016790A on smooth muscle cells contraction in rat's colon with experimental Parkinson`s disease.

The PD was induced by single unilateral stereotaxic injection of 12 μg 6-OHDA. The percentage of destroyed dopaminergic neurons was evaluated in apomorphine test (0.5 mg/kg, i.p.) at 1 and 2 weeks after surgery. The water content in faeces was evaluated on the 1st day, then at the 3rd week and 7th month of the experiment. The daily volume of water consumption and GI transit time were evaluated at the 3rd week and 7th month after surgery. The expression of TRPV4 channels was evaluated by qRT-PCR in muscles and mucosal layer of colon. The action of TRPV4 agonist GSK1016790A (0.3 mmol) on smooth muscle cells of colon was estimated by isometric tension recording.

The apomorphine test showed a progressive increase in the number of turns between the 1st and 2nd week after inducing 6-OHDA-PD. The water content in faeces was increased at the 3rd week ($P<0.05$) *vs.* 1st day of the experiment. The rats with 6-OHDA-PD drank less water *vs.* placebo and intact groups. We observed a 17% delayed GI transit time in 6-OHDA-PD rats ($P<0.01$) *vs.* intact and 21% *vs.* sham-lesioned group of rats 3 weeks after the 6-OHDA treatment. 7 months after the surgery GI transit time was increased more than twice in all studied groups. In 6-OHDA rats, we observed changes in TRPV4 mRNA levels, 50 fold decrease in muscle layer and 2,3-fold increase in mucosa vs sham lesioned rats. TRPV4 agonist action on smooth muscle cells of 6-OHDA-PD rats was reduced by 21% compared to intact group and by 46% in sham-lesioned group ($P<0.05$).

Pharmacological activation of TRPV4 ion channels by their selective agonist GSK1016790A decreased the contractile activity of colon smooth muscle cells in 6-OHDA rats' model of Parkinson's disease.

[1] Carrasco, A. J. P., Timmermann, L. & Pedrosa, D. J. Management of constipation in patients with Parkinson's disease. *NPJ Parkinsons Dis.* **4**, 6, 2018.
[2] Luo J, Qian A, Oetjen LK, Yu W, Yang P, Feng J, et al. TRPV4 Channel Signaling in Macrophages Promotes Gastrointestinal Motility via Direct Effects on Smooth Muscle Cells. Immunity. 2018; 49: 107-119.

CRYSTALISATION OF CRISPR-CAS RELATED TOXIN

Konstanty Keda[1], Giedre Tamulaitiene[1], Irmantas Mogila[1],
Virginijus Siksnys[1], Gintautas Tamulaitis[1]

[1] Institute of Biotechnology, Life Science Center, Vilnius University, Lithuania
konstanty.keda@gmc.stud.vu.lt

Type III CRISPR-Cas system provides prokaryotes with adaptive defence against viruses. It was recently noted that these systems employ specialized cell signalling pathways to combat infections. When CRISPR-Cas effector complex recognizes foreign RNA it starts to synthesize cyclic oligoadenylates from ATP [1]. These molecules activate diverse CRISPR ancillary proteins which consist of signal recognition domain and effector domain: RNase, DNase, ATPase, protease or others [2]. Functions and structures of several effector domains have been elucidated: for example, the RNase activity of HEPN domains [3, 4] and the DNase activity of restriction endonuclease-like effectors [5, 6]. However, many other effector domains have not yet been studied. Recent sequence analysis revealed that a group of such effectors are similar to translation-inhibiting toxins from bacterial toxin-antitoxin systems [2]. In this study we present crystallization results for toxin related to CRISPR-Cas system and discuss possible future strategies.

[1] Kazlauskiene, M., Kostiuk, G., Venclovas, Ļ., Tamulaitis, G. and Siksnys, V. (2017) A cyclic oligonucleotide signaling pathway in type III CRISPR-Cas systems. *Science*, 357(6351), p. 605-609.

[2] Makarova, K.S., Timinskas, A., Wolf, Y.I., Gussow, A.B., Siksnys, V., Venclovas, Ļ. and Koonin, E.V. (2020). Evolutionary and functional classification of the CARF domain superfamily, key sensors in prokaryotic antivirus defense. *Nucleic acids research*, 48(16), p. 8828-8847.

[3] Smalakyte, D., Kazlauskiene, M., F. Havelund, J., Rukšėnaitė, A., Rimaite, A., Tamulaitiene, G., FÞrgeman, N.J., Tamulaitis, G. and Siksnys, V. (2020) Type III-A CRISPR-associated protein Csm6 degrades cyclic hexa-adenylate activator using both CARF and HEPN domains. *Nucleic acids research*, 48(16), p. 9204-9217.

[4] Garcia-Doval, C., Schwede, F., Berk, C., Rostøl, J.T., Niewoehner, O., Tejero, O., Hall, J., Marraffini, L.A. and Jinek, M. (2020) Activation and self-inactivation mechanisms of the cyclic oligoadenylate-dependent CRISPR ribonuclease Csm6. *Nature communications*, 11(1), p. 1-9.

[5] McMahon, S.A., Zhu, W., Graham, S., Rambo, R., White, M.F. and Gloster, T.M. (2020) Structure and mechanism of a Type III CRISPR defence DNA nuclease activated by cyclic oligoadenylate. *Nature communications*, 11(1), p. 1-11.

[6] Rostøl, J.T., Xie, W., Kuryavyi, V., Maguin, P., Kao, K., Froom, R., Patel, D.J. and Marraffini, L.A. (2021) The Card1 nuclease provides defence during type-III CRISPR immunity. *Nature*, p.1-9.

INVESTIGATION OF *GARDNERELLA SPP.* CNA PROTEIN USING IMMUNOLOGICAL METHODS

Raminta Reġkeviļ iÎ tā, Indrā Dalgādienā, Aurelija Çirblienā, Milda Pleļ kaitytā

Vilnius University, Life Sciences Center, Institute of Biotechnology,
Department of Immunology and Cell Biology
raminta.reskeviciute@gmc.vu.lt

Bacterial vaginosis (BV) is one of the most common vaginal infections associated with impaired vaginal microflora that affects women of childbearing age. BV is associated with various adverse outcomes not only relating to womenôs fertility, reproductive health, or pregnancy, but also womenôs mental health [1]. *Gardnerella spp.* is the most associated bacterium with BV and has been detected in almost all vaginal samples from women suffering from BV [2].

Adhesins are cell-surface components that are responsible for the recognition of host cells and adhering to them. Studies on other bacteria show that various adhesins are proven virulence factors that are significant in bacteriaôs pathogenesis [3, 4]. However, the adhesins of bacterium *Gardnerella spp.* are very little studied and described.

After the amino acid sequence of *Gardnerella spp.* collagen adhesin (CNA) protein determination, a hypothesis was proposed that CNA allows *Gardnerella spp.* to bind to host extracellular matrix (EM) proteins.

The interaction between recombinant *Gardnerella spp.* CNA and selected EM proteins was investigated by various ELISA method variations and other immunochemical methods. Monoclonal antibodies (MAbs) against recombinant CNA protein were created using hybridoma technology. Anti-CNA MAbs were used to investigate the interaction between the CNA and EM proteins: type I, III, IV collagens, fibronectin, and fibrinogen. Using indirect ELISA method we detected that CNA interacts with all EM proteins used in the experiment (Fig. 1).

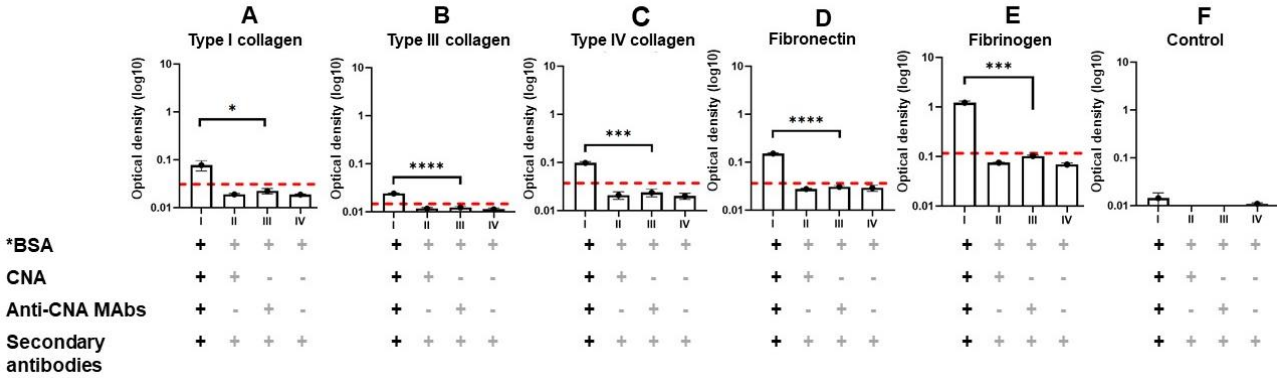

Fig. 1. The investigation of interaction between *Gardnerella spp.* CNA protein and selected EM proteins: A ï type I collagen; B ï type III collagen; C ï type IV collagen; D ï fibronectin; E ï fibrinogen; F ï control, no EM proteins were adsorbed. The *t* test was applied, where *p < 0.05, ***p < 0.001, ****p < 0.0001 (n = 4). The red line indicates the mean of an optical density plus three standard deviations. *BSA ï bovine serum albumin.

Results and created molecular tools, anti-CNA MAbs, raise new questions and hypotheses. In the future, we seek to use more complex model systems to investigate the interactions between native CNA and epithelial cells *in vitro*. This would allow to investigate and understand molecular *Gardnerella spp.* pathogenesis mechanisms.

[1.] Jones, A. (2019) Bacterial Vaginosis: A Review of Treatment, Recurrence, and Disparities, *Jnp-Journal for Nurse Practitioners.* **15**, 420-423.
[2.] Schwebke, J. R., Muzny, C. A. & Josey, W. E. (2014) Role of Gardnerella vaginalis in the Pathogenesis of Bacterial Vaginosis: A Conceptual Model, *Journal of Infectious Diseases.* **210**, 338-343.
[3.] Rhem, M. N., Lech, E. M., Patti, J. M., McDevitt, D., Hook, M., Jones, D. B. & Wilhelmus, K. R. (2000) The collagen-binding adhesin is a virulence factor in Staphylococcus aureus keratitis, *Infection and Immunity.* **68**, 3776-3779.
[4.] Elasri, M. O., Thomas, J. R., Skinner, R. A., Blevins, J. S., Beenken, K. E., Nelson, C. L. & Smeltzer, M. S. (2002) Staphylococcus aureus collagen adhesin contributes to the pathogenesis of osteomyelitis, *Bone.* **30**, 275-280.

PH DEPENDENT SELF-ASSEMBLING OF H_2TPPS_4 IN AQUEOUS SOLUTIONS

Kornelija Buivydaitė[1,2], Marijus Pleļ kaitis[1,2,3], Riļ ardas Rotomskis[1,3]

[1] Biomedical Physics Laboratory, National Cancer Institute, P. Baublio str. 3b, LT-08406 Vilnius, Lithuania
[2] Life Sciences Center, Vilnius University, Saulėtekio av. 7, LT-10257 Vilnius, Lithuania
[3] Biophotonics group of Laser Research Centre, Vilnius University, Saulėtekio av. 9, LT-10222 Vilnius, Lithuania
kornelija.buivydaite@gmc.stud.vu.lt

Recently, supramolecular assemblies of porphyrins have been of growing interests because the aggregate packing structure can be easily tuned through ionic interactions among the cationic core, charged substituents and/or the nature of the inorganic anion. Controlling the packing structure of functional dye molecules by supramolecular methods is a challenging task for tailoring functional materials with desired properties.

The association in aqueous solutions tetrasodium 5,10,15,20-tetrakis(4-sulfonatophenyl) porphyrin (H_2TPPS_4), which was detected by visible spectra has been not clarified. In acidic media it has been described that new species appear with absorptions at 490 and 706 nm. This behaviour in the acidic region has even been described as very complicated. As a result of interchromophoric interactions, perturbations in the absorption and fluorescence spectra of dyes occur. In terms of excitonic coupling, aggregated dyes with blue- and red-shifted absorption bands are referred to as H- and J-aggregates. Due to the distinct optical properties, control of the formation of H- and J-aggregated states of dyes has attracted much research interest.

H_2TPPS_4 is a water-soluble tetrapyrrole molecule (with four sulfo group substitutes), interconnected at Ŭatom via methine bridges. H_2TPPS_4 molecule form changes accordingly to the pH of the solution. In alkaline solutions H_2TPPS_4 is in tetra-anion form with no additional protons attached to the free nitrogen atoms in the center. However, in acidic solutions it can form J-aggregates as it starts self-assembling from its zwitterionic form. The J-aggregates form when positively charged porphyrin rings and negatively charged sulfo groups begin to interact.

In this study, we investigated how different pH affects the formation of ionic species of H_2TPPS_4 molecules, their absorption and fluorescence spectra. The solutions were made by diluting H_2TPPS_4 in deionized water and then changing pH accordingly, with aqueous NaOH (for the pH 7), HCl (for pH 4 to pH 1), or H_2SO_4 (for pH -1) solutions. At the pH 7 tetra-anion form of H_2TPPS_4 was observed with Soret band at 414 nm and Q bands at 516, 553, 594 and 634 nm, respectively. Under 414 nm excitation, fluorescence was observed at 644 nm and 702 nm. By lowering to the pH 4, the H_2TPPS_4 changed to diacid form as two additional protons attached to the free nitrogens at the center of H_2TPPS_4 molecules. Bathochromic shift of the Soret band (435 nm) was observed in the absorption spectrum and the Q bands were reduced to 645 nm with the shoulders around 550 nm, 594 nm. H_2TPPS_4 diacid form under 435 nm excitation had a fluorescence peak at 670 nm. By lowering the pH even more at pH 1 the H_2TPPS_4 formed the zwitterionic form with not only the center nitrogens blocked with protons, but two substitute sulfo groups as well. In this form the H_2TPPS_4 molecules start to actively self-aggregate forming J-aggregates with a distinguished absorption spectrum and Soret band at 490 nm, and Q band at 708 nm. Under 490 nm excitation, the fluorescence peak of the J-aggregates measured at 714 nm. Then, using H_2SO_4 the H_2TPPS_4 solution of pH -1 was reached and at this pH no self-aggregation was observed, as not only all the center nitrogens, but even all the substitute sulfo groups of H_2TPPS_4 were blocked by protons. This led to an absorption spectrum with the Soret band at 438 nm and Q band at 649 nm (bathochromic shift compared to the diacid form of the H_2TPPS_4) and fluorescence (under 434 nm excitation) peak at 682 nm.

The results showed that at certain acidic conditions H_2TPPS4 can form J-aggregates due to positive electrostatic interactions, however if pH gets too low, all SO_3^- groups are blocked and the aggregates can no longer form.

INTRINSIC THERMODYNAMIC PARAMETERS OF HUMAN CARBONIC ANHYDRASE II AND ACETAZOLAMIDE INTERACTION

Eglã VitkÎ naitã and Lina Baranauskienã

Department of Biothermodynamics and Drug Design, Institute of Biotechnology, Life Sciences Center, Vilnius University, Vilnius, Lithuania

egle.vitkunaite@gmc.stud.vu.lt

Carbonic anhydrases (CAs) are metalloenzymes which catalyse reversible reaction of carbon dioxide hydration *in vivo*[1]:

$$CO_2 + H_2O \rightleftharpoons HCO_3^- + H^+ \quad (1)$$

There are twelve catalytically active Ŭ-CA isoforms in humans. Some of them are associated with human diseases such as glaucoma, oedema, epilepsy, cancer. Ŭ-CA isoforms inhibition with small molecule drugs, containing unsubstituted sulfonamide group, is used to control some of these diseases. Nonetheless, none of the currently used drugs is specific for anyone target-CA isoform, and inhibition of others, off-target CAs causes undesired adverse effects. Therefore, the design of new isoform-selective CA inhibitors is still a challenging task.

Human CA II is a cytosolic isoform which has the highest enzymatic activity of all human CAs and is widely distributed in different organs and tissues. In addition to importance as drug target, hCA II is often used as a model protein for analysis of protein-ligand interactions [2]. hCA II is a small, monomeric, non-glycosylated protein, which is readily available and has a wellï studied 3D structure. Analysis of CA binding to its ligands is not straightforward ï CA binding to sulfonamide group bearing compound is linked to several concomitant reactions which occur in addition to binding itself. The binding mechanism includes protonation and deprotonations reactions. Therefore, the observed binding affinity and enthalpy depends on reaction conditions[4]. However, only intrinsic thermodynamic parameters, i. e. independent on reaction conditions, can be directly linked to crystallographic information, and then such results of structure-thermodynamics relationships analysis can be used for rational drug design [3].

In this study we focus on intrinsic thermodynamic parameters of hCA II ï acetazolamide interaction. We used two biophysical methods: isothermal calorimetry titration and fluorescence thermal shift assay. We analysed this reaction by performing experiments in various pH, buffers and temperature. According to dependence of observed binding parameters on reaction conditions we calculated the intrinsic binding parameters (K_d, qH, C_p).

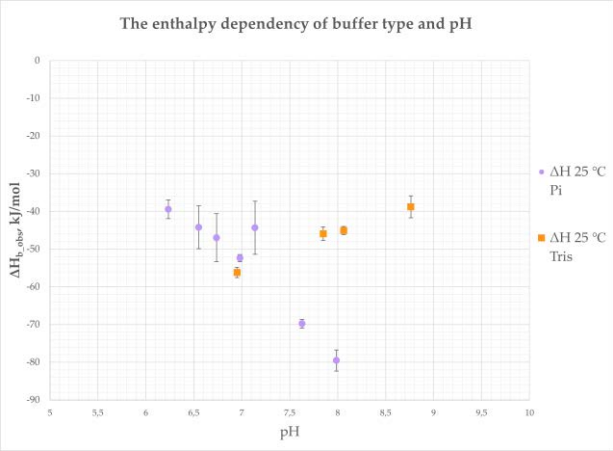

Fig. 1. The dependence of observed enthalpy of hCA II and acetazolamide interaction on buffer type and pH. The experiments were performed at 25 temperature in 0.05 M phosphate buffer with 0.1 M NaCl (purple circles) or 0.05 M Tris buffer (orange squares), with 0.1 M NaCl.

[1] C. L. Lomelino, J. T. Andring, and R. McKenna, ócrystallography and Its Impact on Carbonic Anhydrase Researchô, *International Journal of Medicinal Chemistry*, vol. 2018, pp. 1ï21, Sep. 2018, doi: 10.1155/2018/9419521.

[2] V. M. Krishnamurthy *et al.*, óCarbonic Anhydrase as a Model for Biophysical and Physical-Organic Studies of Proteins and Proteinï Ligand Bindingô, *Chem. Rev.*, vol. 108, no. 3, pp. 946ï1051, Mar. 2008, doi: 10.1021/cr050262p.

[3] V. Linkuvienã *et al.*, óThermodynamic, kinetic, and structural parameterization of human carbonic anhydrase interactions toward enhanced inhibitor designô, *Quart. Rev. Biophys.*, vol. 51, p. e10, 2018, doi: 10.1017/S0033583518000082.

[4] V. MorkÎ naitã *et al.*, óIntrinsic thermodynamics of sulfonamide inhibitor binding to human carbonic anhydrases I and IIô, *Journal of Enzyme Inhibition and Medicinal Chemistry*, vol. 30, no. 2, pp. 204ï211, Mar. 2015, doi: 10.3109/14756366.2014.908291.

ONFLOW: A SOFTWARE TOOL THAT PREDICTS LATERAL FLOW ASSAY PARAMETERS

Denis Baronas[1], Auksė Kazlauskaitė[2], Paulius Sasnauskas[3], Povilas Šėporaitis[3,4], Kamilė Vainiūtė[3]

[1]Department of Biothermodynamics and Drug Design, Institute of Biotechnology, Life Sciences Centre, Vilnius University, Saulėtekio al. 7, Vilnius, LT-10257, Lithuania
[2]Institute of Biosciences, Life Sciences Centre, Vilnius University, Saulėtekio al. 7, Vilnius, LT-10257, Lithuania
[3]Faculty of Mathematics and Informatics, Vilnius University, Naugarduko g. 24, Vilnius, LT-03225, Lithuania
[4]Sector of Microtechnologies, Institute of Biotechnology, Life Sciences Centre, Vilnius University, Saulėtekio al. 7, Vilnius, LT-10257, Lithuania
denis.baronas@gmc.vu.lt

Lateral flow assay (LFA) tests are becoming more popular each year because of their ability to rapidly and cheaply detect small amounts of analyte[1]. However, straightforward questions, for instance, the appropriate concentration of capture sites and optimal test line location can be answered only by experimentation. Thus, the development of LFA tests is very tedious and can exhaust the most valuable resources – time and money. To facilitate the development process of LFA strip tests we have created a universal software tool – onFlow. Our software can accurately predict where to spray probes in order to obtain the most visible results on the strip. onFlow is easy to use as we have provided detailed documentation, default values and integrated an existing molecular interactions platform KOFFI to facilitate user experience as well as an API that makes it accessible to other workflows.

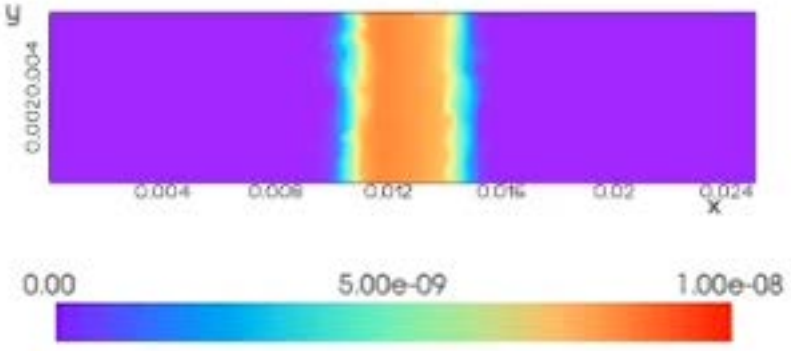

Fig. 1. Simulation of the advection-diffusion-reaction PDE for the concentration of the complex of analyte, detection probe and capture probe throughout the membrane.

The software is based on the mathematical LFA test model that provides a basis for a fast and open-source application that gives recommendations for the design of lateral flow assays. The backbone is a simulation and optimisation of a system of diffusion-advection-reaction partial differential equations[2]. The model uses the finite element method platform FEniCS[3] to simulate a partial differential advection-convection-reaction equation system Eq. (1) and predicts the optimal location of a test line and the required concentrations of reactants to provide a visible signal (Fig. 1).

$$\begin{cases} \frac{\partial [A]}{\partial t} = D_A \Delta [A] - V(t) \cdot \nabla [A] - k_1 [A][P] + k_{-1}[C], \\ \frac{\partial [P]}{\partial t} = D_P \Delta [P] - V(t) \cdot \nabla [P] - k_1 [A][P] + k_{-1}[C], \\ \frac{\partial [C]}{\partial t} = D_C \Delta [C] - V(t) \cdot \nabla [C] + k_1 [A][P] - k_{-1}[C], \\ \frac{\partial [R]}{\partial t} = -k_2 [R][C] + k_{-2}[S], \\ \frac{\partial [S]}{\partial t} = +k_2 [R][C] - k_{-2}[S] \end{cases} \tag{1}$$

[1] Gasperino, D., Baughman, T., Hsieh, H. V., Bell, D. & Weigl, B. H. Improving Lateral Flow Assay Performance Using Computational Modeling. Annual Rev. Anal. Chem. **11**, 219–244 (2018).
[2] Qian, S. & Bau, H. H. A mathematical model of lateral flow bioreactions applied to sandwich assays. Analytical Biochemistry **322**, 89–98 (2003).
[3] Alnæs, M. et al. The FEniCS Project Version 1.5. Archive of Numerical Software **3**, (2015).

PRODUCTION OF RECOMBINANT MOUSE CARBONIC ANHYDRASES Car I, Car II, Car III, Car VII AND Car XIII

Edvardas Timoğlenka, Aurelija Mickeviļiîtă, Lina Baranauskienă

Department of Biothermodynamics and Drug Design, Institute of Biotechnology, Life Sciences Center, Vilnius University, Lithuania

edvardas.timoscenka@gmc.vu.lt

Reversible hydration of carbon dioxide to bicarbonate is catalysed by a family of carbonic anhydrase (CA) enzymes. In mammals, they often exist in multiple isoforms and participate in various physiological processes, including CO_2 and HCO_3^- transport in blood, regulation of pH and electrolyte homeostasis, and some metabolic pathways. Because of their high involvement in physiological processes, human carbonic anhydrases are associated with several diseases, e.g., CA I is linked to haemolytic anaemia, and CA II ï to glaucoma, among others [1]. Their inhibitors are used to control some of these diseases. For medical research purposes, CAs are challenging targets due to high homology and structural similarity between isoforms. The CA isozymes have different levels of kinetic activity, sulphonamide inhibition [2], and are expressed in different tissues. Of particular importance are cytosolic CAs because they are the most abundant class of isoforms. To expand comprehensive views on mammalian CA, research on mice CA (Car) and ligand interactions is performed. Information about Car and small molecule ligand binding could contribute to filed of the drug development for specific CAs.

Here we will present cytosolic Car cloning strategy, expression, purification, and small molecule binding examined by the fluorescent thermal shift assay. The cloning of all Car proteins started with amplification of DNA sequence by PCR, creation of sticky ends with restriction by endonucleases, ligation into pET-15b plasmid, and transformation of *Escherichia coli* bacteria. Growing conditions for a sufficient amount of recombinant Car were optimized by shuffling the *E. coli* strain and varying the protein expression conditions, e.g., amount of added ITPG or using different kinds of zinc salts. The proteins were purified using immobilized nickel ion affinity chromatography. The fluorescent thermal shift assay was used to assess the protein thermal stabilization [3] by binding small molecule ligands. Figure 1A presents optimized results of Car XIII expression and purification, while 1B shows its binding to dichlorophenamide by fluorescent thermal shift assay.

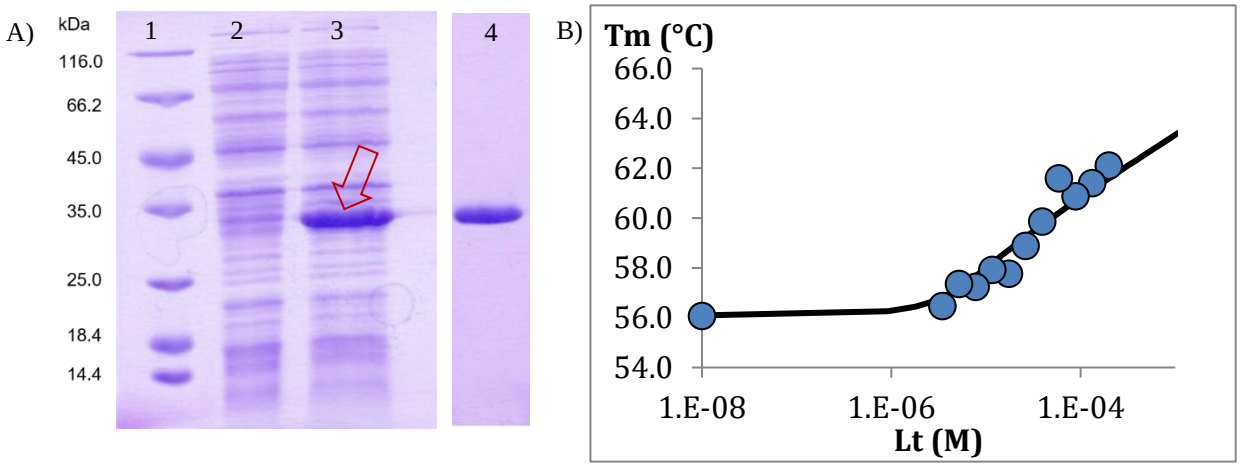

Fig. 1. Car XIII expression, purity and functional activity. A) SDS-PAGE of Car XIII: lane 1 ï MW markers, 2 ï bacterial lysate before induction, 3 ï bacterial lysate after induction, 4 ï purified Car XIII. B) fluorescent thermal shift assay results of Car XIII binding to dichlorophenamide ï symbols correspond to experimental data and line present fitting using K_d determination model.

[1] Susan C. Frost Robert McKenna . Carbonic Anhydrase: Mechanism, Regulation, Links to Disease, and Industrial Applications. DOI: 10.1007/978-94-007-7359-2.

[2] Carta, Fabrizio. A class of sulfonamide carbonic anhydrase inhibitors with neuropathic pain modulating effects. DOI: 10.1016/j.bmc.2015.02.027

[3] Redhead M., Satchell R., Morkî naită V., Swift D., Petrauskas V., Golding E., Onions S., Matulis D., Unitt J. A combinatorial biophysical approach; FTSA and SPR for identifying small molecule ligands and PAINs. June 2015, Anal. Biochem, 63ï 73.

FLAVONE OXIDATION DERIVATIVES ACT AS INHIBITORS OF AMYLOID-BETA AGGREGATION

Andrius Sakalauskas, Vytautas Smirnovas

Institute of Biotechnology, Life Sciences Center, Vilnius University, Lithuania
andrius.sakalauskas@gmc.vu.lt

Protein accumulation into highly dense structure aggregates is associated with multiple neurodegenerative disorders [1]. Alzheimerôs disease (AD) was recognized to be the most prevalent condition that affects over 35 million people worldwide and is projected to increase up to 76 million by 2030 [2]. Typically, Alzheimerôs disease onset at the age of 60 or later, with leading symptoms of progressive decline in memory and other distinct cognitive capabilities [3]. The pathology of this disease is linked to the aggregation of amyloid-beta (Aб) and the formation of Tau neurofibrillary tangles. Aб aggregates are found at the very early stage of the disease, thus the inhibition of this peptide formation and aggregation has profound attention of scientists [4]. Over the years, various compounds were suggested for treatment, however, the effort to find disease-modifying drugs were not rewarding leaving more than 99.5% of clinical trial unsuccessful [5]. Yet, in this research, we focus on the flavones as the potential inhibitors of Aб aggregation. Flavones are natural antioxidants and exhibit neuroprotective and anti-inflammatory effects. The flavones belong to the group of acetylcholinesterase inhibitors, which is shown to have the best positive effect on the treatment of AD symptoms [6]. Although many protein aggregation experiments *in vitro* using flavone derivates show positive results, the *in vivo* results are not flattering. This may be related to a different oxidation mechanism at physiological conditions *in vivo* and *in vitro* leading to environmentally distinct oxidation products [7], [8].

In this study, we show the link between flavone hydroxy-groups position and the oxidation derivatives that possess Aб and insulin amyloid aggregation inhibition effect (Fig. 1). The insulin amyloid aggregation was added to this research to analyze flavone inhibition potential at the conditions where auto-oxidation does not occur, thus both non-oxidized and oxidized flavone particles were tested. The absorbance spectrum data reveal that not all tested flavones undergo auto-oxidation at the experimental conditions. The Aб and insulin aggregation kinetic data show the extreme change of aggregation halftime after compound auto-oxidation. In addition, the atomic force microscopy images display the morphology of the fibrils formed during the experiment.

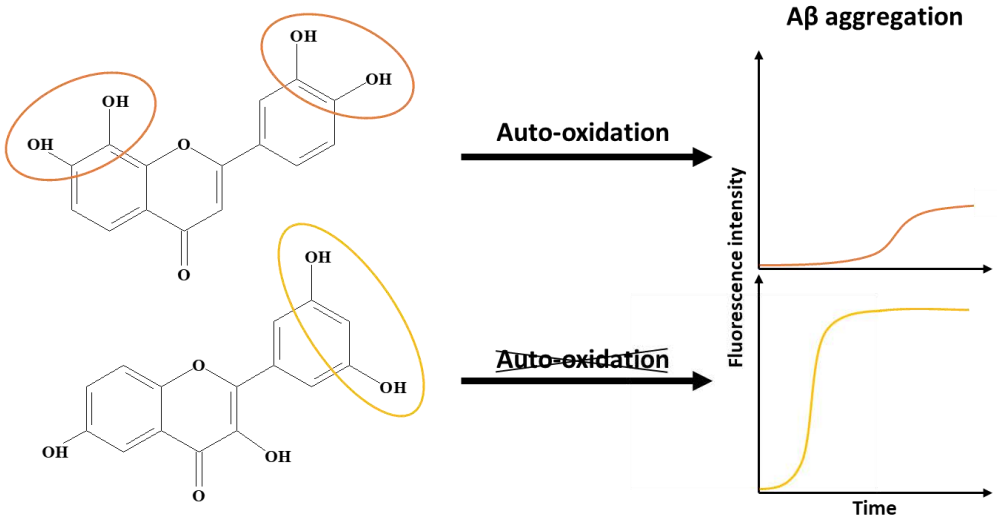

Figure 1. Amyloid-Beta aggregation is inhibited by the flavone auto-odixation derivatives

[1] M. Rekatsina, A. Paladini, A. Piroli, P. Zis, J. V. Pergolizzi, and G. Varrassi, ñPathophysiology and Therapeutic Perspectives of Oxidative Stress and Neurodegenerative Diseases: A Narrative Review,ò *Adv. Ther.*, vol. 37, no. 1, pp. 113ï 139, 2020.

[2] World Health Organization, ñDementia Fact Sheet,ò *WHO*, 2020. https://www.who.int/news-room/fact-sheets/detail/dementia.

[3] M. Tanveer *et al.*, ñMachine learning techniques for the diagnosis of alzheimerôs disease: A review,ò *ACM Trans. Multimed. Comput. Commun. Appl.*, vol. 16, no. 1s, 2020.

[4] A. Anand, A. A. Patience, N. Sharma, and N. Khurana, ñThe present and future of pharmacotherapy of Alzheimerôs disease: A comprehensive review,ò *Eur. J. Pharmacol.*, vol. 815, no. August, pp. 364ï 375, 2017.

[5] D. Mehta, R. Jackson, G. Paul, J. Shi, and M. Sabbagh, ñWhy do trials for Alzheimerôs disease drugs keep failing? A discontinued drug perspective for 2010-2015,ò *Expert Opin. Investig. Drugs*, vol. 26, no. 6, pp. 735ï 739, 2017.

[6] I. Uriarte-Pueyo and M. I. Calvo, ñFlavonoids as Acetylcholinesterase Inhibitors,ò *Curr. Med. Chem.*, vol. 18, no. 34, pp. 5289ï 5302, 2011.

[7] H. Nagayoshi *et al.*, ñOxidation of Flavone, 5-Hydroxyflavone, and 5,7-Dihydroxyflavone to Mono-, Di-, and Tri-Hydroxyflavones by Human Cytochrome P450 Enzymes,ò *Chem. Res. Toxicol.*, vol. 32, no. 6, pp. 1268ï 1280, 2019.

[8] T. Sneideris *et al.*, ñThe Environment Is a Key Factor in Determining the Anti-Amyloid Efficacy of EGCG,ò *Biomolecules*, vol. 9, no. 12, p. 855, Dec. 2019.

EFFECT OF IONIC STRENGTH ON THIOFLAVIN-T AFFINITY TO AMYLOID FIBRILS AND ITS FLUORESCENCE INTENSITY

Kamile Mikalauskaite[1], Mantas Ziaunys[1], Tomas Sneideris[1, 2], Vytautas Smirnovas[1]

[1]Institute of Biotechnology, Life Sciences Center, Vilnius University, LT-10257 Vilnius, Lithuania
[2] Department of Chemistry, University of Cambridge, Cambridge CB2 1EW, UK
kamile.mikalauskaite@gmail.com

Conformational changes in proteins and their aggregation in the form of amyloid fibrils have been implicated in many neurodegenerative disorders, such as Alzheimerôs, Parkinsonôs diseases or mammalian spongiform encephalopathy [1]. Currently, there is a lot of research carried out in order to examine how aggregation of amyloid proteins occurs and how various environmental factors may influence the processes of protein aggregation. It is observed that temperature, pH, ionic strength and type of shaking change not only the kinetic parameters of aggregation, but also the conformational structure of the protein, thus forming fibrils of different strains [2,3]. The fluorescent dye thioflavin-T is one of the most widely used dyes in amyloid protein studies [4]. In this work, it was investigated whether ionic strength of the solution affects the binding of thioflavin-T to amyloid fibrils using absorbance and fluorescence spectroscopy.

Insulin (200 ε M protein dissolved in 100 mM NaCl 100 mM phosphate buffer (pH 2.4), incubation 24 h, 60 ÁC), lysozyme (200 ε M protein dissolved in 2 M GuHCl 50 mM phosphate buffer (pH 6), incubation 24 h, 60 ÁC, with shaking, using glass beads), mouse prion-protein (0.5 mg/ml protein dissolved in 0,5 M GuHCl 50 mM phosphate buffer (pH 6), incubation 24 h, 60 ÁC, Ŭ-synuclein (200 ÕM protein dissolved in PBS, incubation 24h, 60 ÁC, with shaking, using glass beads) amyloid fibrils were prepared. After aggregation, the fibrils were centrifuged, resuspended into distilled water and concentrated to 400 ε M). The absorbance of the samples was measured after mixing the fibrils, ThT and NaCl solutions (final protein conc. 100 ÕM) in the range from 300 to 600 nm. Excitation-emission matrices (EEM) of each sample were then scanned using an excitation and emission range from 435 to 500 nm. The samples were then centrifuged for 10 min at 9000 rpm and the supernatant absorbance in the range from 300 to 600 nm was measured.

A direct dependence between the amount of ThT molecules bound to fibrils and the solutionós ionic strength was observed. At higher ionic strength, more dye molecules are attached to the amyloid fibrils, which increases the sample fluorescence intensity (Fig. 1). Similar ionic strength effects were observed using all four amyloid proteins.

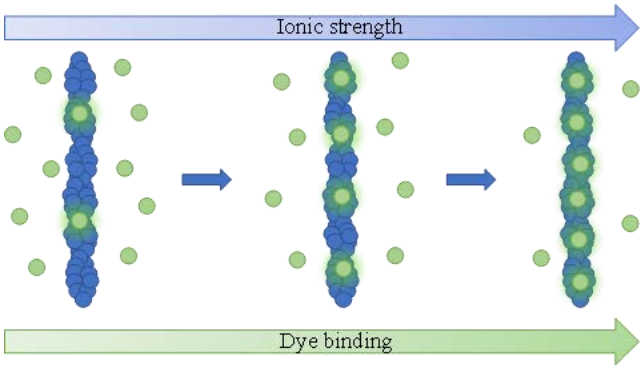

Fig. 1. Higher ionic strength leads to increased fluorescent dye binding.

[1] Knowles TPJ, Vendruscolo M, Dobson CM. The amyloid state and its association with protein misfolding diseases. Nat Rev Mol Cell Biol. 2014 Jun 23;15(6):384ï 96.
[2] Campos-Ram²rez A, M§rquez M, Quintanar L, Rojas-Ochoa LF. Effect of ionic strength on the aggregation kinetics of the amidated amyloid beta peptide Aß (1-40) in aqueous solutions. Biophys Chem. 2017 Sep;228:98ï 107.
[3] Wawer J, SzociŁski M, Olszewski M, PiŇek R, Naczk M, Krakowiak J. Influence of the ionic strength on the amyloid fibrillogenesis of hen egg white lysozyme. Int J Biol Macromol. 2019 Jan;121:63ï 70.
[4] Xue C, Lin TY, Chang D, Guo Z. Thioflavin T as an amyloid dye: fibril quantification, optimal concentration and effect on aggregation. R Soc Open Sci. 2017 Jan 4;4(1):160696.

SELF-ASSEMBLED NANOSTRUCTURES FORMED BY RECOMBINANT PROTEINS OF BACTERIOPHAGE VIRIONS

Laura Kiaugaitā[1], Laurynas Alijogius[1], Eugenijus Gimoliūnas[1], Aurelija Zajanļkauskaitā[1], Martynas Skapas[2], Lidija Truncaitā[1]

1 Vilnius University Life Sciences Center Saulātekio av. 7, Vilnius LT-10257, Lithuania
2 Center for Physical Sciences and Technology, Saulātekio av. 3, Vilnius, Lithuania
laura.kiausaite@gmc.stud.vu.lt

Bacteriophages (phages) are the most widespread and diverse group of viruses that are abundant in microbial ecosystems and specifically infect bacteria. Like other viruses, phages have a nucleic acid genome protected by the proteins of virion. In nature, phages face a wide variety of physical and chemical factors (UV radiation, extreme fluctuations of pH value and temperature). Because of that, the virions of phages are highly robust and stable. This property is very attractive for the development of self-assembled protein nanostructures or phage-like particles.

Phage virion-derived supramolecular nanostructures have a great potential as environment-friendly biomaterials for the development of safe and efficient devices that can be used in technologies and medicine. However, the arsenal of suitable proteins is restricted to only well-studied phages, while the potential of less studied ones remains unknown. Most widespread phages have complex virions designed to recognize and infect host cells. Therefore, prediction of the protein function using only bioinformatic methods can be difficult, and experimental confirmation is needed.

In this study, putative structural proteins of the newly sequenced phages were examined by engineering their recombinant proteins and analyzing the self-assembled protein nanostructures with transmission electron microscope (TEM). For this, we chose three tailed phages from the *Myoviridae* and *Siphoviridae* families, which have the icosahedral heads and tails with the fibers attached to them. The putative tail protein of *Pantoea agglomerans*-infecting phage vB_PagS_MED16, the tail-sheath protein of vB_PagM_AAM22 and the tail-fiber protein from the *Escherichia coli*-infecting phage vB_EcoM_Alf5 were examined.

Our results show that the recombinant proteins of phage virions adopt characteristic forms resembling those of native phages. Therefore, this methodology is suitable for confirmation of the predicted structural function of phage-encoded proteins. Moreover, the resulting nanostructures can serve as basis for engineering of more complex devices that may be utilized depending on their structural and biochemical characteristics.

POLARIMETRIC SECOND HARMONIC GENERATION RESPONSE OF COMPLEX BIOLOGICAL STRUCTURES IN THE FOCAL VOLUME OF THE MICROSCOPE

Mehdi Alizadeh[1*], Fayez Habach[2], Margarete K. Akens[3], Agne Kalnaityte[1], Saulius Bagdonas[1], Virginijus Barzda[1,2,4]

[1] Laser Research Center, Faculty of Physics, Vilnius University, Sauletekio av. 9, LT-10222 Vilnius, Lithuania
[2] Department of Chemical and Physical Sciences, University of Toronto Mississauga, Mississauga, L5L1C6, Canada
[3]Techna Institute, University Health Network, Toronto, M5G 1L5, Canada
[4] Department of Physics, University of Toronto, 60 St. George St, Toronto, M5S1A7, Canada
Mehdi.alizadeh@ff.vu.lt

Polarimetric Second Harmonic Generation (SHG) microscopy can provide extra-molecular information from various non-centrosymmetric biological samples. The results of polarimetric SHG measurements require careful interpretation and modeling when the biological sample has a complex structure in the focal volume. In this study, a numerical modeling [1] has been performed to understand how biophysical parameters such as chiral (C) and achiral (R) susceptibility ratios are affected by different organizations of fibrillar structures in the focal volume. Then the results of numerical modeling have been used to interpret the images obtained from collagenous biological tissues and meso-tetra (4-sulfonatophenyl) porphin (TPPS4) molecules in giant "sea urchin" (GSU) aggregates using polarization-in polarization-out (PIPO) microscopy technique. The numerical modeling shows that in image plane crossing fibers [2] do not have a significant effect on the C ratio. The effect of crossed fibers on the measured R ratio is different for high and low molecular R ratio of individual fibers. In the case of low molecular R ratio, the effective R ratio increases with increasing the crossing angle between two fibers, while the effective R parameter decreases for high molecular R ratio crossing fibers.

On the other hand, tilting fibers out of the image plane affects both R and C ratios [3]. This geometry increases R and C ratios, and the C dependency has a sinusoidal behavior where the sign shows the direction of tilting. These results are in good agreement with the results obtained using PIPO measurements (Fig. 1).

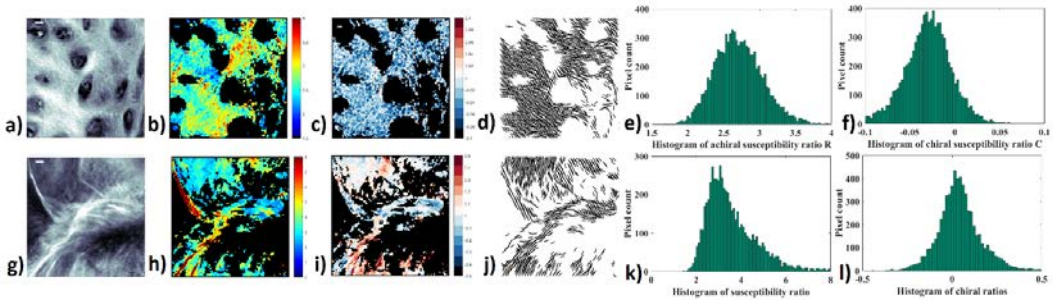

Fig. 1. PIPO microscopy results obtained from cartilage (upper row) and $TPPS_4$ aggregate (lower row) samples. Logarithmic SHG intensity images (a, g). R ratios, (b, h). C ratios (c, i). Cylindrical axis orientation map (d, j) of data in (a) and (g), respectively. Histograms of R values (e, k). Histograms of C values (f, l). Scale bar is 10 μm.

Fig. 1 a) and g) show the logarithmic scaled SHG intensity images of the collagenous and TPPS4 aggregate samples, respectively. Fig.1 b) and h) illustrate the results of R values calculated from Fig.1 a) and g). The $TPPS_4$ has a higher R ratio than cartilage collagen. Fig. 1 c) and i) show the C ratios and Fig.1 d) and j) show the cylindrical orientation maps in the image plane. The histograms of R values are shown in Fig.1 e) and k). The histograms show a higher R ratio for $TPPS_4$. The histograms of C values are shown in Fig.1 f) and l).

There are some regions of interest in the both samples with C ratio close to 0. In some of these regions, different fiber orientations of crossing fibers can be observed at different linear polarization states. In these areas, the value of R increases for low R sample (cartilage), but it decreases for high R sample ($TPPS_4$). Furthermore, there are some regions in the samples without crossing fibers. In these areas, increase in the C values correlates with increase in the R ratio as predicted by the modeling.

In conclusion, biophysical parameters are dependent on the geometry of fibers in the focal volume. PIPO SHG microscopy is a powerful technique to identify different organizations in the focal volume. The results of this study show that PIPO technique enables the reconstruction of complex biological organizations.

[1] D. Sandkuijl, A. E. Tuer, D. Tokarz, J. E. Sipe, and V. Barzda, "Numerical second- and third-harmonic generation microscopy," J. Opt. Soc. Am. B 30, 382 (2013).
[2] M. Alizadeh, D. Merino, G. Lombardo, M. Lombardo, R. Mencucci, M. Ghotbi, and P. Loza-Alvarez, "Identifying crossing collagen fibers in human corneal tissues using pSHG images," Biomedical Optics Express 10, 3875 (2019).
[3] A. Golaraei, K. Mirsanaye, Y. Ro, S. Krouglov, M. K. Akens, B. C. Wilson, and V. Barzda, "Collagen chirality and three-dimensional orientation studied with polarimetric second-harmonic generation microscopy," J. Biophotonics 12, e201800241 (2019).

P8-41

DID NOT PARTICIPATE

OPTICAL STUDY OF PHOTOACTIVE ANTIBACTERIAL AGENTS: RIBOFLAVIN AND CHLOROPHYLLIN.

Rugilã Bareikaitã[1], Deimantã Purytã[1], Irina Buchovec[1]

[1] Institute of Photonics and Nanotechnology, Faculty of Physics, Vilnius University, Lithuania
rugile.bareikaite@ff.stud.vu.lt

Bacteria can be found everywhere: in hospitals, industrial places, food facilities and even spacecraft. The emergence of antibiotic-resistance amongst bacteria is one of the most pressing worldwide issues. One of the promising approaches to treating such bacteria is antimicrobial photoinactivation (API). API is an efficient biophotonic technology based on the interaction of photosensitizer (PS), molecular oxygen, and low doses of light of suitable wavelength to match the PS absorption peak [1]. The interaction of PS and light, in the presence of oxygen results in a plethora of cytotoxic reactions and consequently, induces selective destruction of the target bacteria. Antibacterial efficiency of the API depends on many factors, but most significant on the photophysical properties of used PS. This study focuses on natural PSs - riboflavin (RF) and chlorophyllin (Chl). They are known as human non-toxic and safe for environment photoactive compounds used as food colourants E-101 and E-140ii, respectively [2]. RF (water-soluble Vit B2) is a compound that is quickly degrades by light. According to literature, RF absorption maximums are at 223, 267, 373 and 444 nm. The light-induced RF activation can show potent cytotoxicity and selectively damage different bacteria. Chl is known as a water-soluble, green, negatively charged compound with the main absorption maximum at 405 nm. Therefore, a LED-based light source of light wavelength 405 nm was used in experiments for the optimal excitation of Chl. It is a semi-synthetic porphyrin obtained from chlorophyll that generates reactive oxygen species with antimicrobial activity after exposure to visible light.

Both PSs are known to change the optical absorbance after activation by light. These changes show the activation dependence on excitation dose and can be used to compare the irradiation efficiency by different spectral components. Therefore, the absorption spectra of RF and Chl were investigated after illumination with 450 nm, 405 nm, 4000 K light (Fig.1).

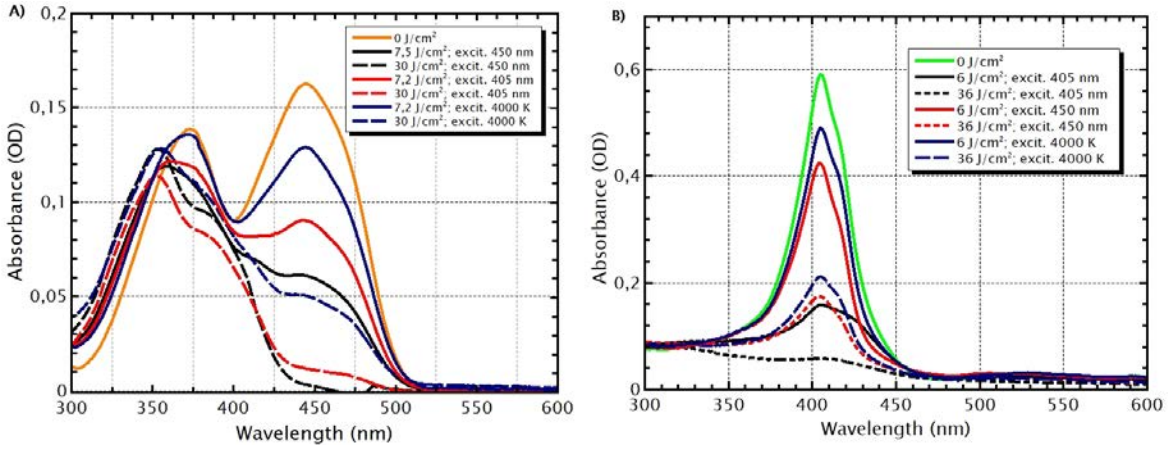

Fig. 1 Photostability as optical absorbance spectra of 1,1Ĭ 10^{-5} M RF (A) and 1Ĭ 10^{-5} M Chl (B) after treatment of different irradiance doses.

The photodegradation effect depicted in Fig. 1A shows that RF can be excited by 450 nm as optimal and by 405 nm and 4000 K light with relative efficiencies of 0,3 and 0,23, respectively. The photodegradation experiments helped assess the RF stability level and revealed itôs photodegradation products after specific illumination exposures. It is known that the aqueous solutions of Chl are also sensitive to light. Our experiments showed that all three irradiance sources (405 nm, 450 nm and white 4000 K) excite Chl, but photoactivation efficiency is different. The photodegradation effect depicted in Fig. 1B shows that Chl can be excited by 405 nm as optimal and by 450 nm and 4000 K light with relative efficiencies of 0,42 and 0,15, respectively. Also, storage stability and photostability of both PSs in the mixture and separate solutions were analyzed. To conclude, RF and Chl are promising natural PSs that can be widely applicable, but the further investigation must be performed.

[1] Buchovec, I et al., (2020). Antimicrobial Photoinactivation Approach Based on Natural Agents for Control of Bacteria Biofilms in Spacecraft. International journal of molecular sciences, 21(18).

[2] T. Maisch *et al.*, ñFast and effective photodynamic inactivation of multiresistant bacteria by cationic riboflavin derivatives,ò *PLoS One*, vol. 9, no. 12, 2014.

MICROBIAL BIOFUEL CELL BASED ON BAKERÔS YEAST TREATED BY 9, 10-PHENANTHRENEQUINONE

Timas Merkelis[1], Kasparas Kizys[2], Antanas Zinovicius[3], Juste Rozene[3], Inga Morkvenaite-Vilkonciene[2,3], Arunas Ramanavicius[1,3]

[1] Vilnius University, Faculty of Chemistry and Geosciences, Naugarduko 24, Vilnius, Lithuania
[2] Vilnius Gediminas Technical University, Faculty of Mechanics, J. Basanavi ius g. 28, 03224 Vilnius, Lithuania
[3] Center for Physical Sciences and Technology, Saul tekio 3, 10257 Vilnius, Lithuania
timas.merkelis@chgf.stud.vu.lt

Over the years alternative energy sources such as microbial biofuel cells (MBFC) are becoming more prevalent. MBFC is an electrochemical device which converts biological energy into usable electric power using biological material as a catalyst for fuel in a redox reaction. Redox mediators used in this system help to transfers electric charge taken from the biological material to the anode [1]. Electrochemical systems that use biological components have desirable traits, such as the ability of cells to self-replicate, regenerate and self-assemble.

BakerÔs yeast can be employed as a catalyst in MBFC. It is a species of single-celled fungi that has great importance in brewing and scientific research. BakerÔs yeast is a simple eukaryotic organism with homology to mammalian and plant cells. Yeast cells are resilient to changing conditions such as pH, anaerobic conditions, temperature. Manipulation of yeast cells is also inexpensive to cultivate and has high metabolic activity, making it very suitable for microbial biofuel cells [**2]**. Although, bioelectrochemical systems have disadvantages, such as low efficiency and the need for redox mediators. Some of these drawbacks can be solved by employing yeast immobilization and modification methods.

In this work we focused on cell treatment by 9, 10-Phenanthrenequinone (PQ) in order to facilitate charge transfer from cells to the anode. PQ passes through the cell walls and sticks to the inner cell membrane [**1].** There it is reduced by the enzymes in the cell and gains 2 electrons which then pass second redox mediator. The second mediator used in our study was potassium ferricyanide ($K_3[Fe(CN)_6]$) due to itôs conductivity and high solubility in water. . After it accepts the electrons from PQ, the redox mediator transfers them to the anode.

It was found that PQ-modified yeast, used in MFBC helps to improve charge transfer from cells to the anode without noticeable effect on cells viability.

[1] Morkvenaite-Vilkonciene I, Ramanaviciene A, Ramanavicius A. 9, 10-Phenanthrenequinone as a redox mediator for the imaging of yeast cells by scanning electrochemical microscopy. Sensors and Actuators B: Chemical. 2016 Jun 2;228:200-6.

[2] Haslett, N. D., Rawson, F. J., Barri re, F., Kunze, G., Pasco, N., Gooneratne, R., & Baronian, K. H. R. (2011). Characterisation of yeast microbial fuel cell with the yeast Arxula adeninivorans as the biocatalyst. Biosensors and Bioelectronics, 26(9), 3742ï3747. doi:10.1016/j.bios.2011.02.011

IDENTIFICATION OF A NOVEL FAMILY OF BACTERIAL LIPOLYTIC ENZYMES

Patricija Izabelė Kaulakytė[1], Lilija Kalėdienė[1], Markas Lukošiūnas[1], Alisa Gricajeva[1]

[1]Department of Microbiology and Biotechnology, Institute of Biosciences, Life Sciences Center, Vilnius University, Sauletekio avenue 7, LT-10257, Vilnius, Lithuania
patricijaizabele@gmail.com

Lipolytic enzymes belong to a large class of enzymes called serine hydrolases that are distinguished by a presence of a nucleophilic serine (nSer) in their active site. Most of the bacterial lipolytic enzymes have the nSer located in a conservative GXSXG pentapeptide (X – any amino acid residue), GDSL motive or less frequently in a motive specific to lipolytic enzymes structurally resembling β-lactamases / DD-peptidases [1]. Conservative amino acid motives and biochemical properties of bacterial lipolytic enzymes are used for their classification [2]. In this work, a putative carboxylesterase (EstAG1) from *Staphylococcus saprophyticus* AG1 [3] with previously uncharacterized pentapeptide and nSer location motive was identified. Enzyme having no close homologues had unconventional GDGTG pentapeptide and nSer located in a SPXYD (Y – hydrophobic residue) sequence previously unspecified for the bacterial lipolytic enzymes. The putatively catalytic nSer and other amino acids related to catalytic function were investigated and validated by site-directed mutagenesis and activity analysis of the mutant recombinant enzymes. Phylogenetic analysis revealed that EstAG1 homologues are found in the other *Staphylococcus* spp. as well. Based on the low amino acid sequence identities, unique conservative amino acid motives and phylogenetic analysis results, EstAG1 belongs to a new family of bacterial lipolytic enzymes.

[1] F. Kovacic, N. Babic, U. Krauss, *Classification of lipolytic enzymes from bacteria* (Springer Nature Switzerland AG: Springer International Publishing, Switzerland, 2019).
[2] T.C.A. Hitch, T. Clavel, A proposed update for the classification and description of bacterial lipolytic enzymes, Peer J **7**, e7249 (2019).
[3] A. Gricajeva, I. Bikutė, L. Kalėdienė, Atypical organic solvent tolerant bacterial hormone sensitive lipase-like homologue EstAG1 from Staphylococcus saprophyticus AG1: synthesis and characterization, International Journal of Biological Macromolecules **130**, 253-265 (2019).

RAMAN LIGHT SCATTERING FROM THE LEAVES PLATES OF AQUATIC MACROPHYTE ELODEA CANADENSIS (MICHX. 1803) UNDER THE INFLUENCE OF MULTILEVEL SALINITY IN VIVO.

Aleksandrs Petjukevičs[1], Natalja Škute[1]

[1] Institute of Life Science and Technologies, Daugavpils University, Daugavpils, Latvia.
aleksandrs.petjukevics@du.lv

An important ecological and physiological parameter for assessing the influence of different salinity levels on plants' growth and development are the changes occurring in the photosynthetic apparatus, significantly the changes of chlorophyll and carotenoid content in the leaves of the plant under the influence of different environmental aspects. Salinity is recognized as one of the leading environmental factors that limit the productivity and development of plants. In general, investigations of the effect of salinity on crops are being studied more actively than other plants. Still, aquatic plants may also experience the adverse effects of NaCl and may be more sensitive to these types of changes or, vice versa, have specific adaptive mechanisms. Therefore, studies in this direction are interesting and promising to clarify this issue and help draw the right conclusions for assessing the effect on plants [2].

During the Raman spectroscopy, the whole leave-plates of the invasive aquatic plant *Elodea canadensis* (Michx.) were examined. It was found that cells exhibit non-uniform distribution of the chlorophyll and carotenoid molecules, which is associated with the different photosynthetic activity rates perhaps caused by various salt concentrations in water. Canadian waterweed was grown in aquarium-tanks with nutrients and various NaCl concentrations: 0 mM, 50 mM, 100 mM in a climate chamber, photoperiod (16 h day / 8 h night, 16°C, relative illumination 2500 Lux).

The Raman spectra were obtained by using the British Renishaw inVia Reflex system at shortened Raman shift range: 1590–850 cm^{-1} (Fig.1.A) and micro-mapping (Fig.1.B), excitation by Ar-ion laser λ = 514.0 nm (~9.2-26.5 mW power at the sample. Obtained Raman spectra were performed with the WiRE 3.3 program, and spectra final correction was carried out using the software package OriginPro 9.2.

The presence of a positive correlation between an increase of NaCl concentration and a decrease of the Raman signal intensity of chlorophyll *a* and chlorophyll *b* (due to overlapping signals of close peaks in some cases, it isn't easy to separate the peaks of Chl *a* from Chl *b*). The 100 mM concentration of NaCl negatively impacted the photosynthetic apparatus's functioning, and at the third week, photosynthetic efficiency decreased significantly [1], [3].

The Raman band's intensity of carotenoids depends on the level of salinity. The peak intensity of the signal of carotenoids was in the range: 395 −16800 a.u. Spectra were similar in general peaks but differ from control samples by the level of shifts signal intensity. Due to the decrease of the total intensity of all peaks in samples (100mM), an increase in the number of low-intensity peaks over the entire length of the spectrum was observed. The band in the region of 1525 cm^{-1} characterizes the stretching vibrations of the double −C=C bonds of the carotenoid molecule and shifts to the high-frequency region when the configuration of the carotenoid molecule changes, the band 1158 cm^{-1} characterizes the stretching vibrations of single C–C bonds. (Fig.1.) The simultaneous shift of the 1525 cm^{-1} band towards lower frequencies and band 1158 cm^{-1} towards higher frequencies may decrease the number of double conjugated bonds in the molecule and processes associated with the changes in the carotenoid molecules. [3]

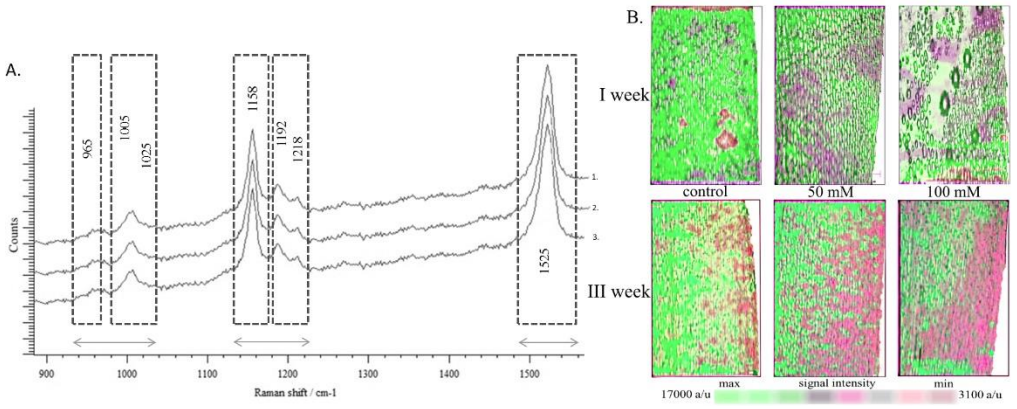

Fig. 1. A The short-range Raman spectra of plant leaves measured directly from leaf surface (- - - Chl *a*, Chl *b,* total carotenoids) **B** - Spatial 2D images of *Elodea canadensis* leaf plate surface with micro-Raman signal intensity maps

[1] A. Petjukevičs, and N. Škute. "Application of Raman scattering in the analysis of the Elodea canadensis genomic dsDNA at different stages of the plant development" Biologia, vol. 72, no. 9, 1017–1022 (2017).
[2] A. Petjukevičs, A. Batjuka & N. Škute. The impact of different levels of sodium chloride on the quantitative changes of chlorophyll and carotenoids in chloroplasts of Elodea canadensis (Michx. 1803). Biologija 61: 34–41(2015).
[3] J. Zeng, J., Ping, W., Sanaeifar, A. et al. Quantitative visualization of photosynthetic pigments in tea leaves based on Raman spectroscopy and calibration model transfer. Plant Methods 17, 4 (2021).

OPTIMIZATION OF GENOME PRIME EDITING IN MURINE EMBRYONIC CELLS

Radvilas Bendorys[1], Bernadeta Masiulionytė[1], Beatričė Milda Balaišytė[1], Stasė Gasiulė[1], Vaidotas Stankevičius[1]

[1]Department of Biological DNA Modification, Institute of Biotechnology, Life Sciences Center, Vilnius University, Lithuania
radvilas.bendorys@gmc.vu.lt

The capability to apply a precise genome editing in cells remains a well-established desire. However, canonical CRISPR‑Cas9 based tools introduce double-strand DNA breaks (DSBs) which can lead to spontaneous INDELs at target site [1]. Prime editing (PE) is the most recent molecular system which consists of a Cas9 nickase fused to a reverse transcriptase. PE is guided by a prime editing guide RNA (pegRNA) which codes both: a guidance to genomic target site and a matrix for the desirable edit [2]. Therefore, PE is able to mediate a targeted mutagenesis without need of DSBs or donor template.

To obtain a desirable base conversion at target site, in this work we adapted and optimized the most recent PE system for genome editing in murine embryonic stem cells. Firstly, plasmids bearing 9 distinct pegRNAs coding SatI restriction site were constructed. Next, the efficiency of genome editing was evaluated by SatI restriction analysis of PCR products which were prepared from cells transfected with plasmids coding PE and corresponding pegRNAs, respectively. Importantly, the analysis revealed that all of selected pegRNA variants showed a significant genome prime editing at the target site. To determine the status of programmable mutagenesis in separate cells, 340 single cell clones were firstly obtained by serial cell dilution. Restriction analysis of each clone unveiled that 27,9% of them obtained a target mutation. Finally, DNA sequencing analysis confirmed that all of the selected 8 clones were bearing a precisely corrected allele and no additional spontaneous mutations were observed in all analysed clones.

In summary, prime editing is a precise and efficient tool for targeted genome mutagenesis in murine embryonic stem cells.

[1] Cong, L., Ran, F. A., Cox, D., Lin, S., Barretto, R., Habib, N., Zhang, F. Multiplex Genome Engineering Using CRISPR/Cas Systems. Science, 339(6121), 819–823 (2013).
[2] Anzalone, A.V., Randolph, P.B., Davis, J.R. *et al.* Search-and-replace genome editing without double-strand breaks or donor DNA. *Nature* 576, 149–157 (2019).

PALMITOXYACETONE, A PRODUCT OF FREE RADICAL LYSOPHOSPHOLIPIDS DESTRUCTION, REGULATES H_2O_2 PRODUCTION BY NEUTROPHILS

Ilya Navitski, Nadezda Amaegberi, Galina Semenkova, Oleg Shadyro

Belarusian State University, Nezavisimosti av., 4, 220030, Minsk, Belarus
ilya.nov42@gmail.com

Lysophospholipids are formed as a result of hydrolysis of glycerophospholipids localized in biological membranes and lipoproteins catalyzed by phospholipases A2 (PLA2) [1]. The products of PLA2 functioning regulate the processes of signal transduction in response to external stimuli. PLA2 plays an important role in the development of pathological conditions associated with oxidative stress formation caused by reactive oxygen species (ROS) hyperproduction. It has been previously shown that ROS induce lysophospholipids destruction. The interaction of lysophosphatidylcholine with ROS is accompanied by lipid molecule fragmentation with the formation of predominantly palmitoxyacetone and stearoxyacetone. The formation of such products from lysophospholipids is possible only through the free radical pathway since the enzymatic systems leading to the accumulation of these compounds have not been found in the human body.

ROS are produced mainly by neutrophils as a result of the enzymes NADPH oxidase and myeloperoxidase activation, which generate superoxide radical anions and hypochlorous acid, respectively [2]. Palmitoxyacetone, formed in the inflammatory focus as a result of ROS-induced free radical fragmentation of lysophospholipids, can change the functional activity of neutrophils, and thus regulate the inflammatory process, which makes this work relevant.

Neutrophils were isolated from the peripheral blood of healthy people in a Histopaque-1077 density gradient according to a standard technique. Cell survival was studied using propidium iodide (λex = 530 nm, λem = 640 nm). ROS generation by neutrophils was determined by the fluorescent method using the H2DCF-DA probe (λex = 488 nm, λem = 530 nm). The cells were stimulated to phagocytosis with the chemotactic peptide fMLP. The measurements were carried out at T = 37 ° C, pH = 7.2.

It has been shown that palmitoxyacetone in the concentration range of 0.1–100 μM doesn't have a toxic effect on cells. It was found that cells incubation with palmitoxyacetone at a concentration of 100 μM for 30 min leads to a decrease, and at a concentration of 1 and 10 μM, to an increase in H_2O_2 production by fMLP-stimulated neutrophils, while 0.1 μM palmitoxyacetone does not affect this process.

Thus, palmitoxyacetone can regulate ROS generation by neutrophils.

[1] G. Lambeau, M. H. Gelb, Biochemistry and physiology of mammalian secreted phospholipases A2, Annu Rev Biochem **77**, 495–520 (2008).
[2] B. M. Babior, Phagocytes and oxidative stress, Am. J. Med. **109,** 33–44 (2000).

THE EFFECT OF INDOLE-CONTAINING STEROIDS ON THE MITOCHONDRIAL MEMBRANE POTENTIAL OF C6 GLIOMA CELLS

Valeriya Klopava [3], Jan Panada [1,2], Tatsiana Kulahava [3,4], Nina Frolova [1], Yaroslav Faletrov [1,2], Vladimir Shkumatov [1,2]

[1] Research Institute for Physical Chemical Problems of the Belarusian State University, Minsk, Belarus
[2] Chemistry faculty of Belarusian State University, Minsk, Belarus
[3] Department of Biophysics, Physics faculty of Belarusian State University, Minsk, Belarus
[4] Institute for Nuclear Problems of the Belarusian State University, Minsk, Belarus
bsu.valeria.kl@gmail.com

Mitochondria are key cellular organelles that play an essential role in various functions such as regulation of cellular metabolism, redox signaling, ionic homeostasis, and cell death [1]. Since tumorigenesis requires flexibility for the tumors to adapt to cellular and environmental alterations, it is not surprising that mitochondria serve a key role in this process [2].

Previously, a series of indole-containing steroids were synthesized: N-(2-(3-indolyl)ethyl)-3β-hydroxyandrost-5-en-17β-amine (IS-1), N-(2-(3-indolyl)ethyl)-3-hydroxyestra-1,3,5(10)-trien-17β-amine (IS-2) and two 20-epimers of N-(2-(3-indolyl)ethyl)-3β-hydroxypregn-5-en-20-amine (IS-3). These compounds were shown to decrease C6 glioma cell proliferation in 10 μM concentration [3], as abiraterone acetate (Abi) anticancer agent did. To examine indole-containing steroid intracellular effects, we investigated the mitochondrial membrane potential (MMP) of C6 glioma cells.

Cells were cultured in DMEM/F-12 medium at 37°C in a humidified 5% CO_2 and 95% air atmosphere. On the third day of growth cells in suspension in HEPES-buffer were incubated with tetraethylbenzimidazolylcarbocyanine iodide (JC-1, 2 μM) for 30 min at 37°C, membrane potential was measured by by spectrofluorimetry. Mitochondrial inhibitors Rotenone (Rot) or Antimicina A (Ana) were added after incubation with JC-1.

We found that Abi at 10 μM decreases the MMP by 62±15%, whereas IS-3R does so by 40±25% (Fig.1 A). IS-1, IS-2, and IS-3S did not affect the MMP. Simultaneous treatment with complex I inhibitor rotenone (Rot) and Abi, IS-1 or IS-3R led to an additional decrease of MMP (Fig.1 B). IS-1 and IS-3R lead to the minor recovery of MMP after inhibition of the third complex by Ana (Fig.1 C).

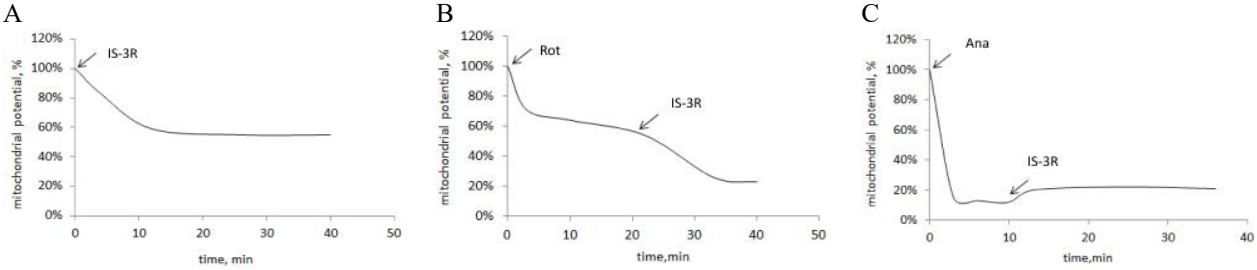

Fig.1. Typical kinetics of MMP changes under the action of IS-3R and complex I (Rot) and complex III (Ana) inhibitors

Although IS-1 is an effective inhibitor of glioma cell proliferation [3], we did not detect it to influence the MMP, contrary to abiraterone, a known apoptosis inducer [4]. The observed effect of the indolesteroid IS-3R on MMP could be related to its interaction with mitochondria on complex III level. Further investigations are underway to examine if apoptosis is involved in indolesteroids' effect on C6 glioma proliferation.

[1] Lalita Guntuku, V, G.M. Naidu, Mitochondrial Dysfunction in Gliomas: Pharmacotherapeutic Potential of Natural Compounds, Curr Neuropharmacol, 14(6): 567–583 (2016).
[2] Altieri D.C., Mitochondria on the move: Emerging paradigms of organelle trafficking in tumour plasticity and metastasis, Br J Cancer. 117:301–305. (2017).
[3] Panada J., Klopava V. et al., New 3β-hydroxysteroid-indolamine conjugates: Design, synthesis and inhibition of C6 glioma cell proliferation, Steroids, 164:108728 (2020).
[4] Lin H.Y., Ko C.Y. et al., CYP17A1 maintains the survival of glioblastomas by regulating SAR-1 mediatedendoplasmic reticulum health and redox homeostasis, Cancers (Basel), 11(9): 1378 (2019).

NEW LINEAR AZOL(IN)E CONTAINING ANTIMICROBIAL PEPTIDE IDENTIFICATION IN THERMOPHILIC BACTERIUM

Justas MartÎnas[1], Alisa Gricajeva[1], Arnoldas Kaunietis[1]

[1] Department of Microbiology and Biotechnology, Institute of Biosciences, Life Sciences Center, Vilnius University, Lithuania
justas.martunas@gmc.stud.vu.lt

Bacteriocins are ribosomally synthesized antimicrobial peptides produced by various bacteria. These antimicrobial peptides are usually stable at high temperatures and over a wide pH range [1]. Bacteriocins have huge potential as both food preservatives, and as next-generation antibiotics targeting the multiple-drug resistant pathogens. It has been suggested that the majority of bacterial species synthesize bacteriocins. The increasing number of reports of new bacteriocins with unique properties indicates that there is still a lot of to learn about this family of peptide antibiotics. Our goal is identification and characterization of novel bacteriocins encoded in thermophilic bacteria. In this study we have identified novel post-translationaly modiefied bacteriocin, belonging to the subclass of linear azol(in)e containing peptides (LAPs), which was encoded in Parageobacillus toebi bacterium. Here we present cloning and expression of this bacteriocin in Escherichia coli. Following the expression, we will purify and characterize its antibacterial effect on various (Para)Geobacillus spp. and other bacteria. Moreover, we will investigate its stability in various temperatures and pH values.

[1] R.H. Perez, T. Zendo, K. Sonomoto, Novel bacteriocins from lactic acid bacteria (LAB): various structures and applications, Microb. Cell Fact. 13 (2014) S3.

ADOMET ANALOGUES WITH FLUORESCENT MOIETIES. RESEARCH ON SYNTHESIS OF FLUORESCEINCARBOXY MOIETY POSSESSING ALKYNE AND PREPARATION OF 6-AZIDOHEX-2-YN-1-YL NOSYLATE

Julija Jurevičiūtė, Martynas Malikėnas

Faculty of Chemistry and Geosciences, Vilnius University, Lithuania
julijaj90@gmail.com

Fluorescent dyes have been a topic of discussion for several decades. Development of new fluorophores has improved sensitivity of biomolecule detection. Some of the most widely used fluorophores are fluorescein and its analogues. Depending on pH fluorescein can exist in "open" or "closed" forms, monoanionic form shifts UV (ultraviolet) spectra in the blue wave direction, comparing with its dianionic form, which has a strong fluorescent emission [1]. Also, fluorescein synthesis has been a topic of debate due to lack of selectivity of Friedel-Crafts acylation (*Fig. 1*). Products that form are structural isomers, their separation requires preparative HPLC (high-performance liquid chromatography) and for this reason pure carboxyfluorescein and its derivatives are costly [2].

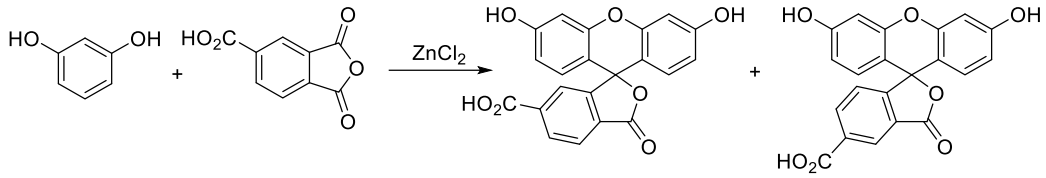

Fig. 1. Synthesis of fluorescein derivatives.

S-Adenosyl-L-methionine (AdoMet) is a commonly used cofactor, which participates in numerous methyl group transfer reactions occurring in living organisms. Sulphur-bound methyl group is transferred onto biomolecules via S_N2 reaction. While methyl group transfer is simple and is catalysed by native methyltransferases (MTases), it has no utility for biomolecule tagging. Despite that, other transferable groups together with engineered MTases are usually applied for tagging in biological systems [3].

In our laboratory, synthesis of fluorescein-6-carboxamide (**1**) has been developed. 6-Carboxyfluorescein, TBTU (2-(1H-Benzotriazole-1-yl)-1,1,3,3-tetramethylaminium tetrafluoroborate), DIPEA (N,N-diisopropylethylamine) and propargyl amine are stirred in N,N-dimethylformamide (DMF). Desired product forms in 78% yield (*Fig. 2*).

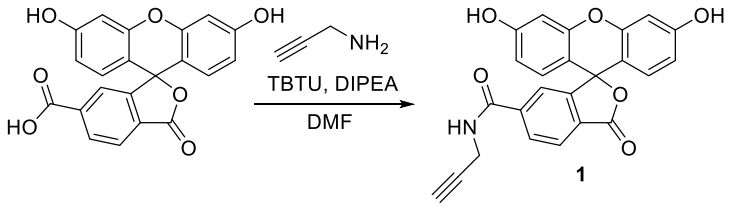

Fig. 2. 6-Carboxyfluorescein reaction with propargyl amine.

Another prerequisite component for the synthesis of AdoMet cofactor analogue has been obtained from 6-azidohex-2-yn-1-ol, 4-nitrobenzensulfonylchloride and a strong base potassium *tert*-butoxide (*Fig. 3*). Synthesis of 6-azidohex-2-yn-1-yl-4-nitrobenzensulfonate (**2**) is accompanied by the formation of ether side product (**3**).

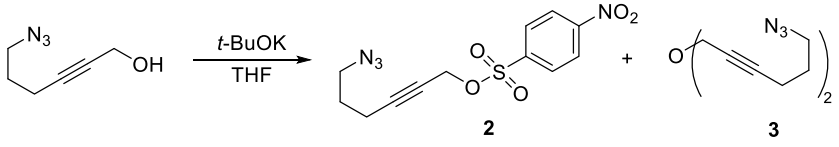

Fig. 3. Synthesis of 6-azidohex-2-yn-1-yl-4-nitrobenzensulfonate.

In the near future we are preparing to synthesise an AdoMet analogue, which, instead of a methyl group, would contain a alkynylazide group. The produced versatile cofactor with a reactive azido group would then be reacted with fluorecein-6-carboxamide (**1**) to form cofactor possessing a fluorescein tag.

[1] M. Rajasekar. *J. Mol. Struct.* **2021**, *1224*, 129085.
[2] Y. Duan, M. Liu, W. Sun, M. Wang, S. Liu, Q. Li. *Mini. Rev. Org. Chem.* **2009**, *6* (1), 35–43.
[3] G. Lukinavičius, M. Tomkuvienė, V. Masevičius, S. Klimašauskas. *ACS Chem. Biol.* **2013**, *8* (6), 1134–1139.

NOTES

NOTES

NOTES

NOTES

OPEN READINGS 2021 ORGANIZERS

Faculty of Physics

SPIE. STUDENT CHAPTER VILNIUS UNIVERSITY

OSA Vilnius University Student Chapter

CENTER FOR PHYSICAL SCIENCES AND TECHNOLOGY

EPS Young Minds

SPONSORS

LIGHT CONVERSION

EKSPLA

BROLIS SEMICONDUCTORS

OPTOGAMA

EKSMA OPTICS

MONO SPEKTRA

Altechna

femtika

PULSAR

HOLTIDA

LIDARIS LIDT Service

TERAVIL

OPTOMAN

IBS HERO

Optoteka

Quantum Light Instruments

3photon

integrated optics

EKSMA

QS LASERS

AgriFood DIH Lithuania

Go Vilnius

THORLABS

Gudobelė

akvilė

BARLEY BROS SOFT BREW